NUREG/CP-0024
Vol. 3

Proceedings of the U.S. Nuclear Regulatory Commission

Ninth Water Reactor Safety Research Information Meeting

Held at
National Bureau of Standards
Gaithersburg, Maryland
October 26-30, 1981

U.S. Nuclear Regulatory Commission

Office of Nuclear Regulatory Research

Available from

GPO Sales Program
Division of Technical Information and Document Control
U.S. Nuclear Regulatory Commission
Washington, DC 20555

Printed copy price: $17.00

and

National Technical Information Service
Springfield, VA 22161

NUREG/CP-0024
Vol. 3

Proceedings of the U.S. Nuclear Regulatory Commission

Ninth Water Reactor Safety Research Information Meeting

Held at
National Bureau of Standards
Gaithersburg, Maryland
October 26-30, 1981

Date Published: March 1982

Office of Nuclear Regulatory Research
U.S. Nuclear Regulatory Commission
Washington, D.C. 20555

FINAL AGENDA

NINTH WATER REACTOR SAFETY RESEARCH
INFORMATION MEETING

AT THE

NATIONAL BUREAU OF STANDARDS
ADMINISTRATION BUILDING 101
GAITHERSBURG, MARYLAND

October 26-30, 1981

TABLE OF CONTENTS

MONDAY, OCTOBER 26, 1981

INTEGRAL SYSTEMS EXPERIMENTS

LOFT Experimental Results

Chairman: G. D. McPherson, NRC

10:30 am -	Introduction	G. D. McPherson, NRC
10:35 am -	Pumps Off (L3-5) and Pumps On (L3-6) Results and Implications	J. H. Linebarger, INEL
11:05 am -	Multiple Failure Loss-of-Feedwater Transient Results and Implications (LOFT Experiment L9-1/L3-3)	C. W. Solbrig, INEL
11:30 am -	Results from LOFT Experiment L6-7/L9-2	J. P. Adams, INEL
11:50 am -	Preliminary Results of Intermediate Break Experiments L5-1 and L8-2	W. H. Grush, INEL
12:05 pm -	A Summary of LOFT Conclusions Relevant to Licensing	R. R. Landry, NRC
12:35 pm -	Blowdown Quench Characteristics of Nuclear and Electric Rods - Influence of Cladding Surface Thermocouples	E. L. Tolman, INEL

Co-Chairmen: G. D. McPherson, W. C. Lyon, NRC

2:00 pm -	Results of Semiscale MOD-2A Upper Head Injection Test Series	A. G. Stephens, INEL

2:35 pm -	Semiscale MOD-2A Natural Circulation Test Series - Preliminary Results	D. J. Shimeck, INEL
3:30 pm -	Break Area Parameter Test Series of ROSA-III for BWR LOCA/ECCS Tests	M. Shiba, JAERI
3:50 pm -	ROSA IV Program at JAERI for PWR Small-Break LOCA Experiments	M. Shiba, JAERI
4:10 pm -	Large Break Integral Test with TBL-1 (Hitachi BWR Integral Facility)	M. Naitoh, Hitachi
4:30 pm -	LOBI* - Influence of PWR Primary Loops on Blowdown - First Results	W. L. Riebold, JRC Ispra
5:00 pm -	PKL-I Findings - PKL-II Plans	D. Hein, KWU, FRG

MECHANICAL/STRUCTURAL ENGINEERING

Load Combinations

Chairman: J. A. O'Brien, NRC

10:30 am -	LOCA-SSE Combination and Asymmetric Blowdown Probability Assessment	C. K. Chou, LLNL
11:10 am -	Piping Reliability Model Validation Based on PWR Feedwater Line Cracking Data	H. Woo, LLNL
11:40 am -	Reliability Approach and Load Combination Criteria	C. A. Cornell, MIT
12:15 pm -	Design Criteria for Shipping Containers Used for Transporting Irradiated Fuel	R. Langland, LLNL

Seismic Safety Margins Research

Chairman: C. W. Burger, NRC

2:00 pm -	Overview	M. Bohn, LLNL
2:30 pm -	Structural Responses (SMACS Code)	J. Johnson, SMA
3:30 pm -	Building and Piping Sensitivity Studies	S. Shukla, LLNL
4:00 pm -	Probability and Risk (SEISIM Code)	J. Wells, LLNL
4:30 pm -	Application of SSMRP to San Onofre Plant	T. Chuang, LLNL

*Loop Blowdown Investigations

5:00 pm -	Ongoing Development	M. Bohn, LLNL

TUESDAY, OCTOBER 27, 1981

SEPARATE EFFECTS

Co-Chairmen: W. B. Beckner, M. W. Young, NRC

9:15 am -	Overview of NRC's BWR Safety Research	W. D. Beckner, NRC
9:25 am -	BWR Blowdown/Emergency Core Cooling Integral Test Program - Final Results from the Two Loop Test Apparatus (TLTA)	G. L. Sozzi, GE
9:40 am -	BWR Refill/Reflood Test Results	J. A. Findlay, GE
9:55 am -	BWR TRAC Model Development and Assessment	J. G. M. Andersen, GE
10:25 am -	TRAC-BWR Heat Transfer	R. E. Phillips and R. W. Shumway, INEL
10:40 am -	Precursory Cooling Effect on the Reflooding of a Hot Vertical Rod	Y. W. Lee, KAERI
11:00 am -	Rod Bundle Heat Transfer Research at ORNL	W. G. Craddick, ORNL
11:20 am -	FLECHT-SEASET Program	L. E. Hochreiter, W
12:00 pm -	Phenomenological Modeling of Two Phase Flow in a Water Reactor at ANL	M. Ishii, ANL
12:20 pm -	Parallel Channel Effects During the Emergency Core Cooling of a BWR	R. T. Lahey, Jr., RPI
12:40 pm -	Countercurrent Flow of Steam and Cold Water in an Inclined Rectangular Channel	S. G. Bankoff, NWU

ADVANCED INSTRUMENTATION

Co-Chairmen: Y. Y. Hsu, A. L. Hon, NRC

2:00 pm -	Introduction	Y. Y. Hsu, NRC
2:10 pm -	Improved Measurements of Cladding Temperature and Fluid Velocity for LOFT	D. J. Hanson, INEL
2:45 pm -	Determining Non-Condensible Gas Concentrations Using Wet Bulb and Dry Bulb Temperature Measurements	P. Griffith, MIT
3:00 pm -	Two-Phase Flow Measurements by Pulsed Neutron Activation Techniques	P. Kehler, ANL

3:30 pm -	Development and Evaluation of Liquid Level Sensors for Use in PWRs	J. E. Hardy, ORNL
4:20 pm -	A Concept for a Fast Neutron, Non-Invasive, Liquid Level and Density Gauge for Nuclear Power Reactors	W. A. Jester, Penn State Univ.
4:35 pm -	Water Spray Studies	R. S. Tankin, NWU
4:50 pm -	Two-Phase Performance Characteristics of of the LOBI Pump	L. Piplies, JRC, Ispra
5:05 pm -	Containment Emergency Sump Studies to Investigate Unresolved Safety Issue A-43	G. G. Weigand, SNL

STRUCTURAL ENGINEERING

Chairman: J. F. Costello, NRC

9:15 am -	Introduction	W. F. Anderson, NRC
9:30 am -	Structural Safety Margins of Containments	W. A. Von Riesemann, SNL
10:30 am -	Design Recommendations Based on Large Scale Testing of Containment Elements	H. G. Russell, PCA
11:00 am -	Safety Margin in Shear Design Criteria for Reinforced Concrete Containments	R. N. White, Cornell U.
11:30 am -	Hydrogen Detonation Loading on Reinforced Concrete Containments	M. N. Fardis, MIT
12:00 pm -	Category I Structures Program	E. G. Endebrock, LANL
12:30 pm -	Containment Buckling Program	C. A. Anderson, LANL
2:00 pm -	Load Combinations for Design of Category I Structures	M. Shinozuka, Columbia U./BNL
2:25 pm -	Errors Resulting from Dynamic Reduction	C. A. Miller, CUNY/BNL
2:50 pm -	Evaluation of Dynamic Testing of Nuclear Power Plant Structures	B. J. Hsieh, ANL
3:30 pm -	Experimental and Analytical Results of Coupled Fluid-Structure Interactions During Blowdown of the HDR Vessel	L. Wolf, KFK, FRG

HUMAN FACTORS RESEARCH

Chairman: R. DiSalvo, NRC

9:15 am -	Welcome and Introductory Remarks	R. DiSalvo, NRC
9:30 am -	A Validated Task Analysis for Reactor Operators	S. Eckel, General Physics
10:30 am -	Time Response Data on Safety-Related Operator Actions	E. Kozinsky, General Physics
11:15 am -	Sandia Human Factors Projects in Nuclear Power	A. D. Swain, SNL
11:45 am -	Results of Graphic Display Evaluation During Transients at the Loss-of-Fluid Test Facility (LOFT)	O. R. Meyer, INEL
2:00 pm -	Results of Control Room Annunciator Systems Evaluations	W. W. Banks, INEL
2:30 pm -	Training Simulator Requirements - A Comparison Among Several Industries	P. M. Haas, ORNL
4:15 pm -	Preliminary Findings of the Human Factors Society Study of Nuclear Reactor Safety Research	H. L. Snyder, VPI

WEDNESDAY, OCTOBER 28, 1981

ANALYSIS DEVELOPMENT

Chairman: S. Fabic, NRC

9:15 am -	RELAP5; Status and Application Experience	V. H. Ransom, INEL
9:45 am -	TRAC-BWR - Transient Reactor Analysis Codes for Boiling Water Reactors	W. L. Weaver III, INEL
10:30 am -	TRAC-PF1 Methods and Models	D. R. Liles, LANL
11:10 am -	Modeling of H_2 Migration in LWR Containments	J. R. Travis, LANL
11:30 am -	Status and Application of COBRA/TRAC and COBRA-TF Codes	M. J. Thurgood, PNL
12:30 pm -	Stability Criteria for PWR Fuel Assemblies in a Baffle Jet Flow	H. Lee, KAERI
2:00 pm -	Status of Code Assessment	F. Odar, NRC

2D/3D PROGRAM

Chairman: L. H. Sullivan, NRC

3:30 pm -	Introduction	L. S. Tong, NRC
3:40 pm -	SCTF Core-I Test Results (System Pressure Effects on Reflooding Phenomena)	H. Adachi, JAERI
4:20 pm -	CCTF Core I Test Results	Y. Murao, JAERI
5:00 pm -	TRAC Analysis Support for the SCTF and CCTF Tests	K. A. Williams, LANL

MECHANICAL ENGINEERING

Chairman: J. A. O'Brien, NRC

9:15 am -	Introduction	J. Richardson, NRC
9:30 am -	Thermal Shock Tests on a Nozzle Corner Performed Within the HDR-Safety Program	W. Muller-Dietsche KFK, FRG
10:30 am -	HDR Analyses (German Standard Problem 4a)	G. E. Howard, ANCO
11:30 am -	Seismic Investigation of HDR Piping	G. L. Thinnes, INEL
12:15 pm -	Computer Code Verification - Mechanical Piping Benchmark Problems	P. Bezler, M. Subudhi, and M. Reich, BNL

Chairman: D. J. Guzy, NRC

2:00 pm -	WIPS: Computer Code for Pipe Whip and Impact Analysis	G. Powell, UCB
2:30 pm -	Two-Phase Jet Loads	S. L. Thompson, SNL
3:30 pm -	Pipe-to-Pipe Impact Tests	M.C.C. Bampton, PNL
4:00 pm -	Characterization of Pressurized Water Reactor Response During Small Break LOCAs	J. A. Hunter, INEL
4:30 pm -	Qualification, Application and Testing of Snubbers	A. T. Onesto, ETEC

INSTRUMENTATION AND CONTROL RESEARCH

Chairman: G. S. Lewis, Jr., NRC

9:15 am -	Instrumentation and Control Program - An Overview	E. C. Wenzinger, NRC

9:40 am -	Demonstration of an On-line Reactor Noise Surveillance System at a PWR	N. E. Clapp, Jr., C. M. Smith, ORNL
10:20 am -	Summary of Studies on Methods for Detecting, Locating and Characterizing Metallic Loose Parts in Nuclear Reactor Coolant Systems	R. C. Kryter, ORNL F. Shahrokhi, U. of Tennessee
10:45 am -	BWR Stability Monitoring Using Neutron Noise	B. R. Upadhyaya, J. March-Leuba, U. of Tennessee
11:10 am -	Feasibility of Detecting and Quantifying PWR Fuel Assembly Vibrations Using Ex-Core Neutron Detectors	F. J. Sweeney, J. A. Reiner, ORNL
11:35 am -	BWR Subcritical Reactivity Monitoring Using the ^{252}Cf Source Driven Neutron Noise Method	J. T. Mihalczo, W. T. King, J. A. Reiner, ORNL
12:00 pm -	Base Neutron Noise in PWRs	G. Kosaly, R. W. Albrecht, D. J. Dailey, U. of Wash. D. N. Fry, ORNL

SELECTED R&D AT EPRI

Chairman: W. B. Loewenstein, EPRI

2:00 pm -	EPRI Safety Program Highlights	W. B. Loewenstein and A. G. Adamantiades, EPRI
2:35 pm -	EPRI Pressurized Thermal Shock Program	T. Marston and K. H. Sun, EPRI
3:30 pm -	Modular Modeling System Code: Review and Qualification	A. B. Long and J. P. Sursock, EPRI
4:00 pm -	Status of EPRI's Dynamic Piping Test Program	H. T. Tang, EPRI
4:30 pm -	Mechanistic Modeling of Two-Phase Flow in Vertical Geometry	G. Lellouche and B. Zolotar, EPRI
5:00 pm -	Early Results of EPRI Research on Hydrogen Combustion and Management	L. Thompson, EPRI

THURSDAY, OCTOBER 29, 1981

FUEL BEHAVIOR RESEARCH

DBA/LOCA - Recent Progress and Status

Chairman: M. Silberberg, NRC
Session Secretary: G. P. Marino, NRC

9:15 am -	Trends in Thermal Calculations for Light Water Reactor Fuel (1971 - 1981)	D. D. Lanning, PNL
9:45 am -	Independent Assessment of FRAPCON-2 and FRAP-T6	E. T. Laats, INEL
10:30 am -	Fuel Rod Bundle Ballooning Test Results from FRG-REBEKA	F. Erbacher, KFK, FRG
11:00 am -	Preliminary Results of MRBT Bundle B-5 (8x8) Test	R. Chapman, ORNL
11:30 am -	LOCA Simulation in NRU	C. Mohr, PNL
12:10 pm -	Results of PBF Appendix K Tests	P. E. MacDonald, INEL
2:00 pm -	Panel Discussion: DBA/LOCA: What Remains to be Done in Fuel Behavior Research	

Panel Chairman: R. Van Houten, NRC
Panel Secretary: G. P. Marino, NRC
Panel Members: R. Meyer, NRC
S. Schultz, Yankee Atomic
P. Rotundo, CE
P. E. MacDonald, INEL

2D/3D Program Workshop

Chairman: L. M. Shotkin, NRC

9:15 am -	Introduction	L. M. Shotkin, NRC
10:30 am -	Flow Reversal Studies During Hot Leg Injection	P. H. Rothe, Creare
11:00 am -	Jet Disintegration in Upper Plenum	J. B. Colson, INEL
11:30 am -	Measurement of Two-Phase Flow at the Core-Upper Plenum Interface Under Simulated Reflood Conditions	D. G. Thomas, ORNL

SEVERE ACCIDENT ASSESSMENT

Co-Chairmen: T. J. Walker, J. T. Larkins, NRC

2:10 pm -	The Large-Scale Melt Facility	T. Y. Chu, SNL

2:25 pm -	Core/Concrete Experiments at Sandia National Laboratories	W. W. Tarbell, Ktech Corp.
3:00 pm -	Core Retention Assessment Program at Sandia National Laboratories	J. D. Fish, SNL
3:30 pm -	CORCON Molten Fuel-Concrete Interactions Code	R. K. Cole, SNL
3:45 pm -	Development of CONTAIN for LWR Containment Analysis	M. J. Clauser, SNL
4:00 pm -	Hydrogen Behavior and Control in Light Water Reactor Accidents	M. Berman, SNL
4:40 pm -	Core-Melt/Coolant Interactions	M. Corradini, SNL
5:10 pm -	SNL Program in Support of LWR Degraded Core Accident Analysis	G. A. Greene, BNL

MATERIALS ENGINEERING

9:15 am -	Introduction, MEB 5-Year Plans, RES & SD	C. Z. Serpan, Jr., NRC

Pressure Vessel Integrity

Chairman: M. Vagins, NRC

9:35 am -	Integrity of Reactor Pressure Vessels During Overcooling Accidents	R. D. Cheverton, ORNL
10:30 am -	Pressurized-Thermal-Shock Tests	G. D. Whitman, ORNL
10:50 am -	Small Specimen Fracture Toughness	R. K. Nanstad, ORNL
11:30 am -	Low Ductile Shelf Intermediate Vessel Test V-8A	R. H. Bryan, ORNL
11:50 am -	Crack Arrest Status	G. R. Irwin, U. of Maryland

Irradiation Effects and Dosimetry

Chairman: M. Vagins, NRC

12:20 pm -	J-R Curve Characterization of Irradiated, Low-Upper Shelf Welds	F. J. Loss, NRL
2:00 pm -	Charpy Toughness of Irradiated High Copper Welds	R. G. Berggren, ORNL
2:20 pm -	IARAR Program	R. Hawthorne, NRL
2:40 pm -	Surveillance Dosimetry of Operating Power Plants	W. N. McElroy, HEDL

3:20 pm -	NRC-EPRI Studies of Pressure-Vessel-Cavity Neutron Fields	J. Grundl, NBS

MATERIALS ENGINEERING

Piping and Crack Growth

Chairman: J. Strosnider, NRC

3:40 pm -	Environmental Effects on Crack Growth	W. Cullen, ENSA-Buffalo
4:05 pm -	J-R Curve Characteristics of Piping Material and Welds	J. Gudas, NSRDC
4:25 pm -	Degraded Pipe Experimental Program	M. Vassilaros, NSRDC
4:45 pm -	Probabilistic Fracture Mechanics for Piping	D. O. Harris, SAI

FRIDAY, OCTOBER 30, 1981

MATERIALS ENGINEERING

Steam Generator Integrity and Corrosion

Chairman: J. Muscara, NRC

9:15 am -	Leak Rate and Burst Strength of Laboratory SCC Steam Generator Tubes	R. A. Clark, PNL
10:30 am -	Environmentally Assisted Cracking in LWRs	W. J. Shack, ANL

Non-Destructive Examination

Chairman: J. Muscara, NRC

11:10 am -	AE Monitoring of Test and Operating Pressure Vessels	P. H. Hutton, PNL
12:25 pm -	ISI Application of SAFT-UT	J. L. Jackson, SWRI
2:00 pm -	Reliability of UT Flaw Detection	F. L. Becker, PNL
2:25 pm -	Improved Eddy-Current Inspection of Power Reactor Steam Generator Tubing	C. V. Dodd, ORNL
2:50 pm -	Possibilities for NDE Round Robin on a Retired-from-Service Steam Generator	R. A. Clark, PNL

RISK ANALYSIS RESEARCH

Chairman: C. E. Johnson, NRC

10:30 am -	Reactor Safety Study - Methodology Applications Program (RSSMAP)	J. J. Curry, NRC
11:00 am -	IREP/NREP Results	J. A. Murphy, NRC
11:30 am -	Reactor Siting Criteria	W. R. Ott, NRC
12:00 pm -	Consequence Analysis Results	R. M. Blond, NRC
2:00 pm -	CORRAL Code Upgrading	P. Baybutt, BCL
2:30 pm -	Overview of Research on Risk Methodology and Data	W. E. Vesely, NRC
3:30 pm -	Reliability Data Analysis	R. L. Dennig, NRC

Severe Accident Sequence Analysis

Chairman: R. T. Curtis, NRC

9:30 am -	Strategies for Managing Potentially Severe Accidents at Large Four-Loop PWRs	N. S. DeMuth, LANL
10:00 am -	BWR Station Blackout Studies - Accident Sequence Analysis	S. A. Hodge, ORNL
10:30 am -	Station Blackout at Browns Ferry Unit 1	R. P. Wichner, ORNL
11:15 am -	Post Meltdown Analyses for PWRs	F. E. Haskin and J. L. Darby, SNL
11:45 am -	Severe Accident Mitigation Studies	H. J. Reilly, INEL
12:00 pm -	Assessment of the MARCH Computer Code	J. B. Rivard, SNL
12:30 pm -	NUREG-0772, Results and Plans in Perspective	R. R. Sherry, NRC

TRENDS IN THERMAL CALCULATIONS FOR LIGHT WATER REACTOR FUEL (1971-1981)

D. D. Lanning
M. E. Cunningham

Presented at the Ninth Water Reactor Safety Research Information Meeting
October 26-30, 1981
Gaithersburg, Maryland

October 1981

Prepared for the U.S. Nuclear Regulatory Commission under a Related Services Agreement with the U.S. Department of Energy under Contract DE-AC06-76RLO 1830

Pacific Northwest Laboratory
Richland, Washington 99352

TRENDS IN THERMAL CALCULATIONS FOR LIGHT WATER REACTOR FUEL (1971-1981)

D. D. Lanning
M. E. Cunningham

I. INTRODUCTION

One significant trend in steady-state thermal calculations in the past ten years has been the steady reduction in calculated values for fuel temperatures and stored energy. This reduction is exemplified in Figures 1 and 2, which show typical results from the NRC codes GAPCON-THERMAL-1 (1973)[1] and FRAPCON-2 (1980).[2] In Figure 1, beginning-of-life temperature profiles for a pressurized PWR are shown; fuel design input was identical for both cases. The FRAPCON-2 temperatures are about 100 K lower throughout most of the fuel volume, resulting in a 15% reduction in the stored energy. In Figure 2, end-of-life FRAPCON-2 predicted temperatures for a fission-gas-saturated BWR (7x7) rod are contrasted with a matching GAPCON-THERMAL-1 (GT1) run. In the GT1 run, both the gas composition and the unrelocated cold gap size were matched to the FRAPCON-2 predictions. Notice that the FRAPCON-2 temperatures are 400 to 500 K lower, along with a 50% decrease in stored energy. In both cases, it is the inclusion of fuel relocation in FRAPCON-2 which lowers the temperatures relative to those in GT1.

How did fuel relocation become so significant? There are two primary reasons: first, the quantity, quality, and comprehensiveness of fuel temperature data has increased dramatically. This has lowered the uncertainty bounds on measured temperatures to the point where the conservatism of the calculated values could be recognized. Second, the partition of total thermal resistance between fuel and gap has been reassessed. The result is that even more gap size reduction is now assumed than is necessary to achieve a match to centerline temperature data. This overestimation is compensated by degrading the fuel conductivity to again achieve agreement to fuel centerline temperature data.

This paper will examine both of the above trends and show the impact upon LOCA (loss-of-coolant accident) calculations due to reducing the input fuel stored energy. We conclude by noting probable future needs in fuel rod thermal/mechanical modeling.

II. FUEL RELOCATION AND REASSESSMENT OF GAP SIZE

The measurement of fuel temperatures has become steadily more precise in the last ten years, and so has the measurement of the local power associated with those temperatures. Whereas previous estimates of local linear heat rating had an uncertainty of ±10% or greater, more precise calibration of assembly power through the addition of more neutron detectors per test assembly has lowered that figure to ±6% in certain cases.[3] In addition, fuel peak temperatures used to be derived from microstructural changes and carried an uncertainty of ±200 K.[4] Now, however, the use of high-temperature thermocouples to measure fuel temperatures has yielded temperature histories with ±20 K precision and ±50 to 100 K uncertainty.*

The comprehensiveness of the fuel temperature data has improved also. In the early 1970s, the most reliable temperature data was only available for helium-filled rods at low burnup (<5,000 MWd/MTM). Measurements have now been extended throughout the ranges listed in Table 1. Most operating conditions for light water reactor (LWR) fuel are now represented in the data set, or spanned by it.

Furthermore, specific fuel designs, enrichments, etc., have been replicated in several instrumented tests at different reactors and produced very similar results. This adds greatly to confidence in the accuracy of the

TABLE 1. Parameter Ranges for Centerline Temperature Measurements

Parameter	Range
Pellet Size	9 to 12 mm diameter
Gap Size	50 to 400 μm diameter
Fill Gas Type	He to Xe; pressures to 7 MPa
Burnup	Up to 30,000 MWd/MTM
Power	Up to 50 kW/m
Temperature	Up to 2700 K

* By "precision" we mean the repeatability of a given measurement in a given rod; by "uncertainty" we mean the repeatability in performance among truly replicate rods; both at the 95%(2σ) confidence level.

measurements. As an example, consider Figure 3, which shows the thermal resistance (slope of temperature versus power plot) of various helium-filled rods at Power Burst Facility (PBF) in Idaho and the Halden Reactor in Norway. These rods were all of the same approximate pellet size, enrichment, and cladding thickness, and only beginning-of-life data is compared. For the low-to-nominal gap sizes at least, the correspondence of the measurements lies within their uncertainty.

Most fuel modeling computer codes of a decade ago envisioned the fuel pellet as a solid cylinder located concentrically within the cladding. Comparison of the early codes to the steadily more precise fuel temperature data revealed the following general trends:

1. Fuel temperatures were overpredicted unless some adjustment was made. Since the gap size was felt to be one of the most unknown parameters in the models, a reduction in gap size was made. This additional gap closure is considered a consequence of fuel cracking and outward movement and is called "fuel relocation."
2. More fractional relocation was needed with large-gap versus small-gap rods to achieve a match to centerline temperature data. This idea is demonstrated in Figure 4. The measured centerline temperatures for two rods of differing gap size are compared to the predictions of GAPCON-THERMAL-3[5] assuming no relocation. Note that the discrepancy between measurement and prediction becomes larger for the larger gap rod.

The choice of gap size as the parameter to be adjusted was arbitrary. Other adjustments have been tried, including accounting for possible pellet eccentricity and contact with the cladding. This has placed suspicion on the adequacy of the basic model for the gap temperature drop. Inadequacy in the basic model, particularly relating to the temperature jump (at the fuel/cladding surfaces) and the contact conductance, could explain the failure of a code to match data.

Carefully controlled measurements of UO_2-Zircaloy conductance at PNL[6,7] have yielded the conclusion that our understanding of gap heat transfer mechanisms is incomplete. Nevertheless, the predicted magnitude from the current models is in agreement with the measurements to such an extent that the discrepancies are small compared to the inferred discrepancies in gap conductance arising from code comparisons to in-reactor fuel temperature data.

This last point is emphasized in Figure 5, where a measured-versus-predicted scatter plot for the ex-reactor gap conductance data is shown. With typical pellet surface heat fluxes for LWR rods lying in the range of 5×10^5 to 10×10^5 W/m^2, the measured/predicted differences in conductance generally amount to only 10 to 50 K in gap temperature drop and are random, whereas the discrepancies noted in Figure 3 are much larger (>100 K) and are biased. So, enhanced gap closure, with perhaps enhanced contact area and contact conductance, definitely seems indicated by in-reactor fuel temperature data.

Another aspect of this inferred relocation is that a significant fraction occurs very early in life. This is emphasized in Figure 6, where centerline temperature data for Rod 1 of test assembly IFA-432 as a function of burnup are presented. (Rod 1 had a 230 μm fabricated gap and stable fuel; it operated at 50 kW/m peak power.) The GAPCON-THERMAL-3 code calculation, which progressively adds relocation as a function of time up to a maximum value, is compared with this data. The calculations are clearly not matched by the data trend.

Comparisons of these types provided the first indications that the behavior of gap size as a function of burnup and power was not well understood. Other sources for such doubts have been the following:

1. Simultaneous centerline and off-center thermocouple measurements from PBF Test GC-2 indicated lower effective fuel thermal conductivity and higher gap conductance than current models would predict.[8] An example of these results is presented in Figure 7.

2. Simultaneous measurements of fuel temperature and rod elongation at both PBF and Halden[9,10,11] indicated that fuel cladding contact

ccurs at powers much lower than that predicted, even with sufficient fuel relocation to match the centerline temperature data.

3. The transient behavior of fuel centerline temperature data, particularly during reactor scrams, usually agrees with calculated results, assuming a constant (full-power) value for gap conductance, rather than assuming a variable conductance commensurate with a shrinking, solid-cylinder pellet.[12] The constant conductance model requires a progressively larger degradation of fuel thermal conductivity at lower powers to match observed pre-scram temperature versus power curves. This degradation is presumed to be due to fuel cracking. An example of this scram data/model comparison is shown in Figure 8.

4. Finally, the carefully observed behavior of fuel temperature in IFA-431/-432 test rods containing densifying fuel raises questions about the applicability of the solid cylinder model. Consider IFA-431, Rod 6 first. This rod contained fuel which was prone to densification, and it was confirmed by postirradiation examination to have densified from the as-built density of 92% TD to a final density of about 96% TD,[13] during its irradiation of 4300 MWd/MTM. The temperature behavior of this rod throughout its life is contrasted with Rod 1 (same as-fabricated, 230 μm initial diametral gap, stable fuel) and Rod 2 (stable fuel, 380 μm initial gap) in Figure 9. According to the solid-cylinder model, the Rod 6 temperatures should have risen to those of Rod 2, which was deliberately sized to simulate 4% instantaneous densification. In fact, this never happened, indicating that the densification <u>did not alter gap size</u>.

   IFA-432 Rod 6(230 μm gap), presumably densified as rapidly as IFA-431 Rod 6, because it contained identical fuel and operated at 50% higher power.[14] It also attained a higher burnup (30,000 MWd/MTM). Its temperature behavior is contrasted to IFA-432 Rod 1 (230 μm gap stable fuel) in Figure 10. The results show that both rods attained saturation of the fill gas with fission gas, after ~12,000 MWd/MTM.

This was confirmed also by pressure transducer readings from these rods throughout their life. According to the solid-cylinder model, the difference between the Rod 1 and Rod 6 temperatures should then be in the range of 300 to 400 K. But in fact, they generally differ by less than 100 K after becoming saturated with fission gas. Again, the indications are that the pellet fuel does not shrink so as to widen the gap. The implications to gap size as a function of power are obvious; if a cracked pellet does not shrink away from the gap due to densification, it probably does not shrink during cooling either.*

In summary, the collection of fuel rod temperature and mechanical data over the past ten years, and the comparison of it to code predictions has led to the following tentative conclusions:

1. Fuel temperatures are definitely lower than predicted by codes which do not account for fuel relocation.
2. Fuel relocation is real and occurs primarily at beginning-of-life.
3. Relocation cannot be invoked merely as an adjustment to gap size within the thermal calculation; it has further implications mechanically in gap closure and pellet-cladding interaction (and fuel compliance) and thermally in degradation of the fuel conductivity.
3. Gap size appears to be remarkably stable as a function of power and burnup.

Modeling improvements in response to these realizations have reduced calculated fuel temperatures and stored energy, in agreement with experimental data. Such a reduction almost automatically leads to a reduction in peak cladding temperatures in a simulated large-break LOCA, at least through the end of blowdown. As an example, during the FRAP-T6 developmental assessment,[15] two identical FRAP-T6 simulations were made for the PBF-LOC-3

* Fuel swelling is no doubt also affecting these results. But note that the correspondence of Rod 1/Rod 6 fuel temperatures begins at ~12,000 MWd/MTM burnup, which, at these temperatures, is quite low to induce swelling that would obliterate the densification effect.

experiment[16] which involved simulated pressurized PWR rods at beginning-of-life. The two FRAP-T6 runs were identical except for the choice of gap conductance model, which resulted in a 160 K initial difference in centerline temperature and a 16% difference in fuel stored energy. At the end of the blowdown period, the case with the higher stored energy had 50 K higher peak cladding temperature (1175 versus 1125 K). Whether this difference would, in fact, continue throughout the heatup and reflood stage depends on when and how ballooning and rupture occur. In the absence of a geometric distortion of the rod, previously presented LOCA simulations with the small code MWRAM indicate that this trend would persist.[17]

III. FUTURE NEEDS IN NRC FUEL CODE DEVELOPMENT

Thermal data for the standard pelletized fuel designs has reached a point where further refinement of fuel codes, while undoubtedly contributing to the understanding of fuel performance, may not, in fact, make significant changes in best-estimate values for the parameters of major interest (fuel temperatures, rod pressures, fuel stored energy, etc.), nor force any change in the conservatism of NRC audit codes. However, there are new innovations in fuel design that are being actively pursued by the industry, and fuel codes will have to be modified to synthesize data for these innovations.

Table 2 lists some of these innovations and the code development tasks which they will create. Many of these tasks relate to the mechanical aspects of fuel rod behavior, but these must be understood in order to predict thermal behavior correctly, because the two are closely interrelated. The same comment applies to the existing pelletized design. As more data accumulate on standard fuel mechanical behavior, it should be assimilated in the fuel codes, if for no other reason than to refine the thermal calculations.

In conclusion, the considerable improvement in fuel thermal data over the past decade has contributed to the refinement of fuel performance codes and a reduction in predicted fuel stored energy; but there are still development needs for the future related to innovations in design and operation.

TABLE 2. Innovations in Fuel Design and Operation

Innovation	Fuel Modeling Development Needs
High Burnup Operation	Changes to gas release and failure predictions.
Niobia Dopant	Adjustment of fuel properties and gas release models.
Zr/Cu Liners on Cladding	Adjustment of cladding thermal-mechanical models.
Annular/Duplex Pellets	Adjustment to fuel compliance and gas pressure calculation; resistance of azimuthal crack; fuel redistribution.
Graphite Clad ID Coating	Adjustment of PCMI models.
Use of Sphere-Pac Fuel	- adjustment of fuel thermal conductivity - restructuring model - crack resistance - adjustment of fuel compliance - new gas release model and gas pressure calculation.

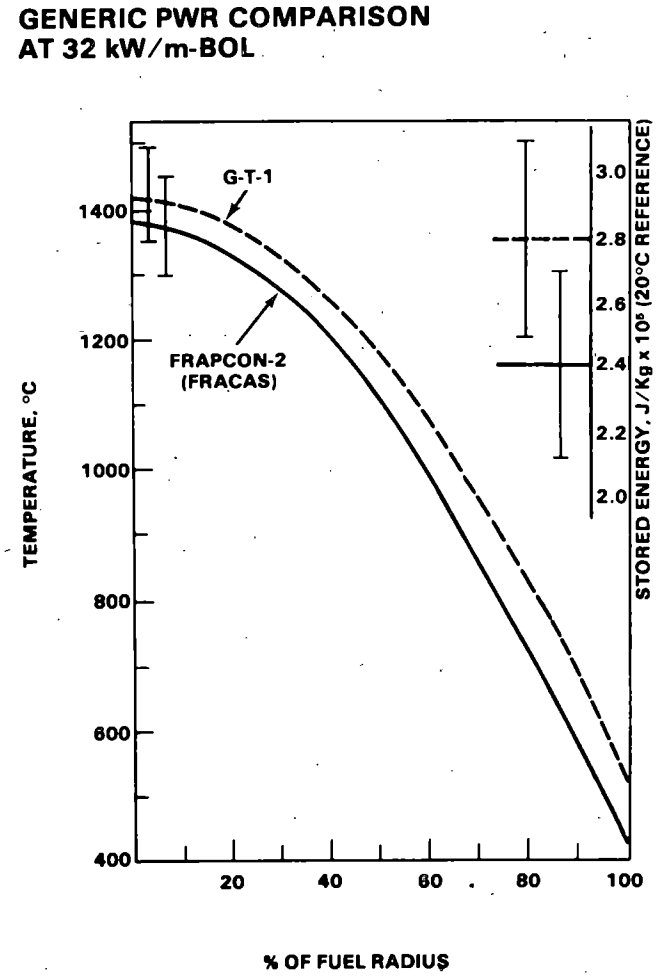

FIGURE 1. Comparison of Temperature Profiles and Stored Energy Predicted by GAPCON-1 and FRAPCON-2 for a PWR Rod at Beginning-of-Life (BOL). (The estimated uncertainty on stored energy is drawn from Reference 18.)

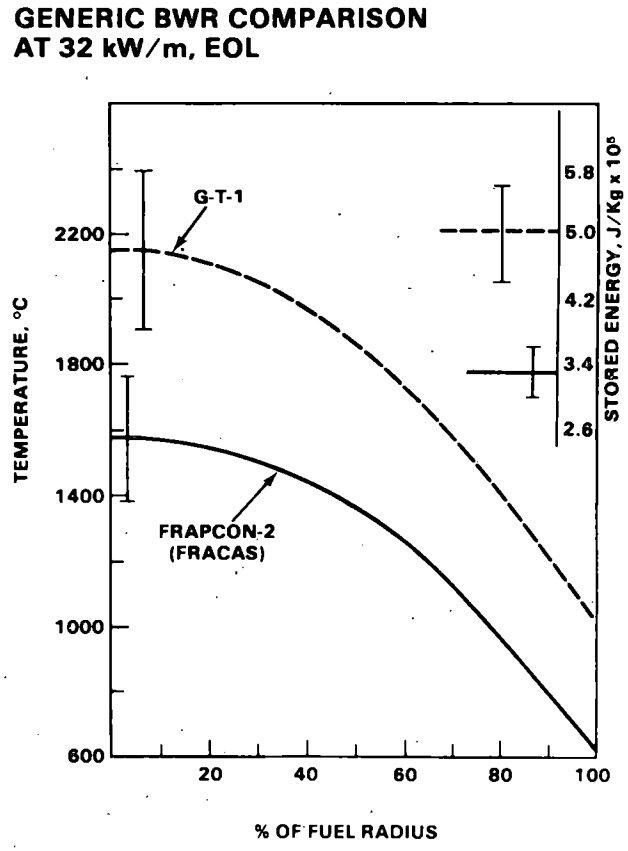

FIGURE 2. Comparison of Temperature Profiles and Stored Energy Predicted by GAPCON-1 and FRAPCON-2 for a BWR Rod Saturated with Fission Gas. (The estimated uncertainty on stored energy is drawn from Reference 18.)

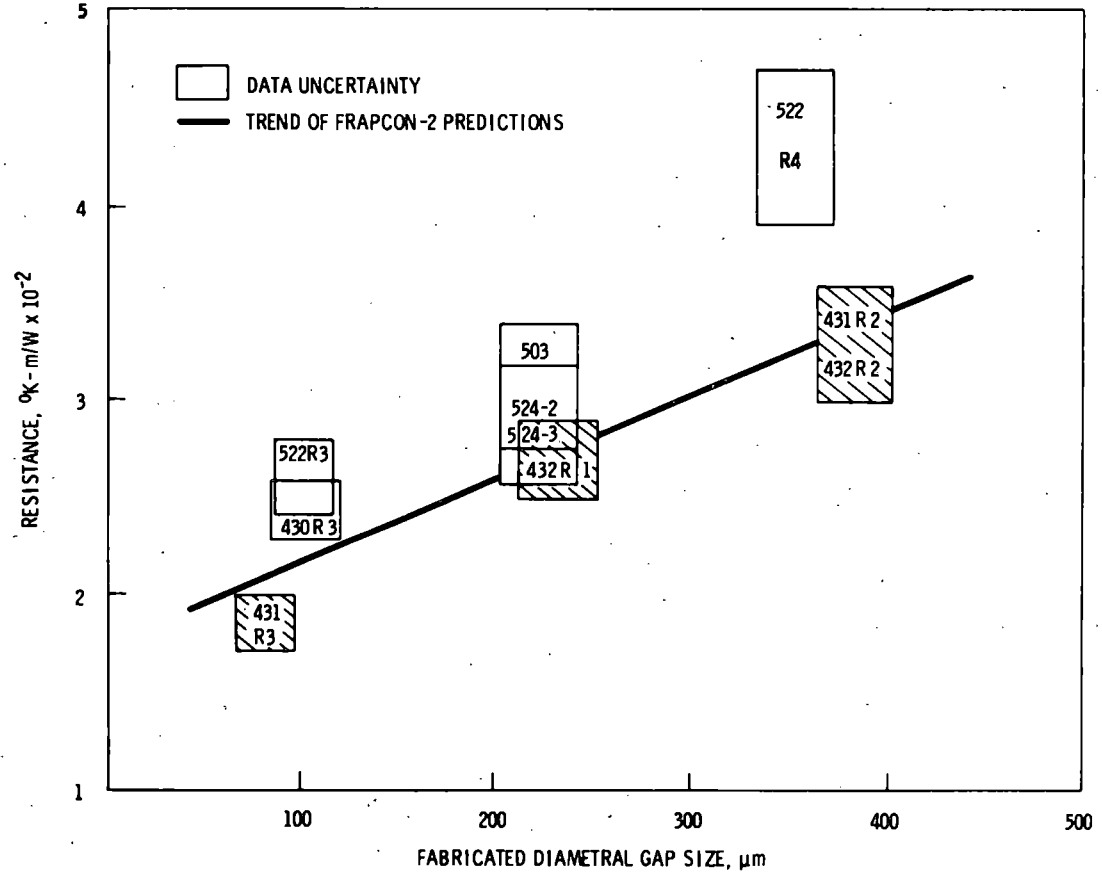

FIGURE 3. Comparison of Thermal Resistances Measured in PBF and Halden for BWR-Sized, 10% Enriched, He-Filled Rods

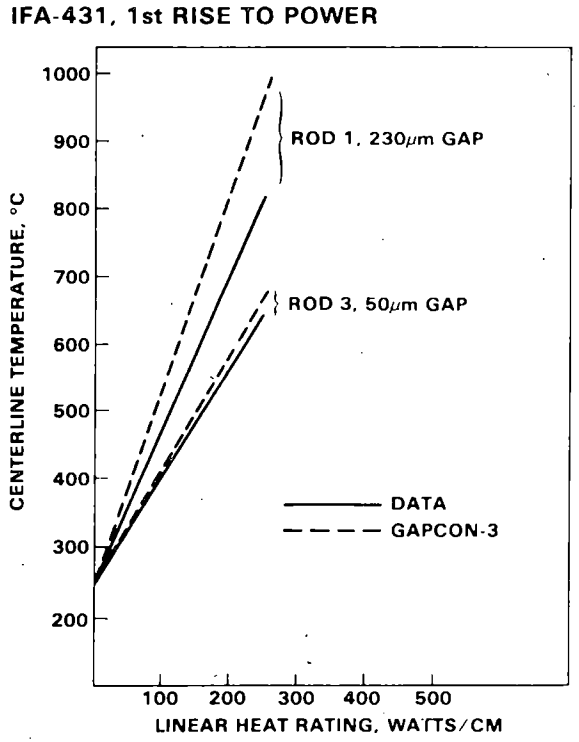

FIGURE 4. Comparison of Measured with Predicted BOL Centerline Temperatures (Assuming no Relocation) for He-Filled Rods of Differing Gap Size

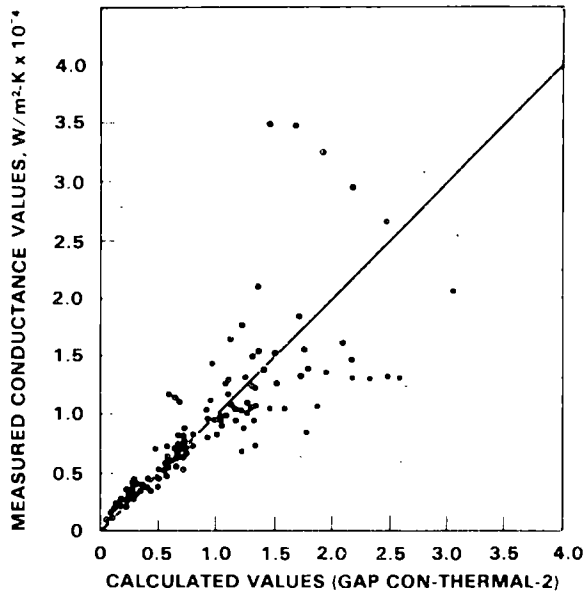

FIGURE 5. Comparison of Measured (Ex-Reactor) Gap Conductances with Predictions of the GAPCON-THERMAL-2 Model (from Reference 6)

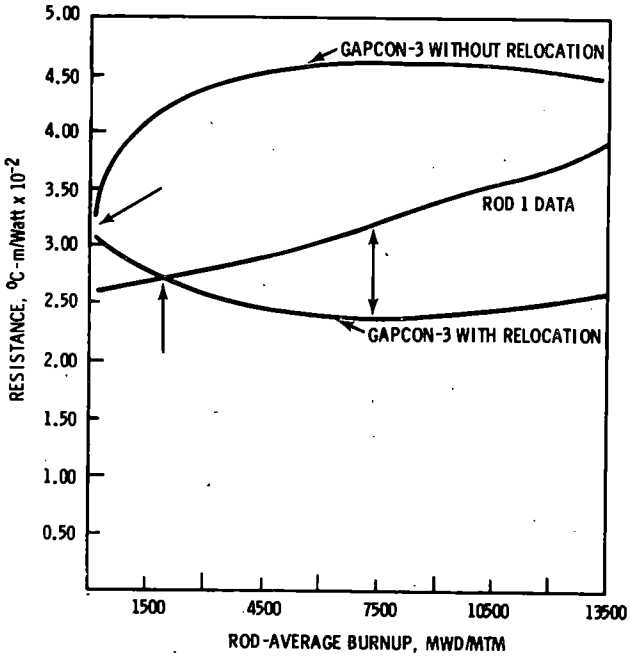

FIGURE 6. Measured Centerline Temperature at Nominal Power Versus Burnup for Rod 1, IFA-432 (230 μm gap, stable fuel), Compared to Predictions by GAPCON-THERMAL-3

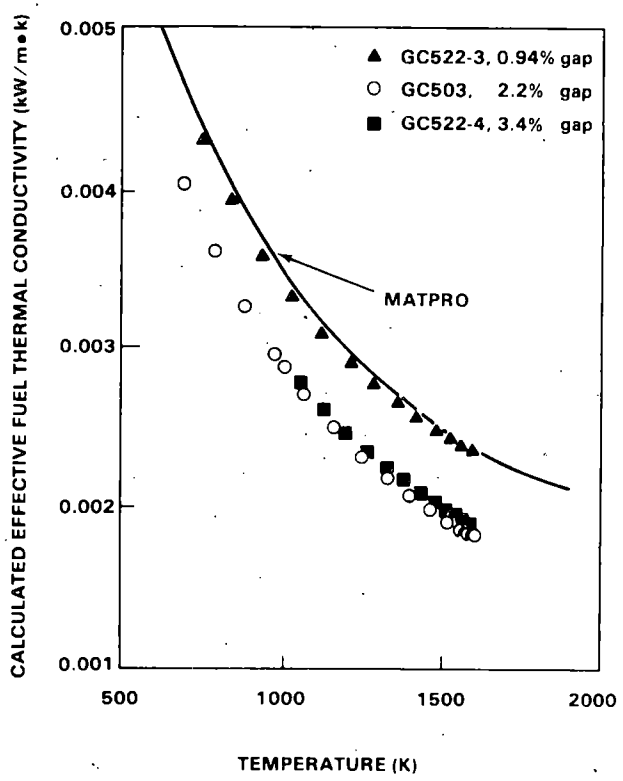

FIGURE 7. Sample Values of Effective Fuel Thermal Conductivity Derived from He-Filled Rods in the PBF Test GC-2 (Reference 8)

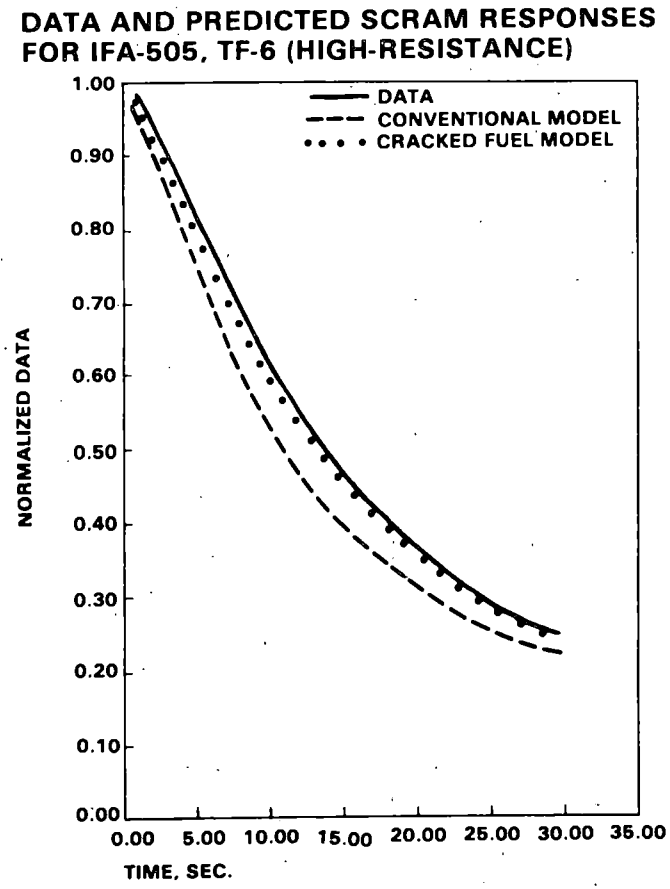

FIGURE 8. Halden Data for Fuel Centerline Temperature Response to Reactor Scram, Compared Cracked Fuel (Constant Conductance) and Solid Fuel (Variable Conductance) Models

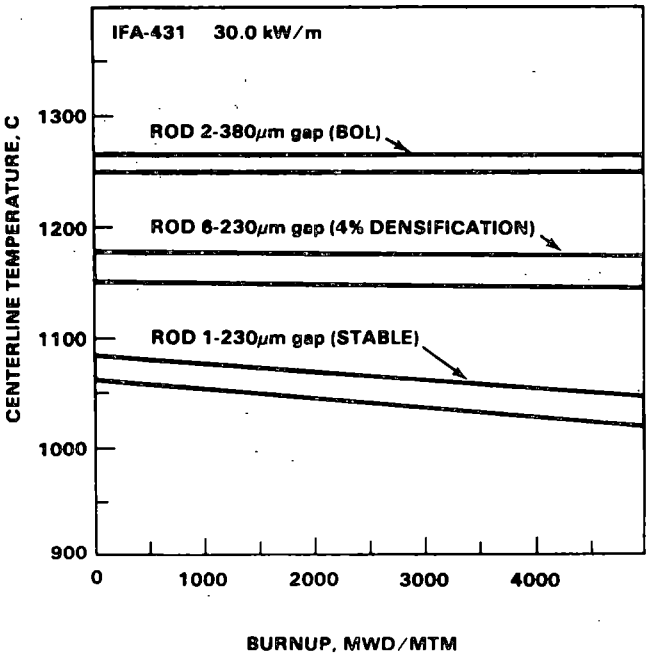

FIGURE 9. Comparison of Centerline Temperature (at Constant Power) Versus Burnup for IFA-431 Rod 1 (230 μm gap, stable fuel) and Rod 6 (230 μm gap, densifying fuel). The BOL temperature level for Rod 2 (380 μm gap, stable fuel) is also shown.

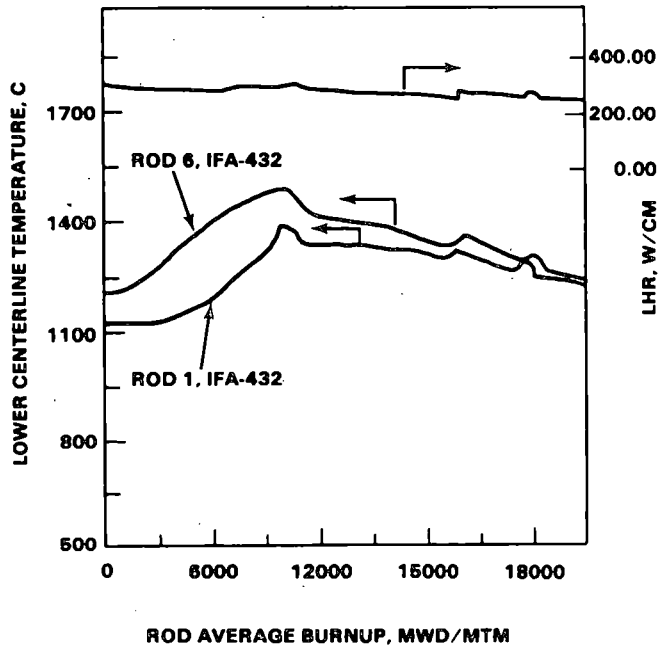

FIGURE 10. Comparison of Centerline Temperature Versus Burnup for IFA-432 Rod 1 (stable fuel) Rod 6 (densifying fuel). The power history was nearly identical for both rods (shown at the top.)

REFERENCES

1. Hann, C. R., et al. September 1973. GAPCON-THERMAL-1: A Computer Code for Calculating the Gap Conductance in Oxide Fuel Pins. BNWL-1778, Pacific Northwest Laboratory, Richland, Washington.

2. Berna, G. A., et al. December 1980. FRAPCON-2: A Computer Code for the Calculation of Steady-State Thermal-Mechanical Behavior of Oxide Fuel Rods. NUREG/CR-1845, Washington, D.C.

3. Hann, C. R., et al. February 1977. A Method for Determining the Uncertainty of Gap Conductance Deduced from Measured Fuel Centerline Temperatures. BNWL-2091, Pacific Northwest Laboratory, Richland, Washington.

4. Lanning, D. D., et al. August 1974. Statistical Analysis and Modeling of Gap Conductance Data for Reactor Fuel Rods Containing UO_2 Pellets. BNWL-1832, Pacific Northwest Laboratory, Richland, Washington.

5. Lanning, D. D., et al. January 1978. GAPCON-THERMAL-3: Code Description. PNL-2434, Pacific Northwest Laboratory, Richland, Washington.

6. Garnier, J. E., and S. Begej. April 1979. Ex-Reactor Determination of Thermal Gap and Contact Conductance Between Uranium Dioxide: Zircaloy-4 Interfaces--Stage I: Low Gas Pressure. NUREG/CR-0330, PNL-2696, Pacific Northwest Laboratory, Richland, Washington.

7. Garnier, J. E., and S. Begej. May 1980. Ex-Reactor Determination of Thermal Gap Conductance Between Uranium Dioxide: Zircaloy-4 Interfaces--Stage II: High Gas Pressure. NUREG/CR-1224, PNL-3232, Pacific Northwest Laboratory, Richland, Washington.

8. Garner, R. W., et al. November 1978. Gap Conductance Test Series 2 - Test Results Report for Tests GC 2-1, GC 2-2 and GC 2-3. NUREG/CR-0330, TREE-1268, EG&G Idaho, Inc., Idaho Falls, Idaho.

9. Peeler, G. B., et al. June 1977. Power-Cooling Mismatch Test Series, Test PCM-4, Test Results Report. TFBP-TR-190, EG&G Idaho, Inc., Idaho Falls, Idaho.

10. Hann, C. R., and R. K. Marshall. July 1977. Comparative Analysis of Pellet-Cladding Interaction from IFA-431 and IFA-432 Halden Reactor Tests. BNWL-2240, Pacific Northwest Laboratory, Richland, Washington.

11. Uchida, M., and M. Ichikawa. November 1980. "In-pile Diameter Measurement of Light Water Reactor Test Fuel Rods for Assessment of Pellet-Cladding Mechanical Interaction." Nuclear Technology 51:33-44.

12. Lanning, D. D., and M. E. Cunningham. June 1980. "Interpretation of Fuel Centerline Thermocouple Response to Reactor Scrams." Paper presented to the Enlarged Halden Program Group Meeting, Lillehammer, Norway, June 1980.

13. Nealley, C., et al. October 1979. Post-Irradiation Data Analysis for NRC/PNL Halden Assembly IFA-431. NUREG/CR-0797, PNL-2975, Pacific Northwest Laboratory, Richland, Washington.

14. Hann, C. R., et al. August 1978. Data Report for the NRC/PNL Halden Assembly IFA-432. NUREG/CR-0560, PNL-2673, Pacific Northwest Laboratory, Richland, Washington.

15. Siefken, L., et al. May 1981. FRAP-T6 Developmental Assessment. EGG-CDAP-5431, EG&G Idaho, Inc., Idaho Falls, Idaho.

16. Yackle, T. R., et al. July 1979. PBF-LOCA Test Series Test LOC-3 Quick Look Report. TFBP-TR-328, EG&G Idaho, Inc., Idaho Falls, Idaho.

17. Lanning, D. D. 1980 "Recent PNL Studies on Gap Conductance and Fuel Stored Energy." Paper presented at the Eighth Water Reactor Research Information Meeting, Gaithersburg, Maryland, October 1980.

18. Cunningham, M. E., et al. October 1980. Application of Linear Propagation of Errors to Fuel Rod Temperatures and Stored Energy Calculations. NUREG/CR-1753, PNL-3539, Pacific Northwest Laboratory, Richland, Washington.

INDEPENDENT ASSESSMENT OF FRAPCON-2 AND FRAP-T6

E. T. Laats

Presented at

The Ninth Water Reactor Safety Research

Information Meeting

October 26 - 30, 1981

Gaithersburg, Maryland

Idaho National Engineering Laboratory

Idaho Falls, Idaho 83415

INDEPENDENT ASSESSMENT OF FRAPCON-2 AND FRAP-T6

E. T. Laats
EG&G Idaho, Inc.

During the last year, the FRAPCON-2 and FRAP-T6 fuel rod behavior codes have been independently assessed by EG&G Idaho, Inc.,[1,2] for the United States Nuclear Regulatory Commission (NRC). FRAPCON-2 is the steady state and FRAP-T6 is the transient fuel rod behavior code,[3,4] each of which is the last version of the code to be issued within the next two to three years. The general goals of these assessments were to characterize code predictive capabilities, to make recommendations for future model development, and to aid the general user when running the codes and interpreting results. These codes, FRAPCON-2 and FRAP-T6, are the bases for the new NRC licensing audit codes in the fuel rod behavior area. Thus, reporting of assessment results was aimed toward fulfilling current and future NRC licensing needs.

For the assessment of FRAPCON-2, code calculations were compared with data from some 700 test rods. First, an analysis was conducted of the rod deformation models (FRACAS-I, FRACAS-II, and PELET) and the fission gas release models (ANS 5.4, FASTGRASS-Mod 2, Beyer-Hann, MacDonald-Weisman, and NRC enhancement), all of which reside in FRAPCON-2. The results indicated that FRACAS-II was overall the most appropriate rod deformation model, and FASTGRASS-Mod 1 was the most appropriate fission gas release model. The ANS 5.4 gas release model also performed commendably.

Emphasis was then placed on assessing FRAPCON-2 capabilities in the areas of thermal, deformation, and internal gas response, when FRACAS-II and FASTGRASS were used concurrently. Overall, the predictive capabilities of FRAPCON-2 were superior to those of its predecessor, FRAPCON-1,

especially in the area of thermal performance. Fuel centerline and off-centerline temperature calculations were in general agreement with experimental data. Best agreement was noted for rods with radial geometries, fill gas composition, and operating power levels that are typical of commercial fuel rods during beginning-of-life operation. The onset of pellet-cladding interaction (PCI) was calculated to occur within the range of the measured values. However, as PCI progressed, pellet strength was calculated to be much stronger than was observed. Fission gas release was most accurately calculated when the measured release was less than 25% of the gas generated. Also, the calculated amount of release was less than the measured amount for rods that attained high burnup levels.

For the assessment of FRAP-T6, code calculations were compared with experimental data to assess code performace in four areas: onset of critical heat flux, cladding failure during power ramp operation, transient fission gas release, and cladding ballooning and rupture. These areas represent the major modeling changes since the assessment of the predecessor FRAP-T5 code. Overall, FRAP-T6 is superior to its predecessor FRAP-T5. The new code has essentially retained the good calculational capabilities of FRAP-T5 while adding new, useful, and computationally accurate capabilities. The LOFT and CE-1 critical heat flux (CHF) correlations for pressurized water reactor power-coolant-mismatch (PCM) conditions and the GE CHF correlation for boiling water reactor PCM conditions most accurately represented the experimental data. For modeling overpower ramp failure tests, the FRACAS-II deformation model and FRAIL rod failure criteria model were most appropriate. Transient fission gas release was most accurately calculated when the pretransient burnup exceeds 15 MWd/kg. Below that burnup, gas release was overcalculated. The cladding burst temperature and pressure replicated the measurements for unirradiated rods. The effects of prior irradiation upon cladding materials properties was not satisfactorally modeled.

REFERENCES

1. E. T. Laats, et al., Independent Assessment of The Steady State Fuel Rod Analysis Code FRAPCON-2, EGG-CAAP-5335, January 1981.

2. R. Chambers, et al., Independent Assessment of The Transient Fuel Rod Analysis Code FRAP-T6, EGG-CAAD-5532, August 1981.

3. G. A. Berna, et al., FRAPCON-2: A Computer Code for The Calculation of Steady State Thermal-Mechanical Behavior of Oxide Fuel Rods, NUREG/CR-1845, January 1981.

4. L. J. Siefken, et al., FRAP-T6: A Computer Code for The Transient Analysis of Oxide Fuel Rods, NUREG/CR-2148, EGG-2104, May 1981.

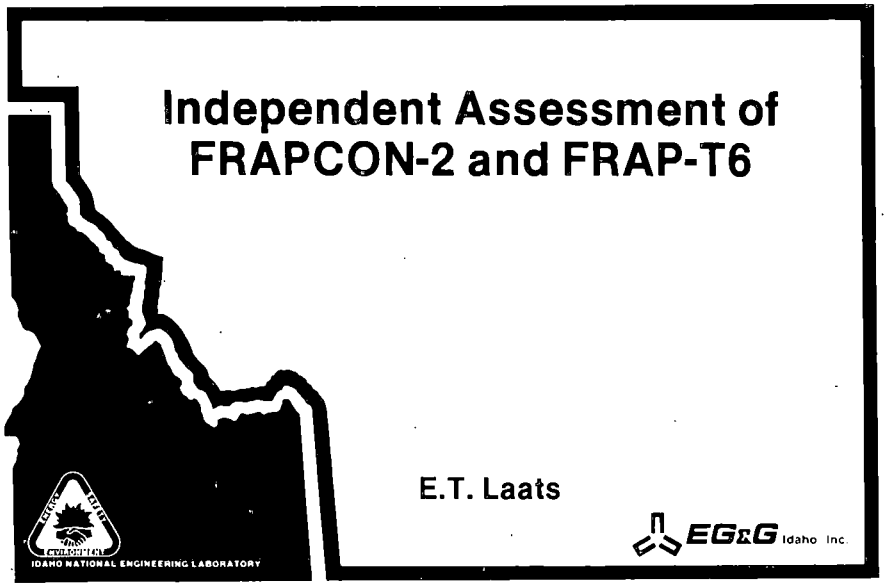

Outline

- Assessment Goals
- FRAPCON-2 Assessment
- FRAP-T6 Assessment
- User Recommendations

INEL-S-34 886

Assessment Goals

- Characterize Calculational Capabilities
- Recommend Future Development
- Aid General User

INEL-S-34 889

FRAPCON-2 Assessment

- Completed January 1981
- Code-to-Data Comparisons Using Data From 700 Test Rods
- Assessment Procedure
  - Selected Deformation and Gas Release Models
  - Characterized Code with Selected Models

INEL-S-34 904

Deformation and Gas Release Models Selection

- Three Deformation Models
  - PELET
  - FRACAS-I
  - FRACAS-II
- Four Fission-Gas Release Models
  - ANS 5.4
  - FASTGRASS Mod 1
  - MacDonald-Weisman
  - NRC
- 300-rod Data Sample
- First Select Deformation Model Using BOL Data Then Gas Release Model

INEL-S-34 884

Selection Procedure

- Developed Criteria List, Assigned Weighting Factors
- Performed Code-to-Data Comparisons
- Determined Score for Each Model
- Selected Model, Based Upon Best Score

INEL-S-34 903

Summary of Gas Release (and Deformation) Model Total Scores

Deformation Model	Gas Release Models			
	ANS 5.4	MacDonald-Weisman	MacDonald-Weisman/NRC	FASTGRASS
PELET	324	338	—	345
FRACAS-I	241	254	222	360
FRACAS-II	358	340	—	368

INEL-S-34 894

Detailed Characterization

- Fuel Temperature
- Onset of Pellet-Cladding Gap Closure
- Fission Gas Release
- Rod Internal Pressure

INEL-S-34 902

Fuel Temperature

- About 160 Instrumented Rods
- Two Code-to-Data Comparison Categories
  - Fuel Centerline
  - Fuel Off-Centerline
- Implied Stored Energy Predictive Capabilities

INEL-S-34 887

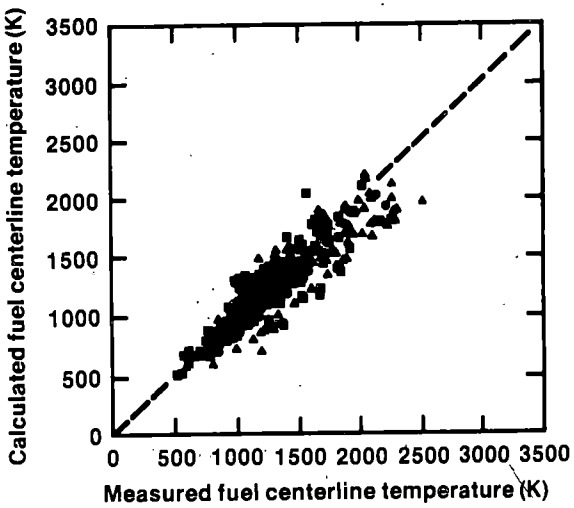

INEL-S-34 896

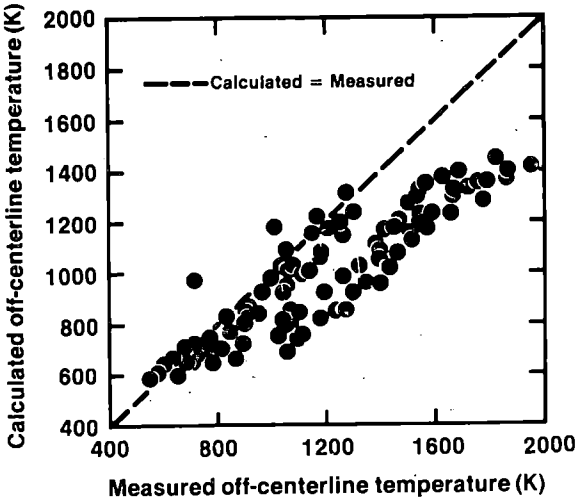

INEL-S-34 881

Implied Stored Energy Calculations

- Best Calculations for Commercial-Type Rods at BOL
- Undercalculations for Non-Helium Filled or Very Large-Gap Rods, and Possibly Commercial Rods at High Burnup

INEL-S-34 901

Results

1. Fuel Centerline and Off-Centerline Temperature Calculations Were in Overall Agreement with Experimental Data

2. Onset of Pellet-to-Cladding Gap Closure Was Calculated to Occur Within the Range of the Measured Values

3. After Attaining the Onset of Gap Closure, Cladding Strain was Overestimated Until Hard Gap Closure was Attained

INEL-S-34 900

Results (cont'd)

4. Calculated Fission Gas Release was Most Accurate When the Measurement was Less Than 25%. Also, Fission Gas Release was Undercalculated at High Burnups

5. Rod Internal Pressure Calculations Were Most Accurate for Rods With a Large Plenum Volume, and Least Accurate for Small-Plenum Pressurized Rods

INEL-S-34 882

FRAP-T6 Assessment

- Completed August 1981
- Code-to-Data Comparisons Using Data From 800 In-Pile and Out-of-Pile Specimen
- Performance Areas Assessed
  - Onset of Critical Heat Flux
  - Power Ramp Failures
  - Transient Fission Gas Release
  - Cladding Burst and Deformation

INEL-S-34 883

Power Ramp Failures

- Two Failure Criteria Models
  - MATPRO-11A
  - FRAIL-6
- Two Deformation Models
  - FRACAS-I
  - FRACAS-II
- 120 Test Rod Sample

INEL-S-34 899

Deformation Model Analysis

- Ability to Calculate Failure Probability of Data Sample Groups
- Ability to Replicate Observed Trends as Function of:
  - Power
  - Ramp Rate
  - Hold Time
  - Burnup
  - Pellet-Cladding Gap Size
  - Cladding Thickness
  - Fuel Density

INEL-S-34 898

Cladding Thickness Effect

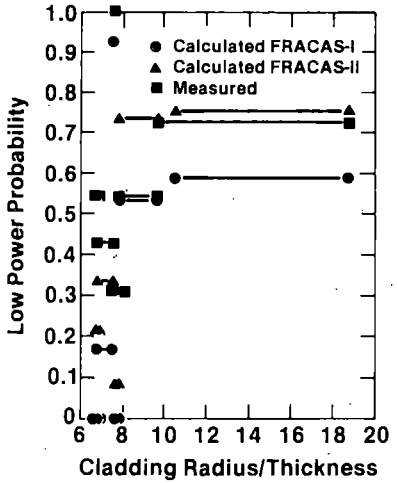

INEL-S-34 905

Maximum Power Effect

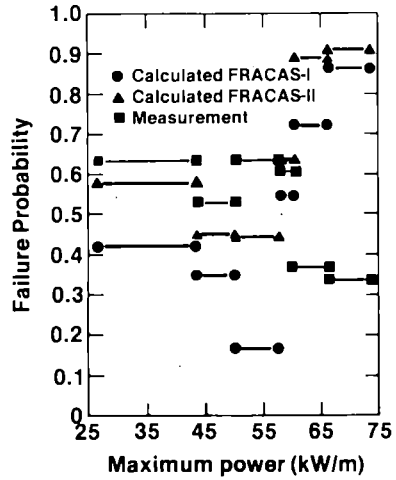

INEL-S-34 893

Power Ramp Failure Results

1. FRACAS-II Performed Better Than FRACAS-I
2. MATPRO Failure Criteria Never Calculated Rod Failure to Occur. FRAIL Was More Realistic
3. Contributions to Failure by Chemical Aggravation Were Hard to Note

INEL-S-34 899

Transient Fission Gas Release

- FASTGRASS-Mod 1 Model
- 40 Test Rod Sample
- Two Deformation Subcodes
  - FRACAS-I
  - FRACAS-II

INEL-S-34 888

Transient Gas Release Comparison

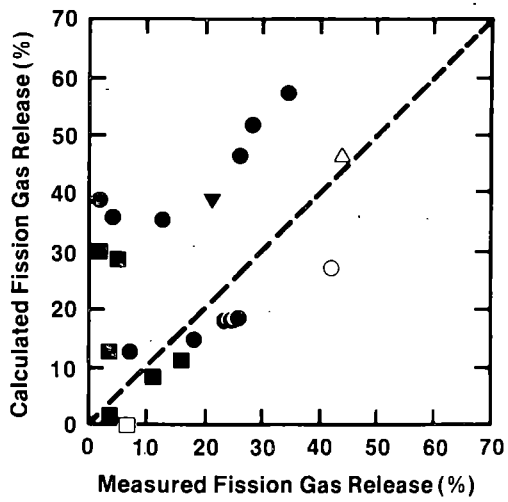

INEL-S-34 891

Transient Gas Release Results

- FASTGRASS Performed Most Credibly With FRACAS-II
- Amount of Gas Release Was Over Calculated for Low Burnups, Tended to Undercalculate at High Burnups

INEL-S-34 892

Cladding Burst and Deformation

- Two Cladding Failure Criteria Models
  - BALON 2
  - FRAIL-6
- Intent was to Isolate and Assess Each Model
  - BALON2 Run with Driver
  - FRAIL-6 Run with Slightly Modified FRAP-T6
- Goal was to Assess Rupture Criteria and Burst Strain
- 600 Rod Data Sample
  - In-Pile and Out-of-Pile
  - Single and Multirod
  - Heatup or Pressurization

INEL-S-34 897

BALON2 Burst Temperature Comparison

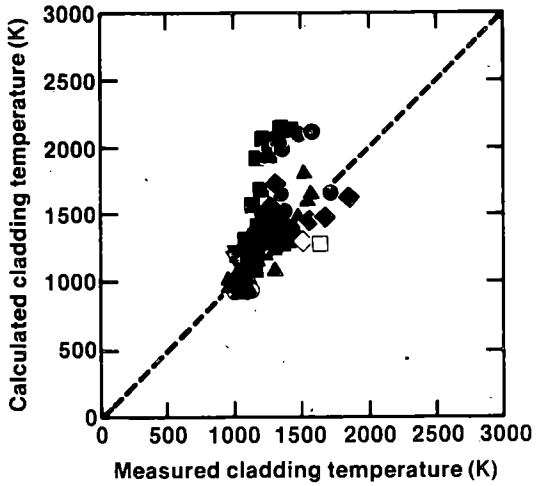

INEL-S-34 921

BALON2 Burst Strain Comparison

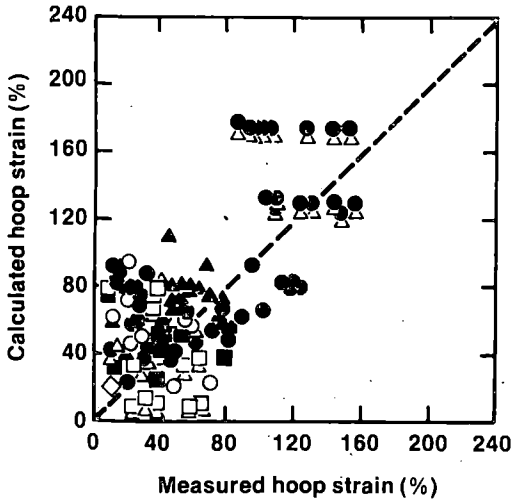

INEL-S-34 920

FRAIL-6 Burst Temperature Comparison

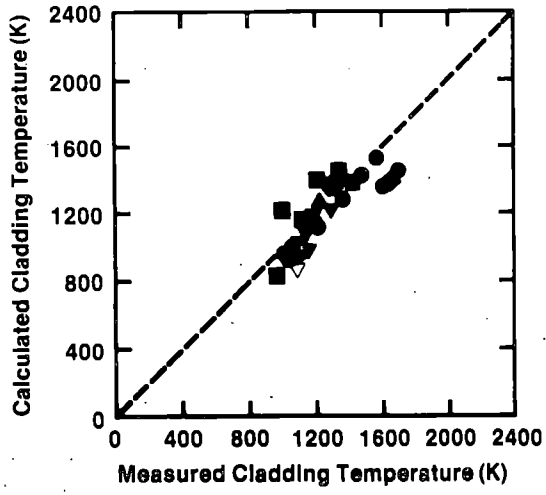

INEL-S-34 886

Cladding Burst and Deformation Results

1. For Unirradiated Rods, Mechanistic BALON2 Calculations Within Scatter of Measurements and FRAIL-6 Empirical Model
2. Effects of Prior Irradiation Overestimated
3. Effects of Prior Irradiation Not Properly Annealed
4. Calculated Burst Strains Exhibit Much Scatter, But General Trends are Correct

INEL-S-34 880

User Recommendations

FRAPCON-2

- Specify FRACAS-II Deformation and FASTGRASS Fission Gas Release Models

FRAP-T6

- Specify FRACAS-II for PCI of Fission Gas Release Analyses. Otherwise, Specify FRACAS-I with Relocation
- Specify LOFT or CE-1 CHF Correlation for High System Pressure PCM Events, GE CHF Correlation for Low Pressure Events
- Always Use FRAIL Failure Criteria for PCI Failure Calculations
- Do Not Use FASTGRASS Unless Fission Gas Release Calculations are Needed

INEL-S-34 890

REBEKA TEST RESULTS

PRESENTED BY

F. J. ERBACHER

KERNFORSCHUNGSZENTRUM KARLSRUHE
INSTITUT FÜR REAKTORBAUELEMENTE
PROJEKT NUKLEARE SICHERHEIT
POSTFACH 3640, 7500 KARLSRUHE 1
FEDERAL REPUBLIC OF GERMANY

NINTH WATER REACTOR SAFETY RESEARCH INFORMATION MEETING,
OCTOBER 26-30, 1981, GAITHERSBURG, MARYLAND, U.S.A.

REBEKA TEST RESULTS

F.J. Erbacher

Kernforschungszentrum Karlsruhe
Institut für Reaktorbauelemente
Projekt Nukleare Sicherheit
Postfach 3640, 7500 Karlsruhe 1
Federal Republic of Germany

SUMMARY

OBJECTIVES

REBEKA is a out-of-pile burst test program to investigate the ballooning and burst behavior of LWR-Zircaloy claddings and the flow blockage in a rod bundle during the refill- and reflood phases of a LOCA. The test results serve to develop and verify fuel rod behavior codes.

The test program is carried out in a number of consecutive test series starting from single rod tests in a steam and helium atmosphere and finishing with bundle tests with flooding. The tests are accompanied by theoretical studies and model development (Fig. 1).

EXPERIMENTAL

Test rigs are available for single rod tests using shortened fuel rod simulators and bundle tests using full-length fuel rod simulators with an axial power profile in bundle arrays up to 7 x 7 (Figs. 2 and 3).

Electrically heated fuel rod simulators have been developed to model the nuclear fuel rod mainly its thermal behavior during reflooding with respect to the heat release, cladding temperature transient and quench time (Figs. 4 and 5).

A fast computer-controlled data acquisition system (PDP 11/03) is used to record all 256 measuring points every 0.1 s.

SINGLE ROD TESTS

A large number of transient single rod burst tests with heated shroud have been performed to investigate the deformation mechanism of Zircaloy cladding tubes in a wide parameter range (Fig. 6).

In parallel with the tests a deformation model has been developed. It is assumed by this model that the time of burst is reached when the actual local stress equals the limiting burst stress. Based on experimental evidence, the burst stress is assumed to depend on the temperature and oxygen concentration of the Zircaloy (Fig. 7).

Figs. 8 and 9 show a comparison between test data and model prediction.

It has been found in single-rod tests without heated shroud that during deformation in the α- and $(\alpha+\beta)$-phases of Zircaloy azimuthal cladding temperature differences decrease the circumferential burst strain substantially (Fig. 10). Azimuthal cladding temperature differences increase during deformation. This is the result of an increased tube bending during deformation due to the anisotropic behavior of the Zircaloy (Fig. 11). This tube bending is an amplifier for increased azimuthal temperature differences and decreased burst strains of the Zircaloy claddings.

BUNDLE TESTS

Up to now four bundle tests using full-length 5 x 5 bundles have been performed. The test procedure and test conditions are designed to simulate the fuel element behavior during the refill- and reflooding phases of a LOCA as representative as possible (Fig. 12). The cladding temperature- and pressure transients develop automatically as a result of the interaction between decay heat, cooling and cladding deformation.

The burst temperatures and burst pressures measured in the bundle tests are in good agreement with the single rod test data (see Fig. 8). The burst strains of the bundle tests are relatively small (see Fig. 9) and caused by azimuthal cladding temperature differences (see Fig. 10).

It has been shown in the bundle tests that two-phase flow cooling during reflooding sets a limit to the cladding deformation by increasing the azimuthal and axial temperature differences on the cladding (Fig. 13).

In a case of an eccentric position of the pellets within the cladding and a resultant temperature difference on the cladding circumference, the increasing cooling efficiency during reflooding enhances the azimuthal differences in temperature. This leads to an increased tube bending and, as a consequence, to a further increase in azimuthal cladding temperature differences. These effects contribute to relatively small circumferential strains.

Fig. 14 illustrates as an example the influence of the cooling efficiency during reflooding on cladding deformation in case of eccentric position of the pellet within the cladding. The diagram demonstrates that the burst strain is decreased when the heat transfer coefficient is increased. In the reflooding phase of a LOCA heat transfer coefficients greater than about 50 W/m^2K are developed. Therefore only bundle tests simulating such heat transfer coefficients produce typical burst strains. Bundle tests using low steam cooling tend to overestimate the burst strains and the resulting flow blockage in a LOCA (Fig. 15).

The two-phase flow during reflooding influences also the axial distribution of cladding deformation. The thermodynamic non-equilibrium results in steam temperature up to about 600 ^{o}C within the two-phase mixture of superheated steam and saturated water droplets. The turbulence and the water droplet dispersion induced by the grid spacers result in an improved mixing of the water droplets with the superheated steam and consequently in a desuperheating

of the steam and a better heat transfer which lowers the cladding temperature downstream of each spacer. Up to the next spacer superheating redevelops again and produces an axial cladding temperature difference. Axial cladding temperature differences up to 50 K between the inner two spacer grids were measured at the time of burst. This results in an axial shift of the maximum strains between two grid spacers and prevents axially extended ballooning.

Fig. 16 illustrates the relatively low burst strains and the axial deformation profile of the bundle test REBEKA 3 which is considered to be most typical. The bursts are axially distributed over 200 mm. A coplanar location of all bursts in one axial level did not occur. The maximum flow blockage at the inner nine rods was 52 %.

Fig. 17 summarizes the test results of the four REBEKA bundle tests performed up to now.

Fig. 18 summarizes in a scenario the interaction between thermohydraulics and fuel clad ballooning in a LOCA.

COMPARISON WITH IN-PILE TESTS

In the FR-2 reactor of KfK single-rod tests in steam were performed using 500 mm long unirradiated as well as irradiated rods. The burst data of these in-pile tests, i. e., the burst pressure, burst temperature and burst strains are in good agreement with the REBEKA out-of-pile test data (see Figs. 8 and 9).

The relatively low burst strains are mainly the result of azimuthal cladding temperature differences. Fig. 19 is a plot of the circumferential burst strain versus the azimuthal difference at maximum clad temperature. It is evident from the diagram that significant temperature variations on the cladding circumference occurred. No influence was found of the fragmented fuel of the irradiated fuel rods on the magnitude of azimuthal cladding temperature difference and an eventual equalization of temperatures on the cladding circumference. The burnup had no influence on the burst data, and neither a difference between the unirradiated and the previously irradiated test rods was observed. In the regions with major clad deformations of the pre-irradiated rods fragmented fuel pellets were found crumbled within the fuel rod. There is experimental evidence that the movement of the fuel fragments occurred at the time of burst and did not influence the deformation behavior.

Based on the FR-2 in-pile tests of KfK it can be concluded that there is no influence of the nuclear environment on cladding deformation.

Some partly preliminary results of other in-pile tests are also plotted in Fig. 9: EOLO tests in ESSOR, tests in PBF and tests in NRU. All results are well within the scatter band of the FR-2 in-pile and REBEKA out-of-pile test results and do hardly indicate a systematic influence of the nuclear boundary conditions on the cladding deformation in a LOCA.

INFLUENCE OF FLOW BLOCKAGES ON COOLABILITY

The REBEKA bundle burst tests under flooding did not show any deterioration of the cooling efficiency due to the ballooned claddings and the resultant flow blockage. To investigate the influence of flow blockages on the cooling mechanism in detail flooding tests have been performed under transient LOCA conditions on a 5 x 5 bundle with conical sleeves simulating the flow blockage (FEBA

program). Fig. 20 shows cladding temperature transients in the blocked and unblocked regions for flooding rates of 3.8 and 2.2 cm/s and a blockage ratio of 62 % in the blocked region. It is evident from the diagram that under the given conditions the effect of water droplet dispersion, which improves the heat transfer, overcompensates the degrading effect of mass flow reduction with the consequence that the cladding temperature downstream of the blocked region is somewhat lower compared to that in the unblocked region for a flooding rate of 3.8 cm/s. Only at the relatively low flooding rate of 2.2 cm/s the cladding temperatures in the blocked regions are almost the same.

Tests on larger bundle sizes (FLECHT/SEASET, 2D/3D) are needed to prove this results for large scale flow diversion.

SUMMARY

The deformation of Zircaloy cladding tubes during a LOCA is governed mainly by circumferential and axial cladding temperature differences which are enhanced by two-phase cooling during reflooding.

Cladding temperature differences prevent large circumferential strains and axially extended ballooning and in this way contribute to a limitation of flow blockage.

Full-length out-of-pile bundle tests performed under representative thermohydraulic boundary conditions exhibited a maximum flow blockage of about 52 %.

Results from flooding tests on blocked geometries suggest that flow blockages up to about 60 % are coolable without any additional cladding temperature increase due to the blockage.

In-pile tests do not indicate a distinct influence of the nuclear environment on cladding deformation.

Out-of-pile bundle tests performed under representative experimental boundary conditions seem to simulate the deformation of nuclear fuel bundles.

CONCLUSIONS

The dominant phenomena of cladding deformation and failure of single rods have been clarified by experiments and can be modeled by computer codes.

More bundle tests under representative boundary conditions are needed to investigate the deformation behavior and the flow blockage in a bundle geometry and to develop and verify flow blockage models.

Burst and flooding tests performed up to now suggest that the coolability of the core can be maintained in a LOCA.

REFERENCES

1. F.J. ERBACHER, H.J. NEITZEL and K. WIEHR, "Studies on Zircaloy Fuel Clad Ballooning in a LOCA, Results of Burst Tests with Indirectly Heated Fuel Rod Simulators", STP 681 Proceedings of the ASTM Fourth International Conference on Zirconium in the Nuclear Industry, June 26-29, 1978.

2. H.J. NEITZEL and H.E. ROSINGER, "The Development of a Burst Criterion for Zircaloy Fuel Cladding under LOCA Conditions", KfK 2893, AECL-6420, October 1980.

3. K. WIEHR, F.J. ERBACHER and H.J. NEITZEL, "Influence of Thermohydraulics on Fuel Rod Behavior in a LOCA", Proceedings of the CSNI Specialist Meeting on Safety Aspects of Fuel Behavior in Off-Normal and Accident Conditions, September 1-4, 1980, Espoo, Helsinki, Finland.

4. K. WIEHR, F.J. ERBACHER and H.J. NEITZEL, "Einfluß eines kalten Regelstabführungsrohres auf das Verformungsverhalten von Zircaloyhüllrohren in der Flutphase eines Kühlmittelverluststörfalles", Jahrestagung Kerntechnik, Berlin, 25.-27. März 1980.

5. P. IHLE et al., "Flutexperimente mit blockierten Anordnungen (FEBA)", PNS-Jahresbericht 1980, KfK-2950, April 1981.

6. E.H. KARB et al, "KfK In-Pile Tests on LWR Fuel Rod Behavior During the Heatup Phase of a LOCA", KfK-3028, October 1980.

7. G. FRIZ et al.,"EOLO-JR: A Single Rod Burst Test Program in the ESSOR Reactor", ANS-ENS Topical Meeting on Reactor Safety Aspects of Fuel Behavior, August 2-6, 1981, Sun Valley, Idaho (USA).

8. P.E. MAC DONALD et al., "Cladding Deformation During a Large Break LOCA", ANS-ENS Topical Meeting on Reactor Safety Aspects of Fuel Behavior, August 2-6, 1981, Sun Valley, Idaho, (USA).

9. C.L. MOHR, Battelle, Pacific Northwest Laboratories, Private Communication (1981).

10. F.J. ERBACHER, "LWR Fuel Cladding Deformation in a LOCA and its Interaction with Emergency Core Cooling", Topical Meeting on Reactor Safety Aspects of Fuel Behavior, August 2-6, 1981, Sun Valley, Idaho (USA).

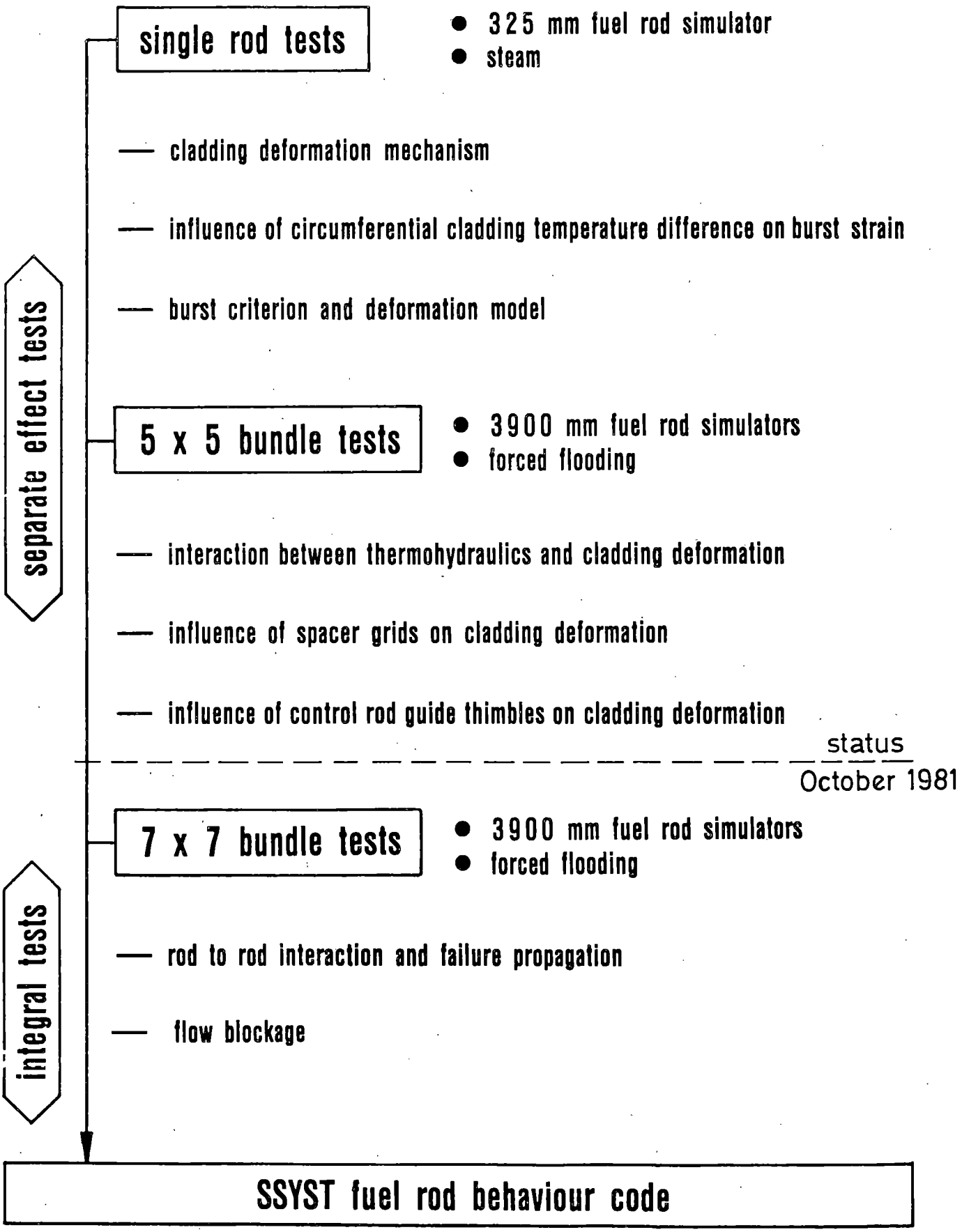

Fig. 1: Test philosophy and test objectives

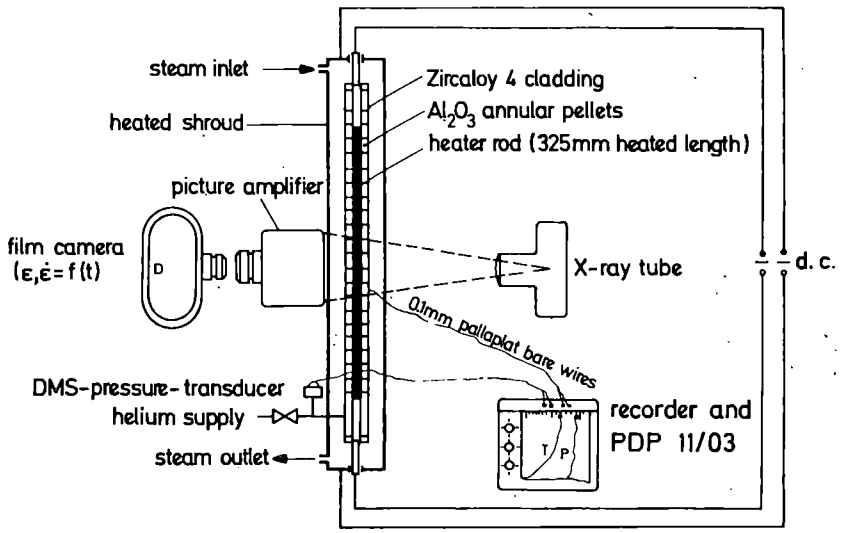

Fig. 2: Test rig for single rod tests

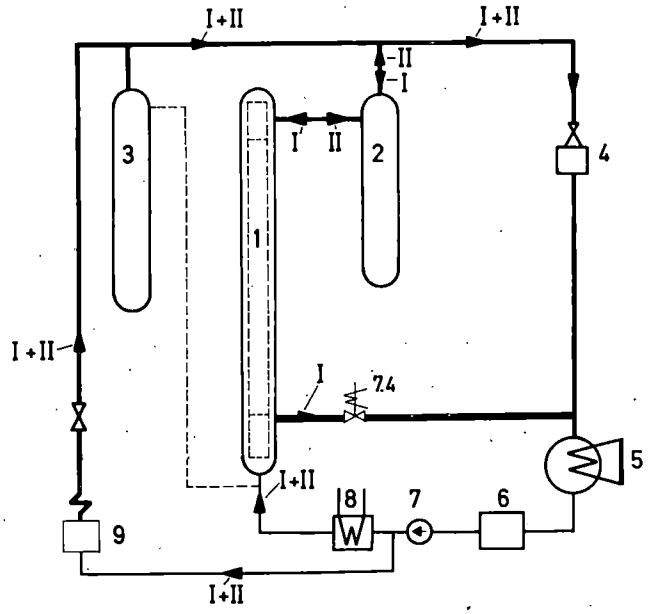

1 test section
2 separation tank
3 containment simulator
4 steam transformer
5 condenser
6 water tank
7 coolant pump
8 heat exchanger
9 steam generator

I refill
II reflood

Fig. 3: Test loop for bundle tests

design criteria (compared to the fuel rod)	design features
thermal behavior	heat capacity and heat transport across the gap adapted to the fuel rod by suitable combination of materials and dimensions
heat transport to the cladding from inside	indirectly heated fuel rod simulator (internal heater, electrically insulated)
axial power profile	approximated by a stepped axial power profile (subsequently a cosine shaped profile)
gas flow in the gap from the plena to the ballooning zone	— full heated length: 3.90 m — original gap width (cold): 50 μm — original plena volumes: upper $\sim$ 9 cm^3, lower $\sim$ 17 cm^3
heat transfer in the gap	materials with similar thermal expansion and emissivity (Al_2O_3 annular pellets, Zircaloy 4 cladding)
Zircaloy 4 cladding	Zircaloy 4 cladding with standard KWU-specification: 10.75 $\varnothing$ x 0.72 mm
internal gas pressure at operating temperature: 70 bar (zero burn-up) 130 bar (max. burn-up)	prepressurized claddings with Helium: 70 to 130 bar (operating temperature)
typical reflood thermohydraulics	full-length fuel rod simulators with original grid spacers

Fig. 4: Design criteria and design features of fuel rod simulator

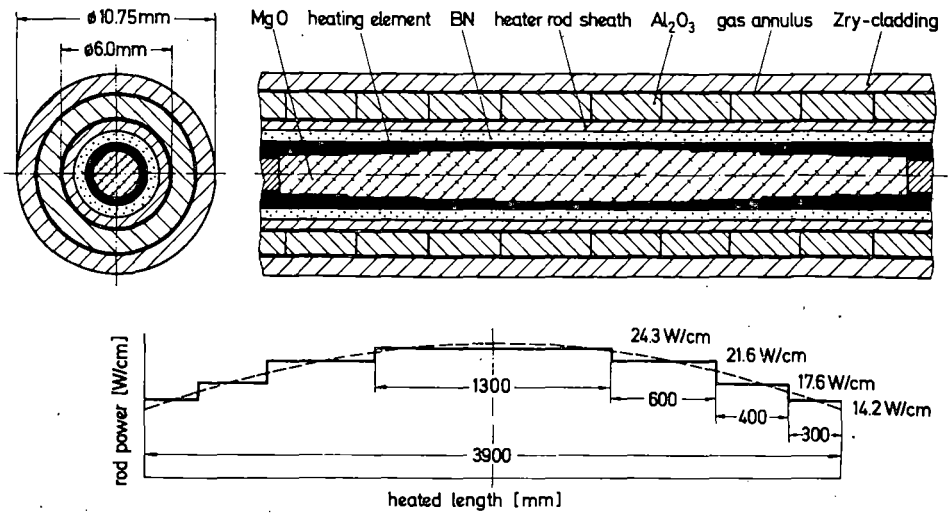

Fig. 5: Fuel rod simulator

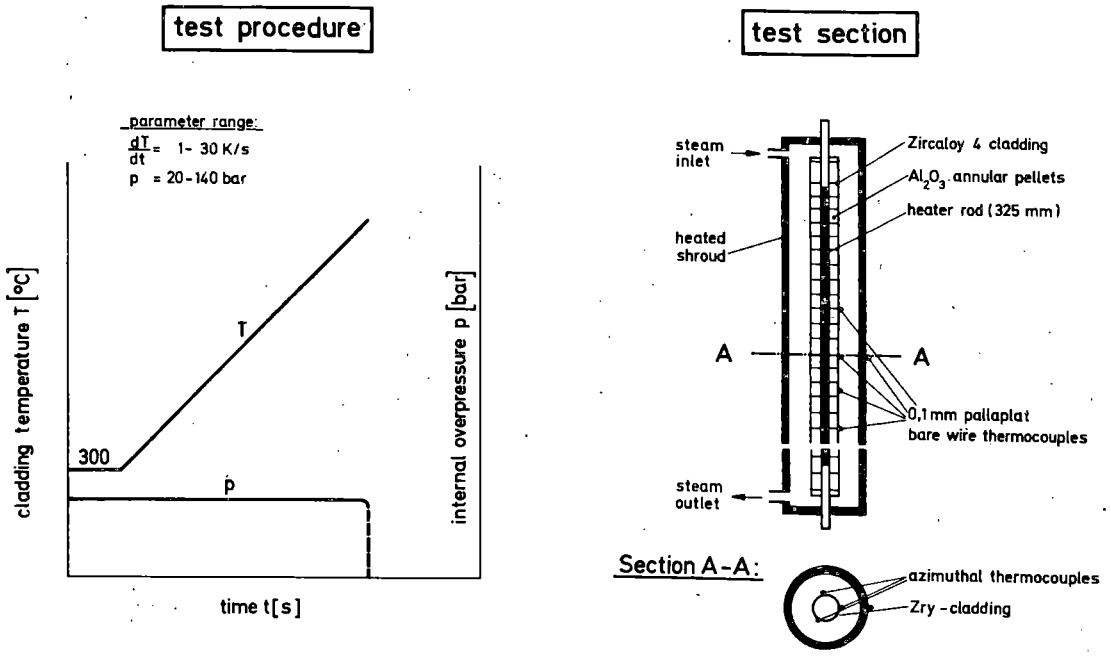

Fig. 6: Transient single rod burst tests in steam

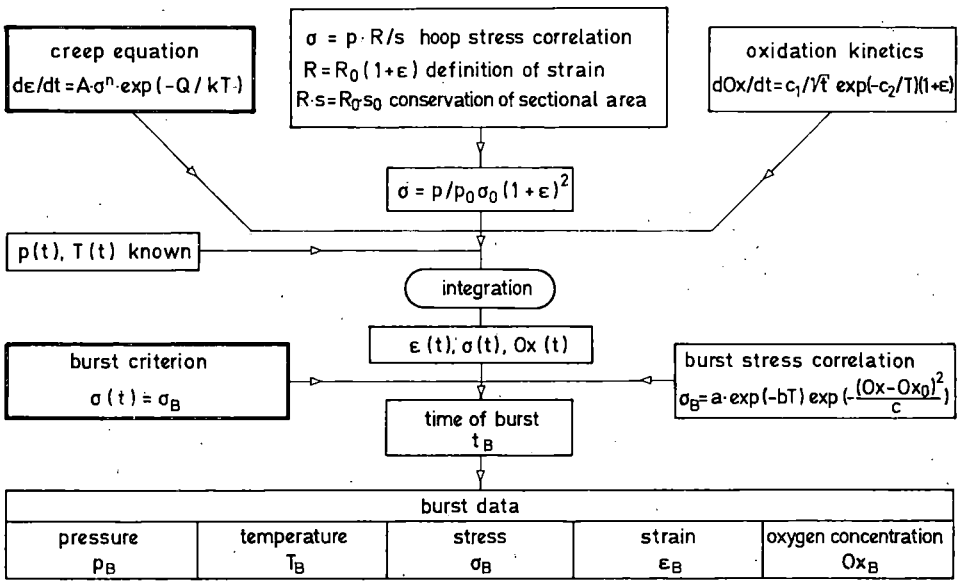

Fig. 7: Burst criterion model (schematic)

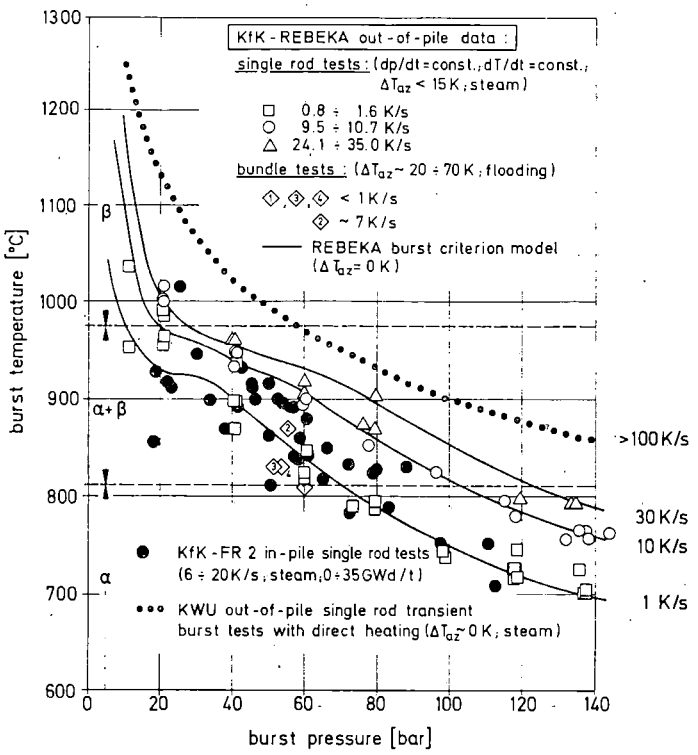

Fig. 8: Burst temperature vs. burst pressure

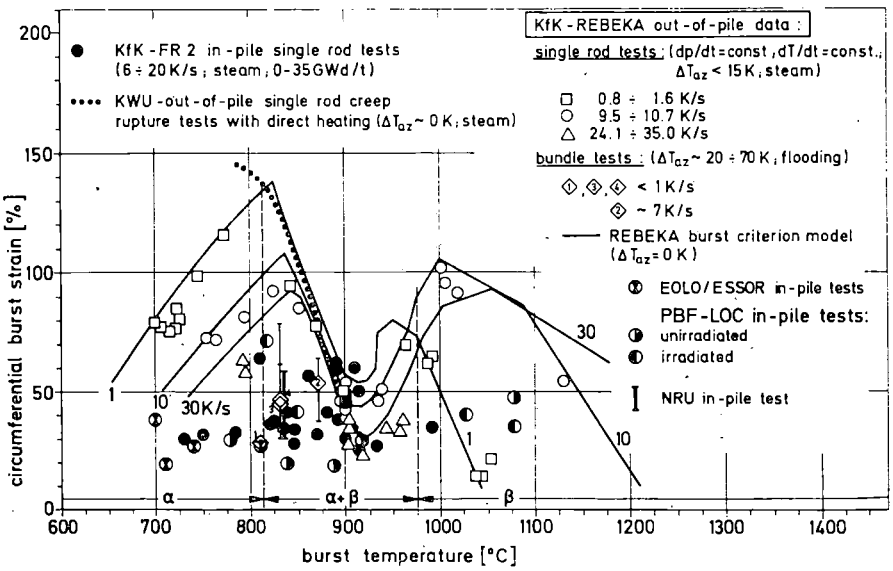

Fig. 9: Burst strain vs. burst temperature

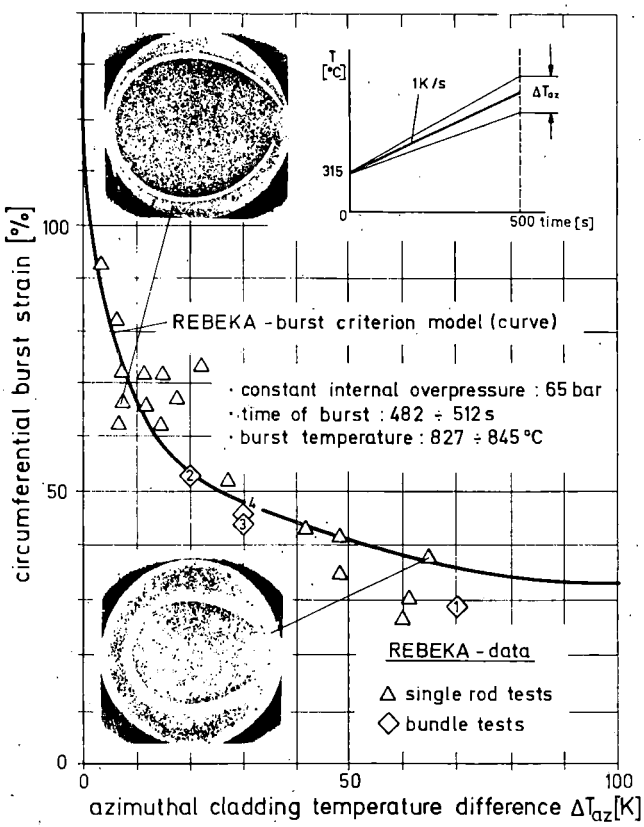

Fig. 10: Burst strain vs. azimuthal temperature difference

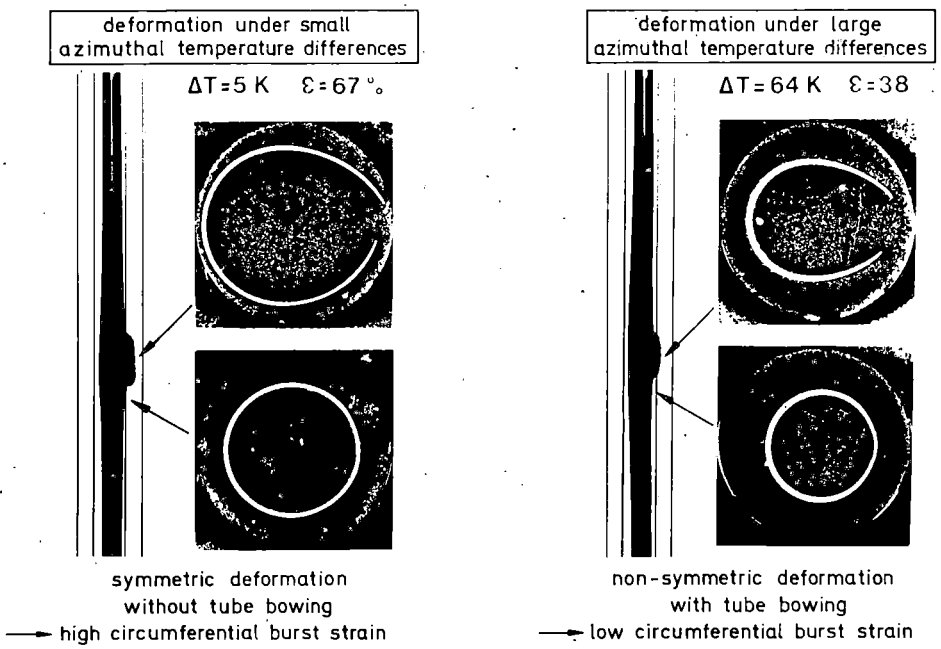

Fig. 11: Deformation mechanism

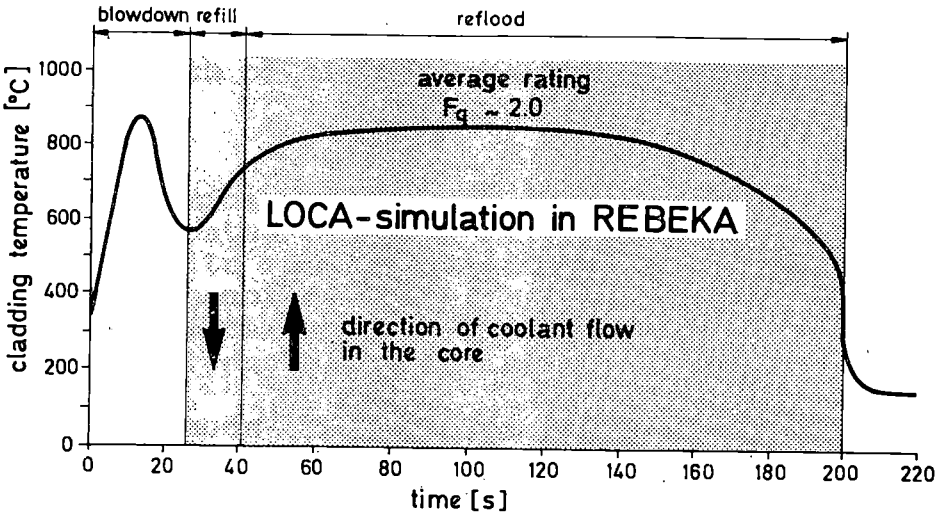

- internal rod pressure (Helium) — 70 bar
- decay heat rating at midpoint — 20 W/cm
- heat transfer during refill by steam flow from top — 30 W/m^2K
- cold flooding rate (forced flooding from bottom) — 3 cm/s
- flooding water temperature — 130 °C
- system pressure — 4 bar
- maximum cladding temperature at start of flooding (test parameter) — 750-850 °C

→ cladding temperature-and pressure histories develop as a result of the interaction between decay heat, cooling and cladding deformation

Fig. 12: Test procedure and test conditions of bundle tests

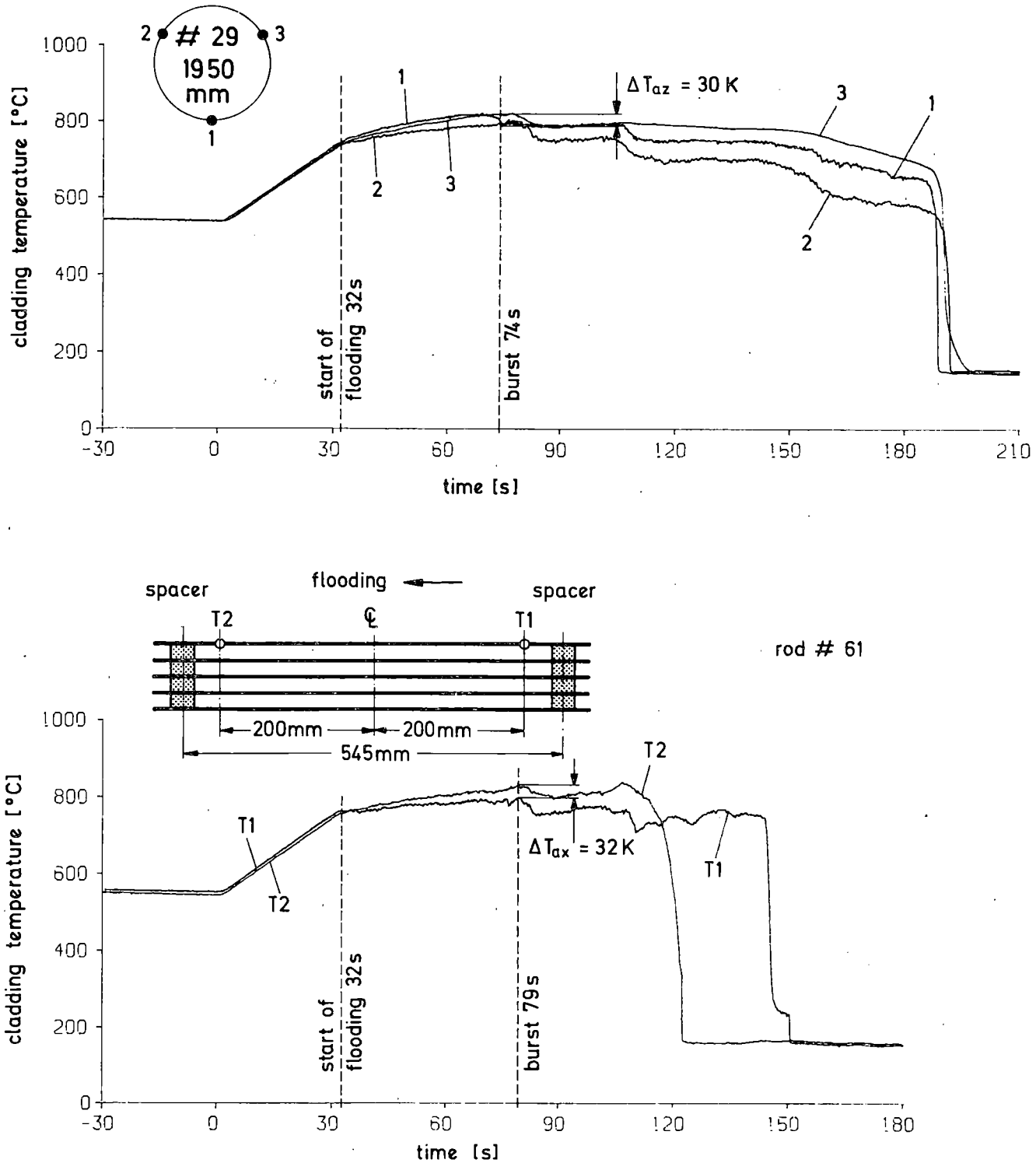

Fig. 13: REBEKA 3: Azimuthal and axial temperature distributions

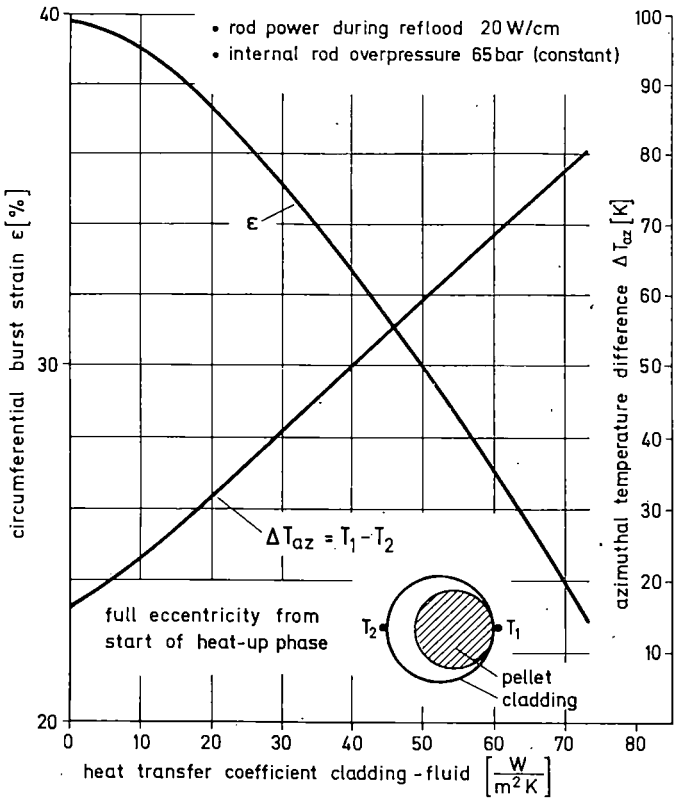

Fig. 14: Influence of heat transfer on cladding deformation

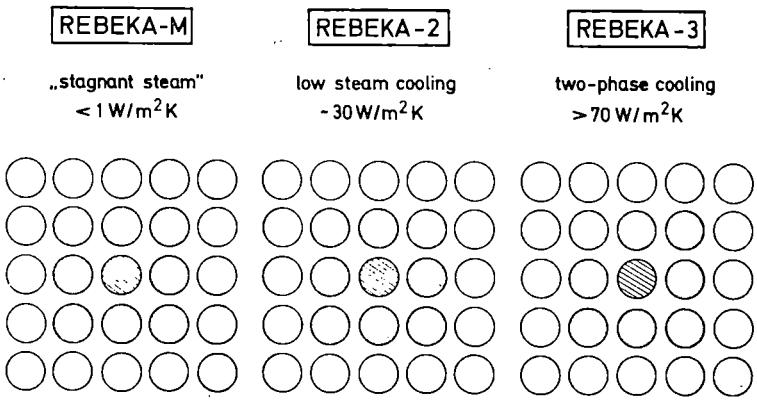

burst strain of centre rod :	~ 89%	~ 52%	~ 37%
mean burst strain of inner ring of rods :	~ 60%	~ 50%	~ 45%
flow blockage at inner 3x3rods :	~ 84%	~ 60%	~ 52%

Fig. 15: Influence of cooling mode on cladding deformation

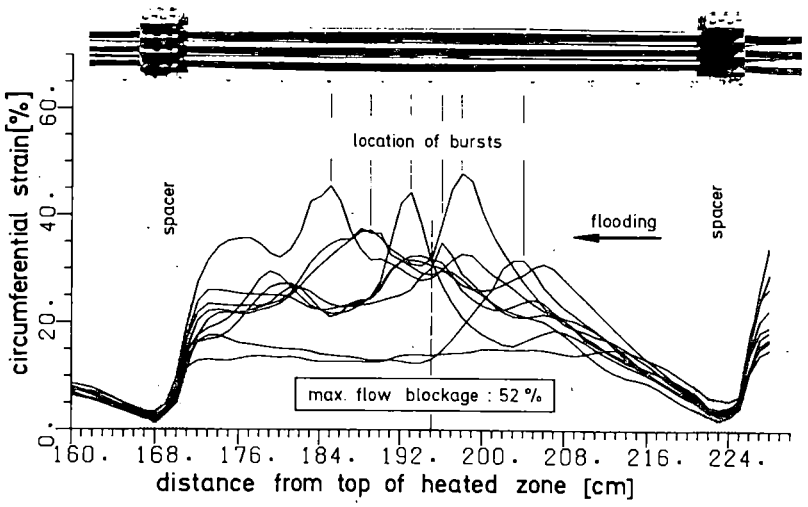

Fig. 16: REBEKA 3: Axial deformation profile

Main characteristic	test 1	test 2	test 3	test 4
main test objective	influence of cooling on deformation			influence of control rod guide thimble on deformation
main test parameter	early flooding	late flooding	early flooding	
flooding rate, cold	-3cm/s (enhanced at start of flooding)		-3cm/s (constant)	-3cm/s (constant)
deformation history	most deformation during reflood (quasi-isothermal)	all deformation during refill (heating rate: 7K/s)	most deformation during reflood (quasi-isothermal)	most deformation during reflood (quasi-isothermal)
max. axial temperature difference at time of burst between two inner grids	50 °C	20 °C	32 °C	40 °C
max. azimuthal temperature difference at time of burst	70 °C	20 °C	30 °C	30 °C / 60 °C
mean burst data	60 bar 810 °C	55 bar 870 °C	51 bar 837 °C	53 bar 830 °C
mean value of circumferential burst strains	29 % (two burst rods)	53 % (without rod 40: pin hole)	44 %	46 %
max. coolant channel blockage ratio	25 %	60 %	52 %	55 %

Fig. 17: Major test data of bundle tests 1, 2, 3, and 4

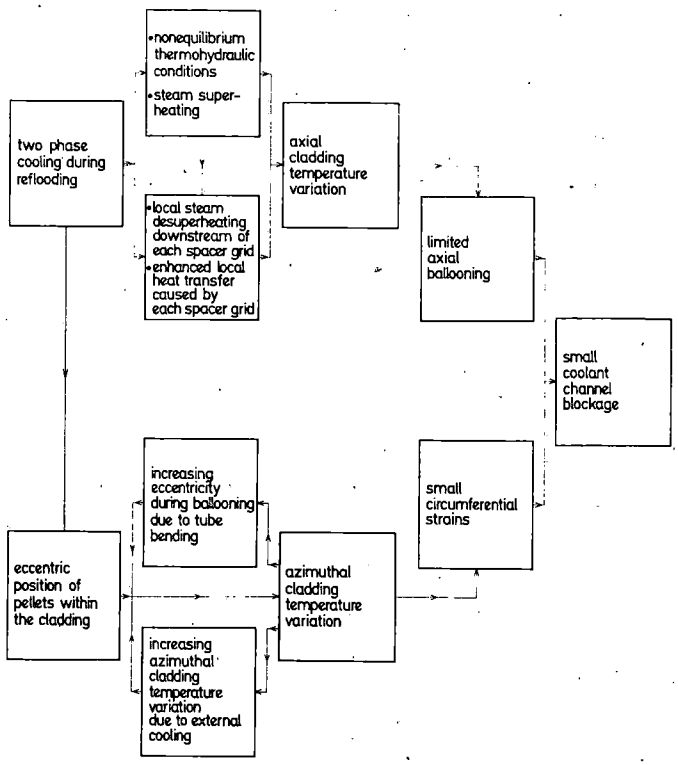

Fig. 18: Interaction between thermohydraulics and fuel clad ballooning (scenario)

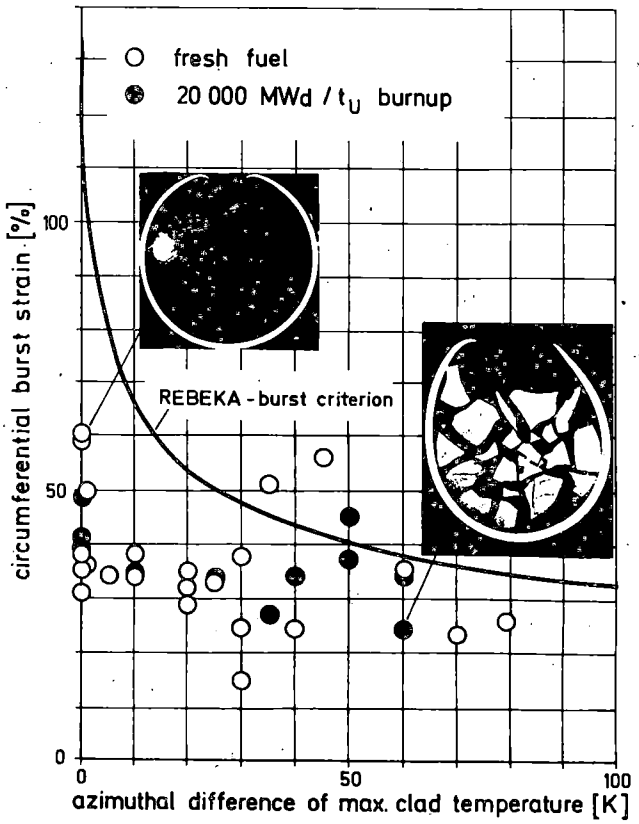

Fig. 19: FR-2 in-pile tests: Burst strain vs. azimuthal temperature difference

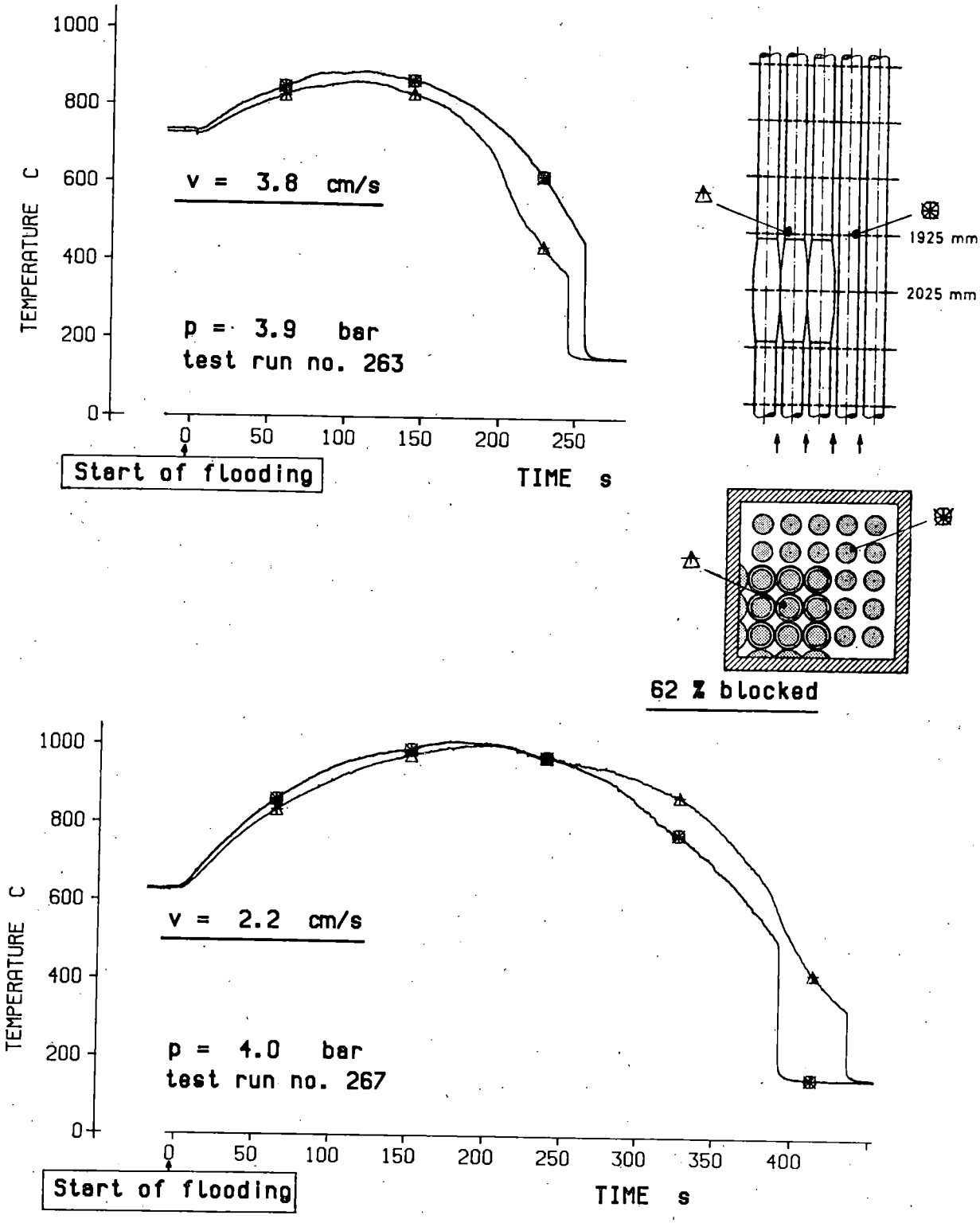

Fig. 20: FEBA flooding tests: Cladding temperatures in a partly blocked 5x5 bundle

PRELIMINARY RESULTS OF MRBT BUNDLE B-5 (8 X 8) TEST*

Robert H. Chapman

Engineering Technology Division
Oak Ridge National Laboratory
Oak Ridge, Tennessee 37830

Presented at the
Ninth Water Reactor Safety Research Information Meeting
October 26-30, 1981
Gaithersburg, Maryland

*Research sponsored by the Office of Nuclear Regulatory Research, Nuclear Regulatory Commission, under Interagency Agreements 40-551-75 and 40-552-75 with the U.S. Department of Energy under contract W-7405-eng-26 with the Union Carbide Corporation.

PRELIMINARY RESULTS OF MRBT BUNDLE B-5 (8 X 8) TEST

Robert H. Chapman

Oak Ridge National Laboratory
Oak Ridge, Tennessee 37830

The Multirod Burst Test (MRBT) Program is investigating the effects of material behavior on LWR cladding deformation in single rod and multi-rod test arrays under conditions representative of refill and reflood phases of a large break LOCA. This research addresses pertinent licensing issues related to ECCS Acceptance Criteria by providing test data for development and validation of deformation models in computer codes. The data are also used by the Nuclear Regulatory Commission to assess and audit licensee models for regulatory purposes.

In these tests internally pressurized, unirradiated Zircaloy-4 tubes containing internal electrical heaters are tested to failure in a low-pressure, superheated-steam environment. The tubes are "uniformly" heated over a 915-mm length; the simulator pressure, due to the small enclosed gas volume, also varies with temperature (and deformation) during the test. The tests are conducted at very low steam flow rates ($200 < Re < 800$) under either constant power or constant heating rate modes of control, as desired.

Over 100 single rod tests have been performed, covering a burst pressure range from 0.77 to 19.2 MPa; the corresponding burst temperatures range from 1170 to 690°C. Heating rates ranging from 0 to 28 K/s have been used. The shroud surrounding the test simulator was unheated in approximately two-thirds of the tests (i.e., in the early phase of the program) and heated to the same temperature as the simulator in the remainder of the tests.

Two 4 X 4 multirod tests (B-1 and B-2), one with and one without shroud electrical heating, have been conducted with a bundle heating rate of ∿29 K/s; initial pressure conditions for these tests were selected to cause failure at about 860°C. An additional 4 X 4 array (B-3) was tested using a bundle heating rate of ∿10 K/s; the shroud was also electrically heated in this test. Initial conditions were adjusted to cause failure at ∿760°C. An 8 X 8 array (B-5) was tested under B-3 test conditions to determine the effect of array size on deformation. The B-5 shroud (unheated electrically) was spaced one-half of a coolant channel away from the outer ring of simulators to provide radial constraint typical of a fuel rod bundle (Fig. 1).

A 6 X 6 array (B-4), with shroud design features identical to the B-5 array, was tested to investigate rod-to-rod interactions and unheated simulator effects. Although it was planned to be a routine ramp test, improper logic in safety control circuits caused premature termination of the test. While primary test objectives were not realized, the data appear useful for model development and validation, particularly for "flat-topped" temperature transients.

Posttest examination (including flow tests) of the three 4 X 4 bundles has been completed and reported. Quick-look results of the 6 X 6 and 8 X 8 tests have also been reported. Posttest examination of these arrays (including flow tests of the 8 X 8 array) is nearly complete; some preliminary 8 X 8 results are included herein.

Temperature uniformity effects in the 4 X 4 bundles were such that the observed deformation was greater than would have been expected from single rod unheated shroud tests but comparable to heated shroud results. However, in addition to these effects, radial constraint in the 8 X 8 bundle test caused greater deformation of the inner 4 X 4 array than was observed for the comparable 4 X 4 bundle test. Based on these results, it was concluded that the equivalent of two rows of guard heaters is needed to simulate radial temperature and mechanical boundary effects in large bundles. Ideally, the guard heaters should also deform to improve the simulation.

A correlation relating burst temperature to pressure and heating rate was derived from the single rod unheated shroud tests. The more recent heated shroud tests tend to be underpredicted by the correlation, particularly for heating rates of 10 and 28 K/s. This is believed to be related to local strain rate effects. Also, correlation predictions for the 8 X 8 test were not as good as for the comparable 4 X 4 test. This is attributed to rod-to-rod interactions (i.e., external support of neighboring rods after contact), causing redistribution of the straining pattern in both the azimuthal and axial directions. These observations indicate that the correlation must be modified to include these effects if improved predictions are to be expected.

Plans are well underway for the B-6 test, currently planned to be the final test in this program, early next year. The test, which will have the shroud design features as in the B-5 test, will be conducted at $\sim$925°C, using a heating rate of $\sim$7 K/s, to investigate deformation in the two-phase region. Flow tests will not be performed.

Work on this program is routinely reported in a series of reports entitled Multirod Burst Test Program Progress Report. Significant results appear in the following reports of this series:

NUREG Report No.	ORNL Report No.	Period Covered
	ORNL/NUREG/TM-36	January-March 1976
	ORNL/NUREG/TM-74	April-June 1976
	ORNL/NUREG/TM-77	July-September 1976
	ORNL/NUREG/TM-95	October-December 1976
	ORNL/NUREG/TM-108	January-March 1977
	ORNL/NUREG/TM-135	April-June 1977
NUREG/CR-0103	ORNL/NUREG/TM-200	July-December 1977
NUREG/CR-0225	ORNL/NUREG/TM-217	January-March 1978
NUREG/CR-0398	ORNL/NUREG/TM-243	April-June 1978
NUREG/CR-0655	ORNL/NUREG/TM-297	July-December 1978
NUREG/CR-0817	ORNL/NUREG/TM-323	January-March 1979
NUREG/CR-1023	ORNL/NUREG/TM-351	April-June 1979
NUREG/CR-1450	ORNL/NUREG/TM-392	July-December 1979
NUREG/CR-1883	ORNL/NUREG/TM-426	January-June 1980
NUREG/CR-1919	ORNL/NUREG/TM-436	July-December 1980

Published topical reports and papers of interest include:

1. R. H. Chapman, et al., Effect of Creep Time and Heating Rate on Deformation of Zircaloy-4 Tubes Tested in Steam with Internal Heaters, ORNL/NUREG/TM-245, October 1978.

2. J. F. Mincey, Steady-State Axial Pressure Losses Along the Exterior of Deformed Fuel Cladding: Multirod Burst Test (MRBT) Bundles B-1 and B-2, NUREG/CR-1011 (ORNL/NUREG/TM-350), January 1980.

3. R. H. Chapman, et al., Zircaloy Cladding Deformation in a Steam Environment with Transient Heating, in Proceedings of Fourth International Conference on Zirconium in the Nuclear Industry, held June 26-29, 1978, at Stratford-on-Avon, England, ASTM STP 681 (1979).

The following limited-distribution data reports have been published:

1. R. H. Chapman, et al., Bundle B-1 Test Data, ORNL/NUREG/TM-322, June 1979.

2. R. H. Chapman, et al., Bundle B-2 Test Data, ORNL/NUREG/TM-337, August 1979.

3. R. H. Chapman, et al., Bundle B-3 Test Data, ORNL/NUREG/TM-360, January 1980.

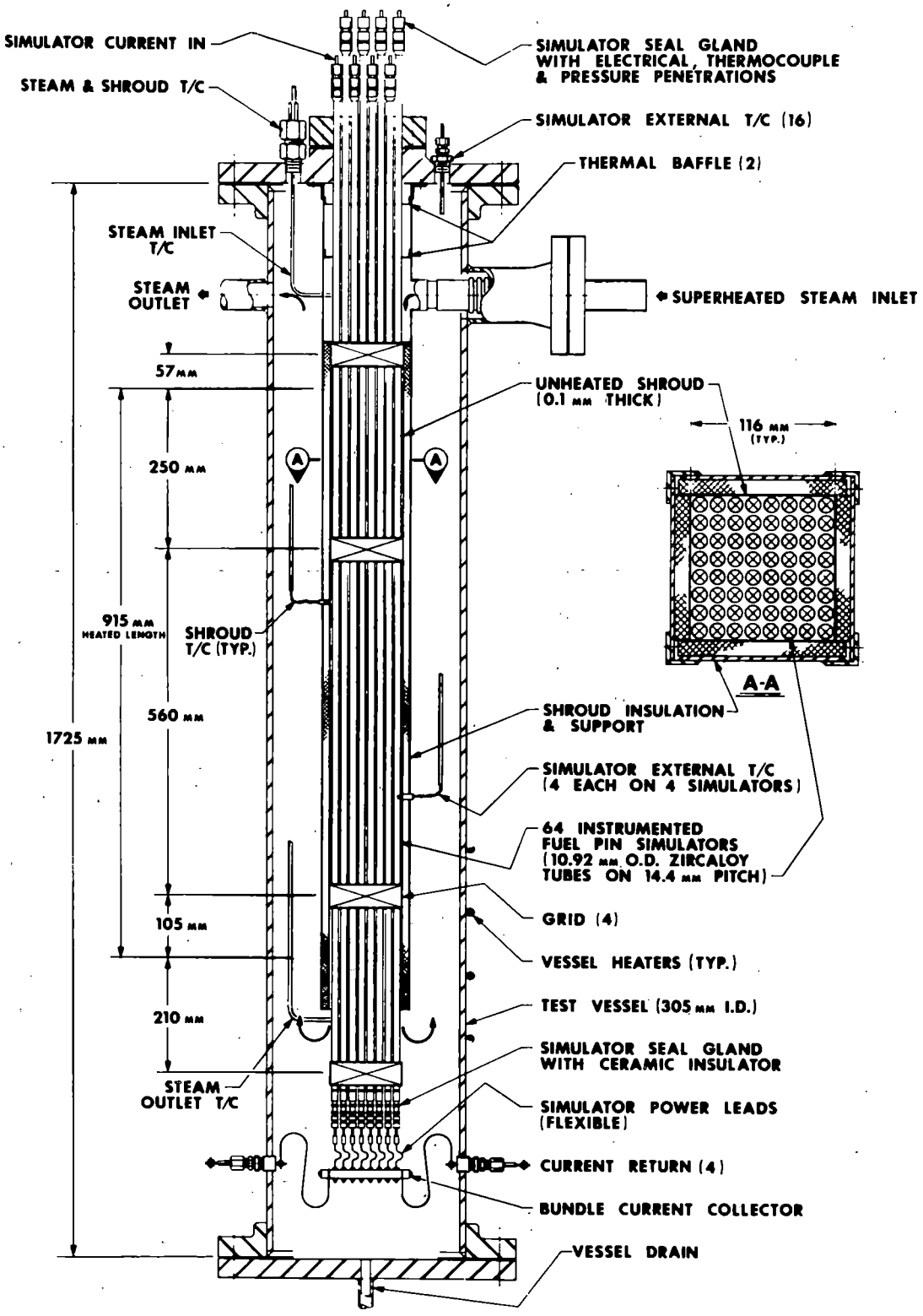

Fig. 1. Schematic of B-5 (8 × 8) bundle test assembly.

UNION CARBIDE ORNL

R. H. CHAPMAN, MANAGER
MULTIROD BURST TEST PROGRAM
OAK RIDGE NATIONAL LABORATORY

PRELIMINARY RESULTS OF MRBT BUNDLE B-5 (8 X 8) TEST

PRESENTED AT
NINTH WATER REACTOR SAFETY RESEARCH
INFORMATION MEETING
GAITHERSBURG, MARYLAND
OCTOBER 29, 1981

UNION CARBIDE ORNL

B-5 TEST ADDRESSES LICENSING ISSUES RELATED TO ECCS ACCEPTANCE CRITERIA

- MINIMUM SIZE OF SIMULATED FUEL BUNDLE
- VALIDITY OF EVALUATION MODELS

UNION CARBIDE ORNL

B–5 (8 X 8) BUNDLE TEST CRITERIA

OBJECTIVE

- TEST CONDITIONS SAME AS B–3 (4 X 4) TO DETERMINE EFFECTS OF ARRAY SIZE ON DEFORMATION CHARACTERISTICS

FEATURES

- TEST AT ~770°C WITH 10 K/s HEATING RATE
- ALL SIMULATORS PRESSURIZED AND HEATED
- OUTER RING OF SIMULATORS RESTRAINED BY CLOSELY SPACED SHROUD
- HIGHLY REFLECTIVE, UNHEATED SHROUD
- FLOW TEST REFERENCE AND DEFORMED BUNDLES

UNION CARBIDE ORNL

SCHEMATIC OF 8 X 8 BUNDLE TEST

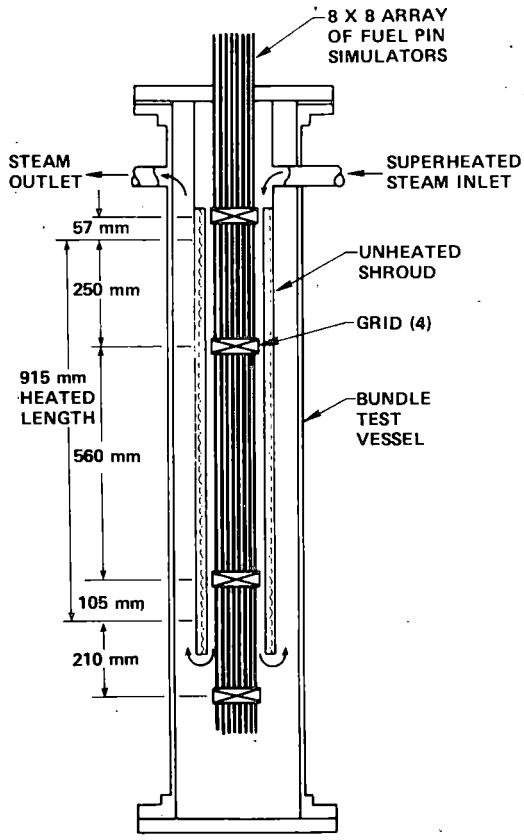

UNION CARBIDE ORNL

COMPARISON OF B-3 AND PRELIMINARY B-5 TEST DATA

	B-3 (4 X 4)	B-5 (8 X 8)
BUNDLE HEAT RATE (K/s)	9.5	9.8
SHROUD HEAT RATE (K/s)	7.1[a]	4.4[b]
INLET STEAM FLOW [$G(s \cdot m^2)^{-1}$]	288	288
INLET STEAM TEMPERATURE (^oC)	320	355
BUNDLE INITIAL TEMPERATURE (^oC)	329 (σ = 2)	335 (σ = 4)
SHROUD INITIAL TEMPERATURE (^oC)	334 (σ = 3)	339 (σ = 4)
INITIAL PRESSURE (kPa)	11610 (σ = 45)	11625 (σ = 30)
MAXIMUM PRESSURE (kPa)	12110 (σ = 55)	12155 (σ = 40)
BURST PRESSURE (kPa)	9425 (σ = 375)	8810 (σ = 525)
BURST TEMPERATURE (^oC)	764 (σ = 9)	775 (σ = 9)
BURST TIME (s)	46.06 (σ = 0.77)	46.29 (σ = 1.05)
BURST STRAIN (%)	58 (σ = 10)	60 (σ = 15)
TUBE VOLUME INCREASE (%)	43 (σ = 7)	50 (σ = 10)
$T_{BUNDLE} - T_{SHROUD}$ AT BURST TIME (^oC)	80[a]	240[b]

[a] SHROUD ELECTRICALLY HEATED

[b] SHROUD NOT ELECTRICALLY HEATED

UNION CARBIDE
ORNL

SMALL UNCONSTRAINED BUNDLES DO NOT PRODUCE SAME DEFORMATION PATTERNS AS LARGE CONSTRAINED BUNDLES FOR SAME TEST CONDITION

B–5 WITH INTERACTIONS

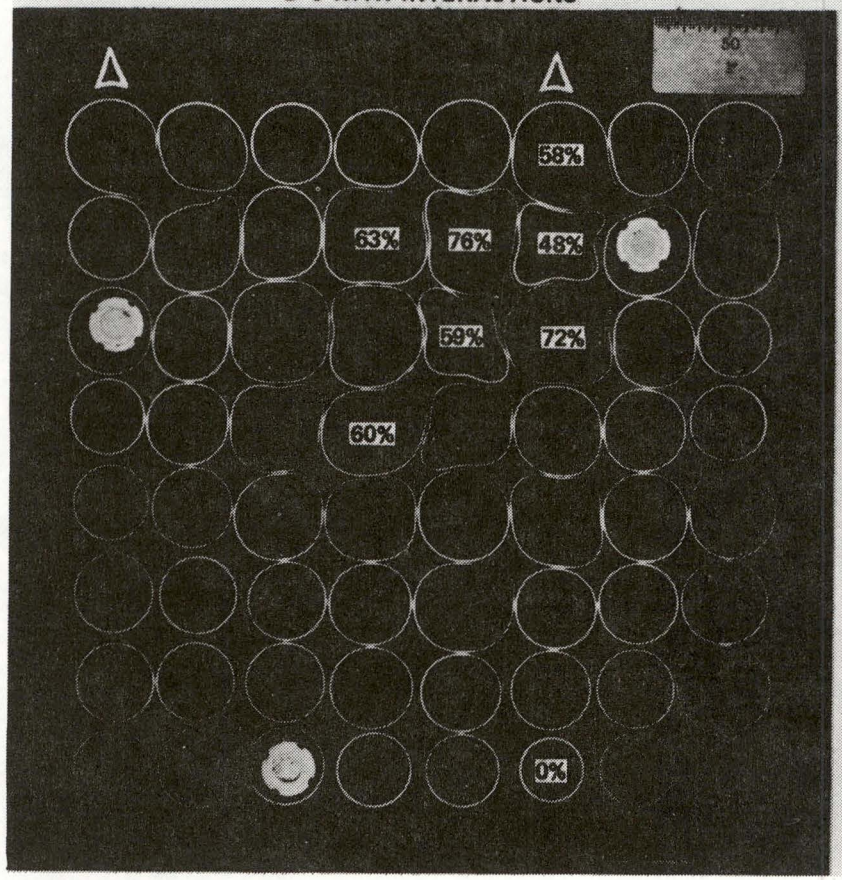

B–3 WITHOUT INTERACTIONS

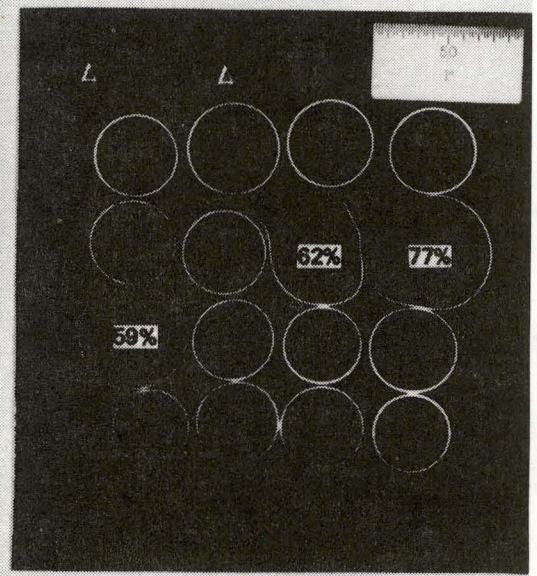

UNION CARBIDE ORNL

B–5 BURSTS WERE PREDOMINATELY TOWARD THE OPEN COOLANT CHANNEL AREAS

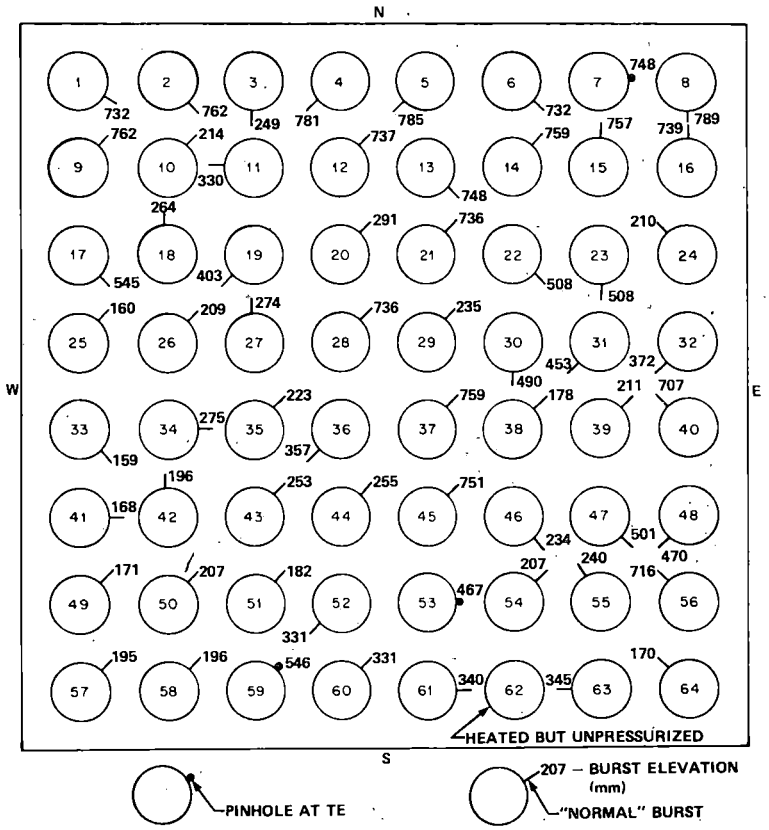

UNION CARBIDE ORNL

TEMPERATURE UNIFORMITY AND ROD-TO-ROD INTERACTIONS CAUSED GREATER DEFORMATION AND LARGER BURST PRESSURE VARIATION IN B–5 (8 X 8) THAN IN COMPARABLE B–3 (4 X 4) TEST

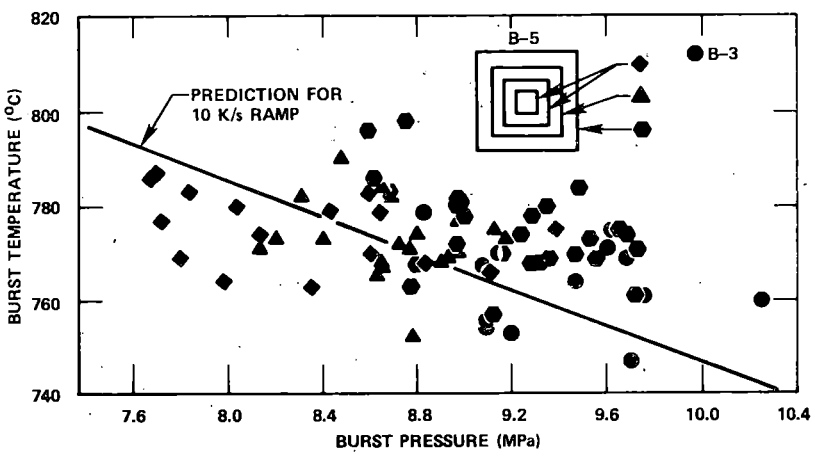

UNION CARBIDE
ORNL

TUBE DILATATION GREATER IN B-5 INTERIOR SIMULATORS THAN IN EXTERIOR SIMULATORS AND GREATER THAN IN COMPARABLE B-3 (4 X 4) TEST

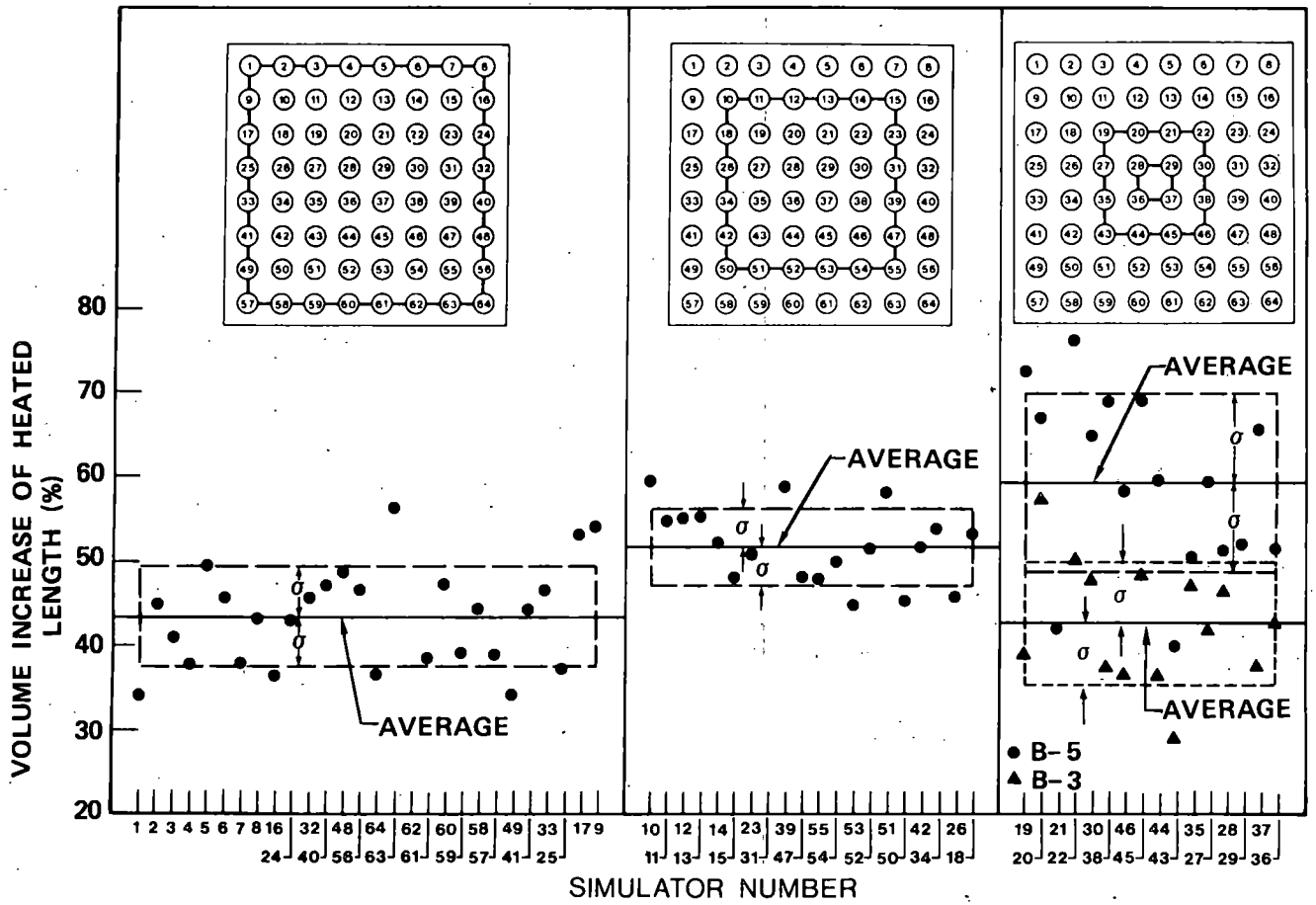

UNION CARBIDE
ORNL

PRELIMINARY DATA SHOW B–5 BURST STRAINS NOT A STRONG FUNCTION OF ROD POSITION AND ONLY SLIGHTLY GREATER THAN B–3 BURST STRAINS

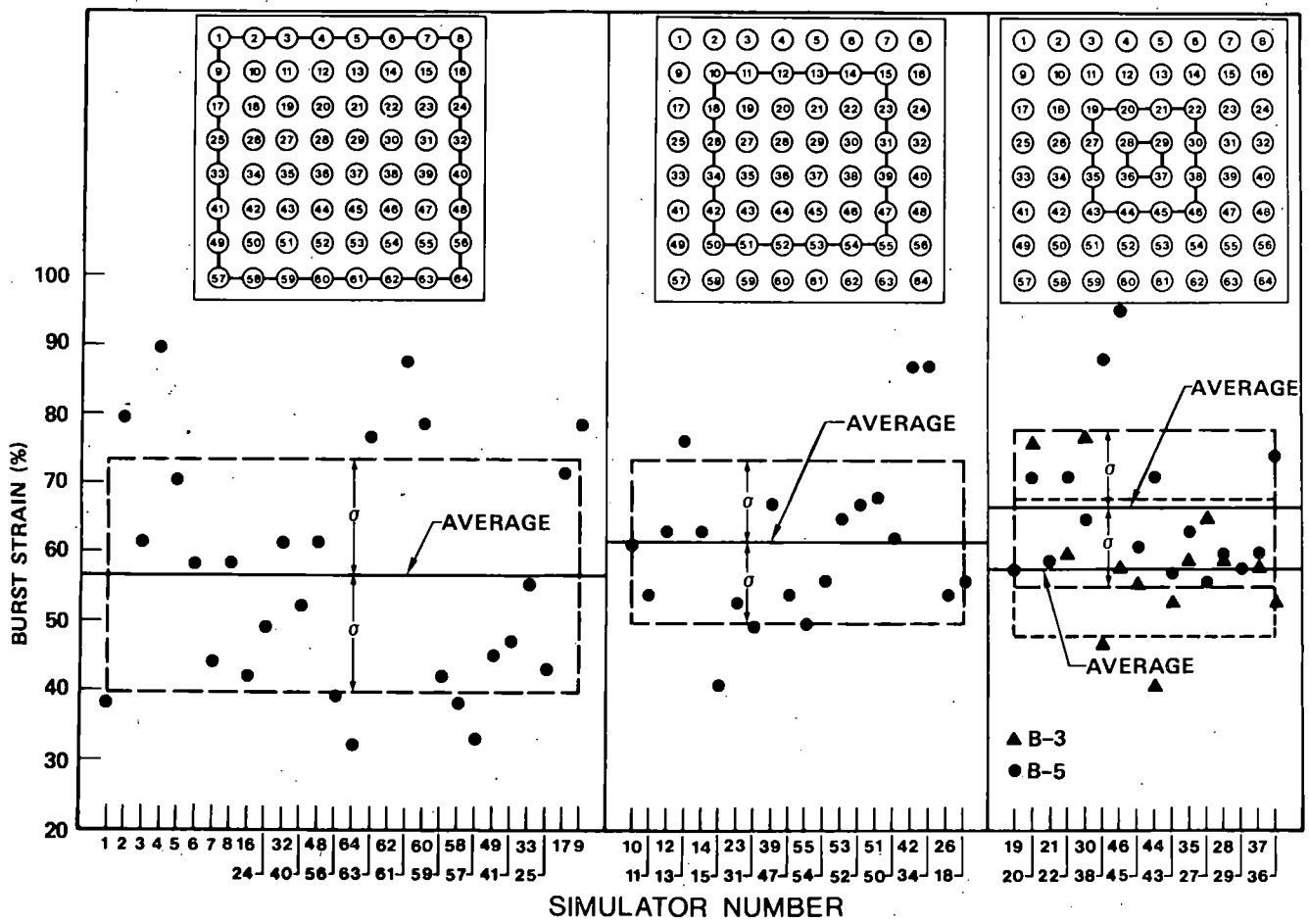

UNION CARBIDE ORNL

SUBDIVISION OF B–5 DATA SHOWS INTERIOR SUBARRAYS HAVE GREATER COOLANT FLOW AREA RESTRICTION

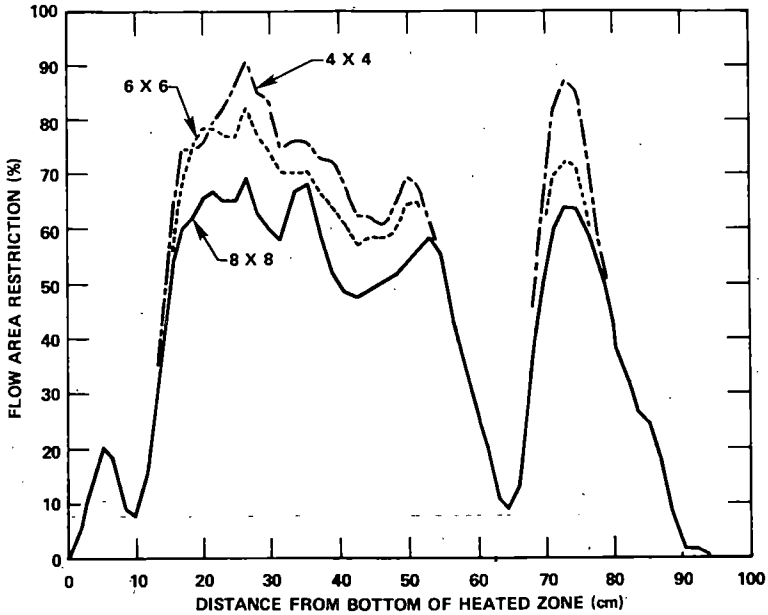

UNION CARBIDE ORNL

PRELIMINARY B–5 DATA SHOW INNER 4 X 4 ARRAY HAS GREATER FLOW RESTRICTION THAN B–3 (4 X 4) ARRAY

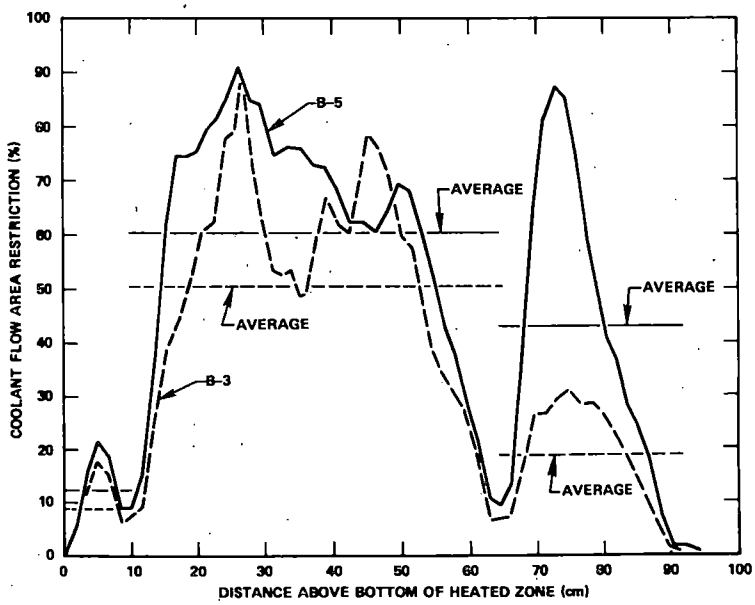

UNION CARBIDE ORNL

PRESSURE TAP ARRANGEMENT IN B–5 FLOW TESTS PERMIT INTERPRETATION OF DATA IN TERMS OF CROSSFLOW

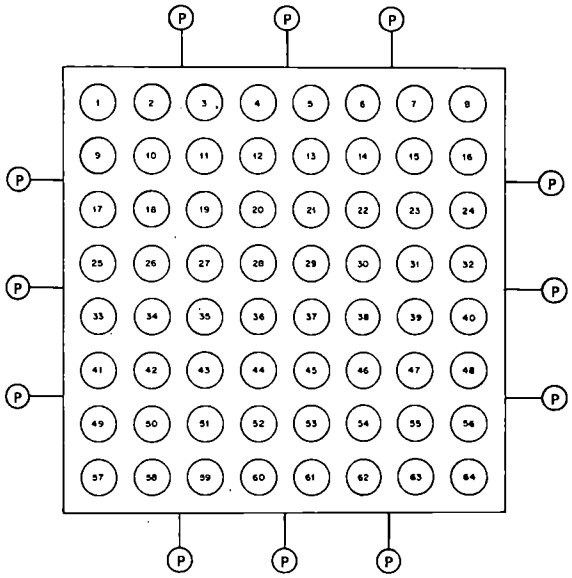

UNION CARBIDE ORNL

COMPARISON OF PRELIMINARY FLOW CHARACTERIZATION DATA ON B–5 AND B–5 REFERENCE BUNDLES AS A FUNCTION OF AXIAL POSITION

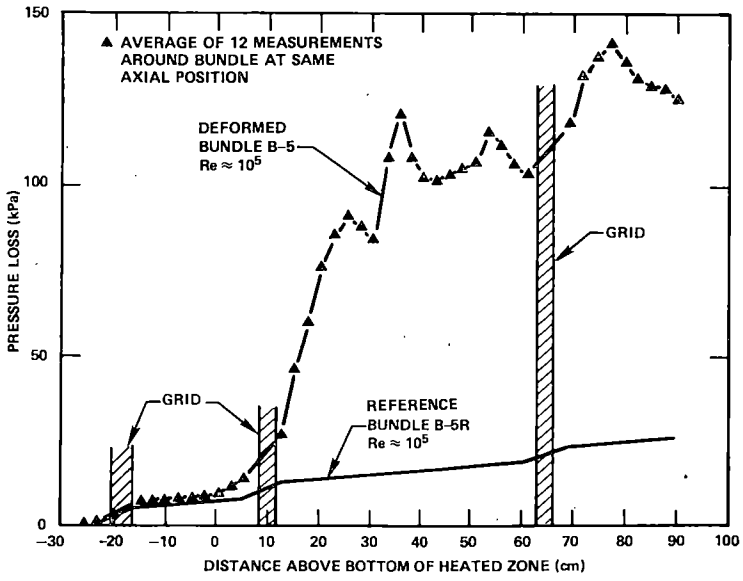

UNION CARBIDE ORNL

COMPARISON OF PRELIMINARY FLOW CHARACTERIZATION DATA ON B-5 AND B-5 REFERENCE BUNDLES AS A FUNCTION OF FLOW RATE

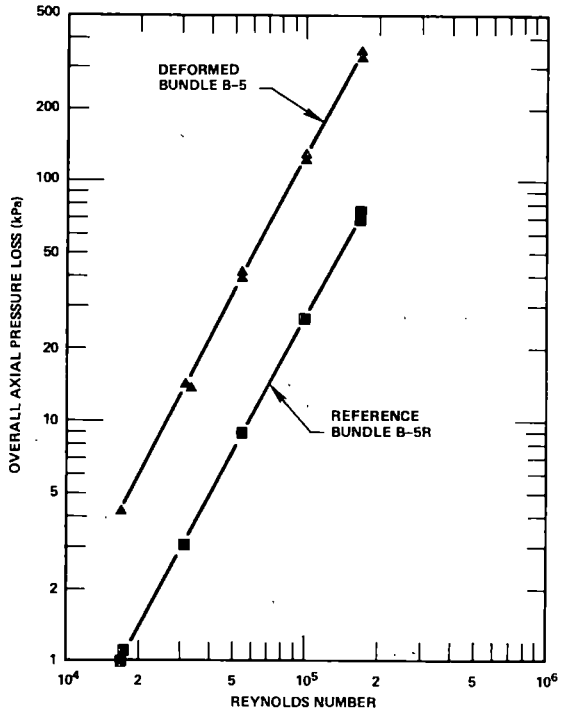

UNION CARBIDE ORNL

PRELIMINARY FLOW AND DEFORMATION DATA SHOW EXCELLENT CORRELATION

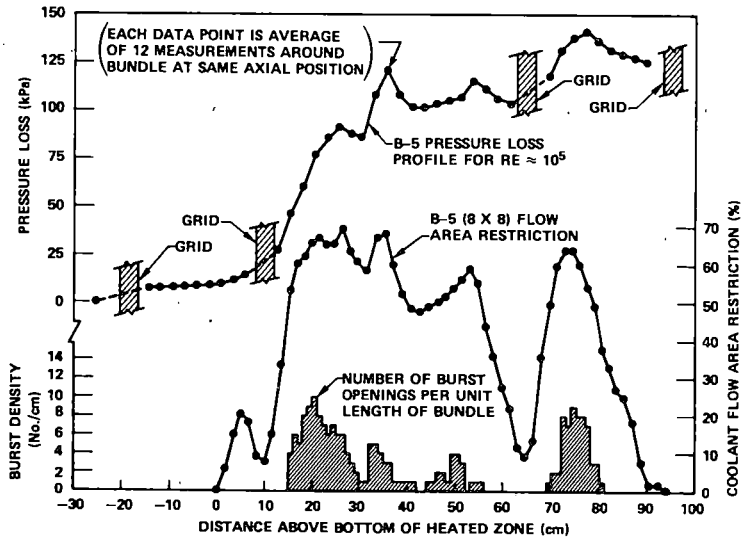

UNION CARBIDE ORNL

CONCLUSIONS APPLICABLE TO TEMPERATURE RANGES IN WHICH HIGH DEFORMATION CAN BE EXPECTED

- 4 X 4 (AND SMALLER) BUNDLE TESTS DO NOT ADEQUATELY SIMULATE TEMPERATURE AND MECHANICAL BOUNDARY EFFECTS OF LARGE ARRAYS
- EQUIVALENT OF TWO ROWS OF DEFORMING GUARD HEATERS NECESSARY TO SIMULATE THESE BOUNDARY CONDITIONS
- BUNDLE FLOW BLOCKAGE CANNOT BE MODELED ON BASIS OF 4 X 4 UNCONSTRAINED BUNDLE DEFORMATION TESTS
- TEMPERATURE UNIFORMITY AND ROD–TO–ROD MECHANICAL INTERACTIONS MODIFY RUPTURE TEMPERATURE–PRESSURE CORRELATION DEVELOPED FROM SINGLE ROD TESTS

LOCA SIMULATION IN NRU

by

C. L. Mohr
G. M. Hesson

October 20, 1981

To be presented at the Ninth Water Reactor Safety Research Information Meeting, October 26-30, 1981, Gaithersburg, Maryland

Pacific Northwest Laboratory
Richland, Washington
Operated by Battelle Memorial Institute

LOCA SIMULATION IN NRU

C. L. Mohr
G. M. Hesson

The LOCA Simulation Project is being conducted in the National Research Universal (NRU) Reactor located at Chalk River Nuclear Laboratory (Atomic Energy of Canada, Ltd. [AECL]) by Pacific Northwest Laboratory. The project is sponsored by the Fuel Behavior Research Branch of the United States Nuclear Regulatory Commission and the United Kingdom Atomic Energy Authority. The project has the major objective of evaluating the thermal-hydraulic and mechanical deformation behavior of a full-length PWR fuel rod bundle during the heatup, reflood, and quench phases of a LOCA. The tests are driven by low-level fission heat and simulate the temperature gradients in the fuel typical of a LOCA.

The NRU-LOCA test variables included the length of the heatup (delay time to reflood) and the reflood rate of the coolant. Additional variables include rod pressurization levels and a variable reflood history.

Currently, four tests have been performed. Two tests (PTH) and (TH-2) have been thermal hydraulic oriented tests while the remaining two tests, MT-1 and MT-2, were materials deformation and rupture tests.

Test Summary

The PTH tests series consisted of 28 separate transient tests using the same test train with unpressurized fuel rods. Reflood rates of 0.8 in./sec to 10.7 in./sec and delay times of 10 sec to 80 sec were used. The results of this test series showed the limits of the FLECHT experiments in predicting the behavior of nuclear heated tests and provided information that showed nuclear rods quench much faster than predicted.

The original intent of the program was to use the PTH test series as the basis for all subsequent materials deformation tests. Specific PTH transients would be selected to determine the incremental effects of deformation and rupture. This philosophy was used in the subsequent MT-1 experiment.

The MT-1 experiment used a pressurized cruciform of eleven rods with one water tube and 20 unpressurized guard rods. The rods were pressurized to 450 psi. The delay time and reflood rate were selected to duplicate the PTH-110 experiment which reached a peak temperature of 1600°F. These conditions were achieved and six of the eleven rods ruptured.

The MT-2 experiment was the second materials deformation test. This test used the same guard rod set and shroud used in MT-1. It was reconstituted in the rod bay under water using a new cruciform test bundle. The test objectives were to perform a low temperature 1500°F (815°C) test using variable reflood rates. A malfunction of the test loop resulted in higher temperature being achieved during this test than desired and was a repeat of the basic MT-1 test conditions.

The most recent test that has been performed was the jointly funded (by NRC and UKAEA) TH-2 test. It used a new thermal hydraulics test bundle reconstituted in the MT-1/MT-2 guard rod and shroud assembly. This test was a thermal-hydraulic test series designed to evaluate the reflood rates necessary to obtain a flat top transient in the 1400°F (760°C) to 1525°F (829°C) range. The time span in this window should be greater than 150 seconds. The PTH test series showed that a single reflood rate or delay time combination could not be used to obtain these conditions and that only a variable reflood rate could potentially be used. The delay time and automatic control system used in this test has shown during the 14 transients performed that it is possible to obtain these kinds of transient conditions. It approaches a steady state boil off condition in which the quench front is in an equilibrium position with the reflood rate.

Deformation Measurement

One of the major features of the program was the development of the Disassembly Examination Reassembly Machine (DERM). This device is designed to disassemble the test bundle and perform single rod profilometry and bundle profilometry under water on an irradiated fuel bundle. It is also designed to reassemble the test train with a new central test bundle cruciform in a previously used shroud and guard rod assembly. The MT-1/MT-2/TH-2 tests have all made use of this machine and demonstrated its usefulness.

Future Test Plans

The immediate test plans are to perform at least one additional alpha temperature range rupture test using the conditions developed in the TH-2 test series. Subsequent tests will include Beta temperature range tests, irradiated rod tests and boil down tests using an insulated shroud.

LOCA SIMULATION TESTS IN NRU

BY

C.L. MOHR *
G.M. HESSON *

NINTH WATER REACTOR SAFETY MEETING
OCTOBER 29, 1981
NATIONAL BUREAU OF STANDARDS
GAITHERSBURG, MD.

* BATTELLE PACIFIC NORTHWEST LABORATORIES

LOCA SIMULATION IN NRU PROJECT

SPONSORS: UNITED STATES NUCLEAR REGULATORY COMMISSION

UNITED KINGDON ATOMIC ENERGY AUTHORITY

LOCA SIMULATION IN NRU PROJECT

OBJECTIVE: EVALUATE THE THERMAL-HYDRAULIC AND MECHANICAL DEFORMATION BEHAVIOR OF A FULL LENGTH PWR FUEL BUNDLE DURING A LARGE BREAK LOCA

SCOPE: BASIC PROGRAM

PTH	THERMAL-HYDRAULIC	OCT 1980
MT-1	ALPHA	APRIL 1981
MT-2	ALPHA	JULY 1981
TH-2	THERMAL-HYDRAULIC	SEPT 1981
MT-3	LONG ALPHA	NOV 1981
MT-4	BETA	MARCH 1982
MT-5	IRRADIATED ROD	JULY 1982
MT-6	INSULATED SHROUD	NOV 1982

CONTENTS

MECHANICAL DESIGN FEATURES

THE FUEL ROD DESIGN VARIABLES

CLADDING MATERIAL SPECIFICATION	ZIRCALOY-4
CLADDING OUTSIDE DIMENSION	0.379 in. (0.963 cm)
CLADDING INSIDE DIMENSION	0.331 in. (0.841 cm)
PITCH	0.502 in. (1.275 cm)
FUEL PELLET DIAMETER	0.325 in. (0.826 cm)
FUEL PELLET LENGTH	0.375 in. (0.953 cm)
ACTIVE FUELED LENGTH	144.0 in. (365.76 cm)
TOTAL SHROUD LENGTH	170.125 in. (423.1 cm)

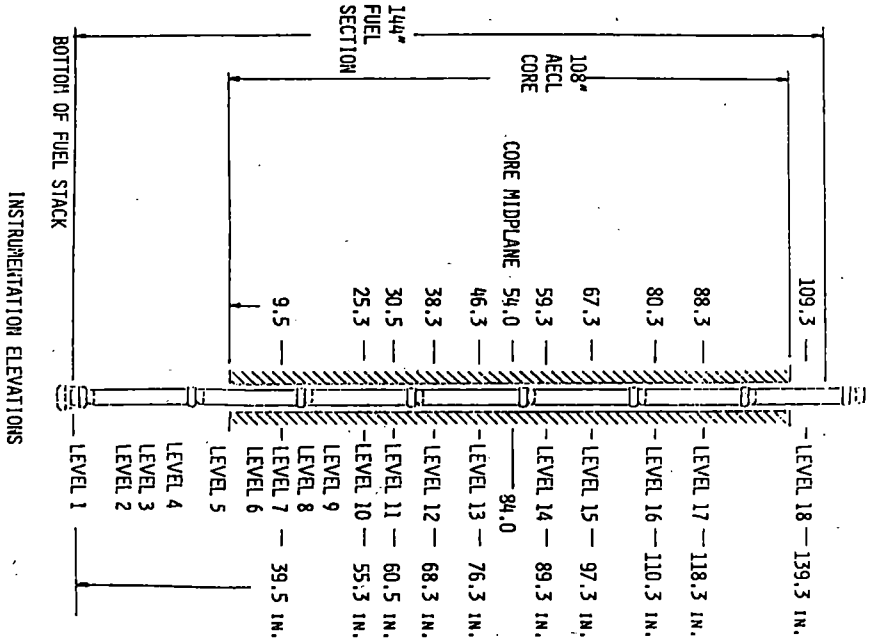

INSTRUMENTATION ELEVATIONS

THERMAL HYDRAULIC TEST DATA

CODE TO CODE COMPARISON

CODE TO DATA COMPARISON

TEST DATA

TEST CONDITION SUMMARY

TEST	DELAY TIME (S)	REFLOOD RATE (IN/SEC)	PEAK TEMP
PTH TEST SERIES (28 TESTS)	3	.8 – 10.7	2040 F
MT–1	31	2.1	1607 F
MT–2	36	.49 – 5.4	1710 F
TH–2 (14 TESTS)	10	.5 – 2.	1550 F

SUMMARY OF INSTRUMENTATION PERFORMANCE

	No. of Failed Thermocouples	SPND's
PTH	28	19
MT1	30	8
MT2	8	1
TH2	17	0

CODE TO CODE COMPARISON

C3–THERM (COMBUSION ENGINEERING)

FRAP–T5 (INEL)

GT3–FLECHT (PNL) COMBINES GAPCON THERMAL 3 WITH EPRI MPC DATA

TRUMP FLECHT

CODE TO CODE COMPARISON

	REFLOOD RATE	DELAY TIME
CASE 1	5.1 cm/sec	20 sec
CASE 2	12.7 cm/sec	0 sec

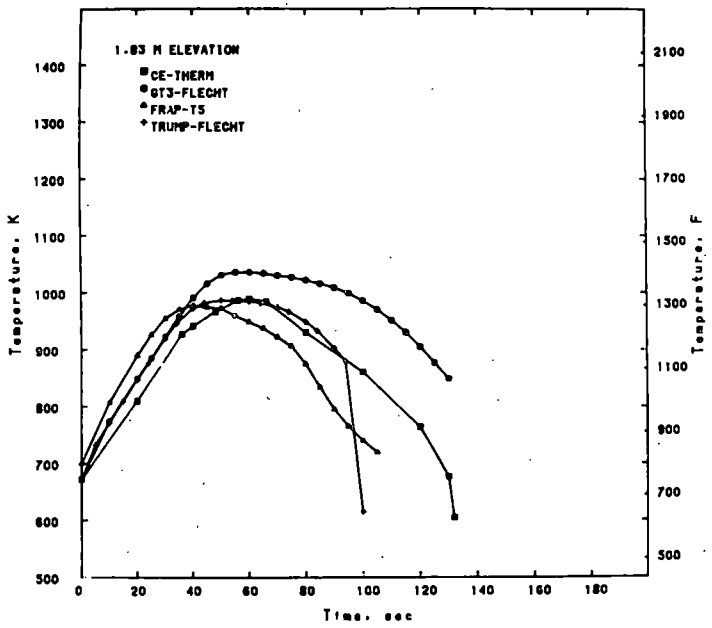
1.83 M ELEVATION
CE-THERM
GT3-FLECHT
FRAP-T5
TRUMP-FLECHT
Temperature, K
Temperature, F
Time, sec

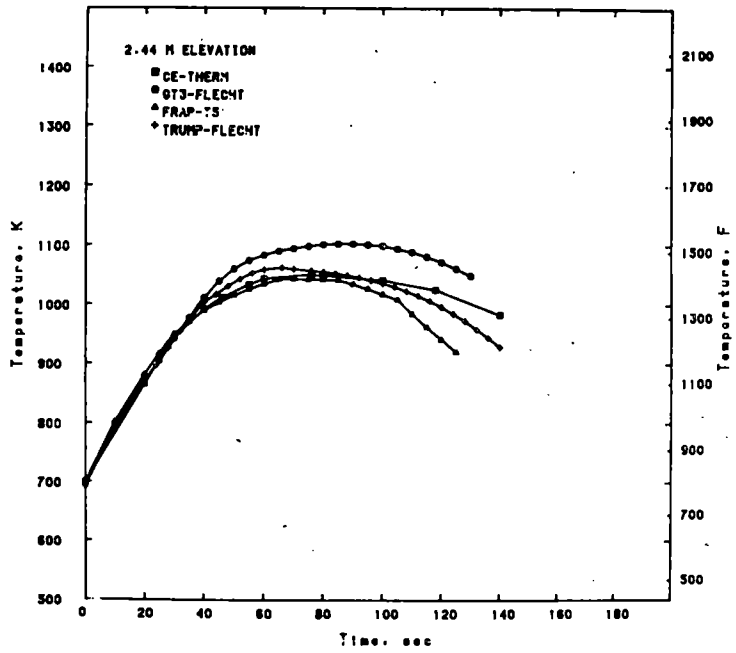
2.44 M ELEVATION
CE-THERM
GT3-FLECHT
FRAP-T5
TRUMP-FLECHT
Temperature, K
Temperature, F
Time, sec

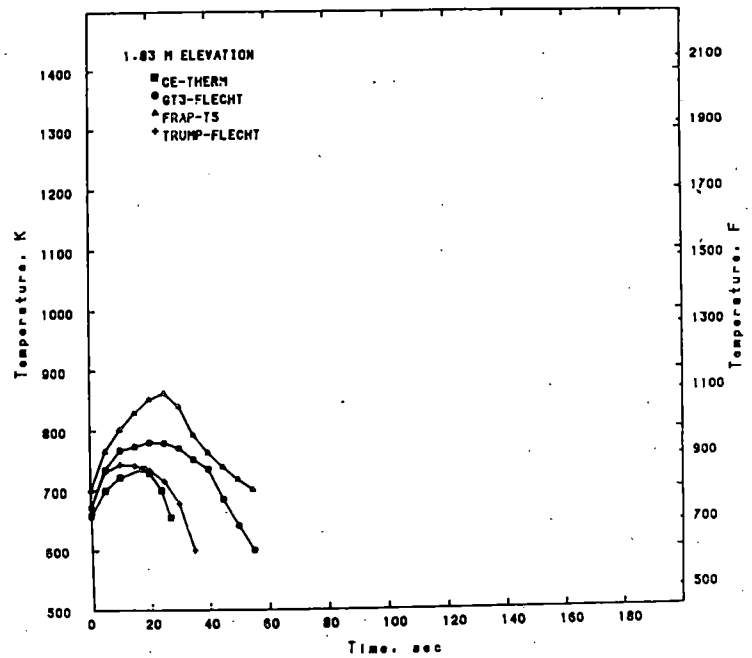
1.83 M ELEVATION
CE-THERM
GT3-FLECHT
FRAP-T5
TRUMP-FLECHT
Temperature, K
Temperature, F
Time, sec

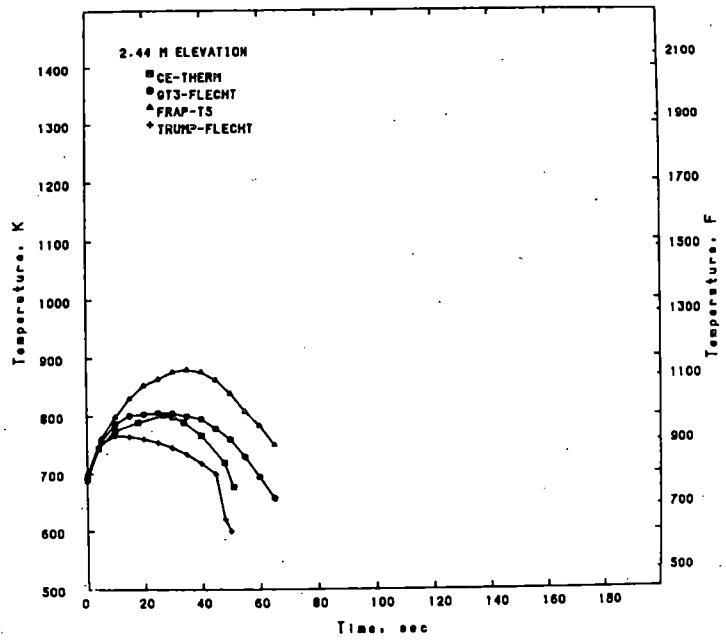
2.44 M ELEVATION
CE-THERM
GT3-FLECHT
FRAP-T5
TRUMP-FLECHT
Temperature, K
Temperature, F
Time, sec

CODE TO DATA

COMPARISON

TEST CASE DESCRIPTION

TEST NUMBER	DELAY TIME (sec)	REFLOOD RATE (cm/sec)	TRANSIENT START TEMPERATURE K (F)
104	38	10.2	701 (802)
108	14	3.9	714 (825)
120	54	15.5	715 (827)
127	3	2.8	765 (917)

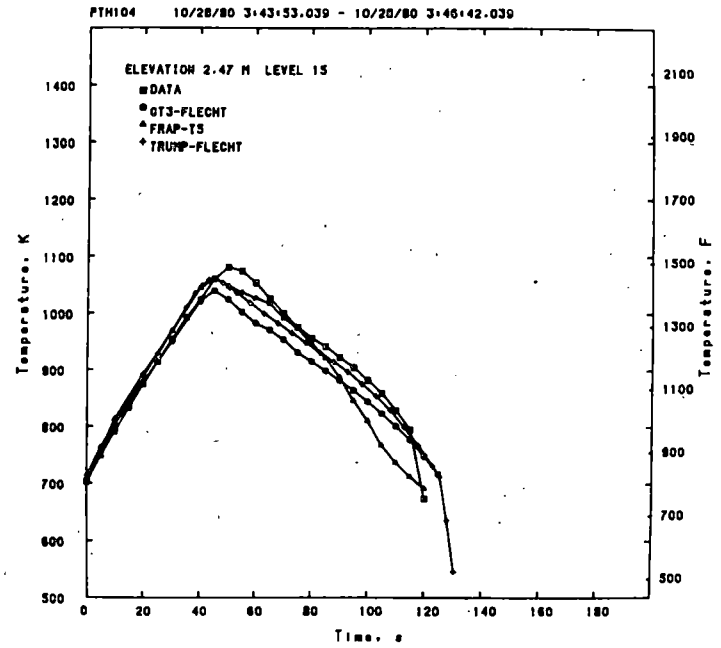

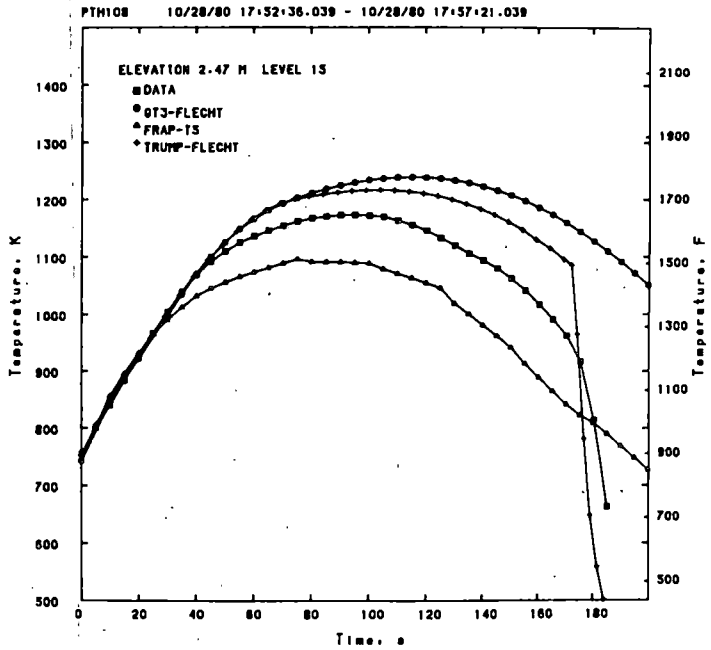

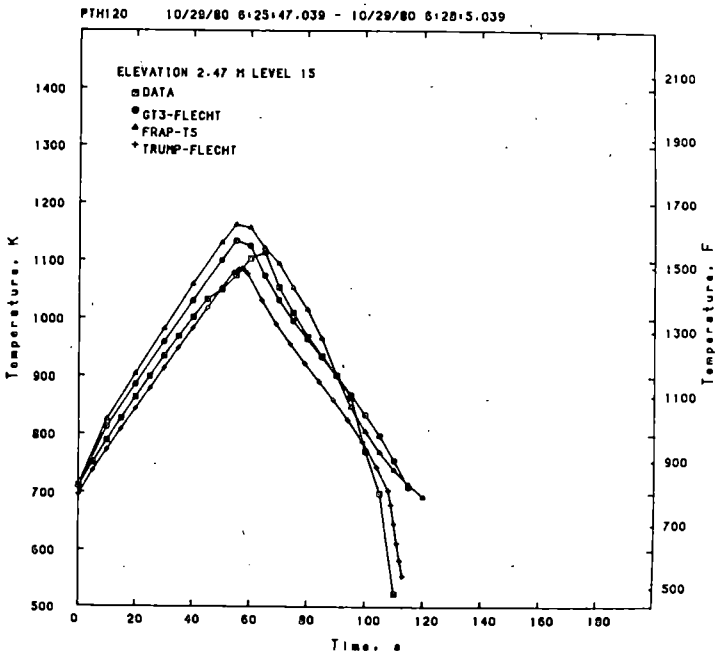

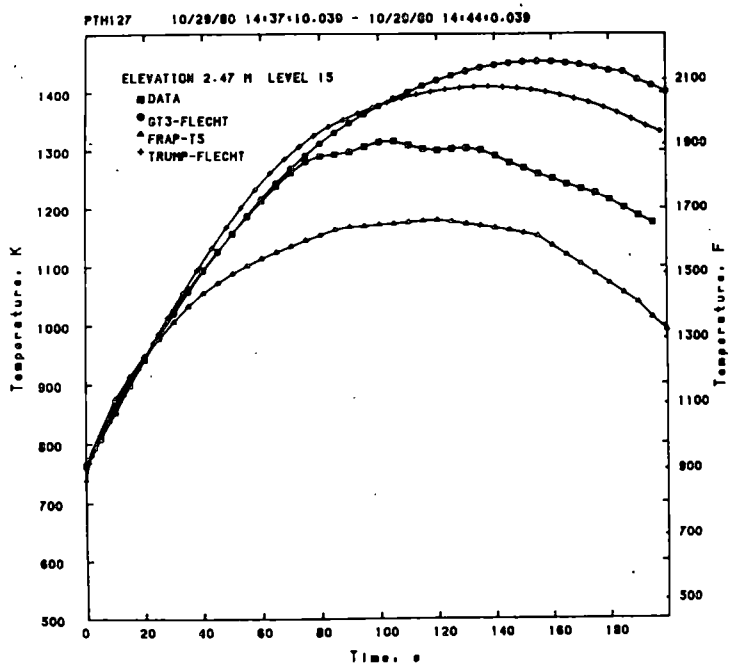

PTH

THERMAL HYDRAULIC TEST

DATA

PTH TEST OBJECTIVES

EVALUATE THE THERMAL PARAMETERS OF REFLOOD RATE AND DELAY TIME ON PEAK TEMPERATURE AND QUENCH

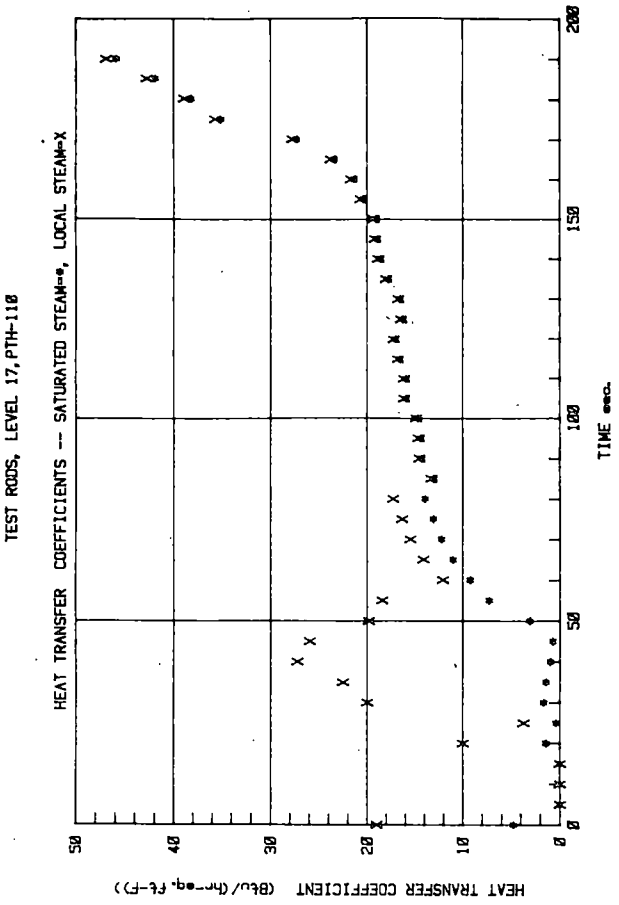

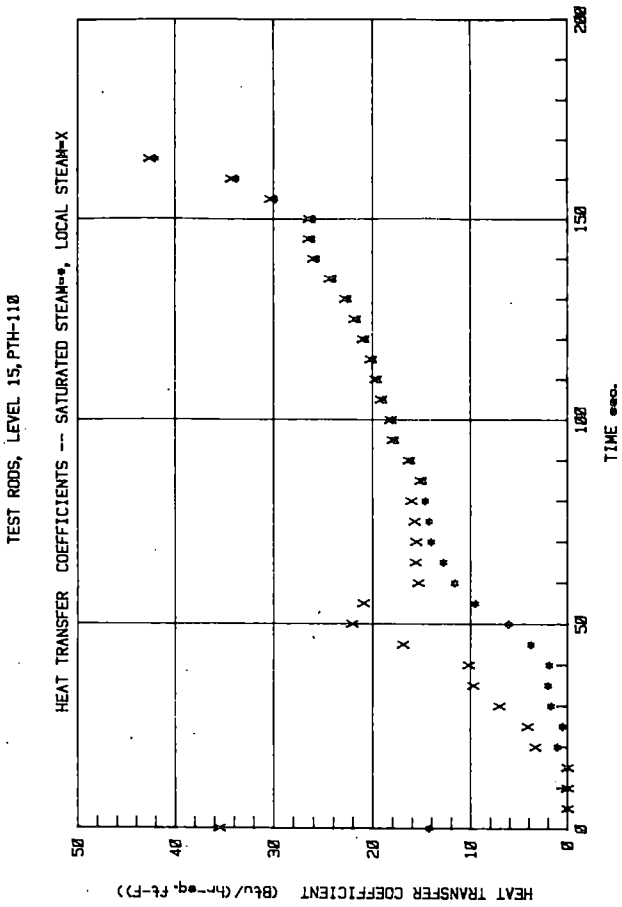

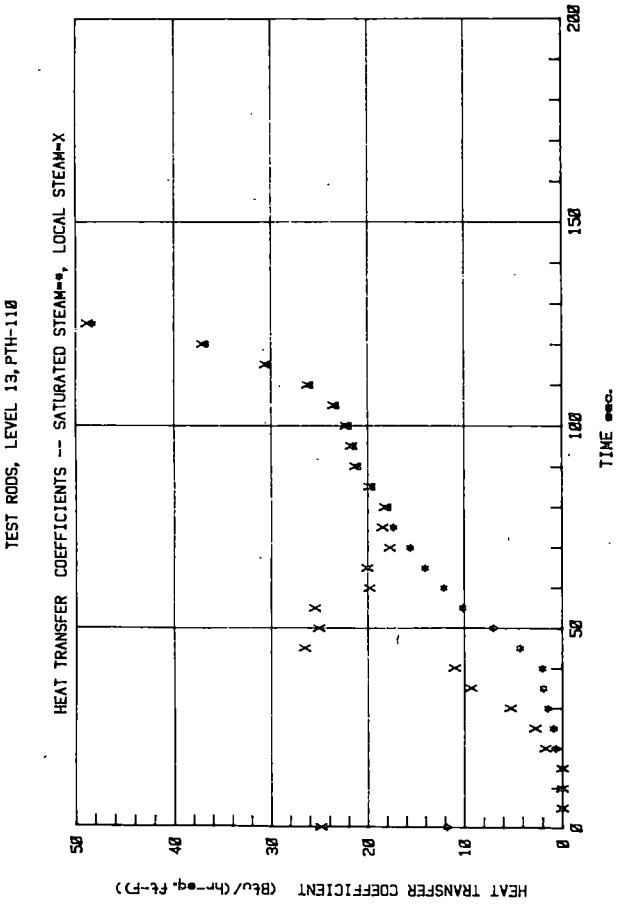

NRU PTH TEST PARAMETERS

TEST NO.	POWER (2) kW/ft (AVERAGE)	REFLOOD RATE (3) in/s		DELAY TIME (3) s		PEAK TEMP DEG F
101	.374	4.9	(3.8)	30	(28)	1403
104 (1)	.363	3.9	(3.9)	38	(37)	1487
105	.337	2.0	(1.9)	10	(7)	1364
106	.362	10.7	(10.5)	20	(20)	1223
107	.365	2.1	(1.9)	20	(20)	1578
108 (1)	.379	1.55	(1.4)	13	(13)	1676
109 (1)	.377	1.55	(1.3)	52	(22)	1881
110 (1)	.375	2.1	(1.9)	30	(30)	1665
111 (1)	.355	1.55	(1.4)	33	(11)	1696
112	.357	4.1	(3.8)	50	(37)	1589
113	.378	7.8	(7.6)	40	(37)	1526
114	.370	7.8	(7.6)	35	(32)	1477
115	.354	9.5	(9.5)	70	(66)	1758
116	.346	4.1	(3.8)	65	(51)	1707
117	.336	4.1	(3.8)	80	(66)	1788
118	.347	3.1	(2.9)	70	(52)	1756
119	.351	3.1	(2.9)	65	(46)	1673
120	.326	6.1	(5.9)	65	(51)	1611
121	.337	4.0	(3.8)	50	(36)	1579
122	.329	7.9	(7.6)	55	(52)	1611
123	.351	3.1	(2.9)	70	(51)	1788
124	.350	6.2	(5.9)	60	(52)	1688
125 (1)	.355	1.65	(1.4)	47	(20)	1802
126 (1)	.310	1.41	(1.2)	31	(3)	1644
127	.402	1.2	(1.0)	35	(3)	1991
128	.363	2.3	(2.0)	80	(50)	1991
129 (1)	.361	1.61	(1.4)	61	(32)	1898
130	.372	.8	(.7)	50	(5)	2040

(1) Values based upon NRU data listings
(2) Average power ratings calculated from NRU PTH test data
(3) Reflood rate and delay times based upon plots of NRU PTH test data. Values iin parentheses are those listing in Table 2 of the report, Prototypic Thermal Hydraulic Experiment in NRU to Simulate Loss of Coolant Accidents

MT – 1

THERMAL HYDRAULIC TEST DATA

MT–1 TEST OBJECTIVE

DUPLICATE PTH–110 AND EVALUATE THE EFFECTS OF DEFORMATION AND RUPTURE ON COOLING AND QUENCH

EVALUATE ELECTRICAL CONNECTOR CONCEPT

EVALUATE LIQUID LEVEL DETECTOR

EVALUATE SINGLE ROD DERM EXAM

TIME OF PRESSURE SWITCH FAILURE MT–1

PS194BC	67 SEC
PS194EC	67
PS192DC	68
PS193EC	67
PS193BC	52
PS192CC	60

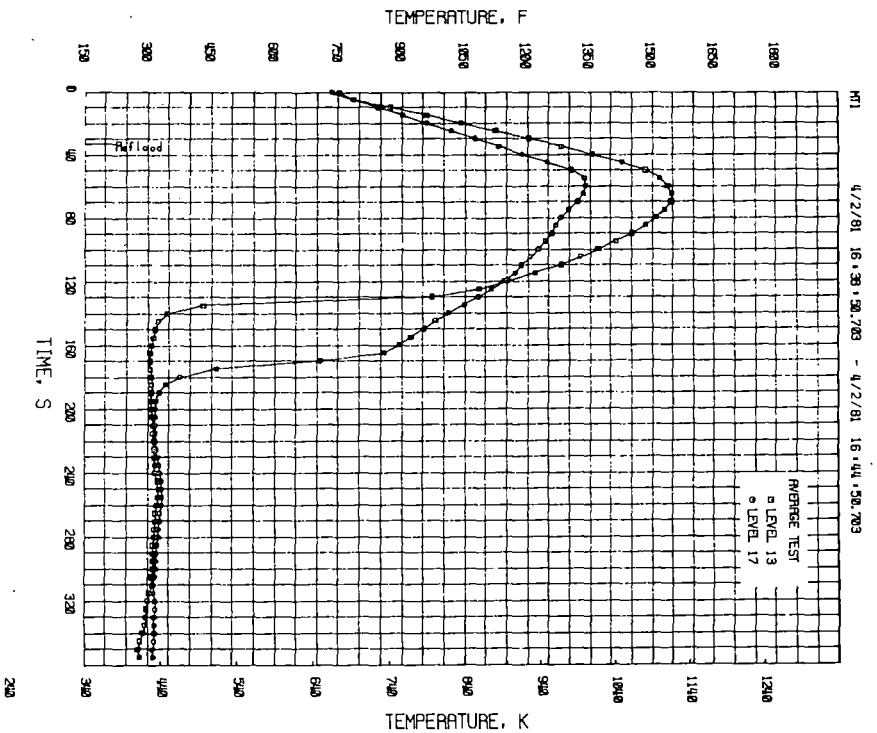

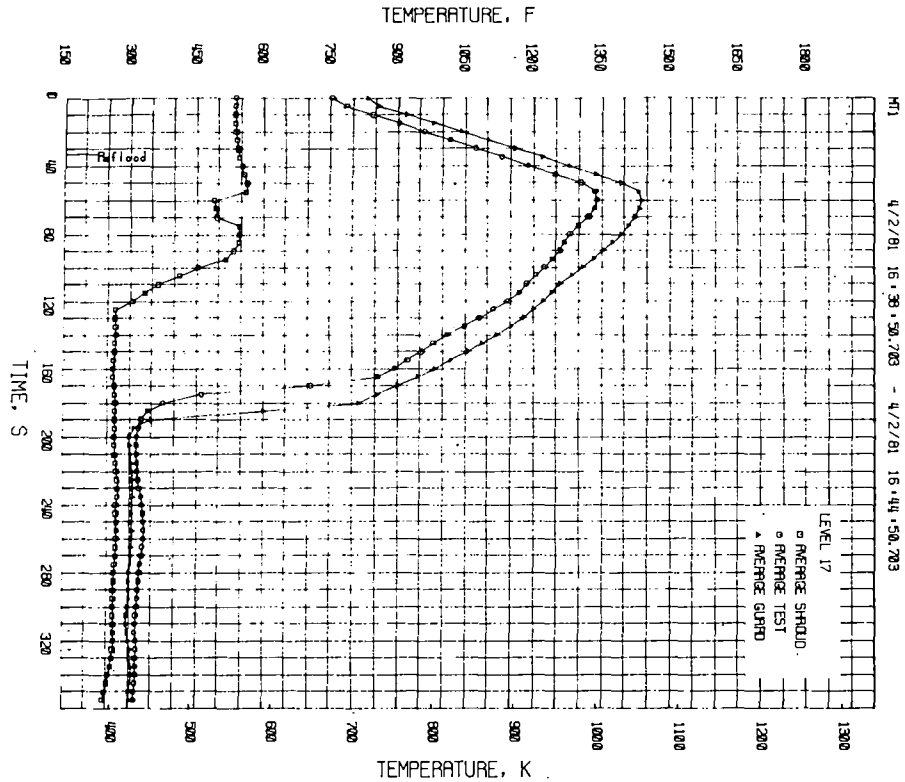
TEMPERATURE, F
Reflood
TIME, S
TEMPERATURE, K
MT1
4/2/81 15:30:50.203 - 4/2/81 16:44:50.203
LEVEL 17
AVERAGE SHROUD
AVERAGE TEST
AVERAGE GUARD

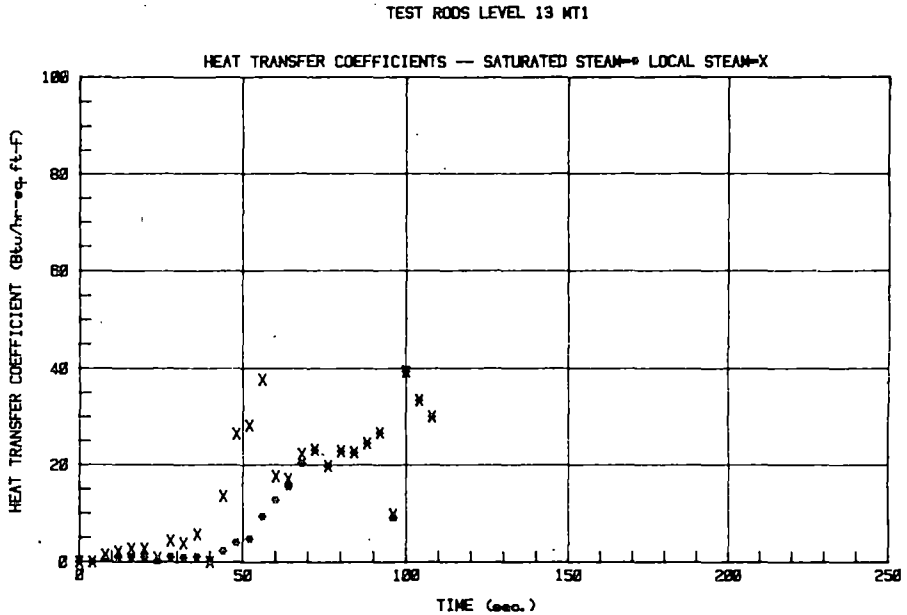
TEST RODS LEVEL 13 MT1
HEAT TRANSFER COEFFICIENTS — SATURATED STEAM-• LOCAL STEAM-X
HEAT TRANSFER COEFFICIENT (Btu/hr--sq. ft-F)
TIME (sec.)

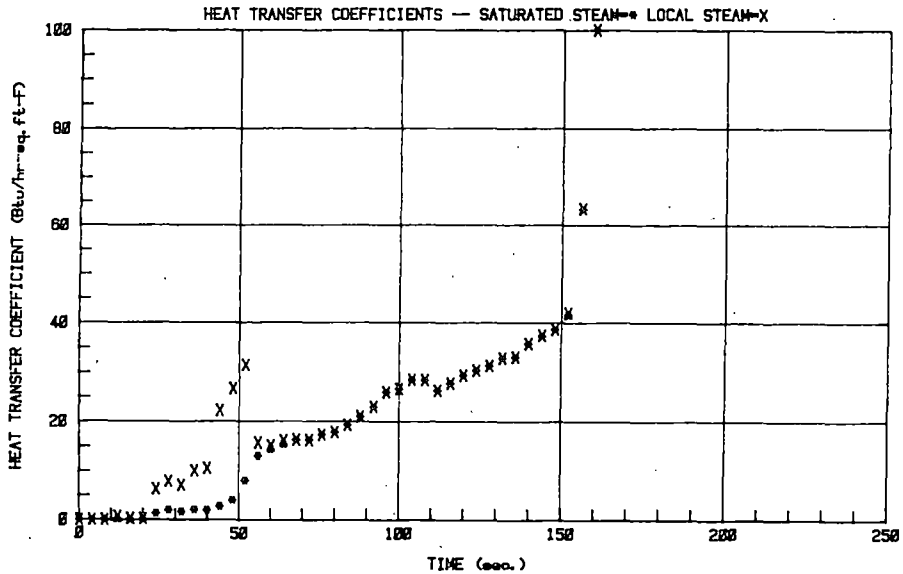
GUARD RODS LEVEL 15 MT1
HEAT TRANSFER COEFFICIENTS — SATURATED STEAM-• LOCAL STEAM-X
HEAT TRANSFER COEFFICIENT (Btu/hr--sq. ft-F)
TIME (sec.)

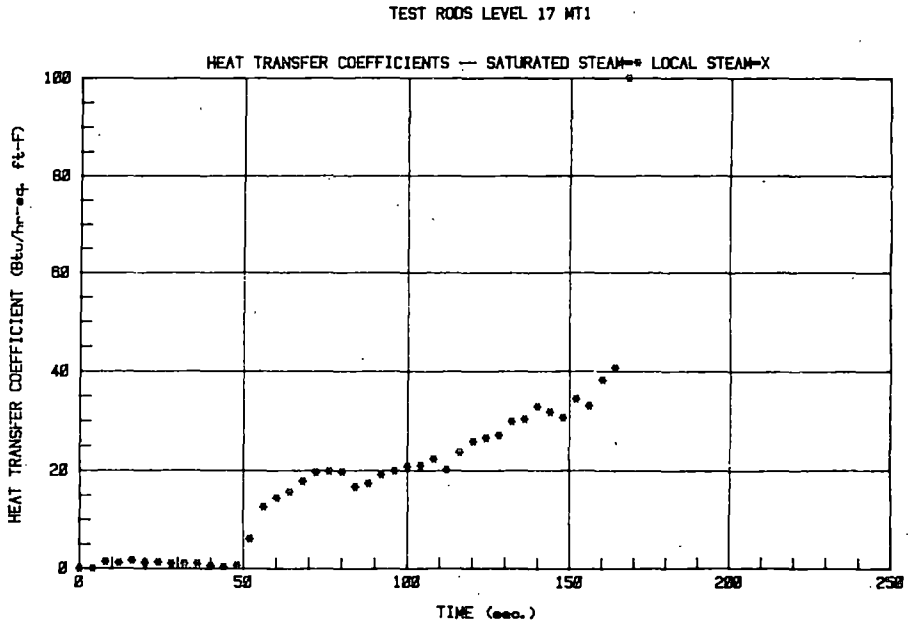
TEST RODS LEVEL 17 MT1
HEAT TRANSFER COEFFICIENTS — SATURATED STEAM-• LOCAL STEAM-X
HEAT TRANSFER COEFFICIENT (Btu/hr--sq. ft-F)
TIME (sec.)

MT – 2

THERMAL HYDRAULIC TEST DATA

MT–2 TEST OBJECTIVES

EVALUATE VARIABLE REFLOOD ON EXTENDED TRANSIENTS

EVALUATE UNDER WATER RECONSTITUTION OF A TEST ASSEMBLY

EVALUATE BUNDLE EXAM

TIME OF PRESSURE SWITCH FAILURE MT–2

PS193DC	65 SEC
PS194BC	65
PS195DC	65
PS194EC	60
PS193EC	65
PS192DC	65
PS193BC	65

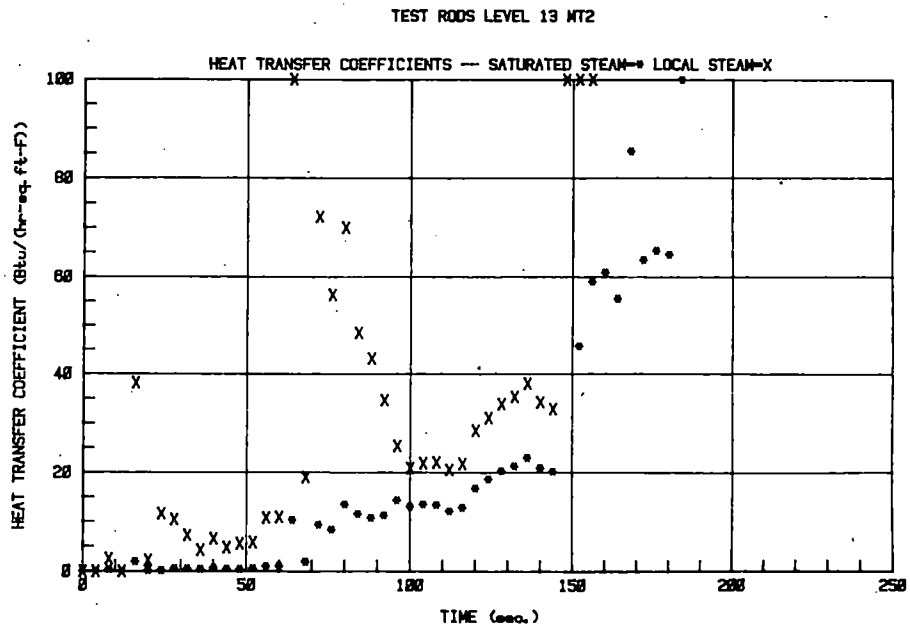

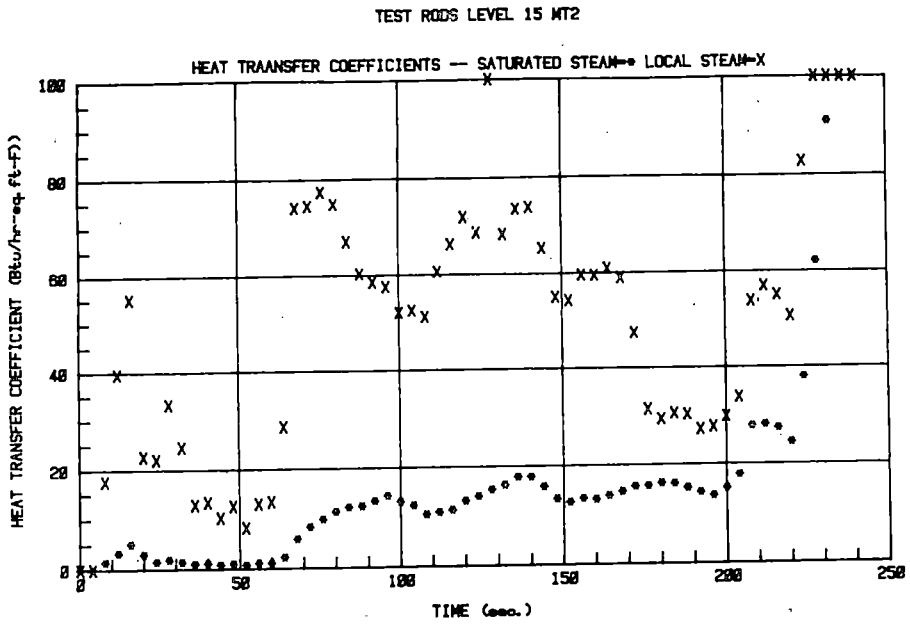
TEST RODS LEVEL 15 MT2
HEAT TRAANSFER COEFFICIENTS — SATURATED STEAM-• LOCAL STEAM-X
HEAT TRANSFER COEFFICIENT (Btu/hr-sq.ft-F))
TIME (sec.)

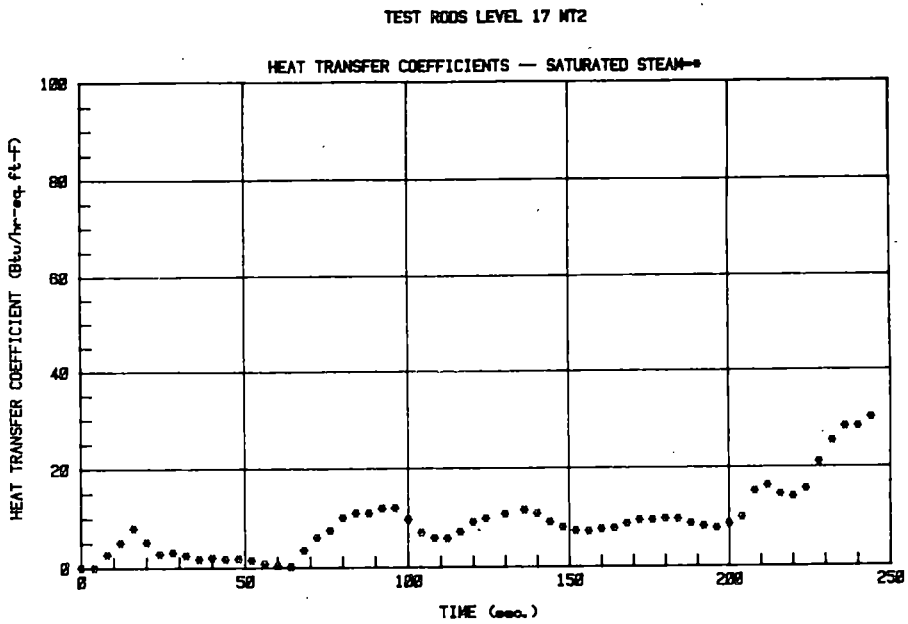
TEST RODS LEVEL 17 MT2
HEAT TRANSFER COEFFICIENTS — SATURATED STEAM-•
HEAT TRANSFER COEFFICIENT (Btu/hr-sq.ft-F)
TIME (sec.)

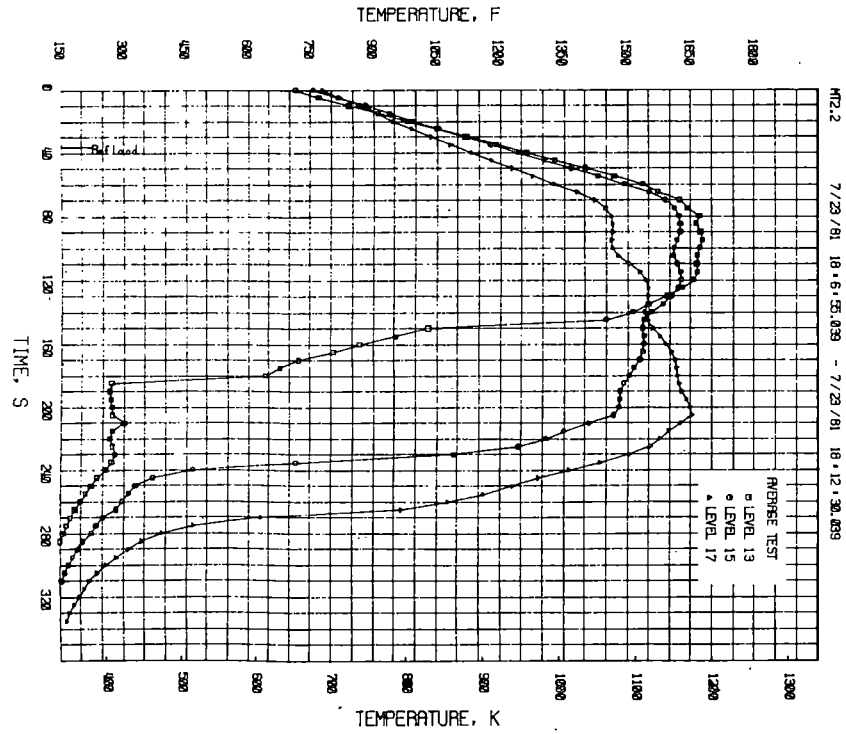
TEMPERATURE, F
TIME, S
TEMPERATURE, K
MT2.2
7/23/81 18:6:55.039 - 7/23/81 18:12:30.039
Refload
AVERAGE TEST
LEVEL 13
LEVEL 15
LEVEL 17

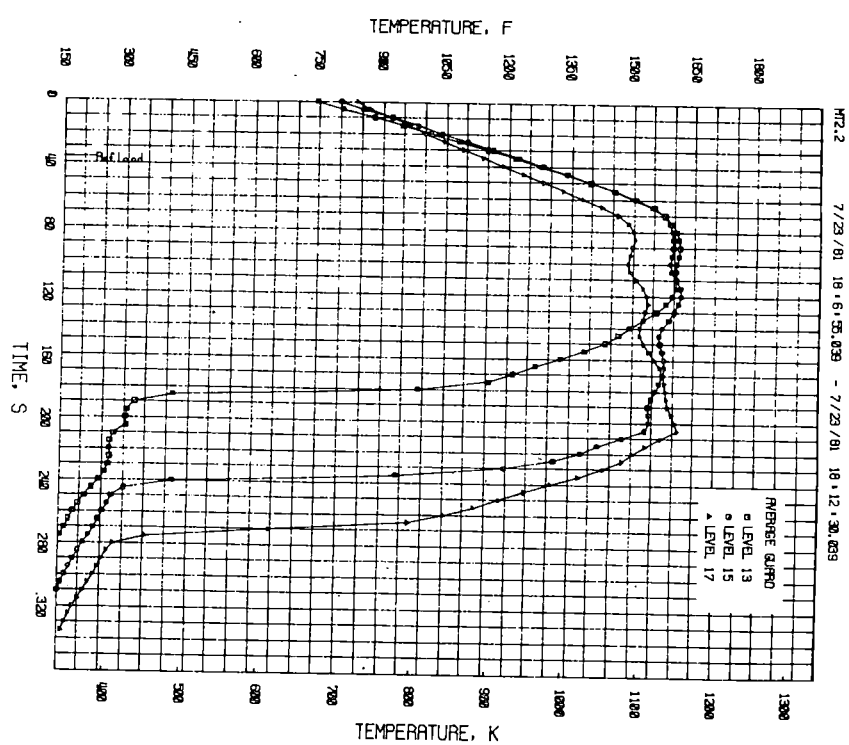
TEMPERATURE, F
TIME, S
TEMPERATURE, K
MT2.2
7/23/81 18:6:55.039 - 7/23/81 18:12:30.039
Refload
AVERAGE GUARD
LEVEL 13
LEVEL 15
LEVEL 17

TH – 2

THERMAL HYDRAULIC FLAT TOP TRANSIENT TEST DATA

TH–2 TEST OBJECTIVES

DETERMINE THERMAL HYDRAULIC PARAMETERS FOR A FLAT TOP TRANSIENT OF 150 SEC+ BETWEEN 750 C TO 820 C

EVALUATE VARIABLE REFLOOD UNDER AUTOMATIC CONTROL

DETERMINE TEST CONDITIONS FOR SUBSEQUENT TESTS

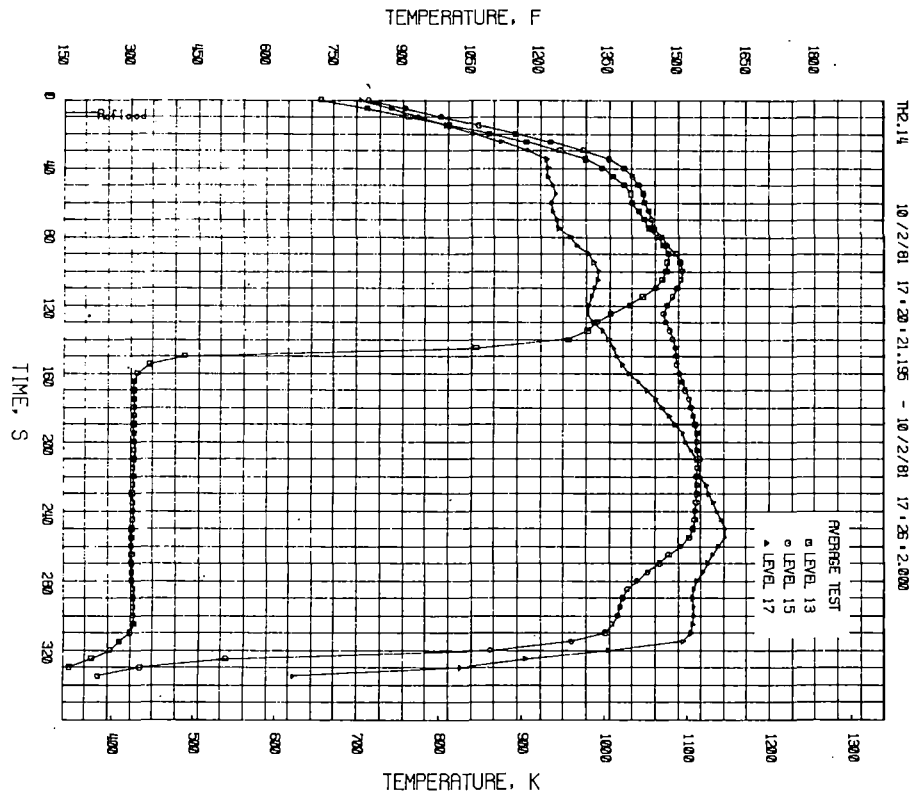

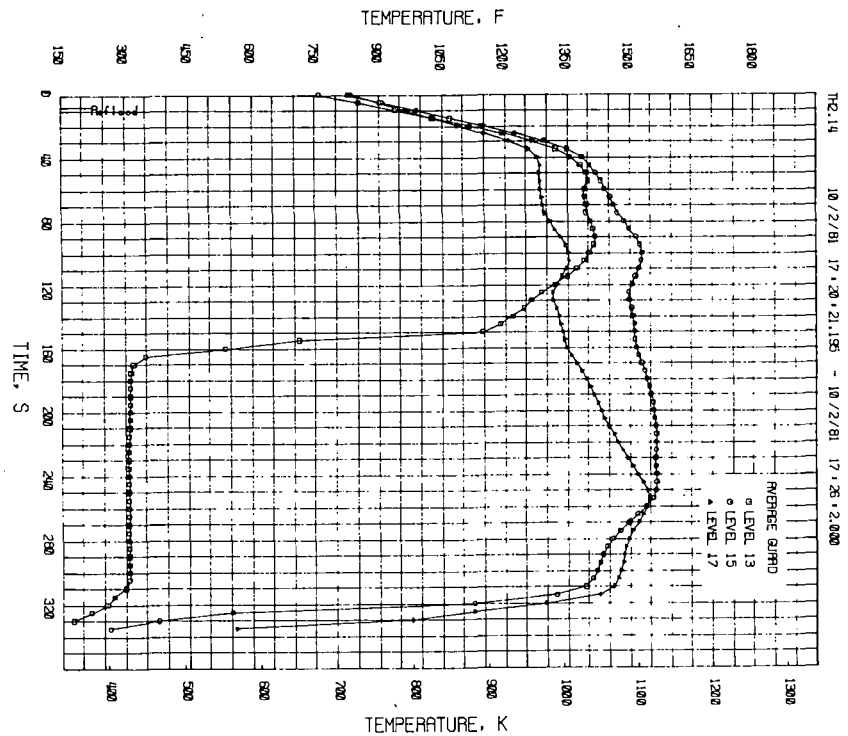

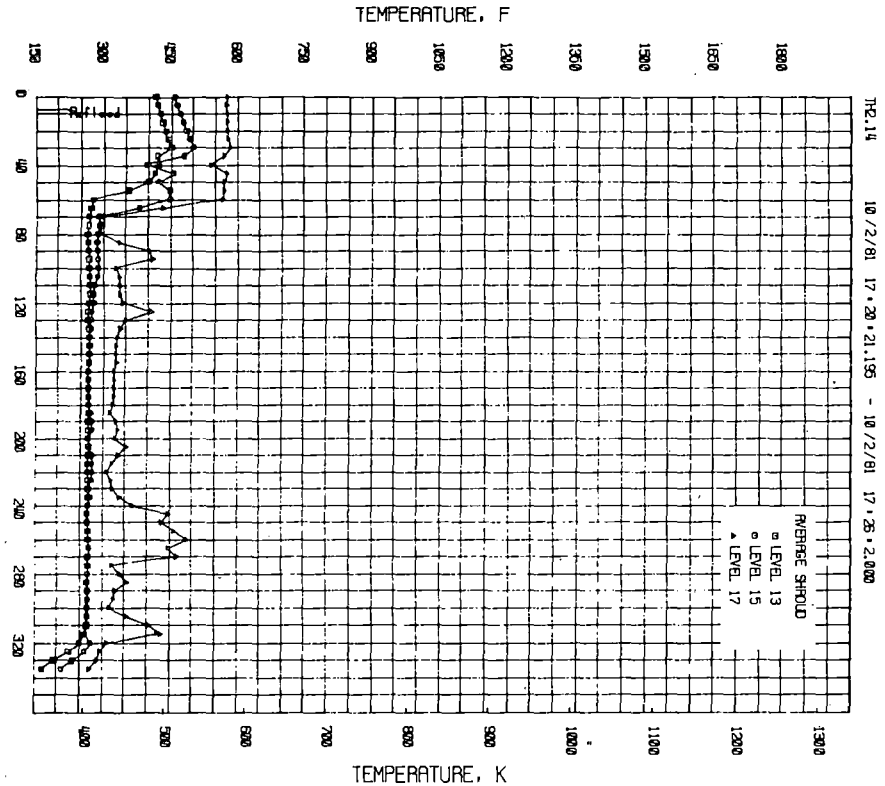

TEST RODS LEVEL 13 TH214

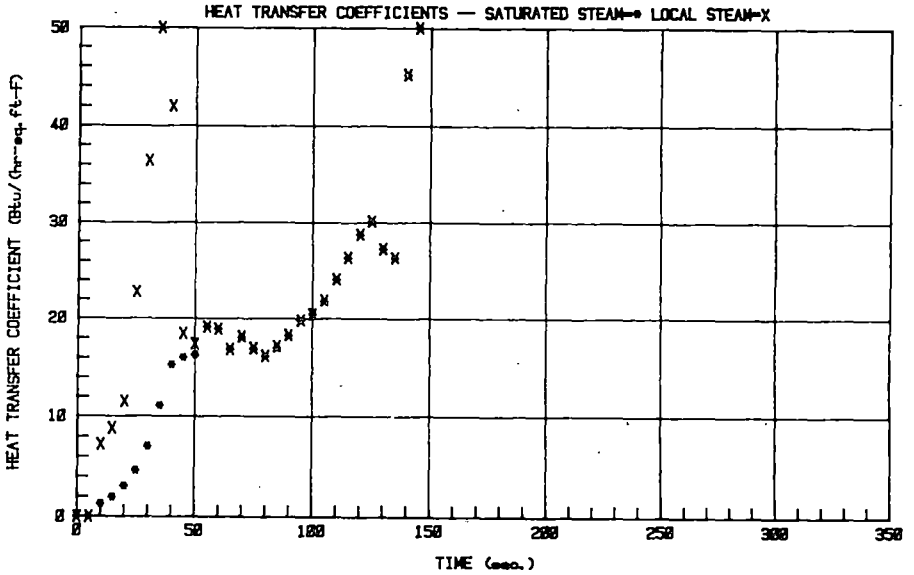

TEST RODS LEVEL 15 TH214

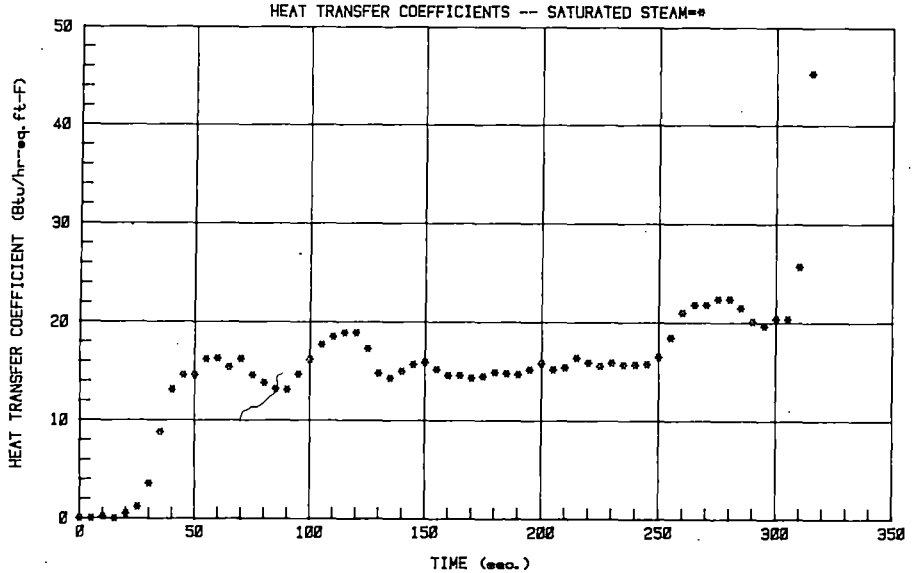

TEST RODS LEVEL 17 TH214

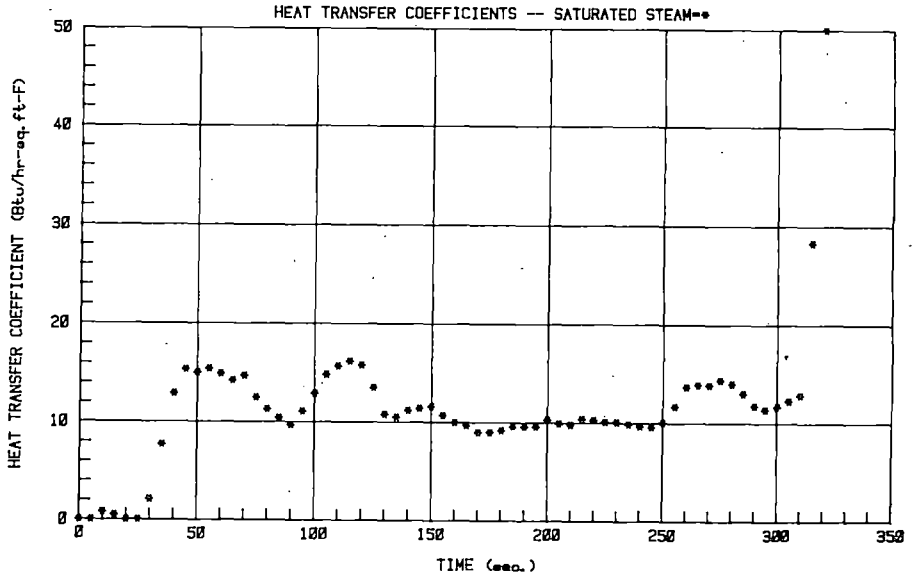

MECHANICAL DEFORMATION RESULTS

PTH

MT–1

MT–2

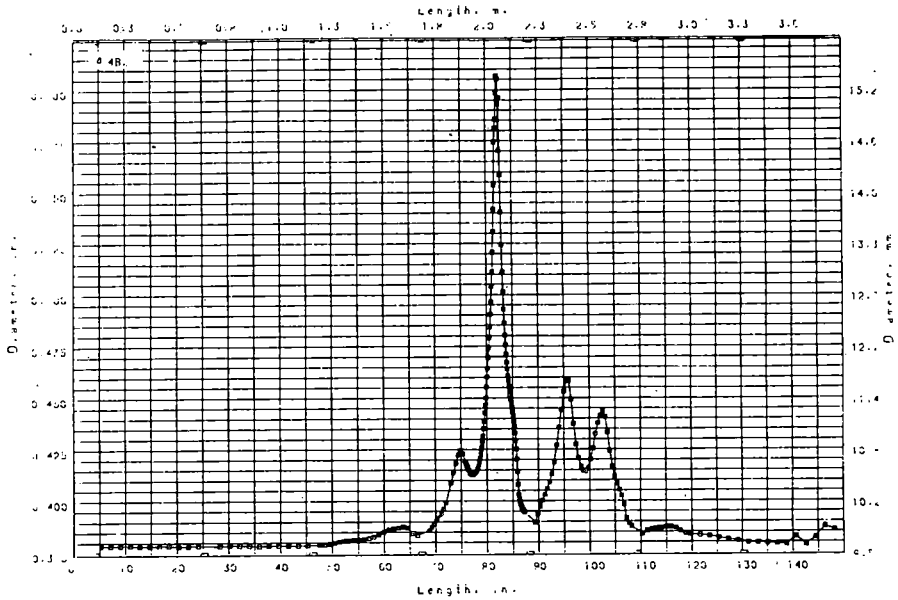

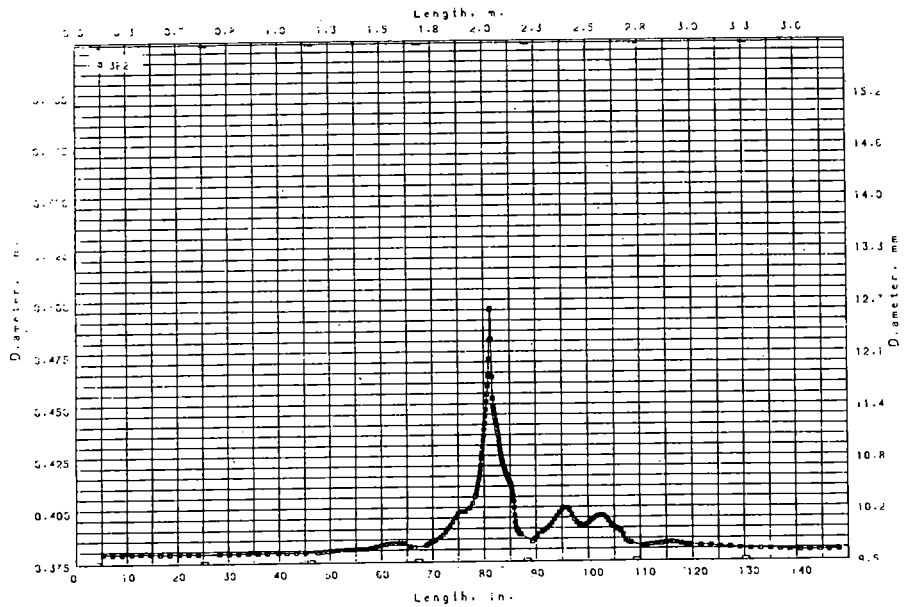

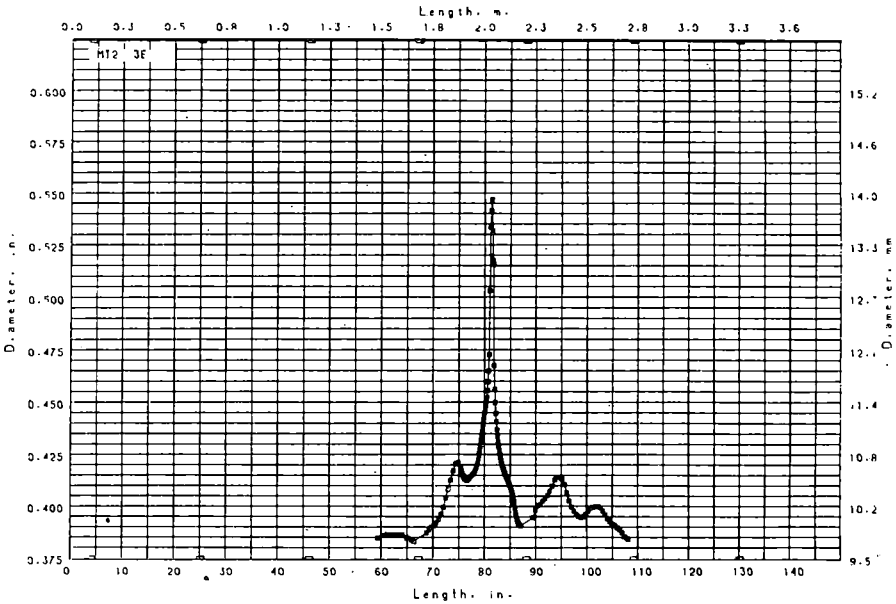

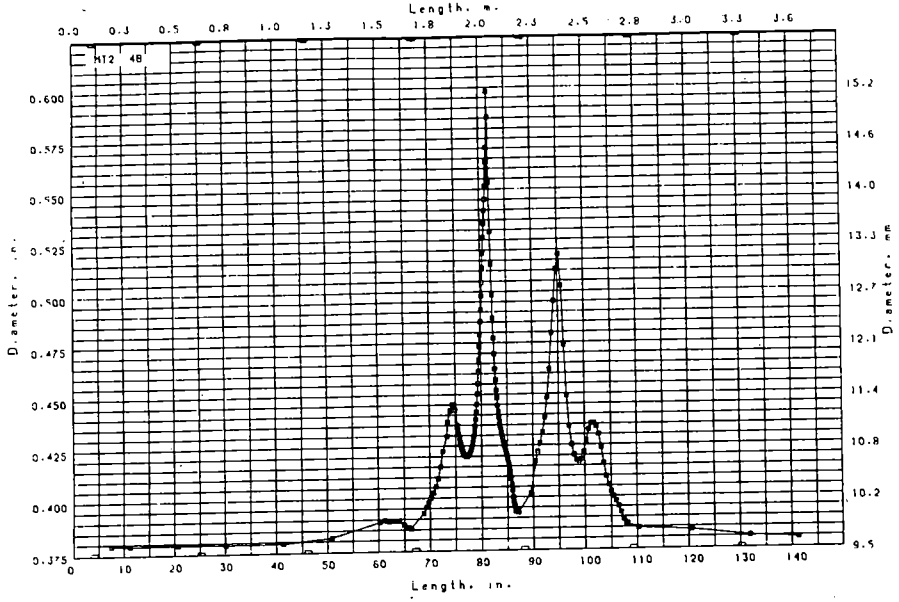

MT1 ROD Z DIMENSION= 82.066

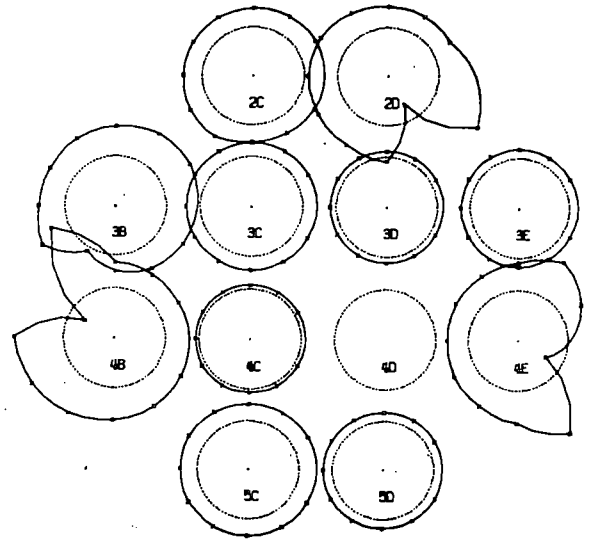

MT2 ROD Z DIMENSION= 82.066

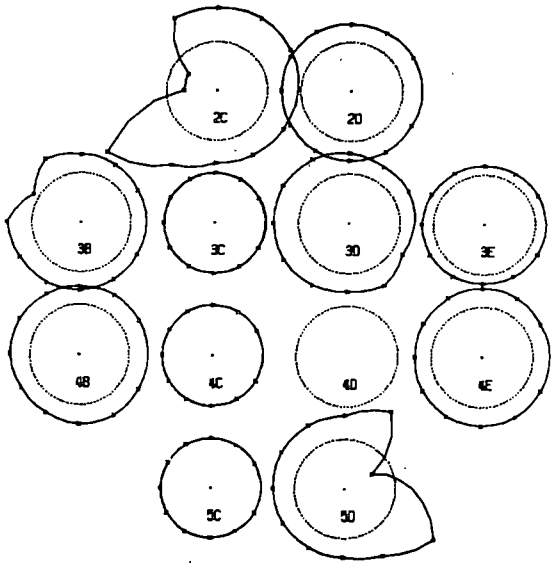

MT2 ROD Z DIMENSION= 80.001

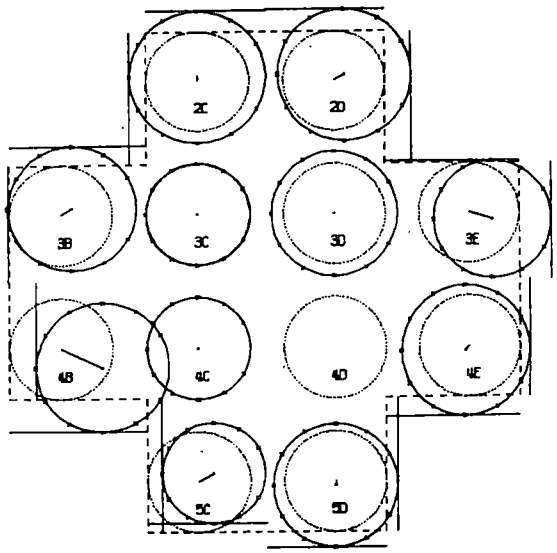

MT2 ROD Z DIMENSION= 82.938

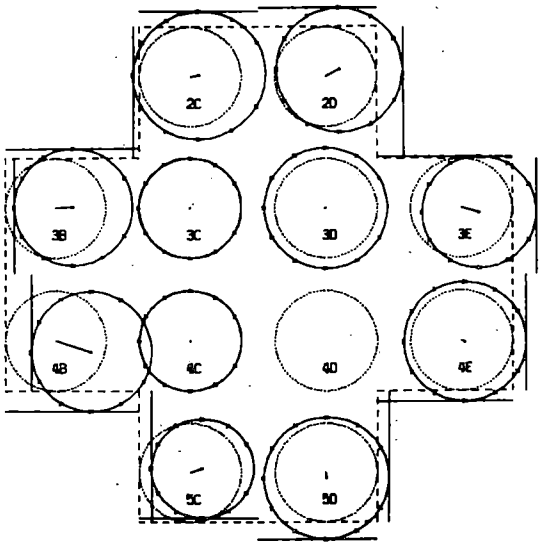

CONCLUSIONS

COMPUTER CODES CAN PREDICT PEAK POWER CONDITIONS

SIMPLE CODES APPEAR TO DO AS WELL AS MORE COMPLEX TRANSIENT CODES

NO CONSISTANT BEHAVIOR IN PREDICTING QUENCH

RUPTURED RODS QUENCH FASTER THAN NON DEFORMED RODS

CONCLUSIONS

FLECHT DATA DOES NOT AGREE FOR UPPER REGIONS ON FUEL ROD OR FOR LOW REFLOOD RATES (OUT OF RANGE)

QUENCH TIMES ARE SHORTER THAN PREDICTED

DERM PROVIDES QUICK ACCURATE PROFILOMETRY

NO SIGNIFICANT EFFECT OF LIFT OFF EXCEPT DURING QUENCH

SIGNIFICANT EFFECT OF LOCAL TEMPERATURES ON ZIRCALOY DEFORMATION

RESULTS OF POWER BURST FACILITY APPENDIX K TESTS

P. E. MacDonald

and

R. K. McCardell

Presented at

The Ninth Water Reactor Safety Research

Information Meeting

October 26 - 30, 1981

Gaithersburg, Maryland

Idaho National Engineering Laboratory

Idaho Falls, Idaho 83415

EG&G Idaho

Idaho Falls, Idaho 83415

RESULTS OF POWER BURST FACILITY APPENDIX K TESTS

P. E. MacDonald

and

R. K. McCardell

EG&G Idaho, Inc.

Introduction

This paper presents an overview of the results of the experimental program conducted in the Power Burst Facility (PBF) from 1975 through 1981 for the United States Nuclear Regulatory Commission (NRC) and discusses the relationship of those results to selected NRC regulations and safety issues. The mission of the NRC fuel behavior research is to help provide the information and phenomenological understanding needed for establishing effective regulatory policies and practices. LWR fuel failure threshold, failure mechanism, loss of coolable geometry, failure propagation, and fuel-coolant interaction data have been obtained from Power-Cooling-Mismatch (PCM) accident, Reactivity Initiated Accident (RIA) and Loss-of Coolant Accident (LOCA) simulations in the PBF. Fuel rod thermal, mechanical deformation, and chemical reaction data have also been obtained and used for computer model development and assessment. In the remainder of this paper we discuss the appropriate NRC regulations and safety issues, key results from the PCM, RIA, and LOCA tests and our evaluation of the NRC regulations.

Power-Cooling-Mismatch Accidents

The NRC requires that U. S. reactors "be designed with appropriate margin to assure that specified acceptable fuel design limits are not exceeded during any condition of normal operation, including the effects of anticipated operational transients."[1] To meet this criterion, a licensee must show that a calculated departure from nucleate boiling ratio[a] (DNBR) exhibits a 95% probability, at the 95% confidence level, that no fuel rod in the core will experience DNB during anticipated steady state or transient operation. This criterion assures that the fuel rod cladding temperatures during normal operation are near the saturation temperature of the water and at safe levels. However, an accidental increase in core power, decrease in coolant flow, or changes in pressure may lead to a loss of continuous liquid coolant-cladding contact (DNB) and a rapid increase in cladding temperatures. Abnormal reactor conditions that can initiate a PCM event include pump failure, loss of electrical power, foreign material in

---

a. The DNBR is the ratio between the linear power at which DNB is expected to occur and the maximum allowable power.

the coolant, cladding swelling, enrichment error, xenon instability or mispositioned control rods. The primary objective of the PCM tests was to determine exactly what would happen and how fast a LWR core would degrade during such events. Specific questions included: (a) what is the margin between DNB occurrence and fuel rod failure? (b) can a coolable geometry be maintained following a severe PCM? (c) what is the propensity for film boiling and fuel failure propagation? and (d) will energetic molten fuel-coolant interactions occur during a severe PCM? The PCM test program was designed as a parametric evaluation of fuel rod response under power cooling imbalance conditions, with test rod peak power, cladding surface temperature, and time in film boiling as the variable parameters. Forty unirradited fuel rods, nine previously irradiated fuel rods, and seven rods with previously irradiated cladding and fresh fuel were tested.

The results from the PCM test program demonstrate that light water reactor fuel rods can depart from nucleate boiling and operate in film boiling for significant times and withstand severe damage prior to failure. Rod-to-rod departure from nucleate boiling and fuel rod failure propagation did not occur. Energetic molten fuel-coolant interactions did not occur and loss of coolable geometry during power-cooling-mismatch type accidents is not expected.

We conclude that the present NRC regulations are quite conservative and it should be possible to develop mechanistic fuel damage criteria which would allow for some increase in core powers or increased operational flexibility.

Reactivity Initiated Accidents

To minimize the extent of damage from postulated inadvertent reactivity initiated accidents in commercial light water reactors, the USNRC has imposed design requirements on reactivity control systems to limit "the potential amount and rate of reactivity increase to assure that the effects of postulated reactivity accidents can neither (a) result in damage to the reactor coolant pressure boundary greater than limited local yielding nor (b) sufficiently disturb the core, its support structure, or other reactor pressure vessel internals to impair significantly the capability to cool the core."[2] The USNRC also requires that the number of fuel rods which will experience cladding failure during various RIAs be estimated and a conservative source term, subsequent transport of activity, and the resulting doses to the public be calculated. The guidelines regarding core cooling and the reactor coolant pressure boundary stresses are assumed to be met if compliance with a 280 cal/g peak-fuel enthalpy limitation is satisfactorily demonstrated. Offsite dose consequences must be calculated assuming that any PWR fuel rod which departs from nucleate boiling fails[2] and any BWR rod subjected to a radial average peak fuel enthalpy of 170 cal/g UO_2 or above fails.[3]

Seven RIA tests have been conducted in the PBF with 6 fresh and 15 previously irradiated test rods to evaluate the 280 cal/g criterion and also the failure threshold criteria (departure from nucleate boiling in a PWR and 170 cal/g radial average peak fuel enthalpy in a BWR). These tests have addressed the following key safety issues: (a) will there be a loss of coolable core geometry when LWR fuel is subjected to a radial average

peak fuel enthaply of 280 cal/g? (b) will energetic molten fuel-coolant interactions (vapor explosions) occur during a severe RIA and result in the production of a significant pressure pulse? and, (c) what is the mechanism and threshold enthalpy for failure of light water reactor fuel during an RIA? The seven PBF tests were all conducted with coolant conditions representative of a boiling water reactor at hot startup.

The experimental results from the RIA test program clearly indicate that energetic molten fuel-coolant interactions will not occur if the radial average peak fuel enthalpy is limited to 280 cal/g. However, the results regarding coolable core geometry and threshold enthalpy for failure are not entirely certain. While all experimental fuel rod debris appears to have been coolable, rod-like geometry was not maintained when single fuel rods were tested at 250 to 285 cal/g, but rod-like geometry was maintained in a nine-rod bundle with the four corner rods tested at 280 cal/g and the remaining rods tested at 235 cal/g or larger. Based on these results the licensing criterion of 280 cal/g UO_2 peak fuel enthalpy should probably be reevaluated. If a new criterion is to be established additional bundle tests using high burnup fuel rods would be required.

The fuel failure threshold also appears to be lower than previously thought. A fuel rod irradiated to 5000 MWd/t failed due to pellet cladding mechanical interaction before the rod departed from nucleate boiling at an energy deposition of 140 cal/g. Other rods tested at 180 to 235 cal/g did not fail. Thus, the rod failure criteria of 170 cal/g UO_2 for a BWR and departure from nucleate boiling for a PWR may be inappropriate. However, recent best-estimate analysis incorporating the effects of void formation and prompt moderator feedback indicate that a BWR-5 rod-drop accident will result in a radial average peak fuel enthalpy of only 110 cal/g UO_2.[4] Therefore, we conclude that an RIA in a light water reactor would pose no real safety concern even though the present regulations are questionable.

Loss-of-Coolant Accidents

The zircaloy cladding on light water reactor fuel rods will plastically deform and rupture during a severe LOCA when the cladding temperatures reach values somewhat above 920 K (a value well below the USNRC licensing criterion of 1477 K). This deformation or "ballooning" may result in blocked flow channels and a loss of coolable geometry. The primary objective of the LOCA tests in the PBF was to determine the magnitude and extent of cladding ballooning during a simulated double-ended cold leg break LOCA. These results are necessary to answer the two key LOCA safety issues: (a) will ballooning during a severe double-ended cold leg break LOCA lead to co-planar blockage and subsequent loss-of-coolable geometry? and (b) which of the out-of-pile ballooning data sets being used in various licensing models is most representative of nuclear fuel rod behavior?

Cladding temperature and pressure differential are the primary parameters that determine cladding circumferential strain during ballooning. The PBF LOCA test program was designed to investigate these two parameters using both fresh and irradiated test fuel rods. Peak cladding temperatures of 1070, 1190, and 1350 K were sought in the tests by varying the rod power history and time of critical heat flux (CHF). These

temperatures correspond to the points of (a) maximum ductility of alpha-phase zircaloy cladding, (b) minimum ductility in the alpha-plus-beta-phase transition, and (c) maximum ductility of beta-phase zircaloy cladding. The effects of prior irradiation and rod internal pressure on cladding ballooning and rupture were also evaluated during the four, four-rod LOCA tests.

Well controlled single rod out-of-pile tests with unheated shrouds have indicated two temperature maximums in the failure strain, approximately 28% total circumferential elongation (TCE) in the alpha phase and about 75% TCE in tne beta phase, with a minimum strain of about 17% TCE in the alpha-plus-beta-phase transition region. The PBF fresh rod results are similar to the out-of-pile results. However, the alpha phase cladding strain of the previously irradiated test rods was more uniformly distributed around the cladding circumference and larger than for similiar unirradiated rods. The deformation of the irradiated rods also extended over a longer axial length. Therefore, the potential for co-planar blockage of coolant subchannels in a bundle of previously irradiated fuel rods is greater than in a bundle of fresh rods. The increased cladding circumferential strain over extended axial lengths of the previously irradiated fuel rods was probably caused by cladding collapse and fuel fragmentation and relocation creating a more circumferentially uniform fuel/cladding gap conductance. The change in gap conductance would decrease local cladding temperature differences, which have been shown in out-of-pile single-rod tests to permit increased cladding strain.

The out-of-pile zircaloy ballooning and burst tests have also shown that rod-to-rod thermal interactions within large bundles of fuel rods reduce the local temperature differences on individual rods such that the rod average TCE within a bundle may be quite large and heated shrouds tend to create a bundle-like thermal environment and induce larger TCEs. In addition, grid spacers within a bundle will tend to concentrate the ballooning in a plane just upstream of the grid, thereby increasing the probability of co-planar coolant subchannel blockages.

Because (a) the PBF unirradiated single rod, unheated shroud data is in good agreement with out-of-pile data for single rods tested in unheated shrouds; and (b) the burst strains from the out-of-pile bundle tests are considerably greater than the burst strains from single rods tested in unheated shrouds; and (c) the burst strains of the previously irradiated PBF rods were greater (at alpha phase temperatures) than the burst strains of the fresh rods, we recommended that large-bundle (at least 64 rods) in-pile tests be performed with previously irradiated rods to properly determine the possibility of co-planar blockage.

REFERENCES

1. Code of Federal Regulations, Title 10, Energy, January 1979.

2. Assumptions Used for Evaluating a Control Rod Ejection Accident for Pressurized Water Reactors, NRC Regulatory Guide 1.77, May 1974.

3. "Fuel System Design, Section 4.2," in Standard Review Plan for the Review of Safety Analysis Reports for Nuclear Power Plants, NUREG-75/087, Rev. 1 (available from NTIS, UB/B/201-004).

4. H. S. Cheng and D. J. Diamond, Thermal-Hydraulic Effects on Center Rod Drop Accidents in a Boiling-Water Reactor, BNL-NUREG-27544, July 1980.

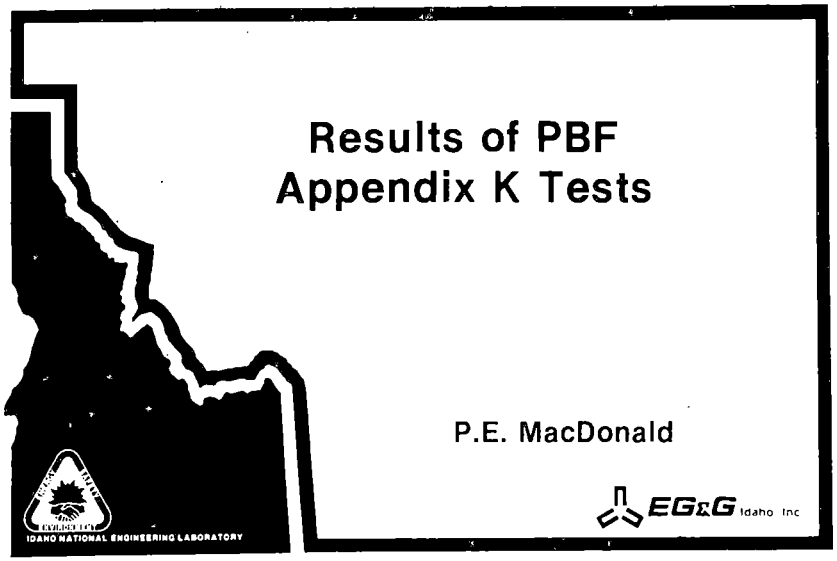

POWER-COOLING-MISMATCH SAFETY ISSUES

- WHAT IS THE MARGIN BETWEEN DEPARTURE FROM NUCLEATE BOILING AND FUEL ROD FAILURE
- CAN A COOLABLE GEOMETRY BE MAINTAINED
- WHAT IS THE PROPENSITY FOR DEPARTURE FROM NUCLEATE BOILING AND FUEL FAILURE PROPAGATION
- WILL ENERGETIC MOLTEN FUEL-COOLANT INTERACTIONS OCCUR

NRC POWER-COOLING-MISMATCH LICENSING CRITERIA

- THE CALCULATED DNBR MUST EXHIBIT A 95% PROBABILITY, AT THE 95% CONFIDENCE LEVEL, THAT NO CORE FUEL ROD WILL DEPART FROM NUCLEATE BOILING.
- CRITERION IMPLIES THAT FUEL RODS OPERATED AT DNBR'S LESS THAN 1.13 TO 1.32 ARE IN FILM BOILING AND FAIL.
- MECHANISTIC FUEL DAMAGE LIMITS ARE NOT PRESENTLY ACCEPTED.

RESULTS OF POWER-COOLING-MISMATCH TEST PROGRAM

- LWR FUEL RODS CAN DEPART FROM NUCLEATE BOILING FOR SIGNIFICANT TIMES AND WITHSTAND SEVERE DAMAGE PRIOR TO ROD FAILURE.
- CLADDING DEFORMATION OCCURS ABOVE 920 K BUT CLADDING RETAINS SUFFICIENT DUCTILITY TO ACCOMMODATE COLLAPSE STRAINS AND PRECLUDE IMMEDIATE FAILURE.
- THE PRIMARY FUEL ROD FAILURE MECHANISM IS OXYGEN EMBRITTLEMENT OF THE CLADDING FROM H_2O- AND UO_2-ZIRCALOY REACTIONS.

RESULTS OF POWER-COOLING-MISMATCH TEST PROGRAM (cont'd)

- ZIRCALOY OXYGEN EMBRITTLEMENT IS PREDICTABLE USING TEMPERATURE-TIME CORRELATIONS DEVELOPED FROM OUT-OF-PILE DATA.
- ENERGETIC MOLTEN FUEL-COOLANT INTERACTIONS DO NOT OCCUR.
- MOLTEN FUEL-CLADDING CONTACT DOES NOT RESULT IN CLADDING MELTING.

KEY REACTIVITY INITIATED ACCIDENT SAFETY ISSUES

- FUEL FAILURE THRESHOLD
- LOSS OF COOLABLE CORE GEOMETRY
- OVERSTRESS OF PRESSURE VESSEL

PEM-7

RESULTS OF POWER-COOLING-MISMATCH TEST PROGRAM (cont'd)

- FUEL GRAIN SEPARATION (POWDERING OR DESINTERING) OCCURS WHEN THE FUEL IS QUENCHED FROM TEMPERATURES ABOVE 1900 K.
- ROD-TO-ROD DNB AND FUEL ROD FAILURE PROPAGATION IS NOT EXPECTED.
- LOSS OF COOLABLE GEOMETRY IS NOT EXPECTED.

APPLICABLE RIA LICENSING CRITERIA

- OFFSITE DOSE CONSEQUENCES WITHIN 10 CFR 100
  - 170 CAL/G - BWRs
  - DEPARTURE FROM NUCLEATE BOILING - PWRs
- RADIAL AVERAGE PEAK FUEL ENTHALPIES BELOW 280 CAL/G
- THESE VALUES WERE BASED ON RESULTS OF EARLY INEL TESTS WITH UNIRRADIATED FUEL RODS

INEL-S-40 017

PROGRESSION OF FUEL ROD DAMAGE EVENTS

- PELLET-CLADDING INTERACTION
- CLADDING PLASTIC DEFORMATION
- FUEL SWELLING AND THERMAL FAILURE
- FAILURE PROPAGATION
- OXIDATION AND EMBRITTLEMENT
- ROD FRAGMENTATION

R810032-4

RIA 1-4 - Rod 1 at 42 cm

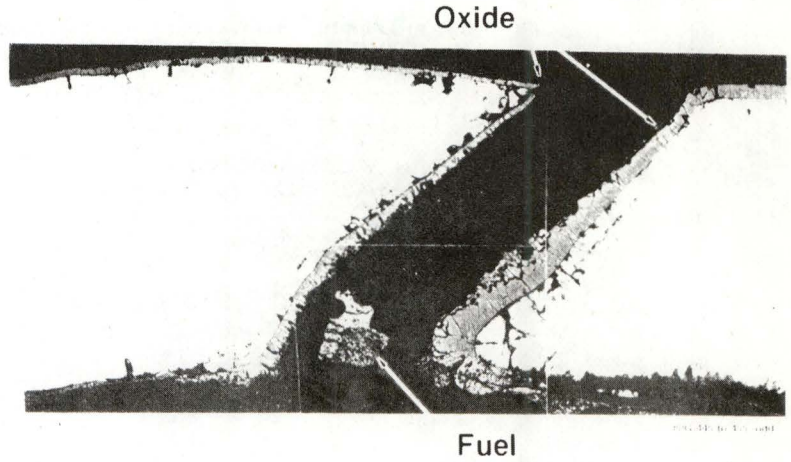

RIA ST-1 Cladding at 0.35-m Elevation

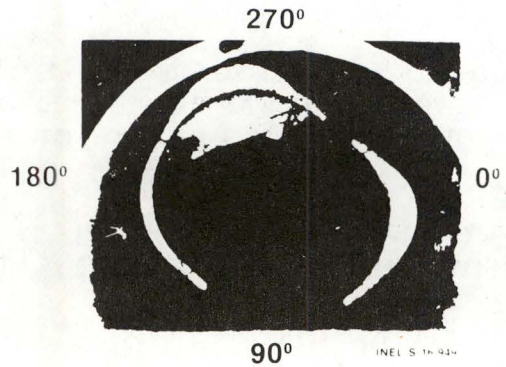

Fuel Swelling in Test RIA 1-4, Rod 1, 42 cm from Bottom

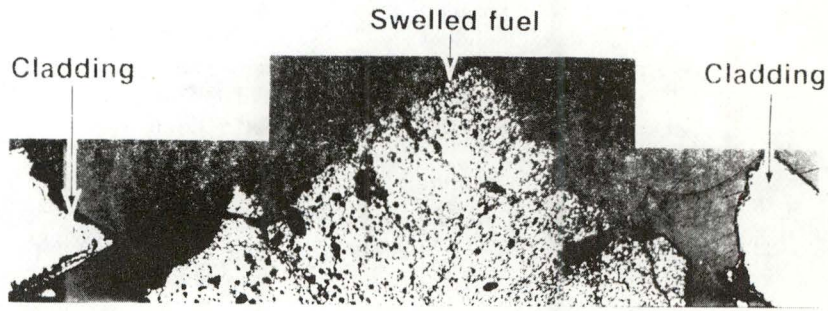

Test RIA 1-1 Rod 801-1

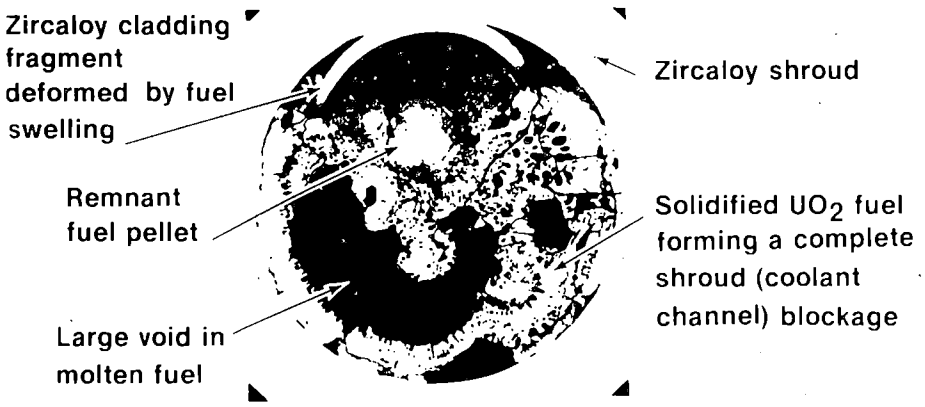

INEL S 18 207

RIA ST-1 (250 cal/g) Fuel Shattering at 0.35-m Elevation, 240° Orientation

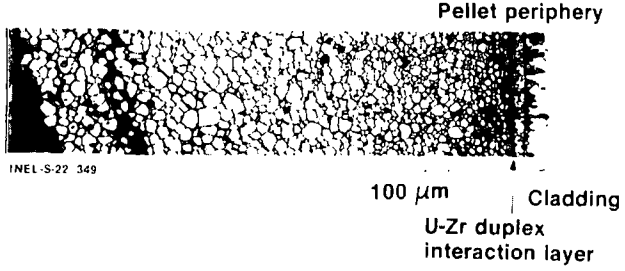

Peak Flux Region of RIA ST-2 (260 cal/g)

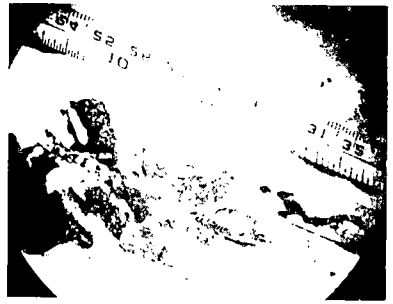

INEL S 14 0-7

RESULTS FROM REACTIVITY INITIATED ACCIDENT TEST PROGRAM

- MODE AND CONSEQUENCES OF ROD FAILURE ARE SIGNIFICANTLY AFFECTED BY PRIOR IRRADIATION
  - IRRADIATED RODS FAIL DUE TO PELLET-CLADDING INTERACTION AT LOW ENERGY DEPOSITIONS
  - EXPANSION OF GASEOUS AND VOLATILE FISSION PRODUCTS INDUCE EXTENSIVE SWELLING OF MOLTEN IRRADIATED FUEL

CONCLUSIONS REGARDING RIA SAFETY ISSUES

- EXPECTED ENERGY DEPOSITIONS IN LWRs ARE WELL BELOW NRC CRITERION. SO WE DO NOT EXPECT LOSS-OF-COOLABLE GEOMETRY OR OVERSTRESS OF PRESSURE VESSEL DURING AN RIA.
- FUEL FAILURE THRESHOLD MAY BE LESS THAN 140 cal/g PEAK FUEL ENTHALPY.

INEL-S-40 019

KEY LOSS-OF-COOLANT ACCIDENT SAFETY ISSUES

- WILL CLADDING BALLOONING DURING A LOSS-OF-COOLANT ACCIDENT LEAD TO CO-PLANAR BLOCKAGE AND SUBSEQUENT LOSS-OF-COOLABLE GEOMETRY?
- IS OUT-OF-PILE BALLOONING DATA REPRESENTATIVE OF NUCLEAR FUEL ROD BEHAVIOR?

CONCLUSIONS REGARDING RIA LICENSING CRITERIA

- ROD FAILURE CRITERIA OF 170 cal/g UO_2 (BWR) AND FILM BOILING (PWR) ARE INAPPROPRIATE.
- LICENSING CRITERION OF 280 cal/g UO_2 PEAK FUEL ENTHALPY SHOULD BE REEVALUATED.
- ADDITIONAL BUNDLE TESTS USING HIGH BURNUP TEST RODS WOULD BE REQUIRED TO ESTABLISH NEW CRITERION.

R810032-7

PBF LOCA PROGRAM CLADDING TEMP HISTORIES

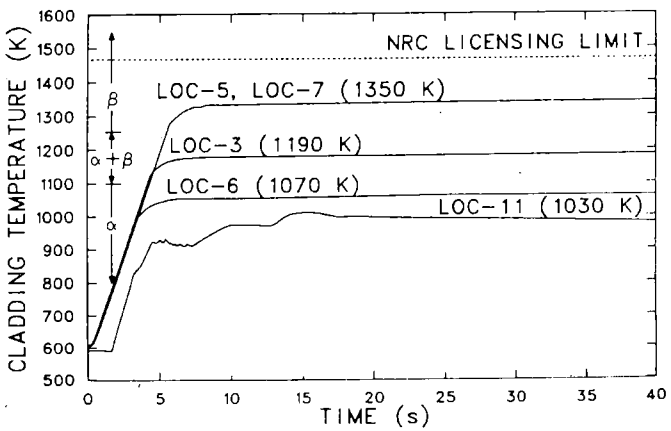

Balloon and Burst Cross Sections of Rods from Test LOC-3

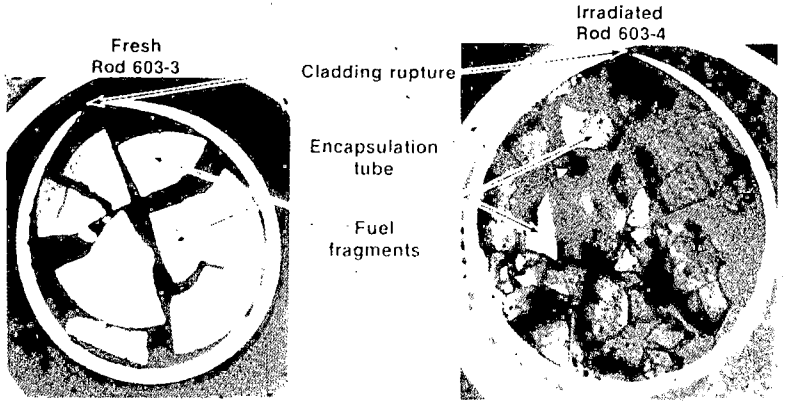

Balloon and Burst Cross Sections of Rods from Test LOC-5

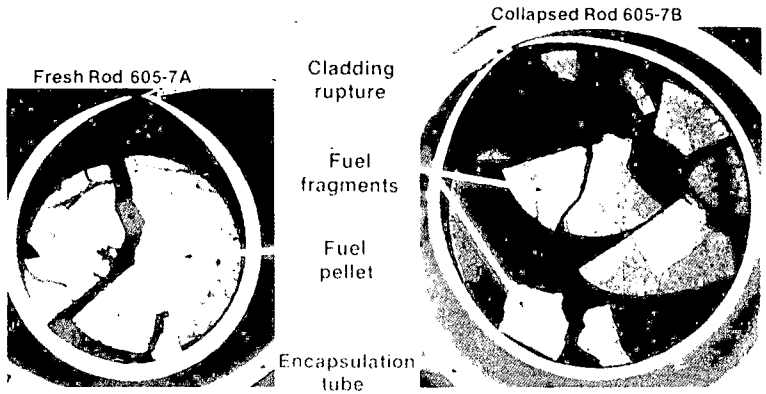

Balloon and Burst Cross Sections of Rods from Test LOC-6

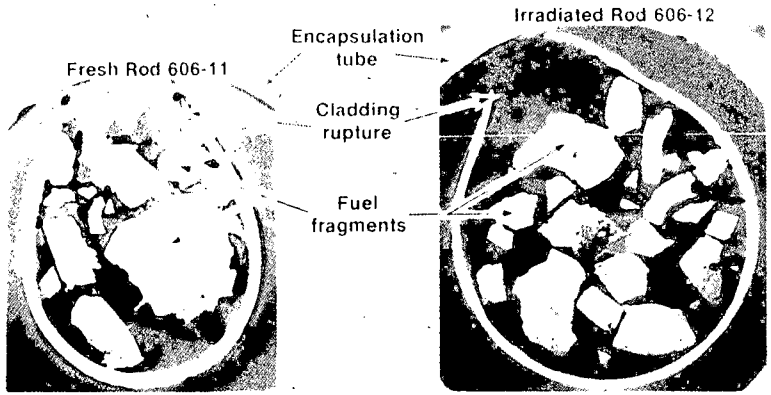

Comparison of Out-of-Pile and In-Pile Burst Test Data

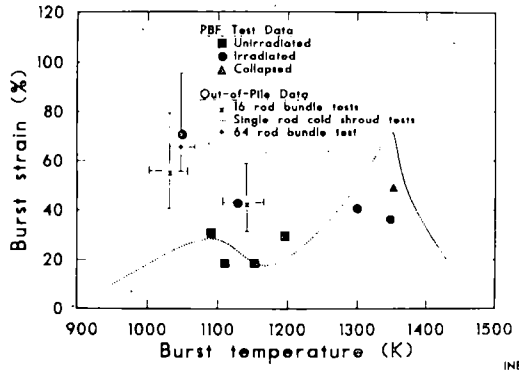

RESULTS FROM THE LOCA TEST PROGRAM

- THE PBF FRESH ROD, UNHEATED SHROUD DATA IS IN GOOD AGREEMENT WITH THE OUT-OF-PILE SINGLE ROD UNHEATED SHROUD DATA
- THE OUT-OF-PILE BUNDLE TEST BURST STRAINS ARE MUCH LARGER THAN THE SINGLE ROD UNHEATED SHROUD BURST STRAINS
- THE PREVIOUSLY IRRADIATED RODS HAD MORE STRAIN TO FAILURE THAN UNIRRADIATED RODS

INEL-S-42 000

CONCLUSIONS

- POWER-COOLING-MISMATCH:
  - IDENTIFIED SIGNIFICANT MARGIN BETWEEN THE PRESENT NRC CRITERIA AND ACTUAL FUEL FAILURE THRESHOLDS.
- REACTIVITY INITIATED ACCIDENT:
  - SHOWN THAT THE NRC CRITERIA MAY BE NON-CONSERVATIVE.
- LOSS-OF-COOLANT:
  - WE STILL DO NOT KNOW WHETHER CO-PLANNER BLOCKAGE AND LOSS-OF-COOLABILITY IS POSSIBLE DURING A LOCA

INEL-S-40 018

CONCLUSIONS REGARDING LOCA SAFETY ISSUES

- WE STILL DO NOT KNOW THE STRAIN TO FAILURE OF IRRADIATED LWR FUEL RODS IN LARGE BUNDLES
- WE DO NOT KNOW THE PRECISE EFFECT OF LARGE CHANNEL BLOCKAGES ON CORE COOLABILITY

INEL-S-40 015

Creare INC.
HANOVER, N.H.

FLOW REVERSAL STUDIES DURING HOT LEG INJECTION

Presented at the Ninth Water Reactor Safety Research Information Meeting

Gaithersburg, Maryland

Thursday, October 29, 1981

by

Paul H. Rothe

CREARE Incorporated
Hanover, NH 03755

INTRODUCTION

The primary purpose of this program was to determine if it is possible for the hot leg pipe to develop flow reversals or flow oscillations in UPTF during hot leg ECC injection. Unlike the cold leg injection geometry, the ECC leaves the injection piping in the hot leg very close to the upper plenum (see Figure 1). Furthermore, the hot leg injector directs the ECC towards the upper plenum at high velocity. Thus, it was initially anticipated that the hot leg ECC would simply flow into the upper plenum. TRAC-PD2 calculations [1] suggested however that both the hot legs and cold legs of GPWRs would plug and that flow oscillations would occur in both legs. These predictions were met with justifiable skepticism in view of several questions on the computer models. Therefore, Creare performed a seven-week program to evaluate the flow behavior independently. Program tasks included:

- Scale Model Hot Leg Injection Separate Effects Experiments and Analysis
- Review and Critique of TRAC-PD2 Calculations of Reference GPWR Hot Leg Behavior
- Assessment of Findings Relative to Operation of UPTF and Development of Recommendations

This presentation concentrates mainly on the results of the experiments [2]. We conclude that hot leg ECC flow reversal is likely in UPTF as presently designed and recommend means to prevent this undesirable result.

Separate Effects Experiments

Because there were very few data in the literature applicable to the geometry of the GPWR hot leg, steam-water separate effects experiments were performed in 1/5 and 1/10 scale transparent models simulating UPTF hot leg injectors (Figures 1 and 2). Both scale models were mounted on our 1/5-scale PWR vessel (used previously in Refill experiments) as shown in Figure 3. The thermal-hydraulic and geometric parameters for GPWRs and the scale models are shown in Figure 4. The reference GPWR information was supplied by LASL [3] and MPR [4]. The diameters of the experimental hot leg and injection pipes were linearly scaled from the reference system. Two scaling concepts were proposed [5] for the distance from the end of the injector to the upper plenum: linear scaling (L/D scaling) or preservation of the transit time in the hot leg ($L/\sqrt{D}$ scaling). Both geometries were tested at each scale. Both Froude-scaled and momentum flux-scaled liquid flows were also tested. The test pressures were approximately atmospheric (15 psia) for most of the tests, however, one series was performed at elevated pressure (60 psia) for comparison purposes. The test matrix is sketched in Figure 5.

In the GPWR hot leg, steam may flow countercurrent to the injection flow as a result of system pressure drops during the LOCA or due to condensation on either the cold leg ECC or even the hot leg ECC itself. In the scale models, the steam flow was varied over the range necessary to achieve complete reversal of the injected flow.

In the order in which they are encountered from highest to lowest steam flow tested, the flow regimes in the experiments are

- the flow reverses completely and the flow pattern is stable (near or above R_T=1)
- the flow reverses completely but some excursions (oscillations) in liquid penetration toward the upper plenum are observed (signified by "R" in the data plots)
- partial delivery to the upper plenum occurs, always with oscillations of a liquid plug in the hot leg
- complete delivery occurs (signified by "D" in the data plots).

The test results for the two injector lengths ($L/\sqrt{D}$ and L/D scaling, respectively) are shown in Figures 6 and 7, and the flow regimes are labelled. The experimental results are presented in terms of gas and liquid Froude numbers in these plots. The primary difference with injection length is that the region of unstable partial reversal becomes smaller as the injection distance becomes smaller (Figure 6 vs Figure 7). The reason for this is that liquid enters the upper plenum during flow oscillations more readily when the distance travelled during the oscillations becomes less. The boundary for complete flow reversal remains about the same because the flow reverses within a couple of inches of the injector. The qualitative observations for the various flow regimes are amplified in Figure 8.

The other salient point to note is that the steam flow necessary for flow reversal is less than linearly dependent on the injection flow rate. Said another way, the flow reversal occurs at a steam flow significantly below R_T=1 at higher liquid flow rates.

The types of flow regimes and experimental trends for complete flow reversal are consistent with the results of countercurrent flow experiments in PWR geometries [6].

It is appropriate to discuss the scaling implications of these data in order to translate the results to UPTF scale. In the past various scaling concepts have been proposed, including Froude (j^*), momentum flux, $j^*\sqrt{\text{scale}}$, and Kutateladze scaling. The data in Figures 6 and 7 were plotted by Froude scaling. In Figures 9 and 10 the data are plotted in terms of superficial velocity which accounts for the major features of the other scaling schemes. Within the experimental uncertainty no single scheme is obviously better than another for these 1/10 and 1/5 scale data.

The situation where the data are somewhat equivocal about the scaling method is comparable to the situation with countercurrent flow in PWR downcomers. To resolve the scaling question, data at low subcooling are required, that is, data should be obtained where the effects of condensation are minimized. It was not possible to obtain such data within the scope of this seven-week program.

In lieu of experimental data at low subcooling, some idea of the magnitude of the effect of condensation may be ascertained by comparison with some Dartmouth experiments [7,8] and the Taitel-Dukler criterion for slug formation in horizontal pipes [9]. For these references the conditions for complete flow reversal (or plug formation) are $j_g^* \simeq 0.7$ compared with $j_g^*=2\pm0.5$ for the Creare experiments with subcooled ECC. This comparison is shown in Figure 11. Given that there is some uncertainty in the scaling methodology, both Froude-scaled and momentum flux-scaled superficial gas velocities are extrapolated to full-scale in Figure 11, based upon the small scale results. At this time then, these are the best-estimates for the range of steam velocities for delivery and flow reversal for hot leg injection at full-scale. The lower bound on these estimates would be improved by the experiments with low ECC subcooling as would the scaling extrapolation.

TRAC-PD2 Calculations

TRAC-PD2 calculations of GPWR behavior, especially hot leg behavior, were reviewed and critiqued by Creare [10]. As shown in Figure 12, the velocities entering the hot leg may approach 100 to 125 ft/sec which will give superficial velocities in the range of values for flow reversal by momentum flux scaling and at the lower end of the Froude scaled range (Figure 11). Thus, it is reasonable that at about 24 seconds, a plug forms at the end of the hot leg in the calculation and is washed downstream (toward the steam generator) as shown by the diagram in Figure 13, which was developed [11] from the TRAC calculations. Plug formation and flow reversal in the TRAC calculations are therefore consistent with check calculations of anticipated steam flows and extrapolated experimental results. The liquid plug velocities are also consistent with simple plug motion analyses.

Assessment of Findings Relative to UPTF

Flow reversal is likely to occur in UPTF as well. It is expected that the flows driven by condensation on injected hot leg fluid alone would approach equilibrium (R_T=1) in the hot leg. Since cold leg injection also occurs simultaneously, the flow in the hot leg might even be twice R_T=1 due to additional condensation in the cold leg. Finally, the reverse steam flow is further enhanced at times by a favorable loop pressure gradient. The combined reverse steam flow is overwhelming. The experimental data presented here show that complete flow reversal always occurs at steam flows less than equilibrium flow rates. Therefore, we expect that flow reversal will occur in UPTF.

The UPTF facility has a large (essentially unheated) volume downstream of the hot leg injector where liquid can collect (unlike the heated steam generator of GPWRs where vapor generation may lead to expulsion of liquid entering the steam generator). Flow reversal may lead to ingestion of water into this volume in UPTF which is unacceptable in view of UPTF objectives to emphasize upper plenum behavior. Steps which minimize loss of ECC into this volume are recommended. Alternatives are flanging off the downstream end of the hot legs, or providing an additional steam flow to keep liquid out of this region. The facility must be designed to withstand the loads due to fluid plug impacts. Scale model experiments with simulated loop features should be considered to assist the design of the UPTF facility, to help design experimental procedures, and to aid in analysis of the results.

Summary

The findings from this work are summarized in Figure 15. Based in part on previous experiments and the separate effects hot leg experiments reported here, the best-estimate range of steam flows for plug formation (no condensation) to complete flow reversal (with condensation) is j_g^*=0.7 to 2.0. By either Froude scaling or momentum flux scaling of hot leg flows, these results may be extrapolated to full-scale UPTF (see Figure 11). TRAC-PD2 calculations indicate that flow velocities will be in this range at full-scale, therefore, plug formation and/or flow reversal are to be expected at full-scale in the UPTF hot leg. This finding leads to several recommendations for the UPTF facility and experiments as identified in Figure 15.

NOMENCLATURE

- D = hot leg diameter
- L = distance from injector discharge to upper plenum
- j_x = superficial velocity of gas or liquid phase, ft/sec
- j_x^* = dimensionless flux of gas or liquid phase, $j_s^*=\rho_x^{1/2} j_x [gD(\rho_f-\rho_g)]^{1/2}$
- R_T = thermodynamic ratio, $R_T = j_f^*/j_g^*$
- T_{ECC} = temperature of injected liquid
- λ = condensation parameter, $c_p(T_{SAT}-T_{ECC})\rho_f^{1/2}/h_{fg}\rho_g^{1/2}$

REFERENCES

1) Motley, F. and Williams, K. A.; TRAC-PD2 CALCULATION OF A DOUBLE-ENDED COLD-LEG BREAK IN A REFERENCE GERMAN PWR; Unnumbered LASL Report, (LAUR), Results presented at 2D/3D Meeting, November 3-6, 1981.

2) Rothe, P. H.; "QUICK STUDIES OF GPWR HOT LEG INJECTION"; Paper presented at 2D/3D Meeting, Erlangen, W. Germany, June 3, 1981.

3) Sample TRAC Calculation Results, Notes given to P. H. Rothe, Creare, during LASL visit of November 20, 1981.

4) Dammerell, P. S.; Comments on Proposed Hot Leg Model Tests, MPR letter from P. Dammerell to C. Crowley, April 7, 1981.

5) Zuber, N.; SCALING OF TRANSITION TO SLUG FLOW DURING ECC HOT LEG INJECTION; US NRC Memorandum, March 5, 1981.

6) Rothe, P. H. and Crowley, C. J.; SCALING OF PRESSURE AND SUBCOOLING FOR COUNTERCURRENT FLOW; Quarterly Progress Report April 1 - June 30, 1978, Creare Technical Note TN-285 (NUREG/CR-0464), October 1978.

7) Richter, H. J. et al.; DEENTRAINMENT AND COUNTERCURRENT AIR-WATER FLOW IN A MODEL PWR HOT LEG; Dartmouth College, US NRC Report NRC-0193-9, Final Report, September 1975.

8) Richter, H. J., Wallis, G. B. and Spears; EFFECT OF SCALE ON TWO-PHASE COUNTERCURRENT FLOW FLOODING; Dartmouth College, US NRC Report NUREG/CR-0312; Final Report, June 1979.

9) Taitel, Y., Lee, N. and Dukler, A. E.; TRANSIENT GAS-LIQUID FLOW IN HORIZONTAL PIPES: MODELING THE FLOW PATTERN TRANSITIONS; AIChE Journal, Vol. 24, No. 3, pp. 920, September 1978.

10) Rothe, P. H. and Crowley, C. J.; QUICK REVIEW OF CALCULATED GPWR ECC OSCILLATIONS; (Creare TM-743), January 1981.

11) Crowley, C. J.; MAGNITUDE OF OSCILLATIONS IN TRAC CALCULATIONS; Creare Memorandum IM-5-269, May 1, 1981.

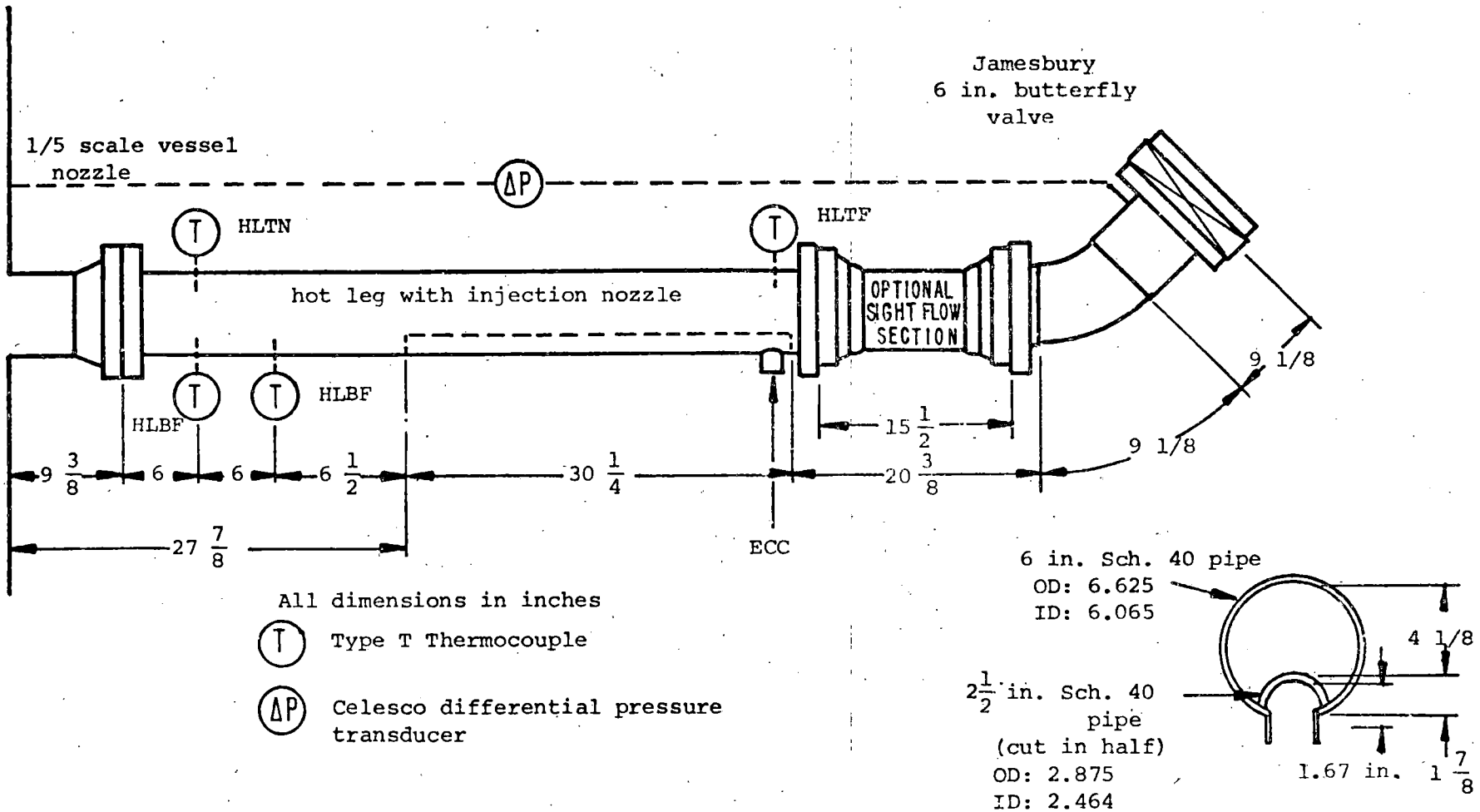

Figure 1. SKETCH OF 1/5-SCALE HOT LEG

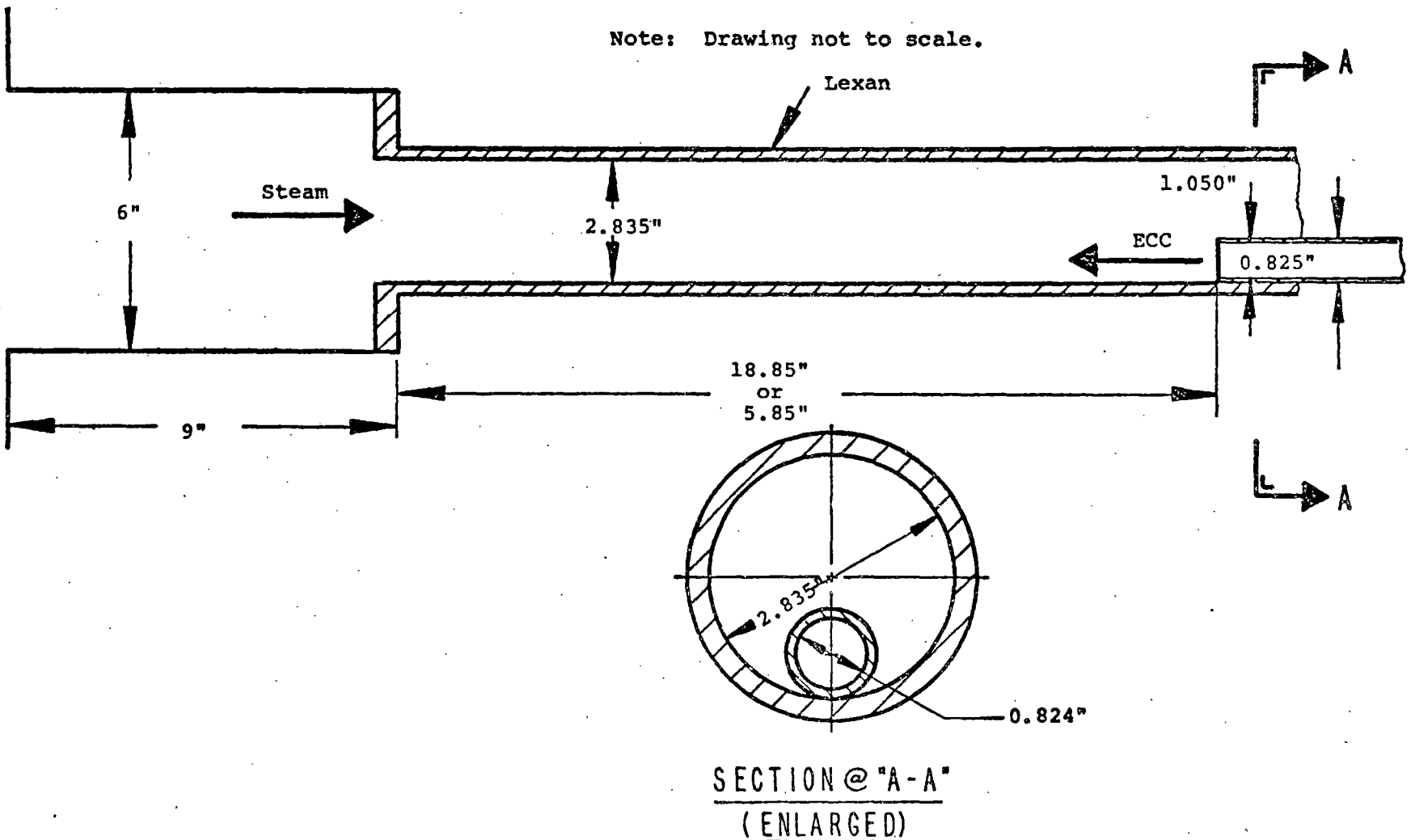

Figure 2. SKETCH OF 1/10-SCALE HOT LEG

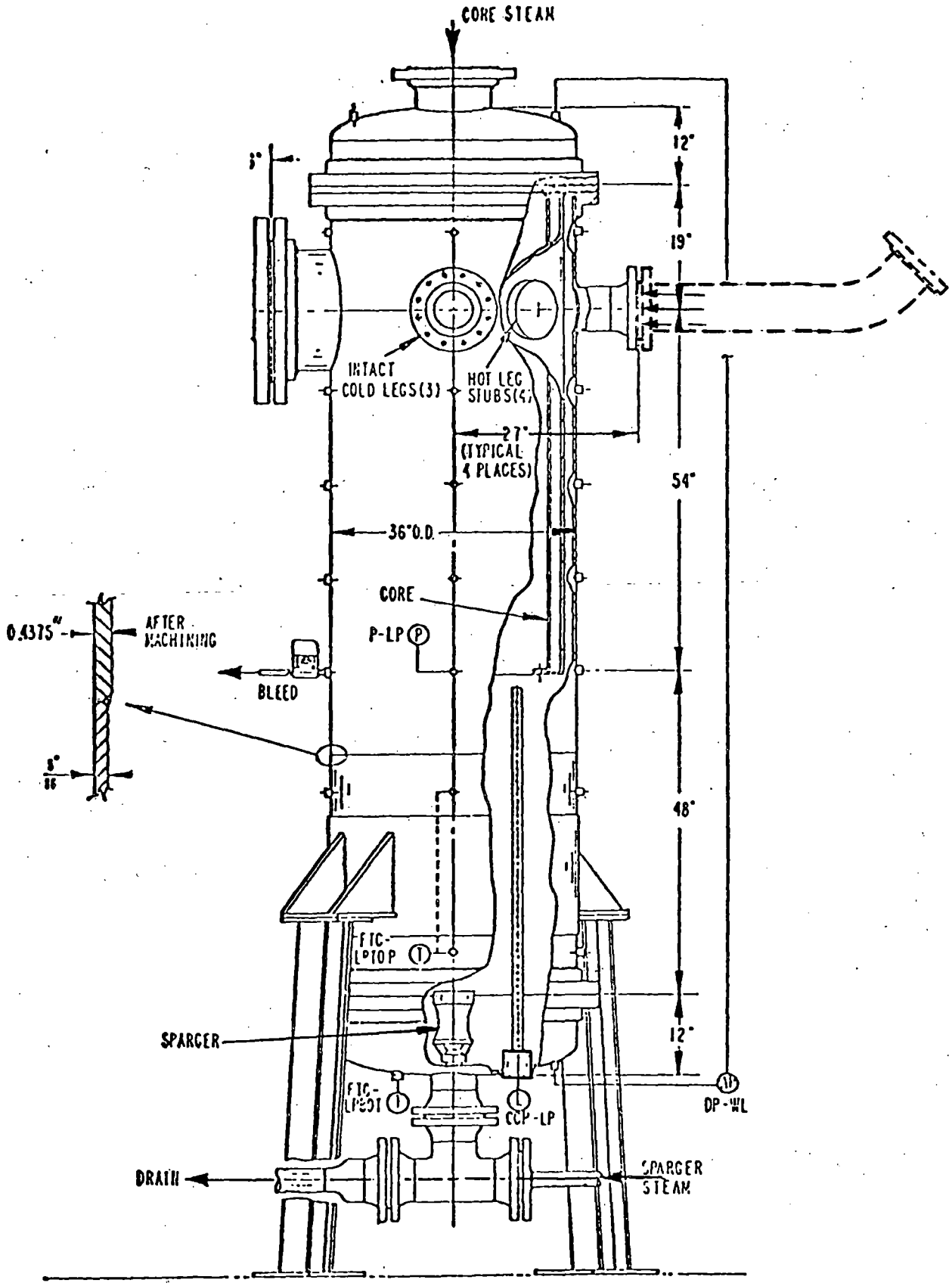

Figure 3. SKETCH OF CREARE 1/5-SCALE VESSEL

Parameter	GPWR		Creare 1/5-Scale	Creare 1/10-Scale
	LASL [3]	MPR [4]		
Pressure	60-220 psia	50-325 psia	15 and 60 psia	15 psia
ECC Flow Per Hot Leg	880 lbm/sec	358-1230 lbm/sec	16.8 lbm/sec (37.1 lbm/sec)	2.6 lbm/sec (5.2 lbm/sec)
Liquid Froude No. in Hot Leg	0.34	0.14-0.48	0.37 (0.74)	0.34 (0.70)
ECC Temperature	86°F	77-95°F	60°F	60°F
ECC Subcooling	207-304°F	186-348°F	152-233°F	152°F
Liquid Velocity At Injection Point	34.7 ft/sec	15-48 ft/sec	14.0 ft/sec [27.8 ft/sec]	10.5 ft/sec [21 ft/sec]
Diameter of Hot Leg	2.46 ft	2.46 ft	0.505 ft	0.236 ft
Area of Hot Leg	4.76 ft^2	4.74 ft^2	0.200 ft^2	0.0438 ft^2
Area of Injector	0.409 ft^2	0.409-0.431 ft^2	0.0215 ft^2	0.004 ft^2
A_{INJ}/A_{HL}	0.086	0.086-0.091	0.108	0.091
Distance From Injector Outlet to Upper Plenum	5.07 ft	4.92 ft	2.32 ft [1.04 ft]	1.57 [0.49]
Length of Hot Leg Diameter Ratio	2.06	2.0	4.59 [2.06]	6.64 [2.06]

( ) Signifies values for area-scaled flows as opposed to nominal F_o scaled

[ ] Signifies values for L/D scaling as opposed to nominal L^2/D scaling.

Figure 4. COMPARISON OF GPWR AND CREARE SCALE MODEL FLOW AND GEOMETRY PARAMETERS

Scale	Pressure	Injector-to-Vessel Length (L/D)	ECC Flow Rate (lbm/sec)	Steam Flow Rate (lbm/sec)	ECC Temperature (°F)
1/5	15	4.59	18.7	1.5-2.8	60
1/5	15	4.59	24.2	1.7-3.2	61
1/5	15	4.59	37.1	2.7-2.9	57
1/5	15	2.06	18.7	1.8-2.2	68
1/5	15	2.06	37.1	2.7-3.6	68
1/5	60	2.06	18.7	2.3-3.6	70
1/10	15	6.64	2.6	0.21-0.48	60
1/10	15	6.64	5.2	0.24-0.48	60
1/10	15	2.06	2.6	0.32-0.48	60
1/10	15	2.06	5.2	0.43-0.48	60

Figure 5. TEST MATRIX FOR HOT LEG INJECTION EXPERIMENTS

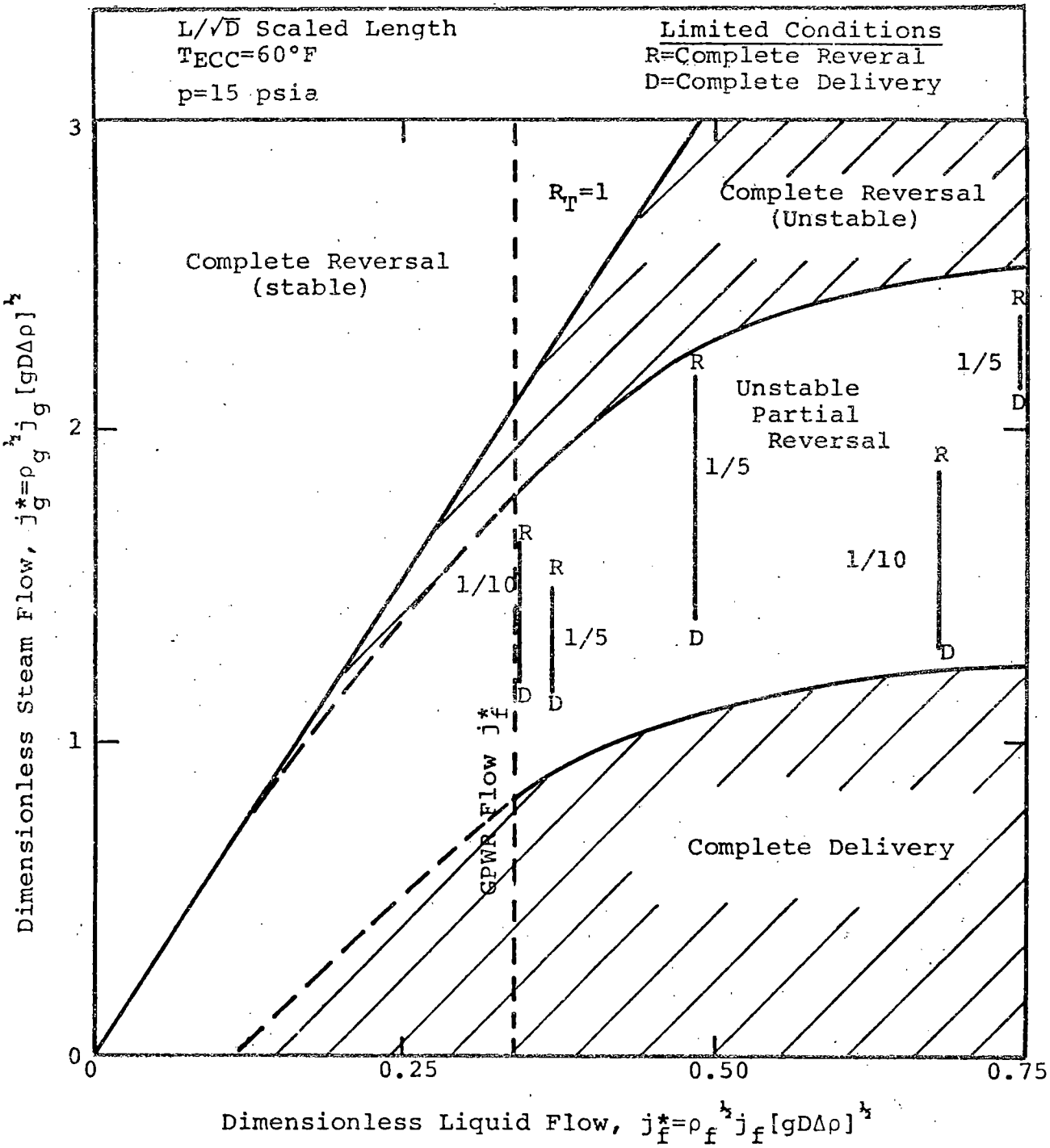

Figure 6. FROUDE NUMBER (CONSTANT j*) MAP FOR L/√D LENGTH DATA

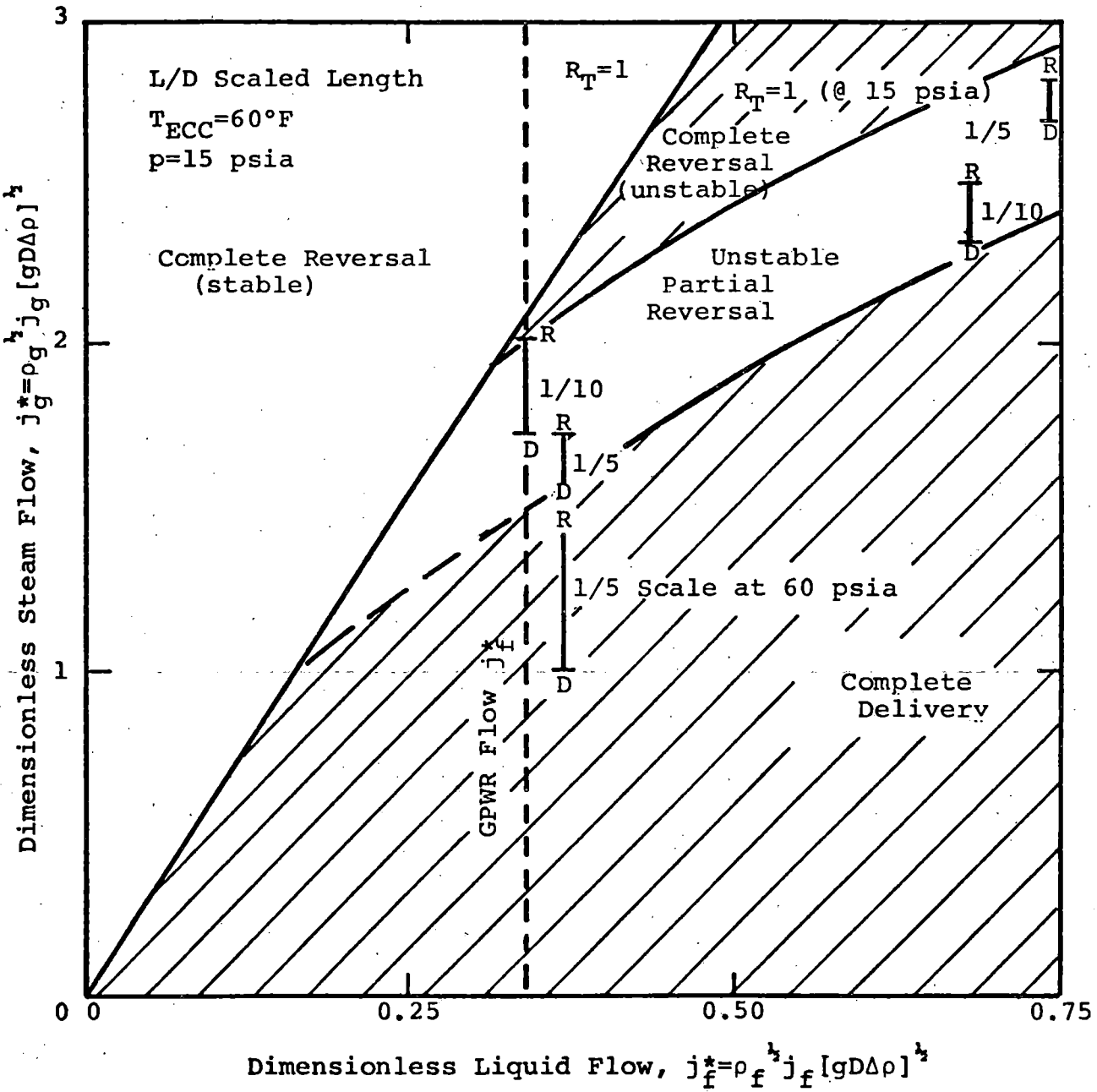

Figure 7. FROUDE NUMBER (CONSTANT j*) MAP FOR L/D LENGTH DATA

1) Test Procedure (@ 15 psia)

   Set Steam Flow (choked)

   Heat up and Air Purge

   Set Initial Vessel Pressure (HL Valve)

   Initiate ECC

   Confirm Complete Flow Reversal

   Confirm Vessel Pressure Above Atmosphere

2) For Successively Decreased Steam Flow, the ECC:

   - Reverses completely, stable near $R_T=1$
   - Reverses completely, some oscillations at data limit shown by "R"
   - Partial reversal, always oscillations
   - Complete delivery, stable at data limit shown by "D"

3) For Stable, Reversed Flow, ECC is Turned Around Within Several Inches of Injection Point. Steam is Observed at Outlet Pressure is always above ambient.

4) For Unstable Reversed Flow, the Minimum Pressure During Oscillations is Above Ambient at High Steam Flows But Becomes Sub-Ambient at lower steam Flows. At the Same Time, Plug Advances Closer and Closer Toward Vessel During Excursions.

5) For Partial Flow Reversal with Oscillations, The Liquid Plug Occasionally Proceeds as Far as Vessel During Excursions.

6) For Complete Delivery, all Steam Appears to be Condensed in Vessel. Pressure is Steady at Ambient Pressure. Injected Liquid Flows Along Bottom of Pipe.

Figure 8. QUALITATIVE OBSERVATIONS IN FLOW REVERSAL TESTS

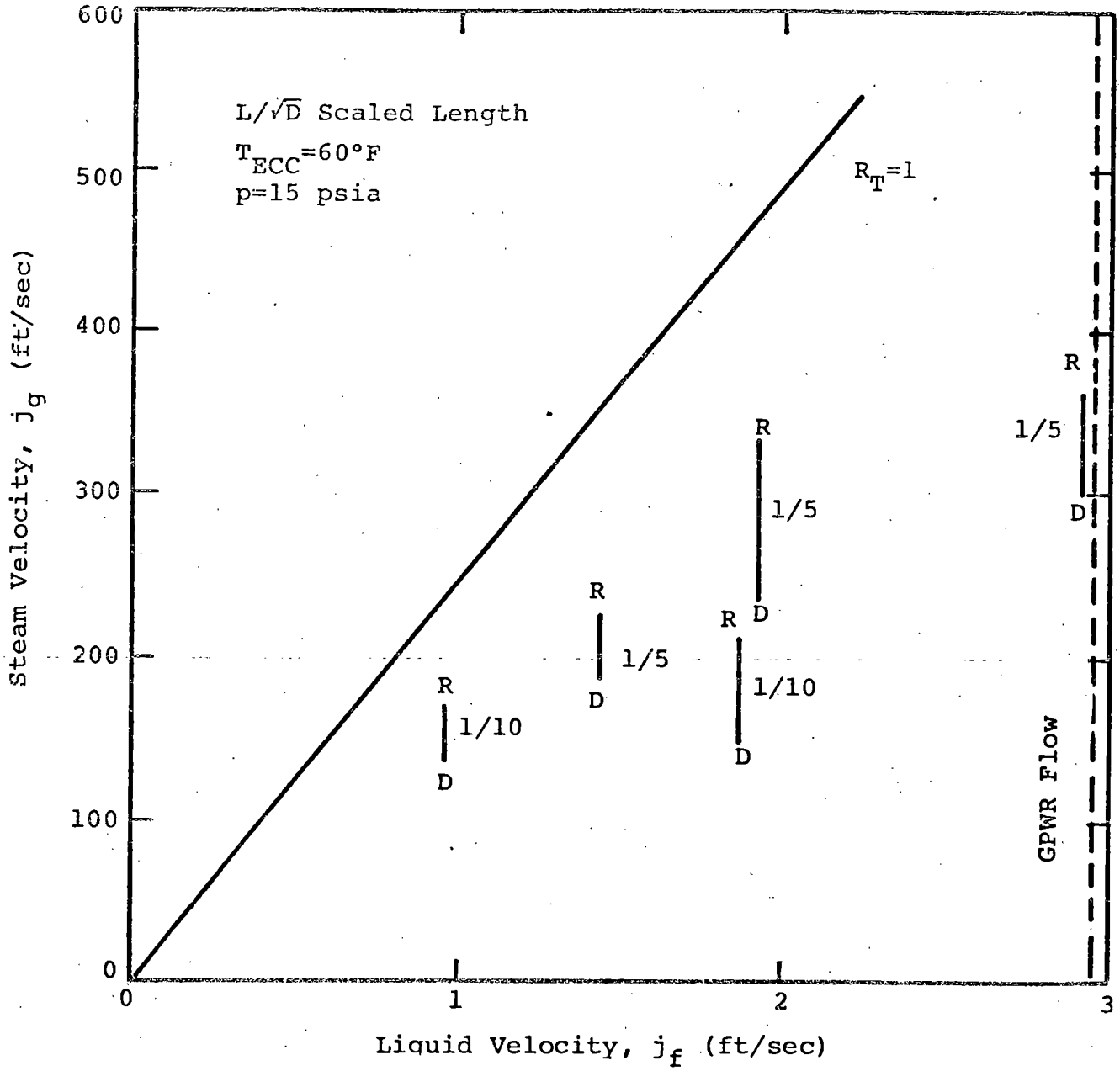

Figure 9. SUPERFICIAL VELOCITY MAP FOR L/√D SCALED LENGTH DATA

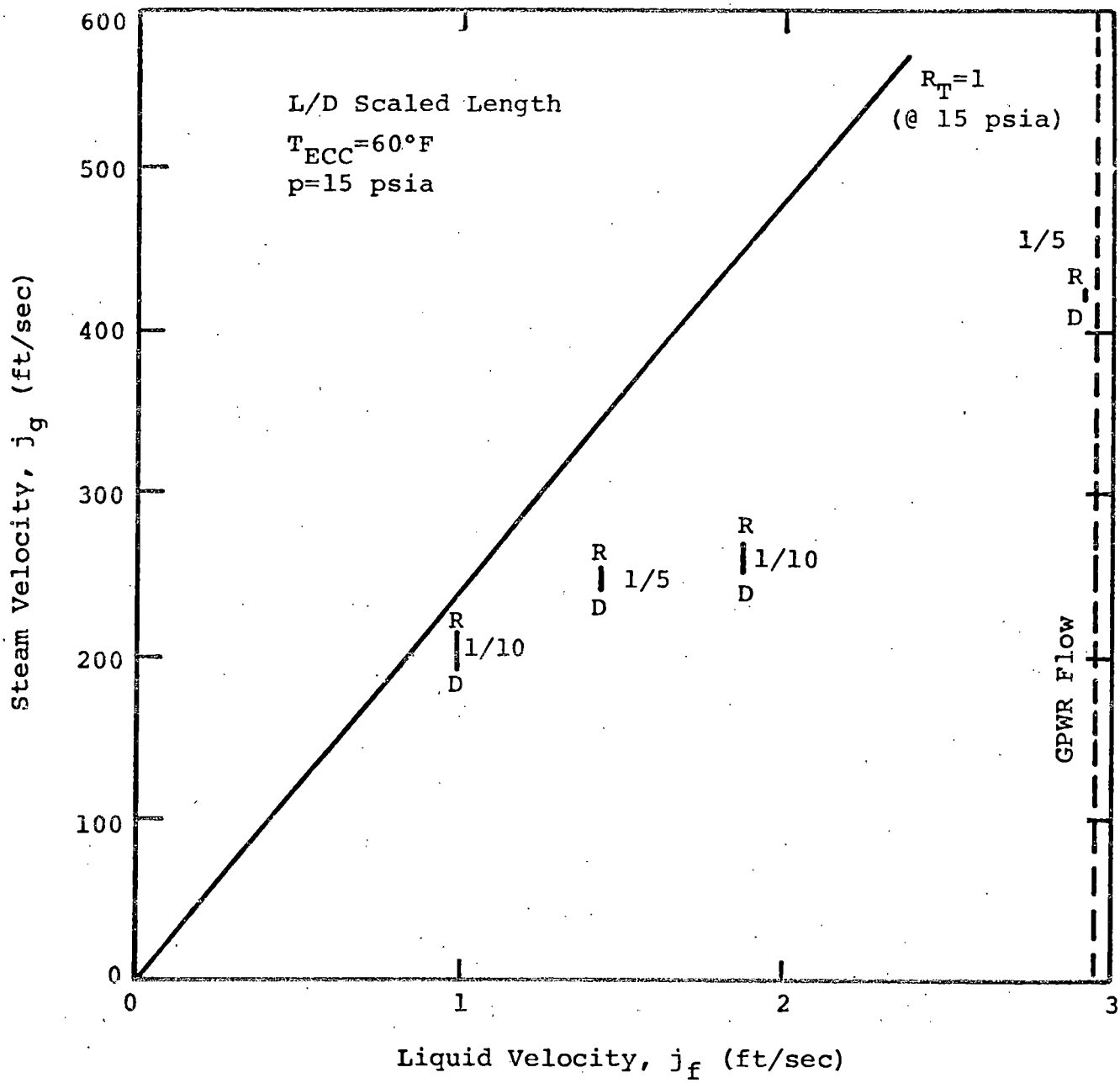

Figure 10. SUPERFICIAL VELOCITY MAP FOR L/D SCALED LENGTH DATA

1) Comparison of Reversal Data (at applicable sizes)

- Creare 1/5-scale hot leg (Steam Water, GPWR Injector) — $J_G^* \sim 2 \pm 0.5$
- Dartmouth Hot Leg [7] (Air-Water, Slow Injection) — $J_G^* \sim 0.7$
- Taitel-Dukler Correlation [9] — $J_G^* \sim 0.75$
- Dartmouth Vertical Tube (Air-Water) [8]
  - Uniform inlet, small tubes — $J_G^* \sim 0.7$
  - Uniform inlet, large tubes — $\rho_G J_G^2 \sim 1.9 \times 10^2$ LBM/FT-SEC^2
  - injector 1 (1 in.), large tube — $J_G^* \sim 1.4$(?)
  - injector 2 (2 in.) Large tube — $J_G^* \sim 0.7$

2) UPTF/GPWR Design Estimates (Based on D=2.46 ft (0.75m), P=60 psia, and F_0=0.35)

	Extrapolated J_G (ft/sec)	
	J^* Scaling	$\rho_G J_G^2$ Scaling
Complete Delivery		
• Dartmouth Tube	75	35
• Taitel-Dukler	130	—
• Creare Hot Leg	185	80
Complete Reversal		
• Taitel-Dukler	130	—
• Dartmouth Tube	185	80
• Creare Hot Leg	275	125

Figure 11. CONDITIONS FOR COMPLETE FLOW REVERSAL

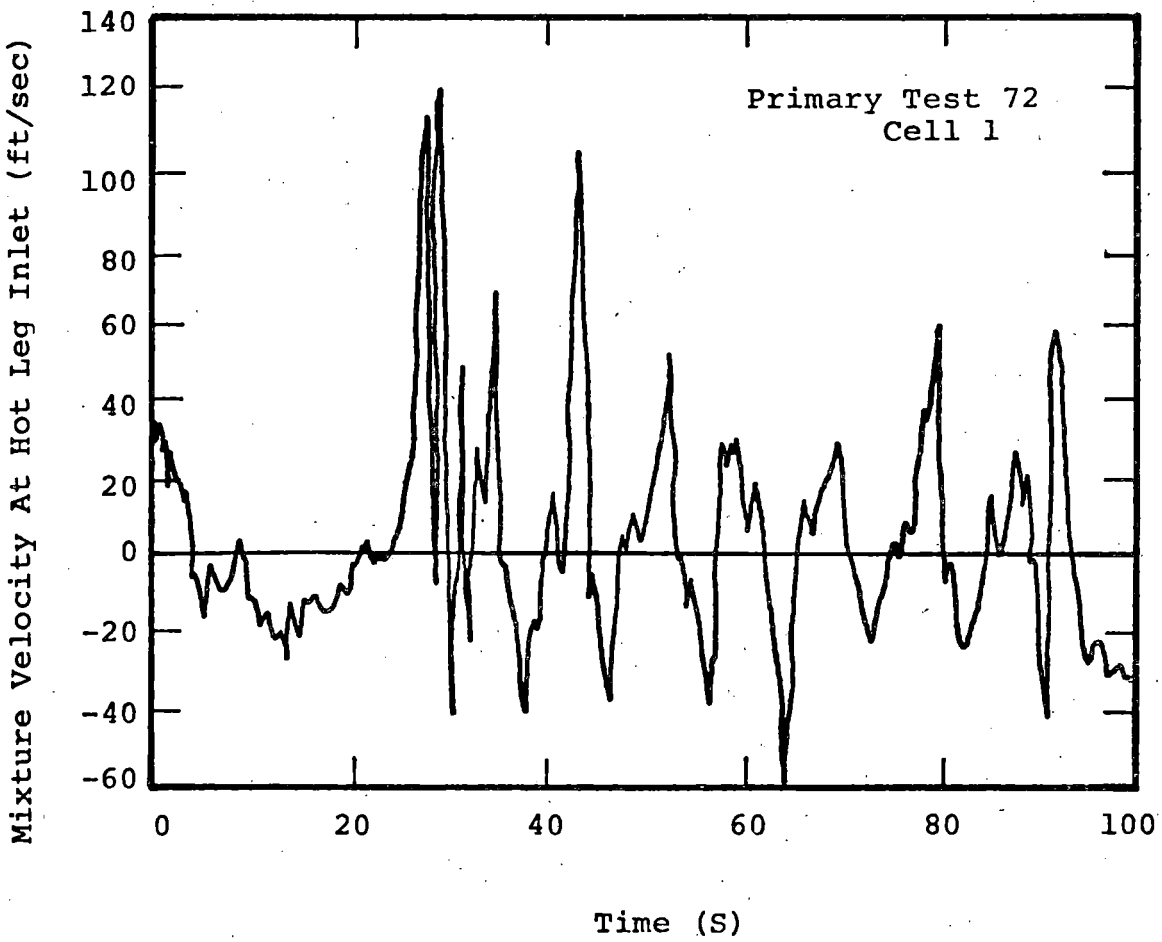

Figure 12. VELOCITY AT HOT LEG INLET FOR GPWR CALCULATED BY TRAC-PD2

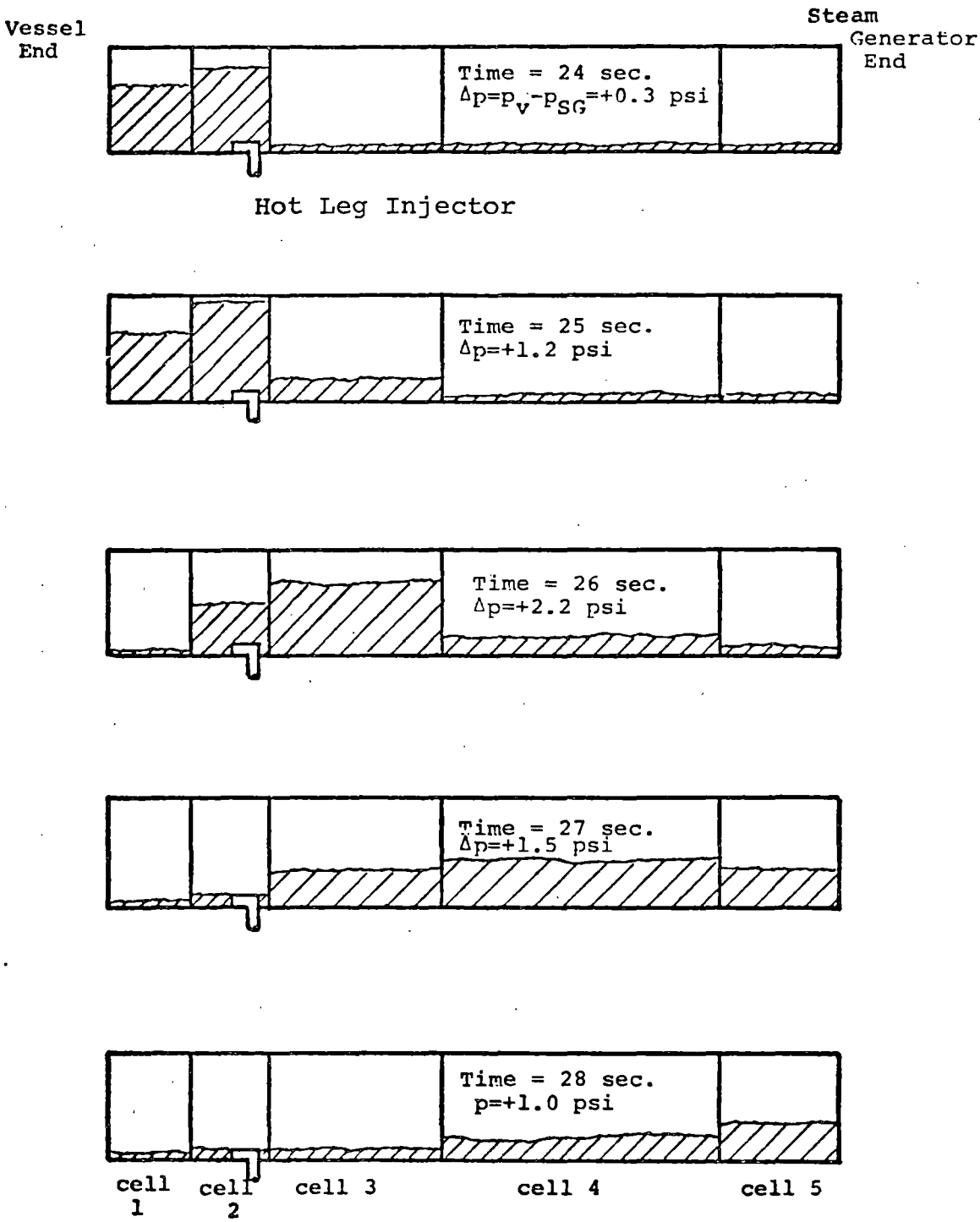

Figure 13. SKETCH OF LIQUID FRACTION IN GPWR HOT LEG CELLS FROM TRAC-PD2 CALCULATION

1) FROM A PURELY EXPERIMENTAL PERSPECTIVE, CREARE SUGGESTS THAT UPTF MIGHT HAVE ENHANCED VALUE BY BEGINNING AS A SIMPLER FACILITY WITHOUT LOOPS (BY FLANGING OFF THE HOT LEGS AND COLD LEGS ON THE LOOP SIDE BY THE ECC INJECTORS). OTHER APPROACHES TO MAKE UPTF A MORE "SEPARATE EFFECTS" FACILITY SHOULD BE DEVELOPED AND EVALUATED.

2) FACILITY MODIFICATIONS ARE RECOMMENDED TO PREVENT FLUID INGESTION INTO STEAM GENERATOR SIMULATOR AND TO PRECLUDE DAMAGE DUE TO FLUID STRUCTURE-INTERACTIONS DURING HOT LEG INJECTION.

3) IF THE LOOPS ARE TO BE A FEATURE OF UPTF, THEN SCALE-MODEL EXPERIMENTS WITH LOOPS SHOULD BE CONSIDERED TO ASSIST UPTF DESIGN AND ANALYSIS.

4) SOME ADDITIONAL SEPARATE EFFECTS EXPERIMENTS WITH LOW ECC SUBCOOLING WOULD CONTRIBUTE TO UNDERSTANDING OF PHENOMENA AND IMPROVE EXTRAPOLATION OF CREARE DATA TO UPTF SIZE.

Figure 14. RECOMMENDATIONS FOR UPTF

1) HOT LEG INJECTION SEPARATE EFFECTS EXPERIMENTS [2]

- 1/5 AND 1/10 SCALE MODEL EXPERIMENTS WERE PERFORMED OVER FROUDE AND MOMENTUM FLUX SCALED ECC FLOWS, AT TWO INJECTOR LOCATIONS (L/D AND $L/\sqrt{D}$ SCALING).
- SEVERAL FLOW REGIMES WERE FOUND, INCLUDING STABLE COMPLETE REVERSAL, UNSTABLE COMPLETE REVERSAL, UNSTABLE PARTIAL REVERSAL, STABLE COMPLETE DELIVERY.
- FOR TEST CONDITIONS CORRESPONDING TO GPWRS, COMPLETE FLOW REVERSAL OCCURRED AT $J_G^*=2.0\pm0.5$ IN THE EXPERIMENTS.
- THE BEST-ESTIMATE RANGE OF STEAM FLOW FROM PLUG FORMATION (COMPLETE DELIVERY) WITHOUT CONDENSATION TO COMPLETE FLOW REVERSAL WITH CONDENSATION IS $J_G^*=0.7$ TO 2.0. (THE LOWER BOUND COULD BE IMPROVED BY ADDITIONAL TESTS WITH LOW ECC SUBCOOLING.)
- EXPERIMENTAL RESULTS ARE EQUIVOCAL ABOUT FROUDE SCALING VS MOMENTUM FLUX SCALING. (THIS UNCERTAINTY COULD ALSO BE REDUCED BY LOW ECC SUBCOOLING TESTS.)
- EXTRAPOLATION OF BEST-ESTIMATE STEAM FLOWS TO FULL SCALE GIVES A RANGE $J_G=75$-275 FT/SEC FOR FROUDE SCALING AND $J_G=35$-125 FT/SEC FOR MOMENTUM FLUX SCALING.

2) CRITIQUE OF TRAC-PD2 CALCULATIONS [10]

- GPWR CALCULATIONS SHOW THAT PLUG FORMATION AND FLOW REVERSAL CAN OCCUR AT FULL-SCALE.
- STEAM VELOCITIES FOR PLUG FORMATION AND FLOW REVERSAL IN TRAC WERE CONSISTENT WITH EXPERIMENTAL EXTRAPOLATIONS AND OTHER CHECK CALCULATIONS.
- LIQUID PLUG VELOCITIES WERE CONSISTENT WITH SIMPLE PLUG MOTION ANALYSES.

3) UPTF OPERATION

- FLOW REVERSAL SHOULD BE EXPECTED IN UPTF AS DESIGNED.
- DESIGN MODIFICATIONS WHICH PREVENT PLUG FORMATION, FLOW REVERSAL, AND FLOW OSCILLATIONS IN THE UPTF HOT LEG ARE RECOMMENDED.
- SCALE MODEL EXPERIMENTS WITH LOOP SIMULATIONS ARE RECOMMENDED TO ASSIST UPTF DESIGN, OPERATION, AND ANALYSIS.

Figure 15. SYNOPSIS: ISSUES AND FINDINGS

JET DISINTEGRATION IN UPPER PLENUM

J. B. Colson,
J. C. Lin,
and
P. D. Wheatley

Presented at
The Ninth Water Reactor Safety Research
Information Meeting

October 26 - 30, 1981
Gaithersburg, Maryland

Idaho National Engineering Laboratory
Idaho Falls, Idaho 83415

JET DISINTEGRATION IN UPPER PLENUM

J. B. Colson, J. C. Lin, and P. D. Wheatley
EG&G Idaho, Inc.

Five tests to qualitatively study jet disintegration and condensation have been completed. The jet disintegration tests were conducted using the Simulated Slab Core (SSC), which was installed in the two-phase loop at the LOFT Test Support Facility. The SSC and hot leg spool piece modeled the upper plenum and hot leg portion of the Slab Core Test Facility operated by the Japan Atomic Energy Research Institute (JAERI).

The objectives of the jet disintegration tests were to (a) determine the coherence of an emergency core coolant (ECC) jet in an upper plenum, (b) evaluate water buildup in the vessel and entrainment into the hot leg, and (c) extend the current data bases for further countercurrent flow limiting (CCFL) model development. Information from these tests can support the development and assessment of advanced computer codes used for best-estimate analyses of transients and accidents, and can help in licensing decisions.

Steam, at about 410 K, was injected into the lower portions of the SSC while liquid, approximately 130 K subcooled, was injected above the upper core support plate (UCSP), just below the hot leg spool piece. The liquid flow rate was approximately 24 kg/s in all of the tests. The steam flow rates for each test were varied from 0 to 8 kg/s. Thermocouples were located at selected openings in the UCSP and on a screen below it. Thermocouple responses were evaluated to determine if steam or subcooled liquid was present. At low to intermediate steam flow rates both sets of thermocouples showed intermittent subcooling, or wetting, indicating CCFL breakdown. As the injected steam flow rate was increased, the duration of CCFL breakdown was decreased. The highest steam flow test indicated very little CCFL breakdown, and nearly all of the ECC fluid was carried to the hot leg.

The mass flows were measured in the hot leg spool piece for each of the five tests. A large flow into the SCC was measured in the hot leg spool piece, for the low steam flow test (3 kg/s), due to steam-water mixing and steam condensation above the UCSP. During the intermediate flow tests, oscillatory flow was measured in the hot leg spool piece. This was caused by unstable countercurrent flow limiting at the UCSP in the slab core. For the high flow test (8 kg/s), a large flow out of the SCC was measured in the hot leg spool piece. The test data indicated that significant ECC fluid can be removed through the hot leg for both intermediate and high steam flows.

Posttest calculations were conducted to evaluate the capability of the TRAC-BD1[1] code to calculate the jet disintegration tests. The calculated fluid temperatures showed trends similar to the experimental data. Timing of the calculated liquid breakthrough did not match the data in all locations, but the magnitude of liquid subcooling was calculated reasonably well.

Several countercurrent flow limiting correlations were reviewed, and the modified Wallis correlations[2] was selected, due to geometric considerations, for comparison with the data. The modified Wallis correlation selected is

$$k_{g,e}^{1/2} + 0.689 k_l^{1/2} = 2.02$$

where

$$k_{g,e} = k_g - \lambda \frac{C_p \cdot \Delta T}{h_{fg}} \left(\frac{\rho_L}{\rho_g}\right)^{1/2} k_{l,in}$$

was suggested by Tien[3] to include the condensation effect.

For the low steam flow test (3 kg/s), the data were below the CCFL correlation. This means that the water penetration was not yet limited by CCFL. For intermediate steam flow tests (4.4 and 6.0 kg/s), the data agreed with the CCFL correlation. This implies that the water penetration was limited by CCFL. For the high steam flow test (8 kg/s), the data were above the CCFl correlation, implying there was no water penetration.

In summary, the selected jet disintegration test matrix spanned a wide range of phenomena at the upper core support plate. The low steam flow test allowed liquid penetration and backflow through the hot leg spool piece. The intermediate steam flow tests showed countercurrent flow limiting at the UCSP, with intermitten breakdown. The high steam flow test indicated CCFL, with large amounts of emergency core coolant liquid being swept out of the hot leg. The jet disintegration test data showed good agreement with the selected CCFL correlation, thus adding to the data base. The TRAC-BD1 computer code also proved capable of calculating the thermal-hydraulic responses of the simulated slab core for tests with steam injection rates similar to those expected in a BWR upper plenum.

REFERENCES

1. J. W. Spore et al., "Development of the TRAC Code for BWR Analysis," Quarterly Technical Progress Report on Water Reactor Safety Programs Sponsored by the Nuclear Regulatory Commission's Division of Reactor Safety Research, July-September 1980, NUREG/CR-1400(3), EGG-2066, November 1980, p. 21.

2. J. K. Jacoby and C. M. Mohr, Final Report on 3-D Experiment Project Air-Water Upper Plenum Experiments, EG&G Idaho, Inc., 3DP-TR-001, November 1978.

3. C. L. Tien, "A Simple Analytical Model for Counter-Current Flow Limiting Phenomena with Vapor Condensation," Letters in Heat Mass Transfer, 4, 3, 1977, pp. 231-238.

Jet Disintegration in Upper Plenum

J.B. Colson

EG&G Idaho Inc

IDAHO NATIONAL ENGINEERING LABORATORY

Contents

- Introduction
- Test objectives
- Jet disintegration test
  - Facility description
  - Test results
  - TRAC-BD1 prediction
- Conclusion

INEL-S-34 017

Test Objectives

- Determine coherence of hot leg ECC jet
- Evaluate CCFL phenomena
- Determine cross flow below UCSP
- Provide TRAC calculation assessment base

INEL-S-34 016

Two-Phase Loop with Slab Core Simulator Installed

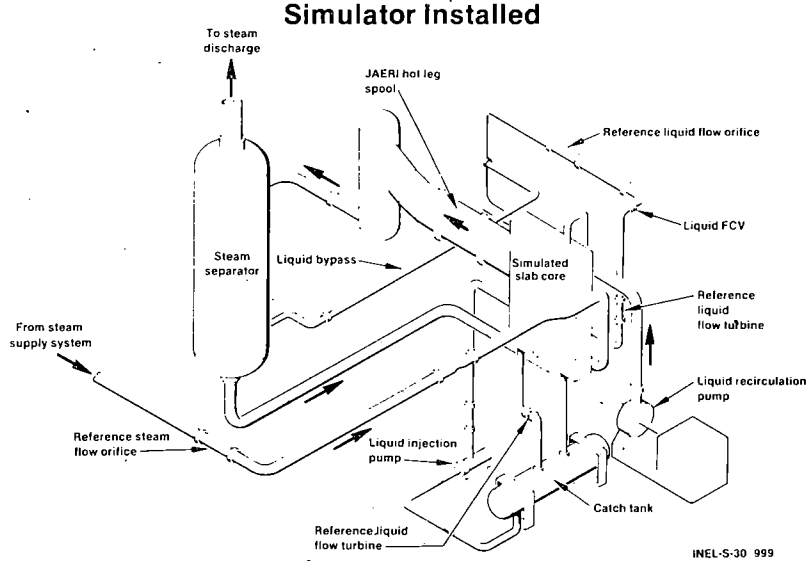

INEL-S-30 999

Simulated Slab Core

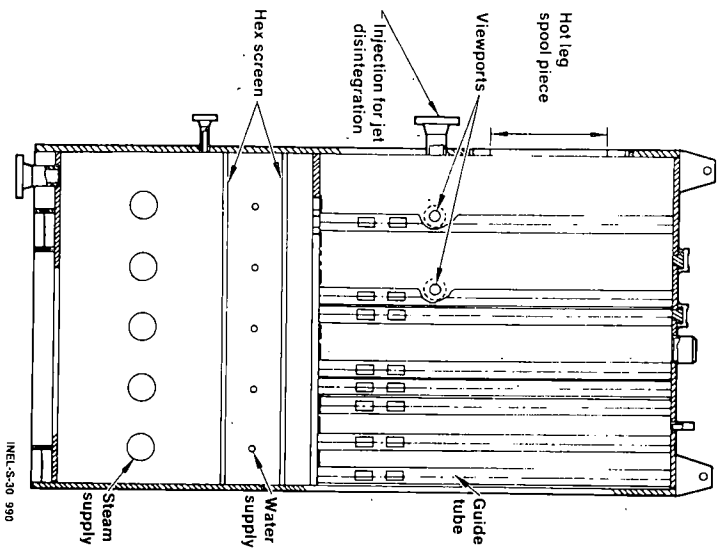

Slab Core Thermocouple Locations

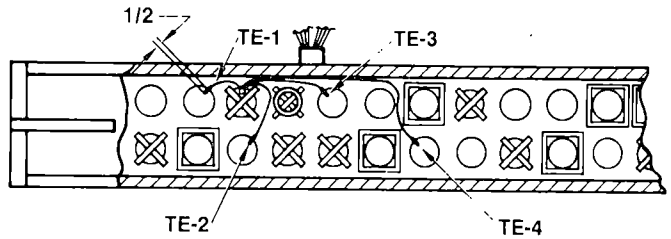

TE-1, -2, -3, and -4 top side of core support plate as shown

TE-5, -6, -7, and -8 to top side of top hex screen (not shown) and lined up with TE-1 through TE-4 respectively

INEL-S-34 018

Hot Leg of the Slab Core

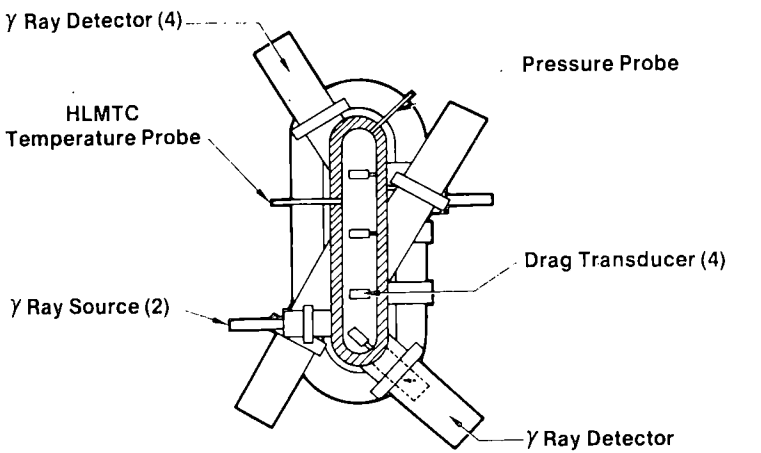

Test Conditions

Test	Steam Flow (kg/s)	Liquid Flow (kg/s)
3D-LD-1	0	23.8
3D-LD-2A	3.03	23.2
3D-LD-3	4.46	23.1
3D-LD-3.5	5.91	23.5
3D-LD-4A	7.81	24.7
Liquid temperature: 130 K subcooled Steam temperature: 410 K		

INEL-S-30 986

Upper Plenum Flow Phenomena

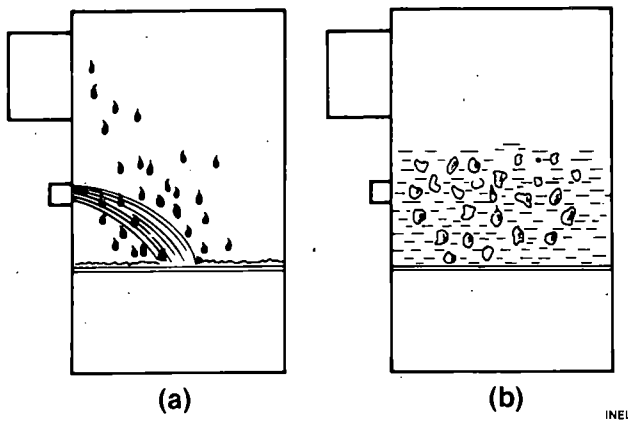

INEL-S-30 981

FLUID TEMPERATURE ABOVE AND BELOW UPPER SUPPORT PLATE FOR NO STEAM FLOW

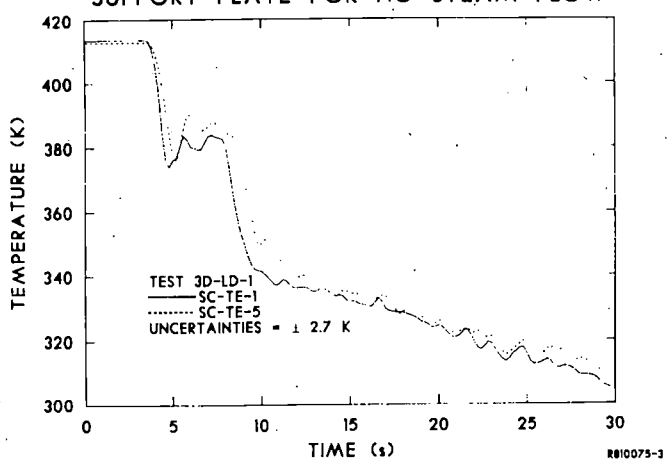

R810075-3

Test Conditions Bracket CCFL Phenomena

- Total penetration
- Periodic penetration
- Total sweepout
- Good agreement with correlation

INEL-S-34 014

FLUID TEMPERATURE ABOVE AND BELOW UPPER SUPPORT PLATE FOR INTERMEDIATE STEAM FLOW

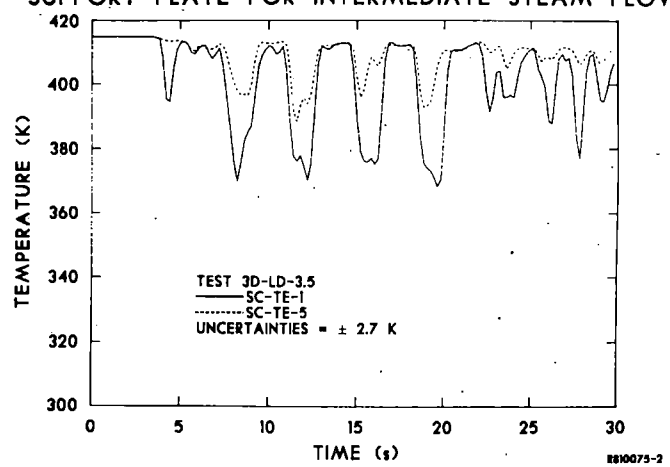

R810075-2

FLUID TEMPERATURE ABOVE AND BELOW UPPER SUPPORT PLATE FOR HIGH STEAM FLOW

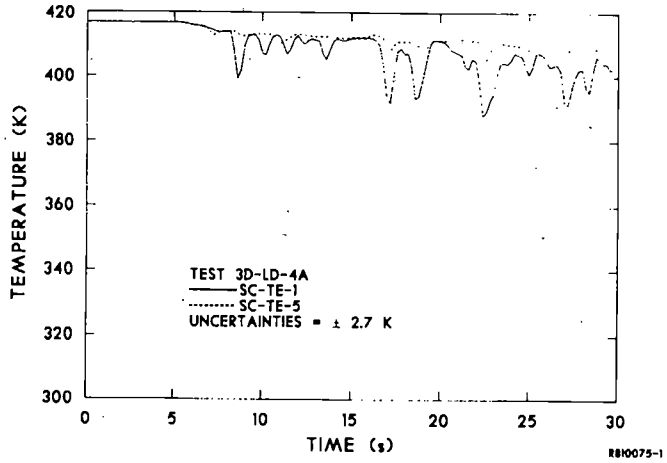

CCFL Correlations and Data

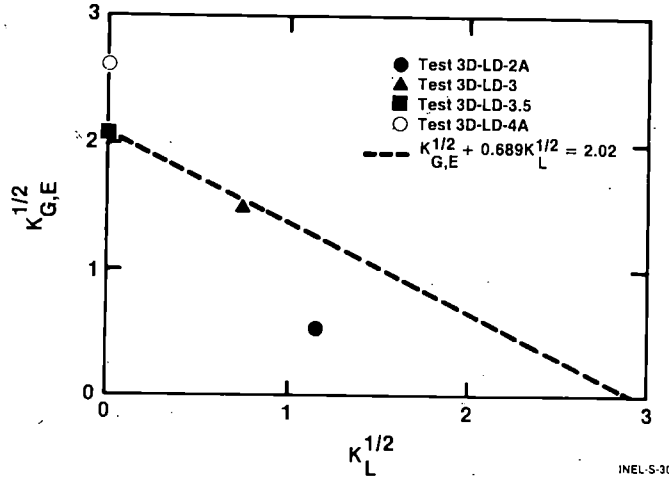

Cross Flow Below UCSP

- None at intermediate to high steam flows
- Evident at low steam flow

INEL-S-34 013

RADIAL TEMPERATURE DISTRIBUTION FOR HIGH STEAM FLOW

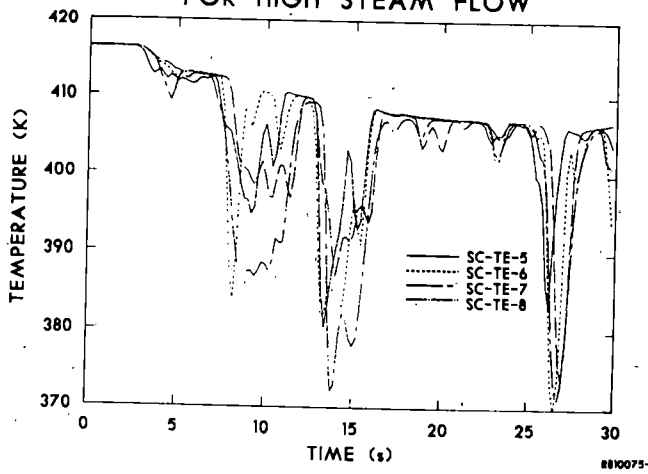

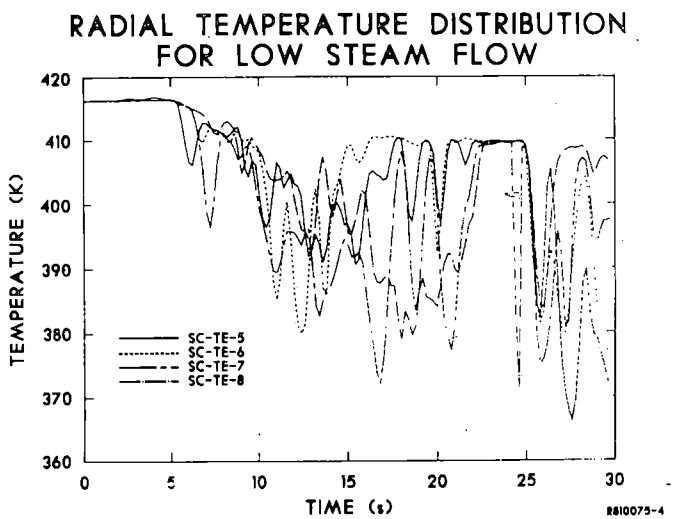

HLSP Mass Flow Consistent

- Reverse flow at low steam flow
- Oscillations at intermediate steam flow
- Positive flow at high steam flow

INEL-S-34 012

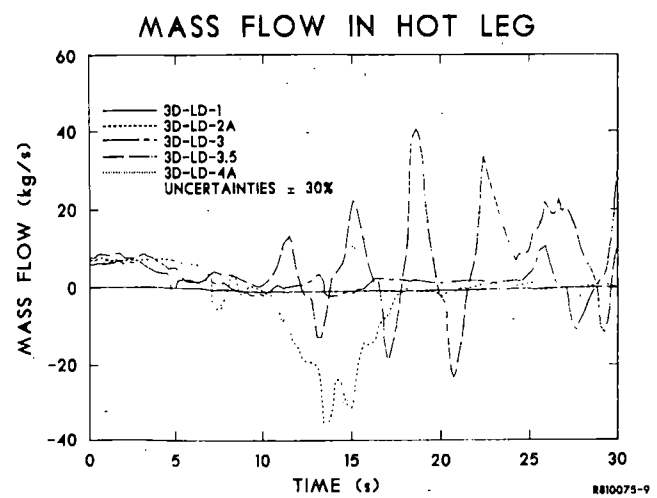

Comparison of TRAC-BD1 Results with Data

- Volume pressure
- Mass flow in hot leg
- Collapsed liquid level in slab core
- Temperature below core support plate

INEL-S-30 983

Hot Leg Spool Piece Pressure Comparison

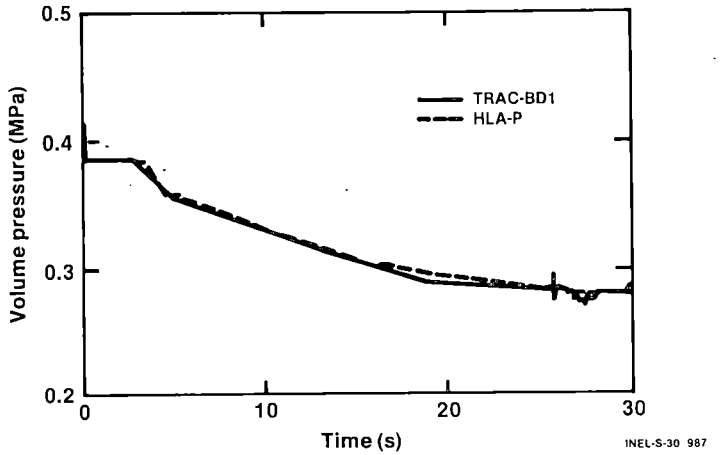

MASS FLOW RATE IN THE HOT LEG

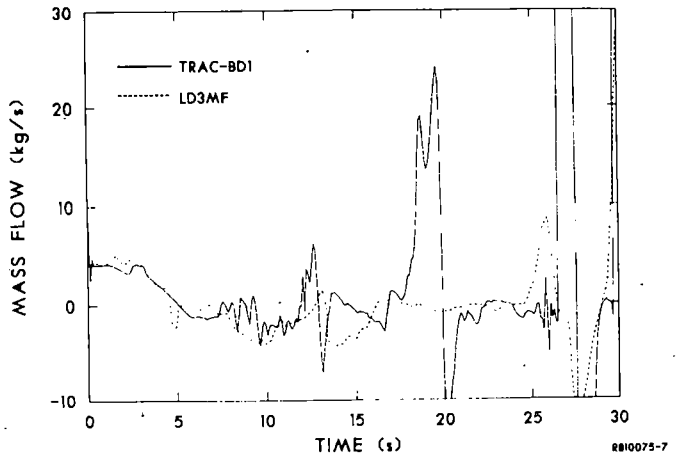

COLLAPSED LIQUID LEVEL

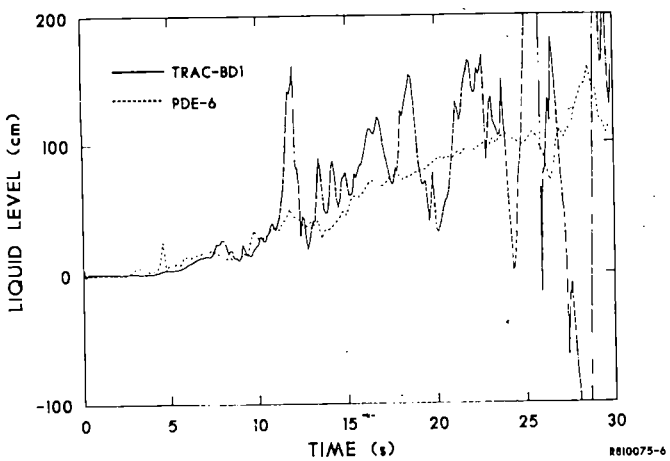

TEMPERATURE COMPARISON

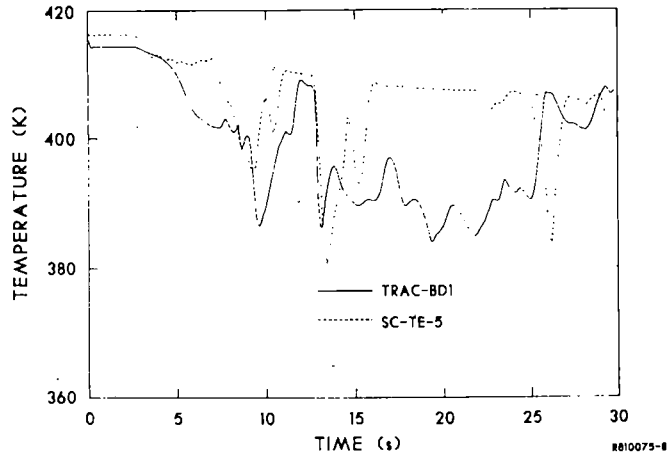

Conclusions

- Jet coherent only until froth buildup
- Test conditions bracket CCFL phenomena
- Evidence of cross flow at low steam flow
- Mixed results in TRAC comparison with data

INEL-S-34 015

JBC-10

UNION CARBIDE
ORNL

DAVID G. THOMAS
S. K. COMBS

INSTRUMENT DEVELOPMENT
LOOP PROGRAM

MEASUREMENT OF TWO-PHASE FLOW AT THE CORE UPPER PLENUM INTERFACE UNDER SIMULATED REFLOOD CONDITIONS

NINTH WATER REACTOR SAFETY RESEARCH
INFORMATION MEETING

GAITHERSBURG, MARYLAND
OCTOBER 26–30, 1981

MEASUREMENT OF TWO-PHASE FLOW AT THE CORE UPPER PLENUM INTERFACE UNDER SIMULATED REFLOOD CONDITIONS*

David G. Thomas and S. K. Combs

Oak Ridge National Laboratory
Oak Ridge, Tennessee 37830

The Instrument Development Loop (IDL) Program is part of the International 2D/3D Refill and Reflood Experimental and Research Program. The principal experimental facilities in the International Program are the Slab Core Experiment in Japan and the Upper Plenum Test Facility (UPTF) in Germany. Among the objectives of the International Program are: the study of the steam binding effect during reflood for various emergency core cooling combinatons; the study of the reflood flow distribution (chimney effect) in a heated core; and the study of the flow hydrodynamics in the core, downcomer, and upper plenum during refill and reflood.

A major problem is coupling the results to be obtained at the two major experiments. One approach is to measure the flows at the interface boundary of the two experiments and attempt to match them as closely as possible. Therefore the two major objectives of the IDL Program were to simulate expected flows at the core/upper plenum interface during the reflood phase of a postulated LOCA and to develop instrumentation systems for mass flow measurement at the core/upper plenum interface.

---

*Research sponsored by Division of Reactor Safety Research, U.S. Nuclear Regulatory Commission under Interagency Agreements DOE 40-551-75 and 40-552-75 with the U. S. Department of Energy under contract W-7405-eng-26 with the Union Carbide Corporation.

Two experimental facilities were used in these studies, a three-bundle air/water loop and a one-bundle steam/water loop. Both loops represent full-scale vertical sections of the UPTF, extending from spray nozzles to the top of the upper plenum and including a short length of dummy fuel rods, upper end boxes, core support plate, and control rod guide tubes.

Three flow regimes were identified and studied: (1) all liquid down, (2) counter-current flow in which gas (or vapor) goes up and liquid goes both up and down, and (3) cocurrent flow in which both gas (or vapor) and liquid go up. Instruments necessary to measure mass flow under these conditions are (1) tie-plate drag body or equivalently ΔP across tie plate, (2) free field turbine meter located above the tie plate or alternatively a string probe located above the tie plate, (3) temperature, (4) pressure, and (5) collapsed liquid level ΔP measurement. The tie-plate drag body was unique because it utilized part of the end box as a drag body and all transducers were contained within structural members of the end box. This meant that this instrument sampled a large amount of the flow with minimum disturbance to the flow.

Some of the significant achievements of the IDL Program include: the tie-plate drag body was developed and tested successfully; measurement with tie-plate drag body was shown to be equivalent to the ΔP measurement; the tie-plate drag body gave a useful measurement in pure downflow situations and the combination of drag/turbine correlates with mass flow for high upflow.

THE OVERALL OBJECTIVES OF THE INTERNATIONAL 2D/3D REFILL AND REFLOOD PROGRAM

- TO STUDY THE STEAM BINDING EFFECT DURING REFLOOD FOR VARIOUS ECCS COMBINATIONS
- TO STUDY THE RELFOOD FLOW DISTRIBUTION (CHIMNEY EFFECT) IN A HEATED CORE
- TO STUDY THE FLOW HYDRODYNAMICS IN THE CORE, DOWNCOMER AND UPPER PLENUM DURING REFILL AND REFLOOD

THE PRINCIPAL EXPERIMENTAL FACILITIES IN THE 2D/3D REFILL AND REFLOOD PROGRAM ARE SLAB CORE AND UPTF

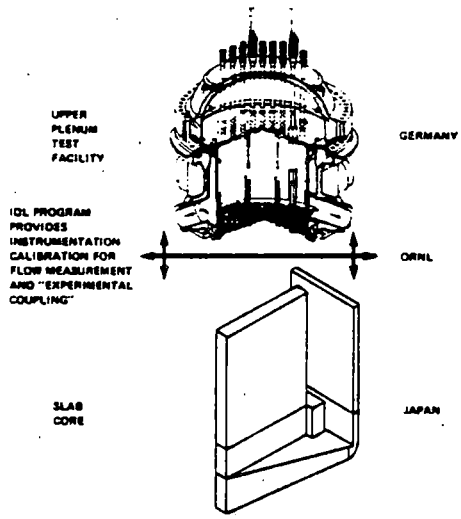

PRINCIPAL OBJECTIVES OF INSTRUMENT DEVELOPMENT LOOP (IDL) PROGRAM

- SIMULATE EXPECTED FLOWS AT THE CORE/UPPER PLENUM INTERFACE DURING THE REFLOOD PHASE OF A POSTULATED LOCA
- SCOPE POSSIBLE INSTRUMENTATION SCHEMES FOR MASS FLOW MEASUREMENT AT CORE-UCSP INTERFACE
- EVALUATE INSTRUMENT ACCURACY
- VERIFICATION OF INSTRUMENT SCHEME MODEL
- PHENOMENOLOGICAL STUDIES

INSTRUMENTATION SCHEME PROPOSED BY THE UNITED STATES

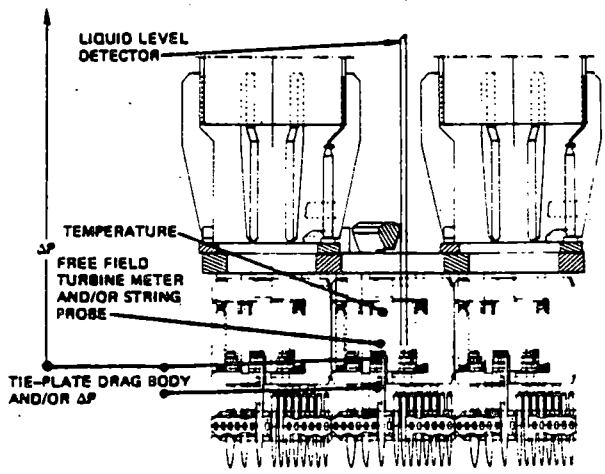

THREE KEY INSTRUMENTS AT CORE UPPER PLENUM INTERFACE ARE TIE-PLATE DRAG BODY, TIE PLATE TURBINE AND TIE PLATE ΔP

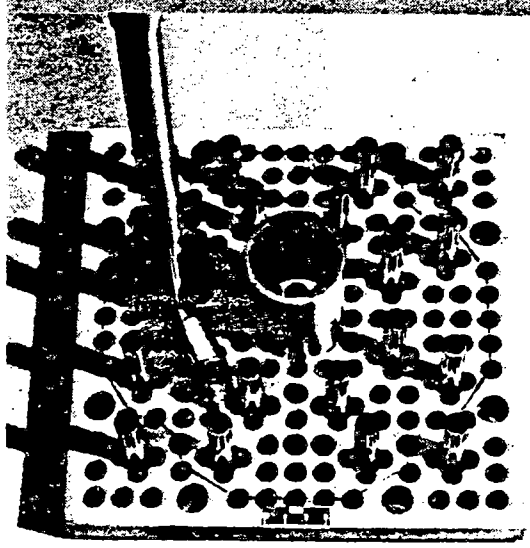

FLUID CARRIED OUT HOT LEG AS A FUNCTION OF CORE SPRAY WATER AND STEAM FLOW RATES AT 65 psia

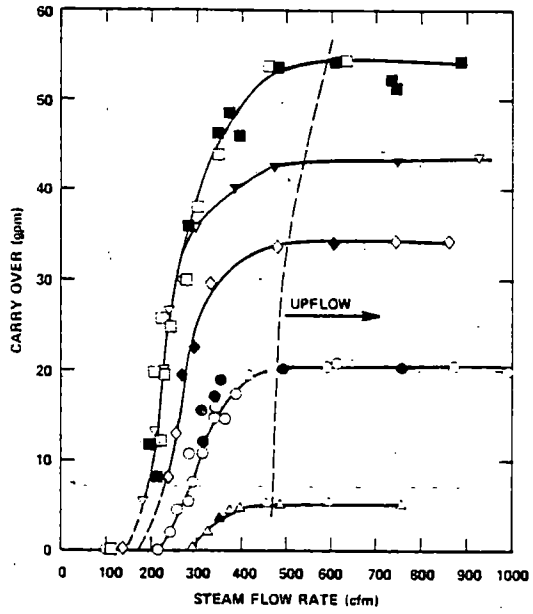

FLUID CARRIED OUT HOT LEG AS A FUNCTION OF CORE SPRAY WATER AND STEAM FLOW RATES AT 100 psia

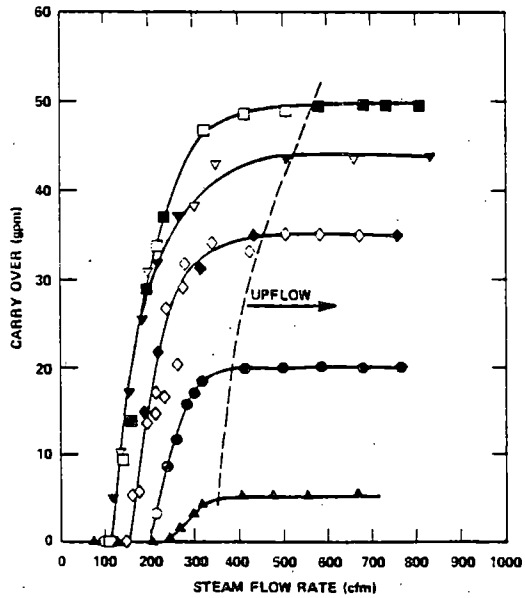

CORE SPRAY COUNTERCURRENT FLOW RESULTS FROM STEAM/WATER LOOP (COMBINED RESULTS FOR PRESSURES OF 30, 65 AND 100 psia)

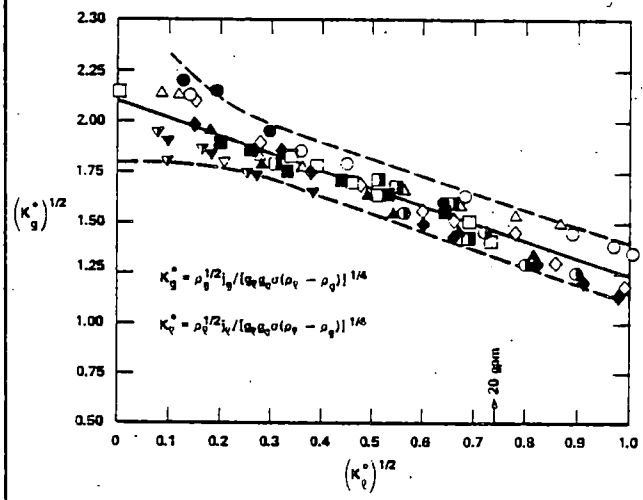

FLOW REGIMES OBSERVED WITH CORE SPRAY IN STEAM/WATER LOOP

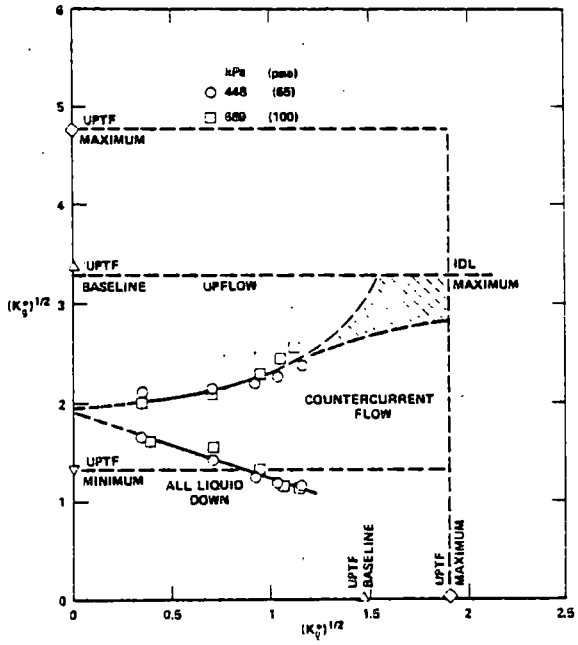

FLOW REGIMES OBSERVED WITH HOT LEG INJECTION IN STEAM WATER LOOP

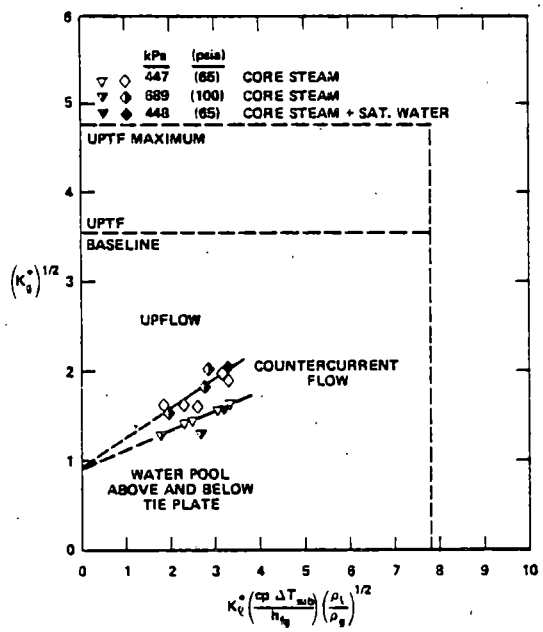

$$K_{gp}^* = K_g^* - f\,K_f^*\left(\frac{c_p \Delta T_{sub}}{h_{fg}}\right)\left(\frac{\rho_f}{\rho_g}\right)^{1/2}$$

MODEL EQUATIONS FOR CALCULATING MASS FLOW RATE THROUGH TIE PLATE

$$\left[G = \frac{lb_m}{(s)\ (module)}\right]$$

PRELIMINARY

- HIGH FLOW UPFLOW

$$G = \frac{2\rho_c}{K_{2\rho}} \frac{AREA}{MODULE} f\left(\frac{F_z}{A_{SDS} V_T}\right)$$

OR:

$$G = \sqrt{\frac{(1-\alpha)\,\rho_f\,g_c\,F_z}{A_{SDS}}} \frac{AREA}{MODULE}$$

- DOWNFLOW
  - NO SEAL ON TIE PLATE

$$G = \frac{g_c F_z}{\sqrt{2g_c h}} \frac{A_{STP}}{A_{SDS}}$$

  - SEAL ON TIE PLATE

$$G = C_1 \rho_f \sqrt{\frac{2g_c F_z}{\rho_f A_{SDS}}} \times \frac{AREA}{MODULE}$$

- COUNTERCURRENT FLOW

$$G = \text{LIQUID DOWN} = C_2 f\left(\frac{F_z}{V_g^{1/2}\,(DP-3)^2\,(1-\alpha)}\right)$$

$$G = \text{MASS FLOW UP} = C_3 f\left(\frac{F_z\,(DP-3)}{1-\alpha}\right)$$

WITH SINGLE PHASE STEAM FLOW THE MOMENTUM FLUX MEASURED BY THE DRAG BODY IS IN EXCELLENT AGREEMENT WITH MOMENTUM FLUX CALCULATED FROM MEASURED INPUT

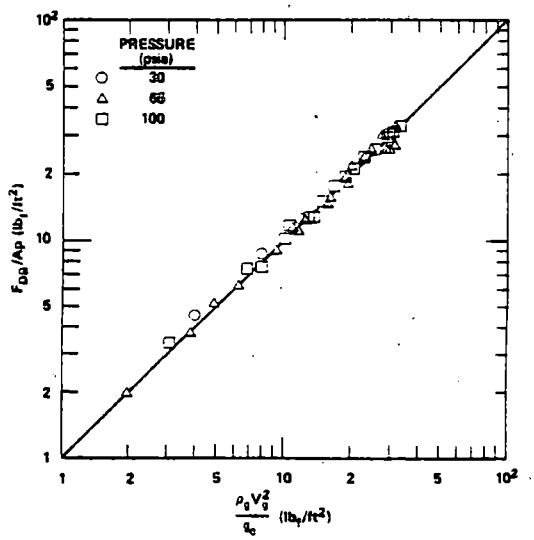

IN HIGH FLOW UPFLOW THE MOMENTUM FLUX MEASURED BY DRAG BODY IS IN GOOD AGREEMENT WITH MOMENTUM FLUX CALCULATED FROM MEASURED INPUTS AND VOID FRACTIONS

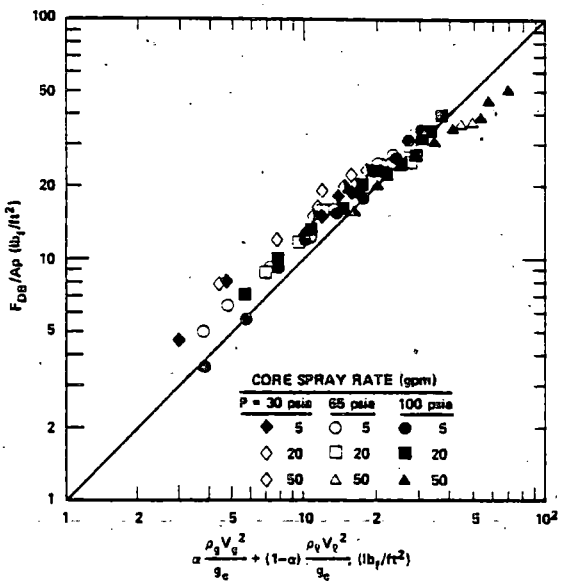

WITH 5 GPM CORE SPRAY THE RESPONSE OF THE TURBINE WAS A FUNCTION OF PRESSURE AND STEAM FLOW RATE

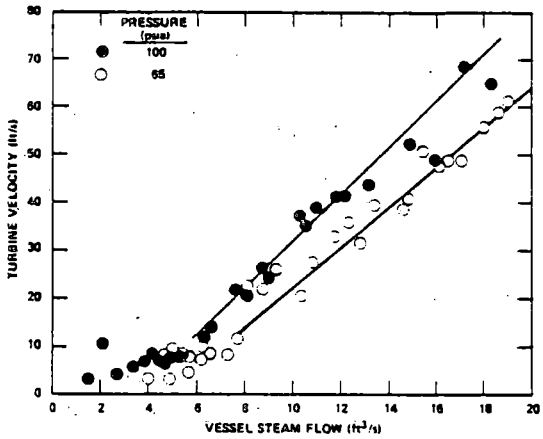

WITH 20 GPM CORE SPRAY THE TURBINE READING WAS SOMEWHAT LESS THAN WITH 5 GPM CORE SPRAY AT A FIXED STEAM FLOW RATE

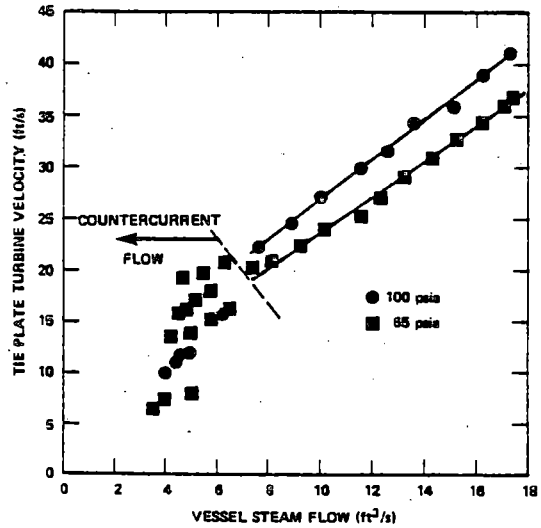

WITH 50 GPM CORE SPRAY THERE WAS A MARKED REDUCTION IN TURBINE READING COMPARED WITH 20 GPM CORE SPRAY AT A FIXED STEAM FLOW RATE

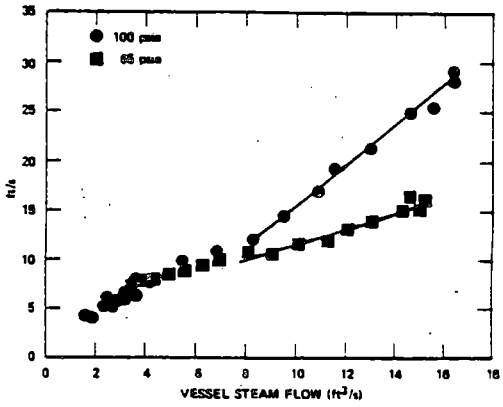

LIQUID FRACTION ABOVE THE TIE PLATE DECREASES MARKEDLY WITH STEAM FLOW RATE WITH 50 GPM CORE SPRAY

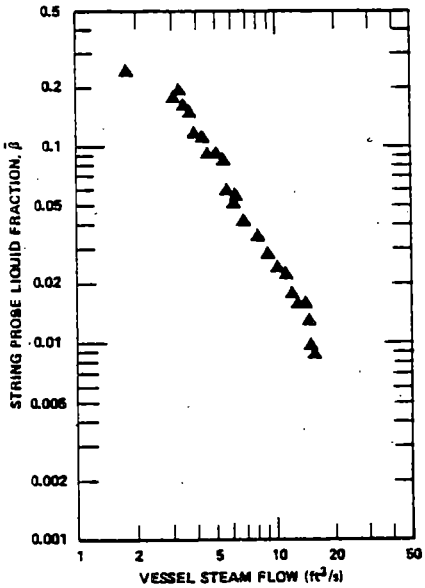

REDUCING THE CORE SPRAY RATE TO 20 GPM HAS LITTLE EFFECT ON THE LIQUID FRACTION–FLOW RATE RELATION COMPARED TO 50 GPM RESULTS

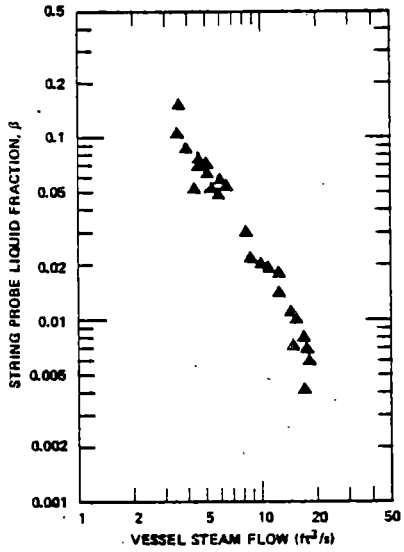

WITH ONLY 5 GPM CORE SPRAY, THE LIQUID FRACTION AT THE TIE PLATE IS CONSIDERABLY SMALLER THAN IN TESTS AT 20 AND 50 GPM AT COMPARABLE STEAM FLOWS

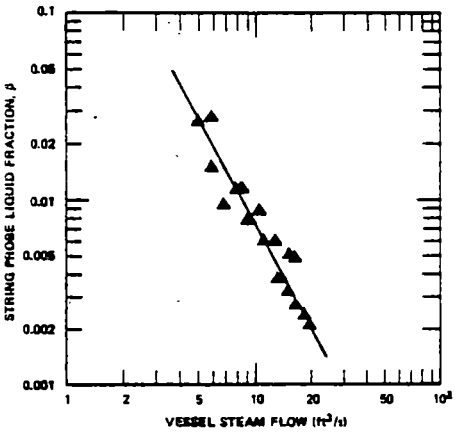

WITH CORE SPRAY, THE COLLAPSED LIQUID LEVEL IS A FUNCTION OF STEAM FLOW RATE AND WATER FLOW RATE AND IS ONLY WEAKLY DEPENDENT ON PRESSURE

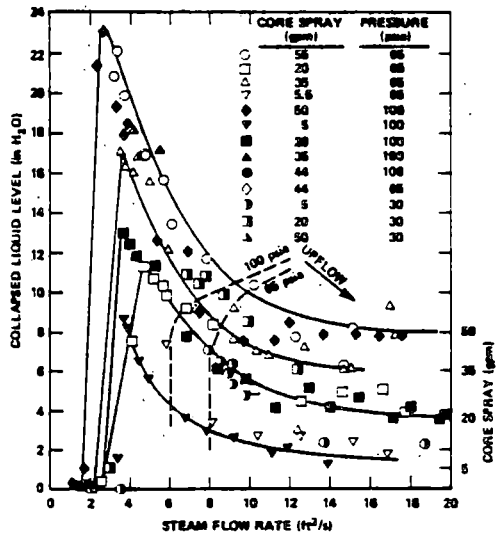

DOWNFLOW CALIBRATION OF TIE-PLATE DRAG BODY IN SINGLE MODULE LOOP

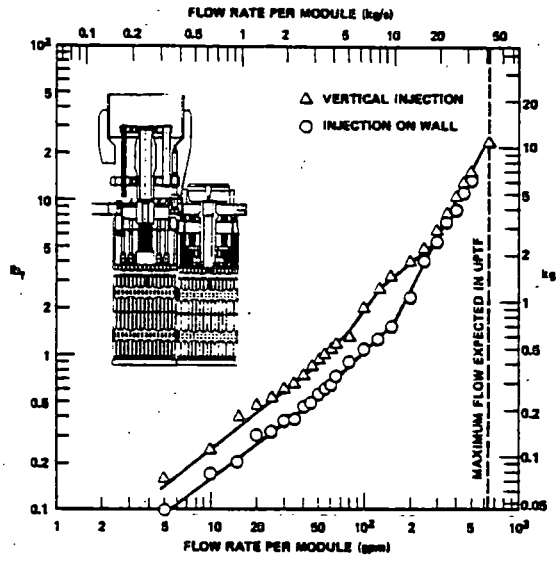

COUNTERCURRENT FLOW LIQUID-DOWN FLOW CORRELATION

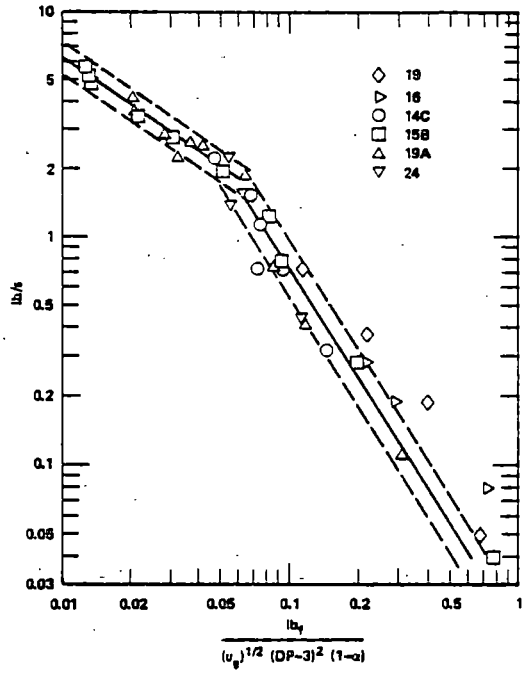

COUNTERCURRENT FLOW CORRELATION FOR MASS FLOW UP

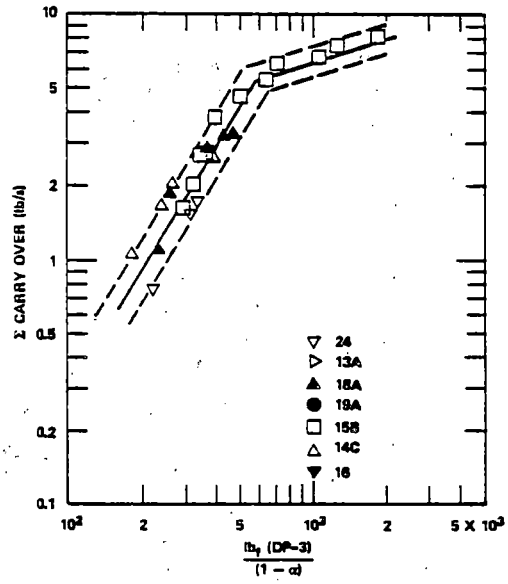

HIGH UPFLOW MASS FLOW RATE CORRELATION FROM SINGLE MODULE STEAM-WATER LOOP USING INEL TURBINE

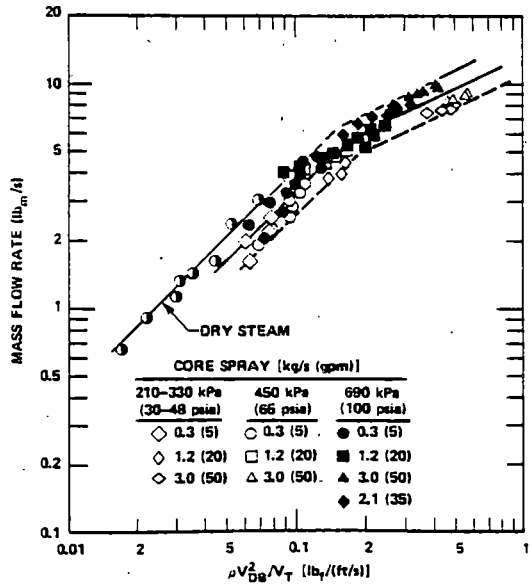

HIGH UPFLOW MASS FLOW RATE CORRELATION FROM STEAM–WATER LOOP USING INEL TURBINE AND PRESSURE DROP ACROSS TIE PLATE (5–50 GPM CORE SPRAY; 35–100 PSIA)

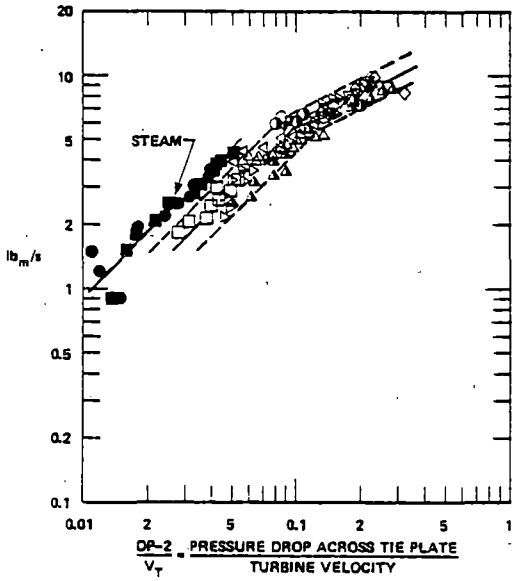

HIGH UPFLOW MASS FLOW RATE CORRELATION FROM STEAM–WATER LOOP USING DRAG BODY AND STRING PROBE VOID FRACTION

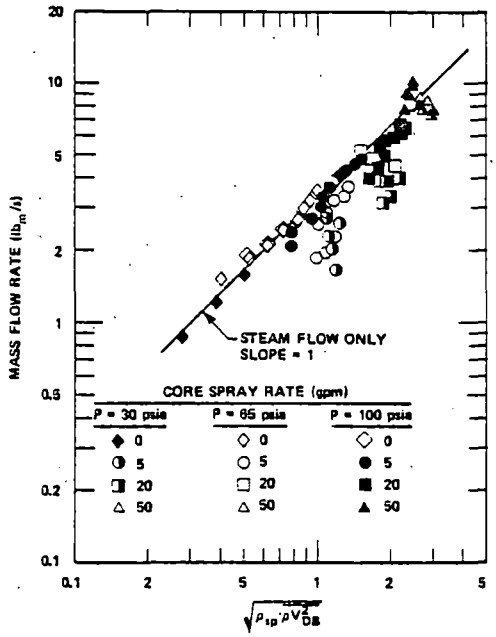

SWITCHING CRITERIA FOR CORE SPRAY ONLY

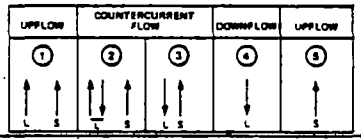

MODEL EQUATION		SWITCHING CRITERIA – CORE SPRAY ONLY	
		START	END
①	YES	REQUIRES FURTHER WORK	NA
②	YES YES	$\dot{m}_g = +$; DP-3 > 0	REQUIRES FURTHER WORK
③	NO	$\dot{m}_g = +$; DP-3 = 0	$\dot{m}_g = +$; DP-3 > 0
④	NO SEAL YES	$\dot{m}_g = +$; DP-3 = 0	$\dot{m}_g = +$; DP-3 > 0
	SEAL YES	$\dot{m}_g = +$; DP-3 > 0	NA
⑤	YES	$\dot{m}_g = +$; DP-3 = 0; $\sqrt{(\dot{m}_g - \dot{m}_{g,t})^2} = ?$	$\dot{m}_g = +$; DP-3 = 0; $\sqrt{(\dot{m}_g - \dot{m}_{g,t})^2} > ?$

HIGH FLOW UPFLOW RESULTS FOR HOT LEG INJECTION COMPARED WITH CORRELATION FOR CORE SPRAY ALONE

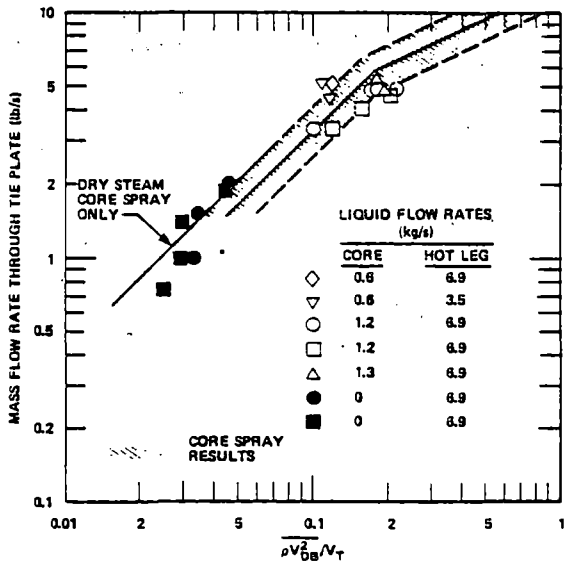

UNION CARBIDE
ORNL

SUMMARY

- IN HIGH FLOW UPFLOW WITH CORE SPRAY THE MASS FLOW RATE ACROSS THE TIE PLATE MAY BE DETERMINED FROM ANY OF THE FOLLOWING:
  - DRAG BODY/TURBINE
  - TIE PLATE ΔP/TURBINE
  - (STRING PROBE LIQUID FRACTION X DRAG BODY)$^{1/2}$
- IT APPEARS THAT THE SAME CORRELATION CAN BE USED FOR HIGH FLOW UPFLOW WITH CORE SPRAY, HOT LEG INJECTION OR CORE SPRAY + HOT LEG INJECTION
- IN COUNTERCURRENT FLOW WITH CORE SPRAY, THE MASS FLOW RATE IS A FUNCTION OF MOMENTUM FLUX (DRAG BODY), COLLAPSED LIQUID LEVEL AND LIQUID FRACTION AT THE TIE PLATE
- IN DOWNFLOW WHEN THERE IS NO BACKPRESSURE FROM STEAM INJECTION THE MASS FLOW RATE CAN BE DETERMINED FROM THE DRAG BODY SIGNAL ALONE

The Large-Scale Melt Facility*

T. Y. Chu
Sandia National Laboratories**
Albuquerque, NM

Abstract:

The Large-Scale Melt Facility is a reactor safety research installation developed at Sandia for the study of core meltdown and degraded core accidents. The facility allows preparation and manipulation of melts of UO_2/ZrO_2 weighing up to 500 kg and at temperatures up to 3000 K. Features of the facility, planned tests, and instrumentation are described.

Large Melt Facility

The facility was designed to produce superheated oxidic melts in the range of 100 kg to 1000 kg for reactor safety related material interaction studies. Currently, the maximum operating temperature of the furnace is 2750°C and the expected superheat of the melt is 175°C. The construction and operation of this facility required significant advances in the state of high temperature material technology and instrumentation.

Facility Design and Operation

The main components of the facility are shown in Figure 1. The induction melting furnace is powered by a 280 kW, 1000 Hz generator. The power is coupled into a graphite susceptor with a coupling efficiency of approximately 60%. Except for a bottom tapping channel, the tantalum alloy crucible for the melt charge is totally enclosed by the susceptor, see Figure 2. The choice of the material and geometry was based on extensive material compatability studies and thermal modelling. To achieve a reasonable packing density and improved thermal properties, the charge, 70% UO_2 and 30% ZrO_2 (stabilized by Y_2O_3) by weight, is hot pressed from powders of raw materials to 70% of theoretical density. The liquidus temperature of the charge was experimentally determined to be 2575°C.

The furnace is located on a platform with an experimental chamber directly under it, Figure 3. During operation both the furnace and the chamber are purged with argon to achieve an inert atmosphere slightly above ambient pressure. Once melting begins, the furnace as well as the experiment are controlled remotely from a building approximately 100 meters away, see Figure 1. The melt is tapped by firing a double barrel 12 gauge shotgun into the bottom of the melt crucible.

Furnace Instrumentation

Because of the low thermal diffusivity of the melt charge, the rate of energy input into the charge is limited; excessive energy input into the susceptor will lead to catastrophic melting of the crucible. Furthermore, the melting phenomenon in the charge is very complex and the melting time cannot be accurately predicted. It is, therefore, extremely important to be able to monitor the temperature in the susceptor and the charge during heating and melting of the charge. For temperatures below 2300°C tungsten rhenium alloy thermocouples are used. For temperatures above 2300°C optical pyrometer is used to monitor the surface temperature of the susceptor. For interior temperature measurements two relatively new methods are used:

a) Ultrasonic thermometers:

The instrument is based on the temperature dependance of the velocity of sound in a sensing wire. This type of sensor has been used successfully in a number of in-pile experiments at Sandia for temperature profile measurements. Additional developments in sensor design, calibration, signal processing and material compatability were required to adapt the sensor to the furnace application. Four tungsten sensors with tantalum sheaths, 3 mm diameter 50-75 cm long with up to 8 sensing elements, are used in the furnace--two in the graphite susceptor and two in the melt charge.

b) Capillary Pyrometer

This device is based on the temperature dependence of gas viscosity. A schematic of the device is shown in Figure 4. The pressure differential

required to push a constant amount of gas through a capillary is monitored. The pressure signal is first amplified by several stages of laminar fluidic amplifiers; the amplified signals are then monitored by conventional pressure transducers. Two will be used--one in the charge and one in the susceptor.

Test Instrumentation

The coming experiment planned for the Large Melt Facility is the interaction of UO_2/ZrO_2 melt with MgO Harklase bricks. The test makes use of a crucible made of these bricks 66 cm deep and 36 cm in diameter, see Figure 5. The main quantitites of interests are thermal responses of MgO, erosion, heat flux partitioning, thermal shock characteristics, gap penetration, brick flotation, aerosol, and gas generation. In addition to standard instrumentations of thermocouples, heat flux gages and pyrometer, Figure 6, two novel techniques were developed for the test:

a) Thick Film Crack Detector

This is used to determine the direction as well as speed of cracking of the bricks. A number of thick film resistive grid networks are deposited on a brick, Figure 7. As a crack crosses a resistor a voltage change is detected in the output circuit. By determining sequences of voltage steps the velocity as well as the direction of the crack propagation can be resolved.

b) Teflon Ablation Heat Flux Sensor

The deposition of aerosol generated during melt/material interaction presents a problem for conventional heat flux gages. To overcome this problem a teflon heat flux gage consisting simply of a 5.1 cm diameter teflon cylinder insulated on the side with the bottom facing the melt is used to measure the upward heat flux from the pool. Since teflon undergoes ablation the exposed surface is continuously renewed. By monitoring the interior temperature of the teflon it is possible to estimate the heat flux at the exposed surface.

Deposition of a large quantity of melt provides an excellent opportunity to study aerosol generation and decay. The experimental chamber is, therefore, equipped with a variety of devices to examine the aerosols.

c) Aerosol Instrumentation

Inertial impactors are used to obtain particle size distributions and filter samplers are used to measure total suspended mass of particles. A two frequency aerosol photometer based on attenuation measurements will be used to obtain mass loading. Two thermophoretic samplers placed next to the crucible are used to collect source aerosols and two canisters are used for collecting larger source particles, see Figure 5. Finally, collection plates will be attached to walls of the chamber to determine deposition mass on walls.

Planned Tests

Two more tests are planned following the MgO test:

a) Melt/Basalt Concrete Interaction

In addition to quantities of usual interests, the experiment will also test one or more filter vent systems and some in-containment cooling devices.

b) Rubble Bed Test

This experiment will test the concept of a thoria rubble bed as a core retention device.

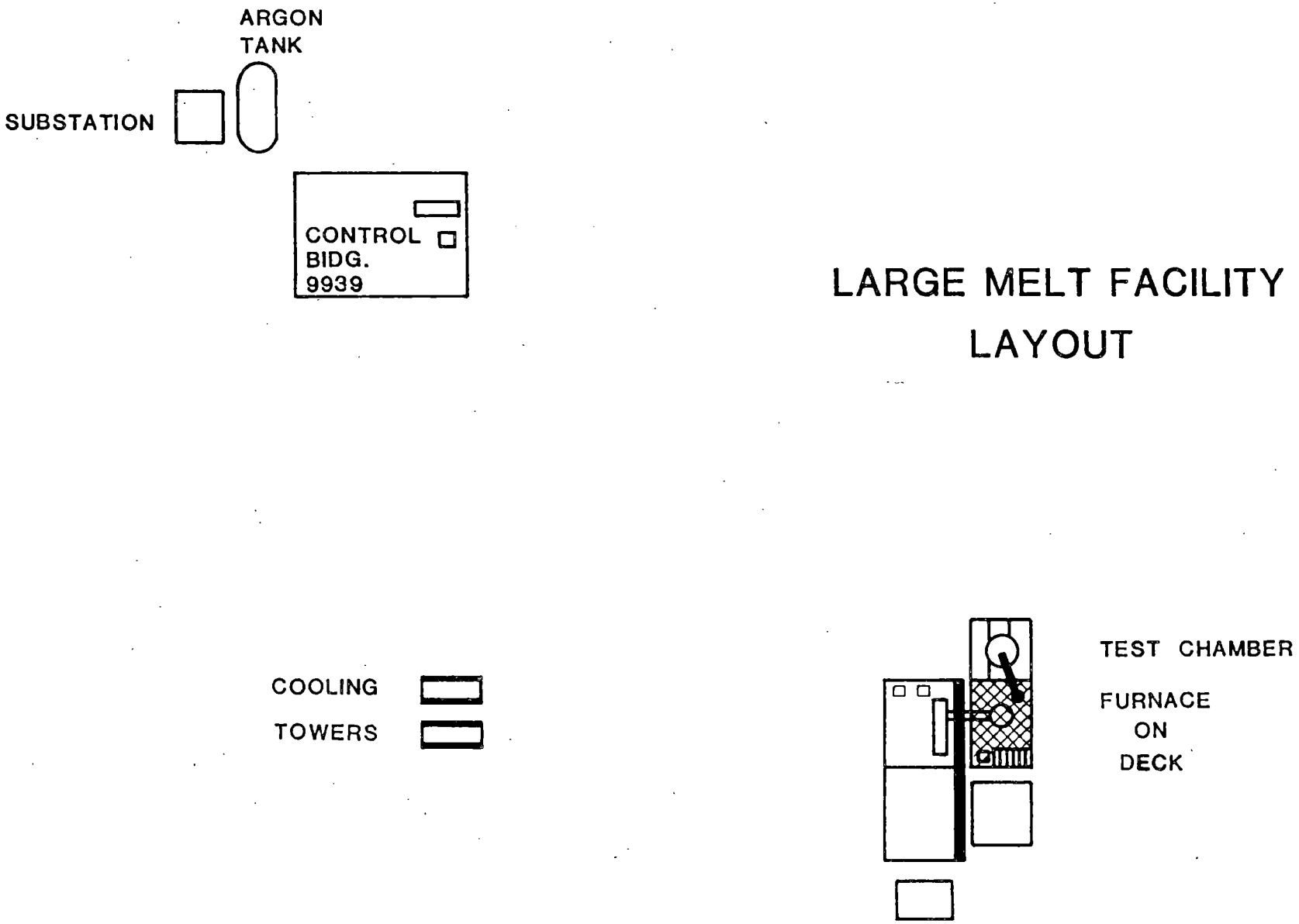

Figure 1 Large Melt Facility Layout.

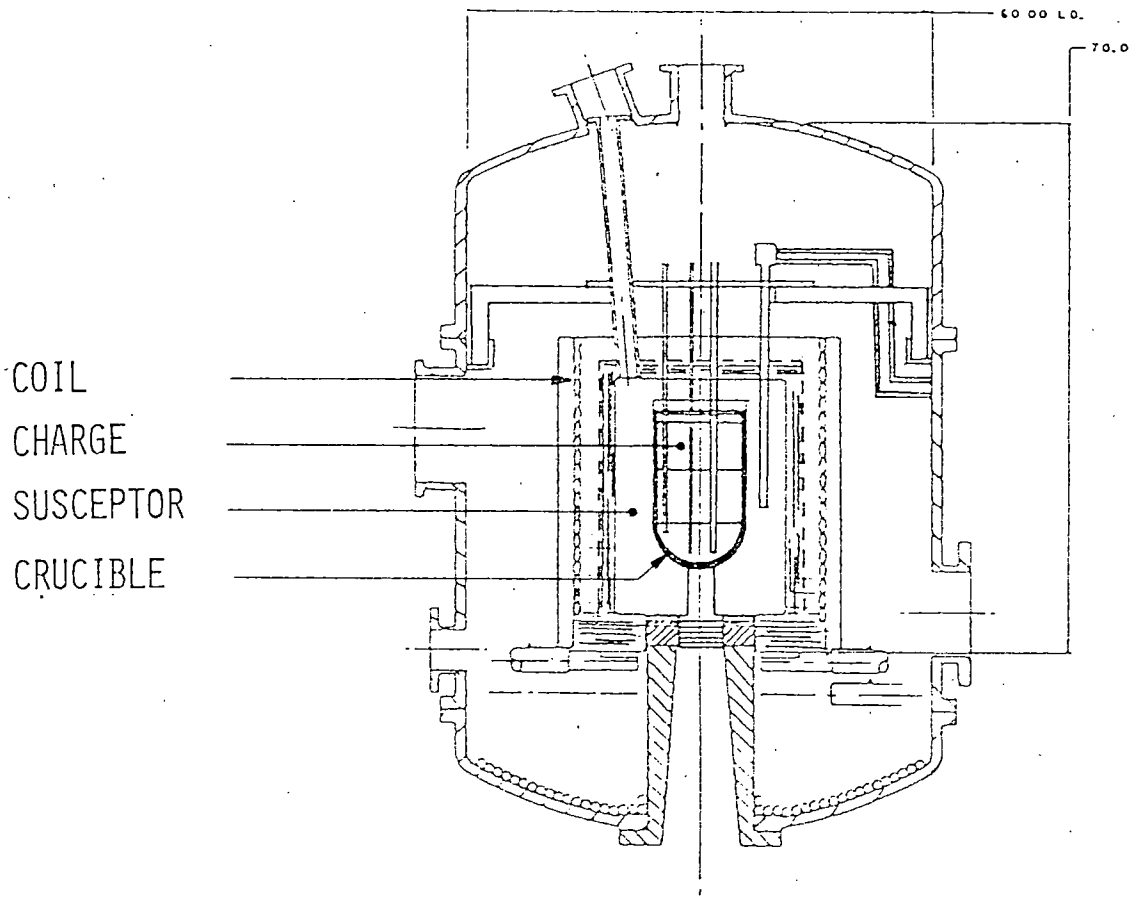

FIGURE 2 FURNACE CROSS SECTION

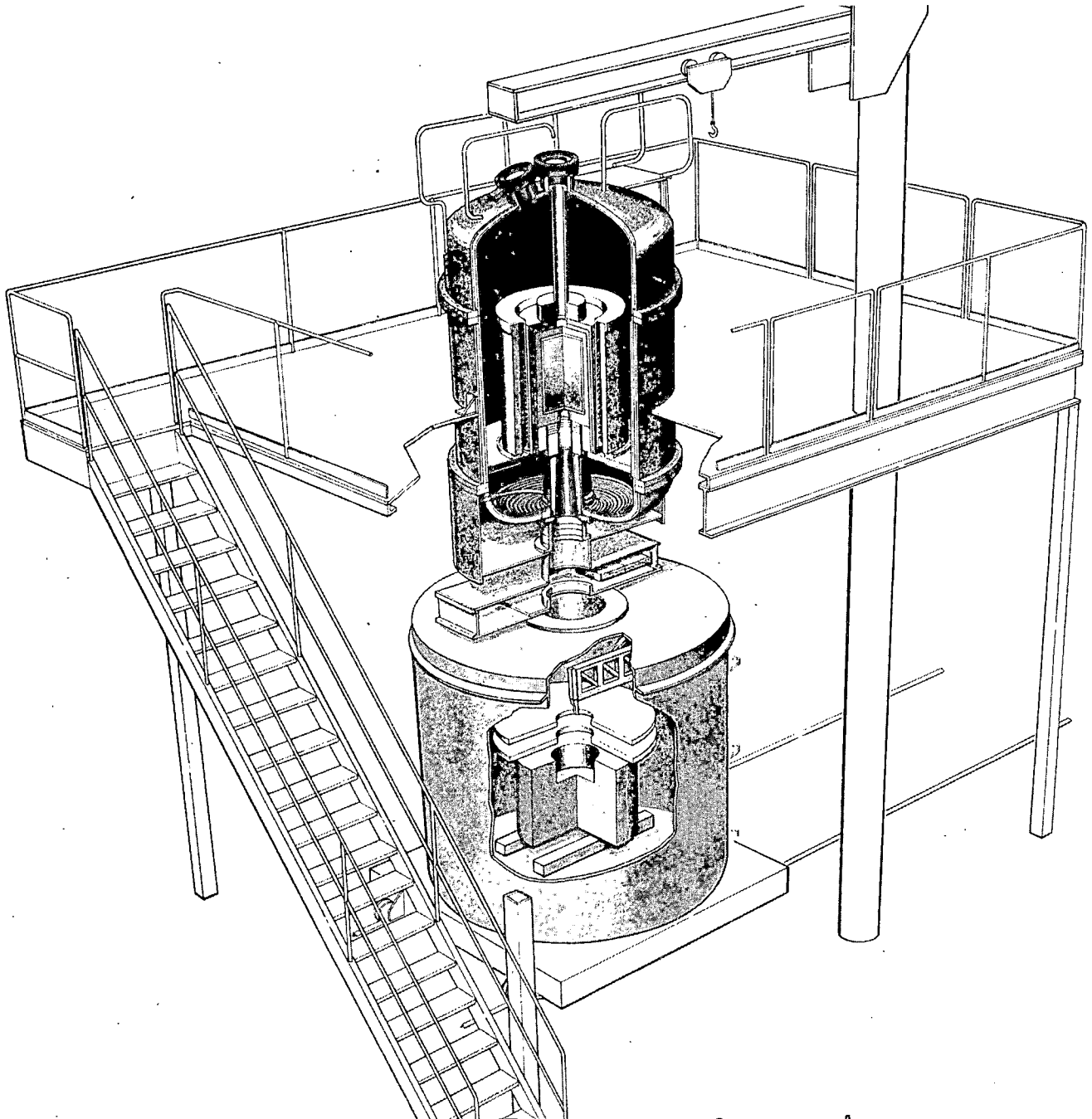

FIGURE 3 FURNACE/EXPERIMENTAL CHAMBER ASSEMBLY

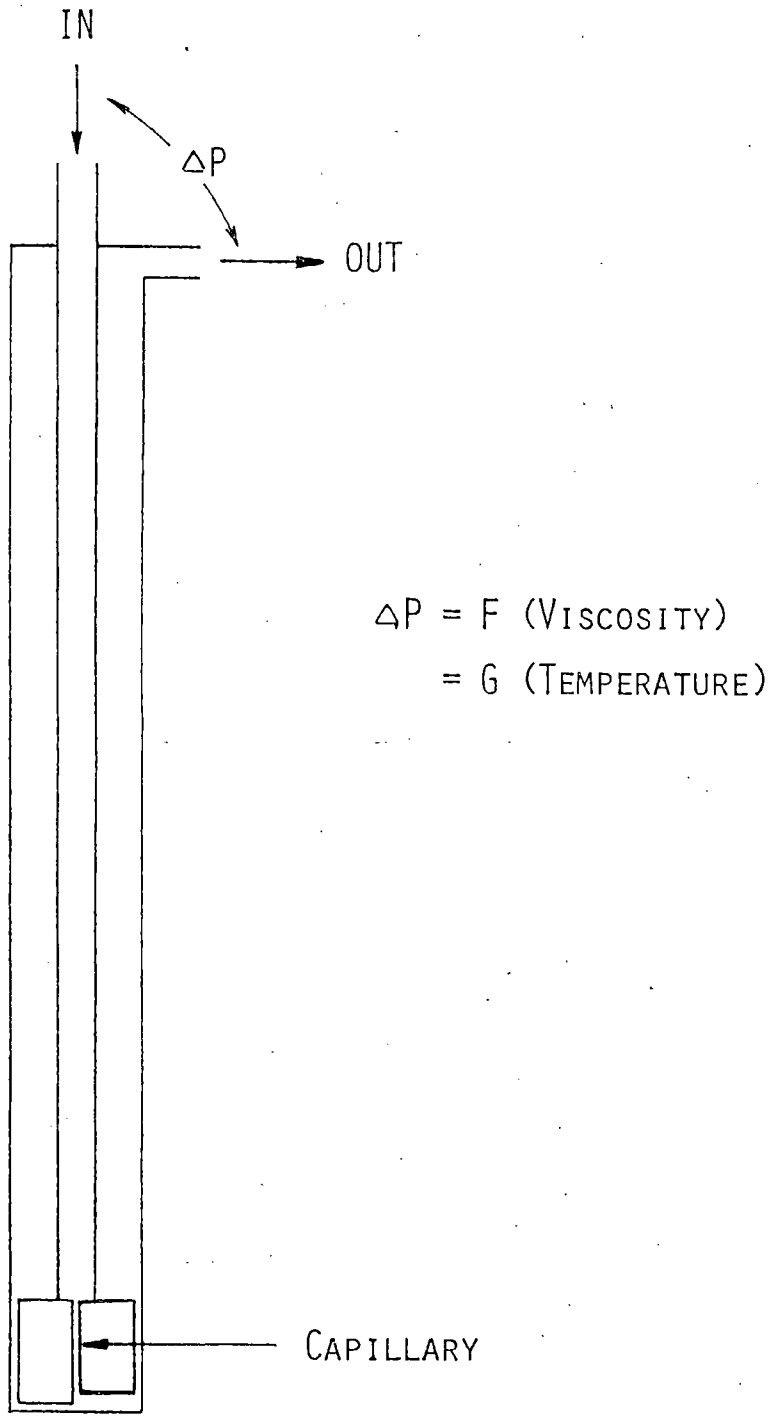

FIGURE 4 SCHEMATIC OF CAPILLARY PYROMETER

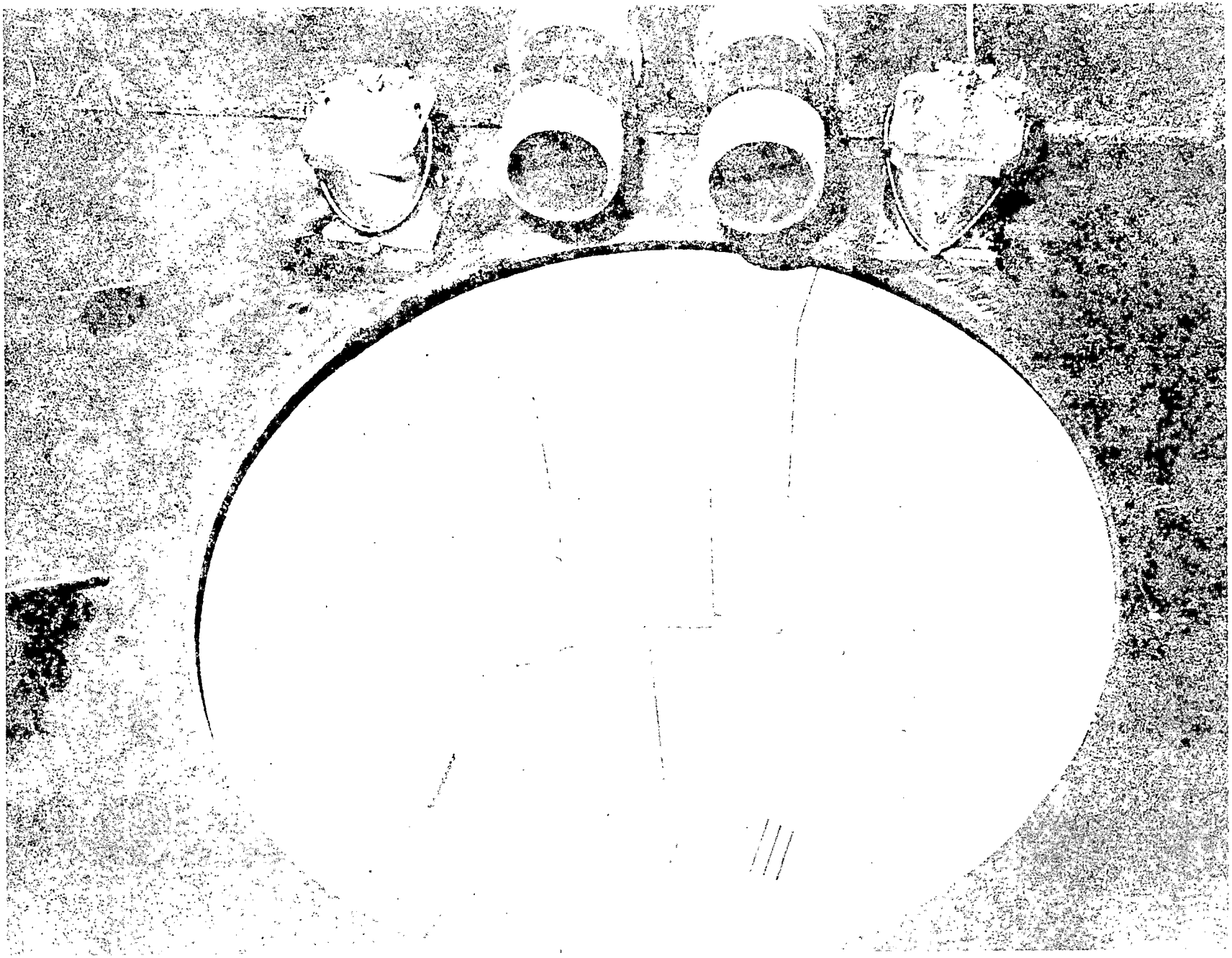

Figure 5 MgO Cavity, also shown are entrance to aerosol samplers and particle collecting canisters

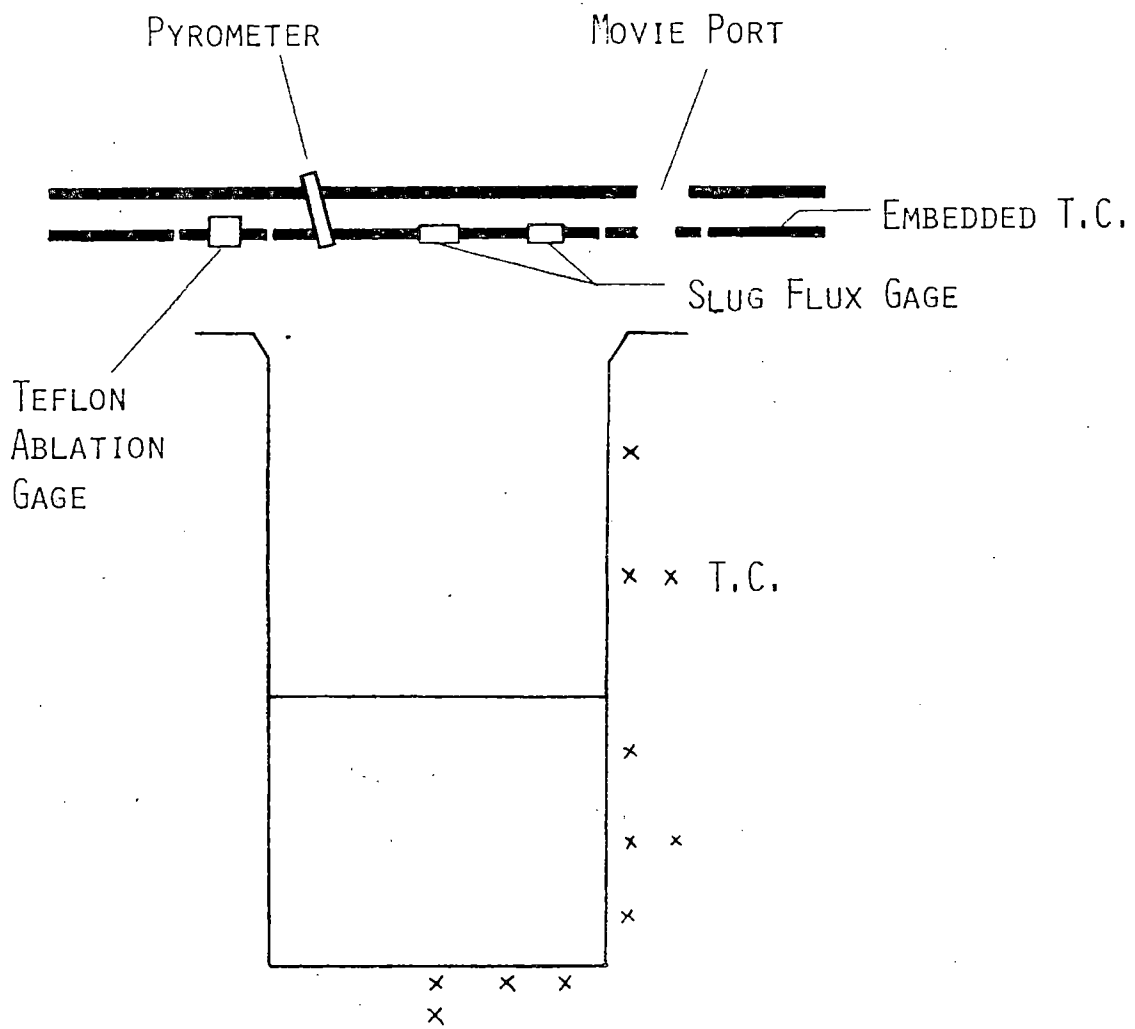

FIGURE 6 THERMAL INSTRUMENTATION OF MgO CRUCIBLE

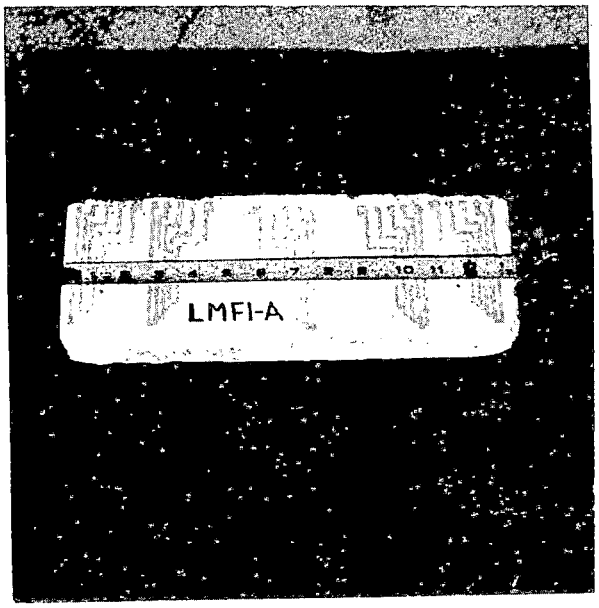

FIGURE 7 THICK FILM CRACK DETECTOR

CORE/CONCRETE EXPERIMENTS AT SANDIA NATIONAL LABORATORIES*

W. W. Tarbell

Ktech Corporation**
Albuquerque, NM 87110

ABSTRACT

An overview of Sandia's core debris/concrete interaction test program is presented. Results from both high temperature (3000°K) and hot-but-not-molten core-concrete tests are given. Gas generation, aerosol production, heat flux from the debris, and concrete erosion data are presented and compared with previous test data. The solubility of core debris in structural materials is discussed. The results indicate that debris materials do not remain in solution at typical cooling rates. Test plans for the future are discussed.

* This work supported by the U.S. Nuclear Regulatory Commission.

** Work performed under contract to Sandia National Laboratories.

INTRODUCTION

Severe reactor accidents can lead to the escape of core debris from the reactor vessel and subsequent attack on containment cavity materials. The objective of this effort is to provide generic data on core debris attack on structural concrete materials. Quantitative data on gas generation, combustible gas production, aerosol generation, heat flux from the debris, and the erosion of concrete are obtained experimentally. The effect of coolant on the debris bed interaction is addressed. Emphasis is placed on conducting experiments with prototypic materials under realistic conditions.

Figure 1 presents a generalized reactor accident temperature-time profile that permits definition of four phases of the melt-concrete interaction. Representation of available data on the curve illustrates the quantitative lack of information in the ultra-high and low temperature regions. These two phases are particularly devoid of information required to develop and optimize models of core debris interactions with concrete.

HIGH-TEMPERATURE PHASE EXPERIMENTS

The ultra-high temperature phase is studied using molten debris simulants generated from metallothermic reactions. Both aluminothermic ($8Al + 3Fe_3O_4 \rightarrow 4Al_2O_3 + 9Fe$) and uranothermic ($2U + Fe_3O_4 \rightarrow 2UO_2 + 3Fe$) reactions have been employed to produce melts up to 30 kg in size at temperatures of 2800 to 3300°K. When brought into contact with basaltic or calcareous aggregate concrete, large quantities of gases, water vapor, and aerosols are released. Instrumentation is employed to quantify the amount and identify the species of the liberated gas and particulate matter. Additional devices monitor the upward heat flux, concrete temperature and pressure within the concrete cavity. Of particular note is the use of enhanced X-ray real-time imaging to monitor the interactions

at the melt-concrete interface. This technique allows direct observation of the attack on the concrete to identify and verify interaction models.

The initial test in the series consisted of 20 kg of iron oxide thermite in a basaltic crucible with a 22-cm diameter x 41-cm deep cavity. Instrumentation included gas flow, temperature and composition, upward heat flux, and cavity overpressure measurement devices. Figure 2 is a plot of the upward heat flux and gas temperature obtained for the test. The initial peak represents the thermite burn front reaching the bottom of the cavity. Gas generation increases until the melt begins to solidify, whereupon the rate decreases.

The gas composition and generation with time are presented in Figure 3. The gas was created by thermally liberating water and carbon dioxide from the decomposing concrete. These species were reduced to carbon monoxide and hydrogen as they passed through the melt.

Figure 4 gives an indication of the relative generation with time based on recovered filter samples. Chemical composition and sizing has yet to be completed. Three formation mechanisms are considered. The first is hydrodynamic, in which particles are produced by melt activity such as bubble bursting and splashing. Particle diameters in excess of one micrometer and concentrations of 10^3 or 10^4 particles per cubic meter would be expected. The other two mechanisms involve the gas phase of the reaction products and could be expected to produce the bulk of the aerosol mass. The first of the two mechanisms is formation by homogeneous or heterogeneous nucleation of material vapor as it cools and becomes super-saturated. The other is a chemical formation involving products from particulate and gas-particulate reactions in which the particle undergoes a change such as breakup.

Aerosol instrumentation for the test described above included an MRI cascade impactor and four filter samples. Preliminary analysis of the data indicates aerosol mass concentration on the order of 10 to 20 g/m^3.

Table 1 outlines the transient tests planned for the future. These experiments are directed toward addressing the effect of geometry on the interaction. Of particular interest is the variation of melt-to-concrete heat transfer over the transition region between the vertical sidewall and bottom of the cavity and the behavior of the non-planar surfaces such as eroded sidewalls.

A large scale test using Sandia's Large Melt Facility (MLF) is planned for the third quarter of FY82. The test will involve 200 kg of UO_2/ZrO_2 melt streaming into a basalt concrete crucible. The crucible will be contained within an enclosure to permit collection of gases and other by-products. The apparatus will employ several filtered-vent systems to assess performance of these devices. There will also be a number of in-containment devices such as heat transfer panels within the experimental chamber to ascertain the degradation in performance produced by the deposition of large quantities of aerosols formed during the melt interaction.

LOW-TEMPERATURE EXPERIMENTS AND TESTS WITH COOLANT

This test series is designed to study the reaction of hot-but-not-molten core debris attacking concrete. The objective of the low-temperature phase of the program is to address four main questions: (1) at what point does the attack on concrete cease? (2) what is the relationship between input power and concrete attack? (3) how does the interaction scale with geometric features and size? and (4) what is the effect of coolant on the interaction? The test matrix addresses the effect of input power, debris geometry, debris mass, and duration during interactions with two generalized concrete types. Table 1 illustrates the experimental matrix and the variation in the experimental parameters that will

be achieved. The program also incorporates direct comparison tests with and without the presence of coolant.

The available data for UO_2 solubility in natural or synthetic silicate compositions is poor and quite inconsistent. Typical solubilities range from 5 to 60 wt. % at 1823°K. Therefore, a series of experiments was made to determine the solubilities of both UO_2 and ZrO_2 (in a 4/1 wt. % ratio which is equivalent to a typical Light Water Reactor [LWR] core) in silicate melts under oxidizing conditions at temperatures ranging from 1473 to 1823°K.

Three types of common silicate rocks were used in these experiments: basalt, granodiorite, and granite (see Table 2 for chemical analysis). Most of the study was directed toward basaltic compositions because of preliminary results which yielded higher UO_2 and ZrO_2 solubilities. The phases observed in the samples after heating for one hour are given in Table 3 along with the UO_2 and ZrO_2 contents of the glass. It is apparent from these results that basaltic melts are better solvents of UO_2 and ZrO_2 than are the more siliceous compositions. Furthermore, silicate melts high in UO_2/ZrO_2 content will quench to glasses only at very fast cooling rates (100°K/sec). At slower cooling rates (even as fast as 2°K/sec), oxide phases like MgU_2O_6 and ZrO_2 precipitate from the melt. Because of the very slow cooling rates hypothesized for a meltdown event, silicate rocks do not appear to be feasible as sacrificial barrier material.

One hot-solid test has been conducted to date. This preliminary experiment involved a 50-kg monolithic solid of 304 stainless steel in contact with a basalt crucible. Cavity size was nominally 22 cm in diameter by 46 cm deep. The objective of the test was to ascertain that the power generation within the debris was sufficient to drive the debris into melt.

Figure 5 depicts the block temperature history. Total heating time was approximately three hours with a nominal power density of 0.1 watt/g. The mean temperature of the block was above the concrete ablation point for approximately 80 minutes. Note that the onset of crust formation coincided with a sharp change in the temperature profile. The crust was purposefully penetrated approximately 20 minutes after formation to determine if it would reappear. Unfortunately the test was terminated prematurely due to shorting of the inductive coils. At the time the power was removed, the crust had reformed across the entire cavity opening. Inspection of the cavity at this point revealed gas escaping and spontaneously igniting through and about the perimeter of the crust. The crust itself appeared to be very viscous with several well formed penetrations.

Approximately 25 minutes after power termination, the cavity above the melt was flooded with tap water. The net effect was a rapid drop in the block temperature with no apparent change in the concrete or in the crust other than a darkening in color. The water did not immediately turn to steam, but was a more gradual process occurring over several minutes. All of the water eventually was boiled off or drained through cracks in the concrete. The process was repeated two additional times with the same net result.

A posttest dissection of the crucible revealed considerable downward and sideward erosion. Figure 6 represents the reconstructed cross-section of the crucible at the point of greatest sideward attack. The final melt shape indicated that the temperature of the block was sufficient to cause some melting. Because the start of sidewall erosion coincided with the original block shape, there was indication that the recession began while the block was still solid.

Diagnostics employed during this test were not adequate to assess the rate of attack. However, if we assume that the movement was linear during the time the block was above the concrete ablation temperature, an erosion rate of 5 to 6 cm/hour downward and 4 to 5 cm/hour in the horizontal direction are obtained. These data can be compared with previous test results (Burn 2 and Burn 3) that demonstrated erosion rates of 3 to 4 cm/hour for debris heated through the low-temperature phase into full melt.

The second test to be conducted consists of a basalt crucible identical to that described above charged with 70 kg of steel spheres. The purpose of the test is to simulate a core debris mass that has fragmented and quenched, with subsequent heating to a temperature above the concrete melting point. Steel spheres 2 to 10 mm in size will be used as the debris. Additional diagnostics will be employed to obtain gas and aerosol generation rates and composition, concrete temperature, heat flux direction and extent, and erosion rate of the concrete. Attempts will be made to determine the onset and strength of crust formation.

A third test is planned to duplicate the second test described above except that coolant will be placed on the debris. The purpose of this experiment will be to determine if the bed will dry out and subsequently begin attacking the underlying concrete. The level of water above the melt will be maintained and mechanisms for condensing the water vapor will be employed. The two tests will allow direct comparison of the effect of coolant on the interaction.

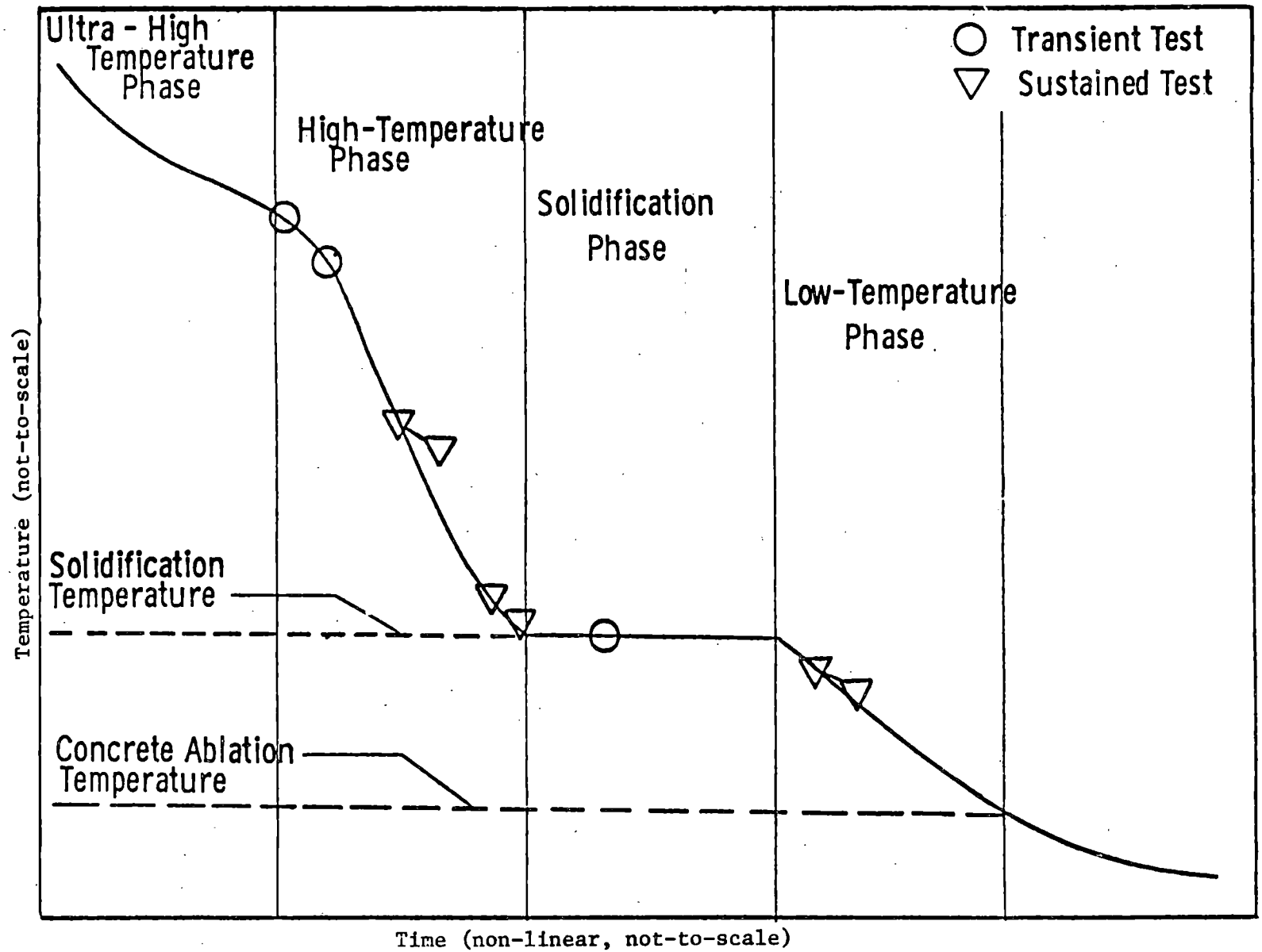

Figure 1. Hypothetical temperature-time history for reactor accident.

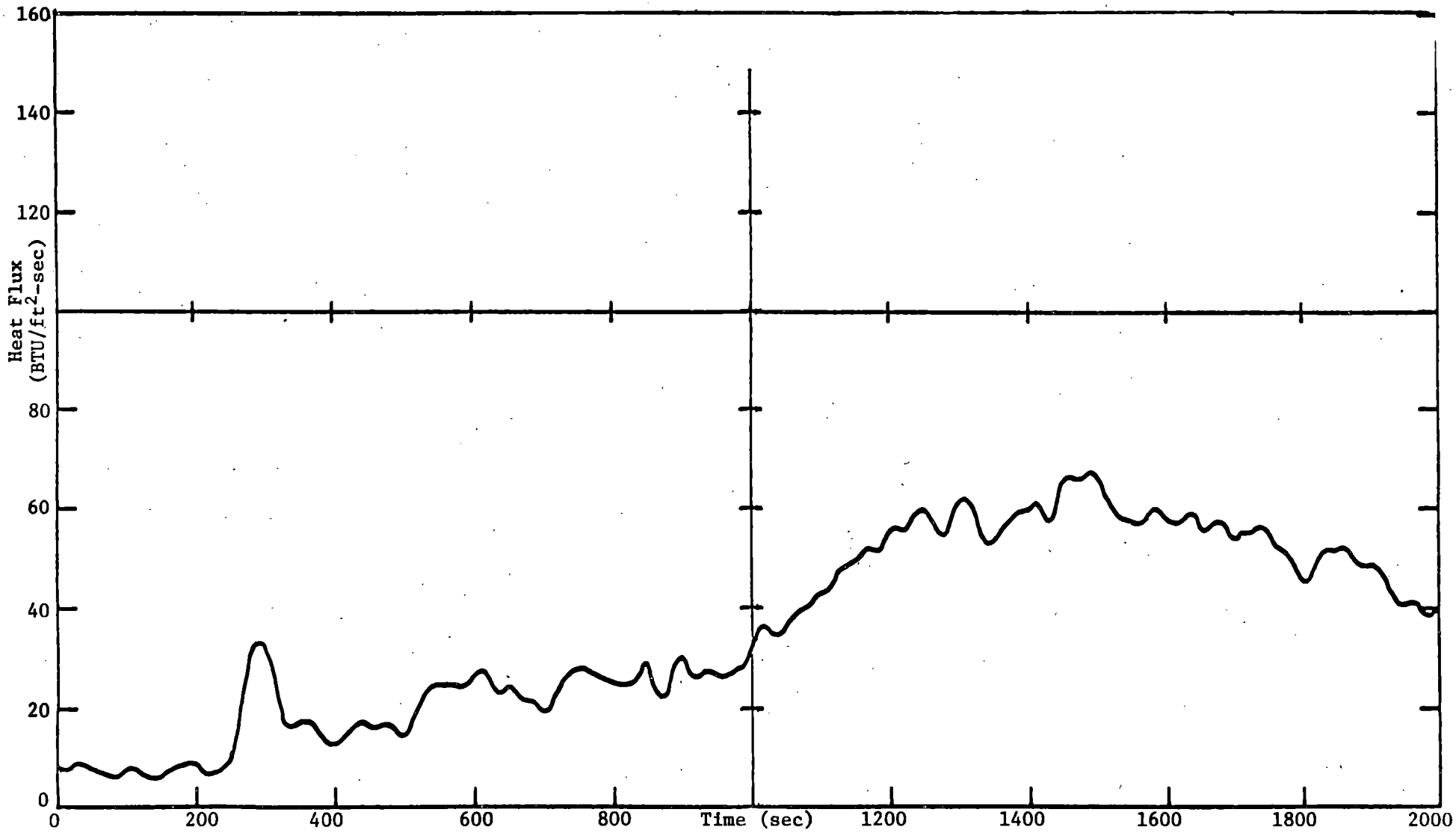

Figure 2. Upward heat flux. High temperature melt-concrete test.

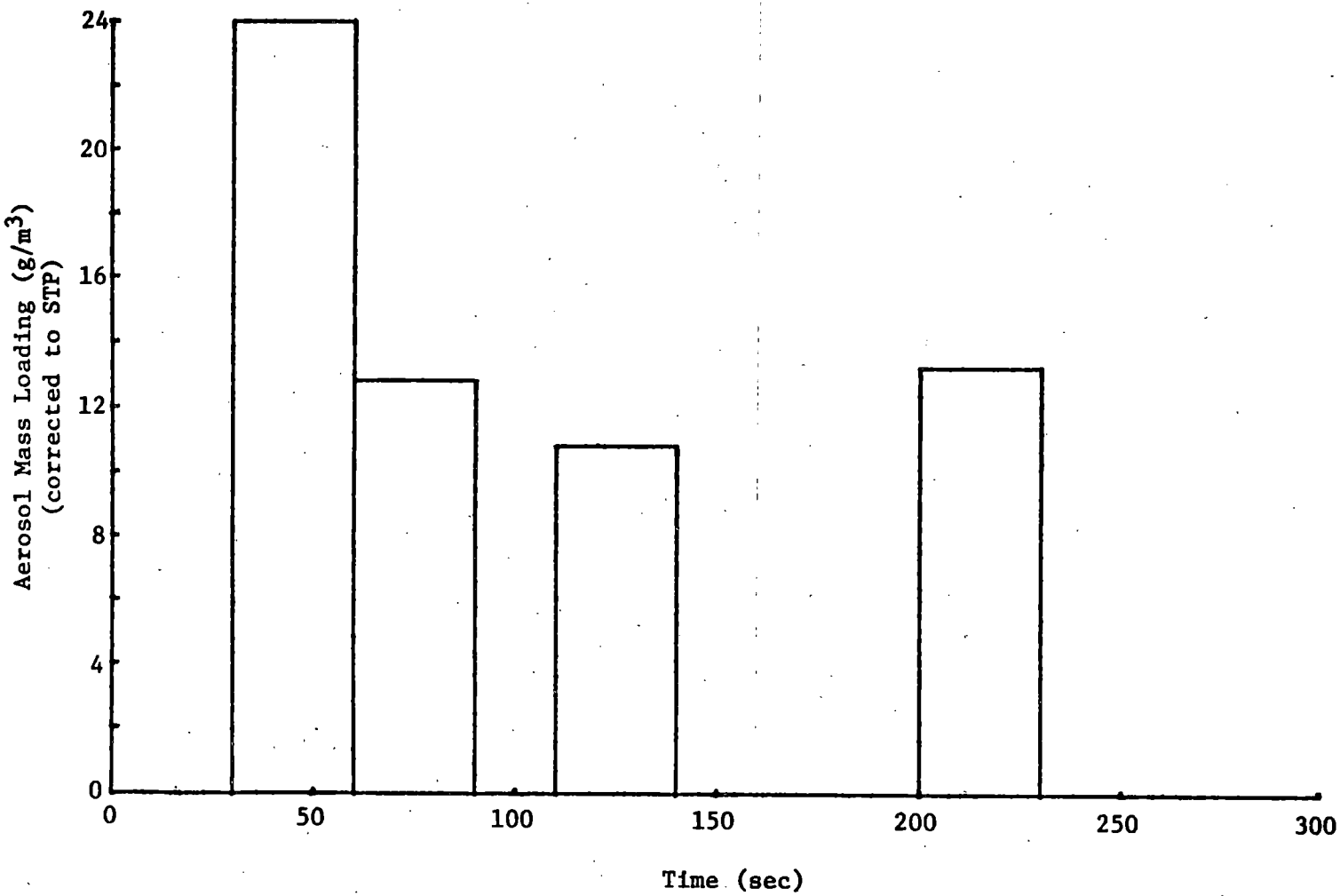

Figure 4. Aerosol mass loading. High temperature melt-concrete test.

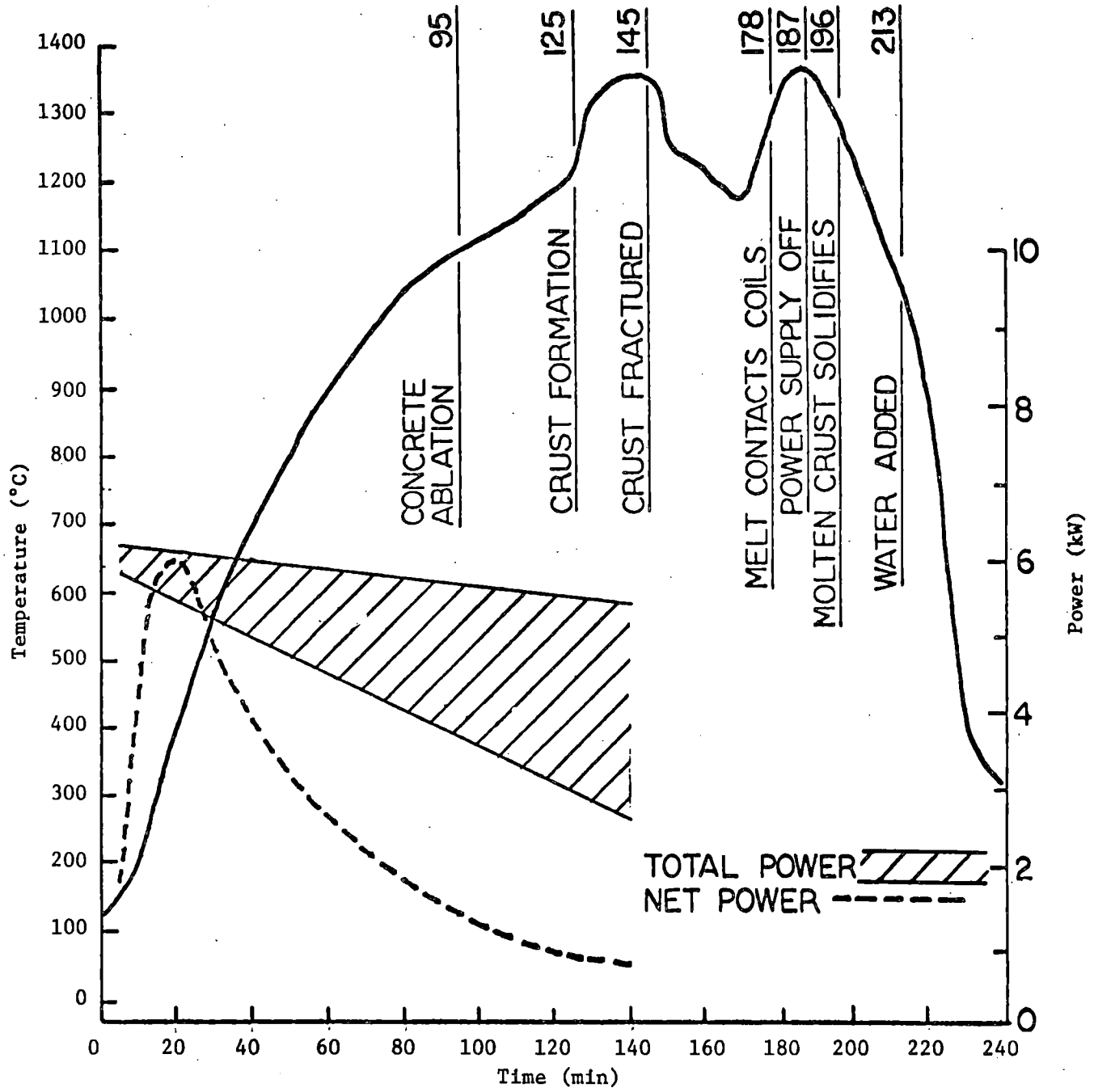

Figure 5. Temperature and input power history. Low temperature melt-concrete test.

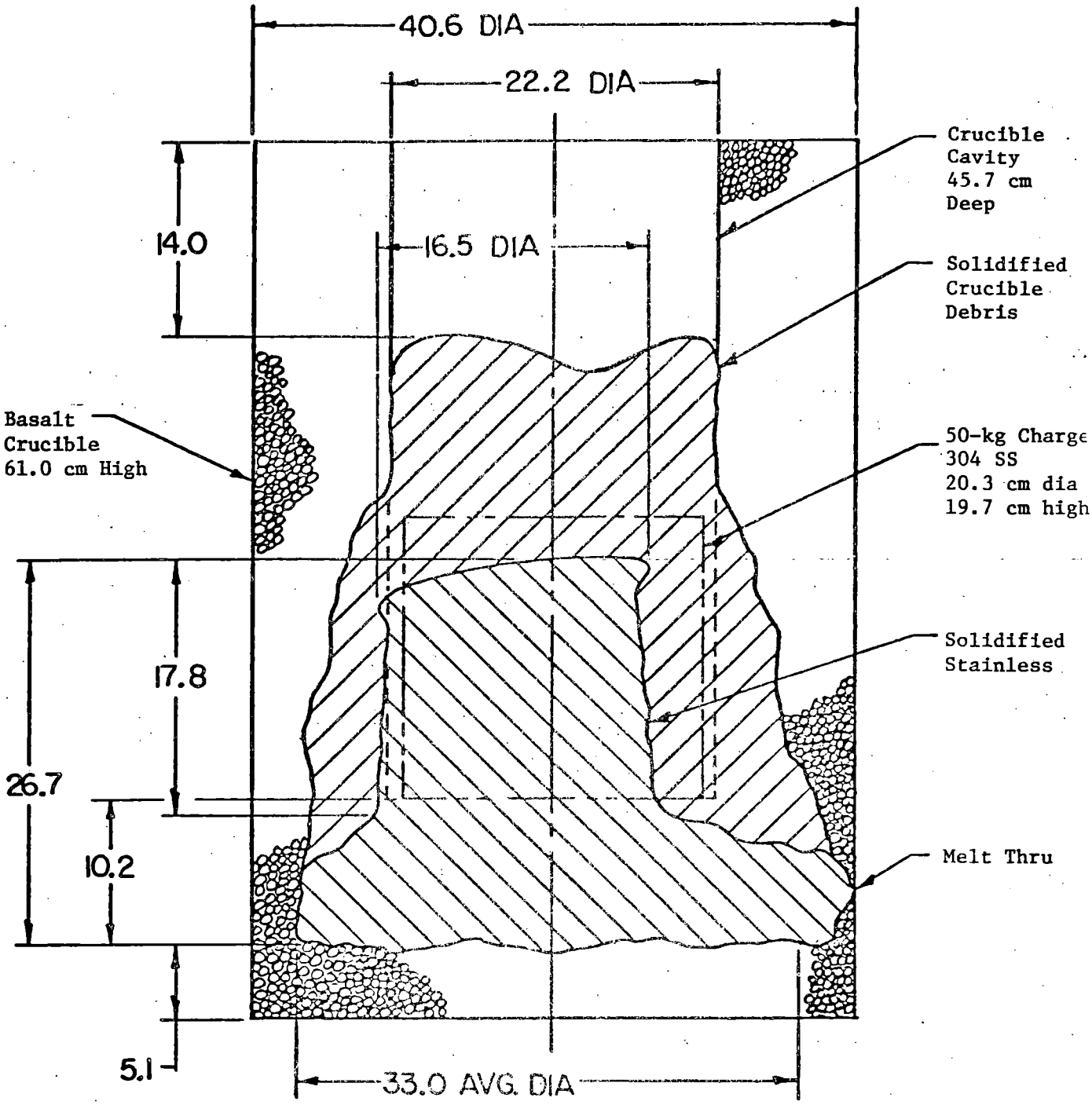

NOTE: All dimensions in centimeters.

Figure 6. Schematic of posttest cross section. Low temperature melt-concrete test.

TABLE 1. HIGH TEMPERATURE MELT-CONCRETE TEST MATRIX

Test No.	Crucible			Melt		Remarks
	Material	Geometry	Size (in)	Material	Quantity (kg)	
1	Limestone Common Sand	Rt. Cyl.	4.75 dia. x 17.75 tall (5154 cc)	Iron-Oxide Aluminum Thermite	10 (L = 6.0 in)	L/D = 1
2	Limestone Common Sand	Spherical cavity	4.13 Sp Rad 3.75 dia. opening (4835 cc)	Iron-Oxide Aluminum Thermite	10	Continuously varying angle at melt-concrete interface
3	Limestone Common Sand	Rt. Cyl.	9.0 dia. x 10.0 tall (10425 cc)	Iron-Oxide Aluminum Thermite	10 (L = 1.7 in)	Repeat Test #1 with L/D = 0.2
4	Limestone Common Sand	Rt. Cyl.	9.0 dia. x 10.0 tall (10425 cc)	Iron-Oxide Aluminum Thermite	20 (L = 3.4 in)	Repeat Test #3 twice melt height
5	Limestone Common Sand	Horizontal Rt. Cyl.	9.0 dia x 4.0 long (4170 cc)	Iron-Oxide Aluminum Thermite	10	Horizontal cylinder varying angle of attack in two planes

TABLE 2. COMPOSITIONS* OF NATURAL ROCK MATERIALS**

Material	Basalt	Granodiorite	Granite
SiO_2	53.27	74.05	73.91
TiO_2	2.16	0.19	0.22
Al_2O_3	14.07	15.24	14.53
FeO***	11.06	1.32	1.76
MgO	6.83	0.47	0.38
CaO	10.57	2.64	1.54
MhO	0.17	0.03	0.03
NiO	0.01	----	----
Na_2O	2.44	4.40	3.56
K_2O	0.44	2.01	5.00
P_2O_5	0.23	0.09	0.09
Total %	101.30	100.44	101.02

* X-ray fluorescence analyses by H. R. Westrich.

** Mixtures of 80/20 wt. % ratio of UO_2/ZrO_2 (65/35 mole % UO/ZrO_2) were added to powdered (<45 μm) rock samples for core debris solubility measurements.

*** Calculated as Fe^{2+}

TABLE 3. RESULTS OF UO_2/ZrO_2 SOLUBILITY EXPERIMENTS[a]

Initial Composition (wt. %)	Temperature (°K)	Cooling[b] Rate (Ks^{-1})	Phases[c] Observed	Glass Composition[d] (wt. % 1σ) UO_2	ZrO_2
50 Basalt, 40 UO_2, 10 ZrO_2	1473	100	Gl, MgU, Zr, Hem	20.27 ± 0.52	1.46 ± 0.14
50 Basalt, 40 UO_2, 10 ZrO_2	1473	2	Gl, MgU, Zr, Hem, ~Zir	19.64[e] ± 1.13	1.44[e] ± 0.15
50 Basalt, 40 UO_2, 10 ZrO_2	1573	100	Gl, MgU, Zr	22.33 ± 0.33	2.73 ± 0.10
50 Basalt, 40 UO_2, 10 ZrO_2	1673	100	Gl, MgU, ~Zr	29.59 ± 0.43	4.17 ± 0.11
50 Basalt, 40 UO_2, 10 ZrO_2	1673	2	Gl, MgU, ~Zr	13.83[e] ± 0.89	1.53[e] ± 0.12
50 Basalt, 40 UO_2, 10 ZrO_2	1773	100	Gl, MgU	38.10 ± 1.08	4.97 ± 0.23
50 Basalt, 40 UO_2, 10 ZrO_2	1823	100	Gl, MgU	41.06 ± 1.29	6.58 ± 0.37
50 Basalt, 40 UO_2, 10 ZrO_2	1823	2	Gl, MgU	13.50[e] ± 1.36	1.58[e] ± 0.15
50 Basalt, 40 UO_2, 10 ZrO_2	1823	0.02	Gl, MgU, Zr	10.54[e] ± 2.63	0.66[e] ± 0.36
25 SiO_2, 15 MgO, 10 Al_2O_3, 40 UO_2, 10 ZrO_2 synthetic basalt	1673	100	Gl, MgU, Zr	29.62 ± 0.44	4.12 ± 0.10
25 SiO_2, 15 MgO, 10 Al_2O_3, 40 UO_2, 10 ZrO_2 synthetic basalt	1673	2	Gl, MgU, U, Zr	16.91[e] ± 2.02	1.45[e] ± 0.42

TABLE 3 (CONCLUDED)

Initial Composition (wt. %)	Temperature (°K)	Cooling Rate[b] (Ks^{-1})	Phases[c] Observed	Glass Composition[d] UO_2 (wt. % 1σ)	Glass Composition[d] ZrO_2 (wt. % 1σ)
50 Granodiorite, 40 UO_2, 10 ZrO_2	1773	100	Gl, Plag, MgU	14.12 ± 0.72	1.71 ± 0.16
95 Granodiorite, 4 UO_2, 1 ZrO_2	1823	2	Gl, Plag, MgU	4.0[e,f]	1.0[e,f]
50 Granite, 40 UO_2, 10 ZrO_2	1773	100	Gl, Plag, MgU	14.20 ± 0.66	1.89 ± 0.14
95 Granite, 4 UO_2, 1 ZrO_2	1823	2	Gl, Plag, MgU	4.0[e,f]	1.0[e,f]

[a] All experiments were held at T for one hour before cooling.

[b] Cooling rates are applicable from T to 1100K.

[c] Phases were identified by optical microscopy and X-ray diffraction and are listed in order of abundance; Gl = glass, MgU = MgU_2O_6, Zr = ZrO_2, Hem = Fe_2O_3, Zir = $ZrSiO_4$, Plag = $CaAl_2Si_2O_8$, U = $UO_{2.9}$

[d] Glass compositions were determined by microprobe techniques.

[e] Exsolution of MgU_2O_6 + ZrO_2 phases from glass upon cooling.

[f] Visual estimate of grain mount.

Core Retention Assessment Program at Sandia National Laboratories*

J. D. Fish
Sandia National Laboratories**
Albuquerque, NM 87185, USA

Abstract

An overview of the Core Retention Assessment Program at Sandia is presented. Results of tests on castible ceramics, steel liners, sacrificial beds, refractory brick crucibles, and rubble bed retention devices are reported. Test plans for the next year are described briefly.

Introduction

Both experimental and analytical investigations of core retention concepts are being carried out at Sandia under the auspices of the Office of Nuclear Regulatory Research. The objective of the program is to provide the generic data base necessary for evaluation and licensing of specific designs.

The primary functional requirement of a core retention device is to prevent the contact of either molten or hot solid core debris with concrete. The core retention device should contain the debris in such a manner that the decay heat can be dissipated without introducing further hazards to the integrity of the reactor containment structure. Specifically, the interaction of core debris with the core retention device should not produce large amounts of hydrogen, aerosols, or energy (from exothermic chemical reactions).

To evaluate the extent to which core retention devices can meet the functional requirement, it is necessary to develop a data base which includes such information as heat transfer and the effect of core retention devices on the distribution of heat within the reactor structure; the coolability of core retention devices under a broad range of scenarios; physical and chemical interactions of core debris and core retention devices with and without coolant present; and the long-term, in-place stability of core retention devices.

The particularly attractive capabilities of the experimental facilities at Sandia are characterized by three aspects:

(1) Large-scale; up to 250 kg melts can be generated routinely. Given the dependence on scale of many of the phenomena of interest, this capability is important.

---

* This work is supported by the U.S. Nuclear Regulatory Commission.
**A U.S. Department of Energy facility.

(2) Sustained melts; melts have been sustained for over two hours in some of the tests that have been carried out. Longer sustained tests are planned. The ability to sustain a melt out-of-pile significantly reduces both complexity and cost of a test compared to running the test in a reactor.

(3) Prototypic materials; use of prototypic reactor materials assures that the phenomena observed in tests are the same as those that would occur in an actual accident.

Five concepts have received preliminary consideration at Sandia: castible ceramics, steel liners, sacrificial beds, refractory brick crucibles, and rubble bed retention devices. Each of these are discussed briefly below. In addition to the experimental program, a penetration model applicable both to brick devices and to rubble bed devices is being developed. This model along with the other interaction models under development will provide the basis: (1) for relating specific experiments to generic phenomena, and (2) for analyzing specific designs without the need to test each and every design.

Castible Ceramics

Castible ceramics are attractive materials for core retention devices, especially for devices to be installed in new plants. In a scoping test,[1] 208 kg of molten steel at 1973 K was teemed onto a high alumina cement crucible. The test was sustained for 1050 s. The high alumina cement was made from calcium aluminate binder (SECAR 250 from Lone Star Lafarge Co.) and brown fused alumina aggregate (DURALUM from Industrial Compound Co.). It was tested in the hydrated form. The hydrated material contains 2.3 weight percent water which is volatilized in two steps of about equal magnitude at 380 and 545 K.

No erosion of the cement either by spallation or by melting occurred during this time. Gases generated during melt interactions consisted mostly of hydrogen. The aerosol concentration in the gas was about 0.45 g/m^3 which was much less than the 9 g/m^3 observed in similar tests with ordinary concrete.[2]

The test results indicate that high alumina cement would be especially attractive as a core retention material if it were dried to minimize gas generation during melt attack. Resistance of this material or other castible ceramics to rehydration over the lifetime of a reactor, however, must be demonstrated.

Steel Liners

Preliminary analyses of tests[3] in which 200 kg stainless steel melts at 1973 K were teemed onto mild steel structures up to 7.62 cm thick indicate that steel liners offer little resistance to melt penetration. The 7.62 cm plate was penetrated in about 25 s by a stream impinging on it with a velocity of 4 m/s.

Extrapolation of results from tests on 1 cm and 1.27 cm plates indicates that the same plate would be penetrated by a quiescent pool of molten steel in about 48 s. Furthermore, back-side cooling of the plate to prevent penetration is not feasible; the heat flux imposed by the melts far exceeds the critical heat flux of either sodium or water coolant.

Sacrificial Beds

Sacrificial core retention devices depend on the interaction of the sacrificial material with the core debris to absorb its heat and to dilute its heat sources.

The feasibility of borax ($Na_2B_4O_7$) as a sacrificial material was tested by teeming 220 kg of molten steel at 1973 K onto a borax crucible.[1] Boiling of the borax produced large quantities of aerosol for the first 25 s of the test. The melt/borax interaction, once aerosol generation ceased, was quite mild. Depending on the accident scenario and the other available mitigation provisions, the copious amount of aerosol that would be generated by the interaction of a borax sacrificial bed and a core debris melt that remained above the 1833 K boiling point of borax for a significant period of time could exacerbate an accident sequence.

Refractory Brick Crucibles

Of the two refractory materials (firebrick and magnesium oxide) tested by teeming molten steel, magnesium oxide (MgO) appears the most promising.[1] The erosion rate for MgO was 6.3×10^{-7} m/s compared to 8.2×10^{-6} m/s for firebrick. Aerosol generation with MgO was also lower. Erosion of MgO by iron oxide, however, was much faster than by steel: 1.05×10^{-5} m/s. The extent to which oxide erosion of MgO is a problem will be tested in the near future at the Sandia Large-Scale Melt Facility by a drop of 250 kg of molten UO_2 with 30% yttria stabilized zirconia into an MgO crucible. Information concerning melt penetration of gaps between bricks, thermal shock, brick flotation, and upward heat flux will also be gained from this test. Feasibility of cooling an MgO device, thermal degradation of structural materials that support and restrain the MgO, and long-term stability of MgO will be determined in later separate-effects tests.

Rubble Bed Retention Devices

For near-term retrofit of existing reactors, the rubble bed concept appears most feasible. This type of protection could be installed easily and quickly into reactor cavities where space is minimal and radiation levels preclude extensive modifications.

Two scoping tests of the rubble bed concept were carried out earlier this year.[4] A significant result of the tests was that melt streaming does not sweep aside the rubble. Considerations related to the rubble bed concept that will be addressed by the series of tests planned for the next year include:

(1) Penetration of a rubble bed by a sustained melt with and without coolant present;

(2) Heat flux distribution of a sustained melt on a cooled rubble bed;

(3) Sizing of rubble particles to assure coolant flow;

(4) Limits on cooling of the debris melt on the rubble;

(5) Hydrogen production by reaction of coolant (i.e., steam in the case of water) with the debris melt;

(6) Thermal shock to the rubble; and

(7) Fabrication and allowable porosity of the rubble particles.

Summary

Quantitative determination of the advantages and disadvantages of various core retention concepts is being actively pursued at Sandia. Castible ceramics, steel liners, sacrificial beds, refractory brick crucibles, and rubble bed retention devices have been examined. Efforts over the next year will concentrate on MgO brick crucibles and thoria rubble beds. Castible ceramics will receive increased attention in the future.

References

1. D. A. Powers, "A Survey of Melt Interactions with Core Retention Material", in Proceedings of the International Meeting on Fast Reactor Safety Technology, Seattle, WA, 19-23 August 1979, p. 379.

2. D. A. Powers, "Sustained Molten Steel/Concrete Interactions Tests", in Proc. Post Accident Heat Removal Information Exchange, Argonne National Laboratory, Argonne, Illinois, November 2-4, 1977, p. 433.

3. D. A. Powers and F. E. Arellano, "Erosion of Steel Structures by High Temperature Melts", Sandia National Laboratories Report SAND81-1755, to be published.

4. W. W. Tarbell, R. Blose, and F. E. Arellano, "Sweepout of a Rubble Bed by a Streaming Melt", Sandia National Laboratories Report, to be published.

CORCON MOLTEN FUEL-CONCRETE INTERACTIONS CODE

PRESENTATION BY

RANDALL K. COLE, JR.

SANDIA NATIONAL LABORATORIES

ALBUQUERQUE, NEW MEXICO

AT

NINTH WATER REACTOR SAFETY RESEARCH INFORMATION MEETING

GAITHERSBURG, MARYLAND

October 29, 1981

SUMMARY

The NRC is supporting research in molten fuel-concrete interactions at Sandia National Laboratories. The objective has been to improve our understanding of the rate and geometry of melt penetration of the reactor basemat, and of the resultant sources of energy, gases, and aerosols within the containment building. This work has led to the development of the CORCON computer code. The MOD1 version of the code has been available since November 1980. A MOD2 version, with significantly extended capabilities, will be available in September 1982.

CORCON treats a number of coupled physical processes taking place in a system composed of a multilayer, stratified liquid pool in an axisymmetric concrete cavity. The atmosphere and surroundings above the pool serve as boundary conditions in MOD1. Their description will be expanded in MOD2, which will also permit an overlying coolant layer, and provide models to describe long-term interaction after significant solidification of the melt has occurred. The necessary material properties and other data and correlations are contained in the code in a modular fashion, freeing the user from extensive input requirements.

Preliminary sensitivity studies have suggested that heat-transfer models are of dominant importance in CORCON-MOD1, as are material properties insofar as they affect heat transfer. Such properties include the viscosities and freezing temperatures of various components of the melt. We are reexamining these models and will upgrade them if possible in MOD2. It must be emphasized that the models and properties are all closely coupled and may contain offsetting errors. Therefore, an improvement in one area is not necessarily an improvement in the code as a whole.

An important assumption in MOD1 is that the pool is liquid and well stirred by bubbles of gas generated by decomposition of concrete. This effectively limits its applicability to the early phase (say, 5 to 10 hours) of the interaction. After this time, significant crusting and solidification is believed to occur. With the loss of bubble agitation, natural convection and conduction determine heat transfer within the pool. We have shown that conventional heat-transfer correlations may be used to calculate heat-transfer in volumetrically heated liquid layers, and demonstrated good agreement with the data of Kulacki, et al.

These methods have been applied to a simple two-layer problem intended to represent a typical pool resulting from a hypothetical core-melt accident in a large PWR. These calculations suggest that, because of its large volumetric heating and small thermal conductivity, most of the oxidic layer will remain molten for many days. Moreover, the results are remarkably insensitive to assumed boundary conditions. In particular, quenching the surface of the pool to the boiling point of water results in a somewhat thicker crust but no significant change in heat flux as compared to cooling by radiation alone.

Recent Pertinent Sandia Reports

1-3. M. Berman, Light Water Reactor Safety Research Program, Quarterly Reports:

July-September 1980:	NUREG/CR-1509/3 of 4
October-December 1980:	NUREG/CR-1509/4 of 4
January-March 1981:	NUREG/CR-2163/1 of 4

4. J. F. Muir, et al., CORCON-MOD1: An improved Model for Molten-Core/Concrete Interactions, July 1981, NUREG/CR-2142, SAND80-2415.

CORCON

MOLTEN FUEL-CONCRETE INTERACTIONS CODE

R. K. COLE, JR.
D. P. KELLY
M. BERMAN

Sandia National Laboratories

CORCON DEVELOPMENT

OBJECTIVE

DEVELOP AND VERIFY A CODE FOR CALCULATION OF THE INTERACTIONS OF MOLTEN CORE MATERIALS WITH CONCRETE. PRINCIPAL CONCERNS INCLUDE

- RATE AND GEOMETRY OF MELT PENETRATION
- RATE AND NATURE OF GAS EVOLUTION
- OTHER SOURCE TERMS TO CONTAINMENT

CORCON DEVELOPMENT

SYSTEM COMPONENTS

- CONCRETE CAVITY OR CRUCIBLE
- MULTILAYER STRATIFIED POOL
- OVERLYING COOLANT[1]
- ATMOSPHERE[2]
- SURROUNDINGS[2]

1. NOT AVAILABLE IN MOD1
2. USER-SPECIFIED BOUNDARY CONDITION IN MOD1

CORCON DEVELOPMENT

PHYSICAL PROCESSES

- ENERGY GENERATION
- CONCRETE DECOMPOSITION AND ABLATION
- HEAT AND MASS TRANSFER
- CHEMICAL REACTIONS
- BUBBLE PHENOMENA, LEVEL SWELL
- CRUST FORMATION AND DEBRIS FREEZING[1]

1. NOT CONSIDERED IN MOD1

CORCON DEVELOPMENT

SCHEDULE AND STATUS

- MOD1
  AVAILABLE SINCE NOVEMBER 1980
  "FROZEN" APRIL 1981
  MAINTENANCE LIMITED TO ERROR CORRECTION

- MOD2
  TO BE AVAILABLE SEPTEMBER 1982
  WILL BE "FROZEN" AFTER INITIAL FIELD TEST

CORCON DEVELOPMENT

MOD1 CHARACTERISTICS

- 8000 SOURCE CARDS
- 100 k_B SCM ON CDC7600, NO LCM
- RUNS IN SINGLE PRECISION ON OTHER MACHINES (TESTED ON 32-bit VAX)
- TYPICAL TIME STEP 10-100 sec
- TYPICAL RUN TIME 0.1sec/STEP on 7600
  PLANT CALCULATION 23 sec for 240 30-sec steps (2 hours)
  CODE COMPARISON TEST 20 sec for 267 15-sec steps (4000 sec)

CORCON DEVELOPMENT

MOD1 CAPABILITIES

- TWO-DIMENSIONAL AXISYMMETRIC CAVITY WITH POINTWISE ABLATION AND RECESSION
- CONSIDERS ONE-, TWO-, OR THREE-LAYER POOL
- HEAT SOURCE FROM INTERNAL DECAY-HEAT MODEL OR USER INPUT
- MATERIAL PROPERTIES INCLUDED FOR MORE THAN 50 SPECIES
- CONCRETE MAY BE ONE OF THREE "STANDARDS" OR USER-SPECIFIED

CORCON DEVELOPMENT

MOD1 LIMITATIONS

- NO CRUST OR SOLID-PENETRATION MODELS
- NO COOLANT LAYER PERMITTED[1]
- ATMOSPHERE AND SURROUNDINGS ARE USER-SPECIFIED BOUNDARY CONDITIONS[1]
- CONSTANT-PROPERTY NON-REACTING GAS FILM[1]
- STEADY-STATE CONCRETE ABLATION ASSUMED
- NO HETEROGENOUS MIXTURES PERMITTED[1]

1. MOD1 CONTAINS PARTIAL CODING OR "HOOKS"

CORCON DEVELOPMENT

MOD1 HEAT TRANSFER

- FILM MODEL FOR POOL/CONCRETE INTERFACE (NOT REFUTED BY CRITICAL VELOCITY ARGUMENT)
- MODIFIED KONSETOV FORM AT LAYER INTERFACES (UNDERPREDICTS DATA OF WERLE AND OF GREENE)
- NO CONDUCTION LIMIT IMPOSED ON CONVECTION
- SURFACE RADIATES THROUGH TRANSPARENT ATMOSPHERE (DOES NOT ACCOUNT FOR AEROSOL OPACITY)

NOTE

- POSSIBLE OFFSETTING ERRORS IN MODELS
- CONSEQUENCES OF IMPROVEMENTS MUST BE TESTED FOR INTERACTIONS

CORCON DEVELOPMENT

EXPECTED MOD2 IMPROVEMENTS

- RESTRUCTURED FOR EASIER COUPLING TO MARCH OR CONTAIN
- RUDIMENTARY ATMOSPHERE AND SURROUNDINGS MODELS FOR STAND-ALONE USE
- ADDITION OF COOLANT LAYER
- INITIAL CRUST AND SOLID-PENETRATION MODELS
- IMPROVED HEAT-TRANSFER MODELS IF AVAILABLE

CORCON DEVELOPMENT

LONG-TERM HEAT TRANSFER

- SOLID CRUST MAY BLOCK BUBBLES
- HEAT TRANSFER IS THEN NATURAL CONVECTION AND CONDUCTION
- OXIDE HAS LARGE VOLUMETRIC HEATING AND SMALL THERMAL CONDUCTIVITY
- BULK OF OXIDE MAY BE LIQUID FOR MANY DAYS UNDER THIN SOLID CRUST

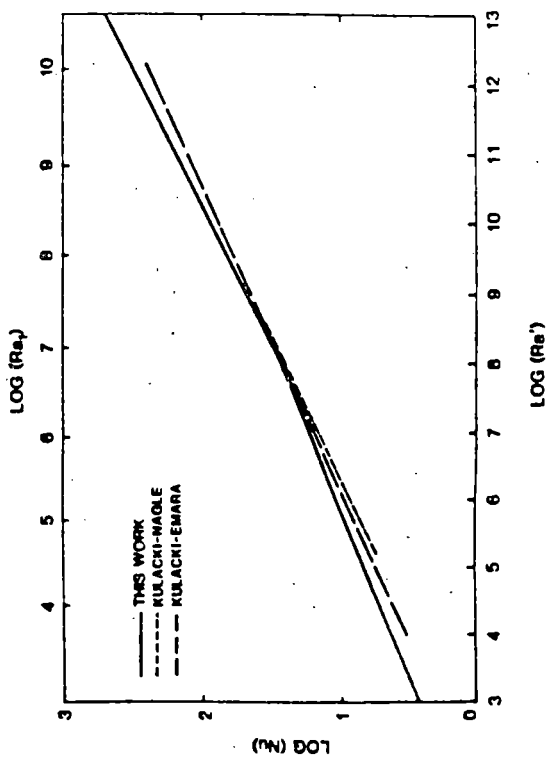

Comparison of Correlations for $T_o - T_m$

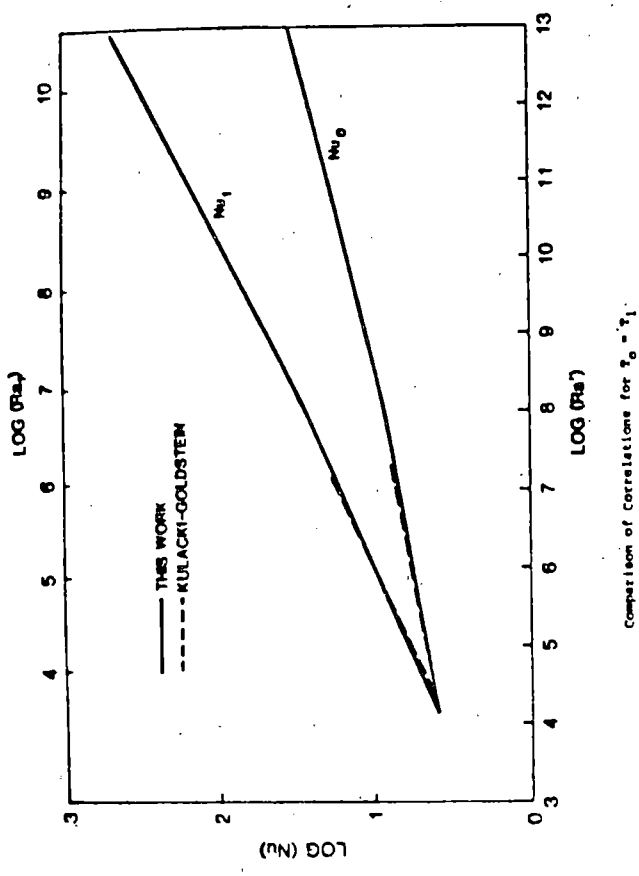
LOG (Ra)
LOG (Nu)
THIS WORK
KULACKI-GOLDSTEIN
Comparison of Correlations for

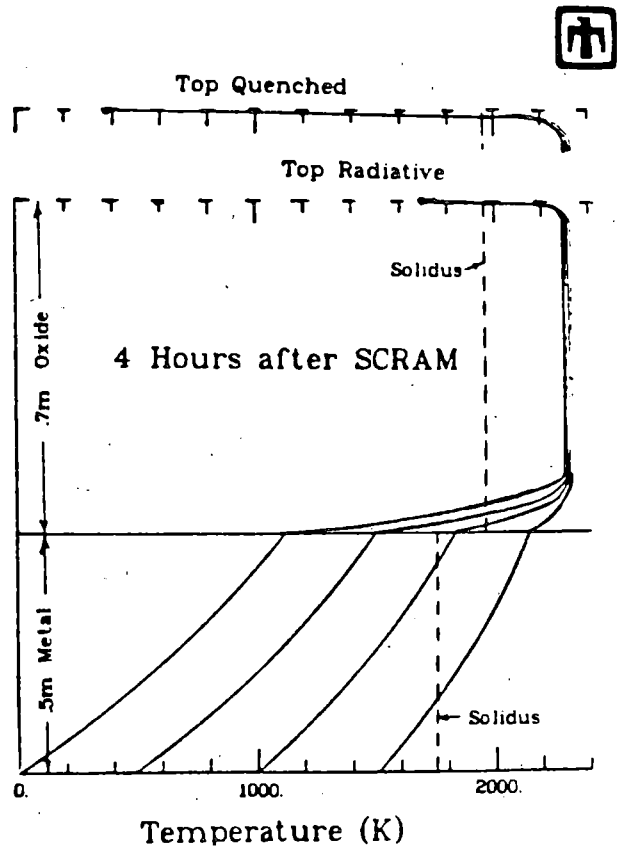
Top Quenched
Top Radiative
Solidus
4 Hours after SCRAM
.7m Oxide
.5m Metal
Solidus
0.
1000.
2000.
Temperature (K)

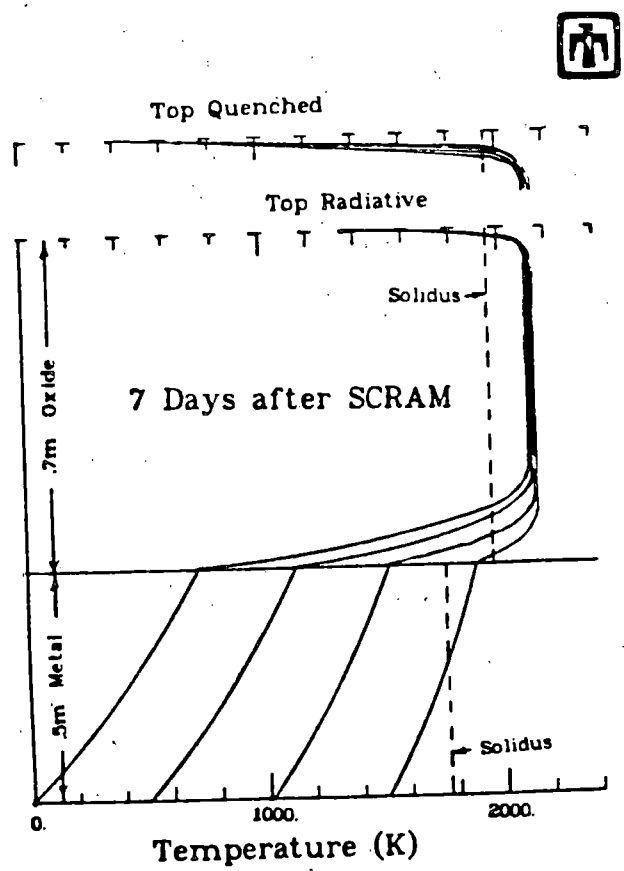
Top Quenched
Top Radiative
Solidus
7 Days after SCRAM
.7m Oxide
.5m Metal
Solidus
0.
1000.
2000.
Temperature (K)

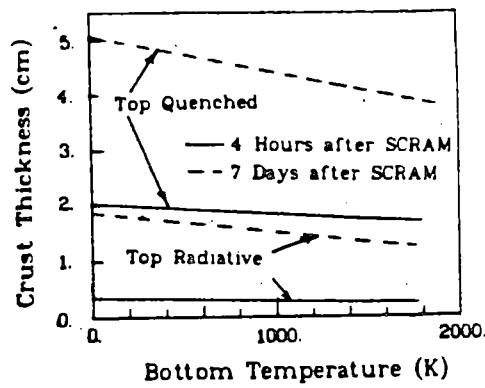
Crust Thickness (cm)
Top Quenched
4 Hours after SCRAM
7 Days after SCRAM
Top Radiative
0.
1000.
2000.
Bottom Temperature (K)

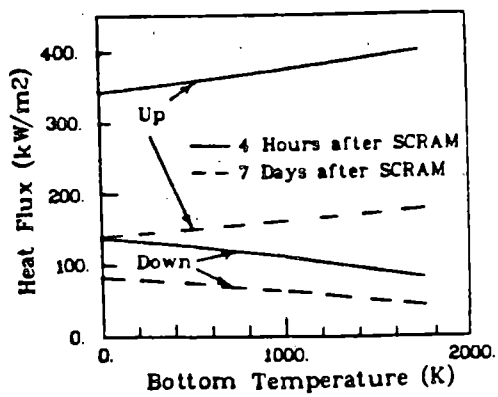
Heat Flux (kW/m2)
Up
4 Hours after SCRAM
7 Days after SCRAM
Down
0.
1000.
2000.
Bottom Temperature (K)

Development of CONTAIN for LWR Containment Analysis*

M. J. Clauser
M. E. Senglaub
J. E. Kelly
J. P. Odom
M. F. Young
P. J. Cooper
K. K. Murata
P. E. Rexroth

Sandia National Laboratories**
Albuquerque, New Mexico 87185

Presentation prepared for the
Ninth Water Reactor Safety Research Information Meeting
Gaithersburg, Maryland
October 26-30, 1981

*This work supported by the U.S. Nuclear Regulatory Commission.
**A U.S. Department of Energy facility.

CONTAIN is a computer code under development for the analysis of phenomena occuring in a reactor containment system during an accident. It is designed to treat the phenomena and system responses that occur over long periods of time (hours or days) inside a reactor containment building and outside of the reactor vessel. The thermal, radiological, chemical, and mechanical consequences of an accident can be tracked throughout the containment building, and the radiological source term for atmospheric dispersal can be established. CONTAIN was initially designed to treat LMFBR accidents, however the models developed for that purpose have been adapted to treat corresponding phenomena in LWR accidents. Models to treat phenomena or systems of special interest to LWRs are currently being developed and implemented. At present, the code[1,2,3] treats most of the phenomena that are common to most types of reactor accidents and provides a framework for incorporation of additional phenomenological and engineered system models needed for specific applications.

CONTAIN treats a containment system as a network of interconnected cells which communicate with each other by gas flow due to pressure differences and by heat flow (thermal conductivity through intervening structures) due to temperature differences. A "reference cell" concept has been implemented in CONTAIN, wherein a complete set of physical processes can be treated in each cell. Those processes actually appropriate for a given cell are specified by the input to the code. Each cell is divided into two parts, an atmosphere and a pool. Within the cell atmosphere the following phenomena of interest in LWR accidents are treated:

- -- Thermodynamics, including condensation.
- -- Heat transfer to structures, walls, etc.
- -- Condensation on structures
- -- Hydrogen combustion
- -- Aerosol behavior, including aglomeration, settling, and vapor condensation
- -- Fission product behavior including decay heating, and release from host materials
- -- Intercell flow of gases, aerosols and fission products

Modeling of other atmospheric chemistry and of various safety systems will be included in the near future.

Aerosols can have a significant effect on containment systems (e.g., vent or filter clogging) and will strongly affect inhalation health consequences. Therefore, significant emphasis has been placed on modeling the physical and chemical processes which govern the evolution of aerosols within the containment system. The MAEROS model[4] was developed as a module of CONTAIN and it provides some capabilities not available in earlier codes. The most important is the ability to deal with multi-component aerosols. It divides the distribution of particle sizes into a series of size classes or sections, and, within each section it keeps track of the amount of each component (chemical species) of aerosol. In this way a collection of, say, large concrete particles and smaller fuel debris particles can be readily distinguished. The effects on the particle size

distribution are calculated that are due to: (1) aglomeration of small particles into large ones, (2) deposition of particles on surfaces due to gravitational settling and thermophoresis, (3) vapor condensation on the aerosols, and (4) time varying sources of particles with different physical and chemical composition. Altogether this should provide a fairly complete treatment of the aerosol behavior.

The pool model is being developed to provide an integrated, self-consistent, and mechanistic model of the various phenomena in the lower part of each cell, particularly the reactor cavity. The heart of this model, SINTER, is intended to provide a framework that treats the mass and energy flow throughout the pool region (which may include the concrete basemat). Within this general framework models for various physical processes provide source terms, heat transfer coefficients, relative velocity correlations, etc. When completed, this model is intended to deal with

-- Core/coolant interactions, both chemical and thermal
-- Core/concrete interactions
-- Water migration and depletion in concrete
-- Debris bed evolution, dryout, melting, etc.
-- Release of gases, aerosols, and energy to the cell atmosphere

CONTAIN presently has at least crude mdoels for these phenomena and work is proceeding to develop both the numerical and physical modeling.

The first version of the code is currently being tested by a limited number of users prior to general release. A draft users' manual which reflects the code's present status has been prepared and is available on an informal basis.

References

1. M. E. Senglaub, J. P. Odom, and P. S. Pickard, "The Multi-Component Drift-Flux Formulation for the SINTER Subsystem of CONTAIN," Proc. of the International Topical Meeting on Advances in Mathematical Methods for the Solution of Nuclear Engineering Problems, 2, 177, Munich, April 27-29, 1981.

2. J. P. Odom, M. E. Senglaub, J. E. Kelly and M. J. Clauser, "CONTAIN: A Computer Code for Simulation of Reactor Accident Containments," ANS Transactions, 38, 328 (June 1981).

3. M. E. Senglaub, J. P. Odom, M. J. Clauser, J. E. Kelly, and P. S. Pickard, CONTAIN, A Computer Code for the Analysis of Containment Response to Reactor Accidents - Version 1A, NUREG/CR-2224, SAND81-1495, Sandia National Laboratories, draft report.

4. F. Gelbard and J. H. Seinfeld, "Simulation of Multicomponent Aerosol Dynamics," J. Colloid Interface Sci. 78, 485 (1980).

CONTAIN Objectives

- Model Phenomena and System Response
  - -- in existing and proposed containment systems
  - -- for water-, sodium-, and gas-cooled reactors
  - -- following a LOCA or CDA
- Predict Conditions Inside Containment that Affect
  - -- containment building
  - -- fission product release
  - -- mitigation devices
  - -- equipment qualification

CONTAIN features

- State-of-the-art physics models
  - -- General cavity debris-pool model (SINTER)
  - -- Multi-component, sectional aerosol model (MAEROS)
  - -- General, detailed fission product decay and transport
- Modular structure
  - -- models readily updated
  - -- physics readily altered
- First version is operational

REFERENCE CELL

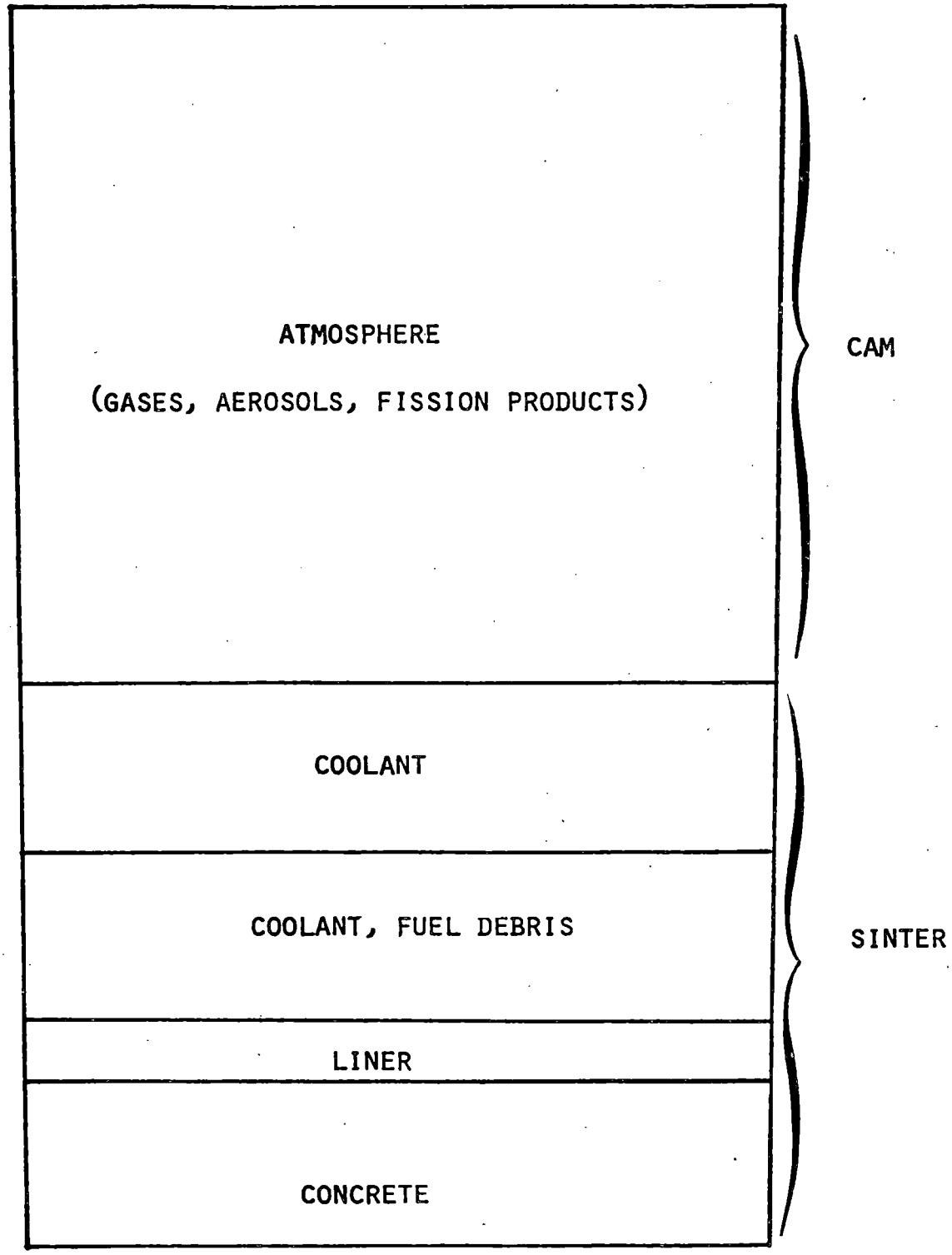

ATMOSPHERE PHYSICS (LWR)

- Two-Phase Thermodynamics
- Surface Heat Transfer
- Surface Condensation
- Hydrogen Burning
- Aerosol Dynamics
- Fission Product Behavior
- Inter-Cell Flow
- Engineered Systems

AEROSOL MODEL (MAEROS)

- Multi-Component
- Multi-Sectional
- Agglomeration Processes
- Deposition on Structures
- Vapor Condensation on Particles
- Aerosol Source Generation

DEBRIS POOL MODEL

- One-Dimensional Multi-Component Drift Flux Formulation
  - One-Dimensional Modeling of Cavity
  - Lumped Component Approach
    (composites: gases, coolant vapor, coolant liquid, other liquids, solid)
  - Assumptions
    - -- tightly coupled motion of components
    - -- thermal equilibrium among gases and liquids
    - -- relative velocities correlations
  - Equations

-- component continuity	-- determines volume fractions
-- mixture continuity	-- determines volumetric flux
-- solid material energy	-- determines solid temperature
-- mixture energy	-- determines fluid temperature

DEBRIS POOL PHYSICS (LWR)

- Concrete Water-Migration (USINT)
- Debris-Concrete Interactions (CORCON)
- Debris-Coolant Interactions
- Chemical Reactions
- Heat Transfer (Conduction, Convection and Radiation)
- Fission Product Heating
- Phase Change (Melting/Freezing, Boiling/Condensing)

HYDROGEN BEHAVIOR AND CONTROL

IN LIGHT WATER REACTOR ACCIDENTS

PRESENTATION BY

MARSHALL BERMAN

SANDIA NATIONAL LABORATORIES

ALBUQUERQUE, NEW MEXICO

AT

NINTH WATER REACTOR SAFETY RESEARCH INFORMATION MEETING

GAITHERSBURG, MARYLAND

OCTOBER 29, 1981

SUMMARY

The NRC is supporting a hydrogen combustion research program at Sandia National Laboratories. The work, begun in FY80, is currently sponsored by several different NRC branches. The overall objective is to quantify the threat posed by hydrogen released during LWR accidents. The research addresses the generation, transport and combustion of hydrogen, including equipment survivability. Schemes for the prevention or mitigation of the effects of hydrogen combustion are also being investigated. The programs contain both theoretical and experimental elements with special emphasis in the following areas:

1. Sources of hydrogen: From corrosion of galvanized material in the containment; from chemical reactions with other coatings (organic and inorganic) and with aluminum.

2. Transport of hydrogen: An analytic investigation of the transport and mixing of hydrogen during LWR accidents using appropriate computer codes.

3. Combustion of hydrogen: This large program element includes theoretical and experimental studies of deflagrations, accelerated flames and detonations. Analytic models and computer codes are being developed to predict the pressures and temperatures which would result from combustion in various containments. Experiments range from small-scale studies (including flame acceleration and detonation research at McGill) to large-scale combustion experiments addressing flammability and detonability limits in multi-component gas mixtures. They include: hydrogen:steam jet behavior; flame acceleration as a function of geometry, obstacles, degree of confinement, ignition source, and hydrogen concentration; and detonations as functions of these same variables. All the experimental work will be accompanied by theoretical analyses aimed at interpreting the experiments and building models to extrapolate the experimental results to LWR accident environments.

4. Mitigation of the effects of hydrogen combustion: Theoretical and experimental studies of mitigation schemes including the intentional burning of hydrogen (deliberate ignition) and the addition of diluents before or after a postulated accident. Recent studies have emphasized the effects of water sprays, fogs, and foams, Halon inerting, deliberate ignition, and flaring from the primary system.

5. The effects of combustion on the functioning and survival of equipment and instrumentation.

The following presentation summarizes the ongoing research, the important results to date, and anticipated results in the coming years. Some of the highlights and recent accomplishments are briefly discussed in the following paragraphs.

The state of knowledge concerning the behavior of hydrogen during LWR accidents was surveyed, evaluated and compiled into a comprehensive document (Ref. 4). We concluded that much of the existing literature dealt with small-scale experiments under laboratory conditions. In contrast, reactor safety questions require information on dynamic accident conditions in large scale, including multiple ignitions, inhomogeneous concentrations, cluttered containments and complex gas and liquid mixtures.

A three-day workshop on the Impact of Hydrogen on Water Reactor Safety was conducted in January, 1981. Forty-four papers were presented to about 200 participants representing nine countries. The Proceedings of the workshop have been published in four volumes (Ref. 7-10). The workshop was an effective vehicle for transmitting information on the status of international research on hydrogen generation, transport, detection, combustion and mitigation. Other topics included regulatory perspectives, a TMI-2 update, and a presentation of the major hydrogen research planned by laboratories and institutions.

The status of commercially available instrumentation for the detection of hydrogen gas in containment was reviewed and evaluated. The results of this review will be published in Ref. 11. We determined that instrumentation improvements are needed, and that detector response times might be reduced using only simple modifications.

Three hydrogen combustion mitigation schemes were evaluated for postulated degraded core accidents in the Sequoyah nuclear power plant. The proposed interim distributed ignition system (deliberate ignition) was shown to be beneficial for some hypothetical accidents. Suggestions were made to improve its performance under certain conditions. Water fogs were shown to be capable of large potential benefits; the major questions concerned the production and maintenance of high density fogs. Halon inerting was shown to be a feasible scheme; however, potential problems might arise concerning containment overpressurization, the potential for corrosion, and the ultimate disposal of the hydrogen.

We recently initiated a review of the hydrogen igniter system (HIS) proposed by Mississippi Power and Light Company for the Grand Gulf nuclear station. We expect to complete this review by January 1, 1982.

MARCH calculations were performed for several accident scenarios for the Zion, Sequoyah and Grand Gulf nuclear plants. Some results have already been reported in quarterlies (Refs. 1-3) and topicals (Ref. 5). MARCH predictions are very sensitive to input assumptions, and results must be used with great caution and restraint.

Codes have been developed to predict pressure and temperature histories during and after combustion events. Heat transfer models have been developed for radiation, conduction into solids, natural and forced convection with and without condensation on surfaces, and for evaporation of water sprays. We found that sprays (if they are on) dominate the heat transfer after combustion; radiation is the next most important heat transfer mechanism. The codes will be used to specify the environments that equipment will undergo during combustion.

The RALOC code has been obtained from the Gesellschaft fur Reaktorsicherheit (GRS) in Germany. We are currently evaluating the code's ability to predict the transport and mixing of hydrogen generated by metal water reactions (note that the code was originally developed to consider only radiolytically-generated hydrogen and its transport). The code is now operational at Sandia, and several assessment calculations have been performed. Qualitative agreement has been demonstrated between code predictions and experimental data.

The CSQ code has been modified to determine the dynamic loads which could result from hydrogen detonations during hypothetical LWR accidents. Calculations have been performed for the Zion, Sequoyah and Grand Gulf nuclear plants. The results have alerted us to the potential for load enhancement from local detonations due to shock reflections and containment symmetries. A draft report has been written (Ref. 13).

Work was initiated on the preparation of a hydrogen behavior manual which could be used by plant designers as a guide for preparing plant-specific operators' manuals. A contract was awarded to General Physics Corporation to assist in the writing of several chapters of the manual.

A detailed experimental program plan was developed which outlined the anticipated experimental tests which will be performed in the various facilites.

Some laboratory experiments on water fogs have been completed. The average fog density was measured with an x-ray absorption system; the parameters varied included nozzle type, nozzle manifold configuration, nozzle height above the beam, and flow rate. The density varied approximately as the square root of the flow rate. This indicates that significant droplet agglomeration was occurring (without agglomeration, the density would vary linearly with flow

rate). Experiments will continue to evaluate other diagnostic systems (lasers, hot wire anemometers, etc.) and to find means of increasing the fog density (surface tension alteration, increased flow rates, etc.).

Laboratory-scale experiments have begun to investigate the effects of water foams on combustion.

Seventy-seven tests have been conducted in the VGES 16-ft tank. These experiments addressed the effects on hydrogen combustion of hydrogen concentration, gas motion, igniter type and location, low initial air pressure, excess nitrogen (partial pre-inerting), and addition of excess CO_2 (inerting and steam simulation). No significant differences were observed in peak pressures for a given hydrogen concentration for all of the variables except pre-burn gas motion, which enhanced the pressure rise for concentrations below about 8%. The tank will soon be reconfigured for experiments on water fogs and foams, flame acceleration, critical tube diameter, and detonations.

A facility to investigate the combustion of hot hydrogen:steam jets is being constructed. Autoignition experiments will begin within a few months.

The design of modifications to the FITS facility has been completed. Experimentation on hydrogen:steam:air combustion is expected to begin in January 1982.

Many experiments on hydrogen accelerated flames and detonations were completed at McGill University under the direction of Prof. John Lee, McGill faculty, and students. Important results include: the generation of further experimental data which support the hypothesis that the critical tube diameter is roughly equal to 13 times the detonation cell size; the observation of significant flame acceleration for deflagration in tubes and channels with obstacles present even for concentrations below the "nominal" detonability limit of 18% (e.g., flame speeds in excess of 200 m/s have been observed for a concentration of 12%, and the flame was still accelerating at that time).

A program plan has been developed to investigate the functionability and survivability of equipment in hydrogen combustion environments. Some models have been developed to characterize the temperature and pressure environments.

A vessel for performing corrosion tests has been designed, built and tested. We have begun the investigation of the rate of hydrogen generation from the corrosion of galvanized materials. A study of the zinc inventories in various containment was completed (Ref. 12).

Recent Pertinent Sandia Reports

1-3. M. Berman, Light Water Reactor Safety Research Program, Quarterly Reports:

July-September 1980:	NUREG/CR-1509/3 of 4
October-December 1980:	NUREG/CR-1509/4 of 4
January-March 1981:	NUREG/CR-2163/1 of 4

4. M. P. Sherman et al., The Behavior of Hydrogen During Accidents in Light Water Reactors, August 1980, NUREG/CR-1561, SAND80-1495.

5. M. Berman et al., Analysis of Hydrogen Mitigation for Degraded Core Accidents in the Sequoyah Nuclear Power Plant, March 1981, NUREG/CR-1762, SAND80-1762.

6. J. F. Muir et al., CORCON-MOD1: An Improved Model for Molten-Core/Concrete Interactions, July 1981, NUREG/CR-2142, SAND80-2415.

7-10. Proceedings of the Workshop on the Impact of Hydrogen on Water Reactor Safety, edited by M. Berman, 4 Volumes, August/September 1981, NUREG/CR-2017, SAND81-0661.

11. E. C. Neidel, J. G. Castle, Jr., A Review of Hydrogen Detection in Light Water Reactor Containments, NUREG/CR-2080, SAND81-0326, to be published.

12. J. E. Womelsduff, V. M. Loyola, Zinc Inventories in Containment for Some PWR and BWR Power Plants, March 1981, NUREG/CR-2021, SAND81-0688.

13. R. K. Byers, CSQ Calculations of Hydrogen Detonations in the Zion and Sequoyah Nuclear Plants, NUREG/CR-2358, SAND81-2216, to be published.

HYDROGEN BEHAVIOR AND CONTROL
IN LIGHT WATER REACTOR ACCIDENTS

PRESENTATION BY

MARSHALL BERMAN
SANDIA NATIONAL LABORATORIES
ALBUQUERQUE, NEW MEXICO

AT

NINTH WATER REACTOR SAFETY RESEARCH INFORMATION MEETING
GAITHERSBURG, MARYLAND

OCTOBER 29, 1981

HYDROGEN BEHAVIOR AND CONTROL IN LWR ACCIDENTS

- THE NATURE AND EXTENT OF THE PROBLEM
- THE IMPORTANT UNRESOLVED ISSUES
- SANDIA'S CONTRIBUTIONS TO THE RESOLUTION OF IMPORTANT QUESTIONS

HYDROGEN BEHAVIOR AND CONTROL
IN LWR ACCIDENTS

UNRESOLVED QUESTIONS REMAIN IN THE AREAS OF

- H_2 AND O_2 GENERATION AND TRANSPORT
- H_2 AND O_2 DETECTION
- COMBUSTION
- MITIGATION AND PREVENTION

IMPORTANT QUESTIONS

H_2 AND O_2 GENERATION AND TRANSPORT

- DEPENDENCE ON PLANT TYPE AND ACCIDENT SCENARIO.
- QUANTITIES AND RATES OF H_2 GENERATED BY MAP, RADIOLYSIS, CORE CONCRETE INTERACTIONS, AND CORROSION.
- TRANSPORT IN CONTAINMENT. MIXING TIMES, POTENTIAL FOR HIGH LOCAL CONCENTRATIONS

IMPORTANT QUESTIONS

H_2 AND O_2 DETECTION

- CAPABILITIES AND LIMITATIONS OF EXISTING EQUIPMENT. SPATIAL RESOLUTION, RESPONSE TIME, ACCURACY, RELIABILITY, SURVIVABILITY.
- IF NECESSARY, DESIGN AND TEST NEW EQUIPMENT.

IMPORTANT QUESTIONS

HYDROGEN COMBUSTION

- DEFLAGRATIONS: LIMITS IN GAS MIXTURES (DYNAMIC ACCIDENT CONDITIONS VS. STEADY LABORATORY ENVIRONMENT), EFFECTS OF TURBULENCE, MULTIPLE IGNITIONS, REPEATED BURNS, INHOMOGENEITIES, FOGS.
- DETONATIONS: LIMITS IN GAS MIXTURES, IMPULSIVE LOADING, DECAY, FOGS.
- ACCELERATED FLAMES AND TRANSITION TO DETONATION EFFECTS OF CONCENTRATION, SCALE, OBSTACLES, TURBULENCE, PEAK LOADS, FOGS.
- EFFECTS ON EQUIPMENT FUNCTIONING AND SURVIVAL.

MITIGATION SCHEMES

- DELIBERATE IGNITION AND FLARING
- DILUENTS — SPRAYS, FOGS, FOAMS
- PRE-ACCIDENT INERTING
- POST-ACCIDENT INERTING — HALON, CO_2 ENGINES
- CHEMICAL GETTERING — PRIMARY SYSTEM, CONTAINMENT
- RECOMBINERS

IMPORTANT QUESTIONS

MITIGATION SCHEMES

- EFFICACY
- COST VERSUS BENEFIT
- POTENTIAL PROBLEMS
- INTERACTIONS WITH OTHER SYSTEMS
- NET RISK REDUCTION

HYDROGEN BEHAVIOR AND CONTROL

IN LWR ACCIDENTS

- SANDIA'S CONTRIBUTIONS TO THE RESOLUTION OF

IMPORTANT QUESTIONS -

SANDIA NATIONAL LABORATORIES

HYDROGEN PROGRAM

OBJECTIVE:

QUANTIFY THE THREAT POSED BY HYDROGEN RELEASED DURING LWR ACCIDENTS AND GENERATE INFORMATION, PROCEDURES AND CONCEPTS WHICH WILL PREVENT OR MITIGATE THAT THREAT.

MAJOR END PRODUCTS:

1. ASSESSMENT OF THREAT FOR SEVERAL CLASSES OF PLANTS.
2. ASSESSMENT OF ADEQUACY OF EXISTING SAFETY SYSTEMS AND MITIGATION STRATEGIES.
3. IDENTIFICATION AND CONCEPT DEMONSTRATION OF IMPROVED MITIGATION AND DETECTION SYSTEMS.
4. PUBLICATION OF OPERATOR STRATEGIES, TRAINING AND EMERGENCY MANUALS.
5. CODES FOR ADDRESSING THE TRANSPORT AND COMBUSTION OF HYDROGEN IN CONTAINMENTS.

SANDIA HYDROGEN PROGRAMS

DIRECT:

- COMBUSTIBLE GAS IN CONTAINMENT
  RES-A1255
- HYDROGEN BURN SURVIVAL
  ANALYSIS AND MODELLING - NRR-A1306
  EXPERIMENTS - RES-A1270
- HYDROGEN BEHAVIOR
  RES-A1246
- HYDROGEN COMBUSTION MITIGATION AND PREVENTION
  RES-BB05?
- REVIEW OF GRAND GULF HYDROGEN IGNITER SYSTEM
  NRR-A1306

INDIRECT:

- MOLTEN CORE-CONCRETE INTERACTIONS
  RES-A1014
- MOLTEN CORE-COOLANT INTERACTIONS
  RES-A1030
- CORE MELT TECHNOLOGY
  RES-A1018
- CONTAINMENT ANALYSIS
  RES-A1198
- SAFETY MARGINS FOR CONTAINMENT
  RES-A1249
- CODE ASSESSMENT AND APPLICATIONS
  RES-A1205

HYDROGEN BEHAVIOR

PROGRAM MANAGER: M. BERMAN

PROJECT LEADER: J. C. CUMMINGS

PRINCIPAL INVESTIGATORS:

ANALYSIS AND MODELLING

M. R. BAER, J. BOCCIO (BNL), B. W. BURNHAM, R. K. BYERS, A. L. CAMP, S. E. DINGMAN, S. K. GRIFFITHS, M. P. SHERMAN

EXPERIMENTAL PROGRAM

W. B. BENEDICK, J. C. CUMMINGS, J. H. S. LEE ET AL. (MC GILL UNIVERSITY), S. F. MOLLER, J. E. SHEPHERD

HYDROGEN BEHAVIOR PROGRAM
ACCOMPLISHMENTS THROUGH FY81

- COMPENDIUM PUBLISHED.
- HYDROGEN DETECTOR DRAFT REPORT RELEASED.
- HYDROGEN WORKSHOP HELD, PROCEEDINGS PUBLISHED.
- SEQUOYAH MITIGATION STUDY COMPLETED, REPORT PUBLISHED.
- GRAND GULF MITIGATION STUDY INITIATED.
- COMPREHENSIVE PROGRAM PLAN DEVELOPED.
- ACCIDENT ANALYSES FOR VARIOUS LWR CONTAINMENTS INITIATED.
- DEFLAGRATION, DETONATION, HEAT TRANSFER CODES DEVELOPED.
- BALOC CODE OBTAINED, EVALUATION BEGUN.
- CSQ DETONATION CALCULATIONS FOR ZION AND SEQUOYAH.
- WORK INITIATED ON HYDROGEN EMERGENCY MANUAL.
- EXPERIMENTAL TEST PLAN DEVELOPED, PRESENTED, APPROVED.
- LABORATORY EXPERIMENTS INITIATED ON FOGS AND FOAMS.
- VGES 16"-TANK TS #1 THROUGH 8 COMPLETED.
- H_2-STEAM JET FACILITY TO BE DESIGNED AND CONSTRUCTED.
- FITS-TANK TO BE MODIFIED.
- EXPERIMENTS ON ACCELERATED FLAMES AND DETONATIONS INITIATED AT McGILL UNIVERSITY.

HYDROGEN BEHAVIOR PROGRAM
EXPECTED RESULTS IN FY82

- CSQ REPORT ON ZION/SEQUOYAH TO BE PUBLISHED.
- HYDROGEN DETECTOR REPORT TO BE PUBLISHED.
- COMPLETE ACCIDENT ANALYSES WITH MARCH.
- COMPLETE DEFLAGRATION CODE (2D, INHOMOGENEOUS).
- COMPLETE BALOC CODE ASSESSMENT.
- PERFORM CSQ DETONATION CALCULATIONS, AS NECESSARY.
- PERFORM PRELIMINARY ASSESSMENT OF MISSILE THREAT.
- PUBLISH MANUAL ON HYDROGEN BEHAVIOR DURING LWR ACCIDENTS.
- INITIATE EFFORT AIMED AT MODELLING ACCELERATED FLAMES.
- COMPLETE MODIFICATION OF FITS FACILITY AND PERFORM TESTS ON DEFLAGRATIONS AND DETONATIONS IN TERNARY MIXTURES OF HYDROGEN-AIR-STEAM.
- COMPLETE CONSTRUCTION OF STEAM-HYDROGEN FACILITY AND PERFORM TESTS ON AUTOIGNITION (AND INTENTIONAL FLAME UNDER BROSE).
- PUBLISH REPORT ON FY81 EXPERIMENTS IN VGES 16"-TANK.
- CONTINUE EXPERIMENTS IN VGES 16"-TANK (MITIGATION, FLAME ACCELERATION, DETONATION).
- CONSTRUCT FLAME ACCELERATION FACILITY. INITIATE EXPERIMENTATION.
- CONTINUE EXPERIMENTS ON FLAME ACCELERATION AND DETONATION AT McGILL UNIVERSITY.

HYDROGEN COMBUSTION MITIGATIVE AND PREVENTIVE SCHEMES

OBJECTIVES: TO PROVIDE THE NRC WITH INFORMATION TO EVALUATE PROPOSED EQUIPMENT, CONCEPTS AND OPERATIONAL SCHEMES TO PREVENT OR MITIGATE THE EFFECTS OF HYDROGEN COMBUSTION DURING LWR ACCIDENTS.

HYDROGEN COMBUSTION MITIGATION
PROGRAM TASKS

1. EVALUATE THE EFFECTIVENESS AND FEASIBILITY OF THE FOLLOWING CONTROL METHODS UNDER ACCIDENT AND POST-ACCIDENT CONDITIONS:
   A) DELIBERATE IGNITION
   B) PRE- AND POST-ACCIDENT INERTING WITH HALON, CO_2 OR N_2
   C) OXYGEN DEPLETION PRIOR TO OR DURING AN ACCIDENT
   D) WATER FOGS AND FOAMS
2. IDENTIFY AND ASSESS NEW CONTROL MEASURES
3. PLAN AND CONDUCT LAB AND INTERMEDIATE SCALE TESTS ON CONTROL SCHEMES (VGES, FITS)
4. INVESTIGATE DELIBERATE FLARING IN THE STEAM-H_2 JET FACILITY
5. IDENTIFY ADVANTAGES AND DISADVANTAGES OF THE VARIOUS SCHEMES (ENGINE, MDT, ETC.)
6. COORDINATE RESEARCH WITH OTHER H_2 PROGRAMS.

HYDROGEN COMBUSTION MITIGATIVE
AND PREVENTIVE SCHEMES

EXPECTED RESULTS IN FY82

- CONTINUE EVALUATION OF PROPOSED MITIGATION SCHEMES (DELIBERATE IGNITION, WATER FOGGING, PRE- AND POST-ACCIDENT INERTING, FLARING).
- IDENTIFY NEW HYDROGEN CONTROL MEASURES.
- CONDUCT LABORATORY AND INTERMEDIATE SCALE TESTS ON MITIGATION SCHEMES (IN VGES JET TANK, FITS TANK, LAPSE FLAME ACCELERATION FACILITY, STEAM/HYDROGEN JET FACILITY.

HYDROGEN BURN SURVIVAL

OBJECTIVES:

- DETERMINE THE THERMAL AND MECHANICAL LOADS WHICH COULD BE DELIVERED TO EQUIPMENT DURING HYDROGEN COMBUSTIONS IN TYPICAL LWR ACCIDENTS.
- DETERMINE THE EFFECTS OF THOSE LOADS ON EQUIPMENT, I.E., SURVIVAL, DEGRADATION OF FUNCTION OR FAILURE.

PROGRAM MANAGER: LOUIS D. CROFF

PROJECT LEADER: WILLIAM McCULLOCH

HYDROGEN BURN SURVIVAL

MAJOR EIC PRODUCTS

1. ANALYTICAL TOOLS FOR CALCULATING THE THERMAL AND MECHANICAL ENVIRONMENTS LIKELY TO RESULT FROM HYDROGEN DEFLAGRATIONS AND DETONATIONS.
2. PREDICTIONS OF THE EFFECTS OF COMBUSTION ON EQUIPMENT.
3. EXPERIMENTAL INVESTIGATION OF THE EFFECTS OF TRANSIENT LOADS ON REPRESENTATIVE PIECES OF SENSITIVE EQUIPMENT.

HYDROGEN BURN SURVIVAL

ACCOMPLISHMENTS THROUGH FY81

- DEVELOP A PROGRAM PLAN.
- SELECT COMPONENTS TO BE TESTED.
- DEVELOP MODELS TO CHARACTERIZE THE TEMPERATURE AND

PRESSURE ENVIRONMENTS.

HYDROGEN BURN SURVIVAL

EXPECTED RESULTS IN FY82

- DEFINE AND ASSESS MODELS TO CHARACTERIZE THE CONTAINMENT BURN ENVIRONMENT (INHOMOGENEOUS CONCENTRATIONS, MULTIPLE BURNS, ETC.)
- DEVELOP MODELS TO PREDICT RESPONSES OF COMPONENTS TO BURNS
- ASSESS ABOVE MODELS AGAINST EXPERIMENTAL DATA (VESS, HITS, BAC AND MEAT FACILITY, ETC.)

COMBUSTIBLE GAS IN CONTAINMENT

OBJECTIVE: DETERMINE THE RATES AND QUANTITIES OF HYDROGEN WHICH CAN BE GENERATED BY THE CORROSION OF ZINC AND OTHER COATINGS IN CONTAINMENT AFTER A HYPOTHETICAL LWR ACCIDENT

PROJECT LEADER: JOHN CUMMINGS

PRINCIPAL INVESTIGATOR: VINCENT LOYOLA

SOURCES OF HYDROGEN

FROM CORROSION

- ZINC-BASED PAINTS/PRIMERS
- ZINC GALVANIZING
- ALUMINUM
- ORGANIC MATERIALS
- OTHER MATERIALS

QUESTIONS TO BE ANSWERED

- INVENTORY IN "TYPICAL" CONTAINMENTS
- RATE OF HYDROGEN EVOLUTION

COMBUSTIBLE GAS IN CONTAINMENT

ACCOMPLISHMENTS THROUGH FY81

- PERFORMED LWR CONTAINMENT ZINC INVENTORY.
- PERFORMED LITERATURE REVIEW.
- DESIGNED, BUILT AND TESTED STEEL REACTOR VESSEL FOR CORROSION TESTS.
- OBTAINED GALVANIZED STEEL COUPONS AND BEGAN TEST PROGRAM (pH, TEMPERATURE, BORIC ACID CONCENTRATION).

COMBUSTIBLE GAS IN CONTAINMENT

EXPECTED RESULTS IN FY82

- COMPLETE BASIC EXPERIMENTAL SERIES
- CONDUCT ADDITIONAL TESTS (NITROGEN, SPRAY, ETC.)
- PERFORM MORPHOLOGICAL ANALYSIS OF DEBRIS AND PARTICULATES (TO ESTIMATE EFFECTS ON PUMPS)
- PREPARE TOPICAL REPORT ON ZINC STUDIES
- PREPARE PLAN TO INVESTIGATE ORGANIC COATINGS (PERHAPS ALSO INCLUDING A RADIATION ENVIRONMENT)

THE BEHAVIOR OF HYDROGEN DURING ACCIDENTS IN LIGHT WATER REACTORS

OBJECTIVES OF REPORT:

1. PROVIDE A COMPENDIUM (BRIEF SUMMARY) OF INFORMATION PERTINENT TO HYDROGEN BEHAVIOR DURING LWR ACCIDENTS
2. DETERMINE THE STATE OF KNOWLEDGE AND IDENTIFY IMPORTANT UNCERTAINTIES AND UNKNOWNS WHICH AFFECT REACTOR SAFETY.

HYDROGEN DETECTION AND CONTROL IN NUCLEAR POWER PLANTS

- SURVEY OF COMMERCIAL HYDROGEN DETECTION SCHEMES
  - LIST OF INSTRUMENT TYPES
  - IDENTIFY PRINCIPLE OF OPERATION
  - VULNERABILITY TO WATER, STEAM AND GASES
  - ACCURACY AND RELIABILITY
  - EFFECTS OF RADIATION
  - LIFETIME CHARACTERISTICS

IS IT ADEQUATE FOR POWER PLANT APPLICATION?
CAN IT BE MODIFIED TO MAKE IT ADEQUATE?

- SURVEY OF UTILITIES

  PLANS FOR HYDROGEN DETECTION
  PLANS FOR HYDROGEN MITIGATION

IF COMMERCIAL TECHNOLOGY IS INADEQUATE

- DEVELOP ADVANCED HYDROGEN DETECTION AND MITIGATION SYSTEM

Sandia National Laboratories

WORKSHOP ON THE IMPACT OF HYDROGEN ON WATER REACTOR SAFETY

BNL/SANDIA

ALBUQUERQUE, NEW MEXICO

JANUARY 26, 27, 28, 1981

- REGULATORY PERSPECTIVES ON H_2 CONTROL
- H_2 BEHAVIOR DURING LWR ACCIDENTS
- H_2 SOURCES AND DETECTION
- COMBUSTION EXPERIMENTS AND ANALYSIS
- H_2 MITIGATION
- TMI-2
- H_2 RESEARCH PROGRAMS

HYDROGEN PROGRAM

SEQUOYAH MITIGATION SCHEMES

DELIBERATE IGNITION

BENEFICIAL FOR MANY ACCIDENTS
CAN BE IMPROVED

WATER FOGS

LARGE POTENTIAL BENEFITS FOR
COMBUSTION, STEAM
OVERPRESSURIZATION, AEROSOLS

HALON

FEASIBLE SCHEME
POTENTIAL PROBLEMS WITH OVER-
PRESSURIZATION, CORROSION,
HYDROGEN REMOVAL

SEQUOYAH MITIGATION EFFORT
DELIBERATE IGNITION - SUMMARY

ADVANTAGES:

- RELATIVELY INEXPENSIVE, EASY TO RETROFIT
- GOAL IS TO PRODUCE MANAGEABLY SMALL RISES IN PRESSURE AND TEMPERATURE
- SHOULD BE BENEFICIAL FOR MANY ACCIDENT SCENARIOS
- IF ACCIDENTAL IGNITION IS INEVITABLE, EARLY, CONTINUOUS IGNITION IS USUALLY BENEFICIAL

DISADVANTAGES:

- COULD BE DETRIMENTAL FOR SOME ACCIDENT SCENARIOS WHICH INVOLVE:
  1. HIGH HYDROGEN RELEASE RATES FROM THE PRIMARY SYSTEM
  2. FORMATION OF POCKETS OF HIGH HYDROGEN CONCENTRATION
  3. EXHAUSTED ICE TRAYS
  4. INOPERABLE SPRAYS OR FANS
  5. CORE MELT

QUESTIONS:

- FLAME ACCELERATION IN ICE CONDENSER REGIONS
- EQUIPMENT SURVIVABILITY

SEQUOYAH MITIGATION EFFORT
WATER FOG MITIGATION -- SUMMARY

- WATER FOGGING APPEARS TO BE A WORKABLE MITIGATION SCHEME
- DROPLET SIZES <100 μm WILL BE REQUIRED.
- DROPLETS >20 μm WILL VAPORIZE EXTERNAL TO THE FLAME ZONE, BUT RAPIDLY ENOUGH TO VALIDATE THE THERMODYNAMIC RESULTS.
- MINIMAL EFFECTS ON FLAMMABILITY LIMITS ARE EXPECTED FOR DROPLETS >10 μm - PERMITS INTEGRATION WITH DELIBERATE IGNITION.
- CONVENTIONAL NOZZLE SYSTEMS WILL PRODUCE THE REQUIRED DROPLET SIZES.
- MAJOR UNRESOLVED QUESTION IS DROPLET RESIDENCE TIME AND LOSS RATES.

SEQUOYAH MITIGATION EFFORT
HALON MITIGATION
SUMMARY

PROS

- EXTENSIVE EXPERIENCE AND DATA
- INERTING CAPABILITY PROVEN
- MOST QUESTIONS FOR NUCLEAR REACTOR APPLICATIONS ANSWERED
- WITHOUT DECOMPOSITION, GAS WILL STABLE FOR LONG PERIOD

CONS

- INCREASE IN CONTAINMENT PRESSURE
- ACIDITY OF CONTAINMENT WATER, CORROSION
- TREATMENT OF POST-ACCIDENT GASES PROBABLY REQUIRES NEW OR MODIFIED RECOMBINER
- CONCENTRATION MUST REMAIN ABOVE INERT LEVEL

UNKNOWNS

- EFFECT OF DECOMPOSITION PRODUCTS
- TREATMENT OF POST-ACCIDENT CONTAINMENT ATMOSPHERE
- MIXING OF HALON WITH CONTAINMENT ATMOSPHERE W AND W/O FORCED CONVECTION (FANS)

COMBUSTION AND HEAT TRANSFER MODELLING

OBJECTIVE: DEVELOP A CAPABILITY TO PREDICT TEMPERATURE AND PRESSURE HISTORIES IN CONTAINMENT DURING AND AFTER A HYDROGEN COMBUSTION.

- DEFLAGRATIONS: CODE TO PREDICT ADIABATIC, ISOCHORIC Ps AND Ts, INCLUDING CO_2, CO, AND WATER FOG EVAPORATION.
- DETONATIONS: CODE TO PREDICT CHAPMAN-JOUGUET Ps AND Ts, INCLUDING INCREASES AFTER NORMAL REFLECTION.
- HEAT TRANSFER: CODES WHICH ADDRESS RADIATION, CONVECTION WITH OR WITHOUT CONDENSATION, CONDUCTION INTO SURFACES, AND EVAPORATION OF SPRAYS.

HYDROGEN TRANSPORT MODELLING

OBJECTIVE: DEVELOP A CAPABILITY TO PREDICT THE CONCENTRATIONS OF HYDROGEN, AIR AND STEAM IN CONTAINMENT AS FUNCTIONS OF POSITION AND TIME FOR HYPOTHETICAL LWR ACCIDENTS.

- ASSESSMENT OF RALOC
- ASSESSMENT OF OTHER CODES
- TRANSPORT AND MIXING EXPERIMENTS
  1. BATTELLE - FRANKFURT
  2. EPRI - HEDL
  3. IN SITU TESTING WITH HELIUM BEFORE LICENSING
  4. SANDIA EXPERIMENTS

CURRENT STATUS

- CODE WAS BEEN CONVERTED TO CDC COMPUTER SYSTEM (FROM ARDAHL).
- FOUR TEST PROBLEMS HAVE BEEN REPRODUCED SATISFACTORILY (SANDIA VS. GRS).
- PLOT CAPABILITY DEVELOPMENT WAS BEEN COMPLETED.
- CODE WAS BEEN MODIFIED TO RESTART PROPERLY DURING FULLY IMPLICIT INTEGRATION.
- PLOT/RESTART FREQUENCY CONTROLS HAVE BEEN MODIFIED.
- SEVERAL ASSESSMENT CALCULATIONS USING BATTELLE CONFIGURATIONS 2, 6, 10 AND 19 HAVE BEEN PERFORMED.
- PRELIMINARY GRAND GULF PLANT MODALIZATION WAS BEEN DEVELOPED AND SIMPLE SENSITIVITY STUDIES HAVE BEEN PERFORMED.

FY80 SCOPE

- ASSESS RALOC CODE AGAINST AVAILABLE TEST DATA ON HYDROGEN TRANSPORT WITHIN CONTAINMENT.
- PERFORM RALOC CODE IMPROVEMENTS WHERE NECESSARY.
- COOPERATE WITH LANL IN IDENTIFYING BENCHMARK CASE FOR COMPARING RALOC AND LANL MULTIDIMENSIONAL ANALYSIS.
- MODEL LARGE DRY PWR CONTAINMENT
  ICE CONDENSER PWR
  BWR
- PERFORM SMALL BREAK AND LARGE BREAK ANALYSIS.

CSQ CODE MODELLING

OBJECTIVE DETERMINE THE IMPULSIVE LOADS WHICH COULD RESULT FROM DETONATIONS IN VARIOUS CONTAINMENTS DURING HYPOTHETICAL LMF ACCIDENTS.

- MODIFICATIONS TO CSQ
- CALCULATIONS OF GLOBAL DETONATIONS IN ZION
- CALCULATIONS OF VARIOUS LOCAL DETONATIONS IN SEQUOYAH
- REPORT BEING WRITTEN

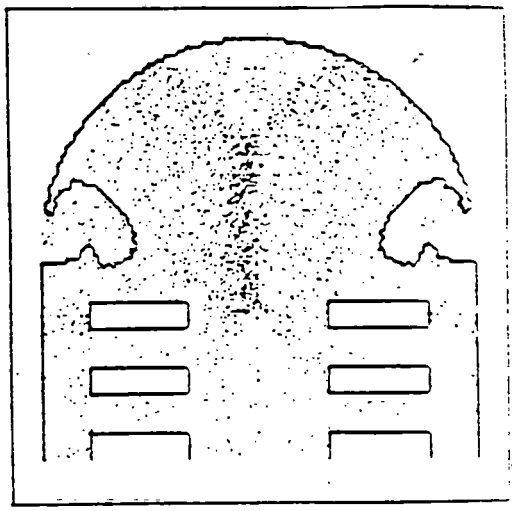

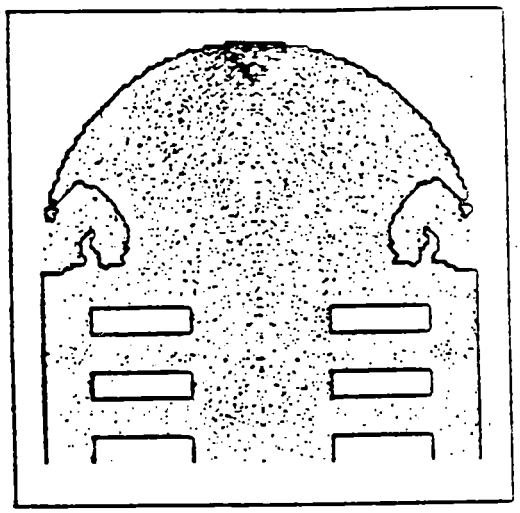

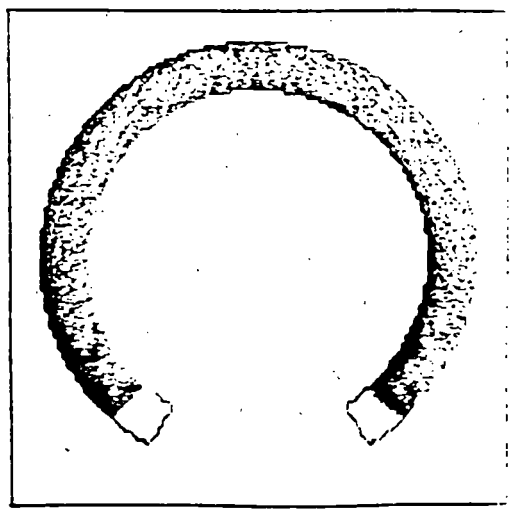

HYDROGEN EXPERIMENTAL PROGRAM

OBJECTIVES

1. CONFIRM EARLIER ANALYTIC AND EXPERIMENTAL WORK.
2. PROVIDE A DATA BASE FOR MODEL DEVELOPMENT AND ASSESSMENT.
3. ANSWER QUESTIONS TOO COMPLEX TO MODEL ANALYTICALLY.
4. EVALUATE EQUIPMENT SURVIVAL AND MITIGATION SCHEMES UNDER CONDITIONS SIMULATING LWR ACCIDENTS.
5. INDICATE THE EFFECTS OF SCALE TO PERMIT RESULTS TO BE EXTRAPOLATED TO REACTOR-SCALE ACCIDENTS.

2-PRONGED EXPERIMENTAL APPROACH

I. VARIABLE GEOMETRY EXPERIMENTAL SYSTEM (VGES)

- SMALL TO LARGE SCALE (2 - 100,000 cu ft.)
- BOTH CRUDE AND SOPHISTICATED INSTRUMENTATION
- INCLUDES LABORATORY APPARATUS, STEEL TANKS, HEATED JETS, BALLOONS, TRENCHES, ETC.
- SOME SYSTEMS ARE IMMEDIATELY AVAILABLE

II. MODIFIED FITS FACILITY

- SMALL TO INTERMEDIATE SCALE (25 - 200 cu ft.)
- INEXPENSIVE RETROFIT
- HIGHLY INSTRUMENTED

EXPERIMENTAL PROGRAM FACILITIES

OPERATIONAL:

- LABORATORY-SCALE (FOG & FOAM)
- VGES 16-FT TANK
- MCGILL TESTS

OPERATIONAL IN FY82:

- FITS TANK
- STEAM-HYDROGEN JET
- VGES ACCELERATED FLAME FACILITY

PLANNED ACCORDING TO NEED:

- VGES PLASTIC BAG DETONATIONS
- THUNDER TUBE
- VGES TRENCH (VERY LARGE SCALE)

HYDROGEN PROGRAM

FLAME ACCELERATION STUDIES

MC GILL UNIVERSITY:	SMALL SCALE EXPERIMENTS AND ANALYSIS
SANDIA	LARGE SCALE EXPERIMENTS, ANALYSIS AND COMPUTER MODELLING.

ACCELERATED FLAMES

McGILL SUPPORT, JOHN LEE ET AL.

- NEAR TERM EFFORTS WILL PROVIDE QUALITATIVE EXPERIMENTAL DATA TO DETERMINE THE SENSITIVITY OF OFF-STOICHIOMETRIC HYDROGEN-AIR MIXTURES TO
  1. FLAME ACCELERATION BY OBSTACLES,
  2. TRANSITION TO DETONATION IN AN OBSTACLE ENVIRONMENT.

McGILL EXPERIMENTS

PRELIMINARY RESULTS - FLAME ACCELERATIONS

- WITHOUT OBSTACLES: FLAME QUICKLY ACCELERATES TO STEADY STATE SPEED (ABOUT 0.2 - 15 M/S FOR 4 - 16% H_2)
- WITH OBSTACLES:
  1. 6.4 CM DIAM TUBE, 50% BLOCKAGE
     - 8% H_2: $v > 20$ M/S AND INCREASING
     - 12% H_2: $v > 220$ M/S AND INCREASING
     - 16% H_2: $v > 500$ M/S AND INCREASING
     - 16% H_2: $\Delta P \sim 7$B AND INCREASING

     A MIXTURE OF 16% H_2 IN AIR HAS AN ACCELERATION SIMILAR TO STOICHIOMETRIC METHANE-AIR.
  2. METHANE-AIR IN 12.7 x 20.3 CM CHANNEL
     - STAGGERED OBSTACLES ARE VERY EFFICIENT AT ACCELERATING FLAMES
     - ACCELERATION VERY SENSITIVE TO DEGREE OF CONFINEMENT

McGILL EXPERIMENTS

PRELIMINARY RESULTS - DETONATIONS

- A MAXIMUM TURBULENT FLAME SPEED MAY EXIST WHICH IS A FUNCTION OF CONCENTRATION, GEOMETRY AND OBSTACLES (E.G., $V_{MAX} \sim$ 800 M/S FOR 20% H_2-AIR, 6 MM SCHELKIN SPIRAL, 5 CM DIAM. TUBE).
- A MINIMUM FLAME SPEED MAY BE REQUIRED FOR TRANSITION TO DETONATION (ABOUT 1500 M/S FOR ABOVE CONDITIONS).
- THE CRITICAL TUBE DIAMETER, D_c, EQUALS ABOUT 13 DETONATION CELL WIDTHS FOR H_2 AND MANY OTHER HYDROCARBONS. D_c = 20 CM FOR STOICHIOMETRIC H_2-AIR, D_c = 2.0 M FOR 18% H_2.
- DETONATIONS IN MIXTURES CONTAINING LESS THAN 18% HYDROGEN APPEAR VERY UNLIKELY UNDER THESE LABORATORY CONDITIONS

ACCELERATED FLAMES

McGILL SUPPORT, JOHN LEE ET AL.

- LONG TERM EFFORTS INCLUDE SMALL SCALE EXPERIMENTS AND MODELLING TO ADDRESS
  1. THE EFFECTS OF REPEATED OBSTACLES (DIFFERENT GEOMETRIES AND SPACINGS) AND VARYING DEGREES OF CONFINEMENT ON FLAME ACCELERATION,
  2. THE TRANSITION DISTANCE AS A FUNCTION OF OBSTACLE ENVIRONMENT AND DEGREE OF CONFINEMENT,
  3. STRONG (JET) IGNITION AND DIRECT INITIATION OF DETONATIONS,
  4. THE TRANSMISSION OF DETONATIONS THROUGH TUBES AND OTHER GEOMETRIES,
  5. THE LEAN LIMITS OF DETONABILITY FOR VARYING DEGREES OF CONFINEMENT.

VGES : LABORATORY EXPERIMENTS

FOG GENERATION AND MAINTENANCE

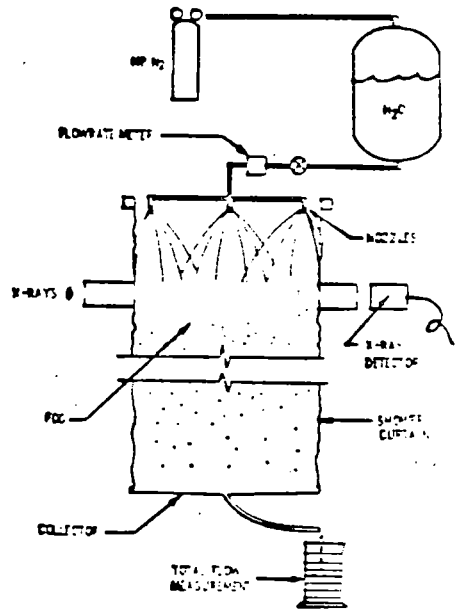

VGES : LABORATORY EXPERIMENTS

FOG GENERATION AND MAINTENANCE

CONCEPT FEASIBILITY DEMONSTRATION

DIRECT DENSITY MEASUREMENT - X-RAY OR OPTICAL BEAM ATTENUATION

INSTRUMENTATION DEVELOPMENT

COMBUSTION IN FOAM

FLAME TUBE - GLOBAL FLAME PROPAGATION, CHARACTERISTICS

VGES 16.04 - FT TANK

SIZE	14-16 ft. in length 4 ft. in diameter 175-200 ft^3 (5.0-5.7 m^3) in volume
STRENGTH	200 PSI (Safety Factor 4
INSTRUMENTATION	Pressure Transducers Thermocouples Gas Sampling
INFORMATION	Scoping
EXPERIMENTS	Hydrogen Concentration Igniter Type, Location Turbulence Water Fogs Obstacles, Ducts Halon Shock Ignition CO_2 Equipment Survivability Additional Tests (Foams)

VGES : 16.04 - FT TANK

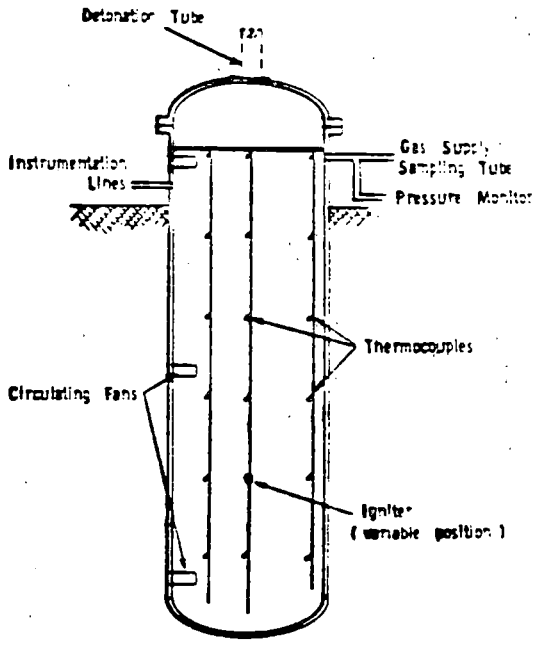

1.22 m (4 ft) diameter 4.27 m (14 ft) tall

5.0 m^3 (175 ft^3) volume

VSES 16 (14) FT TANK EXPERIMENTS

OBJECTIVE: QUICKLY PROVIDE SCOPING DATA AT INTERMEDIATE SCALE. RESULTS HELP TO ASSESS THREATS (DEFLAGRATIONS, DETONATION, ACCELERATED FLAMES) AND MITIGATION SCHEMES.

TESTS:
- HYDROGEN CONCENTRATION
- IGNITER TYPE
- IGNITER LOCATION
- QUIESCENT/TURBULENT
- DETONATIONS
- OBSTACLES
- WATER FOG/FOAMS
- CARBON DIOXIDE
- HALON

VSES 16-FT TANK STATUS

- COMPLETED TEST SERIES 1 - 8.
- 77 DEFLAGRATION TESTS
- MEASURES: P(t), T(t), FLAME SPEED, COMBUSTION COMPLETENESS
- DATA REDUCTION: CONTOUR PLOTS, α-t, $\Delta P/\Delta t$, V_{max}
- EXAMINED: HYDROGEN CONCENTRATION
  - IGNITER TYPE
  - IGNITER LOCATION
  - QUIESCENT/TURBULENT BURN
  - OXYGEN-DEPLETED AIR
  - 14-VOLT GLOW-PLUG IGNITER
  - LOW-PRESSURE COMBUSTION
- NEAR-TERM FUTURE:
  - WATER FOAMS
  - FLAME ACCELERATION
  - DETONATIONS

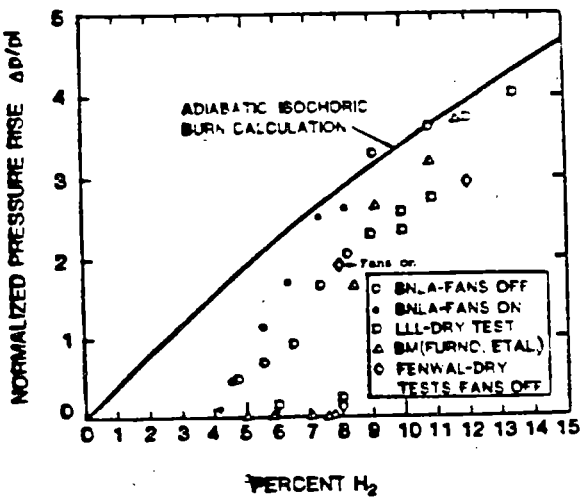

STEAM-HYDROGEN JET

SIZE:	SMALL ORIFICE (0.3-3CM) INITIALLY
FLOW:	CONTINUOUS OR PULSED UP TO SONIC STEAM SUBSONIC TO SUPERSONIC
TEMPERATURE:	VARIABLE UP TO 2000 K INITIALLY
PRESSURE:	VARIABLE UP TO 300 PSI INITIALLY
INSTRUMENTATION:	THERMOCOUPLES LASER SHADOWGRAPHY PHOTOGRAPHY INFRARED TELEVISION PITOT PROBES GAS SAMPLING
INFORMATION:	SCOPING AND DETAILED DATA
EXPERIMENTS:	HYDROGEN CONCENTRATION JET TEMPERATURE JET MOMENTUM IGNITION THRESHOLDS AUTOIGNITION FLAMEHOLDERS, OBSTACLES

HYDROGEN-STEAM JET FACILITY

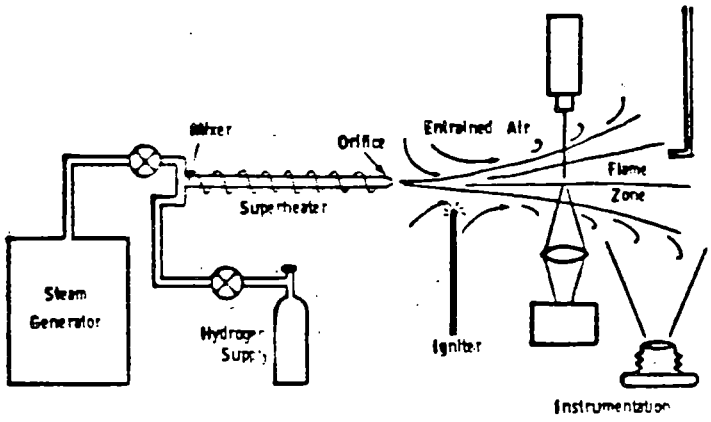

FITS TANK

SIZE:	11 ft. in length 5 ft. in diameter ~200 ft.^{3} (5.6 M^3) in volume
STRENGTH:	300 PSI (Safety Factor 4)
INSTRUMENTATION	Pressure Transducers Thermocouples Gas Sampling Laser Shadowgraphy Photography Infrared Television Strain Gages
INFORMATION EXPERIMENTS	Detailed Data Hydrogen Concentration Initial Temperature Igniter Type, Location Steam Deflagrations Detonations Obstacles, Ducts Shock Ignition Mitigation Schemes Hydrogen Mixing Transport Inhomogeneous Combustion

MODIFIED FITS TANK

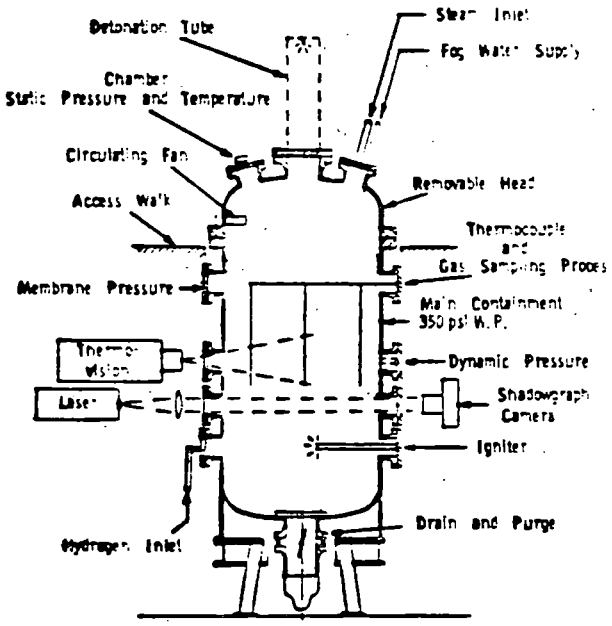

1.5 m (4.9 ft) diameter 3.4 m (11.2 ft) length
5.6 m^3 (195 ft^3) volume

SCHEMATIC OF ICE CONDENSER UPPER PLENUM REGION

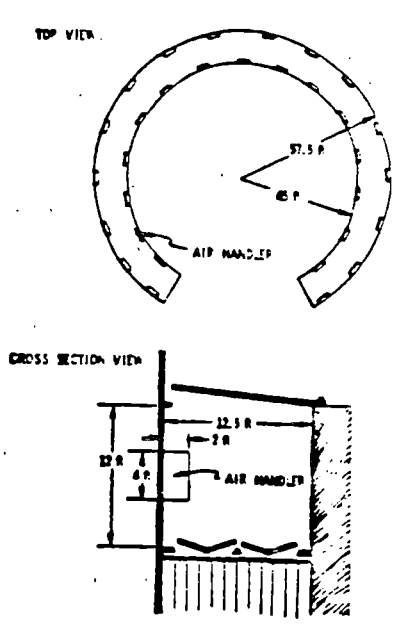

FLAME ACCELERATION FACILITY

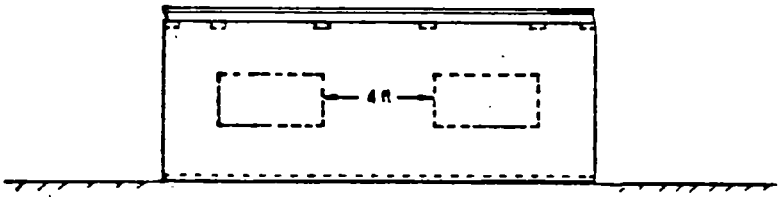

TYPICAL 16 ft SECTION-TOTAL LENGTH 96 ft

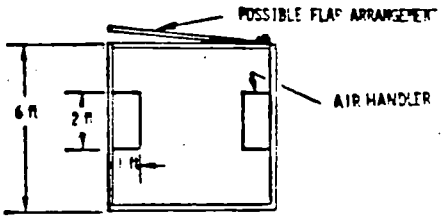

END VIEW

VGES TRENCH, ETC.

SIZE	Very large $\sim 10^5$ ft^3 ($\sim 3 \times 10^3$ m^3) in volume
STRENGTH	Frangible cover of negligible strength
INSTRUMENTATION	Pressure Transducers Thermocouples Gas Sampling (Automatic) Photography Infrared Television
INFORMATION	Scoping
EXPERIMENTS	Hydrogen Concentration CO_2 (Steam Simulant) Obstacles Buoyancy Equipment Survivability Mitigation Schemes Hydrogen Mixing Transport Inhomogeneous Combustion

VGES: VARIABLE GEOMETRY TRENCH

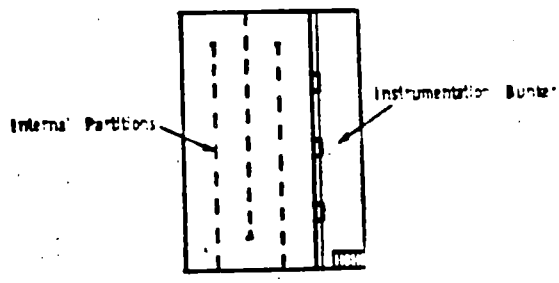

PLAN VIEW

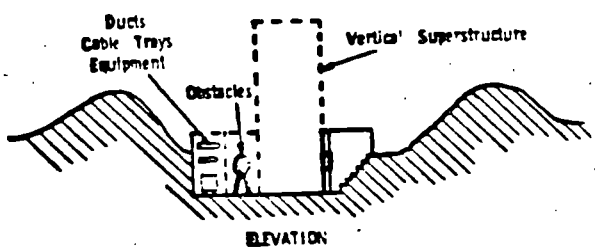

ELEVATION

CORE-MELT/COOLANT INTERACTIONS

PRESENTATION BY

M. L. CORRADINI*

SANDIA NATIONAL LABORATORIES

ALBUQUERQUE, NEW MEXICO

AT

NINTH WATER REACTOR SAFETY RESEARCH INFORMATION MEETING

GAITHERSBURG, MARYLAND

October 28, 1981

*Currently Assistant Professor of Nuclear Engineering, University of Wisconsin, Madison, WI 53706

CORE-MELT/COOLANT INTERACTIONS

M. Berman, M. L. Corradini*, N. A. Evans, D. E. Mitchell,
L. S. Nelson, D. V. Swenson

Light Water Reactor Safety Department
Sandia National Laboratories
Albuquerque, NM 87185

The objective of the core-melt/coolant interactions program is to develop an understanding of the nature of molten-fuel coolant (MFC) interactions during LWR accidents sufficient to: estimate the probability and consequences of in- and ex-vessel steam explosions, and to describe the phenomena associated with non-explosive MFC interactions both in- and ex-vessel.

In 1975, the Reactor Safety Study (WASH-1400)[1] estimated the probability of containment failure via missile generation caused by a steam explosion to be 0.01. Since that time, our research work [2-15] has indicated that the MFCI is a complex process which can affect containment response in a variety of ways; fuel-coolant mixing and rapid steam generation, fuel debris formation, dynamic pressures from a steam explosion, and possibly generation of missiles (the least probable event). We are investigating these physical processes to accurately assess the containment response and the risk from a core-melt accident.

Energetic MFCIs (Steam Explosions)

A steam explosion can be conceptually divided into four phases of energy transfer: (1) fuel-coolant contact and mixing, (2) triggering of the rapid heat transfer, (3) propagation of the explosion causing dynamic pressures, (4) expansion of the high pressure steam and possible generation of missiles.

In a core-melt accident, liquid water could be present in the lower plenum of the reactor vessel [2] and in the reactor cavity [11]. Intermediate scale experiments [3, 14] indicate that fuel-coolant mixing may be a function of the water depth and the fuel-coolant mass ratio. In large water depths ($\geq$ 0.6 m) fuel mixing down to 10 mm diameters occurs in a short time (~ 0.2 s), while in small water depths ($\leq$ 0.2 m) the fuel cannot mix completely with the water before it either reagglomerates on the chamber base, or there is an explosion in the part that does mix. This mixing process is still not well understood.

Experimental data at small and large scale [3-8, 14] indicate that steam explosion triggering is a function of a variety of initial conditions (fuel composition and temperature, coolant temperature, ambient pressure), any one of which may reduce the explosion efficiency. Experiments also support the hypothesis [9] that these initial condition effects can be overcome by introducing an external trigger or increasing its energy. For example, a larger bridgewire trigger pulse reinduces small scale steam explosions [3] at high ambient pressure, high water temperatures and low fuel temperatures near the solidus point. Also, introduction of an external

---

*Currently Assistant Professor of Nuclear Engineering,
University of Wisconsin, Madison, WI 53706

detonator trigger pulse reinduced an intermediate scale explosion [3, 14] at high ambient pressure (1.1 MPa). These results suggest that triggering of a steam explosion may be a stochastic process governed by the probable strength of realistic triggers during the accident and by the possible set of initial conditions; e.g., water reflood onto a molten fuel pool.

Small and intermediate scale experiments resulting in explosions [3, 6, 8, 14]using fuel simulants ($Fe-Al_2O_3$) and actual fuel compositions (UO_2, ZrO_2,SS) consistently produce conversion ratios between 0.1-3% (conversion ratio is the ratio of the measured work to the fuel thermal energy). The peak pressures from these explosions are in the range of 2-30 MPa with propagation velocities of 200-600 m/s. To analyze the experimental results, we have developed a mechanistic one-dimensional model and an empirical two-dimensional explosion model [3, 10, 13]. Both models show good qualitative agreement with the data [14]. In particular, the 2-D model shows good quantitative agreement when the ratio of the mass of fuel to the mass of coolant in the mixing zone is in the range 1 to 2. This result is similar to the initial mixing conditions of the FITS tests [3, 14].

Using the experimental results previously discussed, we have developed a simple probabilistic analysis technique [15] to predict the probability of containment failure due to solid missile generation caused by an in-vessel steam explosion. We limit our assumptions to the most basic physical conditions of the core melt accident and prescribe these initial conditions with frequency distributions. A Monte Carlo solution technique is employed to calculate output frequency distributions for steam explosion energy, reactor vessel response, and resulting missile velocities; a simplified steam explosion model and structural calculation is used. Based on current results, we estimate the probability of containment failure by missile generation caused by an in-vessel steam explosion is one to two orders of magnitude smaller than the WASH-1400 estimates.

Non-Energetic MFCI's (Steam Generation-Debris Formation)

During the past fiscal year, two intermediate scale scoping experiments were conducted (FITS-1G and 2G)[3], the purpose being to provide pressure and temperature data in the FITS chamber for molten fuel-coolant interactions in the absence of a steam explosion. The test results indicated three major physical events:

(i) The fuel melt (20 kg of $Fe-Al_2O_3$) enters the water, rapidly generates hydrogen, and subsequently undergoes combustion in the atmosphere.

(ii) The fuel melt mixes with the water; the degree of mixing depends on the water depth. The melt settles under gravity to the chamber base and eventually quenches, forming discrete debris particles as well as a single large solidified fuel mass.

(iii) As the melt quenches, it begins to decompose and erode the chamber base; this is conceptually similar to a molten core-concrete interaction.

These physical events can take place concurrently during the test. The peak pressures in the FITS atmosphere were 0.35-0.4 MPa; these values are at least a factor of two below thermodynamic values indicating that condensation is an important phenomenon. The fuel debris was of the order of 1-10 mm; this is quite large in comparison to debris from a steam explosion (~ 100-200 μm mass average).

We developed a quenching model which accurately predicted the pressure rise in the FITS chamber. The key elements were a boiling-condensation model and the assumption that fuel, which had formed solid debris, had an average diameter of 10 mm. Based on these results, the peak steam generation rate from the FITSG experiments was calculated to be 0.05 kg/s of steam per kilogram of fuel melt. Modelling of the hydrogen burn and the chamber base erosion are still underway.

Conclusion

Based on current experimental results and analysis, we estimate the probability of containment failure due directly to an energetic MFCI to be at least one to two orders of magnitude below WASH-1400 estimates. We do not mean to imply that explosive and non-explosive molten fuel-coolant interactions can be disregarded; rather research will now be directed toward understanding the nature and impact of such interactions throughout the course of a core melt accident. During this fiscal year, small and intermediate scale experiments and supporting analysis will continue to increase our understanding of these phenomena.

REFERENCES

1. WASH-1400-Reactor Safety Study, NUREG-75/0114, Appendix VIII, Nuclear Regulatory Commission, (October 1975).

2. L. D. Buxton, Molten Core/Water Contact Analysis for Fuel Melt Accidents, SAND77-1842, NUREG/CR-0391, Sandia Laboratories, (February 1979).

3. M. Berman, LWR Safety Research Program, Quarterly Report, Sandia Laboratories
   Jan-March 1979; SAND79-1542 (Dec 1979)
   April-June 1979; SAND79-2057 (Feb 1980)
   July-September 1979; SAND79-2290 (September 1980).
   October-December 1979; SAND80-0927 (July 1980)
   January-December 1980; SAND80-1304; No. 1, 2, 3, 4 (May 1980)
   January-September 1981; SAND81-1216, No. 1, 2, 3 (Oct 1981)

4. L. S. Nelson, L. D. Buxton, Steam Explosion Triggering Phenomena: Stainless Steel and Corium-E Simulants Studies with a Floodable Arc-Melting Apparatus, SAND77-0998, NUREG/CR-0122, Sandia Laboratories (May 1978).

References Continued

5. L. S. Nelson, L. D. Buxton, H. Planner, Steam Explosion Triggering Phenomena Part 2: Corium-A and Corium-E Simulants and Oxides of Iron and Cobalt Studied with a Floodable Arc-Melting Apparatus, SAND79-0620, NUREG/CR-9633, Sandia Laboratories (February 1980).

6. L. S. Nelson, P. M. Duda, Steam Explosion Experiments with Single Drops of Iron-Oxide Melted with a CO_2 Laser, SAND81-1346, NUREG/CR-2295, Sandia Laboratories (September 1981).

7. L. D. Buxton, W. B. Benedick, Steam Explosion Efficiency Studies, SAND79-1399, NUREG/CR-0947, Sandia Laboratories (November 1979).

8. L. D. Buxton, W. B. Benedick, M. L. Corradini, Steam Explosion Efficiency Studies: Part II - Corium Experiments, SAND80-1324, NUREG/CR-0324, Sandia Laboratories (December 1980).

9. M. L. Corradini, Phenomenological Modelling of the Small Scale Vapor Explosion Experiments, SAND79-2003, NUREG/CR-1105, Sandia Laboratories, (February 1980).

10. M. L. Corradini, Analysis and Modelling of Steam Explosion Experiments, SAND80-2121, NUREG/CR-2213, Sandia Laboratories (June 1981).

11. M. L. Corradini, D. V. Swenson, M. Berman, Chapter II, Report of the Zion/Indian Point Study: Volume I, SAND80-0611/1, NUREG/CR-1410, Sandia Laboratories (July 1980).

12. M. L. Corradini, R. L. Woodfin, L. E. Voelker, Preliminary Analysis of the Containment Failure Probability by Steam Explosions Following a Hypothetical Core Meltdown in an LWR, SAND79-2002, NUREG/CR-1104, Sandia Laboratories (February 1980).

13. M. L. Corradini, D. V. Swenson, Probability of Containment Failure by Steam Explosion Following a Postulated Core Meltdown in an LWR, SAND80-2132, NUREG/CR-2214, Sandia Laboratories (July 1981).

14. D. E. Mitchell, M. L. Corradini, W. W. Tarbell, Intermediate Scale Steam Explosion Phenomena: Experiments and Analysis, SAND81-0124, NUREG/CR-2145, Sandia Laboratories (September 1981).

15. D. V. Swenson, M. L. Corradini, Monte Carlo Analysis of LWR Steam Explosions, SAND81-1092, NUREG/CR-2037, Sandia Laboratories (October 1981).

CORE-MELT/COOLANT INTERACTIONS

PROGRAM MANAGER: M. BERMAN

PROJECT LEADER: N. A. EVANS

PRINCIPAL INVESTIGATORS:

N. A. EVANS: M. L. CORRADINI:	MODELLING AND ANALYSIS
D. E. MITCHELL:	LARGE-SCALE EXPERIMENTS
L. S. NELSON:	SMALL-SCALE EXPERIMENTS
D. V. SWENSON:	STRUCTURAL ANALYSIS AND STATISTICS

CORE-MELT/COOLANT INTERACTIONS

OBJECTIVE: DEVELOP AN UNDERSTANDING OF THE NATURE OF MOLTEN-FUEL COOLANT (MFC) INTERACTIONS DURING LWR ACCIDENTS SUFFICIENT TO:

1. ESTIMATE THE PROBABILITY AND CONSEQUENCES OF IN- AND EX-VESSEL STEAM EXPLOSIONS; AND TO
2. DESCRIBE THE PHENOMENA ASSOCIATED WITH NON-EXPLOSIVE MFC INTERACTIONS BOTH IN- AND EX-VESSEL.

MOLTEN-CORE COOLANT INTERACTIONS

PROGRAM ELEMENTS

- SMALL SCALE EXPERIMENTS
  - ARC MELTER
  - SINGLE DROPLET
- INTERMEDIATE SCALE EXPERIMENTS
  - OPEN GEOMETRY
  - FITS AND EXO-FITS
- MODELLING AND ANALYSIS
  - SIMPLE MODELS
  - 1D AND 2D HYDROCODES
  - STRUCTURAL ANALYSIS
  - PROBABILISTIC STUDIES

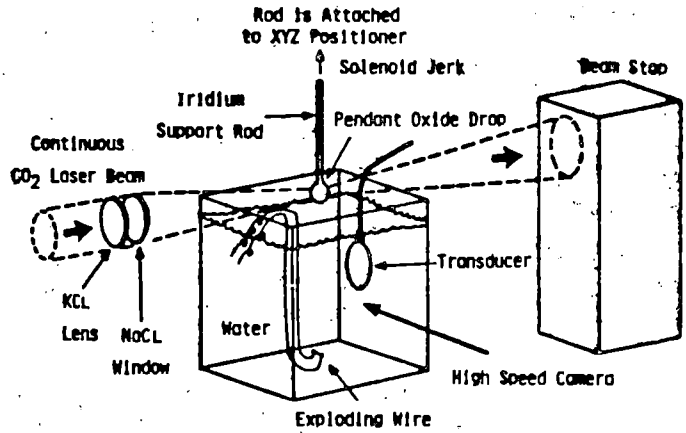

TECHNICAL PROGRESS

SMALL-SCALE EXPERIMENTS

- AMBIENT PRESSURE EFFECTS @ FIXED COOLANT TEMPERATURE, T_c
  - EXPLOSION CAN BE SUPPRESSED AS P_∞ INCREASES
  - EXPLOSION IS REINDUCED AS P_T INCREASES
  - EXPLOSIVITY INCREASES @ INTERMEDIATE PRESSURES

    COMPETING EFFECTS P_∞, T_c

    COLLAPSE MORE LIKELY AT INTERMEDIATE PRESSURES

- AMBIENT PRESSURE EFFECT @ FIXED SUBCOOLING, ΔT_c
  - EXPLOSION CAN BE INDUCED WITH SMALLER TRIGGER AS ΔT_c INCREASES

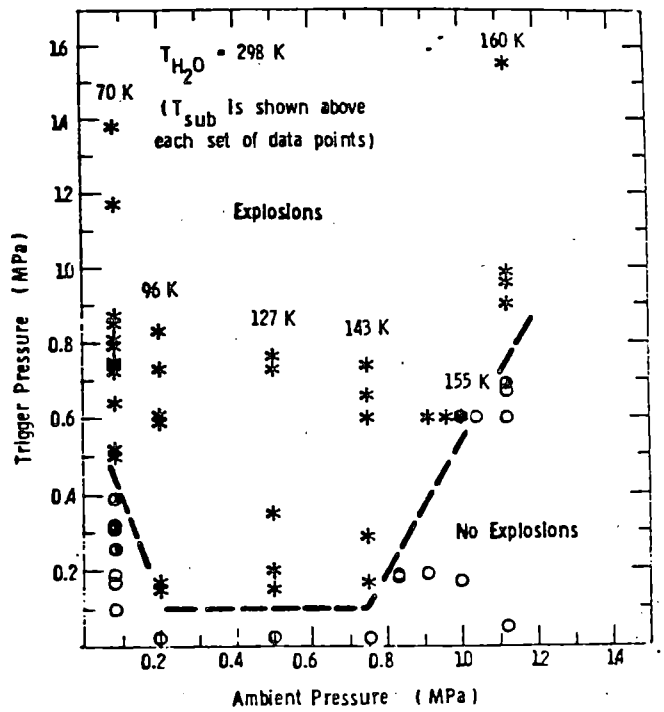

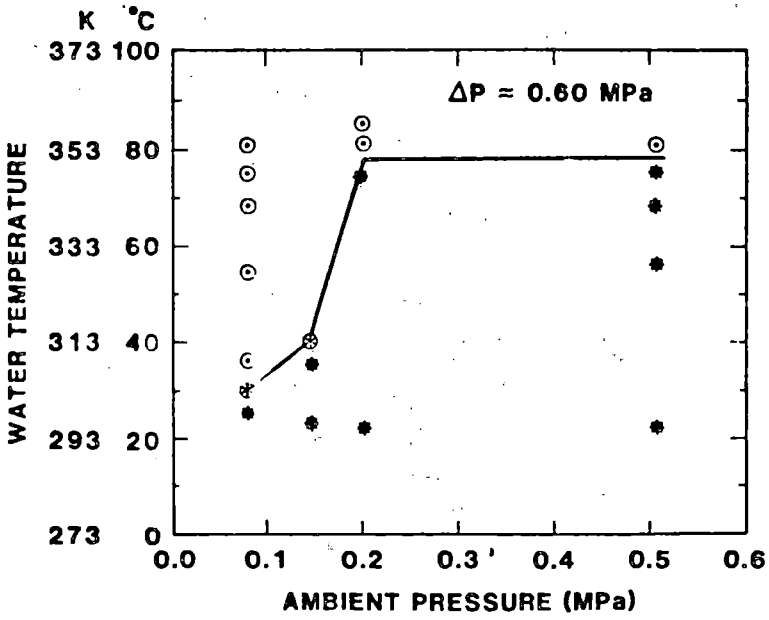

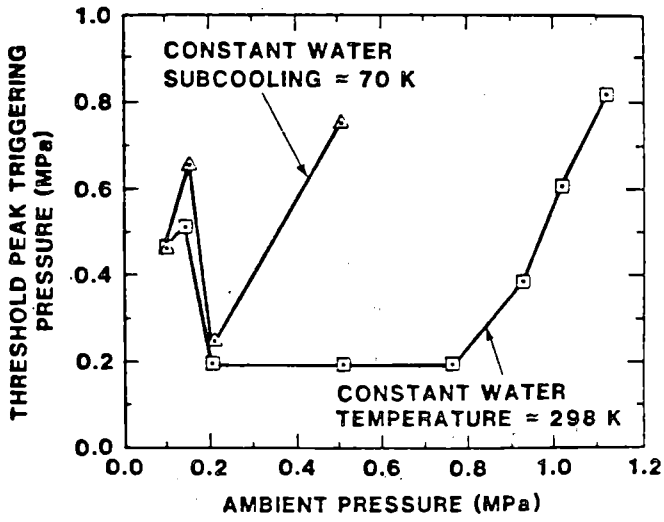

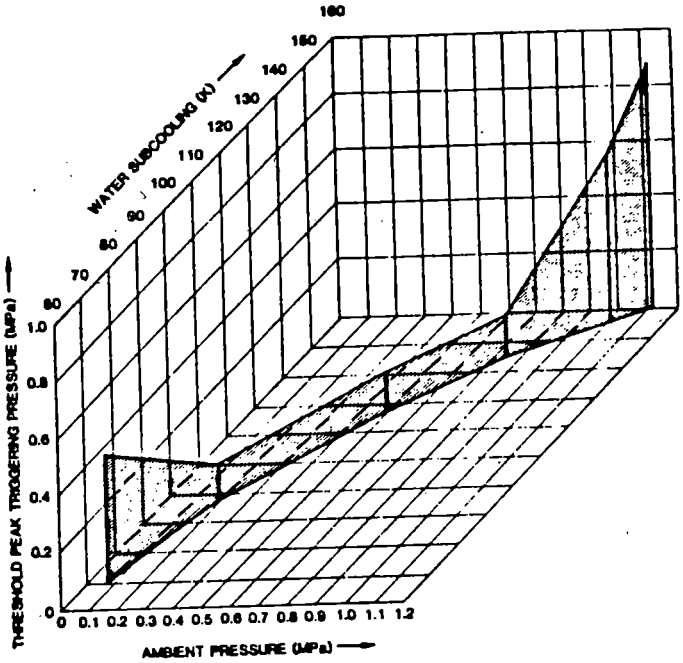
WATER SUBCOOLING (K)
THRESHOLD PEAK TRIGGERING PRESSURE (MPa)
AMBIENT PRESSURE (MPa)

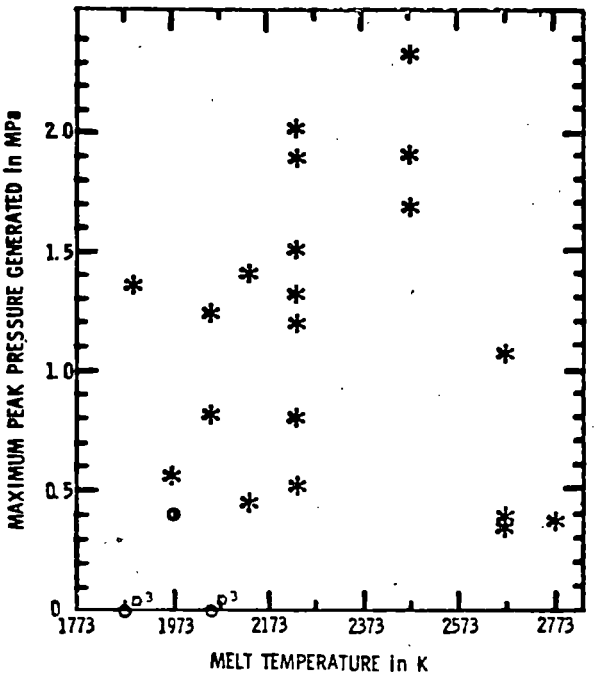
MAXIMUM PEAK PRESSURE GENERATED in MPa
MELT TEMPERATURE in K

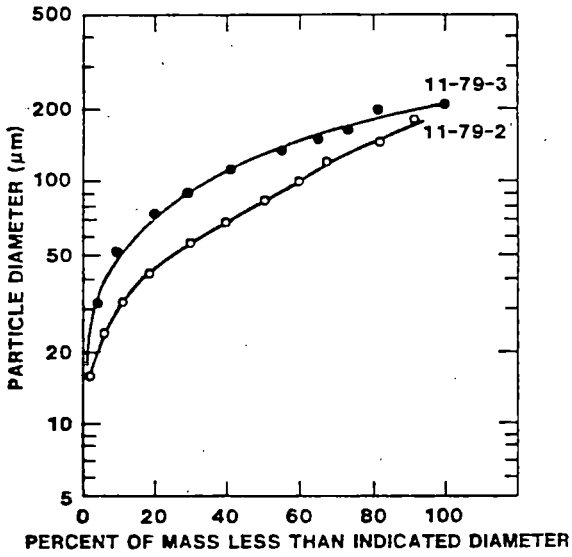
11-79-3
11-79-2
PARTICLE DIAMETER (μm)
PERCENT OF MASS LESS THAN INDICATED DIAMETER

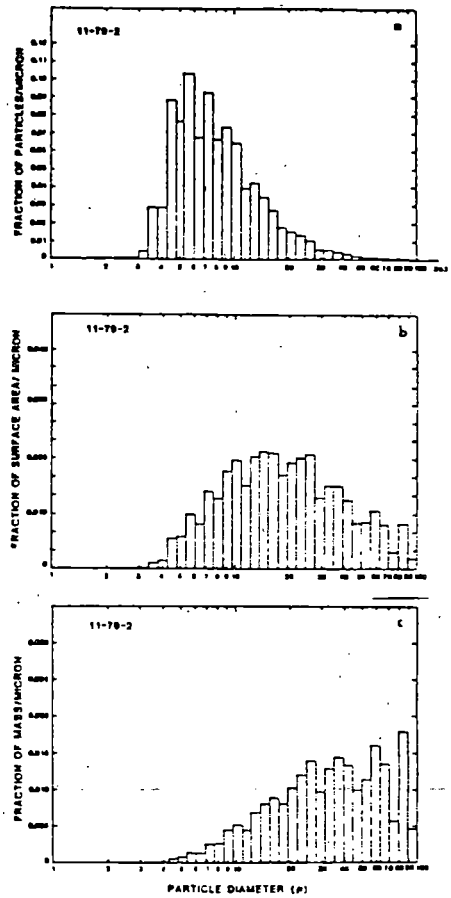

INTERMEDIATE SCALE EXPERIMENTS
OPEN GEOMETRY

VARIABLES: M_F : 1-25 KG

P_∞ : 0.83 B

T_C : 300-370

POUR RATE

FE-ALUMINA, CORIUM A+R

IMPORTANT RESULTS:

CONVERSION RATIO: 0-1.4%

CORIUMS MUCH LESS EXPLOSIVE

MULTIPLE EXPLOSIONS COMMON

LITTLE EFFECT OF WATER TEMPERATURE

FITS AND EXO-FITS

IMPROVEMENTS OVER OPEN GEOMETRY

- COLLECT 100% OF DEBRIS
- VISUAL DATA ON MIXING AND PROPAGATION
- IMPROVED CONTROL OF INITIAL FUEL MASS DELIVERED AND ENTRY VELOCITY
- CONTROL OF AMBIENT ATMOSPHERE (PRESSURE, TEMPERATURE, COMPOSITION)
- IMPROVED INSTRUMENTATION - SHORT AND LONG TERM DATA RECORDING, SLUG IMPACT, ETC.
- FUEL TEMPERATURE MEASUREMENTS

OBJECTIVES

- Quantify Mechanical to Thermal Energy Conversion Ratio as a Function of:
  - Scale
    1 to 25 Kg
  - Melt Composition
  - Water/Melt Mass Ratio
  - Debris
  - Chamber Pressure
- Study Types of Loadings on RPV's Due to FCI's
  - Shock Damage
  - Water/Debris Slug Motion and Impact
  - Overpressurization
- Provide a Data Base for Modeling
  - Kinetic Behavior
  - Detonation Behavior

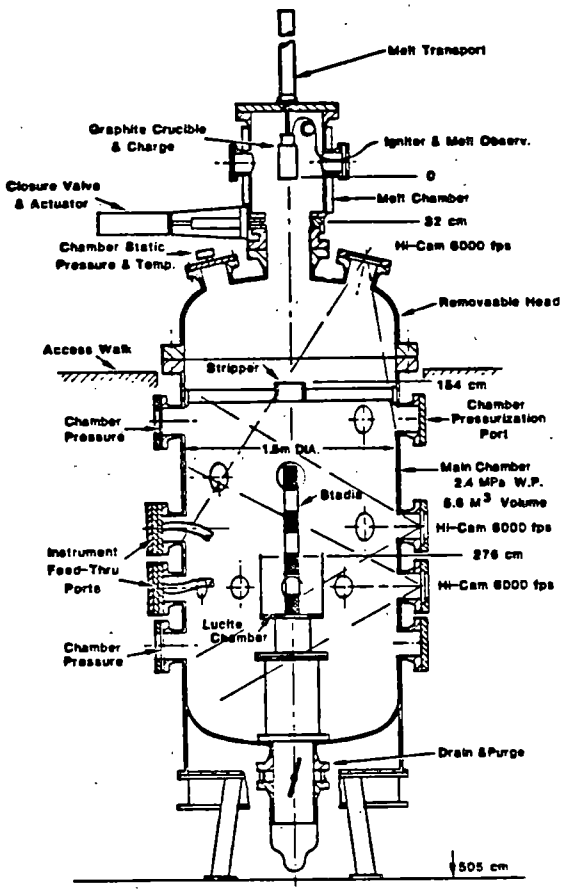

FITS CHAMBER

TYPICAL INSTRUMENTED WATER CHAMBER

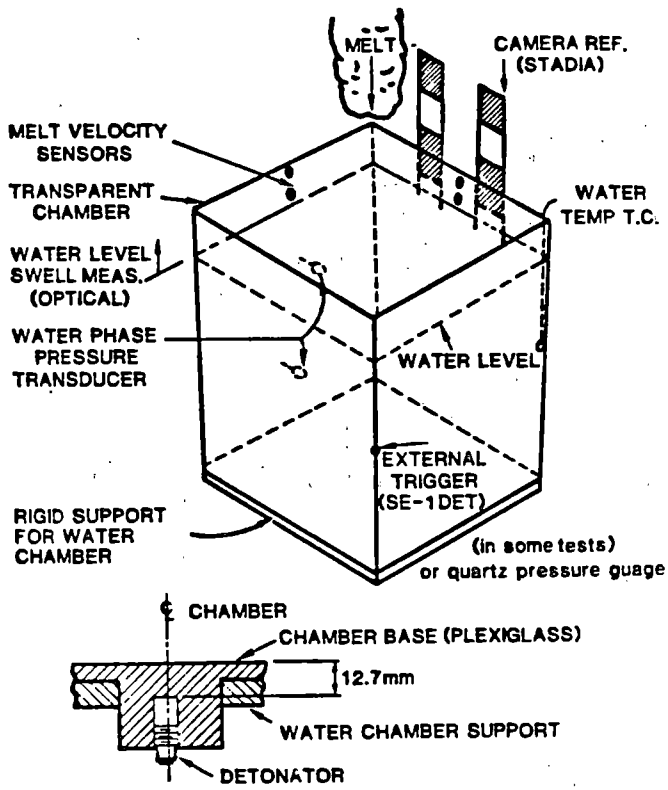

DETONATOR MOUNTING (NOT USED IN ALL TESTS)

PARAMETERS STUDIED OR INCLUDED

- Melt Mass
- Water-Melt Mass Ratio
- Ambient Pressure
- Water Temperature
- Entry Conditions
- Triggering
- Geometry
- Melt Composition

OVERVIEW OF EXPERIMENTAL WORK

● Primary Variable
O Other Variable Effect Observed Or Suspected

	VARIABLE							
EXPT. SERIES	Melt Mass	Mass Ratio	Amb. Press.	Water Temp.	Melt Entry	Triggering	Geometry	Composition
MD (13)	●	O			O		O	
FITSA (5)	O		●			O		
FITSG (2)		O		●				
MDC (13)							O	●
FITSB (6)		●		O	O	O	O	
FITSC (5)								●

IRON ALUMINA SYSTEM

MELT MASS	OBSERVATION
< 1.8 kg	- No Spontaneous Explosions - Mixing Similar To Larger Masses
1.8 to 5.5 kg	- Spontaneous Explosions - Trigger Site At Leading Edge Of Melt - Propagation Through The Melt-Water Mixture - Velocity Depends On Mixture Geometry - 10 To 20 mm Droplets Before Trigger - Time From Melt Entry To Explosion Averages 150 ms - Explosiveness Depends On Average Mixture Density - Explosion Suppressed At 1Mpa Amb. Press. But Can Be Triggered By An External Source - Conversion Ratio KE/Q ≈ 2%
13.6 to 18.7 kg	- Spontaneous Explosions Occur Independent Of Water-Melt Mass Ratio And Water Depth - Triggers (time And Location) Vary - No Spontaneous Explosions In Sat. Water. Reason Unknown - Conversion Ratio Not Yet Determined - Propagation Phase Not Clearly Observed

MDC SERIES SUMMARY

Expt.	Melt Mass (kg) Init.	Del.	Water Mass (kg)	Fuel Type	Major Result
MDC1	5.0	<3.8	152	Corium1	No explosion - dispersed melt delivery
MDC2	5.0	4.0	154	Corium1	Base triggered spontaneous explosion
MDC3	5.0	-	153	Corium2	Crucible failure - no melt delivered
MDC4	6.0	0	152	Corium2	Crucible failure - no melt delivered
MDC5	6.0	4.7	151	Corium2	No explosion - melt dispersed at water entry
MDC6	6.2	-	152	Corium3	Crucible failure
MDC7	5.0	4.48	109	Fe/Al_2O_3	Crucible test - propagating explosion
MDC8	5.0	4.58	104	Fe/Al_2O_3	Crucible test - propagating explosion
MDC9	6.9	-	152	Corium3	Crucible base failure
MDC10	5.0	-	77	Corium2	Crucible base failure
MDC11	5.0	-	152	Corium1	Crucible base seal failure
MDC12	5.0	3.9	77	Corium1	Partial reaction - spontaneously triggered
MDC13	20	15	95.4	Fe/Al_2O_3	Pre-FITSB check out - partial reaction

Corium1 Stn stl as powder
Corium2 Stn stl as sheet
Corium3 No stn stl

CORIUM SYSTEM (LIMITED DATA)

Two Compositions At Fixed Melt Mass (4 kg)

COMPOSITION	OBSERVATION
1	- Mixing Similar To Iron-Alumina - Explosiveness Varies 1 Spontaneous 1 Partial Reaction 1 Non Explosive Interaction may be due to mass threshold - Conversion Ratio 0<KE/Q< 2%
2	- 1 Partial Reaction

FITSB SERIES SUMMARY
IRON-ALUMINA

Expt	Melt Mass Delivered kg	Water Volume Dimensions cm	Water Mass kg	Mass Ratio	Major Result
FITS1B (8/12/81)	18.7	61 sq , 61 deep	226	12.1	spontaneous surface trigger 142 ms after melt entry, second explosion 133 ms later, melt in a stream 8 cm dia.
FITS2B (8/26/81)	18.6	61 sq , 30 deep	113	6.1	spontaneous surface triggered explosion 84 ms after melt entry, coherent melt mass
FITS3B (9/9/81)	18.6	43 sq , 30 deep	57	3.1	spontaneous base triggered explosion 77 ms after melt entry, coherent melt mass
FITS4B (9/23/81)	18.7	61 sq , 61 deep	226	12.1	weak surface triggered explosion followed by base triggered explosion, coherent melt mass preliminary data.
FITS5B (10/15/81)	----	43 sq , 30 deep	57	---	Murphy s Law

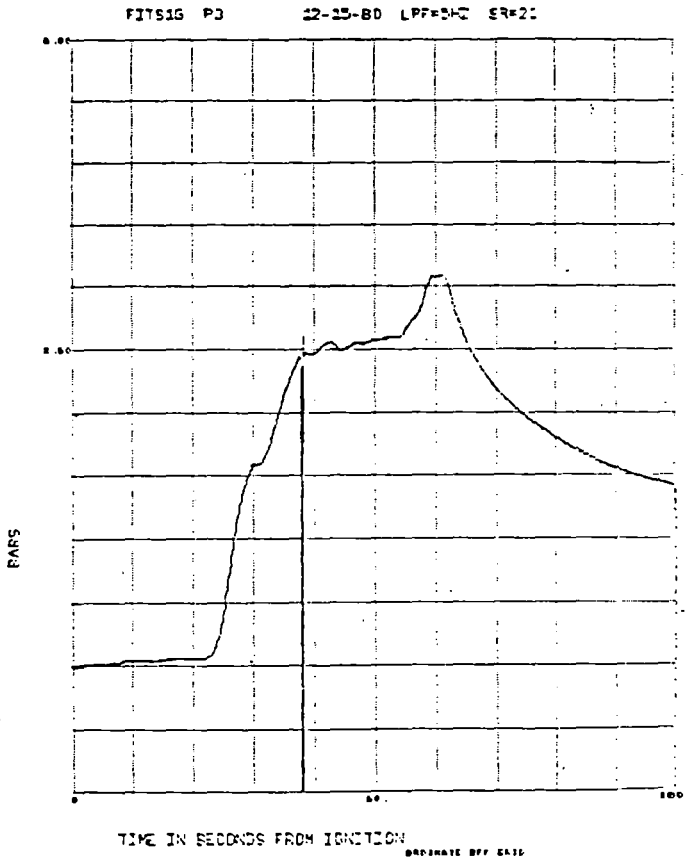

CHAMBER AIR PRESSURE
STEAM SPIKE

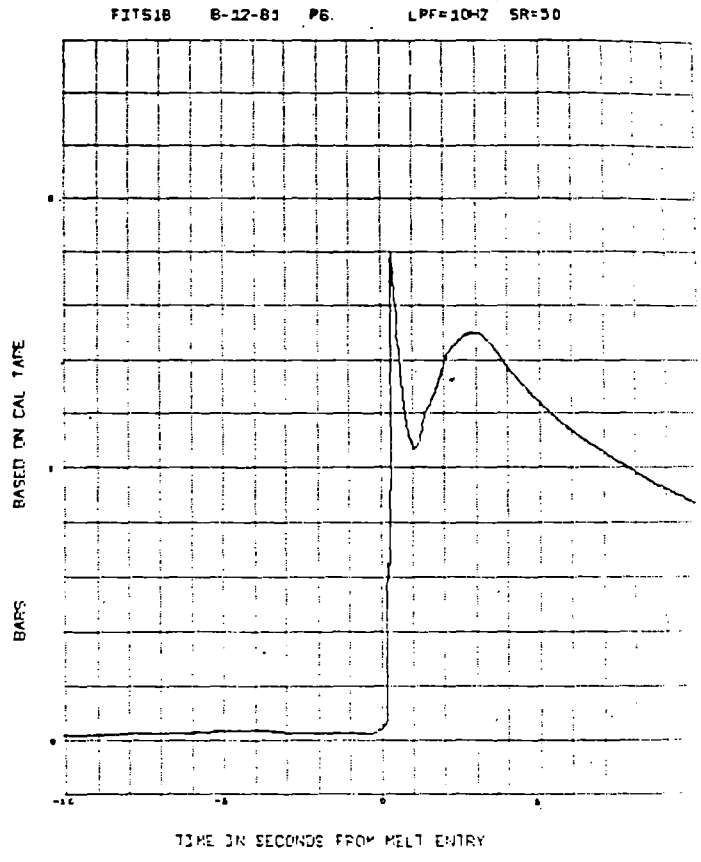

CHAMBER AIR PRESSURE

ANALYSIS AND MODELLING

- TRIGGERING AND FILM COLLAPSE
- 1-D EXPLOSION PROPAGATION
- 2-D EXPLOSION/FLUID/STRUCTURE INTERACTION
- STEAM GENERATION ANALYSIS
- CONTAINMENT FAILURE PROBABILITY

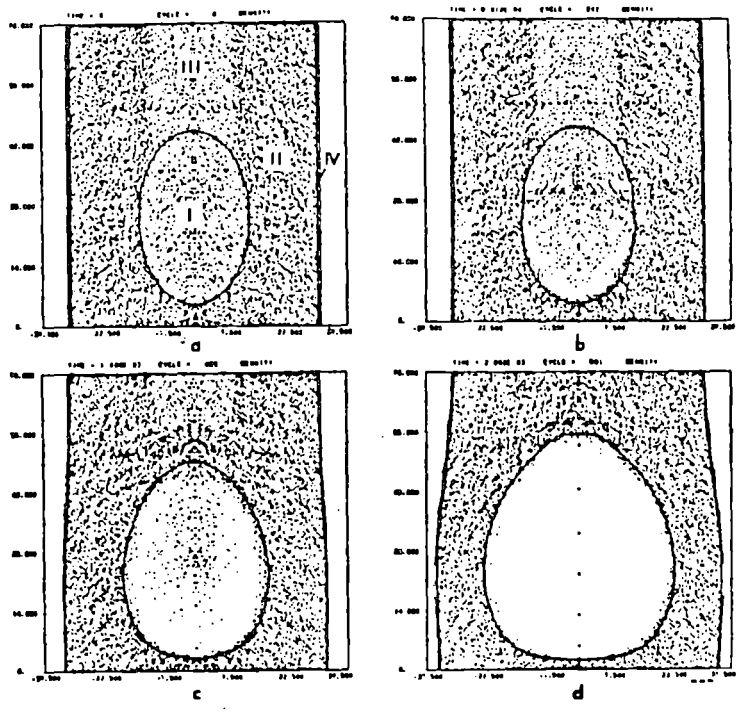

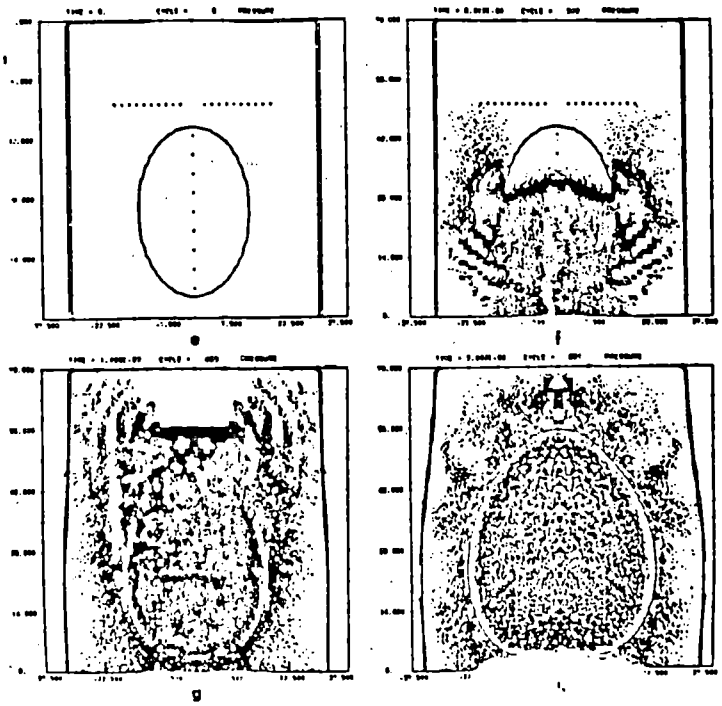

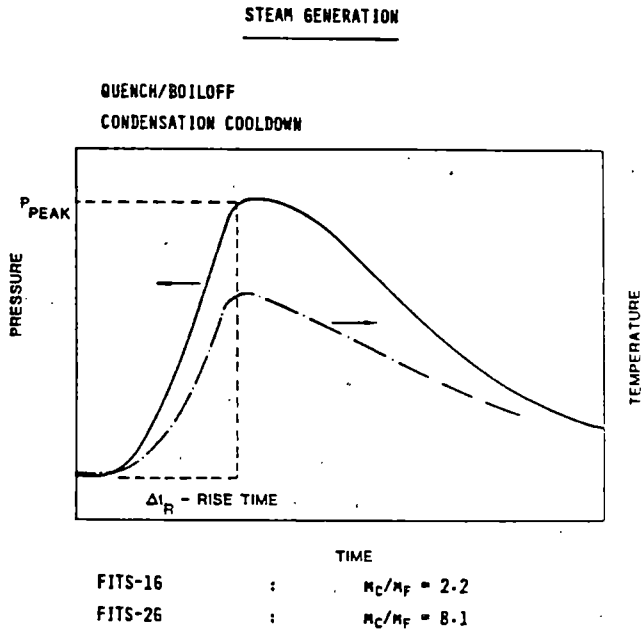

FITS-16 : M_C/M_F = 2.2

FITS-26 : M_C/M_F = 8.1

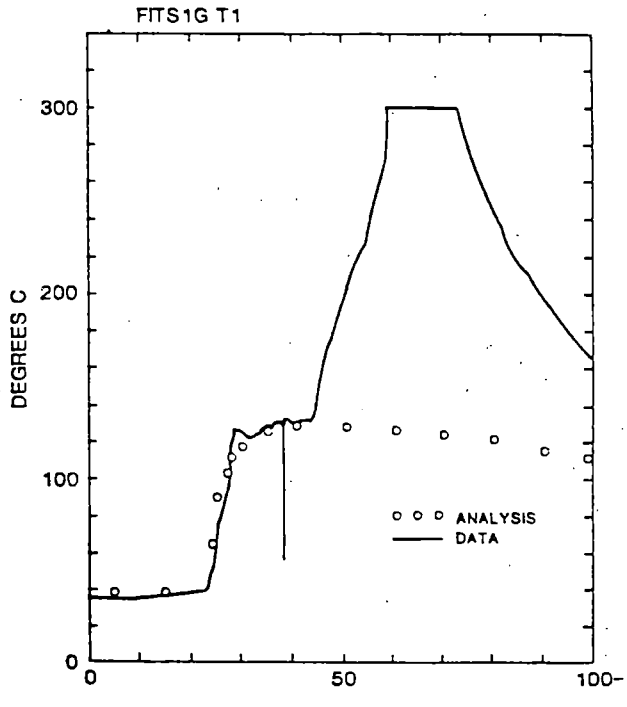

Figure 2.22 Time in seconds from ignition.

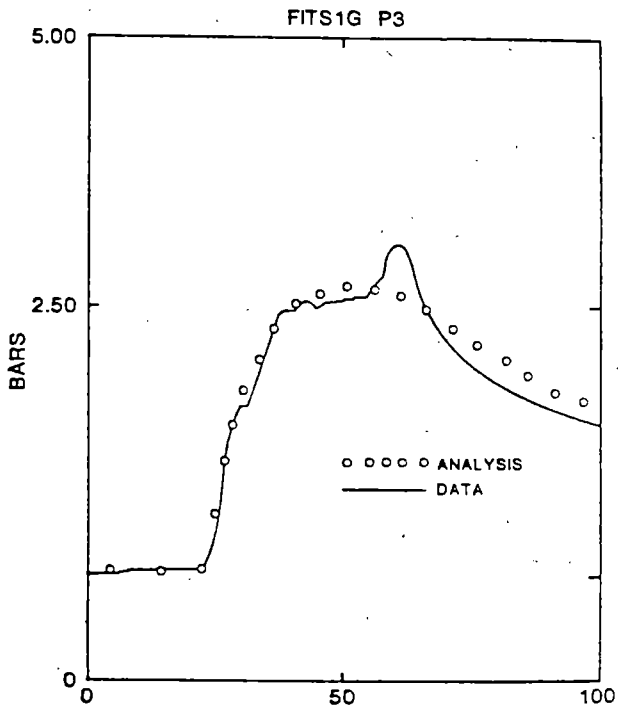

Figure 2.23 Time in seconds from ignition.

STATISTICAL FAILURE MODEL

- WE HAVE DEVELOPED A SIMPLE THERMAL-MECHANICAL MODEL TO CALCULATE PROBABILITY DISTRIBUTIONS OF
  - STEAM EXPLOSION ENERGY
  - REACTOR VESSEL RESPONSE
  - RESULTING MISSILE VELOCITIES
- IT USES A MONTE-CARLO SOLUTION TECHNIQUE
  - RANDOM SAMPLING DETERMINES A SET OF INITIAL CONDITIONS FROM ASSUMED DISTRIBUTION
  - 10,000 CALCULATIONS ARE CONSIDERED
- BASED ON THESE RESULTS, WE ESTIMATE PROBABILITY OF CONTAINMENT FAILURE FOR AN IN-VESSEL EXPLOSION TO BE LESS THAN
  - 0·0001 FOR A PWR (ZION)
  - 0·002 FOR A BWR (BROWNS FERRY)

a. FRACTION OF CORE MOLTEN

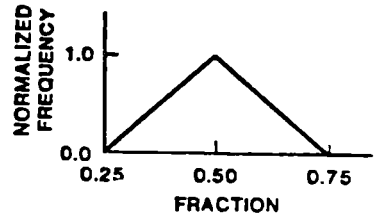

b. FRACTION OF MOLTEN CORE THAT MIXES

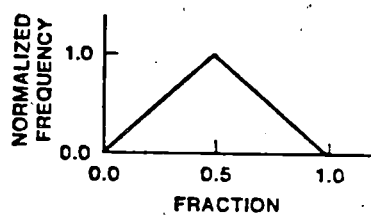

c. FRACTION OF WATER THAT MIXES

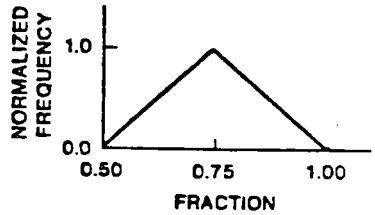

a. ENERGY CONVERSION RATIO

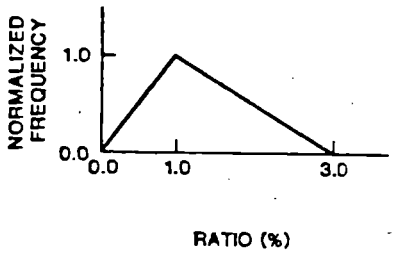

b. FRACTION OF REMAINING UIS

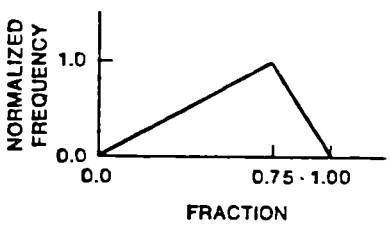

a. PORTION OF VESSEL MODELLED

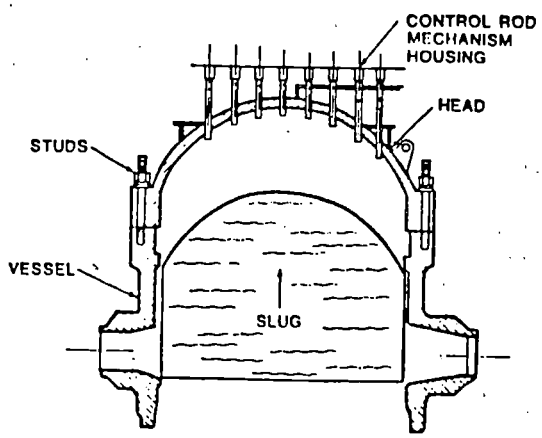

b. 6 DOF STRUCTURAL MODEL

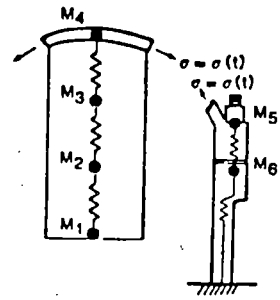

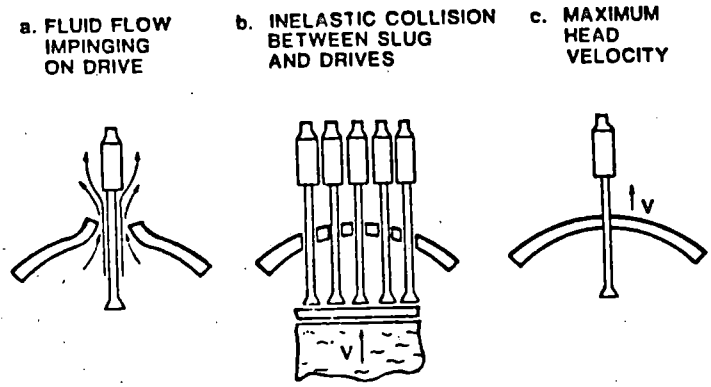
a. FLUID FLOW IMPINGING ON DRIVE
b. INELASTIC COLLISION BETWEEN SLUG AND DRIVES
c. MAXIMUM HEAD VELOCITY
V
V

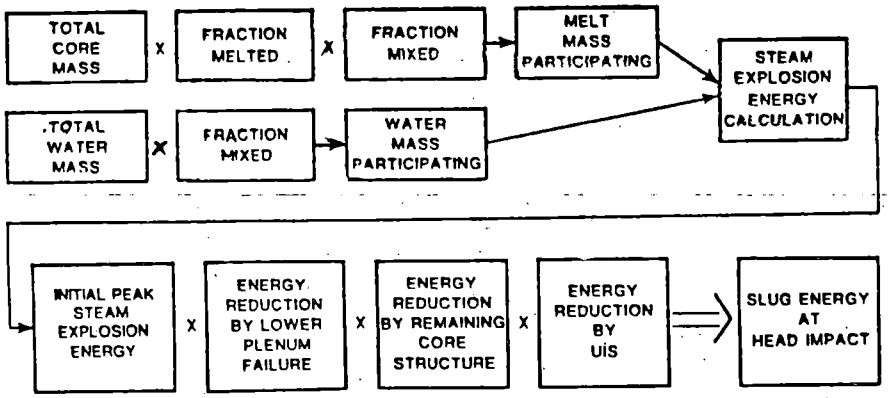
TOTAL CORE MASS
X
FRACTION MELTED
X
FRACTION MIXED
MELT MASS PARTICIPATING
TOTAL WATER MASS
X
FRACTION MIXED
WATER MASS PARTICIPATING
STEAM EXPLOSION ENERGY CALCULATION
INITIAL PEAK STEAM EXPLOSION ENERGY
X
ENERGY REDUCTION BY LOWER PLENUM FAILURE
X
ENERGY REDUCTION BY REMAINING CORE STRUCTURE
X
ENERGY REDUCTION BY UIS
SLUG ENERGY AT HEAD IMPACT

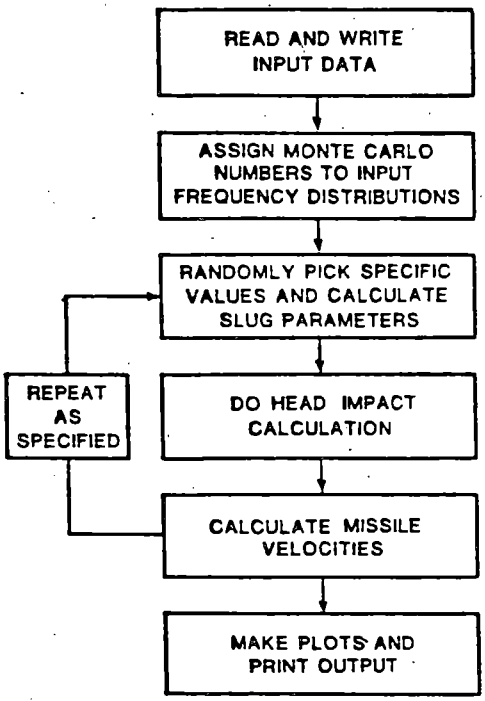
READ AND WRITE INPUT DATA
ASSIGN MONTE CARLO NUMBERS TO INPUT FREQUENCY DISTRIBUTIONS
RANDOMLY PICK SPECIFIC VALUES AND CALCULATE SLUG PARAMETERS
REPEAT AS SPECIFIED
DO HEAD IMPACT CALCULATION
CALCULATE MISSILE VELOCITIES
MAKE PLOTS AND PRINT OUTPUT

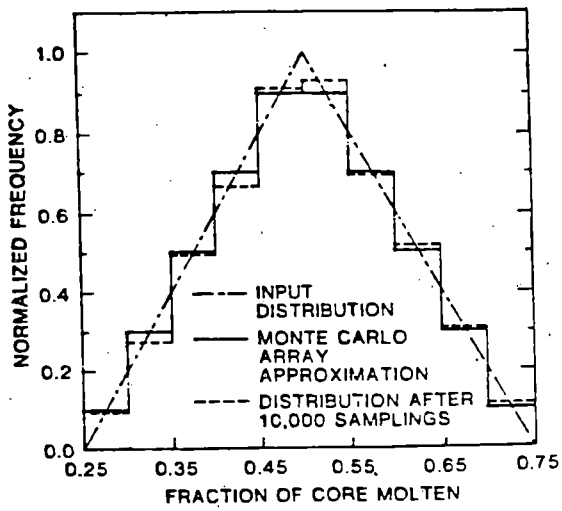
NORMALIZED FREQUENCY
1.0
0.8
0.6
0.4
0.2
0.0
INPUT DISTRIBUTION
MONTE CARLO ARRAY APPROXIMATION
DISTRIBUTION AFTER 10,000 SAMPLINGS
0.25
0.35
0.45
0.55
0.65
0.75
FRACTION OF CORE MOLTEN

a. STEAM EXPLOSION ENERGY

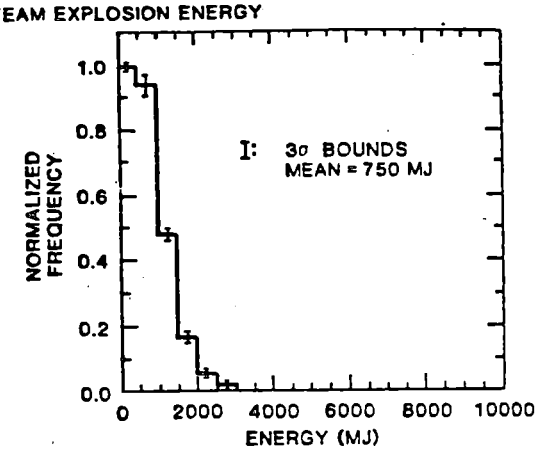

b. SLUG ENERGY AT IMPACT

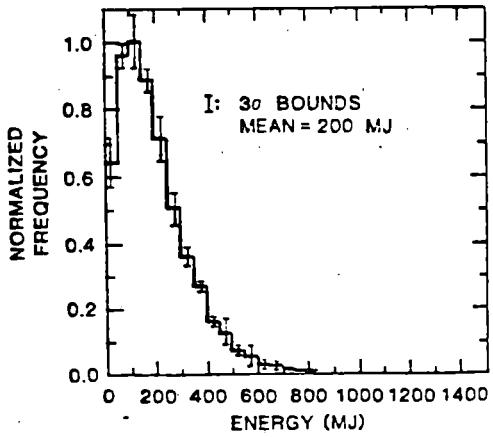

SMALL MASS MISSILE VELOCITIES

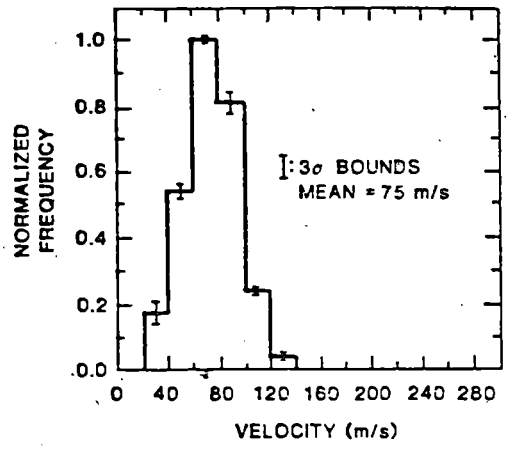

PROBABILITY OF CONTAINMENT FAILURE

CURRENT ESTIMATES

$P = P_{FCC}\ P_F\ P_C$

	WASH-1400 (APP. VIII)	BEST ESTIMATE
P_{FCC}	1.	1.
P_F	0.1	0.5
P_C	0.1	0.0002
P	0.01	0.0001

$_{FCC}$ - FUEL-COOLANT CONTACT (> 20%)

$_{F}$ - FUEL FRAGMENTATION < 5 mm

$_{C}$ - DIRECT CONTAINMENT FAILURE

FY82 PLANS

SMALL SCALE

SINGLE DROPLET STUDIES

SEPARATE AND COMBINED CORIUM CONSTITUTED

INTERMEDIATE SCALE

FITS-B ADDITIONAL TESTS

- SATURATED WATER
- m_C/m_F = 1.5

FITS-C TESTS

CORIUM MELTS FOR COMPARISON TO IRON-ALUMINA MELTS

ANALYSIS

- CONTINUE MODELLING STEAM EXPLOSION PROCESSES
- EVALUATE POSSIBLE ACCIDENT SCENARIOS

BNL PROGRAM IN SUPPORT OF LWR DEGRADED CORE ACCIDENT ANALYSIS

by

G. A. Greene and T. Ginsberg

Program Contributors: J. Klein, J. Klages, C.E. Schwarz
Y. Sanborn, J. C. Chen

Brookhaven National Laboratory
Department of Nuclear Energy
Experimental Modeling Group
Upton, N.Y. 11973

Presented at the

Ninth Water Reactor Safety Research Information Meeting
October 26-30, 1981
Gaithersburg, Maryland

BNL PROGRAM IN SUPPORT OF LWR DEGRADED CORE ACCIDENT ANALYSIS

G. A. Greene and T. Ginsberg

1. INTRODUCTION

Analyses of the response of light water reactor containment buildings to degraded core accidents are currently being sponsored by the Nuclear Regulatory Commission (Yang, 1981; Pratt, 1981; Murfin, 1980). Two important loadings on dry pressurized water reactor containments are:

(i) Molten core-concrete interactions.

The interactions lead to pressurization of the containment as a result of generation of concrete decomposition products and potential combustion of flammable gaseous products. In addition these interactions lead to penetration of the core melt into the containment basemat.

(ii) Steam generation from molten core-water thermal interactions.

Experiments are in progress at BNL in support of analytical model development related to aspects of the above containment loading mechanisms. The work supports development and evaluation of the CORCON (Muir, 1981) and MARCH (Wooton, 1980) computer codes. Progress in the two programs is described below.

2. HEAT TRANSFER IN CORE-CONCRETE INTERACTIONS

Complete meltdown of an LWR core may lead to rapid penetration of the pressure vessel and thermal interaction between core materials and concrete in the reactor cavity in the absence of intervention by engineered reactor safety features. Subsequent core-concrete interactions impact upon containment integrity by containment pressurization, production of combustible gases, and basemat erosion. The CORCON code represents the state of the art calculational tool for calculating the consequences of the attack of molten core materials upon concrete. One of the more dominant but, as yet, least understood heat transfer mechanisms modeled by CORCON is interfacial liquid-liquid heat transfer between immiscible overlying liquid layers with transverse noncondensible gas flow.

In order to measure the heat transfer between overlying liquid layers with gas agitation, the experimental apparatus shown in Figure 1 was constructed. It consists of a rectangular lexan enclosure, open at the top, with a replaceable porous frit in the base for distribution of the gas flux. The lower half has opposing electrodes for resistance heating of one fluid layer. A traversable vertical thermocouple rake is installed with twelve thermocouples separated nominally by one inch. The instrumentation is connected to an automated data acquisition system and data are recorded at steady state (time-integration), 10 Hz and 100 Hz. Liquids employed were silicone oil, and

copper sulfate or zinc sulfate solutions.

The overall interfacial heat transfer coefficient was calculated by the electrical power (W) divided by the cross-sectional area (m^2) and the overall temperature difference (K) between the liquid layers. The superficial gas velocity (m/s) is the volume gas flux divided by the cross-sectional area of the pool. Two series of data were taken. The tests with zinc sulfate-silicone oil (Series 100) had a density ratio of $\sim$.80 and the copper sulfate-silicone oil (Series 200) tests had a density ratio of $\sim$.65. These data are plotted in Figure 2 along with the available data of Werle who used silicone oil-water with a density ratio $\sim$.90. The data points in some cases indicate an average of up to twenty separate experiments.

Examination of the data reveals that within calculated uncertainty and observed scatter, the three separate experiments are in good agreement and there is no noticeable trend between them. At the lowest gas velocity (less than 1 mm/s), there is an apparent increase in the heat transfer coefficient of approximately an order of magnitude over the well-established natural convection asymptote (Haberstroh, 1978). The heat transfer coefficient increases rapidly with increasing gas flux and preliminary observations indicate that mixing becomes significant in the vicinity of 5 mm/s. Below this limit the liquids are predominantly stratified with little or no mixing. Above 5 mm/s, mixing increases with increasing gas velocity and a mixing zone develops, as indicated by detailed transient temperature profile measurements. This enhances the heat transfer more effectively and is evidenced by the apparent steeper slope of the data above 5 mm/s compared to the data below that limit. Eventually, at the highest gas velocity achieved in these tests (1 cm/s), the upper liquid (silicone oil) became totally mixed with entrained fluid from below. This fluidized state may be expected to represent an approximate upper limit to the heat transfer for these experiments. For gas velocities above this limit, the heat transfer coefficient is expected to increase asymptotically to infinity, which would represent a condition in which the liquids were totally mixed and there no longer exists an interface between the two layers.

A preliminary comparison of the experimental data from these experiments as well as the KFK data (Werle, 1978) to the modified Konsetov model (Blottner, 1979) which is currently used in CORCON (Muir, 1981) was performed. It was found that the experimental data exceeded the predicted heat transfer coefficient from the modified Konsetov model by almost three orders of magnitude at bubbling rates as low as 1 cm/s. The trend was divergent for gas velocity greater than this value.

Calculations with CORCON were performed to test the sensitivity of the code to this heat transfer model. The interfacial liquid-liquid heat transfer models in the HPOOL subroutine, HCINTT and HCINTB, were modified to reflect the observations of higher heat transfer from the nonreactor materials experiments. It was found that if the correlations were simply increased by a factor of ten, the concrete ablation rate was decreased and the molten debris was found to have cooled by more than 100 K over the sample problem case

(Zion) with the unmodified correlations. This was for a time of two hours following initial core-concrete interactions. At this time the oxide layer was found to be at a temperature intermediate to the calculated solidus and liquidus temperatures.

3. STEAM SPIKE PHENOMENOLOGY

A number of LWR core meltdown accident sequences have been identified (Murfin, 1980) during which hot core debris would contact and thermally interact with cold water. The mode of contact is accident sequence dependent. Core debris may fall into a pre-existing pool of water in the reactor cavity; or, on the other hand, the debris may initially fall into a dry cavity and be followed by introduction of cold water. The resulting thermal interaction and steam generation lead to pressurization of the reactor containment building. The pressurization rate depends on the relative magnitudes of debris-water heat transfer, on the cooling supplied by passive cold structure or active cooling devices, and/or on the rate of containment venting. This task is directed towards development and experimental evaluation of analytical models for prediction of the rate of steam generation during quenching of core debris under postulated LWR core meltdown accident conditions.

An experiment has been designed and implemented to measure the transient rate of heat transfer resulting from the thermal interaction of simulated hot core debris with cold water. Spherical simulated debris have a well controlled particle size. The surface area available for heat transfer is a known quantity. This enables us to separate the question of fragmentation dynamics and fragment size distribution from that of heat transfer. A schematic of the apparatus is shown in Figure 3. A photograph of the apparatus is presented in Figure 4. A glass pipe serves as the test vessel. The spherical particles are heated in a furnace which sits over the test vessel. Water in the vessel is preheated to the desired temperature. A release mechanism is actuated and the particles are dropped into the water (or the reverse).

A series of initial particle drop experiments are in progress. The parameters of the first series of experiments are shown in Table 1.

TABLE 1. EXPERIMENTAL PARAMETERS

Test Vessel Diameter	101 mm (4 in)
Particle Material	302 S.S.
Particle Diameter	3 mm
Mass of Particles	5 kg
Particle Temperature	533-977 K (500-1300 F)
Mass of Water	4 kg
Water Temperature	361 K (190 F)

Measurements have been made of the average particle "quench time", . This time is defined as the period between initial contact of hot particles with water and the time the particles are effectively quenched. The particles are assumed quenched when vapor production is observed to cease. At this point in the experiment, the particles' temperature is at the water saturation temperature. The quench time is used together with the initial stored energy of the particles, ΔE, to compute the average heat flux for the quench process. The heat flux is defined by $q'' = \Delta E / A_{BED}$ where A_{BED} is the cross-sectional area of the bed. Analysis of the data is underway at the present time.

REFERENCES

Blottner, F.G., "Hydrodynamics and Heat Transfer Characteristics of Liquid Pools with Bubble Agitation," SAND 79-1132 (1979).

Haberstroh, R.D., and R. D. Reinders, "Conducting-Sheet Model for Natural Convection Through a Density Stratified Interface, "J. Heat Mass Transfer, 17, pp. 307-311 (1978).

Muir, J. F. R.K. Cole, M. L. Corradini and M. A. Ellis, "CORCON-MOD1: An Improved Model for Molten Core/Concrete Interactions," SAND 80-2415 (1981).

Murfin, W.B., "Report of the Zion/Indian Point Study: Volume 1," Sandia National Laboratory, SAND 80-0617/1 (August 1980).

Pratt, W. T. and R. A. Bari, "Containment Response During Degraded Core Accidents," Brookhaven National Laboratory, BNL-NUREG-51415 (July 1981).

Werle, H., "Modellexperimente zum Kernschmelaen, "Halbjahresbericht 1978/1, PNS 4332, Kerforschung zentrum Karlsruhe FRG.

Yang, J. W., "Cooling of Core Debris and the Impact on Containment Pressure," Brookhaven National Laboratory, BNL-NUREG-51376 (July 1981)

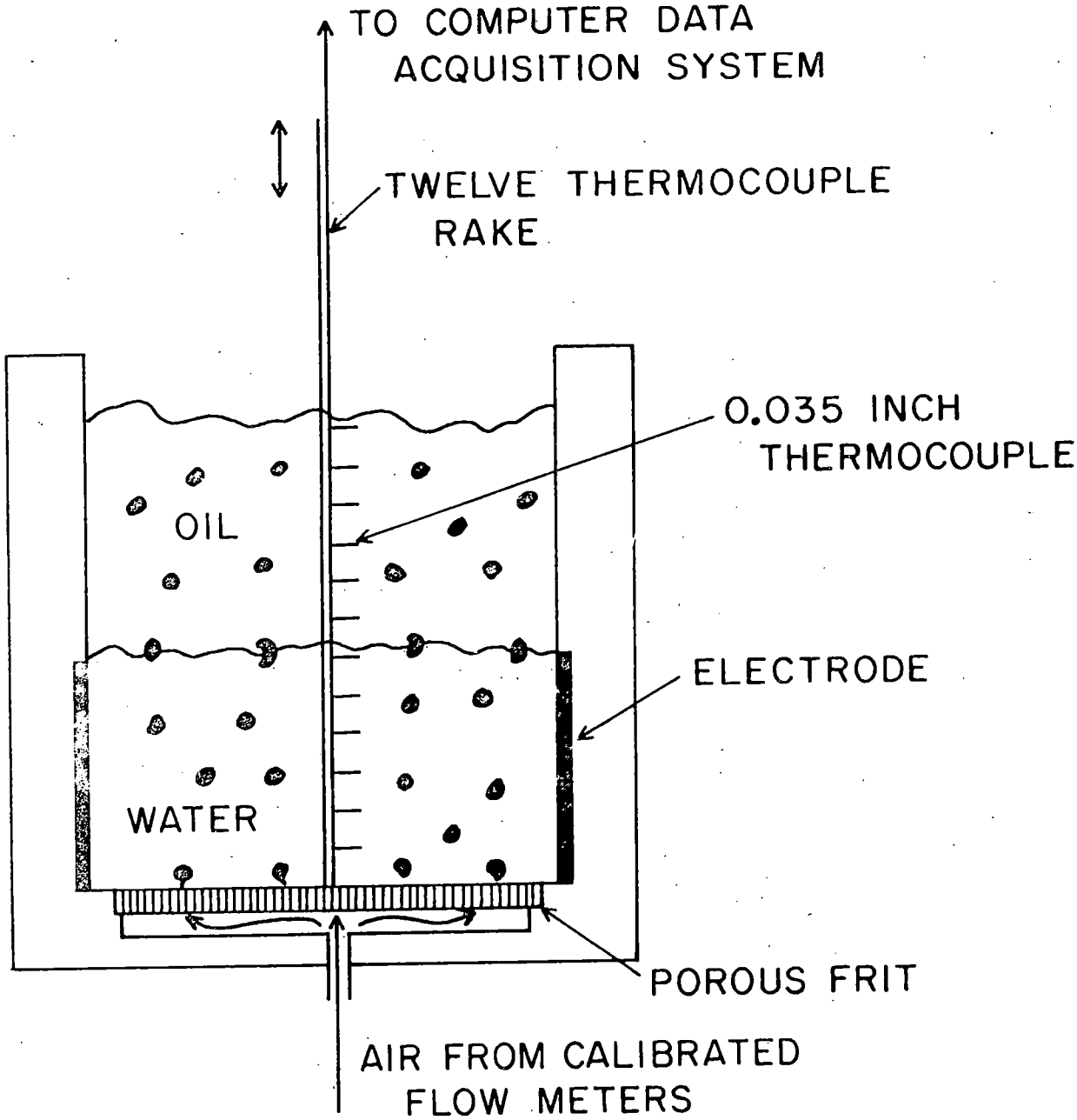

FIGURE 1. SCHEMATIC DIAGRAM OF BUBBLING HEAT TRANSFER APPARATUS

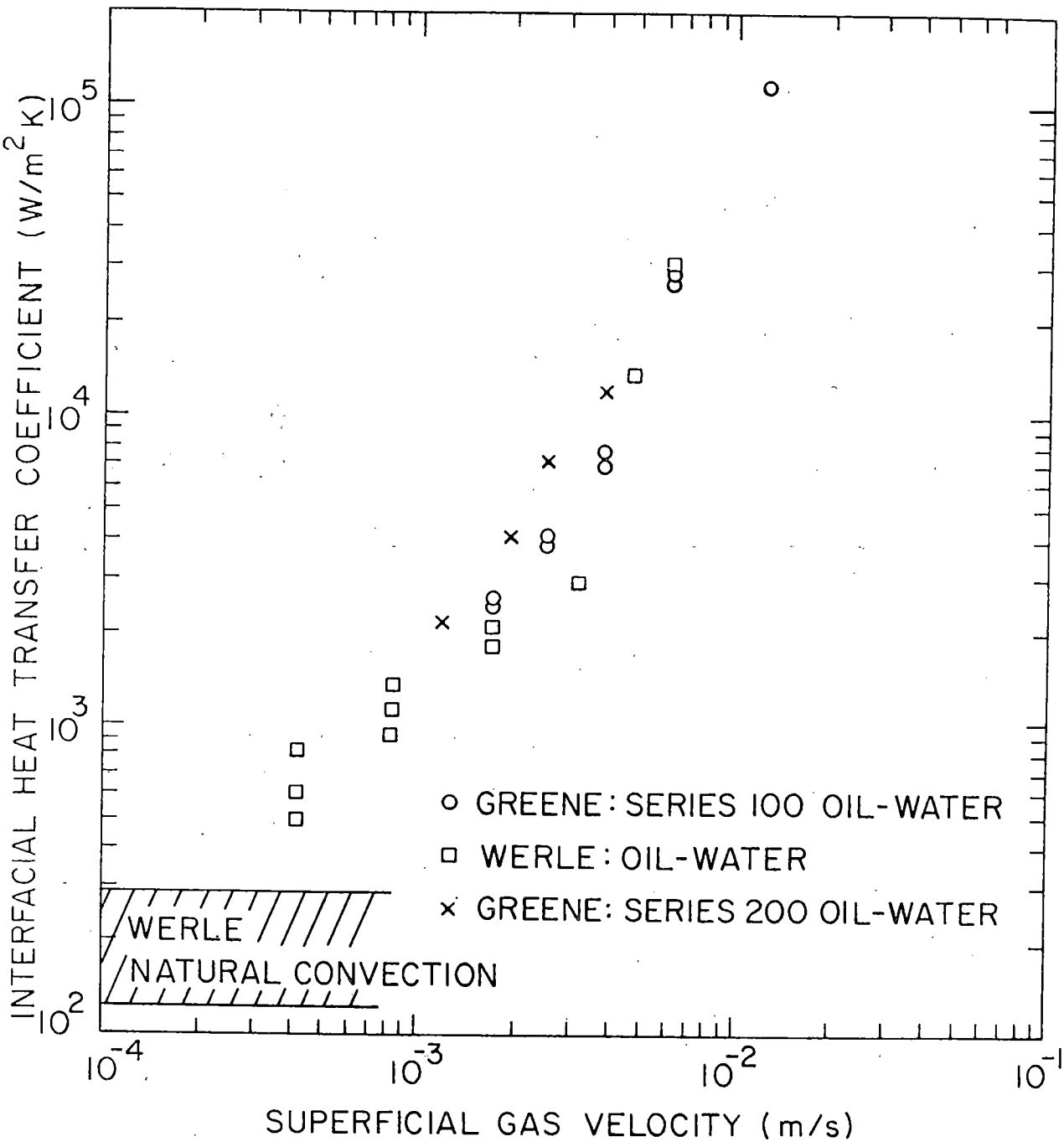

FIGURE 2. LIQUID-LIQUID INTERFACIAL HEAT TRANSFER COEFFICIENT VS. SUPERFICIAL GAS VELOCITY

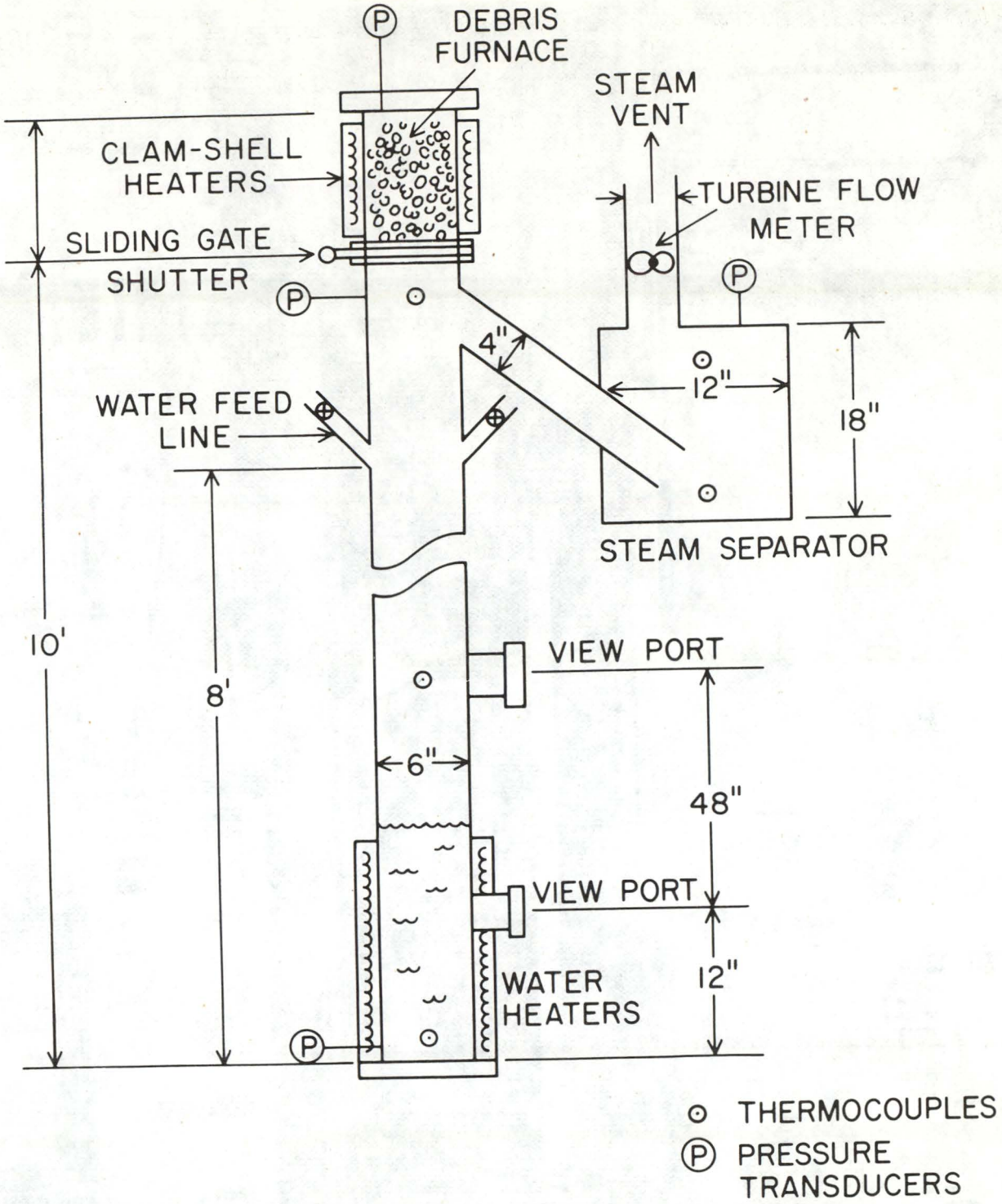

FIGURE 3. SCHEMATIC OF STEAM SPIKE PHENOMENOLOGY EXPERIMENT

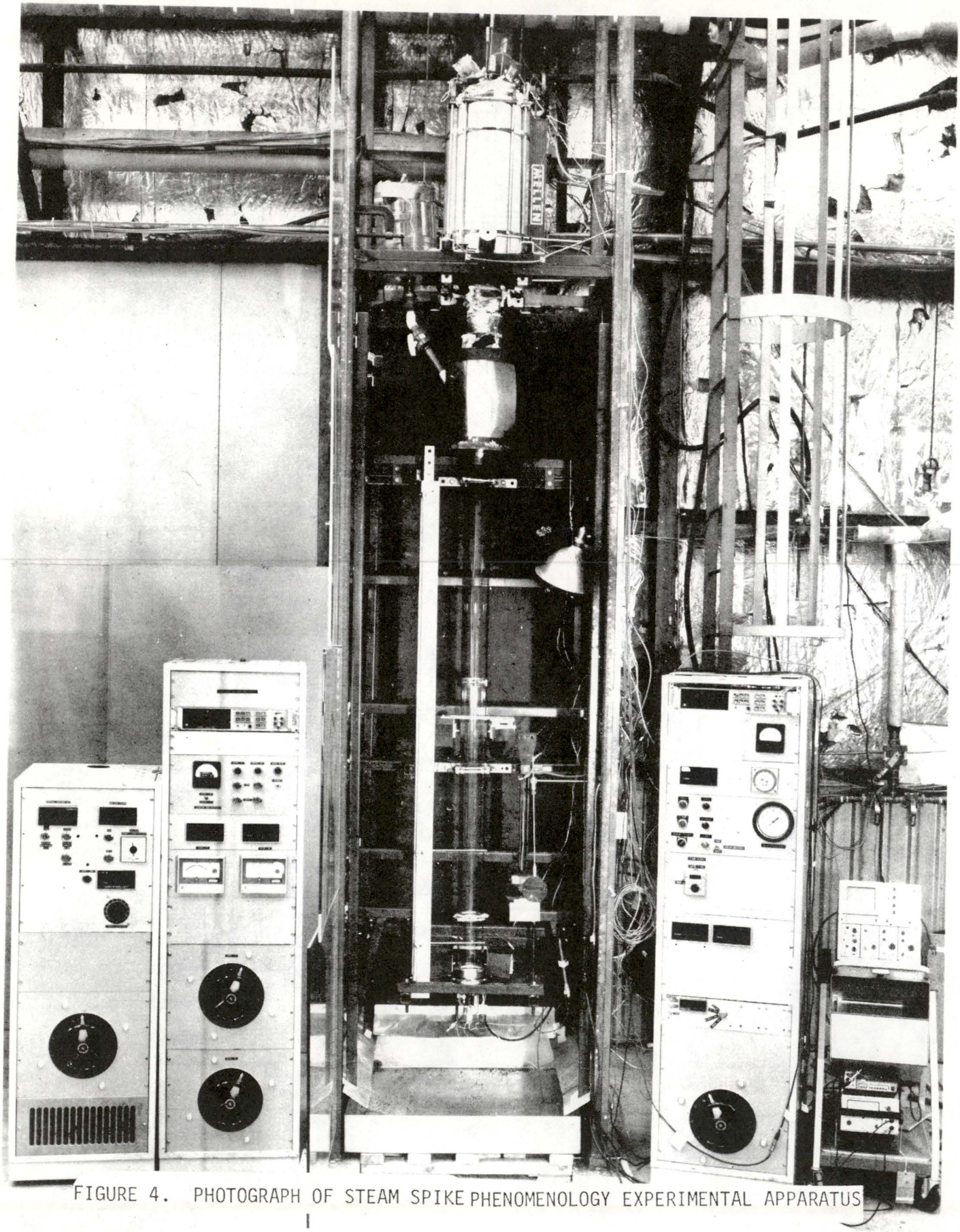

FIGURE 4. PHOTOGRAPH OF STEAM SPIKE PHENOMENOLOGY EXPERIMENTAL APPARATUS

SCOPE OF BNL LWR PROGRAM

LWR TASK	ACCIDENT PHASE	ISSUE	RELEVANT CODES
• HEAT TRANSFER IN CORE-CONCRETE INTERACTIONS	CORE MELT-CONCRETE THERMAL INTERACTIONS	CONTAINMENT INTEGRITY	CORCON
• STEAM SPIKE PHENOMENOLOGY	CORE MELT-WATER THERMAL INTERACTIONS IN LOWER PLENUM AND REACTOR CAVITY	CONTAINMENT INTEGRITY	MARCH

STEAM SPIKE PHENOMENOLOGY

- NRC LICENSING NEEDS

  - PREDICT CONTAINMENT PRESSURIZATION BY STEAM PRODUCED AS A RESULT OF QUENCHING OF MOLTEN CORE DEBRIS IN LOWER PLENUM AND REACTOR CAVITY FILLED WITH WATER.

- BNL PROGRAM OBJECTIVES

  - DEVELOP EXPERIMENTAL DATA BASE FOR EVALUATION OF MARCH CODE MODELING OF DEBRIS-WATER INTERACTION.

  - DEVELOP VERIFIED MATHEMATICAL MODEL FOR USE IN MARCH CODE FOR PREDICTION OF STEAM GENERATION RATE FROM DEBRIS-WATER INTERACTION.

- BACKGROUND

  - MARCH CALCULATIONS INDICATE MAJOR UNCERTANTIES IN CONTAINMENT PRESSURE-TIME HISTORY DEPENDING ON THERMAL INTERACTION ASSUMPTIONS.

STEAM SPIKE EXPERIMENT

- OBJECTIVE
  - MEASURE STEAM GENERATION RATE FROM INTERACTION OF KNOWN DIAMETER PARTICLES WITH WATER

- APPROACH
  - HEAT SPHERES TO TEMPERATURE
  - DROP INTO COLD WATER
  - MEASURE STEAM GENERATION AND QUENCH TIME
  - COMPARE RESULTS WITH MODEL PREDICTIONS

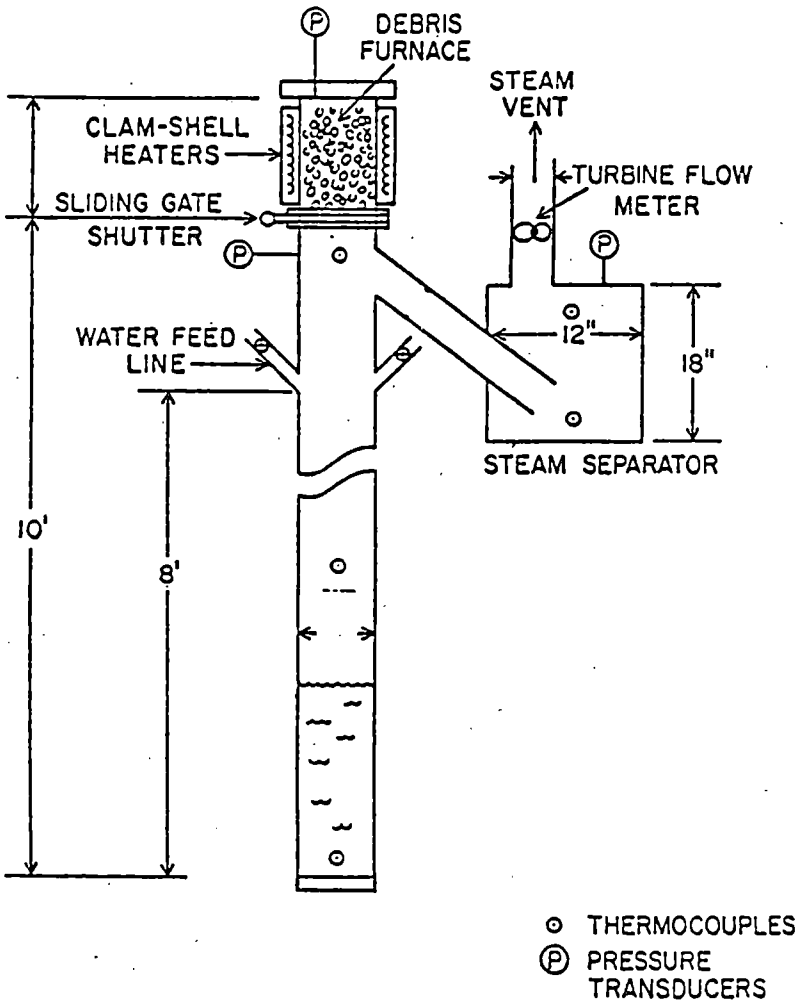

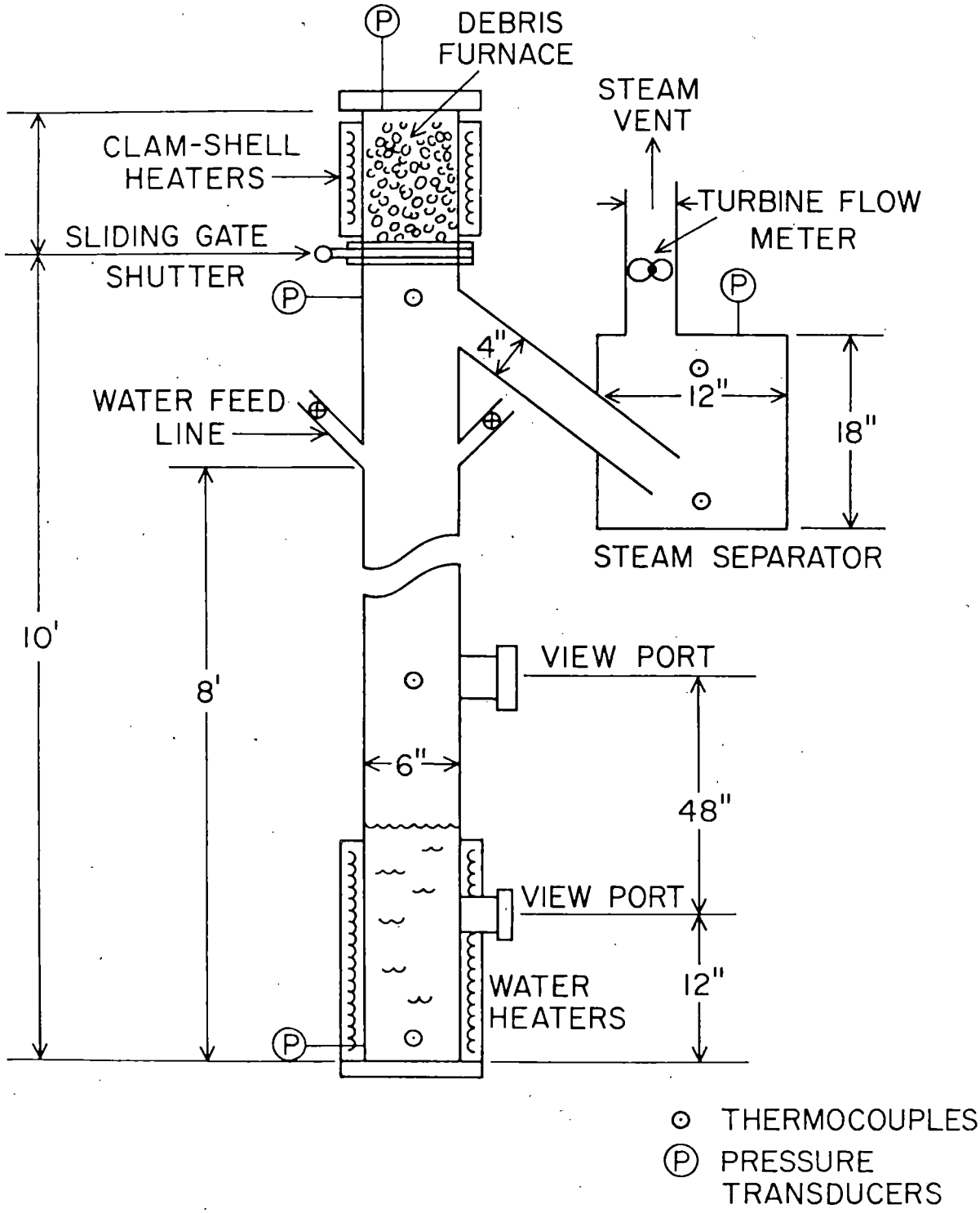

SCHEMATIC OF STEAM SPIKE PHENOMENOLOGY EXPERIMENT

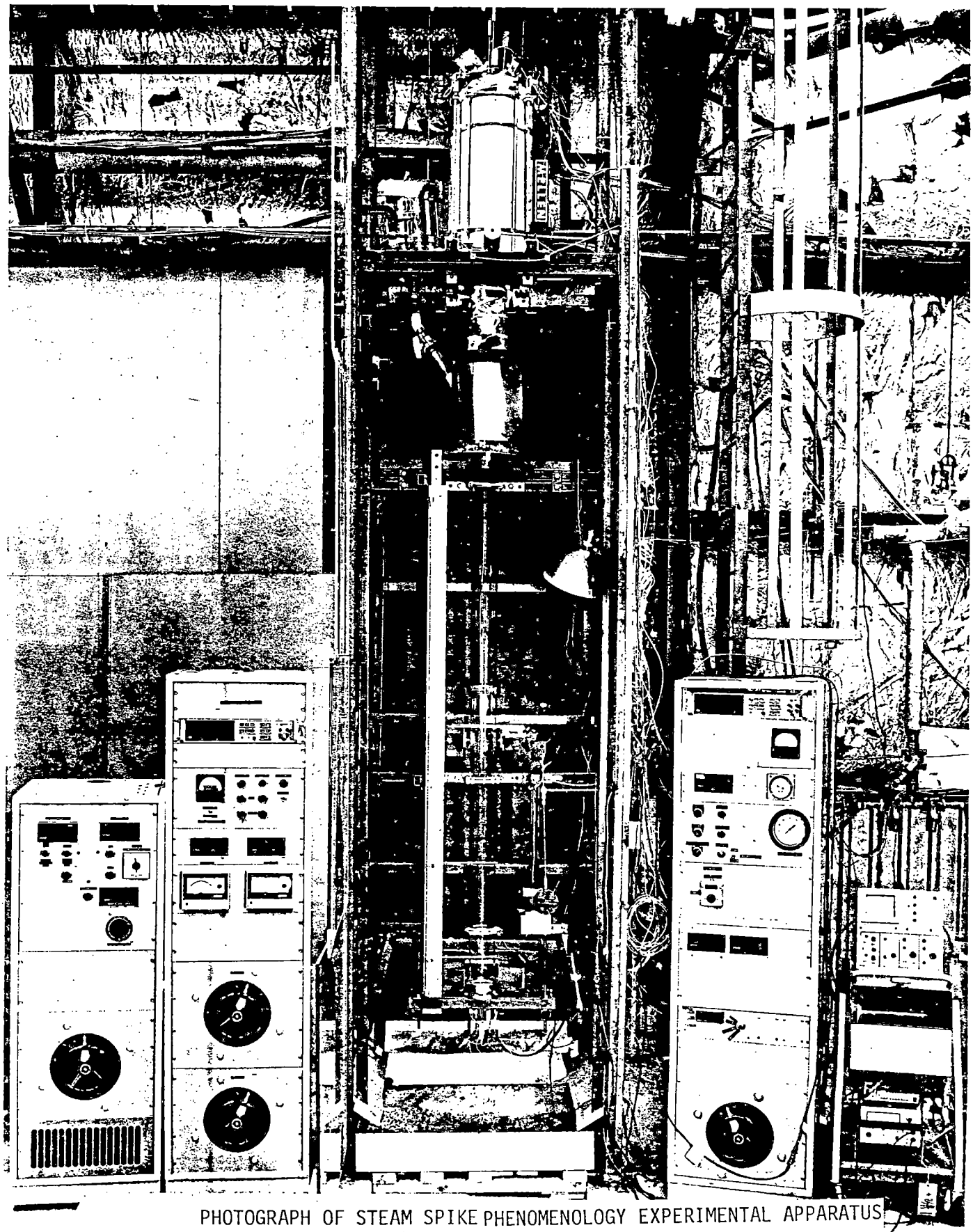

PHOTOGRAPH OF STEAM SPIKE PHENOMENOLOGY EXPERIMENTAL APPARATUS

LIQUID-LIQUID HEAT TRANSFER WITH GAS BUBBLING

- METAL AND OXIDE LAYERS IMMISCIBLE.
- INTERFACIAL HEAT TRANSFER ENHANCED BY GAS BUBBLING FROM CONCRETE.
- HEAT BALANCE, UPWARD VS DOWNWARD, DEPENDENT ON INTERFACIAL HEAT TRANSFER MECHANISMS.
- AVAILABLE DATA: WERLE (KFK).
- AVAILABLE MODELS:
  - SZEKELY
  - KONSETOV
  - GRIEF

LIQUID-LIQUID HEAT TRANSFER

- MODELS ARE NOT IN AGREEMENT.
- AS MUCH AS TWO ORDERS OF MAGNITUDE DIFFERENCE BETWEEN DATA AND MODELS.
- MODELS DO NOT PREDICT SUDDEN INCREASE IN DATA.
- MODEL STRUCTURES DISAGREE.
- RANGE OF GAS VELOCITY TWO ORDERS OF MAGNITUDE LESS THAN PROTOTYPE CASE.
- IMPACT ON CONCRETE PENETRATION CALCULATIONS:

  POSSIBLE THAT CONCRETE PENETRATION RATE AND GAS GENERATION RATES ARE TOO HIGH.

  BY HOW MUCH?

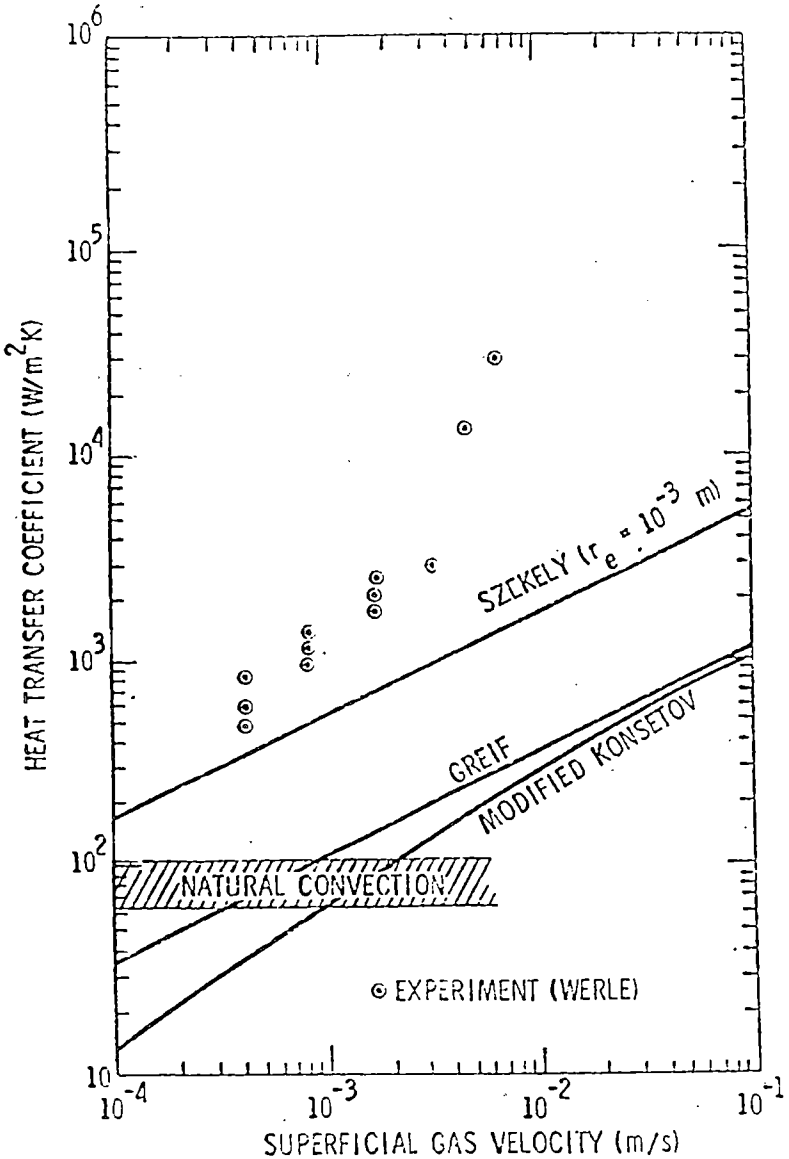

LIQUID-LIQUID HEAT TRANSFER EXPERIMENT

- RECTANGULAR POOL FULLY INSULATED.
- ELECTRODES FOR INTERNAL HEATING-VARIABLE POWER.
- INTERCHANGEABLE POROUS BASE FOR GAS GENERATION-VARIABLE BUBBLE SIZE AND SUPERFICIAL VELOCITY.
- TRAVERSABLE THERMOCOUPLE RAKE-TWELVE CALIBRATED TC'S VERTICALLY ORIENTED.
- AUTOMATED DATA ACQUISITION FACILITY - LOW, INTERMEDIATE, HIGH SPEED DATA SCAN.
- STATISTICAL ANALYSIS PACKAGE

OBJECTIVE: MEASURE HEAT TRANSFER COEFFICIENT OVER A RANGE OF GAS VELOCITY APPLICABLE TO CORE-CONCRETE INTERACTIONS.

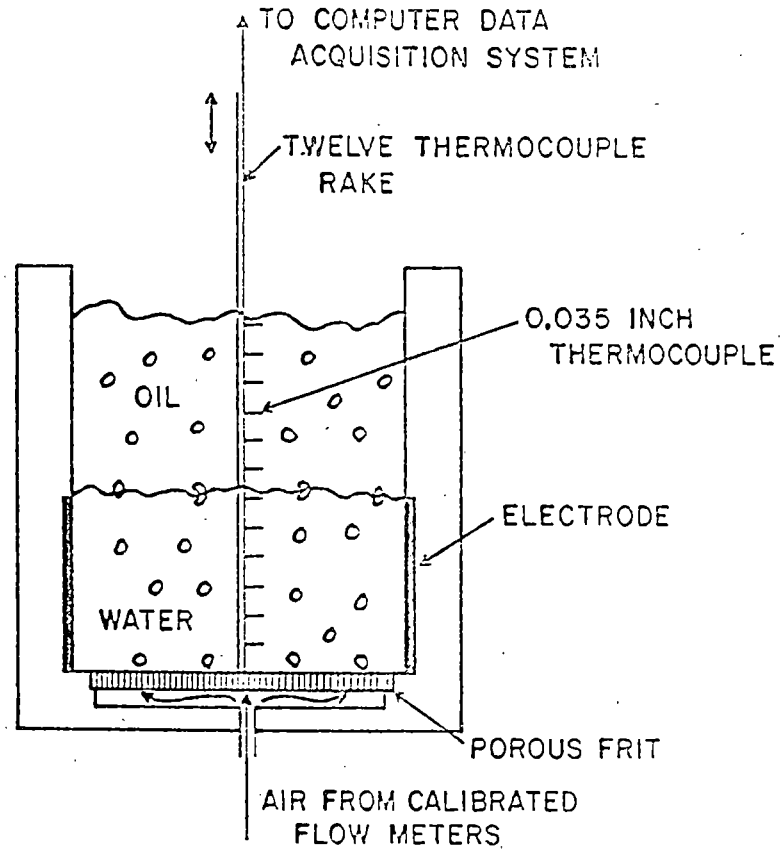

BROOKHAVEN NATIONAL LABORATORY
ASSOCIATED UNIVERSITIES, INC.

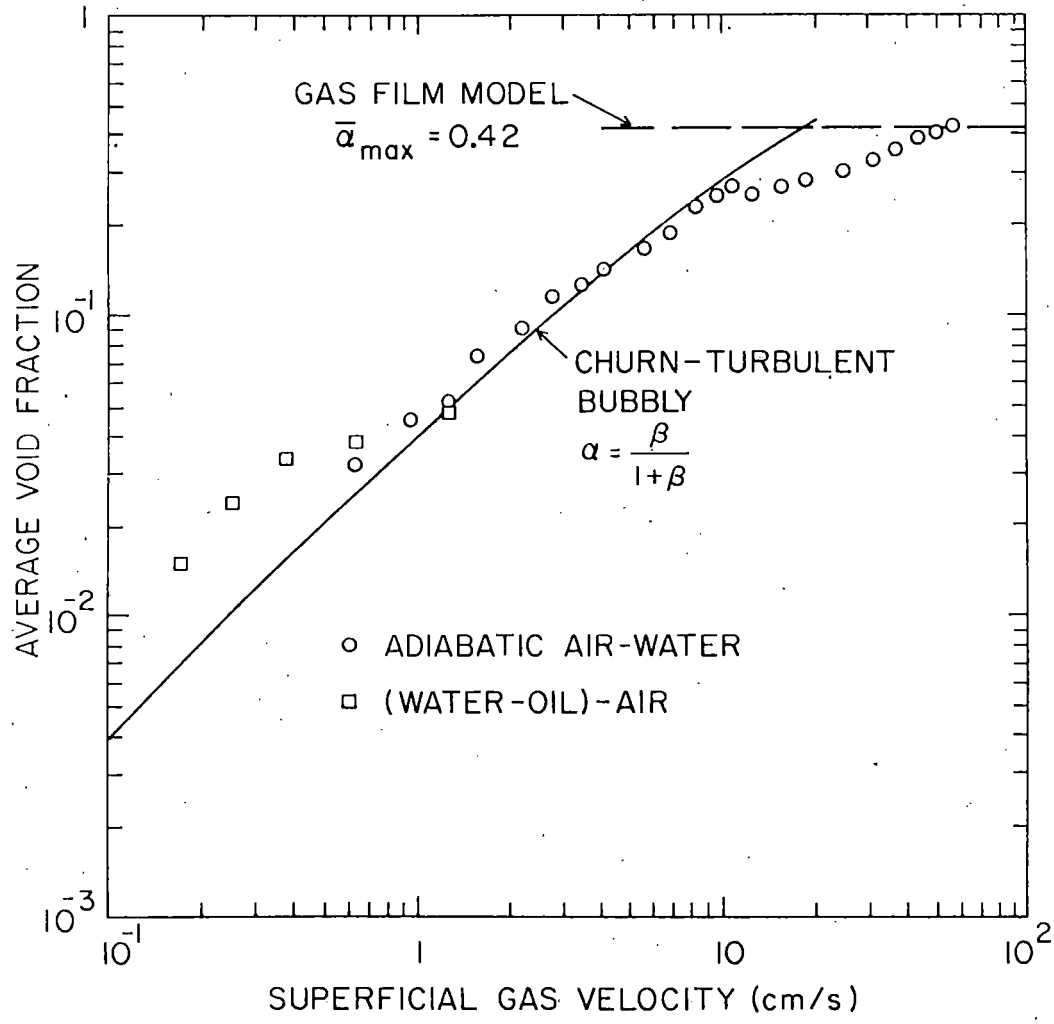
GAS FILM MODEL
$\bar{\alpha}_{max} = 0.42$
CHURN-TURBULENT
BUBBLY
$\alpha = \frac{\beta}{1+\beta}$
ADIABATIC AIR-WATER
(WATER-OIL)-AIR
AVERAGE VOID FRACTION
SUPERFICIAL GAS VELOCITY (cm/s)
1
10^{-1}
10^{-2}
10^{-3}
10^{-1}
1
10
10^{2}

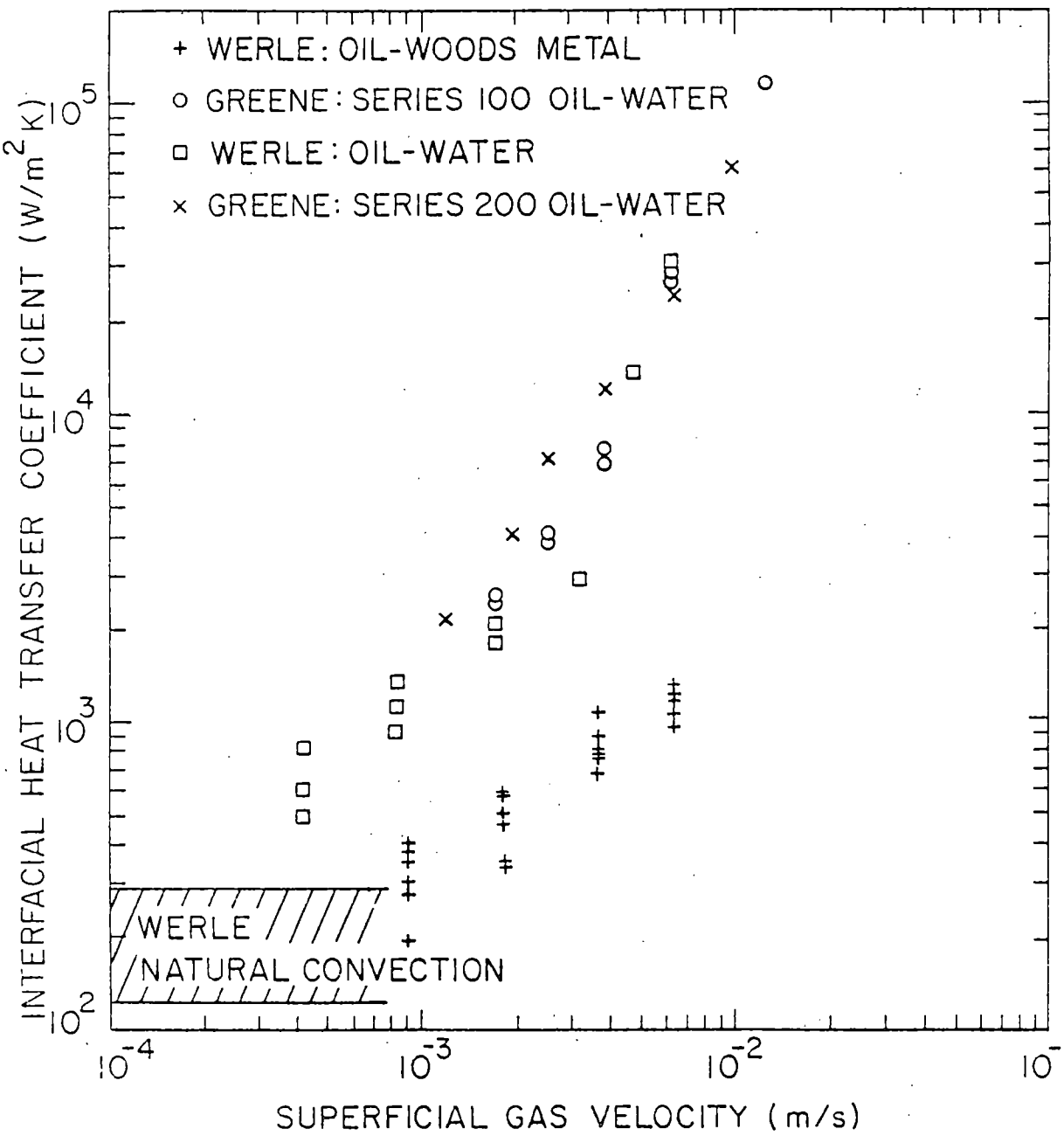
+ WERLE: OIL-WOODS METAL
o GREENE: SERIES 100 OIL-WATER
□ WERLE: OIL-WATER
× GREENE: SERIES 200 OIL-WATER
WERLE
NATURAL CONVECTION
INTERFACIAL HEAT TRANSFER COEFFICIENT (W/m²K)
SUPERFICIAL GAS VELOCITY (m/s)
10⁵
10⁴
10³
10²
10⁻⁴
10⁻³
10⁻²
10⁻¹

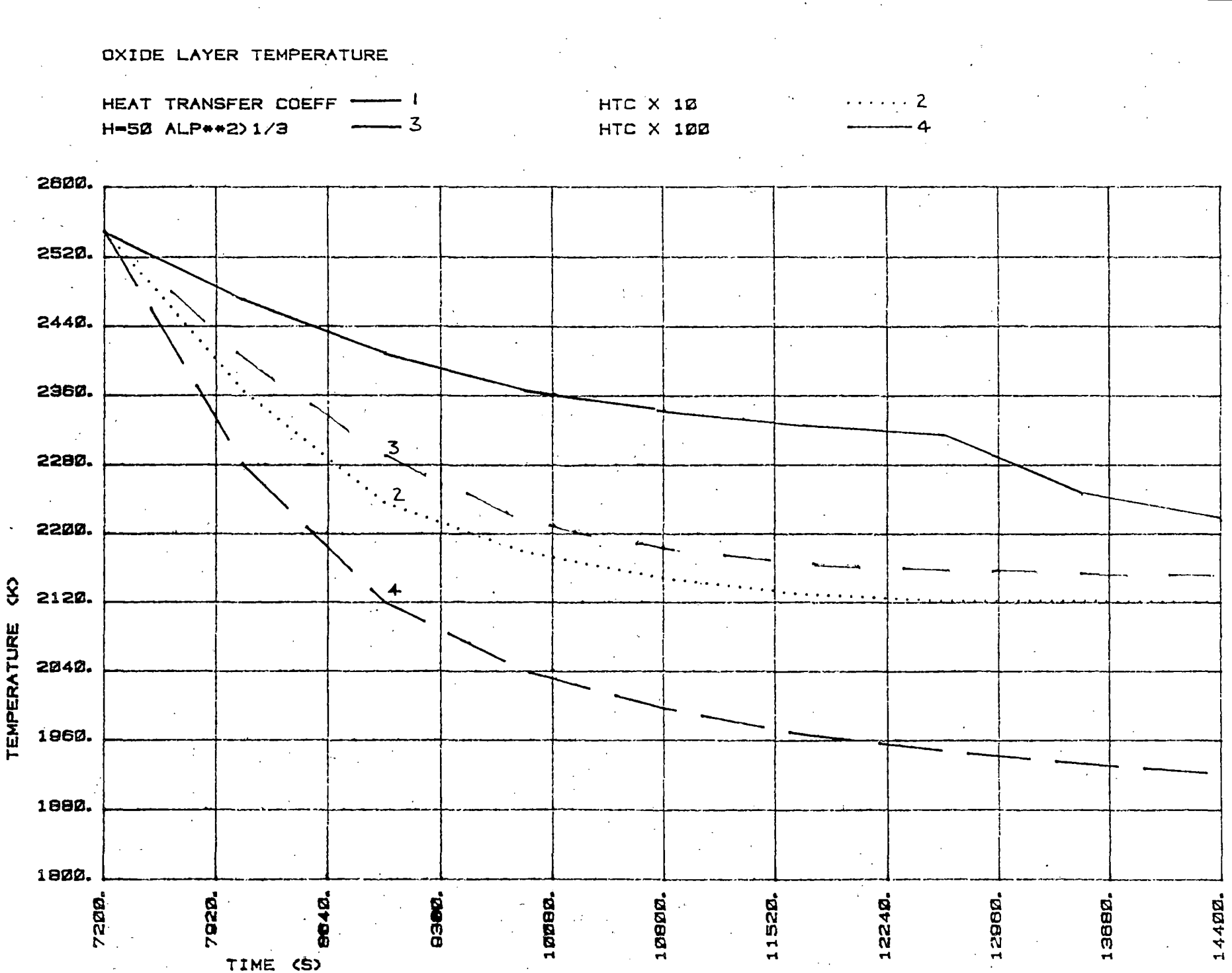
OXIDE LAYER TEMPERATURE
HEAT TRANSFER COEFF
H=50 ALP**2) 1/3
1
3
HTC X 10
HTC X 100
2
4
2600.
2520.
2440.
2360.
2280.
2200.
2120.
2040.
1960.
1880.
1800.
TEMPERATURE (K)
7200.
7920.
10080.
10800.
11520.
12240.
12960.
13680.
14400.
TIME (S)

METALLIC LAYER TEMPERATURE

HEAT TRANSFER COEFF — 1
H=50 ALP**2)1/3 — 3
HTC X 10 2
HTC X 100 ——— 4

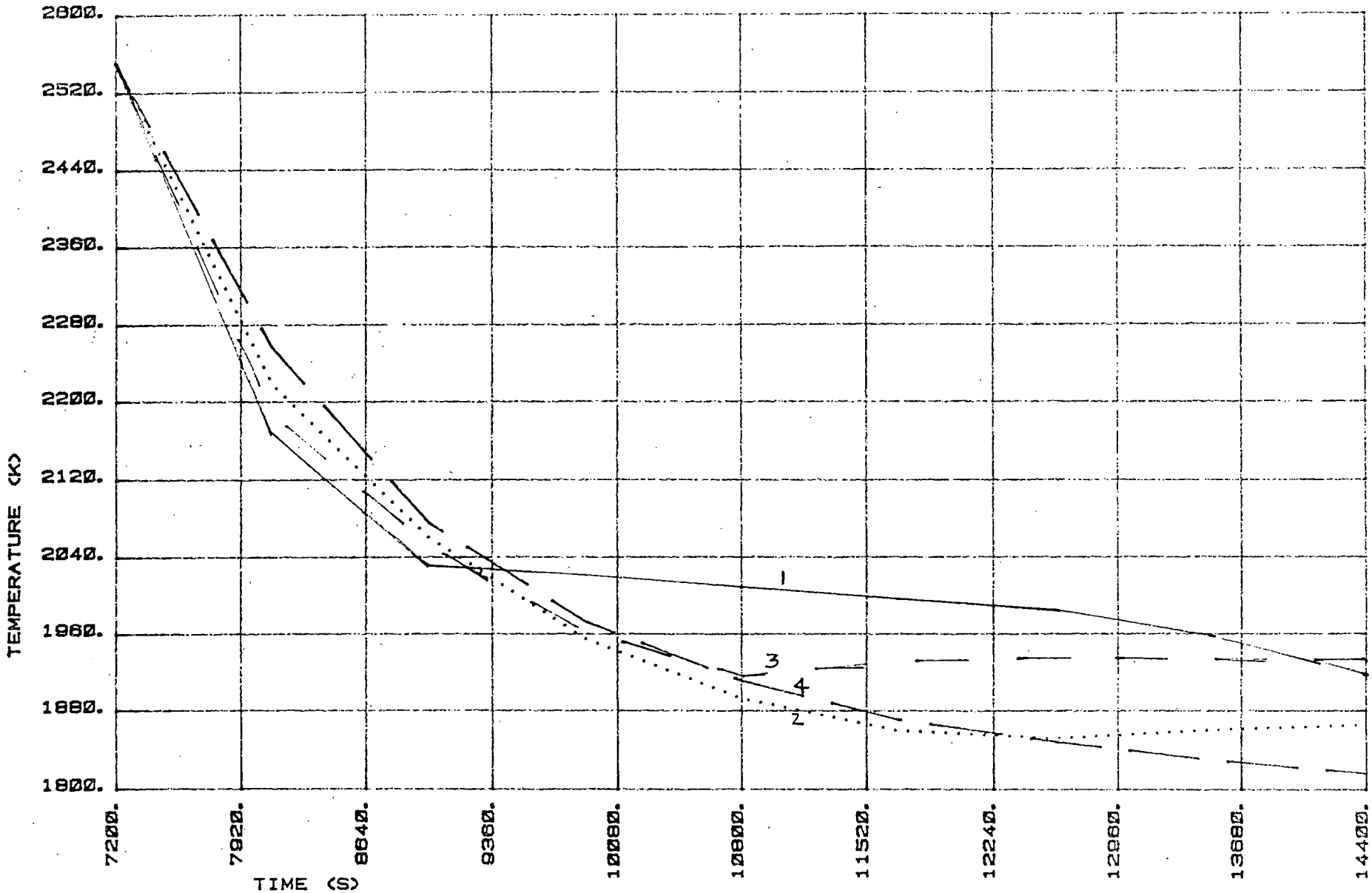

Materials Engineering Branch 5-Year Plans - Research and Standards

Charles Z. Serpan, Jr.
Materials Engineering Branch
U.S. Nuclear Regulatory Commission

Ninth Water Reactor Safety Research Information Meeting
October 29, 1981
Gaithersburg, Maryland

In the Spring of 1981, the NRC Offices of Nuclear Regulatory Research and Standards Development were merged into a single office, with the name of the Office of Nuclear Regulatory Research being retained. The former Metallurgy and Materials Research Branch, and part of the former Structures and Materials Branch (in Standards Development) were merged into the new Materials Engineering Branch in the new Division of Engineering Technology. Thus, we now have the efficiency of both research activities and standards development (including preparation of Regulatory Guides and regulations) being done in the same branch and in some cases by the same person. With time, we expect greater effectiveness in our operations as the needs for information for guides or regulations are being generated immediately in the area where the appropriate research information is being developed; furthermore, as the results are developed, positions being taken can more easily and accurately be modified to the best advantage of the licensing process.

The standards development activities of the branch were developed over the years through close cooperation with the licensing staff and are in direct response to their needs. The plan for these activities is periodically revised to meet the priorities and exigencies of the staff. The current program of standards development plus a schedule for issuance or completion is as follows:

1. Regulatory Guide, "Ultrasonic Testing of Class 1 & 2 Austenitic Pipe Welds During ISI," (develop guide in early 1983 and subsequent revision by mid-1986);

2. Regulatory Guide 1.150, "Ultrasonic Testing of Reactor Vessel Welds During Preservice and ISI," (revision not currently scheduled);

3. Regulatory Guide 1.83, "Inservice Inspection of Steam Generator Tubes," (Revision 2 issued early to mid-1983);

4. Regulatory Guide 1.121, "Bases for Plugging Degraded Steam Generator Tubes," (Revision 1 issued mid-1983);

5. Regulatory Guide, "Acoustic Emission Examination of Reactor Components," (development delayed to 1984-1985 pending completion of research);

6. Regulatory Guide 1.44, "Control of the Use of Sensitized Stainless Steel," (Revision 1 issued early-1983);

7. Regulatory Guide 1.56, "Maintenance of Water Purity in BWRs," (Revision 1 issued in late-1982);

8. Regulatory Guide 1.99, "Predicting Radiation Damage to Reactor Vessels, Regulation 10 CFR 50, Appendices G and H," (revisions periodically as required by new data);

9. Regulatory Guide, "Reference Toughness Curves, Regulation on Fracture Toughness Requirements During Accidents," (development delayed pending availability of personnel);

10. Regulatory Guide 1.84, "Code Case Acceptability for Design and Fabrication," Regulatory Guide 1.85, "Code Case Acceptability for Materials," Regulatory Guide 1.147, "Code Case Acceptability for Inservice Inspection," (periodic revisions to be continued); and

11. Regulation 50.55a: Broaden coverage of ASME Code: Include Class 2 & 3 Components (included in mid-1982 and all other parts of code in subsequent years).

The research activities of the branch, as envisioned for the years FY 1983 through FY 1987, were published earlier this year in NUREG-0740, "Long Range Research Plan, FY 1983-1987," March 1981. As had been the practice in previous years, we will continue to update this research plan on a yearly basis. The research activities continue to be organized in three area: Fracture Mechanics, Operating Effects on Materials, and Nondestructive Examination. The objectives of these three areas for the time period noted are as follows:

Fracture Mechanics

1. To develop and validate experimentally fracture-analysis procedures and design criteria for predicting the stress levels and flaw sizes required for crack initiation and subsequent propagation and arrest in LWR pressure vessels and primary piping under elastic, elastic-plastic, and fully plastic conditions;

2. To show that slow-load fracture toughness, rapid-load fracture toughness, and crack-arrest-toughness results obtained from small laboratory specimens are truly representative of the toughness characteristics of the material behavior in pressure vessels and piping in both unirradiated and irradiated material conditions;

3. To provide definitive experimental validation for the analytical methods used in the prediction of crack initiation, propagation, and arrest that could occur in a hot reactor vessel subjected to the injection of cold ECC water following a large or small LOCA;

4. To provide experimental and analytical procedures for determining the structural adequacy of the LWR reactor pressure vessels (RPVs) subject to postulated overcooling transients such as a main steam line break; to critically examine the entire generic area of the RPVs subjected to a pressurized thermal shock;

5. To develop analytical procedures and experimentally verify procedures for the analysis of degraded (cracked) pipe subjected to normal and upset loading conditions; to critically examine present criteria for postulated pipe rupture and to evaluate the leak-before-break concept for nuclear piping systems; and

6. To develop and experimentally validate analytical procedures for the evaluation of postulated post-pipe-rupture consequences; to critically examine present criteria for piping system restraint locations and configurations.

Operating Effects on Materials

1. Development of changes in the fracture toughness of steels, welds, and components that result from radiation, thermal aging, and environmental embrittlement and development of methods for mitigating this embrittlement, including annealing;

2. Development of methods for calculating, measuring, and predicting neutron flux and fluence in vessel surveillance capsules and the vessel wall itself;

3. Establishment of crack-growth rate of reactor pressure vessel steel, welds, and piping;

4. Identification and studies of the environmental parameters that cause cracking in PWR and BWR piping systems;

5. Studies of the environmental factors that cause degradation of steam generator tubing, support plates, and tube sheet;

6. Studies of the factors causing failures in turbines;

7. Evaluation of BWR and PWR water chemistry parameters and of the effects of changes caused by operating and offnormal conditions; and

8. Evaluation of repair welding in piping.

Nondestructive Examination

1. To quantify the reliability of current inservice inspection techniques for primary system components and to establish the required parameter modification in these techniques to obtain improvements in the reliability of inservice inspections;

2. To develop, evaluate, and validate advanced techniques for flaw detection and evaluation during inservice inspection of primary system components and steam generator tubes; and

3. To develop and validate new techniques for the continuous online monitoring of crack initiation and growth in reactors during operation and for leak detection.

THE OBJECTIVES OF THE PROGRAM ON

STANDARDS DEVELOPMENT ARE:

1. REGULATORY GUIDE, "ULTRASONIC TESTING OF CLASS 1 & 2 AUSTENITIC PIPE WELDS DURING ISI," (DEVELOP GUIDE EARLY 1983 AND SUBSEQUENT REVISION BY MID-1986);

2. REGULATORY GUIDE 1.150, "ULTRASONIC TESTING OF REACTOR VESSEL WELDS DURING PRESERVICE AND ISI," (REVISION NOT CURRENTLY SCHEDULED);

3. REGULATORY GUIDE 1.83, "INSERVICE INSPECTION OF STEAM GENERATOR TUBES," (REVISION 2 ISSUED EARLY- TO MID-1983);

4. REGULATORY GUIDE 1.121, "BASES FOR PLUGGING DEGRADED STEAM GENERATOR TUBES," (REVISION 1 ISSUED MID-1983):

5. REGULATORY GUIDE, "ACOUSTIC EMISSION EXAMINATION OF REACTOR COMPONENTS," (DEVELOPMENT DELAYED TO 1984-1985 PENDING COMPLETION OF RESEARCH);

6. REGULATORY GUIDE 1.44, "CONTROL OF THE USE OF SENSITIZED STAINLESS STEEL," (REVISION 1 ISSUED EARLY 1983);

7. REGULATORY GUIDE 1.56, "MAINTENANCE OF WATER PURITY IN BWRs," (REVISION 1 ISSUED IN LATE 1982):

8. REGULATORY GUIDE 1.99, "PREDICTING RADIATION DAMAGE TO REACTOR VESSELS REGULATION 10CFR50, APPENDICES G AND H," (REVISION PERIODICALLY AS REQUIRED BY NEW DATA):

9. REGULATORY GUIDE, "REFERENCE TOUGHNESS CURVES," (DEVELOPMENT DELAYED PENDING AVAILABILTIY OF PERSONNEL);

10. REGULATORY GUIDE 1.84, "CODE CASE ACCEPTABILITY FOR DESIGN AND FABRICATION," REGULATORY GUIDE 1.85, "CODE CASE ACCEPTABILTIY FOR MATERIALS," REGULATORY GUIDE 1.147, "CODE CASE ACCEPTABILITY FOR INSERVICE INSPECTION," (PERIODIC REVISIONS TO BE CONTINUED); AND

11. REGULATION 50.55A BROADEN COVERAGE OF ASME CODE: INCLUDE CLASS 2 & 3 COMPONENTS (INCLUDED IN MID-1982; ALL OTHER PARTS OF CODE IN SUBSEQUENT YEARS).

THE OBJECTIVES OF THE FRACTURE MECHANICS PROGRAM ARE:

1. TO DEVELOP AND VALIDATE EXPERIMENTALLY FRACTURE-ANALYSIS PROCEDURES AND DESIGN CRITERIA FOR PREDICTING THE STRESS LEVELS AND FLAW SIZES REQUIRED FOR CRACK INITIATION AND SUBSEQUENT PROPAGATION AND SRREST IN LWR PRESSURE VESSELS AND PRIMARY PIPING UNDER ELASTIC, ELASTIC-PLASTIC, AND FULLY PLASTIC CONDITIONS;

2. TO SHOW THAT SLOW-LOAD FRACTURE TOUGHNESS, RAPID-LOAD FRACTURE TOUGHNESS, AND CRACK-ARREST-TOUGHNESS RESULTS OBTAINED FROM SMALL LABORATORY SPECIMENS ARE TRULY REPRESENTATIVE OF THE TOUGHNESS CHARACTERISTICS OF THE MATERIAL BEHAVIOR IN PRESSURE VESSELS AND PIPING IN BOTH UNIRRADIATED AND IRRADIATED MATERIAL CONDITIONS;

3. TO PROVIDE DEFINITIVE EXPERIMENTAL VALIDATION FOR THE ANALYTICAL METHODS USED IN THE PREDICTION OF CRACK INITIATION, PROPAGATION, AND ARREST THAT COULD OCCUR IN A HOT REACTOR VESSEL SUBJECTED TO THE INJECTION OF COLD ECC WATER FOLLOWING A LARGE OR SMALL LOCA;

4. TO PROVIDE EXPERIMENTAL AND ANALYTICAL PROCEDURES FOR DETERMINING THE STRUCTURAL ADEQUACY OF THE LWR REACTOR PRESSURE VESSELS (RPVs) SUBJECT TO POSTULATED OVERCOOLING TRANSIENTS SUCH AS A MAIN STEAM LINE BREAK; TO CRITICALLY EXAMINE THE ENTIRE GENERIC AREA OF THE RPVs SUBJECTED TO A PRESSURIZED THERMAL SHOCK;

5. TO DEVELOP ANALYTICAL PROCEDURES AND EXPERIMENTALLY VERIFY PROCEDURES FOR THE ANALYSIS OF DEGRADED (CRACKED) PIPE SUBJECTED TO NORMAL AND UPSET LOADING CONDITIONS; TO CRITICALLY EXAMINE PRESENT CRITERIA FOR POSTULATED PIPE RUPTURE AND TO EVALUATE THE LEAK-BEFORE-BREAK CONCEPT FOR NUCLEAR PIPING SYSTEMS; AND

6. TO DEVELOP AND EXPERIMENTALLY VALIDATE ANALYTICAL PROCEDURES FOR THE EVALUATION OF POSTULATED POST-PIPE-RUPTURE CONSEQUENCES; TO CRITICALLY EXAMINE PRESENT CRITERIA FOR PIPING SYSTEM RESTRAINT LOCATIONS AND CONFIGURATIONS.

THE OBJECTIVES OF THE PROGRAM ON
OPERATING EFFECTS ON MATERIALS ARE:

1. DEVELOPMENT OF CHANGES IN THE FRACTURE TOUGHNESS OF STEEL, WELDS, AND COMPONENTS THAT RESULT FROM RADIATION, THERMAL AGING, AND ENVIRONMENTAL EMBRITTLEMENT AND DEVELOPMENT OF METHODS FOR MITIGATING THIS EMBRITTLEMENT, INCLUDING ANNEALING;

2. DEVELOPMENT OF METHODS FOR CALCULATING, MEASURING, AND PREDICTING NEUTRON FLUX AND FLUENCE IN VESSEL SURVEILLANCE CAPSULES AND THE VESSEL WALL ITSELF;

3. ESTABLISHMENT OF CRACK-GROWTH RATE OF REACTOR PRESSURE VESSEL STEEL, WELDS, AND PIPING;

4. IDENTIFICATION AND STUDIES OF THE ENVIRONMENTAL PARAMETERS THAT CAUSE CRACKING IN PWR AND BWR PIPING SYSTEMS;

5. STUDIES OF THE ENVIRONMENTAL FACTORS THAT CAUSE DEGRADATION OF STEAM GENERATOR TUBING, SUPPORT PLATES, AND TUBE SHEET;

6. STUDIES OF THE FACTORS CAUSING FAILURES IN TURBINES;

7. EVALUATION OF BWR AND PWR WATER CHEMISTRY PARAMETERS AND OF THE EFFECTS OF CHANGES CAUSED BY OPERATING AND OFFNORMAL CONDITIONS; AND

8. EVALUATION OF REPAIR WELDING IN PIPING.

THE OBJECTIVES OF THE PROGRAM ON
NON-DESTRUCTIVE EXAMINATION ARE:

1. TO QUANTIFY THE RELIABILITY OF CURRENT INSERVICE INSPECTION TECHNIQUES FOR PRIMARY SYSTEM COMPONENTS AND TO ESTABLISH THE REQUIRED PARAMETER MODIFICATION IN THESE TECHNIQUES TO OBTAIN IMPROVEMENTS IN THE RELIABILITY OF INSERVICE INSPECTIONS;

2. TO DEVELOP, EVALUATE, AND VALIDATE ADVANCED TECHNIQUES FOR FLAW DETECTION AND EVALUATION DURING INSERVICE INSPECTION OF PRIMARY SYSTEM COMPONENTS AND STEAM GENERATOR TUBES; AND

3. TO DEVELOP AND VALIDATE NEW TECHNIQUES FOR THE CONTINUOUS ONLINE MONITORING OF CRACK INITIATION AND GROWTH IN REACTORS DURING OPERATION AND FOR LEAK DETECTION.

INTEGRITY OF REACTOR PRESSURE VESSELS DURING OVERCOOLING ACCIDENTS

R. D. CHEVERTON

HSST THERMAL-SHOCK PROGRAM
OAK RIDGE NATIONAL LABORATORY

PRESENTED AT

NINTH WATER REACTOR SAFETY RESEARCH
INFORMATION MEETING

NATIONAL BUREAU OF STANDARDS
GAITHERSBURG, MARYLAND

OCTOBER 29, 1981

PWR PRESSURE VESSEL INTEGRITY DURING OVERCOOLING ACCIDENTS*

R. D. Cheverton

Oak Ridge National Laboratory
Oak Ridge, Tennessee 37830

Pressurized water reactors are susceptible to certain types of hypothetical accidents that under some circumstances, including operation of the reactor beyond a critical time in its life, could result in failure of the pressure vessel as a result of propagation of crack-like defects in the vessel wall. The accidents of concern are those that result in thermal shock to the vessel while the vessel is subjected to internal pressure. Such accidents, referred to as pressurized thermal shock or overcooling accidents (OCA), include a steamline break, small-break LOCA, turbine trip followed by stuck-open bypass valves, the 1978 Rancho Seco and the TMI accidents and many other postulated and actual accidents. The source of cold water for the thermal shock is either emergency core coolant or the normal primary-system coolant. In the latter case the coolant temperature is reduced by depressurization of the primary system or by the secondary system after it has been cooled by depressurization and/or excessive feedwater.

ORNL performed fracture-mechanics calculations for a steamline break in 1978 and for a turbine-trip case in 1980 and concluded on the basis of the results that many more such calculations would be required. To meet the expected demand in a realistic way a computer code, OCA-I,[1] was developed that accepts primary-system temperature and pressure transients as input and then performs one-dimensional thermal and stress analyses for the wall and a corresponding fracture-mechanics (FM) analysis for a long axial flaw. The cladding is included in the thermal analysis but not in the stress or FM analysis. Thus, if the flaw is assumed to extend through the cladding, the calculated stress

---

*Research sponsored by the Office of Nuclear Regulatory Research, U.S. Nuclear Regulatory Commission under Interagency Agreements 40-551-75 and 40-552-75 with the U.S. Department of Energy under contract W-7405-eng-26 with the Union Carbide Corporation.

intensity factors (K_I) are somewhat low, and if the flaws are assumed to be under the cladding, the calculated K_I values are much too large.

A superposition technique was used for calculating the K_I values, and largely because of this feature the operating cost for OCA-I is very low, making parametric and sensitivity studies feasible. The accuracy of the K_I calculation has been checked against a finite-element-analysis code[2] for crack depths ranging from 3 to 90% of the wall thickness and found to be within 1%.

Another convenient feature incorporated in OCA-I is a plotting package that provides critical-crack-depth curves as well as more conventional plots.

Taking advantage of the parametric-type features in OCA-I, a limit analysis was conducted for OCA's to provide a "handbook" assessment capability. Six exponential coolant-temperature transients (decay constants ranging from 0.015 min^{-1} to ∞) and two coolant-temperature asymptotes (66 to 121°C) were used to represent a wide range of temperature transients. For a given thermal transient the pressure was held constant, but several different values in the range of 3 to 17 MPa were included. Two copper concentrations (0.1 and 0.35%) and a wide range of fast-neutron fluences were also included. Critical-crack-depth and K_I vs time-and-crack-depth curves are included in the handbook for over five hundred cases.

An OCA generic study was conducted with OCA-I, and some important flaw-behavior trends were revealed. It appears that very shallow flaws ($\geq$3 mm) will initiate, and in some cases complete penetration of the wall will result. This is worrysome because shallow flaws are more likely to occur and more difficult to detect. The analysis indicates that the thermal shock initiates propagation of a shallow flaw, and failure occurs by plastic instability. In some cases arrest may take place on the upper shelf, but the methodology for including such an event is not yet a part of OCA-I. Another observation from the overall OCA study is that for some accidents there will probably be enough energy stored in the coolant above 100°C to result in a large opening in the vessel wall, if and when a long flaw penetrates the wall.

The generic analysis also indicated that if an OCA were to take place the OCA would be much more likely to result in vessel failure than would the double-ended-pipe-break LOCA, which was the postulated PWR accident that triggered the HSST thermal-shock investigations.

A few specific-plant analyses were also performed and these included the 1978 Rancho Seco accident,[3] a postulated main-steamline-break accident[4] and a postulated accident involving a turbine trip followed by stuck-open bypass valves.[5] The appropriate copper concentration and initial RTNDT were 0.31% and 40°F, and the fluence rate was 0.046×10^{19} n/cm^2/EFPY. OCA-I results for this specific-plant analysis indicated a potential for vessel failure at 20 EFPY for the Rancho Seco accident, and about 4 EFPY for the other two.

The Rancho Seco case did not require a systems analysis since the actual temperature and pressure transients were recorded and were used as input to OCA-I. However, the temperature and pressure transients for the other two cases were derived from a systems-analysis code that is believed to be quite conservative (IRT). There may also be significant conservatism included in the OCA-I analysis, and suspect areas that will be evaluated further include the effect of cladding on flaw extension and propagation, radiation damage to cladding, flaw behavior on the upper shelf and the size of the opening in the wall.

References

1. S. K. Iskander, R. D. Cheverton and D. G. Ball, OCA-I, A Code for Calculating the Behavior of Flaws on the Inner Surface of a Pressure Vessel Subjected to Temperature and Pressure Transients, ORNL/NUREG-84, August 1981.

2. S. K. Iskander, Two Finite-Element Techniques for Computing Mode I Stress Intensity Factors in Two- and Three-Dimensional Problems, ORNL/NUREG/CSD/TM-14, February 1981.

3. Letter to R. D. Cheverton, ORNL, from J. Strosnider, NRC, January 30, 1981.

4. Letter to R. Kryter, ORNL, from R. J. Cerbone, BNL, August 14, 1981.

5. Letter to R. D. Cheverton, ORNL, from M. M. Levine, BNL, August 11, 1980.

INTEGRITY OF REACTOR PRESSURE VESSELS DURING OVERCOOLING ACCIDENTS

R. D. CHEVERTON
HSST THERMAL-SHOCK PROGRAM
OAK RIDGE NATIONAL LABORATORY

PRESENTED AT
NINTH WATER REACTOR SAFETY RESEARCH INFORMATION MEETING
NATIONAL BUREAU OF STANDARDS
GAITHERSBURG, MARYLAND
29 OCTOBER 1981

OVERCOOLING ACCIDENTS (THERMAL SHOCK AND PRESSURE) MORE OF A THREAT TO INTEGRITY OF PWR VESSELS THAN LARGE-BREAK LOCA

- LBLOCA: FLAWS WILL NOT PENETRATE WALL
- OCAs: POTENTIAL FOR PENETRATION AND LARGE OPENING IN WALL

PURPOSE OF OCA ANALYSIS: DISCOVER FLAW BEHAVIOR TRENDS THAT NEED BETTER DEFINITION THROUGH ANALYTICAL AND EXPERIMENTAL STUDIES

BASIS FOR METHODS OF ANALYSIS FOR OCA STUDIES PROVIDED AND VALIDATED BY HSST THERMAL-SHOCK PROGRAM

- LEFM VALIDATED
- CRACK ARREST CONCEPT VALIDATED
- WARM PRESTRESSING DEMONSTRATED
- LARGE SCATTER IN LAB K_{Ic} DATA DISCOVERED
- LOWER-BOUND TOUGHNESS BEHAVIOR OF LONG FLAWS REVEALED
- TENDENCY FOR SHORT FLAWS TO BECOME LONG FLAWS CONFIRMED

OCA ANALYSIS BASED ON CONSERVATIVE ASSUMPTIONS AND MODEL

- LONG AXIAL FLAWS
- ONE-DIMENSIONAL THERMAL AND STRESS ANALYSES
- CLADDING THERMAL RESISTANCE BUT NOT MECHANICAL RESTRAINT INCLUDED
- LOWER-BOUND TOUGHNESS (ASME XI)
- ΔRTNDT FROM REG GUIDE 1.99
- VESSEL FAILURE DEFINED AS CRACK PENETRATION

NEED FOR PARAMETRIC AND SENSITIVITY STUDIES PROMPTED DEVELOPMENT OF OCA-I CODE

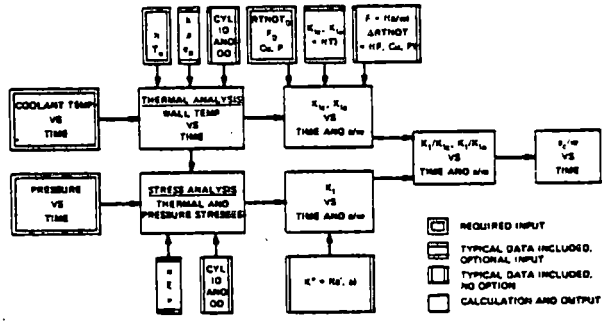

CRITICAL-CRACK-DEPTH CURVES OBTAINED FROM OCA-I USEFUL IN PREDICTING BEHAVIOR OF FLAW

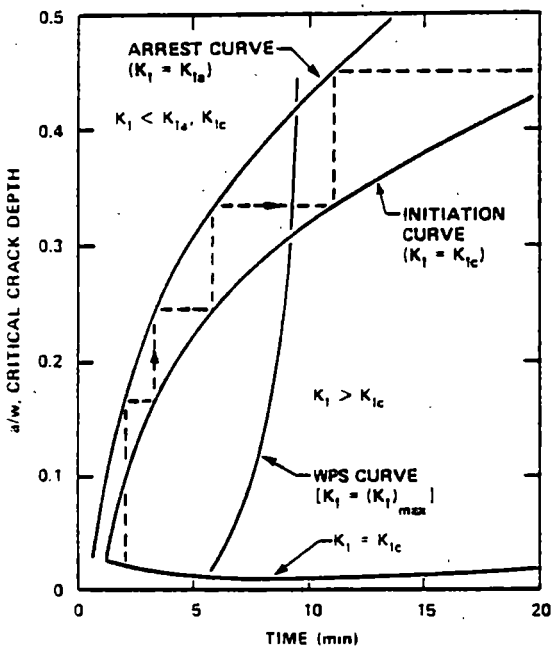

OCA LIMIT ANALYSIS PERFORMED TO PROVIDE "HANDBOOK" ASSESSMENT CAPABILITY

- PERMITS ESTIMATE OF THRESHOLD FLUENCE FOR FAILURE
- PERMITS ESTIMATE OF MAX PERMISSIBLE PRESSURE FOR GIVEN FLUENCE

OCA LIMIT ANALYSIS INCLUDES ~500 CASES

- SIX EXPONENTIAL TEMPERATURE TRANSIENTS ($\omega = -\infty$ TO -0.015 min^{-1})
- TWO TEMPERATURE ASYMPTOTES (66 AND 121°C)
- WIDE RANGE OF CONSTANT PRESSURES (3 TO 17 MPa)
- TWO COPPER CONCENTRATIONS (0.10 AND 0.35%)
- WIDE RANGE OF FAST-NEUTRON-FLUENCE VALUES

GENERIC ANALYSIS OF OCAs HAS REVEALED IMPORTANT FLAW-BEHAVIOR TRENDS

- VERY SHALLOW FLAWS WILL INITIATED ($a \geq 3$ mm)

  SHALLOW FLAWS MORE LIKELY

  DIFFICULT TO DETECT
- THERMAL SHOCK INITIATES PROPAGATION; FAILURE RESULTS FROM PLASTIC INSTABILITY
- FOR SOME CASES ARREST ON UPPER SHELF MAY OCCUR
- LARGE OPENING IN VESSEL WALL POSSIBLE IF FLAW PENETRATES WALL AND COOLANT TEMPERATURE IS ABOVE 100°C

1978 RANCHO SECO ACCIDENT NOT AS SEVERE AS SOME OTHERS ANALYZED

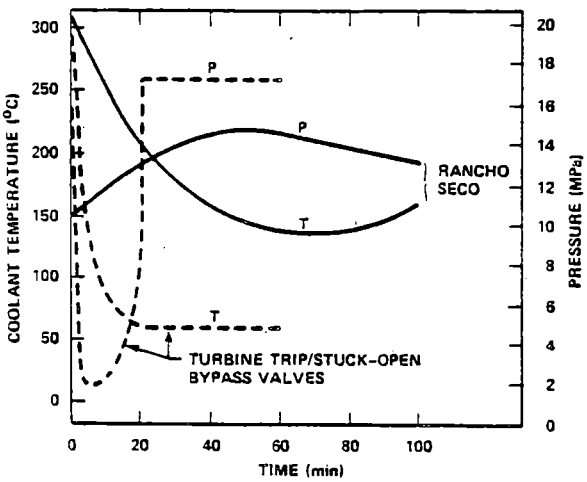

RANCHO SECO THRESHOLD FLUENCE FOR CRACK INITIATION (WITH WPS) $\simeq 1.8 \times 10^{19}$ n/cm^2: CRACK DOES NOT ARREST

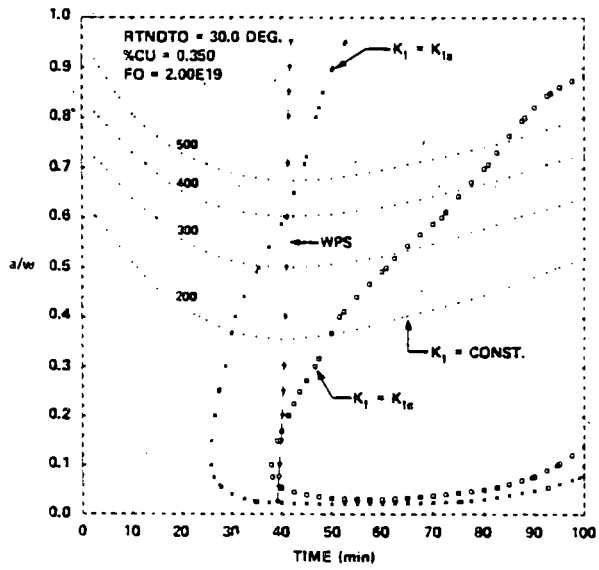

RANCHO SECO THRESHOLD FLUENCE FOR CRACK INITIATION (WITHOUT WPS) $\simeq 0.8 \times 10^{19}$ n/cm^2: CRACK DOES NOT ARREST

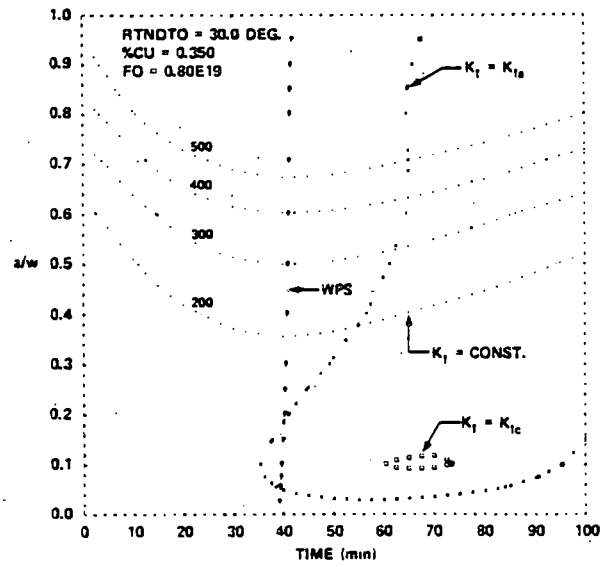

RESULTS OF RANCHO SECO ANALYSIS, ASSUMING Cu = 0.35% AND $RTNDT_o = -1^oC$, INDICATE POTENTIAL FOR PREMATURE FAILURE

	WPS	w/o WPS
THRESHOLD FLUENCE FOR INITIATION AND FAILURE, n/cm^2 x 10^{19}	1.8	0.8
CORRESPONDING TIME IN EFPYs (B&W PLANT)	39	17
CRITICAL CRACK DEPTH, a/w	0.1	0.1
TIME IN TRANSIENT, min	40	65

RESULTS OF ANALYSIS FOR OTHER POSTULATED OCAs INDICATE MUCH SHORTER THRESHOLD TIMES

- MORE SEVERE TRANSIENTS
  - MAIN STEAMLINE BREAK
  - TURBINE TRIP WITH STUCK-OPEN BYPASS VALVES
- GREATER FLUENCE RATE (FLUENCE/EFPY)

SUMMARY: OCA STUDIES INDICATE

- POTENTIAL FOR PREMATURE FAILURE
- CALCULATIONAL MODELS TEND TO BE CONSERVATIVE
- NEED FOR MORE REALISTIC MODELS
  - 2-D THERMAL AND STRESS ANALYSIS
  - CLADDING EFFECTS
  - CLADDING RADIATION DAMAGE
  - FLAW BEHAVIOR ON UPPER SHELF
  - SIZE OF OPENING IN VESSEL WALL

PRESSURIZED-THERMAL-SHOCK TESTS

G. D. WHITMAN

OAK RIDGE NATIONAL LABORATORY

NINTH WATER REACTOR SAFETY RESEARCH
INFORMATION MEETING

OCTOBER 29, 1981

PRESSURIZED-THERMAL-SHOCK TESTS*

G. D. Whitman
Oak Ridge National Laboratory
Oak Ridge, Tennessee 37830

Pressurized-thermal-shock experiments are required to validate methods of fracture analysis to establish the degree of conservatism or accuracy involved in predictions of flaw behavior under certain accident conditions. By using methods and facilities developed for this purpose we can simulate materials and loading regimes to evaluate the integrity of flawed reactor pressure vessels subjected to pressurized-thermal-shock transients. These accidents involve small-break loss-of-coolant accidents, steamline breaks, and other similar overcooling accident senarios involving combined temperature and pressure transients.

Among the objectives we plan to achieve are the simulation of representative conditions of stress state, material combinations and material properties which would be applicable to pressurized water reactor pressure vessels. Flaw behavior involving both noninitiation and initiation and arrest are of interest. Particular attention will be paid to conditions where the outer portions of the vessel wall remain ductile but with low upper-shelf energy fracture toughness so as to determine the propagation or arrest of a running crack moving into a ductile material.

Cladding effects are to be evaluated to determine the influence of stainless steel on small flaw behavior under thermal and pressurized-thermal-shock conditions. Materials properties are to be evaluated and recommendations made for studies of stainless steel cladding including irradiation effects to develop data required for the analysis of flaw behavior. Crack arrest properties and fracture toughness of irradiated primary pressure vessel base materials and weld metal are also being studied, and recommendations are being developed to perform additional investigations.

---

*Research sponsored by the Office of Nuclear Regulatory Research, U.S. Nuclear Regulatory Commission under Interagency Agreements 40-551-75 and 40-552-75 with the U.S. Department of Energy under contract W-7405-eng-26 with the Union Carbide Corporation.

A modification to the existing HSST intermediate vessel test facility is being studied to utilize an HSST intermediate vessel as a pressurized-thermal-shock test specimen. Flaws will be placed in the external mid-region of the cylindrical section of a vessel. Pressure loading will be established by using existing equipment, and thermal loading will be established by suddenly cooling with prechilled liquid (40% wt methanol, 60% wt water) the external surface of a preheated vessel.

The features of this thermal-shock test facility will strongly resemble the now disassembled facility which was used to test the thermal-shock cylinders, TSE-1, 2, 3 and 4. Essential components will include: (1) a refrigeration unit to prechill the coolant; (2) a storage tank for the coolant; (3) a pump to provide flow; and (4) quick-opening valves to divert flow from a bypass to the specimen. The intermediate test vessel will be contained within a low pressure flow duct and heater support to achieve the initial temperature conditions required and to develop the thermal shock desired. This duct will be located within an existing test cell. In order to satisfy the energy limitations for this cell, ballast material in the form of graphite will be inserted in the test vessel. Inadvertent spills of the methanol/water liquid mixture employed to achieve low temperatures will be collected in a cell liner.

In addition to proceeding with the analysis and design of the test facility, we are examining the capability of the intermediate vessel to serve as an adequate test specimen. The conditions that we desire to impose upon the vessel as a specimen were not anticipated in its original design. In addition to verifying the structural design acceptability of the head and access nozzle subassembly, we are also examining ways to overcome the temperature limitation of the closure seal and the instrumentation lead penetration fittings to permit operation up to a temperature of 288°C (550°F).

The use of an external flaw simplifies the cooling system requirements since the system can operate at a much lower pressure to greatly reduce the cost of the components. The predicted behavior of the externally flawed vessel which would be pressured internally and cooled externally produces data which is quite representative of the pressurized water reactor behavior under pressurized-thermal-shock transients. Finite length flaws, long flaws

and cladding effects could be evaluated with an intermediate vessel, and multiple flaws could be evaluated in a single test to greatly enhance the data developed with this concept. Work is continuing on the design of the facility and vessel configuration.

THE MAJOR OBJECTIVES OF A PRESSURIZED-THERMAL-SHOCK EXPERIMENT ARE

- SIMULATION OF CONDITIONS OF MATERIAL TOUGHNESS AND STRESS STATE REPRESENTING PRESSURE AND THERMAL LOADINGS IN A REACTOR VESSEL
- DEVELOPMENT OF DATA FOR VALIDATION OF ANALYTICAL MODELS OF FLAW BEHAVIOR FOR THE CONDITIONS OF INTEREST

EXPERIMENTAL PROGRAM PLANNING INCLUDES

- MATERIALS EVALUATIONS
- SIMPLIFIED STRUCTURAL TESTS
- THERMAL SHOCK TESTS ON CYLINDERS
- PRESSURIZED–THERMAL–SHOCK TESTS ON INTERMEDIATE VESSELS

EVALUATION OF PRESSURIZED-THERMAL-SHOCK IS TO INCLUDE BEHAVIORAL STUDIES OF

- LONG AXIAL FLAW
- CIRCUMFERENTIAL FLAW
- FINITE (SHORT) FLAW EXTENSION
- EFFECTS OF STAINLESS STEEL CLADDING ON FLAW EXTENSION

PRESSURIZED-THERMAL-SHOCK TRANSIENTS INVOLVE COOLDOWNS WITH SIGNIFICANT PRESSURE LOADS ON THE SYSTEM

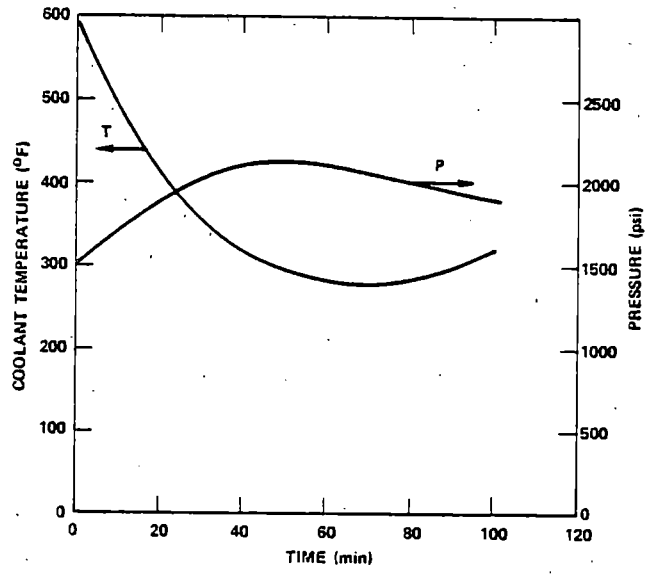

CRITICAL CRACK DEPTH CURVES FOR A REFERENCE PWR VESSEL INDICATE DEEP PENETRATION OF A FLAW UNDER SOME PRESSURIZED–THERMAL-SHOCK LOADINGS

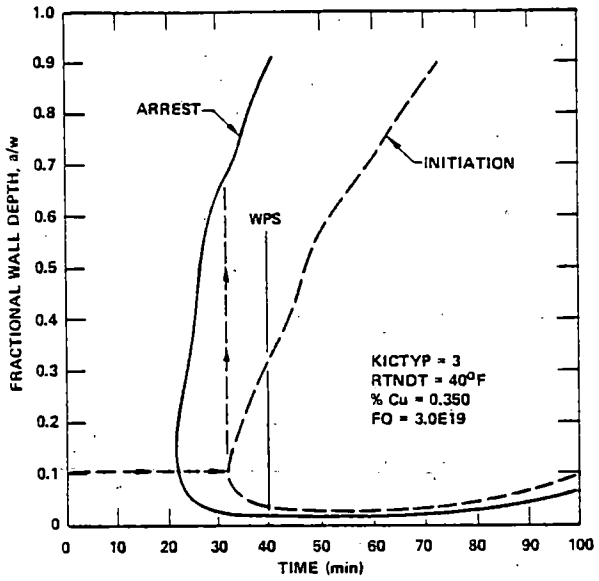

INTERMEDIATE VESSEL TESTS WILL PROVIDE DATA ON

- CRACK ARREST ON UPPER SHELF
- SHORT FLAW BEHAVIOR
- CLADDING EFFECTS
- WARM PRESTRESSING

CURRENT SCOPE OF ACTIVITIES FOR UTILIZATION OF INTERMEDIATE PRESSURE VESSEL

- SPECIMEN ANALYSIS: VALIDATION OF THE FEASIBILITY OF PERFORMING A REPRESENTATIVE PRESSURIZED–THERMAL–SHOCK EXPERIMENT
- LOOP ANALYSES: FLEXIBILITY, FLUID FLOW, HEAT TRANSPORT
- ANALYSIS OF INTERMEDIATE TEST VESSEL TO VALIDATE PERFORMANCE FUNCTIONS OF SEAL AND HEATING PROCEDURE
- EQUIPMENT LAYOUT

PRESSURIZED THERMAL SHOCK EXPERIMENTS ARE IN PLANNING USING HSST INTERMEDIATE VESSELS TO VALIDATE PREDICTIONS OF FLAW BEHAVIOR UNDER COMBINED LOADS

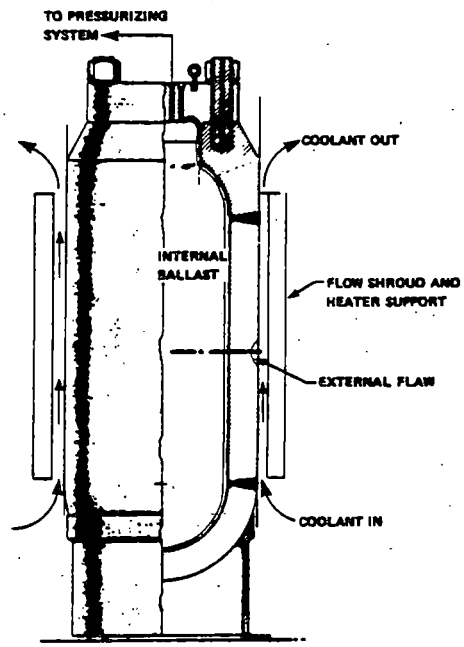

FLAW LOCATION IN CYLINDRICAL SECTION OF AN HSST INTERMEDIATE PRESSURE VESSEL COULD BE CONTAINED IN SPECIAL TEST MATERIAL

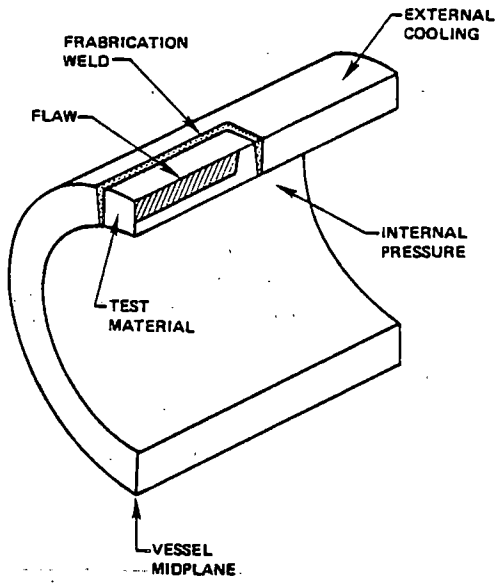

HSST PROGRAM PRESSURIZED-THERMAL SHOCK FACILITY FLOW DIAGRAM

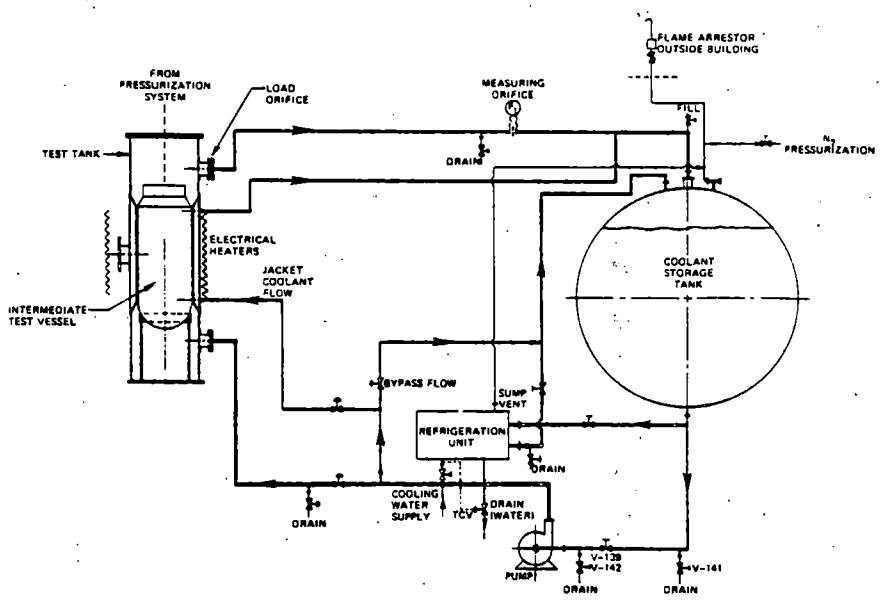

SECTION ELEVATION OF HSST PROGRAM PRESSURIZED-THERMAL-SHOCK FACILITY

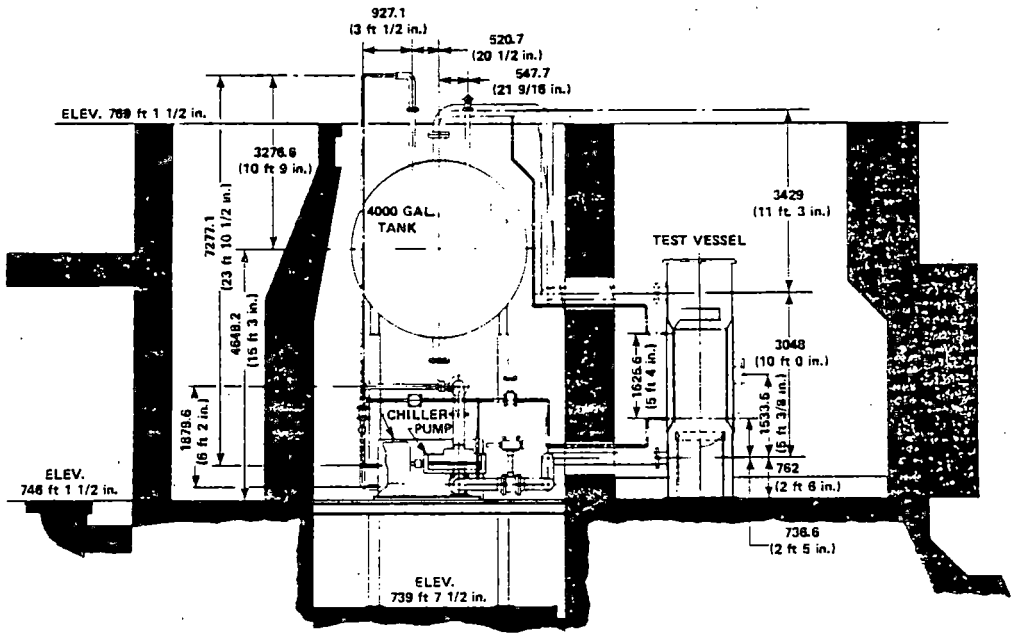

K_I FOR LONG INSIDE AND OUTSIDE FLAWS IN AN INTERMEDIATE TEST VESSEL FOR THERMAL SHOCK ONLY AT TIME OF APPROXIMATE MAXIMUM K_I DECREASE WITH DEEP EXTENSIONS

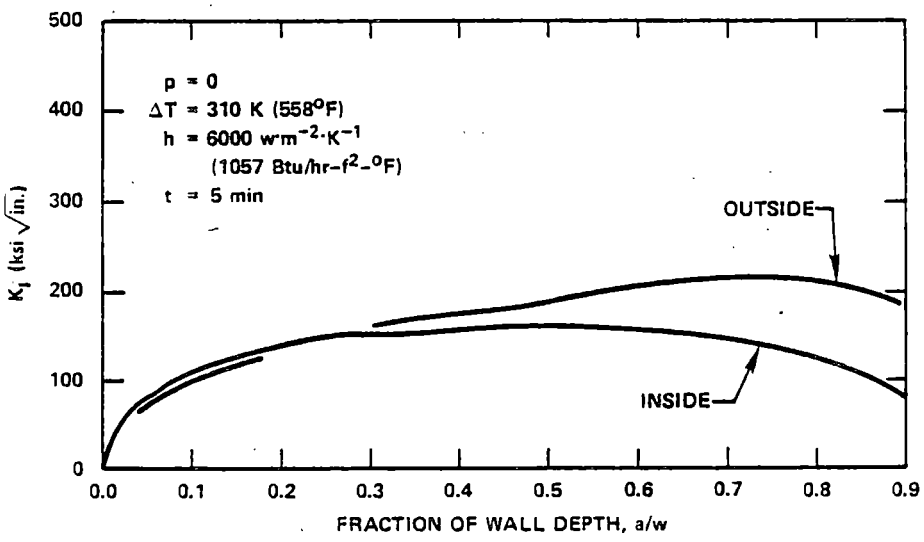

K_I FOR INSIDE AND OUTSIDE FLAWS IN AN INTERMEDIATE TEST VESSEL FOR COMBINED PRESSURE AND THERMAL-SHOCK LOADING AT TIME OF APPROXIMATE MAXIMUM K_I CONTINUE TO INCREASE WITH FLAW EXTENSION

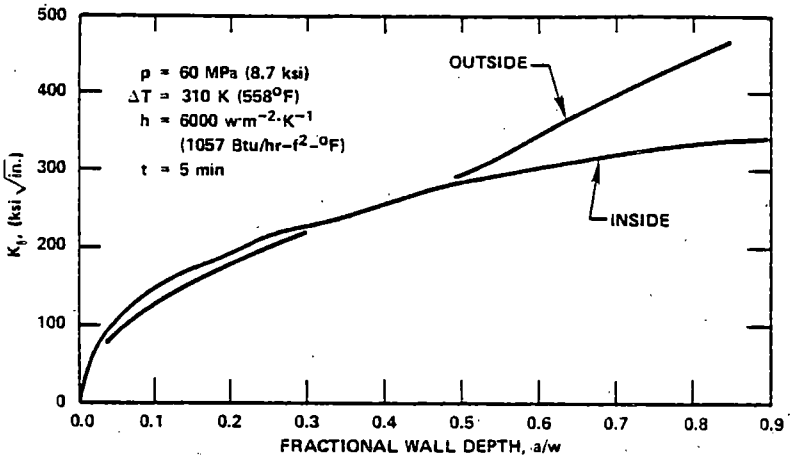

CRITICAL CRACK DEPTH VS TIME AND WARM PRESTRESSING CURVES FOR OUTSIDE FLAW IN INTERMEDIATE TEST VESSEL FOR COMBINED PRESSURE AND THERMAL-SHOCK LOADINGS ARE SIMILAR TO PWR VESSEL RESULTS

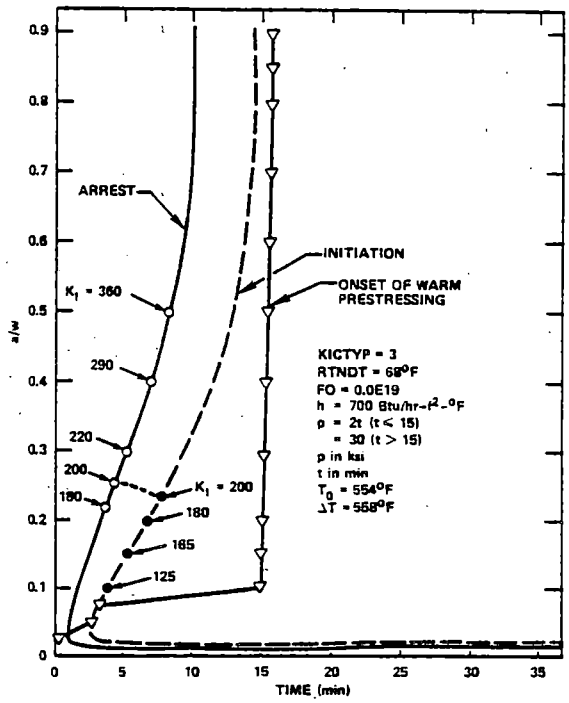

EXPERIMENTS CAN BE PERFORMED TO MEET THE OBJECTIVES OF DETERMINING

- SHORT FLAW GROWTH PATTERNS
- CRACK ARREST BEHAVIOR
- STAINLESS STEEL CLADDING EFFECTS
- DEMONSTRATION OF SUBCRITICAL FLAW SIZES AND CONFIGURATIONS
- VALIDATION OF ANALYTICAL METHODS

RANDY K. NANSTAD

WALTER J. STELZMAN

PRESSURE VESSEL TECHNOLOGY GROUP

METALS AND CERAMICS DIVISION

OAK RIDGE NATIONAL LABORATORY

FRACTURE TOUGHNESS TESTS FOR THERMAL SHOCK EXPERIMENTS DEMONSTRATE NEED FOR LOWER BOUND PREDICTIONS IN TRANSITION REGION*

NINTH WATER REACTOR SAFETY RESEARCH

INFORMATION MEETING

GAITHERSBURG, MARYLAND

OCTOBER 29, 1981

---

*Research sponsored by the Office of Nuclear Regulatory Research, Nuclear Regulatory Commission, under Interagency Agreements DOE 40-551-75 and 40-552-75 with the Department of Energy under contract W-7405-eng-26 with the Union Carbide Corporation.

SUMMARY

The Heavy-Section Steel Technology (HSST) Program is investigating the behavior of light-water nuclear reactor pressure vessels under loss-of-coolant conditions. With the injection of relatively cold emergency-core-cooling water, the large temperature difference (~270 K) between coolant and vessel wall results in a severe thermal shock to the vessel wall, producing inner-surface stresses close to the initial yield strength of the material. If a flaw exists near the inner surface, the abnormally high stress and the relatively low toughness of the material, because of the low temperature and radiation embrittlement, could result in initiation and propagation of the flaw deep into the wall. Since radiation embrittlement increases with increasing copper content, this situation is of particular interest with some of the early pressurized water reactor (PWR) pressure vessels because they contain relatively high copper in welds and/or base material. As part of the thermal shock pressure vessel testing project, a material characterization program provides the fracture toughness information necessary for design of the vessel test conditions.

Thermal shock experiment 5 (TSE-5) resulted in three initiation-arrest events as predicted but the final crack depth indicated a material toughness substantially less than laboratory specimen results had indicated. Additional tests indicated a large scatter in the data not previously obtained. Furthermore, the results indicated that the lower-bound toughness is the material property that governs flaw behavior in the temperature transition region. From an experimental point of view, the number of specimens needed to adequately define the lower-bound toughness is excessive.

A number of laboratory tests were conducted in an attempt to reduce the scatter and allow for a reliable prediction of the lower-bound toughness. Tests that have been conducted include (1) larger compact specimens, (2) side-grooved compact specimens, (3) dynamic precracked Charpy specimens, (4) spring loading in series with the load train of the test machine, and (5) crack arrest specimens. Additionally, an initial statistical examination has been performed. Results of the testing and analyses to date have not provided a test method or an analysis method for prediction of lower-bound fracture toughness in the transition region. The program is continuing and current activities are emphasizing statistical analyses as well as correlative testing with small specimens.

HEAVY-SECTION STEEL TECHNOLOGY PROGRAM
THERMAL SHOCK EXPERIMENTS EVALUATE INTEGRITY OF LWR PRESSURE VESSELS UNDER LOSS-OF-COOLANT CONDITIONS

1. Inside vessel surface:
   - High radiation damage $\rightarrow$ low K_{Ic}
   - Cold H_2O $\rightarrow$ high σ_{th} $\rightarrow$ high K
   - $K > K_{Ic}$: crack initiation

2. Short crack resides in a region of highest thermal stress and lowest toughness.

3. Thermal shock experiments with vessel evaluate material behavior, analytical techniques, correlation of laboratory specimens, and component.

MATERIALS STUDY TO PROVIDE DESIGN INFORMATION FOR THERMAL SHOCK TEST AND POST-TEST EVALUATION

1. Tempering study conducted to vary strength and toughness to produce material with proper response to test conditions.

2. Tensile and fracture toughness properties evaluated pre- and post-test using tensile, Charpy, compact, and drop-weight NDT specimens.

3. Fractographic analyses of specimens and vessel to analyze behavior.

TSC-2 PROLONGATION DOES NOT SATISFY SA-508, CLASS 2

BECAUSE OF ROOM TEMPERATURE ULTIMATE STRENGTH

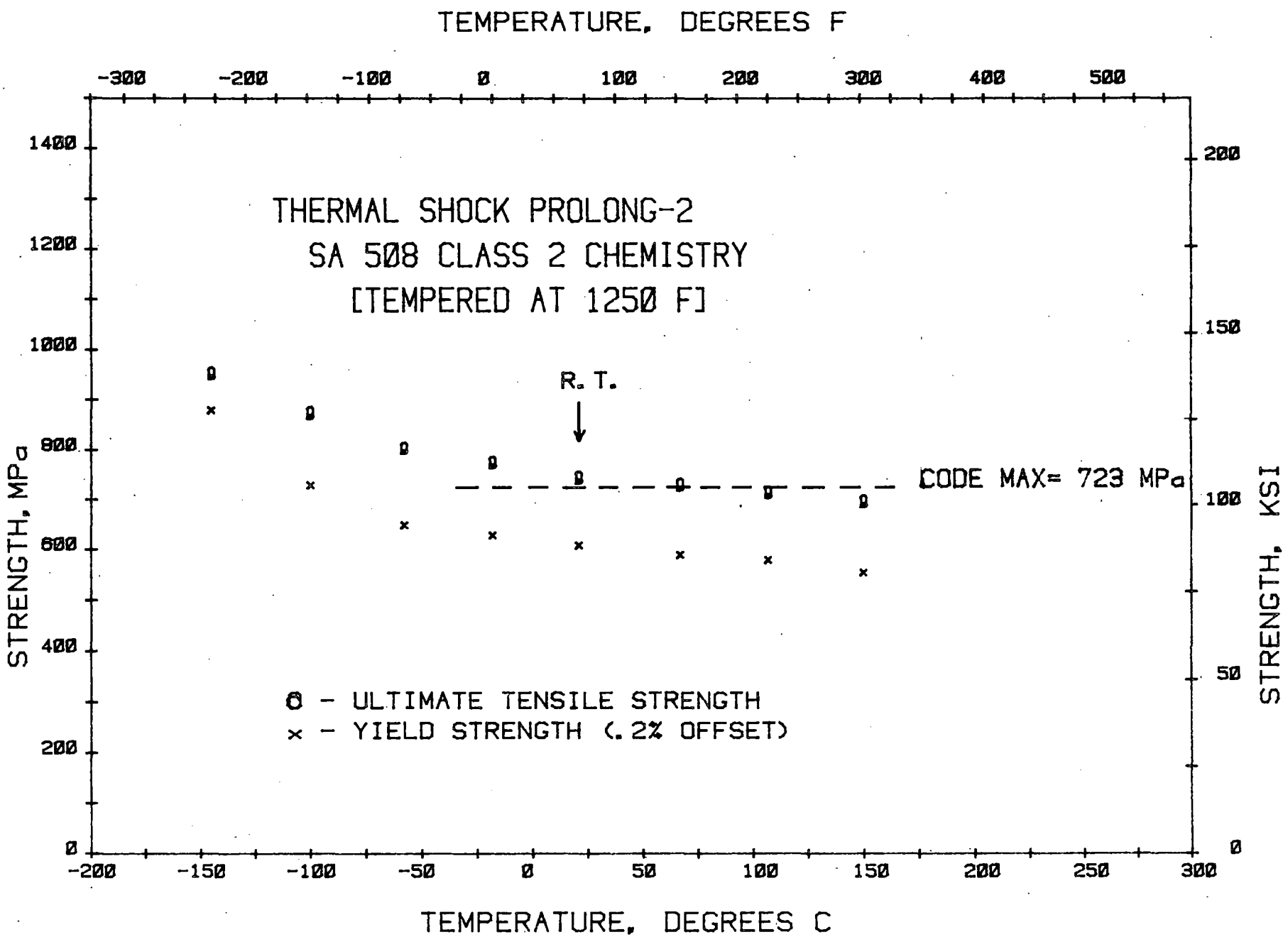

TSC-2 PROLONGATION EXHIBITS AT LEAST 68 j (50 FT/LBS)

AT NDT (10°C)

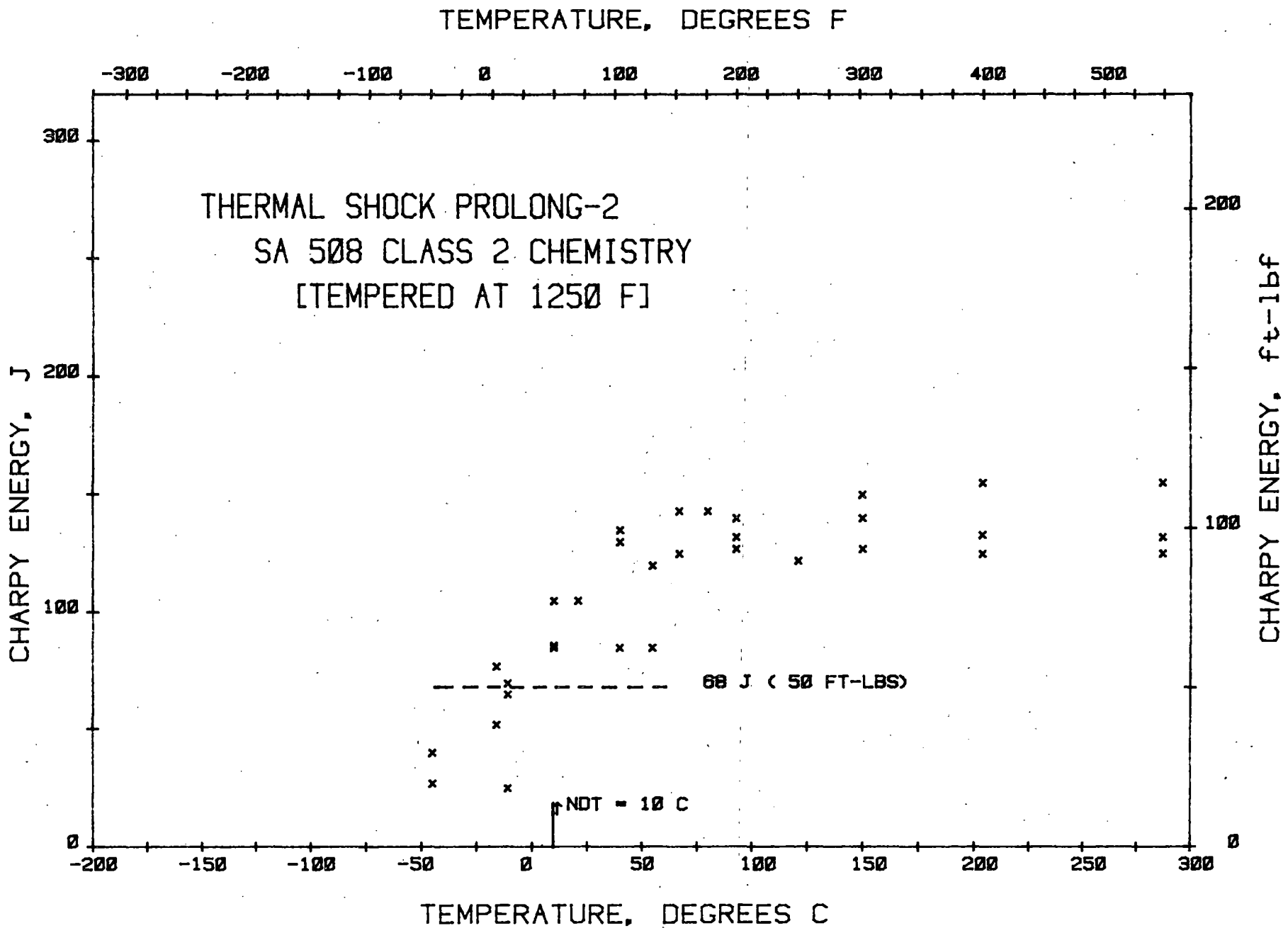

THERMAL SHOCK EXPERIMENT 5 (TSE-5) EXHIBITED CRACK INITIATION AT STRESS INTENSITIES MUCH BELOW LABORATORY PREDICTIONS

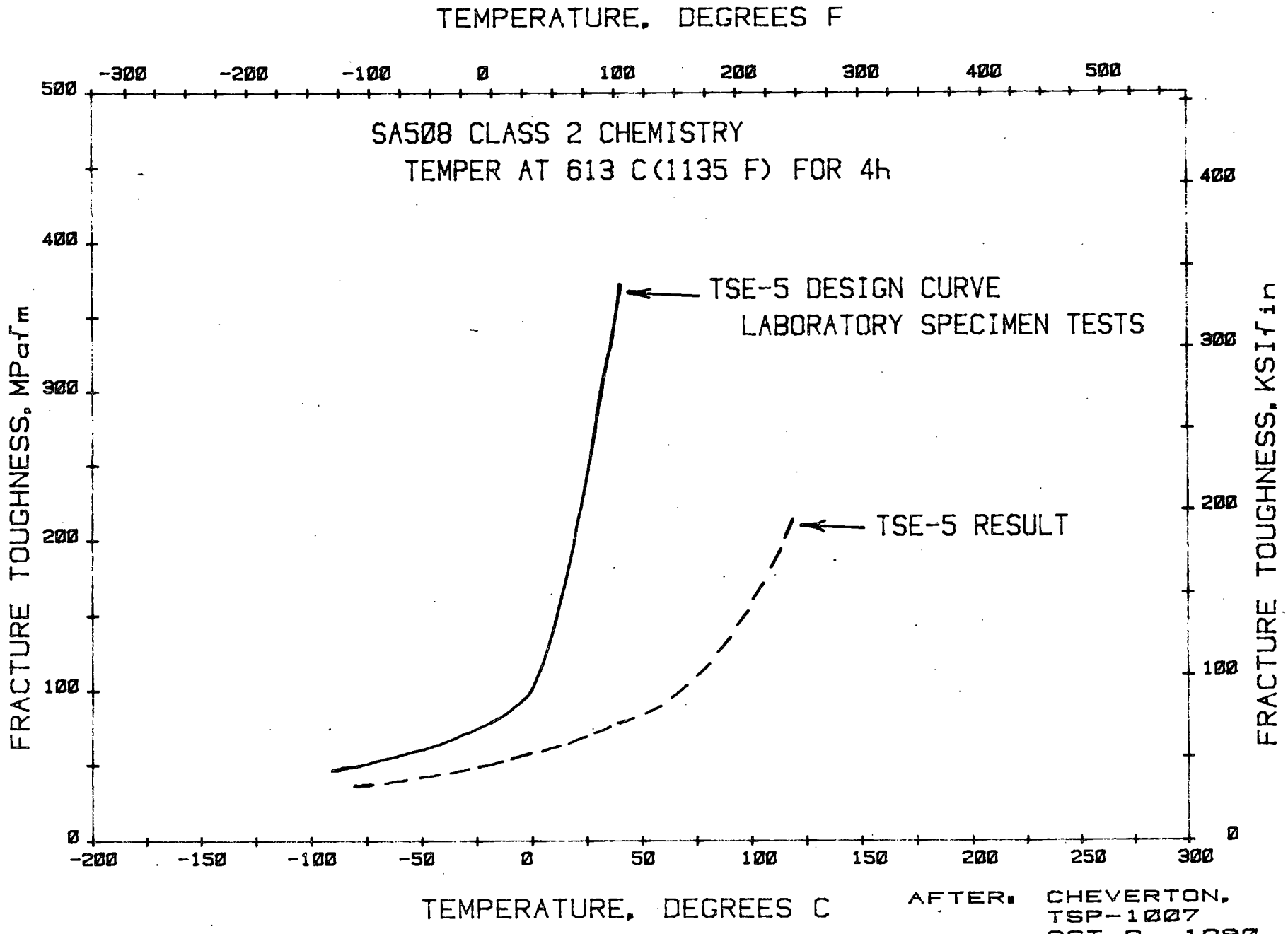

AFTER: CHEVERTON, TSP-1007 OCT 9, 1980

VERIFICATION TESTING WITH ADDITIONAL SPECIMENS RESULTED IN

LARGE SCATTER AND SUBSTANTIAL DECREASE

IN LOWER BOUND CURVE

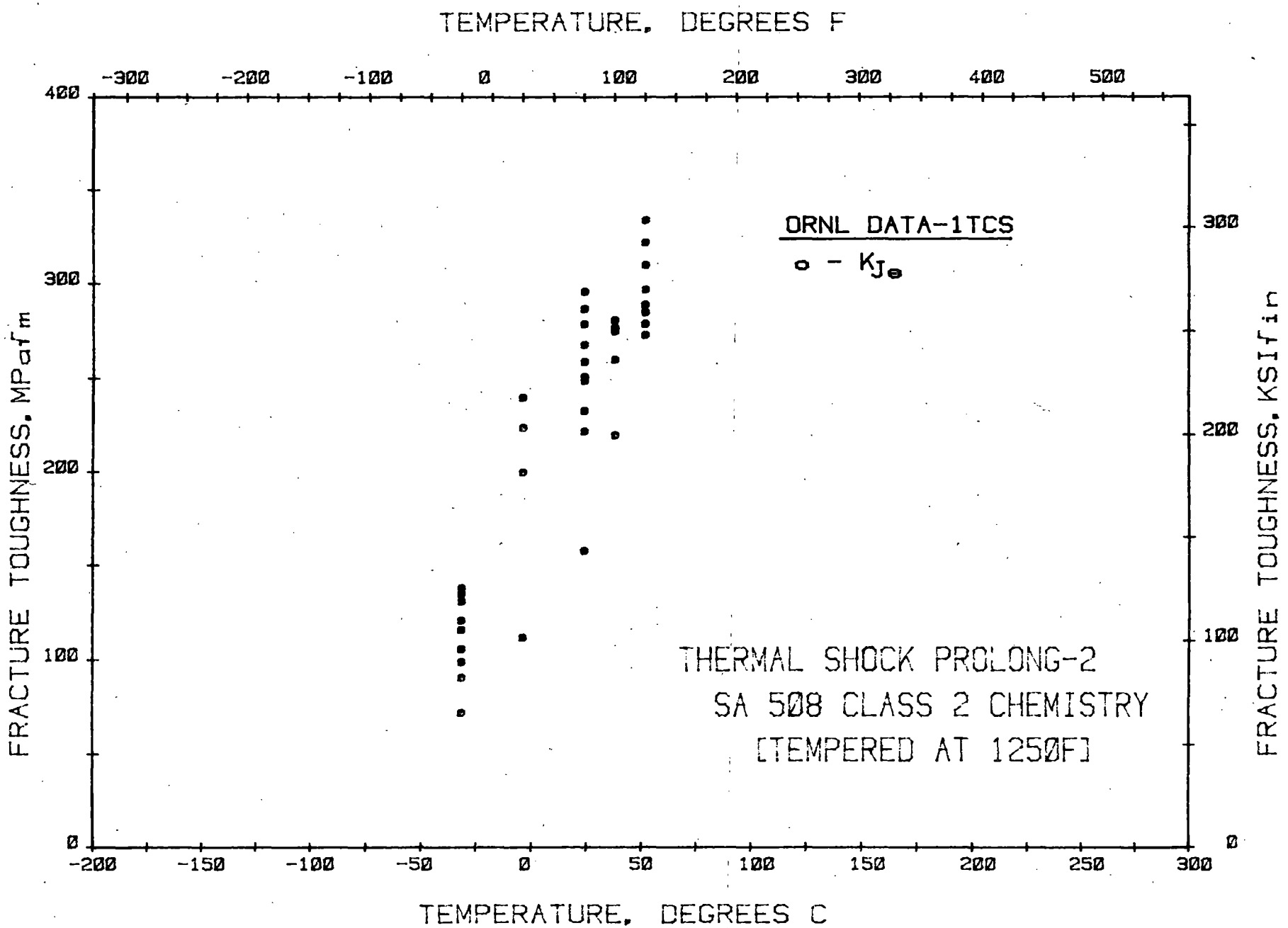

VARIOUS TEST TECHNIQUES WERE EXAMINED FOR REDUCING SCATTER AND DEFINING LOWER BOUND

1. Prolongation and vessel material compared.
2. Larger specimens (2T compact specimens).
3. Side-grooving of 1T compact specimens.
4. Spring-loading in series with test machine.
5. Dynamic precracked Charpy specimens.
6. Crack arrest tests for comparison.

TESTING ITCS WITH SIDE GROOVES DOES NOT SUBSTANTIALLY REDUCE SCATTER

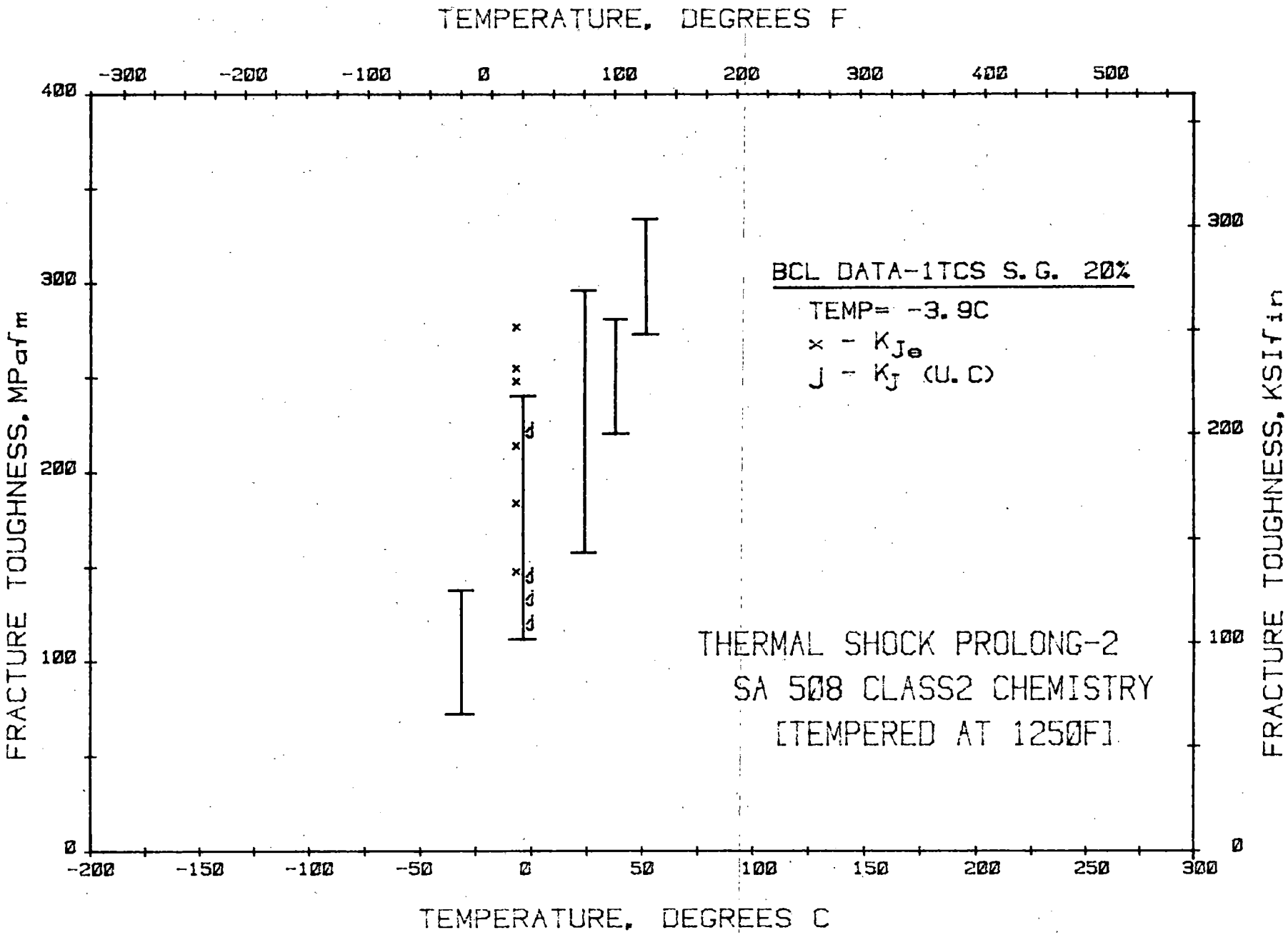

TESTING WITH A SPRING IN SERIES DOES NOT

SUBSTANTIALLY REDUCE SCATTER

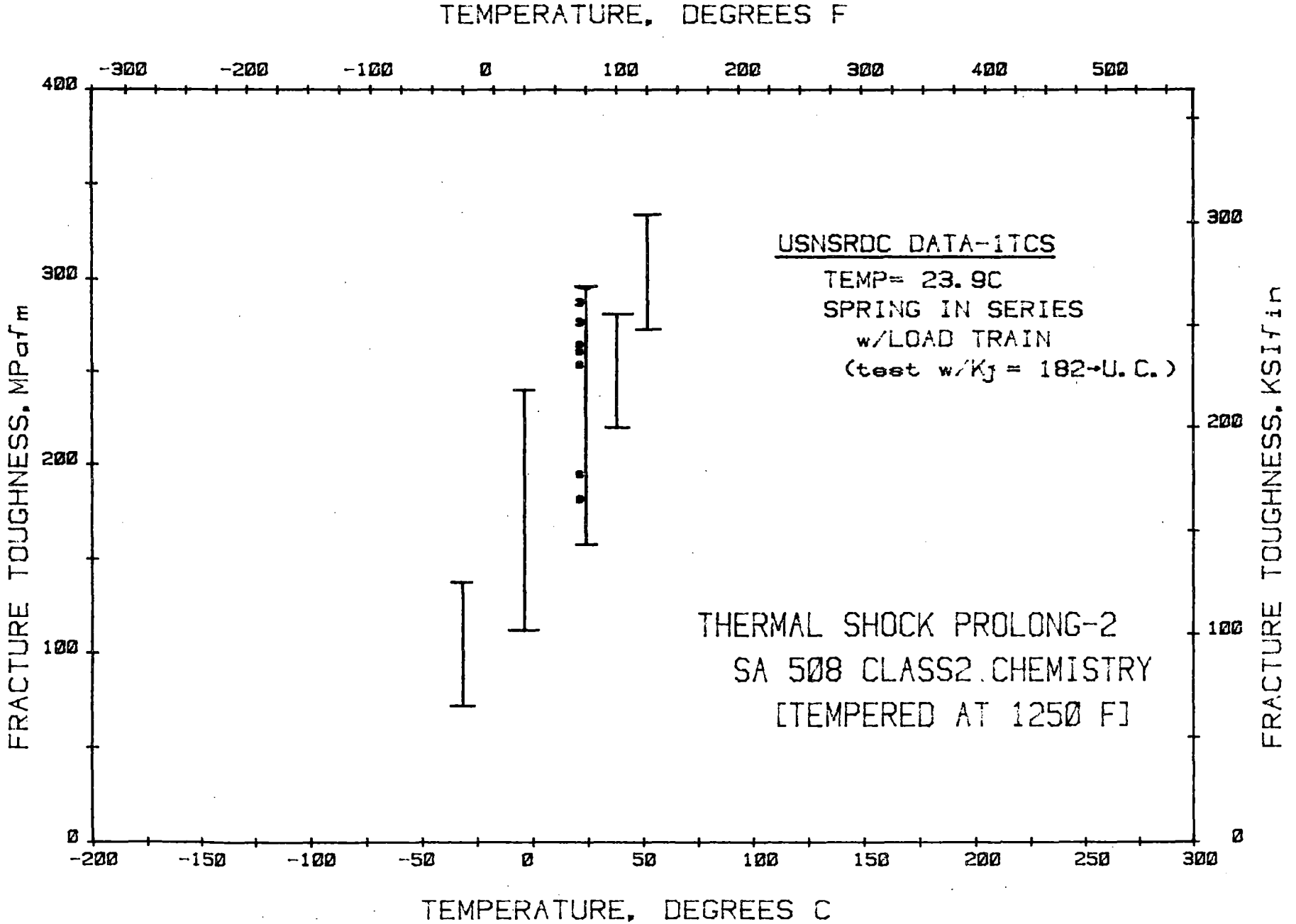

MULTIPLE TESTING WITH DYNAMICALLY LOADED PRE-CRACKED CHARPY SPECIMENS SUBSTANTIALLY INCREASES SCATTER AND SUBSTANTIALLY DECREASES LOWER BOUND

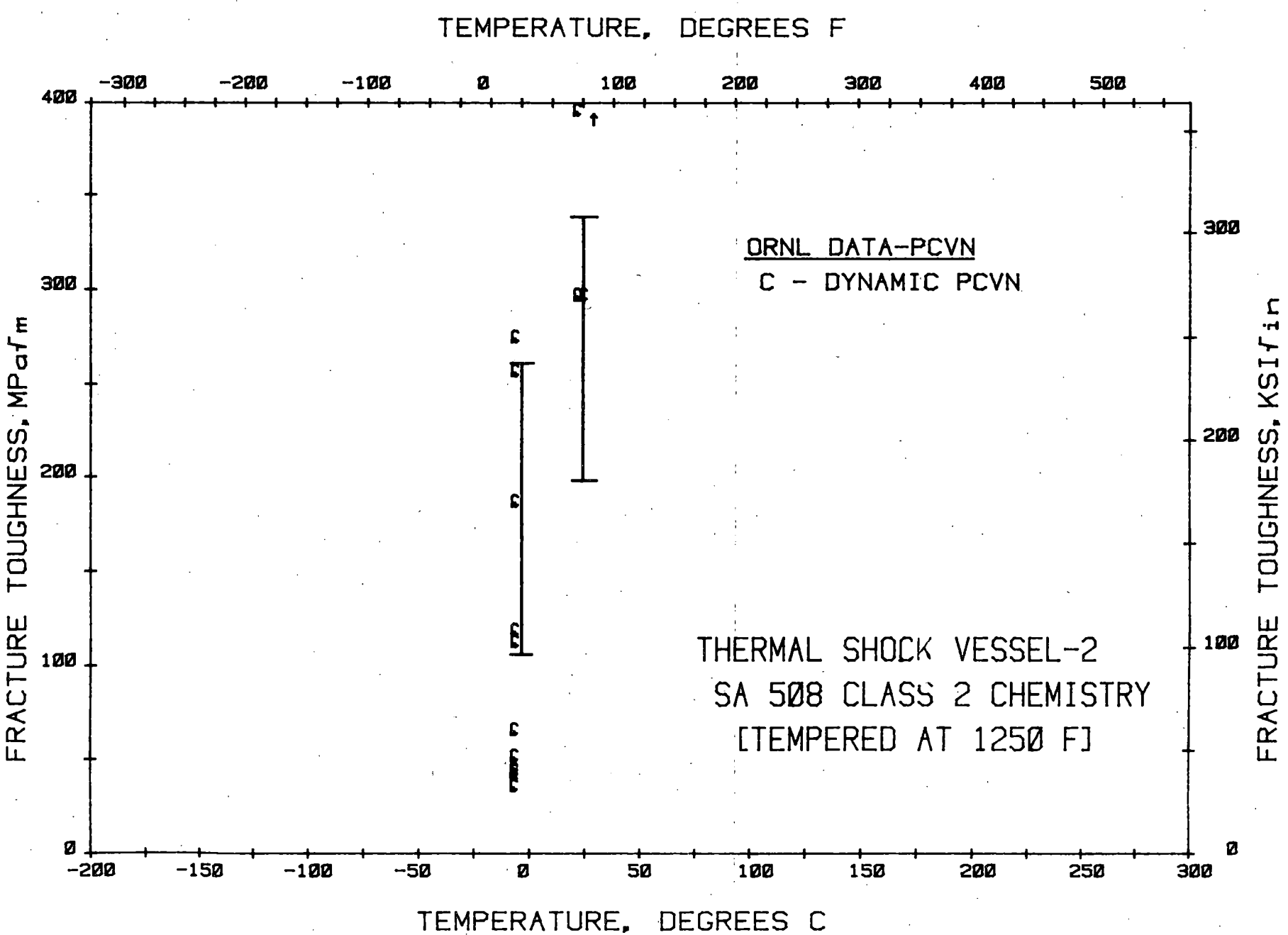

CRACK-ARREST TESTS EXHIBIT TOUGHNESS VALUES BELOW

THE INITIATION TOUGHNESS LOWER BOUND

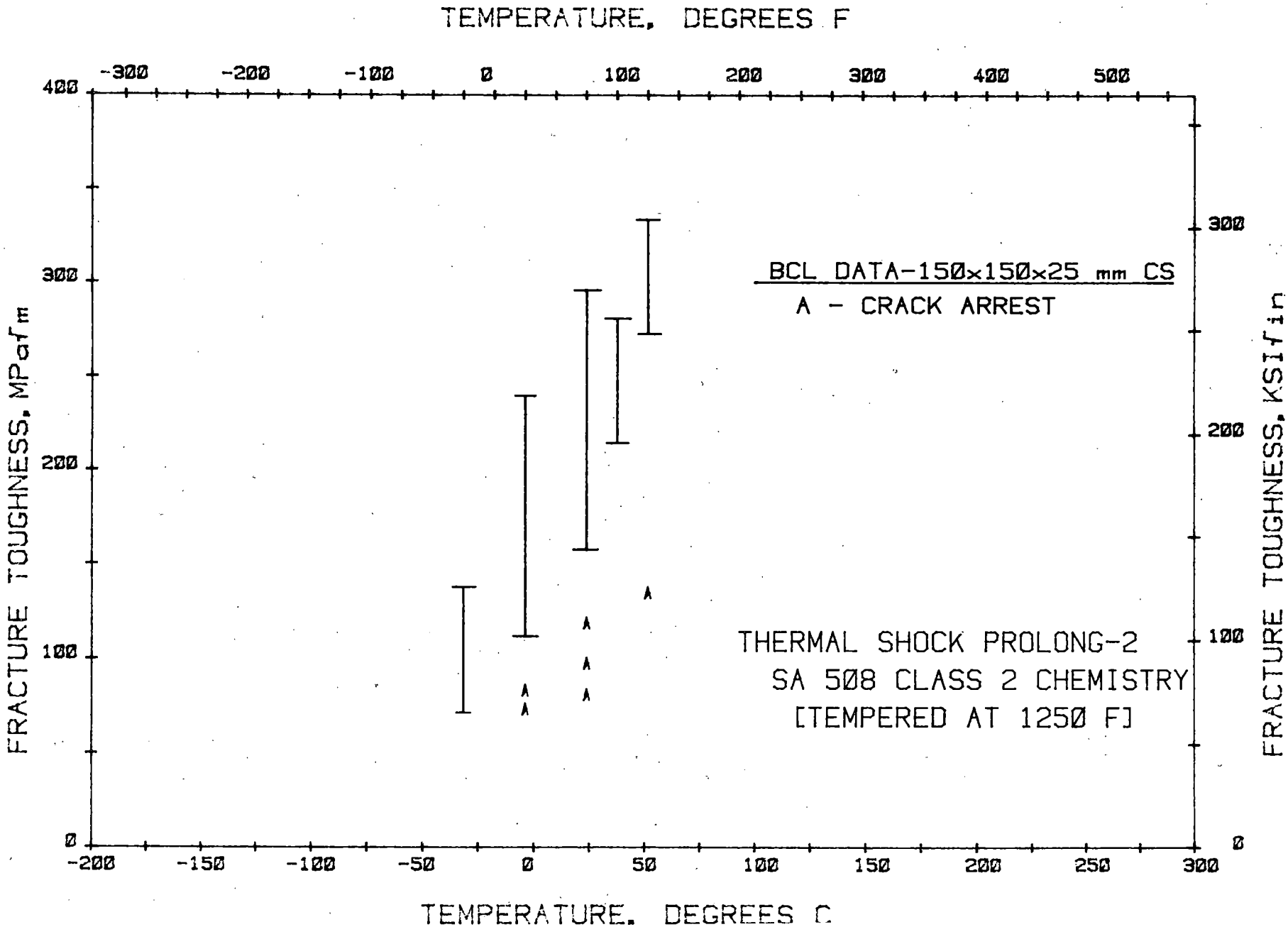

CRACK INITIATION AND ARREST EVENTS IN TSE-5A OCCURRED BELOW SPECIMEN LOWER BOUND PREDICTIONS

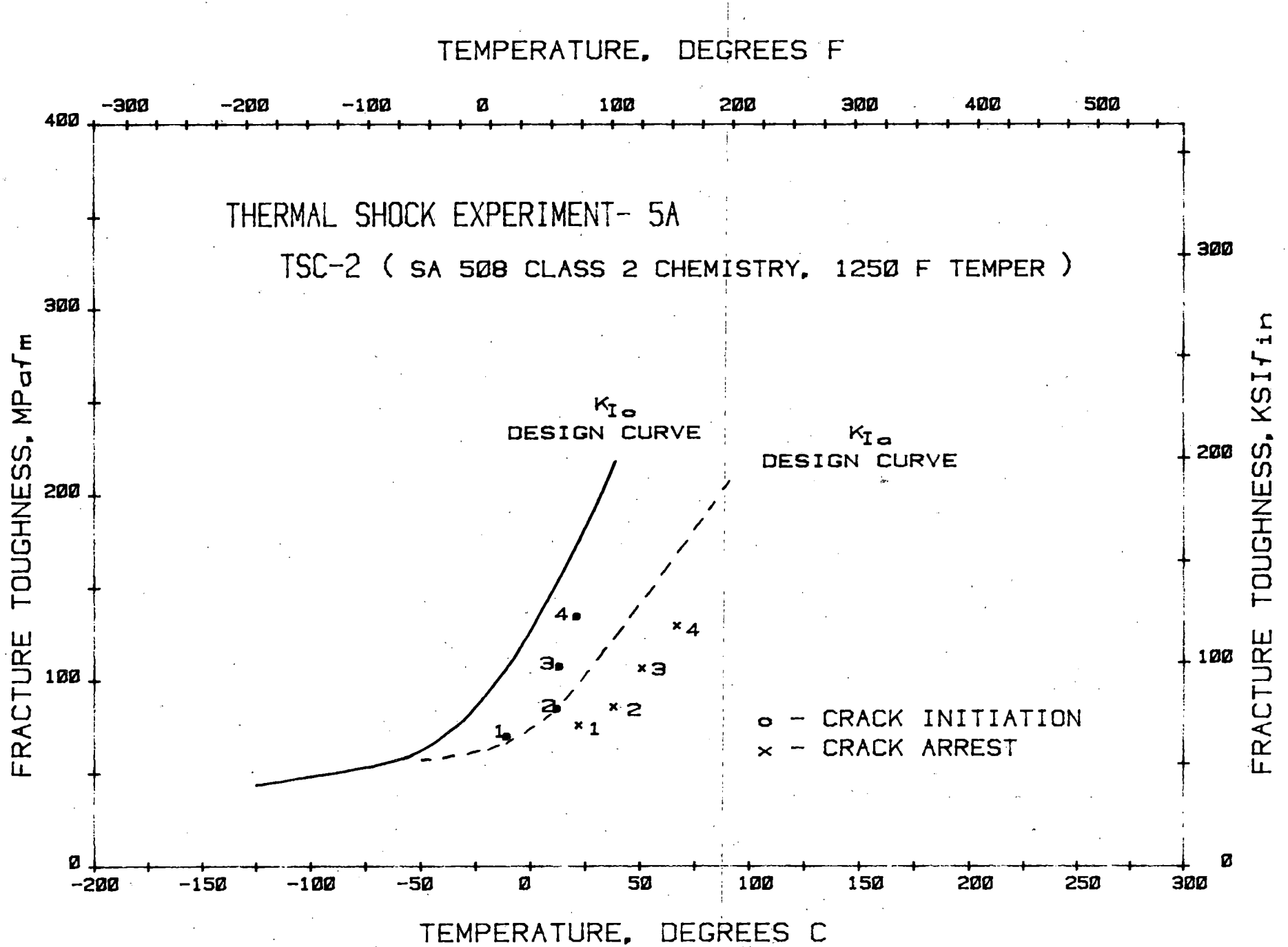

TRANSITION REGION TOUGHNESS TESTS SHOW LARGE VARIATION IN J AND CRACK EXTENSION MEASURED AT FAILURE

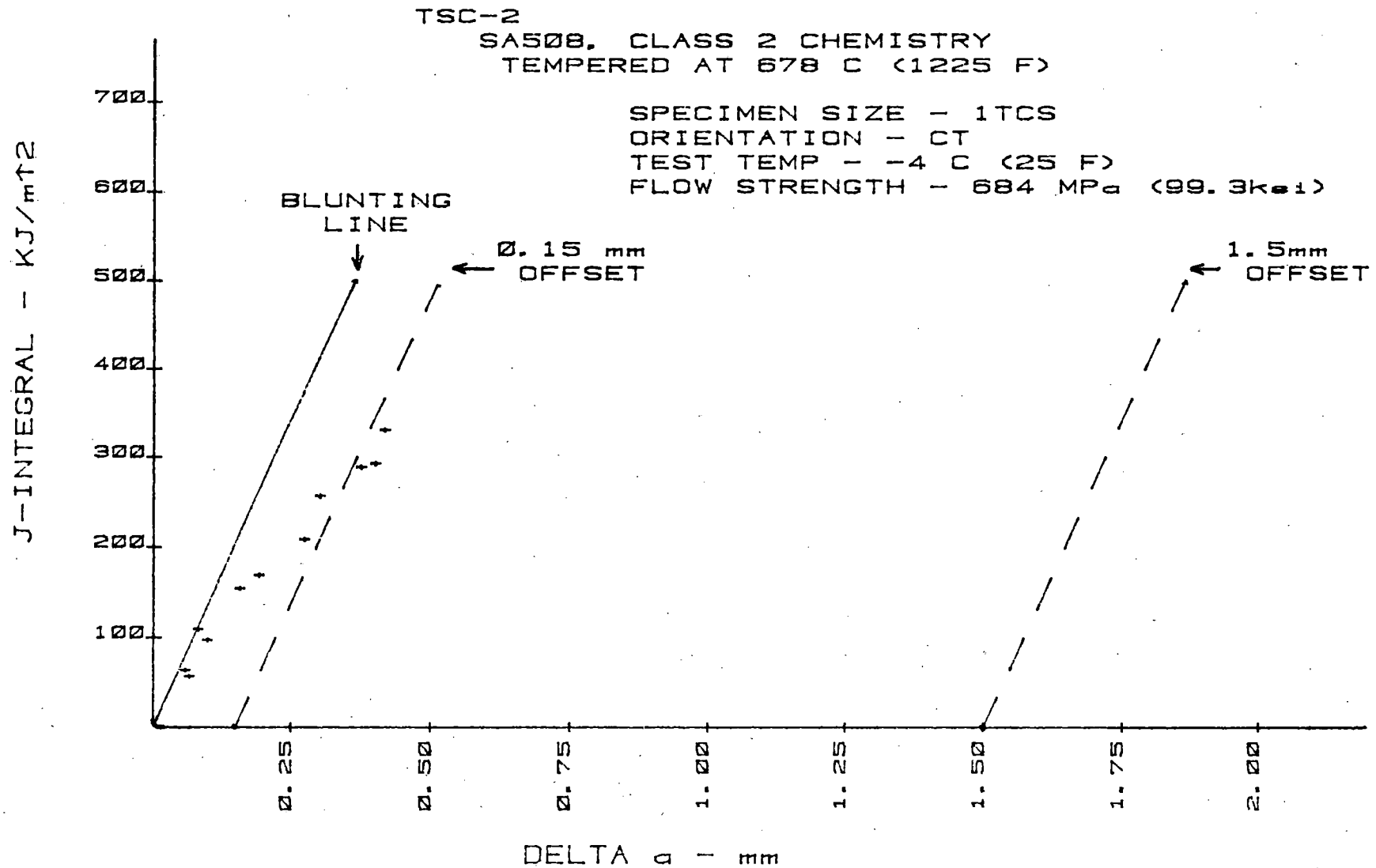

STATISTICAL ANALYSES HAVE BEEN APPLIED WITH SMALL AND LARGE SPECIMEN TOUGHNESS INFORMATION

1. Landes and Shaffer applied Weibull analysis to demonstrate statistical nature of variation (low toughness sites).

2. Iwadate et al. statistically analyzed over 300 specimens to develop experimental method for lower-bound prediction.

3. Ohtsuka using dimensional analysis techniques and J_{in} ($\Delta a \ll 0.5$ mm) for lower-bound prediction.

4. Seidl available energy model uses elastic energy at mode conversion.

5. Many statistical techniques to consider ($C_V \rightarrow K_{Ic}$).

IWADATE ET AL. OBSERVED LARGE SCATTER WITH SMALL SPECIMENS RELATIVE TO LARGER (4T) SPECIMENS

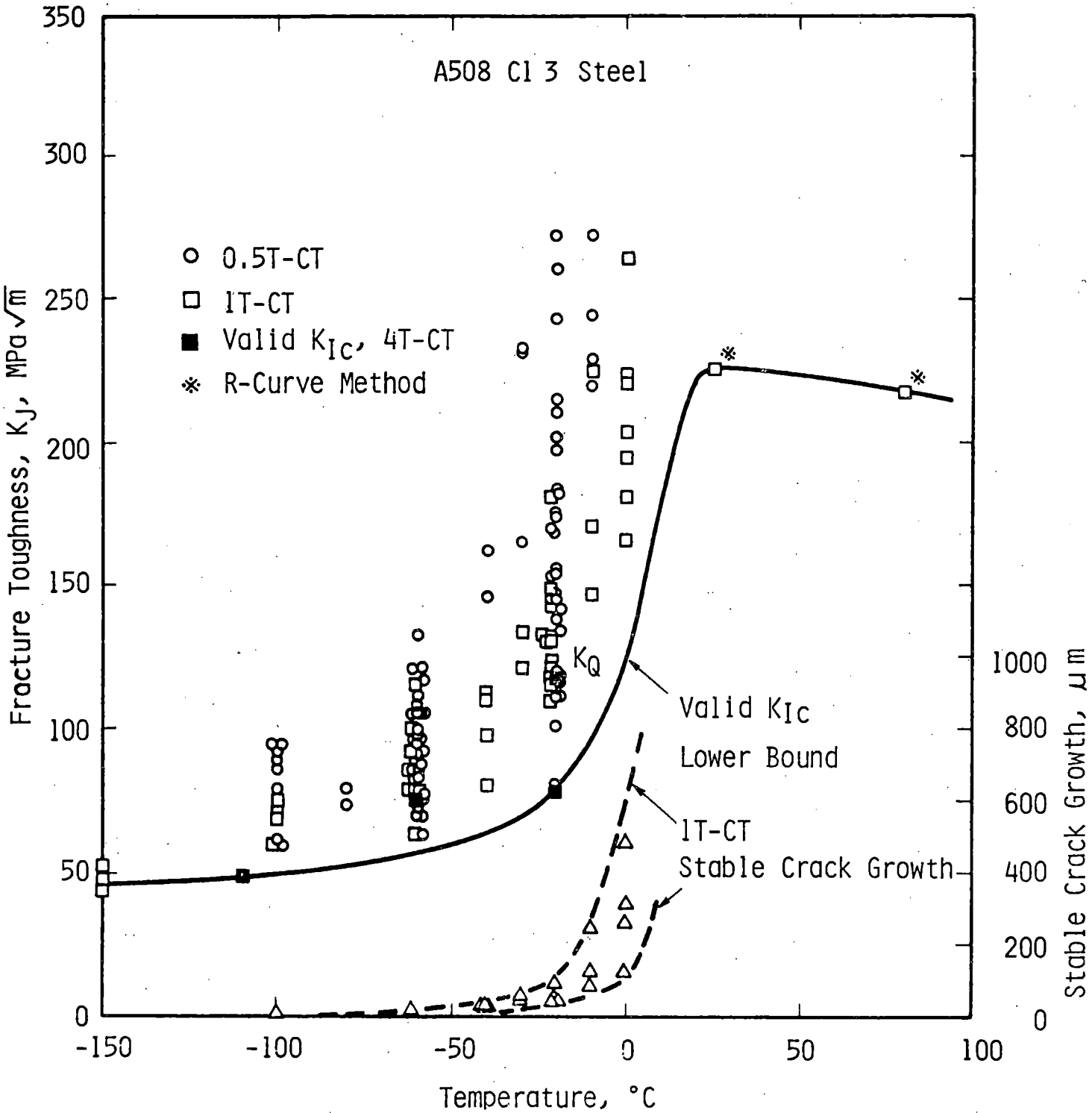

After: T. Iwadate et al., Second International Symposium on EPFM, Philadelphia, October 1981.

IWADATE ET AL. PERFORMED STATISTICAL ANALYSIS (>7300 SPECIMENS), DEVELOPED PROCEDURES FOR LOWER-BOUND PREDICTIONS IN TRANSITION REGION

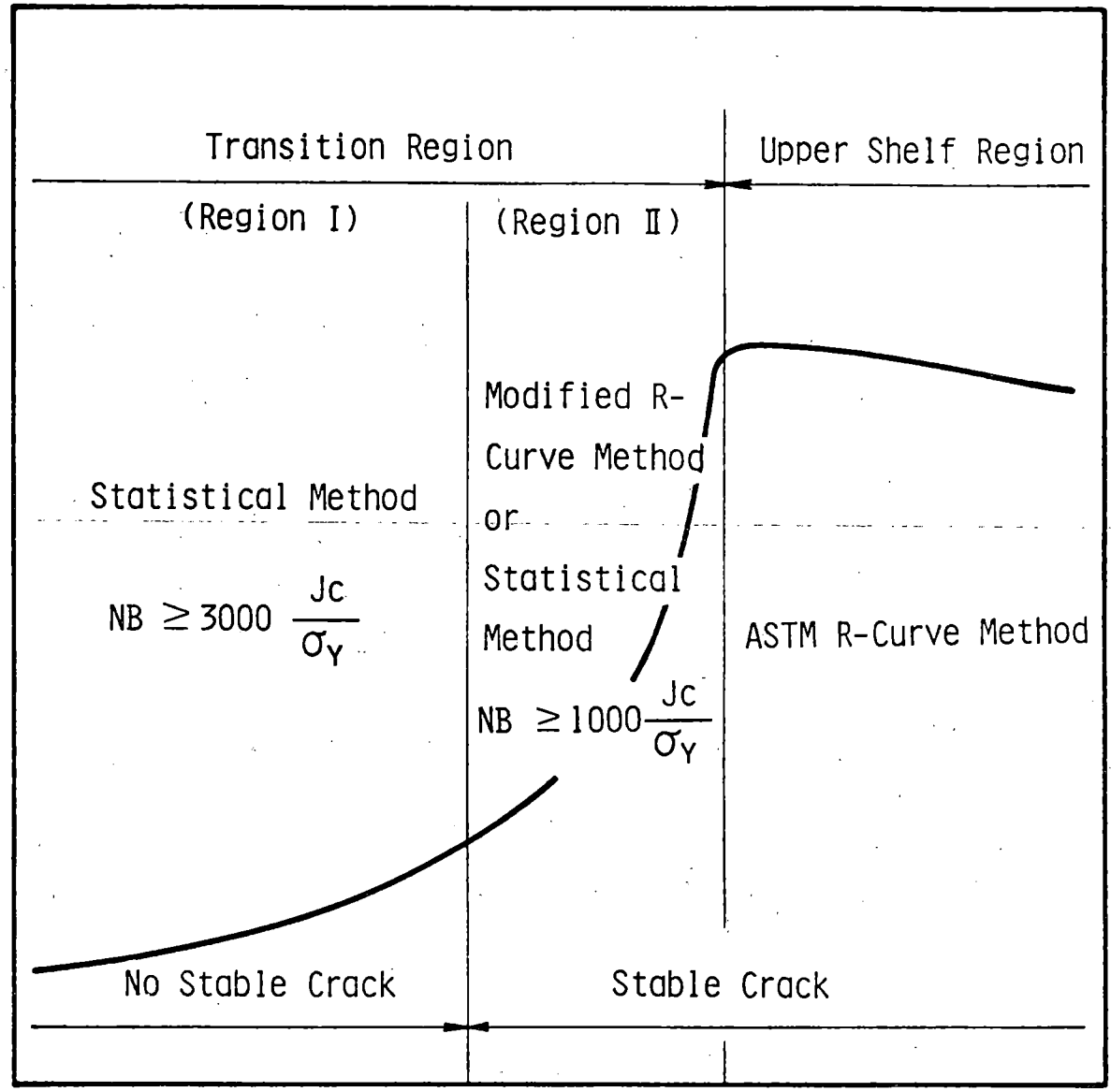

After: T. Iwadate et al., Second International Symposium on EPFM, Philadelphia, October 1981.

TSC-2 PROLONGATION AND VESSEL EXHIBIT SIMILAR CHARPY TOUGHNESS AND SCATTER

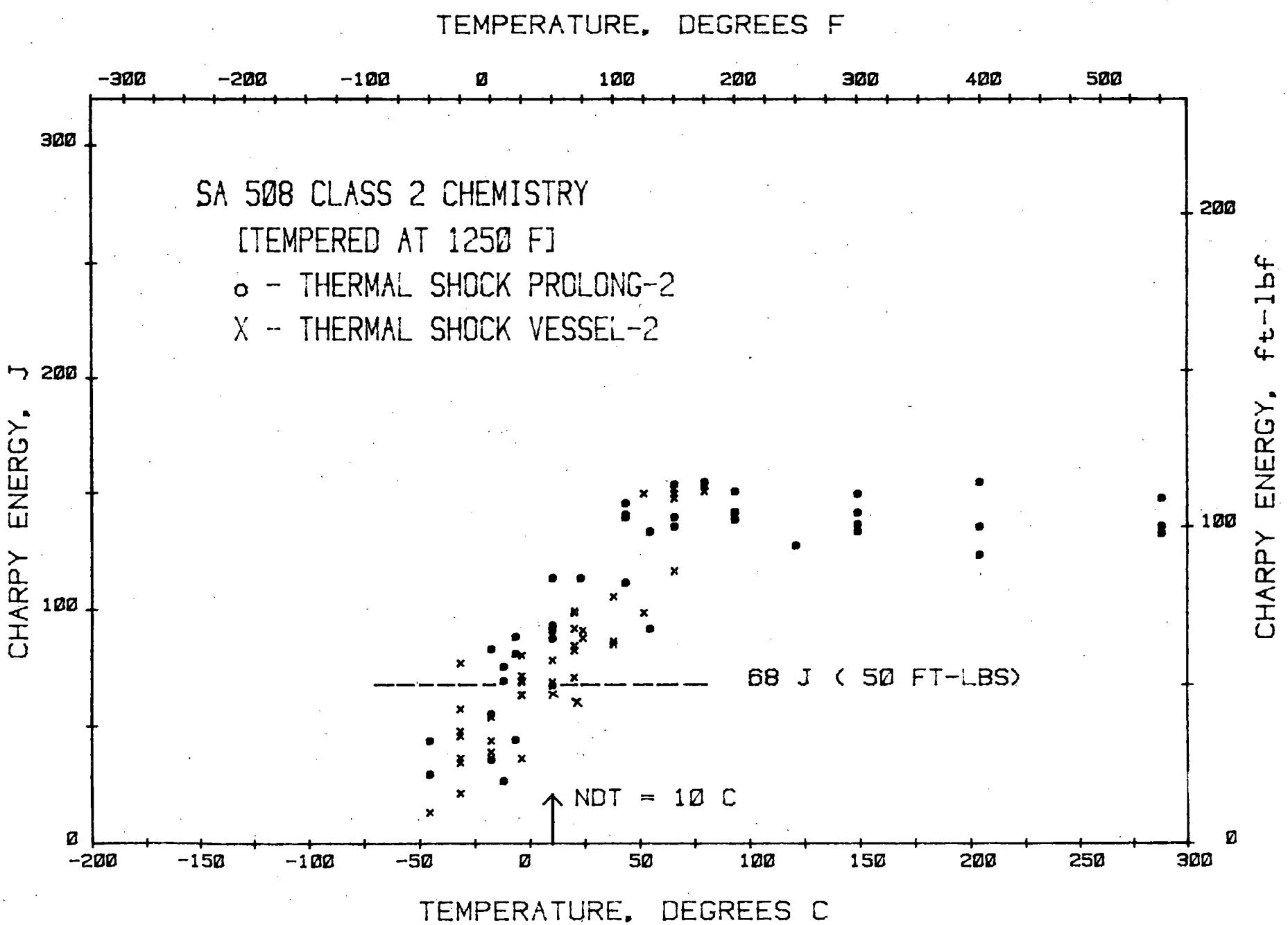

FRACTURE TOUGHNESS TESTS FOR THERMAL SHOCK EXPERIMENTS DEMONSTRATE NEED FOR LOWER-BOUND PREDICTIONS IN TRANSITION REGION

1. Crack initiation events in TSE-5A occurred below lower bound of laboratory specimen data (10 per temperature).

2. Multiple 1T compact specimens were required to define lower-bound behavior.

3. 2T compact specimens did not appear to reduce scatter or lower bound.

4. Side-grooving of 1T CS did not reduce scatter or lower bound.

5. Spring-loading in series did not reduce scatter or lower bound.

6. Dynamic precracked Charpy did not reduce scatter but reduced lower bound below that of vessel initiation.

7. Crack arrest specimens appear to better define lower bound for arrest with less specimens.

8. Charpy impact data show scatter in transition region similar to compact specimen data.

9. Statistical analyses and extrapolation techniques have had minimal success to date in predicting lower bound with a low number of specimens.

LOW DUCTILE SHELF INTERMEDIATE VESSEL TEST V-8A

R. H. Bryan
Oak Ridge National Laboratory

NINTH WATER REACTOR SAFETY RESEARCH
INFORMATION MEETING

National Bureau of Standards
Gaithersburg, Maryland

October 26-30, 1981

LOW DUCTILE SHELF INTERMEDIATE VESSEL TEST V-8A*

R. H. Bryan
Oak Ridge National Laboratory
Oak Ridge, Tennessee 37830

The tests of six 152-mm-thick HSST intermediate test vessels with part-circular surface flaws demonstrated the useful application of linear-elastic fracture mechanics (LEFM) to the analysis of flawed vessels for cases in which fracture toughness is low enough that fast fracture precedes the onset of gross yielding in the structure. However, in tests conducted at high-transition and upper-shelf temperatures, for which toughness is high, tearing and local plastic instability are important mechanisms associated with failure.

Attempts to apply elastic-plastic fracture mechanics (EPFM) methods to the latter types of tests were complicated by extensive yielding and vessel deformations that preceded failure. Further, in the early tests, the means of detecting and measuring stable tearing in a flawed vessel had not been developed. Even so, these tests, which were conducted at 54°C or above, clearly showed that a deeply flawed vessel could sustain through-the-thickness yielding without failing.

All of the intermediate vessel tests involved materials with high-upper-shelf toughness typical of steels in reactor pressure vessels of current design, while some vessels in operating plants contain high-copper welds of lower toughness and greater sensitivity to neutron embrittlement. After some period of operation, the toughness of these welds is expected to be degraded to the extent that practical operating temperature limits may not be definable in accordance with present regulatory guidelines, which essentially would not allow operation of a vessel with a Charpy impact energy upper shelf of less than 68 J. However, no one has actually demonstrated that a vessel with such a low toughness does not have adequate resistance to tearing.

---

* Research sponsored by the Office of Nuclear Regulatory Research, U.S. Nuclear Regulatory Commission under Interagency Agreements 40-551-75 and 40-552-75 with the U.S. Department of Energy under contract W-7405-eng-26 with the Union Carbide Corporation.

Intermediate test vessel V-8 is being prepared for a test in which flaw behavior in low-upper-shelf material will be investigated at upper-shelf temperature. The test program is expected to reveal the modes of flaw growth and to test the capabilities of EPFM in predicting flaw behavior. In addition, the test will be a direct demonstration of the behavior of a flaw in a thick vessel under conditions that may be typical of some future reactor vessel accident conditions.

The plan for the low-upper-shelf test (test V-8A) is to repair vessel V-8, place a longitudinal seam weld of low-upper-shelf toughness in the test section, place a flaw in the weld, and pressurize the vessel at an upper-shelf temperature.

Specifications for the repair and seam weld preparation were developed. The weld should have properties similar to those of irradiated high-copper weld specimens in the second HSST irradiation study. The upper-shelf impact energy should preferably be in the range 54 to 68 J and the yield strength 448 to 621 MPa. Since these values are not typical of welds being made today in pressure vessel steels, a special welding process was required.

The Babcock & Wilcox Company (B&W) developed an acceptable procedure for producing the special seam weld, as demonstrated by Charpy impact, tensile, and J-R curve tests of trial weld material. B&W also repaired vessel V-8 and placed the special seam weld by an automatic submerged arc process with a prolonged postweld heat treatment. In addition to this vessel weld, B&W made additional seam welds by the same process to provide stock for specimens to characterize the vessel, particularly with respect to Charpy impact and J-R curve behavior.

Vessel V-8A will have a fatigue sharpened flaw with a part-circular profile placed in the special seam weld. The size of the flaw will be selected on the basis of measured properties of the low upper shelf material with the objective of carrying out the pressurization program without attaining gross yield. The vessel will be heated to a temperature ($\sim$150°C) at which cleavage would not be expected and pressurized slowly while observations of flaw behavior are made. The onset of stable tearing, progressive stable tearing with increasing pressure, and tearing instability will be observed. Crack geometry will be observed by a variety of means, including crack-opening displacement measurements, ultrasonics, and post-test flaw measurements.

Preliminary estimates of flaw behavior have been made by means of Merkle's tangent modulus method of elastic-plastic analysis of flaws. Stable and unstable tearing are assumed to be controlled by J-R curves derived from trial weld data. Final pretest estimates will be made by means of three-dimensional finite element analysis and the ORVIRT-3D code, by which elastic-plastic behavior may be taken into account.

PURPOSES OF TEST V-8A

- To demonstrate the fracture behavior of low toughness material at upper shelf temperature.
- To compare elasto-plastic fracture mechanics predictions of stable and unstable tearing with full-scale test results.

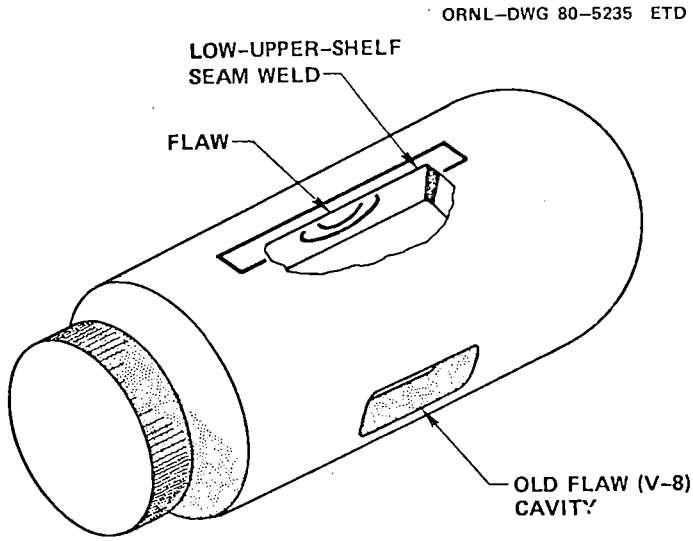

ITV-8A

ORNL–WS 8619 ETD

V-8A TEST CONDITIONS – FLAW AND MATERIALS

PROPERTIES OF FLAWED REGION

- UPPER SHELF CHARPY ENERGY LIKE IRRADIATED HIGH-COPPER WELDS

FLAW GEOMETRY

- PART-CIRCULAR OUTSIDE SURFACE FLAW $\sim <$ HALF THICKNESS DEEP
- SIZED TO INITIATE TEARING PRIOR TO YIELDING (IF PRACTICABLE)

TEST TEMPERATURE

- UPPER SHELF
- SELECTED TO PRECLUDE TEARING – CLEAVAGE MODE CONVERSION

ORNL–WS 8613 ETD

STEPS IN VESSEL PREPARATION BY B&W

- TRIAL WELDS
- SHOP DETAILS AND PROCEDURES
- FLAWING PRACTICE WELDMENT
- CHARACTERIZATION WELDS
- VESSEL WELDS

ORNL PHOTO 3397-81

WELD V8-42 CROSS SECTION (COURTESY B&W)

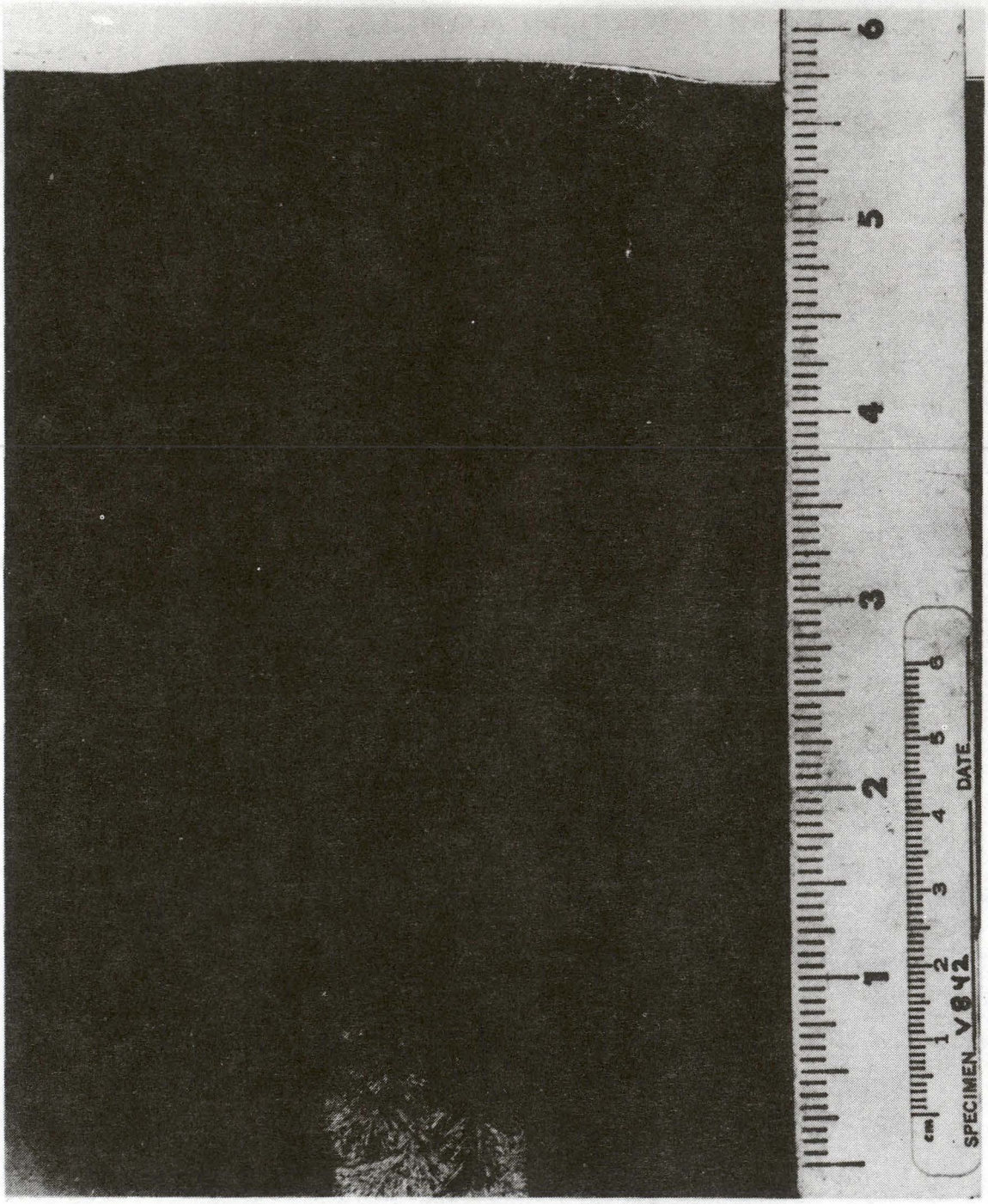

V-8A SPECIAL SEAM WELD PARAMETERS

ELECTRODE	1/8-in. diam SFA 5.23 EF-2 (MnMoNi, Cu-coated)
FLUX	75% Linde 60, 25% Linde 80
PWHT	
Range	566–593°C
Hold time	50 h

ORNL–DWG 81–8210 ETD

SPECIMEN ORIENTATION

CHARPY (C) SPECIMENS
(WL ORIENTATION)

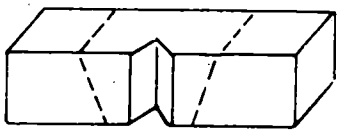

BEND (B) SPECIMENS
TRANSVERSE

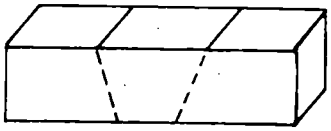

DROP (D) WEIGHT SPECIMENS
(WL ORIENTATION)

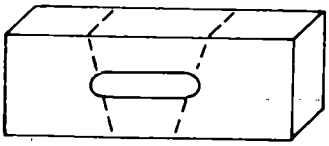

CHEM. ANAL. (A) & MACRO STRUCTURE (M)

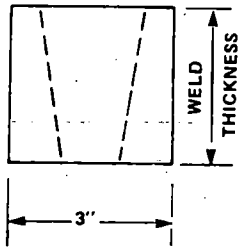

ALL WELD METAL TENSION (T)

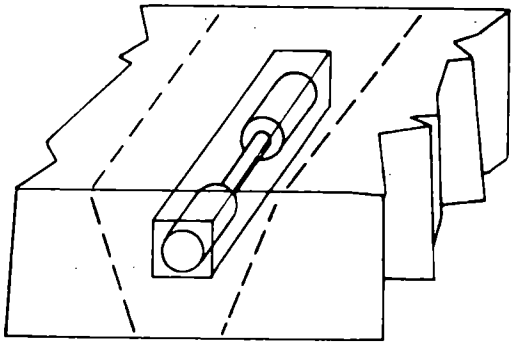

FRACTURE (F) TOUGHNESS OR
J-INTEGRAL (J)
(WL ORIENTATION)

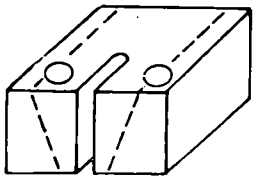

FRACTURE (W) TOUGHNESS
(WT ORIENTATION)

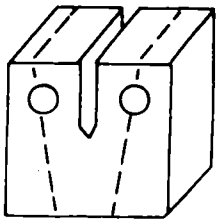

ORNL–DWG 81–8211 ETD

SIDE VIEW WELD V842 CUTTING DIAGRAM

A – CHEMICAL ANALYSIS
B – BEND TEST
C – CHARPY TEST
D – DROP WEIGHT TEST
J – J-INTEGRAL TEST
M – MACRO STRUCTURE
S – SPARE MATERIAL
T – TENSION TEST

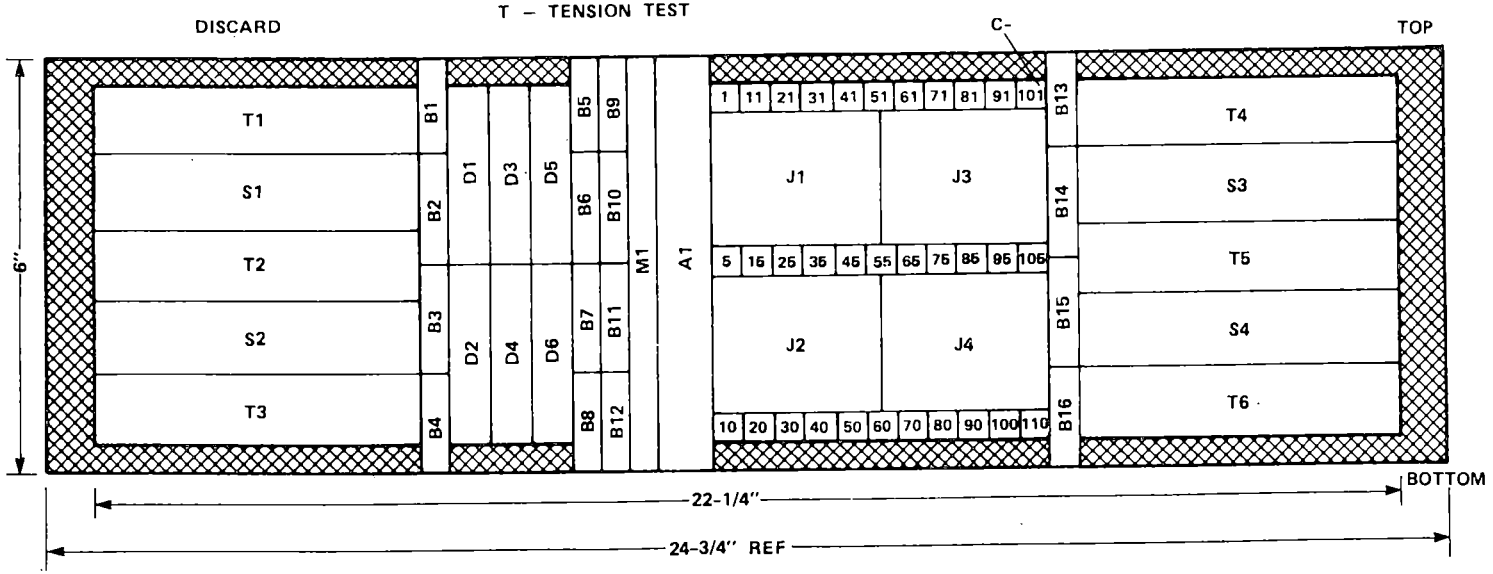

B&W TRIAL WELD (V8-42)

PROPERTY	SPECIFIED ACCEPTABLE VALUE	MEASURED VALUE
IMPACT ENERGY ON UPPER SHELF (J)		
RANGE	47 to 75	50.8 to 63.7
AVERAGE		56.9
YIELD STRENGTH AT RT (MPa)		
RANGE	448 to 621	456 to 466
AVERAGE		460

ORNL–DWG 81–8090A ETD

CHARPY IMPACT TEST RESULTS FOR TRIAL WELD V8–42

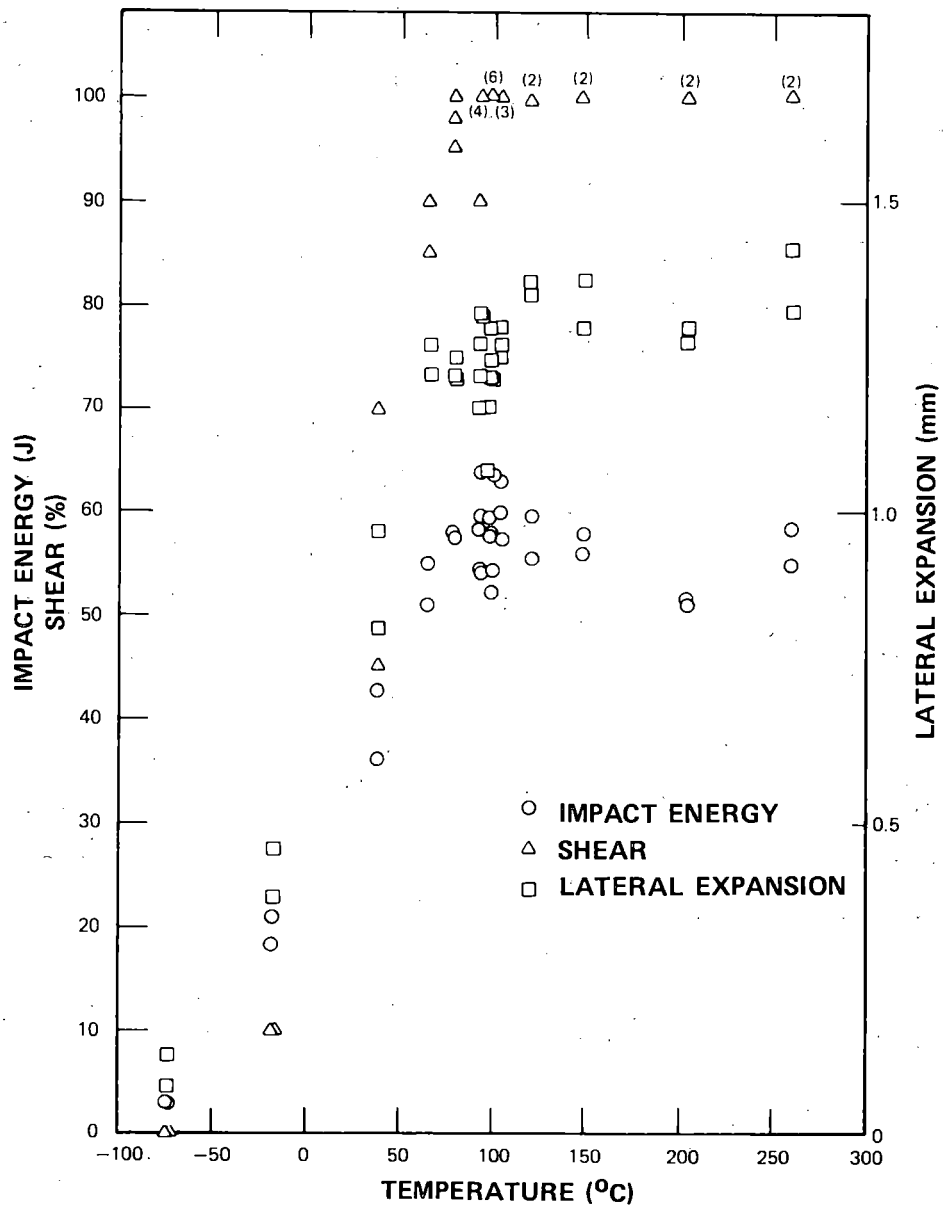

ORNL–DWG 81–8091A ETD

J–R DATA (ADJUSTED) FOR TRIAL WELD V8–42

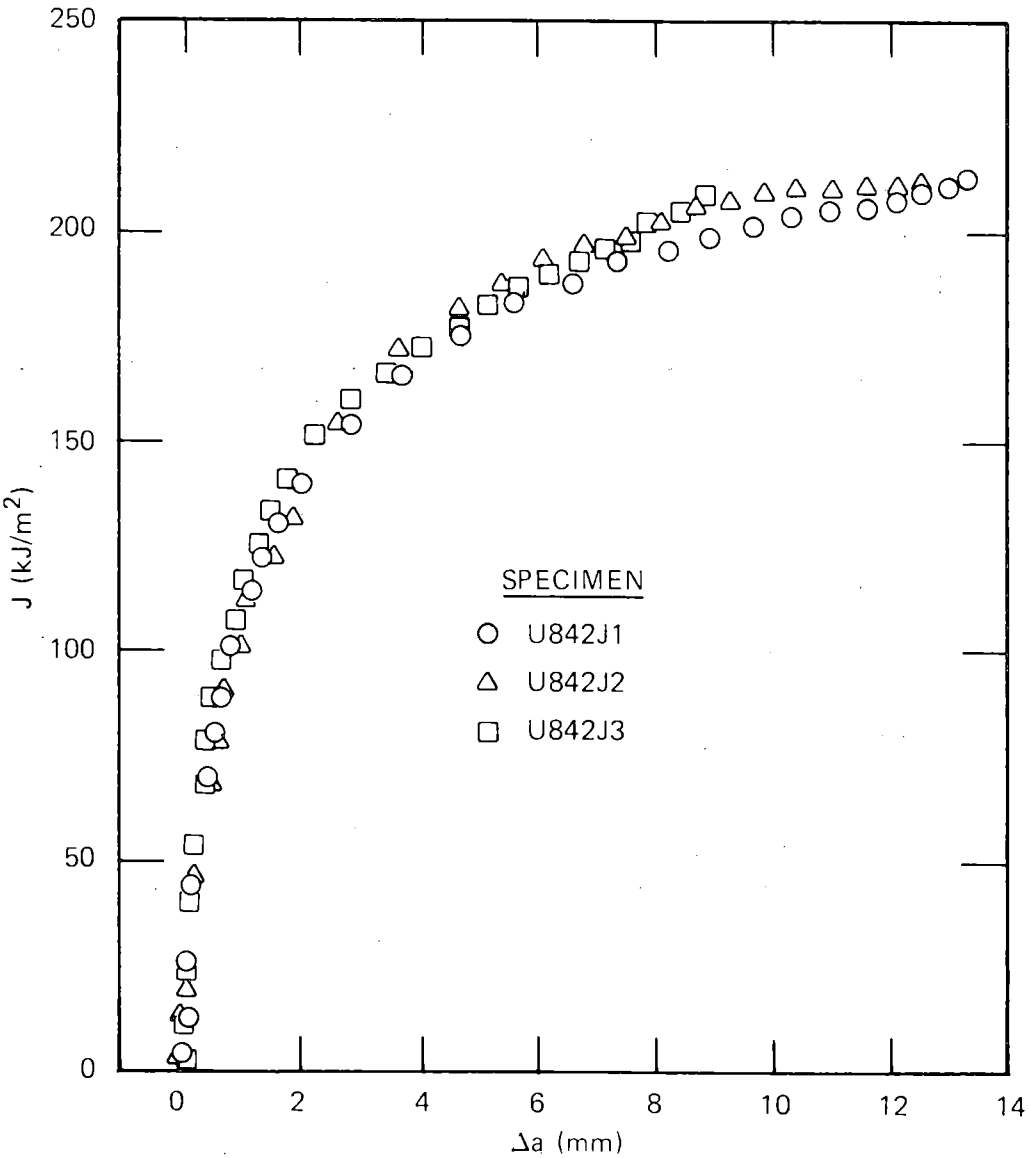

B&W TRIAL WELD (V8-42)[a]

SPECIMEN	TEST TEMPERATURE (°C)	J_{Ic} (kJ/m^2)
V842J1	121	65.6
V842J2	121	65.1
V842J3	116	70.5

[a]Corrected for Δa and rotation.

POWER LAW PARAMETERS FROM LEAST-SQUARES FIT OF J-Δa DATA FROM B&W WELD V8-42 WITH J CONSIDERED RANDOM VARIABLE ($J = C\ (\Delta a)^n$

SPECIMEN	Δa RANGE (mm)	n	C $kJ \cdot m^{-2}/(mm)^n$
J1	0.282–1.509[a]	0.3687	114.10
J2	0.278–1.713[a]	0.3692	109.83
J3	0.246–1.642[a]	0.3606	120.26
J1	0.282–13.193	0.2687	111.06
J2	0.278–12.380	0.2948	108.73
J3	0.246– 8.753	0.2824	115.95

[a]Exclusion range for J_{IC} determination.

ORNL–DWG 81–8092A ETD

COMPARISON OF J–R DATA FOR TRAIL WELD AND IRRADIATE HIGH–COPPER WELDS

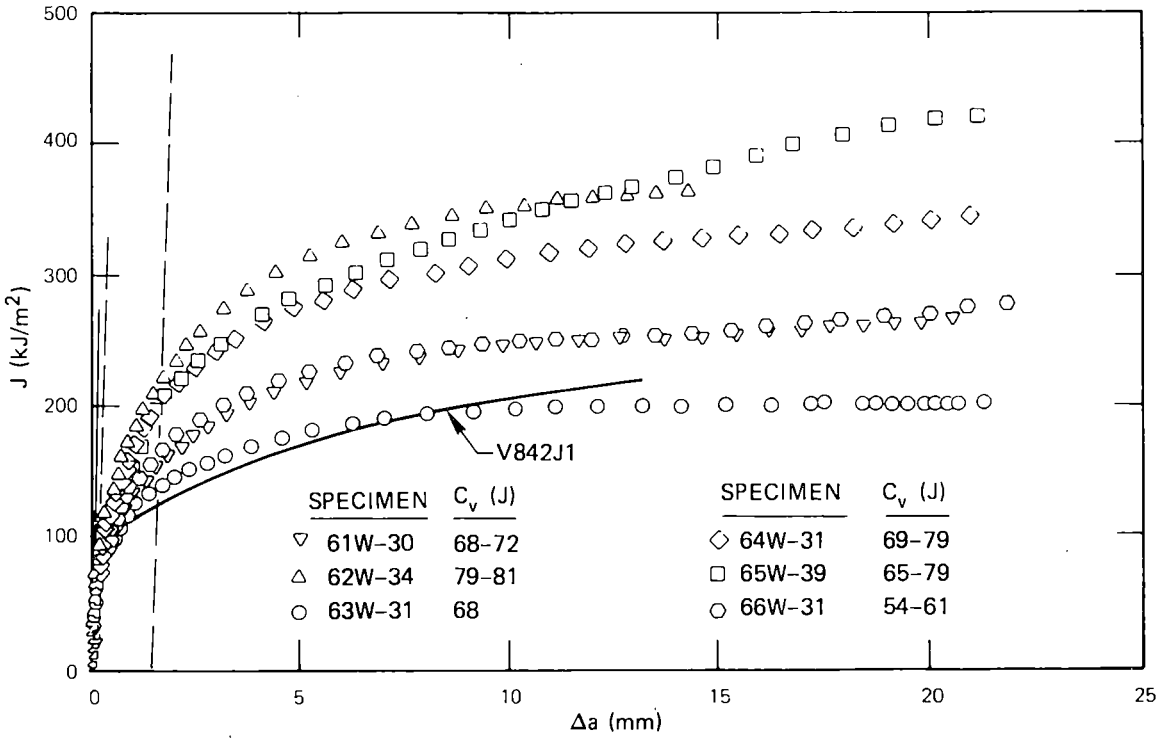

B&W BASE METAL TENSILE PROPERTIES OF HEAT-TREATED V-8 PROLONGATION (58 h at 566 to 593°C)

PROPERTY	TEMPERATURE (°C)	SPECIFIED VALUE[a]	MEASURED VALUE	
			RANGE	AVERAGE
YIELD STRENGTH (MPa)	RT	345 min.	448.8–454.4	452.2
	121		412.9–414.9	414.1
ULTIMATE TENSILE STRENGTH (MPa)	RT	550–690	595.1–600.5	598.6
	121		546.8–552.3	549.3
ELONGATION (%)	RT	18.0 min.	27.5–28.0	27.8
	121		25.0–26.0	25.7
REDUCTION OF AREA (%)	RT		70.2–70.6	70.4
	121		69.5–70.7	70.0

[a]ASME Code for SA 533 B1.

ORNL–WS 8618 ETD

VESSEL WELDS

V–8 CAVITY REPAIR

SPECIAL SEAM WELD

- LOW–UPPER–SHELF WELD PROCEDURE
- LOCATION ~120° FROM REPAIR AND FABRICATION SEAM WELD

ORNL–WS–17021 ETD

CHARACTERIZATION WELDS

WELDMENTS

- 4 24–IN.–LONG SEAM WELDS

CHARACTERIZATION TESTS

- TENSILE – 6 RT
  – 6 AT SELECTED TEMPERATURES
- C_v IMPACT – TRANSITION CURVE (20) FROM –100 TO 500°F
  – 40 AT SELECTED TEMPERATURES
- CHEMICAL ANALYSIS (2)
- COMPACT TENSION (K_{Ic}) – 23 IT CS, WL ORIENTATION, FROM 0 TO 250°F
  – 2 IT CS, WT ORIENTATION AT RT
- J–INTEGRAL TESTS (J_{Ic} AND J–Δa) AT SELECTED TEMPERATURES – 12 IT CS
  – 10 2T CS
  – 10 PCCV
- DROP WEIGHT – 12

ORNL–WS–17019 ETD

V-8A TEST MEASUREMENT PLANS

EVENTS TO BE OBSERVED

- ONSET OF STABLE TEARING
- ONSET OF UNSTABLE TEARING
  - TEARING INSTABILITY
  - LOCAL PLASTIC INSTABILITY

PARAMETERS RECORDED VS TIME

- PRESSURE
- STRAIN
- COD – 3 OR MORE LOCATIONS
- ACOUSTIC EMISSION

CRACK GEOMETRY MEASUREMENTS

- COD AND UNLOADING COMPLIANCE
- CRACK DEPTH BY ULTRASONICS 5 LOCATIONS
- POST-TEST DESTRUCTIVE EXAMINATION
- OTHERS UNDER CONSIDERATION

ORNL–WS 8620 ETD

V-8A TEST LOADING PLANS

- SLOWLY INCREASING PRESSURE
- INTERMITTENT PARTIAL UNLOADING FOR COMPLIANCE MEASUREMENTS
- SUSTAINED LOAD DURING TEARING, WHEN POSSIBLE
- RAPID UNLOADING TO INTERRUPT UNSTABLE TEARING
- REPRESSURIZATION AFTER INTERRUPTED TEARING
- MAXIMUM PRESSURE LIMITED BY POST-TEST REQUIREMENTS – REUSE OF VESSEL AND EXAMINATION OF FLAW

ORNL–DWG 80–4757A ETD

THE HSST INTERMEDIATE PRESSURE VESSELS HAVE BEEN TESTED OVER A FULL RANGE OF CHARPY ENERGIES

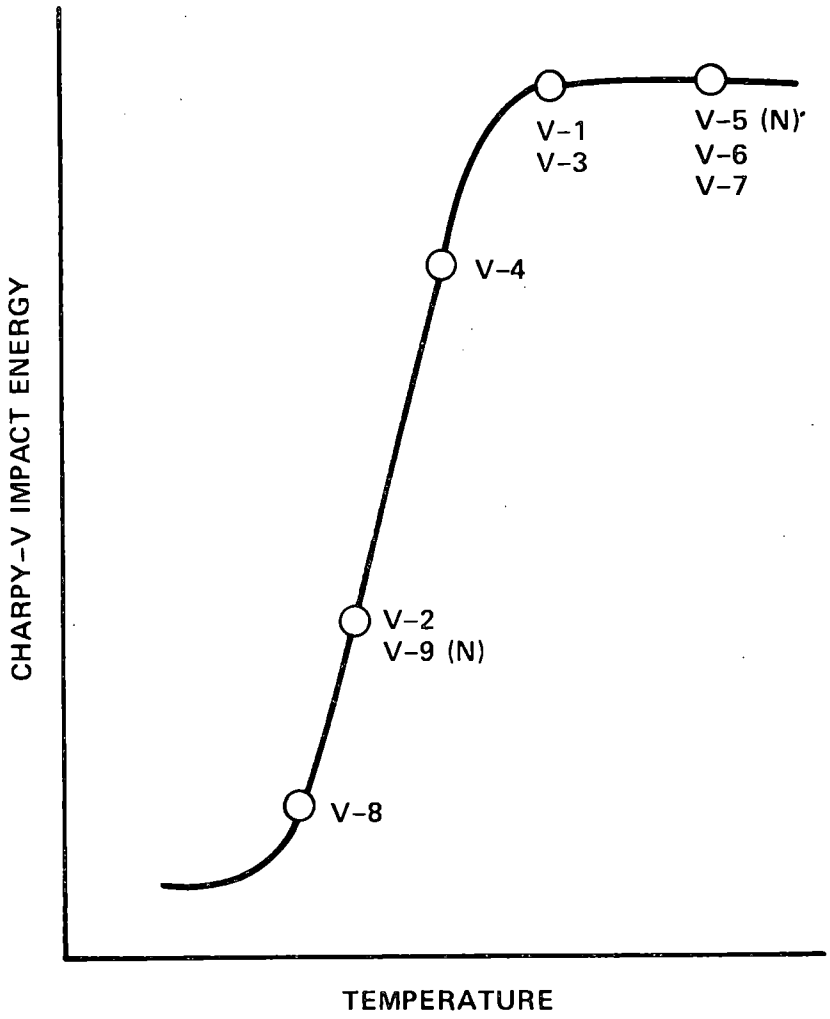

UNION CARBIDE
ORNL

COD–TEARING BEHAVIOR OF INTERMEDIATE TEST VESSELS

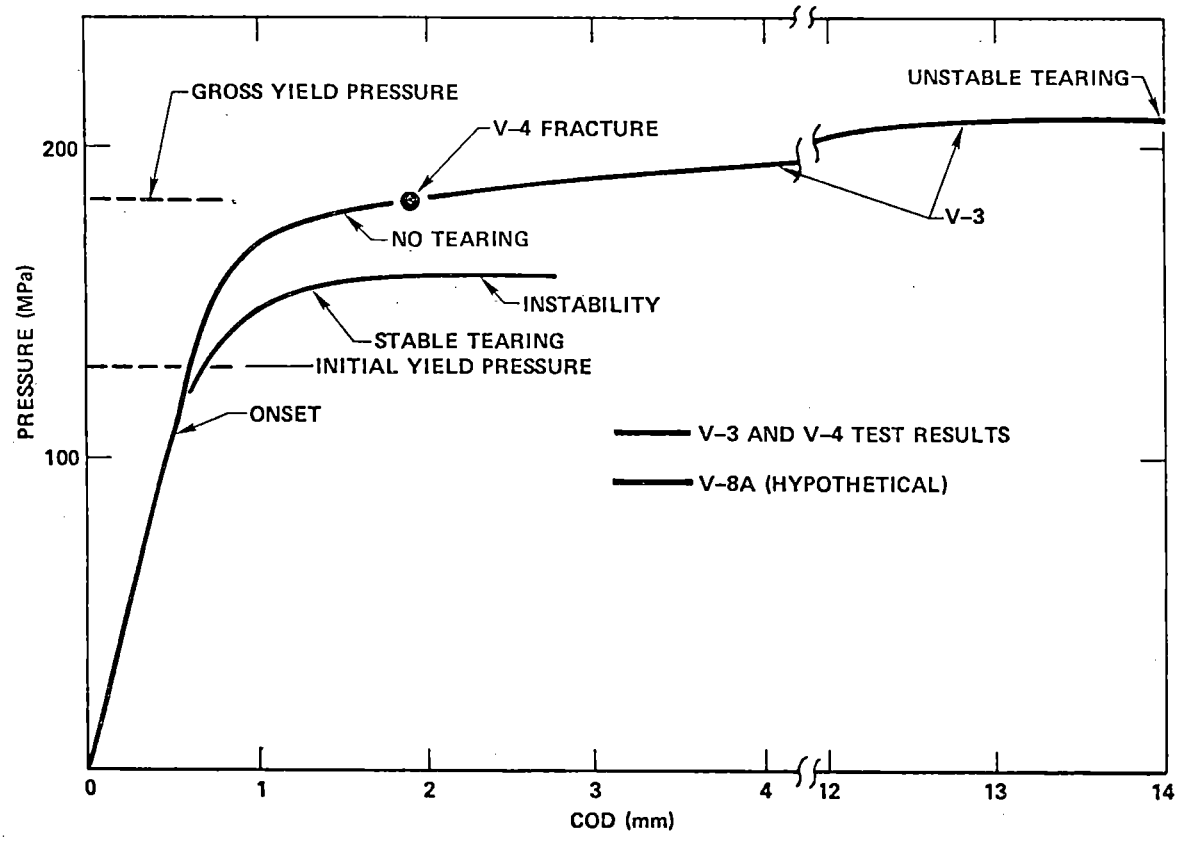

PRELIMINARY V–8A TEARING CALCULATIONS

PROBLEM STEPS

1. ELASTIC – PERFECTLY PLASTIC CYLINDER ANALYSIS
2. J_I SHAPE FACTOR (C) FROM LEFM (NEWMAN'S EQUATIONS, NASA TP 1578)
3. TANGENT MODULUS EQUATION FOR E–P PROBLEMS (MERKLE, ORNL 5059, APP. H; TASK A–11)

$$\sqrt{\rho}\, d\epsilon = 2C\sqrt{a}\sqrt{\frac{Eg}{En}}\, d\lambda$$

   (a) LINEAR ELASTIC CASE RELATES $\int\sqrt{\rho}\, d\epsilon$ TO K_I AND J_I

   (b) $\int\sqrt{Eg}\, d\lambda$ EXPRESSED IN TERMS OF E–P CYLINDER ANALYSIS

RESULT

$$J_I = g^E\, p^2\, C^2\, (a/w) \qquad p \leqslant P_y$$

$$J_I = \left\{ g^E\, p_y{}^2 + g^P\ \ p_p{}^2 \right\} C^2\, (a/w) \qquad p_y \leqslant p < p_{GY}$$

ELASTIC – PERFECTLY PLASTIC CYLINDER ANALYSIS

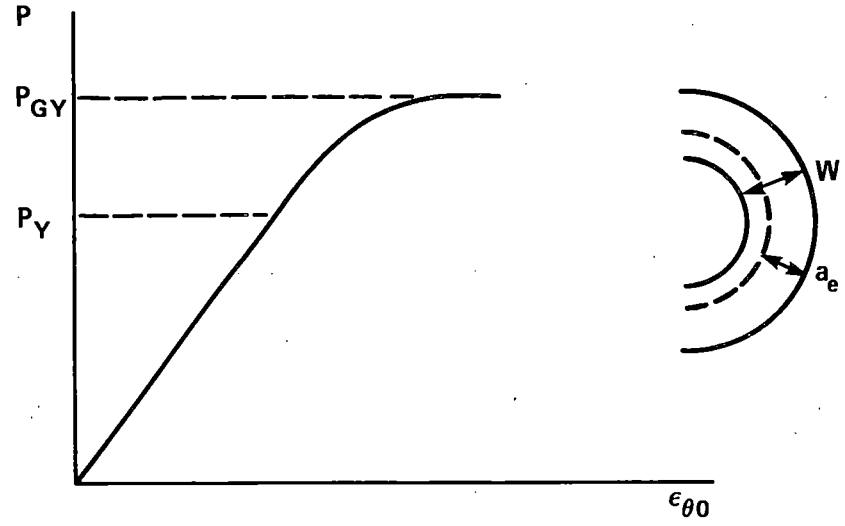

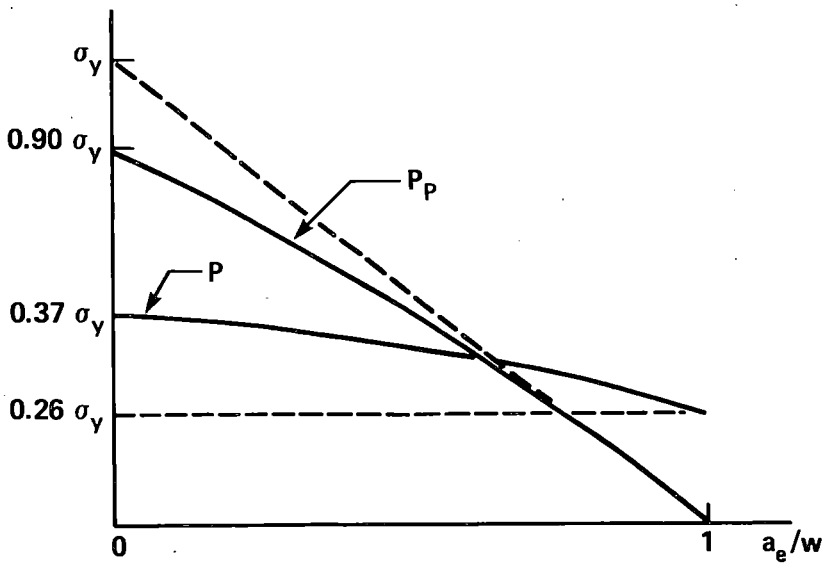

ORNL–DWG 81–16200 ETD

SHAPE FACTOR FOR ITV STRESS GRADIENT

FLAW MODEL

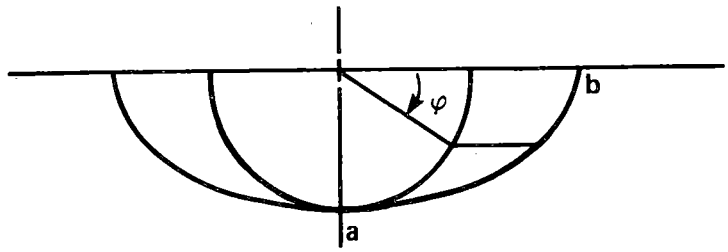

$C = f(\varphi; a/b, a/w)$

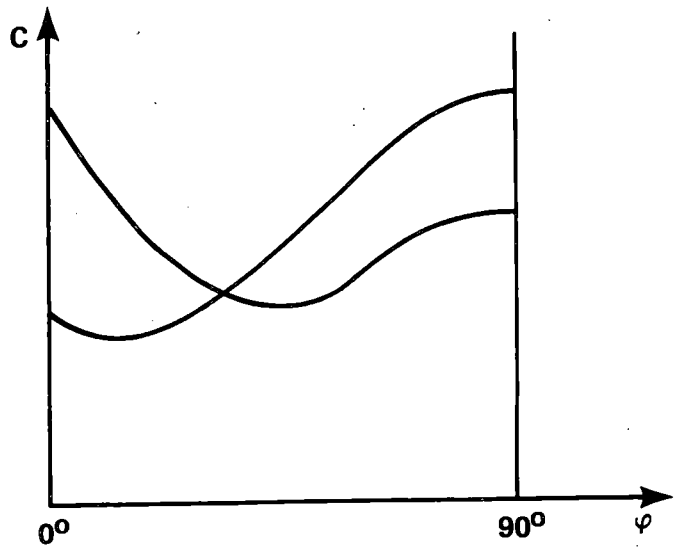

ORNL–DWG 81–16199 ETD

J–CONTROLLED STABLE AND UNSTABLE TEARING

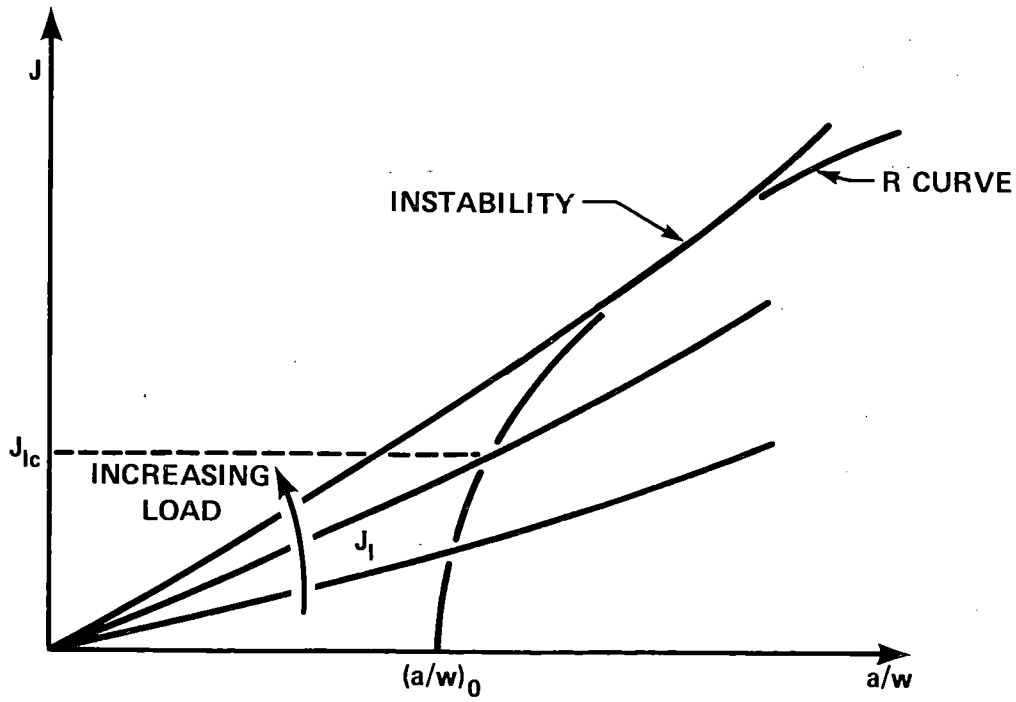

ORNL–DWG 81–16202 ETD

J_I VS PRESSURE AND a/w FOR ITV

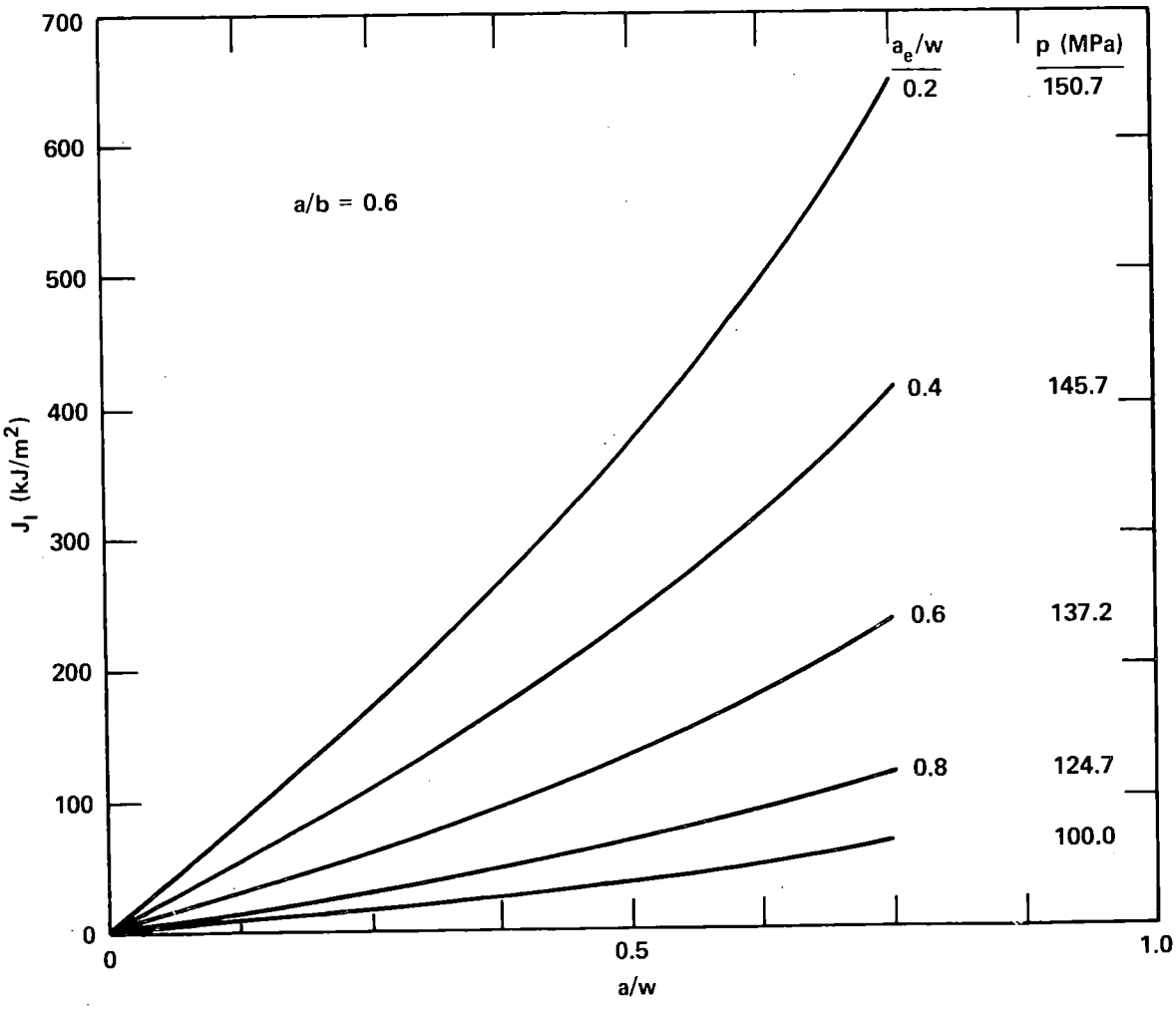

ORNL–DWG 81–16203 ETD

J–R CURVES OF V–8A TRIAL WELD

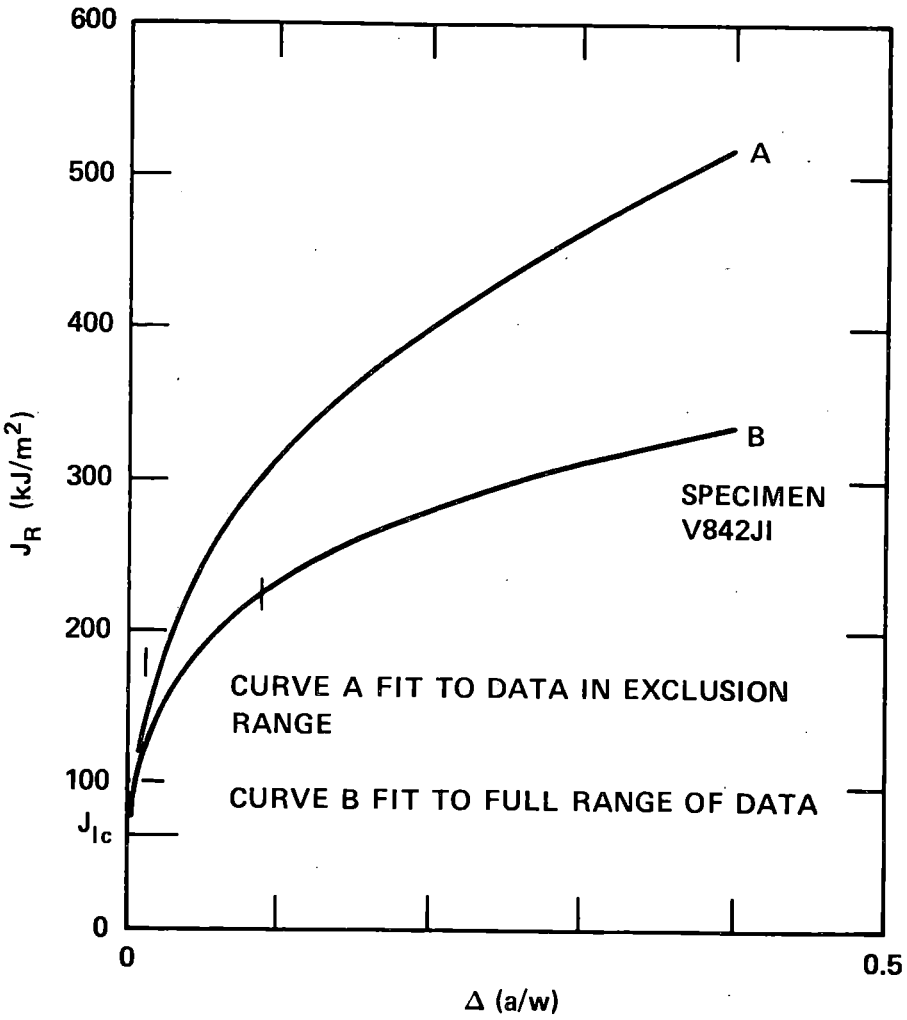

ORNL–DWG 81–16201 ETD

TEARING INSTABILITY ESTIMATE FOR ITV

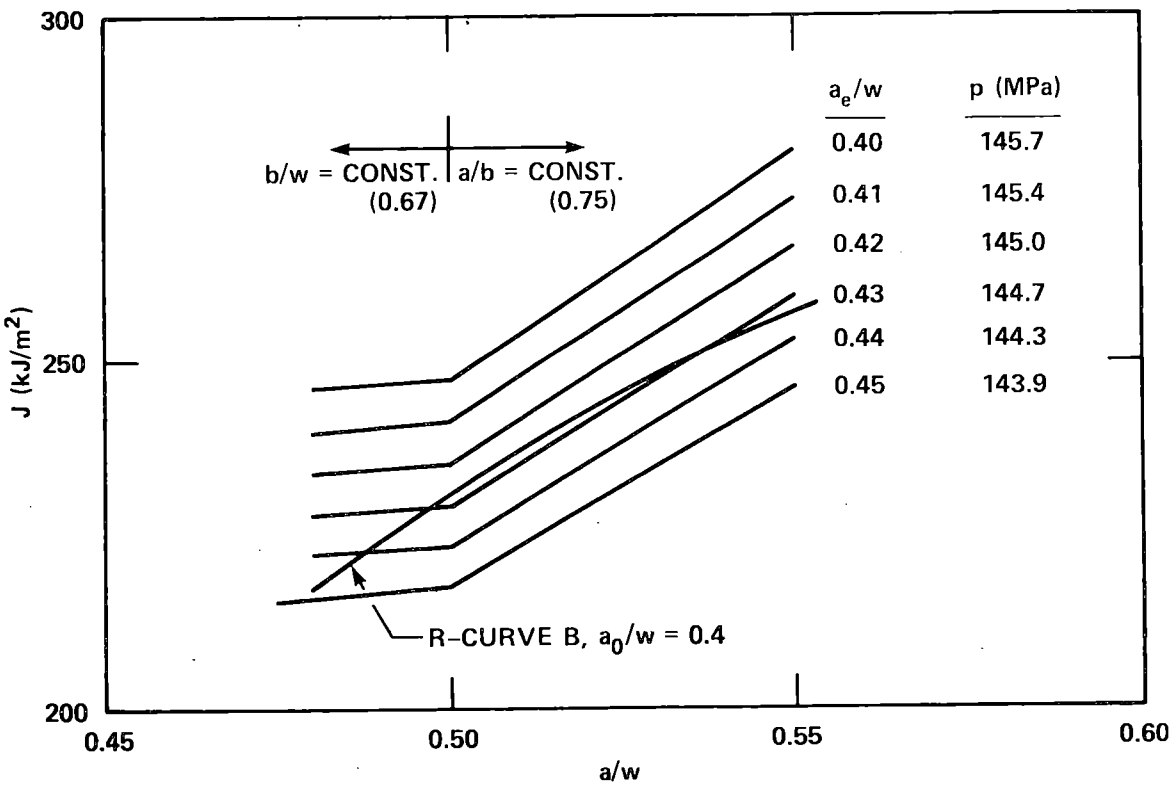

CRACK ARREST

G. R. Irwin
Department of Mechanical Engineering
University of Maryland

(Presented at the Annual Water Reactor Safety Research Review Meeting, NBS, Gaithersburg, MD., October 29-30, 1981)

The outstanding uncertainties pertaining to crack arrest in nuclear vessel steels can be listed under the following topics.

1. Crack Arrest Toughness Evaluations.
2. Modeling Problems at Temperatures Well Above NDTT.
3. Numerical Dynamic Computations

1. Crack Arrest Toughness Evaluations

The results of the Cooperative Test Program on crack arrest as well as successful static analysis predictions of crack arrest for thermal shock tests at ORNL suggested that a substantial amount of energy loss during a run-arrest event occurs away from the crack tip. Reports on these aspects were given at the NRC Research Review meeting in 1980. It was suggested that late breaking elements of the fracture surface, which are increasingly prominent with increase of temperature above NDTT, might provide enough vibration damping to account for a substantial portion of the energy loss away from the crack tip. Other mechanisms were also noted. More careful examinations of past experiments and of the Coop Test Program results now reveal that there is a friction type energy loss mechanism in the current method for K_{Ia} testing which not only assists damping of kinetic energy but also raises significant questions regarding the choice of specimen opening displacement used in calculation of a K_{Ia} test result [1].

The initial trials of a transverse wedge opening loading method for use with compact style specimens were copied from the loading method given in ASTM R-Curve method (E561) as shown in Figure 1. Note that if run-arrest crack extension

causes a load drop, the Hertzian indentations at the load contact regions are free to recover, allowing rapid transfer of load-spring energy accompanied by additional specimen opening displacement. The initial trials of this loading arrangement at MRL gave excessive crack jump lengths. Clearly a reduction of load spring energy (or loading compliance) was needed. This was supplied by changing from a five (5) piece to a three (3) piece wedging method as shown in Figure 2. The success with this arrangement was attributed to reduction of Hertzian load-contact indentations. Note that the loading pin flanges now are compressed against the upper surface of the specimen and the specimen is compressed against a rigid back-up plate. Model-experiment trials in which the pin flange was under rather than over the specimen have recently been made. These show large increases of crack jump size for the same initial opening displacement when the pin flanges are beneath the specimen [1]. Furthermore comparison of final to initial crack opening displacements measured by the 28 participants in the Coop Test Program show strong evidence that the release of load spring energy into specimen displacement was restrained by friction. In addition, the amount of restraint varied widely. With the nearly 8 inch square MRL specimen, the ratio of final to initial opening displacement varied between 1.0 and 1.21. For the BCL specimen, with 25 percent larger in-plane dimensions, this ratio varied between 1.0 and 1.3. Although some correlation with initial K could be seen for a few selected laboratories, for most participants the amount of load-spring response was random. There was no correlation with the K_{Ia} test results. The most plausible conclusion is that the release of load spring energy into the specimen, if it occurred, was sufficiently delayed so as to have no influence upon crack arrest. Although recalculation of Coop Test Program results using the initial rather than final specimen opening has not been done, a sampling of this nature indicates that such a recalculation will have a negligible influence upon data scatter. The main effect will be a reduction on the order of seven (7) percent in the average K_{Ia} value.

From the above comments, the current practice of computing K_{Ia} using the post-arrest specimen opening displacement requires modification. A second problem, related to the specimen displacement, occurs when the size of the initial plastic zone is large enough to cause an appreciable non-recoverable increase of the initial opening displacements. A third testing problem concerns the problem of initiating cleavage cracking at temperatures well above NDTT. In response to these last two problems, the testing practice preferred at BCL uses sequential load-unload steps in the initial load application. This permits an estimated adjustment of the zero-load point of the displacement gage output. In addition the load-unload

steps tend to improve the probability of a successful run-arrest initiation. The BCL sequential loading method is very time consuming. Other methods for solving these problems should be examined as an aid to extending crack arrest toughness evaluations farther above the NDT temperature.

There is an evident need for settlement of crack arrest specimen size requirements, particularly for the thickness requirement which is related to degree of plane strain. Ripling [2] has suggested the inequality

$$B \geq 1.0 \left(\frac{K_{Ia}}{\sigma_{Yd}}\right)^2$$

where σ_{Yd} is estimated by adding 30 ksi (200 MPa) to the slow-load measurement of the yield strength of the steel. K_{Ia} measurements using 1-in and 2-in thick specimens of A36 steel [2] appeared to support this size requirement choice. The unity value of the coefficient in the above inequality may seem small in comparison to the 2.5 value used in ASTM method E399. However, the estimate of an appropriate value for σ_{Yd} is conservative to an uncertain degree. Specimens which fail to satisfy the above inequality would, in any case, possess a strong likelihood of having inadequate thickness.

The measurements of initiation and arrest toughness for the vessel material used in the ORNL test, TSE-5a, are shown in Figure 3. Crack arrest K values for the four arrest events observed in that test have been superimposed on a figure from reference[3]. Relative to the above size requirement, the 1 inch (25 mm) thickness used for the laboratory crack arrest test was adequate for the 3 lowest values of K_{Ia}, nearly adequate for the middle value measured at room temperature, and not adequate for the two largest K_{Ia} values. With this in mind, it is evident that crack arrest K values observed in all of the ORNL thermal shock tests are essentially in agreement with test specimen values measured at BCL. A modest reduction of the K_{Ia} values to eliminate specimen opening displacement due to load-spring energy transfer would not change this conclusion.

2. Analysis Model Used with Experiments

In the cleavage-fibrous transition range the importance of late breaking regions of the fracture surface increases with increase of testing temperature[4,5]. These exert closing forces which reduce the stresses tending to reinitiate cleavage separations ahead of the cleavage crack front. In partial compensation, the abrupt final separations of late breaking regions may assist cleavage initiations in

certain areas of the crack front. It would seem that representation of the closing forces from late breaking regions could be given a more realistic representation by use of a "strip zone" type analysis model and some studies of this have been made. The complexities introduced by so doing must be compared against benefits. At the present time, the practice of using heat tinting in the toughness evaluation test and arrest markings in thermal shock tests have given good agreement and appear to serve well enough when used as indicators of crack size in K_{Ia} computations. However, the tendency of the inferred analysis model to lose realism with increase of temperature above NDTT should be remembered.

Examinations of thermal shock test fractures show that the progressive fracturing direction varies considerably in local regions of the crack front. It is reasonable to question whether 25 mm, or even 50 mm, thickness arrest toughness specimens can model the crack direction behaviors observed in thermal shock testing. In addition the sizes of the unbroken regions behind the crack front seem to be larger in the long-crack-front thermal-shock fractures than in the relatively short-crack-front toughness specimens. A suitable analysis model adjustment for the above features is not currently apparent. Possibly none will be needed if the crack arrest test specimen has adequate thickness relative to a "plane-strain" requirement.

Relative to uncertainties discussed in this section, it is comforting to note [6] that all of the crack arrest data computed for ORNL experiments (TSE 4, 5, and 5A) are above the K_{IR} curve and extend to temperatures not far below the expected temperature for disappearance of cleavage.

3. Numerical Dynamic Computations

Adequate treatment of this topic will not be attempted in this discussion. Computer programs have been developed and tried out at BCL and at the University of Maryland. Predictions in reasonable agreement with a selected run-arrest event in ORNL test TSE5 were obtained. However, the relationship of K_{Ia} to temperature was uncertain and the selected relationship between crack speed and K, basic to these results, requires more study. In addition, the University of Maryland results show an energy balance discrepancy which seems excessive.

(1) Quarterly Progress Report to ORNL, W. L. Fourney, (Mech. Engr. Dept., Univ. of Maryland) Sept. 1981.

(2) "Development of a Standard Test for Measuring K_{Ia} With a Modified Compact Specimen", P. B. Crosley and E.J. Ripling, NUREG/CR-2294, Aug. 1981.

(3) "HSST Program Quarterly Progress Report for Oct.-Dec., 1980", G. D. Whitman and R.H. Bryan, NUREG/CR-1941 pp. 37-49.

(4) "Mechanisms of Fast Fracture and Arrest in Steels", R. G. Hoagland, A. R. Rosenfield, and G. T. Hahn, Metal. Trans. Vol. 3, 1972, pp. 123-136.

(5) "HSST Program Quarterly Progress Report for Jan.-March 1981", G. D. Whitman and R. H. Bryan, NUREG/CR-2141/VI pp. 27-46.

(6) "Lower-Bound K_{Ia} Values", A. R. Rosenfield (BCL), Note with Letter to M. Vagins, NRC, Aug. 13, 1981.

(7) Reference (5) pp. 46-56.

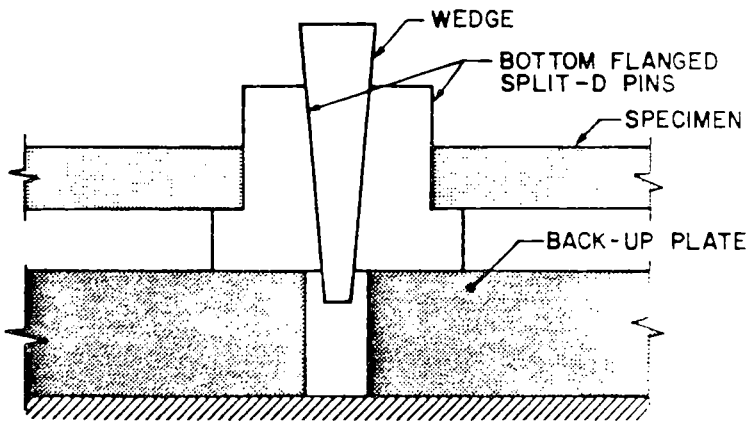

Figure 1 Five-Piece Wedge Arrangement

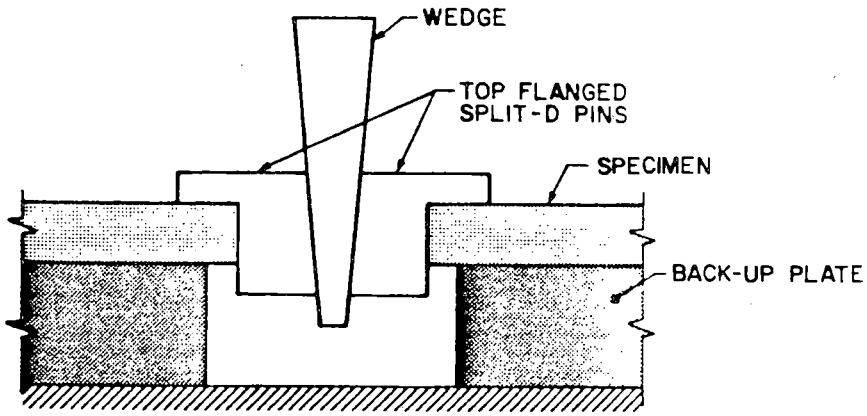

Figure 2 Three-Piece Wedge Arrangement

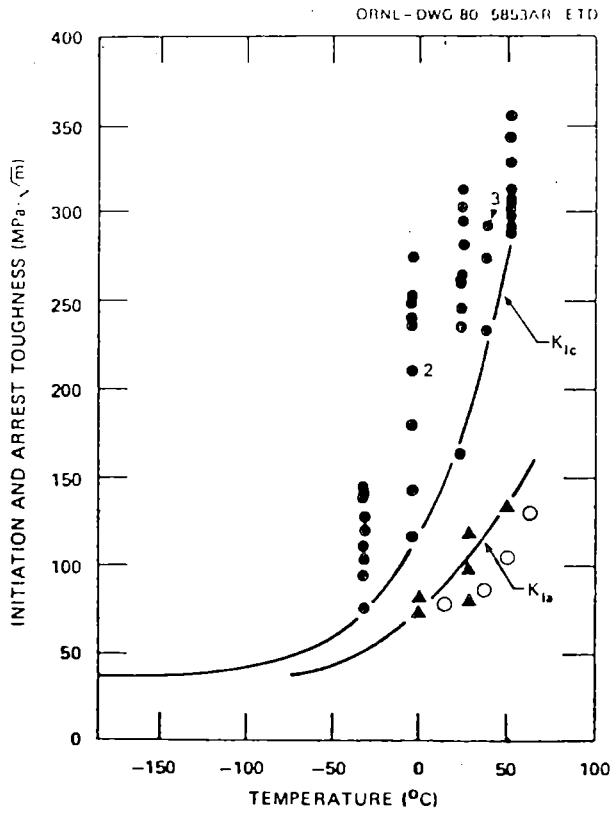

Figure 3 Arrest and Initiation Toughnesses for TSE-5A

J-R CURVE CHARACTERIZATION OF IRRADIATED, LOW-UPPER SHELF WELDS

F. J. Loss
Naval Research Laboratory
Washington, DC 20375

Presented at

9th Water Reactor Safety Research Information Meeting
National Bureau of Standards
Gaithersburg, MD
26-30 October 1981

J-R CURVE CHARACTERIZATION OF IRRADIATED, LOW-UPPER SHELF WELDS

F. J. Loss
Naval Research Laboratory
Washington, DC 20375

BACKGROUND

Previous studies have shown that A533-B submerged arc weld deposits of the type used in the beltline region of some commercial, light water reactor vessels can exhibit low Charpy-V (C_V) upper shelf energy levels after irradiation, that is, energies which lie below 68J (50 ft-lb). In this event, Federal regulations (10 CFR Part 50) require, as one option, the performance of a fracture mechanics analysis which conservatively demonstrates the existence of adequate margins of safety for continued operation. To address this issue, the Nuclear Regulatory Commission (NRC) is sponsoring research studies to: (a) formulate a structural integrity approach based upon elastic plastic behavior, (b) characterize the toughness of low, upper shelf steels in terms compatible with the analysis procedure and (c) verify the approach through structural tests. As part of this NRC-coordinated program, research emphasis at NRL has been placed on characterization of J-R curve trends within the upper shelf temperature regime. This data is essential for use in conjunction with the tearing instability concept being considered by the NRC to assess the margin against failure of the reactor vessel in the presence of assumed defects [1].

In the Heavy Section Steel Technology (HSST) Program seven A533-B submerged arc weld deposits (61W-67W) containing a high copper impurity level have been irradiated to provide a source of materials having low, upper shelf energy. Compact toughness (CT) specimens of various sizes, which include 0.5T-, 0.8T-, 1.6T-, and 4T-CT as well as C_V specimens were irradiated in this program to nominal fluence levels of 0.6 to 1.4×10^{19} n/cm^2 > 1 MeV; postirradiation C_V upper shelf energy levels for these welds ranged from 54 to 81J (40 to 60 ft lb). R curve trends from the testing of the 1.6T- and 4T-CT specimens are summarized here.

SUMMARY OF RESULTS

J-R curves have been obtained by means of the single specimen compliance (SSC) technique [2,3]. This method is capable of producing well-defined R curves having little scatter among the data points. In addition, it has been found that the crack extension must proceed uniformly throughout the specimen thickness in order to achieve an accurate correspondence between this quantity as predicted by the SSC technique and as measured optically after the specimen has been broken apart. Previous studies by the author have shown that side grooving of the specimen by 20% is required to achieve a straight crack-front extension in nuclear vessel steels. This side-groove depth has therefore been applied to the low shelf weld specimen tests reported here.

A typical R curve produced with the SSC technique, as illustrated in Fig. 1, is normally restricted to a small crack extension (Δa) in order to maintain a region of "J dominance." This requirement has been formulated by Hutchinson and Paris [4] as $\omega >> 1$ where $\omega = (b/J)(dJ/da)$. However, R curves associated with longer crack extension, which would violate the ω criterion, may be necessary for a given structural

analysis. Therefore, R curves have been developed in this program which sometimes exceed current crack extension limitations with the expectation that the data may prove useful for future analyses.

The R curve format in Fig. 1 is in accordance with that of the proposed ASTM J_{Ic} standard: J_{Ic} is defined by the intersection of a linear regression fit to the data (i.e., the dashed line between the 0.15 mm and 1.5 mm exclusion lines) with the blunting line, $J = 2 \sigma_f \Delta a$. Using the SSC technique, however, Loss and co-workers [5] have demonstrated that the R curve is nonlinear for small amounts of crack extension (e.g., 2 mm) in structural steels. Consequently, the R curve in the region between the 0.15 mm and 1.5 mm exclusion lines has been described in terms of a power law, $J = C \Delta a^n$, where C and n are constants chosen to optimize the curve fit. To circumvent the potential difficulties associated with the least squares procedure, Loss and co-workers [5] have formulated a new indexing procedure for J_{Ic} which more clearly represents the physical behavior. Specifically, J_{Ic} is taken as that value of J where the power-law R curve crosses the 0.15 mm exclusion line. This is an engineering approach, analogous to that used for the 0.2% yield stress, and it permits a small, but measurable crack extension at the J_{Ic} point. However, it should be noted that for the reactor vessel steels discussed here the magnitude of J_{Ic} given by the author's method is nearly identical to that of the ASTM procedure for reactor vessel steels, as illustrated in Fig. 1.

The SSC technique has been successfully adapted at NRL for the remote testing of irradiated specimens. Figure 2 illustrates typical R curves for 1.6T- and 4T-CT specimen tests of the HSST welds. The lack of scatter among the data points produces well-defined R curves which easily lend themselves to the definition of J_{Ic} as described above. With larger size specimens the SSC method is more difficult to apply because of the increased accuracy that is required in the load and displacement transducers. However, with the experimental technique developed at NRL the "quality" of the R curves from 4T-CT specimens is essentially identical to that of the smaller size specimens.

Figure 3 compares the pre- and post-irradiation behavior for one HSST weld. In general, the HSST welds exhibited a 30-40% decrease in J_{Ic} with irradiation. In this example, however, J_{Ic} is essentially unchanged by irradiation to a fluence of $\sim 1.2 \times 10^{19}$ n/cm^2 > 1 MeV. On the other hand, a large change tearing modulus T is apparent (i.e., T is proportioned to the slope of the R curve). This change in R curve slope is shown more dramatically in Figure 4 for the case of larger crack extensions. Thus, research emphasis directed primarily toward the characterization of J_{Ic} for materials which exhibit a ductile tearing behavior may be of little engineering value in assessing the margin against instability.

Figure 3 also illustrates a "cleavage" popin for the irradiated material. This specimen was unique in that the fracture mode was ductile with the exception of one weld pass in the fracture plane which failed almost entirely by cleavage. While this phenomenon did not appear to markedly reduce the R curve slope in comparison with tests of other specimens from this weld, which failed entirely in a ductile mode, it does illustrate the inhomogeneous behavior which is possible.

A comparison of the pre- and post-irradiation behavior for other HSST welds is presented in Figs. 5-6 (1.6T-CT tests) and Figs. 7-8 (4T-CT tests). The majority of the tests in the program were conducted at 200°C to ensure ductile behavior for both the

irradiated and unirradiated materials. Only a few specimens were available to investigate the R curve behavior at different temperatures. (It should be noted that the R curve slope generally increases with decreasing test temperature.) The relative crack depth (a/w) for all specimens except 65W-37A was 0.5. These results exhibit a surprisingly small variation considering the fact that the tests describe the behavor of seven different welds and the fluence varied by more than a factor of two for the irradiated materials. The small scatter associated with duplicate tests of certain welds can be observed in the figures. The range of J_{Ic} for the irradiated welds is 60-90 kJ/m^2. This is equivalent to a K_{Jc} of 113-139 MPa$\sqrt{m}$ where $K_{Jc} = [EJ_{Ic}/(1-\nu^2)]^{1/2}$ and E and ν are Young's modulus and Poisson's ratio, respectively. It was also noted that J_{Ic} and the initial R curve slope (for a crack extension less than 1.5 mm) exhibit a general correlation with C_v upper shelf energy.

It can be seen that certain R curves in Figs. 6 and 8 exhibit a flattening (and even negative slope) at long crack extensions. The significance of this behavior bears further investigation in that the region of J dominance has been exceeded at the long crack extensions. For example, $\omega = 1$ at a crack extension of 6-8 mm for the 1.6T tests and 15-18 mm for the 4T-CT tests. The negative R curve slope is physically unreasonable and a theoretical explanation must be sought. Finally, it should be noted that the power-law description of the R curve is inappropriate at long crack extensions where a flattening of the R curve is exhibited.

One objective of the present program is to characterize the R curve for a given weld on the basis of CT specimens of similar size, i.e., 0.5T- to 4T-CT. A size independence would suggest that the results from reactor surveillance specimens of small size are indicative of large specimen behavior. While the small size specimens (0.5T- and 0.8T-CT) in the program have not yet been tested, preliminary results with other materials suggest a size independence for R curves measured with side-grooved specimens (Fig. 9). McCabe and Landes [6] have reached a similar conclusion. In contrast to these observations, results from the 1.6T- and 4T-CT tests of the HSST welds exhibit a specimen size dependence whereby higher R curves are produced with the larger of the two specimen sizes (Figs. 10-12). This behavior, while more readily observed with the unirradiated materials, is present in the tests of irradiated material as well. This result is opposite to the expected behavior: because of its higher constraint, the larger specimen would be expected to produce the lower R curve. An explanation of this phenomenon is not currently available. However, it should be noted that the weld seam being tested is of a fixed size so that the larger specimens contain proportionally less weld metal and more plate than is the case with smaller specimens. The difference in flow properties between plate and weld metal may therefore be the cause of the apparent specimen size dependence observed here.

In assessing the margin against failure with the tearing instability approach, it is convenient to plot the applied value of J and the R curve for the material in terms of a J vs. T diagram (Fig. 13). A summary of R curve data from 1T-CT specimens obtained from programs at NRL sponsored by the NRC and the Electric Power Research Institute (EPRI) [7] have suggested a correlation of R curve behavior with C_v upper shelf energy. Figure 14 shows that such a correlation exists over a wide range of C_v energies for plate, weld and forging in both irradiated and unirradiated conditions. This figure also illustrates the apparent specimen size dependence discussed above. In Fig. 14, C_v energy is correlated with the J value at J/T = 8.8 kJ/m^2 (50 in.-lb/in.^{2}). This J-value index is arbitrary and is meant to indicate a J level below which instability will not occur for a large flaw in a reactor vessel. (See Ref. 1 for further details of this procedure.) The

correlation in Figure 14 is expected to enhance the significance of C_v reactor surveillance data with respect to structural integrity.

CONCLUSIONS

The principal conclusions of this study are:

- The SSC technique has been demonstrated as an effective method to characterize the J-R curve of irradiated steels.
- The J-R curves for reactor vessel steels of low upper shelf energy obey a power-law relationship for crack extension increments less than 2 mm. This observation has led the author to propose a new indexing procedure for J_{Ic}.
- The first R-curve data base has been developed for irradiated vessel steels having low shelf energy.
- In certain cases, an apparent specimen size dependence of the R curve has been demonstrated with side-grooved CT specimens having thicknesses between 41 and 100 mm.
- A correlation has been suggested between the R curve parameters and C_v upper shelf energy. If further verified, this finding could enhance the significance of C_v reactor surveillance data with respect to structural integrity.

REFERENCES

1. R. E. Johnson, ed., "Resolution of Reactor Vessel Materials Toughness Safety Issue, Task Action Plan A-11", NUREG-0744, Nuclear Regulatory Commission, Sept. 1981.
2. F. J. Loss, ed., "Structural Integrity of Water Reactor Pressure Boundary Components - Quarterly Progress Report, April-June 1979", NUREG/CR-0943, NRL Memorandum Report 4064, Sept. 28, 1979.
3. F. J. Loss, ed., "Structural Integrity of Water Reactor Pressure Boundary Components, Annual Report, Fiscal Year 1979", NUREG/CR-1128, NRL Memorandum Report 4122, 31 Dec. 1979.
4. J. W. Hutchinson, P. C. Paris, "The Theory of Stability Analysis of J-Controlled Crack Growth", ASTM STP 668, (1979), pp. 37-64.
5. F. J. Loss, B. H. Menke, R. A. Gray, Jr., H. E. Watson, "J-R Curve Characterization of A533-B Weld Metal with Irradiated and Postirradiated Annealing", ASTM STP 725, (1981), pp. 77-91.
6. D. E. McCabe and J. D. Landes, "J_R Curve Testing of Large Compact Specimens", Proceedings of Second International Symposium on Elastic-Plastic Fracture Mechanics", Oct. 6-9, 1981, Philadelphia, PA (to be published as an ASTM STP).
7. J. R. Hawthorne, ed., "NRL-EPRI Research Program (RP886-2), Evaluation and Prediction of Neutron Embrittlement in Reactor Pressure Vessel Materials, Annual Report for CY 1978", NRL Report 8327, Naval Research Laboratory, (Aug. 30, 1979).

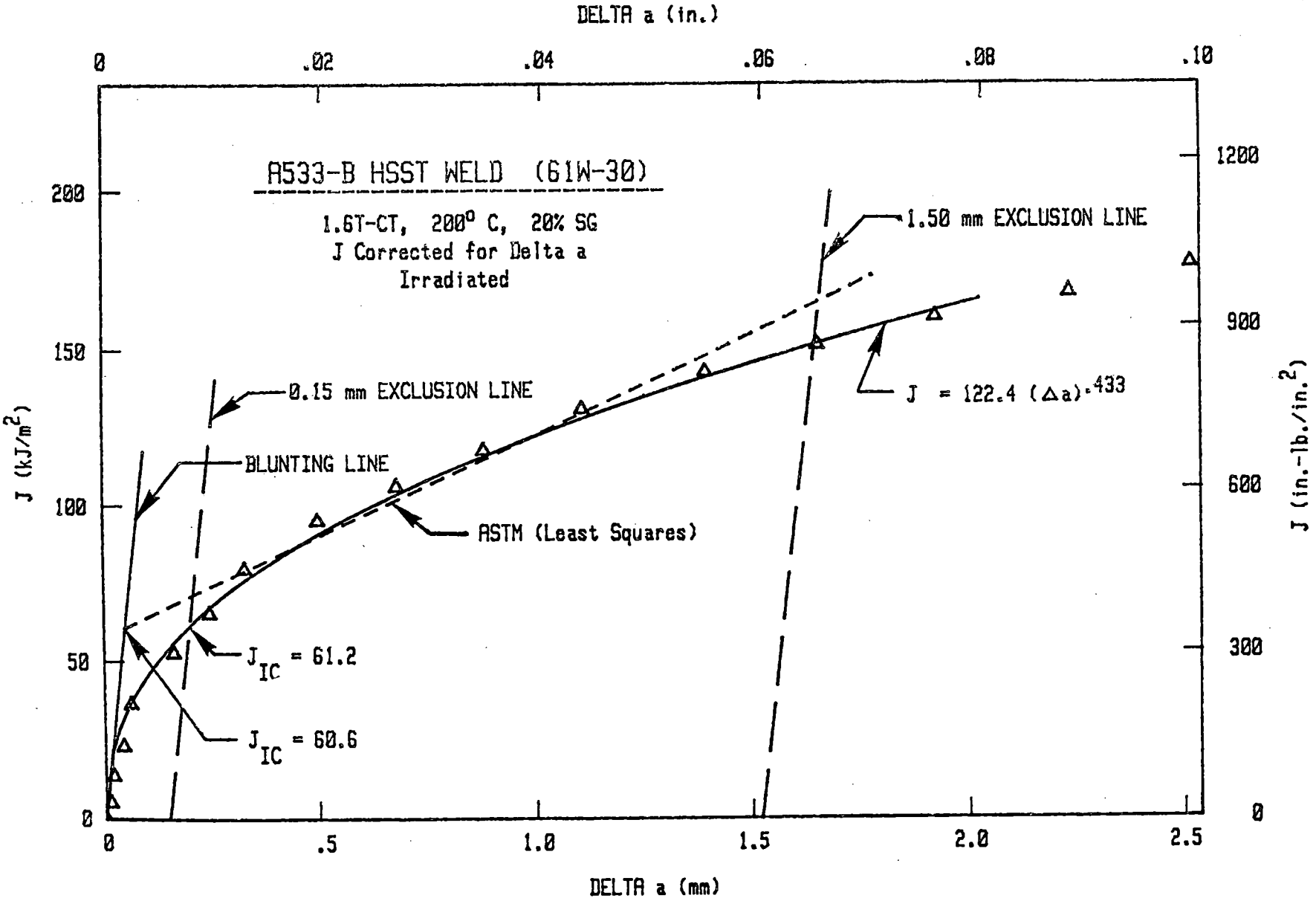

Fig. 1 - Expanded R curve illustrating the power-law behavior exhibited at small crack extension. With the NRL procedure, J_{Ic} is taken as that value where the R curve intersects the 0.15 mm exclusion line. Conversely, J_{Ic} is defined by the proposed ASTM standard as the intersection of the least squares fit of the data (between exclusion lines) with the blunting line.

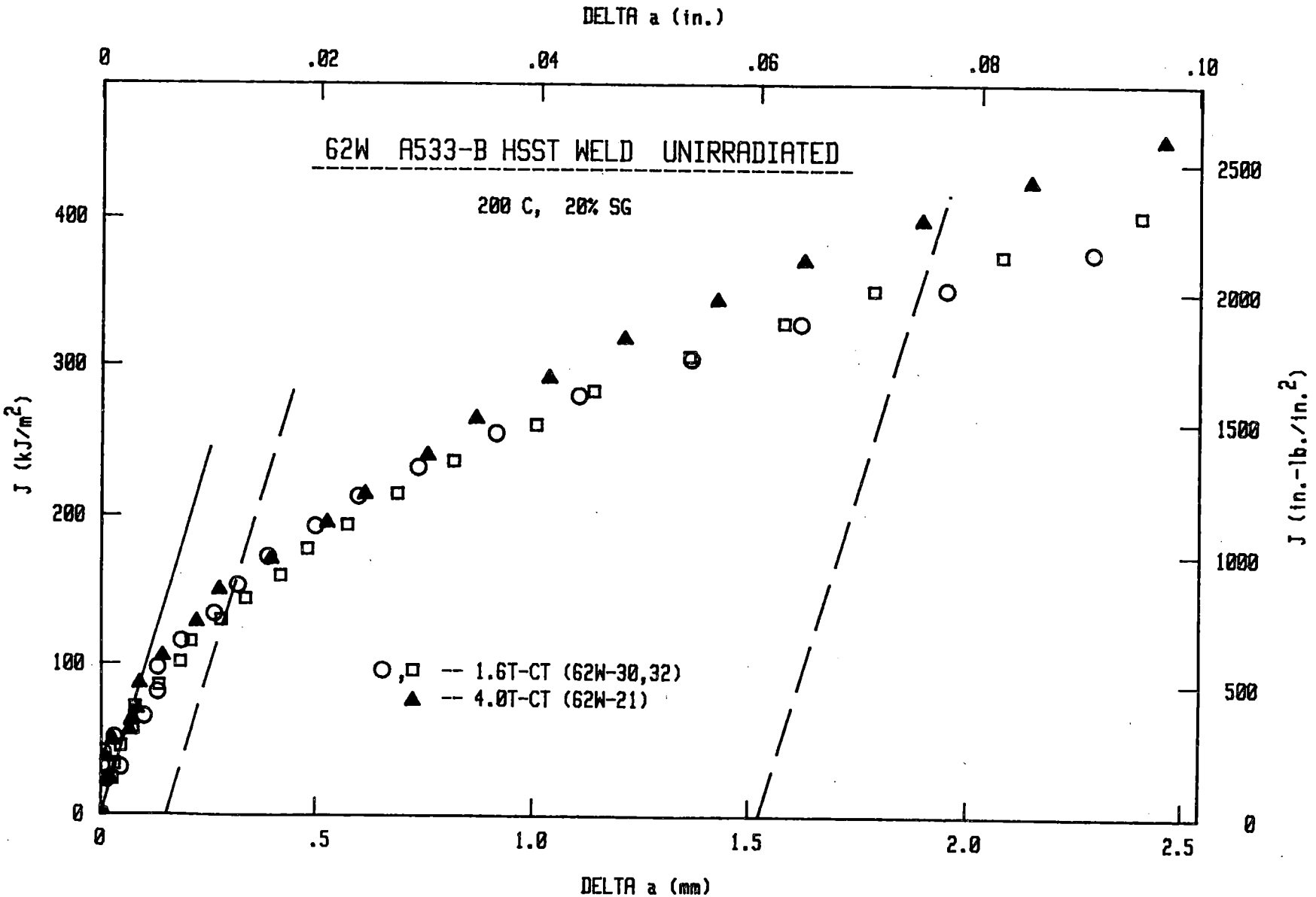

Fig. 2 - Typical R curves defined by 1.6T- and 4T-CT specimen tests. The tests, conducted by remote means in a hot cell, exhibit little scatter among the data points.

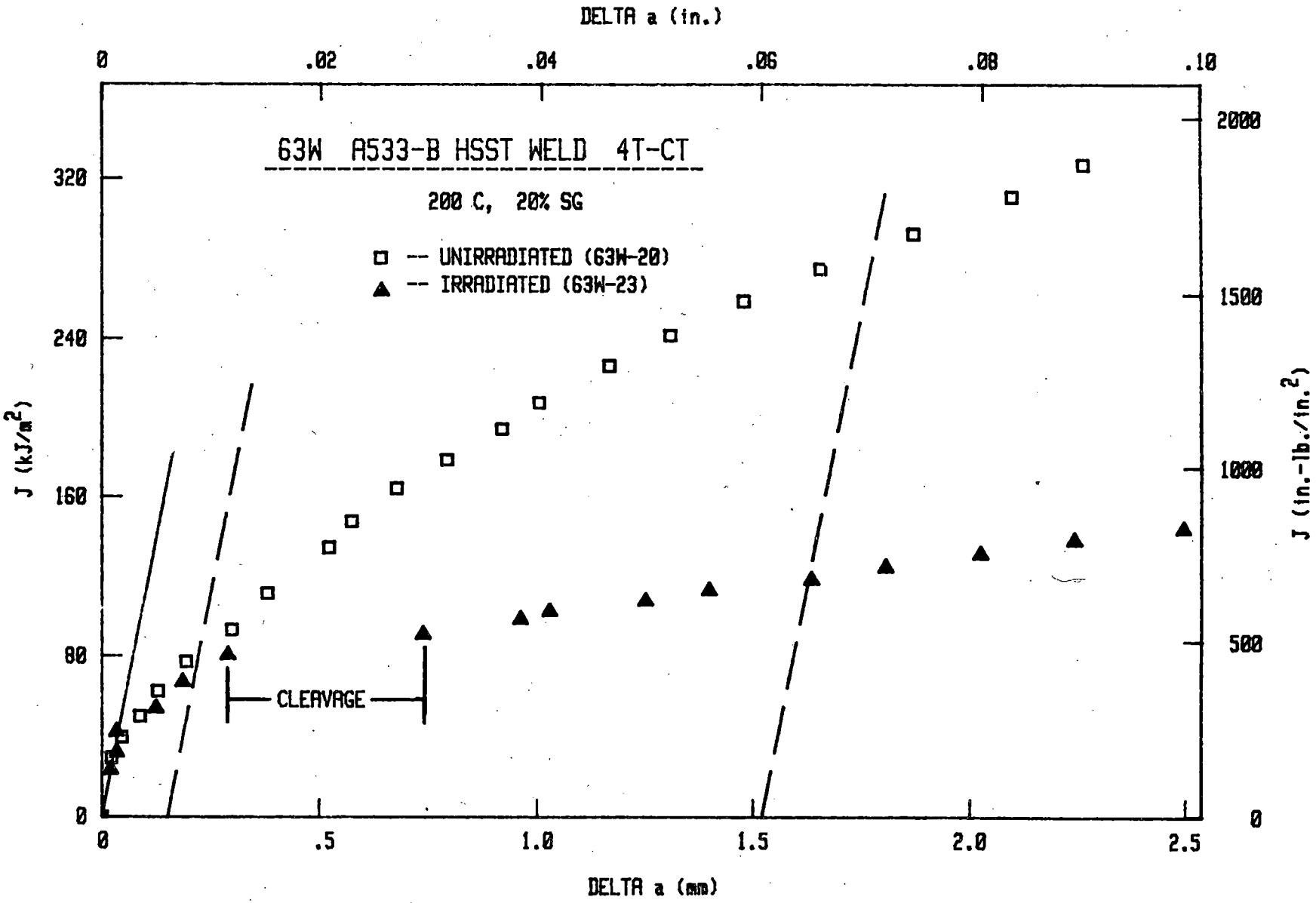

Fig. 3 - Comparison of pre- and post-irradiation behavior, illustrating a case in which J_{Ic} was essentially unchanged by the irradiation.

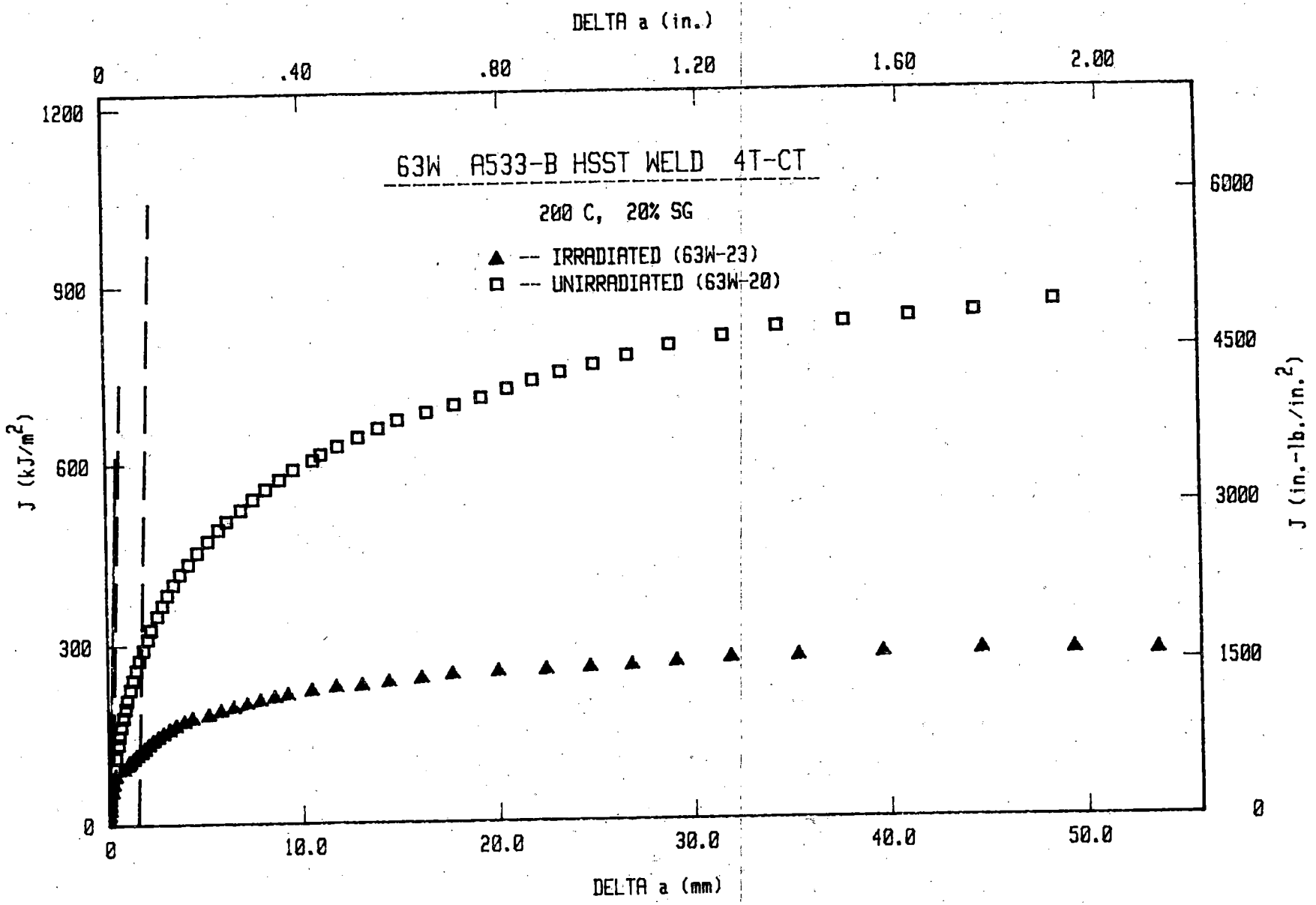

Fig. 4 - Illustrating the R curves for the specimens in Fig. 3 at a large crack extension.

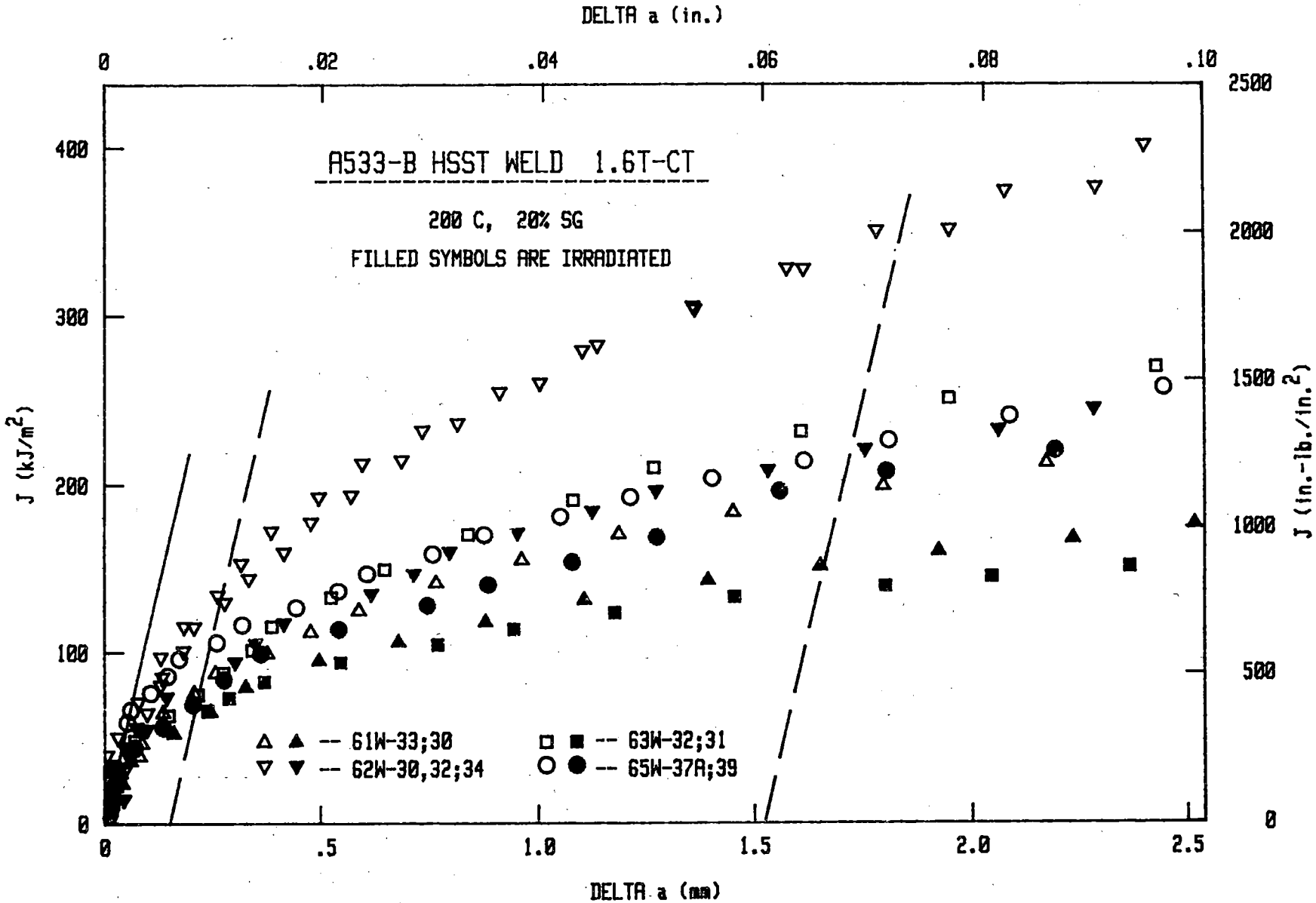

Fig. 5 - R curves from HSST welds tested in the upper shelf regime with 1.6T-CT specimens.

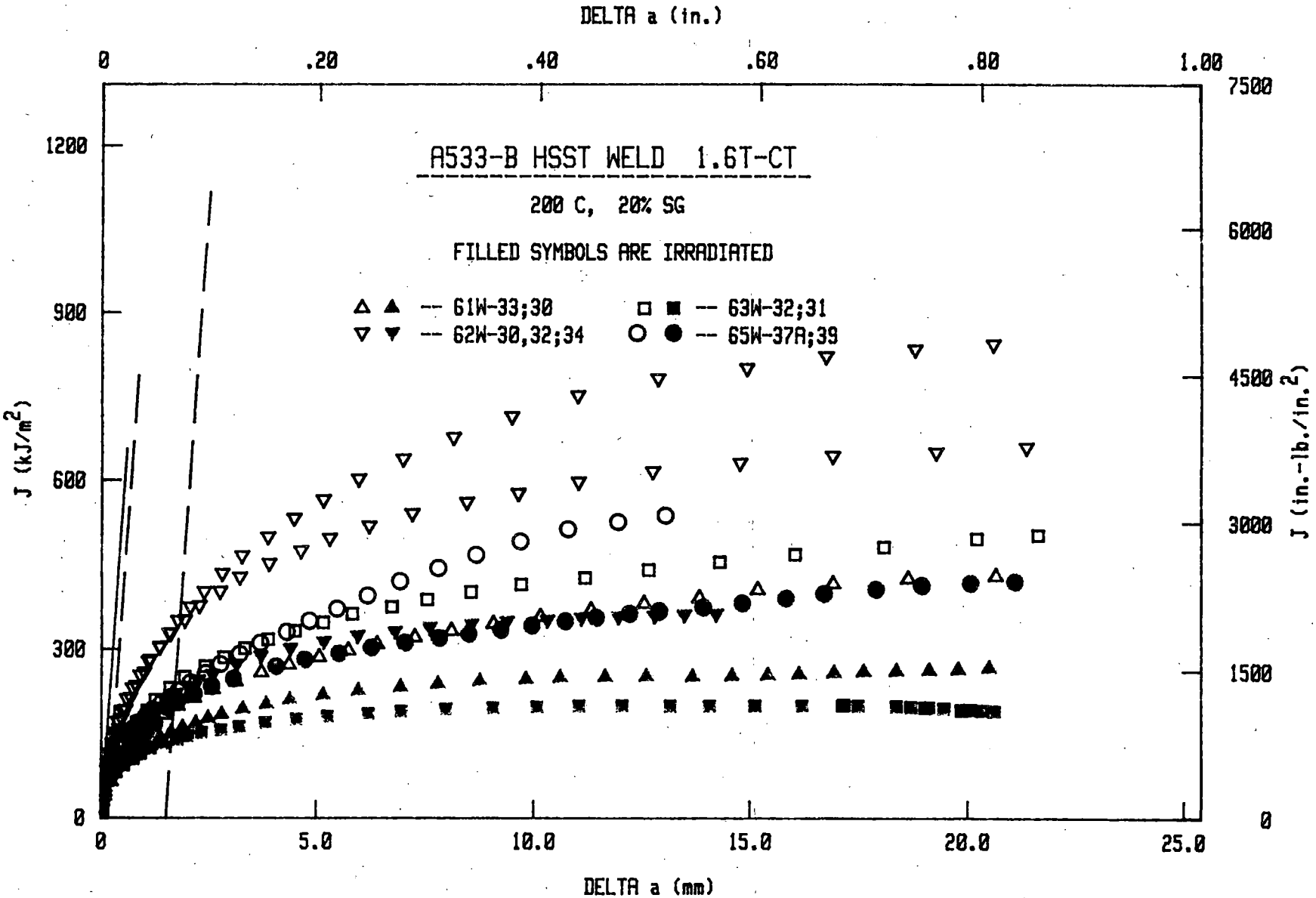

Fig. 6 - Pre- and post-irradiation R curve trends at long crack extension measured with 1.6T-CT specimens.

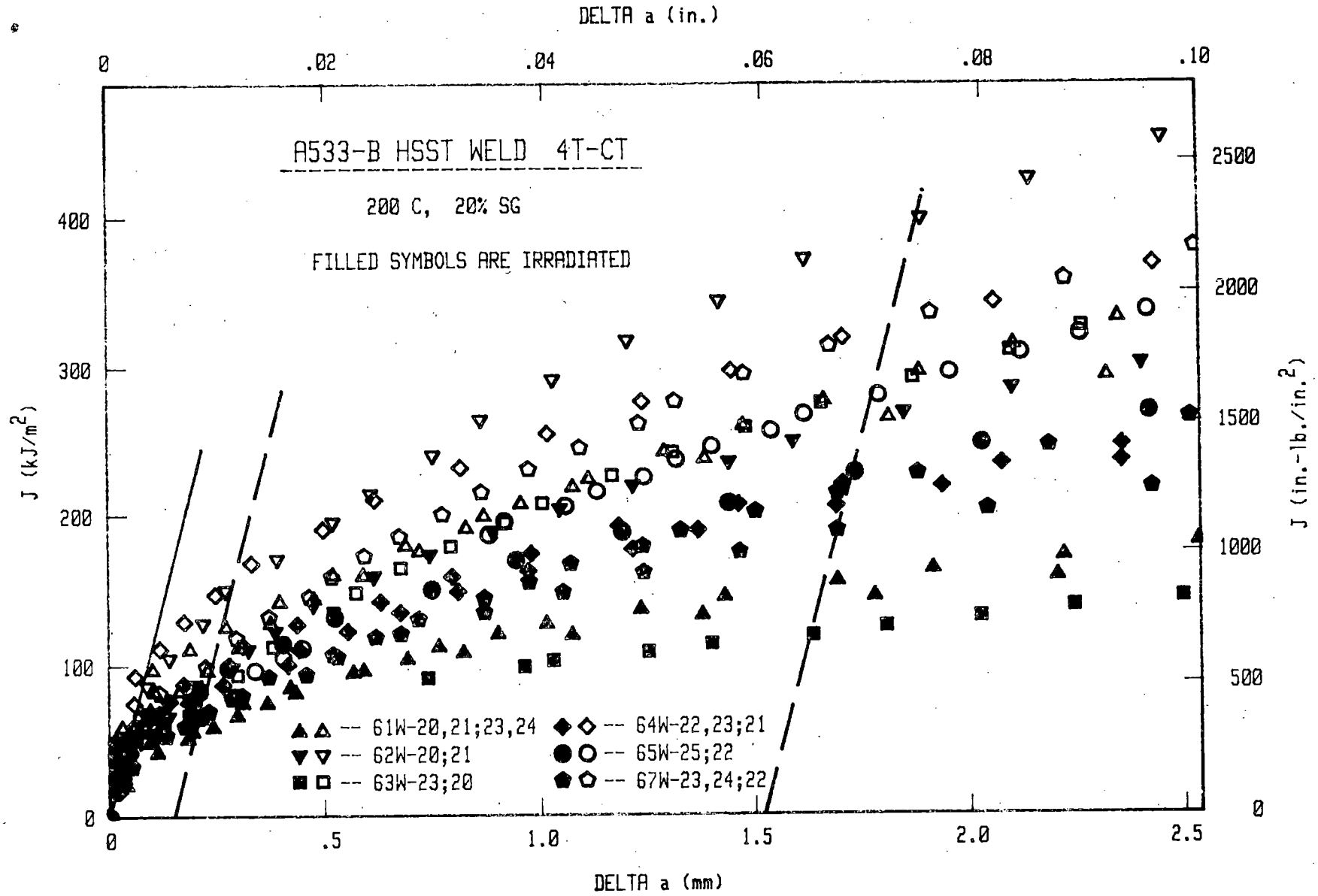

Fig. 7 - R curves from HSST welds tested in the upper shelf regime with 4T-CT specimens.

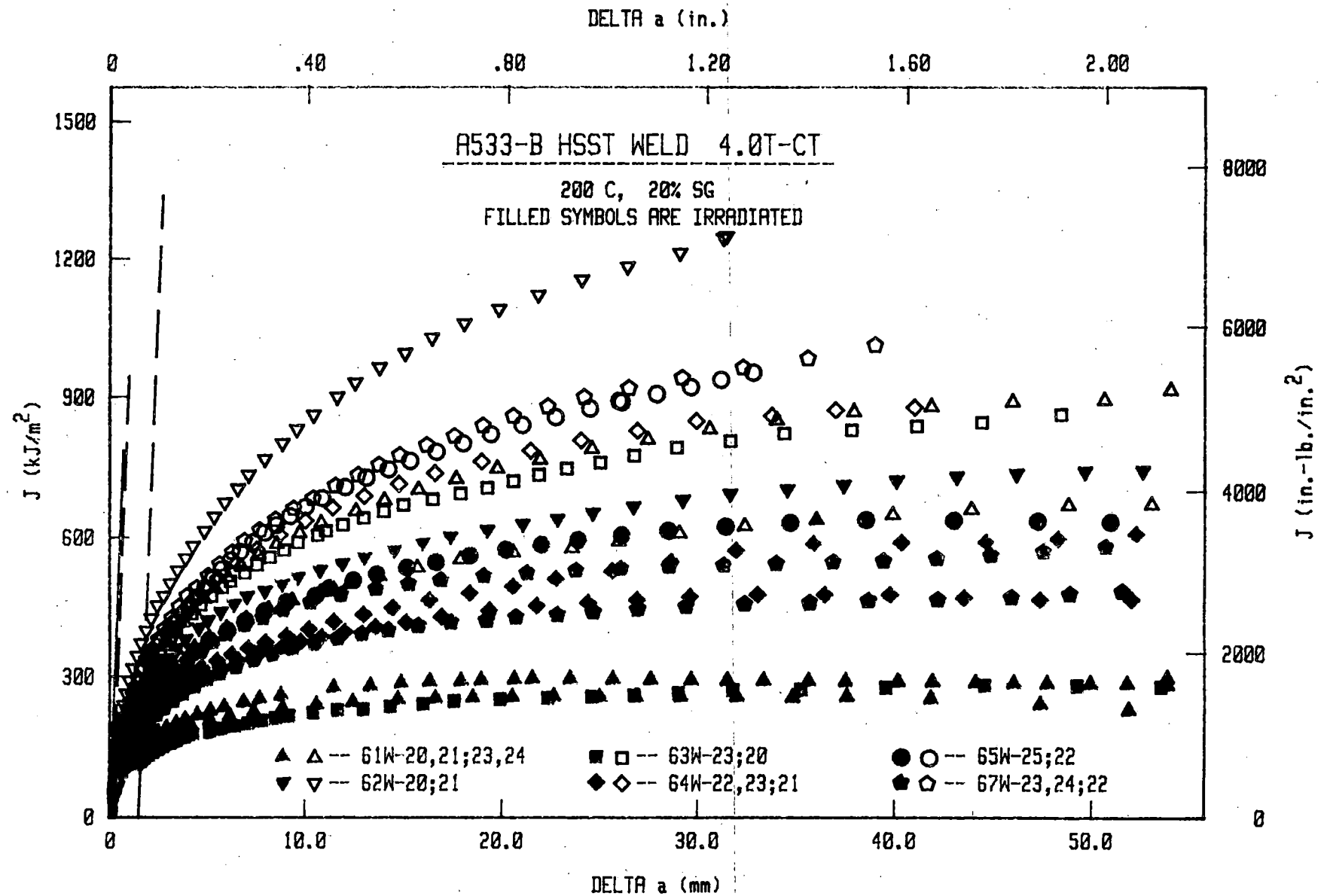

Fig. 8 - Pre- and post-irradiation R curve trends at long crack extension measured with 4T-CT specimens.

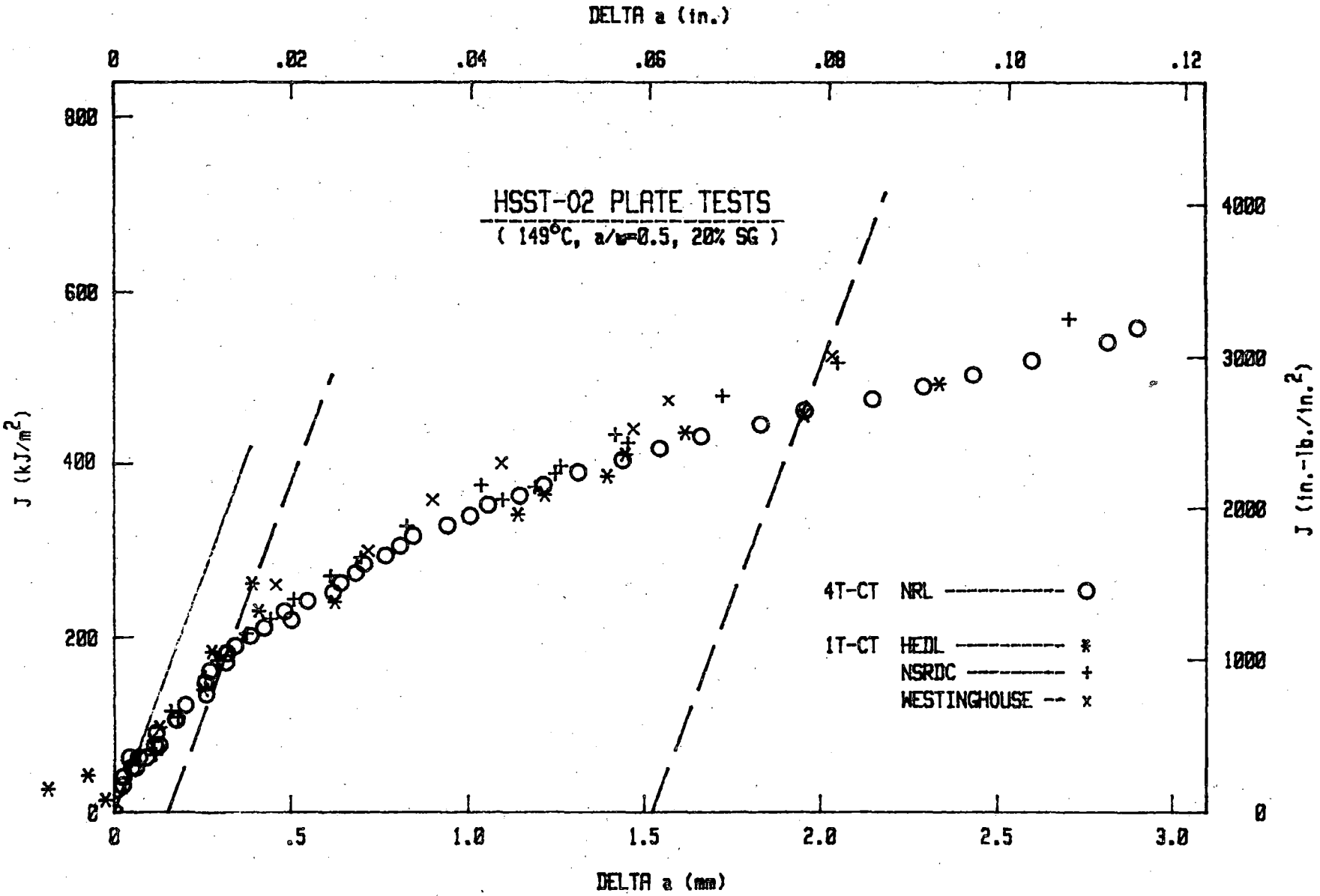

Fig. 9 - Comparison of R curves measured by four laboratories using different size specimens cut from a plate of A533-B steel.

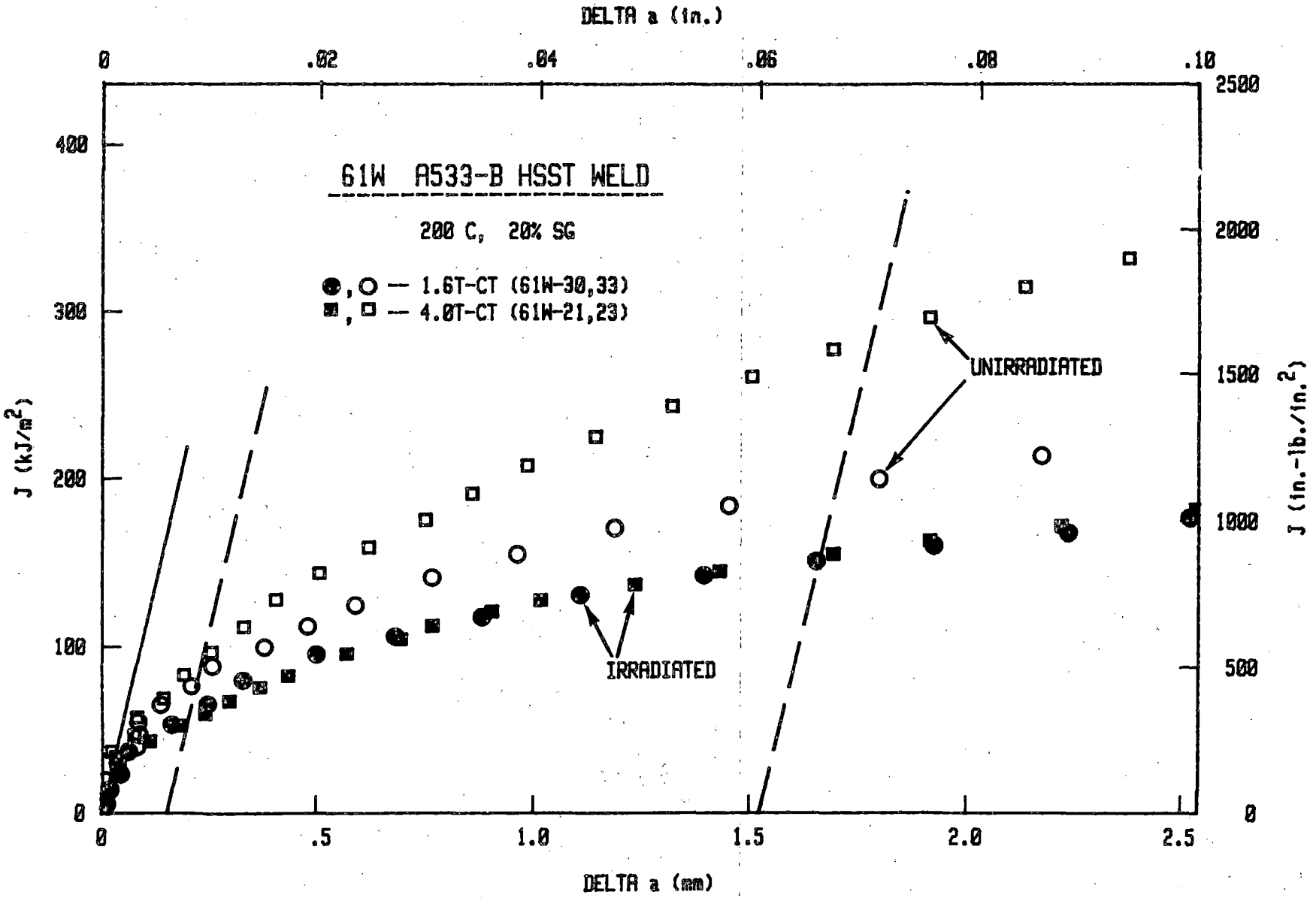

Fig. 10 - Comparison of R curves for HSST weld 61W in the pre- and post-irradiated condition with two specimen sizes. An apparent specimen size dependence is exhibited by the unirradiated material.

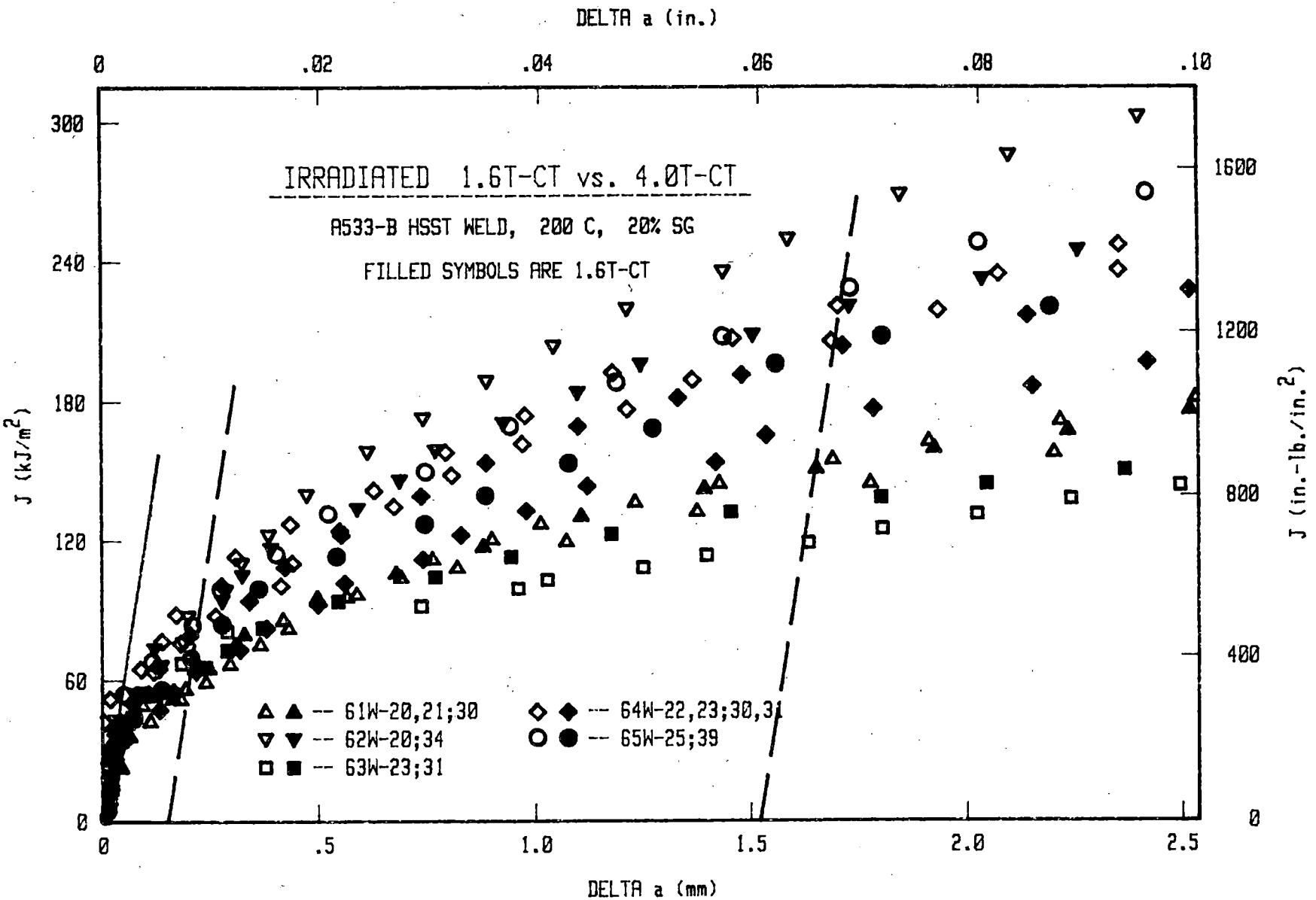

Fig. 11 - Comparison of R curves measured with 1.6T- and 4T-CT specimens for irradiated HSST welds. A general trend toward higher R curves is exhibited by the larger size specimens.

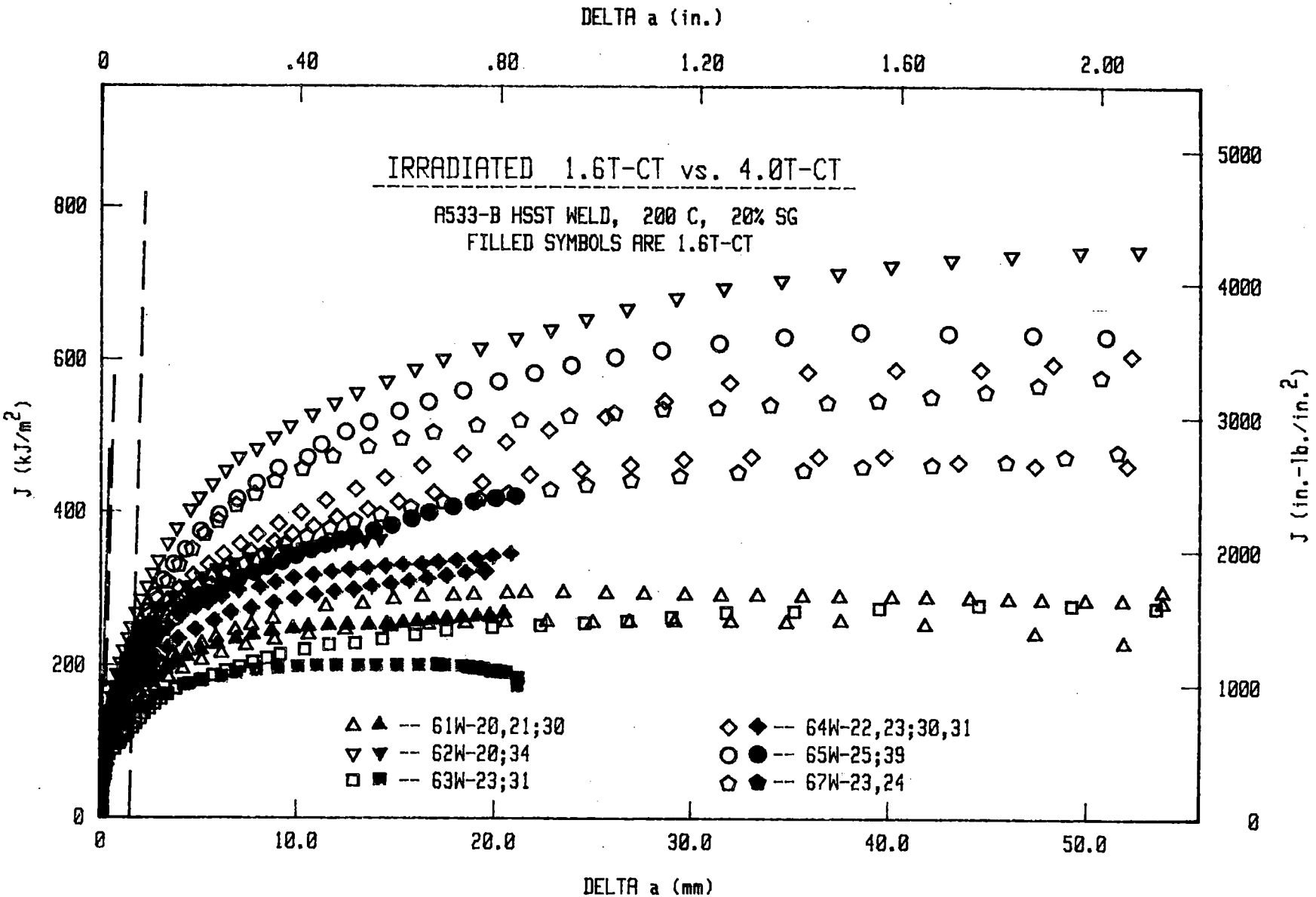

Fig. 12 - Comparison of R curves measured with 1.6T- and 4T-CT specimens at large crack extensions. The trend toward higher R curves by the larger specimen size is clear.

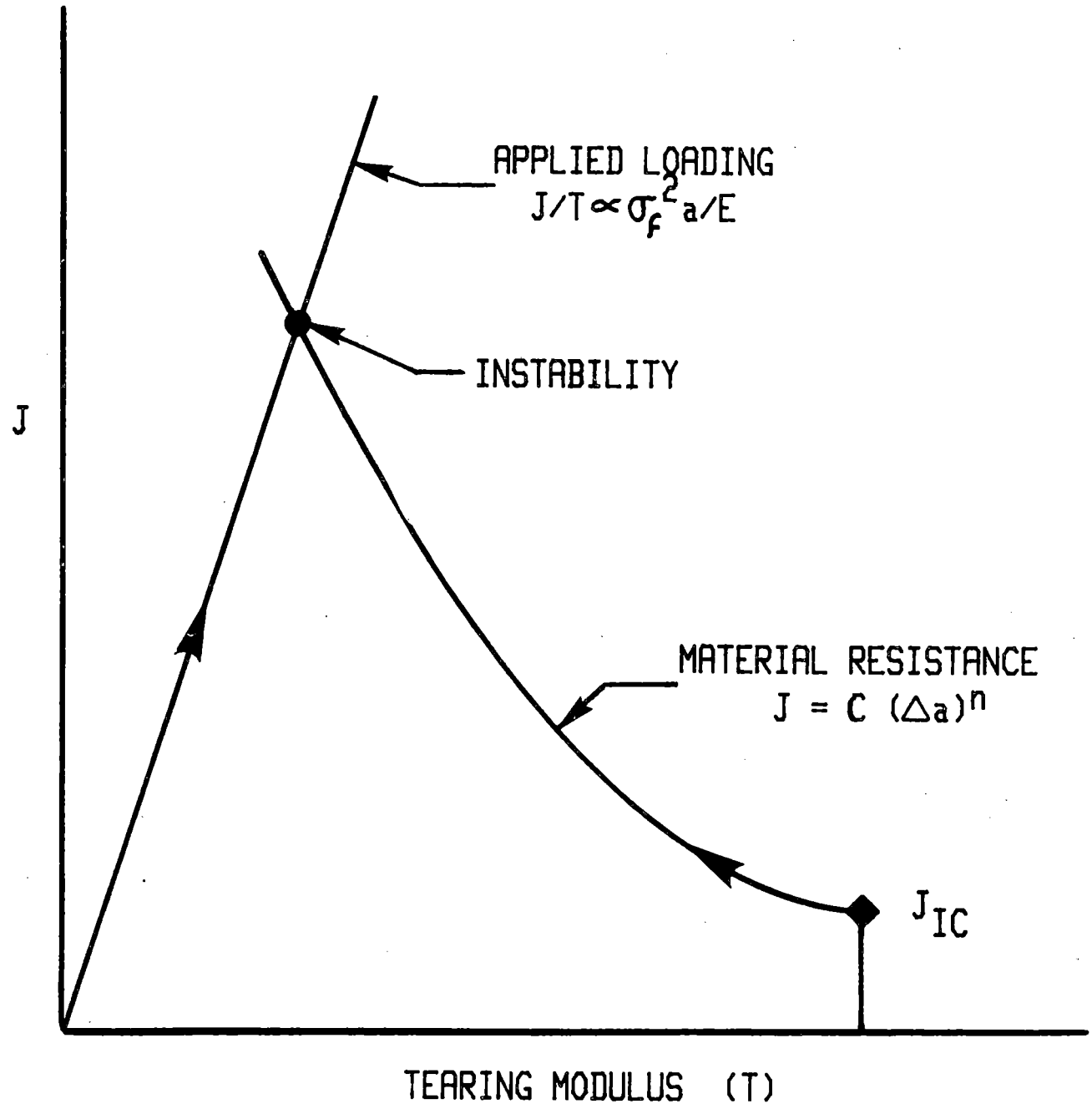

Fig. 13 - Instability diagram illustrating the interactions of material and structural parameters.

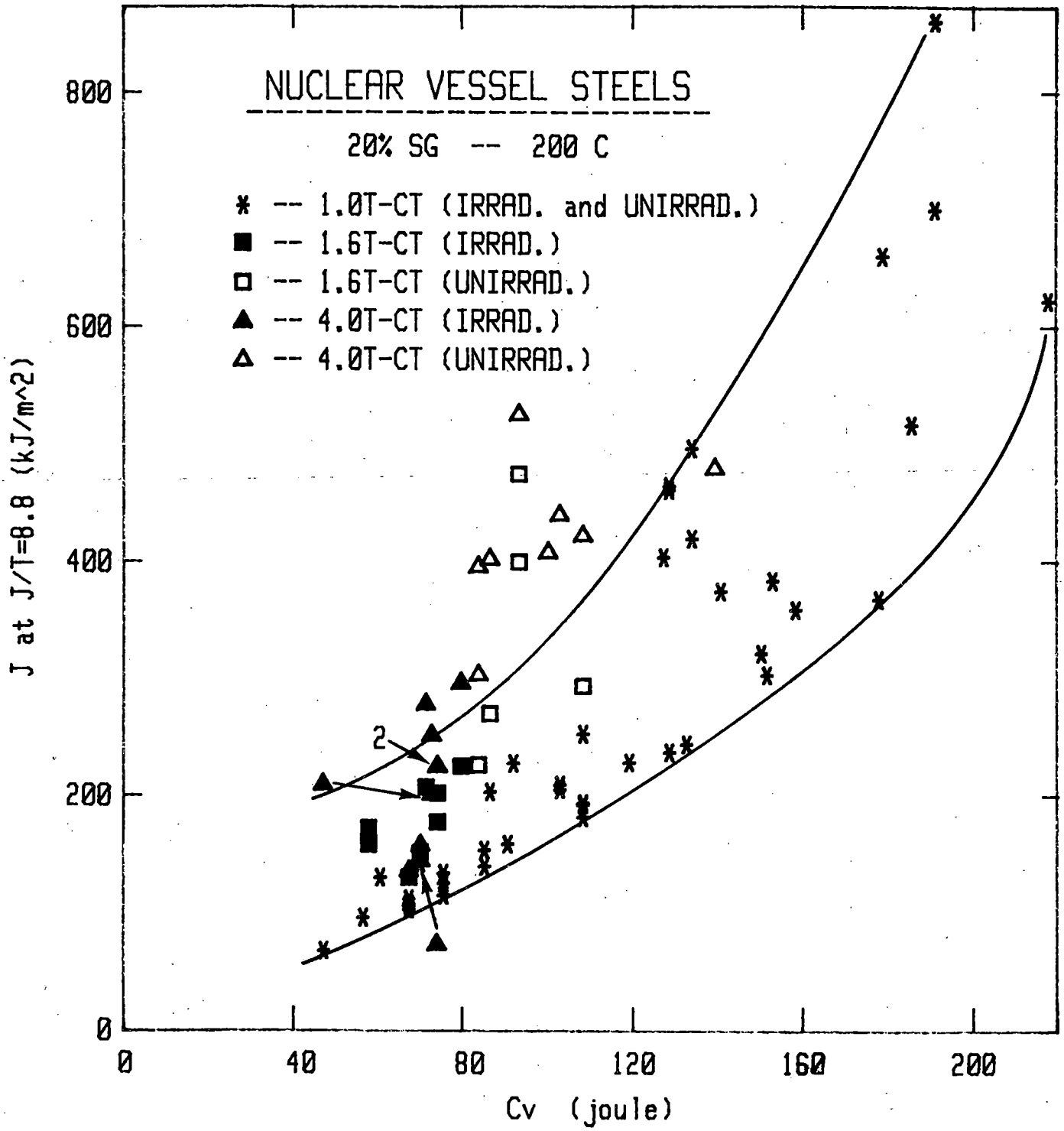

Fig. 14 - Correlation between C_v upper shelf energy and J at a fixed value of J/T.

CHARPY TOUGHNESS OF IRRADIATED HIGH COPPER WELDS*

R. G. BERGGREN

METALS AND CERAMICS DIVISION

OAK RIDGE NATIONAL LABORATORY

PRESENTATION TO

NINTH WATER REACTOR SAFETY RESEARCH

INFORMATION MEETING

OCTOBER 29, 1981

---

*Research sponsored by the Office of Nuclear Regulatory Research, Nuclear Regulatory Commission, under Interagency Agreements DOE 40-551-75 and 40-552-75 with the Department of Energy under contract W-7405-eng-26 with the Union Carbide Corporation.

SUMMARY

The Heavy-Section Steel Technology (HSST) irradiation program was initiated under NRC sponsorship to study fracture toughness of irradiated pressure vessel materials in the upper transition region and to investigate the applicability of small specimen test results to thick-section materials. The irradiation experiments contained fracture toughness specimens 4 in. thick (4T-CS) and a number of smaller specimens of "low-shelf" weldments. Temperatures at the crack fronts of the 4T-CS specimens were controlled during irradiation. Since the smaller specimens were installed in holes and crevices of the 4T-CS specimens, we were unable to independently control the irradiation temperatures of the smaller specimens. Thus, the smaller specimens were exposed to a varied neutron fluence and temperature history and analysis of test data is complex.

Charpy V-notch impact test results for weldments 61W through 67W are summarized in the table.

The figure shows considerable scatter of individual test results typical of most of these submerged-arc welds. In the table summarizing the results of Charpy impact tests, the "Observed Transition Temperature Shift" (estimated) is, in most cases, based on very few data points near the 30-ft-lb index and, therefore, should be considered an approximate value. The "Guideline Transition Temperature Shifts" are from Fig. 1 of NRC Regulatory Guide 1.99 (RG 1.99) with no adjustment for temperature of irradiation. No observed transition temperature shifts exceeded the guideline shifts. There is no discernible relationship of transition temperature shift

with median irradiation temperature. We tried a graphical study of this relationship and found no constant trend of transition temperature shift with median irradiation temperature.

The observed decreases in shelf energy were less than the guideline decreases from Fig. 2 of RG 1.99 in all but one case (HSST weld 65W). The sixth entry for weld 65W is a double entry: eight specimens gave a 24% (average) decrease of upper-shelf energy (less than the guideline value) but two specimens gave a 41% decrease of upper-shelf energy, which is in excess of the guideline value. Both specimens were from the same depth in the thick weldment and may represent an off-average weld pass.

F. W. Stallman has attempted statistical (computer) fitting of the Charpy data from HSST welds 61W through 67W. In these analyses, transition region data and upper-shelf data were analyzed separately by linear regression. The analyses conducted thus far assumed independent linear effects of fast neutron fluence, median irradiation temperature, and copper content about median values for each parameter and the results are presented in the summary table. Standard deviations for the coefficients in the transition temperature estimation were about 10% of the value of each coefficient. However, standard deviations for the coefficients in the upper-shelf energy estimation ranged from 10% for copper content to 83% for irradiation temperature.

SUMMARY OF CHARPY IMPACT DATA FROM THE SECOND AND THIRD HSST 4T-CT IRRADIATION EXPERIMENTS

Median Irradiation Temperature[a] (°F)	Fluence, 10^{18} n/cm^2 (E > 1 MeV)	Transition Temperature Shift, °F			Decrease in Shelf Energy, %		
		Observed[b]		Guideline[c]	Observed[b]		Guideline[c]
Weld 61W: 0.29% Cu Average (0.24–0.34)							
570[d]	9	[e]	179	260	21	31	42
570[d]	13	[e]	238	300	11	39	44
590	6	115	119	215	15	25	38
590	8	[e]	148	250	24	28	41
590	13	165	223	300	24	38	44
600	9	85	155	260	3	30	42
610	8.3		130	245		30	41
610	13	105	207	300	24	38	44
615	3	125	54	150	15	18	33
625	6	100	91	215	5–24[g]	24	38
650	3	75	27	150	17	17	33
Weld 62W: 0.21% Cu Average (0.16–0.26)							
510	8.5	110	190[f]	175	24	31	33
546[d]	6	125	125	145	17	25	31
560[d]	9.0		159	180		30	34
560[d]	13.5	140	226[f]	220	20	38	38
580	6	90	98	145	19	25	31
595	14	100	206	280	21	38	41
Weld 63W: 0.30% Cu Average (0.27–0.33)							
535[d]	9	180	210	260	29	33	42
555[d]	9	180	194	260	29	32	42
580	6	150	130	215	27	26	38
583	8.1		150	255		31	42
590	6	170	122	215	29	26	38
590	10	140	182	275	27	33	42
600	11	130	189	290	29	35	43
Weld 64W: 0.35% Cu Average (0.31–0.39)							
465	4.2	160	212	215	18–36[g]	26	38
525[d]	4.0	130	162	210	21–32[g]	24	37
540[d]	3.7	150	145	200	23	23	37
549[d]	3.6	170	137	200	27	23	37
551[d]	5.6	[e]	180	250	30	27	39

SUMMARY OF CHARPY IMPACT DATA FROM THE SECOND AND THIRD HSST 4T-CT IRRADIATION EXPERIMENTS
(Continued)

Median Irradiation Temperature[a] (°F)	Fluence, 10^{18} n/cm^2 (E > 1 MeV)	Transition Temperature Shift, °F			Decrease in Shelf Energy, %		
		Observed[b]		Guideline[c]	Observed[b]		Guideline[c]
Weld 65W: 0.22% Cu Average (0.18–0.25)							
523	3.3	[e]	107	110	28	21	28
532[d]	3.4	90	101	115	28	21	28
535[d]	3.3	70	97	110	13	21	28
537[d]	3.6		101	170		21	28
542[d]	4.1	80	104	125	23	22	29
543[d]	3.4	100	92	115	23–41[f,g]	21	28
546[d]	5.3	100	118	140	23	24	31
Weld 66W: 0.42% Cu Average (0.35–0.49)							
515	5.5	210	216	245	37	29	39
530[d]	5.0		199	235		28	38
535[d]	4.5	190	186	220	34	26	38
544[d]	5.8	150	198	250	27	29	40
Weld 67W: 0.27% Cu Average (0.22–0.32)							
517	3.8	[e]	136	155	17	23	33
534[d]	5.0		140	175		25	35
540[d]	4.5	150	128	175	18	24	34
543[d]	8	120	178	220	16	30	39

[a]Median irradiation temperature for total irradiation period.

[b]Left column indicates estimate from data plot, right column indicates statistical analysis of all data (welds 61W through 67W).

[c]From Fig. 1 or 2 of RG 1.99. Guideline values were not adjusted for irradiation temperature.

[d]These entries fall within the 550 ± 25°F range of RG 1.99.

[e]Insufficient data.

[f]This value exceeded RG 1.99.

[g]Dual entries indicate large spread in results.

ORNL-DWG 81-16082

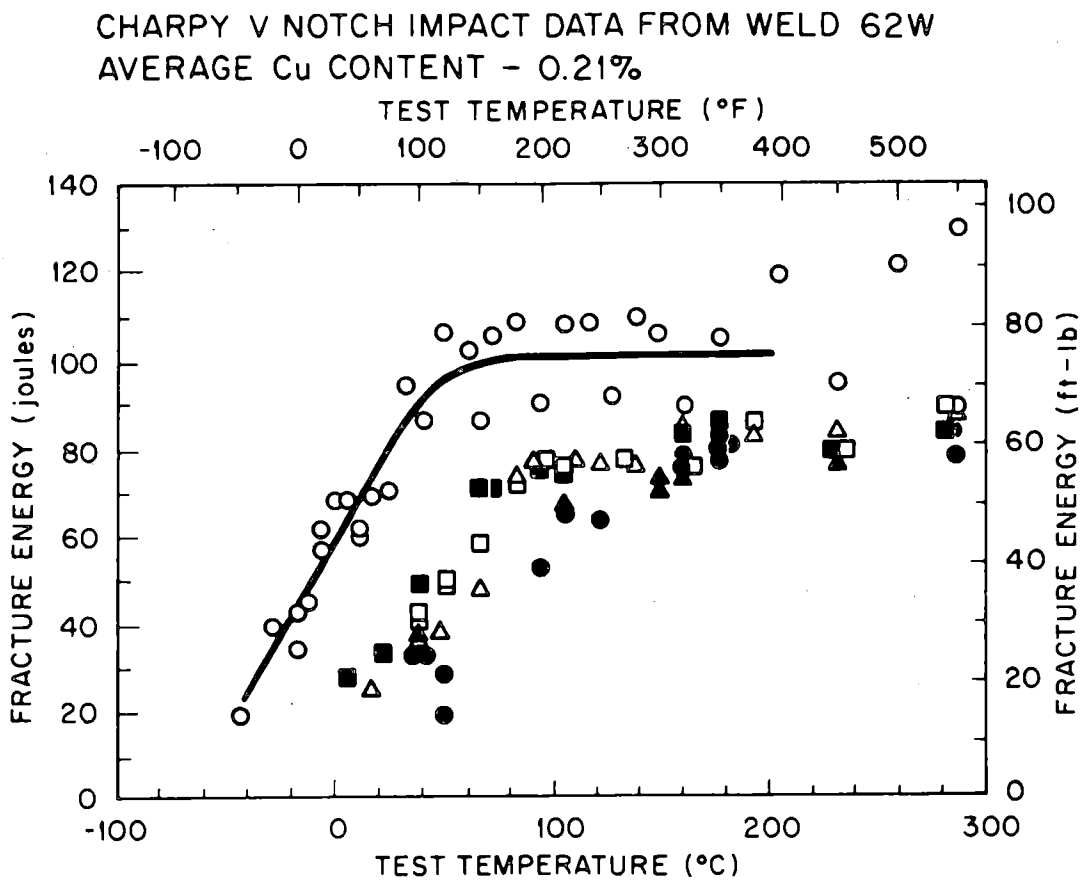

	MEDIAN IRRAD. TEMP. (°F)	FLUENCE 10^{18} n/cm^2 E > 1 MeV
○	UNIRRADIATED - (CONTROLS)	
▲	510	8.5
△	540	6
●	560	11-16
■	580	6
□	595	14

STUDIES IN SUPPORT OF IRRADIATION-ANNEALING-REIRRADIATION (IAR) INVESTIGATIONS AND RADIATION SENSITIVITY VARIABLES DETERMINATIONS

J. R. HAWTHORNE
Naval Research Laboratory

Presented to:

9th Water Reactor Information Meeting
of the
U. S. Nuclear Regulatory Commission

National Bureau of Standards
Gaithersburg, Maryland
29 October 1981

STUDIES IN SUPPORT OF IRRADIATION-ANNEALING-REIRRADIATION (IAR) INVESTIGATIONS AND RADIATION SENSITIVITY VARIABLES DETERMINATIONS

J. R. Hawthorne
Naval Research Laboratory

SUMMARY

High copper, high nickel content welds are the primary focus of attention in IAR investigations because of the high sensitivity to radiation-induced embrittlement shown by these pressure vessel materials. Questions of the nature of the nickel content contribution to radiation sensitivity development (and conceivably to postirradiation heat treatment response) have been raised in view of the significantly lower radia tion sensitivity levels reported for high copper, low nickel content welds.

This report describes a series of investigations in which the influence of progressive increases in nickel and copper content on irradiation and annealing response were determined. The study employed A302-B steel plates made from laboratory melts (split melt practice) having statistical variations in the content of the two elements. Notch ductility property changes with 288°C irradiation and with 399°C annealing served as the basis for intercomparisons. The results clearly show that an increase in nickel content from 0.3 to 0.7% elevates radiation sensitivity for 0.16% and 0.28% copper steels. More importantly, if viewed in conjunction with observations of low sensitivity in low copper, high (up to 1%) nickel content welds, the results confirm the suspected dependence of the nickel effect on copper content in radiation sensitivity development. In postirradiation annealing tests, an influence of nickel level on residual embrittlement level after 168 hr at 399°C was noted for the 0.28% Cu steel but not for the 0.16% Cu steel.

Mechanical property evaluations of materials from Surveillance Specimen Capsule No. 1 (SSC-1) irradiated in the ORNL Pool Side Facility by the LWR Pressure Vessel Surveillance Dosimetry Improvement Program are also reported. Very high radiation sensitivity was observed for one weld and underscores the importance of considering nickel content as well as copper content in making radiation embrittlement projections.

Finally, radiation embrittlement data for low copper content steels and welds from the IAEA Coordinated Program on Advanced Steels are reported. NRL observations confirm the adequacy of USA-developed specifications/guidelines for producing radiation resistant materials overseas and show further that the NRC Regulatory Guide 1.99 applies equally well to these materials.

SELECTED REFERENCES

1. J. R. Hawthorne, "Evaluations of IAEA Coordinated Program Steels and Welds for 288°C Radiation Embrittlement Resistance," presented to the IWG-RRPC Coordinated Program Review Meeting, Vienna, Austria, 22-23 October 1981, NRL MEMORANDUM Report 4655 (to be published).

2. J. R. Hawthorne, "Status of Knowledge of Radiation Embrittlement in USA Reactor Pressure Vessel Steels," presented to IAEA Specialists' Meeting on "Irradiation Embrittlement and Surveillance of Reactor Pressure Components," Vienna, Austria, 19-21 October 1981 (proceedings to be published).

TOPICS

- DEMONSTRATION OF Ni + Cu INTERACTION RADIATION SENSITIVITY
- OBSERVATIONS ON ANNEALING VARIABLES
- PRESSURE VESSEL IRRADIATION SURVEILLANCE DOSIMETRY PROGRAM
- IAEA COOPERATIVE PROGRAM ADVANCED STEELS, WELDS

Ni + Cu INTERACTION STUDY

OBSERVATIONS

HIGH NICKEL, HIGH COPPER - HIGH SENSITIVITY

HIGH NICKEL, LOW COPPER - LOW SENSITIVITY

OBJECTIVE

TEST FOR Ni + Cu INTERACTION

APPROACH

LABORATORY MELTS

STATISTICAL Ni + Cu COMBINATIONS

288^{o}C IRRADIATION

NICKEL CONTENT vs RADIATION SENSITIVITY
(NICKEL + COPPER INTERACTION)

	%Ni	%Cu	
MELT 1 (A302-B)			
	.05	.05	
	.30	.05	
	.30	.15	
	.70	.15	
MELT 2 (A302-B)	.05	.30	
	.30	.30	
	.70	.30	
	.70	.30	(+ .35%Si)

POSTIRRADIATION FINDINGS (MELT 2)

EXPOSURE CONDITION - 2.6×10^{19} N/CM^2 AT 288^{0}C

%Ni	ΔC_V 41J (^{0}C)	ΔC_V USE (J)
.05	86	30
.30	81	30
.70	108	48
.70 (+ .35%Si)	103	41

.28%Cu AND .22%Si BASE COMPOSITION

POSTIRRADIATION FINDINGS (MELT 1)

EXPOSURE CONDITION - 2.4×10^{19} N/CM^2 AT 288°C

%Ni	ΔC_V 41J (°C)	ΔC_V USE (J)
.05	17	~ 0
.30	17	~ 0
.30 (+ .16%Cu)	64	~ 0
.70 (+ .16%Cu)	89	~ 0

.005%Cu and .21%Si Base Composition

NICKEL + COPPER + PHOSPHORUS INTERACTION STUDY

(NRL/HEDL COOPERATIVE)

MELT	CAST	%Ni	%Cu	%P
7	A	.70	.05	.005
	B	.70	.05	.015
	C	.70	.05	.026
8	A	.70	.30	.005
	B	.70	.30	.015
	C	.70	.30	.026

POSTIRRADIATION ANNEALING (399°C-168 HR)*

(Ni + Cu INTERACTION STUDY)

PLATE	RECOVERY (ΔT_{41J})	RESIDUAL (ΔT_{41J})	RECOVERY (% USE)
.16 Cu, .27 Ni	47	17	~100
.16 Cu, .68 Ni	67	22	~100
.28 Cu, .05 Ni	58	28	~100
.28 Cu, .27 Ni	58	28	~100
.28 Cu, .69 Ni	67	42	~100

*After 2.4 to 2.6 x 10^{19} at 288°C

POSTIRRADIATION ANNEALING OBSERVATIONS

(A533-B STEEL - 0.20 Cu, 0.63 Ni)

EXPOSURE - $\sim 2 \times 10^{19}$ N/CM^2 AT 288^{0}C

OBSERVATIONS	ΔT (^{0}C)	ΔUSE (J)
AS IRRADIATED	117	54
ANNEALED		(RECOVERY)
399^{0}C - 24 HR	72 (62%)	30
399^{0}C - 168 HR	89 (76%)	54
427^{0}C - 168 HR	100 (85%)	54

LWR - PVI SURVEILLANCE DOSIMETRY IMPROVEMENT PROGRAM

- MOCKUP - REACTOR VESSEL + THERMAL SHIELD
- POOL SIDE FACILITY (PSF) - ORR REACTOR
- NEUTRON DOSIMETRY
- MECHANICAL PROPERTIES

NRL RESPONSIBILITIES
(PSF IRRADIATIONS)

- REFERENCE MATERIALS
- MECHANICAL PROPERTIES
- PRE-POSTIRRADIATION TESTING
  (Cv, CT, TENSILE)

SURVEILLANCE SPECIMEN CAPSULE NO. 1 (SSC-1)

(LWR-PVI SURVEILLANCE DOSIMETRY PROGRAM)

EXPOSURE - $\sim 2 \times 10^{19}$ N/CM^2 AT 288^{0}C

	MATERIAL	ΔT (41J)	ΔT (0.9 MM)	ΔUSE (J)
(NRL)	A533-B (HSST 03)	61	69	35
(NRL)	A302-B (ASTM REF)	78, 86	83, 94	14, 31
(EPRI)	A533-B WELD .22 Cu	108	119	34
(RR)	A533-B WELD .24 Cu, 1.58 Ni	222	-*	99
(MOL)	A508-3 .05 Cu, .75 Ni	19	19	0
(KFA)	22NiMoCr37 .12Cu, .96Ni	61	67	43

*NOT DETERMINED.

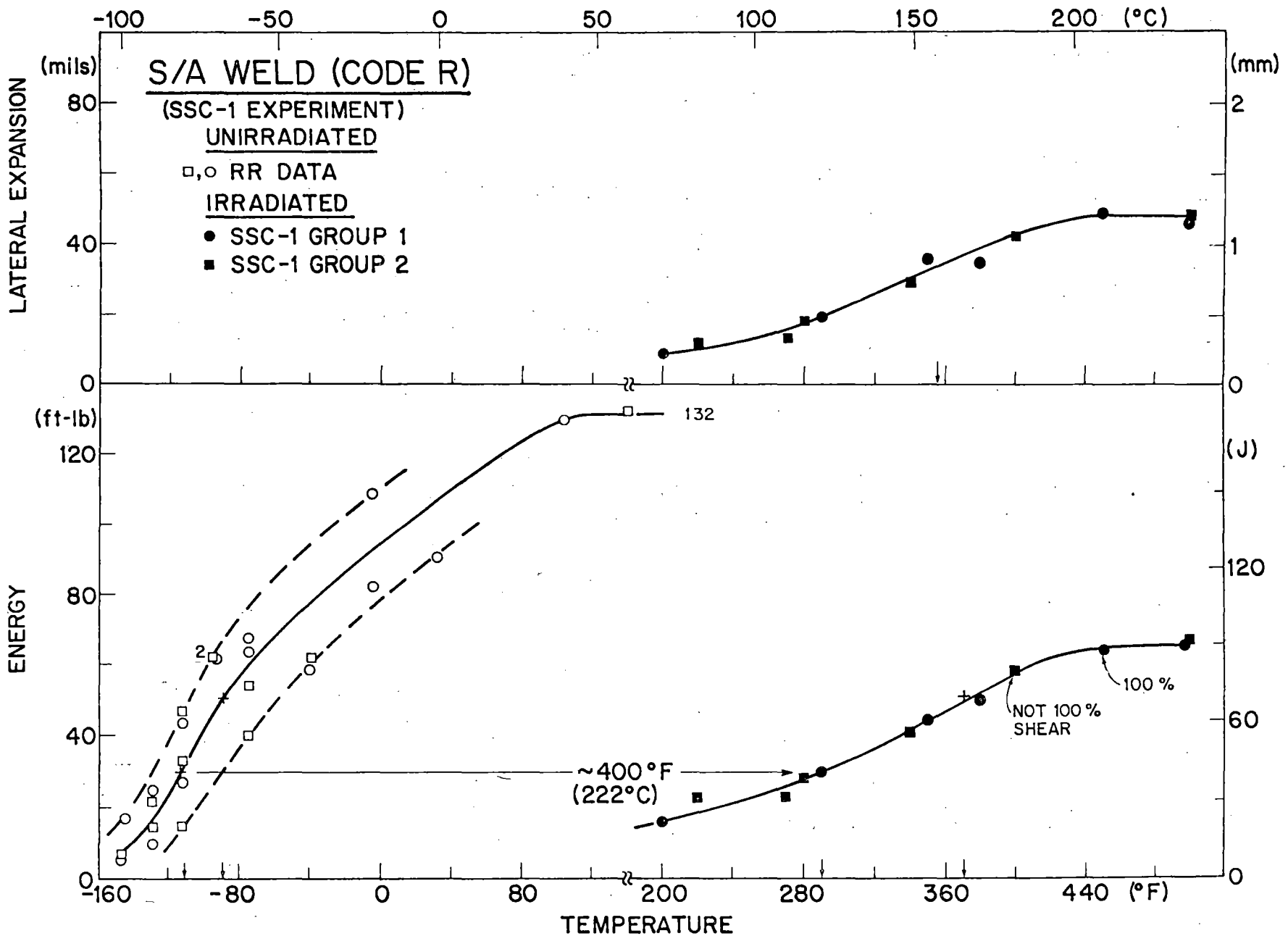
S/A WELD (CODE R)
(SSC-1 EXPERIMENT)
UNIRRADIATED
□,○ RR DATA
IRRADIATED
● SSC-1 GROUP 1
■ SSC-1 GROUP 2
LATERAL EXPANSION
(mils)
(mm)
ENERGY
(ft-lb)
(J)
132
~400°F
(222°C)
NOT 100 % SHEAR
100 %
TEMPERATURE
(°C)
(°F)

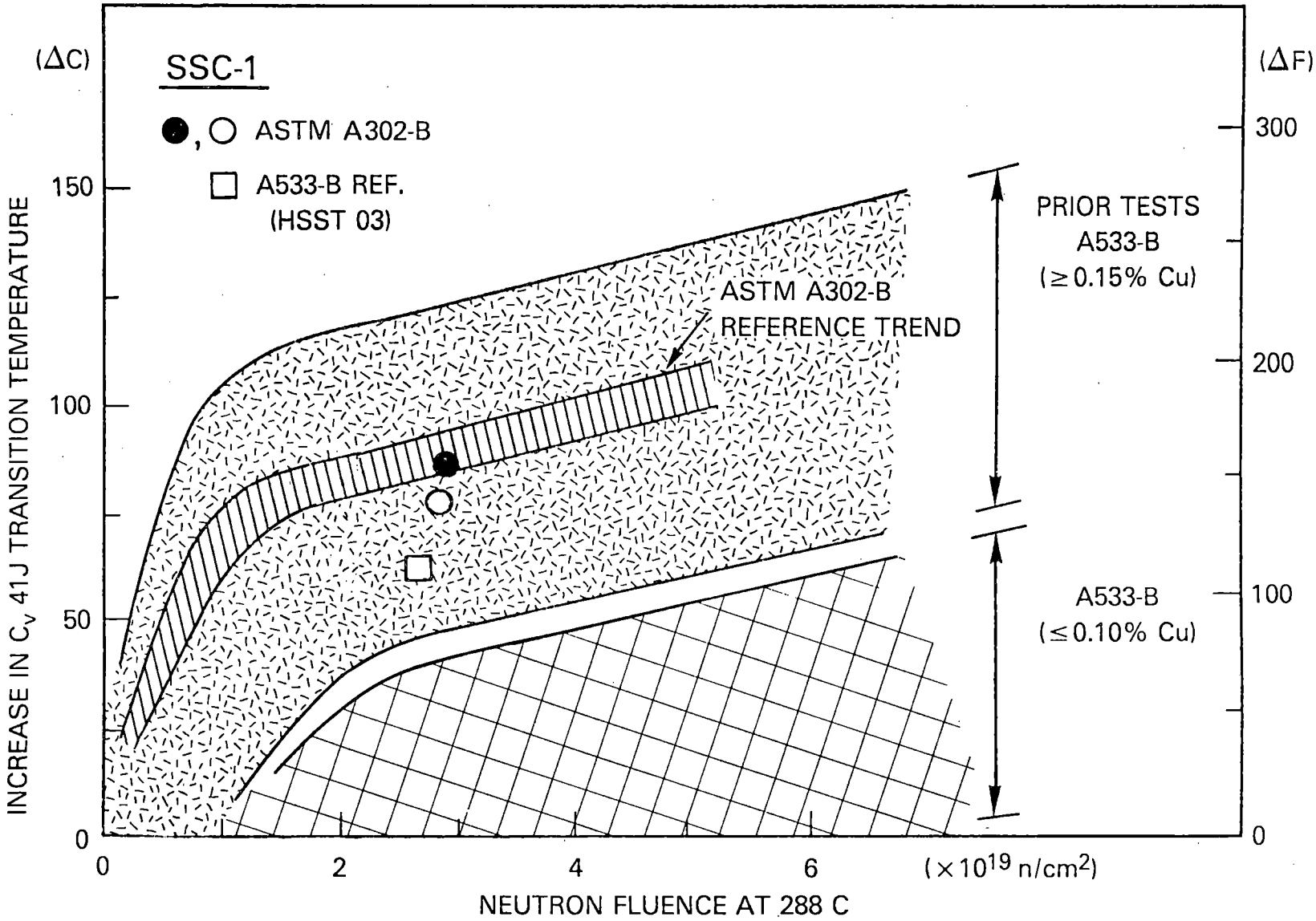
SSC-1
(ΔC)
(ΔF)
● , ○ ASTM A302-B
□ A533-B REF.
(HSST 03)
ASTM A302-B
REFERENCE TREND
PRIOR TESTS
A533-B
(≥ 0.15% Cu)
A533-B
(≤ 0.10% Cu)
INCREASE IN C_v 41J TRANSITION TEMPERATURE
NEUTRON FLUENCE AT 288 C
(×10^19 n/cm^2)
0
50
100
150
200
300
2
4
6

LWR PVI SURVEILLANCE DOSIMETRY PROGRAM

STATUS

UNIRRADIATED REF. TESTS

C_V, T, CT - COMPLETED

SSC-1 CAPSULE TESTS

C_V - COMPLETED

CT, T - UNDERWAY

SSC-2 CAPSULE

DISCHARGED REACTOR

IWG-RRPC OBJECTIVES

- ADEQUACY SPECIFICATIONS/GUIDELINES FOR IMPROVED RADIATION RESISTANCE

- CAPABILITY FOR ROUTINE PRODUCTION RADIATION RESISTANT PLATE, WELD, FORGING

NRL ADDITIONAL OBJECTIVES

- COMPARISON NON-USA vs USA PRODUCTION

- APPLICABILITY NRC REG GUIDE 1.99 TO OVERSEAS MATERIALS

IWG - RRPC PROGRAM MATERIALS

MATERIAL[A]	SUPPLIER	%Cu	%P	%Ni
S/A WELD	FRG	.03	.011	.93
PLATE	FRANCE	.03	.007	.65
FORGING	FRANCE	.07	.009	.69
S/A WELD	FRANCE	.06	.011	.73
PLATE	JAPAN	.01	.007	.66
FORGING	JAPAN	.04	.007	.76
S/A WELD	JAPAN	.04	.008	.89
(BASE PLATE)	JAPAN	(NOT AVAILABLE)		
PLATE (HSST 03, A533-B)	USA	.12	.011	.56

[A] SULFUR CONTENT, .002-.011%

NRL INVESTIGATIONS

(IWG-RRPC MATERIALS)

- NOTCH DUCTILITY, FRACTURE TOUGHNESS
- C_V, PCC_V TEST METHODS
- 288^0C IRRADIATIONS (TEST REACTOR UBR)
  $\sim 2 \times 10^{19} N/CM^2$ ($E > 1$ MEV)

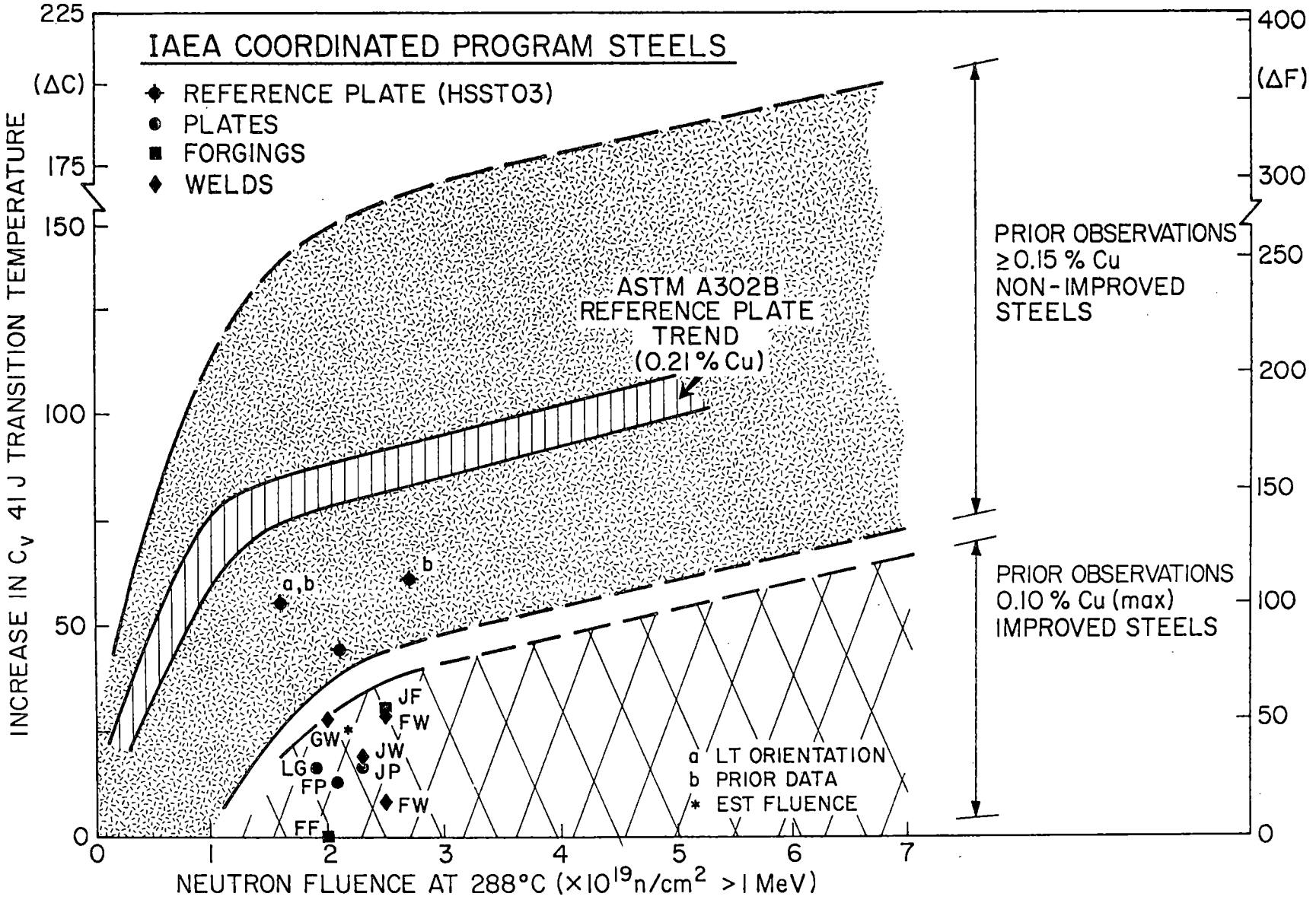
IAEA COORDINATED PROGRAM STEELS
REFERENCE PLATE (HSST03)
PLATES
FORGINGS
WELDS
ASTM A302B
REFERENCE PLATE
TREND
(0.21 % Cu)
PRIOR OBSERVATIONS
≥ 0.15 % Cu
NON-IMPROVED
STEELS
PRIOR OBSERVATIONS
0.10 % Cu (max)
IMPROVED STEELS
a LT ORIENTATION
b PRIOR DATA
* EST FLUENCE
a,b
b
JF
FW
GW
JW
LG
JP
FP
FW
FF
INCREASE IN C_v 41 J TRANSITION TEMPERATURE
(ΔC)
(ΔF)
225
175
150
100
50
0
400
300
250
200
150
100
50
0
0
1
2
3
4
5
6
7
NEUTRON FLUENCE AT 288°C ($\times 10^{19}$ n/cm^2 >1 MeV)

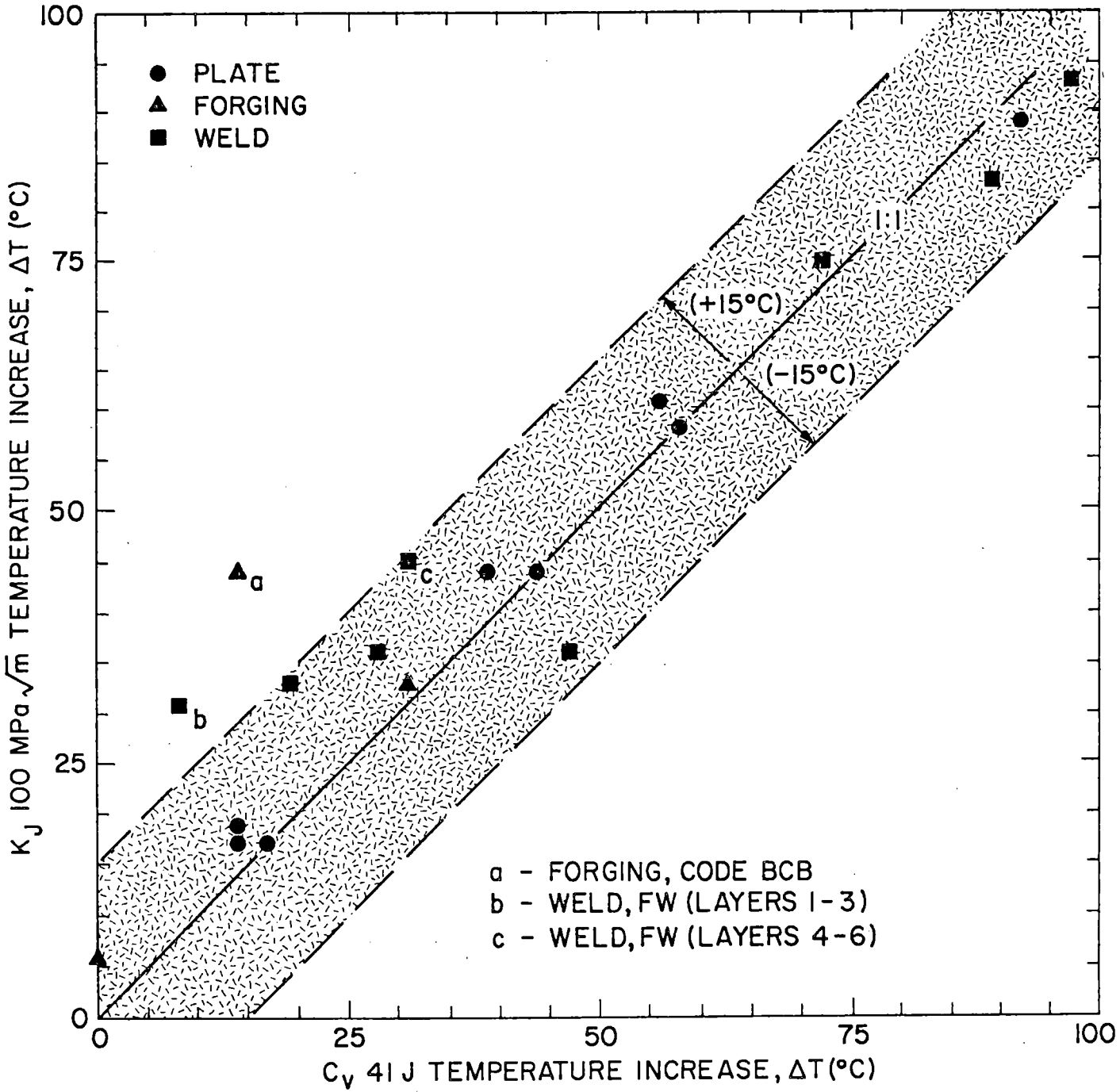
PLATE
FORGING
WELD
1:1
(+15°C)
(-15°C)
a
b
c
a - FORGING, CODE BCB
b - WELD, FW (LAYERS 1-3)
c - WELD, FW (LAYERS 4-6)
K_J 100 MPa$\sqrt{m}$ TEMPERATURE INCREASE, ΔT (°C)
C_V 41 J TEMPERATURE INCREASE, ΔT (°C)
0
25
50
75
100

HEDL-SA 2546

SURVEILLANCE DOSIMETRY OF OPERATING POWER PLANTS

W. N. McElroy, A. I. Davis, R. Gold, G. L. Guthrie, L. S. Kellogg, A. C. Leaf, E. P. Lippincott, D. L. Oberg, F. A. Schmittroth and R. L. Simons (HEDL); F. B. K. Kam, R. E. Maerker and F. W. Stallmann (ORNL); J. A. Grundl and E. D. McGarry (NBS); A. Fabry and H. Tourwe (CEN/SCK); H. Farrar IV and B. M. Oliver (RI).

October 16, 1981

For Presentation at the

NRC 9th Water Reactor Safety Information Meeting

October 26-31, 1981

NBS, Washington, DC

HANFORD ENGINEERING DEVELOPMENT LABORATORY
Operated by Westinghouse Hanford Company, a subsidiary of Westinghouse Electric Corporation, under the Department of Energy Contract No. DE-AC14-76FF02170
P.O. Box 1970, Richland, Washington 99352

SURVEILLANCE DOSIMETRY OF OPERATING POWER PLANTS

W. N. McElroy, A. I. Davis, R. Gold, G. L. Guthrie, L. S. Kellogg, A. C. Leaf, E. P. Lippincott, D. L. Oberg, F. A. Schmittroth, and R. L. Simons (HEDL); F. B. K. Kam, R. E. Maerker and F. W. Stallmann (ORNL); J. A. Grundl and E. D. McGarry (NBS); A. Fabry and H. Tourwe (CEN/SCK); H. Farrar IV and B. M. Oliver (RI).

SUMMARY OVERVIEW

General Design Criterion 31 of Appendix A, "General Design Criteria for Nuclear Power Plants," to 10 CFR Part 50,[1] "Domestic Licensing of Production and Utilization Facilities," requires, in part, that the reactor coolant pressure boundary be designed with sufficient margin to ensure that, when stressed under operating, maintenance, testing, and postulated accident conditions, 1) the boundary behaves in a nonbrittle manner and 2) the probability of rapidly propagating fracture is minimized. Appendix G, "Fracture Toughness Requirements," and Appendix H, "Reactor Vessel Material Surveillance Program Requirements," necessitate the prediction of the amount of radiation damage to the reactor vessel of water-cooled power reactors throughout their service life.

With reference to the United States Nuclear Regulatory Commission (NRC) Regulatory Guide 1.99, Revision 1,[2]* the two main measures of radiation damage are the adjusted reference nil-ductility temperature RT_{NDT} (RT_{NDT} initial + ΔRT_{NDT}) and the decrease in upper-shelf energy level determined from Charpy V notch impact tests. The current measures of neutron exposure most commonly used are fluence > 1 MeV and displaced atoms (dpa).

One category of postulated accidents, thermal shock, is the result of loss of pressure vessel (PV) coolant with the subsequent introduction of colder emergency cooling water, which comes in contact with the inner surface of the initially hot (~550°F) vessel.[3] The resulting decrease in temperature and the development of high thermal stresses at the inner surface introduces the possibility of propagation of pre-existing inner-surface flaws. Figure 1 is a block diagram for a computer code, OCA-I, which was recently developed for calculating the behavior of flaws on the inner surface of a pressure vessel subjected to temperature and pressure transients.[4]

*This is identified as Regulatory Guide 1.99.1 throughout the text.

Of immediate interest for this paper are the surveillance program requirements and what is being done to obtain and document needed information related to: 1) the inner surface neutron fluence (F_0), 2) the 1/4 T neutron fluence, 3) flux levels and fluence and dpa gradients in the PV, 4) the PV steel initial reference nil-ductility temperature, RT_{NDT_0}, and 5) the steel property trend curves of ΔRT_{NDT} and the upper shelf energy decrease versus the fluence (and dpa) derived from test reactor and power reactor surveillance programs.

The NRC established the Light Water Reactor Pressure Vessel (LWR-PV) Surveillance Dosimetry Improvement Program in 1977 to improve, standardize and maintain dosimetry, damage correlation and the associated reactor analysis procedures used for predicting the integrated effects of neutron exposure to LWR-PVs. About the same time, the Electric Power Research Institute (EPRI) established its own experimental and analytic Dosimetry Program.[7] The objective of the program has been to carry out measurements in operating power reactors for use in benchmarking new and improved methods of physics-dosimetry analysis. Of particular interest for both the EPRI and NRC programs has been the development of advanced physics-dosimetry methodologies based on least-squares adjustment procedures.[5,8] A brief overview of these and related programs and an overall program status report are provided in References 5 and 6, respectively. More complete information on the EPRI program work is provided in References 7 and 8. Major benchmark test facilities used or being established for this interlaboratory program work are discussed in References 5 through 8. In Table 1, these as well as other key benchmarks are identified along with the development time frame, participants, and their intended purpose and use. In addition to those in other countries, there are three main US programs to measure the fracture toughness and Charpy properties of irradiated materials, principally high-copper, submerged-arc weldments: 1) the NRC-funded Heavy-Section Steel Technology (HSST) Program, 2) the program funded by the Babcock & Wilcox (B&W) Owners' Group, and 3) the EPRI program.[9]

The main focus of the research efforts presently underway is the LWR power reactor surveillance program in which metallurgical test specimens of the reactor PV and dosimetry sensors are placed in three or more surveillance capsules at or near the reactor PV inner wall. They are then irradiated in a temperature and neutron flux-spectrum environment as similar as possible to the PV itself for periods of about 1.5 to 15 effective full-power years (EFPY)*, with removal of the last capsule at a fluence corresponding to the 30- to 40-year plant end-of-life (EOL) fluence. Because the neutron flux level at the surveillance position is greater than at the vessel, the test is accelerated with respect to the vessel exposure, allowing early assessment of EOL conditions.

*For a surveillance capsule location with a lead factor of ~3, where the lead factor is the ratio of fluence (E > 1 MeV) at the surveillance location to that at the PV wall, see Table 5.

The surveillance capsule metallurgical and dosimetry results are used to verify and/or adjust the final safety analysis report's (FSAR) current and EOL projections of changes in the fracture toughness and embrittlement condition of the PV steel. As discussed in Regulatory Guide 1.99.1 and Reference 9, the derived plant-specific PV steel wall condition is used together with other information to determine the allowable pressure-temperature operating curve to be used for continued operation of the power plant. If however, the RT_{NDT} of the PV steel shifts from an initial beginning-of-life (BOL) value (usually in the range of -50° to 50°F) to a much higher value (in the range above 200°F) as a result of neutron radiation damage, it may be necessary to take corrective action; such as annealing the reactor PV, to obtain a lower operating RT_{NDT} value (i.e., to regain fracture toughness and ductility).* Consideration of other options, such as those involved in changes in the core power distribution to reduce the PV wall neutron exposure rate may also be necessary.

It is currently accepted that uncertainties in the reported values of the neutron exposure parameters of fluence > 0.1 and > 1.0 MeV and dpa should be in the range of ±10% to 30% (1σ).[10-15] To achieve such accuracy on a routine basis, however, it has now been well demonstrated that the reactor physics calculational and dosimetry measurement techniques must be benchmarked [i.e.,verified at the ±5% to 15% (1σ) level.][5,6] This is shown graphically in Figure 2 where the estimated exposure parameter uncertainty range for FSAR and surveillance capsule reports is plotted versus time in years. The dramatic effect (in 1980 to 1981) of proper standardization and benchmarking is apparent, and it is expected that goal accuracies (±10% to 30%) will be routinely achievable after 1985. Thereafter, and depending on the need, some improvement in accuracy may be achieved; but no better than a ±10% to 20% (1σ) level of uncertainty is anticipated.

PROGRAM RESULTS

Figures 2 through 10 and Tables 1 through 14 provide summary highlight information related to surveillance dosimetry for operating power plants, most of which was developed as a result of multilaboratory work during 1981. As appropriate, comments are provided on individual Figures and Tables. In Table 15, an effort has been made to provide a summary of the procedures and requirements for LWR-PV embrittlement surveillance analysis. More detailed comments, information and justification for the present interlaboratory work will be found in two added reference sections on "Surveillance Dosimetry Accuracy Requirements" and "Program Direction and Status."

---

*Here and in Regulatory Guide 1.99.1, RT_{NDT} is used as a measure of PV steel ductility while upper shelf energy is used as a measure of toughness; clearly, it is the steel ductility and toughness that is of concern, not the actual values of RT_{NDT} and upper shelf energy. More information will be found on this subject in Reference 9, where it is concluded that embrittlement limits should be expressed in terms of fracture toughness, not in terms of Charpy impact energy.

SURVEILLANCE DOSIMETRY ACCURACY REQUIREMENTS

The use of RT_{NDT} data for base, heat-affected zone, and weld metal provides overall guidelines for the level of accuracy required of both metallurgy and physics-dosimetry. The uncertainties associated with the determination of RT_{NDT} continue to be studied.[9,14-16] Included in the physics-dosimetry work is not only surveillance capsule but ex-vessel dosimetry for derived values of exposure parameters. Two distinct uses or applications (cases) of RT_{NDT} data can be considered, namely:

1) Plant Safety -- What are the implications of current regulations for accuracy on RT_{NDT} and exposure parameter (fluence > 0.1 and > 1.0 MeV, and dpa) determinations?

2) Standards Development -- What current accuracy is required for the development of standards, procedures, and data needed to define spatial (lead factor) and exposure time (trend curve) extrapolations? These procedures and data are or will be given in Regulatory Guide 1.99.1 and a number of ASTM Standards[10] (Figures 3 and 4); particularly I-C through I-H, II-A through II-F, and III-A through III-E, which are under development.

For Case One, Figure 5, Plant Safety demands a high level of accuracy [generally at a 95% (2σ) or better confidence level] for the exposure parameter variables to avoid premature judgment that controlling property change limits have been reached or surpassed.* Improvement in the accuracy of reported values of the fluence (E > 0.1 and > 1.0 MeV) and dpa variables offer the principal opportunity for avoidance of premature action, since it is currently not possible to reduce the uncertainty on the RT_{NDT} variable (at a fixed position in the PV wall, such as at the surface or 1/4 T locations) below $\sim\pm30°F(2\sigma)$.[14-16] This latter value is typical for a power plant weld metal with a RT_{NDT} value of 100°F after ~5 EFPY of plant operation with a PV inner surface fluence (E > 1.0 MeV) of $\sim6.0 \times 10^{18}$ n/cm^2. This example is based on a weld material with a high nickel and a 0.15% Cu and 0.012% P content and an initial RT_{NDT_o} of 0°F. Based on Pool Critical Assembly/Poolside Facility (PCA/PSF) and recent surveillance capsule studies, Table 5, the best upper and lower limits on measured-calculated values for the exposure variables (fluence > 0.1 and > 1.0 MeV, and dpa) at the surveillance position are ±20% (2σ), and only for benchmarked results.[5,6]

Considering these as best lower- and upper-bound limits, and for this example, a plant-specific controlling trend curve (at the 95% confidence level) can be defined and is shown as the dot-dashed curve in Figure 5.** The

*In Reference 9 it is stated that: "The economic consequences of complying with the federal regulations are demonstrably severe. Therefore, it is necessary to have the most accurate embrittlement predictive methodology possible."

**This is a simplified example which assumes a 95% confidence limit for both the fluence and temperature shift. The actual limits must be set using a statistical combination of these according to the confidence level that is deemed satisfactory.

determination of the intersection of this curve with an acceptable plant-specific upper-bound line that falls in a band of allowable EOL values of RT_{NDT} (for a nominal operating temperature of 550°F for LWR power plants) is required for plant safety. For the present example, a very conservative upper-bound line at RT_{NDT} equals 200°F will be used.* On this basis, the intersection point is at a fluence of $\sim 1.1 \times 10^{19}$ n/cm^2 ($\sim$9.2 EFPY, or 1/4 of the plant life) at the PV inner surface. If instead of a ±20% (2σ) [±10% (1σ)] uncertainty, a ±60% (2σ) [±30% (1σ)] fluence uncertainty had been used (which is more representative of current state-of-the-art values for reported surveillance capsule dosimetry, Table 5), the plant-specific controlling trend curve would shift to the left even further. The result would be that the intersection point would now be at a fluence value of $\sim 5.6 \times 10^{18}$ n/cm^2 ($\sim$4.7 EFPY). Consequently, if the reported fluence value uncertainty had been ±30% (1σ) and an RT_{NDT} value of 200°F were limiting, corrective action, such as annealing the reactor PV, changes in core power distribution to lower the PV neutron exposure rate, etc. would have to be considered immediately. If the reported uncertainty had been closer to ±10% (1σ), however, corrective action could be safely delayed until after another $\sim$4 EFPY of operation. During this period, additional in- and ex-vessel physics-dosimetry measurements and calculations could be performed to verify, certify, and improve the accuracy of the original FSAR and second (and subsequent) surveillance capsule reported values of exposure parameters (fluence > 0.1 and > 1.0 MeV, and dpa). The use of dpa, to better account for spatial effects, might further increase or decrease the allowed current and EOL fluence values, see Figure 10.

The shape of the Charpy shift curve used in current regulations is based on trend curves with a power law dependence of N = 1/2 for the fluence variable.[2] Hence, for Case 2, Standards Development efforts will produce improved and more reliable trend curves, such as those now being established for the ASTM Standard Guide E706(II-F), Figures 3 and 4. The importance of the trend curve in time exposure extrapolations can be seen in Figure 5. Extrapolation uncertainty, whether spatial (lead factor) or temporal (trend curve) depends upon how accurately the curve has been defined as well as how far the extrapolation extends. For example, using MPC, EPRI and NRC data bases, it now appears that the power law approximation of the trend curve possesses an exponent N $\sim$ 1/3 for most PV steels; see Figure 6.[14] This would represent a 33% change in the exponent relative to that used in Regulatory Guide 1.99.1. Clearly the error introduced through ill-definition of the trend curve cannot be neglected given representative ±10% to 30% (1σ) uncertainties for both dosimetry and Charpy data in power plant surveillance capsule work. Consequently, through proper Standards Development efforts, one can fully

*For new plants, Regulatory Guide 1.99.1 states that the PV steel beltline materials should have the content of residual elements such as Cu, P, S and V controlled to low levels such that the EOL, 1/4 T position, RT_{NDT} is less than 200°F. In Reference 9, it is indicated that a ΔRT_{NDT} shift of, say, 252°F may cause real operational difficulty late in life (in startup and shutdown) for some PWR power plants. This, however, would be dependent on a number of factors, including the initial BOL RT_{NDT} value.

expect the generation of more accurate extrapolation procedures. For the more accurate definition of exposure time trend curves, well controlled special research and power reactor metallurgical tests must generate higher quality data.[6,9,14-24] Here it is essential that ΔRT_{NDT} be determined at the ±10% (1σ) uncertainty level or better and that state-of-the-art reactor physics-dosimetry be carried out to a comparable accuracy.

For plant safety, then, a knowledge of the uncertainty in the shape of the trend curve (N = 1/2, 1/3, or less) is essential for defining the point of intersection of a 2σ (plant-specific) trend curve with a plant-specific upper-bound line in the band of allowable EOL values of the adjusted RT_{NDT} (Figure 5). It is well to also note here that whether 10% (1σ), 30% (1σ) or higher values of uncertainty are accepted for derived values of exposure parameters, the routine acceptance of the validity of any exposure parameter value and its quoted uncertainty will be dependent on the periodic benchmarking of the applied experimental physics and dosimetry methodology. As discussed later in this paper, under Program Direction and Status, special benchmark facilities (Table 1) are being or have been established to provide the necessary validation and certification of both the accuracy and precision of the applied physics and dosimetry techniques. Proven and accepted techniques are and will be needed for the definition of values and uncertainties for spatial (lead factor) and exposure time (trend curve) extrapolations.

Although our presentation has focussed on trend curves, similar considerations obviously must arise for extrapolations based on spatial and metallurgical lead factors. Indeed the accuracy and limitations of these different extrapolation procedures have yet to be rigorously defined, let alone compared.

Consequently, comparable Standards Development efforts must go forward to accurately define spatial and metallurgical lead factors. With reference to Table 2, the present discussion has considered effects arising solely from reactor physics-dosimetry (Variables 3 - 10). Analogous considerations must be applied for Variable 1 (steel chemical composition and microstructure) and Variable 2 (steel irradiation temperature) for metallurgical lead factor extrapolations. Even though it is not the purpose of this paper to address metallurgical lead factor extrapolation methodology and uncertainties, some of the main elements involved in this methodology are summarized in Table 3.

In summary, the need for extrapolation in PV and support structure surveillance is an overriding concern. Within this framework, the selection of a "controlling variable", be it metallurgical or reactor physics-dosimetry related, is irrelevant. For example, in Figure 5, a horizontal extrapolation of the ±30°F error bars (to the left for the -30°F bar and to the right for the +30°F bar) results in a fluence band of $\sim 3.0 \times 10^{18}$ to $\sim 1.0 \times 10^{19}$ n/cm^2. Consequently, if the RT_{NDT} property change uncertainty of ±30°F were considered limiting (e.g., material variability in chemistry and microstructure) for a specific PV steel, then knowing the fluence value within a factor of ~3 might be considered adequate. This argument, however, has little relevance to setting safe (95% confidence level or better) current and EOL fluence operating limits for individual pressurized water reactor (PWR) power

plants. It is also clear that high accuracy exposure values are needed for establishing the value of "N" and its uncertainty for the slope (exposure time extrapolation variable) of a trend curve for a specific plant and PV steel. The "exposure time extrapolation" variable plays an extremely important part in extrapolating, in time, plant-specific surveillance capsule derived exposure and metallurgical results. In this context, the reason fluence (or dpa) is used as the extrapolating (independent) variable is that it obviously can be determined as or more accurately than the associated metallurgical (dependent) variable.

PROGRAM DIRECTION AND STATUS

The ASTM Standard E706-81,[10] "Master Matrix for LWR-PV Surveillance Standards," describes a series of 18 standard practices, guides and methods for the prediction of neutron-induced changes in LWR-PV and support structure steels throughout a PV's service life. Figures 3 and 4 provide updated information on the interrelationship of 19 standards (20 including the Master Matrix) and the schedule for their preparation, balloting, acceptance, validation and revision. Some of these are existing ASTM standards, some are ASTM standards that have been modified, and some are newly proposed ASTM standards. The scope of each standard and the general requirements for content and consistency are discussed in the Master Matrix as well as writers' and users' information, justification, and specific requirements for the practices, guides and methods. Information is also provided on applicable documents and references.

Reactor physics and dosimetry analysis and interpretation are discussed in Section 4 of E706-81. Specific subsections deal with:

a) Required Accuracies and Benchmark Field Referencing

b) Power Plant Reactor Physics Analysis and Interpretation

c) PCA Blind Test

d) PWR and Boiling Water Reactor (BWR) Generic Power Reactor Tests

e) Operating Power Reactor Tests

Currently, the NRC is supporting a significant amount of multilaboratory work associated with all five items at HEDL, ORNL, BNL and NBS. Additional work is being supported at a number of laboratories in Europe and elsewhere, the most significant effort being at CEN/SCK, Mol, Belgium. EPRI and reactor vendors are also supporting significant multilaboratory work related to Items a), b), d) and e). Three of the U.S. vendors (Westinghouse, B&W and CE), two U.S. service laboratories (SWRI and BMI), as well as six other U.S. and foreign laboratories participated in the "PCA Experiments and Blind Test." This test was intended to provide a "necessary" but not "sufficient" test of the adequacy of reactor physics tools, procedures and data used for predicting FSAR flux-spectral values. These data are used, in turn, in the analysis of surveillance capsule dosimetry sensor reaction rates and in the

subsequent determination of values of neutron exposure parameters 1) in surveillance capsules, 2) at the inner surface and through vessel walls, and 3) in ex-vessel cavity locations. The initial results of the "PCA Experiments and Blind Test" are now available in a NUREG Report.[5] This PCA benchmark test has established that the limiting accuracy of reactor-physics, dosimetry-derived values of group fluxes and exposure parameters are in the range of ±5% to 30% (1σ) and ±5% to 15% (1σ), respectively, if properly benchmarked; otherwise, errors can be a factor of two or more, see Figure 2.

Relative to Item (c) and by the end of 1982, HEDL, ORNL, NBS and CEN/SCK will complete the final work and documentation for the PCA for the 8/7, 12/13, 4/12 and 4/12 (SSC) configurations for this mockup physics-dosimetry test of a PWR power plant.* The 4/12 and 4/12 (SSC) results will be used primarily in support of the analysis of the physics and dosimetry for the PSF metallurgical test.[5,6] One important aspect of this combined metallurgical/physics/dosimetry test will be to provide benchmarked data to establish the uncertainties associated with the calculation and use of fluence (E > 1.0 MeV) and dpa to account for flux-spectral (spatial lead factor) effects, see Figures 9 and 10. Another important aspect of this effort will be the general use and application of the PCA experimental and analytical results to test and develop advanced physics-dosimetry methodologies based on least-squares adjustment procedures. Least-squares analyses of reactor dosimetry have been in vogue for some time now, and this approach has general world-wide acceptance.[11-13] Indeed least-squares analyses of PCA experiments and blind test results for NRC have already been conducted by HEDL and ORNL.[5] Initial results of the application of HEDL- PCA tested methodology to the analysis of surveillance capsule-derived exposure-parameter values and uncertainties are discussed herein. Work being supported at ORNL by EPRI is also discussed in this paper and in Reference 8.

Still required for this interlaboratory program effort is to complete the development and establishment of a set of ASTM-accepted generic BWR and PWR physics-dosimetry benchmarks, with required in- and ex-vessel dosimetry measurement verification (Table 4).[5-8,10-13] With Reference to ASTM E706-81,[10] these benchmarks are intended to provide a "necessary" and "partly sufficient" test of the adequacy of a vendor/utility group's power reactor physics computational tools.** The standards recommendation should be that the vendor/utility group's observed differences between their own calculated and the selected PWR or BWR measured integral and differential exposure and reaction rate parameters be used to validate and improve their computational tools and measurement resources (if differences fall outside the selected PWR or BWR experimental accuracy limits). (These C/E accuracy

*8/7, 12/13, etc. are the dimensions of the water gaps in cm between the reactor core edge and thermal shield/the thermal shield and pressure vessel inner wall for the PCA PV mockup facility.

**The successful analysis and interpretation of a number of surveillance capsule results for a specific PWR or BWR power plant, together with an appropriate generic plant, provides a "necessary" and "sufficient" test (see Section 4.4.5 of ASTM E706-81, Reference 10).

limits are identified and discussed in the ASTM E706(II-D) Transport Standard, Figure 3).*

As previously stated, the objective of the EPRI experimental program has been to carry out measurements in operating power reactors for use in benchmarking improved physics-dosimetry methods of analysis;[5,8] see Table 4. The reactors where measurements have been carried out included one BWR: TVA's Browns Ferry Unit 3 where ex-vessel measurements carried out by GE have recently been documented.[25] These measurements complement the in-vessel measurements funded by TVA and documented in Reference 26. Supporting transport calculations are being done by Science Applications Inc. The PWR measurements have been carried out at Arkansas Power and Light's Nuclear One-1 (ANO-1) by the University of Arkansas, NBS and HEDL.[6,27] Supporting transport calculations are being done at the University of Missouri, Rolla and at ORNL. The ANO-1 measurements have been carried out ex-vessel only. A set of in-vessel as well as ex-vessel measurements at Crystal River 3 and ANO-2 is presently under consideration, Table 4. An equivalent set of measurements on Duke Power Company's McGuire Unit 1 plant is awaiting startup of the reactor.

The objective of the EPRI analytic program has been the development of an advanced dosimetry methodology based on a least-squares adjustment procedure.[8,28] The methodology being developed by ORNL for EPRI utilizes direct neutron transport calculations together with dosimetry measurements and their uncertainties (or covariances) to determine the best (in a least-squares sense) estimates of the neutron fluxes and their reduced covariances. One of the most important features of the methodology is its ability to estimate the uncertainties in the adjusted flux spectrum. Other features include the capability of obtaining the fluxes at surveillance points as well as at any desired point within the pressure vessel, and the capability of simultaneous least-squares adjustment of fluxes in multiple fields. By simultaneously analyzing benchmark fields (prototypic fields as well as a particular LWR field of interest), it is possible to improve the accuracy of the prediction for the LWR field since the information "learned" from the former fields is used in the determination of the latter.

To date the EPRI-ORNL methodology has been applied to the analysis of a series of progressively more complex fields, including the NBS ^{252}Cf fission field, the Intermediate-Energy Standard Neutron Field (ISNF), the Federal German Republic-PTB ^{252}Cf fission field, and the PCA pressure vessel prototypic field.[8] (The method is presently being applied to the PCA/PSF. Future plans include the application of the methodology to the ANO-1 and, perhaps, ANO-2 measurements.) Results of both the ORNL and HEDL[5] studies have shown that uncertainties in the PCA flux determination can be considerably reduced by using simultaneous adjusting of all available data. Since the predictions have been found to be rather sensitive to the uncertainty estimates, a considerable amount of effort has been invested by

*A similar statement regarding differences applies to the "PCA Experiments and Blind Test" benchmark (see Section 4.4.3 of ASTM E706-81).

both ORNL and HEDL in the preparation of covariance information for measurements in the benchmark and prototypic fields as well as improvements to the ENDF/B-V covariance files for dosimetry cross sections.[5,8] These covariances together with the ENDF/B-V cross-section files constitute a general data base for any least-squares fitting program. As a matter of interest, Reference 29 describes the status of work related to the preparation of the ASTM E706-81 (II-B) Standard Guide for "Application of ENDF/A Cross Section and Uncertainty Files"; see also Reference 10.

For Item (e) and by the end of 1982, initial studies will have been completed for the NRC program; and more quantitative results will be available to certify the accuracy of surveillance dosimetry for operating LWR power plants. For individual and selected sets of surveillance capsules, results will be available from FERRET-SAND code-derived values of exposure parameters (see Table 5 and Sections 4.2 and 7.3 of Reference 5) for four vendors, two service laboratories, and EPRI surveillance capsule reports submitted for or by utilities to NRC. These results, together with those from physics computations, will be used to 1) define inner PV surface and wall gradient flux level and exposure parameter values, Figures 9 and 10, 2) verify the accuracy of FSAR predictions of current and EOL exposure parameter values (fluence > 0.1 and > 1.0 MeV, and dpa) for individual BWR and PWR power plants (see Table 5), and 3) provide higher accuracy [±10% to 30% (1σ)] values of exposure parameters for establishing improved trend curve shapes for MPC, EPRI, NRC and other metallurgical data bases. Least-squares adjustment procedures, as discussed in ASTM Standards E706(I-C), (I-E), and (II-A) (Figure 3) and for the NRC and EPRI programs, will be used to accomplish the above analysis.[5,8,14-16,17]

More specifically, the MPC, EPRI, and NRC data bases are being used together with test reactor data to develop trend curves to account for neutron radiation damage when plant-specific information is not available or is not completely adequate. That is, updated and new physics-dosimetry data are being used together with available metallurgical data to develop new ASTM ΔRT_{NDT} and upper shelf energy shift versus fluence (E > 0.1 MeV and > 1.0 MeV) and dpa curves to replace those in Regulatory Guide 1.99.1 (see Figure 3, ASTM Standard II-F, and Figure 6). In addition to a series of Westinghouse PWR plants (Table 5), the current emphasis and approximate order of priority of studying existing U.S. power plants under this effort is provided in Table 6. This priority listing is currently based on a need to have plant-specific input data to perform fracture analysis studies, including those using OCA-I, for those power plants with PV steels that are suspected of having high RT_{NDT} values (Table 6). As discussed in the section on Surveillance Dosimetry Accuracy Requirements, the correctness of these estimated RT_{NDT} values is critically dependent on the accurate definition and verification of surveillance capsule exposure parameter values, and capsule-to-PV-wall inner surface spatial (lead factor, see Table 5) and exposure time (trend curve, see Table 6) extrapolations. The determination of these spatial and time lead factors also depends on the proper definition and understanding of surveillance capsule perturbation and long-term core fuel subassembly

loading pattern effects. Figures 7, 9 and 10 and Tables 7 and 8 provide information and preliminary results of studies related to this aspect of surveillance capsule data analysis.

HEDL, ORNL, NBS, CEN/SCK, EPRI contractors, vendors and others are doing and will continue to do dosimetry measurement certification work in support of surveillance programs for operating power plants, Items (d) and (e) (see Figures 6 through 8 and Tables 4 through 14). Further, effort will be put forth in the area of validation/calibration of the Figure 3 ASTM Standard Methods:

III-A Analysis of Radiometric Monitors (RM) for Reactor Vessel Surveillance

III-B Analysis of Solid State Track Recorder (SSTR) Monitors for Reactor Vessel Surveillance

III-C Analysis of Helium Accumulation Fluence Monitors (HAFM) for Reactor Vessel Surveillance

III-D Analysis of Damage Monitors (DM) for Reactor Vessel Surveillance

III-E Analysis of Temperature Monitors (TM) for Reactor Vessel Surveillance

Related to Items (a), (b), (d) and (e), therefore, the participants of the LWR-PV Surveillance Dosimetry Improvement Program will jointly seek 1) to develop and establish a set of PWR and BWR Generic Power Reactor Benchmarks based upon conventional, benchmarked, neutron dosimetry, 2) to obtain ASTM acceptance of these and 3) to complete the necessary validation/calibration (round robin testing) of this set of five ASTM Standard Methods (III-A through III-E), consistent with the procedures to be given in II-E, Benchmark Testing of Reactor Vessel Dosimetry.

In summary and with reference to Figure 2, the five measurement standard methods are essential to provide in and ex-vessel dosimetry and temperature measurement capabilities that vendors, service laboratories and utilities will need to certify to themselves and licensing and regulatory bodies the adequacy of their calculational and measurement tools. Of particular importance is the adequacy of individual power plant FSAR/surveillance-capsule-derived, BOL and EOL predictions of flux-spectra and exposure parameter values (fluence > 0.1 and > 1.0 MeV, and dpa for steel) needed for fracture analysis studies of PV and support structure steels. It is essential for the nuclear industry that errors be assigned to all values of calculated and measured flux-spectra, derived exposure-parameters, lead factors, and trend curve slopes given in surveillance capsule reports; further, it is important that these values are based on a proper weighting of the results of individual dosimetry sensors, which includes uncertainties and neutron energy

response weighting. One needs only to look at recent as well as old surveillance program reports to determine the inadequacy of the present practice of stating that FSAR predictions and surveillance capsule measurements agreed or disagreed, but without stating the uncertainties associated with individual predictions and measurements.

ACKNOWLEDGMENTS

The success of the LWR-PV Surveillance Dosimetry Improvement Program is dependent on the efforts and the free exchange of ideas and views of the technical staffs of a large number of research, service, regulatory and vendor/utility organizations. The information reported herein could not have been developed without the continuing support of the representatives and participants of the following organizations: AERE Harwell, England; ASTM Committee E10; Babcock & Wilcox; Battelle Memorial Institute; Brookhaven National Laboratory; CEN/SCK, Mol, Belgium; Centre D'Etudes Nucleaires de Saclay, France; Combustion Engineering; EG&G Idaho, Inc.; EG&G Ortec, Inc., Oak Ridge; Electric Power Research Institute and its contractors; Fracture Control Corp.; General Electric Co.; HEDL; IKE - Stuttgart, West Germany; IRT Corporation; KFA-ZBB, Julich, West Germany; Kraftwerk Union, West Germany; NBS; NUTECH; Naval Research Laboratory; ORNL; Radiation Research Associates; Rockwell International, Energy System Group; Rolls-Royce & Associates Ltd., England; Science Applications Inc.; Ship Research Institute, Japan; South West Research Institute; US Department of Energy; US Nuclear Regulatory Commission; University of Arkansas; University of California Santa Barbara; and Westinghouse Electric Corporation.

Special acknowledgment is due to C. Z. Serpan of NRC for having identified the need for such national and international collaborative work and making it possible by taking a strong overall support and management lead position. Further, to his and U. Farinelli's credit (as prior chairmen of ASTM Subcommittee E10.05 on Nuclear Radiation Metrology and EURATOM, respectively) are their foresight and joint efforts in establishing and supporting the highly successful series of ASTM-EURATOM International Symposia on Reactor Dosimetry. These symposia now serve as the main reporting base for work associated with the improvement, standardization and maintenance of 1) dosimetry, 2) damage correlation and 3) the associated reactor analysis procedures and data used for predicting the integrated effects of neutron exposure on fuels and materials for LWR, fast breeder reactor (FBR) and magnetic fusion reactor (MFR) nuclear power systems.

Very special acknowledgment is given to J. M. Dahlke, who edited this document, and to the HEDL Publication Services, Graphics and Duplicating personnel who contributed to its production.

REFERENCES

1 Code of Federal Regulations, "Domestic Licensing of Production and Utilization Facilities," 10 CFR 50; "General Design Criteria for Nuclear Power Plants," Appendix A; "Fracture Toughness Requirements," Appendix G; "Reactor Vessel Material Surveillance Program Requirements," Appendix H; US Government Printing Office, Washington, DC, current edition.

2 Regulatory Guide 1.99, "Effects of Residual Elements on Predicted Radiation Damage to Reactor Vessel Materials," Rev. 1, US Nuclear Regulatory Commission, Washington, DC, April 1977.

3. R. D. Cheverton, "Pressure Vessel Integrity," Oak Ridge National Laboratory Review, Oak Ridge National Laboratory, Oak Ridge, TN, p. 34, W'81.

4. S. K. Iskander, R. D. Cheverton, and D. G. Ball, OCA-I, A Code for Calculating the Behavior of Flaws on the Inner Surface of a Pressure Vessel Subjected to Temperature and Pressure Transients, NUREG/CR-2113, ORNL/NUREG-84, Oak Ridge National Laboratory, Oak Ridge, TN, August 1981.

5. W. N. McElroy et al., LWR Pressure Vessel Surveillance Dosimetry Improvement Program: PCA Experiments and Blind Test, NUREG/CR-1861, HEDL-TME 80-87, Hanford Engineering Development Laboratory, Richland, WA, July 1981.

6. W. N. McElroy et al., LWR Pressure Vessel Surveillance Dosimetry Improvement Program: 1980 Annual Report, NUREG/CR-1747, HEDL-TME 80-73, Hanford Engineering Development Laboratory, Richland, WA, April 1981.

7. H. A. Till, "Neutron Radiometric and Calculation Benchmarking for LWR Pressure Vessel Radiation Effects," Proceedings of the Third ASTM-EURATOM International Symposium on Reactor Dosimetry, EUR 6813, European Atomic Energy Community, Brussels, Belgium, p. 1275, 1980.

8. J. J. Wagschal, R. E. Maerker and B. L. Broadhead, "LWR-PV Damage Estimate Methodology," Transactions of the ANS Topical Meeting, 1980 Advances in Reactor Physics and Shielding, Sun Valley, ID, September 14-17, 1980.

9. T. V. Marston and K. E. Stahlkopf, "Radiation Embrittlement: Significance of Its Effects on Integrity and Operation of LWR Pressure Vessels", Nuclear Safety 21 (6), p. 724, November - December 1980.

10. ASTM Standard E706-81, "Master Matrix for LWR Pressure Vessel Surveillance Standards," 1981 Annual Book of ASTM Standards, American Society for Testing and Materials, Philadelphia, PA, 1981.

11. Proceedings of the First ASTM-EURATOM International Symposium on Reactor Dosimetry, EUR 5667, Parts I & II, European Atomic Energy Community, Brussels, Belgium, 1977.

12. Proceedings of the Second ASTM-EURATOM International Symposium on Reactor Dosimetry, NUREG/CR-0004, Vol. 1 - 3, US Nuclear Regulatory Commission, Washington, DC, 1978.

13. Proceedings of the Third ASTM-EURATOM International Symposium on Reactor Dosimetry, EUR 6813, European Atomic Energy Community, Brussels, Belgium, 1980.

14. G. L. Guthrie, "A Determination of the Effect of Irradiation Temperature on the Irradiation Induced Charpy Shift," LWR-PV Irradiation Surveillance Improvement Program Progress Report for January - March 1981, HEDL-TME 81-33, NUREG/CR-2345, Vol. 1, Hanford Engineering Development Laboratory, Richland, WA, October 1981.

15. G. L. Guthrie, "An Investigation of the Dependence of Charpy Trend Curve Saturation on Nickel or Copper Concentration," LWR-PV Irradiation Surveillance Improvement Program Report for October - December 1980, HEDL-TME 80-6, NUREG/CR-1241, Vol. 3, Hanford Engineering Development Laboratory, Richland, WA, October 1981.

16. J. D. Varsik, Evaluation of Irradiation Response of Reactor Pressure Vessel Materials, TR-MCM-110, EPRI RP 1553-1, Semi-Annual Progress Report No. 3, July - December 1980, Combustion Engineering Inc, Winsor, CT, 1981.

17. T. J. Williams and R. L. Squires, Interim Analysis of the Results to Date from a Materials Test Reactor Irradiation Program, RRA/N/3467, Rolls-Royce & Associates Ltd, Derby, UK, November 1979.

18. J. S. Perrin et al., Point Beach Unit No. 2 Pressure Vessel Surveillance Program: Evaluation of Capsule V, Final Report, Battelle Memorial Institute, Columbus, OH, June 10, 1975.

19. J. A. Davidson, S. L. Anderson and R. P. Shogan, Analysis of Capsule T from the Wisconsin Electric Power Company Point Beach Nuclear Plant Unit No. 2 Reactor Vessel Radiation Surveillance Program, WCAP-9331, Westinghouse Nuclear Technology Division, Pittsburgh, PA, August 1978.

20. C. Z. Serpan, "Reliability of Fluence Embrittlement Projections for Pressure Vessel Surveillance Analysis," Nucl. Tech. 12, p. 108, September 1971.

21. S. E. Yanichko, S. L. Anderson, R. P. Shogan and R. G. Lott, Analysis of Capsule R from the Wisconsin Electric Power Company Point Beach Nuclear Plant Unit No. 2 Reactor Vessel Radiation Surveillance Program, WCAP-9635, Westinghouse Nuclear Technology Division, Pittsburgh, PA, December 1979.

22. S. E. Yanichko, S. L. Anderson, R. P. Shogan and R. G. Lott, Analysis of Capsule R from the Wisconsin Public Service Corporation Kewaunee Nuclear Plant Reactor Vessel Radiation Surveillance Program, WCAP-9878, Westinghouse Nuclear Technology Division, Pittsburgh, PA, March 1981.

23. D. Pachur, "Apparent Embrittlement Saturation and Radiation Mechanisms of Reactor Pressure Vessel Steels," Proceedings of the 10th International Symposium on Effects of Radiation on Materials, Savannah, GA, June 3-5, 1980.

24. T. R. Mager et al., Steady-State Radiation Embrittlement of Reactor Vessels, Semiannual Technical Progress Report No. 4, EPRI RP 1021-3, Electric Power Research Institute, Palo Alto, CA, April 1981.

25. G. C. Martin, Browns Ferry Unit 3 Cavity Neutron Spectral Analysis, EPRI NP-1997, Electric Power Research Institute, Palo Alto, CA, August 1981.

26. G. C. Martin, Browns Ferry Unit 3 In-Vessel Neutron Spectral Analysis, NED024793, General Electric Co., San Jose, CA, August 1980.

27. W. N. McElroy et al., LWR Pressure Vessel Surveillance Dosimetry Improvement Program: 1979 Annual Report, NUREG/CR-1291, HEDL-SA 1949, Hanford Engineering Development Laboratory, Richland, WA, February 1980.

28. F. G. Perey, Least-Squares Dosimetry Unfolding: The Program STAY'SL, ORNL/TM-6062, Oak Ridge National Laboratory, Oak Ridge, TN, 1977.

29. E. P. Lippincott and W. N. McElroy, ASTM Standard Recommended Guide on Application of ENDF/A Cross Section and Uncertainty File: Establishment of the File, HEDL-SA 2540, paper presented at IAEA Advisory Group Meeting on Nuclear Data for Radiation Damage and Safety, Vienna, Austria, October 12-16, 1981.

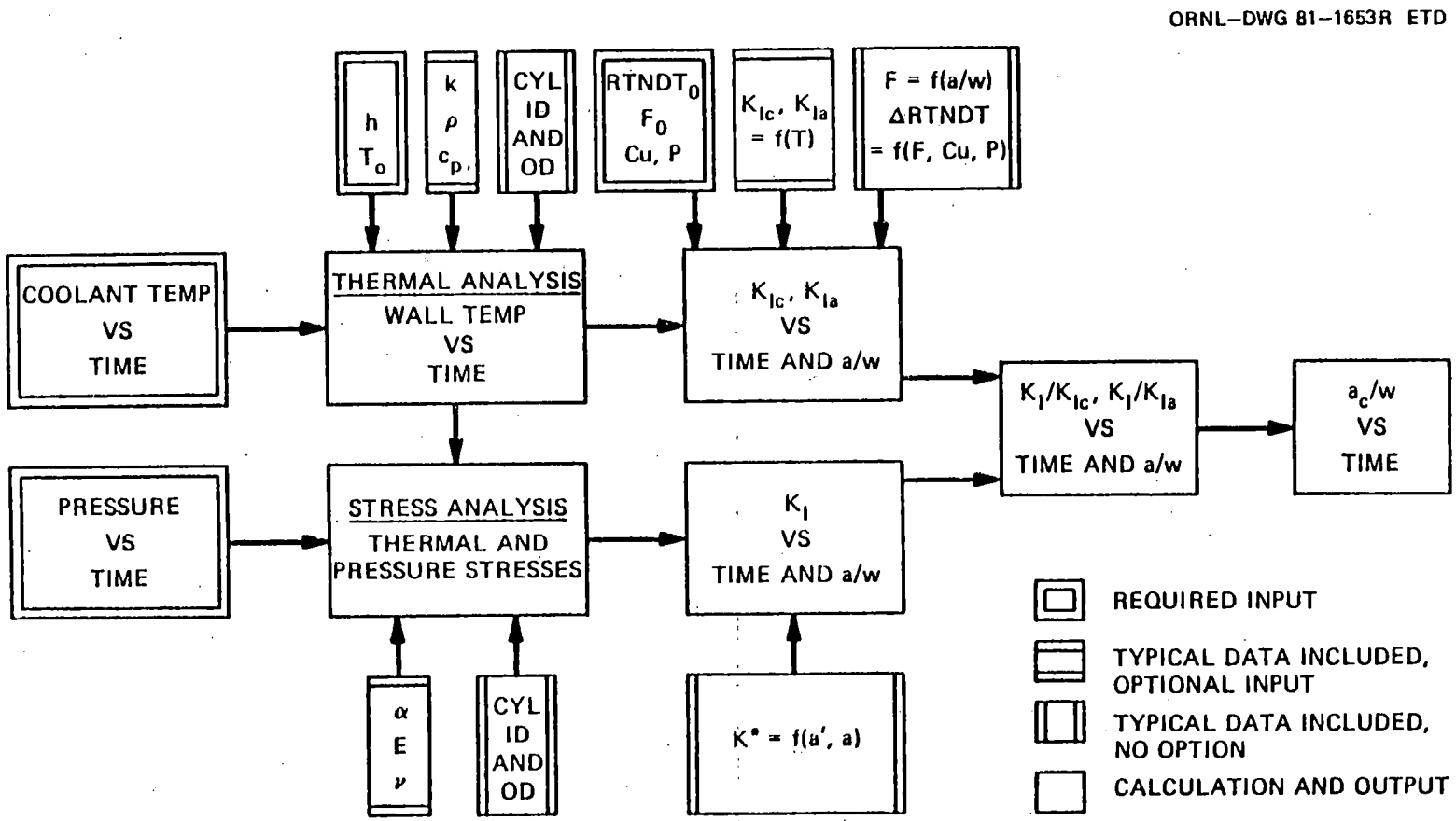

FIGURE 1. Block-Diagram Description of OCA-I, Indicating Basic Input, Calculations and Output.

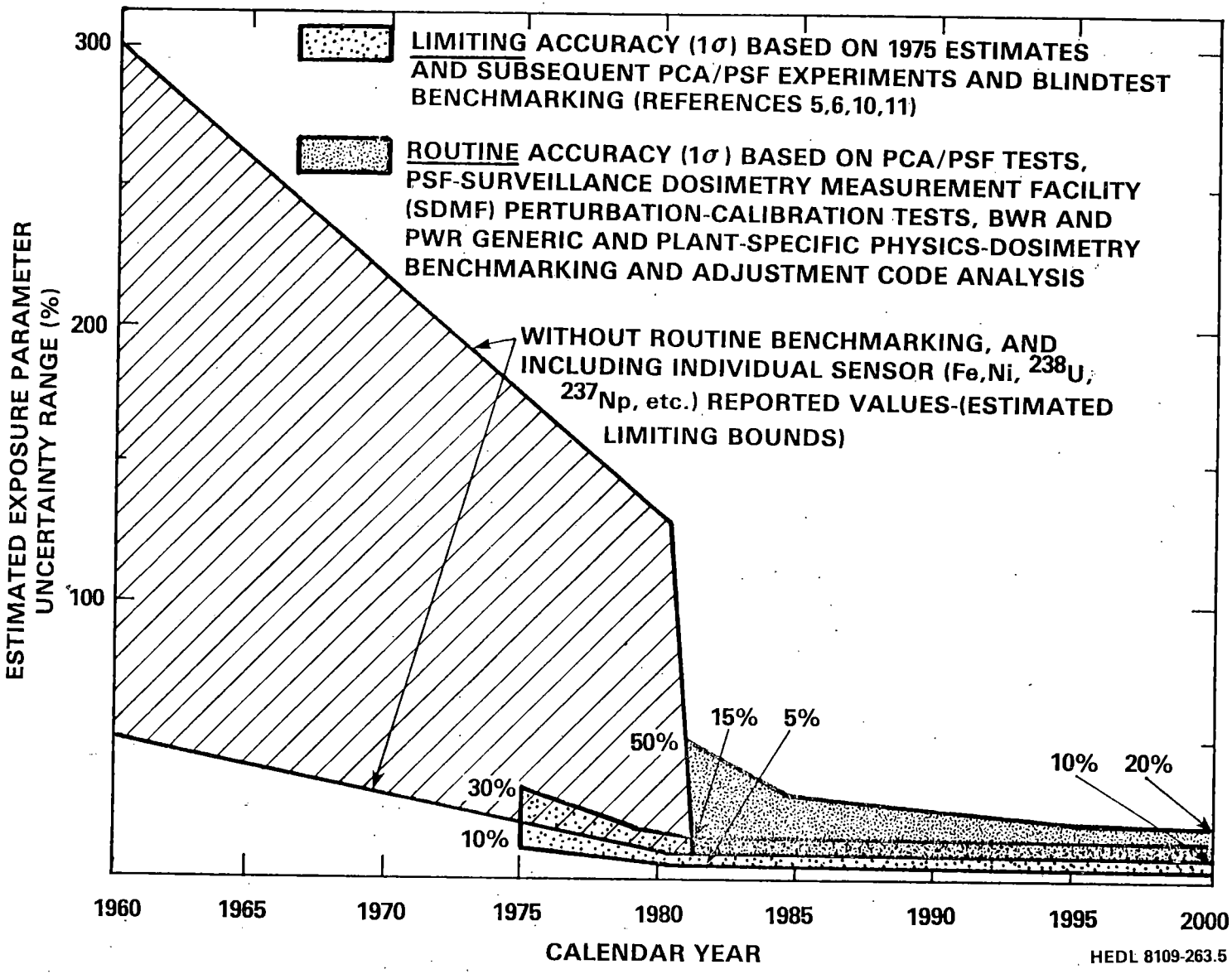

FIGURE 2. Estimated Exposure Parameter Uncertainties Obtained from FSAR and Surveillance Capsule Reports.

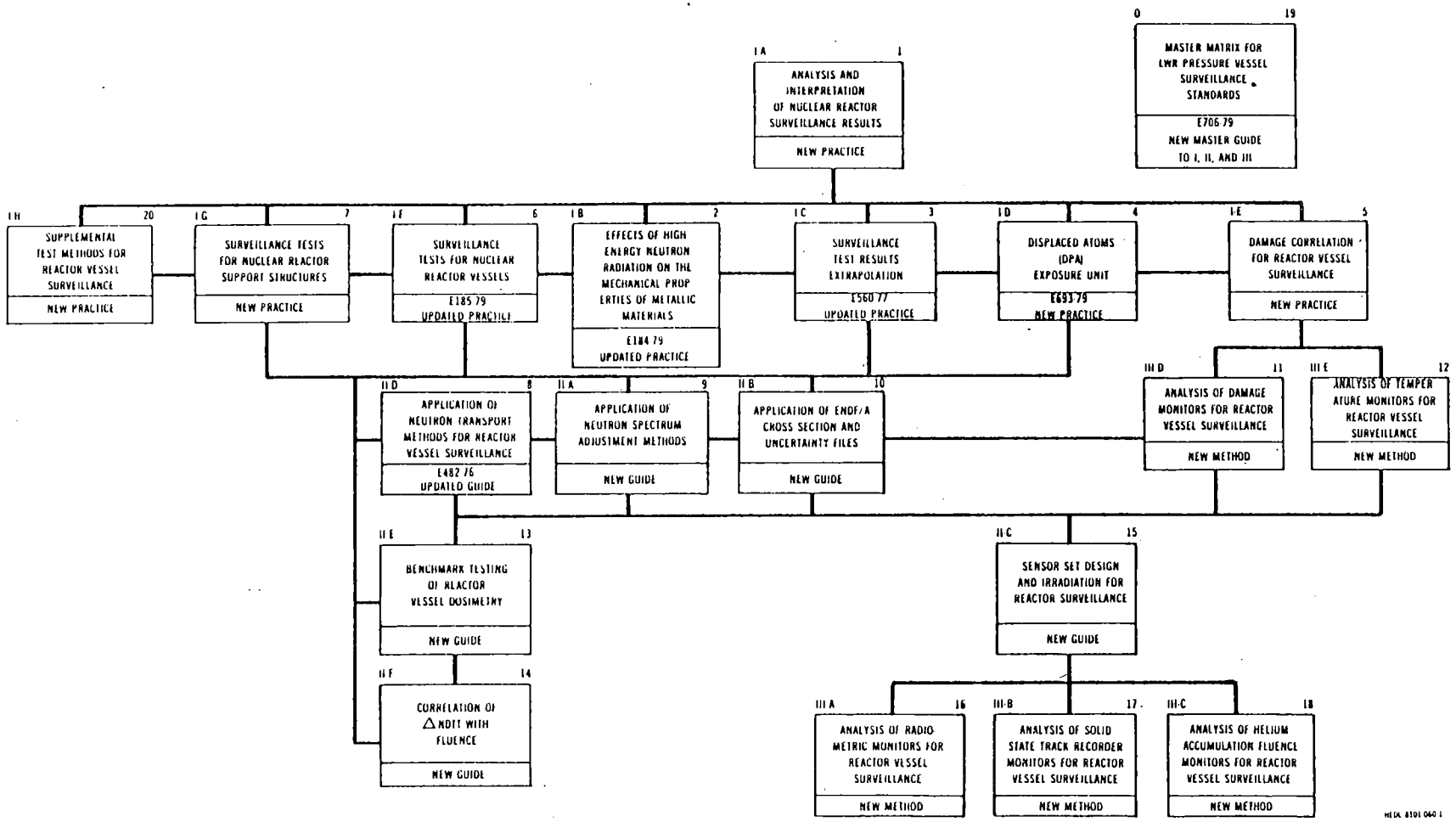

FIGURE 3. ASTM Standards for Surveillance of LWR Nuclear Reactor Pressure Vessels.

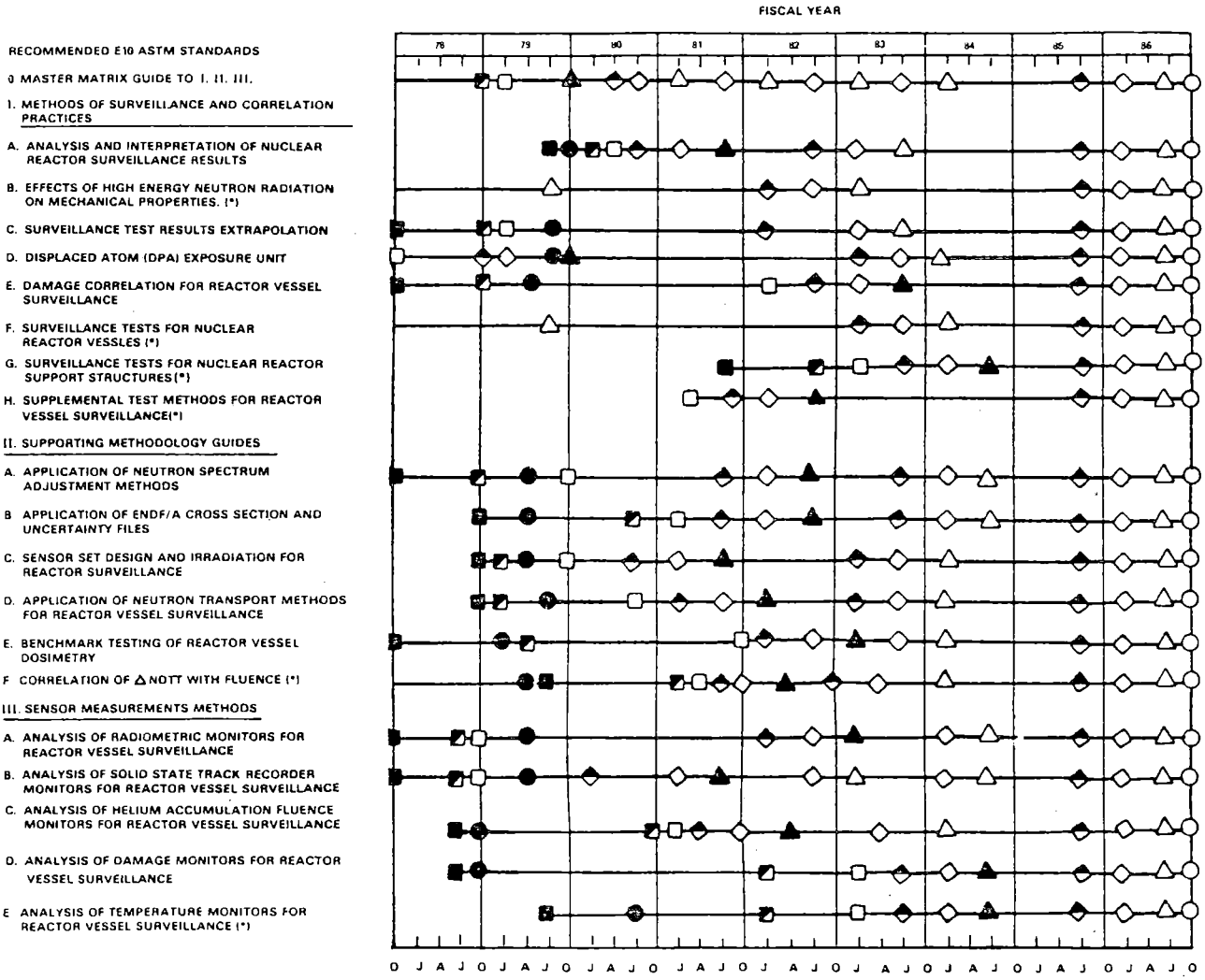

FIGURE 4. Preparation, Validation and Calibration Schedule for LWR Pressure Vessel Surveillance Standards.

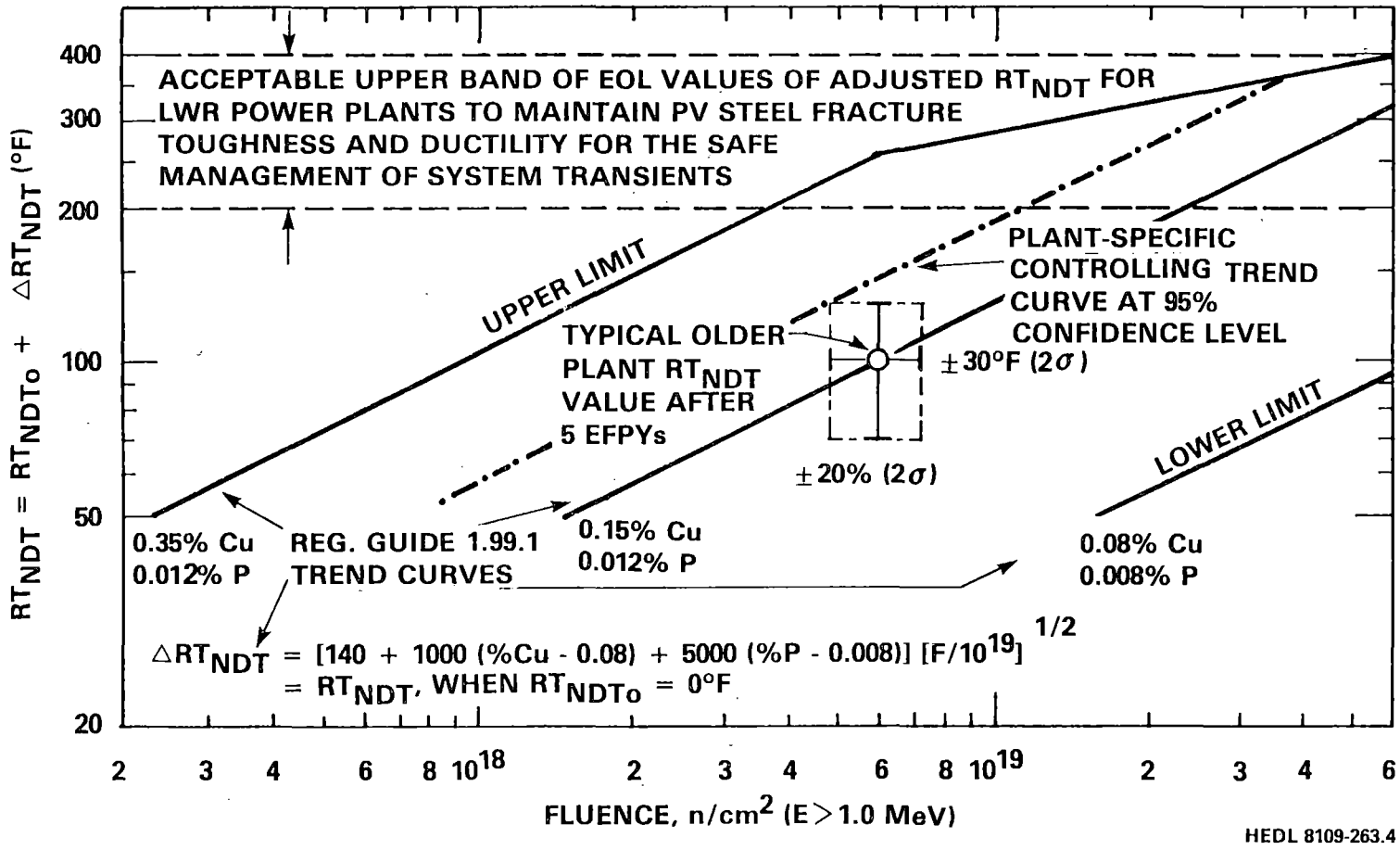

FIGURE 5. Limiting Accuracy of Second Surveillance Capsule Derived Values of RT_{NDT} and Fluence (E > 1.0 MeV) at the PV Wall Inner Surface After ~5 EFPY of Plant Operation for a Typical PWR with an Older Radiation Sensitive Steel.

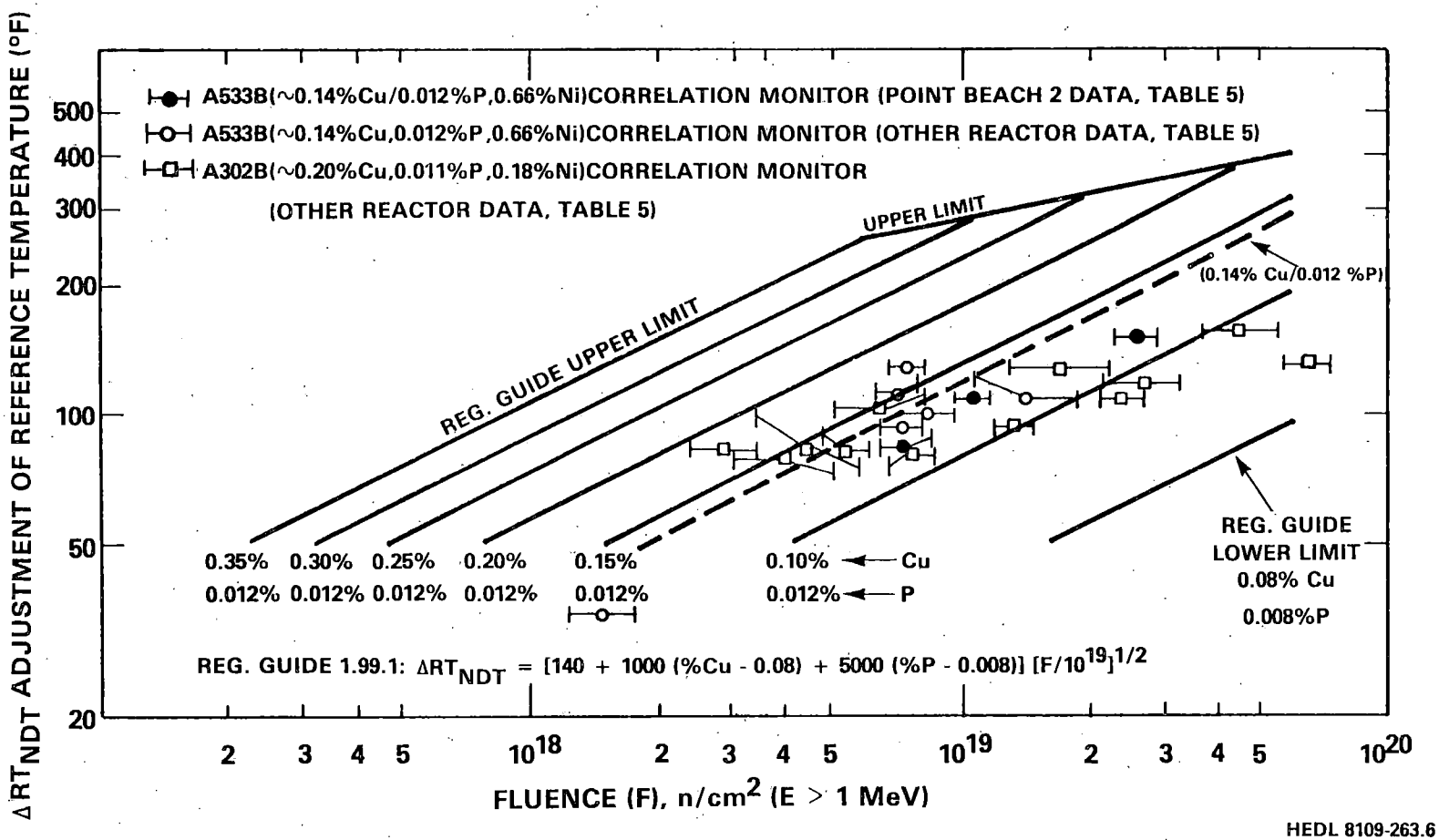

FIGURE 6. ΔRT_{NDT} Trend Curve Results for Correlation Monitor Material with New Exposure Values and Uncertainties.

OAK RIDGE RESEARCH REACTOR (ORR) POOLSIDE FACILITY (PSF)
SIMULATED DOSIMETRY MEASUREMENT FACILITY (SDMF)

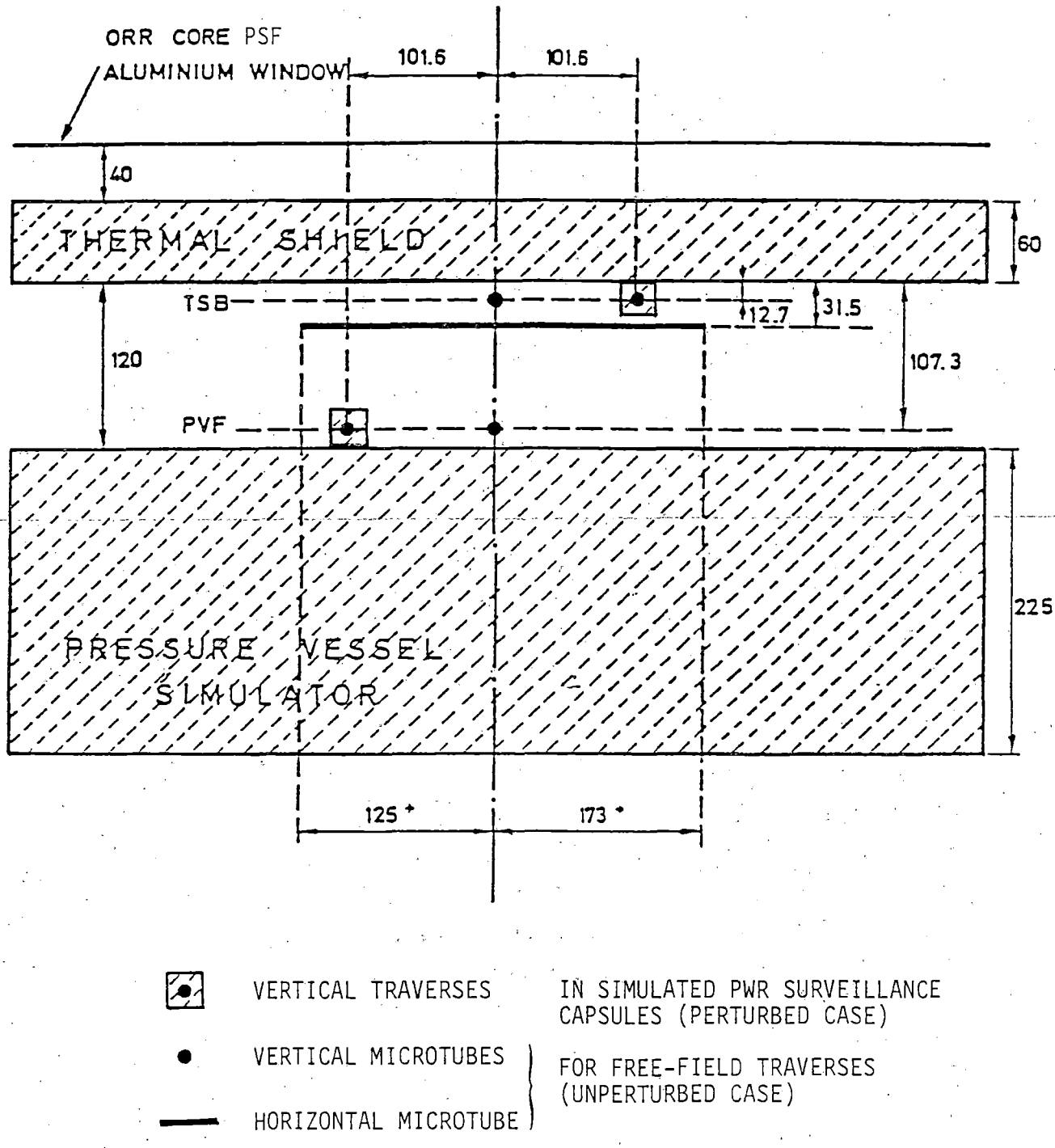

FIGURE 7. PSF-SDMF Perturbation Test Experimental Configuration. (Horizontal Cut at Maximum Axial Flux)

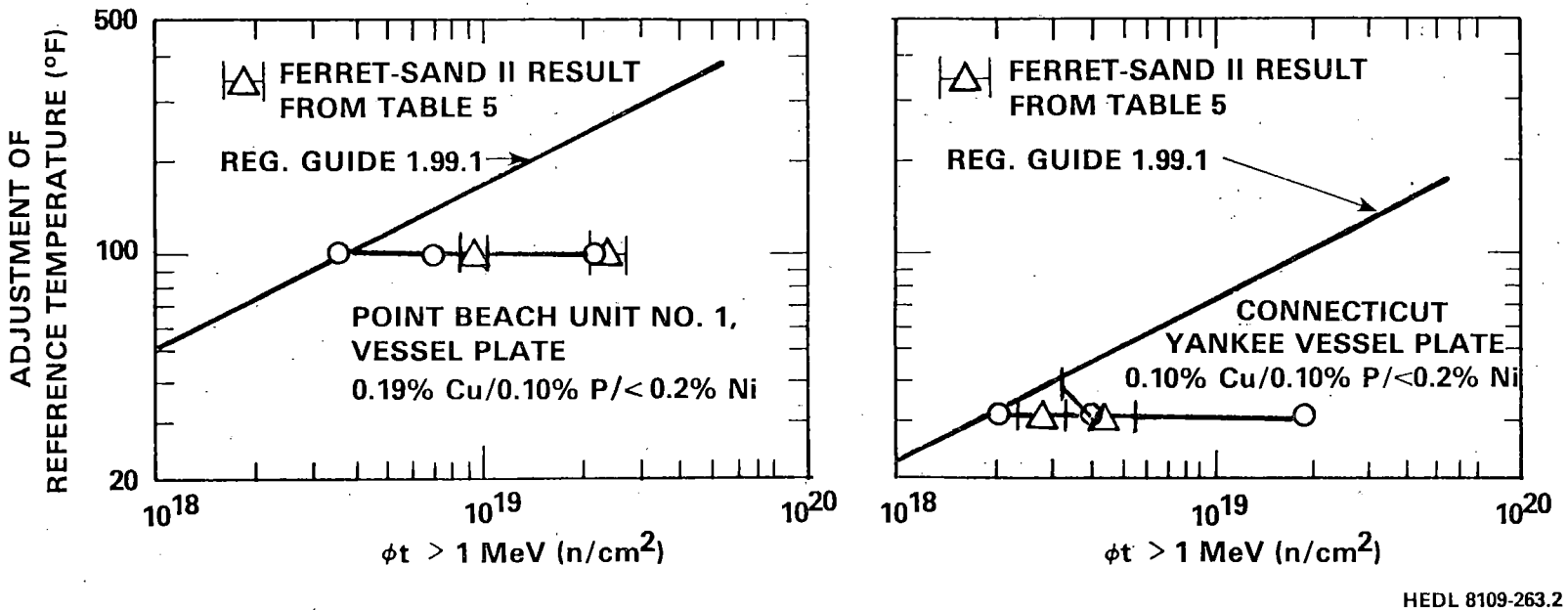

The vessel weldplate, not shown here, also shows apparent saturation. These results fit the hypothesis that materials containing significant amounts of nickel, i.e., greater than 0.5 wt%, do not show saturation in the range of fluence of interest. It appears that materials containing reduced amounts of nickel, i.e., about 0.2 wt%, do reach a saturation embrittlement level.[9] Studies are in progress by Guthrie,[14,15] Varsik,[16] Williams and Squires,[17] Yanichko et al.,[21,22] Pachur,[23] Mager et al.,[24] and others to verify such a hypothesis. It is concluded that there may be an effect of chemical composition on the shape of the trend curve, but data sets investigated to date have not shown any strong evidence of its existence.[14] Limited availability and the poor quality of some of the existing power reactor data are major reasons why this important question has not been answered; see Table 5 and Figure 6.

FIGURE 8. Point Beach Unit No. 1 and Connecticut Yankee Plant Specific Trend Curve Results.

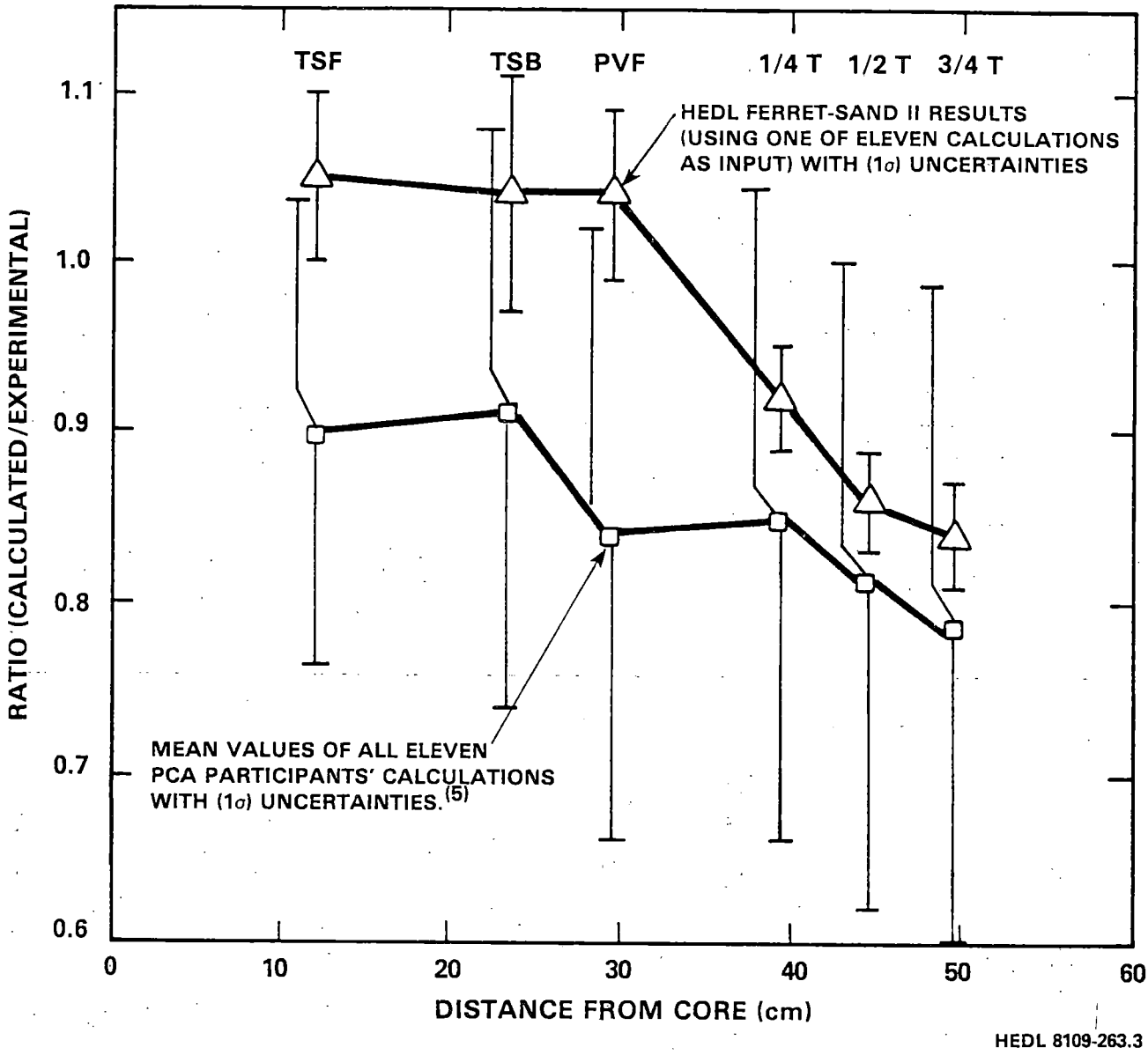

FIGURE 9. Calculated/Experimental Ratios for $\Phi_{E>1.0}$ (PCA 12/13 Configuration) at the Thermal Shield Front (TSF), Thermal Shield Back (TSB), Pressure Vessel Front (PVF), Pressure Vessel 1/4 T, 1/2 T and 3/4 T (Thickness) Positions. (Note that the calculations, generally, underpredicted the magnitude of the flux in passing through the PV wall, by up to an average value of ~20%, at the 3/4 T position; see Reference 5.)

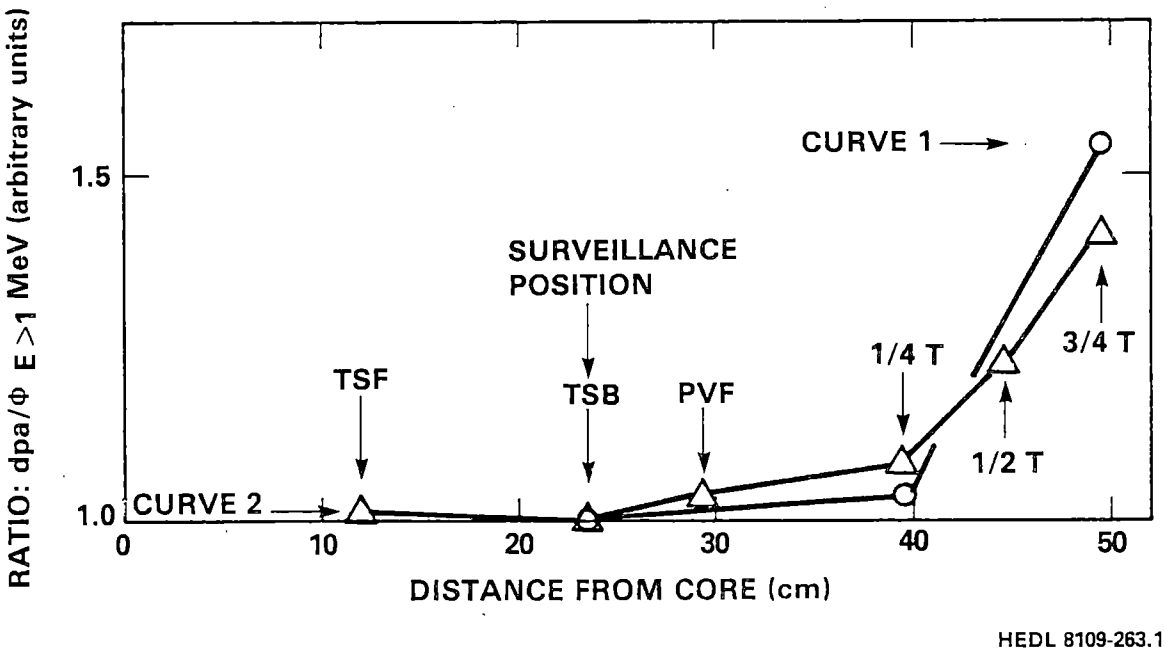

HEDL 8109-263.1

The use of $\phi_{E>1MeV}$ results in a nonconservative estimate of the neutron-produced embrittlement for deep penetration in the PV wall. A better exposure indicator is dpa for steel [using ASTM Standard E706-81 (I-D) (ASTM E693-79) of Figure 3]. The ratio of dpa to $\phi_{E>1MeV}$ is plotted in Curves 1 and 2. Verification of the applicability of dpa versus fluence (E > 1 MeV) will be accomplished via the PSF-PV Metallurgical Test, Table 1.[6,27]

Curve 1 is the result of calculations done for a PWR power plant. Curve 2 is derived from the PCA data used for Figure 9. The calculated neutron flux-spectra used to derive Curve 2 has been adjusted by passive dosimetry integral measurements and active spectrometry differential measurements as described in Reference 5.

Due to the similarity of conditions (i.e., water next to similar amounts of steel), the neutron spectral shapes are similar at higher energies for both the surveillance position and the 1/4 T position. However, deeper penetration in the PV steel causes substantial spectral changes.

The damage produced, as indicated by dpa, is about 50% higher at the 3/4 T position compared to what would be indicated by $\phi_{E>1MeV}$. Thus, the neutron embrittlement beyond one-fourth of the distance through the vessel may be significantly underestimated if $\phi_{E>1MeV}$ is used as a damage parameter.

FIGURE 10. Comparison of Definition and Implications of Spatial Lead Factors ($\phi_{E>1MeV}$ and dpa) at the Thermal Shield Front (TSF), Thermal Shield Back (TSB), Pressure Vessel Front (PVF), Pressure Vessel (PV) 1/4 T, 1/2 T, 3/4 T (Thickness) Positions.

TABLE 1

BENCHMARK FACILITIES*, TIME FRAME, PARTICIPANTS, PURPOSE AND USE

METALLURGICAL CALCULATIONAL BENCHMARK (IRL-PV)	CALCULATIONAL DOSIMETRY CALIBRATION BENCHMARKS	CALCULATIONAL BENCHMARK (PCA-PV)	METALLURGICAL TESTING BENCHMARK (PSF-PV)	SURVEILLANCE CAPSULE BENCHMARK (PSF-SDMF)	CORE SOURCE BOUNDARY BENCHMARK (VENUS)	GENERIC REACTOR BENCHMARKS (BWR-PWR)
1969-1971	1971-2000	1978-1982	1980-1984	1979-2000	1982-1983	1977-2000
1 VENDOR 2 NAT. LAB	MULTILAB FOR FBR-LWR PROGRAMS	MULTILAB VENDORS SERVICE LABS	MULTILAB VENDORS SERVICE LABS	MULTILAB VENDORS SERVICE LABS	MULTILAB VENDORS SERVICE LABS	MULTILAB VENDORS SERVICE LABS
PHYSICS DOSIMETRY METALLURGY SENSOR TESTS	PHYSICS DOSIMETRY SENSOR CALIBRATIONS & QUALITY ASSURANCE	PHYSICS DOSIMETRY SENSOR TESTS & QUALITY ASSURANCE	METALLURGY DOSIMETRY SENSOR LEAD FACTOR TESTS & QUALITY ASSURANCE	SURVEILLANCE CAPSULE PHYSICS DOSIMETRY LEAD FACTOR TESTS & QUALITY ASSURANCE	NEUTRON SOURCE TO SURVEILLANCE & PV WALL POSITIONS TESTS	PHYSICS DOSIMETRY SENSOR LEAD FACTOR IN-VESSEL EX-VESSEL TESTS

*Acronyms:

IRL-PV - Industrial Research Laboratory Pressure Vessel (PV) Mockup Test.[20]
PCA-PV - Pool Critical Assembly Physics-Dosimetry PV Mockup at ORNL.[5]
PSF-PV - Oak Ridge Research Reactor Pool Side Facility Metallurgical-Dosimetry PV Mockup.[6]
PSF-SDMF - PSF Simulated Dosimetry Measurement Facility.[6]
VENUS - Critical Facility at Mol, Belgium.
BWR - Boiling Water Reactor.
PWR - Pressurized Water Reactor.

TABLE 2

PHYSICS, DOSIMETRY AND METALLURGICAL VARIABLES

To account for neutron radiation damage in setting pressure-temperature limits and making fracture analyses, neutron-induced changes in fracture toughness and embrittlement for power reactor PV and support structure steels must be predicted, then checked by extrapolation of surveillance program data during the vessel's service life. Uncertainties in the predicting methodology can be significant. The main variables of concern are associated with:

1) Steel chemical composition and microstructure

2) Steel irradiation temperature

3) Power plant configurations and dimensions - core edge to surveillance to vessel wall to support structure positions

4) Core power distribution

5) Reactor operating history

6) Reactor physics computations

7) Selection of neutron exposure units

8) Dosimetry measurements

9) Neutron spectral effects

10) Neutron dose rate effects

Variables associated with the physical measurement of PV and support structure steel property changes are not considered here.

TABLE 3

MAIN ELEMENTS OF METALLURGICAL LEAD FACTOR DEFINITION

I. Is the Charpy measurement itself in error?

- A. Do results (both pre- and post-irradiation) fall on an S-shaped curve with ±15°F or less uncertainty in both tests?
- B. Were the samples transferred promptly from cold bath to test rig in pre-irradiation case?
- C. Are the thermocouples calibrated in post-irradiated test?
- D. Has the Charpy machine been calibrated? Was it tested at or near the time of measurement?
- E. Are the pre-irradiated results believable for the particular chemistry and heat treatment?
- F. Were sufficient points taken?
- G. Were points outside the transition region used in a computer code to bias the result?
- H. Was the ASTM procedure followed?

II. Are the specimens nonrepresentative?

- A. What are the densities of both pre- and post-irradiated specimens?
- B. Do x-ray tests of pre-irradiated specimens show flaws?
- C. Do the fracture surfaces of the specimens show pre-existing voids (regions of surface texture different from surrounding areas on fracture surface)?
- D. Does a post-irradiation chemistry check indicate misidentified specimens?
- E. Were the specimens marked for identification?

III. Is the temperature correctly known?

- A. Were the specimens tightly packed?
- B. What is the gamma heating rate?
- C. What was the heat transfer gas? Was it actually there?
- D. Were there thermal monitors? What did they show? Did they transmute?
- E. Could the capsule have been running cold due to reduced plant power level?

IV. Can the observed Charpy shift be reconciled to the temperature and neutron exposure by any means?

- A. Can a formula be found to fit?
  1. Use weld formulas for weld metal and plate formulas for plate metal, if possible.
  2. If ex-vessel, take into account lower temperature (Odette formulas).
  3. Check nonconforming formulas to see if the data base used to develop the formulas extended to a composition range and heat treatment that includes that of the specimens. Watch Cu, Ni, V, Mo, Si and C concentrations.
  4. Possible formulas are:
     - Varsik (Plate and weld separate).
     - Guthrie (Plate and weld separate).
     - Guionnet.
     - ASTM recommended practice formulas involving copper, derived from MPC data base.
     - ASTM Practice I-E of Pressure Vessel Surveillance Dosimetry Program (see E706-81 standard).[10]
     - Williams and Squires.
     - Odette.
- B. Is there prior test reactor data on the same or a similar specimen at a similar temperature?
  1. Check data reported by Hawthorne, Williams and Squires, Metals Property Council, EPRI, NRC, and others.
  2. If test reactor data exists, remember rate effects should make surveillance capsule shifts smaller, if there is any significant difference.

V. If formulas don't match data but data appear to be error free, develop plant specific curves for reactor using data produced from surveillance capsules.

VI. Extrapolate to the surface and 1/4 T positions using fluence and dpa ratios developed by dosimetry and reactor calculations. Take ratio of surveillance capsule position to the surface and 1/4 T positions to determine lead factors. Use plant-specific curve of Charpy shift versus fluence or dpa to get allowed EOL fluence.

- A. Validate reactor calculations using PCA data base.
- B. Validate reactor calculations using BWR or PWR generic-plant data base.
- C. Validate reactor calculations using plant-specific data.

TABLE 4

BWR AND PWR GENERIC BENCHMARK FACILITIES

Generic Reactor Benchmark Field	Measurements: Primary Funding Organization	Measurements: Primary Laboratory	Measurements: Verification Funding Organization	Measurements: Verification Laboratory	Calculations: Funding Organization	Calculations: Laboratory
Browns Ferry 3 In-Vessel (General Electric)	TVA GE	GE(c)*	NRC	HEDL (RM - 1 capsule)*	EPRI	Science Applications Inc.
Browns Ferry 3 Cavity (General Electric)	EPRI	GE(c)*	CEN NRC/EPRI(p) NRC/EPRI(p)	CEN(c) (RM - 1 capsule)* HEDL (RM - 1 capsule)* HEDL (SSTR - 1 capsule)	EPRI	Science Applications Inc.
Arkansas 1** Cavity (Babcock & Wilcox)	EPRI	Univ of Arkansas(c)*	NRC NRC/EPRI(p)	HEDL (RM - ~3 capsules)* HEDL (SSTR)	EPRI	Univ of Missouri(c) ORNL
Crystal River 3** In-Vessel and Cavity (Babcock & Wilcox)	B&W(p) EPRI?	B&W*	EPRI(p) NRC/EPRI(p)	? (RM)* HEDL (SSTR)	?	B&W(p)
Arkansas 2 (Combustion Engineering)	EPRI(p)	Univ of Arkansas*	EPRI(p) NRC/EPRI(p)	? (RM - 1 capsule)* HEDL (SSTR)	EPRI(p)	Univ of Missouri
McGuire 1 Cavity (Westinghouse)	EPRI(p)	?*	NRC/EPRI(p) NRC/EPRI(p)	HEDL (RM)* HEDL (SSTR)	EPRI(p)	?

(c) = completed; (p) = proposed; ? = unknown

*As appropriate, selected RM sensors (Fe, Ni, 0.1% Co-Al and Cu wires), Charpy specimens, and/or PV wall scrapings can be analyzed for generated helium by RI; see ASTM E706-81 (III-C) Method for Analysis of Helium Accumulation Fluence Monitors (HAFM) for Reactor Pressure Vessel Surveillance.

**Arkansas 1 and Crystal River 3 are both B&W 177-type plants; therefore, the test results from both are expected to be combined to establish a single set of data to be published for a 177 plant.

TABLE 5

RE-EVALUATED EXPOSURE VALUES FOR SURVEILLANCE CAPSULES

Reactor Unit	Capsule	Fluence ($\phi t > 1$ MeV) Old[a]	Fluence ($\phi t > 1$ MeV) New[b]	1σ% Uncer	Ratio New/Old	dpa[b] Value	dpa[b] 1σ% Uncer	Ratio dpa/ϕt New	dpa/s[b]	Time (s)	Cor. Mon. Charpy Shift (°F)	Weld Metal Charpy Shift (°F)	Weld Metal RT_{NDT}[c] (°F)	Weld Metal %Cu/%P/%Ni	Lead Factor[d]
WESTINGHOUSE															
Turkey Point 4	S	1.25 E+19	1.41 E+19	29	1.13	0.0215	26	1.52 E-21	1.98 E-10	1.084 E+8	110[e]	--	--	0.30/0.014/0.60	1.61
Turkey Point 4	T	6.05 E+18	8.22 E+18	15	1.36	0.0126	12	1.53 E-21	3.27 E-10	3.840 E+7	100[e]	225	225	0.30/0.014/0.60	2.48
Turkey Point 3	S	1.41 E+19	1.69 E+19	28	1.20	0.0244	25	1.44 E-21	2.33 E-10	1.047 E+8	130	--	--	0.31/0.011/0.57	1.61
Turkey Point 3	T	5.68 E+18	7.68 E+18	10	1.35	0.0112	12	1.46 E-21	3.23 E-10	3.473 E+7	80	162	165	0.31/0.011/0.57	2.48
H. B. Robinson 2	S	3.02 E+18	3.96 E+18	28	1.31	0.00640	25	1.61 E-21	1.46 E-11	4.385 E+7	80	--	--	0.34/0.021/ --	1.61
H. B. Robinson 2	V	4.51 E+18	6.41 E+18	27	1.42	0.00976	24	1.52 E-21	9.20 E-11	1.061 E+8	102	185	110	0.30/0.021/ --	0.79
Prairie Island 1	V	5.21 E+18	7.00 E+18	11	1.34	0.0120	13	1.71 E-21	2.77 E-10	4.350 E+7	113[e]	27	-32	0.13/0.017/<0.2	2.5
Prairie Island 2	V	5.49 E+18	7.45 E+18	9	1.37	0.0128	11	1.71 E-21	2.87 E-10	4.454 E+7	130[e]	63	-10	0.08/0.019/0.072	2.5
Point Beach 1	S	--	9.28 E+18	9	--	0.0155	10	1.67 E-21	1.34 E-10	1.163 E+8	--	--	--	0.24/0.019/0.57	1.4
Point Beach 1	R	2.22 E+19	2.41 E+19	11	1.11	0.0419	11	1.74 E-21	2.57 E-10	1.632 E+8	110	165	120	0.24/0.019/0.57	2.5
R. E. Ginna 1	R	7.60 E+18	1.32 E+19	9	1.73	0.0232	11	1.75 E-21	2.68 E-10	8.628 E+7	95	183	140	0.23/0.012/0.56	2.5
R. E. Ginna 1	V	5.32 E+18	5.55 E+18	12	1.04	0.00996	15	1.79 E-21	2.54 E-10	3.923 E+7	83	153	112	0.23/0.012/0.56	3.3
Kewaunee	V	5.59 E+18	7.13 E+18	9	1.28	0.124	11	1.72 E-21	2.97 E-10	4.167 E+7	95[e]	175	115	0.20/0.016/0.77	2.5
San Onofre 1	A	1.20 E+19	2.65 E+19	19	2.21	0.0445	18	1.68 E-21	7.42 E-10	5.846 E+7	120	80	60	0.19/0.17/<0.2	4.8
San Onofre 1	D	2.36 E+19	4.40 E+19	20	1.87	0.0742	19	1.69 E-21	8.32 E-10	8.914 E+7	155	--	--	0.19/0.17/<0.2	5.1
San Onofre 1	F	5.14 E+19	6.45 E+19	12	1.25	0.110	15	1.71 E-21	4.49 E-10	2.451 E+8	130	135	113	0.19/0.17/<0.2	1.8
Point Beach 2	T	9.45 E+18	1.04 E+19	9	1.10	0.0165	10	1.59 E-21	1.50 E-10	1.098 E+8	110[e]	154	154	0.25/0.014/0.59	1.6
Point Beach 2	V	4.74 E+18	7.24 E+18	12	1.53	0.0120	11	1.66 E-21	2.48 E-10	4.859 E+7	85[e]	165	165	0.25/0.014/0.59	2.5
Point Beach 2	R	2.01 E+19	2.56 E+19	11	1.27	0.0438	11	1.71 E-21	2.72 E-10	1.609 E+8	151[e]	230	230	0.25/0.014/0.59	3.37
Conn. Yankee	A	2.08 E+18	2.92 E+18	17	1.40	0.00424	13	1.47 E-21	7.89 E-11	5.377 E+7	85	95	45	0.22/0.020/0.05	6.1
Conn. Yankee	F	4.04 E+18	4.38 E+18	30	1.08	0.00645	26	1.47 E-21	8.35 E-11	7.728 E+7	85	--	--	0.22/0.020/0.05	1.3
Conn. Yankee	H	1.79 E+19	--	--	--	--	--	--	--	--	127	--	--	0.22/0.020/0.05	1.57
COMBUSTION ENGINEERING															
Maine Yankee	1	1.30 E+19	--	--	--	--	--	--	--	2.99 E+7	145[e]	270	240	0.36/0.015/0.78	30.0
Maine Yankee	2	8.84 E+19	1.01 E+20	12	1.14	0.155	13	1.53 E-21	1.07 E-9	1.446 E+8	--	345	315	0.36/0.015/0.78	--
Maine Yankee	263	6.90 E+18	6.72 E+18	8	0.97	0.00988	9	1.47 E-21	6.84 E-11	1.446 E+8	--	222	192	0.36/0.015/0.78	1.76
BABCOCK & WILCOX															
Oconee 1	F	8.70 E+17	6.35 E+17	17	0.73	0.00090	14	1.40 E-21	3.52 E-11	2.625 E+7	14[e]	--	--	0.18/0.014/0.52	1.6
Oconee 1	E	1.50 E+18	1.48 E+18	17	0.99	0.0020	14	1.39 E-21	4.20 E-11	5.166 E+7	35[e]	65	75	0.32/0.016/0.58	1.65

Fluence Scale Adjustment Range (Maxima/Minima) = 3.03

(a) Surveillance capsule report values based on previous standards and recommended procedures and data.
(b) Preliminary FERRET-SAND II derived new values based on current standards and recommended procedures and data; an estimate of possible total bias uncertainties (physics-calculational, sensor QA, photofission, etc. corrections) is not included at present; see Table 10 and Figure 9.
(c) $RT_{NDT} = RT_{NDT_0} + \Delta RT_{NDT}$ [41 J (30 ft-lb)].
(d) Calculated ratio of surveillance capsule to pressure vessel wall maximum fluence ($E > 1.0$ MeV) values.
(e) A533B steel (%Cu/%P/%Ni = 0.14/0.012/0.66, except for Oconee which is 0.17/0.013/0.64), otherwise A302B steel (0.20/0.011/0.18); 41 J (30 ft-lb) Charpy shift (ΔRT_{NDT}).

TABLE 6

OPERATING REACTORS WITH HIGH FLUENCE EXPOSURE

Plant	Manufacturer Plant	Manufacturer Vessel	Percent Copper Circ. Welds	Percent Copper Long. Welds	Time (EFPY)	Fluence[a] (E > 1.0 MeV) x 10^{18} n/cm^2 Circ. Welds	Fluence[a] (E > 1.0 MeV) x 10^{18} n/cm^2 Long. Welds	RT_{NDT} at PV Front Face (°F) Calculated[b] Circ. Welds	Calculated[b] Long. Welds	Measured[c] Circ. Fluence	Measured[c] Long. Fluence	Surveillance Capsule ID
Fort Calhoun	CE	CE	0.35	0.35	4.8	8.2	8.2	280	280	--	--	--
H. B. Robinson	W	CE	0.34	0.34	6.8	11.7	10.8	290	290	175	165	V
Turkey Point 3	W	B&W	0.31	--	5.7	11.2	--	290	--	200	--	T
Turkey Point 4	W	B&W	0.30	--	5.2	10.2	--	280	--	250	--	T
San Onofre 1	W	CE	0.19	0.19	8.8	15.4	15.4	270	270	41	41	A
San Onofre 1	W	CE	0.19	0.19	8.8	15.4	15.4	270	270	44	44	F
Maine Yankee	CE	CE	0.36	0.36	5.5	4.7	4.7	240	240	160	160	2[d]
Maine Yankee	CE	CE	0.36	0.36	5.5	4.7	4.7	240	240	156	156	263
Calvert Cliffs 1	CE	CE	0.30	0.30	4.1	6.0	6.0	230	230	--	--	--
TMI 1	B&W	B&W	0.35	0.31	3.5	2.1	2.1	180	160	--	--	--
Oconee 1	B&W	B&W	0.26	0.31	4.9	2.6	2.3	150	170	76	71	E
Palisades	CE	CE	0.25	0.25	3.9	4.6	4.6	190	190	--	--	--
Yankee Rowe	W	B&W	(0.20 for plate)		14.1	(11.0 for plate)		(200 for plate)		--	--	--
Zion 1	W	B&W	0.35	0.31	4.3	2.7	0.9	170	90	--	--	--
Arkansas 1	B&W	B&W	0.31	0.31	3.9	2.4	1.7	170	150	--	--	--
Indian Point 2	W	CE	(0.25 for plate)		4.0	(2.0 for plate)		(140 for plate)		--	--	--
Rancho Seco	B&W	B&W	0.31	0.31	3.3	2.1	1.9	160	150	--	--	--
Surry 1	W	B&W	0.25	0.18	4.5	7.0	1.5	190	60	--	--	--
Crystal River 3	B&W	B&W	0.35	0.31	2.2	1.3	1.2	150	130	--	--	--

(a) As of May 1, 1981.

(b) RT_{NDT} was calculated by P. N. Randall using known chemistry, presently believed fluence at PV front face and Regulatory Guide 1.99.1.

(c) RT_{NDT} was determined using measured Charpy shifts for surveillance-capsule weld material and new values of fluence (E > 1.0 MeV), Table 5. The Regulatory Guide 1.99.1[2] fluence dependency (N = 1/2) was used to scale the accelerated surveillance capsule results back to the column 7 and 8 values of fluence.

(d) The Reg. Guide 1.99.1 upper-limit fluence dependency, Figure 6, was used to scale back the Maine Yankee accelerated Capsule 2 results.

TABLE 7

PSF-SDMF PERTURBATION TEST RESULTS

Reaction	Unperturbed-to-Perturbed Reaction Rate Ratios					
	Thermal Shield Back (TSB)			Pressure Vessel Front (PVF)		
	Experiment	Calculation	C/E	Experiment	Calculation	C/E
$^{237}Np(n,f)$	0.756	0.749	0.991	--	0.798	--
$^{93}Nb(n,n')$	0.833	--	--	0.895	--	--
$^{238}U(n,f)$	0.852	0.840	0.986	--	0.871	--
$^{58}Ni(n,p)$	0.919	0.922	1.003	0.962	0.942	0.979
$^{54}Fe(n,p)$	0.887	0.937	1.056	0.936	0.953	0.974
$^{46}Ti(n,p)$	0.971*	0.990	1.020	0.978*	0.993	1.015
$^{63}Cu(n,\alpha)$	1.042	1.006	0.965	--	1.004	--

*The reaction listed was Ti(n,x) by experimenter.

TABLE 8

TYPICAL SINGLE PLANT RATIOS (MAXIMA/MINIMA) FOR MEASURED SURVEILLANCE CAPSULE REACTION RATES FOR INDIVIDUAL SENSORS AS A RESULT OF DIFFERENCES IN CORE SOURCE DISTRIBUTIONS

Sensor Reaction	Approx Maxima/Minima* Reaction Rate Ratio
$^{58}Ni(n,p)^{58}Co$	1.6
$^{54}Fe(n,p)^{54}Mn$	1.4
$^{63}Cu(n,\alpha)^{60}Co$	1.3
$^{238}U(n,f)^{137}Cs$	1.5
$^{237}Np(n,f)^{137}Cs$	1.4

*Based on core fuel subassembly replacement calculational and measurement studies. The fluence > 1 MeV at the inner PV surface will, generally, follow these ratios. It is noted that a substantial part of the PCA program has addressed the neutronic validation of LWR-PV lead factors in a slab arrangement of thermal shield and pressure vessel simulator, driven by a clean, well-characterized MTR-type core. It has focused upon the deep-penetration projection uncertainties in this lead factor issue. Actual LWR lead factors also involve significant azimuthal flux variations, whose calculational accuracy depends upon:

- Correct estimates of core source distributions, on a pin-to-pin basis for the last fuel row, in terms of the total absolute core power, and
- Correct modeling of core boundary heterogeneity effects and, in more recent plants, of the heterogeneity effect of neutron pads attached to the core barrel (thermal shield).

The LWR-PV VENUS and BWR and PWR generic benchmarks (Table 1) are concerned with these issues.

TABLE 9

DOSIMETRY/PHYSICS RESULTS FOR POINT BEACH 2

	Capsule V	Capsule T	Capsule R
INITIAL ANALYSIS	4.74×10^{18} ($n/cm^2 > 1.0$ MeV)(a)	9.45×10^{18}(b)	20.1×10^{18}(c)
AFTER WESTINGHOUSE REANALYSIS	6.53×10^{18}	8.29×10^{18}	20.1×10^{18}
RATIO: AFTER/INITIAL	1.37	0.88	1.0
RELATIVE SWING	Capsule V/T = 1.37/0.88 = 1.56		Capsule R/T = 1.0/0.88 = 1.14
AFTER HEDL REANALYSIS(d)	$7.24 \times 10^{18} \pm 12\%$ (1σ)	$1.04 \times 10^{19} \pm 9\%$ (1σ)	$2.56 \times 10^{19} \pm 11\%$ (1σ)
RATIO: AFTER/INITIAL	1.53	1.10	1.27
RELATIVE SWING	Capsule V/T = 1.53/1.10 = 1.39		Capsule R/T = 1.27/1.10 = 1.15

CONCLUSION: All surveillance reports and test reactor reports must be reanalyzed to define new exposure values and uncertainties using current standards and recommended procedures and data.

(a)Surveillance Capsule Report V, June 10, 1975.(18)
(b)Surveillance Capsule Report T, August 1978.(19)
(c)Surveillance Capsule Report R, December 1979.(21)
(d)Preliminary FERRET-SAND II results, taken from Table 5.

TABLE 10

HEDL ANALYSIS POINT BEACH 2 CAPSULE R SURVEILLANCE DOSIMETERS[a]
COMPARISON WITH WESTINGHOUSE ANALYSIS

Reaction and Axial Location[b]	R[b] (cm)	Saturated Activity (dps/g) HEDL	Saturated Activity (dps/g) Westinghouse[b,c]	(West. - HEDL/HEDL) Comparison (%)
$^{59}Co/Al(n,\gamma)$, Bare				
Top		11.67 E+10	11.8 E+10	+1.08
Mid Top		8.297 E+10	8.20 E+10	-1.17
Middle		8.639 E+10	8.67 E+10	+0.32
Mid Bottom		--	--	--
Bottom		11.53 E+10	11.47 E+10	-0.58
$^{59}Co/Al(n,\gamma)$, Cadmium-Covered				
Top		4.575 E+10	4.59 E+10	+0.26
Mid Top		4.426 E+10	4.43 E+10	+0.02
Middle		4.233 E+10	4.27 E+10	+0.80
Mid Bottom		5.055 E+10	5.09 E+10	+0.62
Bottom		4.794 E+10	4.82 E+10	+0.54
$^{63}Cu(n,\alpha)$				
Top	158.33	4.382 E+5	4.28 E+5	-2.33
Mid Top	158.33	3.880 E+5	3.87 E+5	-0.25
Mid Bottom	158.33	4.318 E+5	4.28 E+5	-0.89
Bottom	158.33	4.593 E+5	4.54 E+5	-1.14
$^{54}Fe(n,p)$[d]				
V-13	157.33	6.16 E+6	6.18 E+6	+0.30
E-23	157.33	5.752 E+6	5.72 E+6	+0.56
E-13	157.33	5.183 E+6	4.96 E+6	-4.30
H-9	158.33	4.893 E+6	4.66 E+6	-4.76
R-14	158.33	4.904 E+6	4.77 E+6	-2.73
W-16	158.33	4.936 E+6	4.61 E+6	-6.60
$^{58}Ni(n,p)$				
Middle	158.33	7.390 E+7	7.45 E+7	+0.81
$^{237}Np(n,f)^{137}Cs$				
Middle	158.10	7.180 E+7	6.79 E+7	-5.43
$^{238}U(n,f)^{137}Cs$[e]				
Middle	158.10	9.534 E+6	9.03 E+6	-4.95

[a] Samples of Co/Al and Cu are being shipped to Rockwell International for He analysis. The remaining samples are to be shipped to CEN/SCK for additional radiometric analysis. Discussions have been held with NBS, and certified fission flux standard samples will be prepared by NBS and submitted to HEDL for analysis.

[b] Distance from core center, data from EPRI Progress Report, WCAP-9635, December 1979.[21]

[c] Westinghouse-reported values for Co/Al samples were reported per weight of alloy dosimeter material. Reported values were multiplied by 1/0.0025 to obtain activity per gram cobalt. QA confirmation of the Co alloy content is planned by neutron activation at NBS and calculation from both the certified thermal flux supplied by NBS and the relative ratio with SRM 953.

[d] Calculations for this reaction were made using the iron content as determined by HEDL for the specific solutions received from Westinghouse, see Table 10 continued.

[e] Calculations are based on the ^{238}U solution content determined by HEDL, see Table 10 continued. Corrections have not been made for ^{235}U impurity, $^{238}U(n,\gamma)^{239}Pu$ buildup or photofission contributions. Preliminary calculations at HEDL indicate corrections of as much as ~6% for ^{235}U and ~16% for ^{239}Pu may be required. Rough calculations at Westinghouse indicate <3% correction for photofission contribution.

TABLE 10 (Cont'd)

HEDL ANALYSIS POINT BEACH 2 CAPSULE R SURVEILLANCE DOSIMETERS
QA OVERCHECKS

Analyzing Laboratory	Analysis of	^{238}U Content (mg/200 mℓ)	Isotopic Analysis (at.%) ^{233}U	^{234}U	^{235}U	^{236}U	^{238}U
ORNL-Westinghouse	$^{238}U_3O_8$ Dosimeter Solution	11.91	<0.0001	0.0004	0.0322	0.0001	99.9673
HEDL (by IDMS*)	$^{238}U_3O_8$ Dosimeter Solution	12.10		<0.001	0.034	<0.001	99.963
		Fe Content (mg/mℓ)					
HEDL (by Atomic Absorption)	Fe Charpy Solution						
	Sample No. 2450	2.436					
	Sample No. 2451	4.053					
	Sample No. 2452	7.665					
	Sample No. 2453	4.433					
	Sample No. 2454	6.459					
	Sample No. 2455	4.858					
		Co Content (wt%)					
Vendor Certification	Co/Al Alloy	0.15					
HEDL (by Neutron Activation)	Co/Al Alloy						

Irradiation will be made at NBS with subsequent analysis at HEDL. Comparative calculations will be made from both relative ratios to SRM 953 material irradiated simultaneously, and from the thermal cross section and certified flux-fluence.

*Isotope dilution mass spectrometry.

TABLE 11

REPORTED SURVEILLANCE CAPSULES SINGLE FOIL
FLUX/FLUENCE VALUES (ϕ_i > 1 MeV) RELATIVE TO $^{54}Fe(n,p)$ RESULT

Reactor Name (Vendor-Type, Country, Operation Date)	Service Laboratory Report	Single Foil Flux/Fluence > 1 MeV			
		$\phi_{^{58}Ni(n,p)}$	$\phi_{^{63}Cu(n,\alpha)}$	$\phi_{^{238}U(n,f)(f)}$	$\phi_{^{237}Np(n,f)(f)}$
Point Beach 1	BMI (1973)[a]	1.09	1.63	1.61	2.17
(West. PWR, USA, 12/70)		[Reported[e] Surveillance Value: 1.0(Fe)]			
Same (Angle A)	West. (1979)[b]	0.80	1.51[c]	1.03	1.25
Same (Angle A + 180°)	West. (1979)[b]	1.01	1.41[c]	1.13	1.01
		[Reported[e] Surveillance Value: 1.0(Fe)]			
Average Values for Seven West. Power Plants	West. (1979)[b]	0.97	1.25[c]	1.08	1.15
Humboldt Bay 3	GE (1967)[a]	0.88	0.80	--	--
(GE BWR, USA, 8/63)		[Reported[e] Surveillance Value: 1.0(Fe)]			
San Onofre 1	SWRI (1971)[a]	1.00	1.27	1.10	1.42 (BNW Spectrum 1)
(West. PWR, USA, 1/68)	SWRI (1971)[a]	1.05	0.88	1.29	1.45 (BNW Spectrum 2)
		[Reported[e] Surveillance Value: 0.85 (SAND II, multiple foils)]			
Oconee 1	B&W (1975)[a,b]	1.18	--	2.50	2.70
(B&W PWR, USA, 7/73)		[Reported[e] Surveillance Value: $\frac{1.0 + 2.5}{2}$ = 1.76(Fe+U)]			
Doel 1	CEN/SCK (1979)	1.09	1.51[c]	--	2.41
(Belgium-West. PWR,	CEN/SCK (1979)	1.09	1.06[d]	--	2.41
Belgium, 1/75)		[Reported[e] Surveillance Value: ~1.09(Ni)]			

(a) The results reported in Columns 3-6 are based on the application of old standards, procedures and data and are, therefore, not representative of current capabilities and technology (see Table 5).

(b) Surveillance capsule flux perturbation corrections were calculated by Westinghouse to provide necessary correlations between the U, Np, Cu, Ni and Fe results. No other results shown in the table were corrected for perturbation effects. The current Westinghouse and B&W analyses (Table 5) have made use of newer standards and recommended procedures and data and are, therefore, more representative of current capabilities and technology.

(c) ENDF/B-IV $\sigma(E)$ for $^{63}Cu(n,\alpha)$.

(d) Mann-Schenter $\sigma(E)$ for $^{63}Cu(n,\alpha)$.

(e) These reported surveillance capsule measured fluence values are used for correlating the surveillance capsule metallurgical data with other test and power reactor data. They are also used for making localized predictions of expected PV lifetime neutron exposures and/or can be used to simply confirm the correctness of one-, two- and three-dimensional reactor physics computations.

(f) Based on ^{137}Cs analysis; the Ni, Fe and Cu provide experimental fluence data for time periods up to about 1 year, 5 years and 25 years with a knowledge of the surveillance capsule flux level time history. This information is not needed, however, for a reliable interpretation of fission foil ^{137}Cs ($t_{1/2} \sim 31$ years) results.

TABLE 12

RESULTS OF FAST NEUTRON DOSIMETRY FOR CAPSULES V AND R FOR KEWAUNEE
(Demonstration of the Value of Using Multiple Sensor and
Benchmarked Reactor Physics Results)

Capsule	Reaction	Adjusted Saturated Activity (dis/s)		ϕ (E > 1.0 MeV) (n/cm^2-s)		ϕ (E > 1.0 MeV) (n/cm^2)	
		Measured	Calculated	Measured	Calculated	Measured	Calculated
V	$Fe^{54}(n,p)Mn^{54}$	5.30×10^6	5.65×10^6	1.36×10^{11}	1.45×10^{11}	5.36×10^{18}	5.71×10^{18}
	$Cu^{63}(n,\alpha)Co^{60}$	4.51×10^5	3.86×10^5	1.69×10^{11}		6.66×10^{18}	
	$Ni^{58}(n,p)Co^{58}$	7.27×10^7	8.37×10^7	1.26×10^{11}		4.96×10^{18}	
	$Np^{237}(n,f)Cs^{137}$	7.84×10^7	7.01×10^7	1.62×10^{11}		6.38×10^{18}	
	$U^{238}(n,f)Cs^{137}$	8.89×10^6	7.72×10^6	1.67×10^{11}		6.58×10^{18}	
R	$Fe^{54}(n,p)Mn^{54}$	3.77×10^6	5.65×10^6	9.68×10^{10}	1.45×10^{11}	1.37×10^{19}*	2.06×10^{19}
	$Cu^{63}(n,\alpha)Co^{60}$	4.94×10^5	3.86×10^5	1.86×10^{11}		2.64×10^{19}	
	$Ni^{58}(n,p)Co^{58}$	8.50×10^7	8.37×10^7	1.47×10^{11}		2.09×10^{19}	
	$Np^{237}(n,f)Cs^{137}$	not determined	7.01×10^7	not determined		—	
	$U^{238}(n,f)Cs^{137}$	8.33×10^6	7.72×10^6	1.56×10^{11}		2.22×10^{19}	

*The $^{54}Fe(n,p)^{54}Mn$ results obtained from Capsule R are inconsistent with the remaining dosimetry from Capsule R as well as with the iron data from Capsule V. The iron data from Capsule V agree with the overall average (within 12%), while, for Capsule R, the iron data are low by 51%. The reason for this discrepancy is not known.[22] This demonstrates the value of having multiple sensor, more than one surveillance capsule, and benchmarked reactor physics results so that "bad" sensor data points may be easily identified and assigned higher uncertainty values.

TABLE 13

INTERLABORATORY COMPARISON OF RADIOMETRIC (RM) ANALYSIS PROCEDURES AND DATA[a]
[Range Evaluation (Maxima/Minima) of RM Results Based on First PSF-SDMF Test]

Sensor[b] Set No.	$^{58}Ni(n,p)$ Ratio 1	Ratio 2	Ratio 3	Labs	$^{46}Ti(n,p)$ Ratio 1	Ratio 2	Ratio 3	Labs	$^{63}Cu(n,\alpha)$ Ratio 1	Ratio 2	Ratio 3	Labs	$^{54}Fe(n,p)$ Ratio 1	Ratio 2	Ratio 3	Labs
HNF - 1	1.14 C/B	1.10 D/B	1.06 D/C	6	1.39 C/B	1.16 C/B	1.04 C/I	6	1.11 F/B	---	1.09 F/E	6	1.38 C/B	1.11 C/B	1.04 C/F	6
HNF - 3	1.28 C/B	1.09 A/B	1.05 A/C	6	1.48 C/B	1.21 C/B	1.04 C/A	6	1.05 C/I	1.06 C/F	---	6	1.27 C/B	1.10 A/B	1.04 A/F	6
HNF - 2	1.25 C/B	1.13 F/B	1.06 F/E	6	1.42 C/B	1.19 C/B	1.08 C/I	6	1.06 C/E	1.09 C/E	---	6	1.46 C/B	1.12 A/B	1.06 A/E	6
HNF - 4	1.28 C/B	1.14 F/B	1.06 F/E	6	1.41 C/B	1.09 C/B	1.08 C/F	6	1.08 C/E	1.09 F/E	---	6	1.43 C/B	1.13 C/B	1.04 C/F	6

	$^{58}Fe(n,\gamma)$ Ratio 1	Ratio 2	Ratio 3	Labs
HNF - 1	1.15 C/A	1.03 E/A	1.03 E/A	3[c]
HNF - 3	1.02 C/E	1.02 A/E	1.02 A/E	3
HNF - 2	1.23 C/A	1.04 E/A	1.04 E/A	3
HNF - 4	1.12 C/E	1.01 A/E	1.01 A/E	3

Sensor Set No.	$^{59}Co/Al(n,\gamma)$ Ratio 1	Ratio 2	Ratio 3	Labs
HF - 3	1.15 C/B	1.09 C/B	1.06 C/F	6
HF - 5	1.15 C/B	1.11 C/B	1.04 C/D	6
HF - 4	1.06 F/B	1.09 C/B	1.05 C/F	6
HF - 6	1.23 C/B	1.17 C/B	1.07 C/E	6

	$^{235}U(n,f)^{140}Ba$ Ratio 1	Ratio 2	Ratio 3	Labs	$^{235}U(n,f)^{103}Ru$ Ratio 1	Ratio 2	Ratio 3	Labs	$^{235}U(n,f)^{95}Zr$ Ratio 1	Ratio 2	Ratio 3	Labs	$^{235}U(n,f)^{137}Cs$ Ratio 1	Ratio 2	Ratio 3	Labs
HF - 3	1.06 A/E	---	---	3	1.19 C/D	1.22 A/C	1.08 A/D	4	1.09 D/C	1.22 D/C	1.08 D/E	5	---	1.11 E/C	---	3
HF - 5	1.19 A/D	---	---	3	1.73 C/D	1.19 C/D	1.07 C/E	4	1.51 C/B	1.29 C/B	1.12 C/E	5	---	1.31 C/D	---	3
HF - 4	1.05 A/D	---	---	3	1.30 C/D	1.09 A/C	---	4	1.13 D/C	1.14 D/C	1.07 A/C	5	---	1.05 F/C	---	3
HF - 6	1.13 A/D	---	---	3	1.43 C/D	1.14 A/D	---	4	1.15 C/E	1.11 A/C	1.07 A/B	5	---	1.07 C/D	---	3

	$^{237}Np(n,f)^{140}Ba$ Ratio 1	Ratio 2	Ratio 3	Labs	$^{237}Np(n,f)^{103}Ru$ Ratio 1	Ratio 2	Ratio 3	Labs	$^{237}Np(n,f)^{95}Zr$ Ratio 1	Ratio 2	Ratio 3	Labs	$^{237}U(n,f)^{137}Cs$ Ratio 1	Ratio 2	Ratio 3	Labs
HF - 1	1.10 A/F	---	1.04 A/D	4	1.37 C/F	1.11 A/C	---	5	1.16 A/E	1.21 B/C	1.16 A/E	6	---	1.09 D/C	---	4
HF - 2	1.13 A/E	---	---	4	1.27 C/F	1.12 A/F	---	5	1.14 D/F	---	---	6	---	1.12 F/D	---	4

	$^{238}U(n,f)^{140}Ba$ Ratio 1	Ratio 2	Ratio 3	Labs	$^{238}U(n,f)^{103}Ru$ Ratio 1	Ratio 2	Ratio 3	Labs	$^{238}U(n,f)^{95}Zr$ Ratio 1	Ratio 2	Ratio 3	Labs	$^{238}U(n,f)^{137}Cs$ Ratio 1	Ratio 2	Ratio 3	Labs
HF - 1	1.09 A/D	---	1.04 D/E	4	1.44 C/F	1.11 A/F	---	5	1.16 C/F	1.13 D/C	1.06 B/F	6	---	1.08 E/C	---	4
HF - 2	1.09 A/E	---	---	4	1.27 C/F	1.07 A/E	---	5	1.13 D/E	---	---	6	---	1.06 D/E	---	4

(a)Four vendors and two service laboratories participated in this test. All laboratories remain anonymous for these intercomparisons and are identified only as Laboratories A, B, C, D, E and F.[6] The table evaluation shows the present laboratory-to-laboratory comparative status but also shows the improvement in the data comparisons (Ratios 2 and 3) as a result of interim evaluations and discussions with participants. Ratio 2 was obtained after discussions with participants and subsequent reworking of data by participants. For Ratio 3, and for the case of nonfissile sensors, the results from Laboratory B appeared to be consistently biased low and were, therefore, not used. In the case of the fissile sensors, if a participant appeared to be definitely biased, those results were not used in Ratio 3.

(b)HNF-X and HF-X are sensor set identification numbers for specific perturbed locations in 1-in. x 1-in. stainless steel simulated surveillance capsules for this first PSF-SDMF test; see Table 7 for a preliminary comparison of C/E ratios.

(c)Results for the $^{58}Fe(n,\gamma)$ reaction were not reported by one laboratory after preliminary recalibration of their counting system.

TABLE 14

COMPARISON OF RESULTS OF INTERLABORATORY CONSISTENCY IN MEASURING NICKEL FLUENCE STANDARDS[a]

Nickel Foil ID	^{235}U Fission Spectrum Fluence in $10^{15} m/cm^2$ Reported Value[b]	NBS Value[c]	Ratio of Reported to NBS Value
AP	1.48 ± 5.5 %	1.51 ± 2.5%	0.98
AR	1.479 ± 0.84%	1.47 ± 2.7%	1.01
AS	1.491 ± 1.2 %	1.49 ± 2.7%	1.00
AU	1.672 ± 2.8 %	1.58 ± 3.6%	1.06
BL	2.85 ± 4.0 %	2.66 ± 2.5%	1.07
BM	2.60 ± 2.26%	2.65 ± 2.7%	0.98
BN	2.388 ± 0.07%	2.74 ± 2.8%	0.87
BV	2.479 ± ---	2.36 ± 2.8%	1.05
BW	2.25 ± 2.0 %	2.23 ± 3.0%	1.01
BY	2.17 ± 4.0 %	2.23 ± 3.2%	0.97
BX(1)[b]	2.286 ± 3.1 %	2.20 ± 3.2%	1.04
BX(2)	2.232 ± 1.2 %	(2.20 ± 3.2%)	1.01
CA	1.964 ± ---	2.10 ± 3.2%	0.94
CD(1)[c]	2.08 ± (1.8 %)	2.12 ± 3.5%	0.98
CD(2)	2.10 ± (1.7 %)	(2.12 ± 3.5%)	0.99
CD(3)	2.13 ± (1.7 %)	(2.12 ± 3.5%)	1.00
CG	1.61 ± 3.0 %	1.66 ± 2.9%	0.97
CI	1.96 ± 1.6 %	1.73 ± 3.2%	1.13
CJ	2.14 ± ---	2.30 ± 2.7%	0.93
CL	2.26 ± 3.3 %	2.23 ± 2.9%	1.01
	Fluence Scale Adjustment Range (1.13 ÷ 0.87) =		1.30

(a) Prepared by activation of the $^{58}Ni(n,p)^{58}Co$ reaction in the NBS Cavity ^{235}U Fission Spectrum.

(b) All laboratories remain anonymous for these intercomparisons, as they do for the PSF-SDMF Test (Tables 7 and 13). Similar comparison of results for other sensors [$^{54}Fe(n,p)^{54}Mn$, $^{238}U(n,f)F.P.$, $^{237}Np(n,f)F.P.$, etc.] will be reported in the future by the LWR Surveillance Dosimetry Improvement Program participants.

(c) Accuracies differ within various sets because of positioning uncertainties in foil stacks and flux gradients. They also differ for various irradiations.

(d) One laboratory reported two values: One for Ge(Li) and one for NaI counting.

(e) Three different groups counted this foil but did not report fluence but specific activity on January 29, 1979: Group 1 reported 8164 ± 1.7% dps; Group 2 reported 8257 ± 1.8% dps; Group 3 reported 8373 ± 1.8% dps. Fluence values were derived using a cross section of 102 mb.

TABLE 15

SUMMARY OF THE PROCEDURES AND REQUIREMENTS FOR RPV EMBRITTLEMENT DOSIMETRY SURVEILLANCE ANALYSIS

1.0 Dosimetry - Physics

1.1 Flux, Fluence, MWt, EFPY from surveillance capsule measurements. (E_is).

1.2 Flux, Fluence, MWt, EFPY for EOL prediction (calculation) from FSAR. (C_is).

1.3 Make (C_i/E_i) comparisons, i = 1, ...n. If $C_i/E_i < 0.70$ (30% discrepancies) start over and bring calculations into agreement with measurements using benchmarking methodology. [Note: The actual value (0.70) will depend on the variable "i" of interest; also see ASTM E706 (II-D).[10]]

2.0 Calculate ratios of $\phi > 1$ MeV, dpa [using ASTM E706 (I-D)]. ($\phi \equiv$ fluence, n/cm^2)

2.1 Accel. surveillance location; vessel wall surveillance location; vessel wall; 1/4 T; 3/4 T; ex-vessel locations (if necessary for support structures and physics verification).

2.2 Plot and tabulate results of azimuthal ϕ for accel. surveillance; vessel wall surveillance; vessel wall; 1/4 T; 3/4 T; ex-vessel locations.

3.0 Plot $\phi > 1$ MeV and dpa vs ΔRT_{NDT} for surveillance capsule. Plot also appropriate Regulatory Guide 1.99.1 and ASTM E706 (II-F) curves.

3.1 Determine acceptable (conservative?) trend curve (for example, Figure 5).

3.2 If plant-specific curve is selected, the errors in ΔRT_{NDT}, ϕ and dpa, must be sufficiently small so that this curve can be accepted instead of Regulatory Guide 1.99.1[2] or ASTM E706 (II-F).

- ΔRT_{NDT} errors must be resolved using ASTM E706: I-A, I-C, I-E, I-F, I-G, I-H, II-F, III-D, and III-E (as required).
- ϕ errors must be resolved using ASTM E706: I-A, I-C, I-D, II-A, II-B, II-D, II-E, III-A-D (as required).
  Otherwise, use Regulatory Guide 1.99.1 or ASTM E706 (II-F) curve.

4.0 Revise/update PV wall and 1/4 T ΔRT_{NDT} vs ϕ and dpa curves.

5.0 Draw new MPT (minimum pressure-temperature) curve and determine remaining safe life. If it is less than FSAR predication (e.g., typically 30 to 40 years):

5.1 Consider replacing corner/edge fuel elements.

5.2 Consider annealing vessel.

5.3 Consider other options.

6.0 Additional data needed in Surveillance Reports in support of Steps 1.0 through 5.0.

6.1 Tabulated, with assigned uncertainties and correlations, spectrum (group fluxes) from core edge through surveillance capsule, vessel wall, 1/4 T, 1/2 T, 3/4 T and ex-vessel cavity locations.

6.2 Power-time history for surveillance capsule and cavity positions.

6.3 Fuel subassembly power distribution for physics computations.

6.4 Verification of FSAR values by BWR and PWR generic and PCA/PSF (SDMF)-PV mockup results and update of original FSAR values using surveillance capsule and cavity results (i.e., by application of appropriate ASTM E706 Standards, Figure 3).

6.5 Tabulated and verified dimensions and location of surveillance capsules and pertinent reactor internals, i.e., during normal PV inspections for flaws.

6.6 Tabulated physical dimensions, description and layout of surveillance capsule contents.

NRC-EPRI STUDIES OF PRESSURE-VESSEL-CAVITY NEUTRON FIELDS

J. Grundl, C. Eisenhauer, G. Lamaze, E. D. McGarry
National Bureau of Standards

C. Cogburn
University of Arkansas

N. Tsoulfanidis
University of Missouri

L. Kellogg, W. McElroy
Hanford Engineering Development Laboratory

For Presentation at the
NRC Ninth Water Reactor Safety Information Meeting
October 26-30, 1981
NBS, Washington, D. C.

1. INTRODUCTION

Steel-embrittlement trends in power-reactor pressure vessels are established on the basis of neutron dosimetry and metallurgical testing. For individual vessels this information is obtained only at fixed intervals: nominally one, four, and five years after reactor start-up. Furthermore, the required dosimetry and metallurgy samples are installed in the reactor during construction and, generally, it is not practical or even possible to update or supplement this measurement scheme. New concerns for pressure vessel embrittlement, as well as long-standing efforts to improve neutron exposure surveillance, establish a need for additional neutron field measurements with improved dosimetry methods and more readily accessible locations. This need is emphasized for older reactors where vessel surveillance questions are most severe.

A possible site for this supplementary dosimetry is the pressure vessel cavity. The cavity region is immune to serious safety considerations, and measurements there are relatively inexpensive compared to in-vessel arrangements. In addition, more positions and more kinds of dosimetry can be employed in the unconfined space of the cavity. These clear advantages are often submerged by the looming question of whether cavity neutron fields are sufficiently relevant for the problem of establishing pressure vessel embrittlement trends and limits.

This paper will address the last issue with a brief compendium of cavity neutron field characteristics, dosimetry detector response parameters, and an outline of measurement experience at one operating power plant. Only PWR systems, and for them the core-midplane region, will be under consideration in this short review.

2. CHARACTERISTICS OF OUT-OF-CORE NEUTRON FIELDS

Neutron transport calculations for out-of-core regions have been carried out at the University of Missouri--Rolla (U-Mo.) for Arkansas

Power and Light, Unit #1 (ANO-1), a B&W reactor located at Fayetteville, Arkansas. Under EPRI auspices both 1-D and 2-D, DOT-IV computations have been completed for a modeling that includes all out-of-core structures, the pressure vessel, and the concrete shield.[1] A plan view of ANO-1 at core midplane in Figure 1 shows the primary out-of-core structures and the radial position of detector capsules suspended for irradiation during single reactor cycles. The 1-D calculations of this reactor configuration are used almost exclusively in this review. Its adequacy when compared with the 2-D calculations (the latter with the usual reduced energy resolution), and with PCA calculations obtained from ORNL will be noted in course.

2.1 Neutron-Energy Distributions for Water-Steel Penetration

It is convenient to display these spectra in two regions: (1) a semi-log plot of $\phi(E)/\sqrt{E}$ above 1 MeV, where the fission-source spectrum is modulated by hydrogen scattering; and (2) a log plot of $E\phi(E)$ below 1 MeV where steel scattering resonances are superimposed on a "1/E" water-moderation distribution. A schematic of this display option is shown in Figure 2. An ideal equilibrium-moderation spectrum (i.e. the 1/E-spectrum) appears as a horizontal line below 1 MeV and the fission spectrum as a line of fixed slope above 1 MeV. A bar chart of the dpa cross section, arranged arbitrarily in this schematic, indicates the neutron energy region responsible for 90% of atom displacements in steel; the boundaries, line-break and hash marks delineate four percentile regions of the dpa response: 0.95-0.75-0.5(median)-0.25-0.05. The dpa-response range is an essential orientation for the evaluation and comparison of out-of-core neutron fields since it shows which portions of the neutron spectrum are effective in producing ductility changes in steel.

2.1.1 Neutron spectrum at the 1/4 T position. The quarter-thickness depth in the pressure vessel is the normal focus of attention for determining

steel embrittlement trends and limits. For example, lead factors assigned to the embrittlement of steel samples placed at the surveillance position outside of the thermal shield are defined relative to the 1/4 T position in the vessel. The neutron spectrum at the 1/4 T position in ANO-1 is shown in Figure 3 along with a dpa-response bar chart and a ^{235}U fission spectrum slope. Each region of the spectrum is normalized to unity separately so that the step at 1 MeV is the reciprocal of flux greater than 1 MeV.

Above 1 MeV the fall-off of the hydrogen scattering cross sections yields characteristic changes in the fission neutron source spectrum: a softer-than-fission spectrum below $\sim$ 3 MeV followed by a harder-than-fission spectrum above 4 MeV. Below 1 MeV the relaxation into a near-1/E distribution is strongly modulated by the iron resonances. This is especially important in the first energy decade below 1 MeV where about one third of the atom displacements occur. The dpa response range stretches from 7 MeV down to 140 keV, notably excluding the important iron resonance at 25 keV. Neutrons with energies below 10 keV are not important for steel embrittlement in view of this lower dpa response boundary and this spectrum region will be suppressed in the remaining plots. It may be noted also, in connection with the dpa response energy, that pressure vessel irradiation surveillance can be served well by threshold detectors without a strong requirement for the complications introduced by low-energy detectors.

2.1.2 Neutron spectra at cavity and surveillance positions.

The embrittlement trend of the pressure vessel is presently estimated by extrapolating metal-sample-testing information obtained at the surveillance position (generally the outer surface of the thermal shield) to the 1/4 T position in the vessel. This extrapolation is based largely on neutron transport calculation normalized to dosimetry included with the metal samples at the surveillance position. Dosimetry information from the cavity, if relevant, can provide a valuable check on these calculations.

Furthermore, if the dosimetry at the surveillance position is--or was in the case of older reactors--limited or poorly analyzed, complementary dosimetry could be essential.

The cavity spectrum is shown in Figure 4 along with that of the 1/4 T position and a fission spectrum slope for comparison.

- o Between 1 and 3 MeV a steeper slope versus energy in the cavity spectrum departs from the 1/4 T spectrum by a maximum of $\sim$ 30%.
- o The hardened spectrum components are parallel above 3 MeV, an energy region which encompasses $\sim$ 25% of the 1/4 T dpa response.
- o Below 1 MeV the iron resonance structure within the vessel is preserved in the cavity spectrum.

It may be noted that spectra at positions deeper within the vessel (not shown here) resemble even more closely the cavity spectrum. The spectrum at the surveillance position is shown in Figure 5.

- o Above 1 MeV departures from the 1/4 T spectrum are as large as 20%.
- o Below 1 MeV the iron resonace structure is barely apparent as the spectrum relaxes into a smooth 1/E-distribution.

In Figure 5 a comparison of the U-Mo., 1-D calculation with a more detailed calculation of PCA (12/13 configuration) provided by ORNL shows the degree to which the less sophisticated 1-D calculation is adequate as a calculational base for this survey.

2.2 Concrete Albedo and Spatial Flux Distribution

Calculation results for ANO-1, performed with and without the concrete shield, are shown in Figure 7 for the cavity position. The spectrum differences are not large. These 2-D calculations (the only exception to the use of 1-D results in this paper) indicate that about one third of the flux above 1 MeV at the detector position in the cavity is from the concrete; for a detector position near the outer surface of the pressure vessel about 12% of ϕ(>1MeV) is from the concrete.

Flux traverses for two spectrum components, ϕ(>67keV) and ϕ(>1MeV) are shown in Figure 8. The position of the detector capsule for the ANO-1

measurements was at a radius of 324 cm, closer to the concrete(at 345 cm) than to the vessel. The flux falls rapidly from core edge out thru the vessel and then becomes almost constant in the cavity.

The difficulty of extrapolating with confidence from the surveillance position (outer edge of thermal shield) to the in-vessel positions is well illustrated. The possibility of extrapolating back from the cavity might appear preferable since the extrapolation to 1/4 T is smaller from the cavity (much smaller to 1/2 T) than it is from the surveillance position, and it would be possible in principle to establish in situ the position of a cavity dosimetry capsule relative to the outer surface of the vessel. The mild flux gradient in the cavity is a further aid to meeting the familiar problems of establishing local detector positions and flux perturbations. Whatever the relative merits of cavity and surveillance positions it seems clear that neutron flux measurements on both sides of the vessel would provide essential validation of neutron transport calculations.

2.3 Summary

Calculations of core leakage neutrons diffusing through surrounding water and steel and out into the pressure vessel cavity show that the neutron flux in the cavity, in conjunction with that of the surveillance position, are similar to and bracket well, the neutron flux at the 1/4 T position within the vessel, in terms both of spectrum and flux intensity. They are in important respects complementary. Iron resonance structure within the vessel is preserved in the cavity and the gradients are mild while at the surveillance position the spectrum above 1 MeV matches the 1/4 T spectrum better than in the cavity but the iron resonance structure is undeveloped and gradients are severe. This complementarity could prove useful for establishing confident measurements in support of neutron fluence lead-factors which presently are derived from calculations which often are not plant specific.

2.3.1 Compendium of out-of-core dpa distributions. Bar charts of dpa-response (i.e. the atom displacement cross section) at six locations beginning with the surveillance position and ending with the detector position in the cavity are presented in Figure 9. The pattern of these response ranges provides additional perspectives on the cavity as a dosimetry measurement site:

- o Lower bounds are all within ± 100 keV; median energies are more spread about.
- o Less than 20% of the cavity response range is outside that of the 1/4 T position; for the 3/4 T position less than 10% is outside.
- o Strong shift of the response range at the vessel inner surface may be significant because of concerns for thermal stress and possible surface cracks.
- o The amount of damage exposure below 1 MeV varies within the vessel from 20% to 70% calls for a further review of ϕ(>1MeV) as an adequate "mean effective" damage exposure parameter.

3. CHARACTERISTICS OF DOSIMETRY DETECTORS

Neutron exposure dosimetry is undertaken experimentally almost exclusively by means of neutron detectors which respond to a wide range of neutron energies, i.e. integral detectors and in particular threshold integral detectors. The response characteristics of these detectors can be displayed usefully with a chart of energy response ranges in neutron fields of interest.

3.1.1 Detector response charts for cavity and surveillance positions. A chart of energy response ranges for representative threshold detectors (plus one low-energy capture detector) in the ANO-1 cavity spectrum is shown in Figure 10. The cavity spectrum and dpa response ranges are included in order to help evaluate spectrum coverage features of the detector set.

- o The spectrum itself is not relevant for dosimetry evaluation and not much better incidently is a spectrum truncated to flux above 1 MeV. A spectrum weighting function related to the material property under surveillance is necessary. The dpa cross section serves this purpose, even if by default, for steel embrittlement induced by prolonged exposure to neutrons.

- o Detector set coverage of the dpa response range is >90%, without Np it would drop to 25%.
- o Low energy detectors--$^{58}Fe(n,\gamma)$ is a typical example--are not vital since their response barely reaches the dpa response range.
- o More than about four threshold detectors leads to redundant spectrum coverage in view of the extent of detector response ranges. The ^{58}Ni and ^{54}Fe detectors, for example, are redundant and are employed as a result of experimental conservatism.

The main focus of dosimetry measurement is still the surveillance position. A detector response range chart for representative detectors is given in Figure 11.

- o Detector set coverage and distinctiveness of detector responses is similar to that for the cavity spectrum, even though the dpa response range is somewhat higher.
- o The Np detector is pivotal: with it detector set coverage of dpa is 90%, similar to the cavity; without it, coverage is 50%, much less but still substantially more than in the cavity.

3.1.2 Detector response parameters: spectrum fraction, truncated cross section spectral index. Reaction rate data from dosimetry detectors is often fed directly into spectrum unfolding codes or large-ensemble, least-squares adjustment algorithms (with or without covariance matrices). Even when this procedure is well-understood and the ensemble data (cross sections, realistic starting spectrum, covariance elements and the like) have been validated by application to neutron field benchmarks, a less sophisticated analysis which treats detector results individually is worthwhile as a preamble to the "big machines." This counsel becomes more nearly a necessity when the detector measurements are specifically benchmarked as is planned for the ANO-1 cavity work. The basic features of such a preamble treatment of dosimetry data is to be found in References 2, 3, and 4.

In this paper each detector reaction rate probability will be reduced first to a fission-equivalent flux for comparison with calculation, then to the familiar $\phi(>1MeV)$, and finally to the more recently recommended exposure parameters $\phi(>0.1MeV)$ and dpa. The detector response parameters

required to carry out this analysis are given in Table I, where in order to serve more than the analysis of cavity dosimetry measurements, four out-of-core positions besides the cavity are included. The significance and definition are as follows.

- o spectral index, $S_{\alpha/\beta}$, is the parameter which establishes a measure of the portion of the spectrum between the lower bounds of two detectors α and β, the so-called non-overlap interval. (For Np and U238 fission detectors in the cavity this would be the interval 80 keV to 1.2 MeV--see Figure 10.)

$$S_{\alpha/\beta} \equiv \frac{\sigma_\alpha}{\sigma_\beta} = \int_o^\infty \sigma_\alpha(E)\psi(E)dE / \int_o^\infty \sigma_\beta(E)\psi(E)dE$$

- o truncated cross section, $\bar{\sigma}(>E_{95})$, is the spectrum-averaged detector reaction cross section truncated at the lower bound (E_{95}) of the detector response range. This cross section is a measure of detector reaction rate which is independent of the neutron flux in the energy region where the detector has no response. (In the cavity $\bar{\sigma}(>E_{95})$ for the ^{238}U is 0.52b little different from its value 0.54b in the fission spectrum whereas the full spectrum cross section, $\bar{\sigma}(>0.4eV)$, is 0.049b in the cavity.)

$$\bar{\sigma}(>E_{95}) = \int_{E_{95}}^\infty \sigma(E)\psi(E)dE / \int_{E_{95}}^\infty \psi(E)dE$$

- o spectrum fraction, $\psi(>E_{95})$, is the fraction of the spectrum above E_{95}. It indicates directly the fraction of the spectrum to which the detector responds.

$$\psi(>E_{95}) = \int_{E_{95}}^\infty \psi(E)dE;$$

and

$$\bar{\sigma} = \frac{1}{0.95}\ \sigma(>E_{95})\cdot\psi(>E_{95})\ .$$

Patterns of detector behavior, relevance, and spectrum shifts are evident from even a brief look at Table I.

- o Spectral indexes $S_{Np/Fe}$ and $S_{28/Fe}$ show the large spectrum shift to higher energies at the inner surface relative to 1/4 T; in fact, this inner surface vs. fission spectrum values of $S_{28/Fe}$ indicates a harder-than-fission-spectrum interval around 1 MeV. The spectrum fraction, $\psi(>E_{95})$, for U238 also changes by a factor of 5 in going through the pressure vessel.

- o The truncated cross section, $\bar{\sigma}(>E_{95})$, for ^{238}U does not change drastically in going from the cavity to the surveillance position to the fission spectrum, an indication that cross section and benchmarking uncertainties will be small. Changes as large as a factor of 3 appear in the case of Np.
- o The Ti-detector response parameters at the cavity surveillance positions bracket well the 1/4 T position.

4. MEASUREMENT EXPERIENCE IN A PWR REACTOR CAVITY

Early measurements in the ANO-1 cavity began in 1977 and were for the most part feasibility studies undertaken to explore problems of detector placement and recovery, and to examine the quality of detector response in the cavity. A significant limitation for these experiments was that they could be guided and interpreted only in terms of a generic PWR calculation of restricted scope. Participants in this groundwork effort were the Univ. of Arkansas, NBS, and HEDL; the essential cooperation of the reactor operator, Arkansas Power and Light also must be noted. A demonstration analysis of a portion of the data obtained during this period is reported in Reference 2. More recently these efforts were perfected with regard to cavity access and were expanded under EPRI auspices to include more azimuthal positions and elevations above and below core midplane; and most important, plant-specific calculations were initiated. It is not the purpose of this paper to review this EPRI supported work, some of which is still in progress. Instead, one set of composite dosimetry detector results for the cavity has been distilled from all of the counting data presently available from the Univ. of Arkansas and HEDL. This data set is not to be considered an evaluated result, simply illustrative. Thus, experimental issues which have yet to be resolved to make this data properly consistent are here ignored.

4.1 Reaction Rate Probabilities and Spectral Indexes

The composite result for six threshold detectors is given as reaction rate probabilities*, R/NGT, in column 2 of Table II. The uncertainties

*The reaction rate probability, expressed as dps/nucl, is the measured detector response quantity equal to the spectrum-averaged cross section x neutron flux.

assigned are suggestive based on the spread of the reported data after normalization to a single experiment via the $^{54}Fe(n,p)$ detector.

The simplest spectrum parameter derivable from reaction rate data is the spectral index. Taken here with respect to the Fe detector, this parameter is obtained as the ratio of each reaction rate probability to that of Fe. The result is in column 3 of Table II. The comparison of these observed indexes with the U-Mo. calculation appears in the adjacent column. Rather good agreement is apparent for all but the Cu and Np detectors. The departure of Np is most significant indicating as it does 30% more flux than calculated in the non-overlap range 80 keV to 2.2 MeV--see Figure 10. This result for Np could be indicative of difficulties with the iron resonances just below 1 MeV in the neutron transport calculation (see Figure 4), or in part it could be associated with an error in the subthreshold fission cross section for Np which has yet to be adequately benchmarked.

4.2 Fission-Equivalent Flux

Another parameter which can be derived directly from the observed reaction rate probability without recourse to transport calculations is the fission-equivalent flux. This parameter is most appropriate when dosimetry measurements are benchmarked against the fission spectrum by means of neutron fluence standards or their equivalent. For the present data, only the ^{58}Ni detector has been so benchmarked; however, as a first step all of the data will be reduced to fission-equivalent flux for consistency and to maintain independence from the transport calculation while evaluating detector data.

A fission-equivalent flux, $\phi_{\chi eq}$, is the neutron flux derived from a detector reaction rate probability relative to the corresponding fission-neutron flux which would be required to produce the same reaction rate probability in that detector. The point of this particular flux parameter

is to make explicit the reduction of systematic error inherent in benchmark referencing procedures. (This formulation is unrelated to the old procedure of using a fission spectrum cross section to derive a flux from a detector response in an unknown spectrum.) Functional expressions for deriving $\phi_{\chi eq}$ under two experimental conditions are as follows:

- With a fission neutron flux standard or equivalent (see Reference 3, Section 5):

$$\phi_{\chi eq} \equiv P_s \frac{\phi_\chi}{P_\chi}$$

Where P_s = the reaction rate probability obtained in the spectrum under study, $[R/NGT]_s$, or any detector response quantity corrected for irradiation-specific factors (e.g. a gamma counting rate corrected for irradiation time-history).

P_χ = the reaction rate probability obtained for the neutron fluence standard, $[R/NGT]_\chi$, or any response quantity obtained with the same detection efficiency as applies to P_s.

ϕ_χ = fission neutron flux assigned to the flux standard.

- Without a fission neutron flux standard or equivalent:

$$\phi_{\chi eq} \equiv \frac{[R/NGT]_s}{\bar{\sigma}_\chi}$$

Where $[R/NGT]_s$ = reaction rate probability obtained in the spectrum under study.

$\bar{\sigma}_\chi$ = observed value of the fission-spectrum-averaged detector cross section.

Fission-equivalent fluxes derived according to the above recipe for the composite data from the ANO-1 cavity are presented in Table II. For the Ni detector the value is based on HEDL counting referenced to an NBS neutron fluence standard; for the other detectors, the reaction probabilities of column 2 were divided by observed values of $\bar{\sigma}_\chi$ obtained from Table X-15 of Reference 3. Consistent calculational values of $\phi_{\chi eq}$ are obtained by dividing calculated reaction rate probability [i.e. $\bar{\sigma}_{calc.}$ x $(\text{total flux})_{calc.}$] by the calculated value of $\bar{\sigma}_\chi$ from Table X-13 of Reference 3.

The observed-to-calculated ratios obtained are listed in the last column of Table II.

Four detectors which cover the energy range above 1 MeV (Cu excluded) yield consistent $\phi_{\chi eq}$-values in agreement with calculation. The Np $\phi_{\chi eq}$-value disagrees with calculation by an amount not easily attributable to inaccuracies in subthreshold fission cross sections or even photofission.

4.3 Exposure Parameters: Flux Above 1 MeV and 0.1 MeV, and dpa Probability

In spite of all criticism the neutron flux truncated to above 1 MeV, $\phi(>1\text{MeV})$, remains the conventional neutron flux parameter for pressure vessel irradiation surveillance dosimetry. Recourse to neutron transport calculation is necessary to derive this exposure parameter. The quantity required is the spectrum fraction above 1 MeV, $\psi(>1\text{MeV})$, which from the U-Mo. cavity calculation is 0.048. Combined as follows with fission cross sections from Reference 3, and calculated spectrum fractions and truncated cross sections from Table I, a flux above 1 MeV can be derived for each detector:

$$\phi(>1\text{MeV}) = 0.95 \frac{\bar{\sigma}_\chi}{\sigma(>E_{95})} \cdot \frac{\psi(>1\text{MeV})}{\psi(>E_{95})} \cdot \phi_{\chi eq}.$$

The flux above 0.1 MeV is obtained directly by substituting for $\psi(>1\text{MeV}) = 0.048$, the value $\psi(>0.1\text{MeV}) = 0.42$ from the same calculation. Similarily, the dpa exposure parameter, P_{dpa}, is obtained by replacing $\psi(>1\text{MeV})$ with $\sigma_{dpa} = 152$ barns from the calculation;

$$P_{dpa} = 0.95 \frac{\sigma_\chi}{\sigma(>E_{95})\psi(>E_{95})} \sigma_{dpa} \phi_{\chi eq}.$$

All of these neutron exposure parameters are presented in Table III. Agreement is better than 5% among those parameters which correspond to detectors with response range above 1 MeV (excluding Cu). The Np detector indicates some 30% more flux than the higher energy detectors.

Establishing an average value for these parameters requires a choice of weighting factor. The result for two choices of weighting are given in the lower half of Table III: equal weight for all detectors, and a weight equal to $\psi(>E_{95})$, the spectrum coverage factor. The latter average without the anomalous Np result is included in the Table as are the calculated values for the three exposure parameters. The final result of experimental dosimetry in the ANO-1 cavity as displayed in Table III are seen to agree with the predictions of calculation when the Np detector is ignored; when the Np detector with the full weight of its spectrum coverage factor is included, the measured exposure parameters are 20% to 40% more than those calculated.

5. CONCLUSIONS

The pressure vessel cavity is a readily accessible and appropriate region for supplementary vessel irradiation surveillance dosimetry. As such it complements the conventional limited-scope dosimetry at the surveillance position and makes possible dosimetry measurements which, because they bracket the vessel, provide a much better check of the neutron transport calculations which are used to establish surveillance capsule lead factors.

Out-of-core neutron fields. Neutrons streaming through the vessel dominate the cavity neutron field which preserves important features of the in-vessel neutron spectrum. Comprehensive calculations of out-of-core neutron fields for a specific PWR system (the Arkansas Power and Light, Unit #1, a B&W reactor) illustrate the neutron field characteristics that support this conclusion:

- Shifts of the atom displacement probability distribution in the cavity are modest relative to the 1/4 T and 3/4 T in-vessel positions. Less than 1/3 of the neutron flux above 1 MeV at mid-cavity is from the concrete shield.
- Iron resonance structure that develops within the vessel is preserved in the cavity spectrum.

- o Between 1 and 3 MeV the cavity spectrum departs from the 1/4 T spectrum by up to 30%; above 3 MeV, the hardened fission-spectrum components are parallel.
- o Spatial flux gradients are mild, promising improved accuracy in establishing dosimetry location relative to pressure vessel boundaries.

Based on this survey, which is limited to one set of calculations, the possibility that cavity dosimetry could be put on a par with conventional dosimetry at the surveillance position is not ruled out with regard to establishing 1/4 T exposure.

Detector response survey. A set of threshold integral detectors, not large but including Np(n,f) or its equivalent, can provide spectrum coverage adequate for establishing neutron exposure parameters which are appropriate for monitoring radiation damage in steel (i.e. the parameters flux above 0.1 and 1 MeV, and dpa, the atom displacement probability). In this regard, the survey indicates that the conventional flux above 1 MeV is not really an adequate damage exposure parameter in view of the spectrum variation which occurs around 1 MeV in pressure vessel environments.

Cavity measurement experience. A significant amount of measurement experience in one PWR vessel cavity demonstrates that meaningful experiments can be performed at core midplane and at various elevations and azimuthal positions in the cavity. One composite set of threshold detector results from the cavity has been analyzed with simple detector response parameters and successfully reduced to both conventional and updated neutron exposure parameters. For most of the detectors the spectral indexes and neutron exposure parameters derived from their responses agree with calculation to 15% or better. The notable exception is the Np(n,f) detector for which the measured spectral index and exposure parameters are 30% or more greater than calculated.

Acknowledgements

The authors gratefully acknowlege the cooperation of Arkansas Power and Light in providing access to their reactor for cavity measurements. At the University of Arkansas, the authors thank B. Brandon, R. Culp, and W. Sallee for their work in taking and analyzing the data. The calculations at the University of Missouri were the result of a group effort and the authors gratefully acknowledge the work of D. R. Edwards, D. Frankenbach, L. Kao, and K. Wincel. At the National Bureau of Standards, the authors thank R. Dallatore for the design and fabrication of the early dosimetry capsules and D. Shipe for tireless assistance in the preparation of this manuscript.

References

(1) Nicholas Tsoulfanidis, Private Communication and EPRI Progess Reports (1981).

(2) J. A. Grundl, C. M. Eisenhauer, E. D. McGarry, "Neutron Flux Measurements in the Pressure Vessel Cavity of an Operating U.S. Power Reactor," NBS Internal Document (1978).

(3) "Compendium of Benchmark and Test Region Neutron Fields for Pressure Vessel Irradiation Surveillance, Standard Neutron Field Entry, Fission Neutron Spectra, Part I: ^{252}Cf Spontaneous Fission," LWR Pressure Vessel Dosimetry Progress Report, NUREG/CR-0551 (Sept. 1978). Also available directly from NBS.

(4) J. Grundl, C. Eisenhauer, "Fission Reaction Rate Standards and Applications," Proc. Symp. on Neutron Standards and Applications, NBS Special Publ. 493, Washington, D.C. (1977).

TABLE I. Detector Response Parameters for Out-of-Core Neutron Fields
(University of Missouri Calculation)

	Cavity	Outer Surface	1/4 T Thickness	Inner Surface	Surveillance Position	^{235}U Fission Spectrum
DPA Exposure						
$\psi(> E_{95})$	0.484	0.502	0.593	0.436	0.358	0.834
$\sigma(> E_{95})$(mb)	2.98×10^5	3.18×10^5	3.33×10^5	8.38×10^5	5.32×10^5	9.73×10^5
$^{237}Np(n,f)$						
$\psi(> E_{95})$	0.444	0.465	0.396	0.350	0.290	0.796
$\sigma(> E_{95})$(mb)	466	514	1238	1502	1041	1578
$S\alpha$/Fe	69.2	70.2	27.1	14.5	27.1	17.0
$^{238}U(n,f)$						
$\psi(> E_{95})$	0.0363	0.0421	0.1348	0.200	0.0882	0.527
$\sigma(> E_{95})$(mb)	407	406	534	576	524	532
$S\alpha$/Fe	4.93	5.01	3.98	3.16	4.15	3.79
$^{58}Ni(n,p)$						
$\psi(> E_{95})$	0.0191	0.0223	0.0855	0.136	0.0576	0.362
$\sigma(> E_{95})$(mb)	209	205	276	343	254	264
$S\alpha$/Fe	1.337	1.339	1.305	1.280	1.311	1.297
$^{54}Fe(n,p)$						
$\psi(> E_{95})$	0.0129	0.0147	0.0696	0.1217	0.0474	0.317
$\sigma(> E_{95})$(mb)	232	231	260	298	235	233
$S\alpha$/Fe	1.000	1.000	1.000	1.000	1.000	1.000
$^{46}Ti(n,p)$						
$\psi(> E_{95})$	0.00444	0.00504	0.0285	0.0606	0.0174	0.127
$\sigma(> E_{95})$(mb)	144	148	136	133	115.3	80.6
$S\alpha$/Fe	0.214	0.219	0.214	0.221	0.180	0.139
$^{63}Cu(n,\alpha)$						
$\psi(> E_{95})$	0.0027	0.00313	0.01737	0.0369	0.0097	0.0658
$\sigma(> E_{95})$(mb)	21	22	19	18	15	7.8
$S\alpha$/Fe	0.0194	0.0204	0.0179	0.0180	0.0130	0.0069

$S\alpha$/Fe: spectral index relative to $^{54}Fe(n,p)$

E_{95}: energy above which 95% of detector response occurs

$\psi(> E_{95})$: spectrum coverage factor (fraction of flux above E_{95})

$\sigma(> E_{95})$: truncated cross section (average detector cross section above E_{95})

$\sigma(> E_{95}) \cdot \psi(> E_{95})/0.95$ = full-spectrum-averaged cross section

TABLE II. Results of Cavity Measurements at Core Mid-Plane

(Arkansas P. & L. Unit 1)

Detector	[a]Reaction Probability R/NGT x 10^{17} (dps/nucl.)	[b]Spectral Index Sα/Fe		[c]Fission-Equivalent Flux $\phi_{\chi eq}$ (x 10^{-8})	
		Observed	Obs/Calc	Observed	Obs/Calc
$^{237}Np(n,f)$	105 ± 10%	91 ± 10%	1.3	8.1 ± 10%	1.3
$^{238}U(n,f)$	5.8 ± 15%	5.0 ± 10%	1.01	1.93 ± 10%	.95
$^{58}Ni(n,p)$	1.6 ± 5%	1.51 ± 5%	1.13	1.50 ± 5%	.95
$^{54}Fe(n,p)$	1.16 ± 5%	1.00	-	1.45 ± 10%	.93
$^{46}Ti(n,p)$	0.24 ± 10%	0.20 ± 10%	0.93	2.12 ± 10%	.88
$^{63}Cu(n,\alpha)$	0.017 ± 15%	0.012 ± 15%	0.63	2.8 ± 15%	.64

[a]Composite result from data reported in 1981 by University of Arkansas and HEDL. The uncertainty is suggestive based on the spread of the reported results after renormalization to Experiment #4. (The reaction probability is the detector response quantity equal to the spectrum-averaged cross section x neutron flux.)

[b]Composite result EPRI supported efforts (1980-81) and early exploratory work by University of Arkansas/ NBS/HEDL (1978).

[c]Obtained as quotient of reaction probability (column 2) and the ^{235}U fission-spectrum-averaged cross section, except for $^{58}Ni(n,p)$. For the latter an NBS neutron fluence standard was available making possible a value benchmarked against the ^{235}U fission spectrum.

TABLE III. Neutron Exposure Parameters for the ANO-1 Cavity

Detector	Spectrum Coverage factor $\psi(> E_{95})$	Truncated Flux $\phi(> 1$ MeV)	relative	$\phi(> 0.1$ MeV)	Atom Displacement Probability Rate P_{dpa}
$^{237}NP(n,f)$	0.444	2.3×10^{8}	1.32	2.04×10^{9}	7.4×10^{-13}
$^{238}U(n,f)$	0.0363	1.76	1.01	1.54	5.6
$^{58}Ni(n,p)$	0.019	1.80	1.03	1.58	5.7
$^{54}Fe(n,p)$	0.013	1.74	1.000	1.52	5.5
$^{46}Ti(n,p)$	0.0044	1.73	0.99	1.51	5.5
$^{63}Cu(n,\alpha)$	0.0027	1.33	0.76	1.16	4.2
Average Values					
equal wt.:		1.78×10^{8} (s.d. = ± 15%)		1.56×10^{9}	5.7×10^{-13}
$\psi(> E_{95})$ wt.:		2.22		1.97	7.1
$\psi(> E_{95})$ wt. w/o NP:		1.75		1.54	5.6
Calculated Values					
U-Mo.		1.57×10^{8}		1.67×10^{9}	5.8×10^{-13}

Figure Captions

Figure 1. Plan view of Arkansas Power and Light , Unit #1 at core midplane. Detector capsules were suspended in the wells at the radius shown for one cycle of reactor operation. Measurements also have been made at other elevations and azimuthal positions.

Figure 2. Schematic of display option for water-steel penetration spectra. Above 1 MeV a semi-log plot of $\phi(E)/\sqrt{E}$ is a line of constant slope for a fission neutron spectrum; below 1 MeV a log plot of $E\phi(E)$ is a horizontal line for an equilibrium moderation spectrum. The bar chart indicates the energy region responsible for 90% of atom displacements in steel. Percentile marks divide this dpa-response range into four subregions.

Figure 3. Neutron spectrum at the the 1/4 T position in the ANO-1 vessel from U-Mo. calculations. The dpa response range indicates that $\sim$ 2/3 of the atom displacements come from neutrons above 1 MeV, and also stresses the importance of the iron resonances just below 1 MeV. (The energy regions above and below 1 MeV are separately normalized to unity so that the step at 1 MeV is the reciprocal of the flux greater than 1 MeV.)

Figure 4. Cavity neutron spectrum in the energy range 10^{-2} to 9 MeV along with the 1/4 T spectrum and a fission spectrum slope.

Figure 5. Neutrum spectrum at the surveillance position showing a strong resemblance to the in-vessel spectrum above 1 MeV but little development of the iron resonance structure below 1 MeV.

Figure 6. Comparison of the U-Mo., 1-D calculation at 1/4 T to a high-resolution calculation by ORNL at the same position for the PCA 12/13 configuration.

Figure 7. The cavity spectrum from calculations with and without concrete.

Figure 8. Flux fractions greater than 0.067 MeV and 1 MeV as function of radial distance. The radial position for the foil irradiations is 324 cm; the concrete shield begins at 345 cm.

Figure 9. Compendium of dpa-exposure distributions for out-of-core positions in ANO-1. These distributions, divided into four subregions indicate the neutron energy range responsible for steel embrittlement. The lower energy bound is given for each response range.

Figure 10. Detector response ranges for the neutron field at the cavity position in Arkansas Power and Light, Unit #1 (ANO-1). The cavity spectrum range (which extends down to a lower energy bound of 2.6 eV), and dpa response range are included in order to evaluate features of spectrum coverage for individual detectors.

Figure 11. Detector response ranges for the surveillance position in ANO-1.

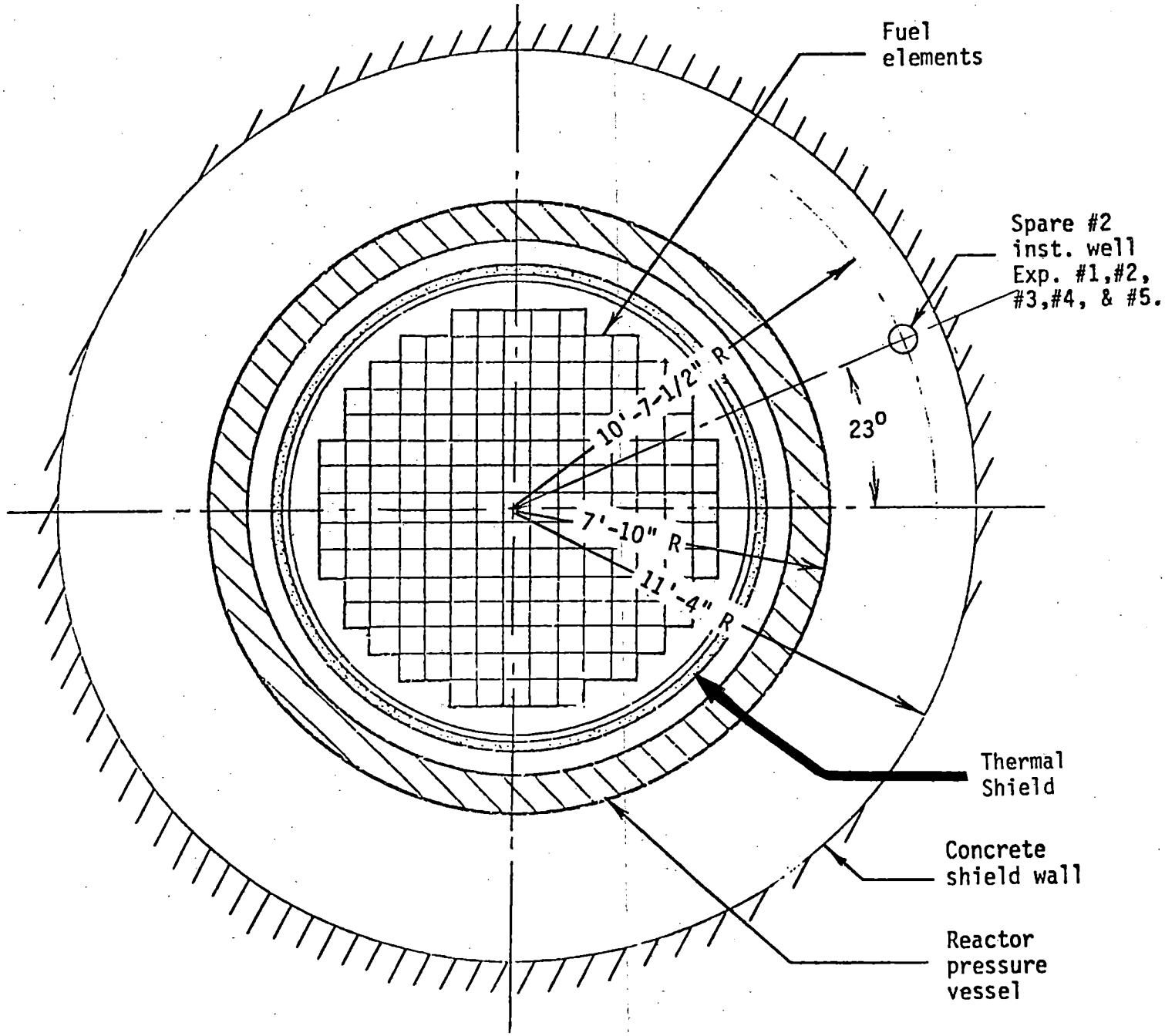
Fuel elements
Spare #2 inst. well Exp. #1,#2, #3,#4, & #5.
23°
10'-7-1/2" R
7'-10" R
11'-4" R
Thermal Shield
Concrete shield wall
Reactor pressure vessel

Figure 1

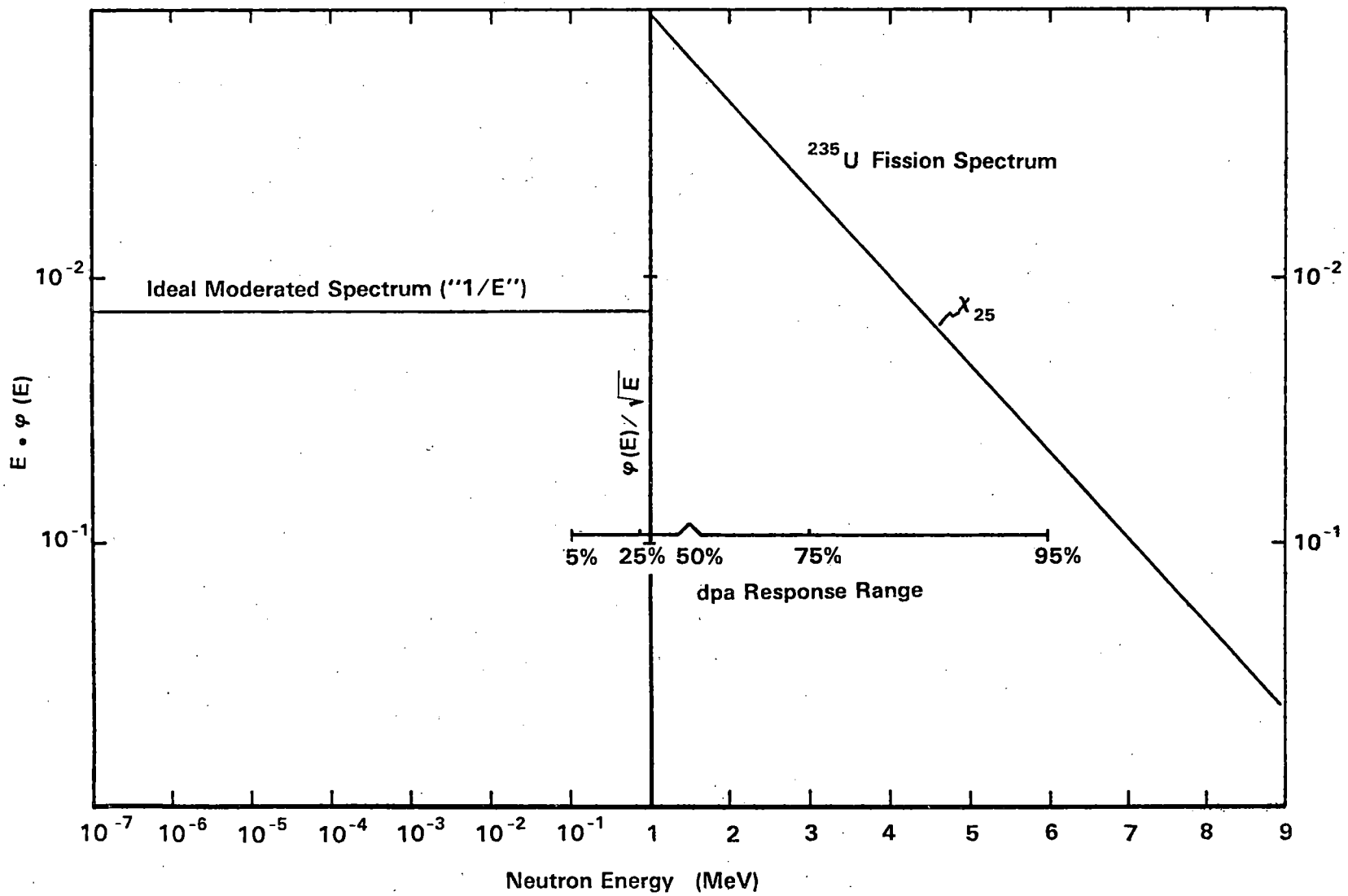
^{235}U Fission Spectrum
Ideal Moderated Spectrum ("1/E")
χ_{25}
$\varphi(E)/\sqrt{E}$
E • φ (E)
10^{-2}
10^{-1}
5% 25% 50% 75% 95%
dpa Response Range
10^{-7} 10^{-6} 10^{-5} 10^{-4} 10^{-3} 10^{-2} 10^{-1} 1 2 3 4 5 6 7 8 9
Neutron Energy (MeV)

Figure 2

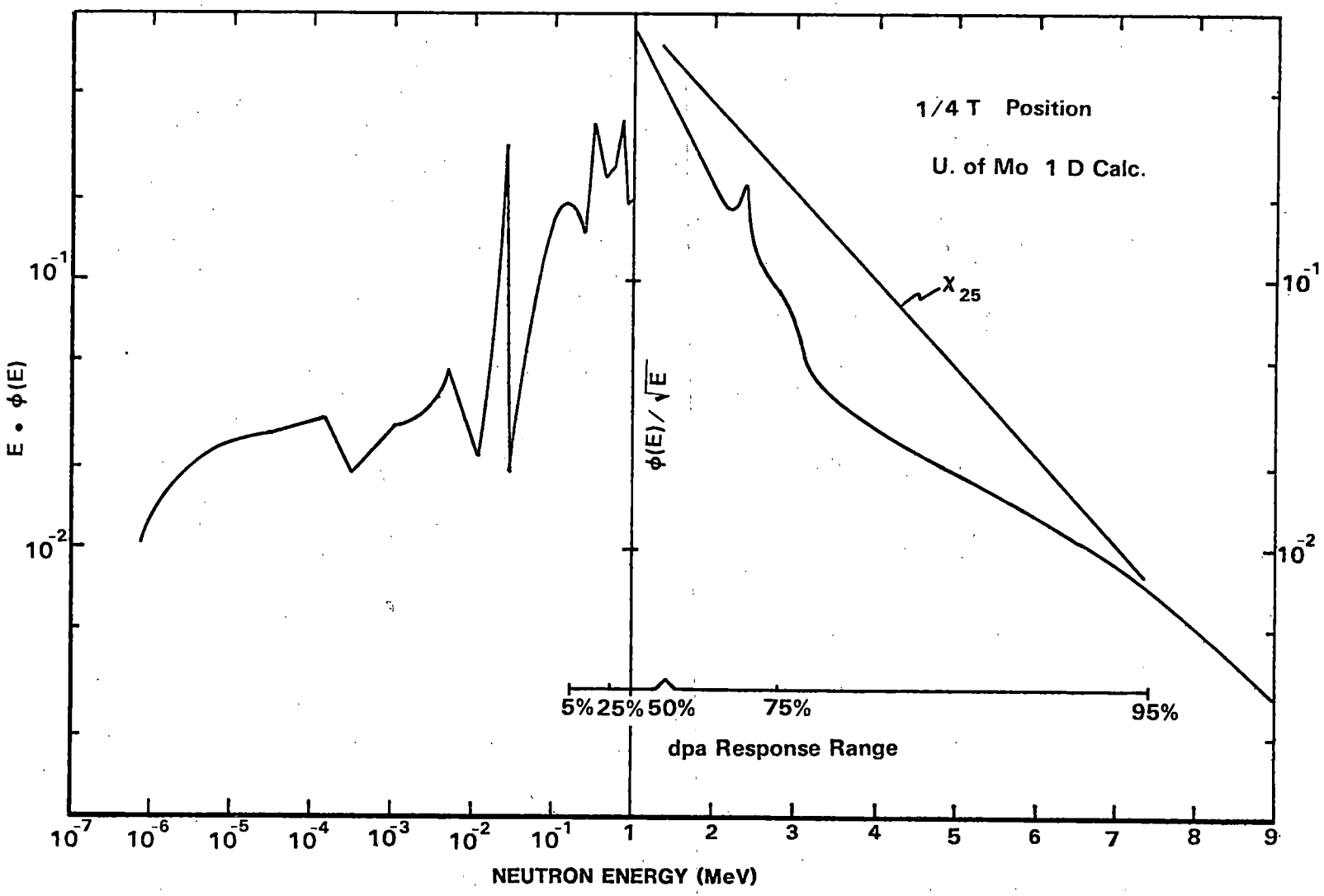
1/4 T Position
U. of Mo 1 D Calc.
χ_{25}
$E \cdot \phi(E)$
$\phi(E)/\sqrt{E}$
10^{-1}
10^{-2}
5% 25% 50% 75% 95%
dpa Response Range
10^{-7} 10^{-6} 10^{-5} 10^{-4} 10^{-3} 10^{-2} 10^{-1} 1 2 3 4 5 6 7 8 9
NEUTRON ENERGY (MeV)

Figure 3

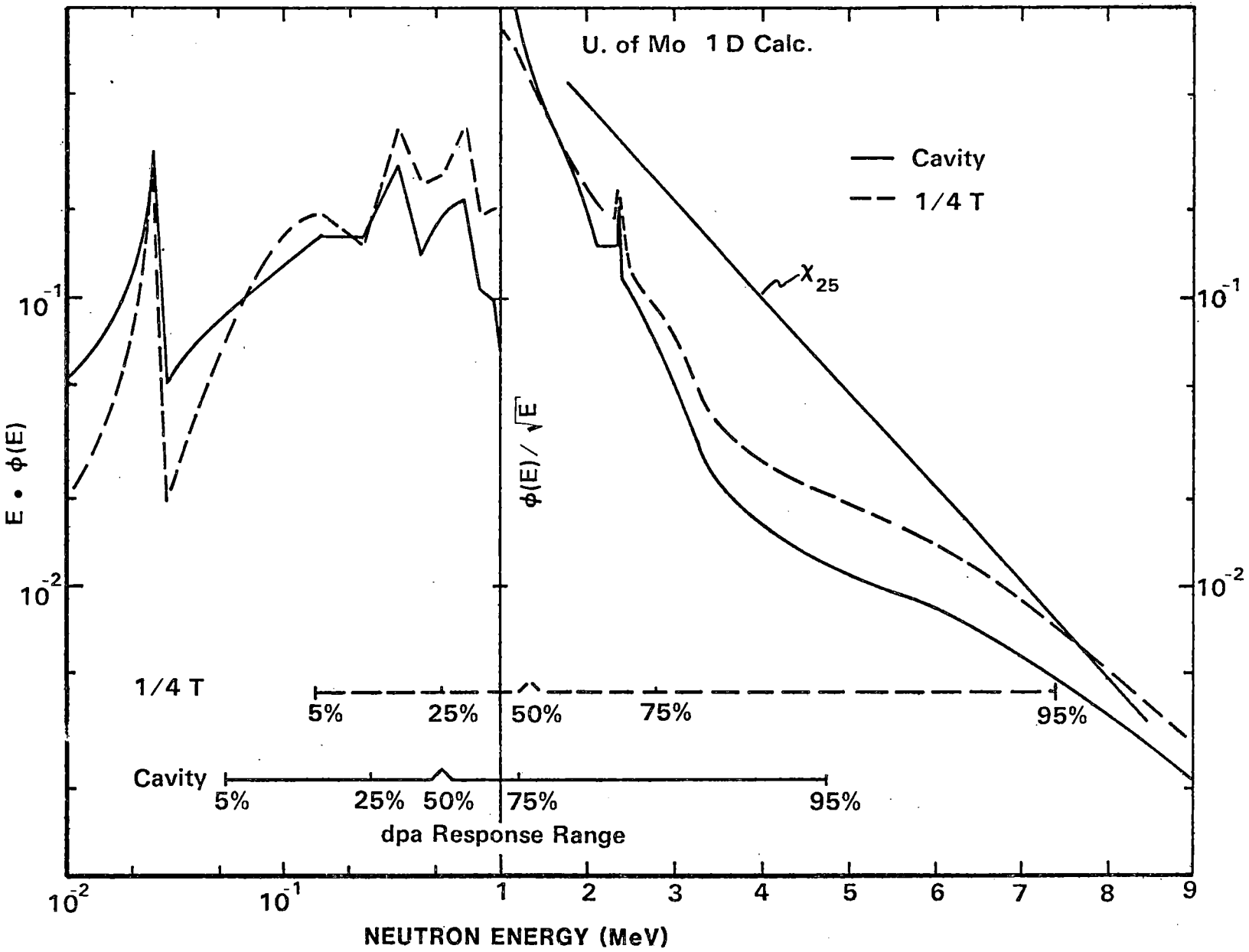
U. of Mo 1 D Calc.
Cavity
1/4 T
χ_{25}
10^{-1}
10^{-2}
E • φ(E)
φ(E) / √E
1/4 T
5%
25%
50%
75%
95%
Cavity
5%
25%
50%
75%
95%
dpa Response Range
10^{-2}
10^{-1}
1
2
3
4
5
6
7
8
9
NEUTRON ENERGY (MeV)

Figure 4

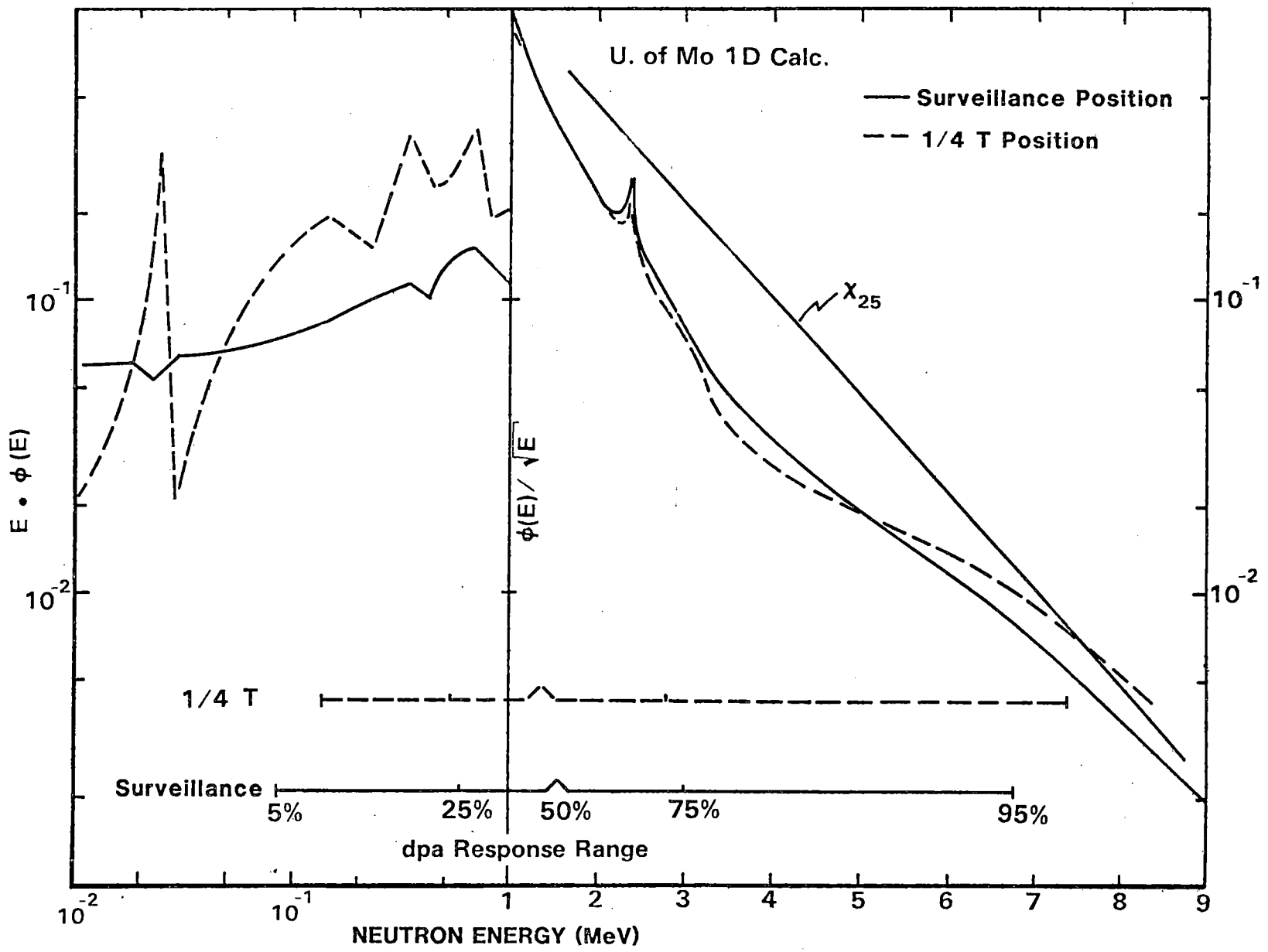
U. of Mo 1D Calc.
Surveillance Position
1/4 T Position
χ_{25}
10^{-1}
10^{-2}
E • ϕ (E)
ϕ(E) / √E
1/4 T
Surveillance
5%
25%
50%
75%
95%
dpa Response Range
10^{-2}
10^{-1}
1
2
3
4
5
6
7
8
9
NEUTRON ENERGY (MeV)

Figure 5

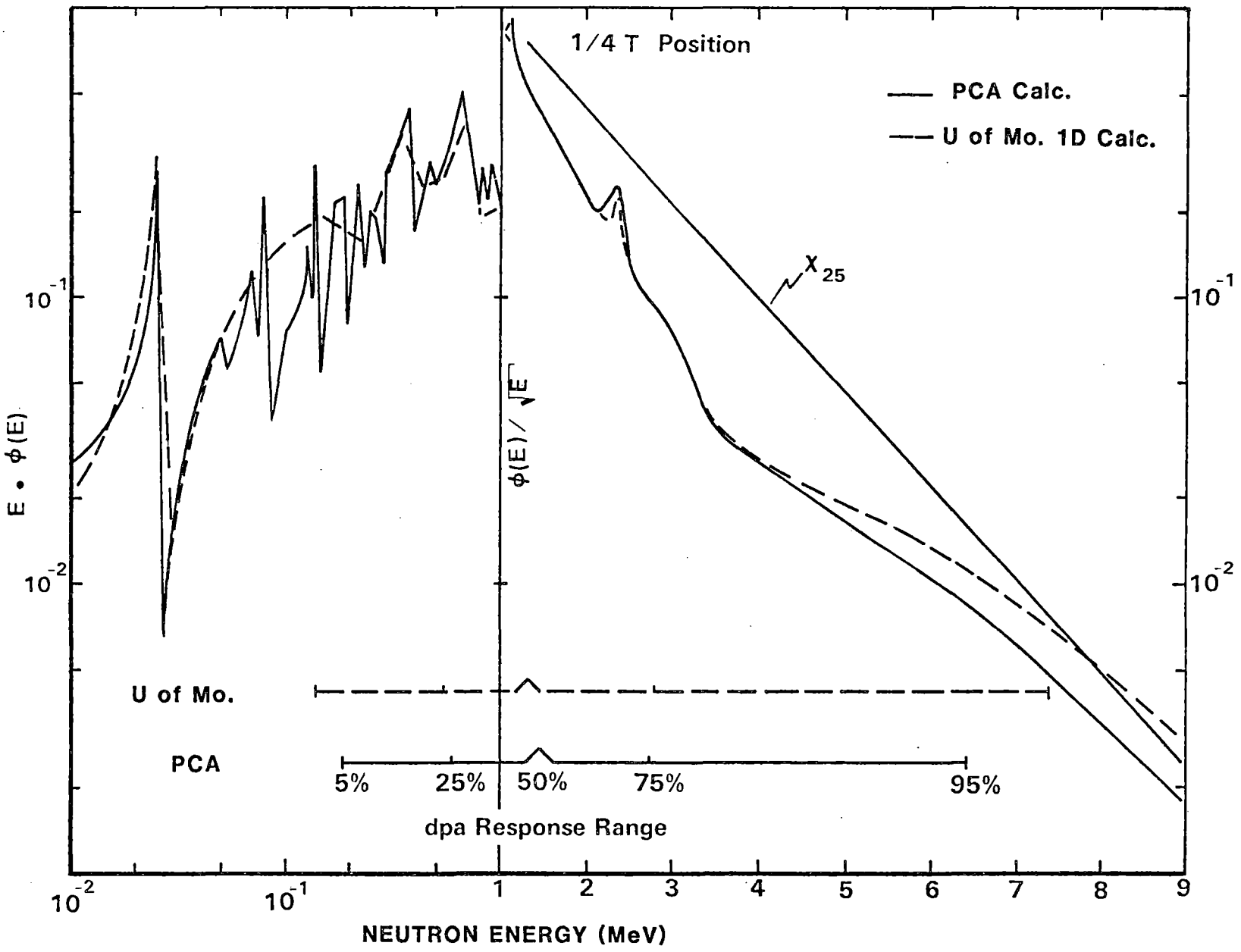
1/4 T Position
PCA Calc.
U of Mo. 1D Calc.
χ_{25}
10^{-1}
10^{-2}
E • φ(E)
φ(E) / √E
U of Mo.
PCA
5%
25%
50%
75%
95%
dpa Response Range
10^{-2}
10^{-1}
1
2
3
4
5
6
7
8
9
NEUTRON ENERGY (MeV)

Figure 6

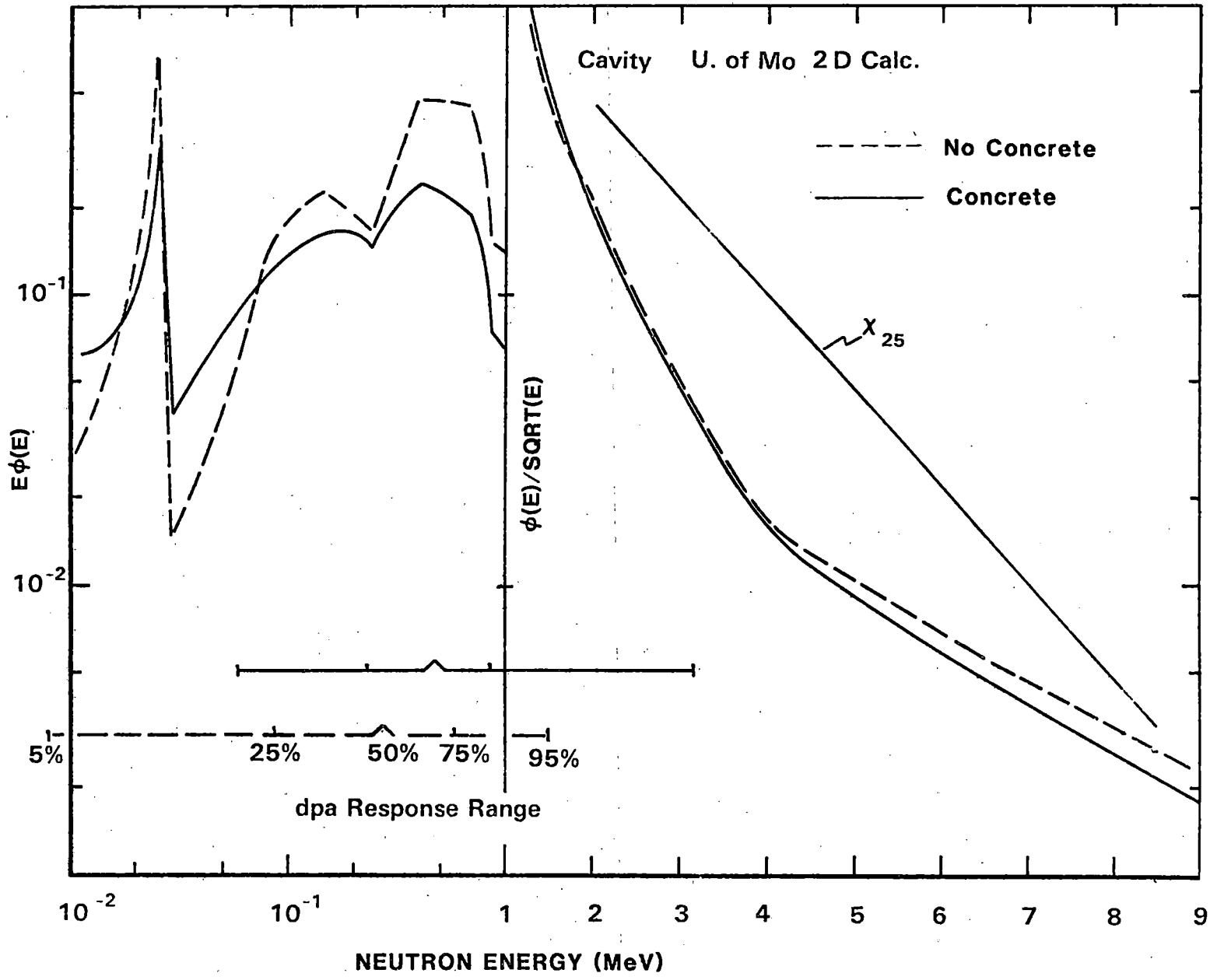
Cavity U. of Mo 2D Calc.
No Concrete
Concrete
χ_{25}
$E\phi(E)$
$\phi(E)/SQRT(E)$
10^{-1}
10^{-2}
5%
25%
50%
75%
95%
dpa Response Range
10^{-2}
10^{-1}
1
2
3
4
5
6
7
8
9
NEUTRON ENERGY (MeV)

Figure 7

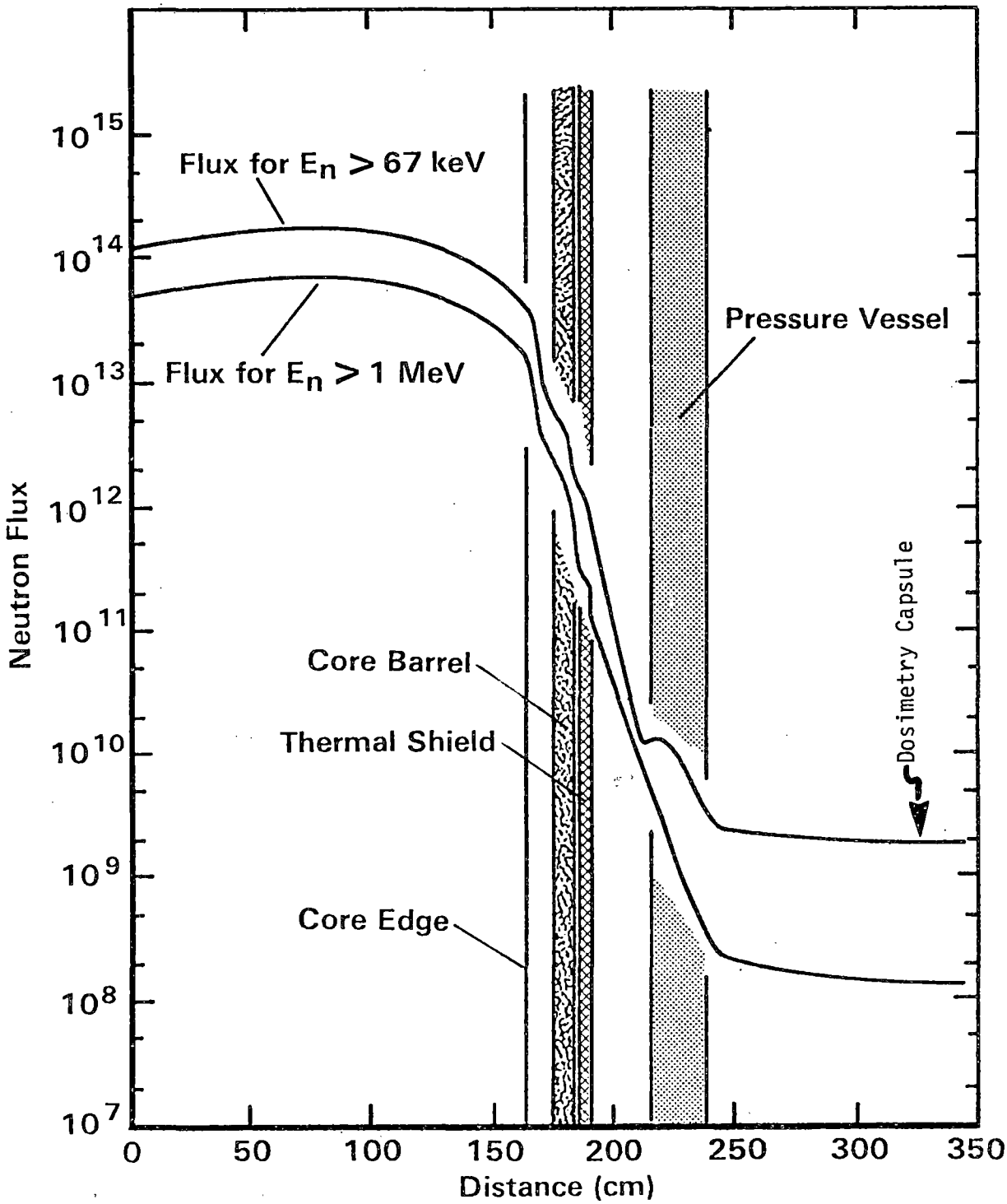
Flux for $E_n > 67$ keV
Flux for $E_n > 1$ MeV
Pressure Vessel
Core Barrel
Thermal Shield
Core Edge
Dosimetry Capsule
Neutron Flux
10^{15}
10^{14}
10^{13}
10^{12}
10^{11}
10^{10}
10^{9}
10^{8}
10^{7}
0
50
100
150
200
250
300
350
Distance (cm)

Figure 8

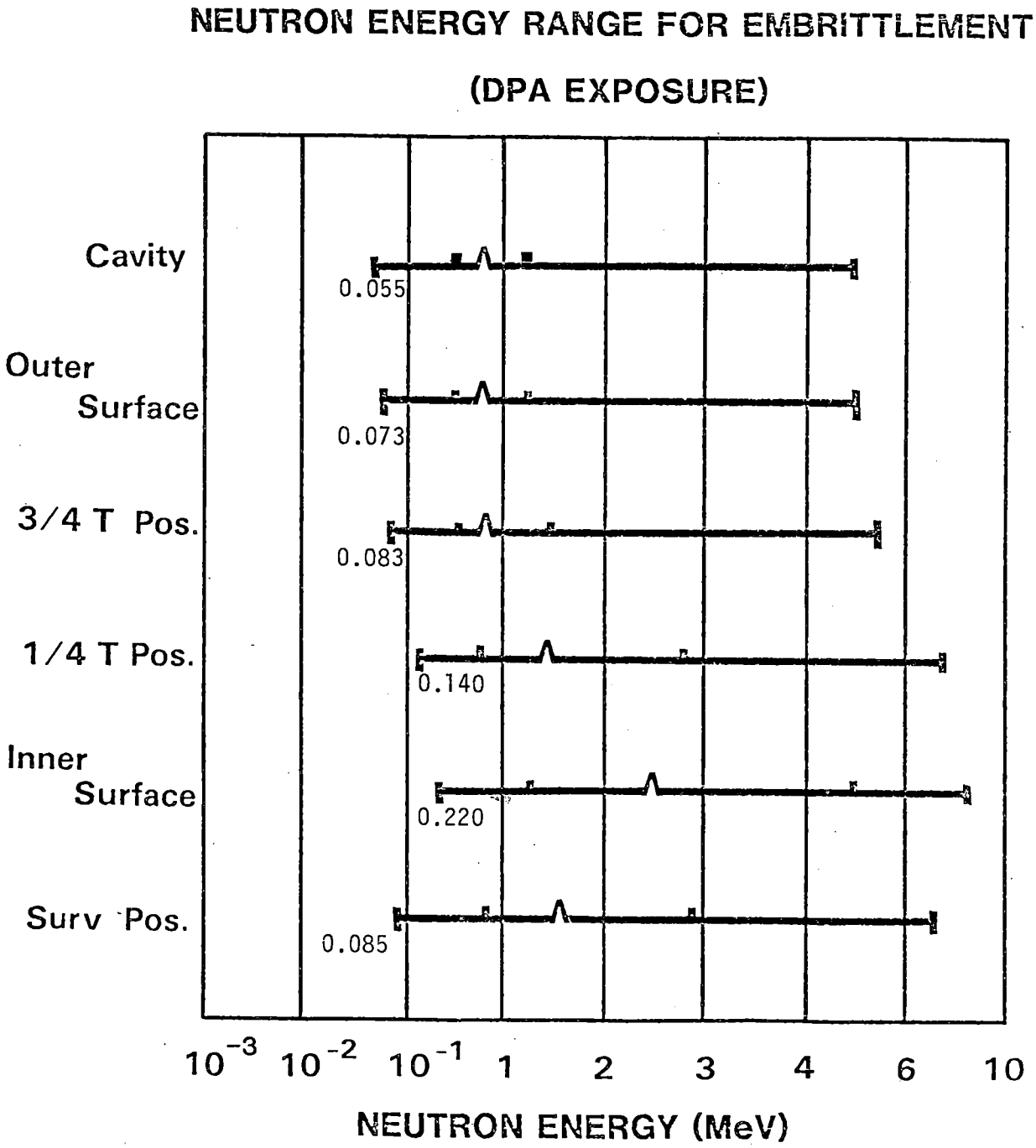
NEUTRON ENERGY RANGE FOR EMBRITTLEMENT
(DPA EXPOSURE)
Cavity
0.055
Outer Surface
0.073
3/4 T Pos.
0.083
1/4 T Pos.
0.140
Inner Surface
0.220
Surv Pos.
0.085
10^-3 10^-2 10^-1 1 2 3 4 6 10
NEUTRON ENERGY (MeV)

Figure 9

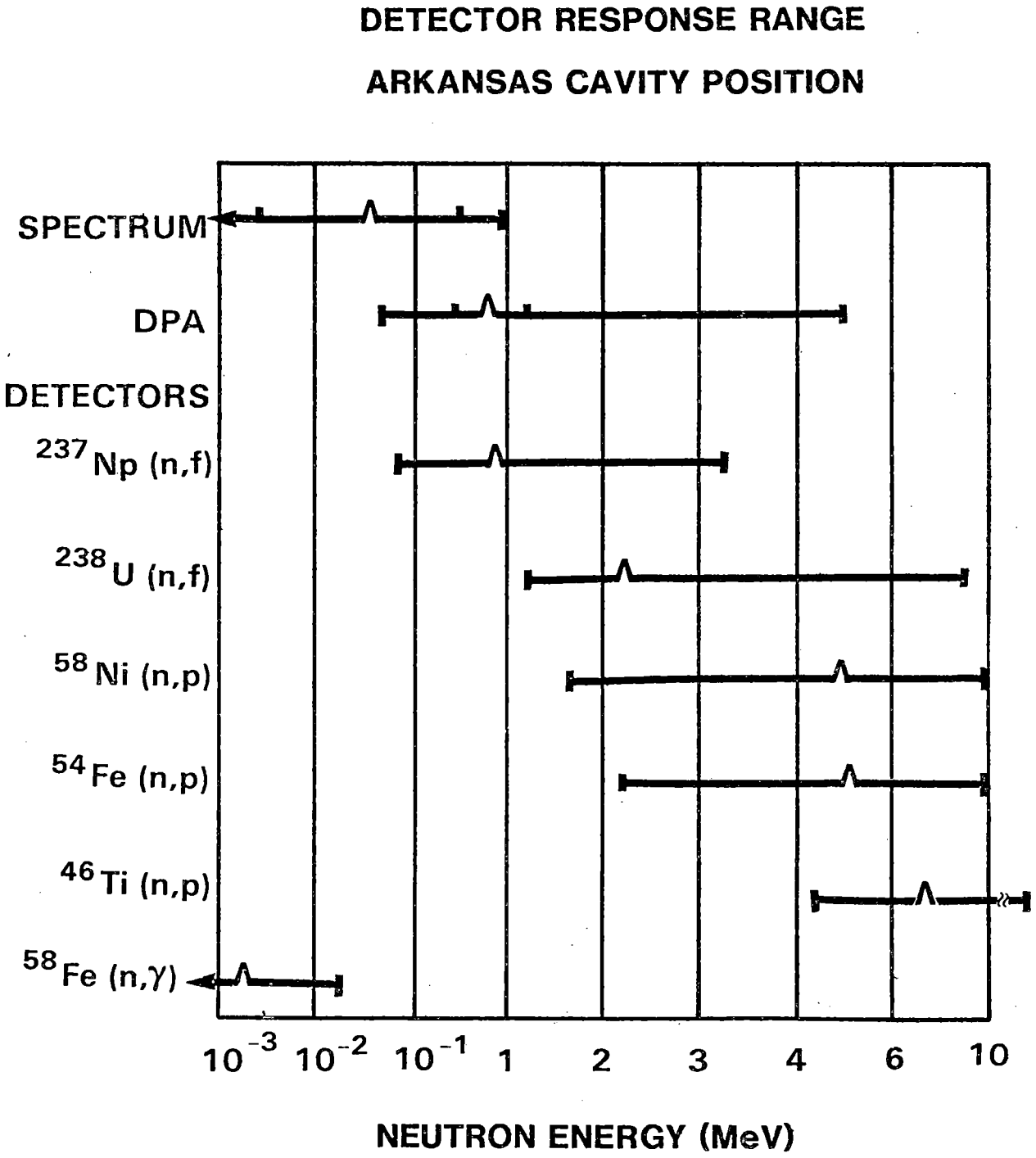
DETECTOR RESPONSE RANGE
ARKANSAS CAVITY POSITION
SPECTRUM
DPA
DETECTORS
237Np (n,f)
238U (n,f)
58Ni (n,p)
54Fe (n,p)
46Ti (n,p)
58Fe (n,γ)
10-3 10-2 10-1 1 2 3 4 6 10
NEUTRON ENERGY (MeV)

Figure 10

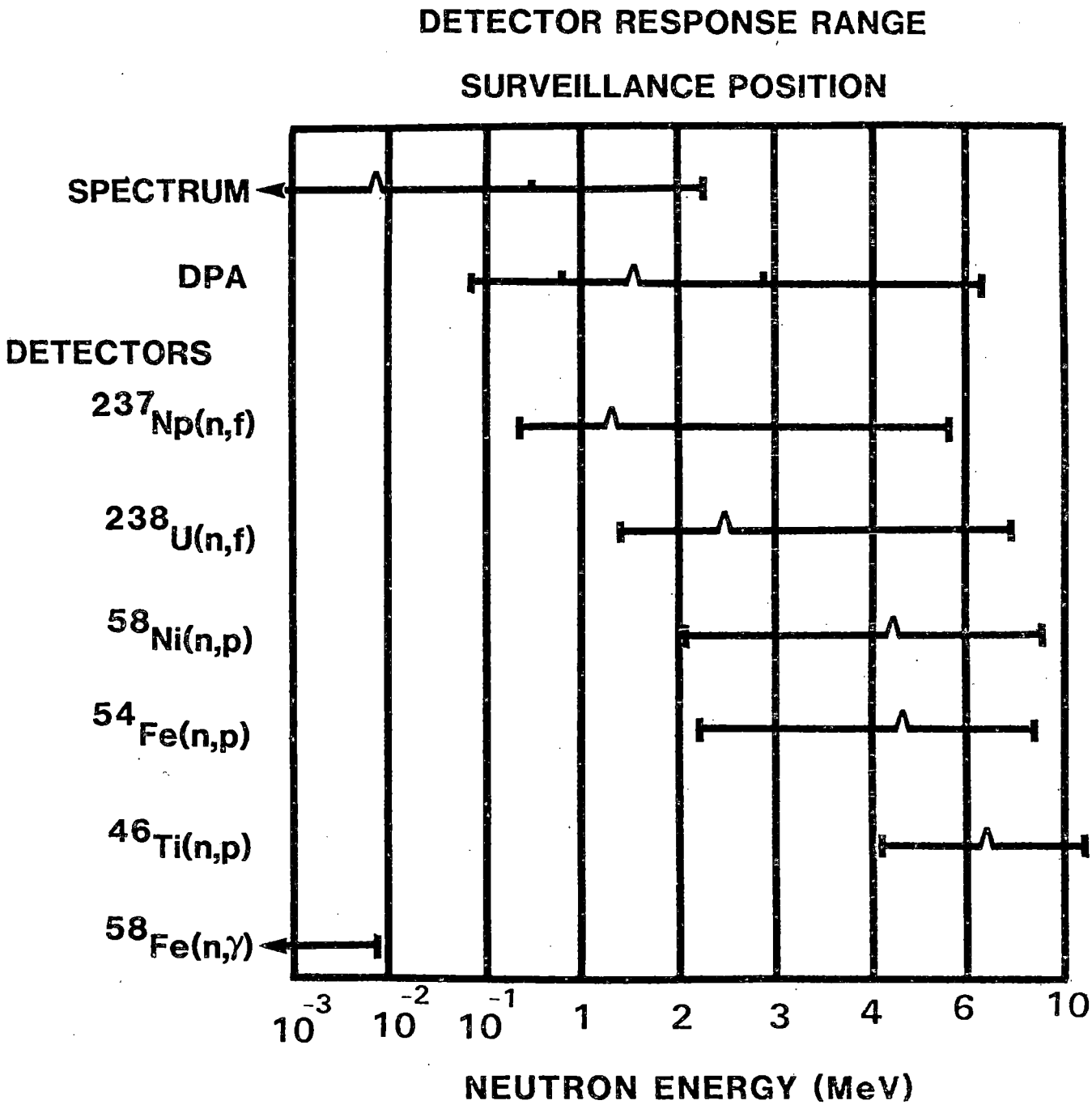
DETECTOR RESPONSE RANGE
SURVEILLANCE POSITION
SPECTRUM
DPA
DETECTORS
237Np(n,f)
238U(n,f)
58Ni(n,p)
54Fe(n,p)
46Ti(n,p)
58Fe(n,γ)
10-3
10-2
10-1
1
2
3
4
6
10
NEUTRON ENERGY (MeV)

Figure 11

INFLUENCE OF CRITICAL VARIABLES ON ENVIRONMENTALLY-ASSISTED CRACK GROWTH RATES OF PVP MATERIALS IN PWR COOLANT ENVIRONMENTS

by

W. H. Bamford and L. J. Ceschini
Westinghouse Nuclear Energy Systems Division
Forest Hills Site, B-300
P. O. Box 855
Pittsburgh, PA 15230

and

W. H. Cullen
ENSA, Inc.
9700B George Palmer Highway
Lanham, MD 20706

and

F. J. Loss and H. E. Watson
Code 6392
Naval Research Laboratory
Washington, D. C. 20375

Presented to:

9th Water Reactor Safety Information Meeting
National Bureau of Standards
Gaithersburg, Maryland
30 October 1980

This research is directed at the determination of the critical variables which influence environmentally assisted crack growth rates of pressure vessel and piping materials. During the past year this program has been carried out through the cooperative efforts of the Naval Research Laboratory and Westinghouse Electric Corporation. Each of the areas of emphasis of the research will be discussed briefly below.

Material Effects Matrix

This test matrix was designed to allow an evaluation of the range of pressure vessel steels and welds found in operating nuclear reactor systems. The tests have been conducted on precracked standard fracture specimens, two inches (5.08 cm) thick, in autoclave chambers with environments designed to simulate the pressurized water reactor environment. The test program has been split between Westinghouse and NRL.

Three different welds were studied in the matrix, and these were made with Linde 80, Linde 124 and Linde 0091 flux. The heat-affected zones from these welds were also characterized; two of these welds were in A533B Cl 1 plate and the other was in A508 Cl 2 forging steel. The specimens tested and the loadings employed are shown in Table 1. Additionally, both plate and forging base metal were studied.

There are two major loading variables which were intended for study in this test matrix, R ratio and loading form. It has long been known that R ratio is a very important variable in this environment, and two values were studied. The second loading variable was the waveform, where a sinusoidal loading form was compared to a ramp-reset condition. Both load forms resulted in a cyclic frequency of 17 mHz.

Testing emphasis during the past year has been directed at completion of the characterization of the welds and heat affected zones of the Linde 0091 flux. Examples of the crack growth rate data are shown in Figures 1 to 3.

One major finding thus far from the matrix is that the material chemistry appears to play an important part in determining its sensitivity to environmental acceleration of crack growth rate. The sulfur content appears to be the key parameter here, with environmental effects much more evident in those materials with high sulfur content. For this reason a new submatrix was devised to study sulfur effects from A533B plate materials. This matrix includes both R ratio and orientation effects. Orientation of the crack with respect to the rolling direction can be important in materials with high sulfur content, so it was included as a test variable.

Studies of Sulfur and Crack Orientation Effects

Three different heats of the same material, A533B Cl plate, were utilized, with the only major difference being the sulfur content. The test matrix was devised to study three parameters, sulfur content, crack orientation, and R ratio. All tests have been designed to use the same specimen size and

exactly the same loadings for a given R ratio. All tests have been run in simulated PWR environment with the same water chemistry, pH = 9 at room temperature. The portion of the matrix which is now complete is shown in Table 3; a schematic of the specimen orientations used in this matrix is shown in Fig. 4.

Results obtained thus far in the matrix of tests, Figs. 5 to 10, have been remarkably consistent with the same trends observed at both high and low R ratio. The trends in the degree of environmental enhancement are the same as those observed earlier for fracture toughness and Charpy energy, where the materials and orientations which display the lowest toughness also display the highest degree of environmental susceptibility.

The highest environmental enhancement was found in the transverse T-L orientation, while the lowest occurred in the L-S orientation. Materials with high sulfur content showed the most enhancement, but the amount of enhancement did not change once the sulfur level exceeded 0.016.

The observed behavior of the L-S, or through thickness orientation was about the same regardless of sulfur content, and was equivalent to the behavior of all three orientations of the low sulfur heat TW. This is an important observation, because the crack orientation which is of most interest from the standpoint of reactor vessel integrity would be propagating in the through-thickness direction.

The effects of orientation and sulfur content on the environmental enhancement of fatigue crack growth demonstrated here help to explain some part of the rather large scatter found in earlier attempts to compile available data.

It seems very likely that even when all the variables which affect corrosion fatigue crack growth are known, a considerable amount of scatter will remain, because the corrosion influence is not a constant factor in a water environment. Crack growth behavior is much more consistent in either an inert environment or a very agressive one, like hydrogen sulfide.

Fractography

Considerable study of the fracture surfaces of the tested specimens has been carried out as a part of this program for a number of years. The dominant feature of the fracture surface has been ductile striations, although areas of brittle-like facets have been found mixed among the striations. Measured striation spacings have correlated well with the macroscopically observed crack growth rate.

One of the main results coming out of the current fractographic studies is the correlation of high sulfur content with the appearance of brittle regions connecting adjacent areas of striated growth that had deviated in elevation from the macroscopic fracture plane. Previous studies had noted the appearance of this component in plate material and in HAZ fracture surfaces.

In the present test matrix on sulfur level and orientation, going from 0.004 to 0.026 sulfur clearly promotes the brittle component in a manner which is independent of orientation. Attempting to correlate the presence of this brittle component with crack growth enhancement is, however, not straight forward, since the low S series of specimens show definite enhancement in

crack growth rate compared to baseline air data. One of the clearest examples of the effect of sulfur level is in the T-L orientation, specimens IN-1, PN-1, and TW-1. Although TW-1 does show enhanced growth at low ΔK, at higher ΔK values the effect diminishes. Apparently in this series of tests the sulfur is making an additional contribution to the crack growth rate so that the higher sulfur specimens are able to sustain a higher growth rate, even though the low S specimen also is enhanced relative to air data.

The mechanism responsible for the development of the brittle areas and the crack growth enhancement of the high sulfur specimens is not clear. Based on the sulfur prints and fractography, it appears unlikely that the effect results from a simple mechanical effect associated with inclusions.

A more likely possibility is the local alternation in crack tip chemistry due to reaction of the sulfide with the water. Apparently this creates a condition at the crack tip that promotes local crack front deviations from the main fracture plane and produces brittle striations. It would be interesting to conduct a series of tests to determine if a low level of sulfur in the water would produce this fractography and if so what level would be required.

Static Load Testing

The behavior of cracks in the pressure vessel steels and welds of interest in PWR environment has been under investigation using bolt-loaded specimens since 1974. The specimens are WOL type, one inch (2.54 cm) thick, and loaded to a fixed displacement by a bolt of the same material. The specimens are positioned in the bottom of two of the operating corrosion fatigue autoclaves.

Cracking under static load has been observed in several of the heat-affected zone materials, and in a single heat of A533B Cl 1 plate. The incubation time for the heat-affected zones has been rather short, less than 2000 hours, but for the plate material the time to first cracking exceeded 27000 hrs. in the environment. No cracking has occurred in the welds or forging material as yet, after nearly sixty thousand hours, forty-five thousand in the environment.

There are presently 14 bolt-loaded specimens under test in the environment, including specimens from A533B Cl 1, A508 Cl 2, a Linde 80 weld, a Linde 124 weld, and four heat-affected zones. The specimens have all been prepared in the same manner. They are precracked in air at low loadings in compliance with ASTM E 399 requirements, then loaded to predetermined value of stress intensity factor, K, which is obtained by tightening the bolt until the face opening of the specimen corresponds to that K as determined by a compliance relationship. If the crack propagates, it should stop at a length which corresponds to the threshold for stress corrosion cracking, K_{ISCC}. This value is easily calculated from the final crack length, because the face opening of the specimen remains constant even though the load drops as the crack propagates. Thus the applied K will decrease as the crack propagates, stopping at $K = K_{ISCC}$. This process is complicated considerably by the fact that incubation times are involved which may be very long in some cases. Even when cracking occurs, as it has in some specimens, it is irregular, and occurs by fits and starts. The method used to expose the specimens to the environment is somewhat deficient because the crack length can only be monitored periodically as the autoclave is opened for specimen insertion or repair of seals. Nonetheless, through numerous removals, considerable information has been obtained on the behavior of these specimens.

Values obtained thus far from the specimens which have cracked have been as low as 45 MPa$\sqrt{m}$, although testing is continuing. The observed tendency is for cracks to propagate unevenly at first, and then for the crack to straighten out. In many cases the crack propagation path has been non planar.

Crack propagation is now occurring in all the heat-affected zone specimens except those from the Linde 0091 weld in the A533B plate material. These have been exposed to the environment for a longer period now than the incubation time for any of the other HAZ specimens.

During the next year a number of new bolt loaded specimens will be inserted into the environment. These are designed to study a number of material effects on the propagation of cracks under static displacement, including sulfur content, weld type, and the type of base metal.

Main Matrix Testing (Irradiated)

Fatigue crack growth rate results are now available for two heats of A508-2, one heat of A533B and one submerged arc weld deposited with Linde 0091 flux. These were conducted with 17 mHz sinusoidal waveforms and load ratios of 0.2. Environmental conditions were PWR-typical, i.e. 288°C (550°F) reactor-grade water (≈1000 ppm boron, 1 ppm lithium) containing <1ppb dissolved oxygen and pressurized to 14 MPa (2000 psi). The specimens were irradiated to typical end-of-life fluences for quarter-thickness locations. The results to date are shown as Figs. 11 through 14.

Taken as a whole, these data sets confirm that for these materials, tested under the specific conditions given above, there is little effect of irradiation on fatigue crack growth rates. Fig. 11 gives results for A533B at two test frequencies. The 1 Hz test frequency generally allows little or no environmental influence, while the 17 mHz test frequency has been shown to provide a near maximization of growth rates in pressure vessel steels in PWR environments [1]. (The reader should note that this is distinctly not the case for BWR environments [2].) From Fig. 11, the 17 mHz results are higher than the 1 Hz results, however, as shown in Fig. 12, the comparison of the irradiated results with companion unirradiated results indicates that the growth rates are about the same in each case. Similar growth rate results, for two heats of A508-2 are shown in Figs. 13 and 14, and for submerged-arc weld metal deposited using Linde 0091 flux, the results are shown in Fig. 15.

The overall similarity of these results points up the basic equivalence in the fatigue crack growth data for pressure vessel steels for which the chemistry is within specification and the sulfur levels are low. They also indicate that the conclusion that irradiation does not increase fatigue crack growth susceptibility, ranges over the general class of reactor-typical materials. However, it must be kept in mind that water chemistry, materials and test conditions have been very nearly optimized in the laboratory, and that materials of degraded chemistry, or long duration upsets in water chemistry may have a very detrimental influence on these results. To specifically address the question, an additional A533B and additional sub-arc weld deposits have been, or are being prepared for irradiation and testing under this aspect of the overall fatigue crack growth program.

Piping Steel Test Matrix

This test matrix is similar to the main test matrix in that it calls for tests to be conducted for two waveforms (17 mHz sinusoidal, 60 sec ramp/reset), two load ratios (0.2, 0.7) and PWR-typical water chemistry. Both stainless and low-carbon, ferritic piping-grade steels are being investigated under this program segment. While the primary goal of this matrix is to determine the dependence of fatigue crack growth on material properties, the concept of material properties has been extended to include orientation effects, which have a stronger influence on crack growth rates in piping steels than in the more texturally homogeneous pressure vessel materials.

Initial results on A106 Gr. C steel, in reactor-grade water at load ratios of 0.2 and 0.7 parallel those results for pressure vessel steels presented in the main matrix section. Crack growth rate results are shown in Fig. 16 (R = 0.2) and Figs. 17 and 18 (R = 0.7). An interesting result based on the data at R = 0.7 is that there appears to be little difference in the crack growth rates between the two test frequencies. Only tests at intermediate or lower frequencies will indicate whether this is a valid conclusion for all frequencies at higher load ratios, or whether the apparent maximization in growth rates at about 17 mHz test frequencies, found for pressure vessel steels, occurs at a different test frequency for piping steels.

Fatigue crack growth data for A516 Gr. 70 steel is shown in Figs. 19 and 20, at R = 0.2, for two orientations. As would be expected, the growth rates for a crack propagating parallel to the longitudinal axis is, on the average, higher than that for a crack propagating in the circumferential direction. Confirmatory tests, and additional tests for other materials and orientations are being planned.

Variable Amplitude Tests

Although this series of tests is actually part of the piping steel test matrix, it is described as a seaparate section because of its unique characteristics. These tests are carried out using a variable-amplitude, variable-frequency waveform which is scaled to that from an operating pressurized water reactor. The specimens are tested in high-temperature reactor-grade water, as in the main and piping steel matrices, but the loading waveform contains seven components of various load ratios and periods. The load ratios are based on measured load ratios for the pressure induced stresses in an operating pressurized water reactor [3].

The load ratios, test frequencies, and cyclic counts for each waveform segment contained in one test "lifetime" are shown in Table 4. In the test program, a segment of which is shown in Fig. 21, these individual cycles are thoroughly mixed. The choice of frequencies is somewhat arbitrary, but the components with the lowest load ratios (start-up, 0.151; hydro-test, 0.139) were assigned 17 mHz frequencies since this had been shown to produce the highest crack growth rates in pressure vessel and piping steels. The other waveform components were assigned frequencies ranging from 33 mHz to 1 Hz, and when the total of 9121 cycles per lifetime are individually multiplied by their periods, the entire reactor "lifetime", for the purposes of this test, is collapsed to a span of twenty hours. A multiple specimen daisy chain, consisting of two specimens of A351 stainless piping steel, and two specimens of A351 matching

weld deposit has been tested. The results of these tests which should not be plotted on the customary da/dN vs ΔK plot as in many of the previous figures, are presented in Tables 5 and 6. These tables give the growth of a flaw during one test "lifetime" for values of the ΔK level which pertained at the beginning of the lifetime.

Overall, these growth increments are not dangerously high, and the next steps of the test program involve devising methods through which these increments can be reasonably accurately predicted from the results of less expensive or complex tests. During the next year, additional variable amplitude tests, as well as a series of constant amplitude tests in direct support of this program, will be carried out.

REFERENCES

1. W. H. Cullen, H. E. Watson, V. Provenzano, "Results of Cyclic Crack Growth Rate Studies in Pressure Vessel and Piping Steels" in Structural Integrity of Water Reactor Pressure Boundary Components, Annual Report, Fiscal Year, 1979, NUREG/CR-1128, NRL Memorandum Report 4122 (Dec. 31, 1979) pp. 43-81.

2. D. A. Hale, J. N. Kass and C. Jewett, "Environmental Fatigue Crack Growth", in BWR Environmental Cracking Margins for Carbon Steel Piping, First Semiannual Progress Report, July 1978 to December 1978, NEDC-24625 (Jan. 1979).

3. M. E. Mayfield, et. a., "Cold Leg Integrity Evaluation" NUREG/CR-1319, available from Division of Technical Information and Document Control, U. S. Nuclear Regulatory Commission, Washington, D. C. 20555.

TABLE 1

WELD AND HEAT-AFFECTED ZONE SPECIMENS COMPLETED

MATERIAL	Test Conditions			
	R = 0.2		R = 0.7	
	One Cycle Per Minute SINE	One Min-Ramp No Hold	One Cycle Per Minute SINE	One Min-Ramp No Hold
Linde 124 Weld (2TWOL)	C-2 C-3	C-7 C-9	C-1 C-6	C-8 C-10
Linde 124 Weld HAZ (In A533B Cl 1 Plate) (2TCT)		C-24-HAZ-1		C-23-HAZ-1
Linde 80 Weld (2TCT)	C-3-WLD C-6-WLD	C-1-WLD	C-4-WLD C-7-WLD	C-2-WLD
Linde 80 Weld HAZ (In A508 Cl 2 Forging) (2TCT)	C-3-HAZ	C-1-HAZ	C-4-HAZ	C-2-HAZ
Linde 0091 Weld (2TCT)	D-1-WLD D-3-WLD	Q342W2	D-2-WLD *D-4-WLD *D-5-WLD	Q342W1
Linde 0091 Weld HAZ (In A533B Cl 1 Plate) (2TCT)	D-1-HAZ		*D-2-HAZ *D-4-HAZ *D-6-HAZ	

*denotes specimens completed during this report period.

TABLE 2

Materials Chemistries

MATERIAL		C	Mn	P	S	Si	Ni	Cr	Mo	Cu	V	Co
Linde 124 Weld "C"		.085	1.32	.013	.012	.48	.91	.14	.49	.05	.005	-
Linde 124 Weld HAZ "C" (adjoining plate plate)		.23	1.33	.009	.014	.22	.58	-	.55	.12	-	-
Linde 80 Weld "C"		.14	1.36	.019	.014	.42	.54	.06	.37	.18	-	-
Linde 80 Weld "C" HAZ adjoining forging		.23	.58	.005	.008	.28	.72	.39	.60	.05	.03	.02
Linde 0091 Weld "D"		.14	1.06	.012	.008	.20	-	-	.48	.15	-	-
Linde 0091 Weld "D-HAZ		.25	1.37	.010	.020	.27	.61	-	.55	.13	-	-
A533B Cl 1	"L83"	.22	1.37	.003	.008	.22	.66	.15	.54	.18	-	-
	"02GF" "2D","02GB"	.22	1.45	.011	.019	.22	.69	.12	.53	-	-	-
	"04A"	.23	1.29	.010	.018	.24	.60	.09	.50	.14	-	-
	"1HT"	.19	1.28	.009	.013	.25	.61	.04	.55	.10	.005	-
	"IN"	.21	1.26	.012	.026	.25	.47	-	.47	.19	-	-
	"TW"	.21	1.38	.008	.004	.21	.67	-	.56	.08	-	-
	"W7"	.23	1.40	.005	.004	.25	.70	-	.57	-	-	-
	"P1"	.21	1.33	.012	.016	.22	.56	-	.54	.13	-	-
A508 Cl 2	"R","R2","R1"	.19	.64	.010	.009	.23	.69	.42	.60	-	-	-
	"F","F1"	.19	.60	.010	.012	.26	.70	.33	.56	-	.02	.008
	"V82"	.20	.60	.013	.012	.20	.73	.35	.56	-	-	-
	"Q71"	.19	.69	.007	.009	.31	.82	.38	.62	.01	-	-

TABLE 3

SPECIMENS COMPLETED IN STUDY OF A533B PLATE

Material: A533B Class 1	Test Conditions					
	R = 0.2			R = 0.7		
Sulfur content/ Orientation	TL	LT	TS	TL	LT	TS
S = 0.004	TW-1 W7-2C7	TW-4	TW-7	TW-2 W7-2C6	TW-5	TW-8
S = 0.016	PN-1	PN-4	PN-7			
S = 0.026	In-1	IN-4	IN-7	IN-2	IN-5	

NOTE: All the above tests were carried out in sumulated PWR environment at 288°C. All specimens were 2TCT, and the applied loadings were identical for all specimens at a given R ratio. Load form was a one cycle per minute sine wave.

TABLE 4A

Material Code	C	Mn	P	S	Si	Ni	Cr	Mo	Cu	V
L83 A533B	.22	1.37	.008	.008	.22	.66	.15	.54	.18	.02
1HT A533B	.21	1.35	.019	.013	.31	.63				
Q71 A508-2	.19	.69	.007	.009	.31	.82	.38	.62	.01	.13
V82 A508-2	.20	.60	.013	.012	.20	.73	.35	.56		
Q93 Sub-arc Weld	.15	1.25	.014	.010	.20	.20	.10	.55	.18	.02

TABLE 4B

Material Code	C	Mn	P	S	Si	Ni	Cr	Mo	Co	V
FOP A106 Gr. C	.25	.88	.016	.017	.22	.25	.10	.033	.007	.003
FOK A516 Gr. 70	.25	1.05	.018	.017	.23	.27	.10	.065	.008	.002

TABLE 5

Material: Stainless Steel-A351

Initial K-Level (MPa $-\sqrt{m}$)	Growth (mm)
30.0	.165
35.0	.203
40.0	.471
45.0	.635
50.0	1.140

TABLE 6

Material: Stainless Weld Metal

Initial K-Level (MPa $-\sqrt{m}$)	Growth (mm)
30.0	.114
35.0	.204
40.0	.281
45.0	.425
50.0	.655
55.0	.886

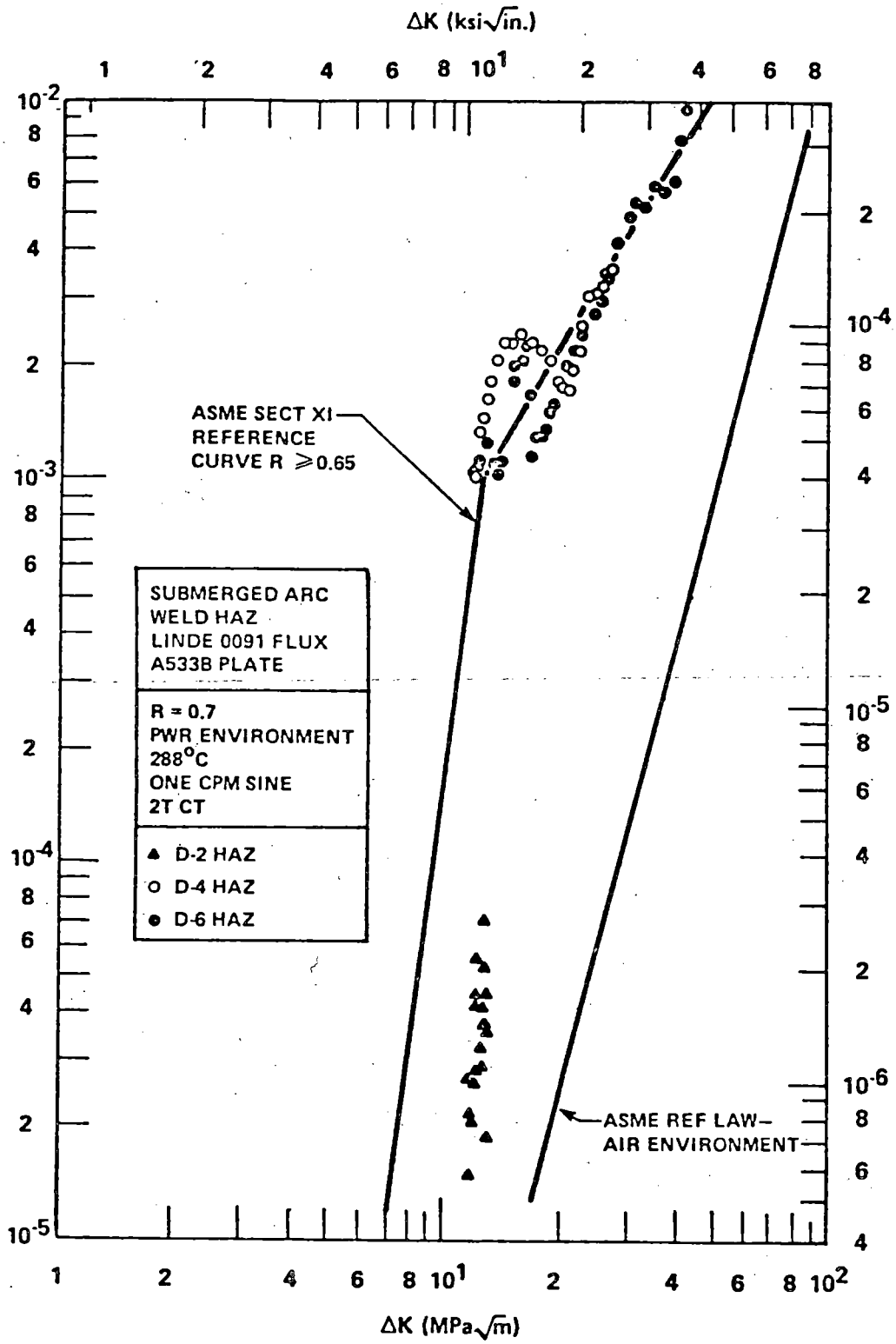

Figure 1 Summary of Results, Linde 0091 Heat Affected Zone Specimens Tested at R = 0.7

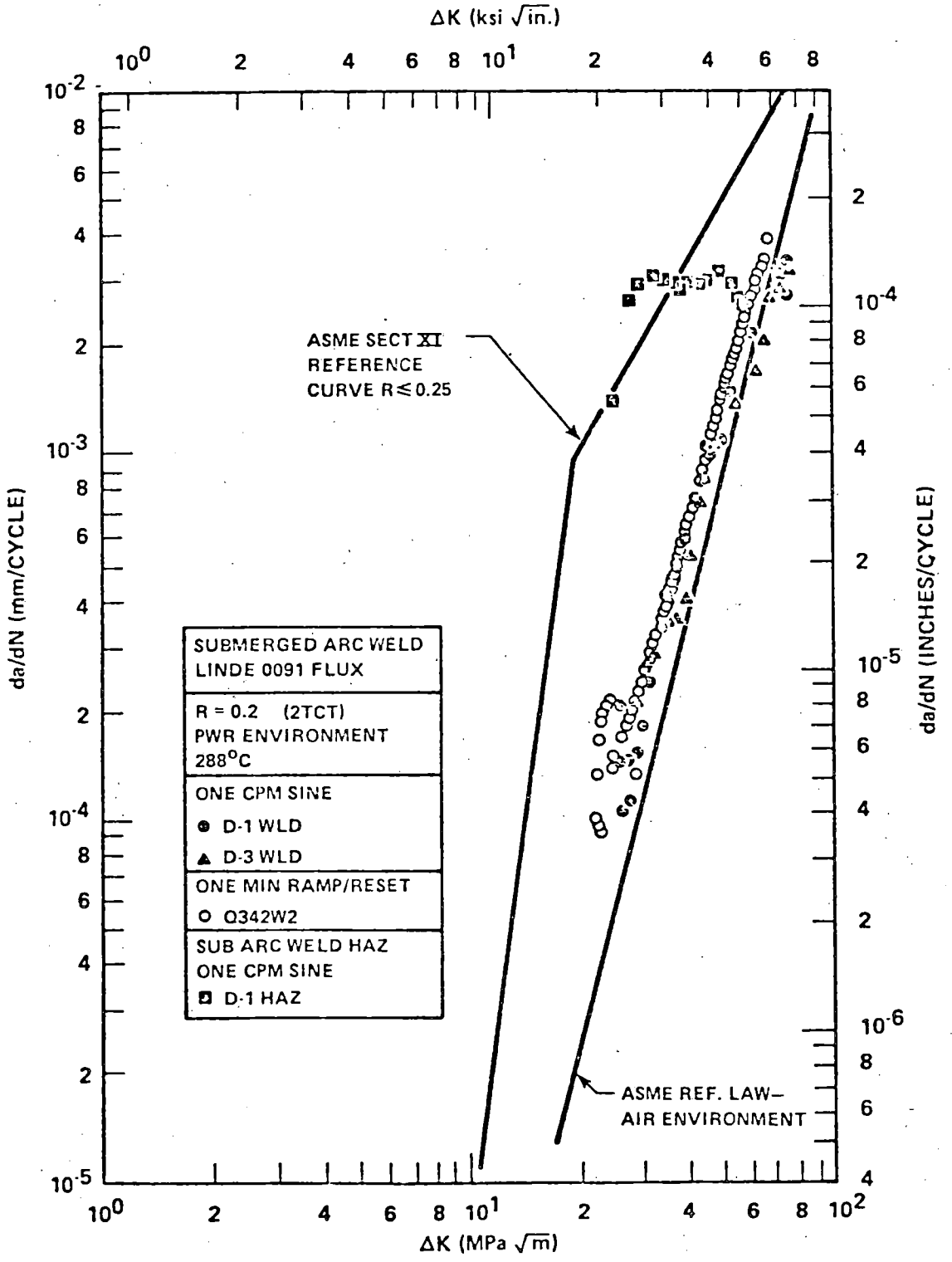

Figure 2 Summary of Previously Obtained Results for Linde 0091 Weld and HAZ at R = 0.2

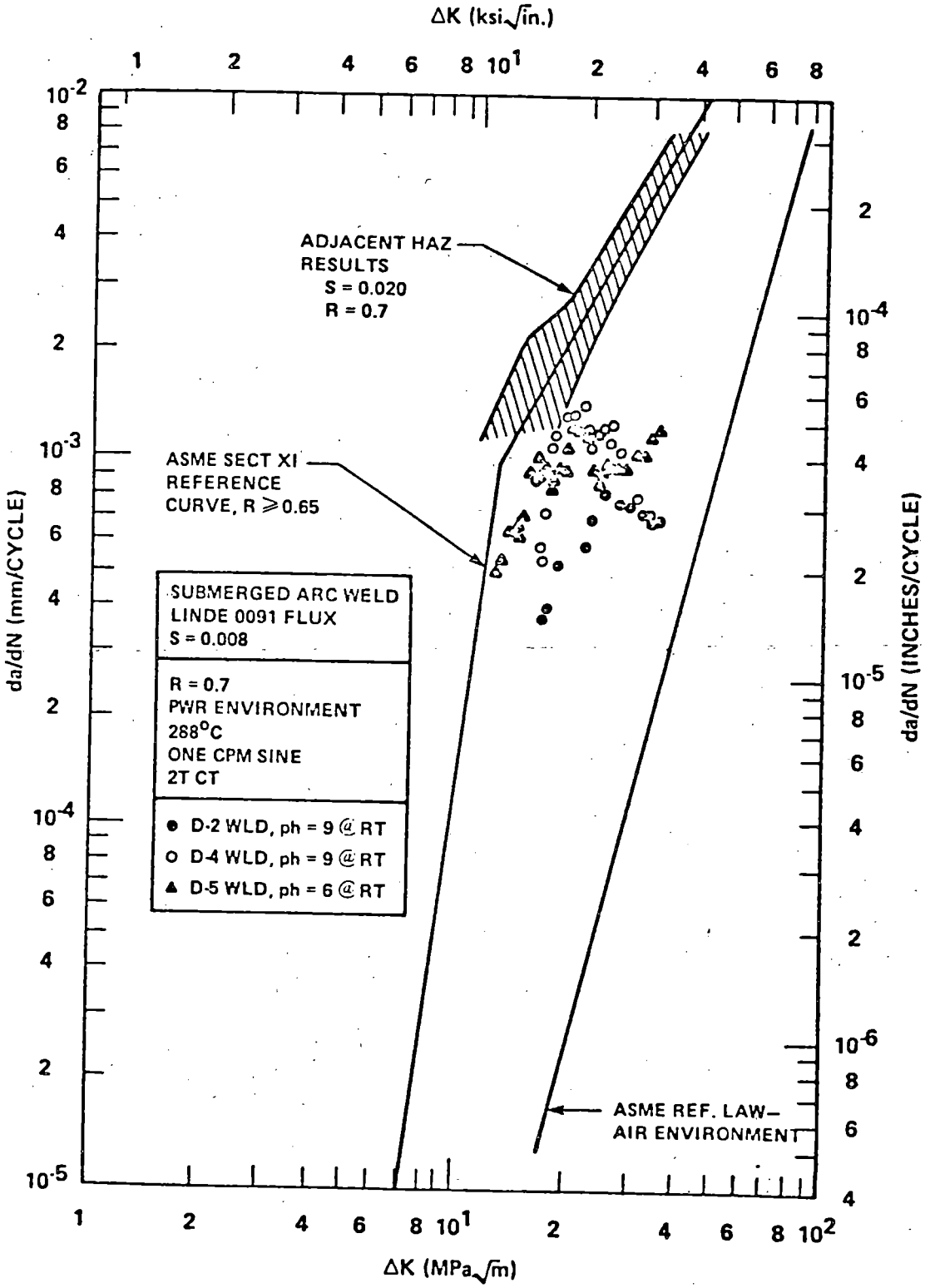

Figure 3 Summary of Results for Linde 0091 Weld at R = 0.7

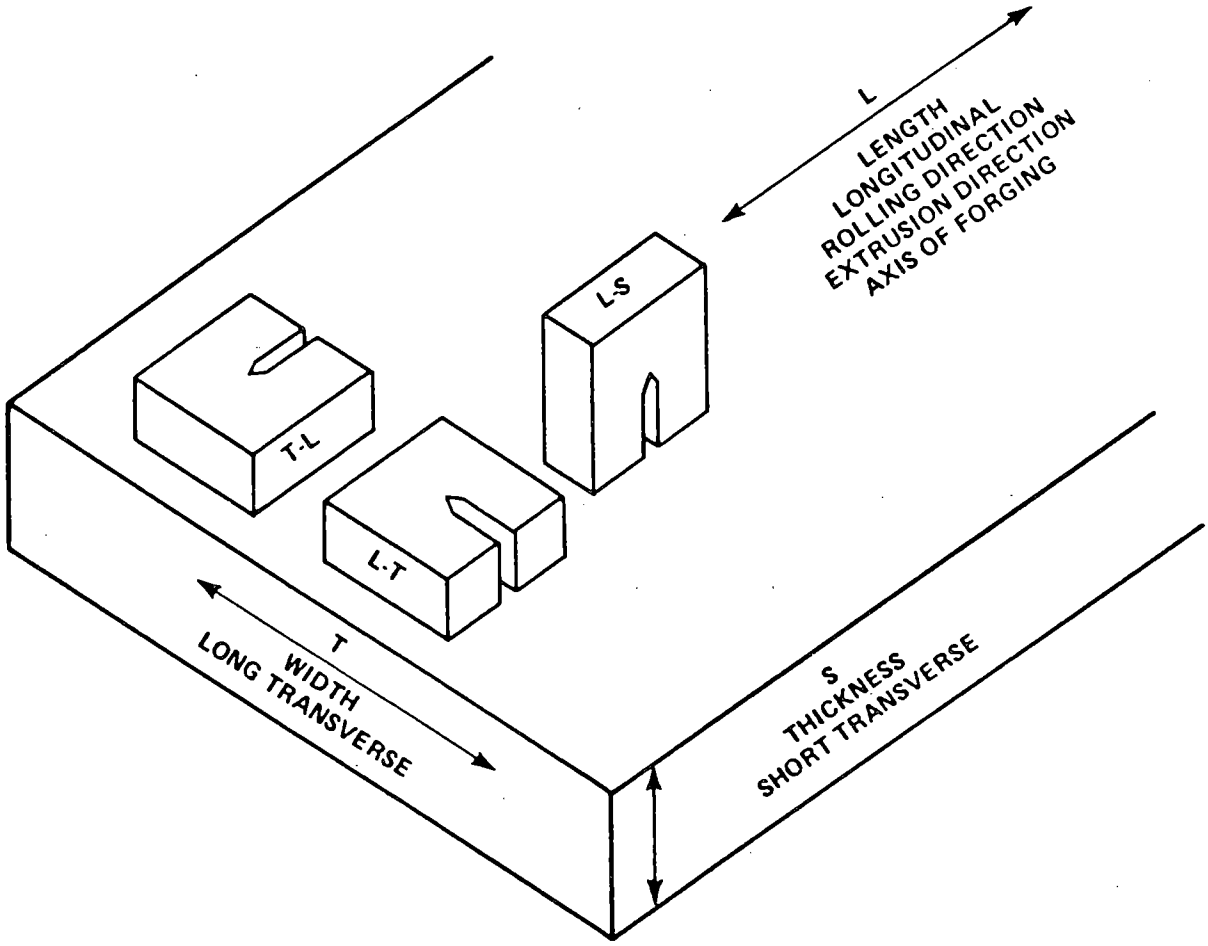

Figure 4 Crack Plane Orientation Identification Code for Plate

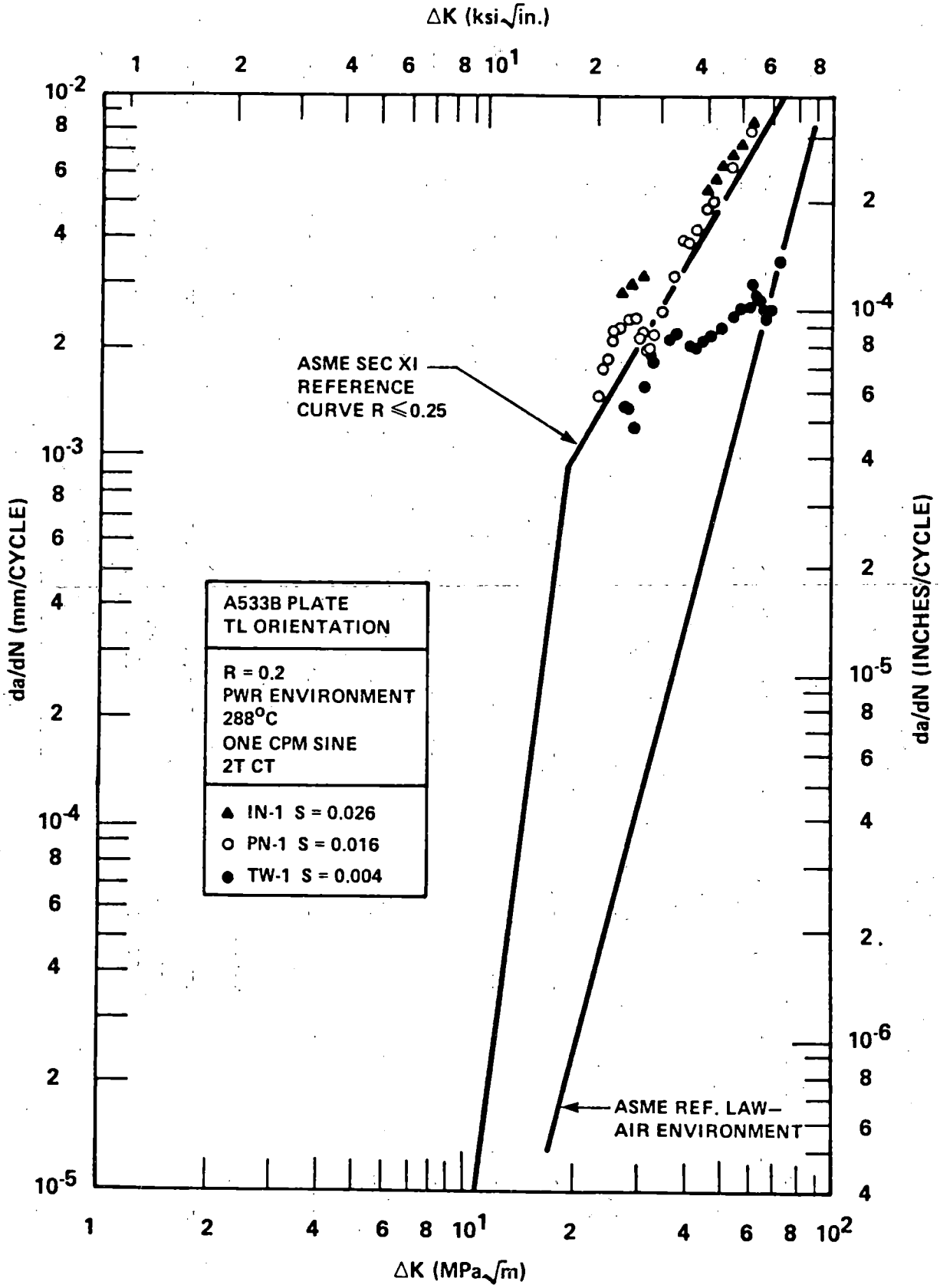

Figure 5 The Effect of Sulfur Content on Fatigue Crack Growth in PWR Environment at R = 0.2, TL Orientation

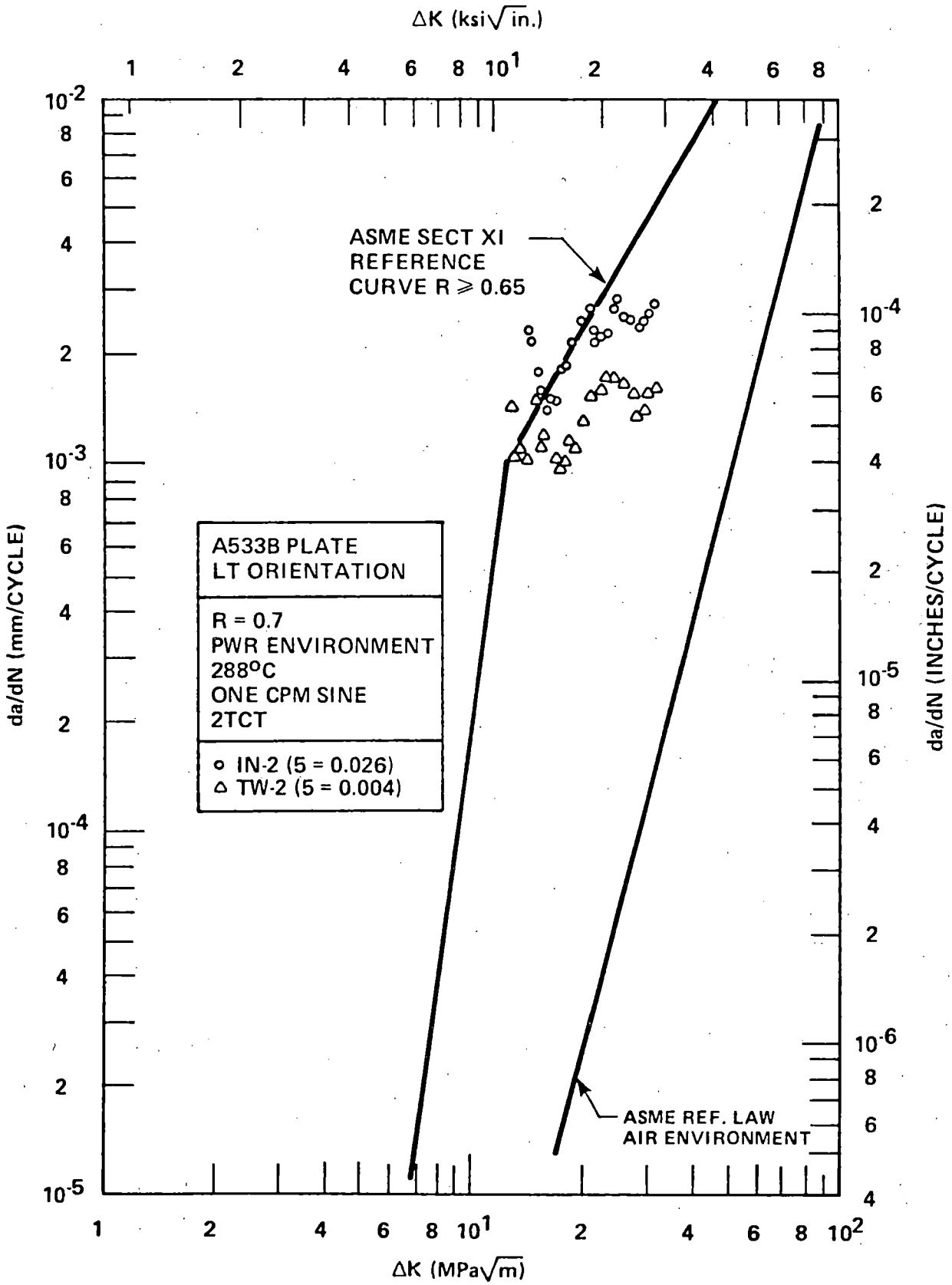

Figure 6 The Effect of Sulfur Content on Fatigue Crack Growth on PWR Environment at R = 0.7, TL Orientation

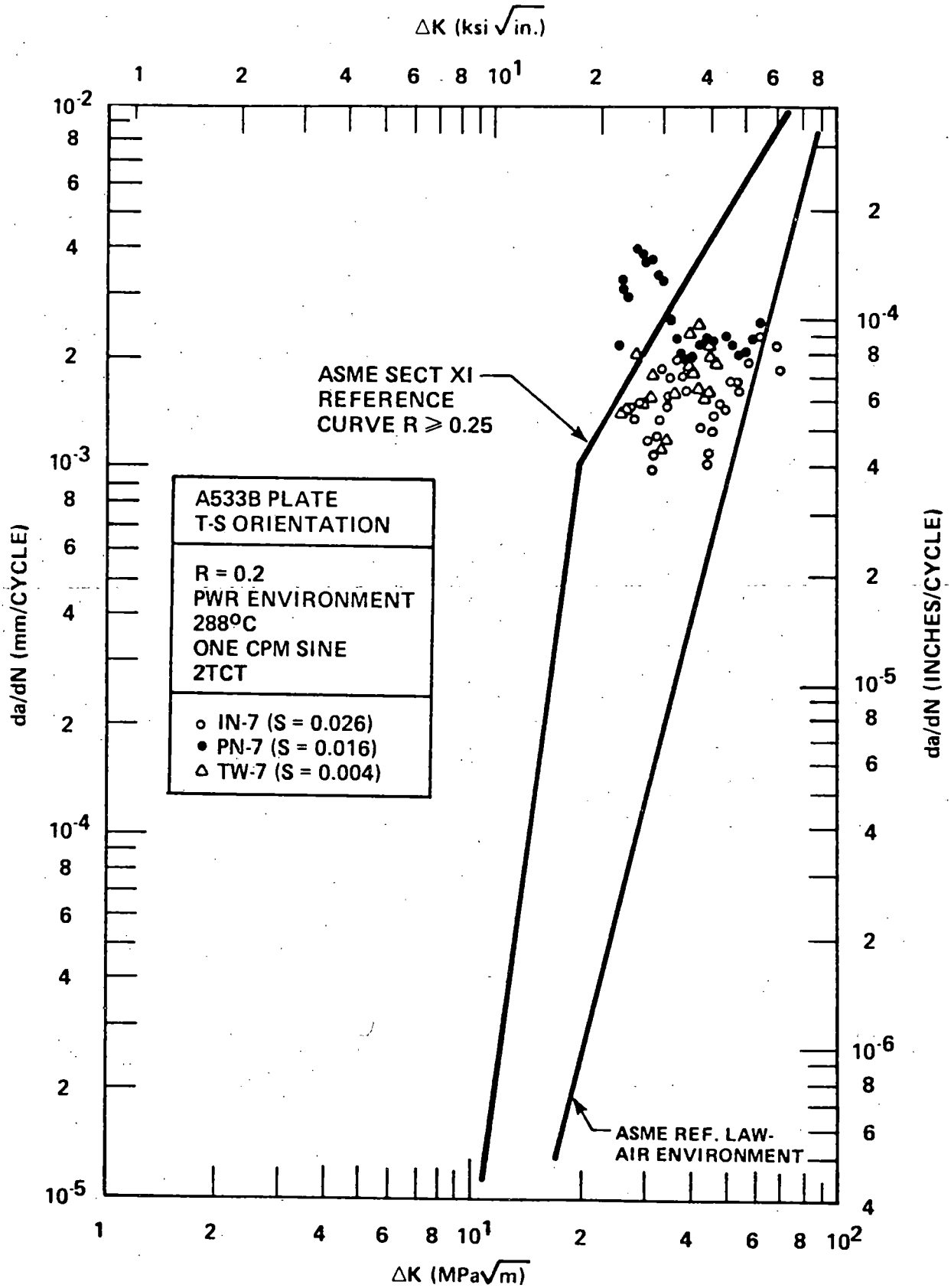

Figure 7 Comparison of Behavior of T-S Orientation at R = 0.2

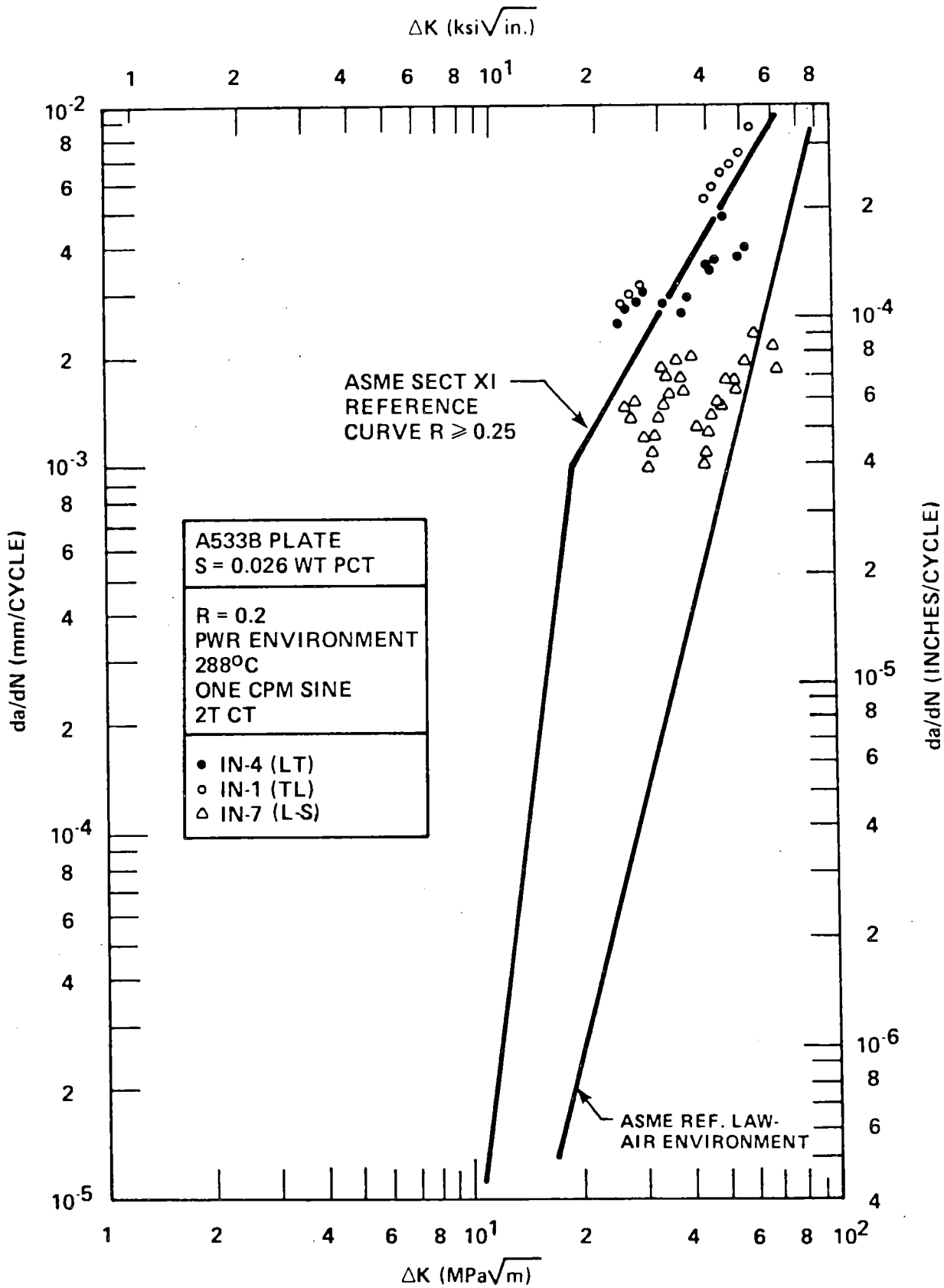

Figure 8 The Effect of Specimen Orientation on Crack Growth, High Sulfur Plate Material

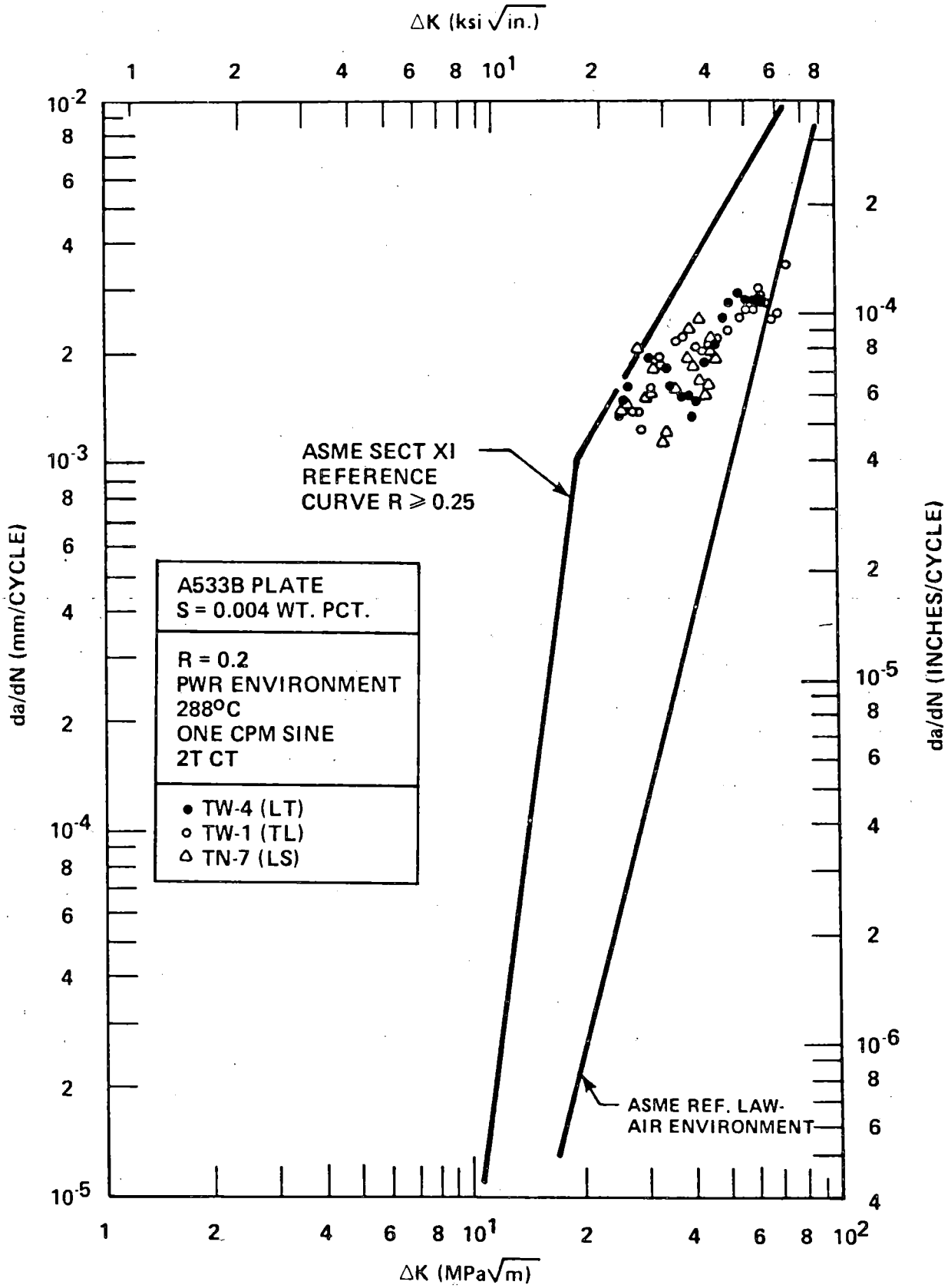

Figure 9 Effects of Specimen Orientation on Crack Growth Rate, Low Sulfur Plate

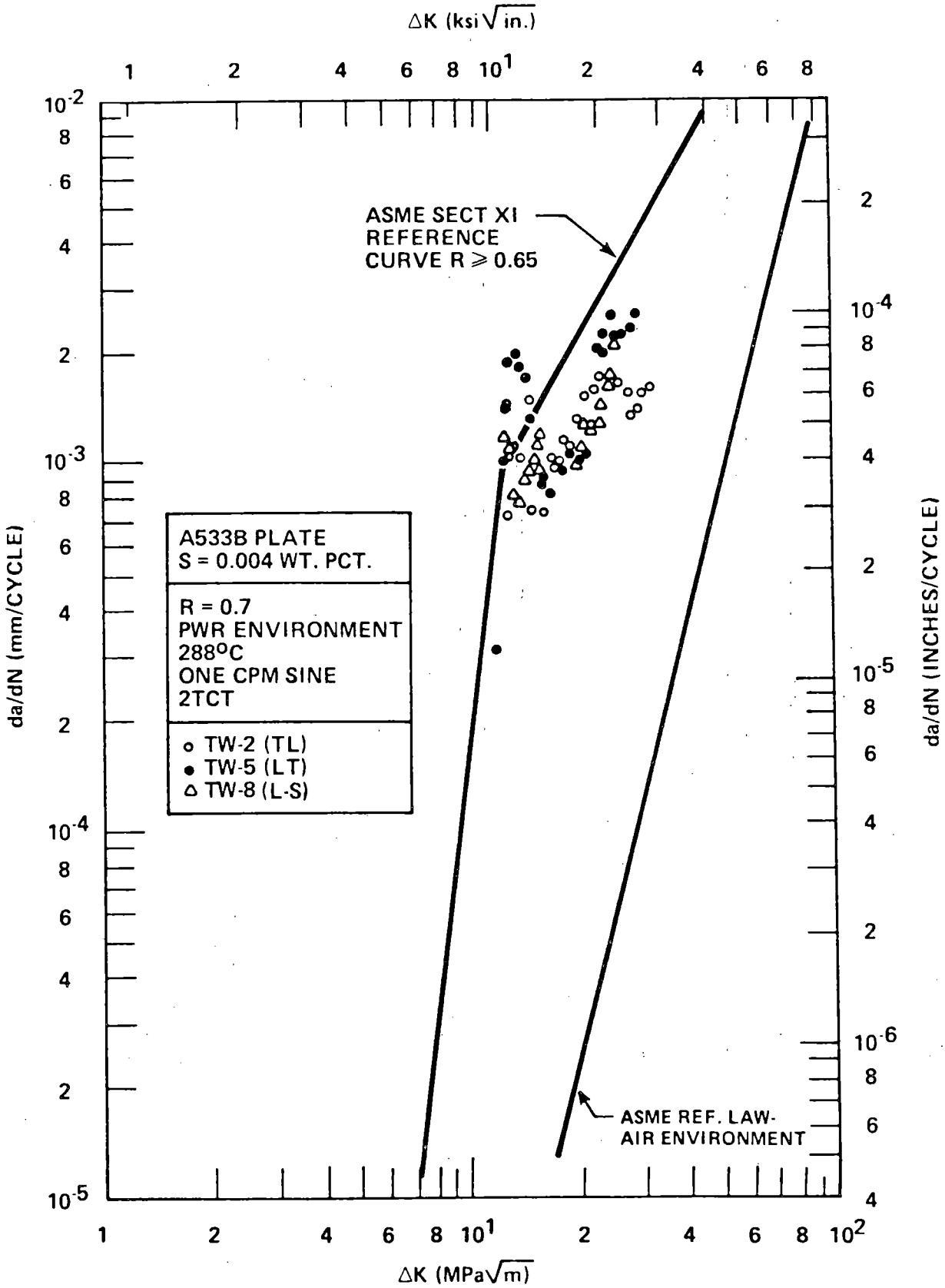

Figure 10 Effect of Orientation at R = 0.7, Low Sulfur Heat

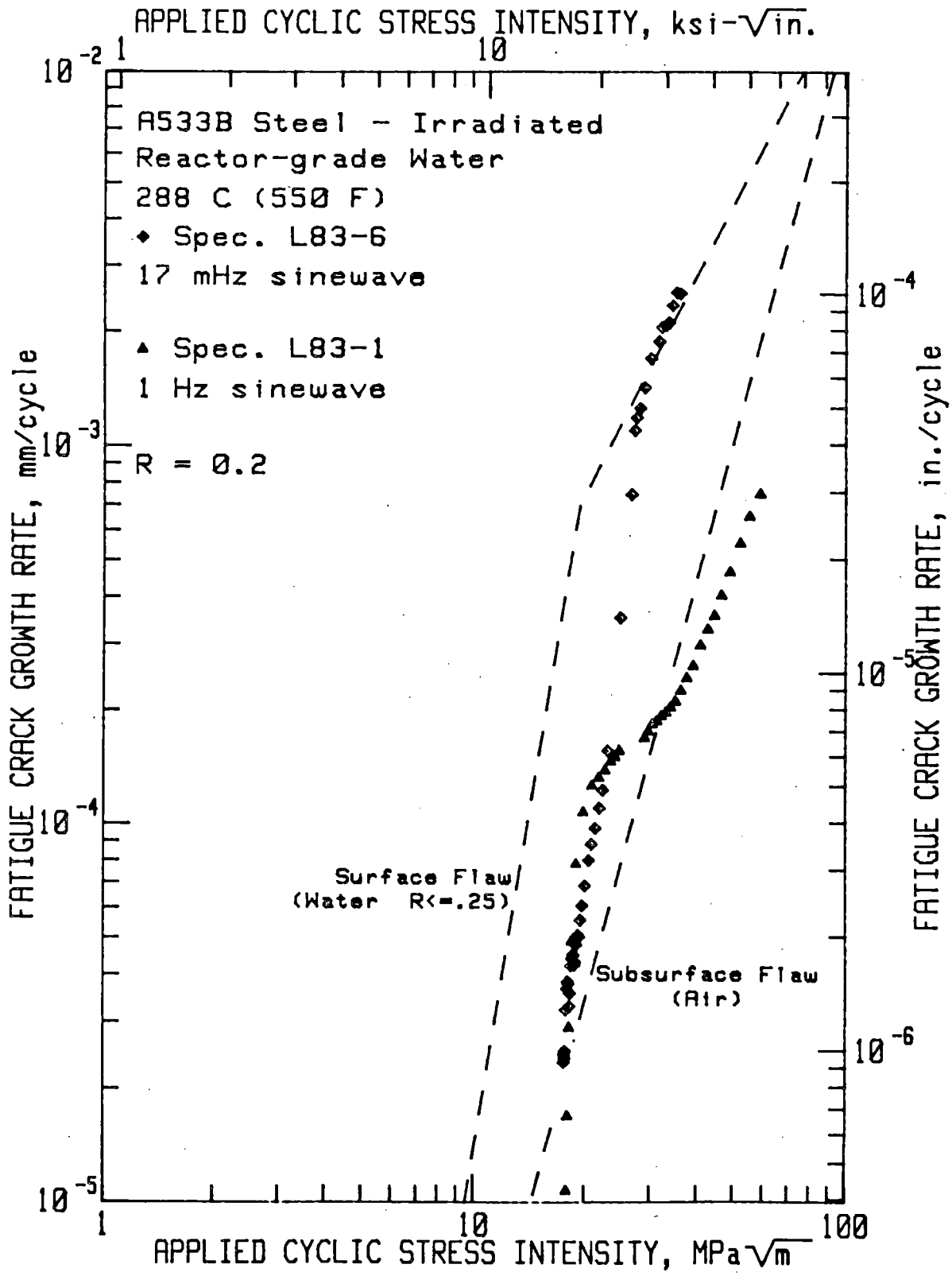

Fig. 11 Fatigue crack growth rates vs applied cyclic stress intensity factor for A533B steel irradiated to end-of-life condition at quarter-thickness (3.4×10^{19} neutrons/cm^2, >1MeV.

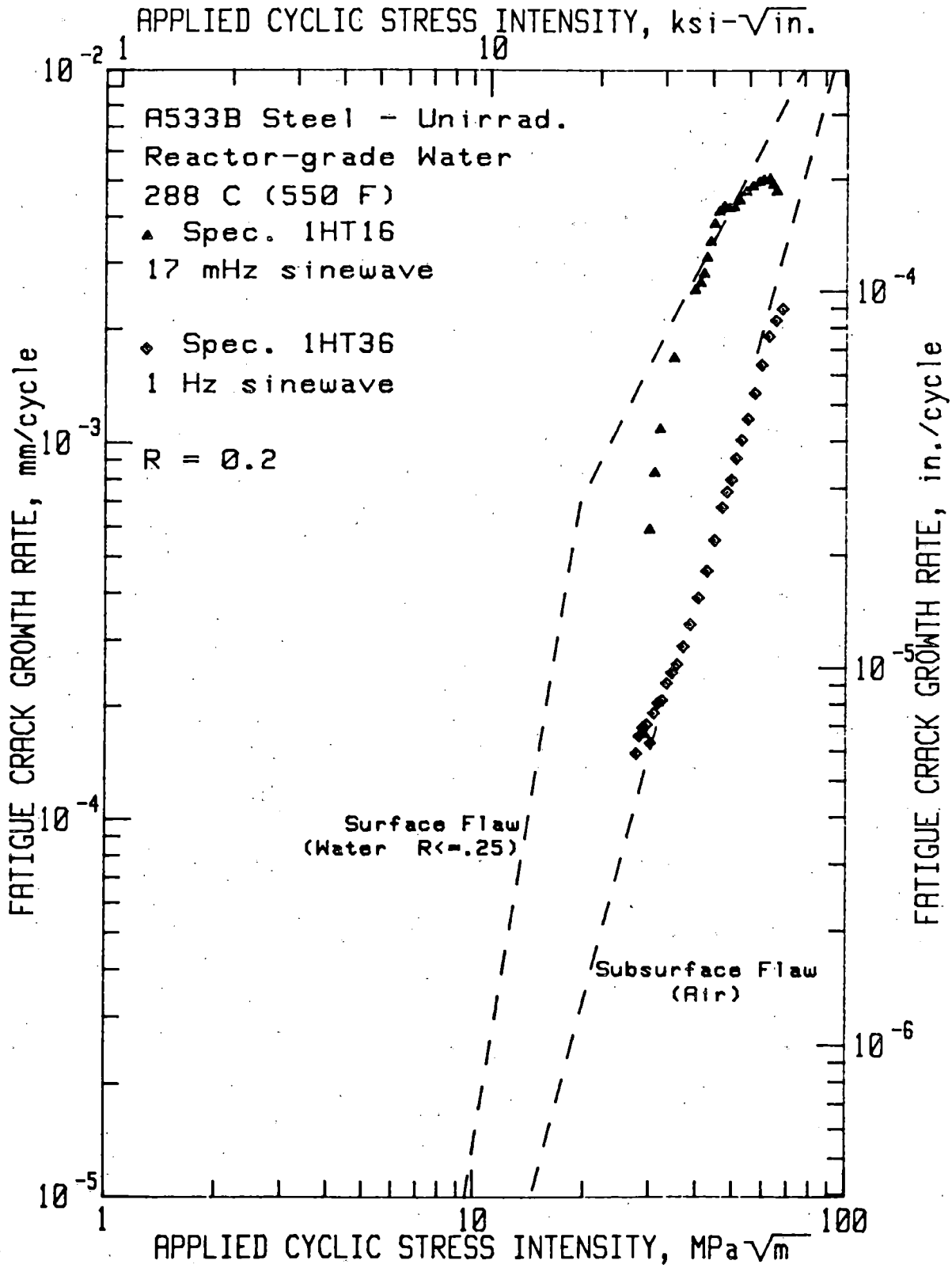

Fig. 12 Fatigue crack growth rates vs applied cyclic stress intensity factor for unirradiated A533B steel. The trends of the growth rates for each of the two frequencies is about the same in Fig. 11, for the irradiated steel, as it is for the unirradiated steel.

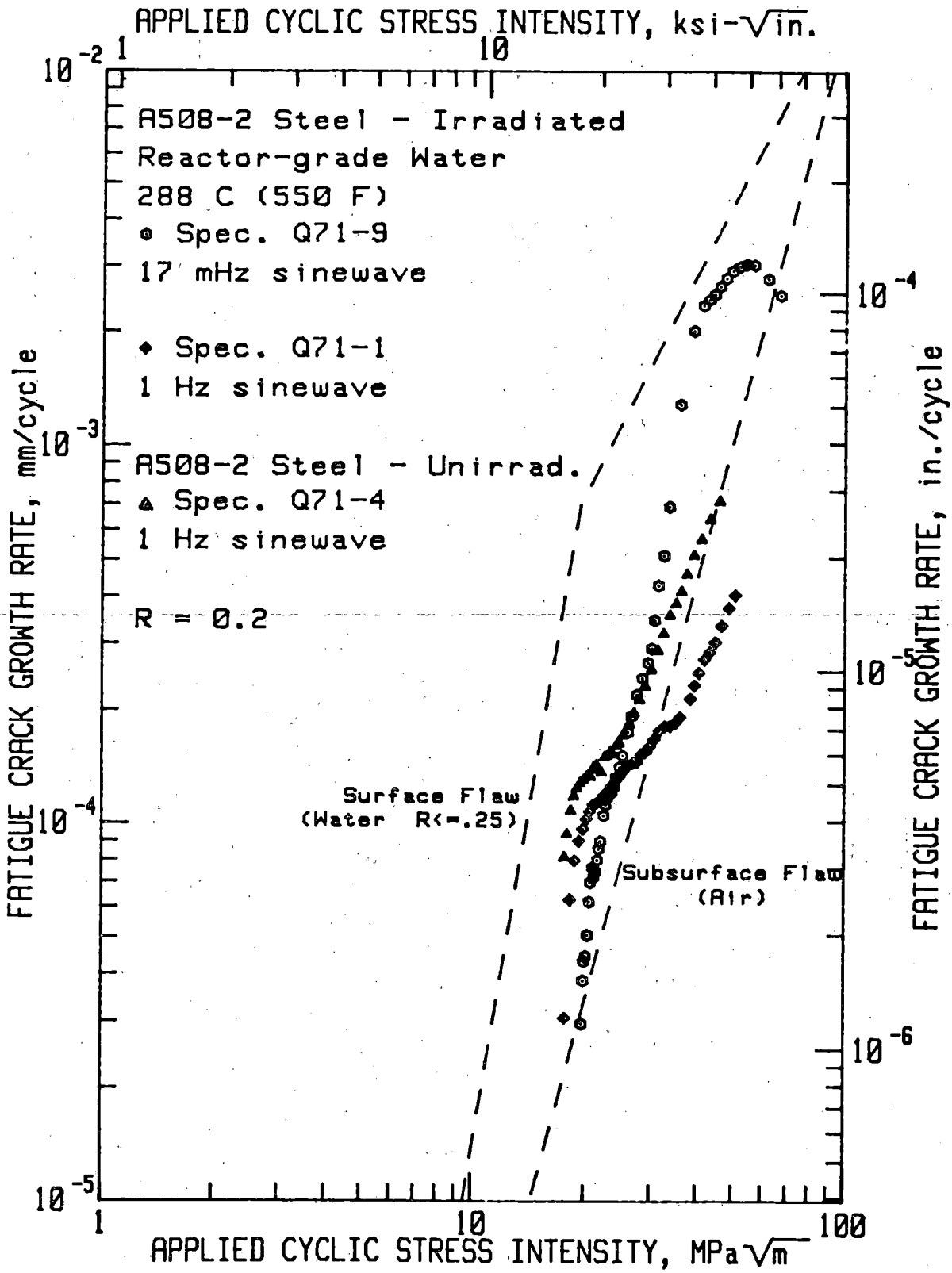

Fig 13 Fatigue crack growth rates vs applied cyclic stress intensity factor for A508-2 steel (code Q71) irradiated to end-of-life condition at quarter-thickness (3.4×10^{19} neutrons/cm^2, >1MeV, for Q71-1; 4.5×10^{19} neutrons/cm^2, >1MeV for Q71-9).

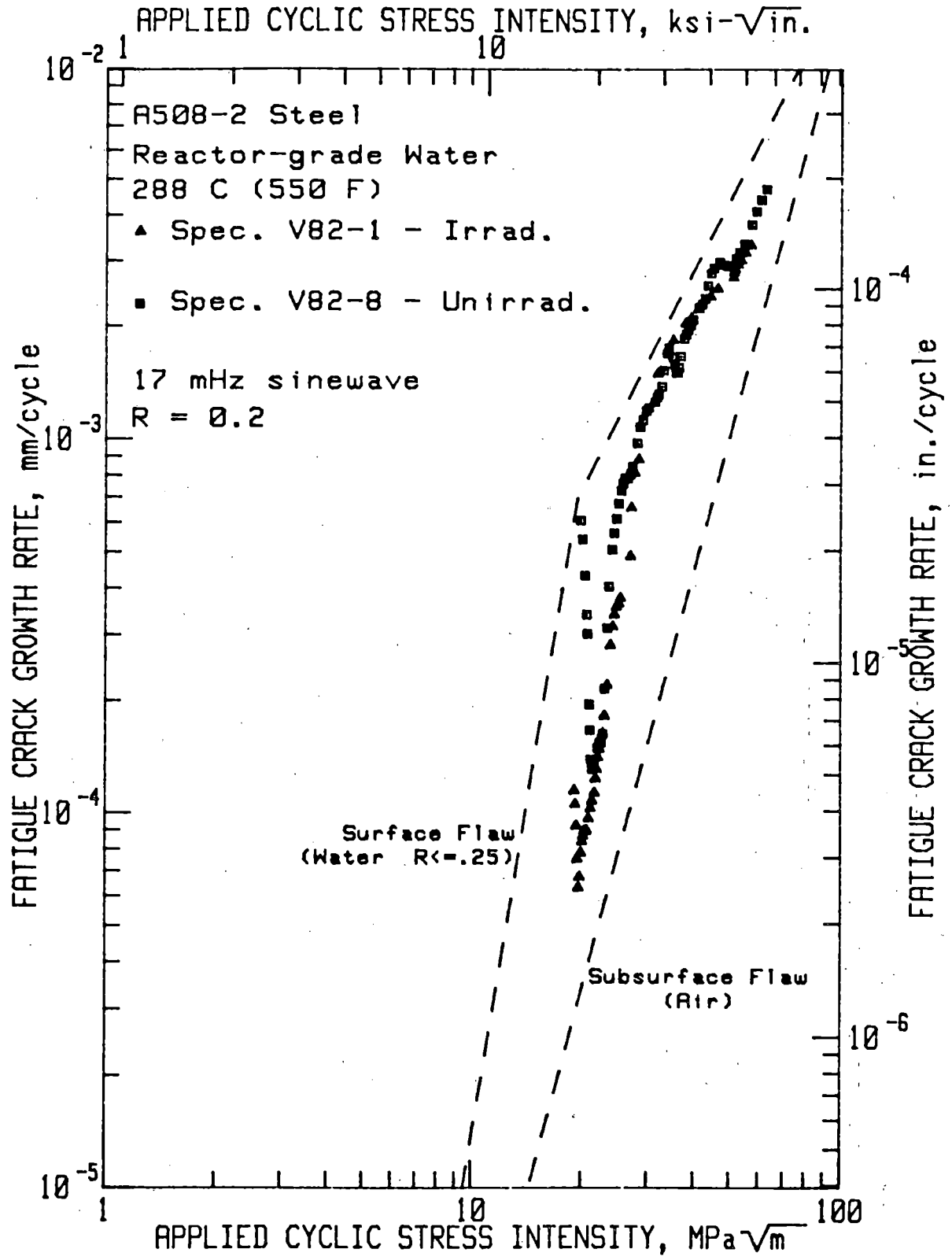

Fig. 14 Fatigue crack growth rates vs applied cyclic stress intensity factor for A508-2 steel (code V82), irradiated to end-of-life condition at quarter-thickness (2.46×10^{19} neutrons/cm^2, >1MeV.

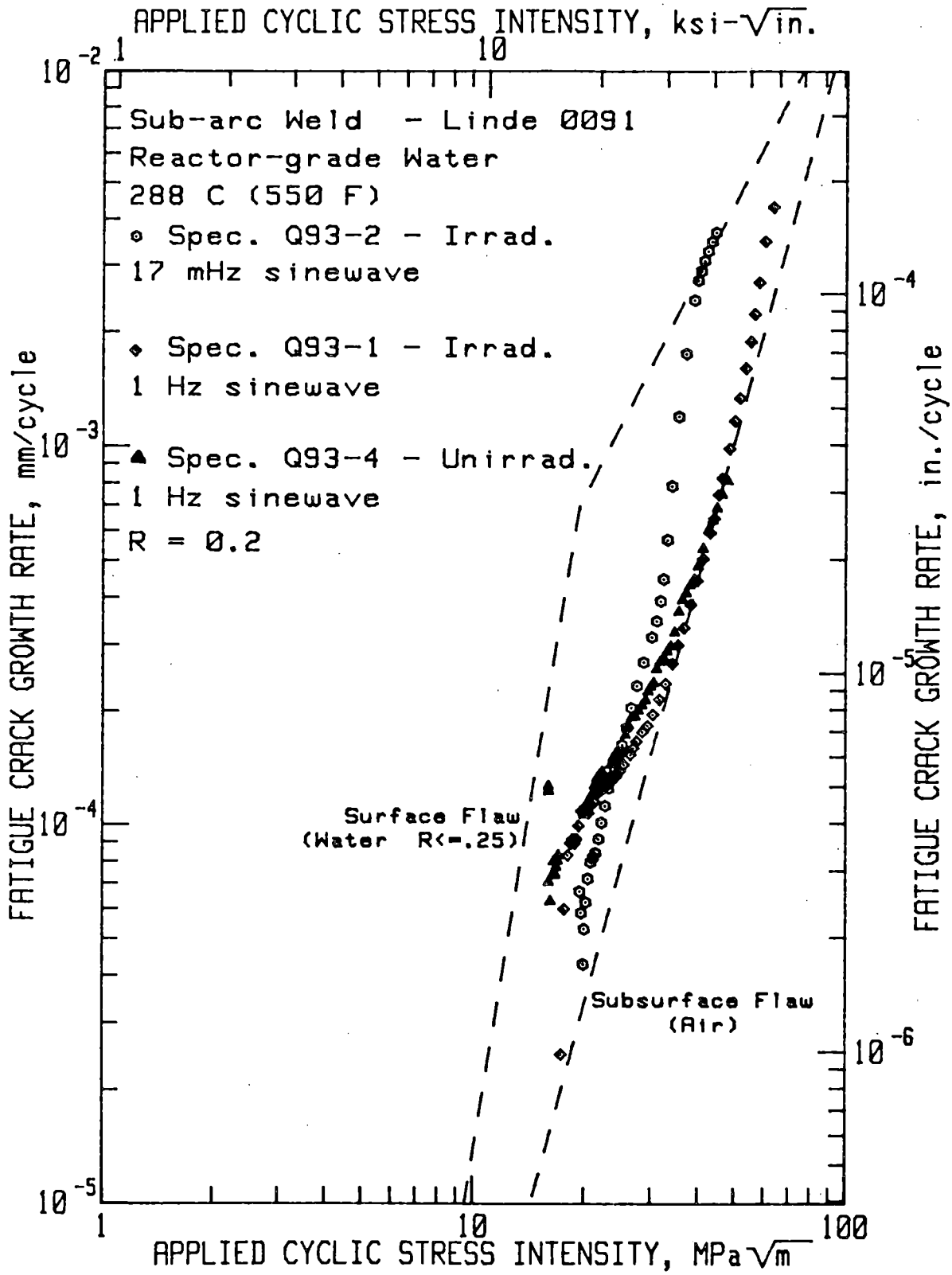

Fig. 15 Fatigue crack growth rates vs applied cyclic stress intensity factor for a submerged-arc weld deposit made with Linde 0091 flux, and irradiated to end-of-life condition at quarter-thickness (3.4×10^{19} neutrons/cm^2 >1MeV for Q93-1; 4.5×10^{19} neutrons/cm^2, >1MeV for Q93-2).

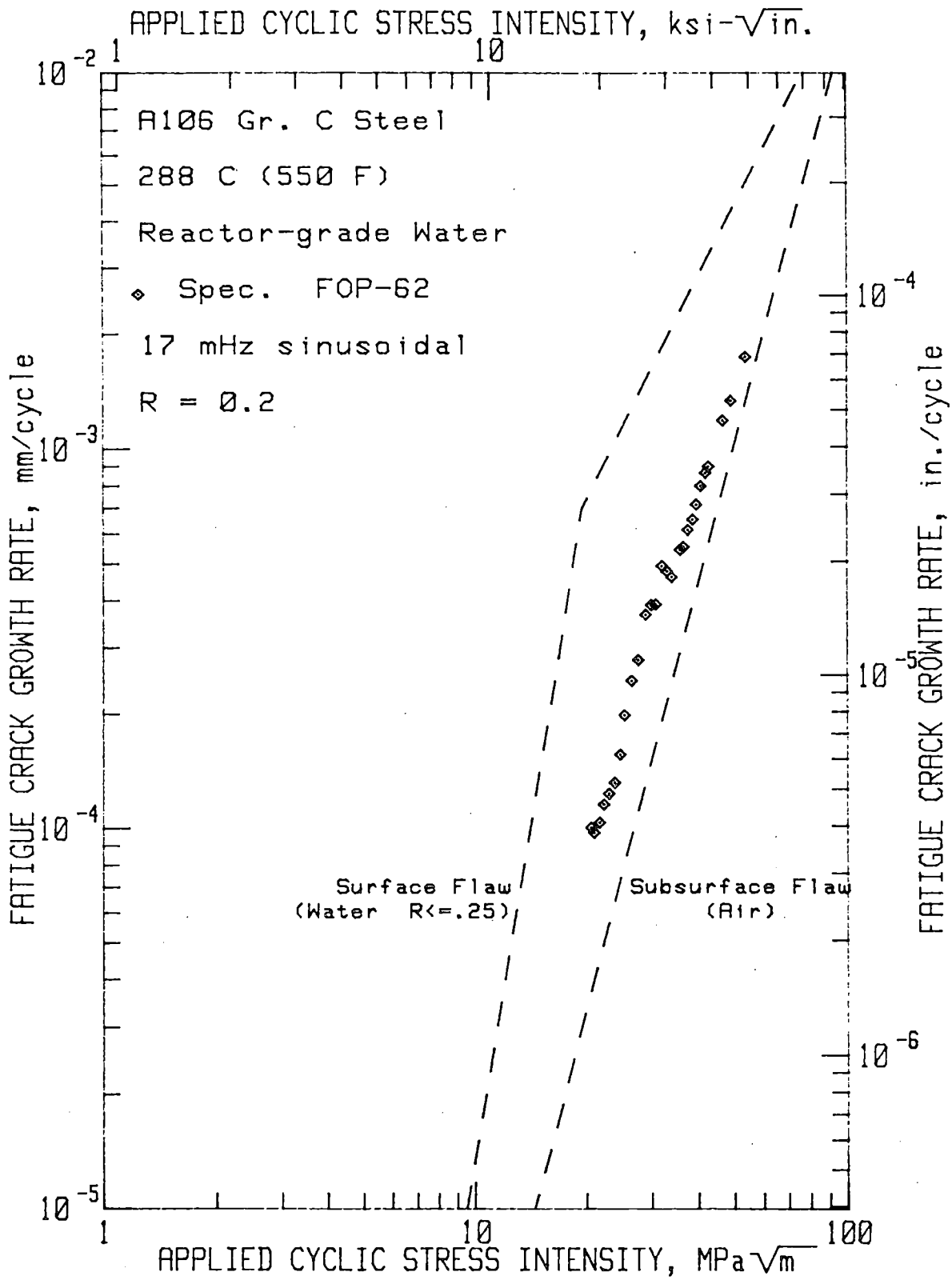

Fig. 16 Fatigue crack growth rates vs applied cyclic stress intensity factor for A106 Gr. C steel, R = 0.2, 17 mHz sinusoidal waveform.

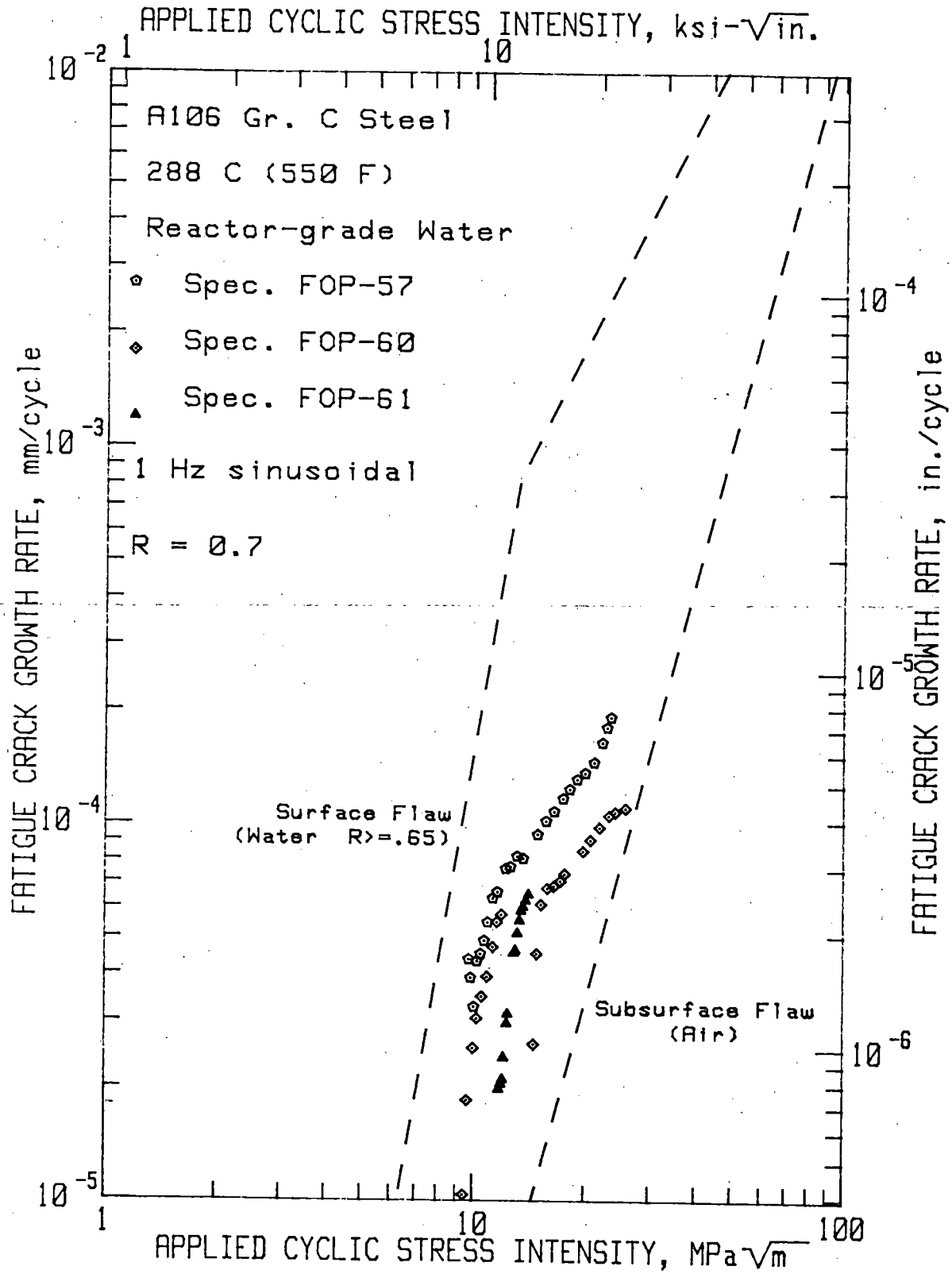

Fig. 17 Fatigue crack growth rates vs applied cyclic stress intensity factor for A106 Gr. C steel, R = 0.7, 1 Hz sinusoidal waveform.

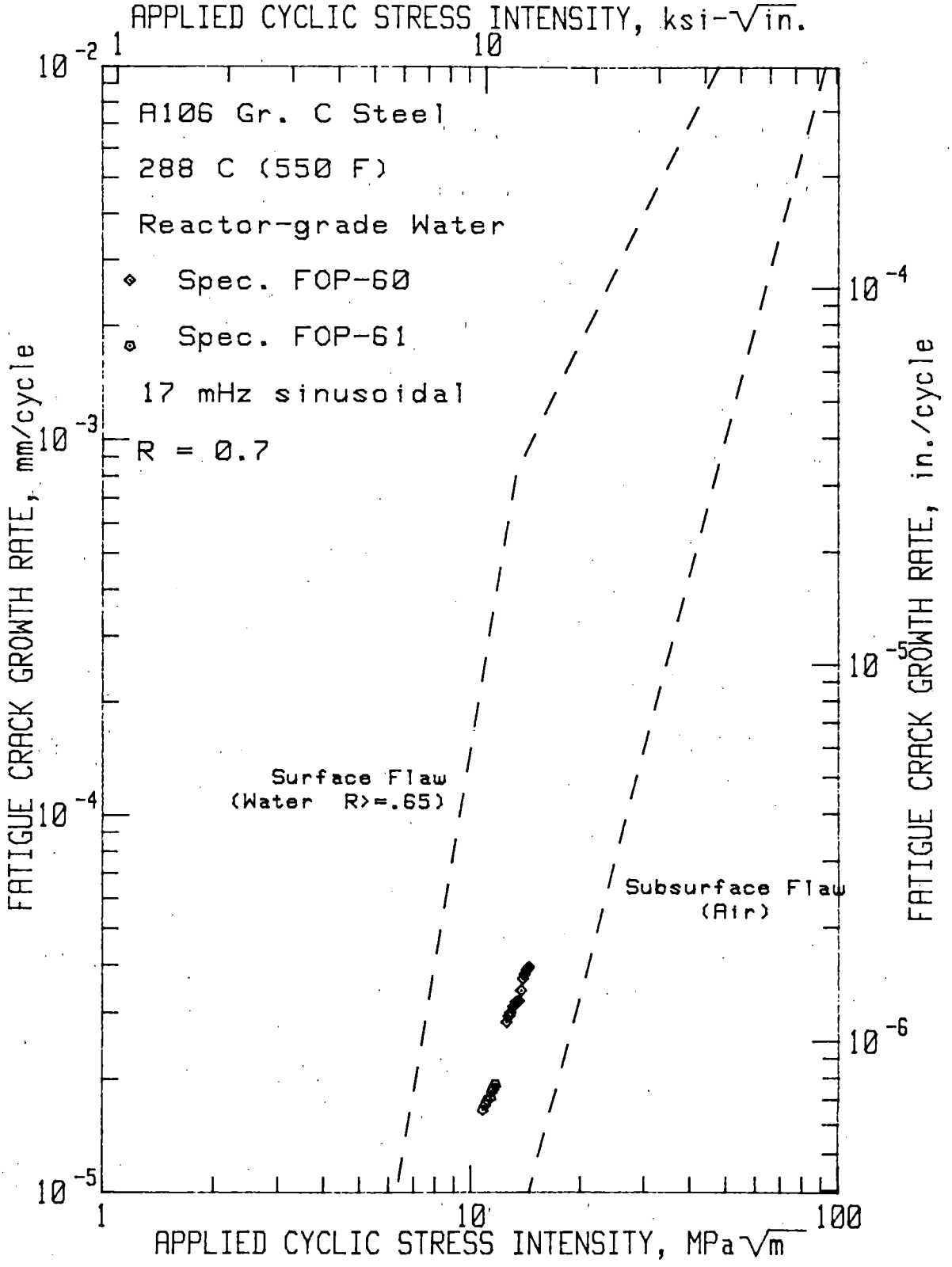

Fig. 18 Fatigue crack growth rates vs applied cyclic stress intensity factor for A106 Gr. C steel, R = 0.7, 17 mHz sinusoidal waveform.

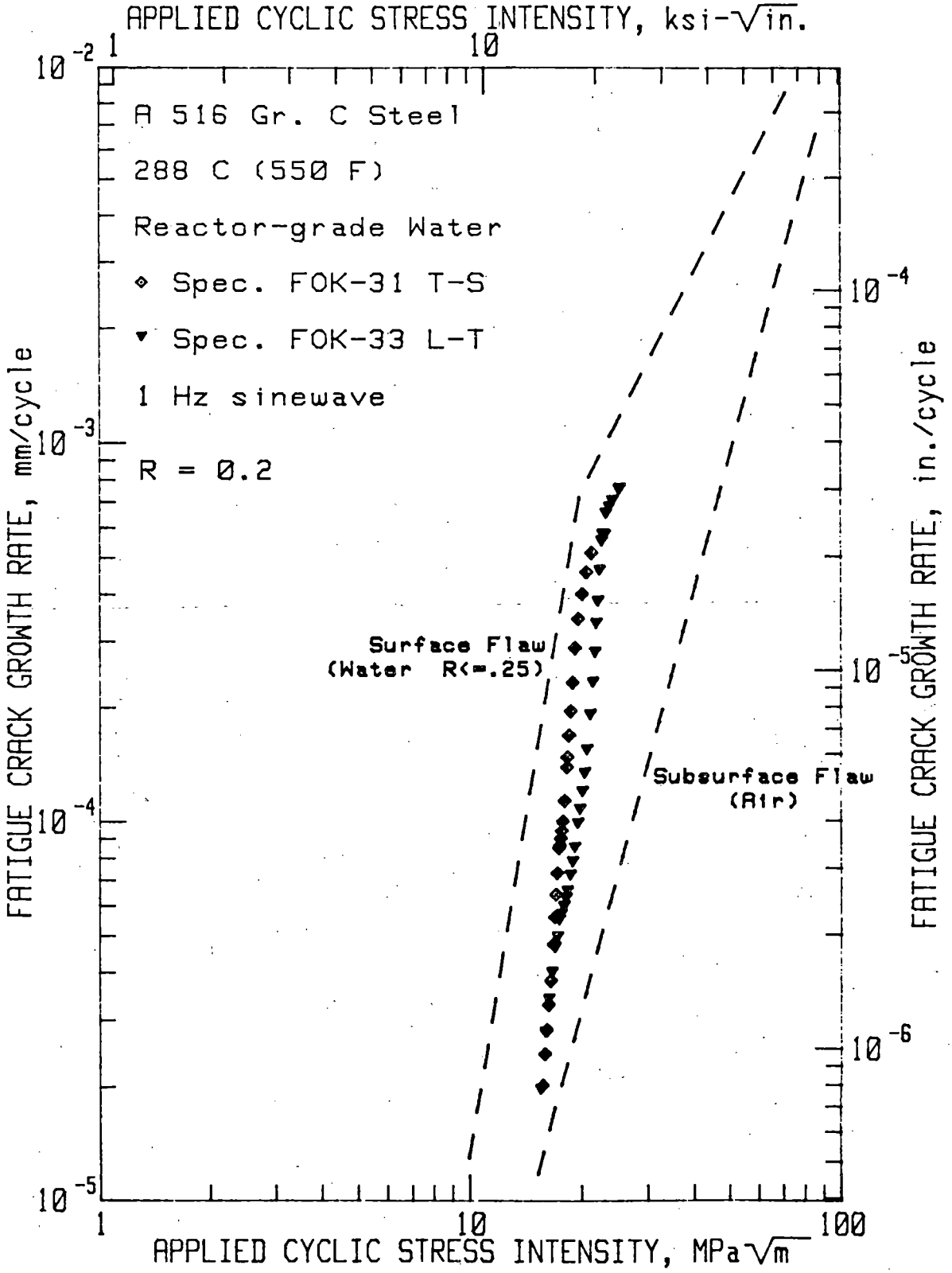

Fig. 19 Fatigue crack growth rates vs applied cyclic stress intensity factor for A516 Gr. 70 steel, R = 0.2, 1 Hz sinusoidal waveform. The growth rates for the T-S orientation are slightly higher than for the L-T orientation.

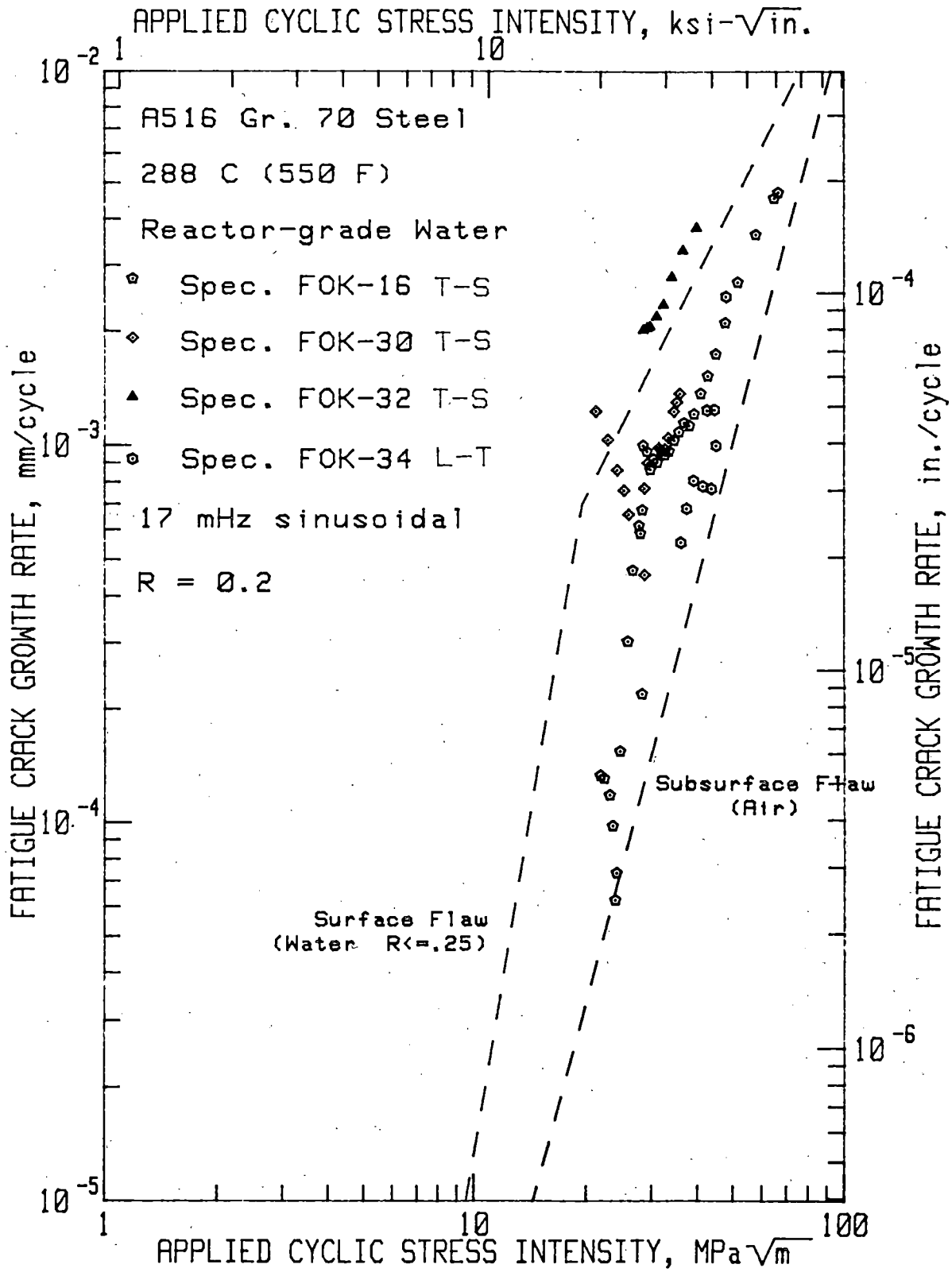

Fig. 20 Fatigue crack growth rates vs applied cyclic stress intensity factor for A516 Gr. 70 steel, R = 0.2, 17 mHz sinusoidal waveform. The growth rates for the three tests in the T-S orientation are all higher than the test in the L-T orientation.

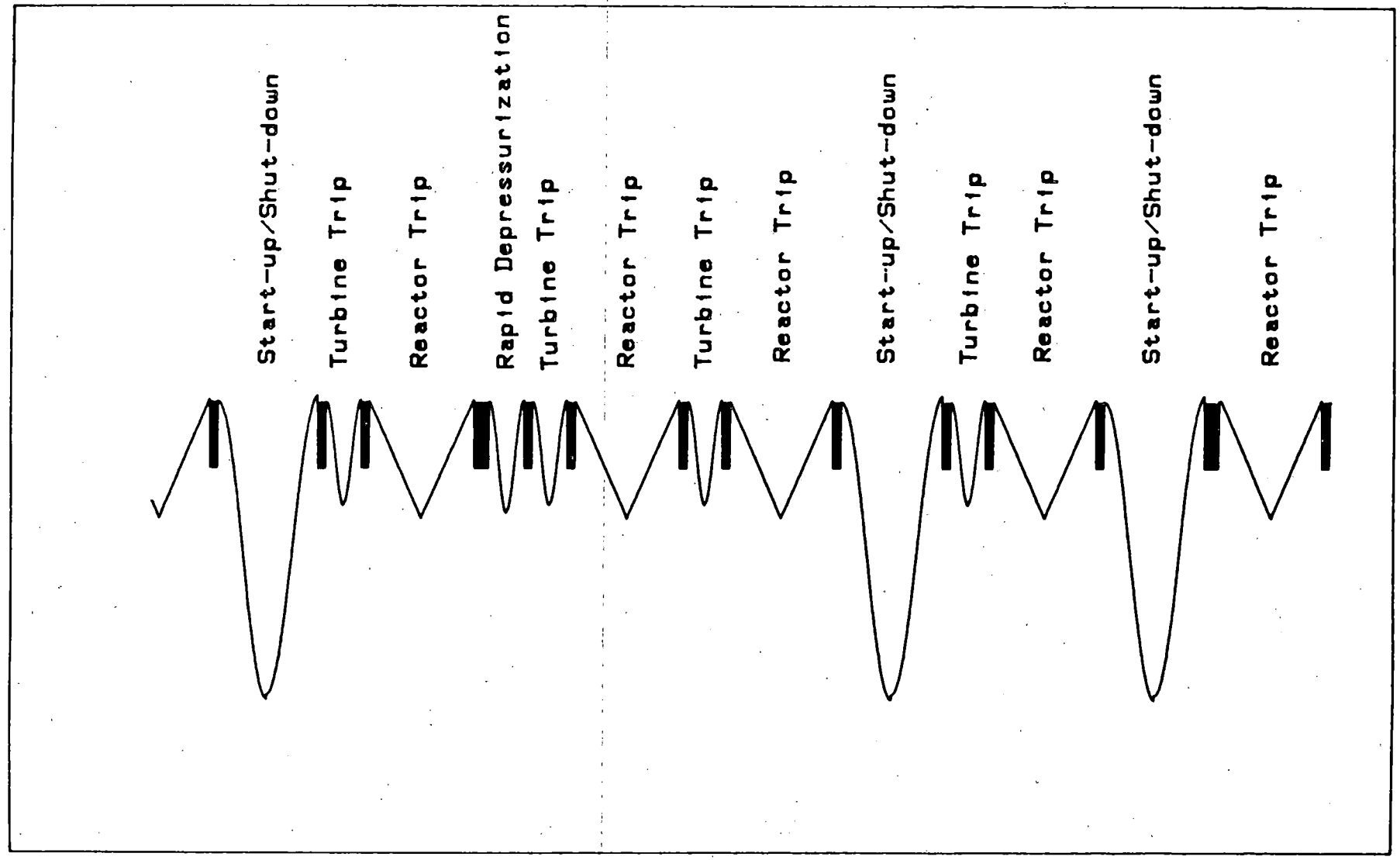

Fig. 21 Schematic of the waveform used in the variable amplitude test program. The different components range in frequency from 1 Hz to 17 mHz, and in load ratio from R = 0.139 to 0.804.

J_I-R CURVE CHARACTERISTICS OF PIPING MATERIAL AND WELDS

J.P. GUDAS
D.R. ANDERSON
DAVID TAYLOR NAVAL SHIP R&D CENTER
ANNAPOLIS, MARYLAND 21402

U.S. NUCLEAR REGULATORY COMMISSION
9TH WATER REACTOR SAFETY RESEARCH
INFORMATION MEETING
WASHINGTON, D.C.
29 OCTOBER 1981

PROGRAM OBJECTIVE

DEVELOP J_{Ic} AND TEARING MODULUS DATA BASE FOR

- —REACTOR PIPING STEELS
- —PIPING WELDMENTS

ASSESS VARIABILITY OF DUCTILE FRACTURE PROPERTIES

DTNSRDC

SCOPE

- —MECHANICAL PROPERTY CHARACTERIZATION
- —J-INTEGRAL TESTS AT: RT, 300°F, 550°F
- —J-INTEGRAL TESTS OF VARIOUS PIPING ORIENTATIONS
- —METALLURGICAL/MICROFRACTURE ANALYSIS

DTNSRDC

MATERIALS

ASTM A516 GR-70 (PLATE)

ASTM A106 GR-C (PIPE)

CENTRIFUGALLY CAST 304 SS (PIPE)

CAST 304 SS WELDMENT(S)

ASTM A516 GR-70 WELDMENT(S)

ASTM A106 WELDMENT(S)

J-INTEGRAL FORMULATION

$$J_{(i+1)} = \left[J_i + \left(\frac{\eta}{b}\right)_i \frac{A_{i,i+1}}{B_N} \right] \left[1 - \left(\frac{\gamma}{b}\right)_i (a_{i+1} - a_i) \right]$$

WHERE:

η = 2 + (0.522) b/W FOR COMPACT SPECIMENS

= 2 FOR 3-POINT LOAD SPECIMENS;

γ = 1 + (0.76) b/W;

$A_{i,i+1}$ = AREA UNDER THE LOAD VERSUS LOAD LINE DISPLACEMENT RECORD BETWEEN LINES OF CONSTANT DISPLACEMENT AT POINTS i AND i+1.

DTNSRDC

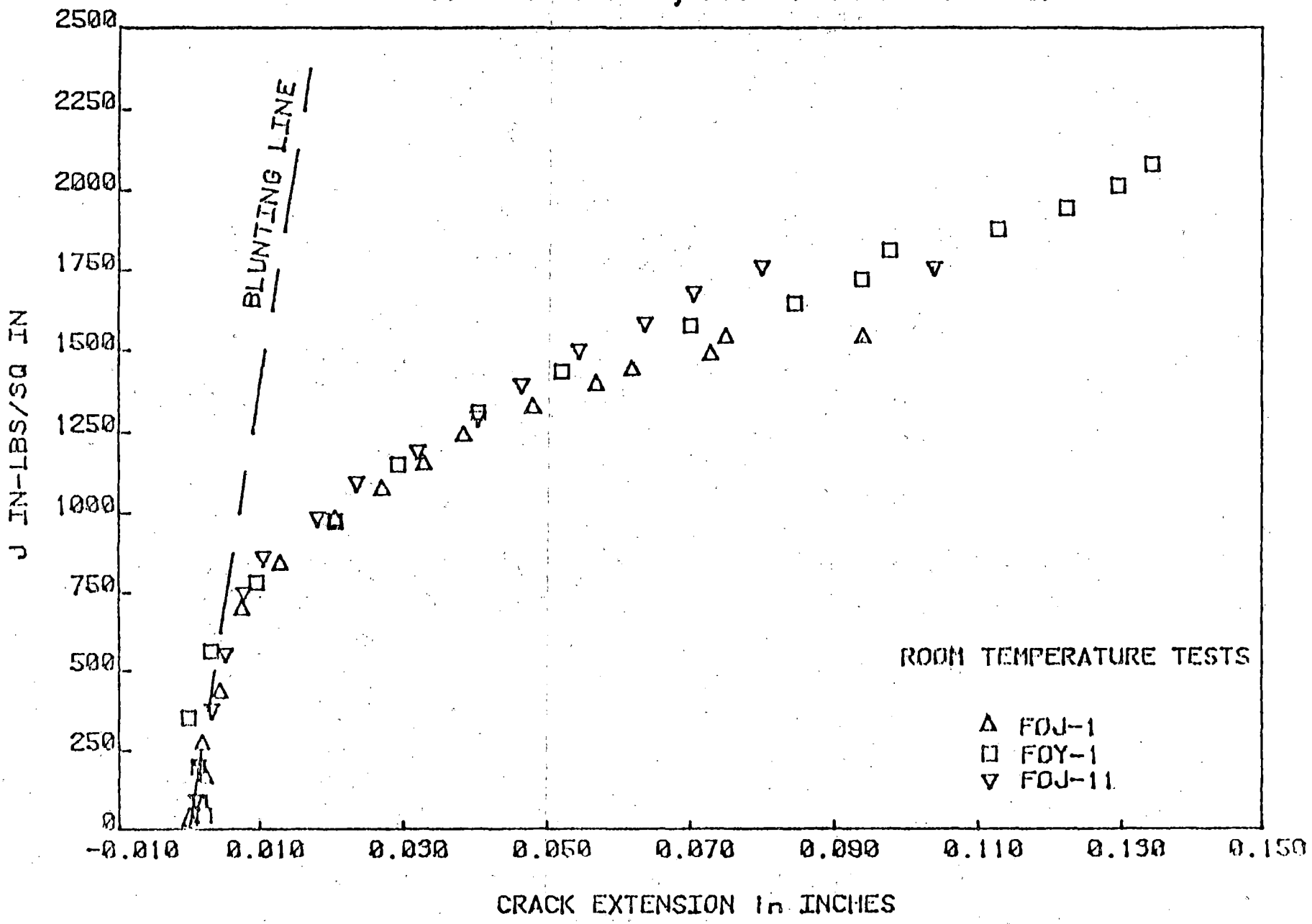
J vs CRACK EXTENSION , A516 (20%SIDE GROOVES)
J IN-LBS/SQ IN
2500
2250
2000
1750
1500
1250
1000
750
500
250
0
BLUNTING LINE
ROOM TEMPERATURE TESTS
FOJ-1
FOY-1
FOJ-11
-0.010
0.010
0.030
0.050
0.070
0.090
0.110
0.130
0.150
CRACK EXTENSION In INCHES

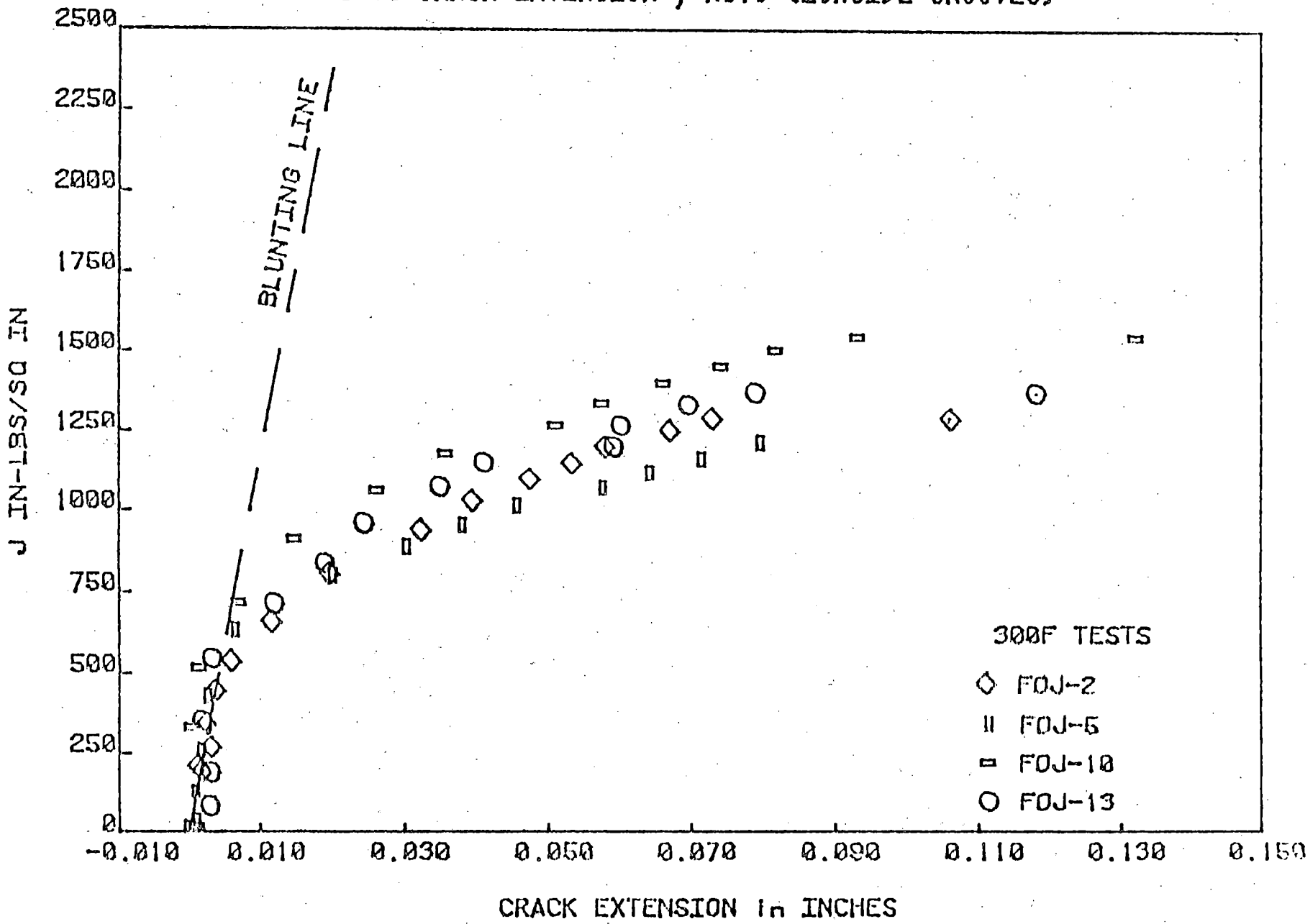
J vs CRACK EXTENSION , A516 (20%SIDE GROOVES)
J IN-LBS/SQ IN
2500
2250
2000
1750
1500
1250
1000
750
500
250
0
BLUNTING LINE
300F TESTS
FOJ-2
FOJ-5
FOJ-10
FOJ-13
-0.010
0.010
0.030
0.050
0.070
0.090
0.110
0.130
0.150
CRACK EXTENSION In INCHES

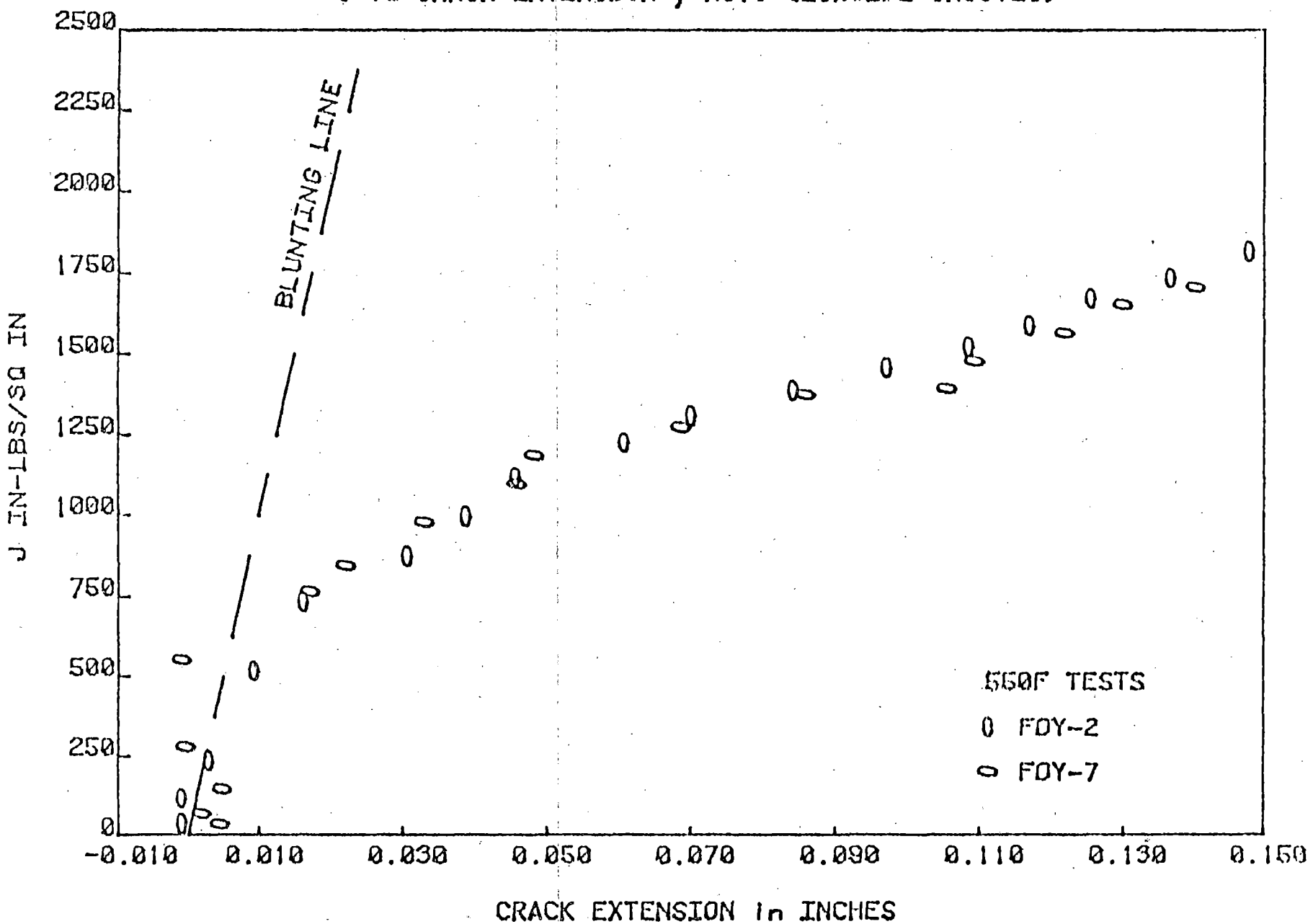
J vs CRACK EXTENSION , A516 (20%SIDE GROOVES)
J IN-LBS/SQ IN
2500
2250
2000
1750
1500
1250
1000
750
500
250
0
BLUNTING LINE
-0.010
0.010
0.030
0.050
0.070
0.090
0.110
0.130
0.150
CRACK EXTENSION In INCHES
550F TESTS
FOY-2
FOY-7

DUCTILE FRACTURE DATA SUMMARY
ASTM A516 GR70 STEEL
1TCT SPECIMENS, 20% S.C.

SPECIMEN I.D.	CRACK ORIENTATION	TEST TEMP (°F)	J_{Ic} (in-lb/in^2)	$\phi J/da$ (lb/in^2)	T	Comments
FOJ-1	T-L	RT	796	12008	73	
FOJ-11	T-L	RT	854	13005	79	
FOY-1	T-L	RT	845	11946	73	
FOJ-2	T-L	300	684	9643	80	
FOJ-3	T-L	300	712	7052	59	
FOJ-10	T-L	300	873	9204	77	
FOJ-13	T-L	300	788	8769	73	
FOY-2	T-L	550	629	11016	128	
FOY-7	T-L	550	695	10180	118	
CF8A S.S. PLATE						
FQR-232	---	RT	*	*	614	
FQR-236	---	RT	*	*	747	

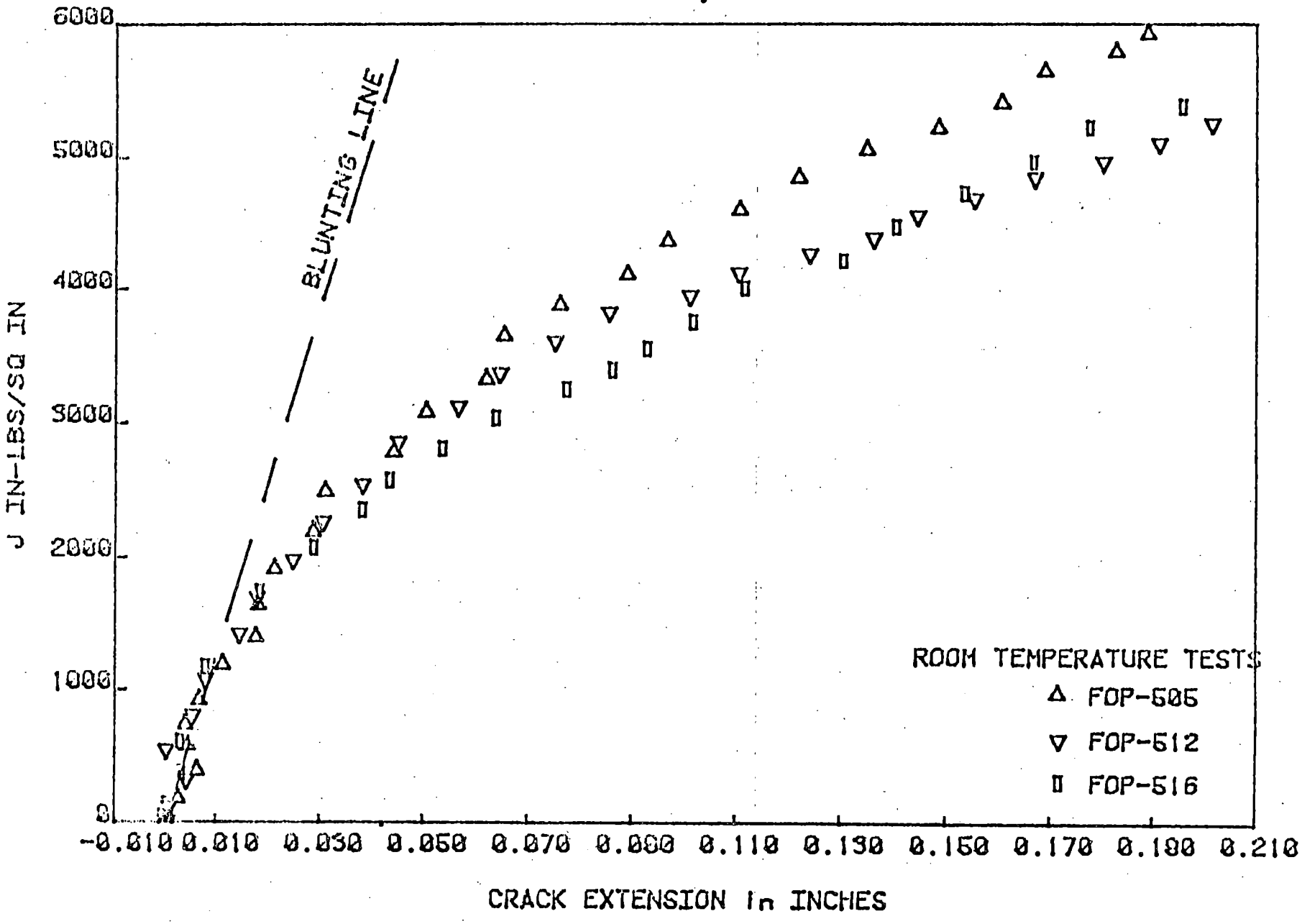
J vs CRACK EXTENSION , A106(L-C Orient.)
J IN-LBS/SQ IN
6000
5000
4000
3000
2000
1000
0
BLUNTING LINE
-0.010 0.010 0.030 0.050 0.070 0.090 0.110 0.130 0.150 0.170 0.190 0.210
CRACK EXTENSION In INCHES
ROOM TEMPERATURE TESTS
FOP-505
FOP-512
FOP-516

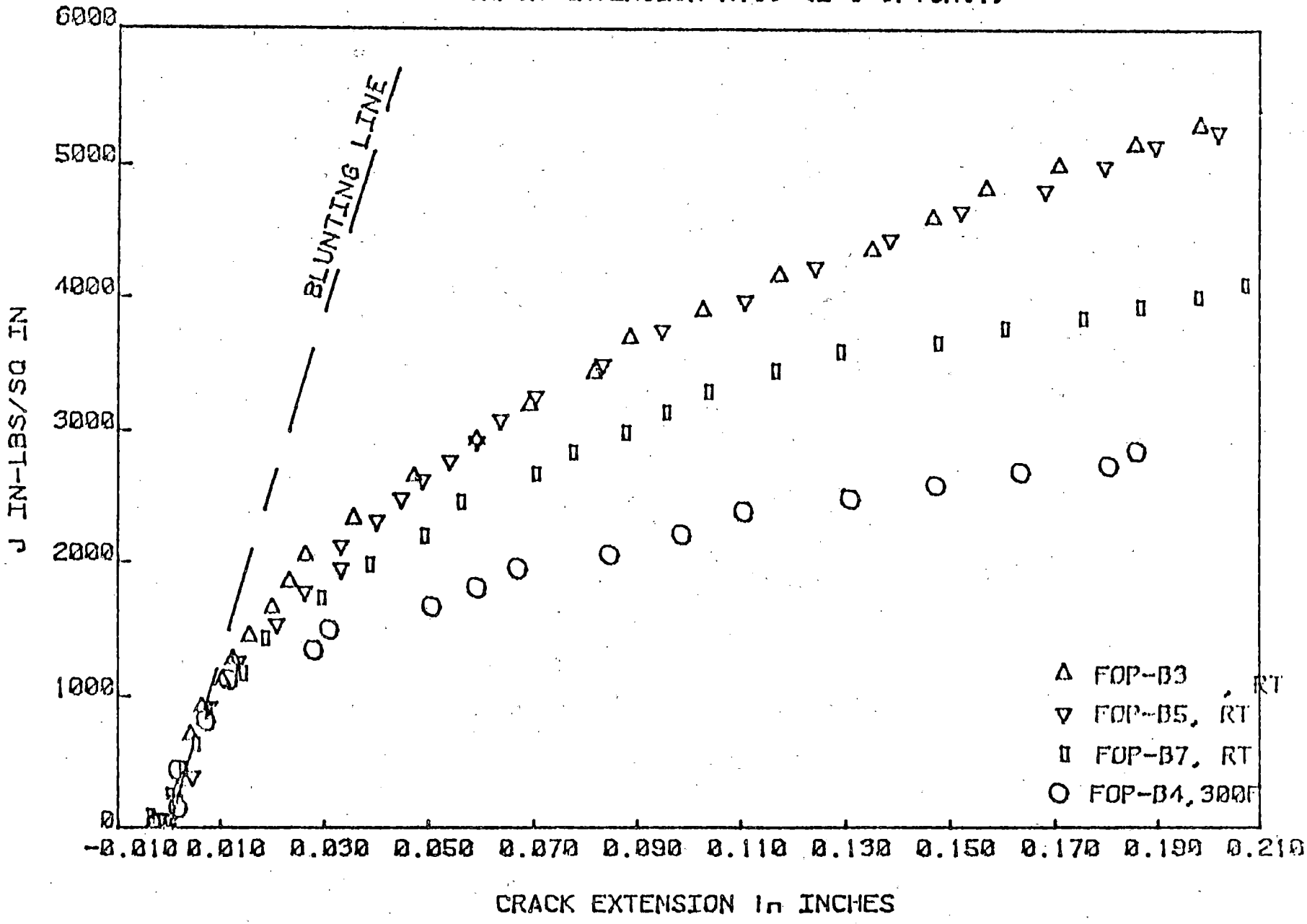
J vs CRACK EXTENSION A106 (L-C Orient.)
6000
5000
4000
3000
2000
1000
0
J IN-LBS/SQ IN
BLUNTING LINE
FOP-B3, RT
FOP-B5, RT
FOP-B7, RT
FOP-B4, 300F
-0.010 0.010 0.030 0.050 0.070 0.090 0.110 0.130 0.150 0.170 0.190 0.210
CRACK EXTENSION In INCHES

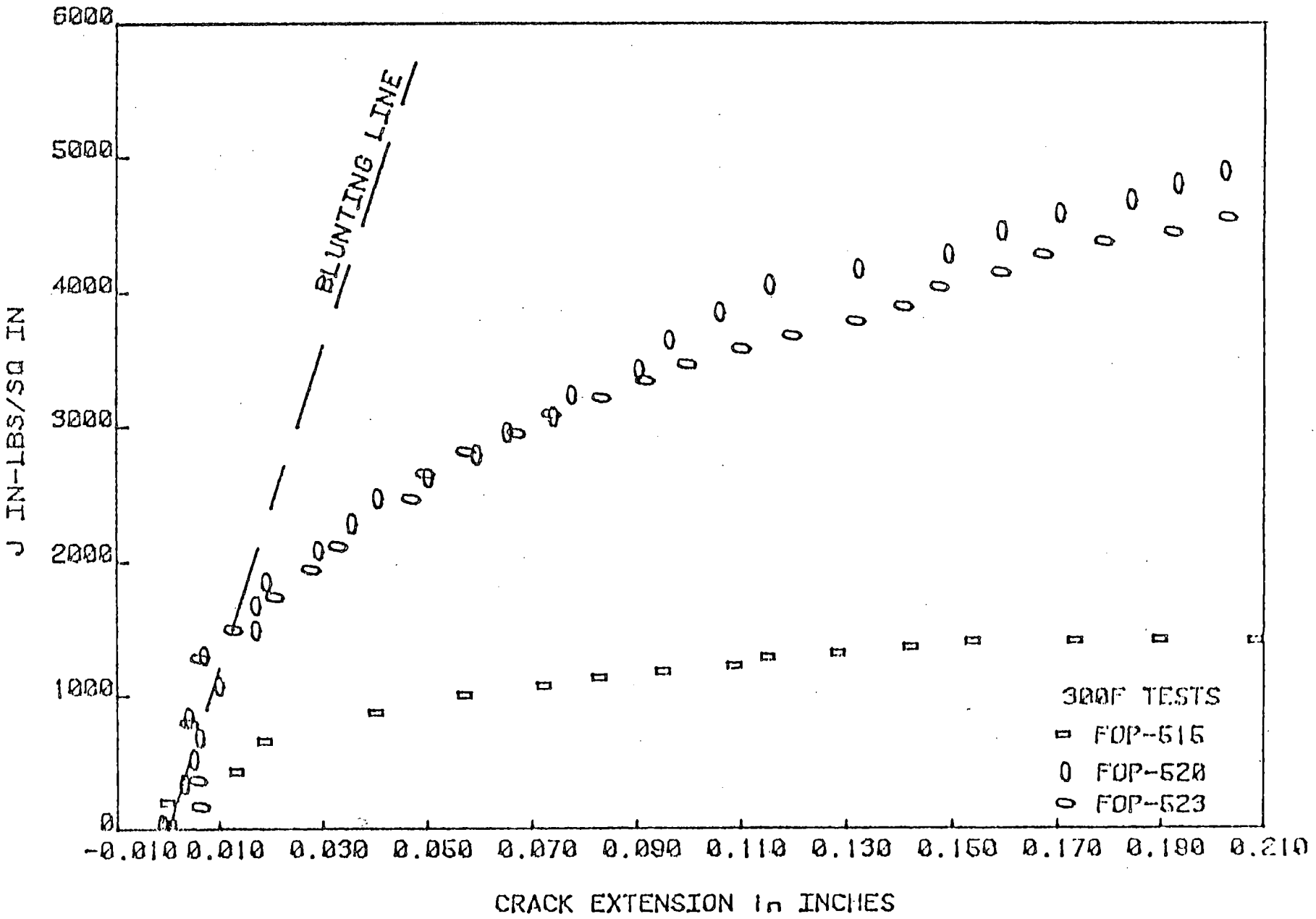
J vs CRACK EXTENSION A106 (L-C Orient.)
6000
5000
4000
3000
2000
1000
0
J IN-LBS/SQ IN
BLUNTING LINE
300F TESTS
FOP-515
FOP-520
FOP-523
-0.010 0.010 0.030 0.050 0.070 0.090 0.110 0.130 0.150 0.170 0.190 0.210
CRACK EXTENSION In INCHES

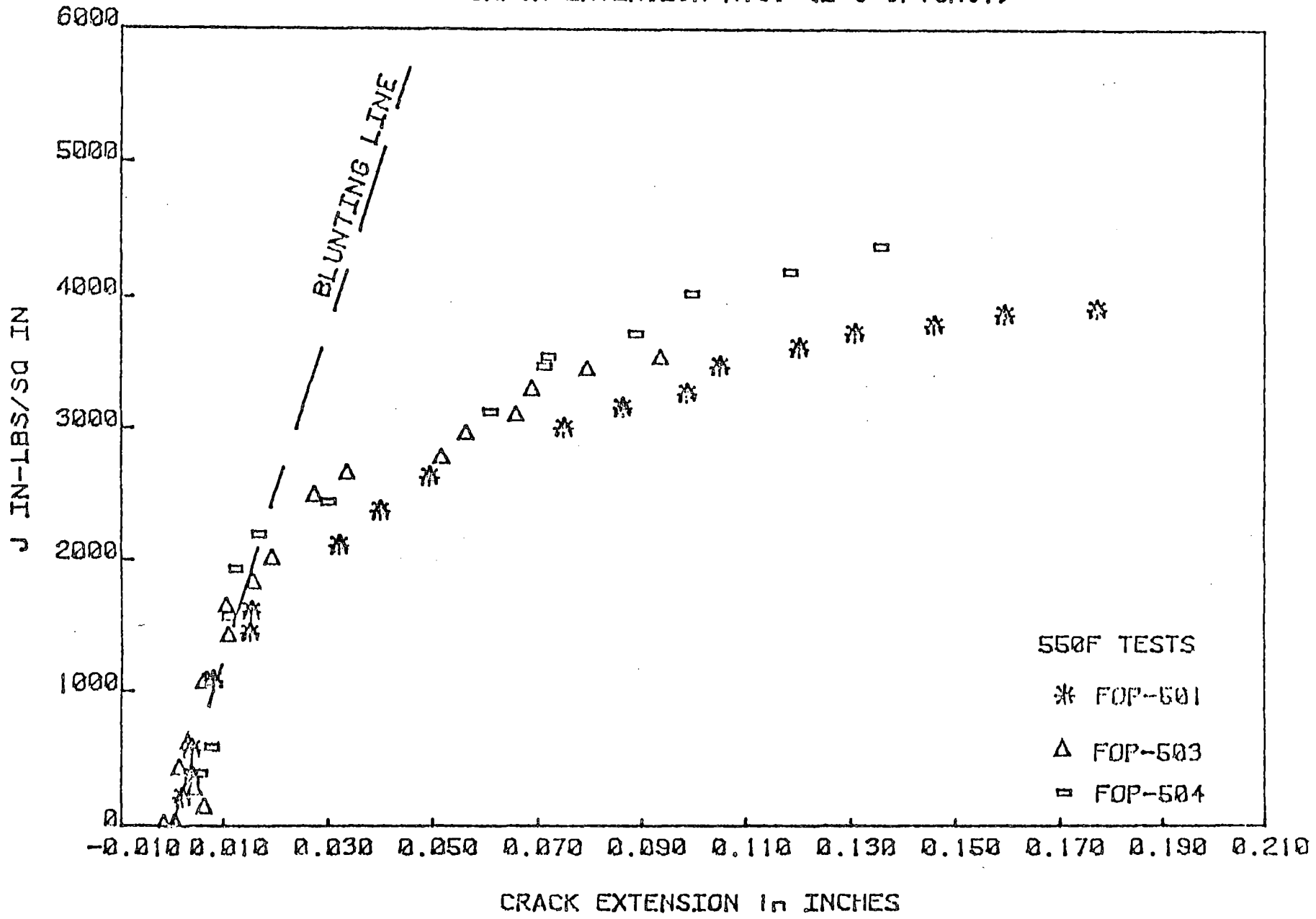
J vs CRACK EXTENSION A106 (L-C Orient.)
6000
5000
4000
3000
2000
1000
0
J IN-LBS/SQ IN
BLUNTING LINE
550F TESTS
FOP-501
FOP-503
FOP-504
-0.010
0.010
0.030
0.050
0.070
0.090
0.110
0.130
0.150
0.170
0.190
0.210
CRACK EXTENSION In INCHES

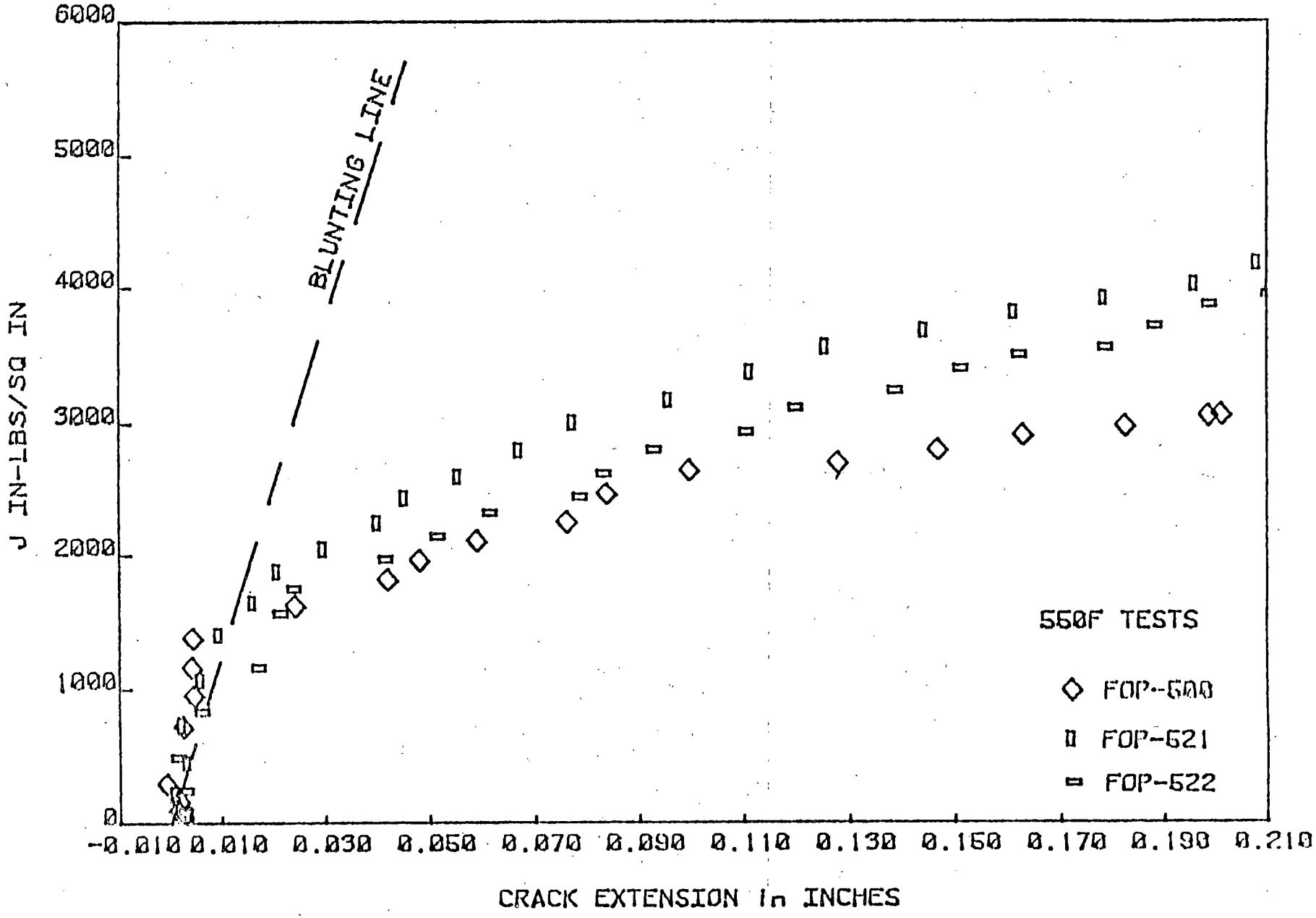
J vs CRACK EXTENSION A106 (L-C Orient.)
6000
5000
4000
3000
2000
1000
0
J IN-LBS/SQ IN
BLUNTING LINE
550F TESTS
FOP-500
FOP-521
FOP-522
-0.010
0.010
0.030
0.050
0.070
0.090
0.110
0.130
0.150
0.170
0.190
0.210
CRACK EXTENSION In INCHES

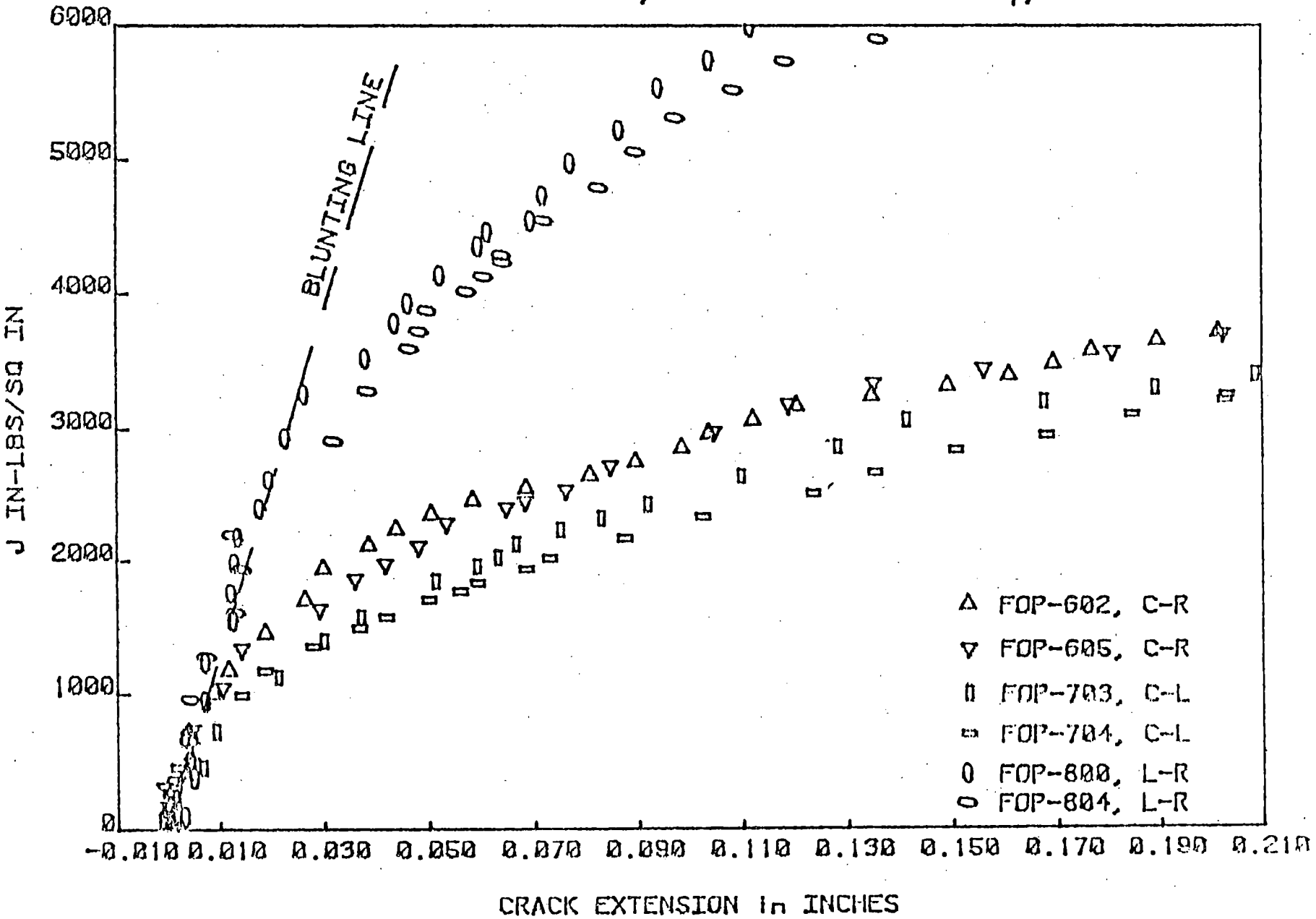
J vs CRACK EXTENSION, A106 Orientation Study,RT
J IN-LBS/SQ IN
6000
5000
4000
3000
2000
1000
0
BLUNTING LINE
FOP-602, C-R
FOP-605, C-R
FOP-703, C-L
FOP-704, C-L
FOP-800, L-R
FOP-804, L-R
-0.010 0.010 0.030 0.050 0.070 0.090 0.110 0.130 0.150 0.170 0.190 0.210
CRACK EXTENSION In INCHES

DUCTILE FRACTURE DATA SUMMARY
ASTM A106 CLASS C STEEL
1TCT SPECIMENS, 20% S.C.

SPECIMEN I.D.	CRACK ORIENTATION	TEST TEMP (°F)	J_{Ic} (in-lb/in^2)	$\partial J/da$ (lb/in^2)	T	Comments
FOP-505	L-C	RT	1563	35919	250	
FOP-512	L-C	RT	1780	29943	209	
FOP-516	L-C	RT	1830	22591	158	
FOP-515	L-C	300	386	11795	96	Slag Inclusions
FOP-520	L-C	300	1821	22132	181	
FOP-523	L-C	300	1640	24261	198	
FOP-500	L-C	550	1466	12476	93	
FOP-501	L-C	550	1837	19931	148	
FOP-503	L-C	550	2292	17940	133	
FOP-504	L-C	550	2162	23098	171.5	
FOP-521	L-C	550	1755	19763	147	
FOP-522	L-C	550	1320	18242	135	
FOP-B3	L-C	RT	1579	27865	194	
FOP-B5	L-C	RT	1302	32220	225	
FOP-B7	L-C	RT	1262	23627	165	
FOP-B4	L-C	300	1126	13980	114	Secondary Cracks
FOP-602	C-R	RT	1426	21668	151	
FOP-605	C-R	RT	1382	18655	130	
FOP-703	C-L	RT	903	20107	140	
FOP-704	C-L	RT	1034	15189	106	
FOP-800	L-R	RT	3159	33335	232	
FOP-804	L-R	RT	2725	34767	242	

Enclosure 1a

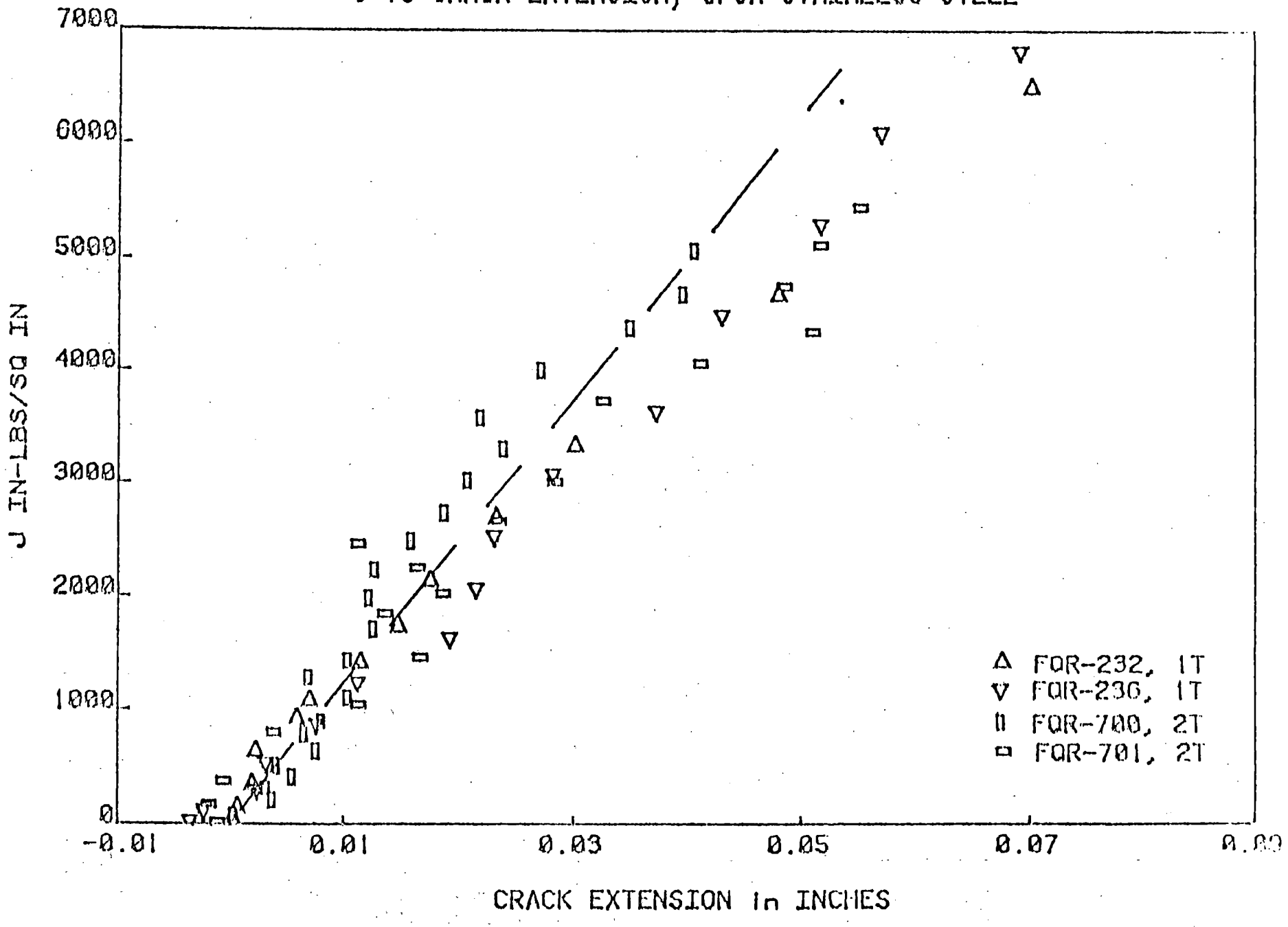
J vs CRACK EXTENSION, CF8A STAINLESS STEEL
7000
6000
5000
4000
3000
2000
1000
0
J IN-LBS/SQ IN
-0.01
0.01
0.03
0.05
0.07
CRACK EXTENSION in INCHES
FQR-232, 1T
FQR-236, 1T
FQR-700, 2T
FQR-701, 2T

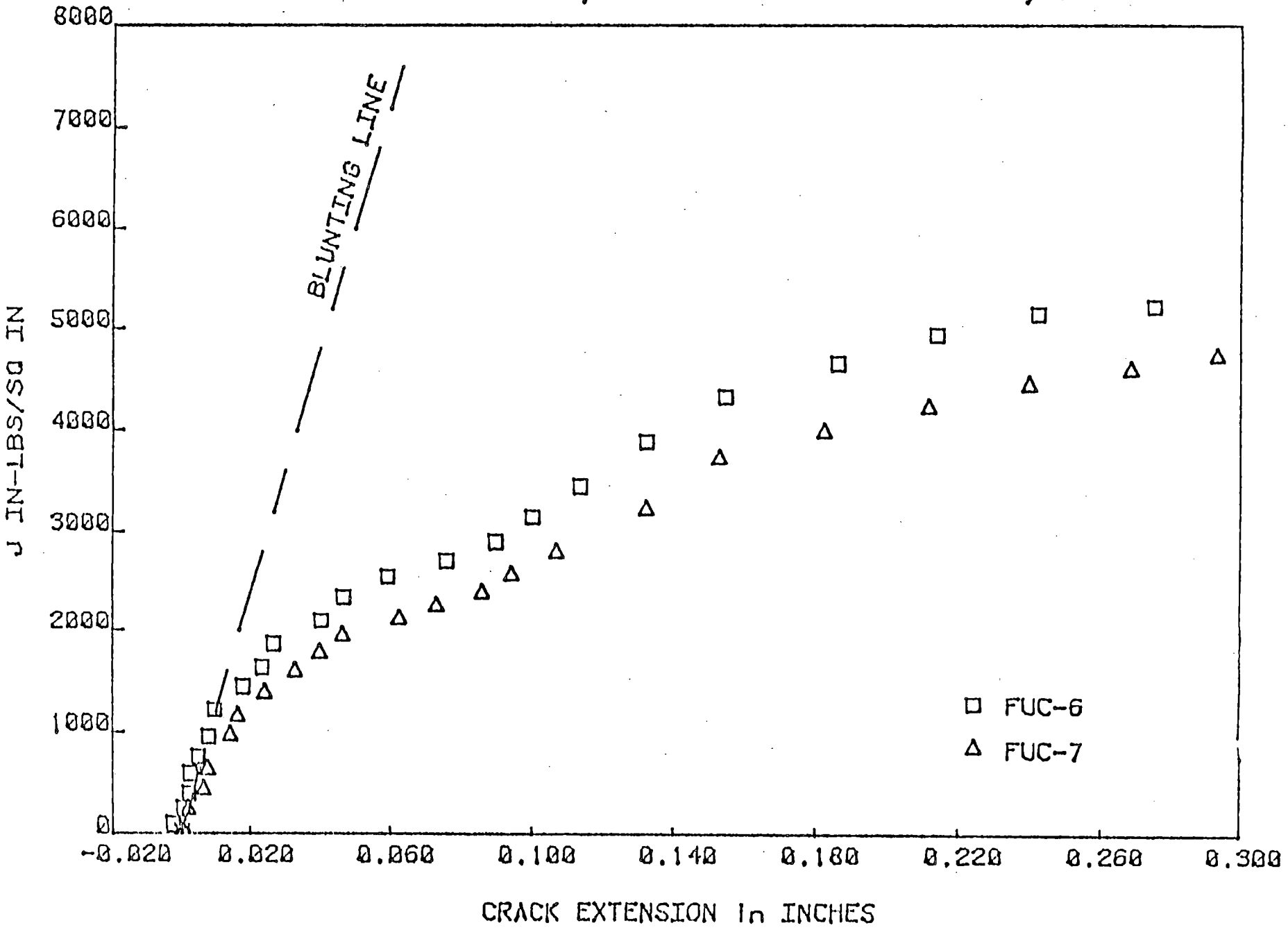

Enclosure (1h)

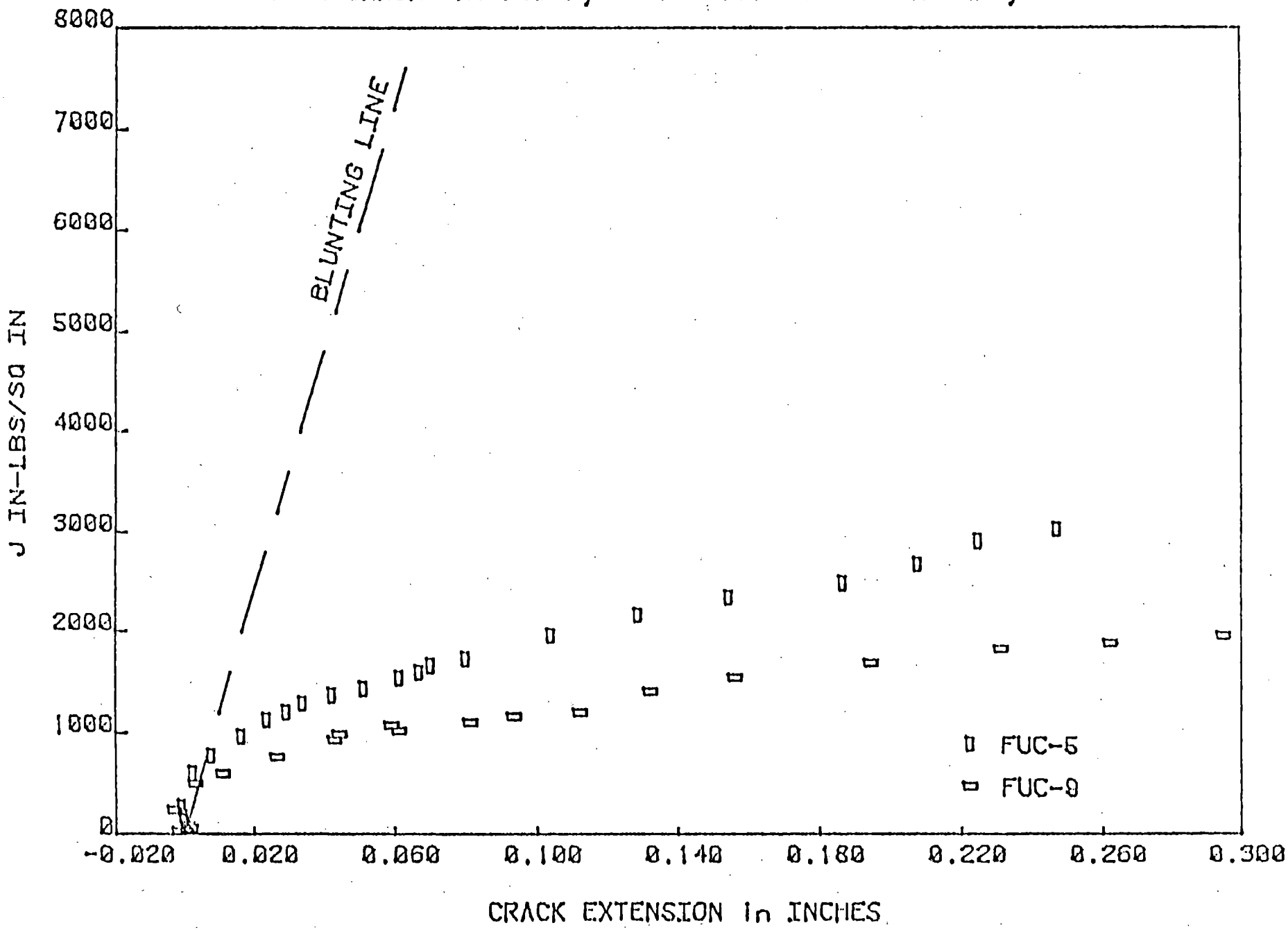

Enclosure (1e)

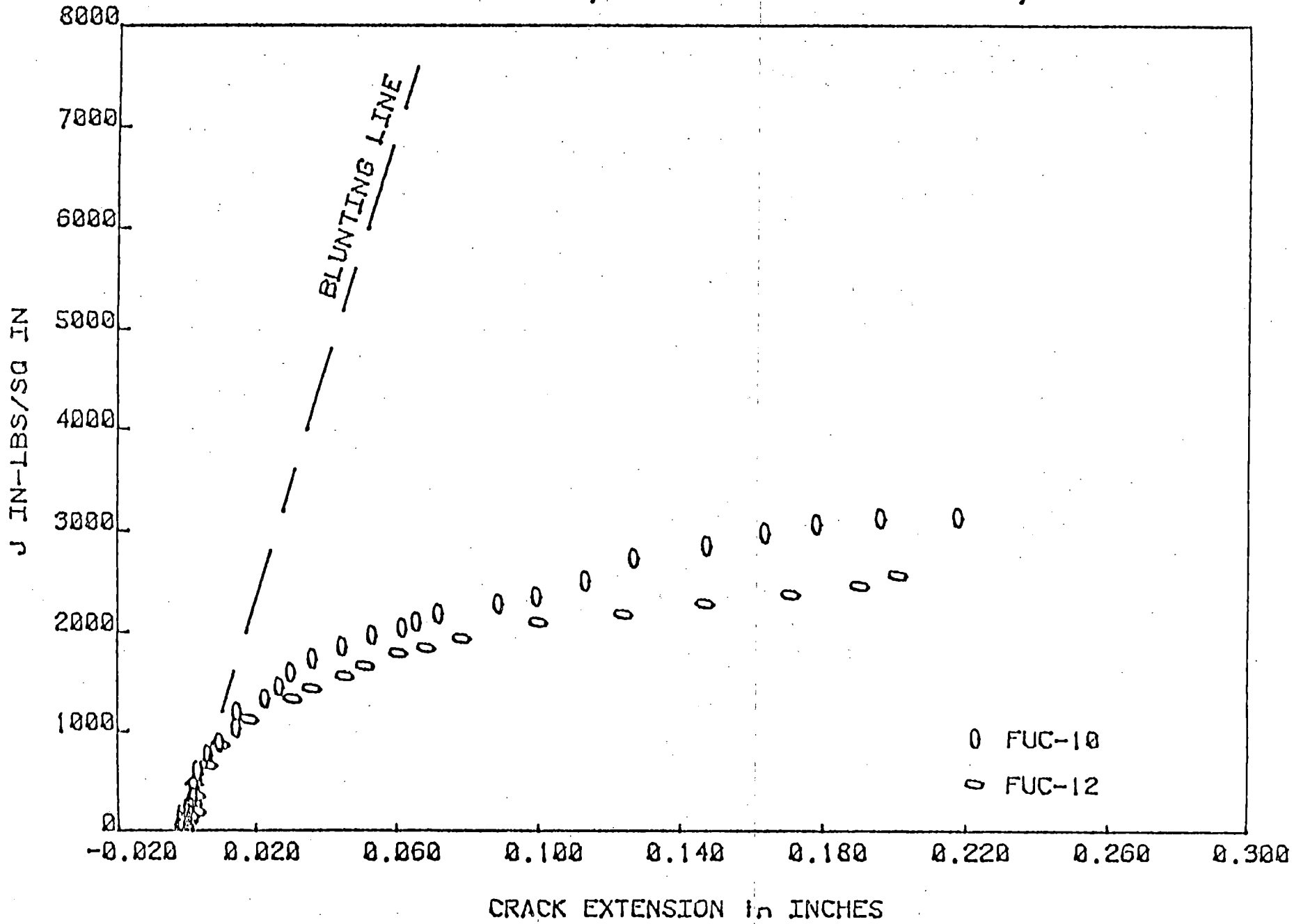

Enclosure (1d)

Summary of Results for J_I-R Curves of
CF8A Stainless Steel Weldments

Specimen Identification	Test Temp	J_{Ic} in-lb/in^2	T	dJ/da in-lb/in^3
FUC-6	RT	1386	108.5	21796
FUC-7	RT	958	104.8	21053
FUC-5	300°F	908	89.0	11636
FUC-9	300°F	547	71.4	9330
FUC-10	550°F	1219	133.6	16328
FUC-12	550°F	992	121.2	14811

Enclosure (1a)

DEGRADED PIPE EXPERIMENTAL PROGRAM

MICHAEL G. VASSILAROS
JOHN P. GUDAS
DAVID TAYLOR NAVAL SHIP R&D CENTER

JAMES A. JOYCE
U.S. NAVAL ACADEMY

U.S. NUCLEAR REGULATORY COMMISSION
9TH WATER REACTOR SAFETY RESEARCH
INFORMATION MEETING
WASHINGTON, D.C.
29 OCTOBER 1981

PROGRAM OBJECTIVE

- EVALUATE TEARING INSTABILITY CONCEPT WITH ASTM A 106 CI C STEEL PIPE IN BENDING

- EVALUATE CRACK INSTABILITY PREDICTIONS FROM WIDELY DIFFERING SPECIMEN GEOMETRIES

$$T = \frac{dJ}{da} \cdot \frac{E}{\sigma_o 2} = \text{CONSTANT}$$

$$T_{MAT} > T_{APPLIED} = \text{STABLE CRACK GROWTH}$$

$$T_{MAT} \leqslant T_{APPLIED} = \text{INSTABILITY}$$

FOR ANY SPECIMEN

$$T = \frac{dJ}{da} \cdot \frac{E}{\sigma_o^2} \leqslant \frac{1}{\alpha}\left\{p(\quad) + \frac{EB}{K_m}\, q(\quad) - \frac{JE}{W\sigma_o^2}\, r(\quad)\right\}$$

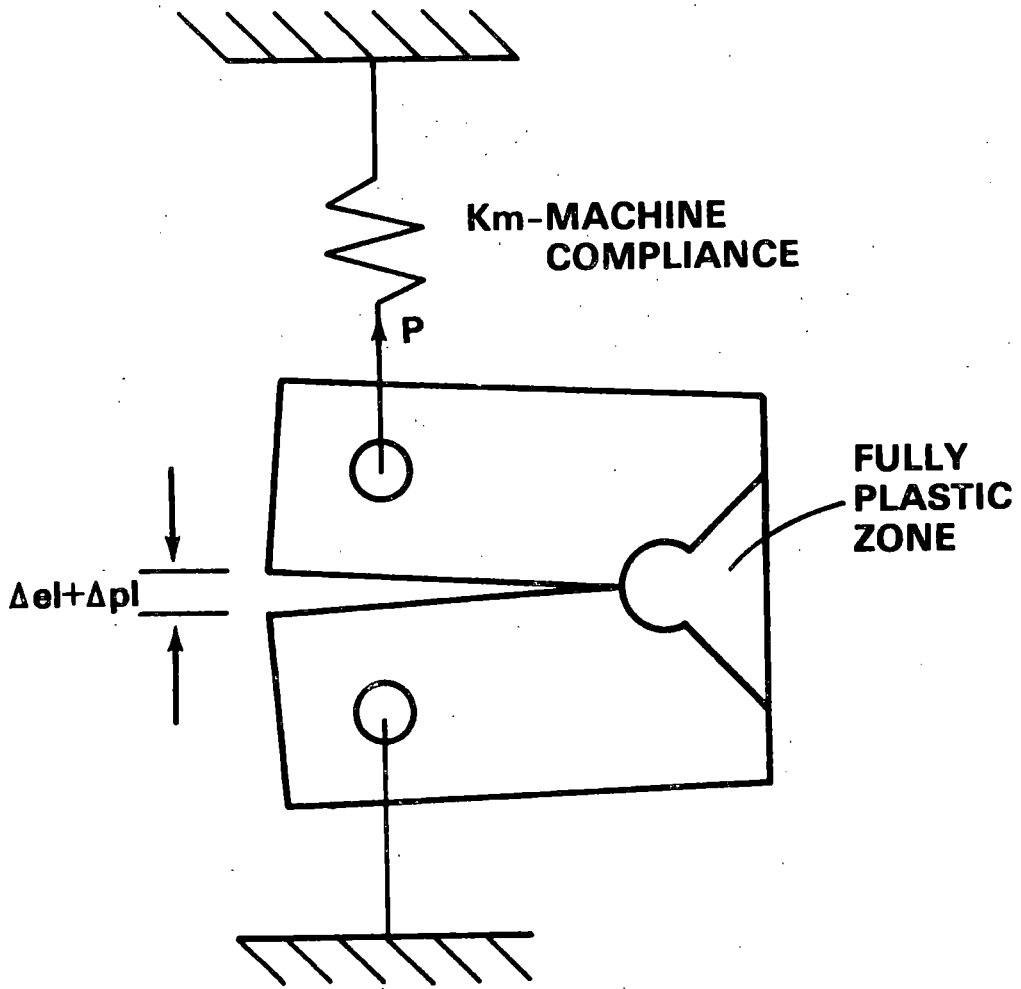
Km-MACHINE
COMPLIANCE
P
FULLY
PLASTIC
ZONE
Δel+Δpl

TEST SETUP FOR TEARING INSTABILITY EXPERIMENTS

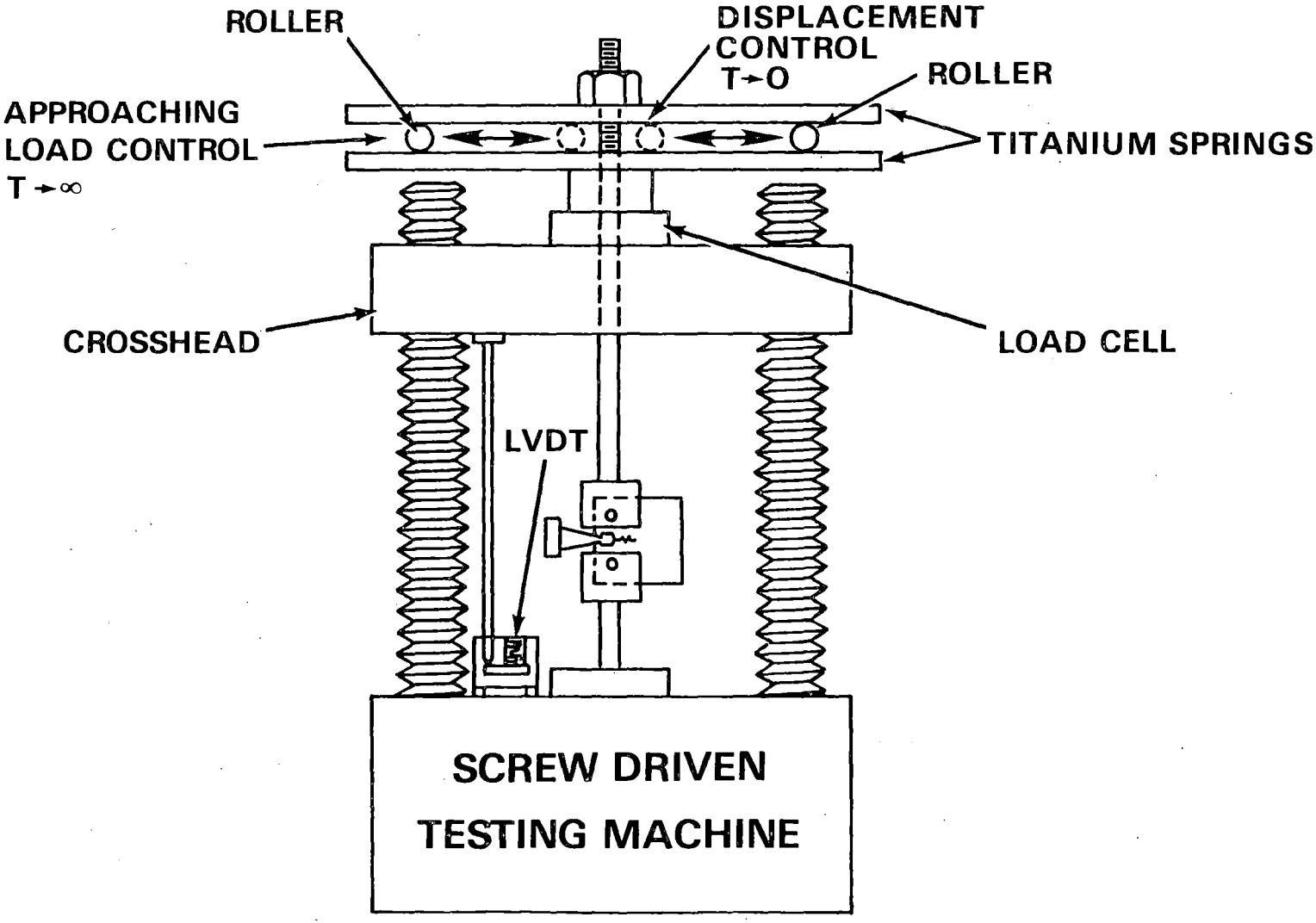

DTNSRDC

TEST MATRIX FOR TEARING INSTABILITY EXPERIMENTS

MATERIAL	A/W	PERCENT SIDE GROOVES	TEST TEMPERATURE
HY-130	0.80	0, 20	R.T.
HY-80	0.65	0, 20	R.T.
ASTM A516	0.65	0, 20	150° C
ASTM A106	0.65	0	R.T.

$T_{APPLIED}$ VERSUS $T_{MATERIAL}$ CALCULATED THE J_I-R CURVE SLOPE TAKEN TO CRACK EXTENSION OF 5.0 mm

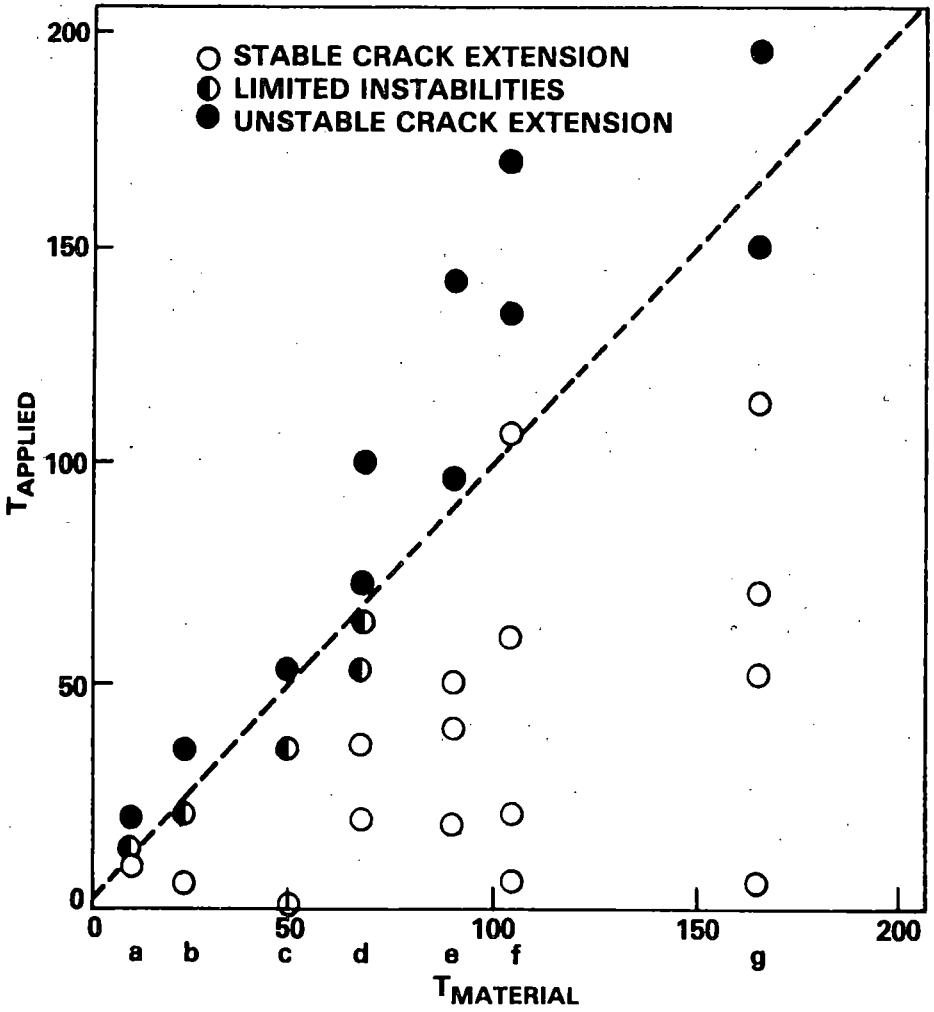

MATERIAL	a/W	% S.G.	TEMP.
a HY-130	0.80	20	RT
b HY-130	0.80	0	RT
c A516	0.65	20	150°C
d HY-80	0.65	20	RT
e A516	0.65	0	150°C
f HY-80	0.65	0	RT
g A106	0.65	0	RT

DTNSRDC

$T_{MATERIAL}$ VERSUS CRACK EXTENSION DATA FOR COMPACT SPECIMENS OF HY-130 AND ASTM A106 STEELS

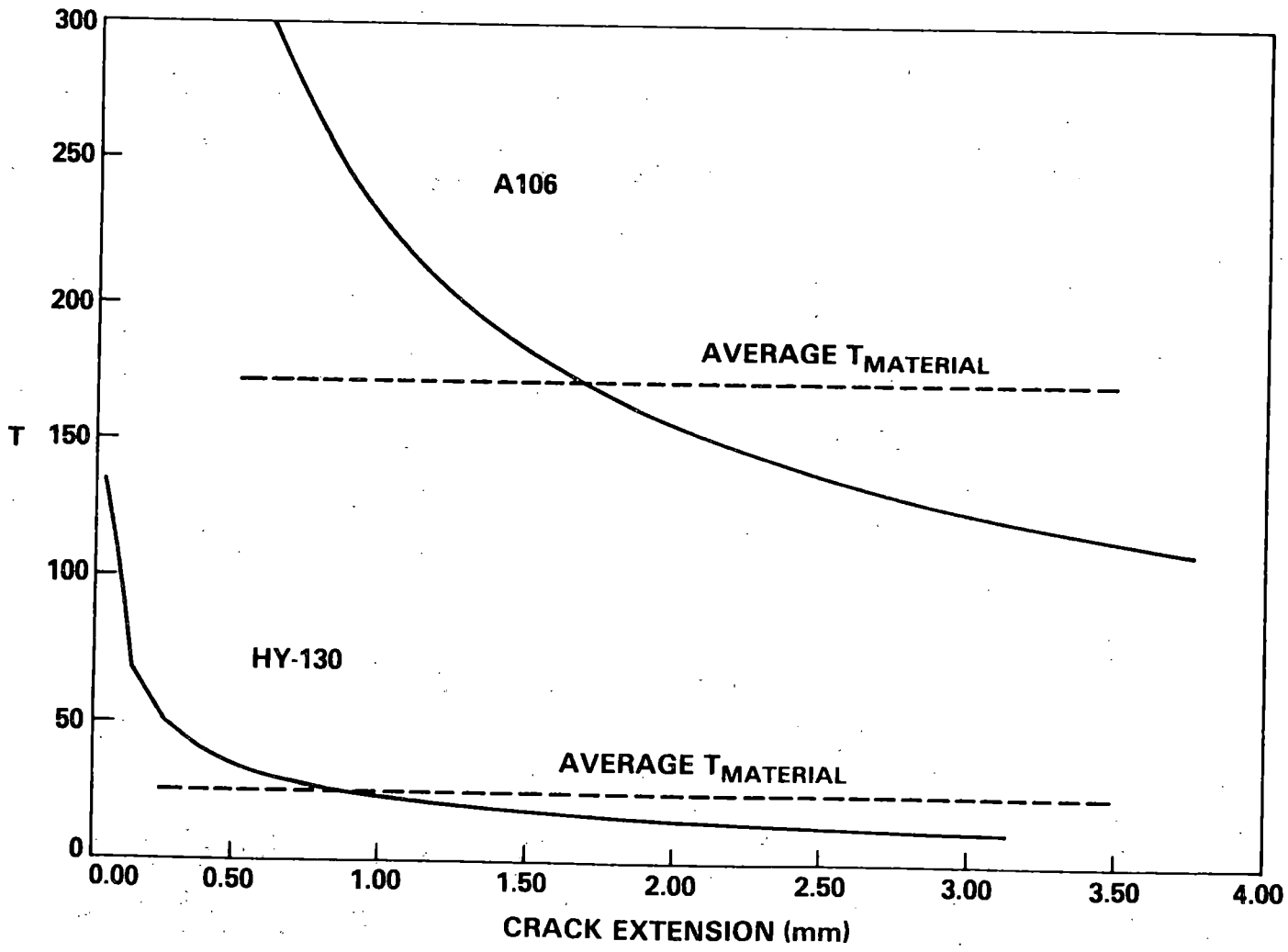

DTNSRDC

POWER LAW FIT OF J-INTEGRAL R-CURVE DATA FOR AN HY-80 STEEL SPECIMEN WHICH EXHIBITED UNSTABLE CRACK EXTENSION

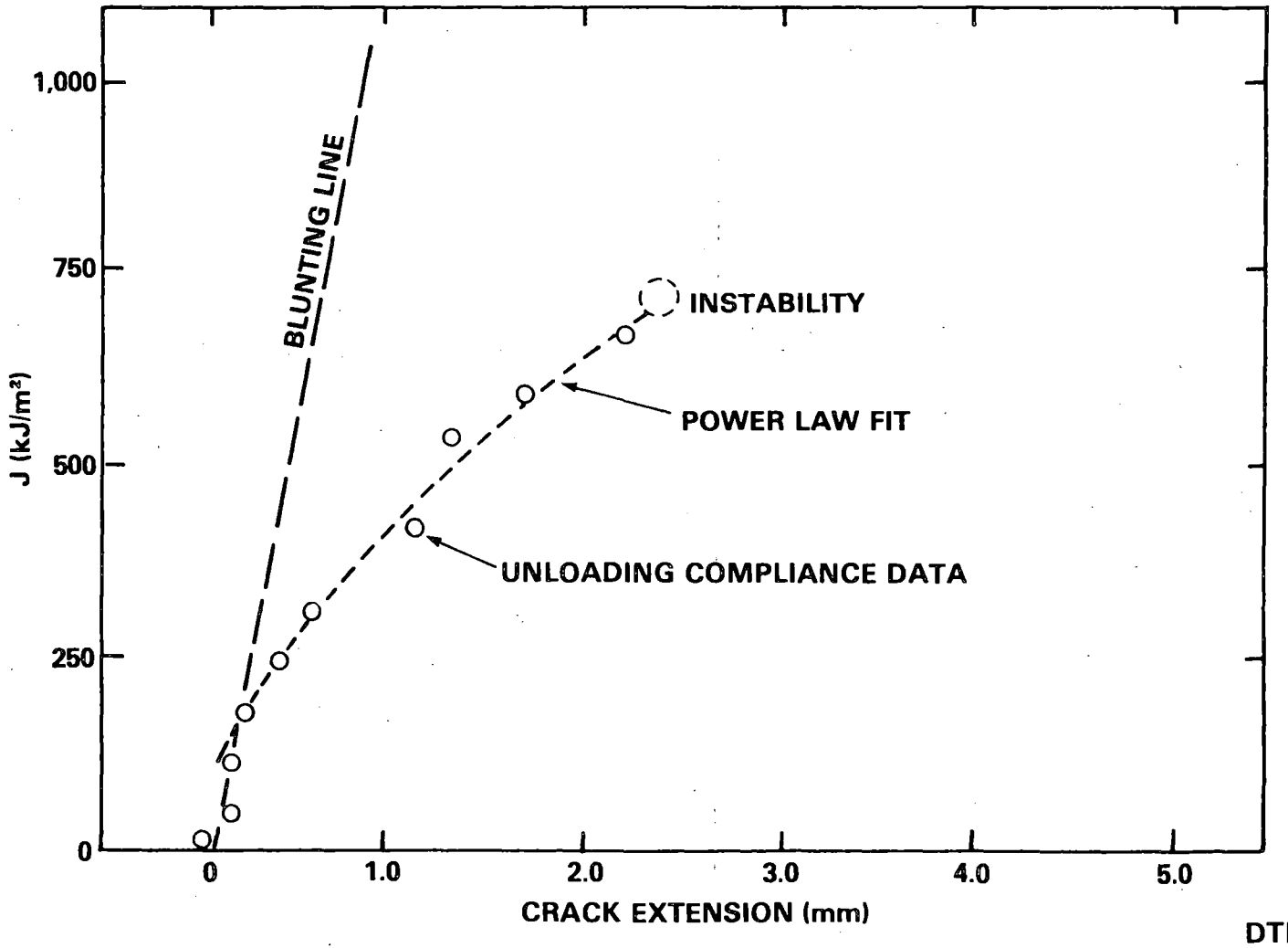

DTNSRDC

$T_{APPLIED}$ VERSUS $T_{MATERIAL}$ CALCULATED AT THE POINT OF INSTABILITY

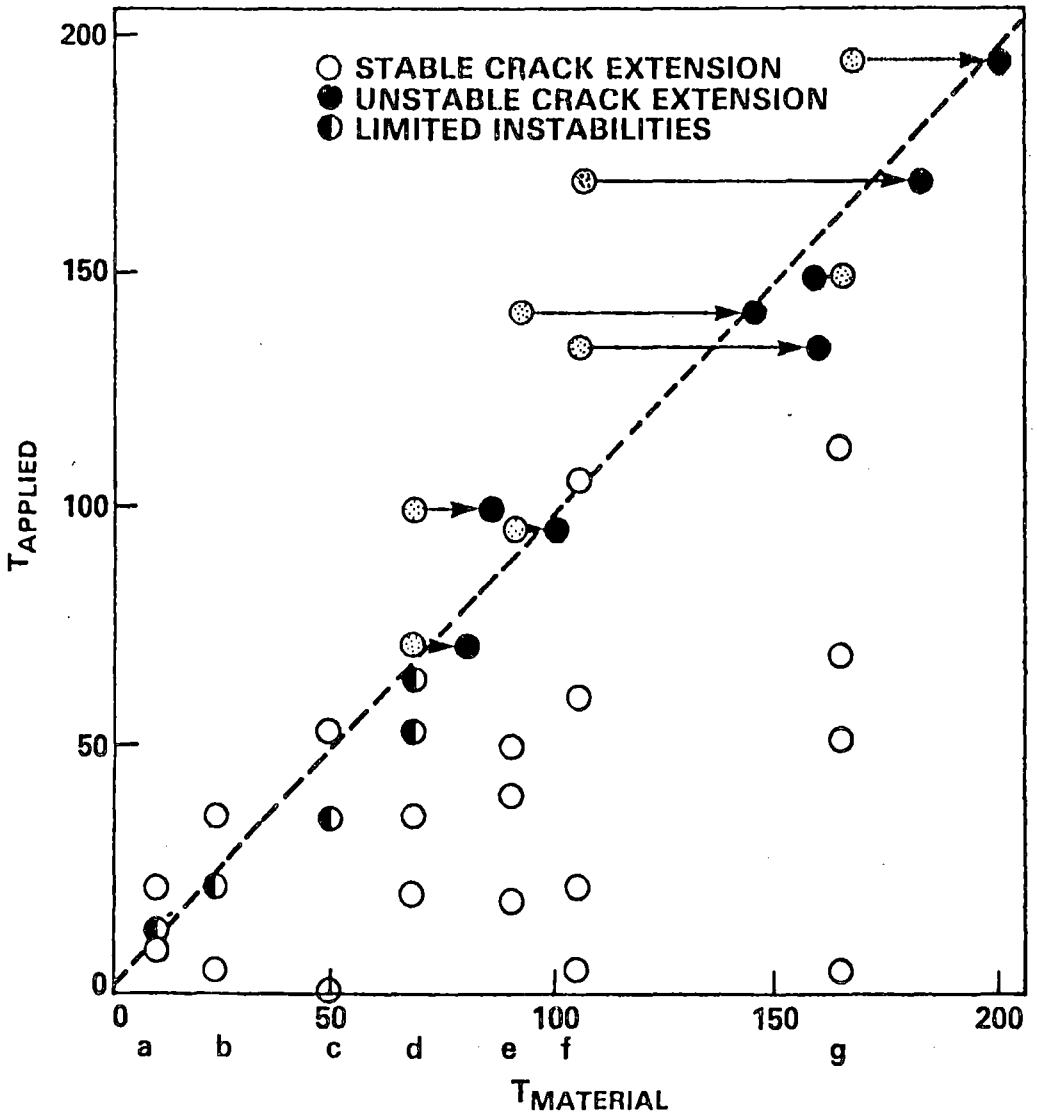

MATERIAL	a/W	% S.G.	TEMP.
a HY-130	0.80	20	RT
b HY-130	0.80	0	RT
c A516	0.65	20	150°C
d HY-80	0.65	20	RT
e A516	0.65	0	150°C
f HY-80	0.65	0	RT
g A106	0.65	0	RT

DTNSRDC

$T_{APPLIED}$ VERSUS CRACK EXTENSION ACCORDING TO THE MODELS OF PARIS AND CO-WORKERS AND ERNST AND CO-WORKERS

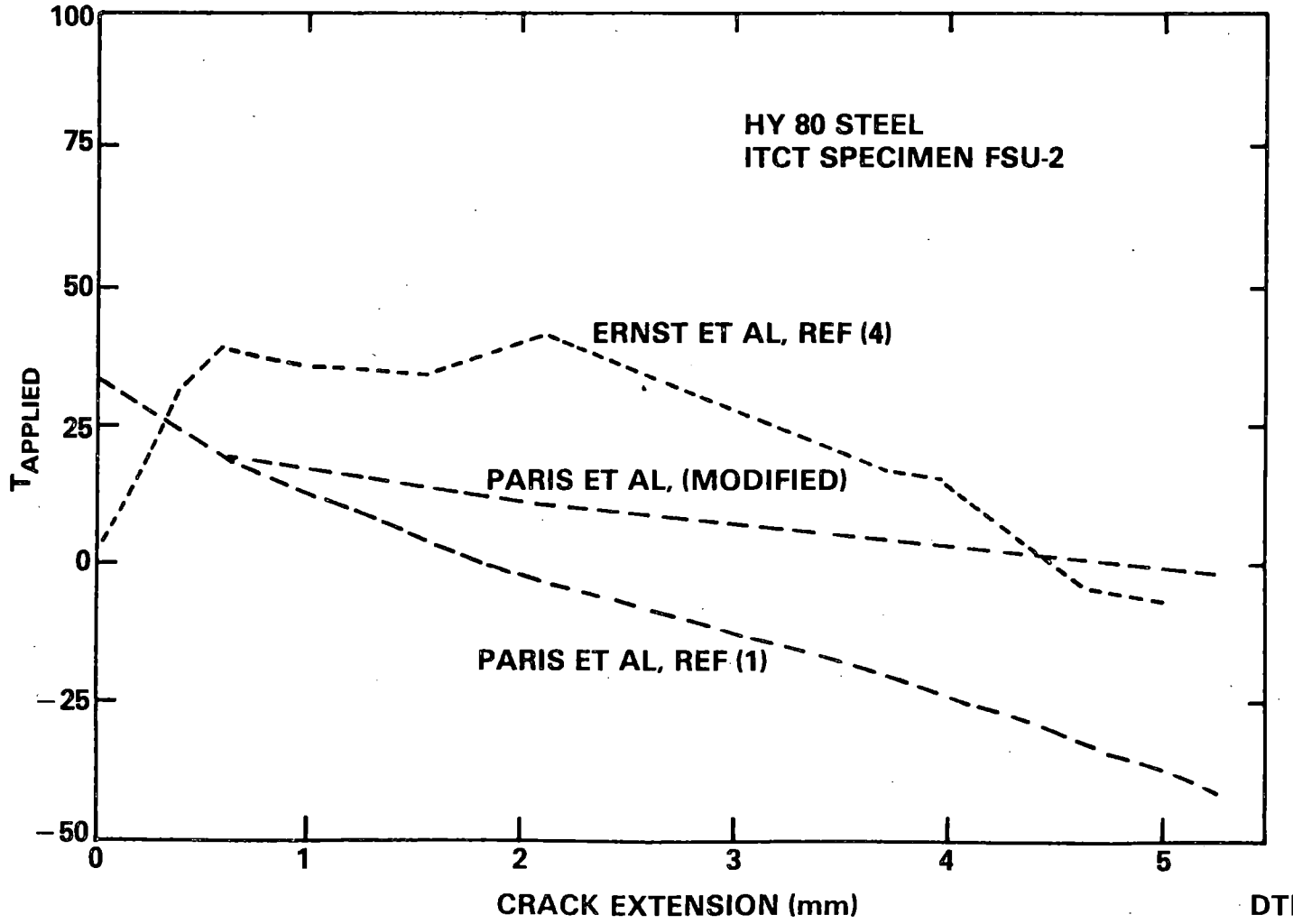

DTNSRDC

J_I VERSUS T FOR ASTM A106 STEEL SPECIMENS

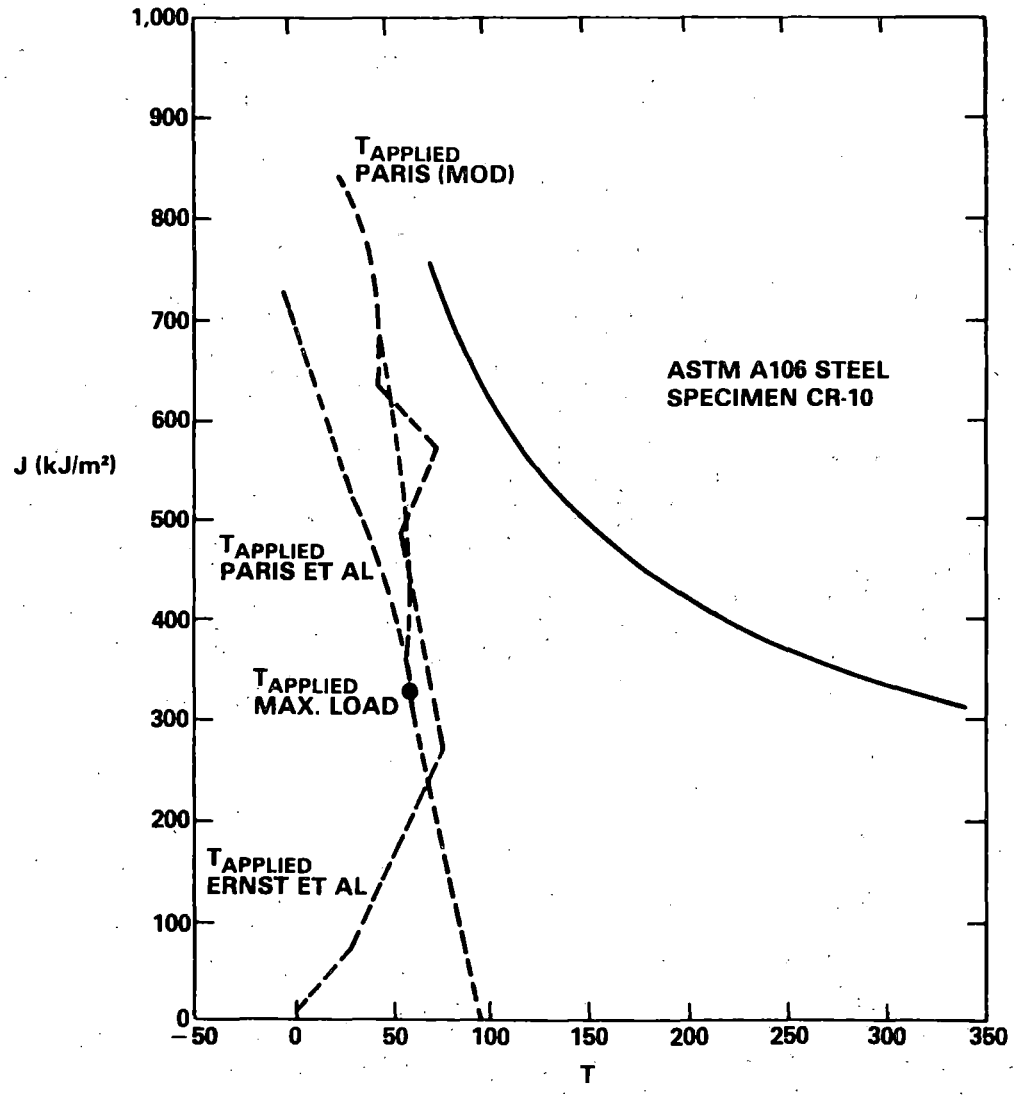

DTNSRDC

J_I VERSUS T FOR ASTM A106 STEEL SPECIMENS

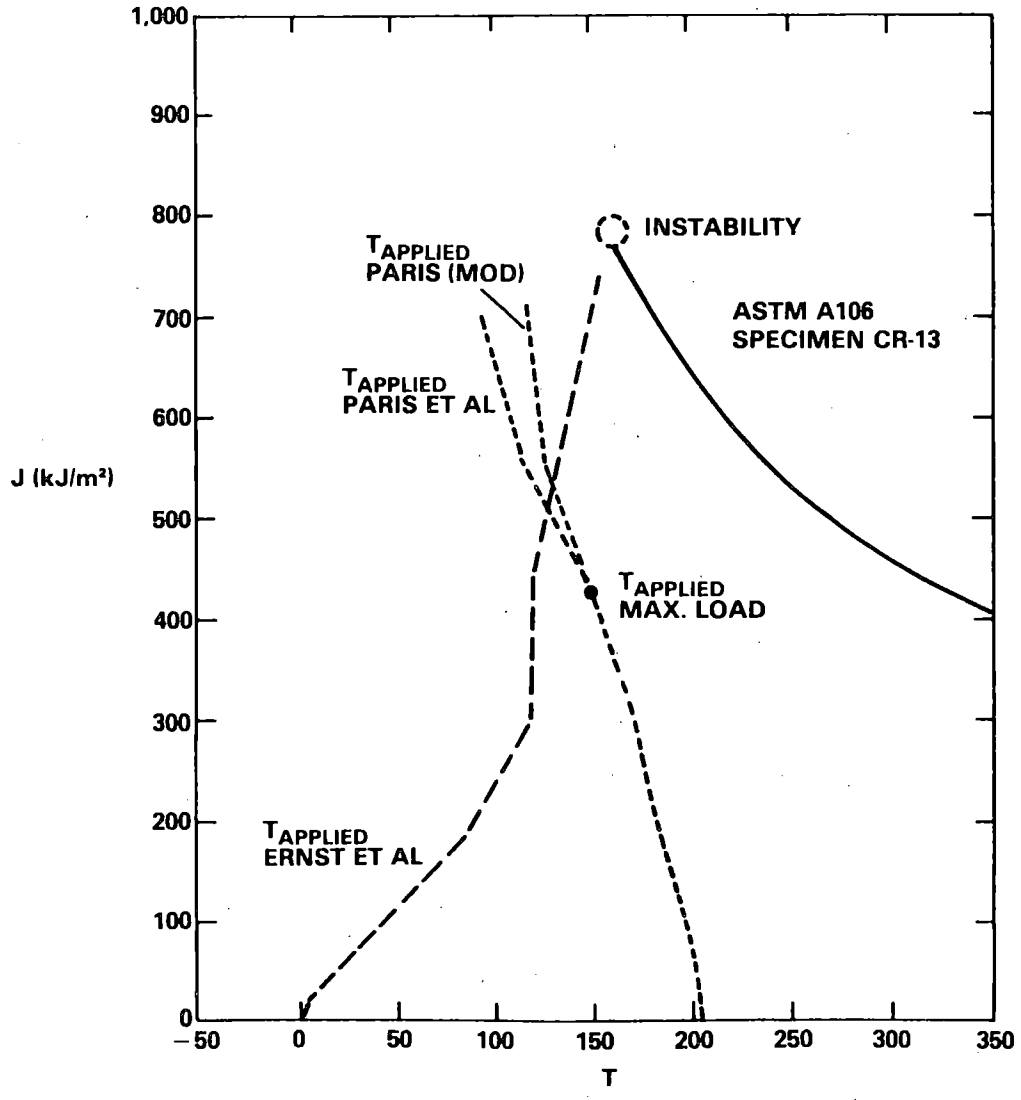

DTNSRDC

APPROACH

A. PROCURE 8-INCH SCHEDULE 80, ASTM A 106 STEEL, AND CHARACTERIZE ROOM TEMPERATURE MECHANICAL PROPERTIES, TOUGHNESS AND J-INTEGRAL DUCTILE FRACTURE PROPERTIES;

B. BUILD TEST FIXTURES FOR CLOSED-LOOP TEST MACHINE TO PRODUCE $T_{APPLIED}$ VALUES UP TO 200;

C. DEVELOP AND VALIDATE CRACKED CYLINDER COMPLIANCE FORMULATIONS WITH Al 6061 AND A 106 CYLINDERS OF PROPORTIONAL GEOMETRIES;

D. DEVELOP OR MODIFY EXISTING J-INTEGRAL FORMULATIONS FOR CRACKED CYLINDERS;

E. PERFORM INSTABILITY TESTS WITH Al 6061 PIPE

F. PERFORM J-INTEGRAL R-CURVE TESTS WITH CRACKED CYLINDERS OF A 106 AT ROOM TEMPERATURE WITH VERY LOW $T_{APPLIED}$ VALUES:

G. PERFORM J-INTEGRAL R-CURVE TESTS WITH CRACKED CYLINDERS OF A 106 AT ROOM TEMPERATURE WITH $T_{APPLIED}$ VALUES VARYING UP TO 200;

H. CORRELATE CRACK STABILITY OBSERVED IN TESTS WITH J-INTEGRAL R-CURVE PREDICTIONS FROM COMPACT SPECIMENS AND CRACKED CYLINDERS.

SCHEMATIC OF TESTING APPARATUS FOR LARGE PIPE TEARING INSTABILITY TESTS

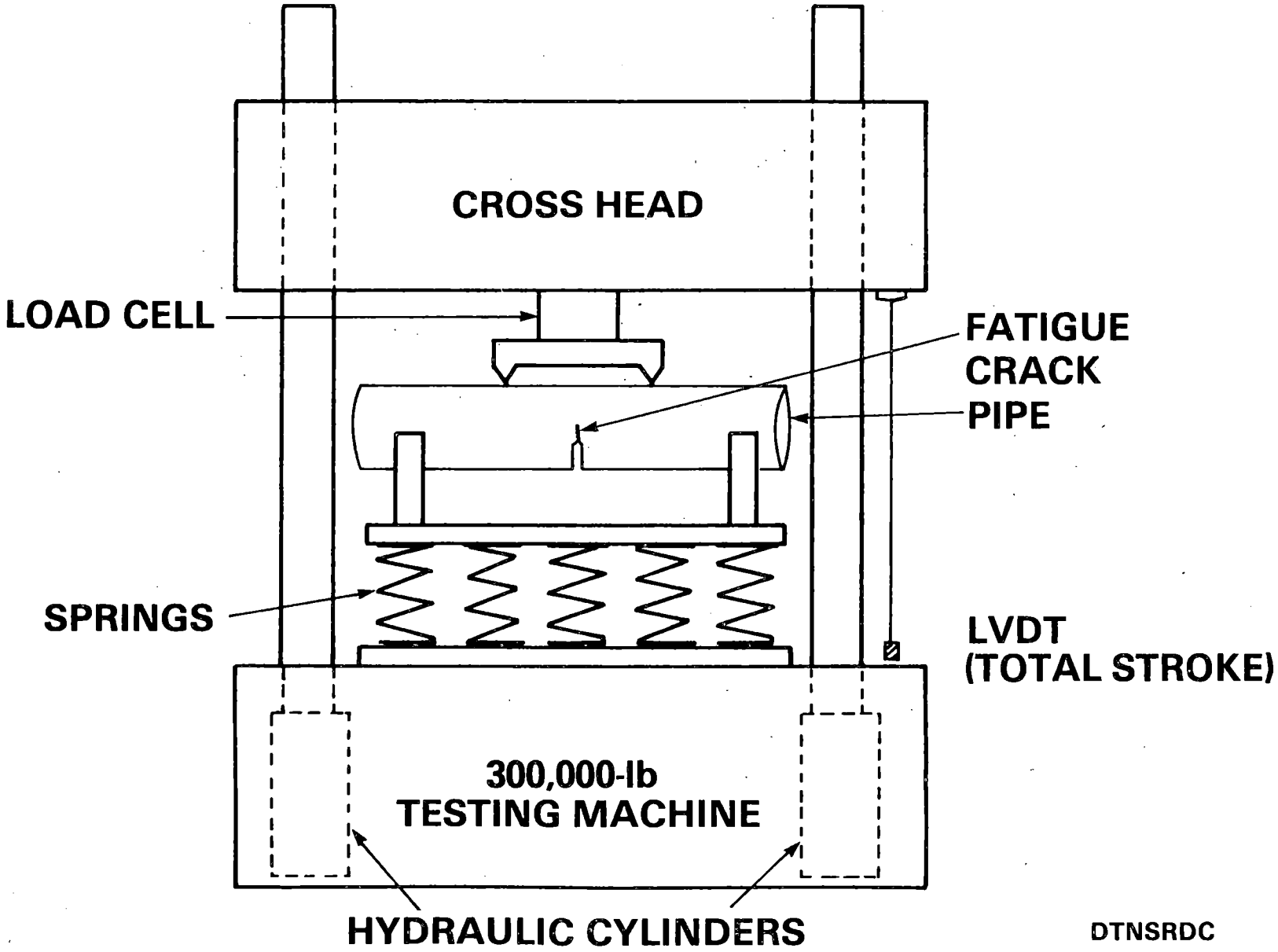

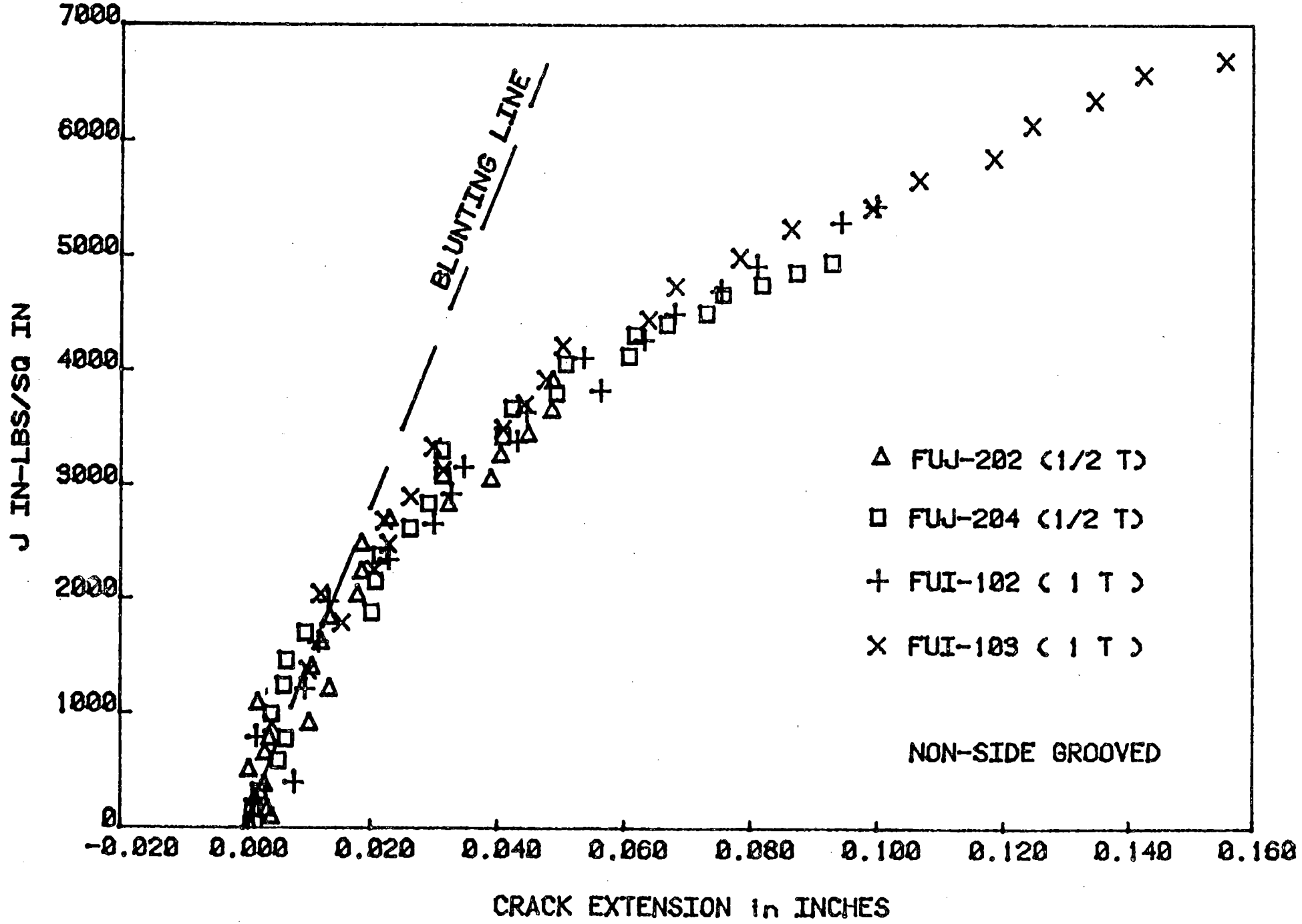
J vs CRACK EXTENSION A106 STEEL
7000
6000
5000
4000
3000
2000
1000
0
J IN-LBS/SQ IN
BLUNTING LINE
FUJ-202 (1/2 T)
FUJ-204 (1/2 T)
FUI-102 (1 T)
FUI-103 (1 T)
NON-SIDE GROOVED
-0.020
0.000
0.020
0.040
0.060
0.080
0.100
0.120
0.140
0.160
CRACK EXTENSION in INCHES

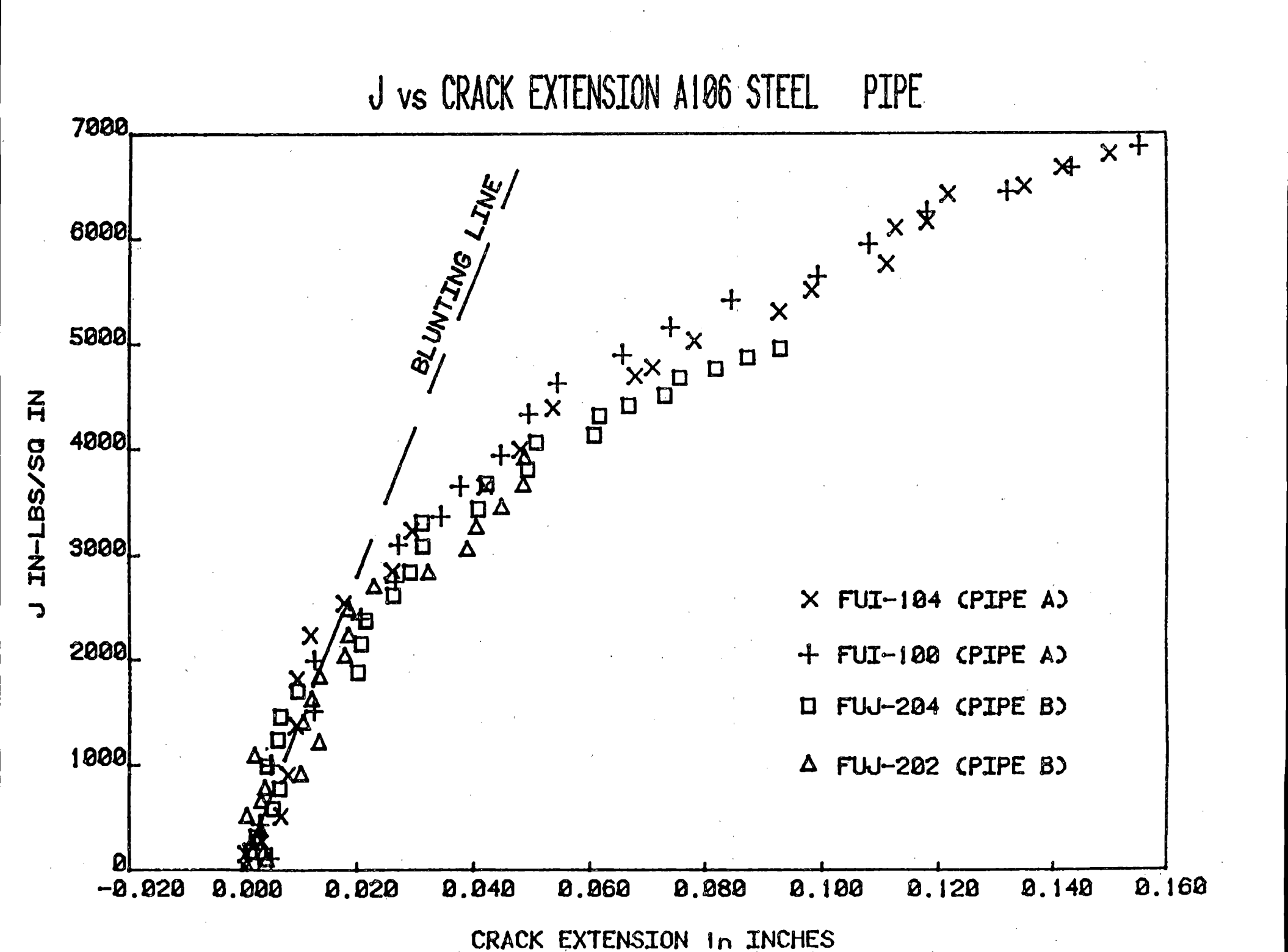
J vs CRACK EXTENSION A106 STEEL PIPE
J IN-LBS/SQ IN
7000
6000
5000
4000
3000
2000
1000
0
-0.020
0.000
0.020
0.040
0.060
0.080
0.100
0.120
0.140
0.160
CRACK EXTENSION In INCHES
BLUNTING LINE
FUI-104 (PIPE A)
FUI-100 (PIPE A)
FUJ-204 (PIPE B)
FUJ-202 (PIPE B)

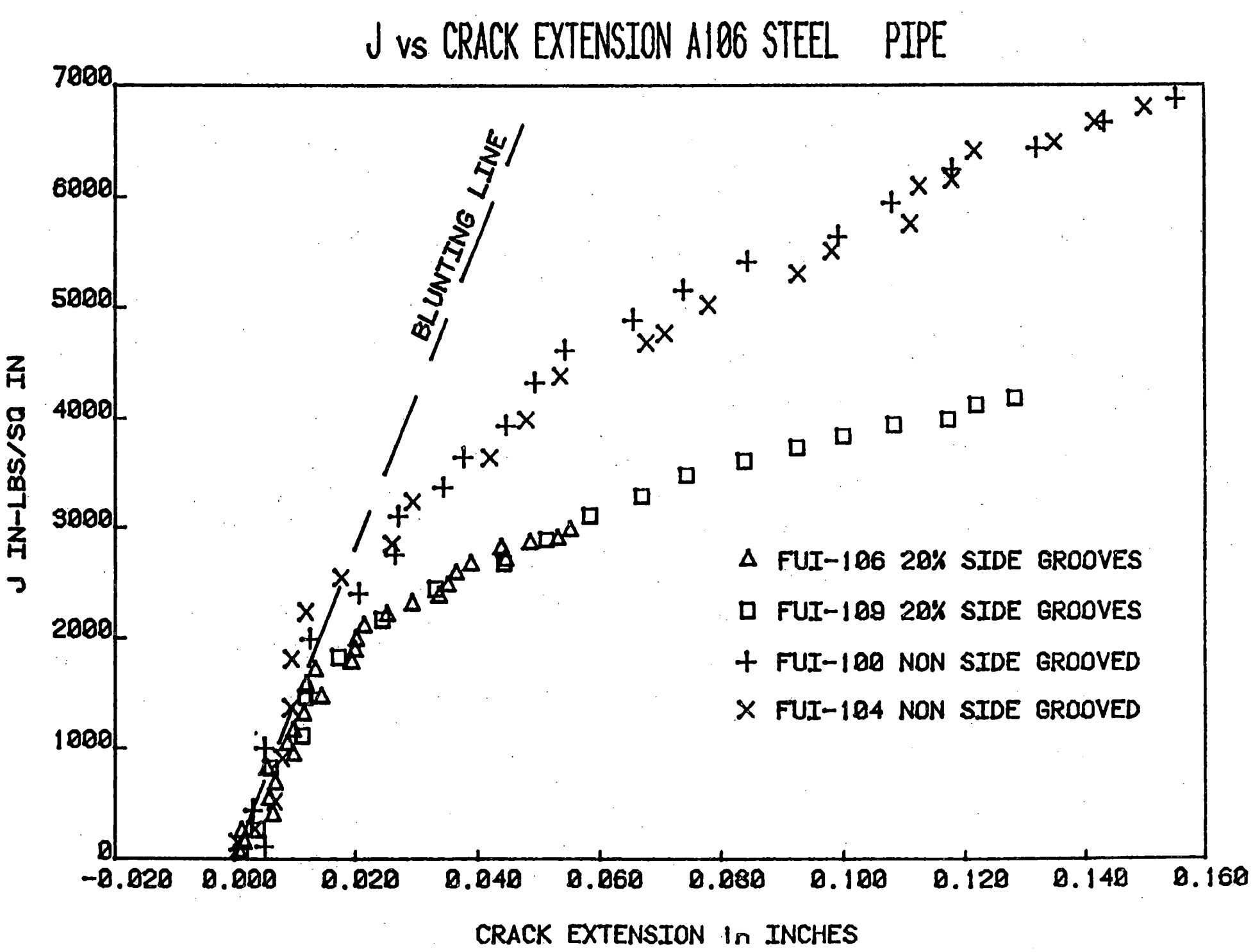
J vs CRACK EXTENSION A106 STEEL PIPE
7000
6000
5000
4000
3000
2000
1000
0
J IN-LBS/SQ IN
BLUNTING LINE
FUI-106 20% SIDE GROOVES
FUI-109 20% SIDE GROOVES
FUI-100 NON SIDE GROOVED
FUI-104 NON SIDE GROOVED
-0.020
0.000
0.020
0.040
0.060
0.080
0.100
0.120
0.140
0.160
CRACK EXTENSION in INCHES

ASME SA 106 GRC PIPE FRACTURE PROPERTIES

SPECIMEN GEOMETRY	% S.G.	AVG JIC (IN-LB/IN^2)	AVG T
1. TCT B = 0.5	0	3,390	306
½ TCT	20	1,527	250

EIGHT INCH SCHEDULE 80 PIPE

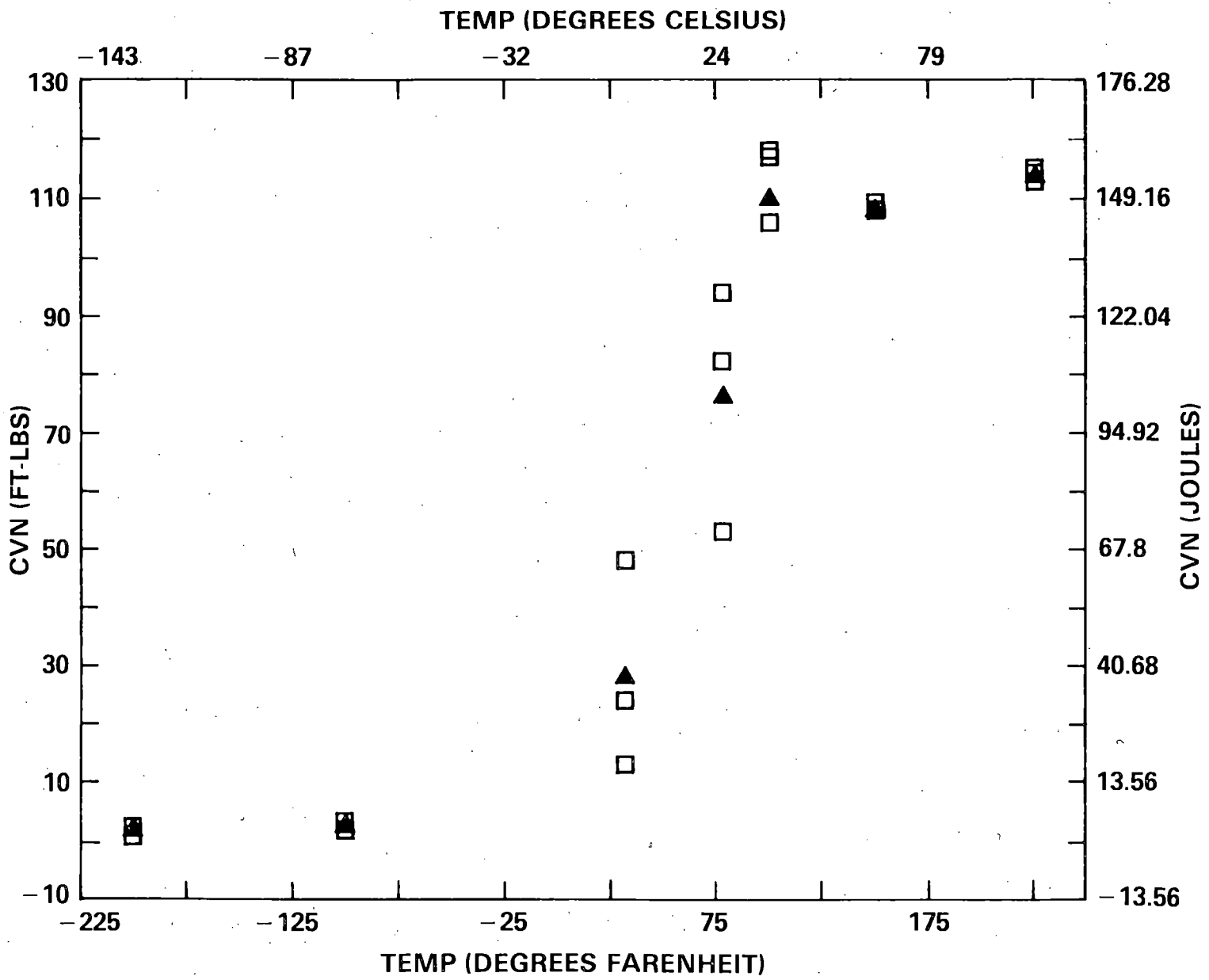

J VS CRACK EXTENSION A106 FUI 1/2 T SERIES

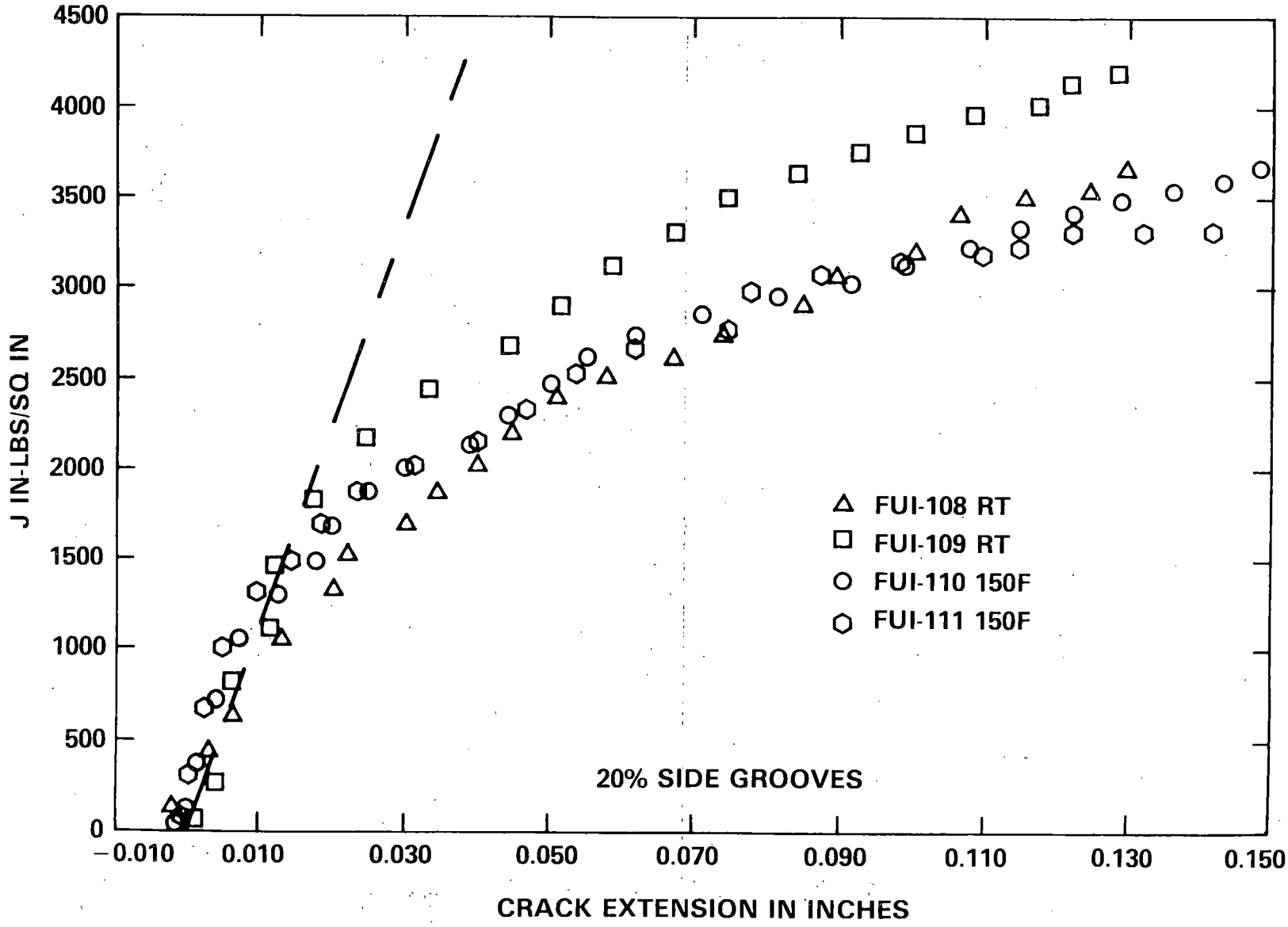

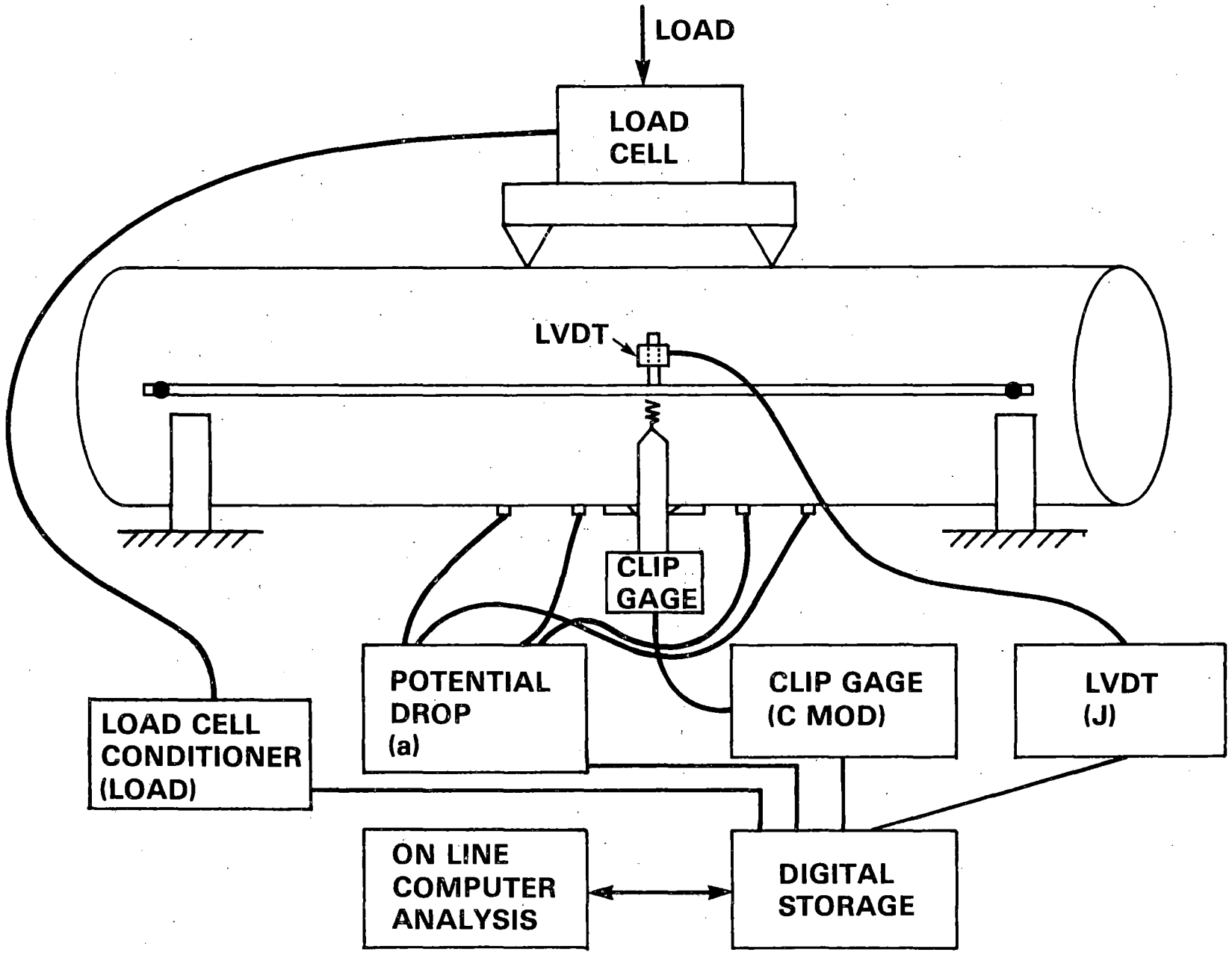
LOAD
LOAD CELL
LVDT
CLIP GAGE
LOAD CELL CONDITIONER (LOAD)
POTENTIAL DROP (a)
CLIP GAGE (C MOD)
LVDT (J)
ON LINE COMPUTER ANALYSIS
DIGITAL STORAGE
DTNSRDC

$$J_{TOT} = J_{ELASTIC} + J_{PLASTIC}$$

$$J_{eL} = \alpha \frac{K_I^2}{E}$$

$$J_{P\ell} = \frac{I}{Rt} \int_o^P \left(\frac{\partial \delta_{PL}}{\partial \phi} \right)_P \, dP$$

$$J_{P\ell} = \beta \int_o^{\delta_{P\ell}} P d\delta_{P\ell} + \int_{\phi_o}^{\phi} \gamma J_{P\ell} \, d\phi$$

ϕ = CRACK ANGLE

ZAHOOR & KANNINEN

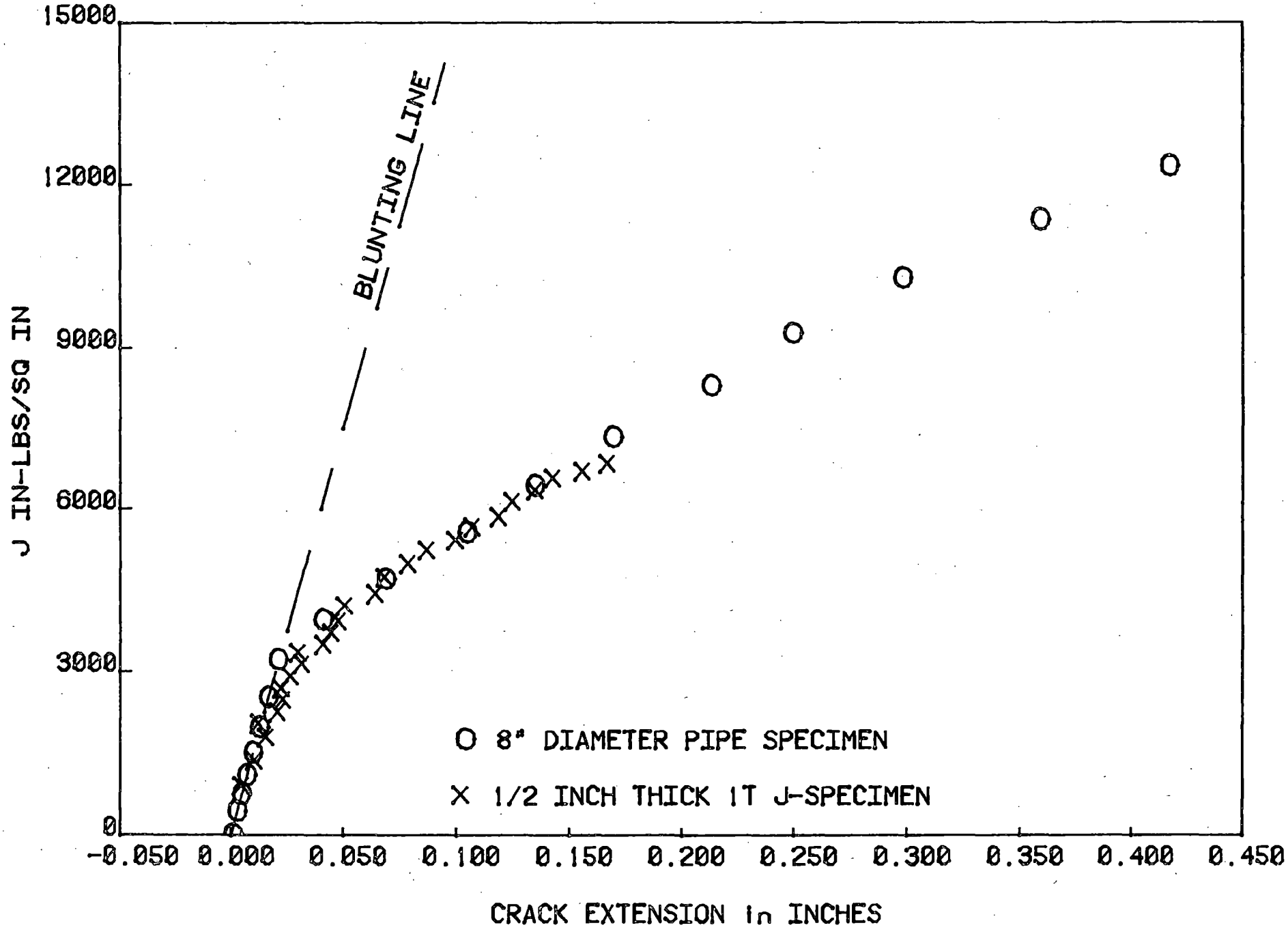
J vs DELTA A FOR A106 STEEL PIPE
15000
12000
9000
6000
3000
0
J IN-LBS/SQ IN
BLUNTING LINE
O 8" DIAMETER PIPE SPECIMEN
X 1/2 INCH THICK 1T J-SPECIMEN
-0.050 0.000 0.050 0.100 0.150 0.200 0.250 0.300 0.350 0.400 0.450
CRACK EXTENSION In INCHES

PROBABILISTIC FRACTURE MECHANICS FOR PIPING*

By

David O. Harris
Science Applications, Inc.
San Jose, California

Presented at
Ninth Water Reactor Safety Research Information Meeting
National Bureau of Standards
Gaithersburg, Maryland
October 29, 1981

A probabilistic fracture mechanics model of structural reliability was developed in earlier phases of this program.[1] The model was developed for reactor piping, and was originally applied to large cast austenitic piping in a commercial PWR. It is assumed that piping failures occur as the result of crack-like defects introduced during fabrication, with the initial crack size being randomly distributed. The manner in which cracks grow during service is calculated by fracture mechanics techniques.

The earlier phase of this work considered fatigue crack growth in austenitic piping and was aimed primarily at assessing the influence of seismic events on the probability of piping failure. Results were generated by a Monte Carlo code called PRAISE that employes stratified sampling.[2]

The efforts for the current year consisted of modifying the PRAISE code to make it more generally applicable so that other piping systems and materials could be easily analyzed. Specifically, PRAISE was modified to allow consideration of other materials and subcritical crack growth characteristics (such as stress corrosion cracking). Additionally, the code was expanded to include factors not originally included, such as residual stresses, vibratory stresses, and longitudinal welds.

The expanded PRAISE code was then applied to a variety of pipe conditions, including various pipe sizes, vibratory & residual stresses and subcritical crack growth mechanisms. Generally speaking, the probability of a sudden and complete pipe severance varied somewhat with the conditions considered, but was invariably very low. In contrast to this, the probability of a leak varied widely, and fairly high values were predicted for some conditions. This supports the "leak-before-break" concept. It was found that vibratory stresses and stress corrosion cracking were detrimental — which is as expected. Residual stresses could be beneficial or detrimental, depending on their sign and spatial distribution.

* Work performed as part of Load Combinations Program, Lawrence Livermore National Laboratory, Livermore, California.

The new version of PRAISE is of much more general applicability than the original version, and results generated by it provide a useful means of assessing the relative importance of the many factors affecting the integrity of piping systems in light water reactors.

References

1. D.O. Harris, E.Y. Lim and D.D. Dedhia, "Probability of Pipe Fracture in the Primary Coolant Loop of a PWR Plant, Vol. 5: Probabilistic Fracture Mechanics Analysis", NUREG/CR 2189, Vol. 5, 1981.

2. E.Y. Lim, "Probability of Pipe Fracture in the Primary Coolant Loop of a PWR Plant, Vol. 9: PRAISE Computer Code User's Manual", NUREG/CR 2189, Vol. 9, 1981.

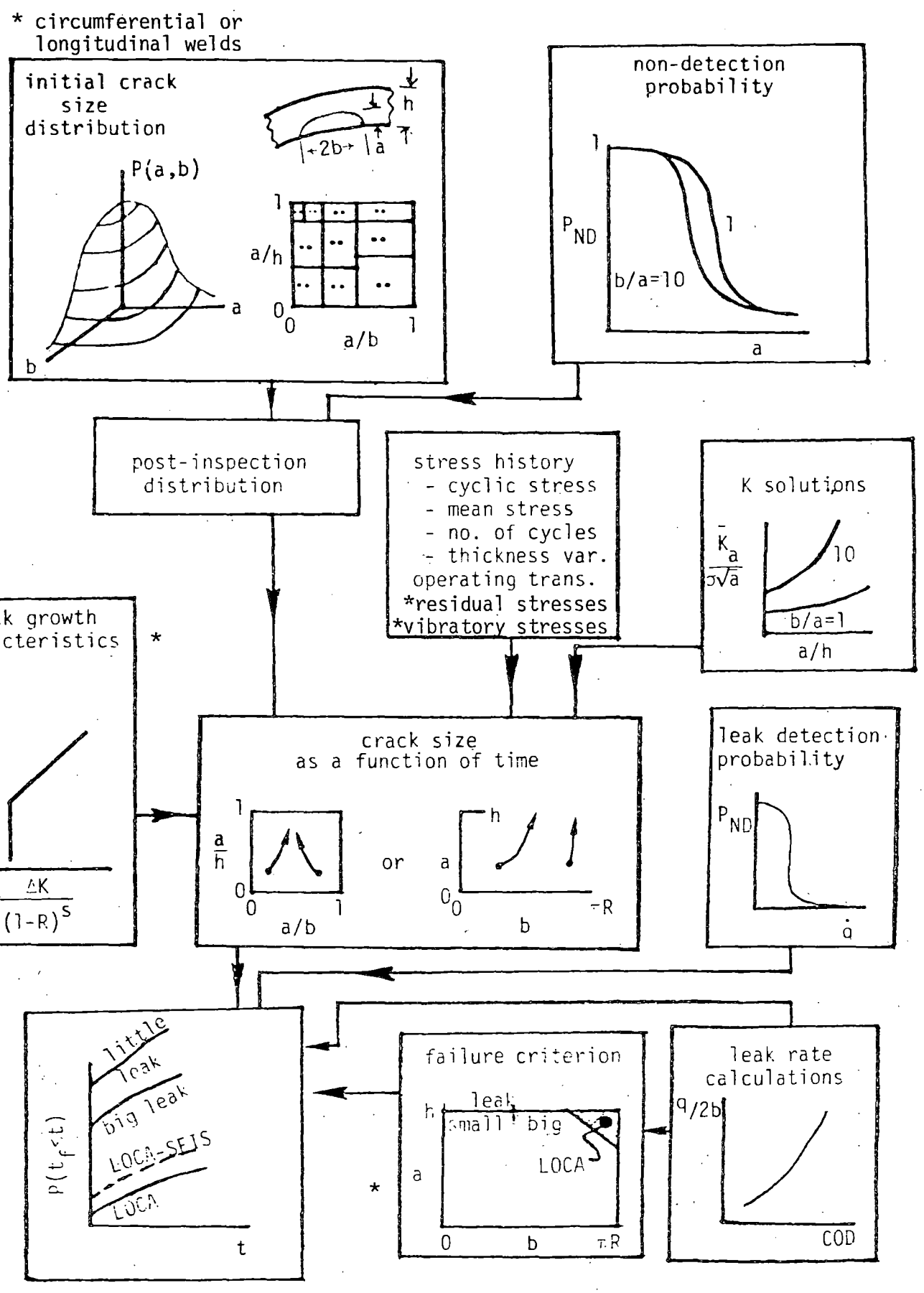

* Items expanded or altered to allow additional capabilities in code

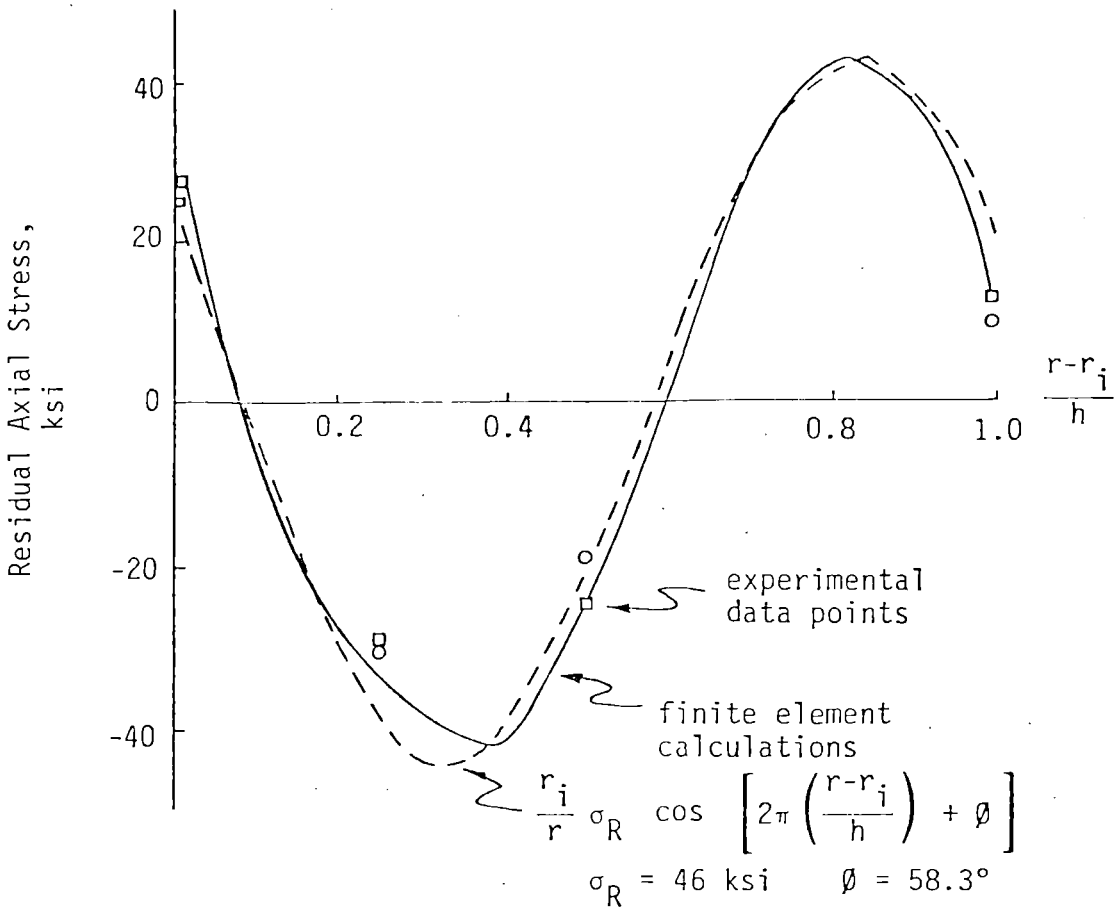

Thickness Variation of Axial Component of As-Welded Residual Stress in a 24 Inch Line.

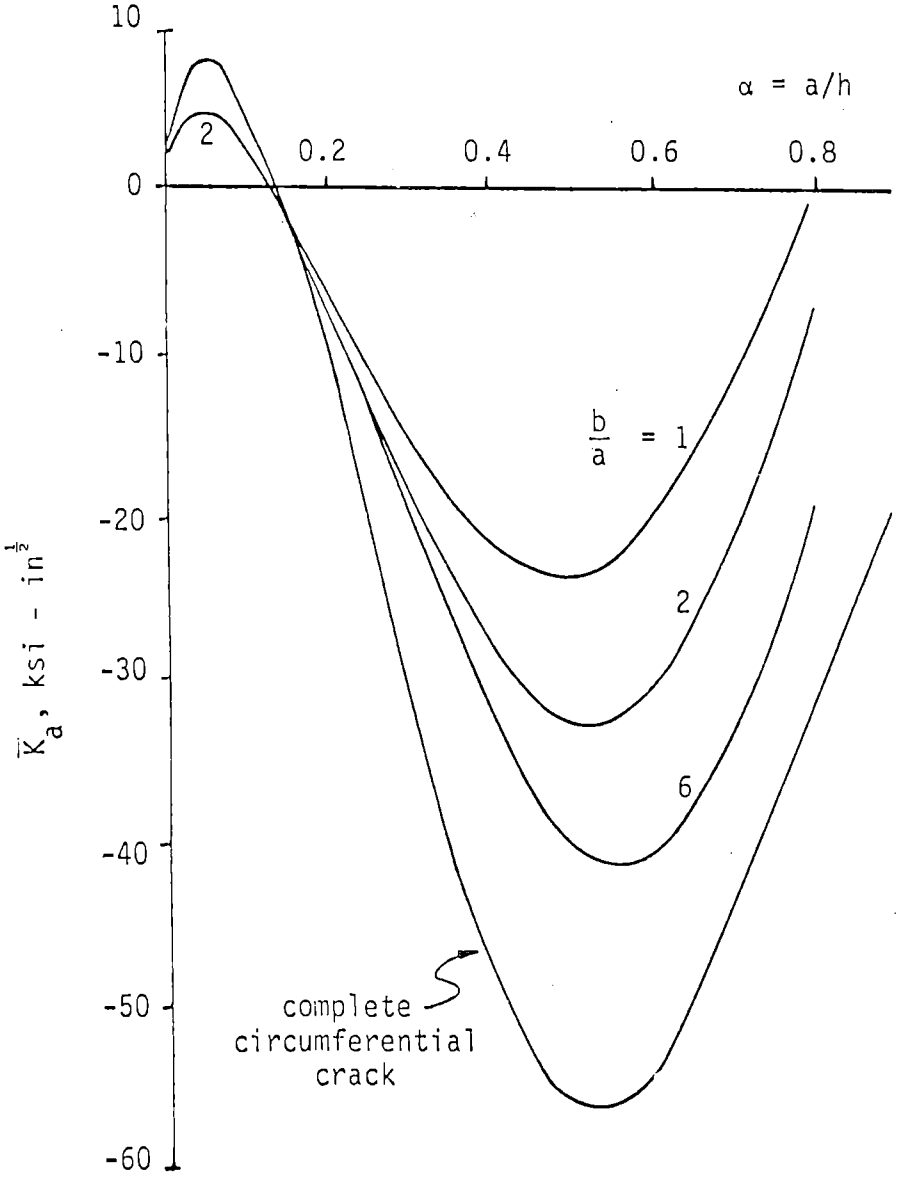

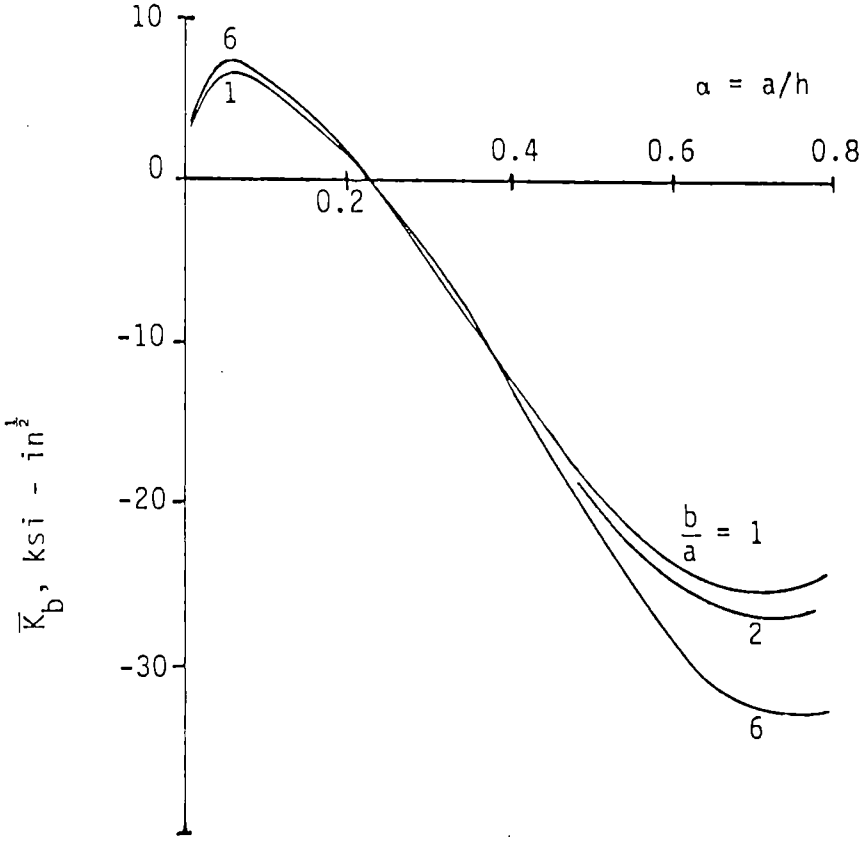

RMS-Averaged Stress Intensity Factors for Part-Circumferential Interior Surface Cracks in 24 Inch Pipe Due to Residual Stresses

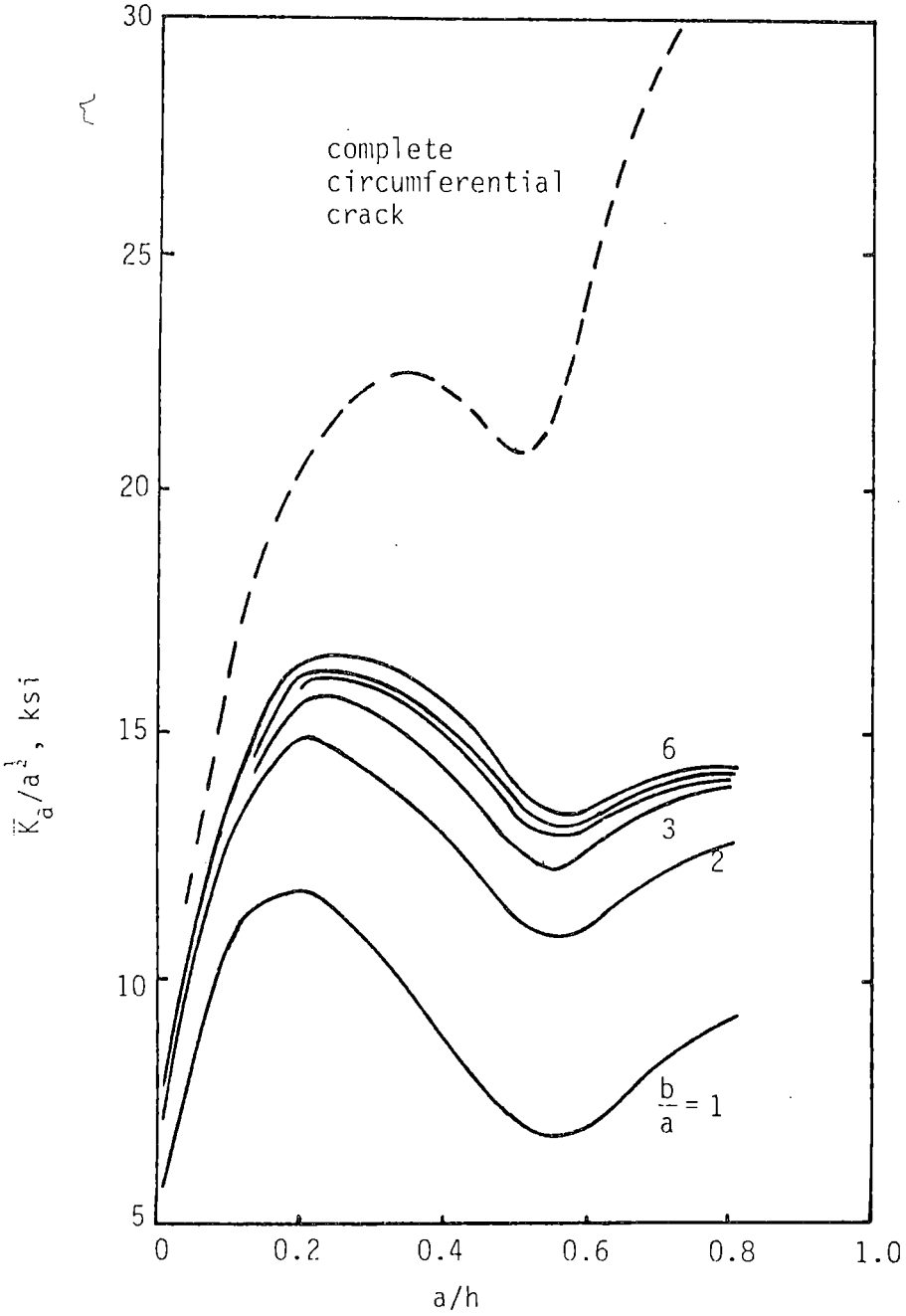

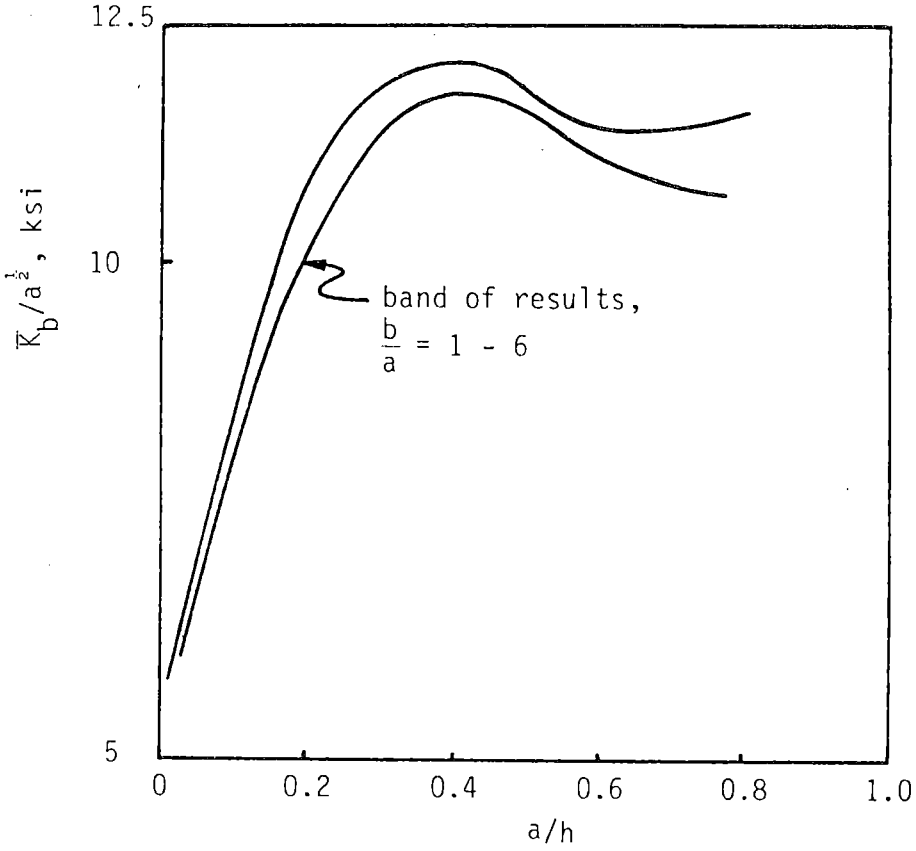

RMS-Averaged Stress Intensity Factors Due to Residual Stresses for Part-Circumferential Cracks at Angular Location Resulting in Maximum Values; 16 Inch Line Heat Affected Zone.

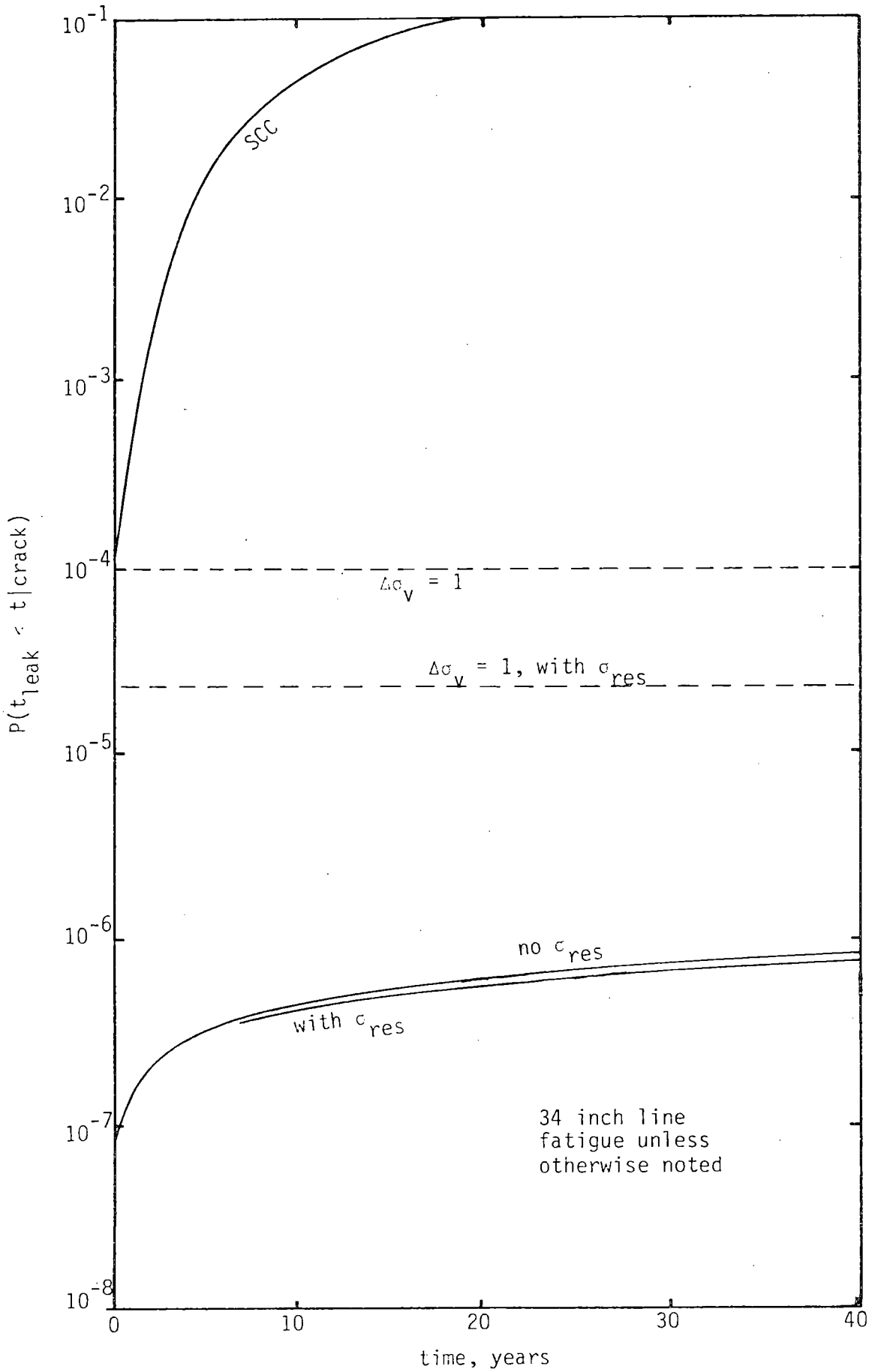

Cumulative Leak Probability for 34 Inch Line Under Various Conditions. Results are Conditional on a Crack Being Initially Present.

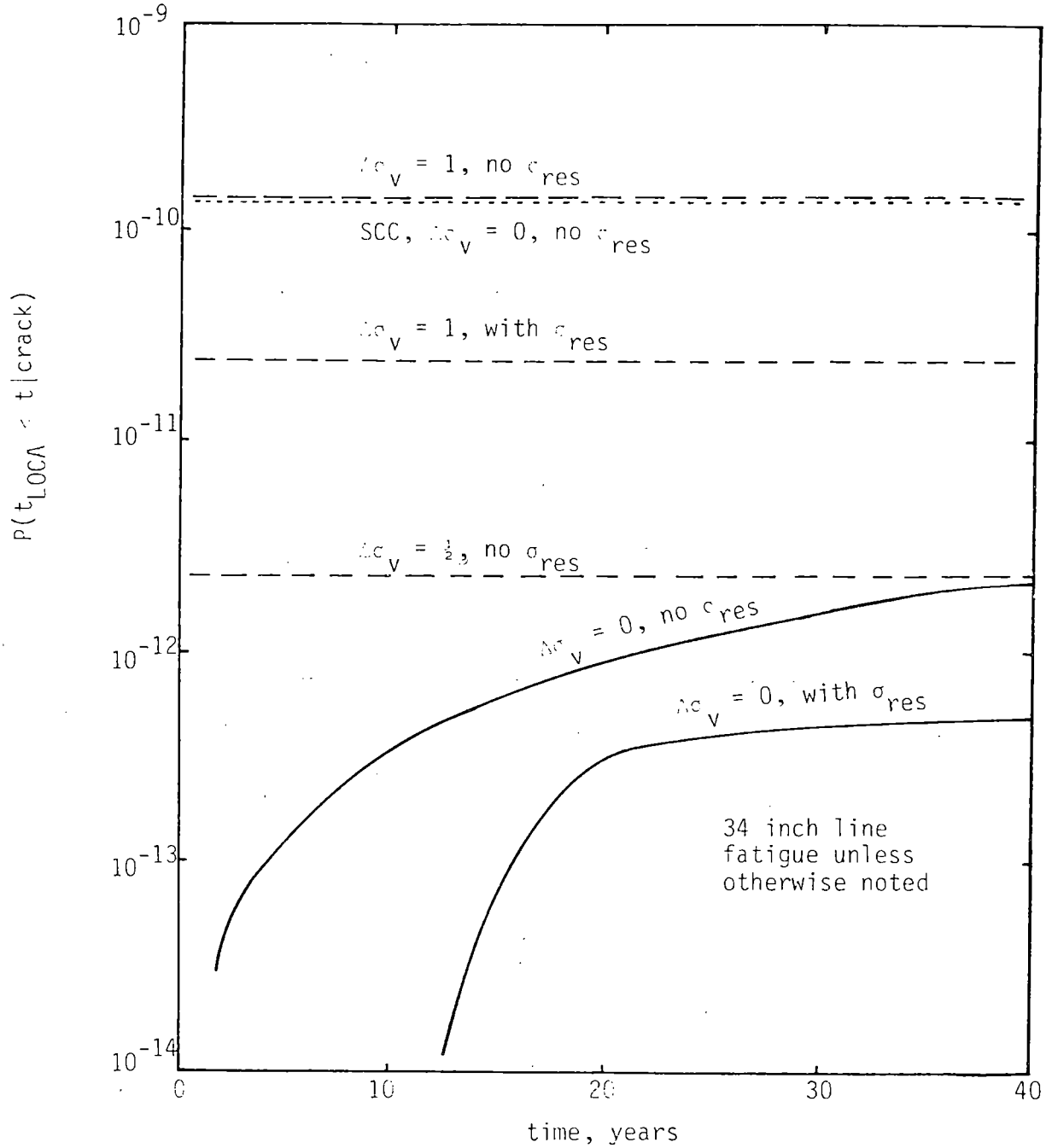

Cumulative Probability of a Sudden and Complete Pipe Severance for the 34 Inch Line Weld Joint Under Various Conditions. Results are Conditional on a Crack Being Initially Present.

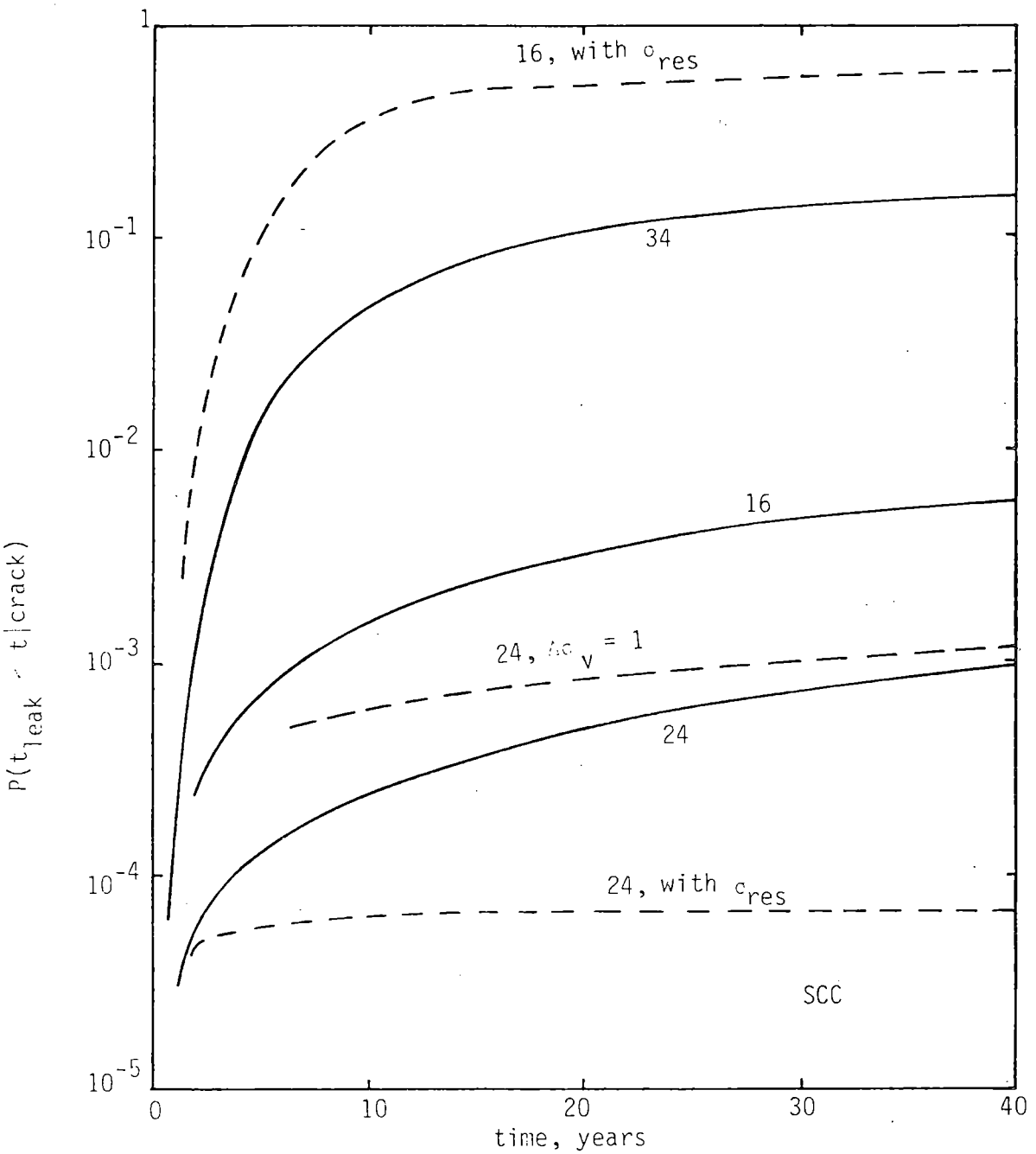

Cumulative Leak Probability in Various Size Lines With Cracks Growing due to Stress Corrosion Cracking. Results are Conditional on a Crack Being Initially Present.

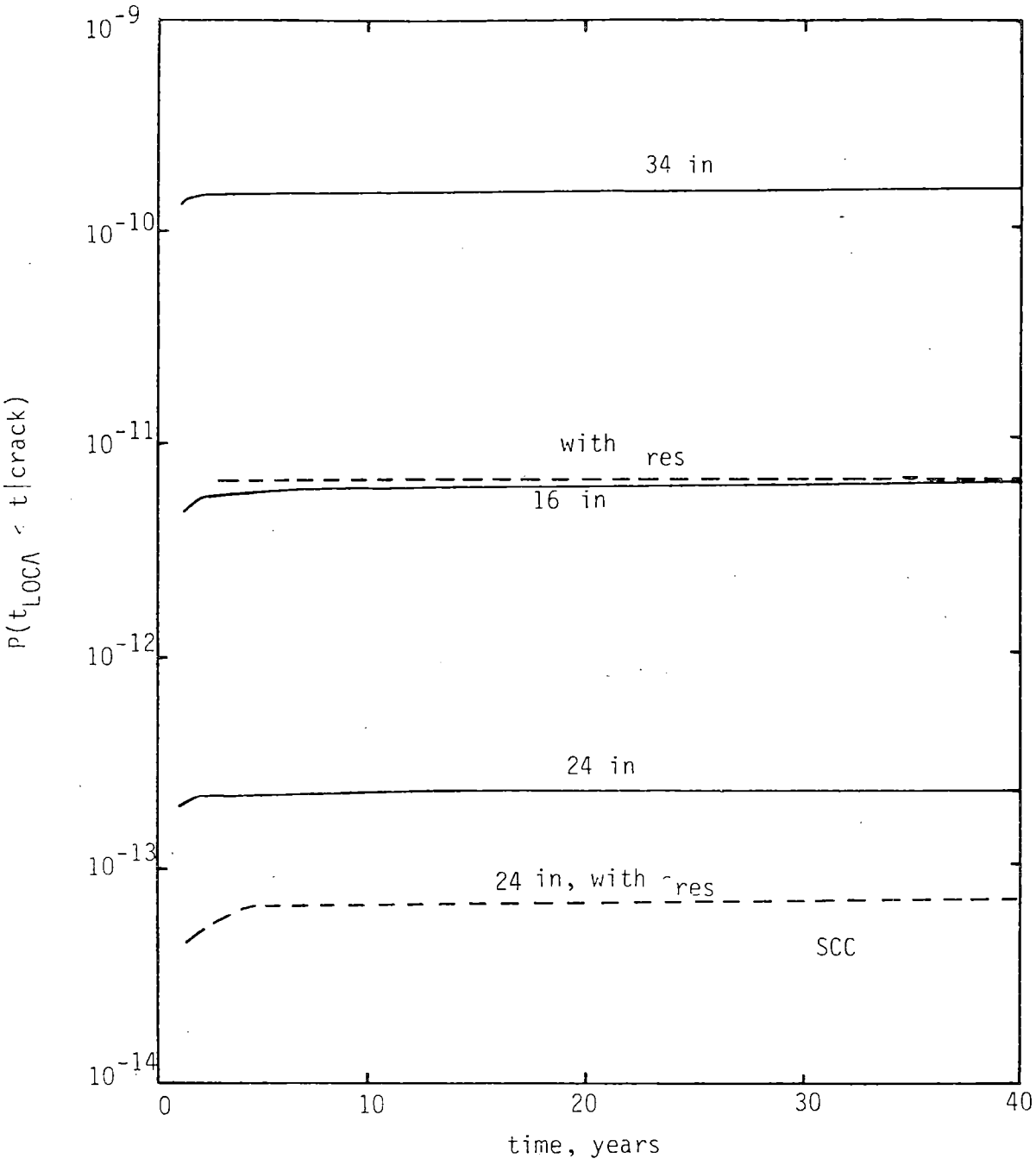

Cumulative Probability of a Sudden and Complete Pipe Severance in Various Size Lines with Cracks Growing due to Stress Corrosion Cracking. Results are Conditional on a Crack Being Initially Present.

CONCLUSIONS

- LOCA PROBABILITIES INVARIABLY LOW.
- LEAK PROBABILITIES VARY WIDELY, DEPENDING ON CONDITIONS.
- STRESS CORROSION CRACKING GREATLY INCREASES FAILURE PROBABILITIES.
- VIBRATORY STRESSES HAVE IMPORTANT (AND DETRIMENTAL) INFLUENCE ON FATIGUE CRACK GROWTH.
- RESIDUAL STRESSES HAVE IMPORTANT INFLUENCE ON STRESS CORROSION CRACK GROWTH (BUT NOT FATIGUE).
- RESIDUAL STRESS CAN BE BENEFICIAL OR DETRIMENTAL, DEPENDING ON THEIR SIGN AND SPATIAL DISTRIBUTION (AXISYMMETRIC GENERALLY MORE FAVORABLE).

PRAISE-B PROVIDES A USEFUL MEANS OF ASSESSING RELATIVE INFLUENCE OF THE MANY FACTORS AFFECTING PIPING RELIABILITY.

PNL-SA-9971

PWR STEAM GENERATOR TUBE INTEGRITY PROGRAM

FY81 PROGRESS: LEAK RATE STUDIES ON LABORATORY SCC STEAM GENERATOR TUBES

R. A. Clark, Project Manager

October 1981

Presented at the Ninth Water Reactor Safety
Research Information Meeting
Gaithersburg, Maryland
October 26-30, 1981

Work Supported by
the U. S. Nuclear Regulatory Commission
NRC FIN No. B-2097
Dr. Joseph Muscara, Program Manager
under a Related Service Agreement with
the U.S. Department of Energy under
Contract DE-AC06-76RLO 1830

Pacific Northwest Laboratory
Richland, Washington 99352

INTRODUCTION

The Steam Generator Tube Integrity Program is part of NRC research efforts concerning primary system integrity. Past programmatic activity has involved fabrication of machined or chemically induced defects in Inconel 600 steam generator tubing simulating service defects. These specimens were subsequently burst or collapse tested at steam generator operating temperatures and a determination made of remaining mechanical strength. Data evaluation allowed development of mathematical formulae relating defect type and size to remaining tube integrity. Eddy current data taken on the laboratory produced defect specimens then allowed development of certainty bands about plots of defect size versus remaining tube integrity. These certainty bands reflect the ability to accurately size a particular defect using single or multifrequency eddy current techniques in the laboratory. Thus, given an ability to determine the type of defect in an operating unit, the remaining integrity of a defected tube can be determined within a certainty dependent on the accuracy of the nondestructive measurement technique.

FY 1981 PROGRESS

Part of the ongoing efforts in this program involve the study of specimens with a tight laboratory produced intergranular stress corrosion crack. A round robin eddy current test is just being completed on a series of cracked specimens which will next be subject to metallographic sectioning. After determination of the most accurate SCC sizing a further series of cracked specimens will be sized then burst tested to relate tube integrity to crack size. This characterization effort is being made because similar morphology machined and chemically produced defects fit the same mathematical relationship of remaining strength versus defect size with the single exception that the mathematical model based on an electro-discharge machined (EDM) slot did not provide a good correlation with the burst strength of SCC containing tubes. SCC specimens burst at considerably lower pressures than predicted by the model. Either the EDM notch is not a good SCC simulation or the sizing of previous SCC's was inaccurate. Because of the potential ramifications of the SCC burst pressures this further characterization study is being carried out.

Along a similar vein leak rate studies were initially conducted on specimens with through-wall EDM notches. These notches were nominally three mils wide at the root. Leakage at a pressure differential of 2200 psig was usually above the 20 gpm limit of the original flow system. With the development of a laboratory SCC simulation an additional leak test matrix using through wall SCC samples was established. These tests will be explained in some detail later in this paper.

About a year and a half ago with the assistance of Virginia Electric and Power Company (VEPCO) the program acquired the 'A' generator being replaced at the Surry 2 nuclear station. This unit was subsequently transported to the Hanford Reservation where it was stored pending construction of the Steam Generator Examination Facility (SGEF). The SGEF is an especially designed containment to house the retired from

service steam generator in its normal vertical position. The SGEF will enable nondestructive primary and secondary side examinations then subsequent specimen removal. Other features include an ability to conduct large scale secondary side cleaning and primary side decontamination experiments. The largest effort of the program during fiscal year 1981 was directed toward construction of the SGEF. Ground breaking was in December 1980. At the end of September the facility was 92% complete, with completion scheduled for November 19, 1981. The Surry generator will be lowered through a roof hatch into the completed SGEF and an extensive research effort initiated utilizing the retired from service unit as a vehicle.

Because of the potentially unique opportunity presented by long term availability of a service degraded steam generator for research purposes, NRC has sought to include other participants in the program. It is believed that vendors, users and foreign regulatory agencies have potentially much to gain from participation. Extensive contacts have resulted in several additional participants including U. S. and European interests joining the program.

LEAK RATE STUDIES

A previously reported laboratory procedure[1] to create localized intergranular stress corrosion cracks in unsensitized Inconel 600 steam generator tubing is being used to produce specimens with near through wall or through wall cracks. These specimens are then subject to internal pressurization with 300°C deionized water and leakage rates to ambient air measured. Figure 1 schematically depicts the test system used. A large autoclave serves as the hot water reservoir. Pressure is maintained in the autoclave by bleeding in a cover gas from high pressure accumulators as the autoclave blows down via a bottom penetration through the test specimen. The blowdown water passes through a high temperature flow meter to the specimen which is instrumented to measure internal pressure and temperature. Each test is started by first opening a vent valve on the specimen and allowing sufficient heated water to pass through the specimen to bring it to test temperatures. The vent valve is then closed and specimen leakage is controlled by a metering valve. In concept the metering valve will enable several pressure differential versus flow data points to be taken. The metering valve is positioned and pressure in the specimen allowed to come to an equilibrium for the particular flow, then the metering valve opened further allowing a new equilibrium pressure to be obtained, etc. This results in data shown in figures 2 and 3. However, several other types of leak rate data were also observed. Figures 4 and 5 show a specimen that leaked at less than 2 gpm, which was about

---

[1] R. A. Clark and R. L. Burr. Technical Note: A Method for Controlled Stress Corrosion Cracking in Nonsensitized Inconel 600 Tubing. Corrosion, Vol. 36, No. 7, pp. 382-383, July 1980.

the minimum controllable flow on the metering valve and the least value measurable with our flow meter. Pressure quickly built up to the system equilibrium (2500 psig) and in this case the leak rate remained at a constant level below the flow meter calibration level. Depicted in figures 6 and 7 is a specimen that initially had a low flow allowing pressure to build up to an equilibrium value, then after one minute the stress corrosion crack opened up leading to a sudden large leak. The data in the previous figures is acquired using a minicomputer which samples each measuring device 15 times a second. A second computer system with graphics capability then creates plots of flow versus time, pressure differential versus time and flow versus pressure differential. In addition a videotape is taken of each test which often allows a correlation of leak rate changes with visible changes in the specimen flaw. In several instances crack growth has been observed by successive 'pop-ins' at the crack tip.

The total matrix of proposed tests is shown in Table 1. This matrix is designed to evaluate potential leakage associated with cracks of different sizes and orientations. More importantly information is generated on what happens to the defect under an accident condition such as a main steam line break (MSLB) during which the pressure differential across the generator tubes is temporarily increased. Data on the tests completed to date suggest some research redirection may be advisable. Specimens with similar dimensioned through wall cracks have not given similar leak rate results, and some specimens have proven impossible to fabricate after close to a year of effort.

Figure 8 shows the most extensive failure to date. This specimen had a 7/16" long crack located in the center of a 2" long area with 60% wall thinning. Figures 9, 10, 11, and 12 show before and after leak test views of more typical specimens. Some specimens show no crack growth or noticeable crack opening during the course of a test. Other similar specimens will show deformation as in figure 12 leading to leakage in excess of 20 gpm. Additional tests need to be conducted to provide a statistical sample before conclusions can be drawn.

As mentioned previously, experience with the tests run to date suggests some redirection. First the method used to produce localized stress corrosion cracks in tube samples does not appear to be capable of producing 100% through wall cracks longer than 1" without deformation in the sample. On the other hand crack growth behavior in 1" long and shorter cracks suggests there is no real benefit in testing the longer cracks. It appears that 1" through wall stress corrosion cracks are not stable at a pressure differential of 2500 psig across an 875" O.D x .050" wall steam generator tube. Second, the experiment as set-up can be improved. Currently we have two interchangeable flow meters, one for the range 2 gpm to 20 gpm and a second for the range 4.5 gpm to 450 gpm. Virtually all tight SCC's initially leak <.2 gpm then many procede rapidly to leakage >20 gpm. A second later test then needs to be conducted using the high flow meter. In addition, pressure

control at the specimen by means of restricted flow is not sufficient to achieve optimum information from the specimen. The following system modifications are being considered. Installation of a pressure regulator near the autoclave source that would allow a gradual and controlled pressure differential to be established across the specimen, and installation of three parallel flow paths that can be successively valved in. These flow paths would have flow meters in the ranges 0.03-0.3 gpm, 2 gpm - 20 gpm, and 4.5 gpm - 450 gpm. A test would be run by slowly increasing the ΔP across a specimen to 1000 psig, approximating the normal operating pressure differential across a steam generator tube. After a period of leakage at this pressure differential sufficient to establish crack stability, the pressure differential would then be increased to a level simulating a MSLB condition. Specimen leakage and crack stability would then be determined for ΔP's in the range 2200 to 2500 psig.

The initial results of these tests suggest that through wall cracks $\leq$1" long with initial leakage <.2 gpm can propagate into leaks of greater than 20 gpm when exposed to a short differential pressure transient of 2500 psig. This information coupled with previous limited burst test results on SCC tubes that showed failures at pressures below a crack model based on EDM notches suggests further work is needed to relate leak rates, crack size and potential for crack instability during an accident transient.

TABLE 1

LEAK RATE TEST MATRIX*

UNIFORM THINNING AND STRESS CORROSION CRACK

Study 1/4", 1/2", 1", and 1-1/2" SCC with uniform thinning twice the crack length and of the following depths: 0%, 35-45%, 55-60%, 75-85%. (Number of tests = 16)

LONG THROUGH-WALL CRACKS

Study 2" and 3" cracks with no uniform thinning. (Number of tests = 2)

0.625" X 0.034" TUBING

Spotcheck tubes with no thinning and varying crack lengths. (Number of tests = 4)

SCC THROUGH-WALL CIRCUMFERENTIAL

Study circumferential cracks of 45°, 90°, 120°, 180°, 270°. (Number of tests = 5)

LEAK IN SIMULATED TUBE SHEET CREVICE

Test 1 SCC and multiple SCC with and without packing. (Number of tests = 4)

LEAK UNDER DENT

Study tubes with 1/8" and 1/4" cracking on each side of support plate. (Number of tests = 2)

*10.875" X 0.050" Tubing Unless Otherwise Noted

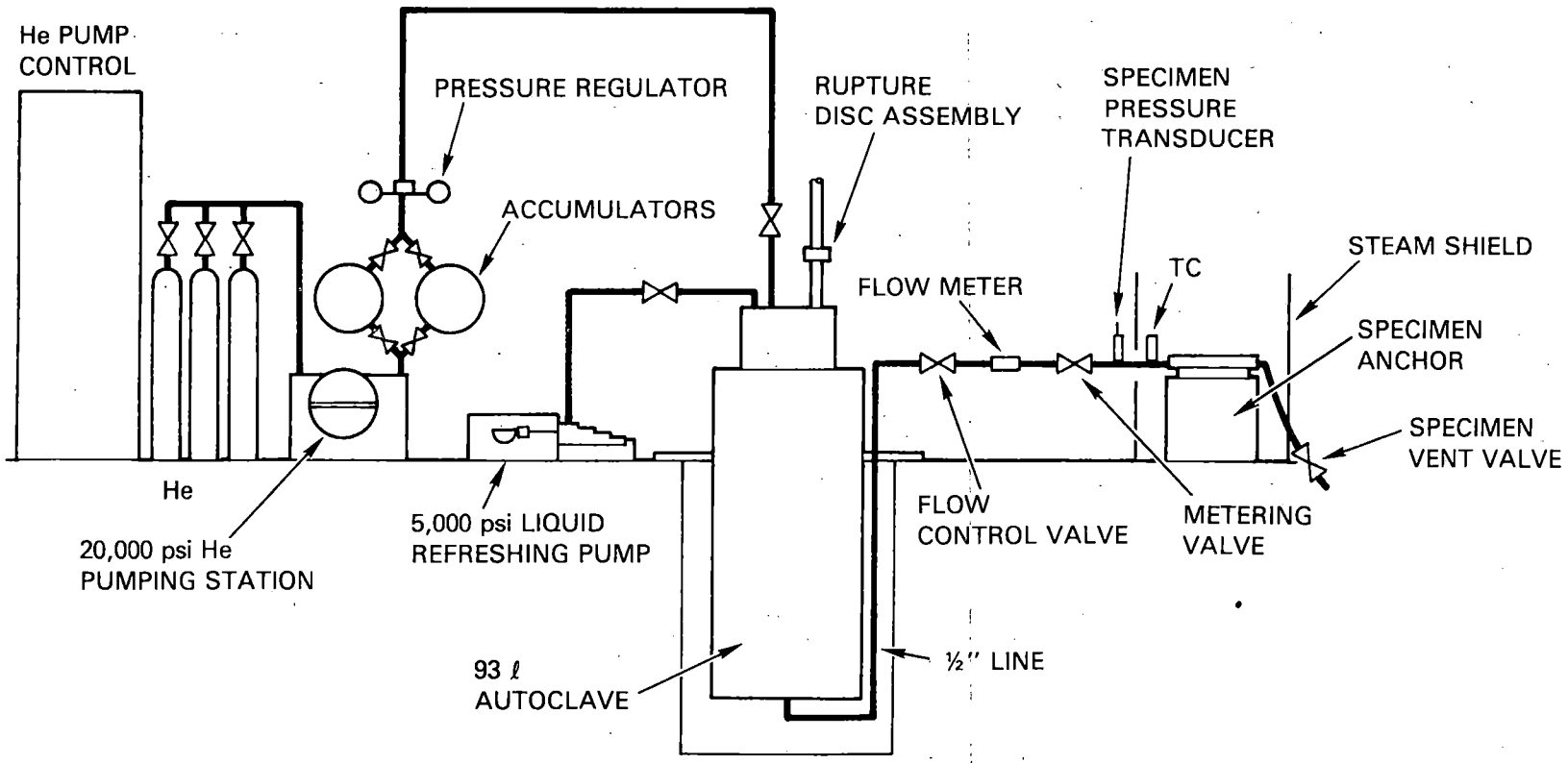

Figure 1. Leak Rate Test Set-Up

Figure 2

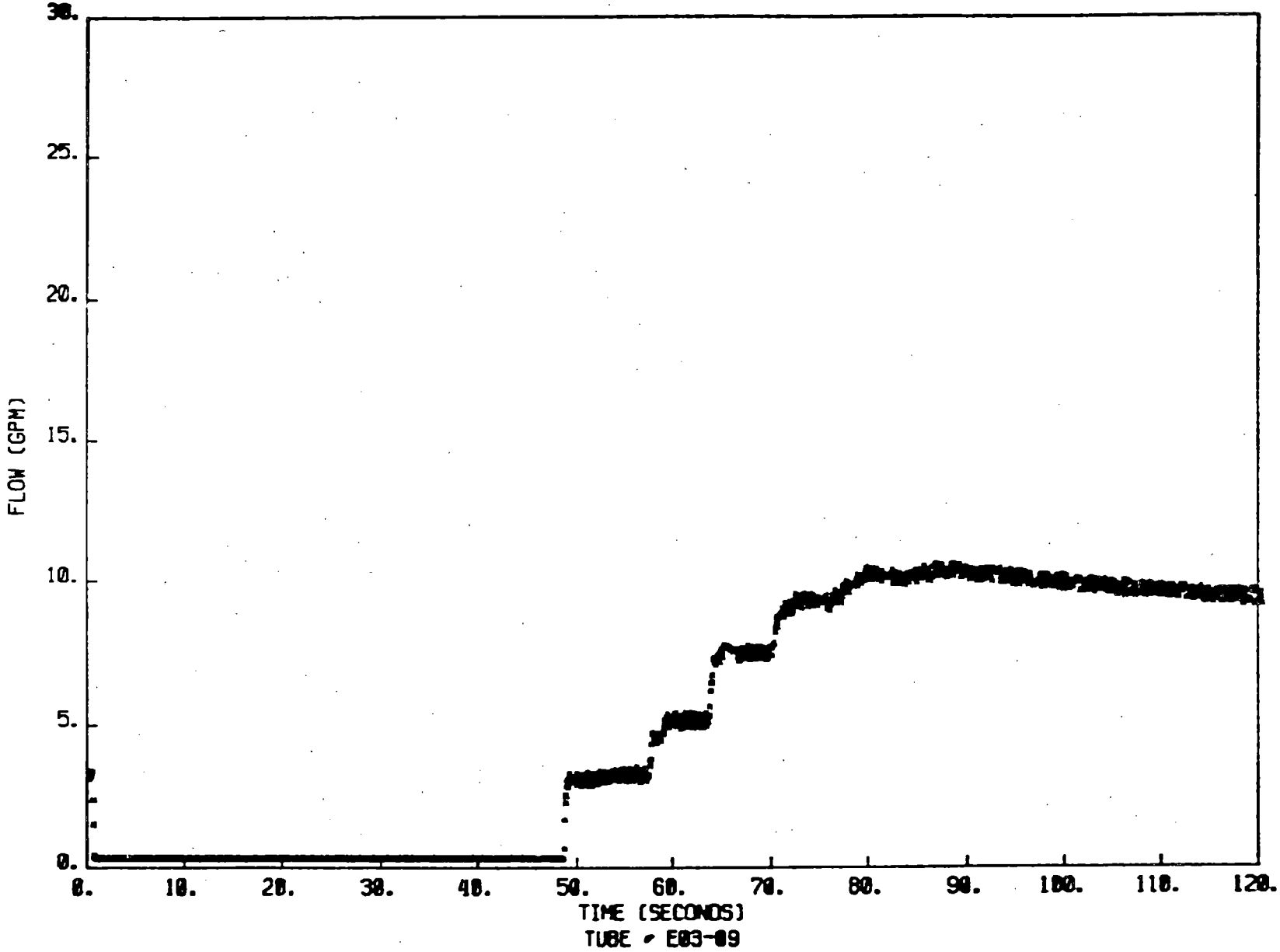
30.
25.
20.
15.
10.
5.
0.
FLOW (GPM)
0.
10.
20.
30.
40.
50.
60.
70.
80.
90.
100.
110.
120.
TIME (SECONDS)
TUBE - E03-09

Figure 3

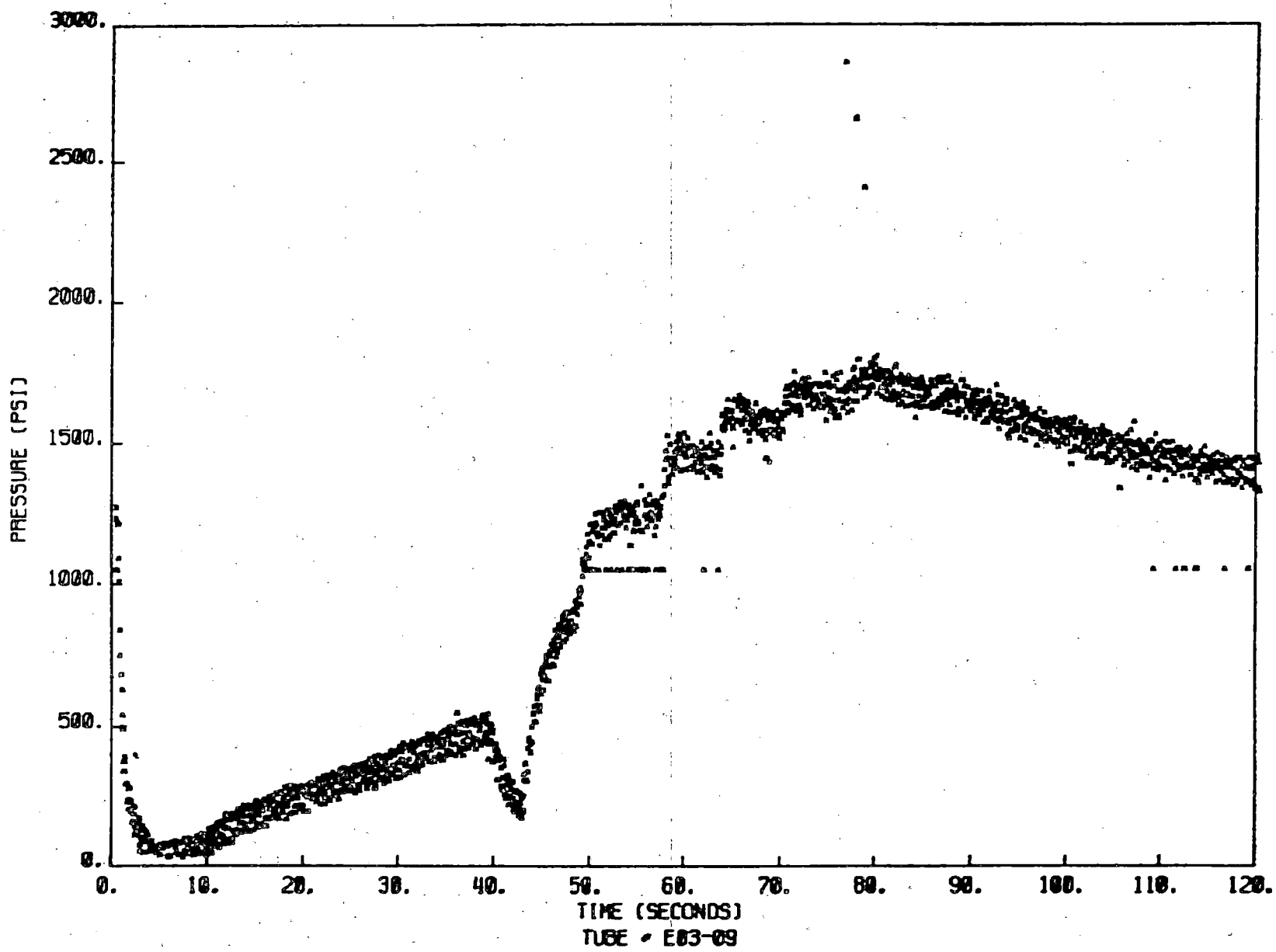
3000.
2500.
2000.
1500.
1000.
500.
0.
PRESSURE (PSI)
0.
10.
20.
30.
40.
50.
60.
70.
80.
90.
100.
110.
120.
TIME (SECONDS)
TUBE - E03-09

Figure 4

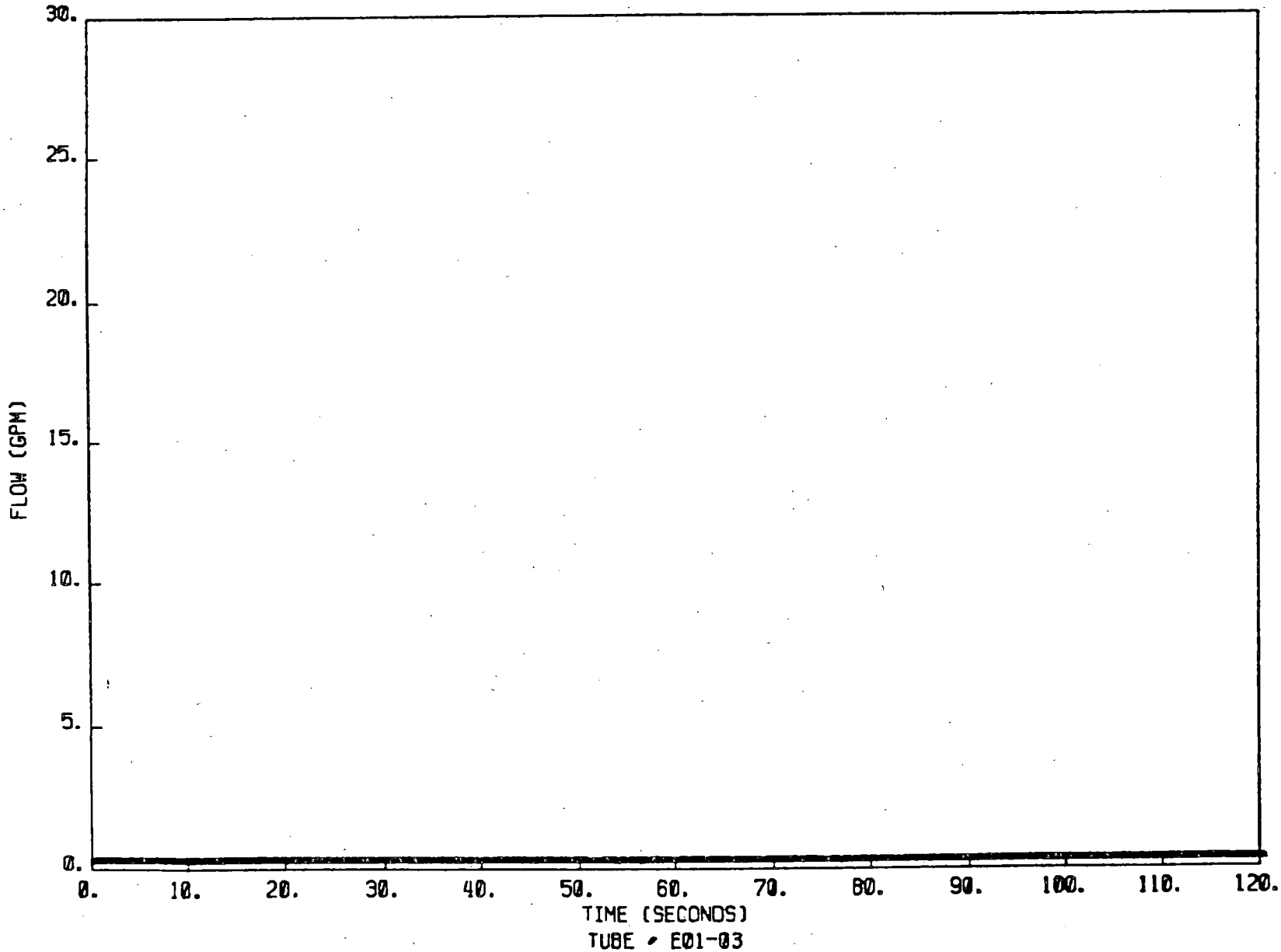
30.
25.
20.
15.
10.
5.
0.
FLOW (GPM)
0.
10.
20.
30.
40.
50.
60.
70.
80.
90.
100.
110.
120.
TIME (SECONDS)
TUBE • E01-03

Figure 5

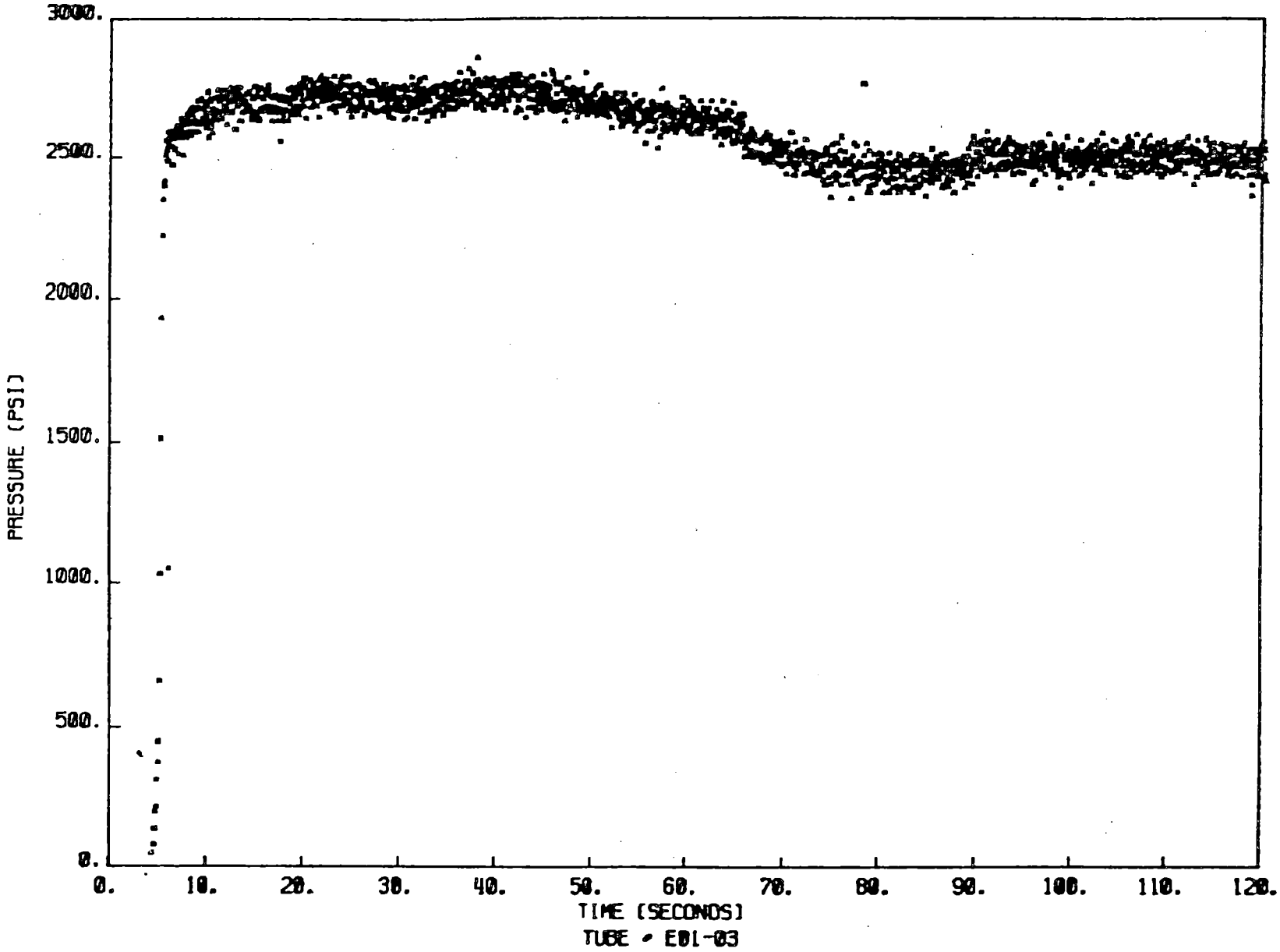
3000.
2500.
2000.
1500.
1000.
500.
0.
PRESSURE (PSI)
0.
10.
20.
30.
40.
50.
60.
70.
80.
90.
100.
110.
120.
TIME (SECONDS)
TUBE - E01-03

Figure 6

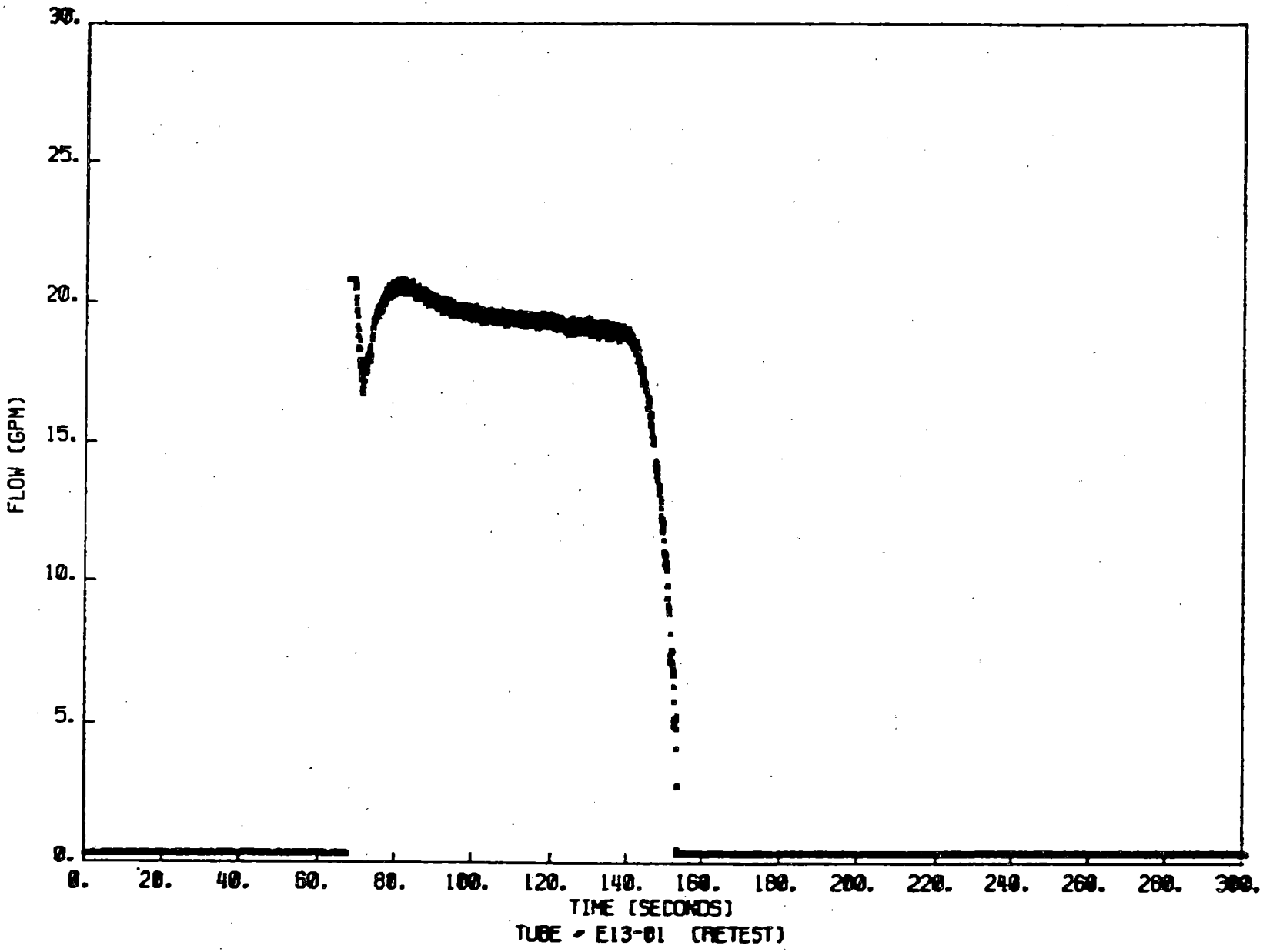
30.
25.
20.
15.
10.
5.
0.
FLOW (GPM)
0.
20.
40.
60.
80.
100.
120.
140.
160.
180.
200.
220.
240.
260.
280.
300.
TIME (SECONDS)
TUBE - E13-01 (RETEST)

Figure 7

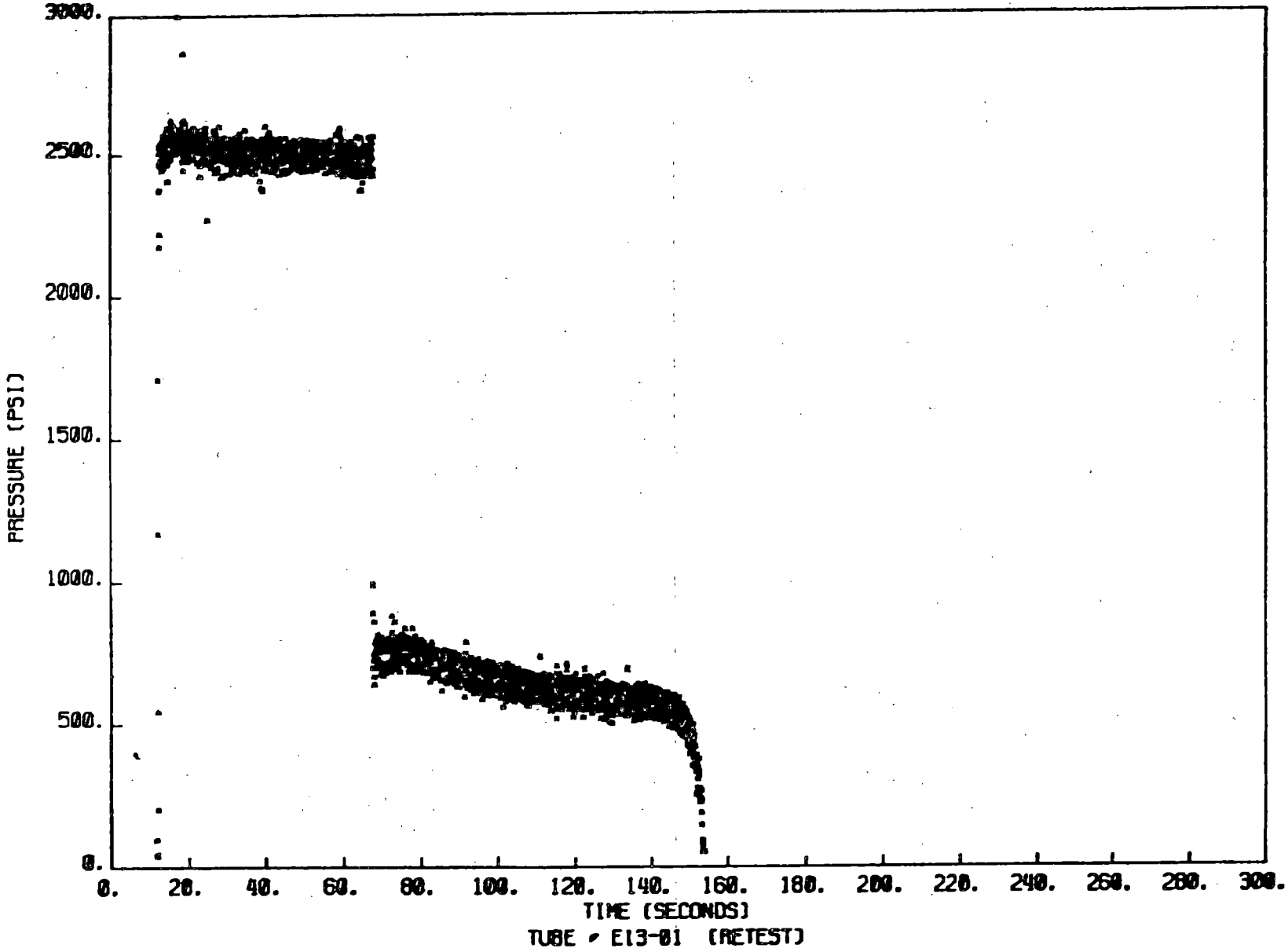
3000.
2500.
2000.
1500.
1000.
500.
0.
PRESSURE (PSI)
0.
20.
40.
60.
80.
100.
120.
140.
160.
180.
200.
220.
240.
260.
280.
300.
TIME (SECONDS)
TUBE # E13-01 (RETEST)

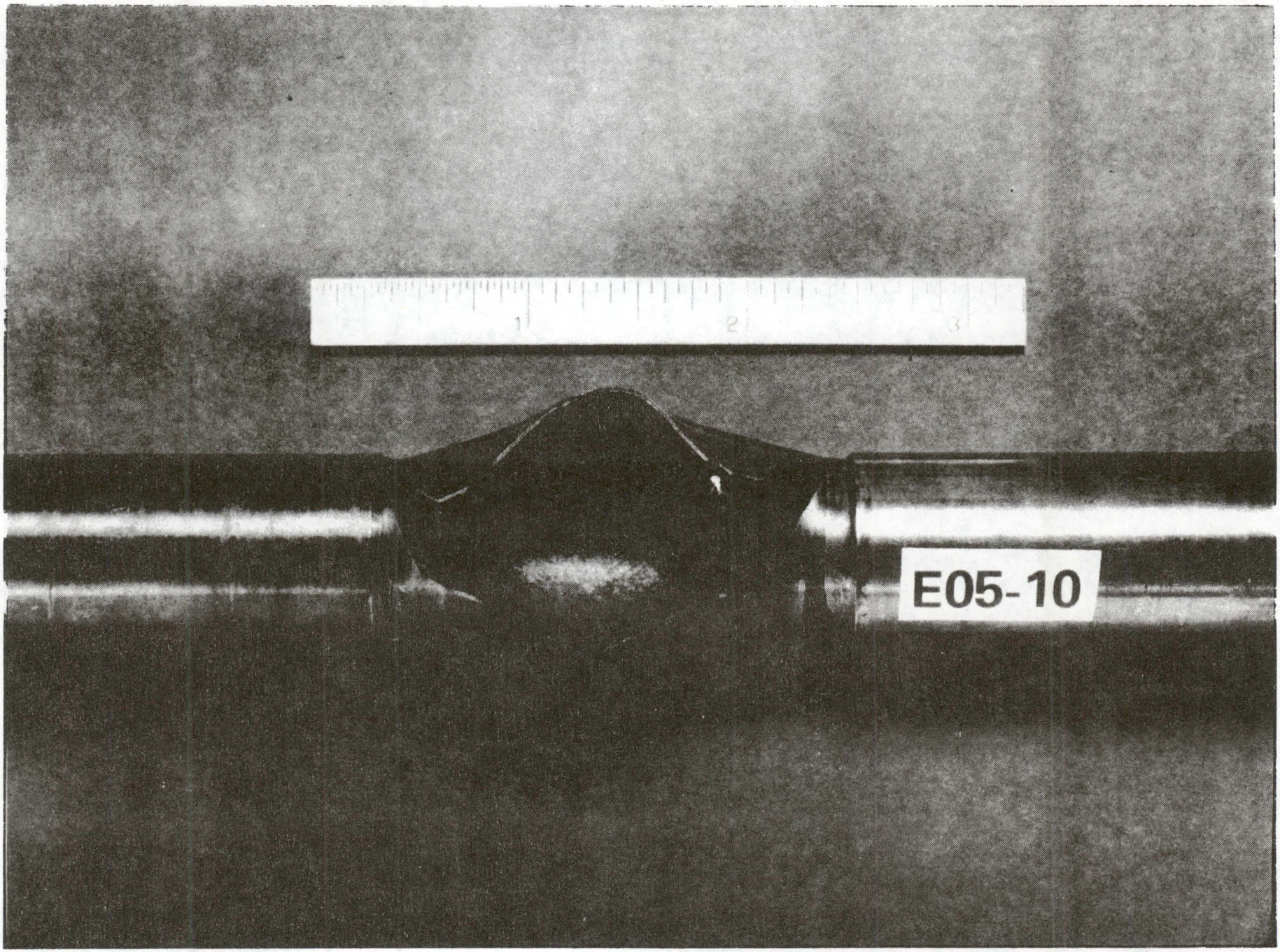

Figure 8 Specimen E-05-10 After Leak Rate Test

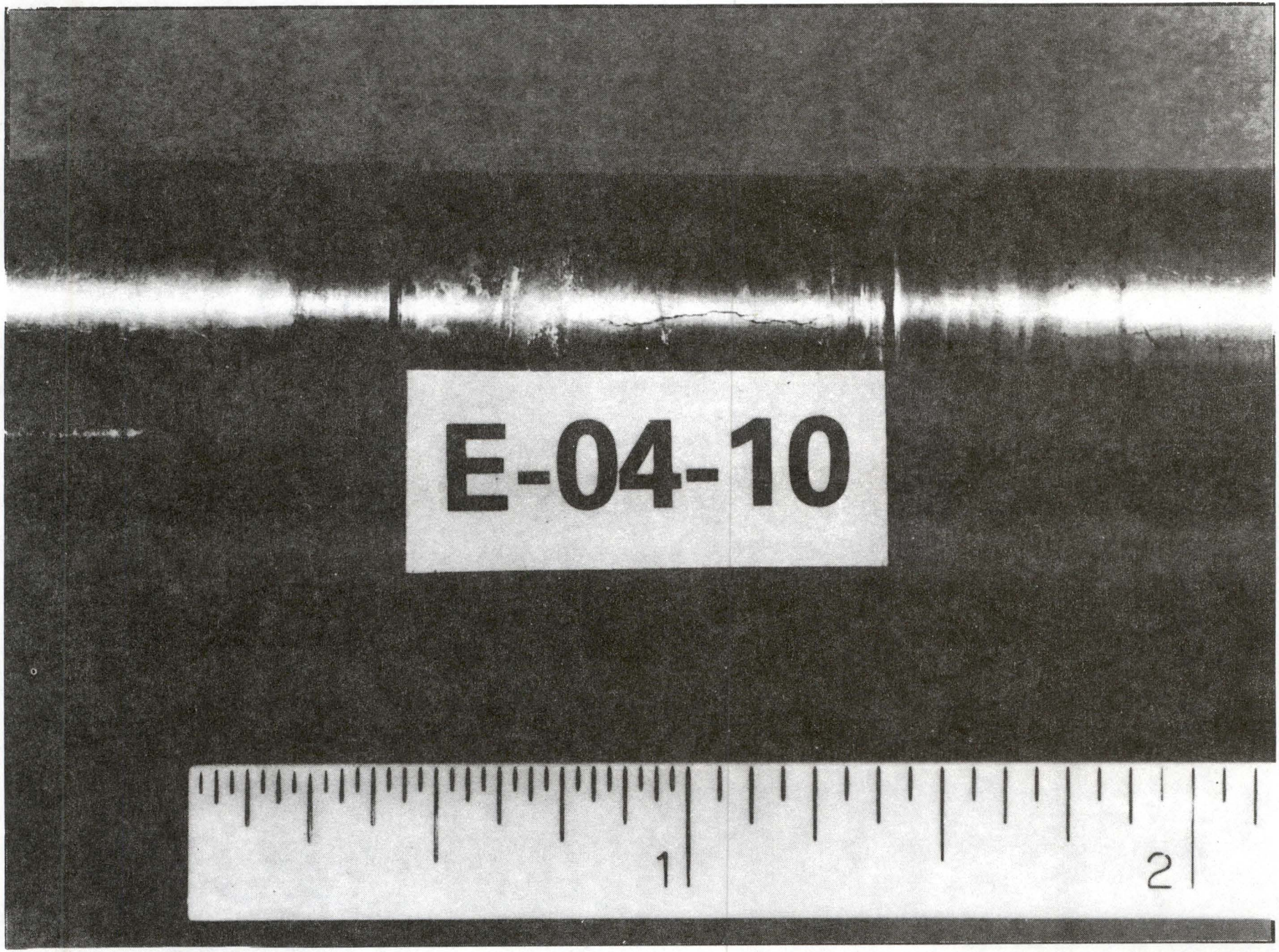

Figure 9. Specimen E-04-10 Before Leak Rate Test

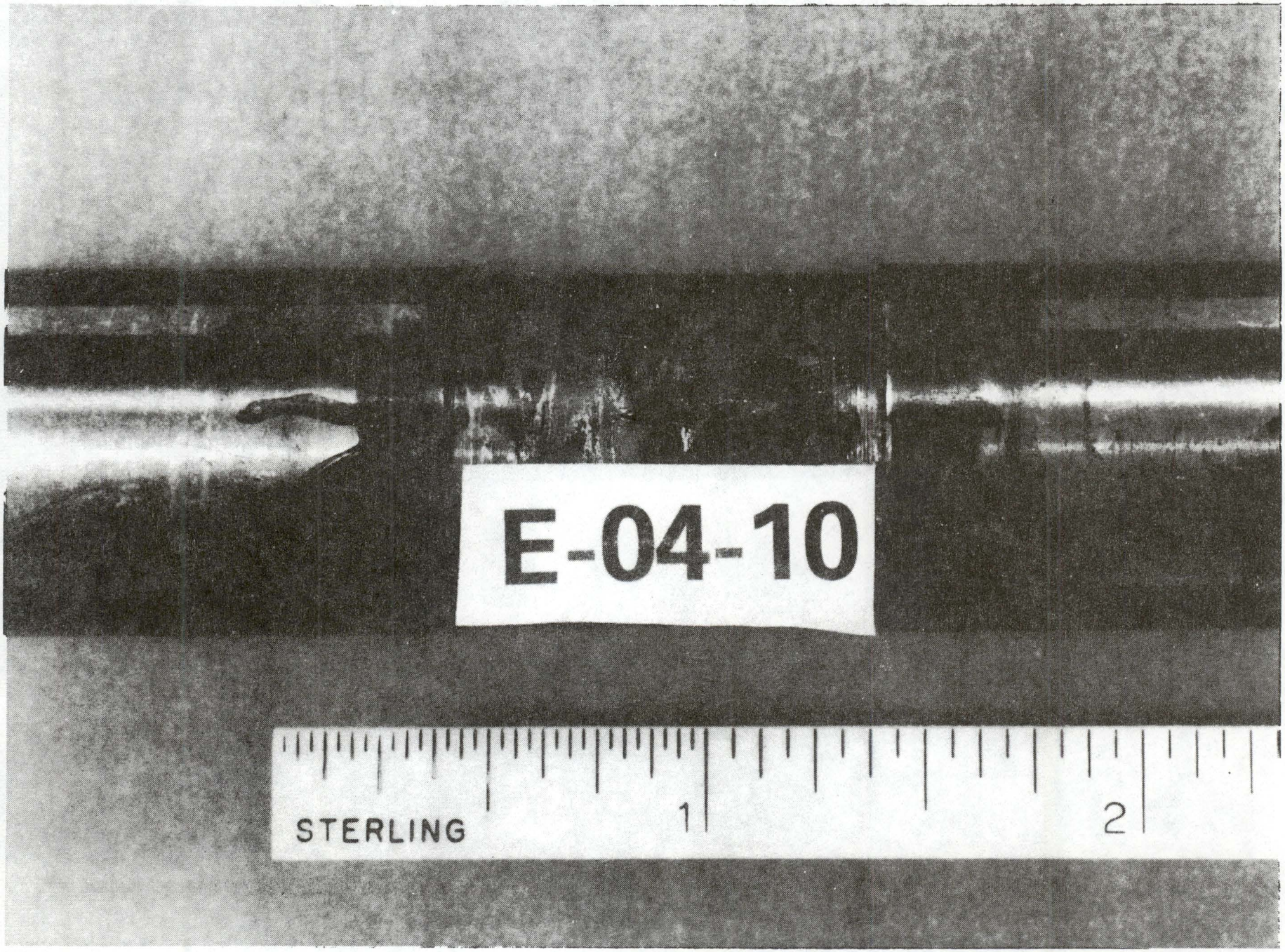

Figure 10. Specimen E-04-10 After Leak Rate Test

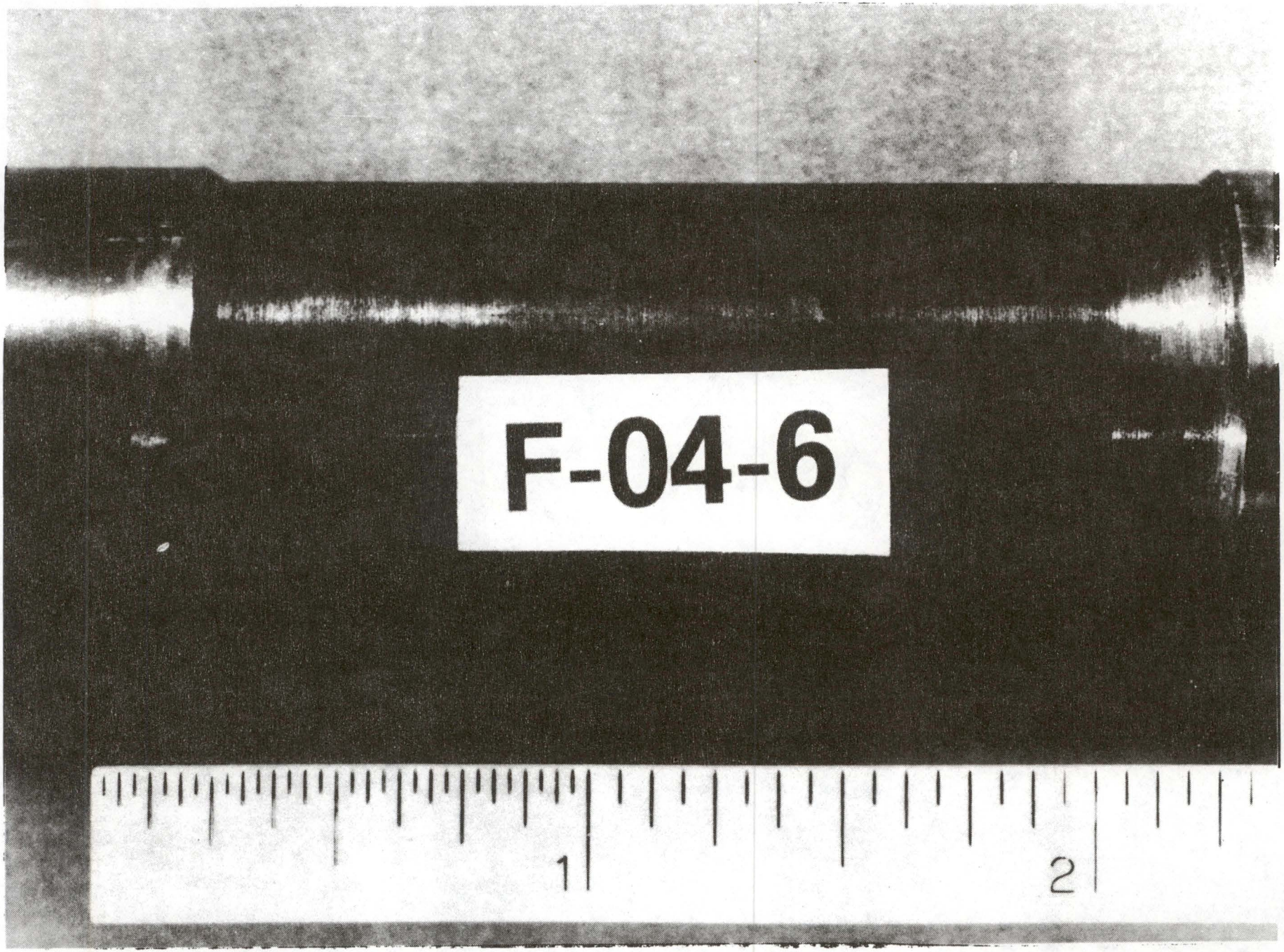

Figure 11. Specimen F-04-6 Before Leak Rate Test

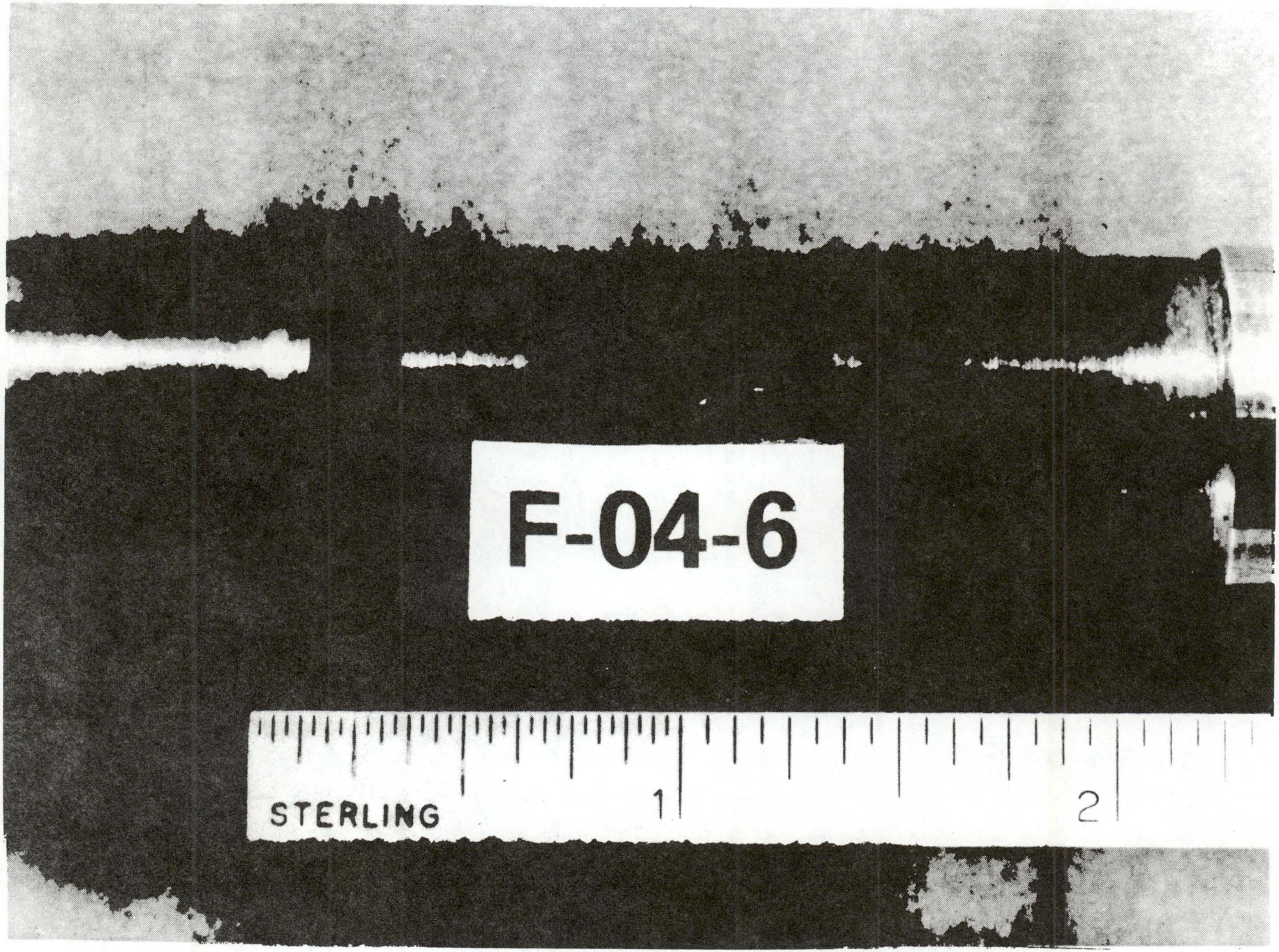

Figure 12. Specimen F-04-6 After Leak Rate Test

ENVIRONMENTALLY ASSISTED CRACKING IN LIGHT WATER REACTORS

Materials Science Division
Argonne National Laboratory
9700 South Cass Avenue
Argonne, Illinois 60439

PRESENTATION FOR THE NINTH WATER REACTOR SAFETY RESEARCH INFORMATION MEETING

October 30, 1981

ENVIRONMENTALLY ASSISTED CRACKING IN LIGHT WATER REACTORS (A2212)

Introduction

The objective of this program is to develop an independent capability for the detection and control of stress-corrosion cracking (SCC) in light-water reactor (LWR) systems and the evaluation of the technical merits of proposed remedies for the problem. Because the EPRI/BWR Owners Group Program is approaching completion and the NRC is being faced with decisions on the remedies developed by the Owners Group, the experimental work will initially concentrate on problems related to intergranular stress corrosion cracking (IGSCC) in BWR systems. However, ongoing research on other environmentally assisted cracking problems involving pressure vessels, nozzles, and turbines will be monitored and assessed, and where unanswered technical questions are identified, experimental programs to obtain the necessary information will be developed to the extent that available resources permit.

The current effort is divided into six subtasks: (A) Leak Detection and Nondestructive Evaluation, (B) Analysis of Sensitization, (C) Crack Growth Rate Studies, (D) Evaluation of Nonenvironmental Corrective Actions, (E) Evaluation of Environmental Corrective Actions, and (F) Mechanistic Studies. The specific objectives of each of the subtasks are discussed in subsequent sections.

A. Leak Detection and Nondestructive Evaluation

The detection of IGSCC through normal in-service inspections is very difficult. As a result, many through-wall cracks have occurred and early detection of leakage is necessary to identify the failed components. Although multiple leak-detection systems are required at present, no current method offers the proper combination of sensitivity, leak-locating ability, and leakage measurement accuracy. Acoustic emission techniques appear to represent the most promising approach for improvement in leak detection and will be the focus of our efforts on leak detection systems. The objectives of this subtask are to (a) determine the sensitivity, specifications, and calibration procedures for a prototype quantitative acoustic leak detection system, and (b) develop an independent capability to assess the effectiveness of current and proposed acoustic techniques to detect, locate, size, and characterize leaks in nuclear reactors.

To establish the effect of variables such as crack geometry and size, applied stress, temperature, and pressure on the structure, strength, and propagation characteristics of acoustic leak signals, laboratory tests will be carried out on a high temperature, high pressure test system (see Fig. 1). The acoustic signals (in the frequency range of practical interest) are generated primarily by the steam flow at the orifice exit. Hence, although the laboratory test system cannot completely simulate the reactor geometry, the acoustic signals should be characteristic of those generated in an operating reactor if the orifice geometry in the laboratory is characteristic of the actual crack geometry. Thus, in addition to simulated flaws where geometry and size can easily be controlled, tests will also be carried out with actual IGSC cracks obtained from field failures so that the signals from

actual cracks can be characterized and used to assess the adequacy of different types of simulated flaws. The complete test program will include tests to (1) characterize transducers, (2) evaluate methods for coupling transducers to piping, (3) determine the effect of orifice geometry and size, (4) determine the effect of pressure and temperature, (5) explore the relationship between leak rate and acoustic signature, (6) measure the attenuation of acoustic waves from leaks, (7) evaluate the capability of acoustic techniques to locate leaks, and (8) characterize the leak test loop to assure that the laboratory results are a valid representation of expected in-service experience.

As note previously the detection of IGSCC before the cracks have grown large enough to cause a leak is a very difficult. IGSCC that can be detected by conventional ultrasonic testing (UT) under laboratory conditions may be missed during a field examination even by the most skilled operator. To help overcome the shortcomings of existing methods, a number of advanced ultrasonic NDE techniques are being developed. However, the effectiveness of these techniques has not been demonstrated conclusively in a field environment. Thus alternate approaches which may be able to overcome these problems will be investigated. These include spatial averaging and detection based on the characterization of beam scattering patterns. These methods could improve detection and identification of cracks in the heat affected zone and increase the effectiveness of through-the-weld inspections by averaging out weld-metal noise.

Another approach which will be investigated is the use of horizontally polarized shear (SH) waves. These are currently difficult to use since a highly viscous or solid couplant must be used, which makes pipe inspection very slow. However, SH wave transducers fixed to the pipe can be used to monitor crack growth or electromagnetic acoustic transducers (EMATs) can be used. Current EMAT devices are not sensitive enough for detection of small IGSCC in stainless steel, but newer devices appear promising and work is planned to evaluate the use of these devices for through-weld inspections and the inspection of cast stainless steels.

B. Analysis of Sensitization

Sensitization of austenitic stainless steels such as Types 304 and 316 occurs in the temperature range of about 400-900°C under normal isothermal heat treatment. However, it has been shown that Type 304 SS may be sensitized at temperatures below the normal isothermal sensitization range if carbide nuclei are present at grain boundaries. This phenomenon is referred to as low-temperature sensitization (LTS). Extrapolation of current laboratory results indicates that in some cases Type 304 SS BWR pipe weldments that were not sensitized during welding could become sensitized, and thus susceptible to IGSCC within reactor lifetimes.

Information on the kinetics of LTS is available only for a few heats of Type 304 SS, and there are large variations in the apparent activation energy for different heats of material and types of specimen. This variation has been attributed to differences in the amount of strain, dislocation density, and/or impurity element content of the material, but at present the susceptibility to LTS of arbitrary heats of material cannot be assessed.

The possibility that remedial thermomechanical treatments, i.e., corrosion-resistant cladding (CRC), induction-heating stress improvement (IHSI), and heat sink welding (HSW), may improve the short term performance but leave the material vulnerable to LTS also needs to be investigated. For example, in the IHSI process, it is possible that the strain induced during the induction-heating cycle may influence long-term kinetics.

The potential for LTS in the proposed "Nuclear Grade" (NG) alternate materials, Types 304NG and 316NG SS needs to be investigated to qualify these materials for long-term service. Sensitization is suppressed in these materials; however, as long as some grain-boundary carbide nuclei are precipitated and remain in the material, the possibility of LTS does exist.

The development of more sensitive tests for sensitization has been an important concern of the NRC. Although not yet established as an ASTM practice, electrochemical tests for sensitization appear promising. The most widely studied test of this type is the electrochemical potentiokinetic reactivation (EPR) technique, the use of which is relatively well established for Types 304 and 316 SS. The applicability of the EPR technique to the alternate materials needs to be investigated. A correlation between IGSCC susceptibility and the degree of sensitization measured by EPR needs to be established and threshold EPR values for alternate alloys should be determined.

The objectives of subtask B then are to establish the importance of LTS of materials under long-term reactor operating conditions, and to evaluate the quantitative capability of the EPR technique to identify the susceptibility of piping material to IGSCC. The investigations to be conducted include: (a) studies on the kinetics of LTS and an assessment of predictive methods for LTS, (b) examination of possible adverse effects of stress-improvement remedies on LTS potential in alternate materials, (c) studies on the effect of LTS on IGSCC susceptibility, and (d) evaluation of the EPR technique and other types of sensitization measurements for applicability to alternate materials.

C. Crack Growth Rate Studies

The early instances of IGSCC in operating BWRs generally occurred in smaller pipes, and the response to the detection of IGSCC generally was to immediately repair or replace the cracked piping. It now appears that for reactors with standard Type 304 SS piping material, cracking can occur anywhere in the recirculation system, including the main recirculation line. Because of the severe economic consequences of long forced outages for repair or replacement, attention has been focused on the assessment of the remaining safe lifetime of flawed piping. Two problems must be considered, the slow growth and development of the crack by IGSCC and the relatively rapid growth and final failure under mechanical loading. Our concern in this program is only with the first problem, since the second problem is being addressed by other NRC programs. Understanding crack-growth behavior is, of course, important for other reasons besides assessing the safety implications of flawed piping. A better understanding would permit a more rational extrapolation of laboratory test results to the prediction of operating-plant behavior.

Current work on the measurement of crack growth rates seeks to characterize these rates in terms of the linear elastic fracture mechanics (LEFM) stress intensity as well as the level of sensitization and the amount of oxygen present in the coolant. However, both current mechanistic studies of crack growth and some experimental data indicate that, contrary to the LEFM model in which the crack velocity depends only on the current value of the crack-tip stress intensity K, the crack velocity depends strongly on the geometry of loading and on the nature of the remote external loading (constant extension rate, constant applied force, and constant displacement).

The work in this subtask is aimed at a evaluation of the validity of LEFM to predict IGSCC growth. The test program will focus on the effect of loading history and specimen geometry on crack growth in sensitized Type 304 stainless steel. Initial data will be generated on 1T compact tension specimens under constant load, slow-fast cyclic waveforms, and trapezoidal loading histories. A more limited range of tests will be carried out on surface-cracked panels.

D. Nonenvironmental Corrective Actions

The fundamental premise of the current efforts to prevent IGSCC in BWR piping is that IGSCC involves a complex interaction between material susceptibility (sensitization), the stresses acting on the material, and the environment, and that by suitably altering or varying these parameters immunity from IGSCC can be produced. Nonenvironmental corrective actions seek to mitigate either the material susceptibility or the state of stress on the inside surface of the weldment. It is convenient to classify the proposed nonenvironmental corrective actions into three groups: improved fabrication techniques, alternate materials, and residual stress improvement (RSI) techniques. The improved fabrication techniques include solution heat treatment, corrosion resistant cladding, and heat sink welding. The alternate materials most extensively studied are the low-carbon, controlled-nitrogen "Nuclear Grade" austenitic stainless steels, and carbon steel.

Current research programs sponsored by EPRI have generated an extensive data base on improved fabrication techniques and alternate materials. Many of the proposed remedies and alternate materials have demonstrated a clear superiority over Type 304 stainless steel in laboratory tests. However, the conditions in the laboratory tests differ from those experienced during in-service reactor operation in many respects. The most important differences appear to be in water chemistry and loading history. The majority of the tests have been carried out in a high-purity-water environment, although impurities such as chlorides and sulfates even at low levels that are within the water quality limits for an operating BWR are known to have a strong effect on the IGSCC susceptibility of sensitized Type 304 stainless steel. Similarly the loading histories employed in laboratory tests differ substantially from those encountered in an operating reactor. In order to carry out tests in a reasonable laboratory time scale the tests impose substantially higher stresses and plastic strains than would be encountered in service.

The primary objectives of this subtask are (1) to determine the effect of minor chemical impurities on the IGSCC susceptibility of Type 316NG stainless steel and Type 304 stainless steel weldments with IHSI treatments, (2) to

develop a better understanding of the effect of loading history on the IGSCC susceptibility of sensitized Type 304 stainless steel and to apply these results to the assessment and development of design rules such as the GE stress-rule, the critical strain/strain-rate model and the sensitive-location index proposed by EPRI, and to the general problem of extrapolating data obtained under laboratory loading histories to more realistic operating histories, and (3) to investigate the feasibility of an accelerated testing procedure which can be used to carry out parametric studies of environmentally assisted crack growth in Type 316NG stainless steel and thus obtain better estimates of the factor of improvement expected under in-service conditions than is currently available from the EPRI/GE program where testing has been carried out under a single set of test conditions.

Testing will focus on impurity levels (primarily chlorides and sulfates) and loading conditions which cause IGSCC in sensitized Type 304 stainless steel, although the relative susceptibility to transgranular SCC of Type 304 stainless steel and the alternate materials will also be checked to ensure that the new materials are at least no worse in this regard. We will investigate not only susceptibility under different loading histories, but will also closely examine deformation characteristics, i.e., how the applied stresses, imposed plastic strains, and residual stress affect the strain rates, since the current mechanistic understanding suggests that strain rate rather than stress or strain per se is the mechanical loading variable most directly related to IGSCC. Current work on the stresses and deformations associated with weldments are based on time-independent plasticity models of mechanical behavior. To develop a unified treatment of IGSCC under different loading histories it is necessary to understand the dependence of the strain rate on applied load and loading rate. Only a very limited amount of data is currently available on the stress/strain/strain-rate behavior of Type 304 stainless steel and additional data will be developed in this program.

E. Environmental Corrective Actions

During the past decade, it has been clearly established that the reactor coolant environment under both normal and off-normal water-chemistry conditions has a profound influence on the performance and reliability of nuclear power-plant components. The problems of intergranular stress corrosion cracking of weld-sensitized Type 304 stainless steel piping in BWRs, the accelerated corrosion of carbon steel support plates and the concomitant cracking of Inconel tubes in pressurized water reactor (PWR) steam generators, and the environmentally assisted cracking of turbine-disk materials are being evaluated by the NRC, reactor vendors, and electrical utilities relative to plant safety issues.

The objective of this subtask is to evaluate the potential effectiveness of proposed actions to solve or mitigate the problems primarily from the standpoint of water-chemistry modifications. The possibility of defining practical limits on water chemistry during off-normal transients will also be explored. As in the other subtasks, the initial emphasis will focus on stress-corrosion-cracking of austenitic stainless steels in BWRs.

Numerous studies have been undertaken to understand various aspects of the SCC process in sensitized austenitic stainless steels exposed to simulated BWR water environments at elevated temperatures. Information from slow- or

constant-extension-rate experiments has provided useful insight into the effects of temperature, strain rate, material composition, degree of sensitization, and water chemistry (viz, oxygen concentration) on SCC susceptibility; however, the large plastic strains involved in these tests are unduly severe and are not characteristic of reactor loading conditions. Also, the qualitative crack-growth data obtained from these experiments cannot be used with analytical models to determine the conservatism of present design methods regarding crack growth and the magnitude of acceptable initial flaw sizes in reactor components.

Crack-growth measurements on fracture mechanics type specimens in well-characterized, simulated reactor-coolant environments offer the most promise. In particular, the load waveform, frequency, and amplitude should typify conditions during long-term operation as well as during normal startup and other frequently encountered transients. Similarly, the influence of bulk water chemistry on crack initiation and growth during off-normal conditions must be established under chemical control where the corrosion potential of the material and pH of the solution are determined at the test temperature, and the concentrations of impurity anions are consistent with BWR operating experience. The dependence of crack-growth rate on changes in bulk coolant chemistry from off-normal to normal operating conditions will be investigated at several temperatures between ∿120 and 288°C. This information will be useful in establishing optimum procedures for minimizing crack growth during water-chemistry transients.

Since the addition of hydrogen to high-purity water is being considered as a method to suppress radiolytic oxygen and hydrogen peroxide formation in the BWR coolant and to preclude cracking of the material under reactor operating conditions, the influence of hydrogen, (with and without the presence of impurities) on the rate and mode of crack propagation will also be established. These experiments will provide quantitative crack-growth data on Type 304 stainless steel with different degrees of sensitization in simulated BWR environments that encompass the range of normal, alternate (0.5 ppm H_2), and off-normal water-chemistry conditions. The information can be used to determine the potential degree of improvement in SCC resistnce of the steel through implementation of more stringent control of water chemistry and the potential for better material performance through hydrogen additions to the reactor feedwater.

F. Mechanistic Studies

The specific mechanism(s) by which cracks propagate under stress-corrosion conditions remains a matter of considerable controversy. On the other hand, a great deal has been learned about the general characteristics of SCC. These developments in turn enable a more rational use and extrapolation of experimental test results and provide the framework for the development of predictive models for specific systems of material and environment.

SCC occurs under a specific range of conditions in which the relative rates of straining (leading to fracture of protective films) and repassivation (i.e., reforming the protective film) are the critical factors in crack growth. Thus, studies of the actual processes of deformation at crack tips, the mechanical properties of the protective films, and the actual solution chemistry within the crack (which strongly influences the properties of the

film and the rate of repassivation) are of fundamental importance regardless of the specific physical mechanism by which crack advance occurs in the time period between film rupture and reformation. Understanding of these subprocesses themselves has important practical implications. More detailed knowledge of crack-tip deformation will lead to a better understanding of the role of load history on crack propagation. The relationship between bulk chemistry and chemistry at the crack-tip is important in developing meaningful laboratory tests and in assessing the effectiveness of bulk chemistry control in mitigating SCC.

However, a predictive model for SCC requires an understanding of the specific mechanism for crack advance. There are two principal hypotheses, one, that advance occurs by the anodic dissolution of metal at the crack tip, and another which suggests that the crack tip undergoes hydrogen embrittlement (HE) followed by mechanical fracture.

A method to distinguish between hydrogen embrittlement and dissolution as the predominant crack-advance mechanism involves the effect of hydrostatic tension. All current models for HE in some manner require hydrostatic tension to concentrate the hydrogen atoms in a critical region. On the other hand, the dissolution rate is thought to depend primarily on the local pH/potential condition at the crack tip and not on the state of stress. Thus, studies have been made to compare Mode I (uniaxial tensile) with Mode III (anti-plane shear) loading. In some systems the two modes give equivalent cracking propensity, which seems to rule out HE. However, in other systems susceptibility is considerably reduced in Mode III, indicating a significant but not exclusive role for HE, whereas for still other systems essentially no susceptibility has been reported in Mode III, indicating a dominant HE contribution. Such studies have not yet been reported for austenitic stainless steels. On the other hand, the crack propagation rate for ductile alloys in various aqueous environments is directly proportional to the measured current density on a freshly exposed alloy surface (following rapid straining to fracture the protective film), which strongly supports the anodic dissolution model.

The concept of a critical range of strain rates at the crack tip to obtain susceptibility in a given material/environment system has been strongly supported by the widespread use of the constant-extension-rate tests for both fundamental and screening purposes. The concept also provides a rational method for correlating SCC under fixed load, stress relaxation, or cyclic-load conditions, i.e., the major requirement is to attain the critical strain-rate regime, independent of how it is obtained.

There is evidence that below the critical strain-rate regime, SCC does not occur. This is consistent with the often reported "threshold" stress or stress intensity. However, it is known that application of a cyclic component of load can significantly increase the amount of plastic deformation. This implies that cylic loads can reduce the apparent thresholds, and this has been reported for a number of systems. If the cyclic amplitude is large, the fracture mechanism or mode may change, e.g., IGSCC may change to transgranular corrosion fatigue, but for sufficiently small amplitudes, this should not occur. Also, a significant strain-rate dependence might be expected since creep deformation typically exhibits a strong temperature (and hence strain rate) dependence.

Finally, the entire question of a critical strain-rate requirement in the vicinity of the crack tip brings in the question of how the local stress, strain, strain-rate behavior relates to the applied loading conditions. There is evidence that the local dislocation structure and slip pattern near the crack tip are closely related to the crack advance, and in some systems a possible relationship between "striations" on the crack surface and the spacing of dislocation sources has been observed. The initial investigations in this subtask will include the analytical and experimental study of the relationship between bulk chemistry and crevice or crack chemistry, characterization of passive films as a function of water chemistry and local alloy composition, study of the dislocation structure near stress corrosion crack tips, evaluation of the effect of low-amplitude, low-frequency cyclic loads on threshold stresses and crack propagation rates, and experiments on the effect of crack growth made to determine the relative importance of hydrogen embrittlement in the IGSCC of LWR steels.

Progress

Since the official start of this program in April 1981, the primary focus of our experimental efforts has been on the development of experimental facilities. The leak detection loop is virtually complete. Figure 1 shows a general schematic of the system, which consists of ∿30 feet of 10-in. Schedule 80 piping welded into a "U" shape. One end of the piping, to be used for testing radioactive pipe sections with field-induced leaks, will pass through an exhaust hood to prevent any radioactivity from entering the room during testing. The other end of the pipe run will be used to test nonradioactive pipe sections containing artificial leaks and laboratory-grown cracks.

The conceptual design for supplying pressurized hot water to the leak site is shown at the lower left of Fig. 1. A small cap (∿40 mm in diameter and 6 mm deep) is welded to the inner surface of the pipe section that contains the leak. After tubing is connected to the cap, the section is welded or soldered into an opening in the wall of a 10-in. pipe, which is then welded to the rest of the piping to complete the "U".

Transducers will be placed at several locations along the pipe run to acquire acoustic data from the leaks, and establish attenuation characteristics and leak location capability. Mirror insulation of the type used in reactors will be installed on sections of the piping to determine any effects on acoustic signal generation and attenuation. The pipe will be filled with water; however, for high-temperature tests, the region near the crack will not be in contact with water. This is necessary to reduce the heat sink and permit the cracked region to be heated efficiently.

Two methods of providing high-pressure, high-temperature water are being incorporated into the test facility. One employs a Pulsafeeder pump, which will provide a continuous supply of hot water at high pressure (up to 14 MPa) but at low flow rates (<0.1 gal/min.). High flow rates, when needed, will be provided by a high-pressure, high-temperature reservoir. This higher flow rate can be maintained for a relatively short time (several minutes or less). Acoustic signals will be put on tape or digitized and stored in the computer for signal analysis work. Lines going to the crack or artificial leak will be heated to maintain reactor-like temperatures.

Experimental facilities for conducting IGSCC tests on materails in simulated reactor-coolant environments have been procured and assembled. An Instron machine with low strain-rate capability ($\sim 10^{-7}$ s^{-1}) and an MTS system have been equipped with high-pressure autoclaves and small circulation loops to control the purity of the water. A second MTS system is nearly complete. Instrumentation to monitor water quality (pH, conductivity, and oxygen concentration) at the inlet and outlet of the autoclaves is also in place. A schematic of the loop for the MTS system is shown in Fig. 2. A high-temperature pH sensor and a reference electrode for installation in the autoclaves were assembled and tested. Upon completion of several modifications, a high-temperature pH sensor and reference electrode for monitoring the corrosion potential of the specimen material will be installed in each of the autoclaves. A schematic of the reference electrode is shown in Fig. 3.

Figure 4 shows a schematic of a small-diameter "pipe" autoclave system which is used for experiments on smooth tensile specimens. The reference electrode is located in a "stand off" to avoid any possible Cl^- contamination of the specimen. A similar arrangement is used on the large autoclaves.

Subcontracts have been placed with E. F. Rybicki of the University of Tulsa for analytical studies of the stress redistribution near weldments and with D. Prine of GARD Inc. for characterization studies of the acoustic-emission signals from leaking cracks. A subcontract with Battelle-PNL to carry out the pipe testing portion of the program is nearly complete.

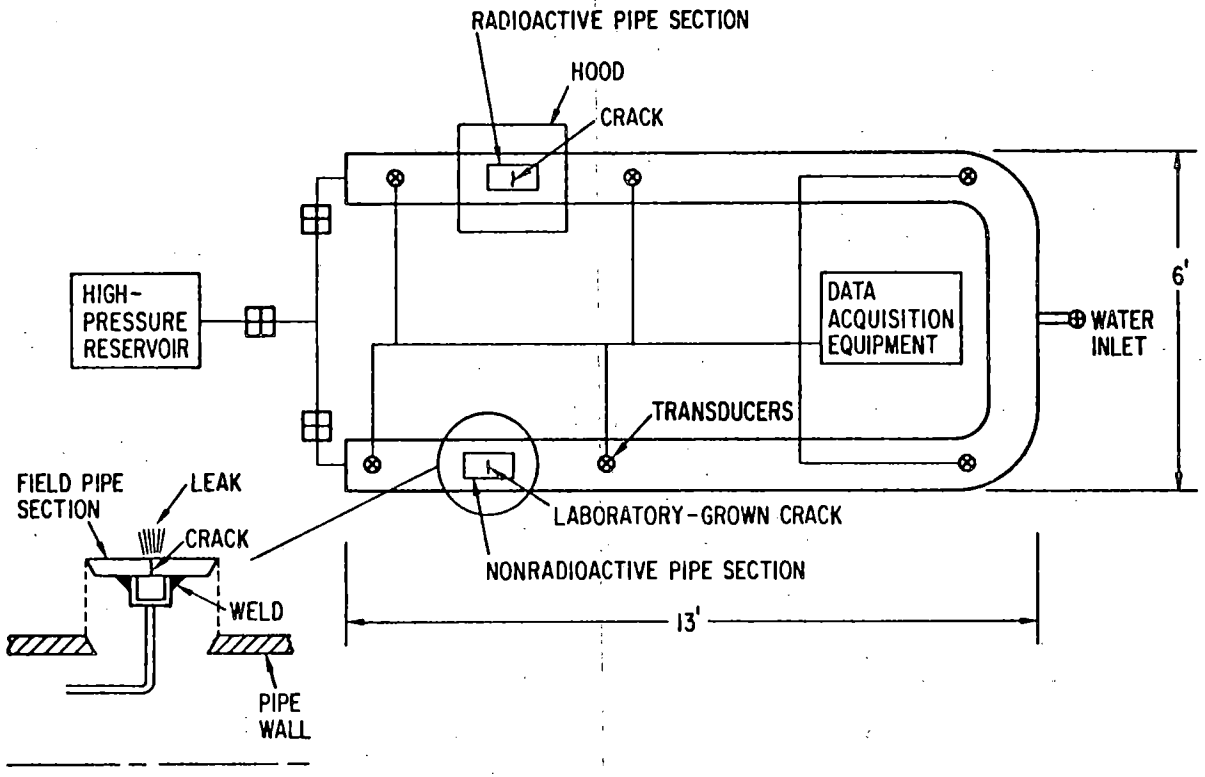

Fig. 1. Schematic of Leak Test Loop.

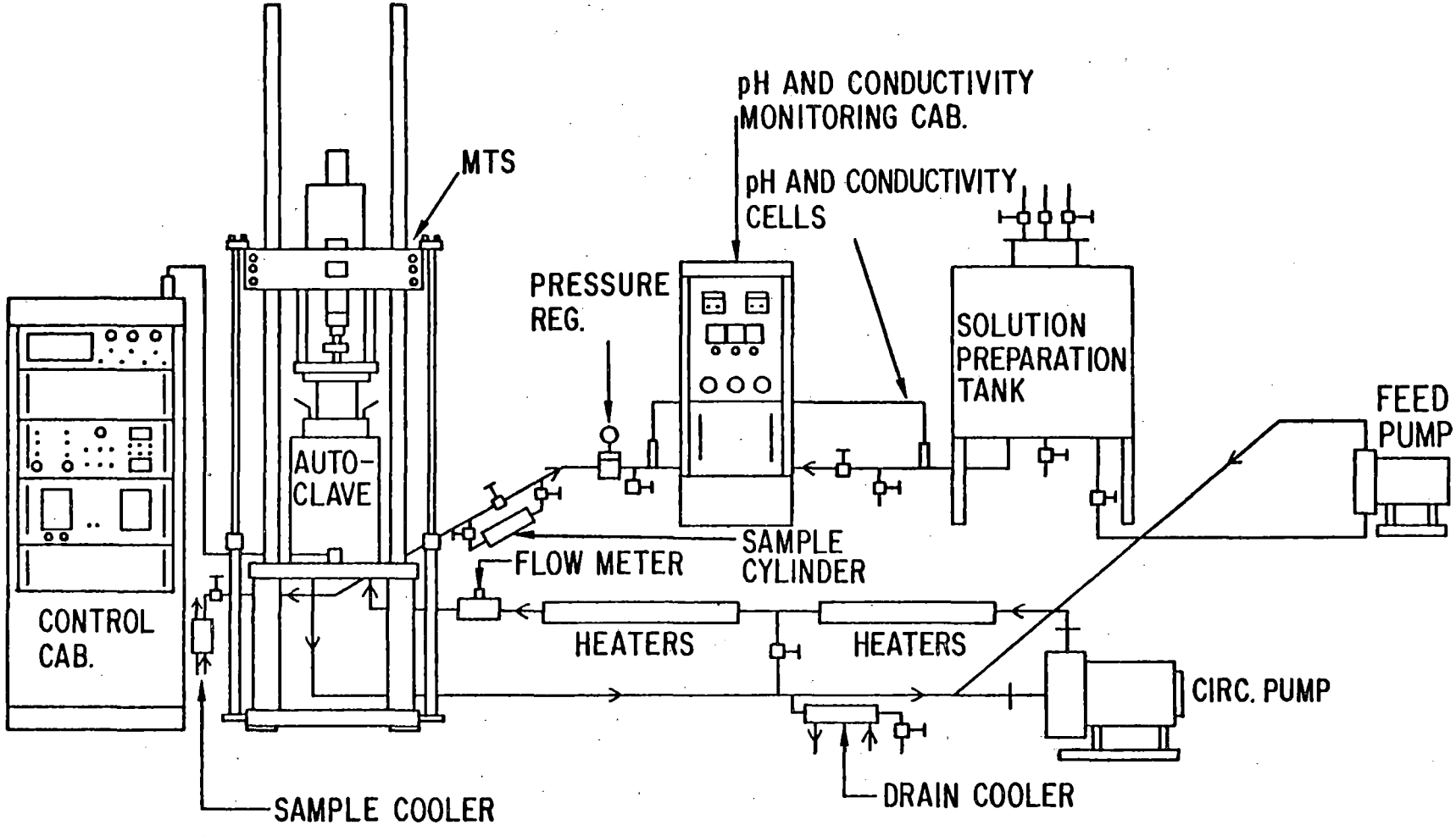

Fig. 2. MTS System and Circulating Loop.

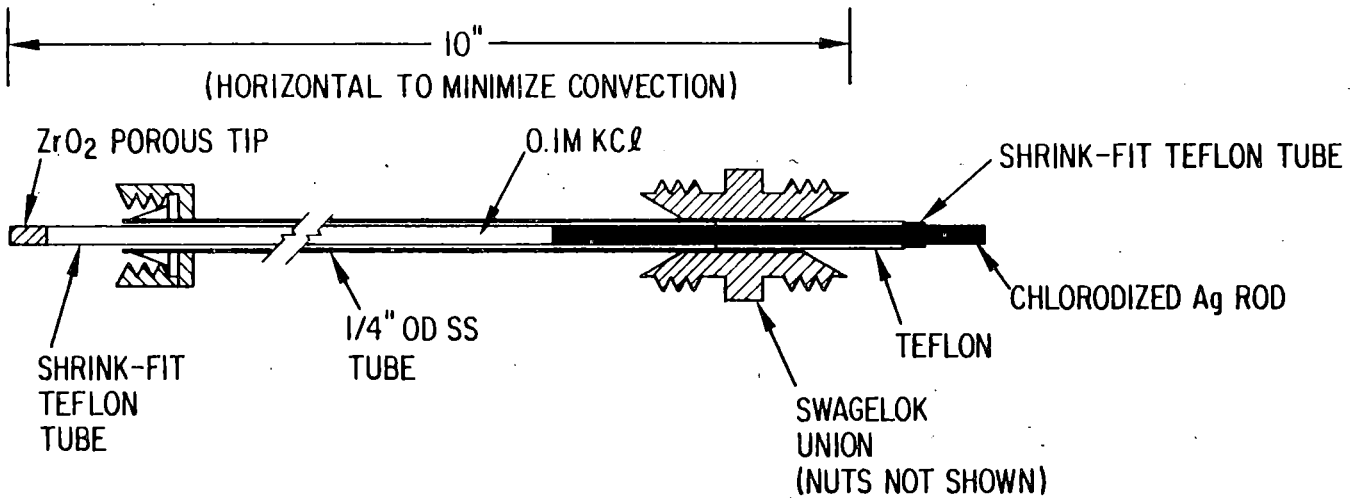

MODIFIED DANIELSON ELECTRODE

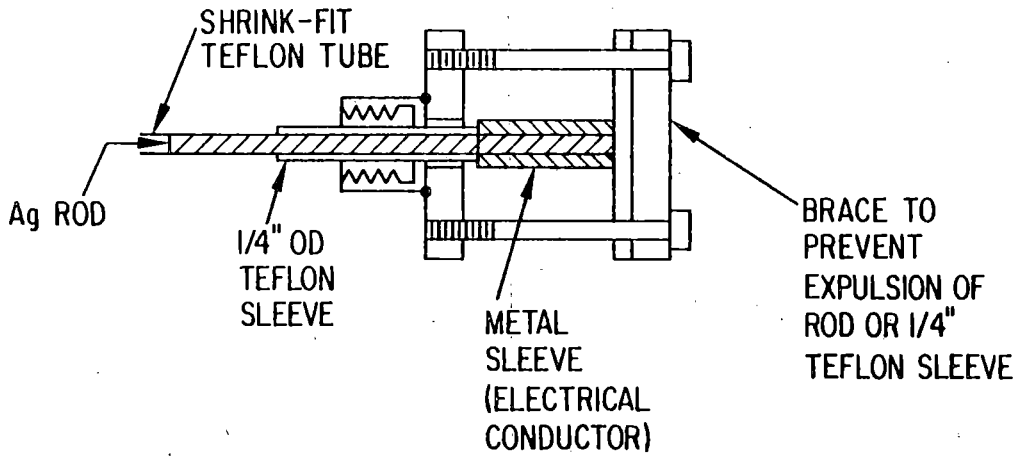

DETAIL OF CLOSURE AROUND SILVER ROD

Fig. 3. Reference Electrode.

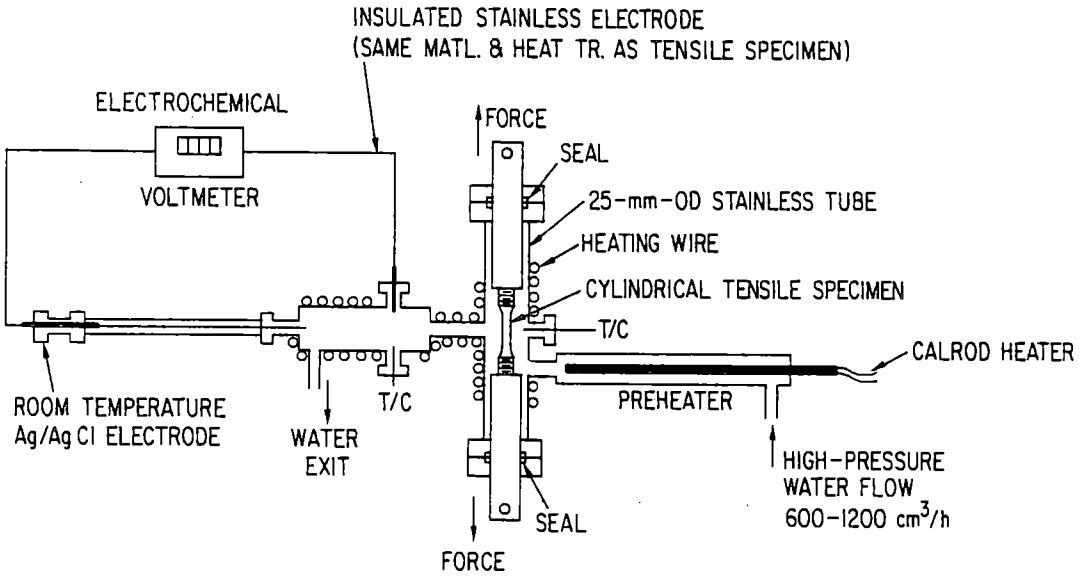

Fig. 4. Small Autoclave for Tensile Specimens.

PNL-SA-9977

ACOUSTIC EMISSION - FLAW RELATIONSHIP FOR INSERVICE MONITORING OF NUCLEAR REACTOR PRESSURE BOUNDARIES

P.H. Hutton, Project Manager
R.J. Kurtz, Assistant Project Manager

October 1981

Presented at the Ninth Water Reactor Safety Research Information Meeting
Gaithersburg, Maryland
October 26-30, 1981

Work Supported by the U.S. Nuclear Regulatory Commission under a Related Services Agreement with the U.S. Department of Energy under Contract DE-AC06-76RLO-1830

Pacific Northwest Laboratory
Richland, Washington 99352

ACOUSTIC EMISSION - FLAW RELATIONSHIP FOR INSERVICE MONITORING OF NUCLEAR REACTOR PRESSURE BOUNDARIES[a]

Contractor: Pacific Northwest Laboratory
P.H. Hutton, Project Manager
R.J. Kurtz, Assistant Project Manager

Sponsor: NRC, Engineering Technology Division
Materials Engineering Branch
Dr. J. Muscara, Program Manager

OBJECTIVE

The objective of the acoustic emission (AE)/flaw characterization program is to provide an experimental feasibility evaluation of using the AE method on a continuous basis (during operation and during hydrotest) to detect and analyze flaw growth in reactor pressure vessels and primary piping. This effort is based on the philosophy that AE shows demonstrated capability for being a valuable addition to current nondestructive inspection (NDI) methods with unique capability for continuous monitoring, high sensitivity and remote flaw location.

NEEDS ADDRESSED

This program addresses the following areas of significance:

- In older reactors, effective inspection of the vessel by conventional methods is extremely difficult. AE can help assure structural integrity by being used to monitor these vessels to detect and locate active flaws, facilitate an estimate of severity based on AE and localize shielding penetration location(s) for flaw inspection by conventional methods.

- Conventional NDI of nozzles and primary piping can be difficult and costly of personnel radiation exposure. AE could detect the presence of an active flaw and maintain surveillance of flaw growth to assure that it remains within safe limits. Availability of such a monitoring system would also reduce personnel exposure by minimizing the need for conventional NDI.

- As a secondary benefit, AE systems provide a sensitive detector of leaks as well as cracking in piping. They can also be adapted to sensing flow - no flow in critical valves.

---

[a] Prepared for the 9th Water Reactor Safety Research Information Meeting, National Bureau of Standards, Gaithersburg, MD, October 26-30, 1981.

SCOPE

The program scope is described by three primary areas of effort:

- Develop a method to identify crack growth AE signals as unique from other innocuous but similar acoustic signals.
- Develop a relationship between measured AE and crack growth which will enable an estimate of flaw severity based on measured AE information.
- Demonstrate the total concept through off-reactor vessel tests and finally, on-reactor monitoring. This includes developing the necessary instrumentation system.

The program started with testing laboratory specimens to determine fundamental feasibility of program objectives using ASTM A533B, Class 1 steel. This first phase is essentially completed. Since theoretical transfer of these results to a full size structure is very questionalbe in this case, the next phase calls for testing on a heavy section (> 100 mm wall) vessel to check laboratory results and establish criteria more directly relatable to a reactor vessel. Vessel testing is to include a simulation of pertinent reactor environment conditions (background noise, flaws exposed to pressurized and heated water, etc.) excluding nuclear radiation. The final phase requires installation and operation of a prototype AE monitor system on an operating reactor on a test basis to check vessel results and finalize application methods and system.

RESULTS

The pattern recognition method for identifying crack growth AE and the AE/fracture mechanics relationship for flaw evaluation developed under Phase 1 were discussed at the 8th Information Meeting in 1980. They will, therefore, not be included again here.

Major new accomplishments this year are:

- Arrangements for performing a vessel test have been completed and preparation for the test is about 75% complete.
- An AE test system has been installed on a new power reactor and monitoring of preservice testing is in progress.
- A specialized AE monitor and analysis system has been completed and laboratory tested.
- Irradiated fracture specimen tests at NRL were AE monitored.
- AE/weld monitoring was demonstrated on fabrication of a Plate Inspection Steering Committee (PISC) 2 test specimen in Germany.

DISCUSSION

Further detail on each of the accomplishments is provided below.

VESSEL TEST

Preparations for testing an intermediate scale pressure vessel in collaboration with the West German Materialprufungsanstalt (MPA) are nearly complete. The test will be performed in Stuttgart and Mannheim, West Germany starting in February 1982, for a period of approximately three to four months.

The MPA test vessel, ZB1, is a 120 mm thick, 1712 mm O.D. cylindrical vessel made from nominally A508 steel (see Figure 1). Since this program is focused on A533B steel, the center 1500 mm of the vessel cylinder has been modified, as shown in Figure 2, to incorporate a patch of this material. The Battelle patch was machined from an 210 mm thick plate and contains three part-circular surface flaws, which have been fatigue presharpened by internal notch pressurization. Two of the flaws are on the inside surface of the patch and one is on the outside surface. The notch geometries for the three flaws are given in Table I.

Table I

Geometry of Notches in A533B Patch

Notch	Location	Depth (mm)	Surface Length (mm)
A	I.D.	22	54
B	I.D.	32	81
C	O.D.	48	190

The notches were precracked to produce approximately 7 mm of crack growth. The aspect ratio of each notch was designed to provide a nearly constant stress intensity along the periphery of the notch root. Different flaw depth-to-wall thickness ratios were chosen for each notch to provide a spectrum of stress intensity factor ranges for constant pressure vessel loading conditions. The longitudinal axes of the flaws are perpendicular to the circumferential stress in the vessel.

The test sequence (see Figure 3) was designed to investigate flaw detection and evaluation by AE methods under both operating and hydrotest conditions.

To simulate reactor pressure vessel loading conditions, the test vessel will be internally pressurized with water at temperatures of 90 and 288°C. The water pressurization system will provide constant amplitude cyclic, as well as monotonic mechanical stressing of the vessel. The cyclic frequency will be about 1 cycle per minute. Blocks of pressure cycles will be applied at R - ratios (R = minimum pressure/maximum pressure) of 0.1 and 0.6. These high and low R - ratio loading blocks will be alternated and are designed to produce approximately equal amounts of crack growth at each R - ratio. Hydrotests will also be performed during the test. Successive overpressures will start at 1.0 and increase to 1.4 times the maximum cyclic pressure (see Figure 3).

One of the important objectives of the vessel test is to evaluate the effect of various reactor background noises on AE monitoring. This relates to both basic detection of the AE signal and to identification of crack growth AE signals from innocuous noise signals.

One major source of noise is the reactor coolant circulation system. Measurements of this noise taken on operating reactors shows it to be very high relative to AE signal levels at low frequencies (< 100 kHz). However, with increasing frequency, it diminishes until at about 400 kHz, it is down near the electronic noise level of the measurement system. The planned approach to simulating reactor flow noise at a localized area is to drive a transducer located on the inside surface of the vessel with a shaped electrical input.

Mechanical rubbing of thermal insulation on the exterior of the vessel is a potential noise source to be simulated by covering the vessel with blanket-type glass fiber insulation except for an approximately 200 mm wide band of mirror insulation around the vessel cylinder.

Mechanical stressing of weld slag inclusions may produce noise similar to acoustic emission. To investigate this, a 100 mm long strip of slag inclusions shall be incorporated in the A533B insert-to-vessel weld denoted in Figure 2. The size of the slag inclusions will be measured prior to vessel testing by nondestructive means (e.g., x-ray and UT) and confirmed by post-test destructive testing.

Potential base metal-to-weld cladding interface noise will also be investigated. To simulate this potential noise source, a 4 mm thick patch of stainless steel weld overlay cladding will be deposited on the inside surface of the 750 mm circular repair plug (see Figure 2). Two 50 x 100 mm areas of intentionally defective weld cladding will be included on the plug. One area will contain underclad cracks and the other will have poorly bonded clad. The two defective areas will be separated from each other by at least 500 mm.

Electrical transients will also be introduced by methods such as spark discharge or turning electric motors on and off.

REACTOR MONITORING

Arrangements were made with the Tennessee Valley Authority to perform AE testing on their Watts Bar Unit 1 reactor. Figure 4 identifies the areas to be monitored. The bases for their selection are:

- No. 2 Inlet Nozzle

  Nozzle regions are a generic area of high stress. In addition, the No. 2 nozzle contains a Code acceptable level of underclad cracking.

- Safety Injection Pipe

  The safety inspection pipe adjacent to the No. 2 cold leg represents a convenient location to install a crack growth specimen in an area exposed to reactor hydraulic noise. The specimen will be acoustically coupled to the pipe and thus simulate a crack growth condition in the pipe. This is an important element of the test to demonstrate detection of crack growth AE in the reactor environment.

- Vessel Wall

  Installing sensors to monitor a segment of the vessel wall will test the capability to monitor this very limited access portion of the vessel. This section of the vessel contains a fabrication girth weld which is extremely difficult to inspect directly by other NDI methods.

Installation of wave guide sensors at the three locations was completed between September 24 and October 7. Figures 5, 6 and 7 show the specific sensor arrangement. Figure 8 shows the 50 mm thick crack growth specimen installed on the safety injection pipe.

Temporary signal leads have been strung to a central point from which preservice pressure testing can be monitored. Permanent leads for reactor operational monitoring will be installed later.

Monitoring of cold hydrostatic testing was started October 15.

The objectives of reactor monitoring include:

- Test the AE system integrity in the true reactor environment.
- Evaluate the ability to distinguish between background noise and crack growth AE.
- Demonstrate the ability to detect and evaluate AE from crack growth.
- Determine that false flaw indications can be avoided.

AE MONITOR SYSTEM

The AE monitor system designed to validate advanced data processing and analysis methods developed under Phase 1 has been completed. In Figure 9, the system is shown during laboratory testing with sensor arrays on a section of 660 mm diameter pipe. This system will be used for monitoring the ZB-1 vessel test and also for initial reactor monitoring.

The Dunegan/Endevco 1032 AE monitor is used to determine AE source location and associated signal parameters such as peak time, duration, etc. This information together with the parametric features is stored on floppy disks and it also goes to the Digital Equipment Corporation PDP 11/03 computer for on-site analysis.

Digitized signal waveforms are recorded on tape in parallel with processing through the D/E 1032 system. These waveforms are then played back to the PDP 11/03 for evaluation by pattern recognition.

The PDP 11/03 is also used to sort pattern recognition information on the basis of a source location derived from the D/E 1032 system. Data identified by pattern recognition as crack growth AE and associated with a specific location will be used to estimate flaw severity.

An important feature of the system is the provision for storing all of the basic data (source location, signal features and digitized waveforms). This will facilitate post test analysis to improve and refine AE signal identification and interpretation models.

IRRADIATED FRACTURE SPECIMENS

A series of irradiated and unirradiated 4T compact tension fracture specimens of A533B weldment were tested at NRL in FY81. This provided an opportunity to evaluate the effect of irradiation on detectable AE from fracture in A533B.

Figure 10 gives the preliminary results from AE monitoring two of the irradiated specimens. The specimen arrangement is also shown on the right. The two irradiated specimens show fairly similar AE responses with the total number of signals somewhat low in both cases. Load, crack opening displacement and crack length data for both specimens has been requested from NRL to facilitate a more meaningful analysis of AE versus fracture mechanics.

We plan to obtain AE data from an unirradiated specimen for comparison during FY82.

AE/WELD MONITORING

In process AE monitoring of welding to detect flaws was demonstrated during fabrication of a PISC-2 test specimen in Germany. This work was performed as part of the NRC-German technical exchange agreement.

The demonstration was performed by GARD, Inc. under a subcontract from this program. An instrument system developed earlier under NRC sponsorship was used. The specimen (Figure 11) will comprise one of the PISC 2 specimens for evaluating weld flaw detection by various NDI methods. The entire weld is to be inspected nondestructively at the Institut für Zerstörungsfreie Prüfverfahren (IzfP) in Saarbrucken, West Germany. A 300 mm length of one end of the weld is then to be destructively tested at Materialprüfungsanstalt (MPA) in Stuttgart, West Germany. We are awaiting these examination results to complete an evaluation of the AE monitoring effectiveness. Preliminarily, however, based on the intended flaws inserted, the following results were obtained:

- Detection: All cracks, three of four porosity zones, and the one slag inclusion were all detected. There appeared to be no "overcalls" - i.e., indication of nonexistant flaws.

- Classification: The classifier used classifies all defects as either a crack or slag. All cracks were correctly classified. The porosity zones were classified 67% as cracks and 33% as slag. The one slag inclusion was called a crack.

The preliminary assessment is quite encouraging. Ultimately, the AE results can be weighed in light of results obtained with other NDI methods under PISC 2.

FY82 PLANS

The major tasks planned for FY82 are:

- Perform the ZB-1 vessel test and analyze the results.

- Monitor preservice pressure tests at Watts Bar, Unit 1, evaluate results and prepare for inservice monitoring.

- Develop an engineering prototype AE monitor/analysis system.

- Characterize AE from piping material and relevant piping failure mechanisms.

- Guided by ZB-1 vessel test results, perform laboratory tests as needed to provide definition of the reliability of AE/flaw detection during inservice hydro testing.

PUBLICATIONS

Quarterly Report, October 1 - December 31, 1980, P.H. Hutton, R.J. Kurtz, NUREG/CR-1454, PNL-3380-4, Vol. 4, April 1981

Quarterly Report, January 1 - March 31, 1981, P.H. Hutton, R.J. Kurtz, NUREG/CR-2127, PNL 3801-1, Vol. 1, July 1981.

Quarterly Report, April 1 - June 30, 1981, P.H. Hutton, R.J. Kurtz, NUREG/CR 2127, PNL 3810-2, Vol. 2, September 1981.

Quarterly Report, July 1 - September 30, 1981, P.H. Hutton, R.J. Kurtz, NUREG/CR-2127, PNL 3810-3, Vol. 3, November 1981 (anticipated).

CREDITS

Primary among other Battelle staff members contributing to this work are: J.R. Skorpik, T.T. Taylor, J.F. Dawson, D.K. Lemon, L.J. Busse, R.P. Gribble, R.A. Pappas, R.B. Melton and P.G. Doctor. Their contributions are gratefully acknowledged.

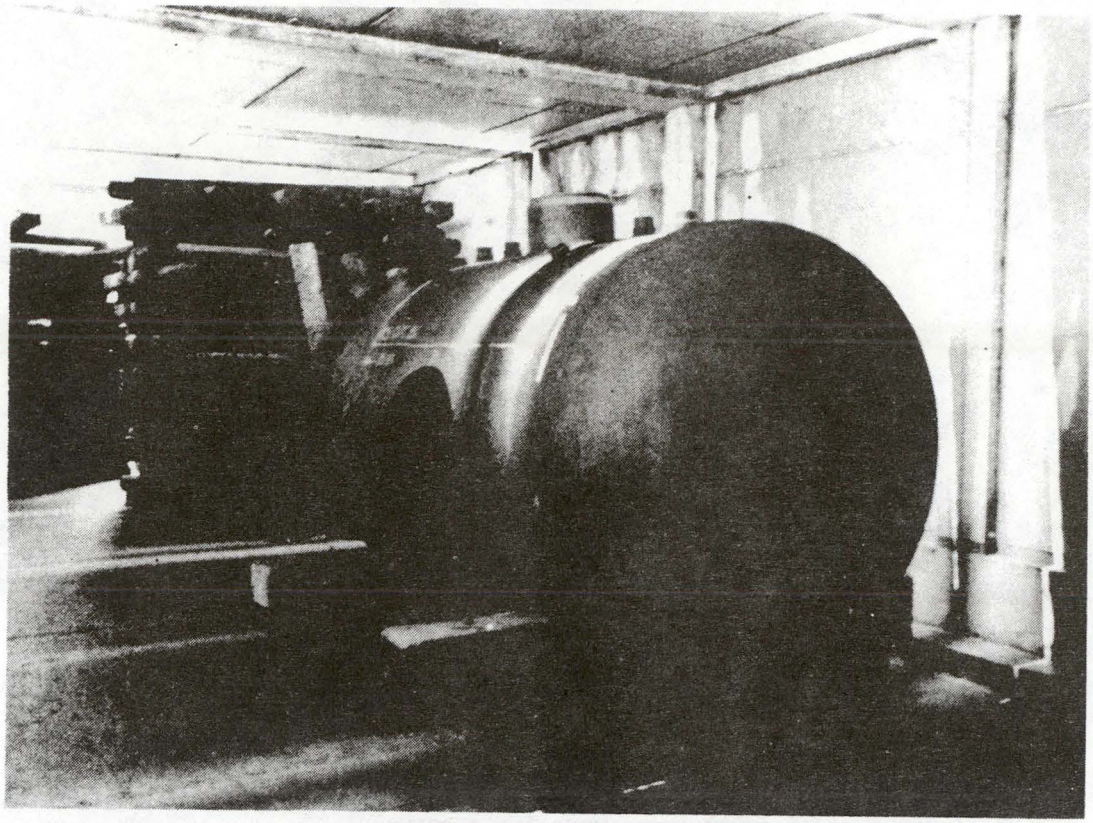

Figure 1. ZB-1 Test Vessel Unmodified.

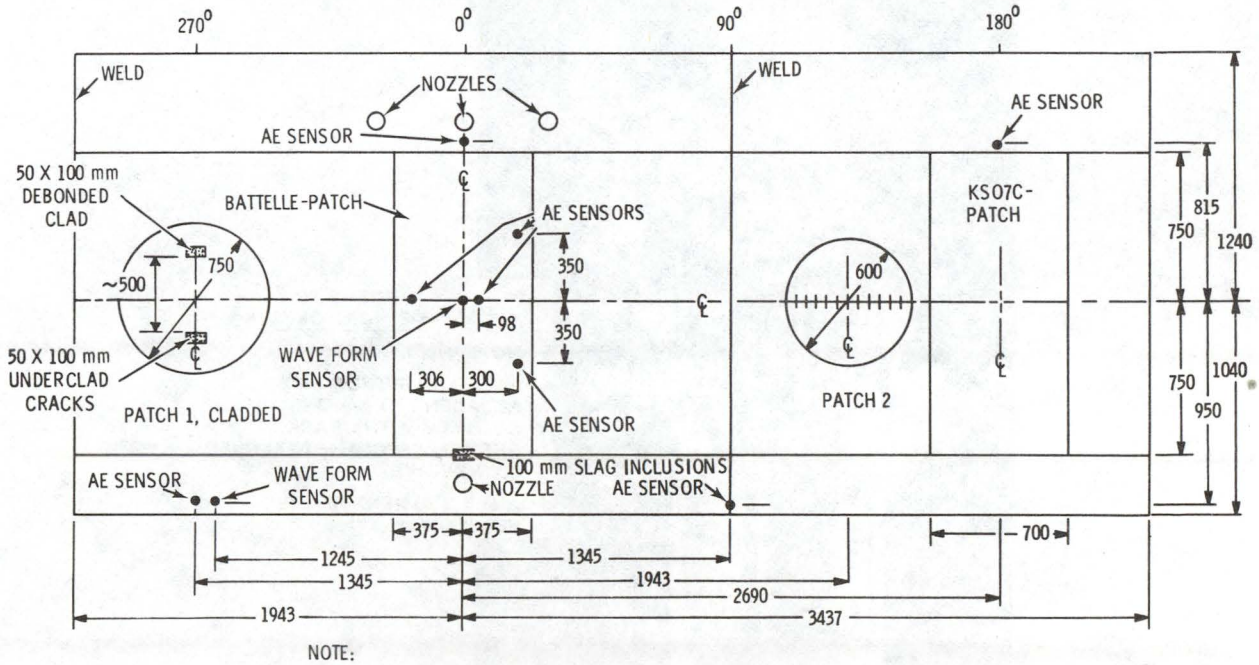

NOTE:

1) DIMENSIONS IN MILLIMETERS
2) AN ULTRASONIC NOISE SIMULATION TRANSDUCER WILL BE MOUNTED ON THE INSIDE CENTER OF THE PATCH
3) ALL AE SENSORS WILL BE METAL WAVE GUIDES
4) AE SENSORS ON THE PATCH WILL BE MOUNTED IN DRILLED AND TAPPED HOLES. ALL OTHER SENSORS WILL BE PRESSURE COUPLED USING MAGNETIC MOUNTS

Figure 2. ZB-1 Vessel Test Configuration.

TYPE OF LOADING	R-RATIO	TEST TEMP. °C	COMMENTS
HYDRO	-	**20-90**	$P_h = 1.0\ P_o$
CYCLIC	0.1	20-90	
CYCLIC	0.6	20-90	CRACK MARK
HYDRO	-	**20-90**	$P_h = 1.02\ P_o$
CYCLIC	0.1	20-90	
CYCLIC	0.6	20-90	CRACK MARK
HYDRO	-	**20-90**	$P_h = 1.04\ P_o$
CYCLIC	0.33	288	
CYCLIC	0.6	288	CRACK MARK
HYDRO	-	**20-90**	$P_h = 1.06\ P_o$
CYCLIC	0.33	288	
CYCLIC	0.6	288	CRACK MARK
HYDRO	-	**20-90**	$P_h = 1.10\ P_o$
CYCLIC	0.33	288	
HYDRO	-	**20-90**	$P_h = 1.40\ P_o$
HYDRO	-	**20-90**	**STABLE CRACK GROWTH**
HYDRO	-	**20-90**	**BURST**

NOTE: P_o = MAX CYCLIC TEST PRESSURE
P_h = HYDROTEST PRESSURE

Figure 3. Test Sequence for ZB-1 Vessel Test.

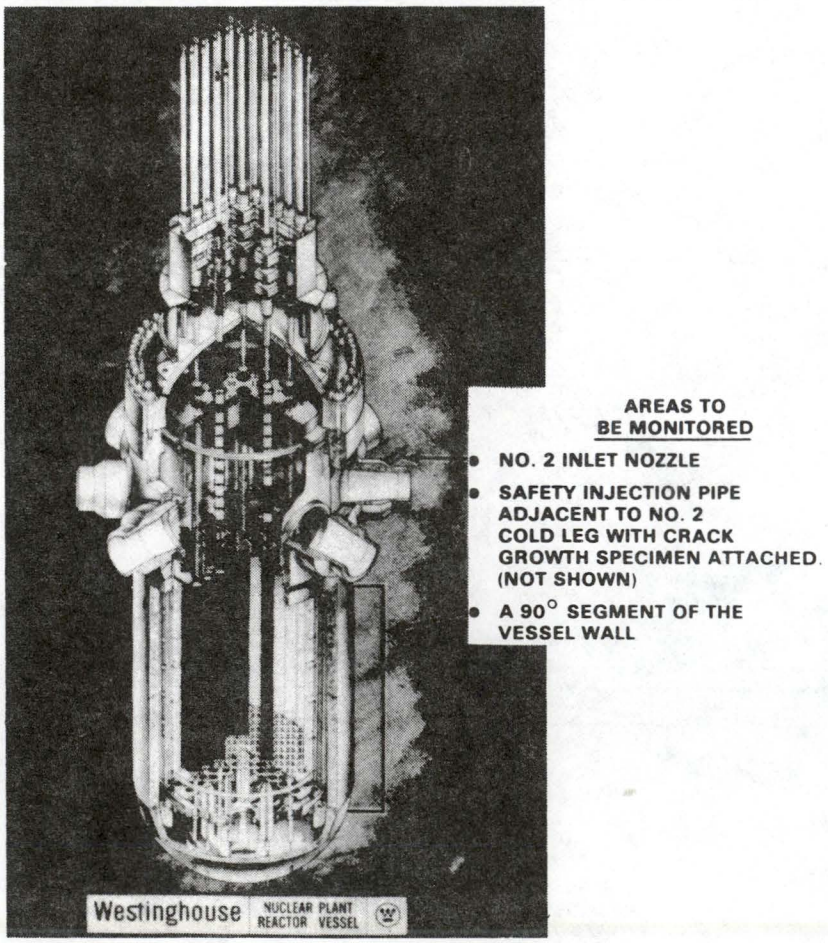

Figure 4. AE Monitoring - Watts Bar Unit 1 Reactor

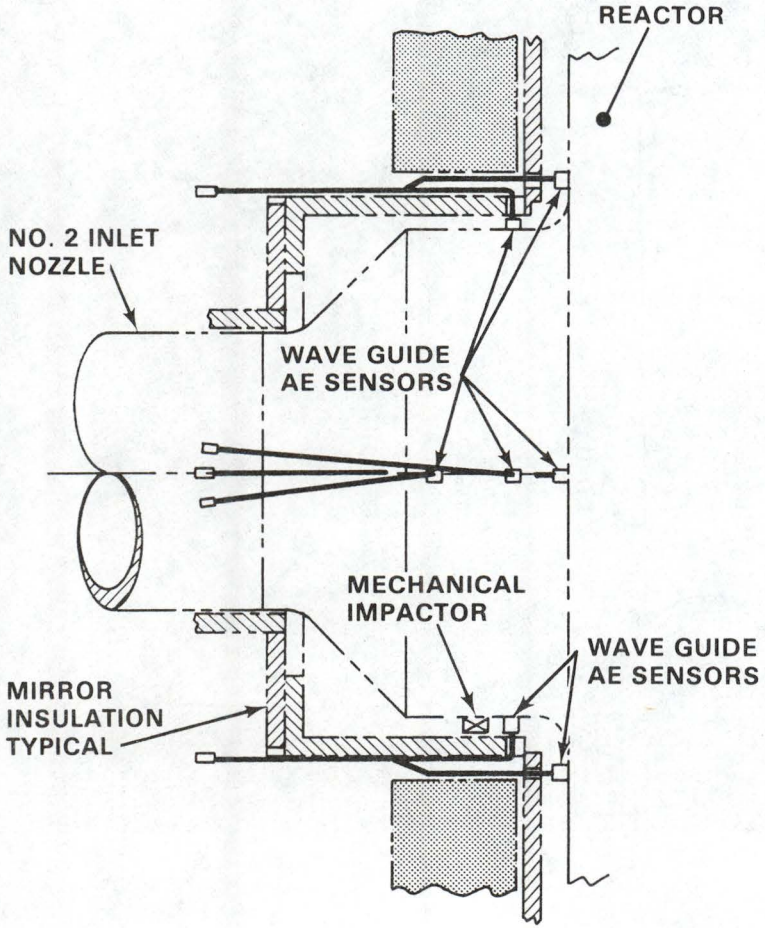

Figure 5. AE Sensor Installation - No. 2 Inlet Nozzle - Watts Bar Unit 1.

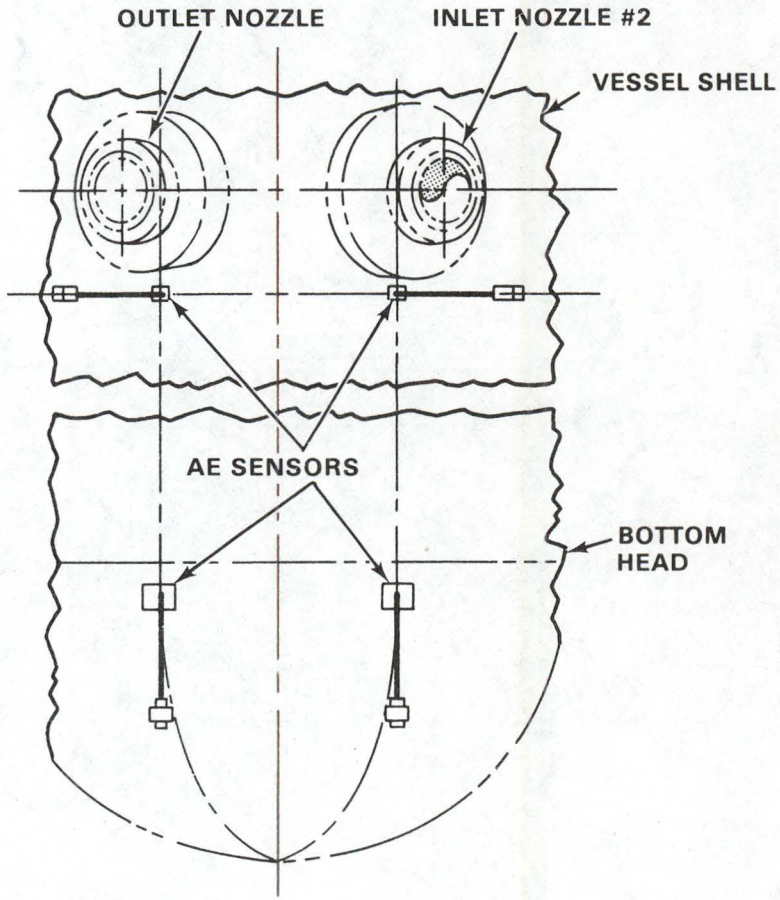

Figure 6. AE Sensor Installation - Vessel Wall - Watts Bar Unit 1.

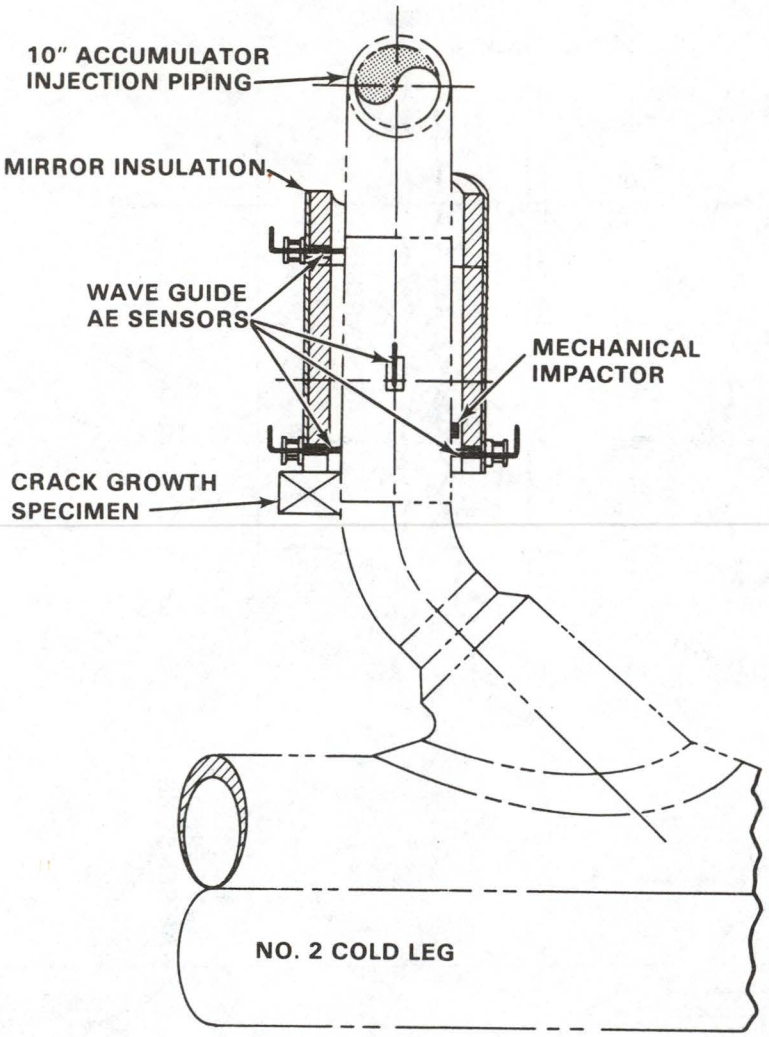

Figure 7. AE Sensor Installation - Safety Injection Pipe - Watts Bar Unit 1.

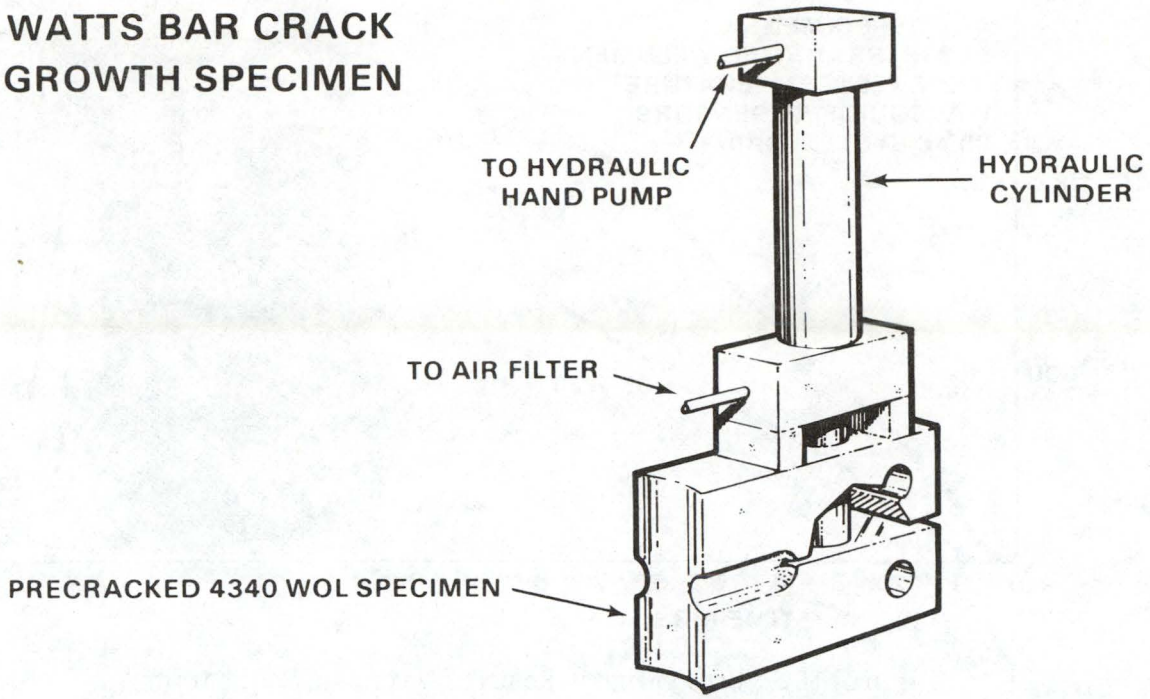

Figure 8. Watts Bar Crack Growth Specimen.

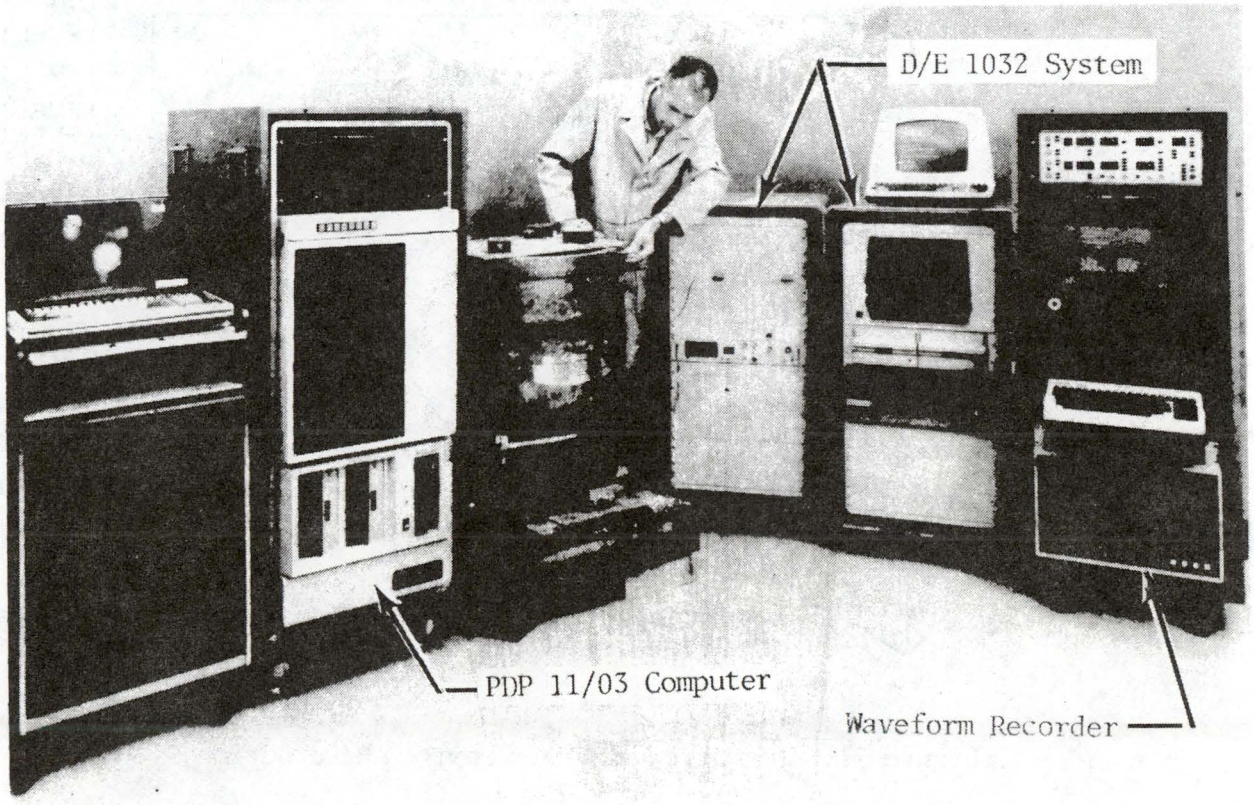

Figure 9. AE Detection/Analysis System.

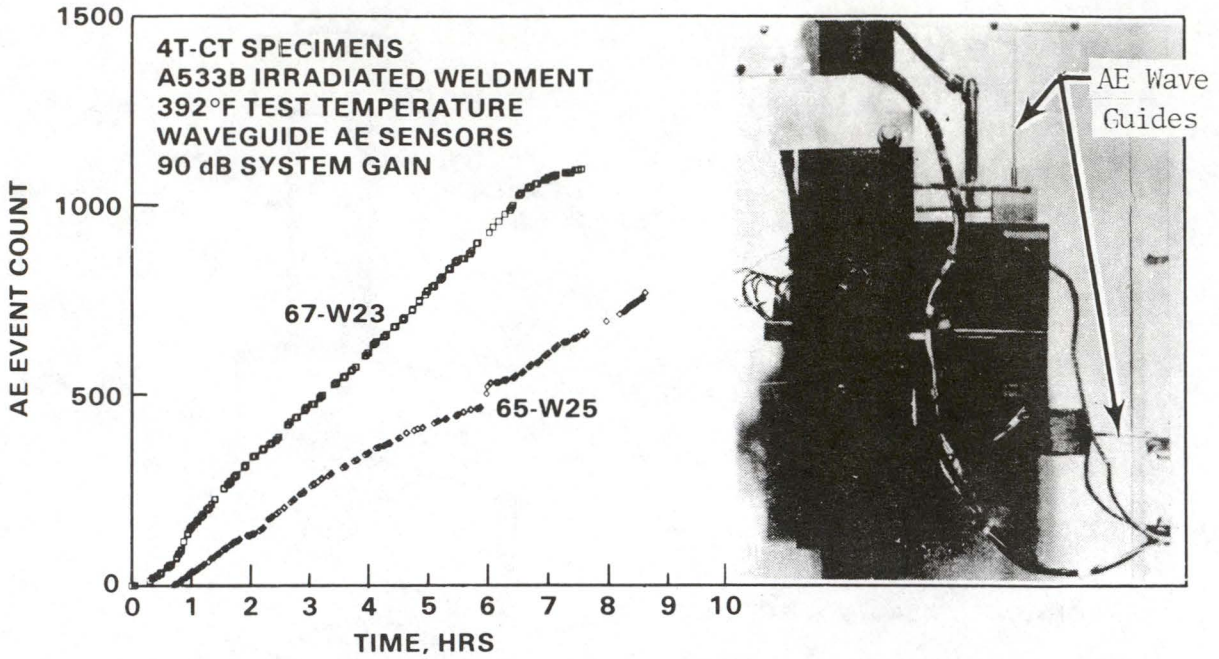

Figure 10. Preliminary Results from AE Monitoring Irradiated Fracture Specimen.

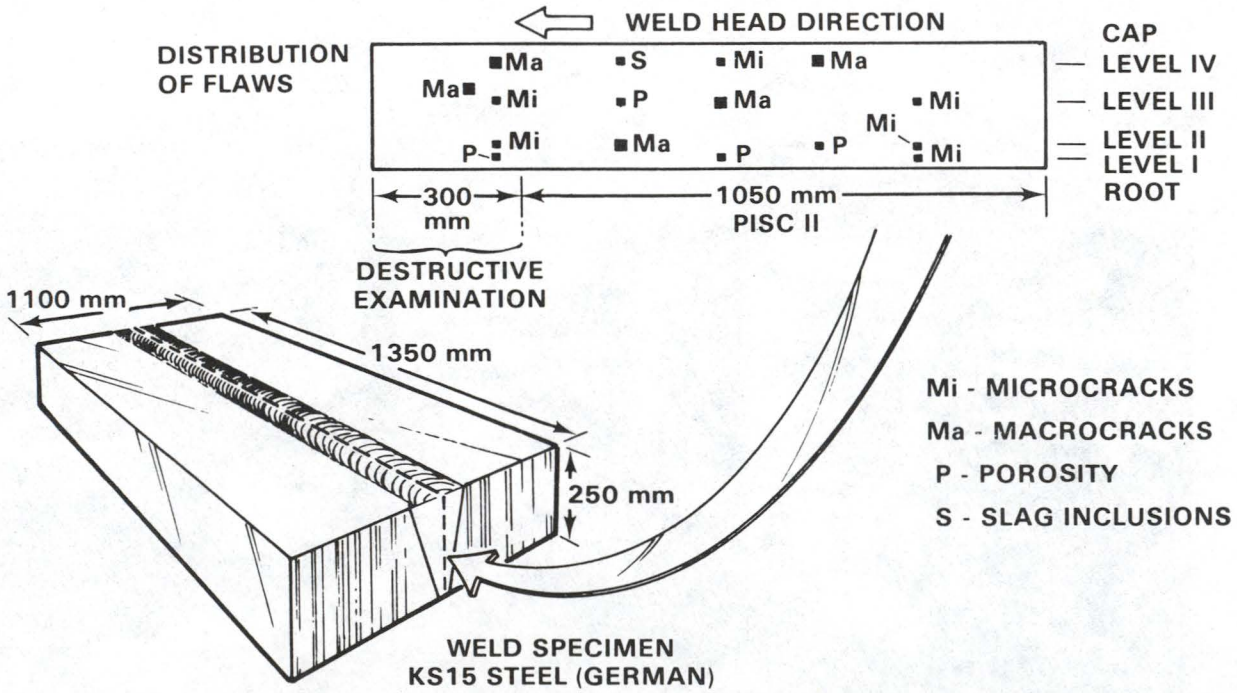

Figure 11. Demonstration Specimen - AE Detection of Weld Flaws.

INSERVICE INSPECTION APPLICATION OF THE SYNTHETIC APERTURE FOCUSING TECHNIQUE FOR ULTRASONIC TESTING (SAFT UT)

Jerry L. Jackson
Assistant Director
Research and Development

and

Dennis R. Hamlin
Senior Research Engineer
Quality Assurance Systems and Engineering Division
Southwest Research Institute

Presented at

Ninth Water Reactor Safety Research Information Meeting

October 26-30, 1981
National Bureau of Standards (N85)
Gaithersburg, Maryland

Work Sponsored by

Metallurgy and Materials Research Branch
Division of Reactor Safety Research
Nuclear Regulatory Commission
NRC Contract NRC-04-77-145

INSERVICE INSPECTION APPLICATION OF THE SYNTHETIC APERTURE FOCUSING TECHNIQUE FOR ULTRASONIC TESTING (SAFT UT)

Jerry L. Jackson
Assistant Director
Research and Development

and

Dennis R. Hamlin
Senior Research Engineer
Quality Assurance Systems and Engineering Division
Southwest Research Institute

I. BACKGROUND

Southwest Research Institute (SwRI) is conducting a project entitled "Program for Field Validation of the Synthetic Aperture Focusing Technique for Ultrasonic Testing (SAFT UT)." The project's purpose is to continue the development of SAFT UT and to validate its usefulness for inservice inspection applications. SAFT UT is an ultrasonic imaging method for accurately measuring the spatial locations and extent of flaws contained in structural components and weldments in nuclear power reactor systems. The increased measurement accuracy offered by SAFT UT, when compared with that provided by measurement methods now in use, will improve the reliability of flaw severity assessments with resultant safety and economic benefits to the nuclear power industry.

This project is one part of a team effort being conducted by the University of Michigan (U of M) and SwRI. Although the two groups are working under separate contracts, their efforts are integrated and synergetic. The U of M group is concentrating on theoretical aspects of SAFT UT while SwRI, working with information and advice supplied by U of M, is contributing the engineering and performance evaluations necessary to produce and validate a practical field tool.

The objectives of this program are to:

- Produce a SAFT UT system in a form useful for field test.
- Validate the performance of that system for characterizing both real and simulated flaws in realistic test specimens.
- Conduct field trials using the system on actual structures.
- Estimate the reliability and confidence level for SAFT UT examinations and compare those results with similar estimates made for conventional ultrasonic methods.

The ultimate goal is to produce a field-rated system for highly accurate flaw size measurements and to conduct sufficient testing of that system to promote its acceptance by industrial and regulatory authorities.

Work accomplished to date during this contract period has (1) provided solutions to several technical problems encountered during previous efforts, (2) provided solutions to some technical problems discovered in the course of laboratory tests, and (3) permitted SAFT UT examinations of numerous test specimens containing actual or simulated weld defects typical of those encountered in nuclear power reactor plants. The rest of this report will summarize these accomplishments.

II. TECHNICAL OVERVIEW

During a previous program, SwRI designed and constructed a system for performing SAFT UT. When testing the system's performance, it was determined that the signal-to-noise ratio (SNR) of the computed images was not adequate. The earlier program was concluded by an engineering analysis that estimated the probable causes for the low SNR and by recommendations of methods to solve the problem. The present program, which is the subject of this report, was designed to:

(1) Improve the SNR and

(2) Validate the performance of SAFT UT as an accurate tool for characterizing flaws contained in components and weldments used in nuclear power reactor systems.

A. Progress to Date

In planning the current project, maximum emphasis was placed on accomplishing large improvement to the SNR of the existing SAFT system. For this purpose, and in accordance with recommendations reached within the earlier program, the following subjects were investigated and optimized:

(1) Transducer design parameters and construction methods,

(2) Improved methods and equipment for the visual display of computed images,

(3) Application of signal processing methods, and

(4) Careful review of the system design and diagnostic tests to validate proper system operation.

Each of these four areas are discussed in the following four subsections.

1. Transducer Improvements

Significant increases were obtained in the SNR of SAFT images, principally by improved transducer performance. This was largely due to a change from the use of highly focused transducers to transducers that had only moderate or weak focusing. Original experiments were conducted using transducers containing lenses with a power of F/1 to F/2. In these experiments, the desired signals from flaws were weak and the undesired signals (noise) produced by spurious reverberations within the transducer were quite strong. The result was a low SNR.

During the current program, it was found that the SNR is a sensitive function of the lens F/- number. In effect, as the F/- number increases (as focusing becomes weaker), two advantageous effects occur simultaneously: the flaw signals become stronger while noise signals become weaker. Changing from an F/1 lens to an F/4 lens improves the SNR by 15 to 20 dB. Further improvements in SNR and resolution were made by selecting a 5-MHz test frequency instead of 2-1/4 MHz. Currently, a 3/4-inch diameter, 3-inch focal length lens (F/4) operating at 5 MHz is being used. This transducer was obtained from Panametrics and is providing very good results.

2. Improved Display

The second objective, to improve the display, depended upon execution of the image reconstruction algorithm. During reconstruction, the examined area of the inspected component is modeled in a digital computer as a three-dimensional volume. This volumetric region is subdivided into pixels (cells) upon which the reconstruction algorithm operates using the ultrasonic test data obtained during scanning. Upon completion of processing, every cell in the volumetric region will contain an amplitude value representing that cell's contribution to the reconstructed image. The final image is formed by displaying the computed signal amplitude as a function of cell location within the volume. The image is then interpreted by noting the locations of high signal amplitude. It should be noted that the reconstruction algorithm does not attempt to directly determine the size and location of reflectors (flaws). Flaw size and location are deduced by operators from the patterns formed by cells that show evidence of containing a reflector.

Based on display studies conducted at the U of M, SwRI implemented a Ramtek® color-graphics display system for use with the SAFT UT inspection characteristics derived at the U of M. The amplitude range associated with the collection of cells composing the image display is quantitized into 32 parts. Each part is represented by a distinct color on the display screen. A rainbow-type color sequence is used to represent the amplitude, with blue colors depicting low amplitudes and red colors representing high amplitudes. Five basic colors are used - red, orange, yellow, green, and blue; and the color intensity and hue are modulated so that each color gradually transitions into the next. Division of the amplitude display range into 32 parts provides enhancement of subtle amplitude changes within the display. Use of bright (red) colors for high amplitudes and dark (blue) colors for low amplitudes draws immediate attention to maximum amplitude cell patterns within the display. This method has proven to be very effective for presenting SAFT UT data to operators in a form promoting rapid assimilation.

3. Application of Signal Processing Methods

Moderate, but useful, improvement to the SNR is obtained by incorporating several computer programs to perform signal-processing functions on SAFT data. These steps are designed to remove constant terms and out-of-band noise, which sometimes contribute to background noise and clutter. The routines that have been added include:

(1) Envelope detection of the processed RF signal.

(2) High pass filtering to remove low frequency terms in raw data and also in processed data. Instances were encountered of aliasing resulting from the sampling process inherent to the reconstruction algorithm. The signals resulting from aliasing add noise to the image. As a matter of convenience, this noise was removed by filtering rather than by removing the source of the aliasing.

(3) An option to permit operators to review the frequency spectrum of selected data for diagnostic purposes. There is benefit in studying the frequency spectrum of processed data for the purpose of detecting equipment malfunctions and performance reductions caused by aliasing.

4. Validating System Operation

This subsection presents the results of combining the improved transducer performance, the signal-processing methods, and the Ramtek colorgraphics display system with the image reconstruction algorithm. A test specimen was designed and fabricated containing machined reflectors of known size, location, and orientation. This test specimen was examined by the SAFT UT inspection system, and the resulting images achieved were compared to the actual machined reflectors.

a. Test Description

An aluminum test block containing six bottom-drilled holes was used as a convenient test piece for evaluating the signal-processing method and for estimating accuracy, resolution, and the SNR. The dimension of this block and image display orientations are shown in Figures 1 and 2 while Figures 3 and 4 are the processed SAFT UT image of the holes. Figure 3 is a top view (looking in the direction of the hole axis). Note the well defined images of the ends of the six holes and the excellent resolution as evidenced by the separate indications of the two most closely spaced holes. Figure 4 is a side view derived from the same data used to produce the top view. Again, the spacing between all six hole ends are clearly defined (1.27 mm) increments, which are precisely the dimensions used in fabrication and thus constitute convincing evidence of the high range-resolution abilities of SAFT. Such high range resolution is distinctly superior to the resolution of acoustical holography. The SNR of this image is in excess of 30 dB.

b. Point Spread Function

The image resolution exhibited by the SAFT UT system correlates well with theoretical predictions. Using results by Norton (1), the point spread function for a pulse-echo synthetic aperture focusing system can be determined from the following equation.

---

[1]Norton, Stephen John, "Theory of Acoustic Imaging." A dissertation submitted to the Department of Applied Physics and the Committee on Graduate Studies of Stanford University, December 1976.

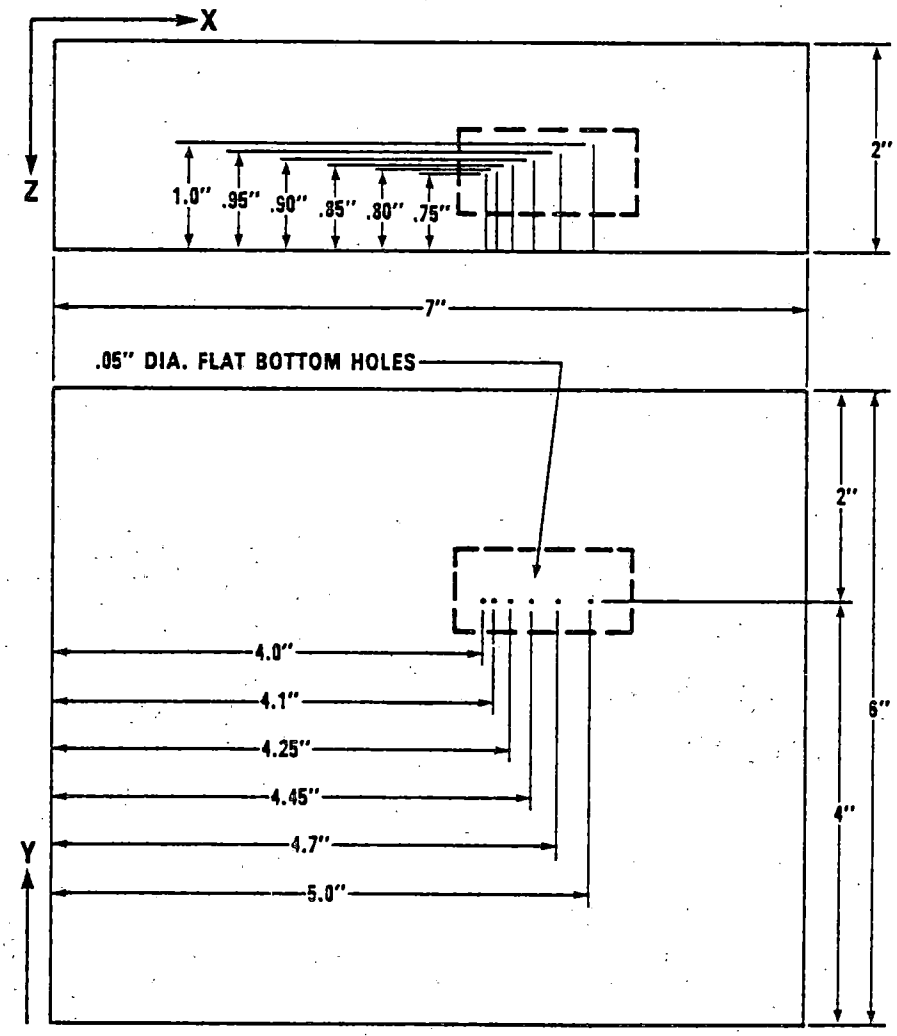

FIGURE 1. ALUMINUM TEST BLOCK DIMENSIONS

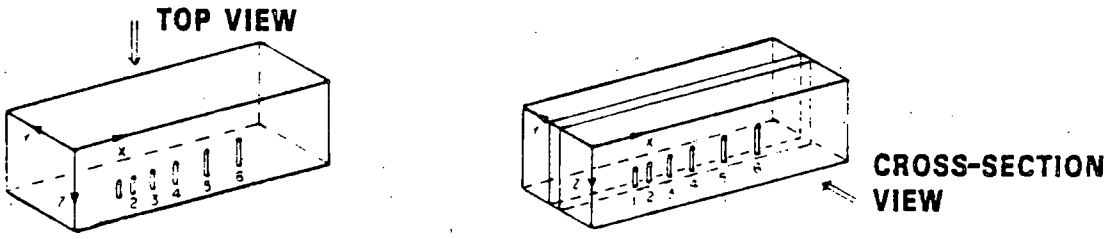

FIGURE 2. PROCESSED DATA ORIENTATIONS

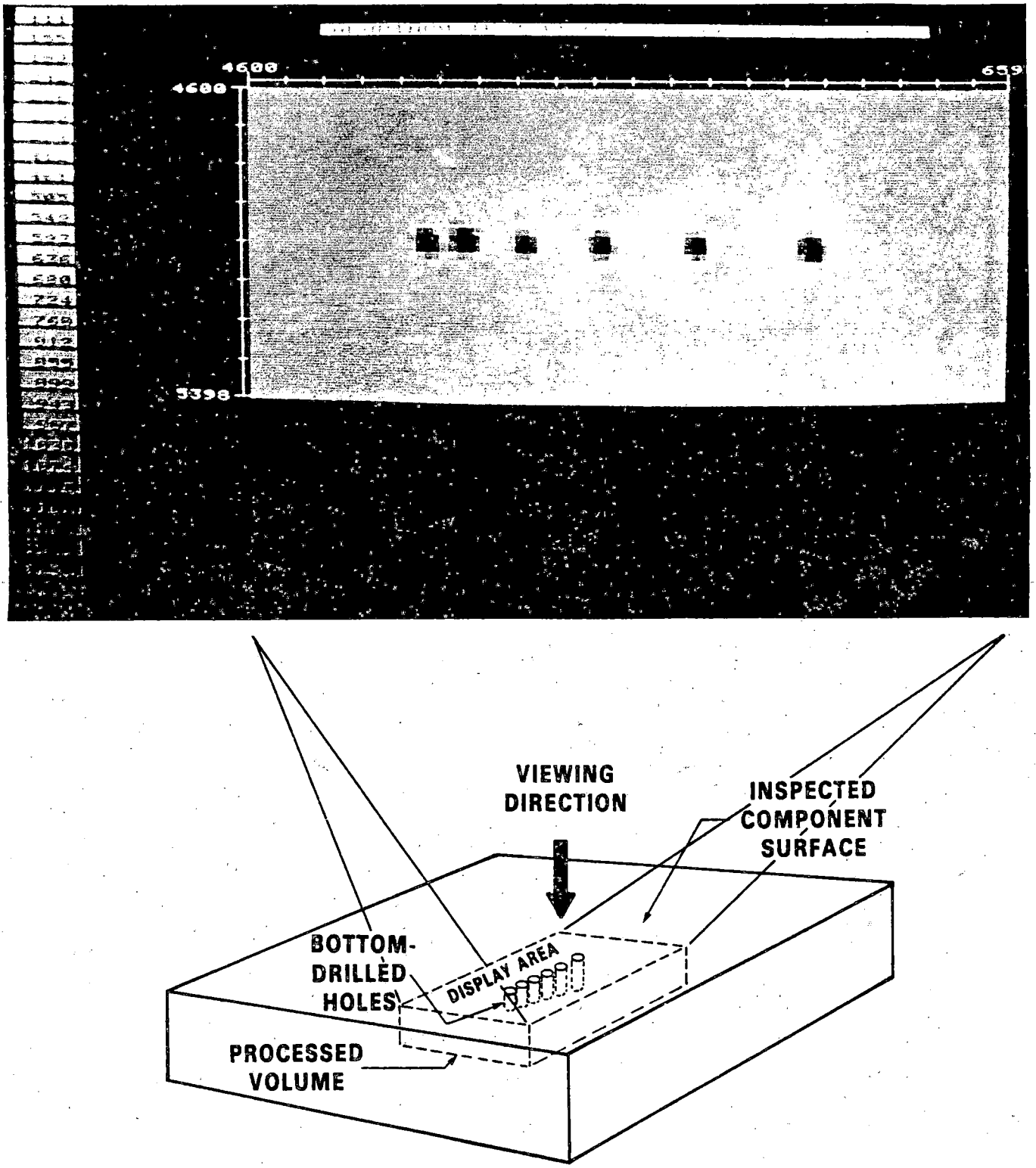

FIGURE 3. ALUMINUM TEST BLOCK C-SCAN VIEW OF BOTTOM-DRILLED HOLES

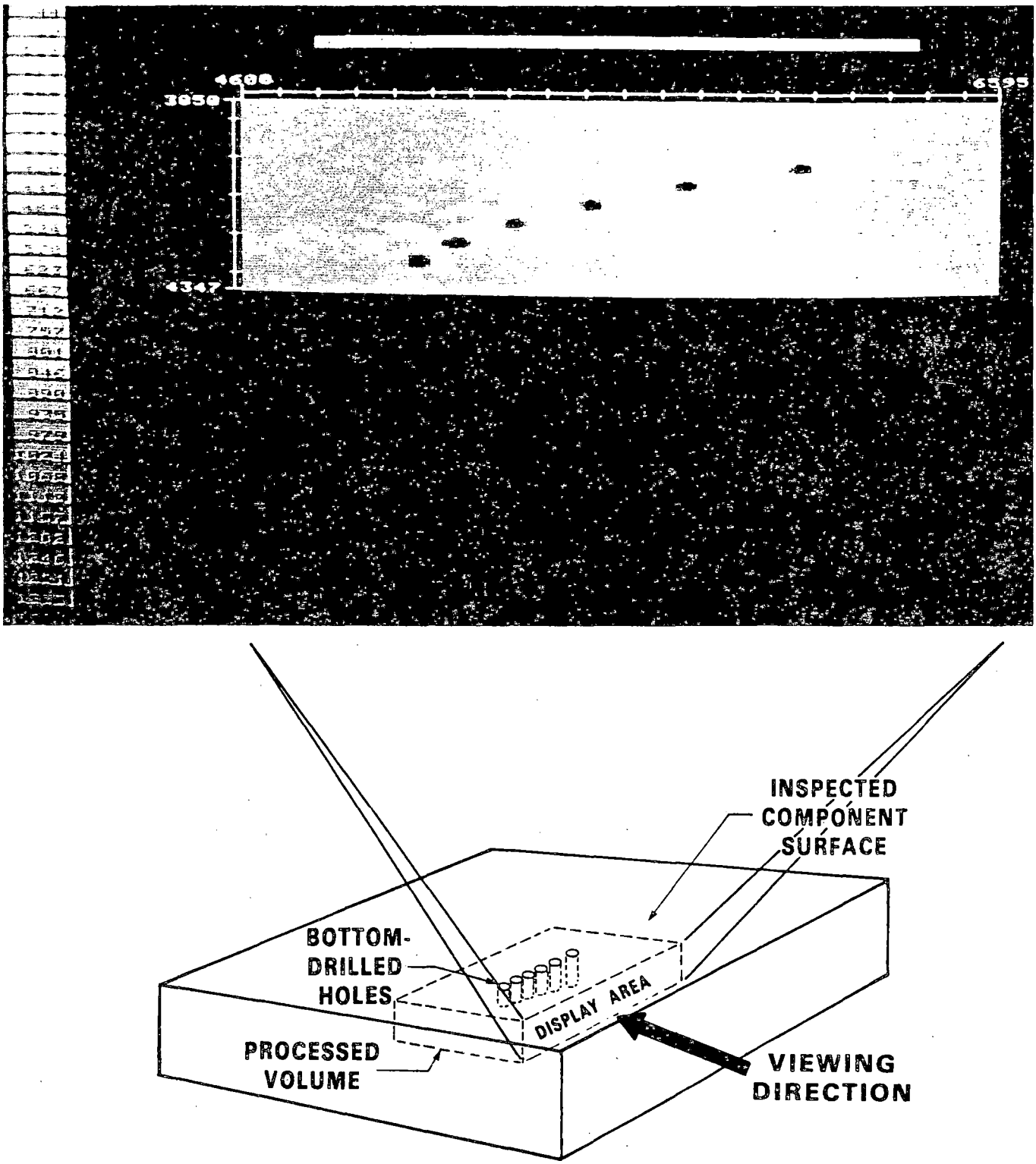

FIGURE 4. ALUMINUM TEST BLOCK B-SCAN VIEW OF BOTTOM-DRILLED HOLES

$$\frac{A_{(p)}}{A_{(o)}} = \frac{2J_1\left(\frac{2\pi\tan\frac{\Theta}{2}}{\lambda} \cdot 2p\right)}{\left(\frac{2\pi\tan\frac{\Theta}{2}}{\lambda} \cdot 2p\right)} \qquad (1)$$

where

$\frac{A_{(p)}}{A_{(o)}}$ = normalized image amplitude for a point target as measured at a lateral distance from the target

$J_1(\ )$ = Bessel function of order one

Θ = included angle of the synthesized aperture

λ = wavelength

Using this expression for the case of a 5-MHz focused transducer (longitudinal wave in aluminum) with Θ equal to 30 degrees produces the predicted point-spread function shown in Figure 5. The experimentally measured point-spread function for a one wavelength reflector in the previously mentioned aluminum test block has been superimposed to allow comparision. It is seen that the experimentally measured point-spread function correlates well with the predicted one; it is slightly broader and has lower sidelobes because of unequal illumination throughout the aperture. The experimental and the predicted functions are slightly displaced because of the volume sampling technique used in the reconstruction process.

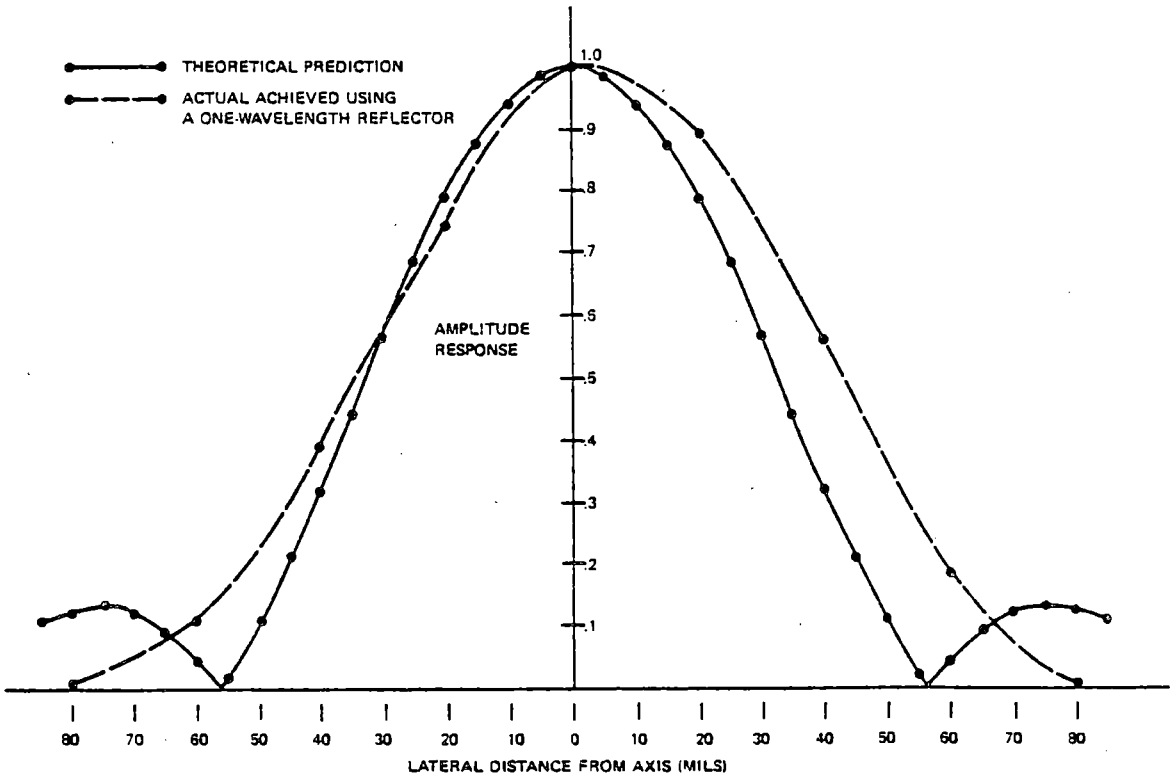

FIGURE 5. POINT SPREAD FUNCTION

B. System Improvements Required to Permit Examination of Cylindrically Shaped Components

The SAFT UT system's ability to conduct examinations of cylindrically shaped surfaces was originally based on using a strongly focused beam transducer that, among other requirements, provided a good front-surface echo over a broad range of incident angles so that the component surface could be properly tracked. This capability ensured that the focal point of the transducer could be precisely positioned on the surface even though the focused beam was angulated relative to the component surface. Another equally important requirement was that the focused transducer provide a SNR sufficient to permit detection of echoes from weakly reflective surfaces within the material. However, as described previously, extensive evaluations conducted during this program established that the SNR is a sensitive function of lens F/- number and that changing from an F/1 lens to an F/4 lens improved the SNR by 15 to 20 dB. Currently, SwRI is operating the system using a 3/4-inch diameter, 3-inch focal length lens (F/4) operating at 5 MHz. As a result of steps taken to ensure good SNR (adoption of less strongly focused transducers), the adaptability of existing scan mechanisms to examine components with moderate-to-strong surface curvature has been reduced. It was necessary, therefore, to make improvements to the existing system so that cylindrical test specimens could be examined.

1. Design Considerations

An engineering evaluation established that the most direct way to avoid limitations imposed by weakly focused transducers was to add either one or two degrees of transducer freedom operating under passive control. In this case, passive control means the use of self-activating mechanical means without the assistance of electronic or software operations.

This was accomplished by retrofitting a different transducer holder to the existing scan mechanism. The holder employs an unusual mechanical design that permits transducer rotation in a single degree of freedom about a point. The point can (by existing controls) be adjusted and controlled to be coincident with the component surface and thus accommodate near-cylindrical and near-flat surfaces. The holder is fitted with two spring-loaded arms contacting the component's surface and exerting forces to cause the holder to assure a position approximately normal to the surface. This action is maintained throughout scan movement over curved surfaces. The holder is shown in Figure 6. The small fixture shown at the lower right serves as an alignment tool, which permits the focused transducer to be installed so that the focal point is coincident with the axis of rotation of the transducer holder. A cylindrical test specimen was fabricated to evaluate the operational effectiveness of this holder. Figure 7, a photograph of the specimen, shows the machined reflectors contained within the specimen. Two sets of six bottom-drilled holes were created identical in size and spacing to the holes machined in the aluminum test block discussed previously. One set of holes was oriented axially while the other set was oriented circumferentially.

2. Cylindrical Test Specimen Examination Results

The wrought stainless steel pipe test component was examined using the new transducer holder. Figures 8 and 9 represent the top and side view of the axially oriented holes. Figures 10 and 11 represent the top and side view

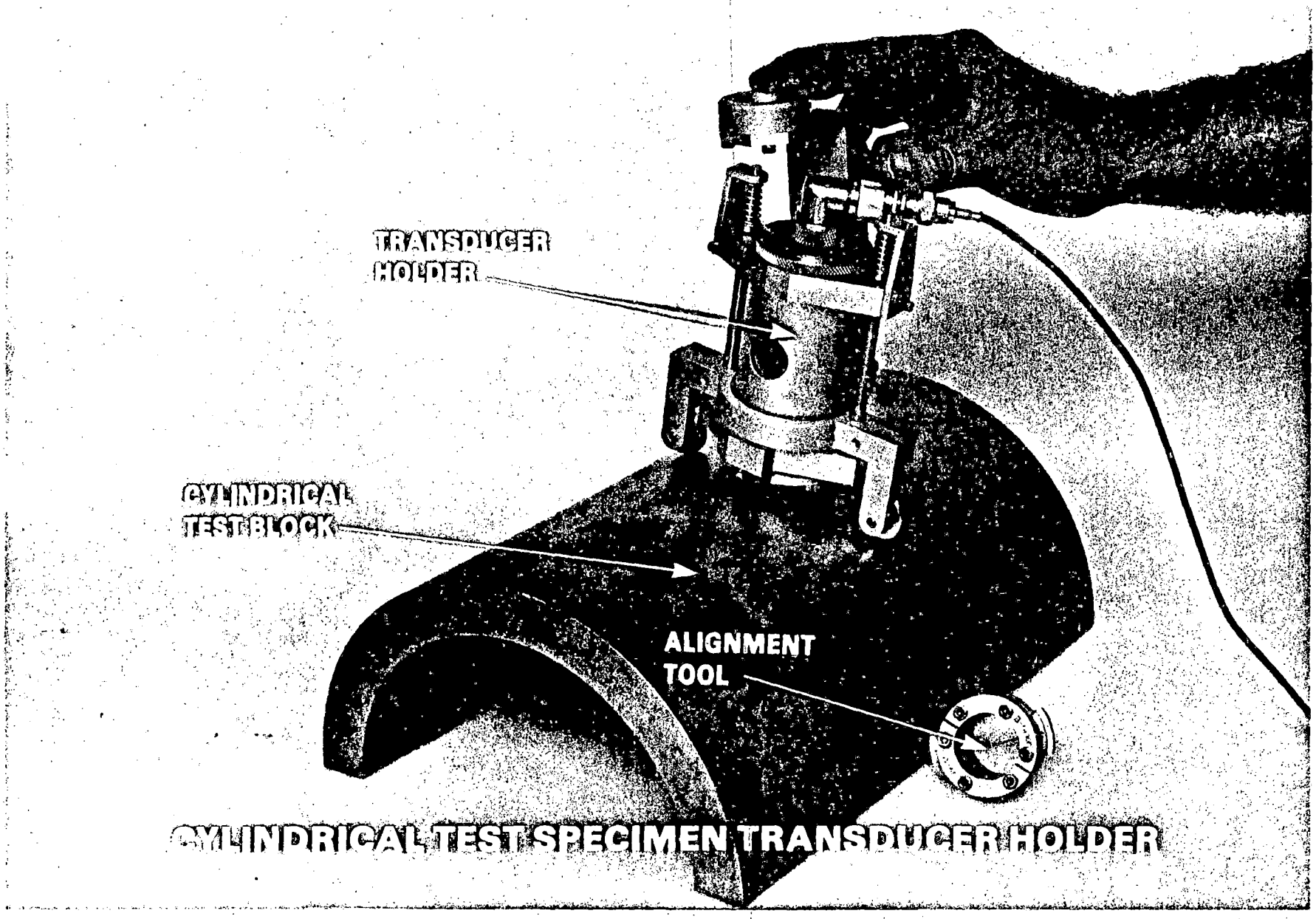
TRANSDUCER
HOLDER
CYLINDRICAL
TEST BLOCK
ALIGNMENT
TOOL
CYLINDRICAL TEST SPECIMEN TRANSDUCER HOLDER

FIGURE 6

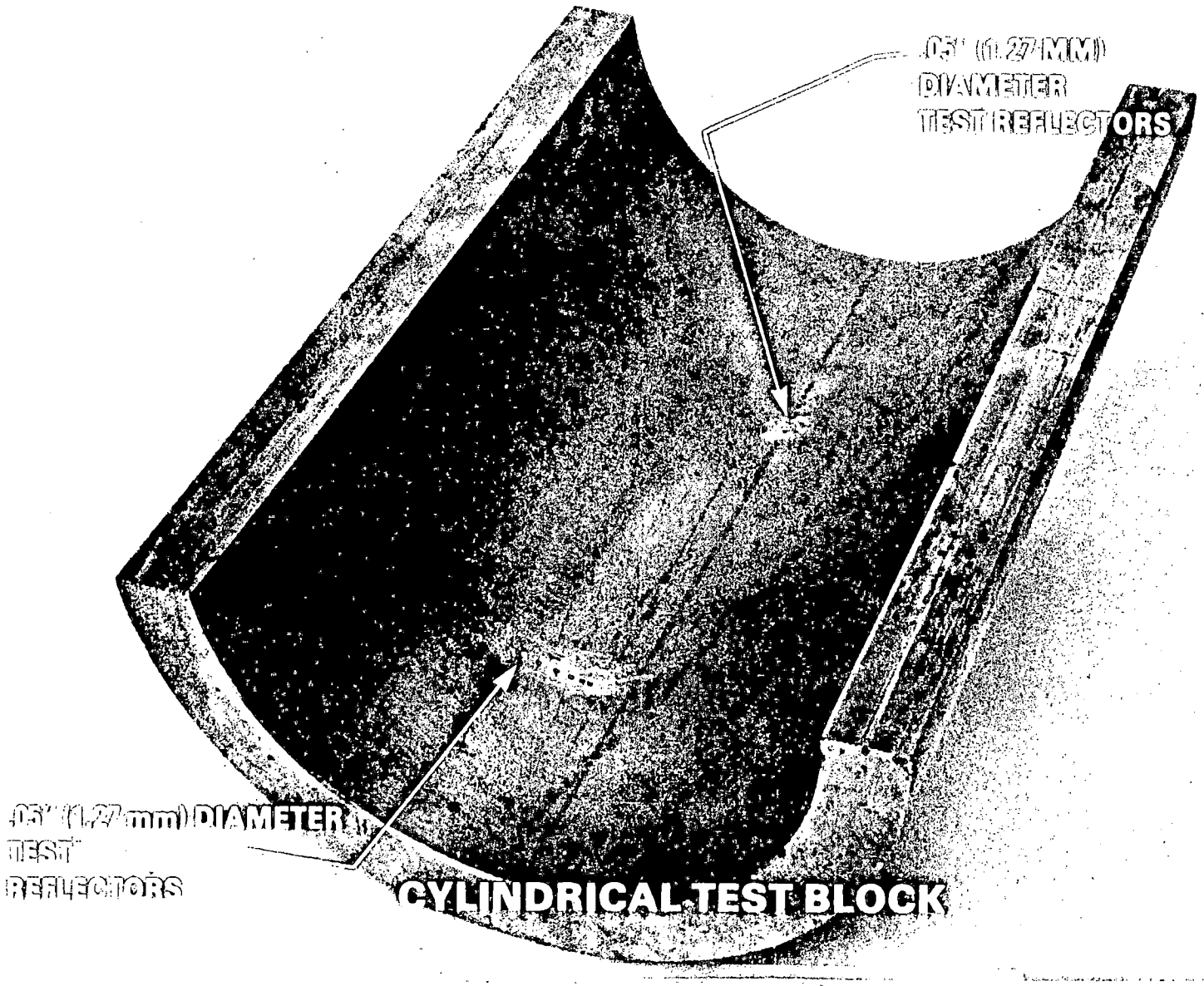
.05" (1.27 MM)
DIAMETER
TEST REFLECTORS
.05" (1.27 mm) DIAMETER
TEST
REFLECTORS
CYLINDRICAL TEST BLOCK

FIGURE 7

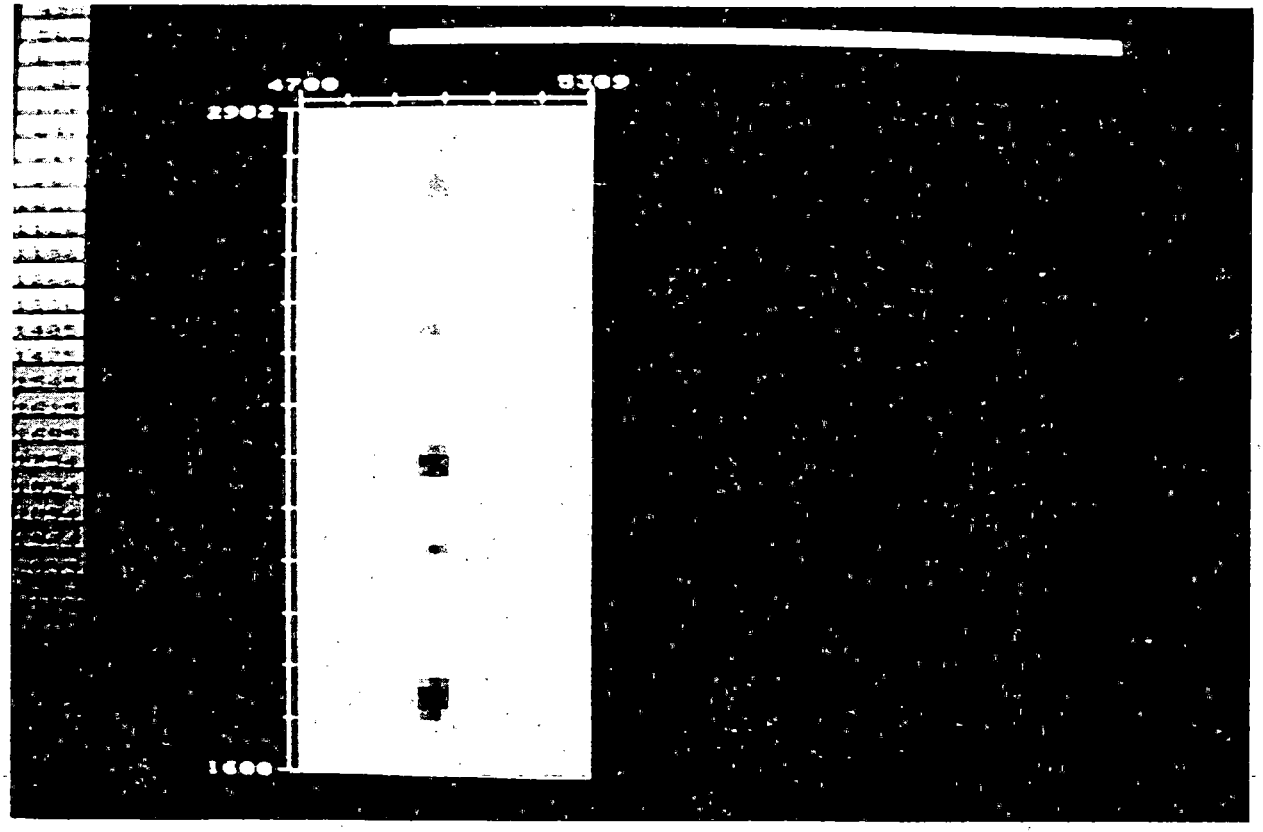

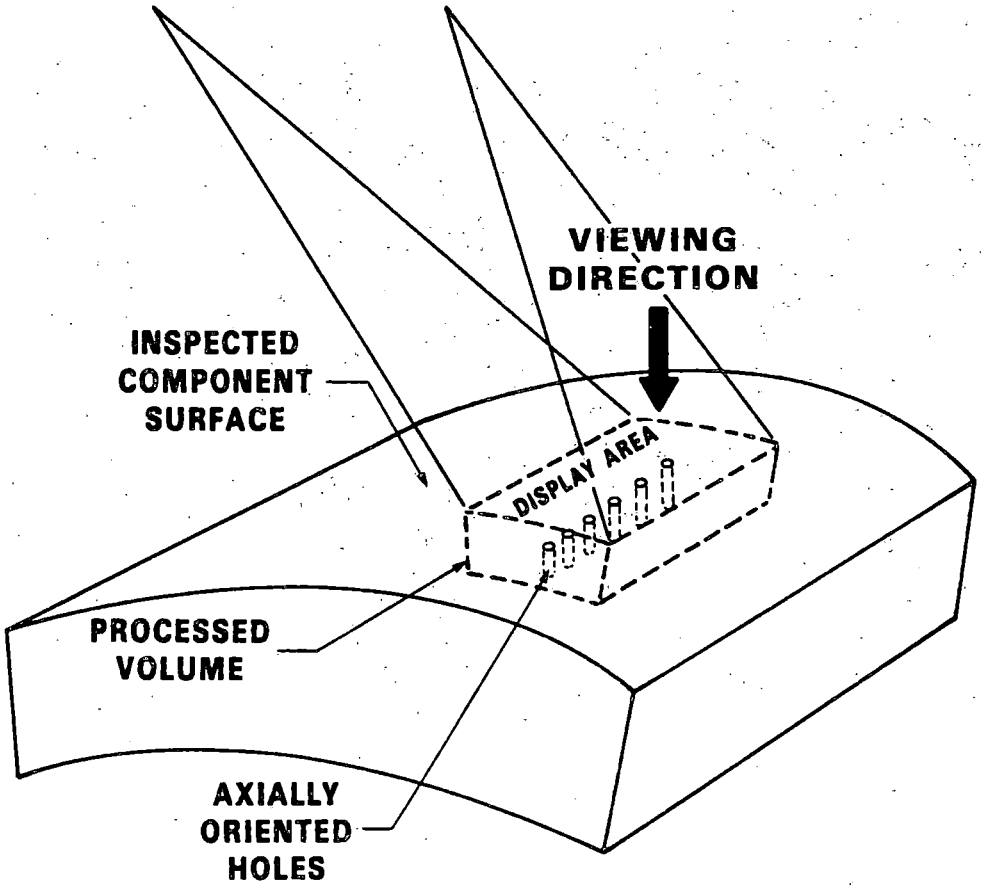

FIGURE 8. CYLINDRICAL WROUGHT STAINLESS STEEL SPECIMEN, C-SCAN VIEW OF AXIALLY ORIENTED HOLES

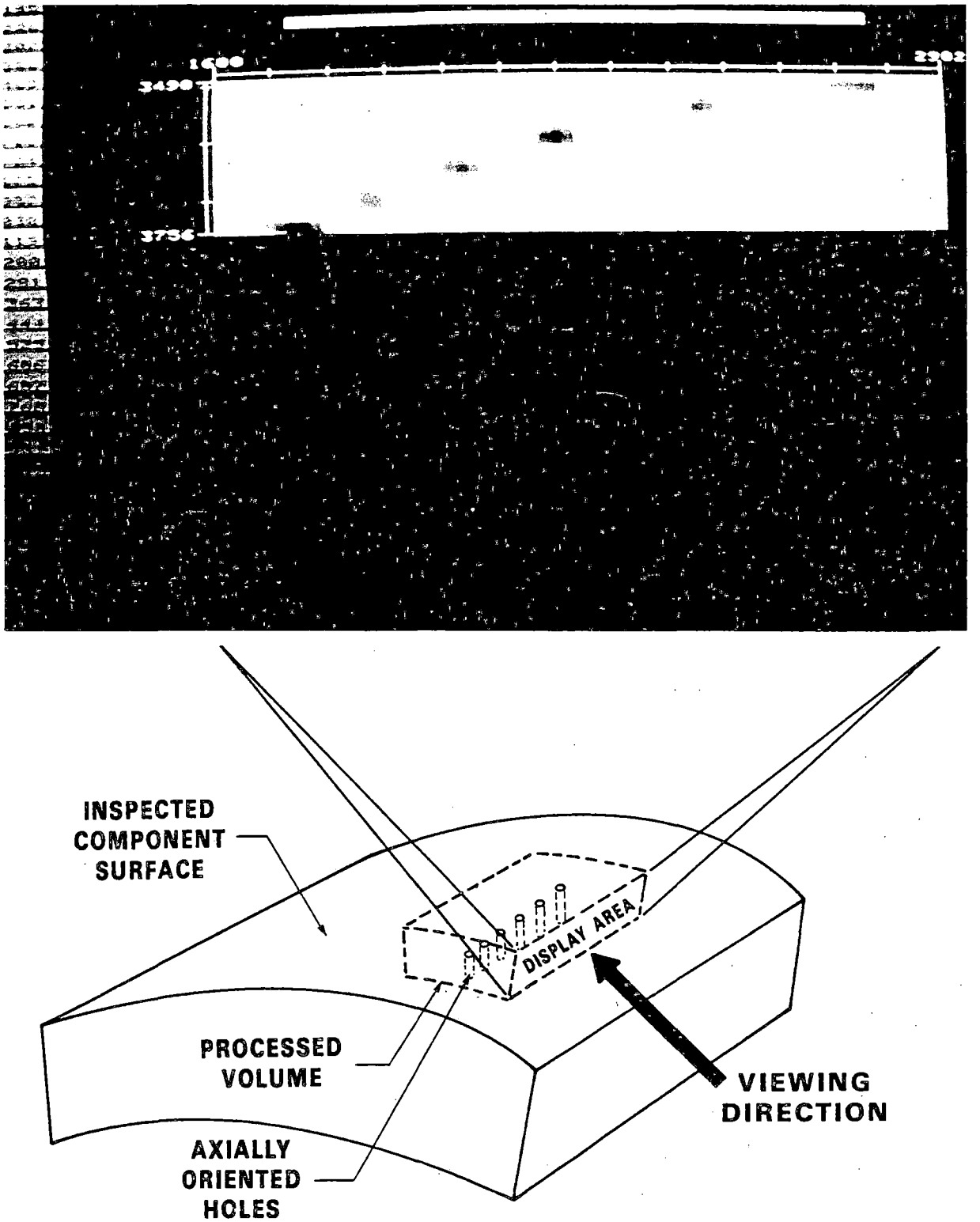

FIGURE 9. CYLINDRICAL WROUGHT STAINLESS STEEL SPECIMEN, B-SCAN VIEW OF AXIALLY ORIENTED HOLES

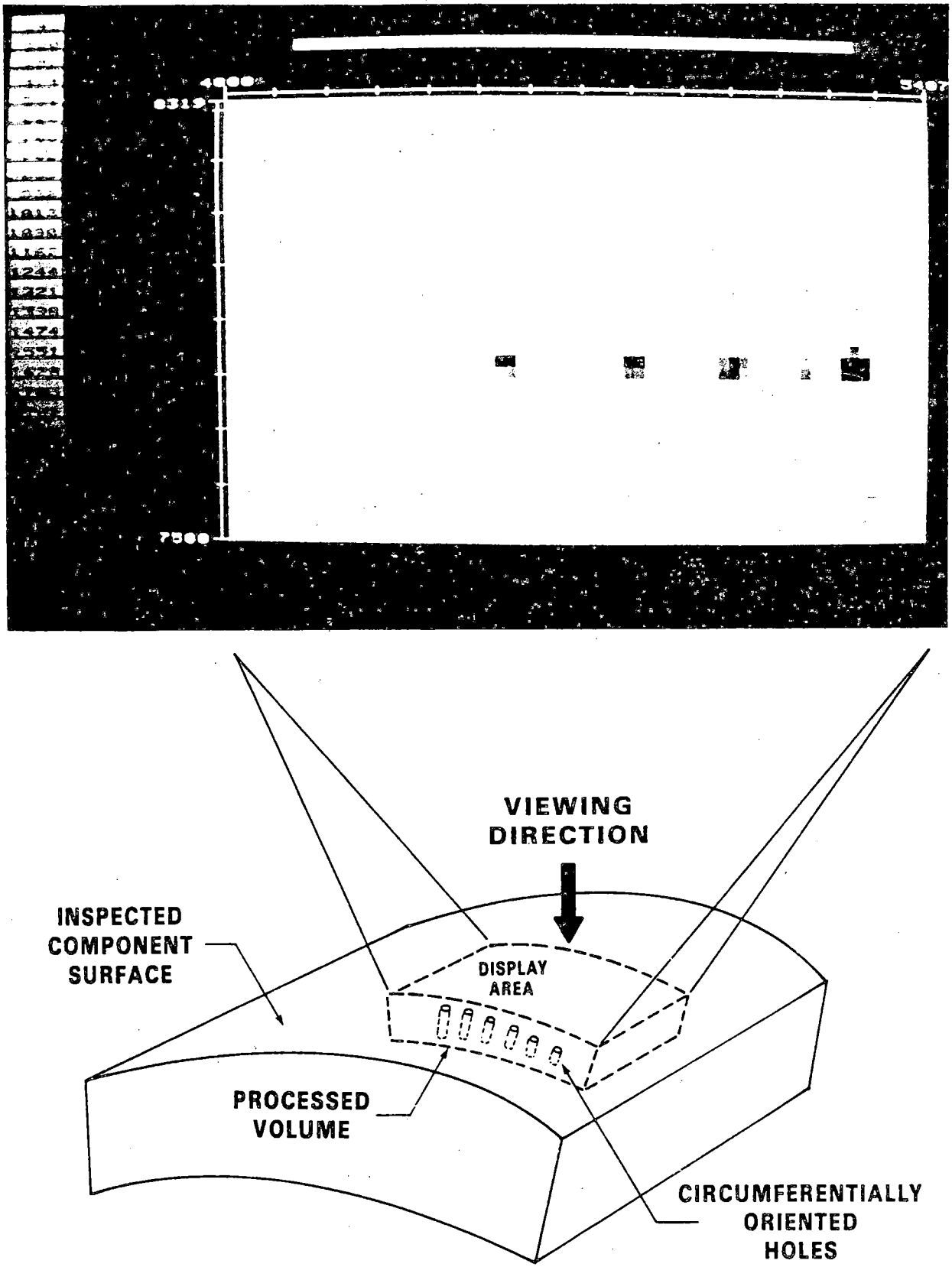

FIGURE 10. CYLINDRICAL WROUGHT STAINLESS STEEL SPECIMEN, C-SCAN VIEW OF CIRCUMFERENTIALLY ORIENTED HOLES

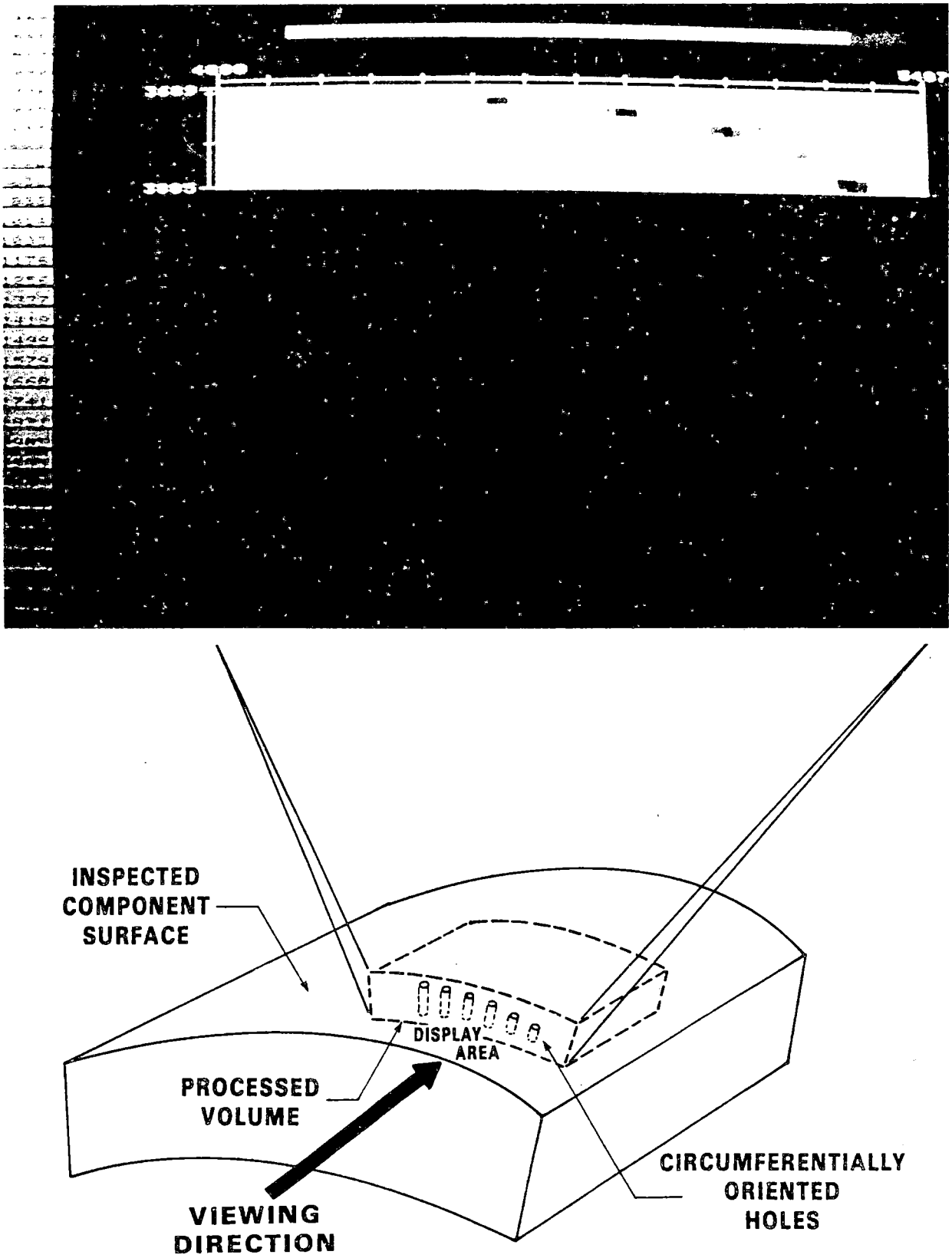

FIGURE 11. CYLINDRICAL WROUGHT STAINLESS STEEL SPECIMEN, B-SCAN VIEW OF CIRCUMFERENTIALLY ORIENTED HOLES

of the circumferentially oriented holes. In both tests, all six hole ends were clearly imaged. The lateral and range-resolution capability of the system was quite evident; however, the SNR and image clarity obtained in the cylindrical wrought stainless steel specimen were not quite as good as those obtained in the aluminum test block. This was due, in part, to the differencies in the acoustic properties of the materials involved and the varying surface geometrics (flat versus cylindrical). Test results do demonstrate the usefulness of the new holder for overcoming a limitation imposed by the use of weakly focused transducers.

C. Current Activities

As a result of the success achieved in validating proper system operation, two activities are receiving emphasis:

(1) Use the SAFT UT inspection system in conducting a test matrix consisting of a series of flat plate and cylindrical test specimens to thoroughly evaluate the system performance under a variety of circumstances.

(2) Perform required system enhancement to permit the existing SAFT UT inspection system to be evaluated during actual field inspection activities.

1. Test Matrix

A series of test specimens are currently being examined with the SAFT UT inspection system. Originally, the test matrix was to consist of a series of three specimens containing fabricated weld defects. However, a variety of additional test specimens were obtained at very low cost to the project and were added to the test matrix.

a. Fabricated Test Specimens

During work conducted previously, three test specimens were constructed containing a variety of welding fabrication flaws and geometry conditions. One specimen was a butt-welded carbon steel plate while the other two consisted of wrought or cast stainless steel pipe coupons. All fabricated defects in the butt-welded carbon steel plate were examined and images produced. This specimen is currently undergoing destructive examination so that the images produced can be compared to the actual defects. The two cylindrical test specimens are presently undergoing SAFT UT examination and will also be destructively examined to permit evaluation of system performance.

b. The Welding Institute Specimens

A series of stainless steel specimens were fabricated by The Welding Institute for a program designed to evaluate the effectiveness of a variety of nondestructive examination techniques to characterize weld defects. These specimens were examined and images produced. The results will be published in the final report. The Welding Institute also plans to destructively examine the specimens and publish the results so that SAFT UT can be evaluated for these defects.

c. General Electric Test Block

A section of nuclear-grade carbon steel plate 6-1/4-inch thick was obtained from General Electric. The specimen, containing a small thermal fatigue crack located near the backwall, also was examined and images were produced. The test will provide useful information on the ability of SAFT UT to image a weak diffused reflector near a strong specular reflector (backwall) in a relatively thick-walled specimen.

d. Palisades Feedwater Nozzle Piping

A ferrite carbon-steel pipe containing suspected fatigue cracks was obtained and is currently being examined. The pipe component was removed from an operating nuclear power reactor plant and represents an actual service-induced defect. Upon completion of the SAFT UT examination, this specimen will be destructively examined to permit evaluation of system performance.

2. Improvements to Permit Field Implementation

Currently, all SAFT UT examinations are performed in a laboratory environment using the immersed-mode UT technique. In order to inspect an actual component of an operational nuclear power reactor plant, a mechanism must be implemented to replace the immersed-mode inspection. To accomplish this task, a water column was designed and fabricated and is currently undergoing testing. The column is designed to be inserted into the transducer holder shown in Figure 6. To eliminate spurious acoustic reverberations, the water column is lined with a sound absorbing compound. The compound is composed of several substances mixed so that the resulting product has an acoustic impedance nearly identical to water and is highly attenuative. Upon successful completion of the water column tests, the SAFT UT system will be capable of performing field inspections.

III. PRELIMINARY CONCLUSIONS OF SwRI SAFT UT SYSTEM EVALUATION

The SAFT UT inspection system has been used to examine a number of laboratory test specimens containing a variety of fabricated weld defects simulating realistic type defects. These specimens will eventually undergo destructive examination so that SAFT UT images of these defects can be compared with the actual defects. This method of analysis should prove to be very effective in establishing the performance capabilities of SAFT UT.

Pending results obtained from the destructive examinations, some preliminary conclusions were formed based on a comparison of existing SAFT UT images to data obtained from radiographic and conventional UT examination methods. In order to summarize these preliminary conclusions, the performance capability of the existing SAFT UT system was evaluated based on specific characteristics of the examined defect. Three classes of defects appear to immerge with uniquely important characteristics relative to SAFT UT examination and defect characterization. These are:

(1) Defects that are not located in the immediate proximity (one or two wavelengths) of the component backwall or weld root region and that are volumetric in nature such as porosity, lack of fusion, and slag or tungsten inclusions,

(2) Defects located within the root area of weldments such as lack of penetration, and

(3) Crack defects.

Conclusions from examinations performed on defects representative of these three classes are discussed below.

A. Volumetric Type Defects

The SAFT UT image of defects classed as volumetric exhibit good clarity and are well defined. These defects apparently provide a reflecting surface favorably oriented to the direction of insonification so that echo signals are returned to the transducer from numerous locations within the synthetic aperture. This results in the production of high quality SAFT UT images, exhibiting good accuracy and resolution in defining the defect location and spatial extent. Destructive examination of the test specimens containing this class of defect is, therefore, expected to confirm high performance. Specimens scheduled for destructive examination and containing this type of defect include:

(1) Butt-welded carbon steel plate

(2) The Welding Institute specimen

(3) Stainless steel (both wrought and cast) piping specimens

An example of the high-quality images obtained for this type of defect is shown in Figure 12. The defect shown was obtained from the slag inclusion region of the 4-inch thick, butt-welded carbon steel plate specimen. The three viewing orientations are also shown in Figure 12.

B. Cracks

The SAFT UT image of defects classed as cracks can be subdivided into two categories based on general crack orientation relative to the direction of the insonifying ultrasound. Good crack images were obtained for cracking that is generally oriented perpendicular to the insonifying ultrasound. For example, good images were obtained for the heat-affected-zone cracking in the butt-welded carbon steel plate specimen. These cracks are expected to run along weld beads and are, therefore, oriented 90 degrees to the ultrasonic beam direction. However, vertically oriented cracks appear to be difficult to image. Limited success was obtained with the intergranular stress corrosion crack defect in the Duane Arnold specimen. In tests conducted on a 6-inch thick vessel plate and a section of the Palisades feedwater pipe, images did not give clear indications of the suspected (but unconfirmed) cracks.

The imaging of vertically oriented cracks using (near) zero-degree incident angles is a technical challenge because of the low reflectivity from that direction. Test results obtained to date cast doubt on the advisability of relying on that examination angle entirely. It would be desirable to repeat these tests using refracted shear wave data processed by SAFT UT to verify an expected improvement in image clarity. Unfortunately, the equipment in use at SwRI does not possess that capability.

C. Root Region Defects

SAFT UT images of defects classed as existing entirely within the root region and deeper than the component backwall are difficult to obtain because they tend to be masked by the strong backwall reflections. Defects of this type were contained in The Welding Institute specimen. In one case, the defect image could be isolated (removed from the surrounding backwall reflector) and evaluated. In the other case, it could not.

The use of a refracted shear wave instead of zero-degree longitudinal wave is expected to improve the performance of SAFT UT for examining the region adjacent (within two wavelengths) of the backwall. As was noted earlier, however, equipment limitations (not limitations of SAFT UT) prevent such tests.

IV. SUMMARY

Experiments for measuring the performance of SAFT UT are continuing. Results are indicating very good performance for characterizing volumetric flaws that are reflective from the zero-degree direction. Improvement seems to be needed for characterizing vertical cracks and shallow, surface-connected flaws. The limitations experienced in characterizing the latter flaw types are attributed to the use of zero-degree insonification. The use of refracted shear waves is believed to offer the needed improvements.

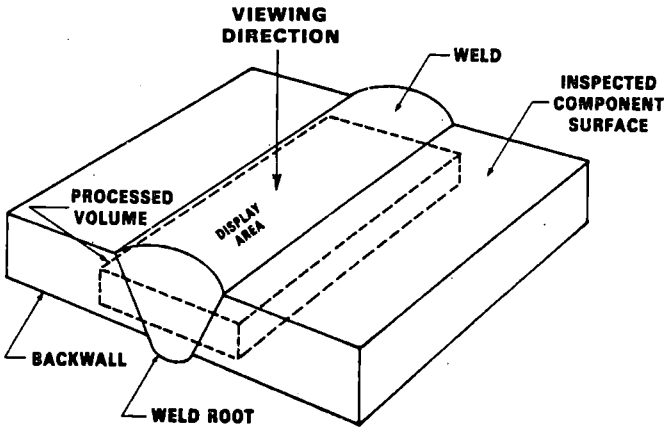

C-Scan View

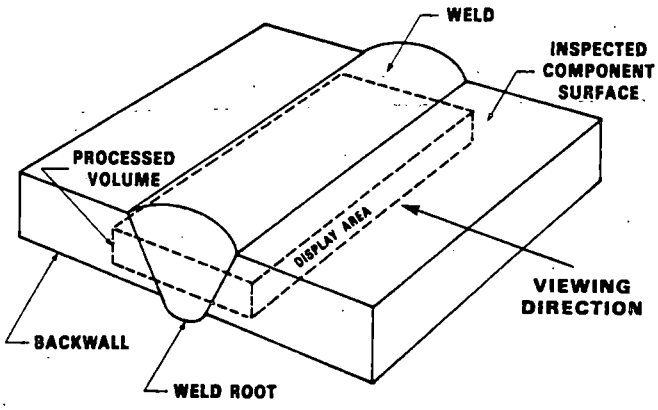

B-Scan View Parallel to Weld

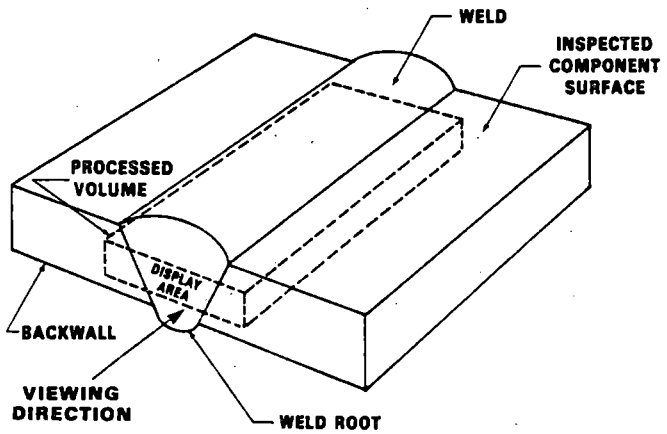

B-Scan View Transverse to Weld

The Schematics Are Adjacent to Their Corresponding CRT Color Display (on the facing page). The Schematics Depict the Viewing Direction, Weld Location, and Processed Volume Imaged. The Color Display Represents the Images Obtained from the Viewing Direction Through the Processed Volume Region.

FIGURE 12. THREE ORIENTATIONS FOR BUTT-WELDED CARBON STEEL PLATE - SLAG INCLUSION

Amplitude
Versus
Color
Index

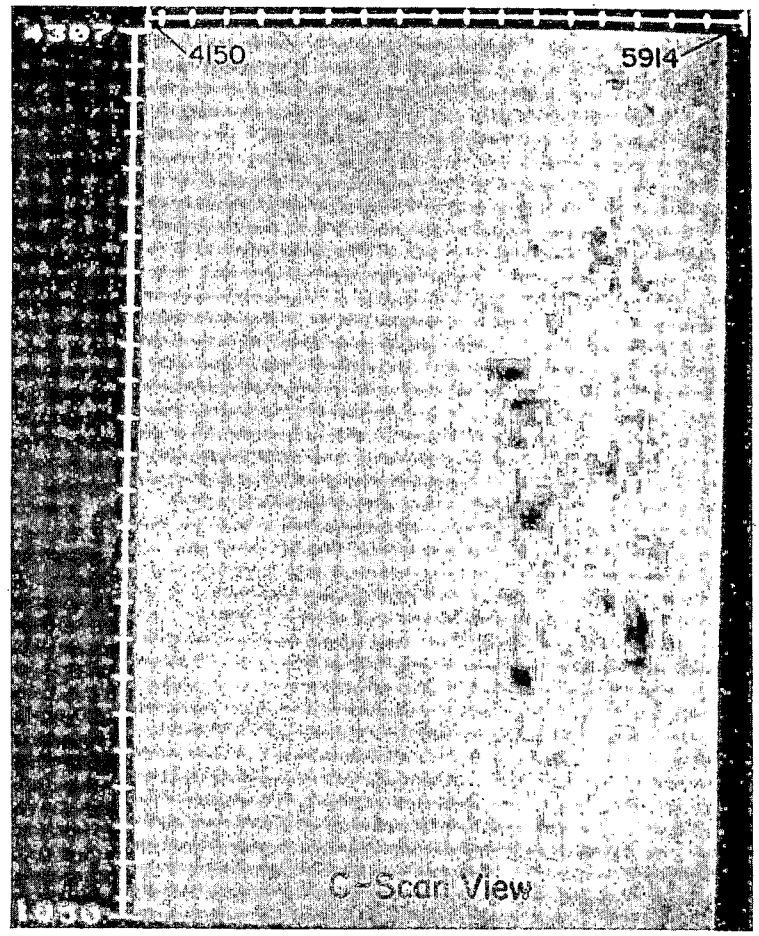

⊢—⊣ = 0.1 inch

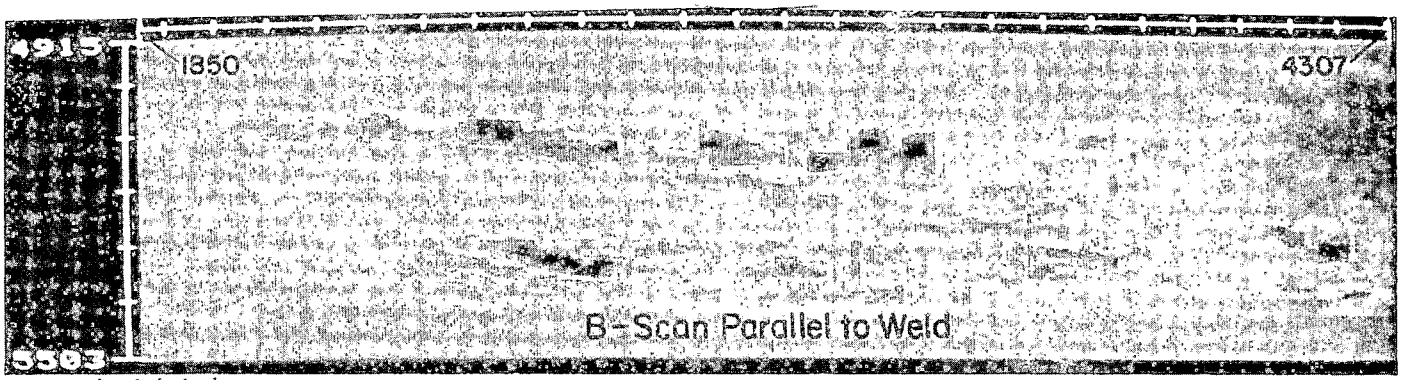

⊢—⊣ = 0.1 inch

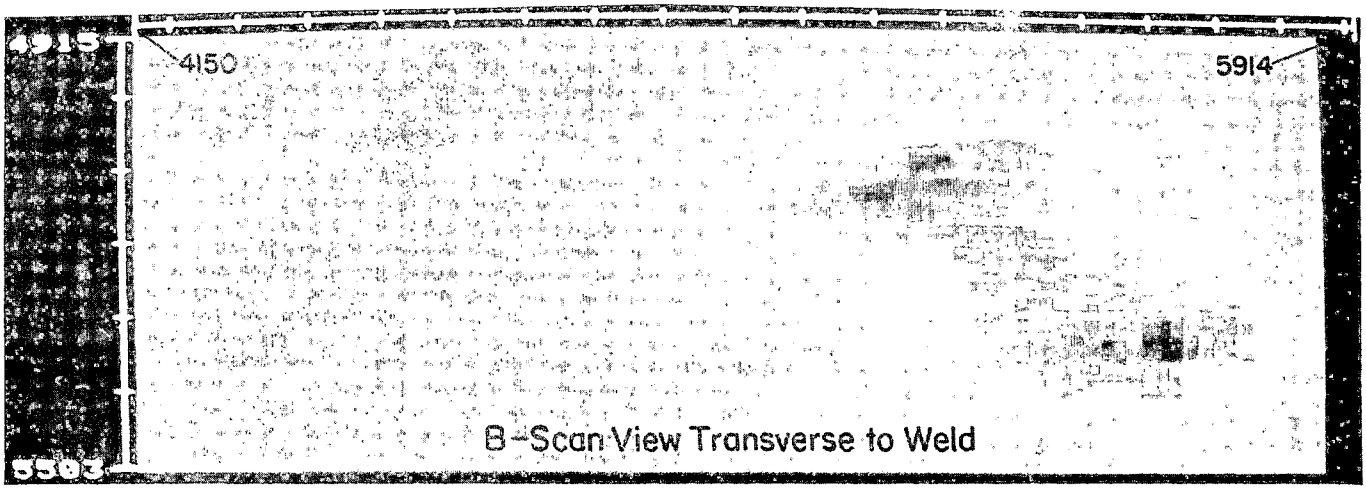

⊢—⊣ = 0.1 inch

PNL-SA-9985

RELIABILITY OF INSERVICE ULTRASONIC FLAW DETECTION

F.L. Becker, Project Manager

October 1981

Presented at the Ninth Water Safety Research Information Meeting
Gaithersburg, Maryland
October 26-30, 1981

Work Supported by the U.S. Nuclear Regulatory Commission Under a Related Services Agreement with the U.S. Department of Energy under Contract DE-AC06-76RLO 1830

Pacific Northwest Laboratory
Richland, Washington 99352

RELIABILITY OF INSERVICE ULTRASONIC FLAW DETECTION

F.L. Becker
Pacific Northwest Laboratory (PNL)
Operated by Battelle

INTRODUCTION

This report summarizes the third year's activities on a seven year program which is being conducted by PNL on behalf of the U.S. Nuclear Regulatory Commission. The objectives of this program are shown in Figure 1. The safety and licensing issues addressed by this program are shown in Figure 2. The first two years of the program were directed toward basic measurements of the influences of material and flaw characteristics on inspection reliability, as well as preparations for the Round Robin which is currently in progress.[1] The primary activity during this third year of the program has been the Round Robin to determine the effectiveness of primary piping inservice inspection. Other activities in support of and in addition to the Round Robin include: instrument and search unit evaluation, state-of-practice review, initiation of vessel application investigations, fracture mechanics evaluations, statistical evaluations and crack making processes. I will briefly review the status of these program components and discuss in more detail the Round Robin and its preliminary results.

STATUS OF MAJOR PROGRAM TASKS

ROUND ROBIN

The Round Robin involves six inspection teams, approximately 1500 test sample measurements on 100 pipe samples and 3,240 inspection man-hours over a period of seven months. The test materials include 10 inch, Schedule 80 stainless steel pipe with intergranular and fatigue cracks, as well as 33 inch, centrifugally cast stainless steel and clad ferritic main coolant pipes with fatigue cracks. The Round Robin was initiated in May 1981. The fifth team is now completing the test matrix. I will discuss later the test results from the first four teams. We expect to publish preliminary results of the Round Robin early in 1982 with detailed analysis and destructive test results available in May or June of 1982.

INSTRUMENT AND SEARCH UNIT EVALUATION

A major contributor towards the effectiveness of an inspection is the operating characteristics of the inspection system. Over the past year, we have developed a laboratory system for measuring these characteristics. The operation of each component of the system is

assessed independently. Measured transmitter parameters include: pulse waveforms into fixed known loads, frequency content and impedance. Measured search unit parameters (independent of pulser characteristics) include: spectral and temporal response, bandwidth, center frequency, peak frequency and insertion loss. Angle beam transducer profiles and amplitude distributions are also measured in steel. Measured receiver-display parameters include: bandwidth, noise, sensitivity, linearity and input impedance. The measurements are, for the most part, performed using a desk-top calculator and plotter which can produce finished four color data sheets. A report describing the system and results of several evaluations is expected to be published in late 1981. Each search unit and instrument used in the Round Robin has been characterized and will be reported.

STATE-OF-PRACTICE REVIEW

As a part of this program, a review of the state-of-practice for inservice inspection of nuclear piping was conducted. Interviews with utility, ISI vendors and NSSS ISI personnel were conducted with detail questions concerning equipment, procedures, materials, geometrical conditions and access. The responses to these questions have been compiled and analyzed. The document is currently in the review process and is expected to be published within two months.

VESSEL APPLICATIONS

Two efforts in the area of vessel examinations have been initiated. These include a short term program to define the effectiveness of near-surface (under clad crack) examinations and a longer term program to assess the effectiveness of the overall vessel inspection program.

The objective of the short term program is to assess the capability of existing and proposed near-surface crack detection techniques to detect .25 to .5 inch deep cracks which could become critical in the event of an overcooling transient in some of the older PWR reactors. Fabrication of a test block with under clad fatigue cracks is in progress. The block will be evaluated using existing and proposed near-surface inspection techniques. Also, as a part of this program, a block will be supplied to the U.S. Pressure Vessel Research Committee (PVRC) for inclusion in a round robin which is expected to be conducted during the summer of 1982.

In the longer range program, both volumetric and near-surface cracks will be considered. Both preservice and inservice inspections will be incorporated. The influence of calibration, clad conditions, flaw orientation, equipment characteristics, as well as geometric conditions will be considered. We expect to cooperate in this effort with both the U.S. PVRC, as well as the International Plate Inspection Steering Committee (PISC).

FRACTURE MECHANICS

The primary objective of the fracture mechanics task is to evaluate the impact of inspection unreliability and to provide recommendations for more appropriate inspection requirements. A program continuing the efforts initiated by Battelle Columbus [2] which was reported here last year, to assess the integrity of the PWR cold leg is nearing completion. This report is expected to be completed and published in 1981.

STATISTICS

Statistical analysis has played an important role in this program, in both designing the test matrix, as well as analyzing the data. It is our expectation that the results of the piping Round Robin test will allow us to model other situations which could not be included in the test matrix. In the pressure vessel inspection reliability area, this program is also providing assistance to the PVRC and PISC programs in the analysis of inspection data.

CRACK MAKING

A key to successful reliability assessments is the defects which are available for evaluation. Over the past two years, we have developed the capability to produce realistic surface connected cracks (both fatigue and IGSCC) in piping samples of complicated geometrical configurations. These, as well as other samples, could provide a sample set which could be used to qualify the effectiveness of procedures and personnel. A report describing these crack making techniques is expected to be published by mid-1982.

ROUND ROBIN INSPECTION PROGRAM

Preparations for the piping Round Robin were completed and the first of six teams completed the examination matrix in May 1981. The fifth team is now completing their examinations during this last week of October. The sixth and last team is tentatively scheduled for November or December 1981.

The objective of the piping Round Robin is to define the reliability and effectiveness of inservice inspection procedures. Procedures based on minimum Code requirements, as practiced field procedures and recommended improved procedures, are being tested. A second objective is to define the source and magnitude of inspection uncertainties. Towards this end, the manual inspection data is being automatically recorded for later analysis. Teams from six industrial ISI organizations are being used to collect the data.

The test matrix is shown in Figure 3. The test matrix consists of two procedure codes (as applied in the field) and improved; four material/flaw type combinations; two inspection environments (laboratory and difficult) and two access conditions (near and far side). The effectiveness of minimum Code requirements will be measured by evaluating recorded data from the field procedures.

The size of each experiment is dictated by the confidence level which is required. The major experiments are the Code procedures under difficult conditions for near side access and are treated by the full ANOVA experiments of 25 observations per team. The results of other experiments are compared to the major experiments and require fewer observations to provide meaningful measures of the differences.

PRELIMINARY ROUND ROBIN RESULTS

Although the data is preliminary, it is appropriate to review it and to make limited conclusions. The data available here is from the first four teams. In drawing conclusions based on this data, one should consider that: (1) the data has been scored by computer and the results may improve or be lowered by the manual analysis now in progress, and (2) the fatigue cracks included are conservative. The IGSCC are not necessarily conservative.

The probabilities reported here as a function of crack depth are of two types; probability of detection (DET) and Correct Rejection (CR). Correct rejection is the simple probability that a flaw of a given depth will be detected and properly classified as a crack without regard to depth sizing. Detection is the probability that the defect was detected but not necessarily properly classified as a crack. The difference between the two is the probability that a crack was called a geometry signal.

Figure 4 depicts the results for 10 inch, Schedule 80 stainless pipe for both fatigue and IGSCC cracks. (There was very little difference in test results between fatigue and IGSCC cracks). Note that for zero size defects, a 37% probability is recorded. This represents the number of blank samples which were improperly called cracked. In Figure 5, the performance of the best, as well as the least effective teams, are shown. Note that the most effective team had a false call rate (blanks called cracks) of only 8% as opposed to 50% for the least effective team. We believe that a false call rate of less than 15 to 20% for this test is an acceptable rate. In field applications, considerably more analysis will be performed before a pipe is cut out.

Figure 6 shows the degree of improvement resulting from the "improved procedure". The degree of improvement is modest. This can be accounted for by two factors. The first being that two of the teams were using sensitivies equivalent to the improved procedure (20% DAC from a 10% notch). The second factor could be that the training time was insufficient to change acquired habits and opinions.

The results for the clad ferritic main coolant pipe are shown in Figure 7. We can see that for this case, performance is considerably improved and that the correct rejection probability for the improved procedure is 100% for all cracks. This degree of improvement can be attributed to the increased sensitivity (20% DAC as opposed to 50%), as well as the trianing provided (approximately four hours).

The results for cast stainless main coolant pipe is not so encouraging. The results from one team using their own field procedure are shown in Figure 8. The remaining teams scored zero or less than 25%. The flaws in this material are conservative (i.e., short and tight), however, they are identical to those in the clad ferritic pipe. The improved procedure did not prove effective, even for the team shown in Figure 8. However, we believe it is possible with training to do better than is shown in Figure 8, particularly in minimizing the number of false calls.

AXIAL POSITION ACCURACY

A key parameter in distinguishing between cracks and geometrical reflectors is the axial position of the defect relative to the root or other geometric discontinuities. Manual plotting is the method generally used for this determination. Table I lists the axial positioning errors for the four teams. The mean error ($\bar{x}$) and the standard deviations (σ) are listed for each team and three of the test material/flaw combinations. Material 1 is the 10 inch, Schedule 80 stianless pipe with fatigue flaws. Material 2 is the same as one except that it contains only IGSCC flaws. Material 3 is the clad ferritic main coolant pipe. The cast stainless steel pipe is omitted due to lack of sufficient data. The primary attribute which should be noted is that the fourth team performed most effectively and Team One was the least effective in performing the Round Robin as measured by their rate of correct rejection. Team Two's performance was close to Team One. While Team Three was close to the performance of Team Four. It can be

Table I
Axial Position Accuracy

Team		Material: 1	2	3
1.	$\bar{x}$	.01 in.	.03 in.	-.06 in.
	σ	.29	.25	.24
2.	$\bar{x}$	-.12	-.18	-.03
	σ	.25	.29	.22
3.	$\bar{x}$	.002	.03	-.05
	σ	.15	.17	.12
4.	$\bar{x}$	.06	.06	-.04
	σ	.14	.12	.10
All	$\bar{x}$	-.004	-.002	-.047
	σ	.223	.211	.176

seen from the table, that the standard deviation for Teams Three and Four is approximately one half of that for Teams One and Two. In addition, it appears that Team Two has systematic errors for

Materials 1 and 2, as indicated by their larger and negative mean error $\bar{x}$. While it may not be sufficient, this data does indicate that axial location accuracy is a good indicator of effective performance.

PERLIMINARY CONCLUSIONS FROM THE ROUND ROBIN

Several conclusions can be drawn from a preliminary review of available Round Robin data. These include the following, which are listed in descending order of confidence:

1. Inspection of clad ferritic main coolant pipes can be highly effective, given that sufficient inspection sensitivity is used.

2. Large differences in performance between teams, all meeting Code, were observed.

3. The care and accuracy of plotting the axial position of indications appears to be an indicator of performance effectiveness.

4. Access to the flaws (near side or far side of the weld) had no statistical significance for the clad ferritic pipe.

5. Little difference was noted between the laboroatory and difficult conditions as applied in this test.

6. Performance improvements resulting from the "improved provedure" were modest, except for the clad ferritic case where improvement was significant.

Conclusions concerning the remaining parameters of the Round Robin must await further data and analysis.

REFERENCES

1. Becker, F.L., et al, Integration of NDE Reliability and Fracture Mechanics, Phase I Report, NUREG/CR-1696, PNL-3469, Vol. 1, prepared for the Nuclear Regulatory Commission by Pacific Northwest Laboratory, Richland, Washington, September 1980 - March 1981.

2. Mayfield, M.E., et al, Cold Leg Integrity Evaluation, NUREG/CR-1319, prepared for the Nuclear Regulatory Commission by Battelle Columbus Laboratories, Columbus, Ohio, February 1980.

NDE/FM

OBJECTIVES

1. DETERMINE THE RELIABILITY OF ULTRASONIC INSERVICE INSPECTION (ISI) PERFORMED ON COMMERCIAL, LIGHT WATER REACTOR PRESSURE VESSELS AND PIPING
2. USING FRACTURE MECHANICS ANALYSIS, DETERMINE THE IMPACT OF NDE UNRELIABILITY ON SYSTEM SAFETY AND DETERMINE THE LEVEL OF INSPECTION RELIABILITY REQUIRED TO ASSURE A SUITABLY LOW FAILURE PROBABILITY
3. EVALUATE THE DEGREE OF RELIABILITY IMPROVEMENT WHICH COULD BE ACHIEVED USING IMPROVED AND ADVANCED NDE TECHNIQUES
4. BASED ON MATERIAL, SERVICE AND NDE UNCERTAINTIES, FORMULATE RECOMMENDED REVISIONS TO ASME SECTION XI AND REGULATORY REQUIREMENTS NEEDED TO ASSURE SUITABLY LOW FAILURE PROBABILITIES

FIGURE 1. Objectives.

NDE/FM LICENSING AND SAFETY ISSUES

I EFFECTIVENESS AND RELIABILITY OF INSERVICE INSPECTION

II ADEQUACY OF CURRENT REQUIREMENTS

- INSPECTION TECHNIQUE
- EXTENT AND FREQUENCY OF INSPECTION
- ALLOWABLE FLAW SIZES AND REQUIRED PROBABILITY OF DETECTION

III RECOMMENDATIONS FOR IMPROVED INSPECTION REQUIREMENTS

FIGURE 2. Licensing and Safety Issues.

ULTRASONIC TESTING PROCEDURE	PIPE TEST MATERIAL	INSPECTION CONDITIONS (ENVIRONMENT)			
		LABORATORY		DIFFICULT	
		NEAR ACCESS	FAR ACCESS	NEAR ACCESS	FAR ACCESS
FIELD / IMPROVED	10-INCH STAINLESS STEEL (SS) FATIGUE	12	12	25 / 16	12
	10-INCH SS WITH IGSCC	12		25 / 16	12
	32-INCH CENTRIFUGALLY CAST SS	3		25 / 16	12
	33.5-INCH CARBON STEEL + SS CLADDING	3		25 / 16	12

Figure 3. Round Robin Test Matrix. Number of Observations for the Field Procedures are Shown Above the Diagonal, Improved Procedures Below.

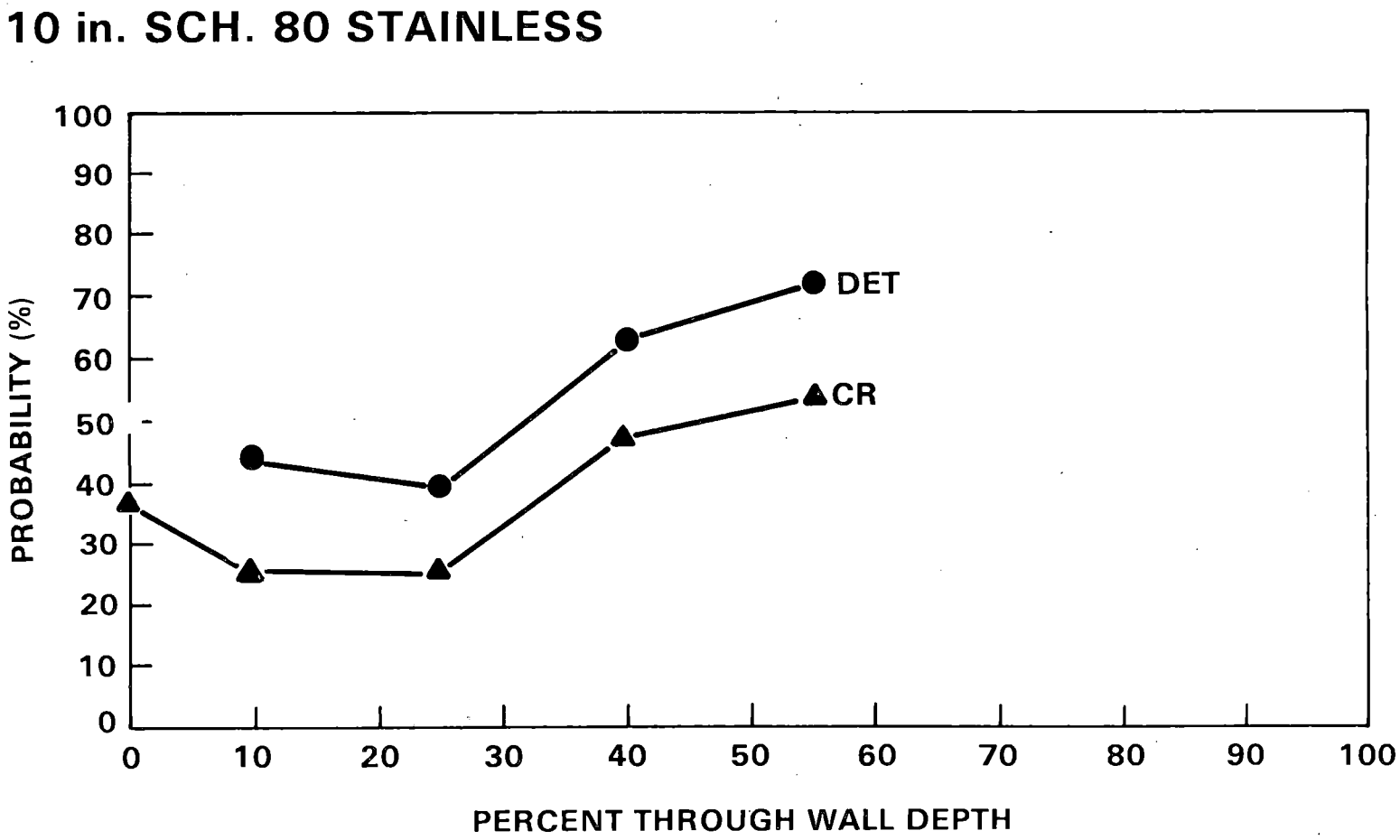

FIGURE 4. Probability of Detection (DET) and Correct Rejection (CR) of Fatigue and IGSCC Cracks in 10 in. Sch. 80 Stainless Steel Pipe as Function of Through Wall Depth, for Four Teams.

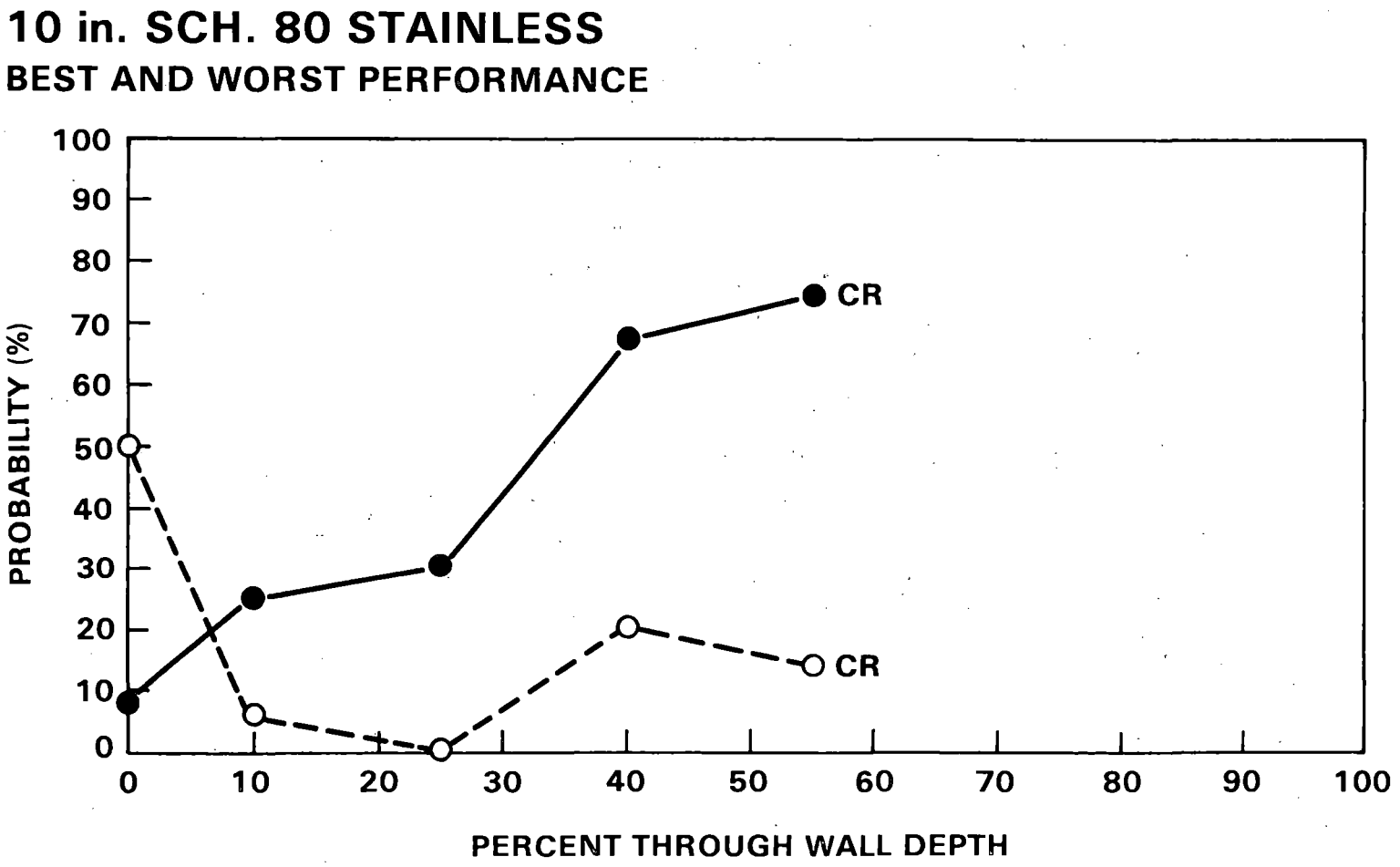

FIGURE 5. Probability of Detection (DET) and Correct Rejection (CR) of Fatigue and IGSCC Cracks in 10 in. Sch. 80 Stainless Steel Pipe as Function of Through Wall Depth, for Most and Least Effective Teams.

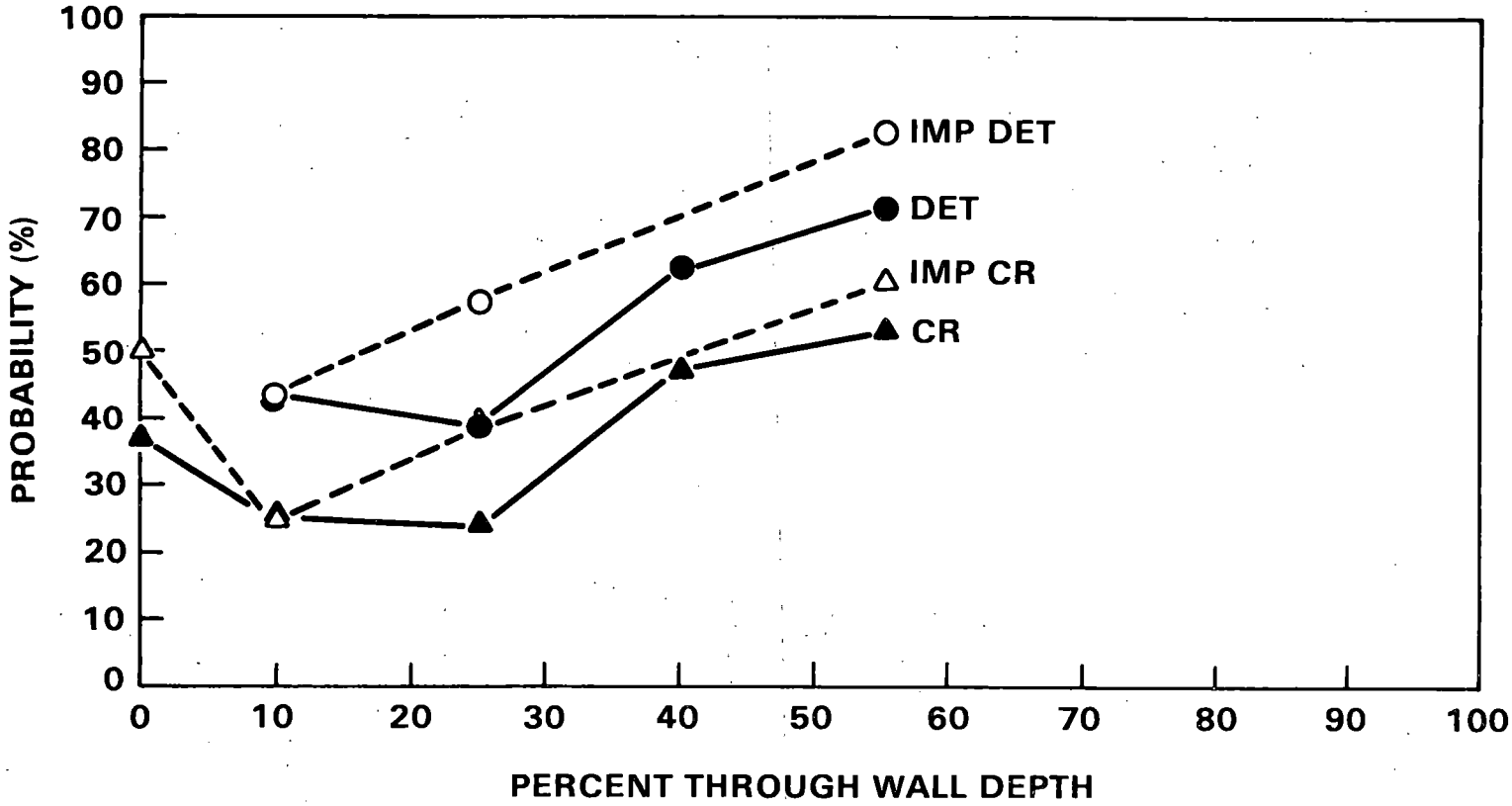

FIGURE 6. Probability of Detection (DET), Correct Rejection (CR), and Improved Inspection Procedure (IMP) of Fatigue and IGSCC Cracks in 10 in. Sch. 80 Stainless Steel Pipe as Function of Through Wall Depth, for Four Teams.

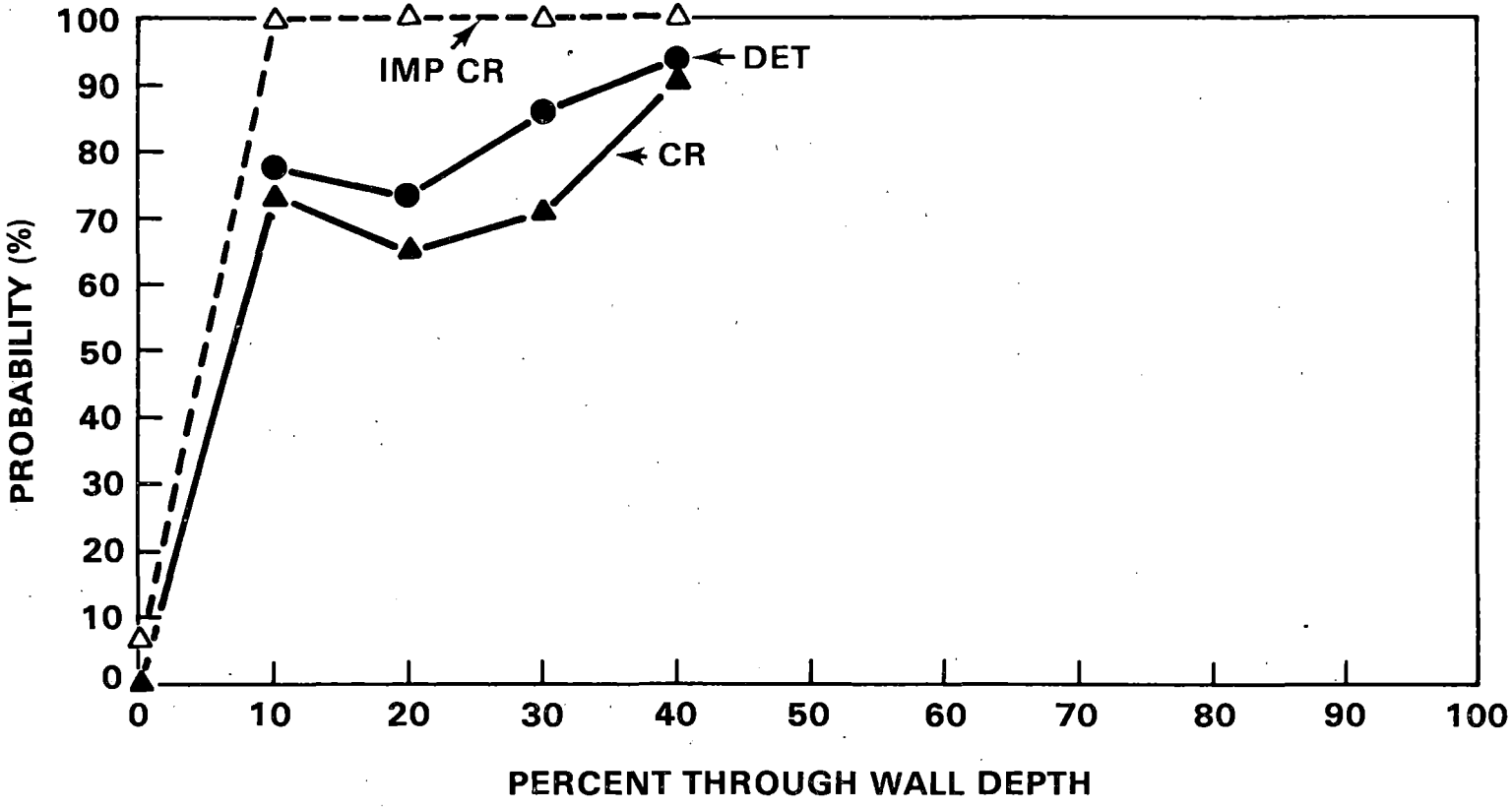

FIGURE 7. Probability of Detection (DET) and Correct Rejection (CR) of Fatigue Flaws in Clad Ferritic Main Coolant Pipe. The correct rejection rate for the improved procedure (IMP CR) is also shown.

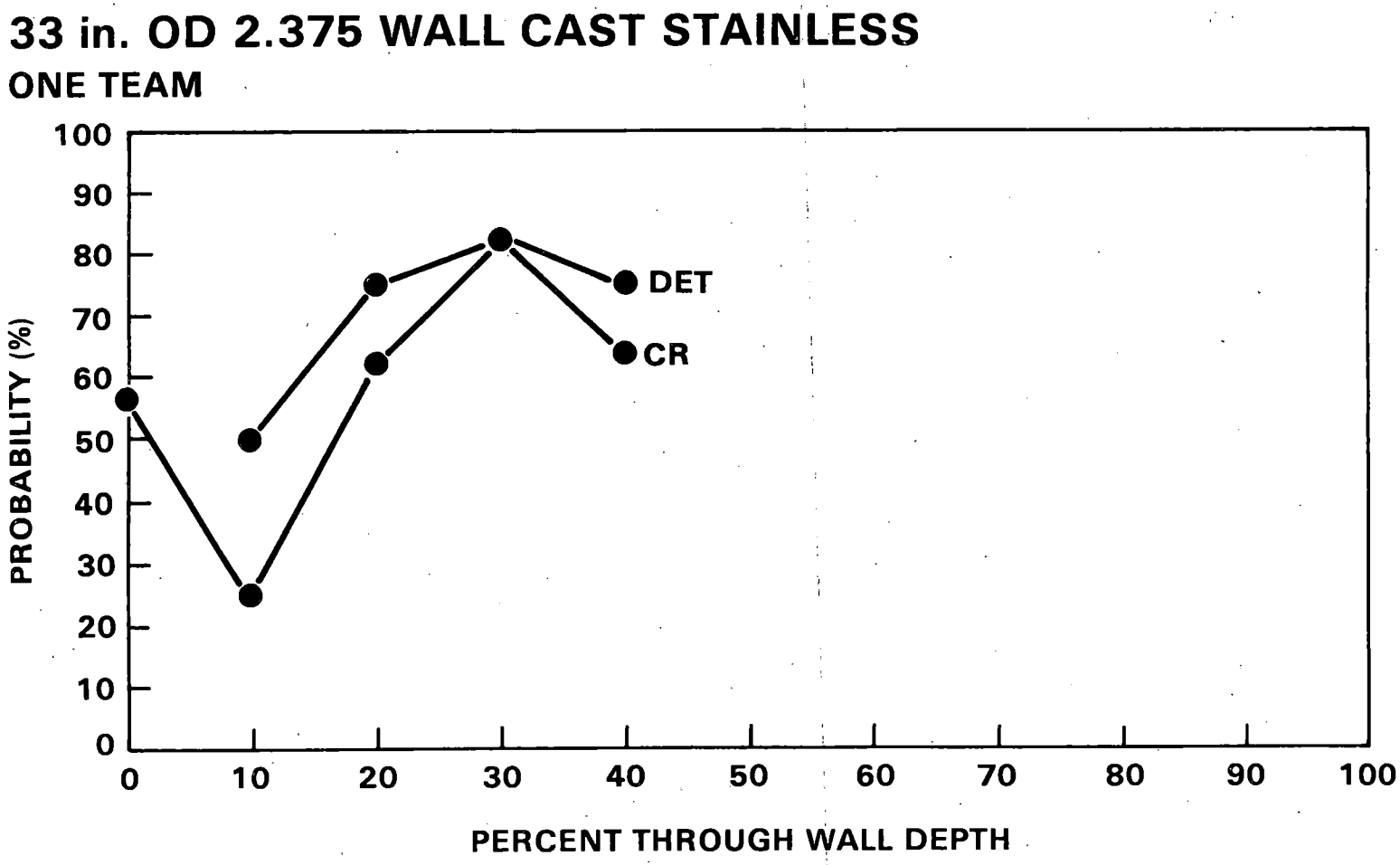

FIGURE 8. Probability of Correct Rejection (CR) and Detection (DET) in Centrifugally Cast Stainless Steel Main Coolant Pipe, for One Team. The remaining teams achieved less than 25% correct rejection rate.

IMPROVED EDDY-CURRENT INSPECTION OF POWER REACTOR STEAM GENERATOR TUBING*

C. V. Dodd

Metals and Ceramics Division
OAK RIDGE NATIONAL LABORATORY
Oak Ridge, Tennessee 37830

SUMMARY

The research branch of the U.S. Nuclear Regulatory Commission requested that the Nondestructive Testing Group of the Metals and Ceramics Division of Oak Ridge National Laboratory undertake a program to improve the eddy-current inspections of steam generator tubing. The initial objective of this program was to improve the accuracy of eddy-current inspections, particularly in the tube-support regions where dents, wall thickness changes, wastage, and cracks have occurred. Later our group was asked to give particular emphasis to the detection and measurement of the depth of the intergranular attack that was occurring in the tube sheet region.

We assumed a very general approach to the multiple-property inspection problem and considered all the options and requirements for designing the best possible inspection system. The system was initially designed using a theoretical model with calculations performed on a minicomputer. After initial design studies defined the best system for the given inspection conditions, an optimum three-frequency eddy-current instrument that can be controlled by its internal microcomputer or the minicomputer in the laboratory was constructed. The instrument was calibrated and tested on laboratory samples using the ModComp IV computer to control the test and reduce the data. During field operations, the operator can remain in a mobile laboratory and remotely run the test, with only the instrument physically located inside containment.

The system was tested in the field at the R. E. Ginna reactor, and then at the Point Beach reactor, two operating plants that had been experiencing intergranular attack. Approximately 100 tubes were scanned up to the first tube support at both plants. The system was operated at Ginna at frequencies of 10 and 100 kHz and 1 MHz. An offset of all the data was observed (the wall thickness gave a value of 63 mils rather than 50 mils). We later learned that this shift in data was caused by temperature and cable differences between the laboratory and Ginna. Other than this shift in data, no significant

---

*Research sponsored by the Office of Nuclear Regulatory Research, Nuclear Regulatory Commission, under Interagency Agreement DOE 40-551-75 with the Department of Energy under contract W-7405-eng-26 with the Union Carbide Corporation.

problems were experienced and vector correction of the raw magnitudes and phases made with the minicomputer restored the thickness readings to their correct values. This correction technique was programmed into the microcomputer for the Point Beach test. The frequencies were then changed to 20, 100, and 500 kHz to reduce the potential for this type of error. These two changes eliminated the offset problem. The results from both Ginna and Point Beach showed slight wall thinning that could be attributed to intergranular attack in some of the tube-sheet regions. The wall thinning was less than that observed in samples removed earlier from the steam generator.

The wall thickness of the Point Beach tubes appeared to be several mils thicker above the tube sheet. After a study of the effects of simulated sludge of different nonconducting ferromagnetic materials, it was speculated that the difference in thickness may result from a small layer of a good conductor such as copper plated out on the tubes. The presence of only a thin layer of the high conductivity would appear like thicker Inconel. After we had reported our findings, Westinghouse personnel acknowledged that they had also seen these "copper signals" in their inspections and that the signals were present in several different generators, with Point Beach being one of the worst. Calibration readings made on standards immediately after the probe was removed from the steam generator at Point Beach agreed very well with the actual values. The tube scans at Ginna were much cleaner and showed little, if any, change in thickness as the tube entered the tube sheet. Tubing samples from Ginna showing intergranular attack have been scanned with the eddy-current instrument and are now being metallographically examined.

This type of multiple-frequency inspection can detect buildup of sludge, deposition of products on the tube walls, magnetite formation, and other detrimental conditions so that corrective action can be taken before wastage, cracks, and other defects detrimental to the safety of steam generators occur.

Preliminary measurements with small dent samples have shown that the system is capable of measuring properties in the presence of these dents. We will attempt to extend these measurements to the detection of stress-corrosion cracks in the presence of large dents. This effort may require the use of multiple regions, spring-loaded pancake probes, or both.

Personnel from Westinghouse and Zetec as well as the personnel operating the reactors were impressed with the system and expressed their desire to incorporate parts of it into their equipment. Therefore, we will release these designs as they are completed.

GENERAL PROGRAM OBJECTIVES

1. Improve the state-of-the-art for steam generator inspection to meet the specific problems that are now present in steam generators.

2. Provide a broad technical base to allow quick response to new steam generator problems as they arise.

3. Provide NRC with an independent evaluation of the eddy-current inspections that the utilities and their vendors are performing.

SHORT-TERM PROGRAM OBJECTIVES

Develop eddy-current inspection techniques for steam generator tubing that will measure or discriminate against simultaneous variations in each of the following parameters:

1. tube diameter, including denting at the supports,
2. probe wobble,
3. presence of supports around the tube,
4. tube wall thickness,
5. location (radial and axial) of defects in the tube wall, and
6. size of defects in the wall.

Apply program to detection of intergranular attack in the tubesheet crevice region and perform field inspection.

THE PRESENTATION WILL COVER THE FOLLOWING

I. BACKGROUND

1. Steam generator problems

2. General eddy-current multiple property technique

II. OAK RIDGE SOLUTION TO THE PROBLEM

1. Analytical studies to determine best conditions

2. Construction of system for laboratory tests

3. Experimental verification of system on laboratory stamples

4. Design of system for field tests

5. Field test of system on Ginna and Point Beach steam generator tubing for intergranular attack

III. FUTURE PLANS

1. Train system to detect small cracks in the presence of large dents

2. Design a pancake probe and test it on the full range of dent standards

3. Field test the system at the PNL steam generator test facility on the tubes with large dents

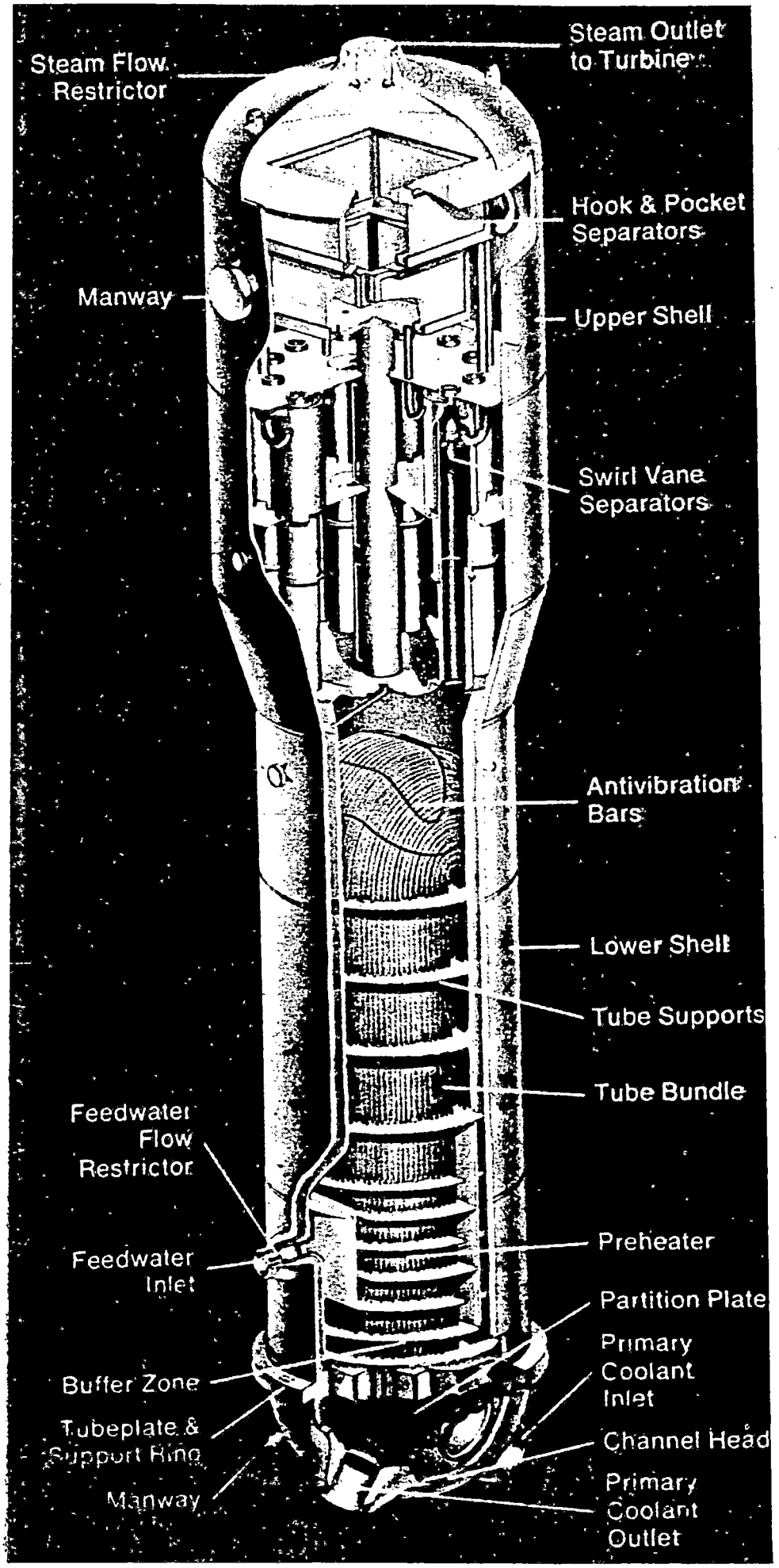
Steam Outlet to Turbine
Steam Flow Restrictor
Hook & Pocket Separators
Manway
Upper Shell
Swirl Vane Separators
Antivibration Bars
Lower Shell
Tube Supports
Tube Bundle
Feedwater Flow Restrictor
Preheater
Feedwater Inlet
Partition Plate
Primary Coolant Inlet
Buffer Zone
Tubeplate & Support Ring
Channel Head
Manway
Primary Coolant Outlet

ORNL-DWG 80-19391

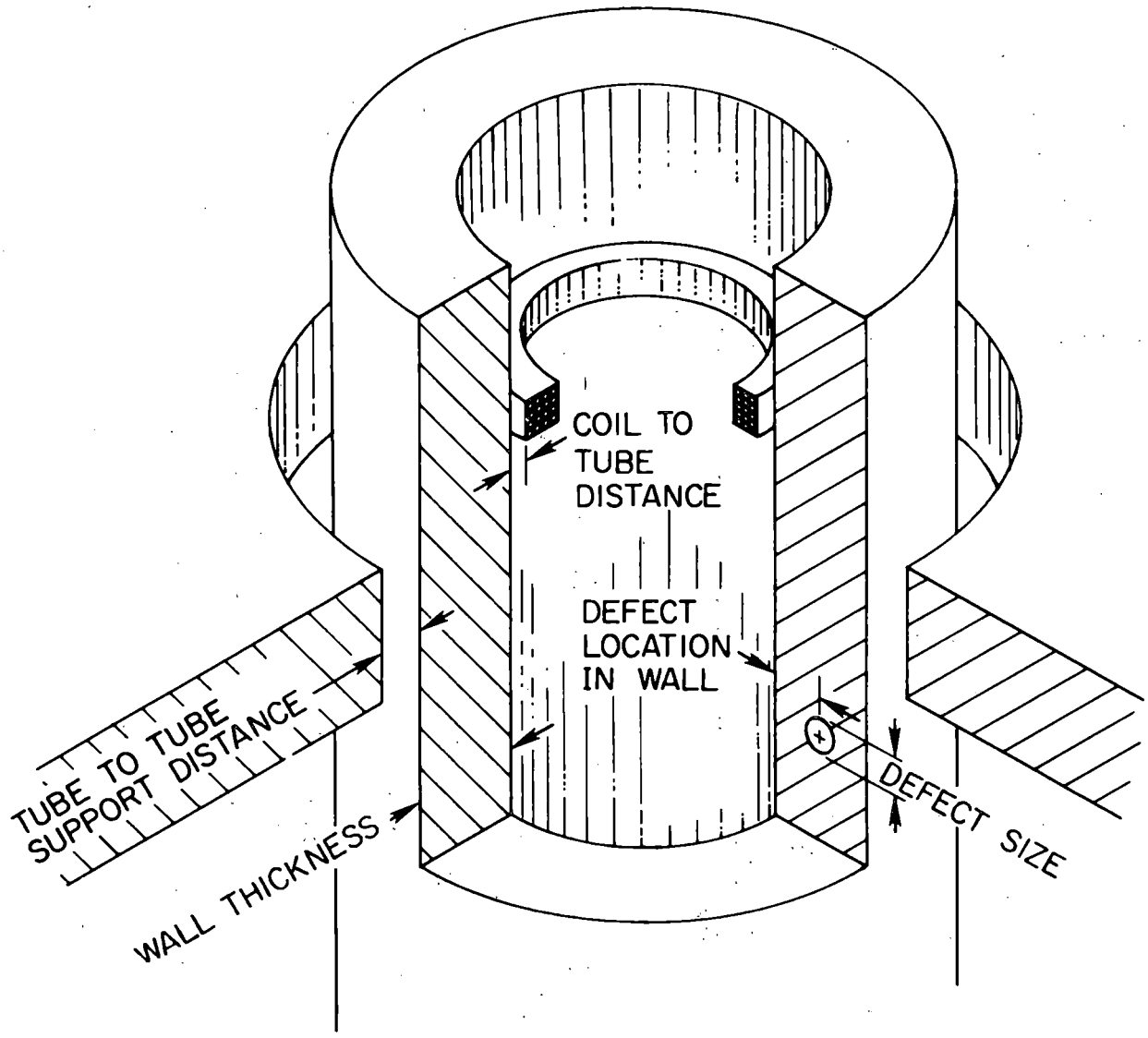

ORNL-DWG 80-19390

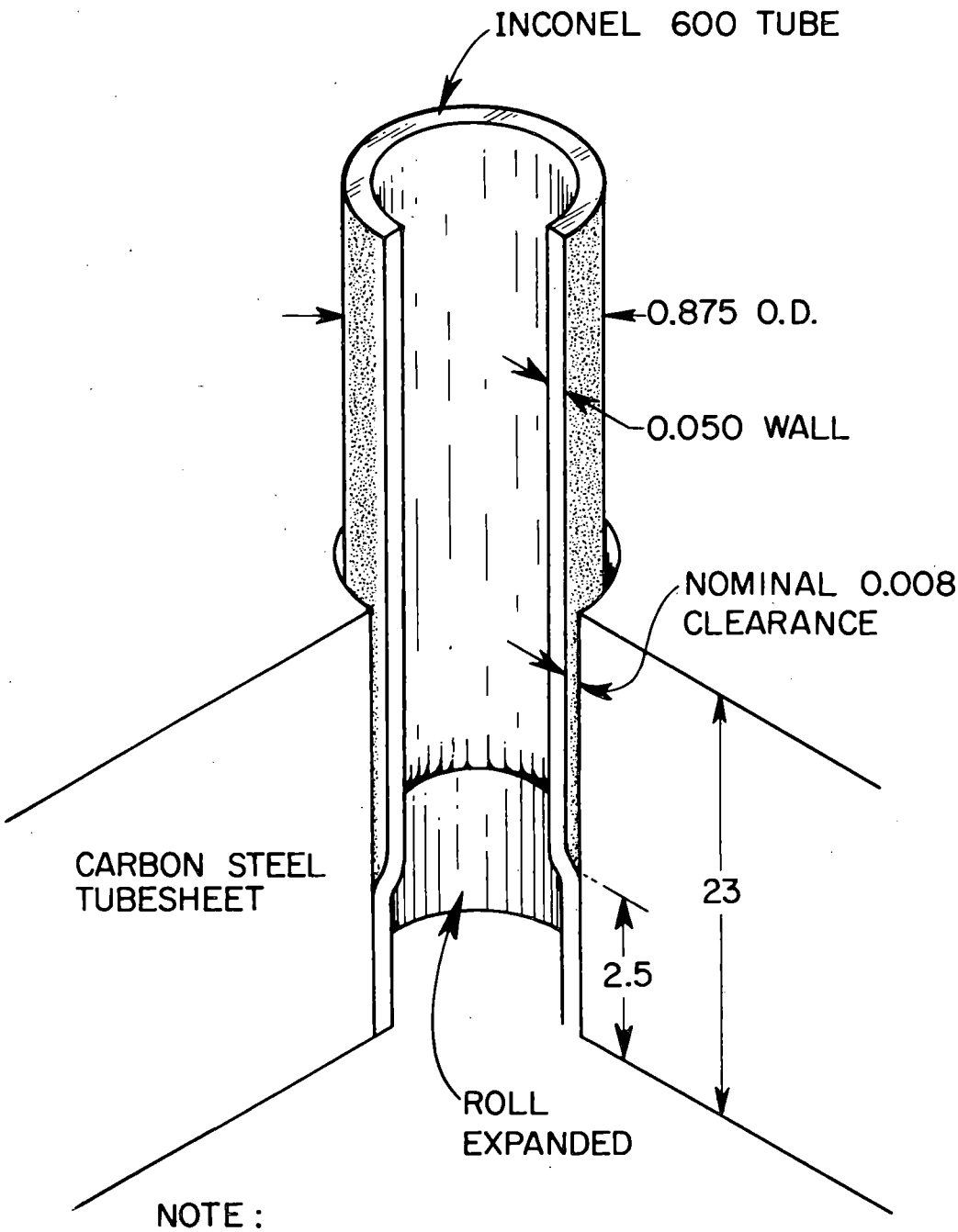

NOTE:
DIMENSIONS IN INCHES

ORNL–DWG 80-19392

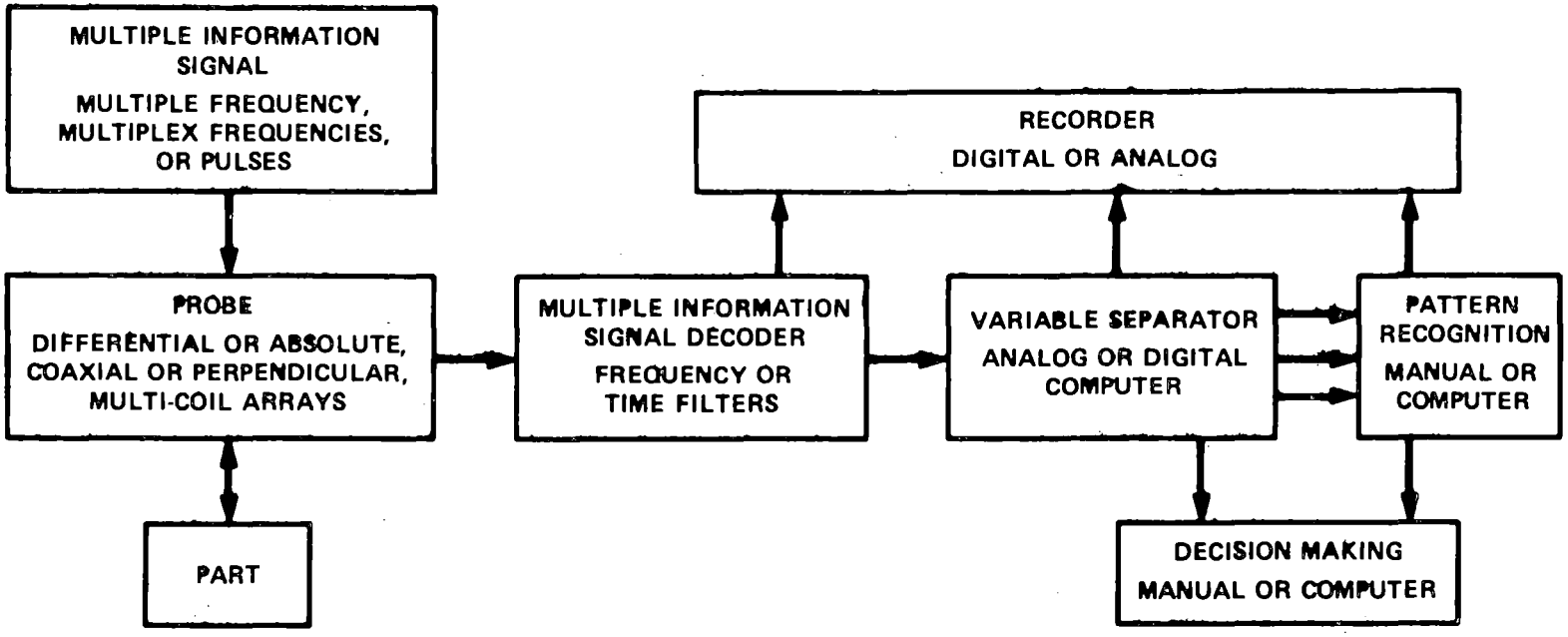

PRESENT TYPES OF MULTIPLE-FREQUENCY INSTRUMENTS

	Organization			
	ORNL	Zetec	Intercontrole	Adaptronics
Signal Source	Multiple Frequency	Multiplex Frequency	Multiple Frequency	-
Probe	Absolute	Differential/ Absolute	Differential/ Absolute	-
Signal Decoder	Filters	Time Delay	Filters	Sequential Scans
Variable Separator	Digital	Analog	Analog	-
Recorder	Digital	Analog	Analog	Analog
Pattern Recognition	-	Manual	Manual	Digital
Cost	-	$16K	$40K	-

ORNL-DWG 78-16168R

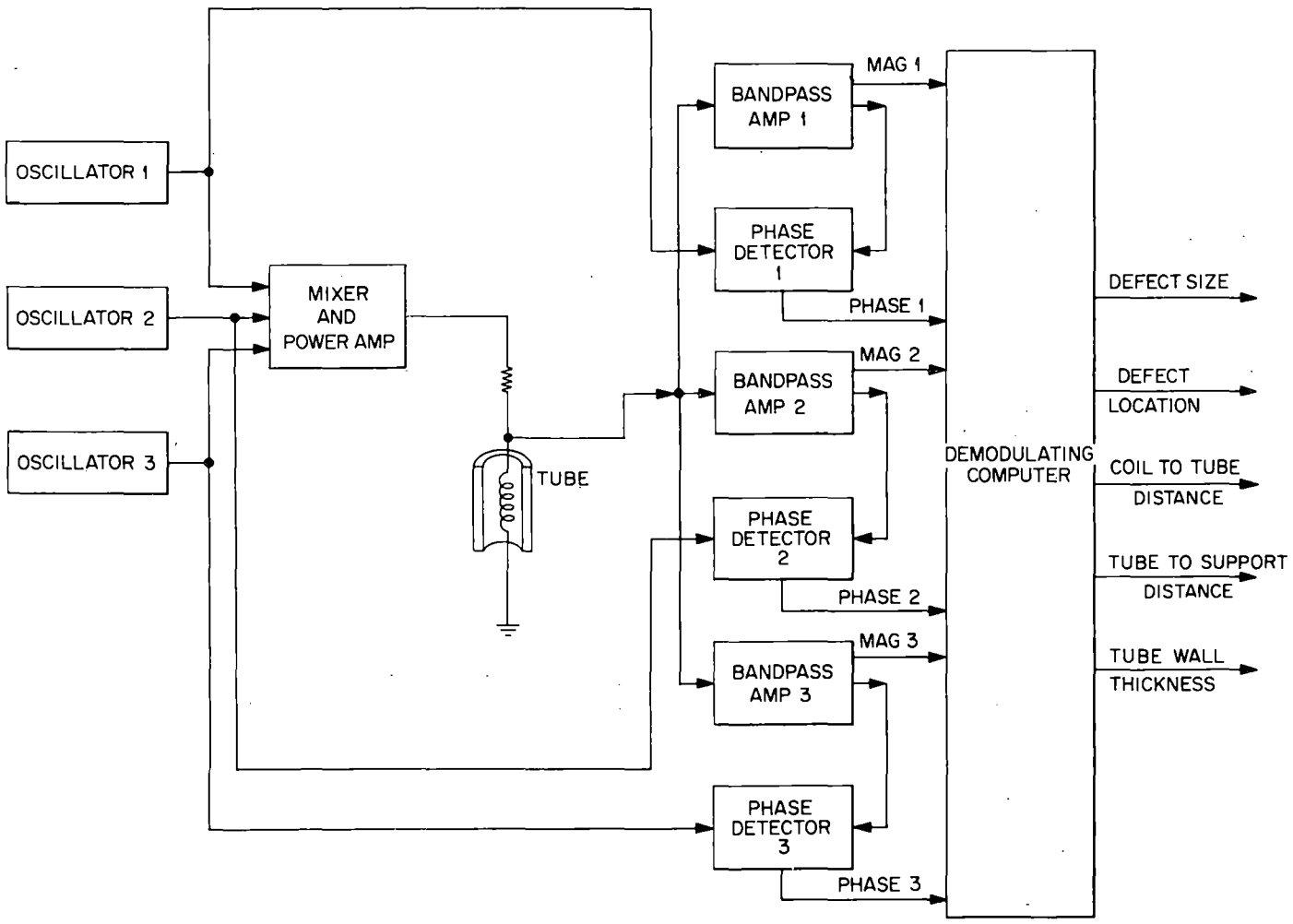

BLOCK DIAGRAM OF A THREE FREQUENCY INSTRUMENT

ORNL-DWG 80-11989

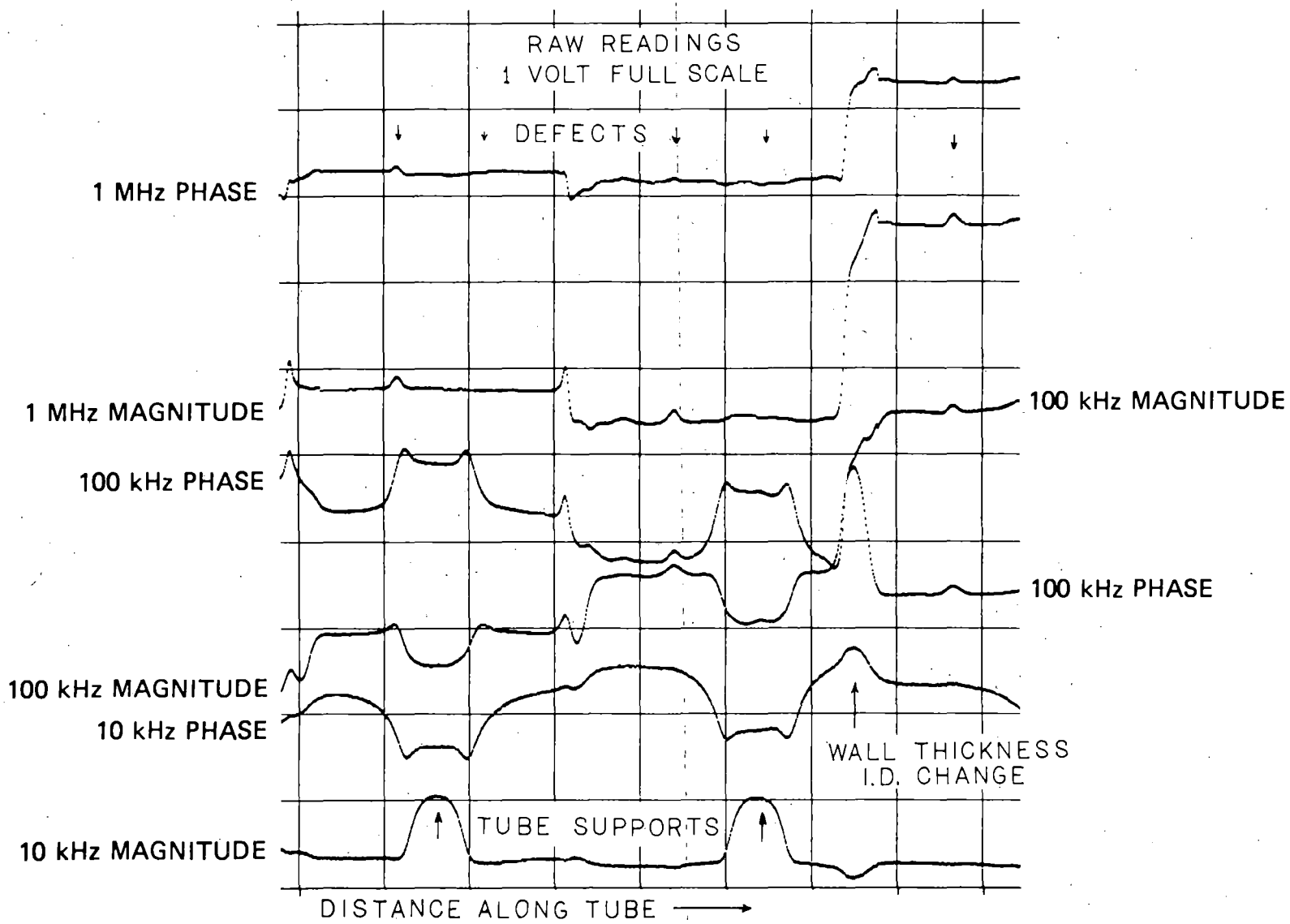

ORNL-DWG 80-11990

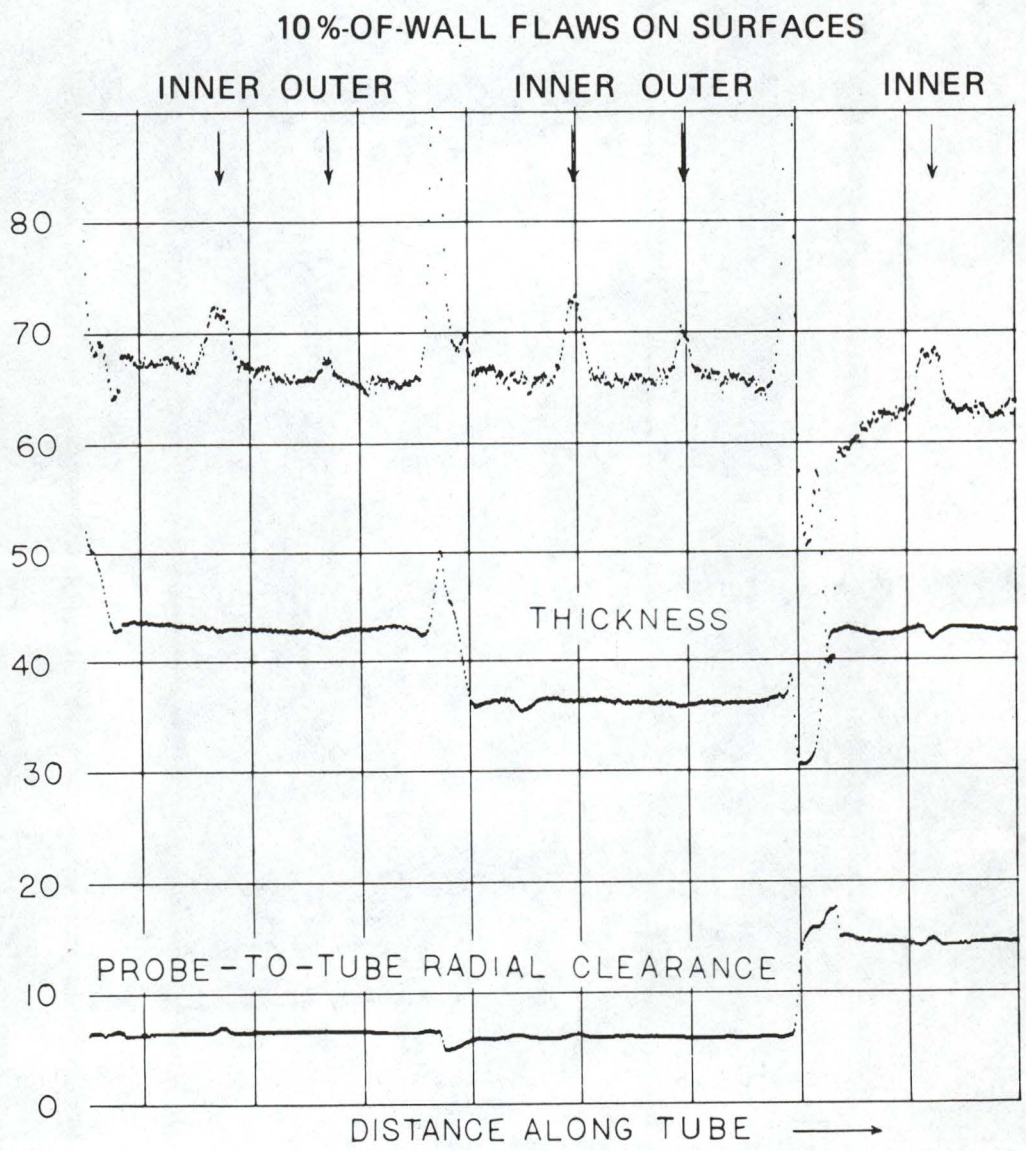

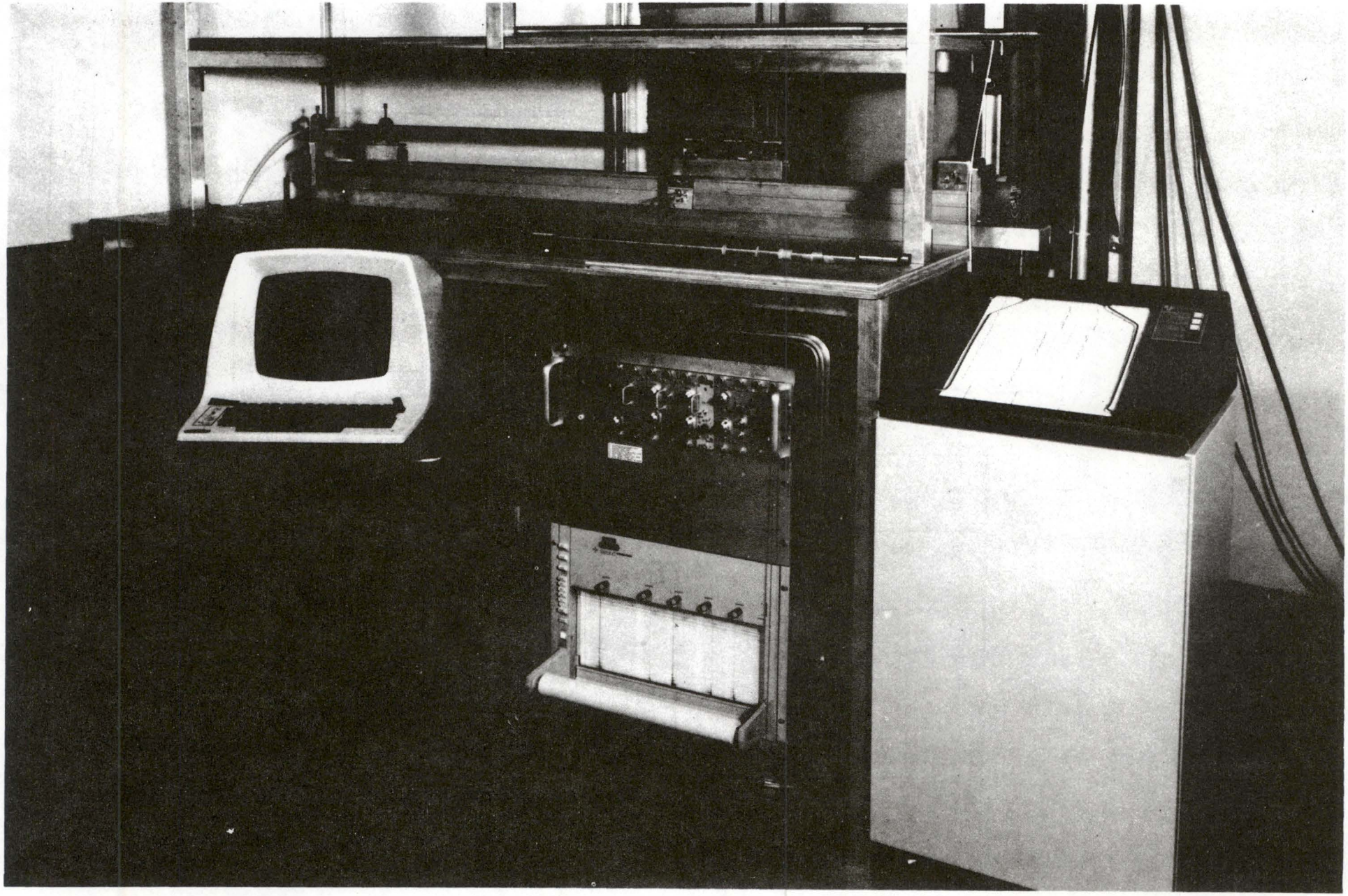

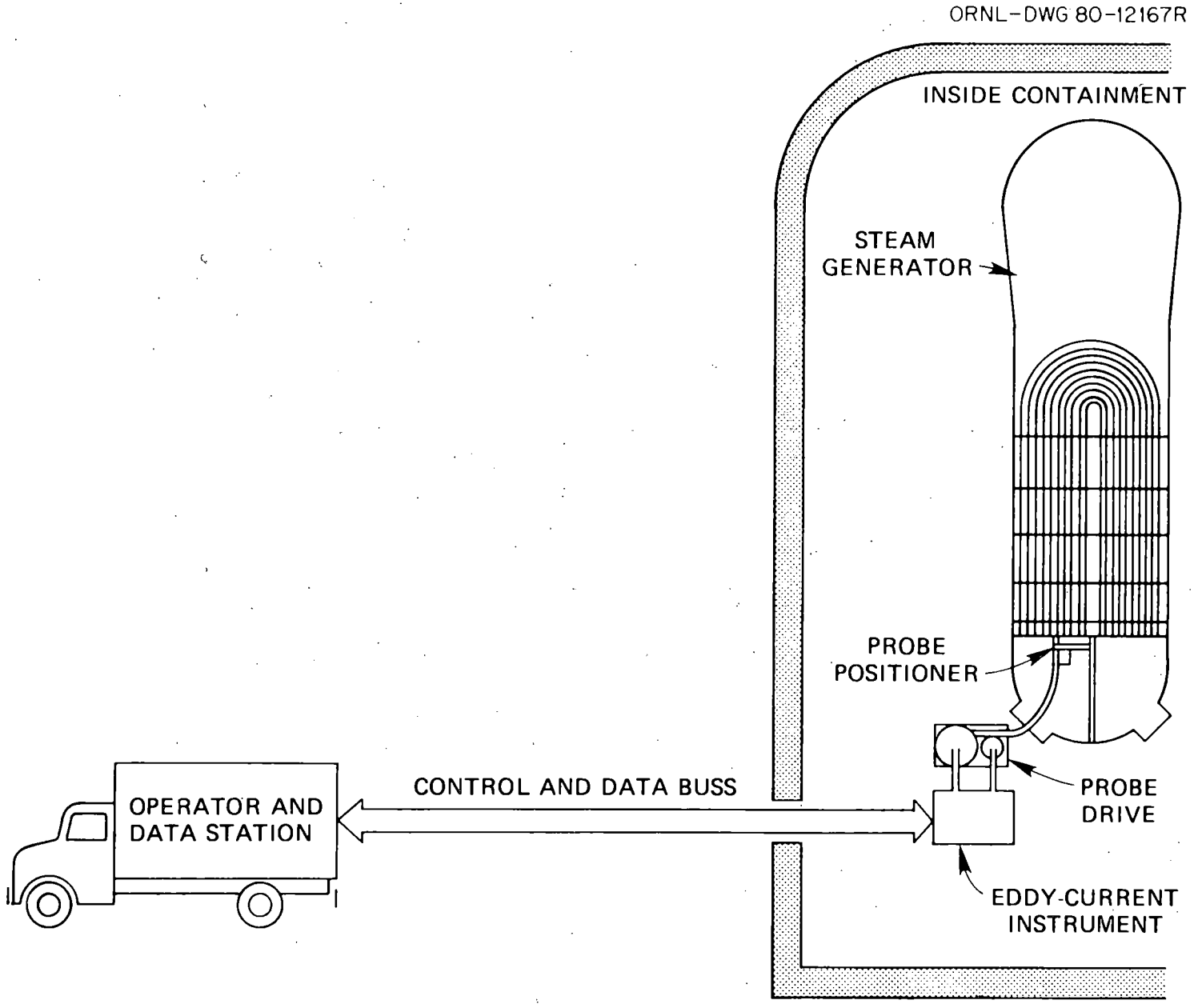
ORNL-DWG 80-12167R
INSIDE CONTAINMENT
STEAM GENERATOR
PROBE POSITIONER
PROBE DRIVE
EDDY-CURRENT INSTRUMENT
CONTROL AND DATA BUSS
OPERATOR AND DATA STATION

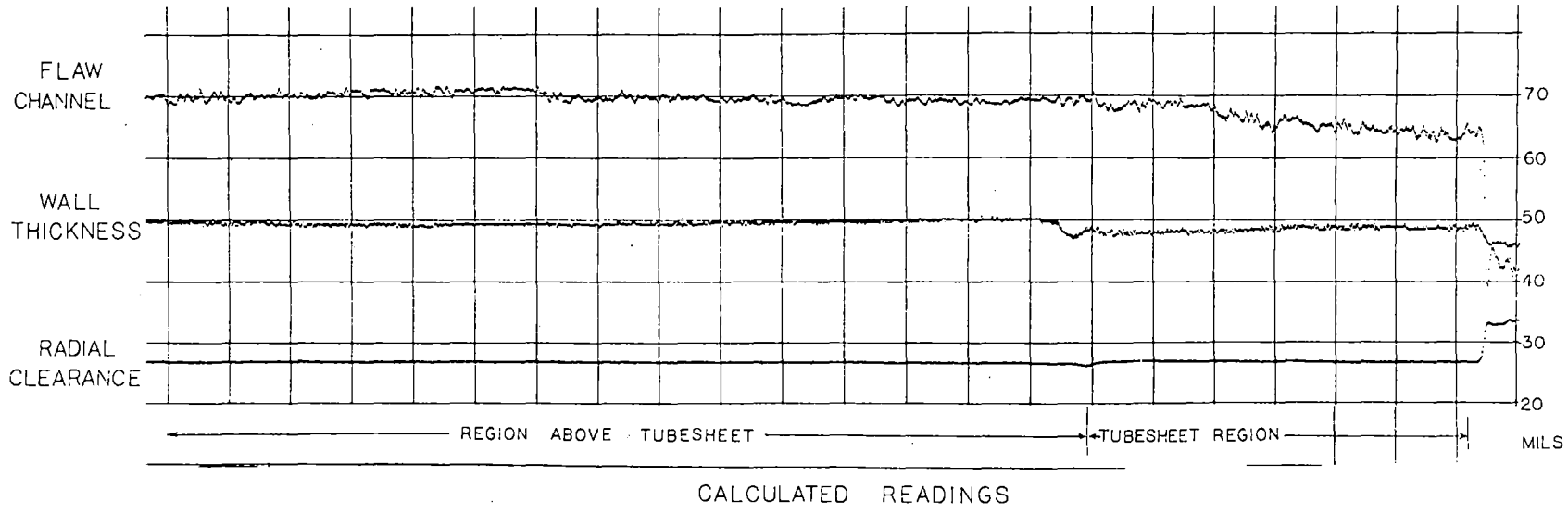

GINNA STEAM GENERATOR

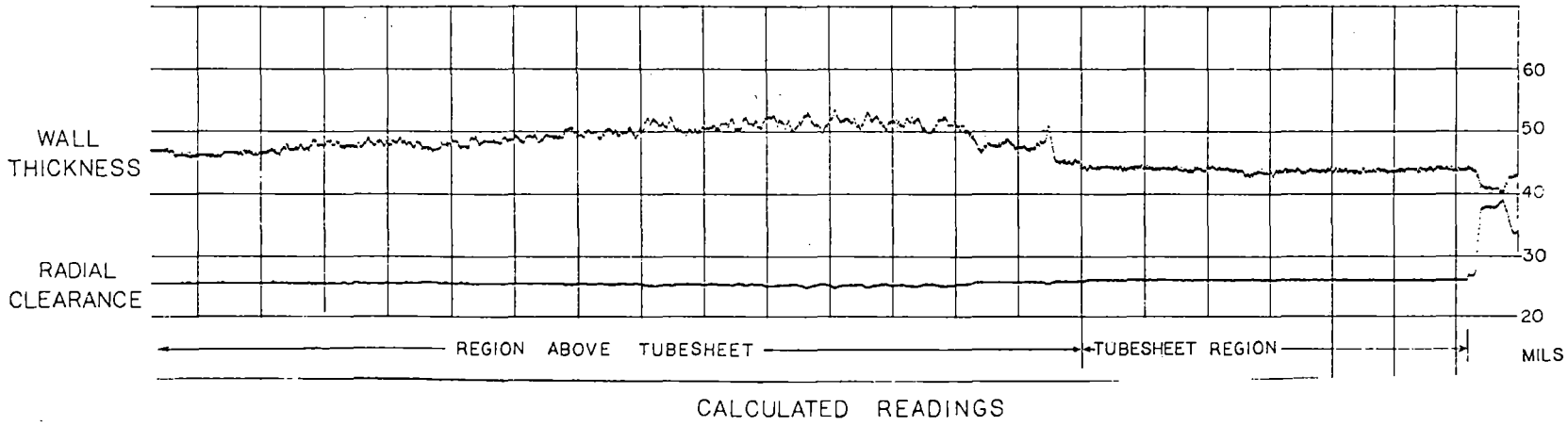

POINT BEACH STEAM GENERATOR

ORNL-DWG 81-10012

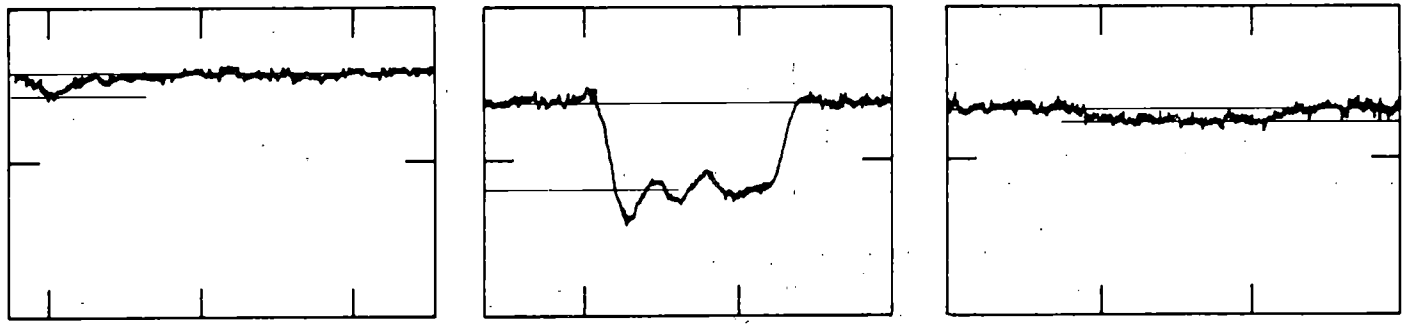

POINT BEACH SAMPLE
1.5 mil

PNL SAMPLE
5.5 mil

GINNA SAMPLE
1.0 mil

SUMMARY OF INSPECTION RESULTS

1. The equipment worked as designed and good raw data were obtained.

2. The IGA produced in the laboratory does not seem to match that produced in the field. The larger grain separation of laboratory samples gives a larger apparent thickness change than the actual steam generator sample.

3. The scans of tubes in the Ginna steam generator appeared similar to scans performed after the tubes had been removed.

4. Metallography is being performed to determine the degree of IGA on "good" and "bad" tubes.

5. Regions of the Point Beach tubes appear to have a metallic copper coating above the tubesheet.

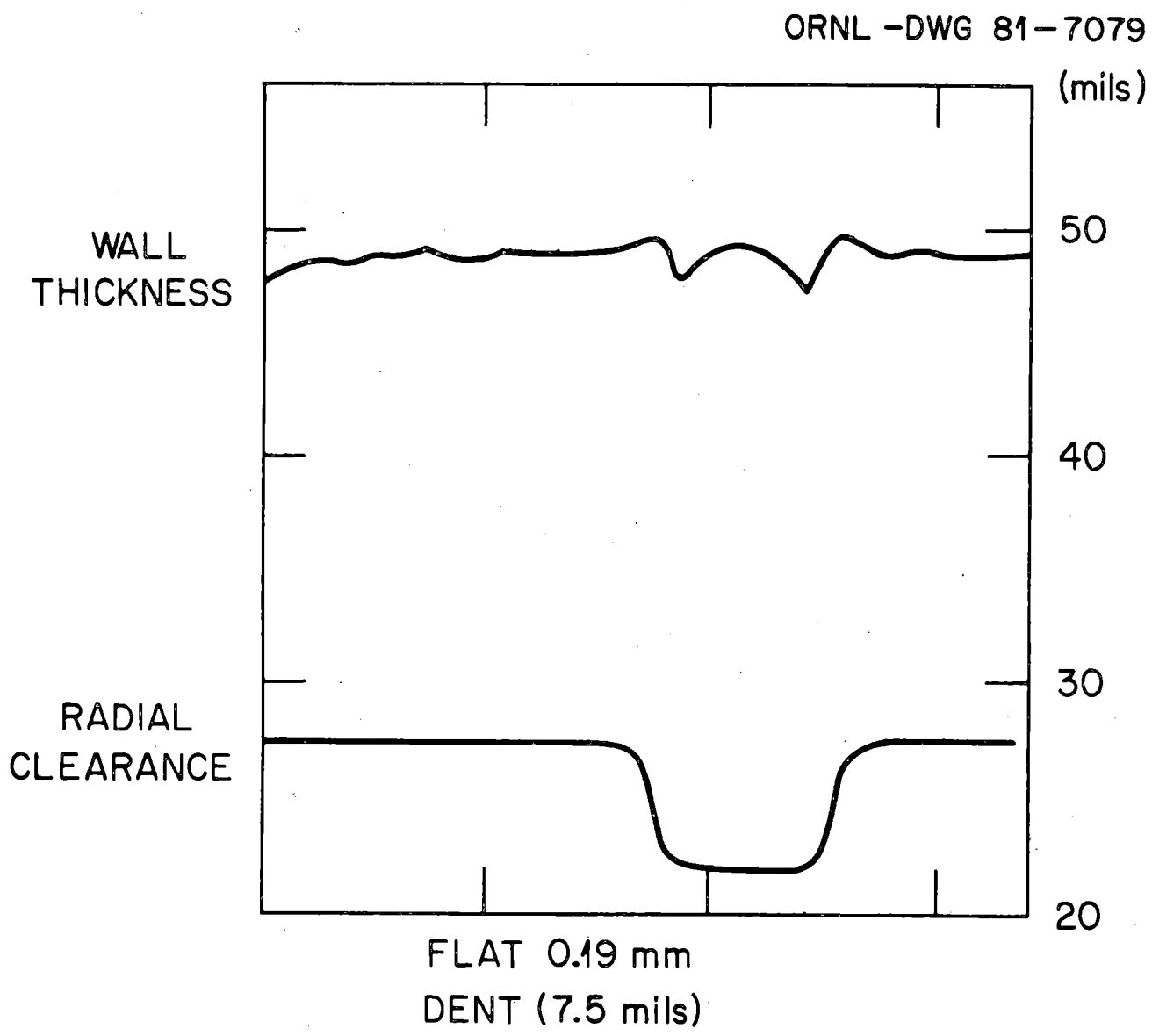
ORNL -DWG 81-7079
(mils)
WALL
THICKNESS
50
40
30
RADIAL
CLEARANCE
20
FLAT 0.19 mm
DENT (7.5 mils)

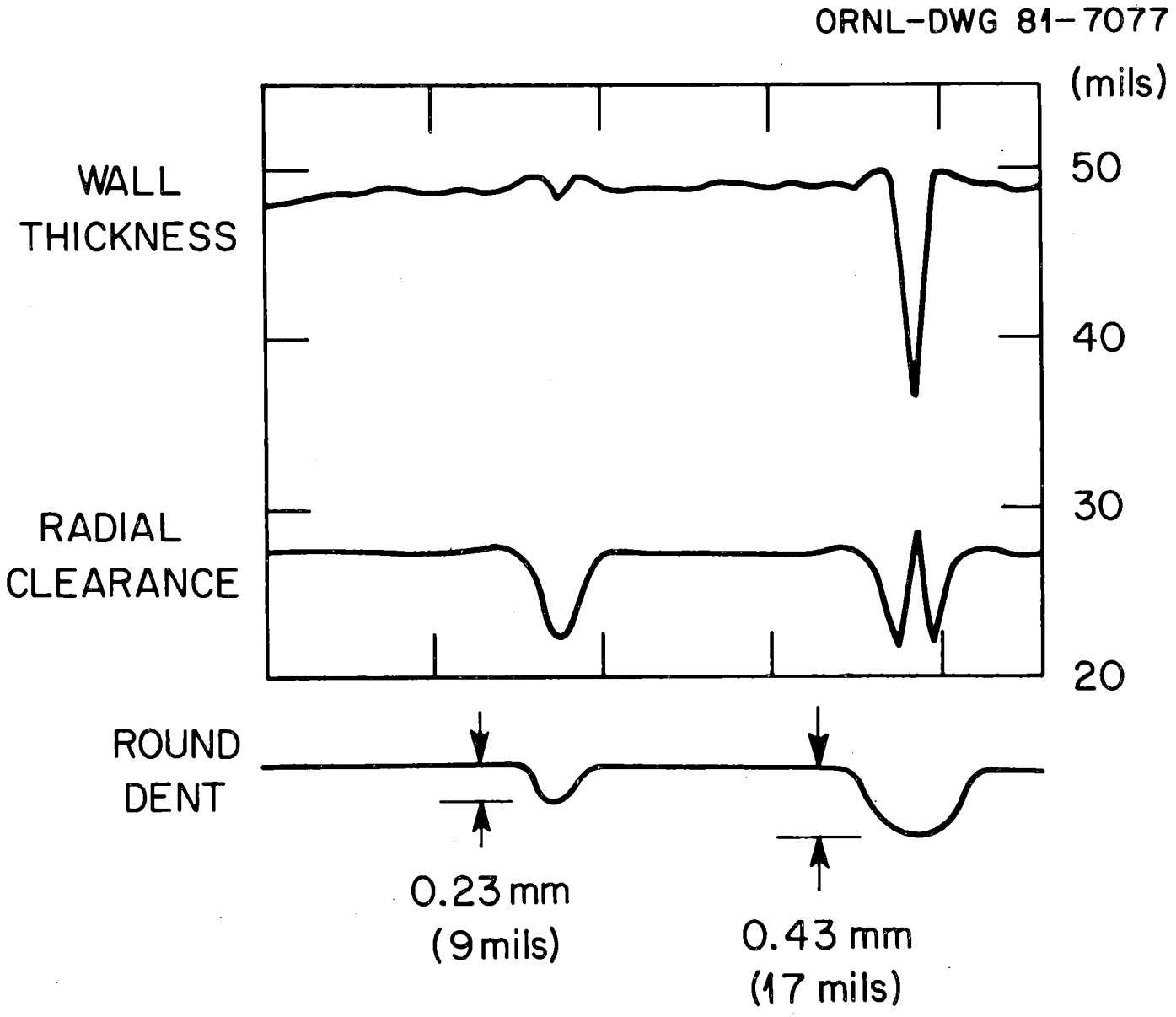
ORNL-DWG 81-7077
(mils)
WALL
THICKNESS
50
40
RADIAL
CLEARANCE
30
20
ROUND
DENT
0.23 mm
(9 mils)
0.43 mm
(17 mils)

FUTURE WORK

1. Extend the range of dents from 0.010 in. to 0.110 in. on the radius. Emphasize the detection of stress-corrosion cracks in this range.

2. Design an optimum pancake coil for steam generator tubing. Test on the entire range of standards available.

3. Test both the circumferential probe and the pancake probe at the PNL steam generator test facility.

PNL-SA-9968

NDE ROUND ROBIN POSSIBILITIES ON A RETIRED FROM SERVICE PWR STEAM GENERATOR

PWR STEAM GENERATOR TUBE INTEGRITY PROGRAM

R. A. Clark, Project Manager

October 1981

Presented at the Ninth Water Reactor Safety
Research Information Meeting
Gaithersburg, Maryland
October 26-30, 1981

Work Supported by
the U. S. Nuclear Regulatory Commission
NRC FIN No. B-2097
Dr. Joseph Muscara, Program Manager
under a Related Services Agreement
with the U.S. Department of Energy
Contract DE-AC06-76RLO 1830

Pacific Northwest Laboratory
Richland, Washington 99352

NDE ROUND ROBIN POSSIBILITIES ON A RETIRED FROM SERVICE PWR STEAM GENERATOR

An extensive research program utilizing a retired from service pressurized water reactor steam generator as a test bed has been initiated at Pacific Northwest Laboratory. This NRC program, because of the unique research opportunities it presents, has been organized to allow participation by other parties. Figure 1 provides a listing of the planned task activities for the total program. This paper deals with specific opportunities for participation in nondestructive examinations.

A recirculating type steam generator was obtained for research purposes by the NRC after its removal from service at Virginia Electric and Power Company's Surry II nuclear station. The steam generator had been in service approximately six years. At the time of removal almost 22% of the generator tubes had been plugged either because of indicated defects or as a preventative measure. Design features of the unit include carbon steel support plates with drilled flow holes, tight inner-row U-bends, and a deep crevice in the tube sheet where the generator tubes are only expanded over 2-1/2" of the 22" tube sheet depth (Figure 2). The generator was operated initially with secondary side water conditioning using sodium phosphate additions. After approximately one and a half years operation a conversion to an all volatile treatment of secondary water was made. Cooling water condensors were tubed with 90:10 Cu:Ni alloy and had a history of leakage. The condensors were cooled using brackish water drawn from the James River.

The unit has experienced extensive denting of the Inconel 600 steam generator tubes due to corrosion of the carbon steel support plates. Resulting stresses on the support plates have led to hour glassing of flow slots, complete closure of flow slots where support plates have cracked at the flow slot corners, and some evidence of support plate disintegration. The strain on the steam generator tubes due to denting has potentially led to crack initiation under the dents. In addition, through-wall cracking and a resultant large leak in an inner-row U-bend led to preventative plugging of the innermost two rows of tubes.

The aforementioned defect conditions plus potential corrosion effects in the tube sheet crevice region, wastage, and stress corrosion cracking make this removed from service unit a useful vehicle for defect characterization studies. A principle programmatic objective is to utilize current practice, advanced practice, and developmental nondestructive techniques and instrumentation to characterize steam generator primary and secondary side conditions. The nondestructive test (NDT) results will then be validated utilizing destructive metallographic sectioning of specimens removed from the generator. A statistically developed sampling plan for destructive assay will allow determination of NDT inspection measurement error and confidence bands.

The program is interested in obtaining information on prospective instrumentation and technologies that could be incorporated into an NDE round robin type test. Nondestructive means for characterizing the generator from the secondary side as well as the primary side are sought. Participation in round robin activities will involve either interested parties conducting examinations at Hanford, Washington, where the steam generator is located or training PNL personnel in use of the appropriate technology.

Primary side access to the generator will become available in April 1982. Secondary side access will be available starting January 1982. The majority of round robin activities will occur between September 1982 and June 1984. It is anticipated the extended period of availability will allow time for new or developmental techniques and devices to be used, with iterative examinations that may be necessary during the course of development. The steam generator will be examined in the Steam Generator Examination Facility (SGEF), shown schematically in Figure 3. This especially designed facility contains the generator in its normal vertical operating position. Operations in the SGEF will be handled similar to procedures for entering operating reactor containments.

In summary, a service degraded test bed will be available for extended NDT studies. Potential steam generator tubing defects include inner and outer diameter initiated stress corrosion cracking, denting, cracking under dents, cracks in tight radius U-bends, wastage, mechanical wear, and intergranular attack in the tube sheet crevice region. Devices that have potential for inservice primary or secondary side NDT are sought for inclusion in the round robin tests. Candidate techniques can include standard, or developmental eddy current approaches, (i.e., specialized eddy current probes), ultrasonics, profilometry, radiographics, optical, etc. Methods for inservice support plate characterization from the primary or secondary side are also of interest. Interested parties should contact PNL Project Manager, R. A. Clark (509) 376-0174.

MILESTONE CHART
SURRY GENERATOR PROGRAM

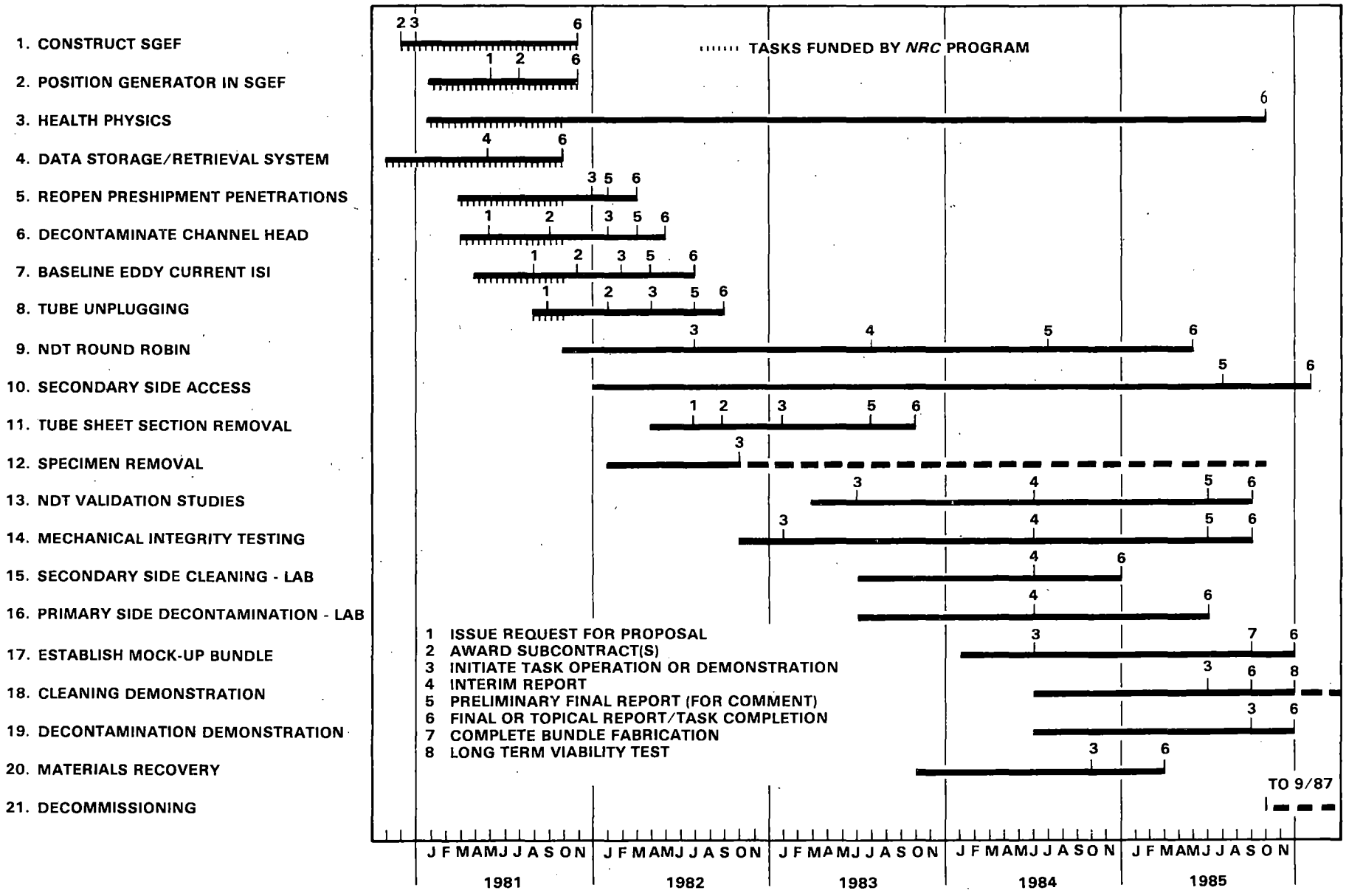

Figure 1

CREVICED TUBE SHEET POSTULATED CORROSION CONDITION

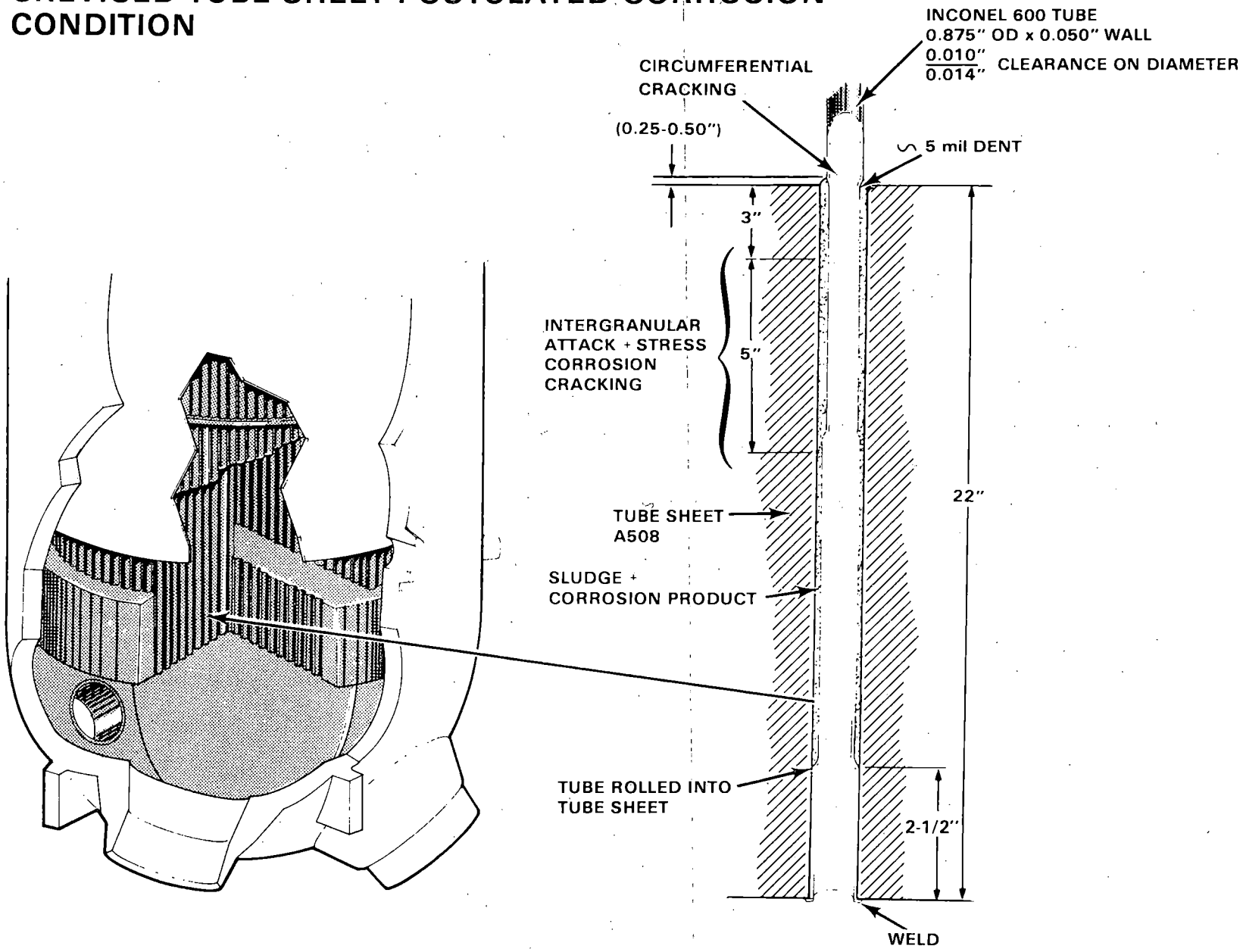

Figure 2

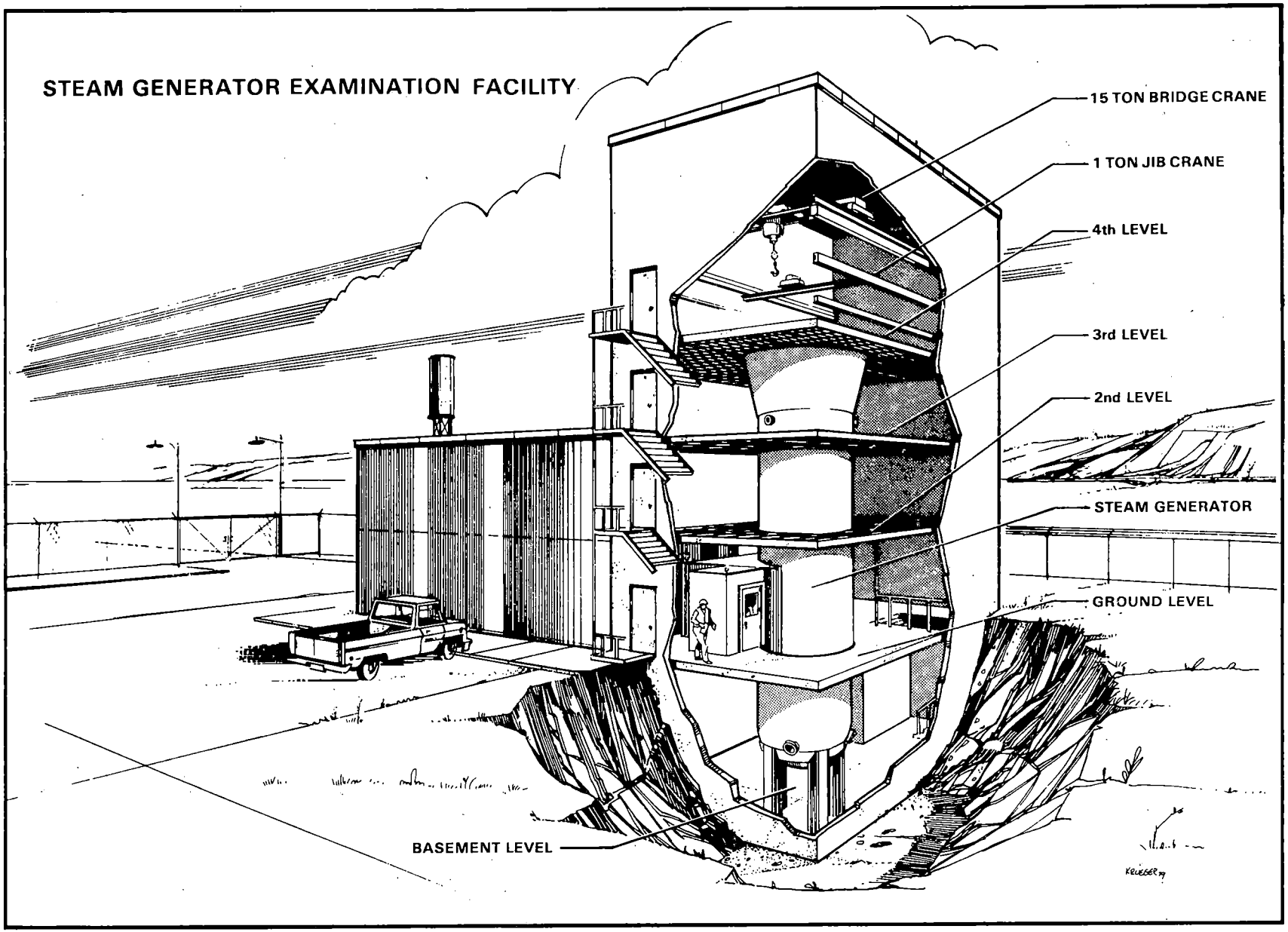
STEAM GENERATOR EXAMINATION FACILITY
15 TON BRIDGE CRANE
1 TON JIB CRANE
4th LEVEL
3rd LEVEL
2nd LEVEL
STEAM GENERATOR
GROUND LEVEL
BASEMENT LEVEL

Figure 3

REACTOR SAFETY STUDY

METHODOLOGY APPLICATIONS PROGRAM

(RSSMAP)

J. J. CURRY
DIVISION OF RISK ANALYSIS
OFFICE OF NUCLEAR REGULATORY RESEARCH
U. S. NUCLEAR REGULATORY COMMISSION

Reactor Safety Study Methodology Applications Program (RSSMAP)
(Summary)

The Reactor Safety Study (RSS, WASH-1400) analyzed the risk of operation of a Westinghouse designed reactor with a large dry containment (Surry) and a GE designed reactor with a MARK I containment (Peach Bottom). To broaden the class of nuclear power plants explicitly analyzed for risk, the RSSMAP study was initiated. The selection of the RSSMAP plants, thus, included designs from CE (Calvert Cliffs #2) and B&W (Oconee #3) as well as significantly differing designs from Westinghouse (Sequoyah, ice condenser containment) and GE (Grand Gulf, MARK III containment).

The methodology used in RSSMAP required the determination of sequence occurrence probabilities and an analysis of their phenomenology up to the point of containment failure. In an effort to minimize the manpower and funding necessary to complete the risk assessments, insights and techniques from the RSS were used whenever possible. The most major of these are: (i) system unavailability is dominated by single and double component unavailabilities, human error and common mode faults; (ii) use of the RSS component data base and point values for estimating system unavailabilities; (iii) use of some system or subsystem unavailability estimates from the RSS, e.g., actuation circuitry, PCS; (iv) use of LOCA and transient initiators and RSS data on their occurrence; and (v) use of the RSS release categories.

Significant differences between the RSSMAP and RSS methodologies exist in the method of sequence quantification and phenomenological modeling. Major differences in the assessment of sequence probabilities involve: (i) the

use of a Boolean expression depicting the dominant unavailability contributors identified in (i) of the previous paragraph instead of a detailed fault tree; (ii) details of system design and operation being determined largely from information available in the Final Safety Analysis Report, Technical Specifications and selected plant procedures; (iii) the use of computer codes to determine dominant cut sets; (iv) the inclusion of complement events in the sequence quantification; and (v) modifications to the event tree structure, e.g., linking of transient and LOCA trees by a stuck open relief valve, greater tree generalization. Modeling of accident phenomenology in RSSMAP to the point of containment failure reflected, in particular, the development of the numerous subroutines of MARCH, not available at the time of the RSS. (Viewgraph VIII). The RSSMAP study did not include consequence modeling.

Final RSSMAP results are stated in terms of core melt probabilities for each of the RSS release categories. The containment failure modes are also indicated. (Viewgraphs X-XII). Although the dominant accident sequences vary for individual designs, the total core melt probabilities for the three plant analyses completed thus far lie in the range of 10^{-4} to 10^{-5} per reactor year.

FOUR PLANT STUDY
(NUREG/CR-1659, VOLS. 1-4)

SEQUOYAH #1	W	2/81
OCONEE #3	B&W	5/81
CALVERT CLIFFS #2	CE	(12/81)
GRAND GULF #1	GE	(11/81)

OBJECTIVES

- IDENTIFY RISK DOMINANT ACCIDENT SEQUENCES FOR ADDITIONAL REACTOR DESIGNS

- COMPARISON OF DOMINANT SEQUENCES TO THOSE IDENTIFIED IN WASH-1400

- DRAW CONCLUSIONS ABOUT EFFECT OF DESIGN DIFFERENCES ON RISK

METHODOLOGY

I. SEQUENCE PROBABILITY ANALYSIS (SNL)

II. SEQUENCE CONSEQUENCE ANALYSIS (BCL)

SEQUENCE PROBABILITY ANALYSIS

RSS SEQUENCE INITIATORS

RSS EVENT TREES MODIFIED

RSS DATA BASE

FSAR SUPPLIED INFORMATION

SYSTEM FAULTS VIA "SURVEY AND ANALYSIS"

SURVEY AND ANALYSIS

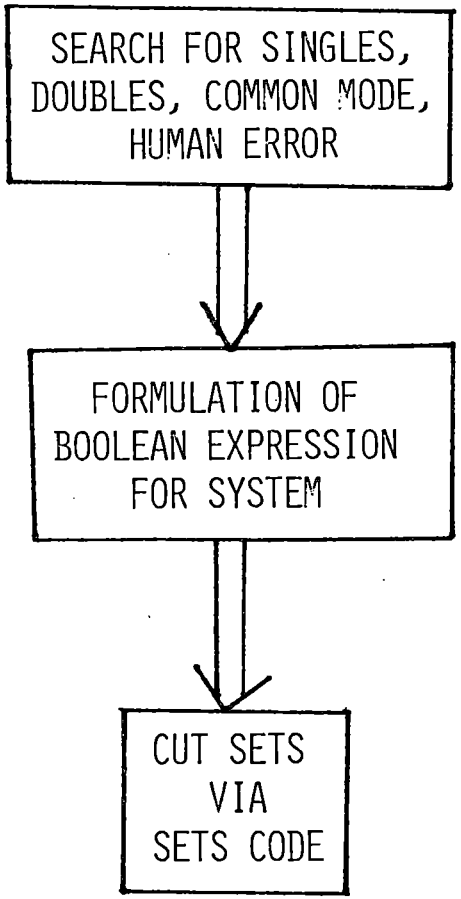

SEQUENCE CONSEQUENCE ANALYSIS

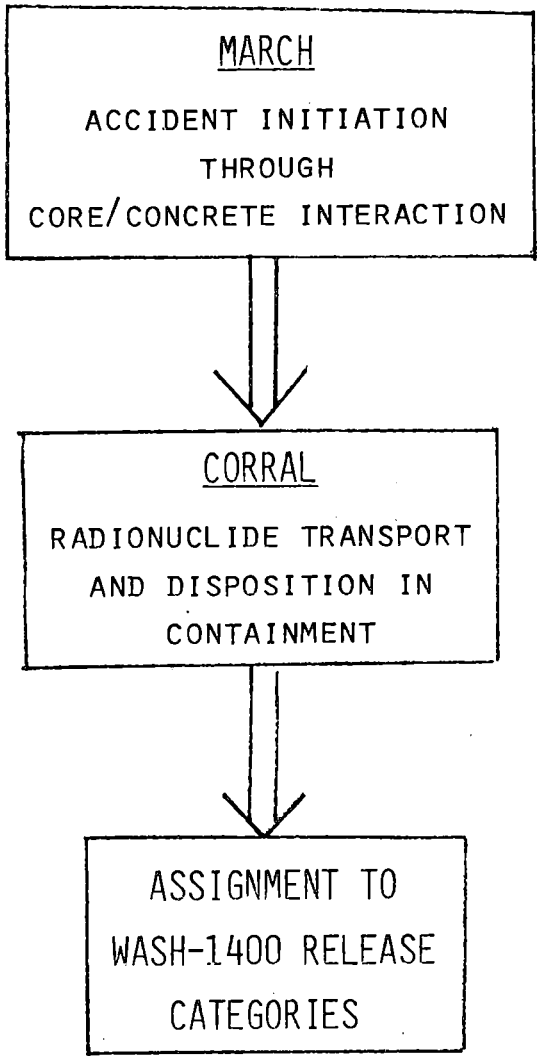

PHENOMENOLOGICAL MODELING

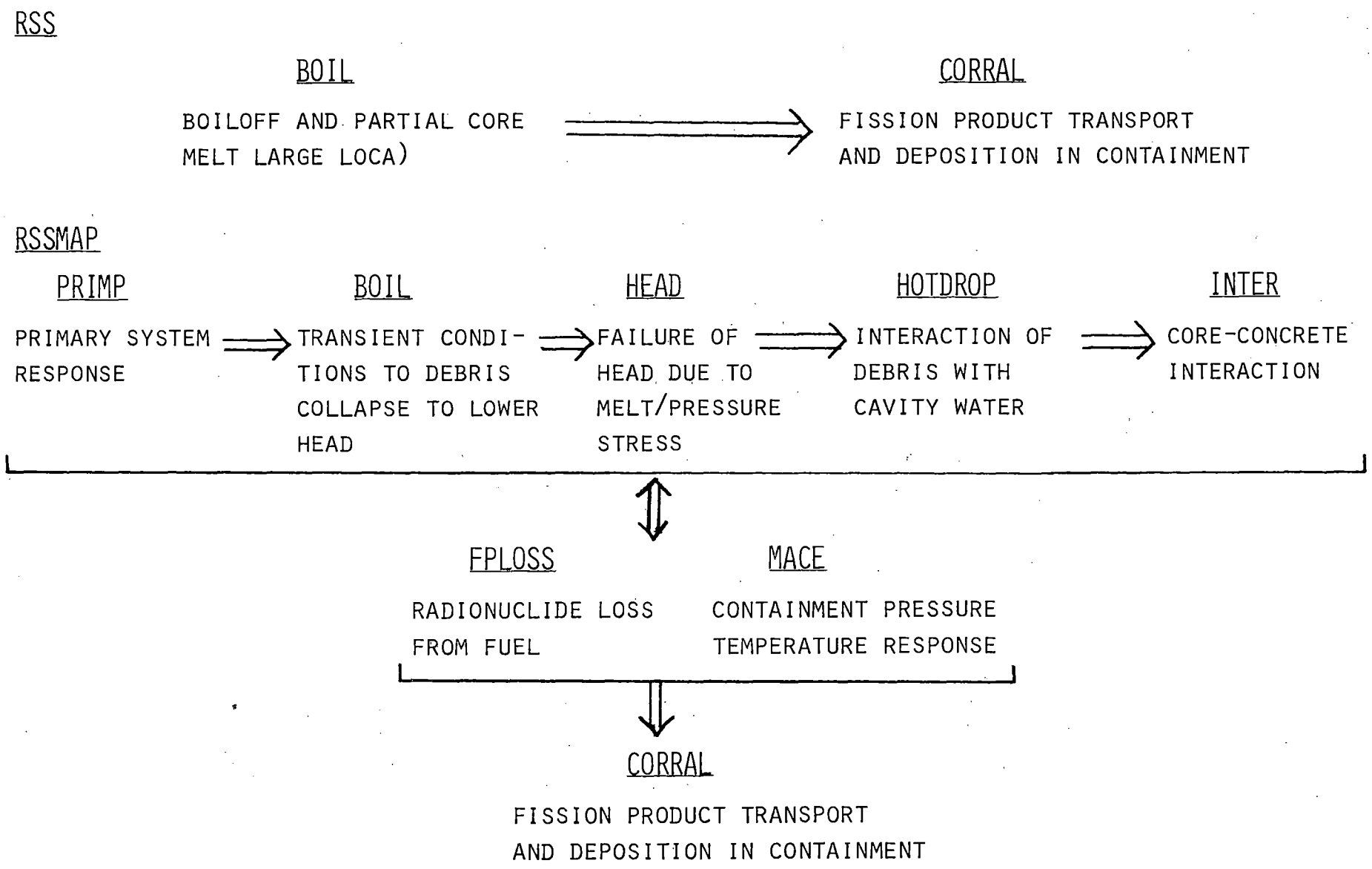

RESULTS

CORE MELT PROBABILITIES

FOR RSS RELEASE CATEGORIES

RSSMAP SEQUOYAH #1 RESULTS

Release Category 1	Release Category 2	Release Category 3	Release Category 4	Release Category 5
$S_1H-\alpha$	$S_2HF-\gamma$	$S_2H-\gamma$	$S_1H-\gamma$	$S_1D-\gamma$
1×10^{-7}	5×10^{-6}	2×10^{-5}	1×10^{-5}	4×10^{-6}
	V	$S_1HF-\delta,\gamma$	$S_2D-\gamma$	
	5×10^{-6}	3×10^{-6}	6×10^{-6}	
		TML-γ		
		3×10^{-6}		

Symbols:

Initiating Events

- S_1 -- Small LOCA (2 in. $\leq$ D $\leq$ 6 in.)
- S_2 -- Small LOCA (< 2 in.)
- V -- Interfacing systems LOCA
- T -- Transient

Containment Failure Modes

- α -- Vessel steam explosion
- γ -- Hydrogen burning
- δ -- Overpressure

System Events

- B -- Electric power system
- C -- Containment spray injection system
- D -- Emergency core cooling injection system
- F -- Containment spray recirculation system
- H -- Emergency core cooling recirculation system
- L -- Auxiliary feedwater system
- M -- Power conversion system

RSSMAP OCONEE #3 RESULTS

RELEASE CATEGORY	1	2	3	4	5	6	7
T_2MLU			$\gamma 6.0\times10^{-7}$		$\beta 8.8\times10^{-9}$		$\varepsilon 6.0\times10^{-7}$
T_1MLU			$\gamma 1.0\times10^{-6}$		$\beta 1.5\times10^{-8}$		$\varepsilon 1.0\times10^{-6}$
V		$V<4.0\times10^{-6}$					
$T_1(B_3)MLU$			$\gamma 1.1\times10^{-6}$		$\beta 1.6\times10^{-8}$		$\varepsilon 1.1\times10^{-6}$
T_2MQ-H			$\gamma 5.5\times10^{-6}$		$\beta 8.0\times10^{-8}$		$\varepsilon 5.5\times10^{-6}$
S_3H			$\gamma 5.0\times10^{-6}$		$\beta 7.3\times10^{-8}$		$\varepsilon 5.0\times10^{-6}$
S_1D	$\alpha 6.7\times10^{-8}$		$\gamma 1.3\times10^{-6}$		$\beta 4.9\times10^{-8}$		$\varepsilon 5.4\times10^{-6}$
T_2MQ-FH		$\gamma 2.5\times10^{-6}$		$\beta 3.7\times10^{-8}$		$\varepsilon 2.5\times10^{-6}$	
S_3FH		$\gamma 2.1\times10^{-6}$		$\beta 3.1\times10^{-8}$		$\varepsilon 2.1\times10^{-6}$	
S_2FH	$\alpha 1.3\times10^{-8}$			$\beta 9.5\times10^{-9}$		$\varepsilon 1.0\times10^{-6}$	
T_2MLUO			$\gamma 4.1\times10^{-6}$		$\beta 5.9\times10^{-8}$		$\varepsilon 4.1\times10^{-6}$
T_2KMU			$\gamma 3.9\times10^{-6}$		$\beta 5.7\times10^{-8}$		$\varepsilon 3.9\times10^{-6}$
S_2D	$\alpha 2.0\times10^{-8}$		$\gamma 4.0\times10^{-7}$		$\beta 1.5\times10^{-8}$		$\varepsilon 1.6\times10^{-6}$
S_3D			$\gamma 7.0\times10^{-7}$		$\beta 1.0\times10^{-8}$		$\varepsilon 7.0\times10^{-7}$
T_1MLUO			$\gamma 2.7\times10^{-6}$		$\beta 3.9\times10^{-8}$		$\varepsilon 2.7\times10^{-6}$
T_3MLUO			$\gamma 5.5\times10^{-7}$		$\beta 8.0\times10^{-9}$		$\varepsilon 5.5\times10^{-7}$
T_2MQ-D			$\gamma 7.5\times10^{-7}$		$\beta 1.1\times10^{-8}$		$\varepsilon 7.5\times10^{-7}$
CATEGORY TOTAL[1]	1.1×10^{-7}	1.0×10^{-5}	2.9×10^{-5}	9.7×10^{-8}	4.6×10^{-7}	7.3×10^{-6}	3.5×10^{-5}

T_1 - Loss of Offsite Power Transient

T_2 - Loss of Power Conversion System Transient Caused by Other Than a Loss of Offsite Power

T_3 - Transients with the Power Conversion System Initially Available

S_1 - Intermediate LOCA ($10'' < D \leq 13.5''$)

S_2 - Small LOCA ($4'' < D \leq 10''$)

S_3 - Small-Small LOCA ($D \leq 4''$)

V - Interfacing Systems LOCA

(B_3) - Emergency Power System

D - Emergency Coolant Injection System

F - Containment Spray Recirculation System

H - Emergency Coolant Recirculation System

K - Reactor Protection System

L - Emergency Feedwater System, Recovery of Power Conversion System and High Head Auxiliary Feedwater System

M - Power Conversion System (Normal Operation)

Q - Reclosure of Pressurizer Safety/ Relief Valves

U - High Pressure Injection System

O - Reactor Building Cooling System

α - Vessel Steam Explosion

β - Penetration Leakage

γ - Overpressure Due to Hydrogen Burning

ε - Base Mat Melt Through

RSSMAP GRAND GULF #1 RESULTS (DRAFT)

DOMINANT ACCIDENT SEQUENCES	BWR Core Melt Release Categories			
	1	2	3	4
T_1PQI	$\alpha 1.6 \times 10^{-8}$	$\delta 1.6 \times 10^{-6}$		
$T_{23}PQI$	$\alpha 3.7 \times 10^{-8}$	$\delta 3.7 \times 10^{-6}$		
T_1PQE			$\gamma 1.2 \times 10^{-7}$	$\delta 1.2 \times 10^{-7}$
$T_{23}PQE$			$\gamma 2.7 \times 10^{-7}$	$\delta 2.7 \times 10^{-7}$
SI	$\alpha 4.6 \times 10^{-8}$	$\delta 4.6 \times 10^{-6}$		
T_1QW		$\delta 6.2 \times 10^{-6}$		
$T_{23}QW$		$\delta 1.2 \times 10^{-5}$		
$T_{23}C$		$\delta 5.4 \times 10^{-6}$		
T_1QUV			$\gamma 7.5 \times 10^{-7}$	$\delta 7.5 \times 10^{-7}$
CATEGORY(1) TOTAL	1.1×10^{-7}	3.4×10^{-5}	1.2×10^{-6}	1.4×10^{-6}

T_1 - A loss of offsite power transient.

T_{23} - Any other transient which requires an emergency reactor shutdown.

S - A small LOCA (the break area is less than one square foot).

C - Failure to render the reactor subcritical.

E - Failure of the Emergency Core Cooling System.

I - Failure of residual heat removal systems after a LOCA (including transient induced LOCAs).

P - Failure of a safety/relief valve to reseat.

Q - Failure of the Power Conversion System.

U - Failure of the High Pressure Core Spray and Reactor Core Isolation Cooling System.

V - Failure of the low pressure ECCS systems to provide core flow.

W - Failure of the residual heat removal systems after a transient.

α - Containment failure due to a steam explosion.

γ - Containment failure due to an overpressure caused by rapid hydrogen burning.

δ - Containment failure due to an overpressure caused by gas generation.

Interim Reliability Evaluation Program

Probabilistic safety analysis and risk assessment techniques are widely believed to offer powerful tools for the safety design and safety evaluation of nuclear power plants. Past attempts to apply such techniques to commercial nuclear plants have provided useful catalogues of accident sequences, identified many strengths and weaknesses in the design and operation of the plants, provided insights into the importance of accident contributors, and provided rough estimates of the likelihood of serious accidents. Recent evidence tends to suggest that plant-to-plant differences in design and operation may give rise to significant differences in the likelihood or course of accidents. Therefore, the extensive application of these safety analysis techniques to many reactor plants appears to be desirable. This need is reflected in the TMI Action Plan (NUREG-0660) in which the Interim Reliability Evaluation Program (IREP) is identified as a high priority effort leading to the systematic risk assessment of all reactors (Section II.C).

The Interim Reliability Evaluation Program is intended to apply probabilistic risk analysis techniques to several nuclear power plants and to develop procedures adequate for the consistent analysis of all plants with the following specific objectives: (1) Identify--in a preliminary way--those accident sequences that dominate the contribution to the public health and safety risks originating in nuclear power plant accidents; (2) Develop a foundation for subsequent, more intensive, applications of probabilistic safety analysis or risk assessment on the subject plants; (3) Expand the cadre of experience practitioners of risk assessment methods within the NRC and the nuclear power industry; and (4) Evolve procedures codifying the competent use of these techniques for use in the extension of IREP to all domestic light water reactor plants.

Phase I of the IREP study consisted of a reliability analysis of the Crystal River Unit 3 facility. A report on that effort will be published shortly. Using methodological insights gained from the Crystal River Study, the Phase II IREP studies were initiated in September 1980. The Phase II studies consist of analyses of four plants:

1. Browns Ferry Unit 1, by a team composed of personnel from EG&G, Idaho and Energy, Inc. and directed by EG&G, Idaho;

2. Arkansas Nuclear One Unit 1, by a team composed of personnel from Sandia National Laboratories, Science Applications, Inc. (SAI), and Arkansas Power and Light Company and directed by Sandia National Laboratories;

3. Calvert Cliffs Unit 1, by a team composed of personnel from Science Applications, Inc., Evaluation Associates, and NRC and directed by SAI; and

4. Millstone Unit 1, by a team composed of personnel from Science Applications, Inc., Northeast Utilities, and NRC, also directed by SAI.

Responsibility for overall technical management of the study rested with Sandia National Laboratories. Periodic reviews to assure the quality of the product were conducted by Sandia National Laboratories and NRC personnel not involved directly with the work of any one team, with the assistance of Energy, Inc.

Reports on each study should be published in the first quarter of CY 1982. Separate reports will also be issued regarding procedures for conducting future analyses of the same scope and breadth as these four studies, and detailing the technical and methodological insights and nuclear safety perspectives gained from this activity.

It is important to note that while it is our opinion that these studies represent the state of the art given their scope, they are incomplete. External events (earthquakes, fires, etc.) are not included and the assignment of accident sequences to release categories was performed in a subjective manner with limited plant-specific calculations. Thus, this portion of the study relied heavily on analyses performed previously on similar facilities. While accident sequence and release category frequencies will be quantified, they are of value primarily in comparative analyses and the absolute values determined should not be used without a clear appreciation of their inherent uncertainties. The principal product to be obtained is the integrated engineering logic presented in the plant and system models, not the specific values computed for accident frequencies.

THE INTERIM RELIABILITY

EVALUATION PROGRAM (IREP)

NEED FOR IREP

- PAST PRA'S GIVE INSIGHTS ON
  - DOMINANT ACCIDENT SEQUENCES
  - IMPORTANCE OF ACCIDENT CONTRIBUTORS
  - ESTIMATES OF LIKELIHOOD OF ACCIDENTS
- EVIDENCE THAT PLANT-TO-PLANT DIFFERENCES MAY BE SIGNIFICANT
- EXTENSIVE APPLICATION OF PRA TECHNIQUES IS DESIRABLE

IREP OBJECTIVES

- IDENTIFY DOMINANT ACCIDENT SEQUENCES FOR PLANTS UNDER STUDY
- DEVELOP FOUNDATION FOR FUTURE ANALYSES
- EXPAND CADRE OF EXPERIENCED PRA PRACTITIONERS
- EVOLVE PROCEDURES FOR FUTURE IREP ANALYSES ON ALL PLANTS

IREP ORGANIZATION

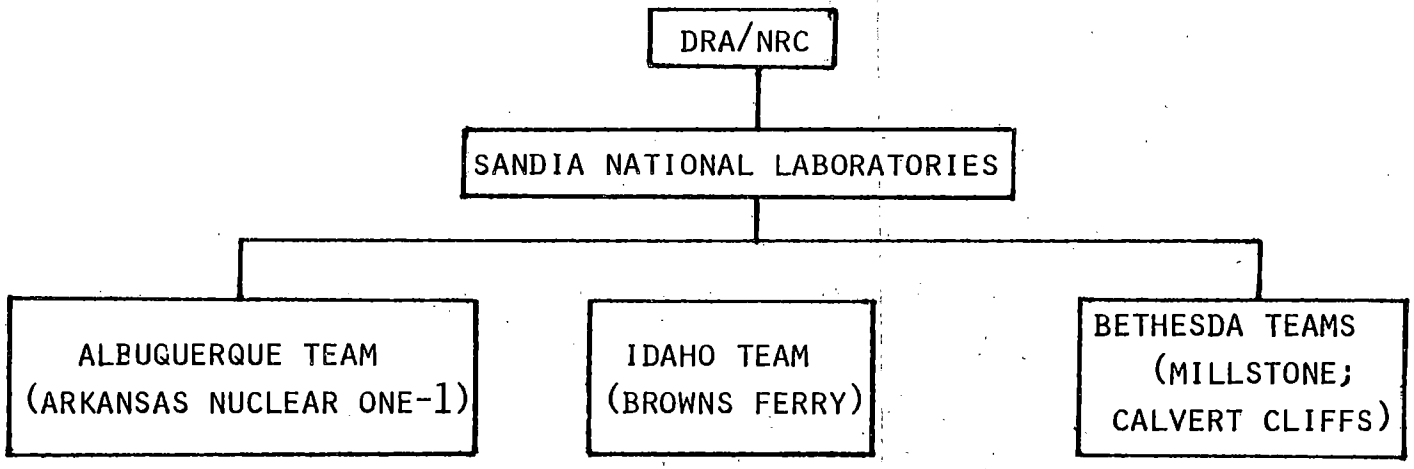

SANDIA NATIONAL LABORATORIES

SAI - ALBUQUERQUE

ARKANSAS POWER AND LIGHT COMPANY

IDAHO NATIONAL ENGINEERING LABORATORY

ENERGY INCORPORATED

SAI - BETHESDA

DRA/NRC

NRR/NRC

BALTIMORE GAS AND ELECTRIC COMPANY

NORTHEAST UTILITIES

SCOPE

- DETAILED SYSTEMS ANALYSIS
- LIMITED CONTAINMENT ANALYSIS
- NO SITE SPECIFIC TRANSPORT/CONSEQUENCE ANALYSIS
- EXTERNAL EVENTS EXCLUDED

TEAM PROFILE

- EXPERIENCED TEAM LEADER
- LESS EXPERIENCED SYSTEMS ANALYSTS
- COMPUTER EXPERT
- UTILITY PERSONNEL (3/4 TEAMS)

MANPOWER

- TOTAL PROJECT: ~ 54 PEOPLE

  ~ 39 MANYEARS

- PLANT ANALYSIS: 9-10 PEOPLE

  ~8 MANYEARS

INFORMATION BASE

- FSAR
- PIPING AND INSTRUMENTATION DRAWINGS
- EMERGENCY, TEST, AND MAINTENANCE PROCEDURES
- UTILITY PERSONNEL/PLANT CONTACT
- PLANT VISITS
- METHODS DOCUMENTS
- EPRI NP-801
- PLANT SPECIFIC AND OTHER LER'S
- WASH-1400
- HUMAN RELIABILITY HANDBOOK

MAJOR IREP TASKS

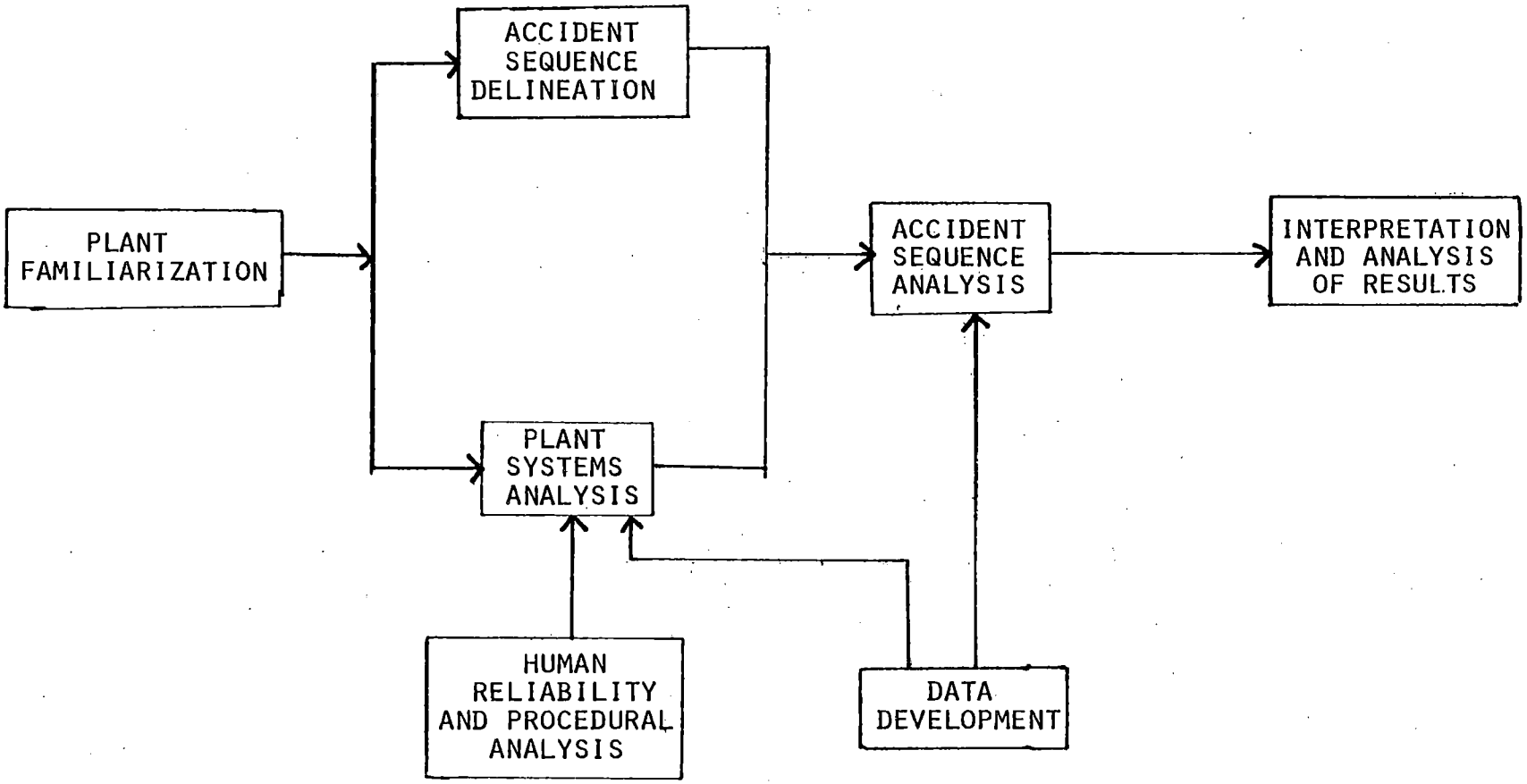

IREP QUALITY CONTROL

- TEAM OF "SPECIALISTS" PERFORMING PERIODIC REVIEW AND VISITATION
- PEER REVIEW OF STATUS REPORTS, DRAFT REPORT
- TEAM LEADER MEETINGS

PRODUCTS

- IDENTIFICATION OF DOMINANT ACCIDENT SEQUENCES AND ENGINEERING INSIGHTS
  - EMPHASIS ON ENGINEERING INSIGHTS, NOT ABSOLUTE NUMBERS

PRODUCTS

- DOCUMENTED PLANT MODELS FOR FUTURE ANALYSES
  - INFORMATION BASE TO EVALUATE REGULATORY ISSUES
  - FOUNDATION FOR PRA METHODOLOGY EXTENSION

PRODUCTS

- REVISED IREP PROCEDURES GUIDE
  - INCORPORATE EXPERIENCE
  - INPUT TO INDUSTRY/NRC EFFORT

QUALITATIVE RESULTS

- SINGLE FAILURES IN SUPPORT SYSTEMS
- INCOMPLETE TESTS
- MINOR PROCEDURAL ERRORS
- SMALL TEST AND MAINTENANCE CONTRIBUTIONS

REVISED IREP PROCEDURES GUIDE

- INCORPORATE EXPERIENCE FROM IREP
- SET FORTH ORGANIZATION, PROCEDURES, METHODS FOR IREP-TYPE ANALYSES

PROCEDURES GUIDE INSIGHTS

- EXPERIENCED TEAM LEADER
- UTILITY INVOLVEMENT
- ASSUMPTION SPECIFICITY
- LOGIC LOOPS
- SEQUENCE EVALUATION

POTENTIAL FUTURE USES OF IREP MODELS

- OPERATOR TRAINING (MULTI-FAULT SEQUENCES, IMPORTANCE OF DIAGNOSIS AND RECOVERY)
- EMERGENCY PLANNING (PRE-PLANNING, PROGNOSIS)
- ADEQUACY OF PROCEDURES
- ADEQUACY AND OPTIMIZATION OF LCO'S
- SYSTEMS INTEGRATION
- SIGNIFICANCE OF COMPONENT RELIABILITY
- SYSTEM RELIABILITY
- RISK IDENTIFICATION AND COST-BENEFIT ANALYSES
- PRECURSOR EVALUATION

- THESE SUGGESTED USES MAINLY RELY ON COMPARATIVE MEASURES OF IMPORTANCE

- FRAMEWORK OF ENGINEERING LOGIC RESULTING FROM AN INTEGRATED CONSISTENT ANALYSIS OF A PLANT IS A TOOL APPLICABLE TO UTILITY AND REGULATORY DECISION MAKING

NATIONAL RELIABILITY EVALUATION PROGRAM

- NRC EXPLORING WAYS TO SYSTEMATICALLY APPLY PRA TO NUCLEAR POWER PLANTS
- ADVICE AND PARTICIPATION OF COMPETENT PARTIES BOTH WITHIN AND WITHOUT THE NUCLEAR INDUSTRY IS NEEDED
- RESOURCES OF IEEE AND ANS USED TO DEVELOP PRA PROCEDURES GUIDE
- PROJECT DIRECTED BY A STEERING COMMITTEE UNDER JOINT CHAIRMANSHIP OF TWO REPRESENTATIVES OF IEEE AND ANS
- REVIEW DRAFT OF GUIDE (NUREG/CR-2300) AVAILABLE AND WAS SUBJECTED TO PEER REVIEW AT IEEE REVIEW CONFERENCE 10/26-28/1981

REACTOR SITING CRITERIA

William R. Ott
Siting and Environmental Branch
Division of Health, Siting, and Waste Management
Office of Nuclear Regulatory Research

10 CFR Part 100, issued in 1962, required (see Figure 1) specification of (1) an exclusion zone of such size that an individual on the boundary for two hours following the onset of a postulated fission product release would not receive doses in excess of 25 rem to the whole body or 300 rem to the thyroid, (2) a low population zone (LPZ) such that an exposed individual on the outer boundary for the entire duration of passage of the release would also be limited by the same doses, (3) a population center distance of one and one-third times the LPZ boundary. Applicants were directed to assume a fission product release, containment leak rate, and meteorological conditions pertinent to the site. TID 14844 (March 23, 1962) was referenced as providing a procedural method and sample calculations for complying with these requirements.

Over the years, use of these reference doses became a mechanism for applicants to qualify larger plants in more populous sites through more realistic calculation of the reference doses. It was never the intent of the AEC or NRC to deemphasize the importance of distance as a contributor to protection of public health and safety. Thus, the NRC is now involved in a rulemaking to specify demographic criteria which is the culmination of several years of review of existing siting practice and extensive examination of the consequences of accidents beyond the design basis event of TID 14844 and the availability of sites under various alternative ways of setting demographic criteria.

An Advance Notice of Rulemaking (ANR) published July 29, 1980, listed several other topics also being considered for rulemaking. This list has been modified as shown in figure 2 based on preliminary staff analyses and analysis of comments on the ANR and a Notice of Intent to prepare an Environmental Impact Statement (NOI) for the rulemaking.

The demographic criteria are the central issue of the rulemaking. Figures 3 and 4 give a feel for the statistics pertinent to existing sites. Figure 5 displays the crucial decisions which the staff feels will determine the nature of the criteria that are finally approved.

Figure 6 gives a basic idea of the considerations involved in making these decisions. Figure 7 presents ways being considered to consider sites which exceed a trip-level as used in decision 3. The decision on numbers relates very strongly back to staff experience. That experience indicates that present guidance as expressed in Reg. Guide 4.7 has given a reasonable degree of protection since its publication. With the removal of Part 100 and its concepts, the preliminary staff analyses indicate that a refinement of present staff practice may be an optimal choice for interim criteria. The ways in which the source terms have been formulated will allow later revisions to be accomplished with minimal additional detailed studies.

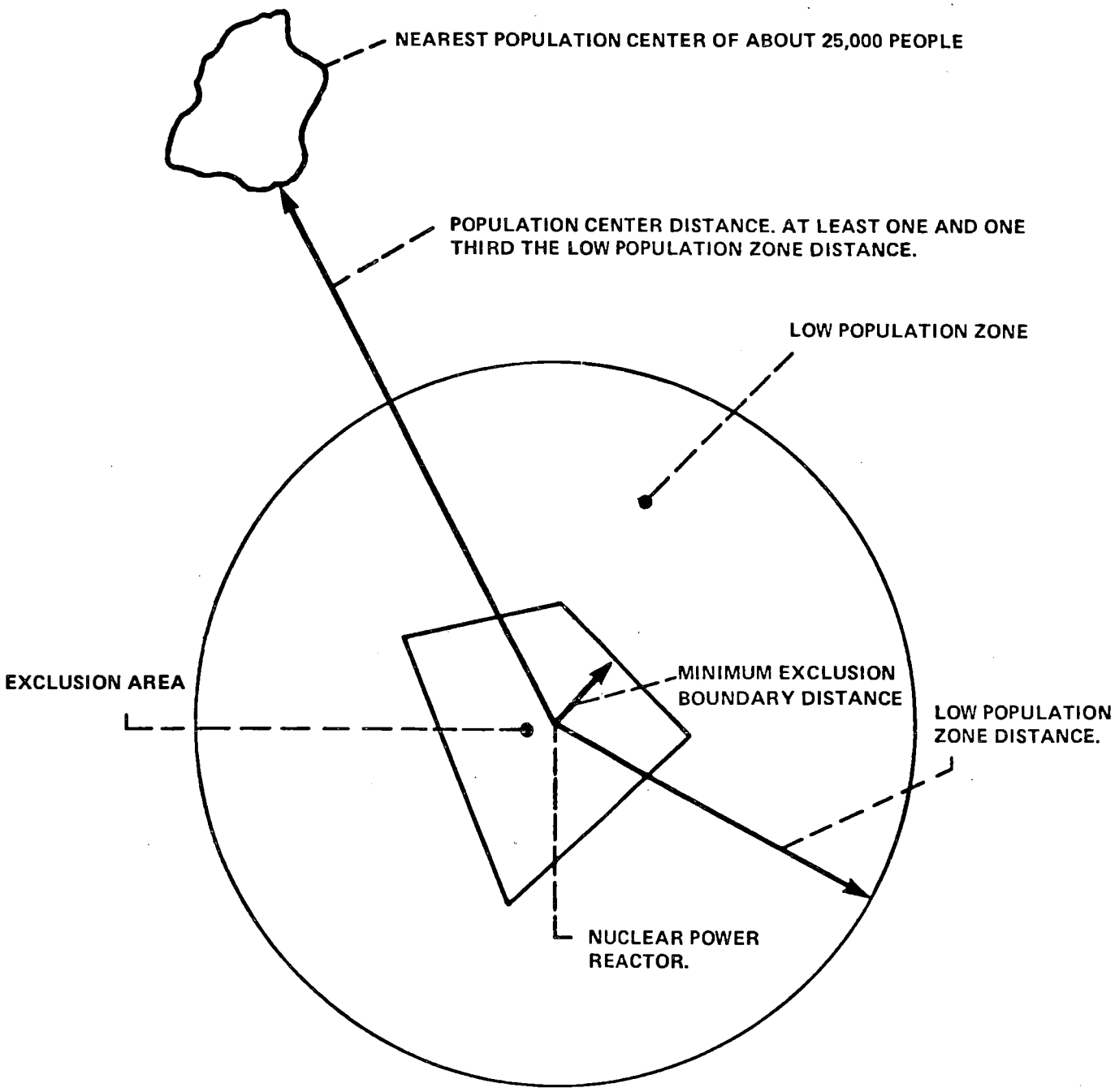

INTERRELATIONSHIP OF PART 100 AREAS AND DISTANCES

FIGURE 1

Scope of Rulemaking

Siting Policy Task Force Recommendation	Action: (Alternatives being analyzed)
1. Establish fixed exclusion and protective action distance and population density and distribution criteria.	Protective action distances set in EP rule. Exclusion distance and population density and distribution limits are being developed.
2. Standoff distance from external hazards.	Information requirement being considered.
3. Groundwater interdiction	Deferred to severe accident rulemaking.
4. Seismic hazards.	Deferred in ANR
5. Post licensing changes in offsite activities.	Notification requirements.
6. No unique or unusual designs to compensate for site deficiencies (Throw into alternative site analysis)	Delete
7. Site approval at earliest decision	Accomplish through stringent criteria for re-opening.
8. Termination of review on State agency disapproved.	Delete
9. Common basis for comparing risk	Deferred in ANR

Figure 2

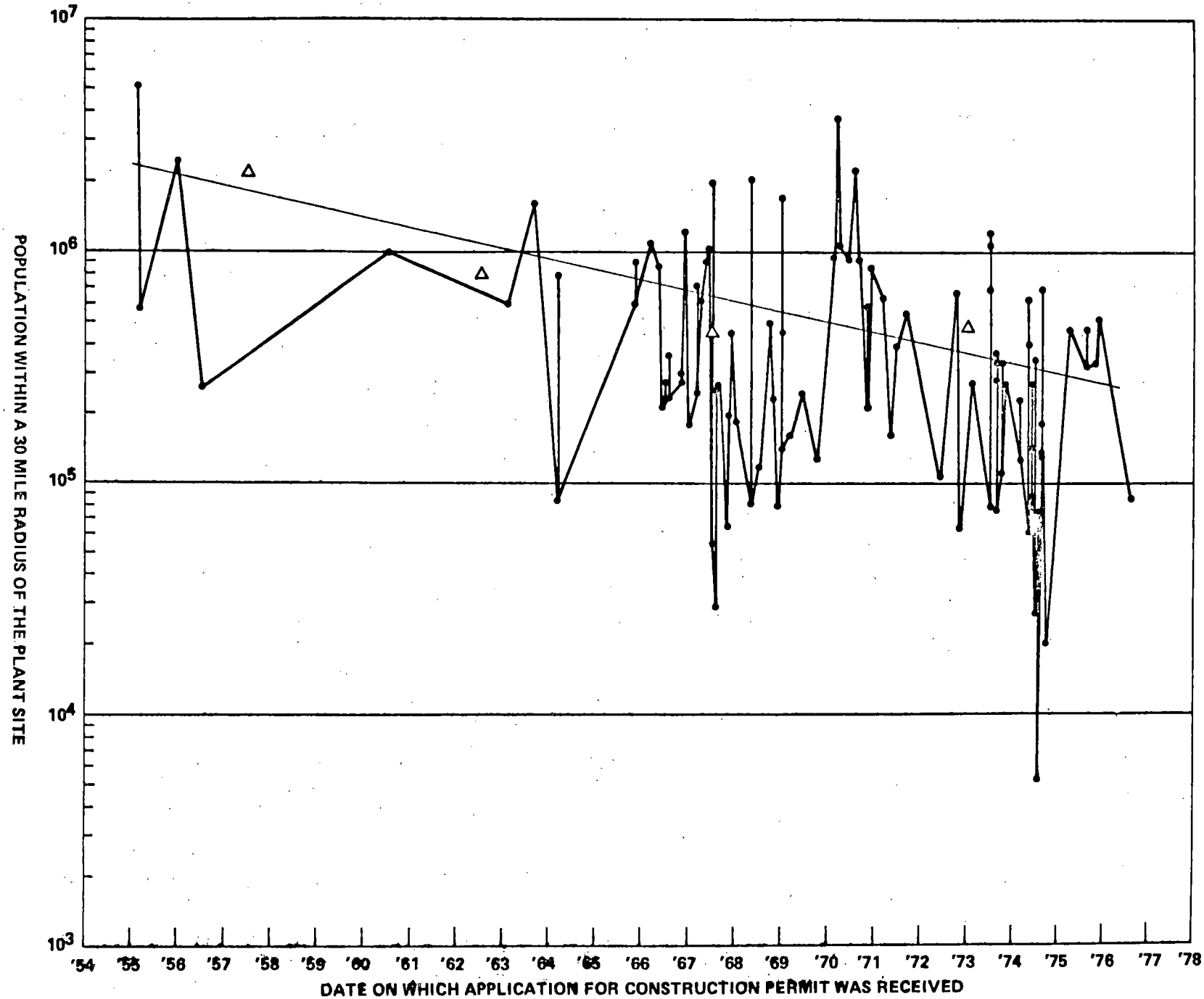
10^7
10^6
10^5
10^4
10^3
POPULATION WITHIN A 30 MILE RADIUS OF THE PLANT SITE
'54 '55 '56 '57 '58 '59 '60 '61 '62 '63 '64 '65 '66 '67 '68 '69 '70 '71 '72 '73 '74 '75 '76 '77 '78
DATE ON WHICH APPLICATION FOR CONSTRUCTION PERMIT WAS RECEIVED

FIGURE 3

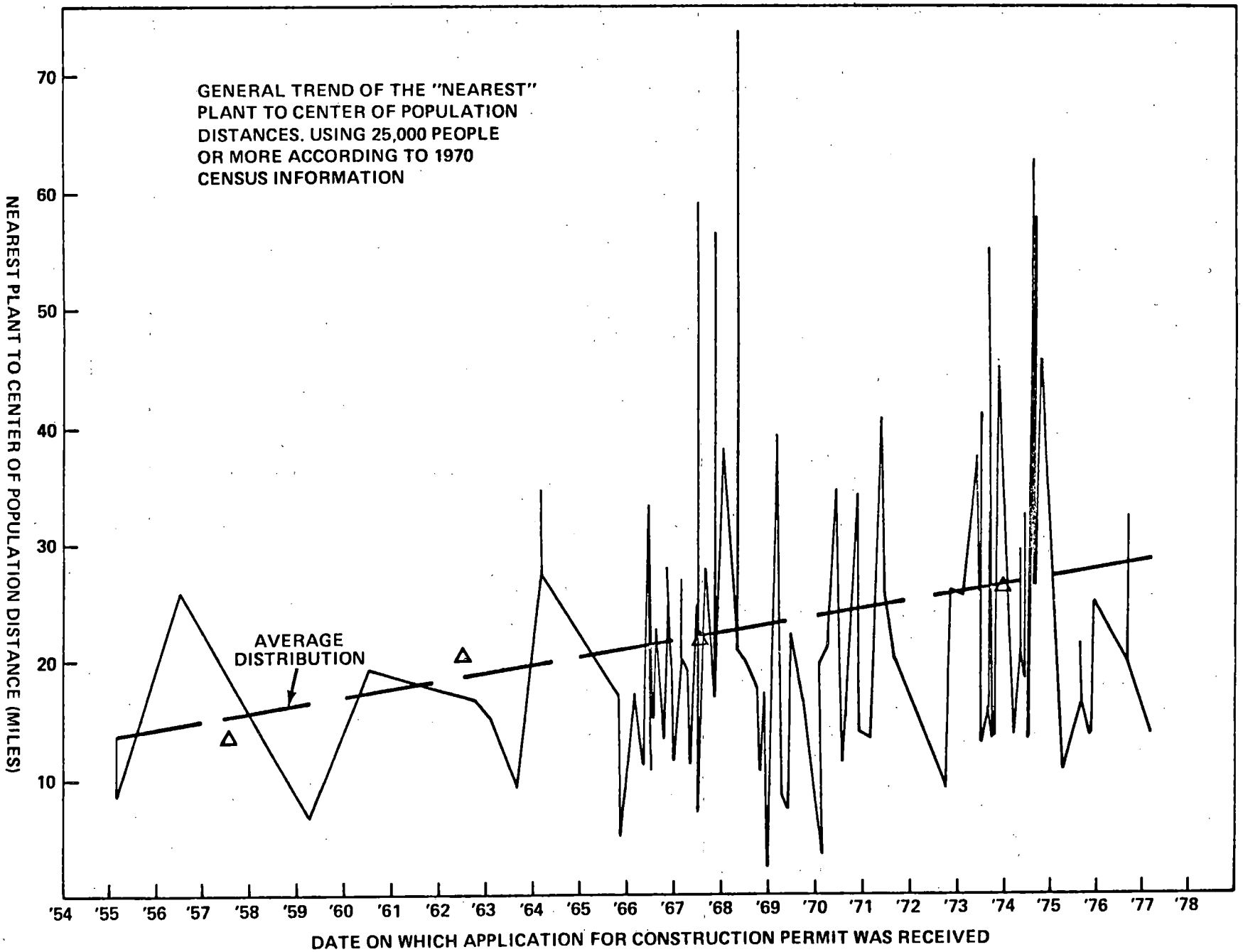
GENERAL TREND OF THE "NEAREST" PLANT TO CENTER OF POPULATION DISTANCES. USING 25,000 PEOPLE OR MORE ACCORDING TO 1970 CENSUS INFORMATION
AVERAGE DISTRIBUTION
NEAREST PLANT TO CENTER OF POPULATION DISTANCE (MILES)
70
60
50
40
30
20
10
'54 '55 '56 '57 '58 '59 '60 '61 '62 '63 '64 '65 '66 '67 '68 '69 '70 '71 '72 '73 '74 '75 '76 '77 '78
DATE ON WHICH APPLICATION FOR CONSTRUCTION PERMIT WAS RECEIVED

FIGURE 4

DECISIONS TO BE MADE IN SPECIFYING CRITERIA

1.	NATIONAL	VS	REGIONAL
2.	RADIAL DENSITY	VS	RADIAL DENSITY PLUS SECTOR RESTRICTION
3.	ABSOLUTE RESTRICTION	VS	TRIP LEVEL 1. INCREMENTAL RELAXATION 2. COMPARATIVE RISK EVALUATION
4.	NUMERICAL VALUE (POSSIBLE RANGE FROM 100 TO 1500)		

Figure 5

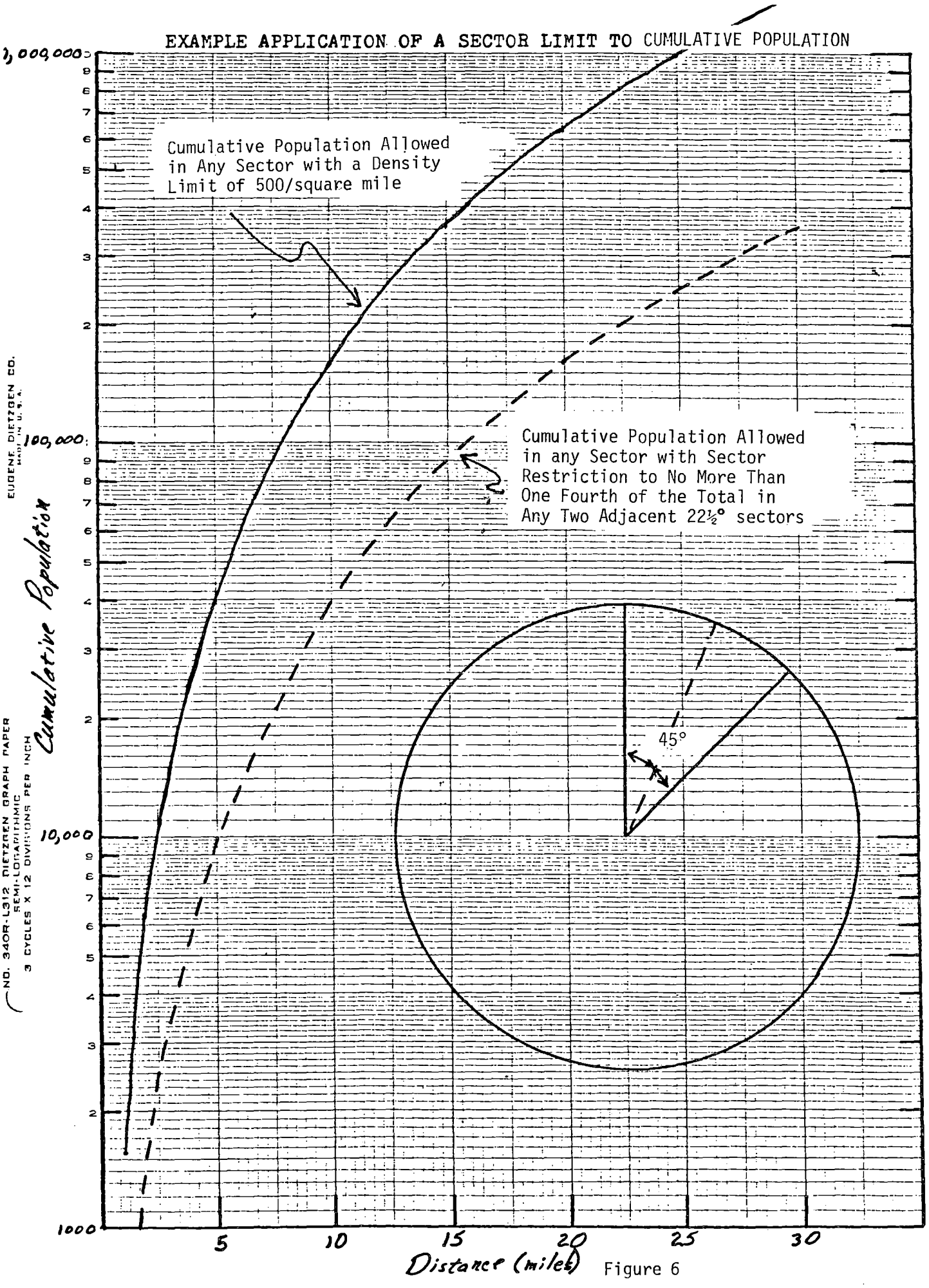
EXAMPLE APPLICATION OF A SECTOR LIMIT TO CUMULATIVE POPULATION
Cumulative Population Allowed in Any Sector with a Density Limit of 500/square mile
Cumulative Population Allowed in any Sector with Sector Restriction to No More Than One Fourth of the Total in Any Two Adjacent 22½° sectors
45°
Cumulative Population
Distance (miles)
1,000,000
100,000
10,000
1000
5
10
15
20
25
30
EUGENE DIETZGEN CO.
NO. 340R-L312 DIETZGEN GRAPH PAPER
SEMI-LOGARITHMIC
3 CYCLES X 12 DIVISIONS PER INCH

Figure 6

INCREMENTAL APPROACH

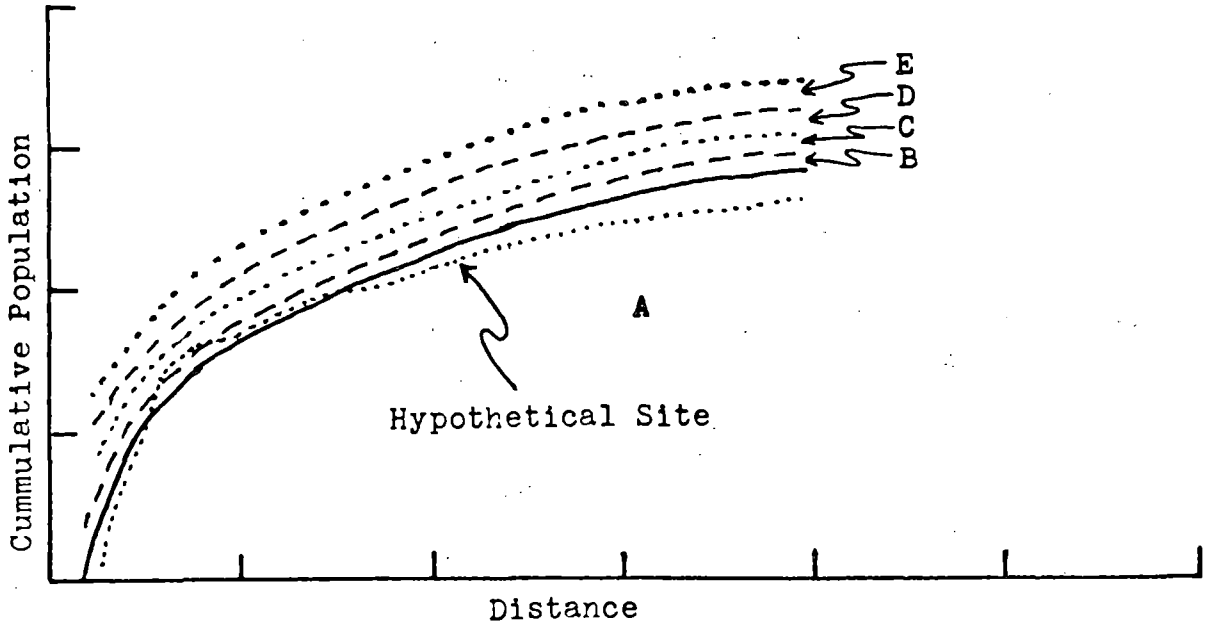

In order to utilize sites in any increment above "A" an applicant must demonstrate that there are no viable sites in "A" or in any other increment which is more restrictive than that of the proposed site.

COMPARATIVE RISK EVALUATION

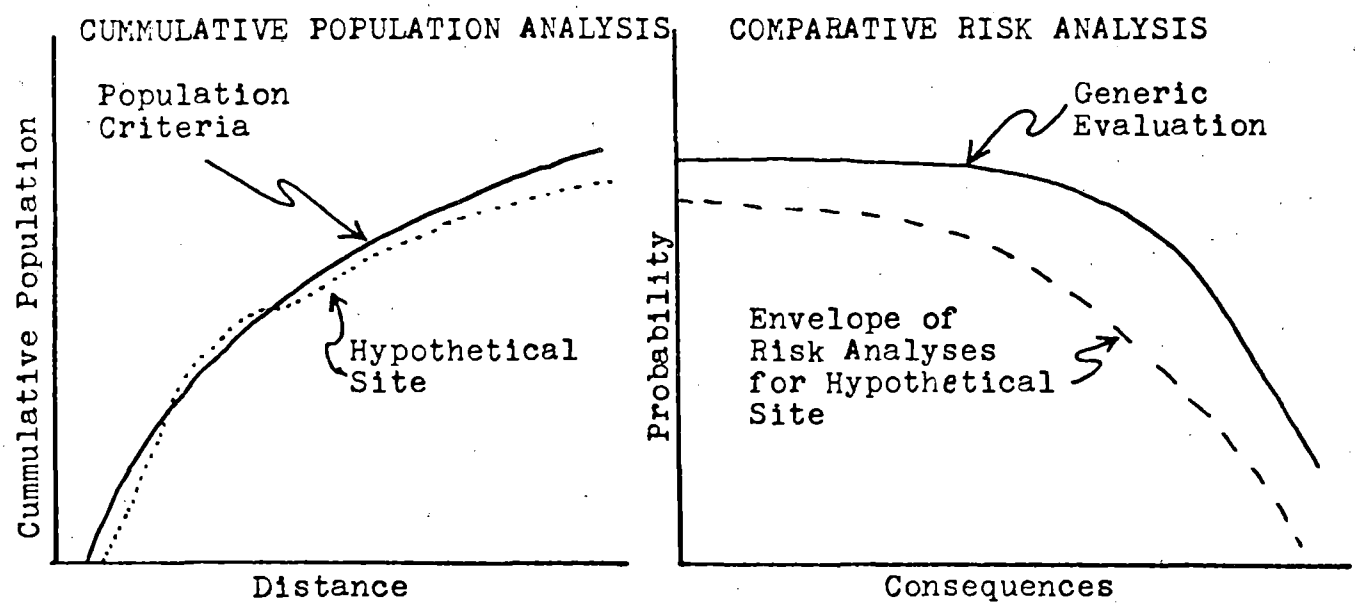

In order to utilize a site which violates the population criteria (e.g. "Hypothetical Site") an applicant demonstrate that (1) no sites are available that meet the criteria and (2) a risk analysis utilizing site specific parameters important to the determination of risk results in a risk envelope within that permitted by the more generic assumptions associated with the development of the criteria.

Figure 7

REFERENCES

"Report of the Siting Policy Task Force," Office of Nuclear Reactor Regulation, U.S. Nuclear Regulatory Commission, NUREG-0625, August 1979.

"Demographic Statistics Pertaining to Nuclear Power Reactor Sites," Office of Nuclear Reactor Regulation, U.S. Nuclear Regulatory Commission, NUREG-0348, October 1979.

"Advance Notice of Rulemaking: Revision of Reactor Siting Criteria," 45 FR 50350 (July 29, 1980).

"Notice of Intent to Prepare an Environmental Impact Statement for Revision of the Regulations Governing the Siting of Nuclear Power Plants," 45 FR 79820 (December 2, 1980).

Consequence Analysis Results

Roger M. Blond
Division of Risk Analysis
Office of Nuclear Regulatory Research

The principle objective of the siting requirements is to establish demographic criteria that will limit potential public health and economic consequences (risk) from a spectrum of postulated reactor accidents while perserving the nuclear option in all regions of the country. To provide the technical understanding necessary to meet this objective, the staff and Sandia National Laboratories undertook an effort to provide: insights into the numerical criteria for population distribution and density surrounding future nuclear power plant sites; and standoff distances for offsite hazards. To gain insights into demographic criteria, analyses were performed in the following areas: accident risk evaluations; site availability impacts; past siting practice; socioeconomic impacts; and safety goal implications.

The first problem that needed to be resolved was to establish the relationships that would be used between the plant design and the site. Five siting source terms (SST) were selected to provide a representative spectrum of potential accident conditions for what can be considered the current light-water-reactor design.

A modified version of the Reactor Safety Study consequence model, CRAC2, was developed to examine the accident risks from these five source terms. Sensitivity studies were conducted to investigate the importance to siting of the

following parameters: meteorology; emergency response; power level; interdiction criteria; design; source term; standoff distances to cities; exclusion radius; and population criteria.

The distances of risk significance were found to be about one half mile for the lesser accidents (justification for exclusion zone); two miles for somewhat bigger accidents; ten miles for most accident conditions; and 30 to 50 miles for the big accidents.

Population density and sector limit considerations were found to have the largest impacts on accident risk of all of the site related parameters. Therefore, the siting demographic criteria will take the form of population density and distribution limits.

SITING POLICY

OBJECTIVE: ESTABLISH DEMOGRAPHIC CRITERIA TO LIMIT POTENTIAL PUBLIC HEALTH AND ECONOMIC CONSEQUENCES (RISK) FROM A SPECTRUM OF POSTULATED REACTOR ACCIDENTS WHILE PRESERVING THE NUCLEAR OPTION IN ALL REGIONS OF THE COUNTRY.

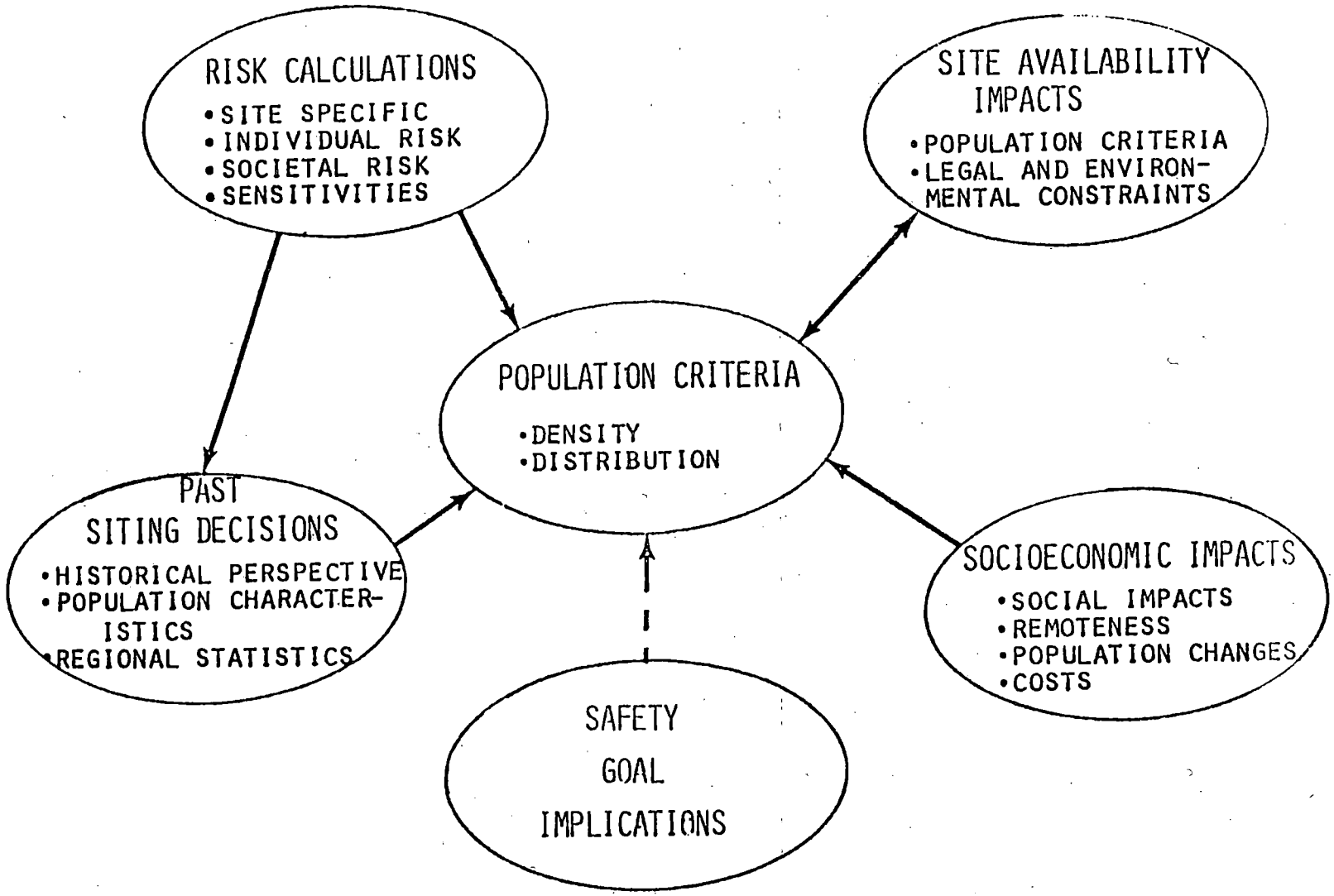
RISK CALCULATIONS
•SITE SPECIFIC
•INDIVIDUAL RISK
•SOCIETAL RISK
•SENSITIVITIES
SITE AVAILABILITY IMPACTS
•POPULATION CRITERIA
•LEGAL AND ENVIRONMENTAL CONSTRAINTS
POPULATION CRITERIA
•DENSITY
•DISTRIBUTION
PAST SITING DECISIONS
•HISTORICAL PERSPECTIVE
•POPULATION CHARACTERISTICS
•REGIONAL STATISTICS
SOCIOECONOMIC IMPACTS
•SOCIAL IMPACTS
•REMOTENESS
•POPULATION CHANGES
•COSTS
SAFETY GOAL IMPLICATIONS

Group 5 - Limited core damage. All systems of containment perform as designed (DBA-LOCA equivalent)

Group 4 - Modest core damage. Containment systems operate but in somewhat degraded mode (TMI-2 equivalent)

Group 3 - Severe core damage. Containment fails by basemat melt-through. All other release mitigation systems have functioned as designed (Analogous to Reactor Safety Study Pressurized Water Reactor, PWR, Categories 6 and 7)

Group 2 - Severe core damage. Containment fails to isolate. Containment release mitigating systems (e.g., sprays, suppression pool, fan coolers) operate to reduce release (Analagous to Reactor Safety Study PWR Categories 4and 5)

Group 1 - Severe core damage. Essentially involves loss of all installed safety features. Severe direct breach of containment (Analogous to Reactor Safety Study PWR Categories 1-3)

SENSITIVITY CALCULATIONS

1. METEOROLOGY
2. EMERGENCY RESPONSE
3. POWER LEVEL
4. INTERDICTION CRITERIA
5. DESIGN
6. SOURCE TERM
7. STANDOFF DISTANCE TO CITIES
8. EXCLUSION ZONE RADIUS

DISTANCES OF RISK SIGNIFICANCE

SOURCE TERM	CONSEQUENCES*	DISTANCE	
		EXPECTED	MAXIMUM
SST1	EARLY FATALITIES	< 5	≤ 25
	EARLY INJURIES	$\lesssim 10$	$\gtrsim 50$
	LAND INTERDICTION	≈ 20	> 50
SST2	EARLY FATALITIES	≈ 0.5	$\lesssim 2$
	EARLY INJURIES	< 2	≈ 5
	LAND INTERDICTION	≈ 2	≈ 10
	LAND DECONTAMINATION	≈ 10	> 50
	DOSES > PAGs	$\lesssim 20$	> 50
SST3	LAND DECONTAMINATION	$\lesssim 0.5$	$\lesssim ?$
	DOSES > PAGs	≤ 0.5	$\lesssim 2$
SST4 & 5	NO OFFSITE DISTANCE RELATIONSHIPS		

*INCLUDES CONSEQUENCES WHICH HAVE RELEVANT DISTANCE RELATIONSHIPS. EFFECTS SUCH AS LATENT CANCER FATALITIES AND GENETIC DAMAGE HAVE NO DISTANCE RELATIONSHIPS.

SITING FACTORS WHICH INFLUENCE RISK

		LIMITS	BY	IMPACT
1.	POPULATION DENSITY	CONSEQUENCES	10	LIMITS TOTAL NUMBER OF PEOPLE
2.	SECTOR LIMIT	CONSEQUENCES	4	LIMITS POPULATION CLUSTERING
3.	DISTANCE/GRID SIZE	CONSEQUENCES	3	LIMITS POPULATION CLUSTERING
4.	POWER LEVEL	CONSEQUENCES	2	LINEAR
5.	EMERGENCY RESPONSE	CONSEQUENCES	10	INDEPENDENT
6.	CORRELATION OF WIND AND POPULATION	PROBABILITIES	3	DATA AND METHOD PROBLEMS
7.	PRECIPITATION OCCURRENCE	PROBABILITIES	3	DATA PROBLEMS
8.	NUMBER AND PROXIMITY OF UNITS	PROBABILITIES	2	LINEAR
9.	SITE METEOROLOGY	PROBABILITIES	1.2	DATA PROBLEMS
10.	DESIGN/SOURCE TERM	PROBABILITIES	100	INDEPENDENT

Assumptions: SST1, NYC weather, Summary Evacuation within 10 miles,
Uniform wind rose

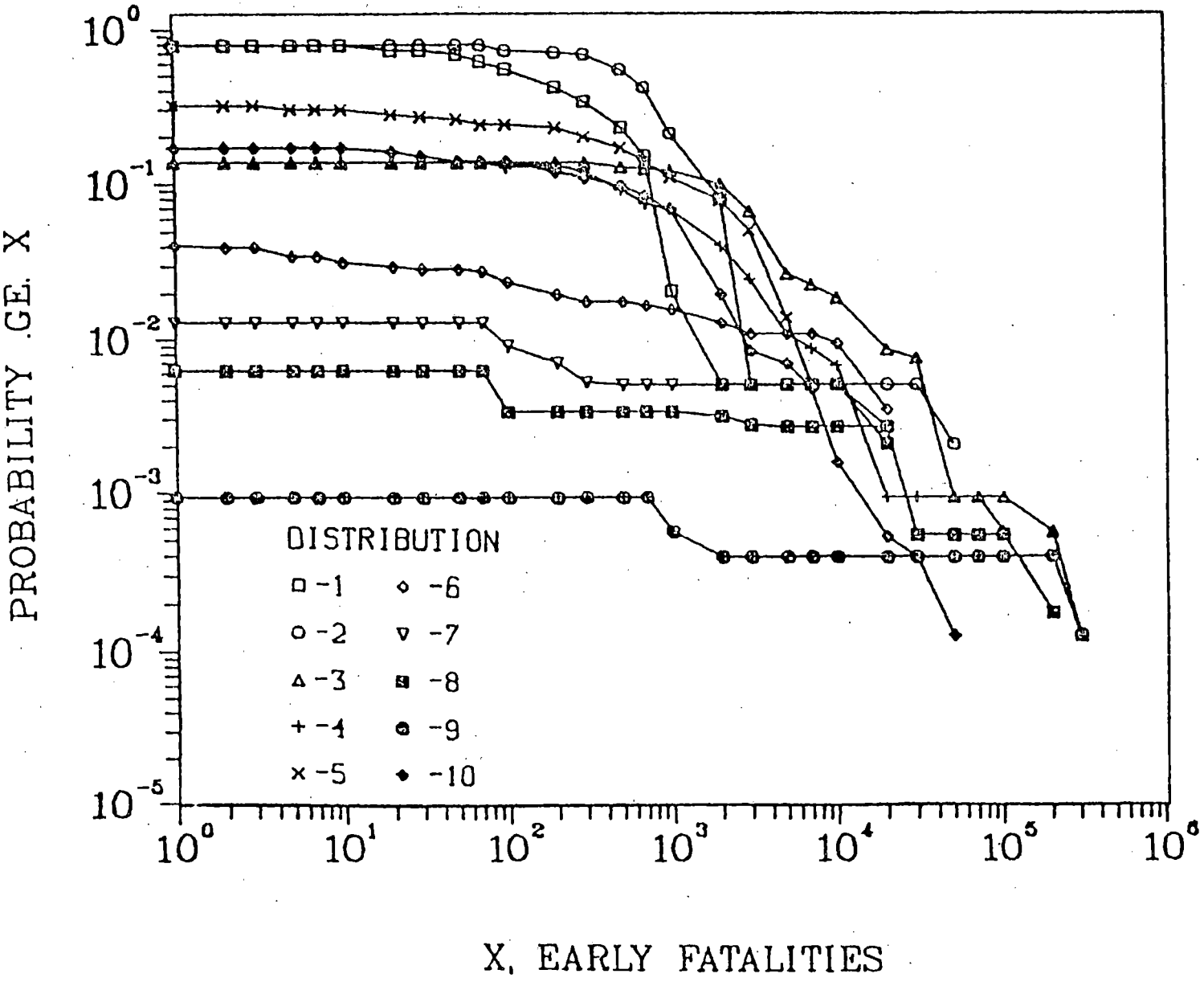

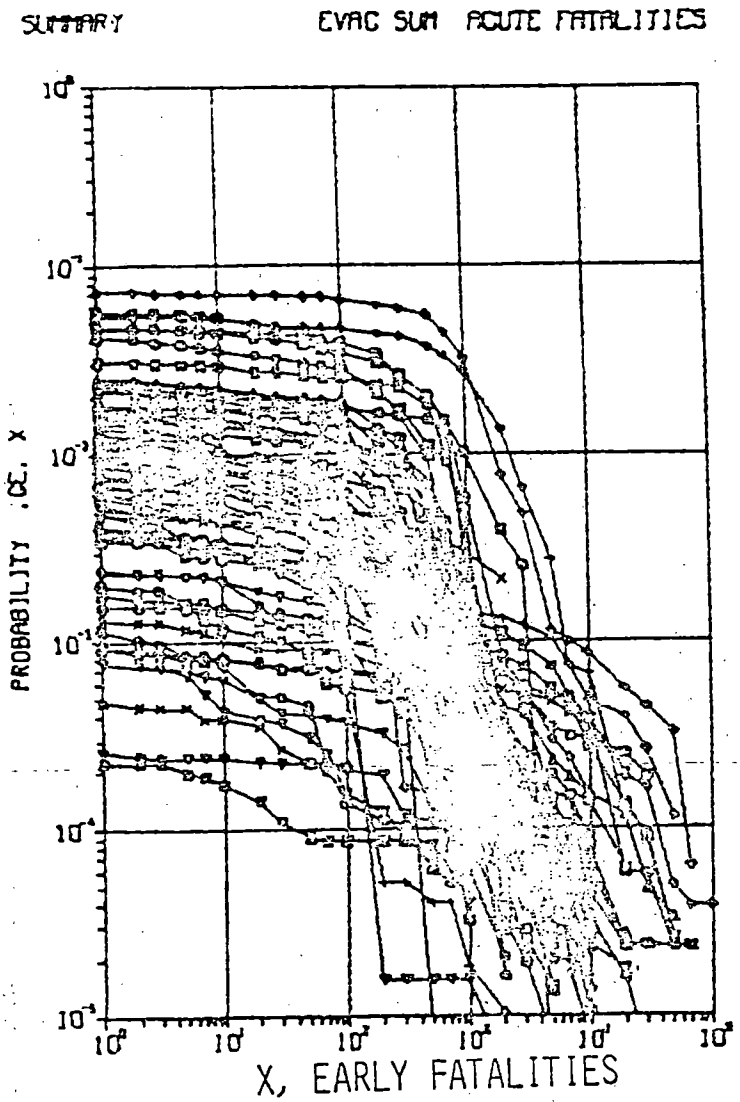

"SITE-SPECIFIC" EARLY FATALITY RISK CURVES FOR 91 SITES

ASSUMPTIONS:

(1) CONDITIONAL ON CORE MELT (SST1, 2, 3)

(2) STANDARD 1120 MWE REACTOR

(3) STANDARD EVACUATION SUMMARY

(4) ACTUAL SITE POPULATION AND WIND ROSE

(5) REGIONAL METEOROLOGY

RADIONUCLIDE BEHAVIOR IN LWR CONTAINMENTS DURING DEGRADED CORE ACCIDENTS: MATADOR, A REPLACEMENT FOR THE CORRAL CODE

PRESENTED AT
THE NINTH WATER REACTOR SAFETY
RESEARCH INFORMATION MEETING

OCTOBER 26-30, 1981
GAITHERSBURG, MARYLAND

P. BAYBUTT AND S. RAGHURAM

BATTELLE, COLUMBUS DIVISION
RISK ASSESSMENT GROUP
COLUMBUS, OHIO 43201

Battelle
Columbus Laboratories

A new computer code called MATADOR (Methods for the analysis of transport and deposition of radionuclides) has been developed to replace the CORRAL computer code which was written for the Reactor Safety Study (WASH1400). MATADOR is suitable for use in system risk studies to analyze radionuclide transport and deposition in reactor containments. The principal output of the code is information on the timing and magnitude of radionuclide releases to the environment as a result of severely degraded core accidents. MATADOR considers the transport of radionuclides through the containment and their removal by natural deposition and the operation of engineered safety systems such as sprays. The code requires input data on the source term from the primary system, the geometry of the containment, and thermal-hydraulic conditions in the containment.

MATADOR was written because the CORRAL2 code contains a number of deficiencies. Some potentially important transport processes are not modelled, for example, diffusiophoretic transport of particles. The validity of some transport models in CORRAL is also questionable, for example, that for transport of I_2. Additionally, the description of the radionuclide source term is rigid. Furthermore, a very simple treatment of particle size is used.

MATADOR provides for a completely general source term description. It allows the treatment of two or more particle sizes and treats explicitly aerosol agglomeration. MATADOR models iodine transport by both natural and forced convection and treats deposition on either dry or wet surfaces. Particle deposition by gravitational settling, and diffusional, thermophoretic, and diffusiophoretic deposition is modeled. Removal of radionuclides by such engineered safeguards or sprays, filters, suppression pools, and ice condensers is included in the code. MATADOR allows for resuspension of radionuclides from filters and also permits degraded filters to be considered. It also treats the attenuation of radionuclides during passage through leak pathways in the containment.

A comparison of results obtained with MATADOR and CORRAL2 is given in the presentation material (see viewgraphs). Comparisons have been made for the PWR accident sequences TMLB' and S_2D, and for the BWR accident sequences TC and AE.

RADIONUCLIDE BEHAVIOR IN LWR CONTAINMENTS DURING DEGRADED CORE ACCIDENTS: MATADOR, A REPLACEMENT FOR THE CORRAL COMPUTER CODE

P. BAYBUTT AND S. RAGHURAM

Battelle
Columbus Laboratories

CONTENTS

- OBJECTIVES
- DESCRIPTION OF CORRAL
- CORRAL DEFICIENCIES
- COMPARISON OF MATADOR WITH CORRAL
- RESULTS

Battelle
Columbus Laboratories

OBJECTIVES

- To completely rewrite CORRAL-2
- To correct deficiencies in CORRAL
- To provide a code for use in system risk studies

Battelle
Columbus Laboratories

DESCRIPTION OF CORRAL

CORRAL ACCOUNTS FOR RADIONUCLIDE TRANSPORT IN LWR CONTAINMENTS DURING MELTDOWN ACCIDENTS

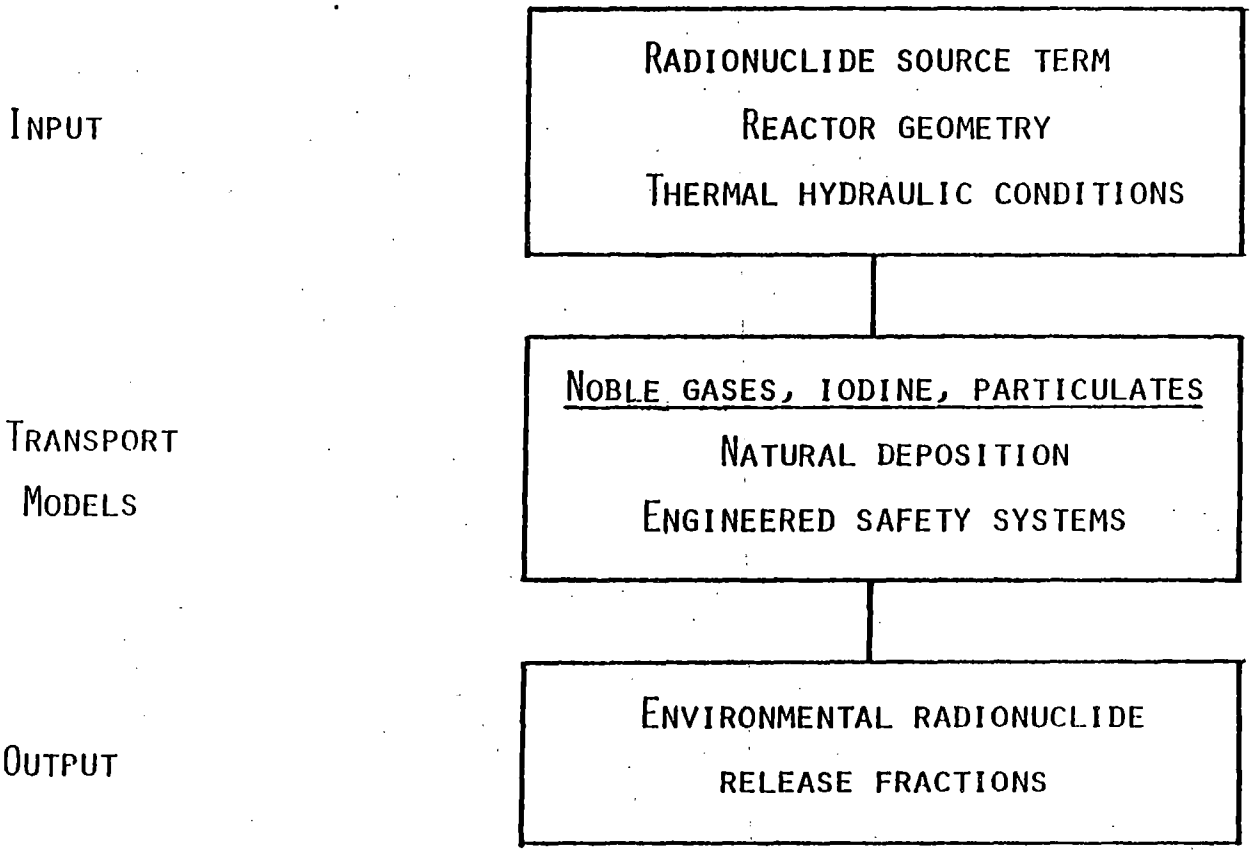

Battelle
Columbus Laboratories

STATUS OF CORRAL

- THE CORRAL CODE WAS WRITTEN FOR THE REACTOR SAFETY STUDY
- CORRAL WAS UPGRADED TO CORRAL-2 IN 1977, BUT NO CHANGES WERE MADE IN THE RADIONUCLIDE BEHAVIOR MODELS
- FURTHER MODIFICATIONS HAVE BEEN MADE TO CORRAL-2 BUT NONE AFFECTING RADIONUCLIDE BEHAVIOR

Battelle
Columbus Laboratories

DEFICIENCIES IN CORRAL-2

- SOME POTENTIALLY IMPORTANT RADIONUCLIDE TRANSPORT PROCESSES ARE NOT MODELED
- THE VALIDITY OF SOME TRANSPORT MODELS IN CORRAL IS QUESTIONABLE
- THE RADIONUCLIDE SOURCE TERM DESCRIPTION IS RIGID
- A VERY SIMPLE TREATMENT OF PARTICLE SIZE IS USED

(MORE)

DEFICIENCIES IN CORRAL-2 (CONTINUED)

- CORRAL-2 NOT VALIDATED
- THE INTERFACE WITH MARCH IS COMPLEX
- THE CONTINUED EVOLUTION AND ADAPTATION OF CORRAL HAS REACHED THE STAGE WHERE FURTHER CHANGES ARE DIFFICULT
- IMPROVEMENTS IN EFFICIENCY CAN BE ACHIEVED

CODE MODELS

- SOURCE TERM
- TRANSPORT AND DEPOSITION
- PARTICLE SIZE

Battelle
Columbus Laboratories

SOURCE TERM

CORRAL	MATADOR
FOUR COMPONENT	UNRESTRICTED
RESTRICTIONS ON TIME DEPENDENCE	COMPLETELY FLEXIBLE
NO INERT MATERIALS	RADIONUCLIDES AND INERT MATERIALS

Battelle
Columbus Laboratories

PARTICLE SIZE

CORRAL	MATADOR
MONODISPERSE AEROSOLS	TWO OR MORE SIZES
LINEAR SIZE DECREASE WITH TIME	AGGLOMERATION

Battelle
Columbus Laboratories

VAPOR TRANSPORT AND DEPOSITION PROCESSES

CORRAL	MATADOR
NATURAL CONVECTION	NATURAL AND FORCED CONVECTION
DRY SURFACES	DRY OR WET SURFACES
SPRAY REMOVAL	SPRAY REMOVAL
FILTERS	FILTERS WITH RESUSPENSION AND DEGRADED FILTER CAPABILITY
POOL SCRUBBING	POOL SCRUBBING
	ICE CONDENSER

Battelle
Columbus Laboratories

PARTICLE TRANSPORT AND DEPOSITION PROCESSES

CORRAL

- GRAVITATIONAL SETTLING
- SPRAY REMOVAL
- FILTERS

MATADOR

- GRAVITATIONAL SETTLING
  DIFFUSIONAL DEPOSITION
  THERMOPHORETIC DEPOSITION
  DIFFUSIOPHORETIC DEPOSITION
- SPRAY REMOVAL
- FILTERS
- LEAKAGE THROUGH CONTAINMENT

Battelle
Columbus Laboratories

COMPARISON OF MATADOR AND CORRAL2 RESULTS - TMLB'

	I	Cs	Te	Ba	Ru	La
CORRAL2	0.41	0.43	0.15	5.0×10^{-2}	2.0×10^{-2}	2.4×10^{-3}
MATADOR	0.49	0.38	0.07	4.8×10^{-2}	1.4×10^{-2}	1.4×10^{-3}
Difference Factor	0.8	1.1	2.1	1.1	1.4	1.7

Battelle
Columbus Laboratories

COMPARISON OF MATADOR AND CORRAL2 RESULTS - S_2D

	I	Cs	Te	Ba	Ru	La
CORRAL2	3.9×10^{-2}	0.12	0.38	9.0×10^{-3}	2.3×10^{-2}	4.5×10^{-3}
MATADOR	4.6×10^{-2}	0.04	0.14	3.5×10^{-3}	8.4×10^{-3}	1.6×10^{-3}
Difference Factor	0.8	2.7	2.8	2.6	2.8	2.8

Battelle
Columbus Laboratories

COMPARISON OF MATADOR AND CORRAL2 RESULTS - TC

	I	Cs	Te	Ba	Ru	La
CORRAL2	0.06	0.13	0.12	1.4×10^{-2}	9.6×10^{-3}	1.5×10^{-3}
MATADOR	0.49	6.7×10^{-3}	1.2×10^{-3}	8.2×10^{-4}	2.5×10^{-4}	2.5×10^{-5}
Difference	0.1	19	95	17	39	62

Battelle
Columbus Laboratories

COMPARISON OF MATADOR AND CORRAL2 RESULTS - AE

	I	Cs	Te	Ba	Ru	La
CORRAL2	4.8×10^{-3}	8.5×10^{-3}	7.0×10^{-3}	1.0×10^{-3}	6.1×10^{-4}	9.3×10^{-5}
MATADOR	5.7×10^{-2}	1.2×10^{-2}	2.4×10^{-3}	1.6×10^{-3}	4.9×10^{-4}	4.9×10^{-5}
Difference Factor	0.1	0.7	1.6	0.6	1.2	1.9

Battelle
Columbus Laboratories

RISK METHODOLOGY AND DATA BRANCH, DIVISION OF RISK ANALYSIS, USNRC

OVERVIEW OF RESEARCH ON

RISK METHODOLOGY & DATA

WILLIAM E. VESELY

NINTH WATER REACTOR SAFETY RESEARCH INFORMATION MEETING

GAITHERSBURG, MARYLAND

OCTOBER 30, 1981

RISK METHODOLOGY AND DATA

SUMMARY

W. E. Vesely

Methods Development for System Interactions and Reliability Analysis

Research to improve upon current capabilities in system interaction analysis, system reliability analysis, and failure mode prediction are slated for FY 1982-1987. Improved mathematical models of system networks will be developed to deal with feedback effects, delayed and conditional fault propagation, and partial failures and to accommodate improved models for human reliability, both human error and human corrective action. Methods such as the "GO" codes, sneak-circuit analysis, logic-circuit simulation, diagraph methods, matrix methods, Markov methods, and dynamic simulation will be explored and adapted to the needs of nuclear safety system reliability analysis.

NRR needs a practical set of techniques to deal with systems interactions in licensing. A focus of the research into improved system reliability analysis techniques will be research to meet this need. A variety of reliability engineering techniques that show promise for systems interaction evaluation will be explored, e.g., fault trees, network models of fault propagation, failure mode effects analysis, and common-cause failure analysis software. Improvements in probabilistic assessment are also planned to better resolve failure modes of equipment. Some types of failures lend themselves to preventive maintenance or to identification and repair before the fault has progressed from incipient failure to total failure. Methods to resolve such failure mode characteristics in data analysis and predictive system reliability analysis--coupled with improved assessments of the risk significance of hypothetical failures developed in applied systems analysis--will be of use to I&E and SD in focusing upon the more effective ways of reducing reactor accident risks, as well as improving safety analysis and risk assessment.

Common-Cause Failure Analysis and Hazardous External Events

The goal of this research work is to develop models, data, and computer codes for the systematic analysis of common-cause failures and external events as they affect safety system reliability and accident probabilities and consequences.

Multiple concurrent component failures and external hazards are of particular importance to reactor safety; they can compromise the redundancy or defense in depth that is entended to ensure safety in the plants. There are several kinds of common-cause failures. Some multiple failures originate in the failure of a common support system; these are treated in network system reliability analysis techniques. Other multiple failures can be traced to common human intervention (operations or maintenance); these are treated in human reliability research. Two other varieties of common-cause failure are the subjects of this research program: (1) multiple faults originating in common design, fabrication, installation, startup, operating history, or service environment, and (2) external events such as earthquakes, site flooding from direct natural forces or the failure of flood prevention features, hurricanes, or tornadoes.

Methods Development for Accident-Sequence Analysis

The development of methods for accident-sequence analysis for reactors is a new program. The first phase is the development of a hierarchical classification scheme for reactor accidents. This scheme is to provide a catalog of LWR accident scenarios of various kinds and degrees of severity that can be used in qualitative, deterministic, and probabilistic safety analysis; in operator training; in planning for emergencies; and in the analysis of operating experiences. One of the principal subtasks will be to continue the study of "precursor events" and their risk significance.

Data Bank Methodology

The objective of this research is to develop computer codes and procedures by which raw data on reactor operating experiences can be transformed into component reliability data.

Different measures of the reliability of components are revised as additional information about reactor operation is accumulated. These reliability parameters include failure probability per demand or per duty cycle, failure rates per hour of service, component unavailability because of testing or maintenance, and repair times. A number of safety-related components are covered. The data is assembled according to the type of component involved, and the average and range of reliability are obtained for generically similar equipment for all commercial LWRs, for all plants of the type, and for individual plants. Data sources include LERs, the NPRDS, and studies of selected plant operations and maintenance logbooks. The data analysis includes quality control of the data base through checks of the consistency of the three sources of data.

PROGRAM AREAS

- SYSTEM UNAVAILABILITY MODELING
- ANALYSIS OF LIMITING CONDITIONS FOR OPERATIONS
- SOFTWARE RELIABILITY MODELING
- COMMON CAUSE ANALYSIS
- FLOOD ANALYSIS
- STATISTICAL AND UNCERTAINTY EVALUATIONS
- RISK MANAGEMENT AND DECISION APPROACHES
- DATA ANALYSIS

SYSTEM UNAVAILABILITY MODELING

OBJECTIVE -

TO CALCULATE DETAILED TIME-DEPENDENT POINTWISE UNAVAILABILITY INCLUDING:

- o VARIABLE TEST INTERVALS
- o TEST INEFFICIENCIES
- o TEST DOWN-TIMES AND REPAIR TIMES

APPLICATIONS -

EVALUATION OF TIME DEPENDENT SYSTEM FAILURE BEHAVIORS

DETERMINATION OF OPTIMAL TESTING SCHEMES

SYSTEM UNAVAILABILITY MODELING (CONT) ------

STATUS:

DEVELOPMENT PHASE WILL TERMINATE IN FY 1982

APPLICATIONS AND LICENSING TRANSFER PHASE BEGAN IN FY 1981

RESULTS:

THREE COMPUTER CODES, METHODOLOGY DESCRIPTION AND ASSOCIATED NUREGS (FOR FRANTIC, FRANDOM AND FRANTIC II CODES)

SYSTEM UNAVAILABILITY

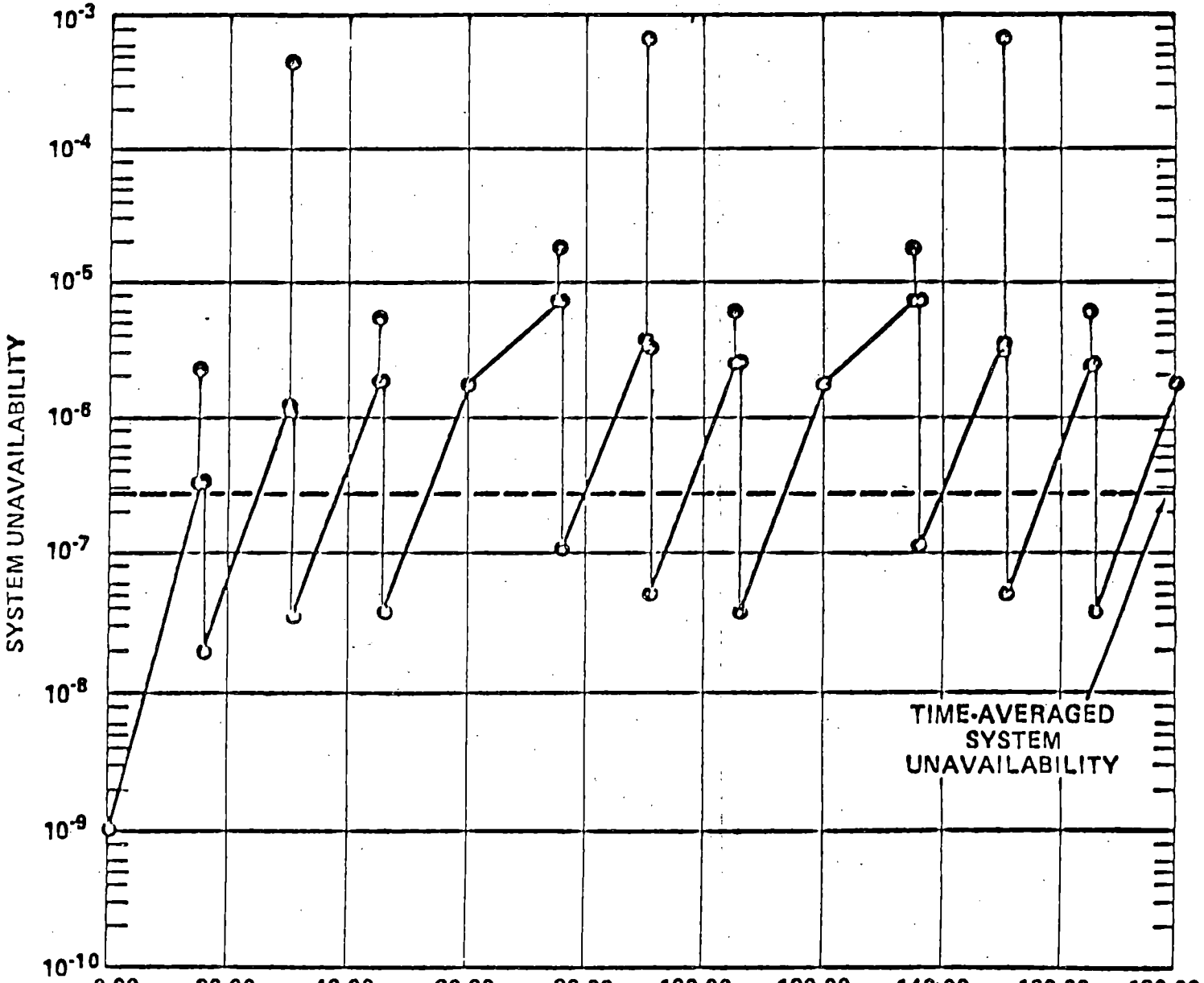

$$Q = [\,1 - (1-Q_1) \cdot (1-Q_2) \cdot (1-Q_3)\,] \cdot Q_4 \cdot Q_5$$

PERIODICALLY TESTED UNAVAILABILITY

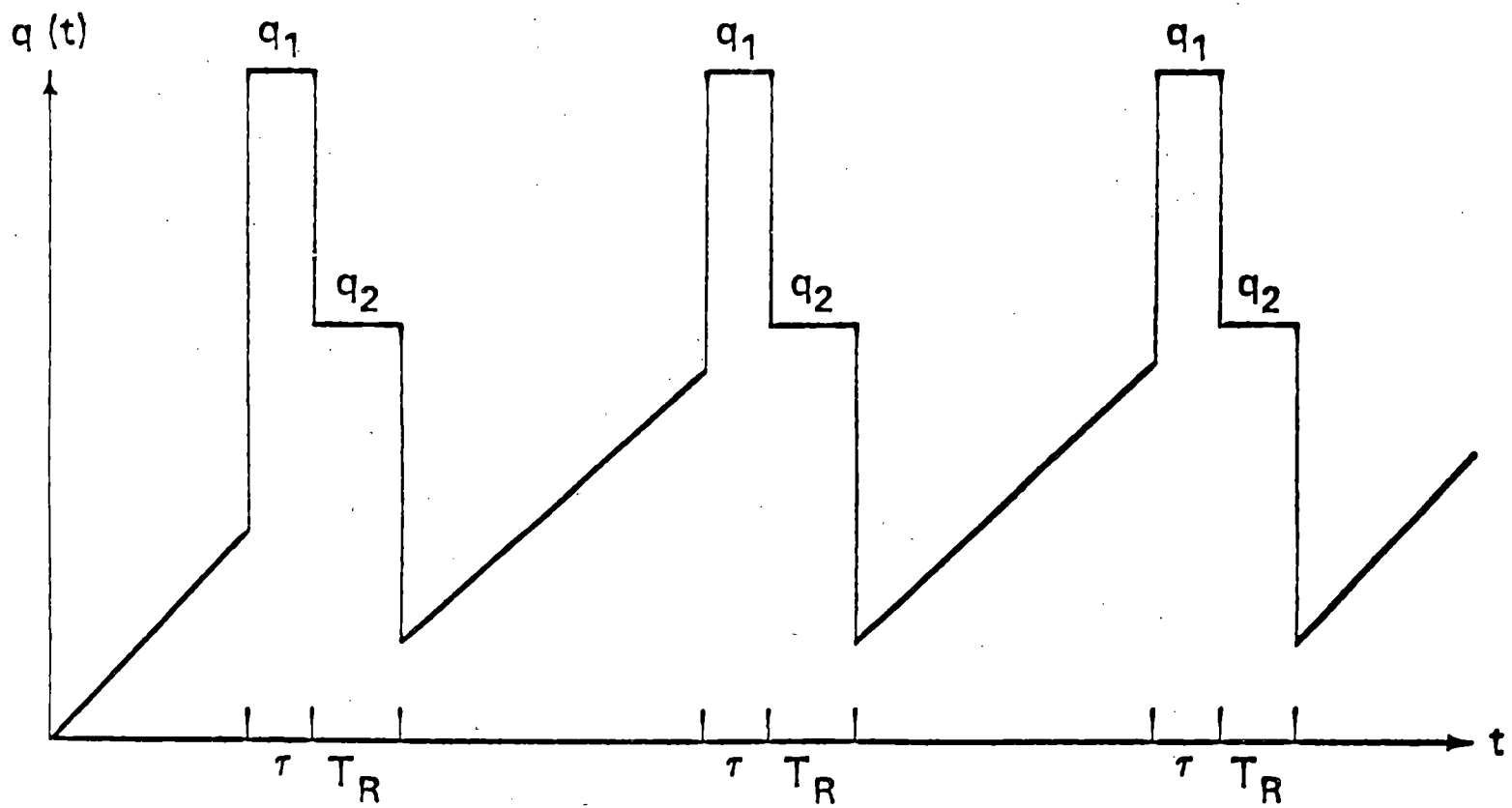

ANALYSIS OF LIMITING CONDITIONS FOR OPERATIONS (LCOs)

OBJECTIVE: TO DEVELOP APPROACHES FOR SETTING ALLOWED DOWNTIMES AND SURVEILLANCE TEST INTERVALS BASED ON RISK EVALUATIONS

APPROACH:

1. DEVELOP THEORETICAL METHODS AND SOFTWARE
2. PERFORM SENSITIVITY STUDIES ON EVALUATIONS OF SPECIFIC DESIGNS (IREP)
3. GENERALIZE TO OBTAIN GENERIC GUIDELINES AND RULES FOR TECH SPECS

LCO METHODS DEVELOPMENT (CONT) ----

PRESENT STATUS:

1. DEVELOPMENT OF THE METHODOLOGY IS COMPLETE AND DOCUMENTATION IS IN PREPARATION

2. UNCERTAINTY AND SENSITIVITY STUDIES ARE PARTIALLY COMPLETE. THIS WORK WILL CONTINUE IN FY 1982

3. AN INTERIM PROGRESS REPORT IS IN PREPARATION AND SCHEDULED FOR COMPLETION ON SEPTEMBER 15, 1981

SEQUENTIAL TEST MONITORING SCHEME

OBJECTIVE: TO DEVELOP A SEQUENTIAL TEST MONITORING SCHEME FOR PERIODICALLY TESTED COMPONENTS

APPROACH: 1. DEVELOP CONTROL LINES FOR PERIODICALLY TESTED COMPONENTS USING SEQUENTIAL PROBABILITY RATIO TEST AND RISK CRITERIA

2. DEVELOP A MONTE CARLO SIMULATION CODE FOR EVALUATING THE PROPERTIES OF THE CONTROL LINES

3. APPLY THE TECHNIQUE TO SPECIFIC COMPONENTS

STATUS: 1. THE TECHNICAL WORK IS COMPLETE

2. A COMPUTER CODE COLINE (CONTROL LINE EVALUATION) HAS BEEN DEVELOPED

3. A DRAFT REPORT IS IN PREPARATION

SEQUENTIAL TEST MONITORING SCHEME (CONT)

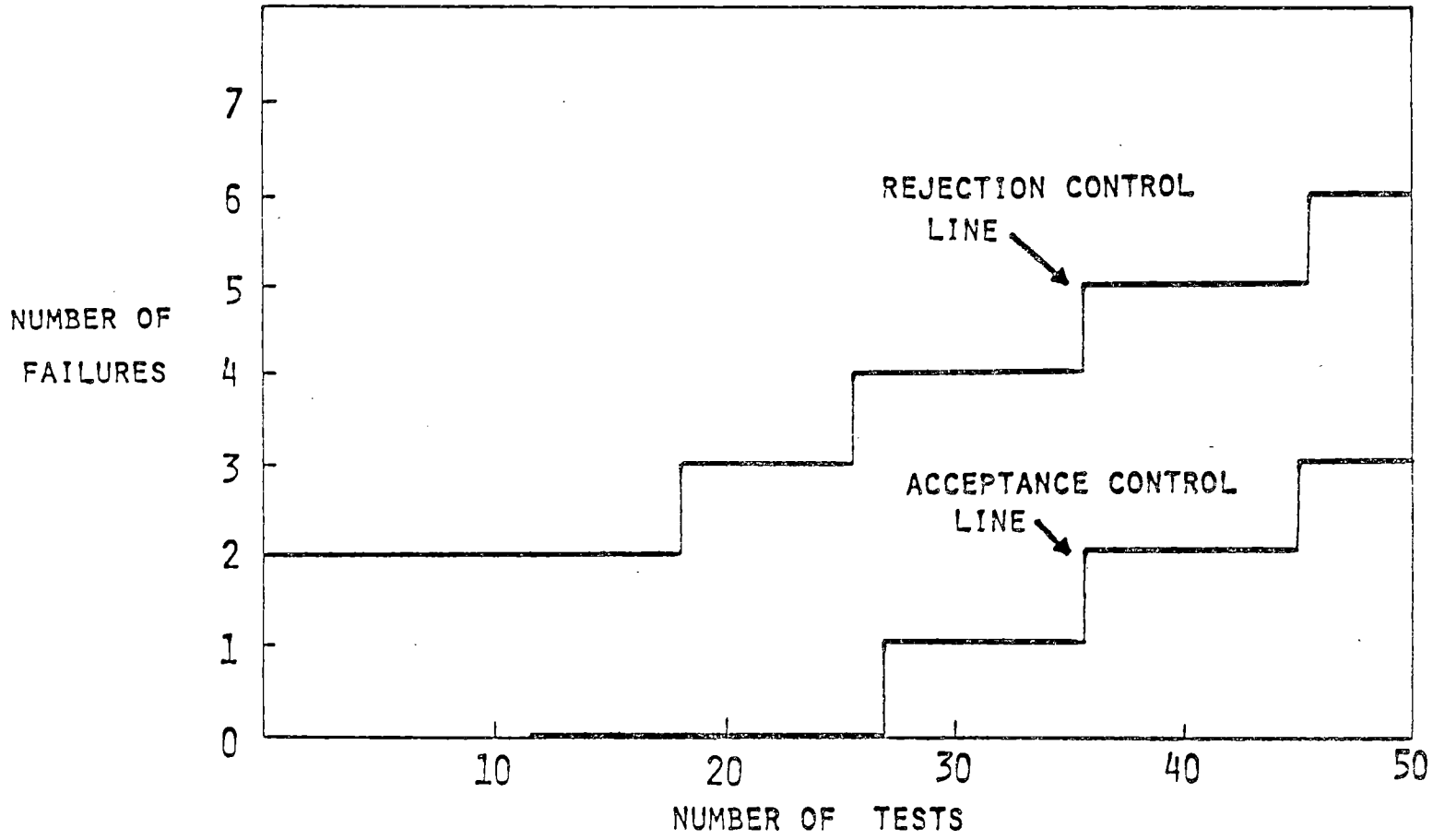

A TYPICAL TESTING SCHEME FOR DIESEL GENERATORS

SOFTWARE RELIABILITY MODELING

OBJECTIVE: TO EVALUATE METHODS AND HISTORICAL DATA FOR SOFTWARE RELIABILITY EVALUATION

TASKS: 1. REVIEW METHODS FOR QUANTITATIVE RELIABILITY EVALUATIONS

2. ASSEMBLE AND ANALYZE HISTORICAL DATA ON SOFTWARE FAILURE RATES

3. DEVELOP QUALITY CONTROL PROCEDURES FOR SOFTWARE VALIDATION

4. DETERMINE APPLICABILITY OF SOFTWARE QUANTIFICATION APPROACHES FOR RISK ANALYSIS

STATUS: 6 MONTH PROGRESS REPORT ISSUED

COMMON CAUSE ANALYSIS

OBJECTIVE: TO DEVELOP SYSTEMATIC APPROACHES FOR IDENTIFYING AND QUANTIFYING COMMON CAUSE CONTRIBUTORS IN RISK ANALYSIS

APPROACH:

1. ANALYZE LER DATA TO OBTAIN STATISTICAL ESTIMATES OF COMMON CAUSE PROBABILITIES

2. DETERMINE AND CATEGORIZE ROOT CAUSES OF COMMON CAUSE FAILURES

3. DEVELOP ENGINEERING METHODS AND RULES FOR SYSTEMATICALLY EVALUATING COMMON CAUSE CONTRIBUTIONS IN RISK ANALYSIS

COMMON CAUSE ANALYSIS (CONT) -----

STATUS: STATISTICAL ANALYSIS COMPLETED ON DIESELS, PUMPS, AND VALVES

WORK BEGUN ON CATEGORIZING ROOT CAUSES AND FACTORS MOST INFLUENCING COMMON CAUSE PROBABILITIES

RESULTS: 1 COMPUTER CODE AND ASSOCIATED NUREG FOR STATISTICAL ANALYSIS AND 3 NUREGS ON DATA EVALUATIONS

ANALYSIS & PREDICTION OF MAJOR FLOOD OCCURRENCES

OBJECTIVE: DEVELOP METHODOLOGY TO PREDICT FLOOD OCCURRENCE PROBABILITIES VERSUS FLOOD LEVEL (INCLUDING UNCERTAINTIES)

TASKS:

1. DEVELOP BAYESIAN TECHNIQUES TO ESTIMATE FLOOD OCCURRENCE PROBABILITIES
2. DEVELOP MODULAR COMPUTER CODE TO IMPLEMENT BAYESIAN FLOOD ESTIMATION TECHNIQUES
3. PERFORM EXTENSIVE SENSITIVITY STUDIES

STATUS

- CODE OPERATIONAL FOR RESTRICTED PROBABILITY MODELS
- DRAFT NUREG PUBLISHED

  FLOE: A PROGRAM FOR BAYESIAN ESTIMATION OF FLOOD PROBABILITIES

PLANNED FOR FY 1982:

- SENSITIVITY STUDIES
- ADDITIONAL MODEL DEVELOPMENT

TITLE: FLOOD RISK SYSTEMS ANALYSIS

OBJECTIVE: DEVELOP METHODOLOGY FOR EVALUATING THE RISK IMPACT OF FLOODS ON LWR NUCLEAR POWER PLANTS

TECH APPROACH:

1. DEVELOP TECHNIQUES TO BOUND THE PROBABILITY THAT A FLOOD CAUSES EXTENSIVE DAMAGE IN A NPP.
2. EXTEND THE CAPABILITIES OF THE NOAH COMPUTER CODE TO: A) ADD CAPABILITY FOR BOUNDING ANALYSIS, AND B) INCORPORATE QUANTITATIVE ANALYSIS CAPABILITY.
3. DEMONSTRATE METHODOLOGY ON THE SURRY PLANT

- COMPUTER PROGRAM EXTENSIONS/CAPABILITIES BY DECEMBER 1981:
  - IDENTIFY FLOOD PROTECTION SETS
  - ANALYZE FLOODS BELOW CRITICAL FLOOD DEPTH
  - PERFORM FLOOD SCREENING ANALYSIS
  - COUPLE QUALITATIVE AND QUANTITATIVE ROUTINES
  - IDENTIFY DESIGN MODS TO REDUCE SYSTEM FAILURES DUE TO FLOODS
  - IDENTIFIES COMPONENTS ROLE IN FLOOD ANALYSIS

STATISTICAL AND UNCERTAINTY EVALUATIONS

OBJECTIVE: TO DEVELOP AND COMPARE APPROACHES FOR SYSTEMATIC TREATMENT OF UNCERTAINTIES

TASKS:

1. DEVELOP DISTRIBUTION APPROACHES FOR MODELING FAILURE RATE VARIATIONS
2. COMPARE BAYESIAN AND CLASSICAL APPROACHES FOR PROPAGATING UNCERTAINTIES (ON WASH-1400, IREP SYSTEM MODELS)
3. DEVELOP GUIDELINES FOR USE AND INTERPRETATION IN RISK ANALYSIS

STATUS: 4 NUREGS WILL BE ISSUED FROM OCTOBER - DECEMBER 1981

THE AMERICAN STATISTICAL ASSOCIATION AD HOC ADVISORY COMMITTEE

OBJECTIVE: TO PROVIDE RES WITH ADVICE AND PEER REVIEW ON PROGRAMS WHICH REQUIRE STATISTICAL AND PROBABILISTIC TECHNIQUES AND APPROACHES

TECH APPROACH:

1. THREE TWO-DAY CLOSED MEETINGS WERE HELD IN THE DC AREA
2. COMMENTS ON QUALITY AND COMPREHENSIVENESS OF VARIOUS REPORTS
3. REFLECT STATE-OF-THE- ART PROCEDURES IN THE REVIEWS
4. SUGGEST NEW APPROACHES AND NEW AREAS OF RESEARCH
5. SUGGEST IMPROVEMENTS AND EXTENSIONS IN EACH REVIEW

RISK MANAGEMENT AND DECISION APPROACHES

OBJECTIVES: TO EVALUATE METHODS OF SYSTEMATICALLY INCORPORATING RISK ANALYSIS IN DECISION MAKING, AND TO EVALUATE ISSUES RELATED TO IMPLEMENTATION OF QUANTITATIVE SAFETY GOALS

MAJOR PROJECTS:

1. DEVELOPMENT AND EVALUATION OF SYSTEMATIC DECISION-THEORETIC APPROACHES
2. DEVELOPMENT OF CRITERIA TO EVALUATE NUMERICAL SAFETY GOALS
3. EVALUATION OF SPECIFIC NUMERICAL SAFETY GOALS

DEVELOPMENT AND EVALUATION OF SYSTEMATIC DECISION-THEORETIC APPROACHES (PART 1)

OBJECTIVES: DEVELOP QUANTITATIVE MODELS FOR PREDICTING LOSS OF BENEFITS FROM NUCLEAR PLANT SHUTDOWNS

APPROACHES:

1. DEVELOP REGIONAL CATEGORIZATIONS OF NUCLEAR POWER PLANTS
2. DETERMINE LOSS OF DIRECT ECONOMIC BENEFITS FROM NUCLEAR POWER PLANT SHUTDOWN
3. CONSTRUCT MODELS FOR INDIRECT LOSSES FROM SHUTDOWN
4. EVALUATE SPECIFIC CASE STUDIES

STATUS: SIX MONTH PROGRESS REPORT SUBMITTED

NUREG TO BE SUBMITTED BY OCT 1981

DEVELOPMENT AND EVALUATION OF SYSTEMATIC DECISION-THEORETIC APPROACHES (PART 2)

TASKS: 1. DEVELOP SPECIFIC APPROACHES FOR SYSTEMATIC UTILIZATION OF RISK ANALYSES

2. EVALUATE SPECIFIC CASE STUDIES TO DEMONSTRATE THE APPROACHES:

A. INDIAN POINT 2 ALTERNATIVES --

- o STATUS QUO
- o VENT/FILTER SYSTEM
- o CORE CATCHER
- o HYDROGEN CONTROL
- o DERATING

B. IREP/UTILITY RISK ANALYSIS ON RECORD

STATUS: ONE PRELIMINARY REPORT AND 6 MONTH PROGRESS REPORT SUBMITTED

ONE NUREG TO BE COMPLETED BY DEC 1981

DEVELOPMENT OF CRITERIA TO EVALUATE NUMERICAL SAFETY GOALS

OBJECTIVE: TO EVALUATE SOCIOLOGICAL AND TECHNICAL ISSUES ASSOCIATED WITH FORMULATIONS OF ACCEPTABLE RISK GOALS

RESULTS TO DATE: NUREG/CR-1614, DTD SEPT 1980, ACCOMPLISHES THE FOLLOWING:

- o DEFINED ACCEPTABLE RISK DECISIONS AND EXAMINED SOME FREQUENTLY PROPOSED SOLUTIONS
- o CHARACTERIZED THE ESSENTIAL FEATURES OF ACCEPTABLE RISK PROBLEMS THAT MAKE RESOLUTION DIFFICULT
- o CREATED A TAXONOMY OF DECISION MAKING METHODS
- o SPECIFIED OBJECTIVES AN APPROACH SHOULD SATISFY TO GUIDE SOCIAL POLICY

FUTURE WORK: BEING PROGRAMMED

EVALUATION OF SPECIFIC NUMERICAL SAFETY GOALS

OBJECTIVE: INVESTIGATE SPECIFIC SAFETY GOALS WHICH HAVE BEEN PROPOSED WITH REGARD TO IMPLEMENTATION ISSUES

RESULT: NUREG/CR-2040, DATED MAY 1981, ACCOMPLISHES THE FOLLOWING:

- DEVELOPS APPROACHES FOR EVALUATING THE CHARACTERISTICS OF PROPOSED NUMERICAL CRITERIA
- INVESTIGATES POTENTIAL WAYS OF RANKING CRITERIA
- EVALUATES RISK IMPLICATIONS OF EMPLOYING VARIOUS CRITERIA
- EVALUATES MODELS AND DATA REQUIRED IN IMPLEMENTING DIFFERENT CRITERIA
- DISCUSSES VARIOUS RISK MANAGEMENT APPROACHES

DATA ANALYSIS BREAKDOWN

RELIABILITY AND STATISTICAL TECH.

DEV. OF DATA BASES FOR RISK ANALYSIS

CONDUCTION OF DATA ANALYSIS FOR AGENCY

DEV. OF FAILURE RATE DATA MANUALS

TITLE: NPRDS ANALYSIS/LER ANALYSIS

FIN NOS. A6290
A6276

OBJECTIVES:

1. DEVELOP STATISTICAL METHODOLOGY AND SOFTWARE FOR APPLICATION TO A RELIABILITY DATA BASE
2. DEVELOP SYSTEMATIC APPROACHES FOR USE OF COMPONENT AND SYSTEM RELIABILITY DATA
3. DETERMINE VALUE OF DATA IN EXISTING NPRDS DATA BASE
4. DETERMINE FAILURE RATES FOR NPP COMPONENTS USING THE LER FILE

TECH APPROACH:

1. DEVELOP A RELIABILITY METHODS/DATA CANDIDATE LIST FOR POTENTIAL UTILIZATION WITH AN IMPROVED NPRDS
2. DEVELOP A MODULAR, SYSTEMATIC RELIABILITY/RISK ANALYSIS NETWORK AND A FIVE YEAR IMPLEMENTATION PLAN
3. COMPLETE DEVELOPMENT OF HIERARCHICAL APPROACH FOR FAILURE RATE POINT ESTIMATES AND ASSOCIATED UNCERTAINTY INTERVALS
4. EVALUATE LER FAILURE DATA ON COMPONENTS AND TABULATE SO THAT FURTHER STATISTICAL ANALYSES MAY BE PERFORMED

TITLE: ANALYSIS OF RELIABILITY DATA FROM NPP

OBJECTIVE: COLLECT AND ANALYZE FAILURE DATA FROM THE IN-PLANT MAINTENANCE FILES OF NPP TO SUPPLEMENT DATA OBTAINED FROM NPRDS AND LERs.

TECH APPROACH:

1. COLLECT COMPONENT POPULATION, FAILURE AND REPAIR DATA FROM IN-PLANT MAINTENANCE FILES
2. DEVELOP GENERIC SYSTEMS DEFINITIONS
3. DEVELOP A DESIGN-RELATED CATEGORIZATION SCHEME
4. ANALYZE DATA

STATUS

REPORTS DUE END OF FY 1981

1. GENERAL METHODOLOGY REPORT

   DATA COLLECTION AND ENCODING METHODS, GENERIC SYSTEMS DEFINITIONS

2. PUMP DATA REPORT - 4 PLANTS

3. VALVE DATA REPORT - 4 PLANTS

PLANNED FOR FY 1982 - EMPHASIS ON DATA COLLECTION AND ENCODING

- ADDITIONAL PLANTS
- ADDITIONAL COMPONENTS

  BATTERIES AND INVERTERS
  DIESEL GENERATORS
  PUMP DRIVERS
  OTHERS TO BE DECIDED

EXAMPLE OF DEVELOPED INSTRUCTION MATERIAL

FAULT TREE HANDBOOK - NUREG-0492

I. BASIC CONCEPTS OF SYSTEM ANALYSIS

II. OVERVIEW OF INDUCTIVE METHODS

III. FAULT TREE ANALYSIS - CONCEPTS AND DEFINITIONS

IV. THE BASIC ELEMENTS OF A FAULT TREE

V. FAULT TREE CONSTRUCTION

VI. PROBABILITY THEORY: THE MATHEMATICAL DESCRIPTION OF EVENT

VII. BOOLEAN ALGEBRA & APPLICATION TO FAULT TREE ANALYSIS

VIII. THE PRESSURE TANK EXAMPLE

IX. THE THREE MOTOR EXAMPLE

X. PROBABILISTIC AND STATISTICAL ANALYSES

XI. FAULT TREE EVALUATION

XII. FAULT TREE CODES

NUREG PUBLICATIONS DURING FY 1980 AND FY 1981

1. NUREG/CR-1110, "BAYESIAN ANALYSIS OF COMPONENT FAILURE DATA," DTD NOVEMBER 1979.

2. NUREG/CR-1205, "DATA SUMMARIES OF LICENSEE EVENT REPORTS OF PUMPS AT U.S. COMMERICAL NUCLEAR POWER PLANTS," DTD JANUARY 1980.

3. NUREG/CR-1331, "DATA SUMMARIES OF LICENSEE EVENT REPORTS OF CONTROL RODS AND DRIVE MECHANISMS AT U.S. COMMERCIAL NUCLEAR POWER PLANTS," DTD FEBRUARY 1980.

4. NUREG/CR-1362, "DATA SUMMARIES OF LICENSEE EVENT REPORTS OF DIESEL GENERATORS AT U.S. COMMERCIAL NUCLEAR POWER PLANTS," DTD MARCH 1980.

5. NUREG/CR-1401, "ESTIMATORS FOR THE BINOMIAL FAILURE RATE COMMON CAUSE MODEL," DTD APRIL 1980.

6. NUREG/CR-1278, "HANDBOOK OF HUMAN RELIABILITY ANALYSIS WITH EMPHASIS ON NUCLEAR POWER PLANT APPLICATIONS," DTD APRIL 1980 (2ND DRAFT PUBLISHED OCTOBER 1980).

NUREG PUBLICATIONS DURING FY 1980 AND FY 1981 CONTINUED

7. NUREG/CR-1363, "DATA SUMMARIES OF LICENSEE EVENT REPORTS OF VALVES AT U.S. COMMERCIAL NUCLEAR POWER PLANTS," DTD JUNE 1980 (3 VOLUMES).

8. NUREG/CR-1539, "A METHODOLOGY AND A PRELIMINARY DATA BASE FOR EXAMINING THE HEALTH RISKS OF ELECTRICITY GENERATION FROM URANIUM AND COAL FUELS," DTD AUGUST 1980.

9. NUREG/CR-1614, "APPROACHES TO ACCEPTABLE RISK: A CRITICAL GUIDE," DTD SEPTEMBER 1980.

10. NUREG/CR-1730, "DATA SUMMARIES OF LICENSEE EVENT REPORTS OF PENETRATIONS AT U.S. COMMERCIAL NUCLEAR POWER PLANTS," DTD SEPTEMBER 1980.

11. NUREG/CR-1819, "DEVELOPMENT AND TESTING OF A MODEL FOR FIRE POTENTIAL IN NUCLEAR POWER PLANTS," DTD NOVEMBER 1980.

12. NUREG/CR-1880, "INITIAL QUANTIFICATION OF HUMAN ERRORS ASSOCIATED WITH REACTOR SAFETY SYSTEM COMPONENTS IN LICENSED NUCLEAR POWER PLANTS," DTD JANUARY 1981.

NUREG PUBLICATIONS DURING FY 1980 AND FY 1981 CONTINUED

13. NUREG/CR-1879, "SENSITIVITY OF RISK PARAMETERS TO HUMAN ERRORS IN REACTOR SAFETY STUDY FOR A PWR," DTD JANUARY 1981.

14. NUREG-0492, "FAULT TREE HANDBOOK," DTD JANUARY 1981

15. NUREG/CR-1916, "A RISK COMPARISON," DTD FEBRUARY 1981.

16. NUREG/CR-1930, "INDEX OF RISK EXPOSURE AND RISK ACCEPTANCE CRITERIA," DTD FEBRUARY 1981.

17. NUREG/CR-1924, FRANTIC II, A COMPUTER CODE FOR TIME DEPENDENT UNAVAILABILITY ANALYSIS," APRIL 1981.

18. NUREG/CR-1740, "DATA SUMMARIES OF LERS OF SELECTED INSTRUMENTATION AND CONTROL COMPONENTS AT U.S. COMMERCIAL NUCLEAR POWER PLANTS," DTD MAY 1981.

19. NUREG/CR-2158, "OPTIMUM TEST INTERVALS FOR ONLINE TESTING," DTD MAY 1981.

NUREG PUBLICATIONS DURING FY 1980 AND FY 1981 CONTINUED

20. NUREG/CR-2040, "A FEASIBILITY STUDY OF THE APPLICATION OF QUANTITATIVE RISK CRITERIA IN THE LICENSING OF NUCLEAR POWER PLANTS IN THE U.S., DTD MAY 1981.

21. NUREG/CR-2259, "FLOE: A PROGRAM FOR BAYESIAN ESTIMATION OF FLOOD PROBABILITIES," DTD JULY 1981.

22. NUREG/CR-2258, FIRE RISK ANALYSIS FOR NUCLEAR POWER PLANTS," DTD JULY 1981.

23. NUREG/CR-2269, "PROBABILISTIC MODELS FOR THE BEHAVIOR OF COMPARTMENT FIRES," DTD AUGUST 1981.

Reliability Data Analysis

R. L. Dennig
U.S. Nuclear Regulatory Commission

Ninth Water Reactor Safety Search
Information Meeting

October 30, 1981

REPORTS IN THE DATA SUMMARIES OF LICENSEE EVENT SERIES:

1. Data Summaries of Licensee Event Reports of Pumps at U.S. Commercial Nuclear Power Plants, January 1, 1972, through April 30, 1978, W. H. Sullivan, J. P. Poloski, EG&G, Idaho, Inc., NUREG/CR-1205, January 1980.

2. Data Summaries of Licensee Event Reports of Control Rods and Drive Mechanisms at U.S. Commercial Nuclear Power Plants, January 1, 1972, through April 30, 1978, W. H. Hubble, C. F. Miller, EG&G Idaho, Inc., NUREG/CR-1331, February 1980.

3. Data Summaries of Licensee Event Reports of Diesel Generators at U.S. Commercial Nuclear Power Plants, January 1, 1976, through December 31, 1978, J. P. Poloski, W. H. Sullivan, EG&G Idaho, Inc., NUREG/CR-1362, March 1980.

4. Data Summaries of Licensee Event Reports of Valves at U.S. Commercial Nuclear Power Plants, January 1, 1976, through December 31, 1978, Vol. 1 -- Main Report, Vol. 2 -- Appendices A through N, Vol. 3 -- Appendices O through Y, W. H. Hubble, C. F. Miller, EG&G Idaho, Inc., NUREG/CR-1363, Vol. 1, 2, 3, June 1980.

5. Data Summaries of Licensee Event Reports of Primary Containment Penetrations at U.S. Commercial Nuclear Power Plants, January 1, 1972, through December 31, 1978, D. W. Sams, M. Trojovsky, EG&G Idaho, Inc., NUREG/CR-1730, September 1980.

6. Data Summaries of Licensee Event Reports of Selected Instrumentation and Control Components at U.S. Commercial Nuclear Power Plants from January 1, 1976, to December 31, 1978, C. F. Miller, W. H. Hubble, D. W. Sams, W. E. Moore, EG&G Idaho Inc., NUREG/CR-2037, April 1981.

7. Data Summaries of Licensee Event Reports of Pumps at U.S. Commercial Nuclear Power Plants, January 1, 1972 through September 30, 1980, M. Trojovsky, EG&G Idaho, Inc., (Supercedes NUREG/CR-1205).

8. Data Summaries of Licensee Event Reports of Valves at U. S. Commercial Nuclear Power Plants from January 1, 1976, through September 30, 1980, (DRAFT)

COMMON CAUSE FAILURE ANALYSIS

1. Common Cause and Individual Failure and Fault Rates for Licensee Event Reports of Diesel Generators at U.S. Commercial Nuclear Power Plants (DRAFT).

2. Common Cause and Individual Failure and Fault Rates for Licensee Event Reports of Valves at U.S. Commercial Nuclear Power Plants (DRAFT).

3. Common Cause and Individual Failure and Fault Rates for Licensee Event Reports of Pumps at U.S. Commercial Nuclear Power Plants (DRAFT).

4. Common Cause and Individual Failure and Fault Rates for Licensee Event Reports of Selected Instrumentation and Control Components at U.S. Commercial Nuclear Power Plants (DRAFT).

5. User's Manual for the BFR Code (DRAFT).

OTHER DATA ANALYSIS

1. Comparison of NPRD and LER-Derived Failure Rates for Selected Valves (DRAFT).

2. Exploratory Data Analysis of NPRD Valve and Pump Data (DRAFT).

PUMPS

1972 - Third Quarter 1980

	Recurring Common Cause	Common Cause	Recurring	Command Fault	Recurring Command Fault	Random	Total
Running	0	3	15	58	13	19	108
Alternating	36	5	121	81	23	98	364
Standby	1	9	62	246	127	174	619
TOTALS	37(3.4%)	17(1.6%)	198(18%)	385(35%)	163(15%)	291(27%)	1091

PUMPS

1972 - Third Quarter 1980

Personnel Errors

Operations	Maintenance	Testing	Total
49	75	28	152

$$\frac{152}{1091} \times 100\% = 14\%$$

STANDBY PUMPS - MD- FAIL TO START

UNITS - 10^{-4}/demand

```
0*      00000000000000000000000000000000    (+20)
1       0024455779
2       167
3       2    (RO2)
4
5
6       3    (KE1)
7
8
9
1**
2
3
4
5
6
7
8
9
1***
```

	WASH-1400
Range	3×10^{-4} - 3×10^{-3}/d
Median	1×10^{-3}/d

STANDBY PUMPS - MD WITH COMMAND - FAIL TO START

UNITS - 10^{-4}/demand

0*	00000000000000000000000000	
1	0222233677	
2	03345778	
3	024456	
4	13688	
5	14488	
6	6	
7	17	
8		
9	5	(RG1)
1**	045	(BR1), (KE1), (RO2)
2	8	(DB1)
3		
4		
5		
6		
7		
8		
9		
1***		

STANDBY PUMP - TD - FAIL TO START

Units - 10^{-4}/demand

0*	00000000000000000000000000000000
1	
2	
3	
4	889
5	
6	45889
7	
8	
9	55 (DR2), (DR3)
1**	2445
2	1224899
3	38 (BV1), (DC2)
4	055
5	37
6	39 (BR1), (BR2)
7	
8	
9	
0***	
2	
3	

WASH-1400

Range 3×10^{-4} - 3×10^{-3}/d

Median 1×10^{-3}/d

STANDBY PUMPS - TD - WITH COMMAND - FAIL TO START

UNITS - 10^{-4} /demand

0*	0000000000000000000	
1		
2		
3		
4	89	(QC1), (VY1)
5		
6	9	(CC1)
7	6	
8		
9	555	
1**	223444449	
2	124899	
3	00278	
4	1337	
5	09	
6	3	
7	5	(SL1)
8	08	
9	134	
1***	3356	(AR2), (BR2), (DC2), (JF1)
2		
3		

VALVES

1976 - 1978

Recurring Common Cause	Common Cause	Recurring	Command Fault	Recurring Command Fault	Random	Total
52(2%)	122(5.3%)	384(16.6%)	460(20%)	83(3.6%)	121(52.5%)	2318

Personnel Errors

Operations	Maintenance	Testing	Total
151	72	32	255

$$\frac{255}{2318} \times 100\% = 11\%$$

MOV - Fail to Operate

UNITS - 10^{-4}/Demand

0*	0000000000000000
1	3355568
2	0000257
3	0112556677
4	000389
5	337
6	19
7	345
8	128
9	68
1**	145
2	2
3	
4	
5	6 (FP1)*
6	
7	
8	
9	
1***	

WASH-1400

Range 3×10^{-4} - 3×10^{-3}/d

Median 1×10^{-3}/d

SELECTED INSTRUMENTATION AND CONTROL COMPONENTS
1976-1978

	Recurring* Common Cause	Common Cause	Recurring	Command Fault	Recurring Command Fault	Random	Total
PWR	36	54	329	41	7	680	1147
BWR	59	126	390	82	21	661	1339
TOTALS	95(4%)	180(7%)	719(29%)	123(5%)	28(1%)	1341(54%)	2486

TOTAL CRITICAL HOURS	
PWR	957,840
BWR	597,240
Total	1,555,080

* Failures only

SELECTED INSTRUMENTATION AND CONTROL COMPONENTS

1976-1978

	Personnel Errors			
	Operations	Maintenance	Testing	Total
PWR	18	34	13	65
BWR	22	111	12	145
TOTALS	40	145	25	210

$$\frac{210}{2486} \times 100\% = 8.4\%$$

I&C LIQUID LEVEL - REDUCED CAPABILITY

Units - 10^{-7}/hour

```
0*      00000000000000000000000000000
1
2       455        (FC2), (HN1), (IP2)
3       27
4       888
5       1
6       3348
7       11
8
9       55
1**     034489
2       559
3       0    (ZI2)
4       3    (BR3)
5
6
7
8
9
1***
2
3
4
```

WASH-1400

Range 3×10^{-6} - 3×10^{-4}/hr

Median 3×10^{-5}/hr

I&C - PRESSURE/VAC - REDUCED CAPABILITY

UNITS - 10^{-7}/hour

0*	00000000000000000000000000
1	699
2	4447
3	22
4	038
5	44
6	033333
7	
8	
9	55555
1**	135669
2	57999
3	2 (MI1)
4	8 (BR2)
5	1 (NA1)
6	
7	
8	
9	
1***	

WASH-1400

Range 3×10^{-6} - 3×10^{-4}/hr

Median 3×10^{-5}/hr

LA-UR - 81-3025

TITLE: STRATEGIES FOR MANAGING POTENTIALLY SEVERE ACCIDENTS IN PWRs

AUTHOR(S): N. S. DeMuth
D. Dobranich
R. J. Henninger

SUBMITTED TO: Ninth Water Reactor Safety
Research Information Meeting
Nuclear Regulatory Commission
October 26-30, 1981

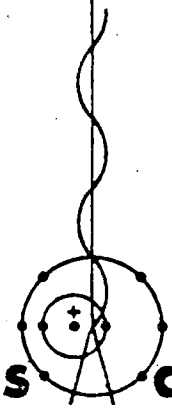

Form No. 836 R2
St. No. 2629
1/78

DEPARTMENT OF ENERGY
CONTRACT W-7405-ENG. 36

STRATEGIES FOR MANAGING POTENTIALLY SEVERE ACCIDENTS IN PWRs

Nelson S. DeMuth

In the aftermath of the Three Mile Island accident, investigators pointed out the need for simulating a wide range of postulated transient or accident conditions including equipment failures and operator actions, for adding and upgrading instrumentation to monitor plant conditions during accidents, and for improving emergency procedures and training to assure proper operator response to various accident conditions. The Nuclear Regulatory Commission (NRC), as part of its response to these needs, initiated the Severe Accident Sequence Analysis (SASA) program to further our understanding both of reactor accident phenomena and of the human-machine interface during a spectrum of accidents. Efforts at Los Alamos for the SASA program have focused on (1) identification of potential accidents involving multiple equipment failures, (2) computer simulations of postulated accident sequences including equipment malfunctions and operator actions, and (3) evaluation of critical safety equipment and operator responses.[1]

Investigations at Los Alamos have used the Transient Reactor Analysis Code (TRAC)[2] to simulate automatic safety equipment and operator response during loss-of-feedwater (LOFW) and steam-generator-tube-rupture (SGTR) transients at a 4-loop Westinghouse nuclear power reactor. Studies of severe LOFW transients were prompted by NRC concerns about the capabilities of primary safety systems to remove decay heat in the absence of secondary cooling and about the operator actions necessary to implement this kind of long-term cooling. Transients involving tube ruptures in the steam generators, as well as other types of interfacing-system loss-of-coolant accidents (LOCAs) differ from LOCAs into containment in (1) the instrumentation response, (2) the automatic actuation of safety features, (3) the potential for radiological releases outside of containment, and (4) the need for operator actions to mitigate their consequences.

A computer model was developed for simulating the response of the plant to LOFW and SGTR transients. This model included detailed representations of the pressurizer relief and safety valves, the atmospheric relief valves on the steam lines, the safety injection and charging pump flows, the pressurizer relief tank and rupture disk, the containment with fan coolers and sprays, and primary-to-secondary flow through broken tubes in the steam generator.[3] Automatic and operator-initiated responses were simulated using the trip logic in TRAC.

The initiator for the feedwater transients was loss of main feedwater and reactor coolant pump trip caused by temporary loss of offsite power. Subsequent automatic actions included reactor scram and closure of main steam isolation valves. Failure of the auxiliary feedwater system coupled with the inability of the operators to restore any cooling to the steam generator secondaries was assumed to produce this severe accident. A number of sequences were analyzed to determine the effect of critical equipment malfunctions and to evaluate possible operator strategies for controlling the accident.

In the initial sequence, the automatic response of engineered safety features was evaluated assuming no operator intervention. This sequence produced dryout of the steam generators after about 1 h, followed by heatup and pressurization of the primary to the setpoint of the power-operated relief valves (PORVs). Opening of these valves maintained the primary pressure near the setpoints as primary coolant was discharged to the pressurizer relief tank. Rising pressure in the relief tank caused rupture disks to open, venting discharge from the primary into the containment. Actuation of emergency core cooling on a containment overpressure signal eventually provided sufficient flow to cool the core with once-through flow provided by the high-head charging pumps. Failure of the high-head charging system to deliver coolant at the PORV setpoint could lead to core damage unless the operator takes action to depressurize the primary.[4]

In another sequence, symptom-oriented emergency procedure guidelines were simulated. These procedures involved operator action to open both PORVs and initiate emergency core cooling. The primary depressurization resulting from opening both PORVs enhanced the high-pressure injection flows and maintained core cooling in a once-through mode until the refueling water storage tank was depleted. The discharge of primary coolant into the containment building caused the fan coolers to begin operating in the emergency mode. Heat removal from three fan coolers was found to be adequate to prevent actuation of containment sprays.

The initiator for rupture of U-tubes in one of the steam generators was assumed to be a break in the main steam line upstream of the isolation valve. The rapid depressurization of the secondary induced rupture of a number of U-tubes, generated a reactor scram signal on excess steam flow, and produced a rapid drop in the primary pressure. Emergency core cooling was automatically initiated on low primary pressure and equilibrated with the leakage flow to prevent core uncovery for double-ended ruptures of five tubes or less. Hot primary liquid flowing out the broken tubes was replaced with cold liquid from the safety injection system, so the core was cooled throughout the transient. For rupture of more than five tubes, the primary pressure dropped to the setpoint for accumulator injection. Isolation of the affected steam generator requires operator action to cool and depressurize the primary further, while removing decay heat through the unaffected steam generators.

REFERENCES

1. R. D. Burns III, "Loss of Feedwater Transients in PWRs", Eighth Water Reactor Safety Information Meeting, USNRC (October 1980).

2. Safety Code Development Group, "TRAC-PD2, An Advanced Best-Estimate Computer Program for Pressurized Water Reactor Loss-of-Coolant Accident Analysis" Los Alamos National Laboratory report LA-8709-MS (May 1981).

3. D. Dobranich, N. S. DeMuth, R. J. Henninger, and R. D. Burns III, "Special Small-break Applications with TRAC", ANS Specialists Conf. on Small Breaks in LWRs, Monterey, CA (August 1981).

4. N. S. DeMuth, D. Dobranich and R. J. Henninger, "Loss of Feedwater Transients for the Zion-1 Pressurized Water Reactor", Los Alamos National Laboratory Report (in preparation).

REACTOR SAFETY ANALYSIS GROUP
ENERGY DIVISION
LOS ALAMOS NATIONAL LABORATORY

STRATEGIES FOR MANAGING POTENTIALLY SEVERE ACCIDENTS IN PWRs

NINTH WATER REACTOR SAFETY
RESEARCH INFORMATION MEETING
NUCLEAR REGULATORY COMMISSION
WASHINGTON, D.C.

OCTOBER 30, 1981

A VARIETY OF MULTIPLE-FAULT ACCIDENT SCENARIOS WERE ANALYZED

TRAC CALCULATIONS FOR SASA-

1. LOSS OF FEEDWATER (LOFW)
2. STEAM GENERATOR TUBE RUPTURE (SGTR)
3. MAIN STEAM LINE BREAK (MSLB)
4. PRESSURIZER VALVE LOCA (PV-LOCA)
5. ANTICIPATED TRANSIENTS WITHOUT SCRAM (ATWS)

LOS ALAMOS

TRAC SIMULATIONS OF LOFW TRANSIENTS AT ZION

LOFW ANALYSES

1. NOMINAL SCENARIO (NO OPERATOR ACTION)
2. ESF ACTUATION ON CONTAINMENT OVERPRESSURE
3. SYMPTOM-ORIENTED EMERGENCY PROCEDURES
4. "BLEED AND FEED" STRATEGIES

LOS ALAMOS

SPECIFIC COMPONENT MODELS

(1) POWER OPERATED RELIEF VALVES
(2) STATIC CHECK SAFETY VALVES
(3) PRESSURE RELIEF TANK (RUPTURE DISKS)
(4) CONTAINMENT (FAN COOLERS AND SPRAYS)
(5) REACTIVITY FEEDBACK (TEMP., α, BORON)
(6) STEAM GENERATOR TUBE RUPTURE

Los Alamos

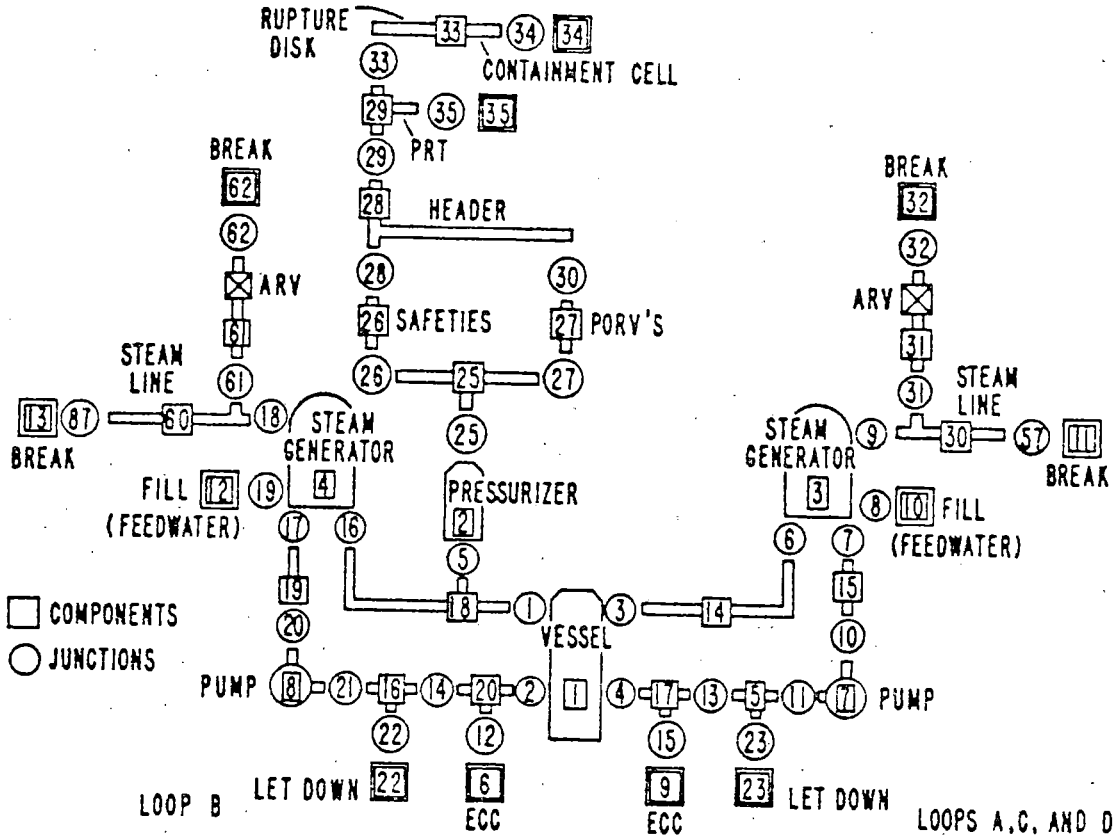

ZION-I PWR TRAC SYSTEM SCHEMATIC

NOMINAL SEQUENCE IS TOTAL LOFW INITIATED BY LOSS OF OFFSITE POWER

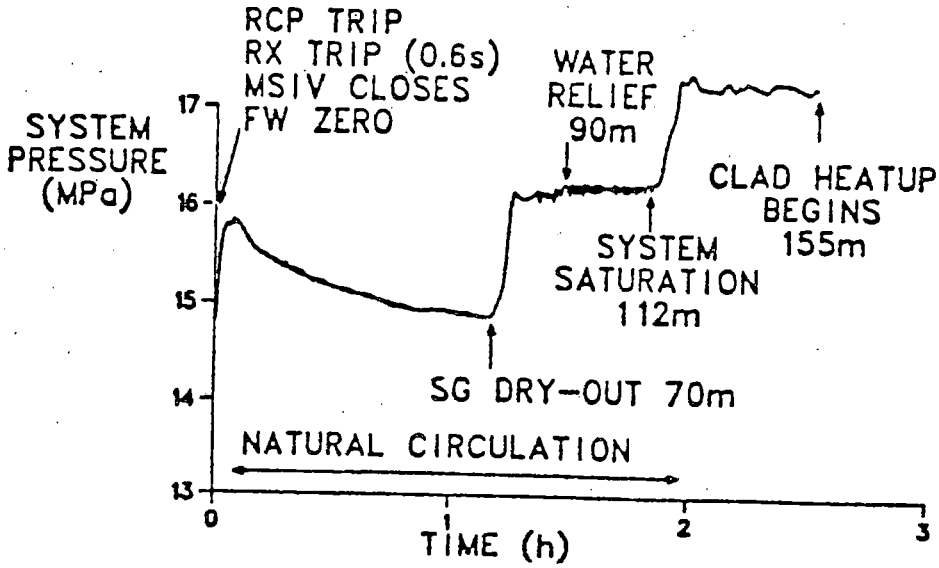

PRIMARY OVERPRESSURE PROTECTION SYSTEM

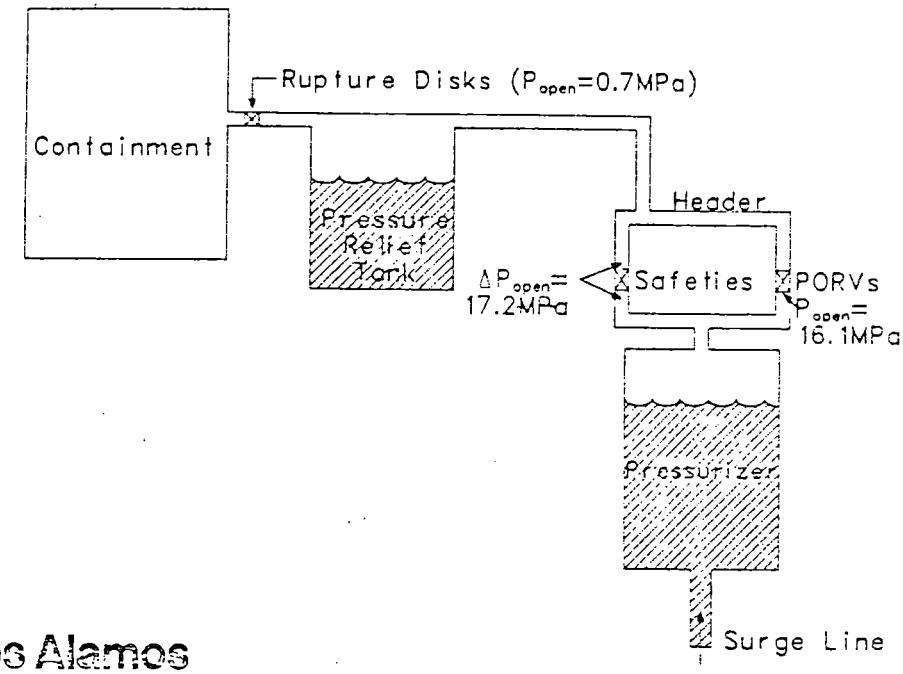

Los Alamos

SAFETY SYSTEMS FUNCTION
TO PREVENT CORE DAMAGE

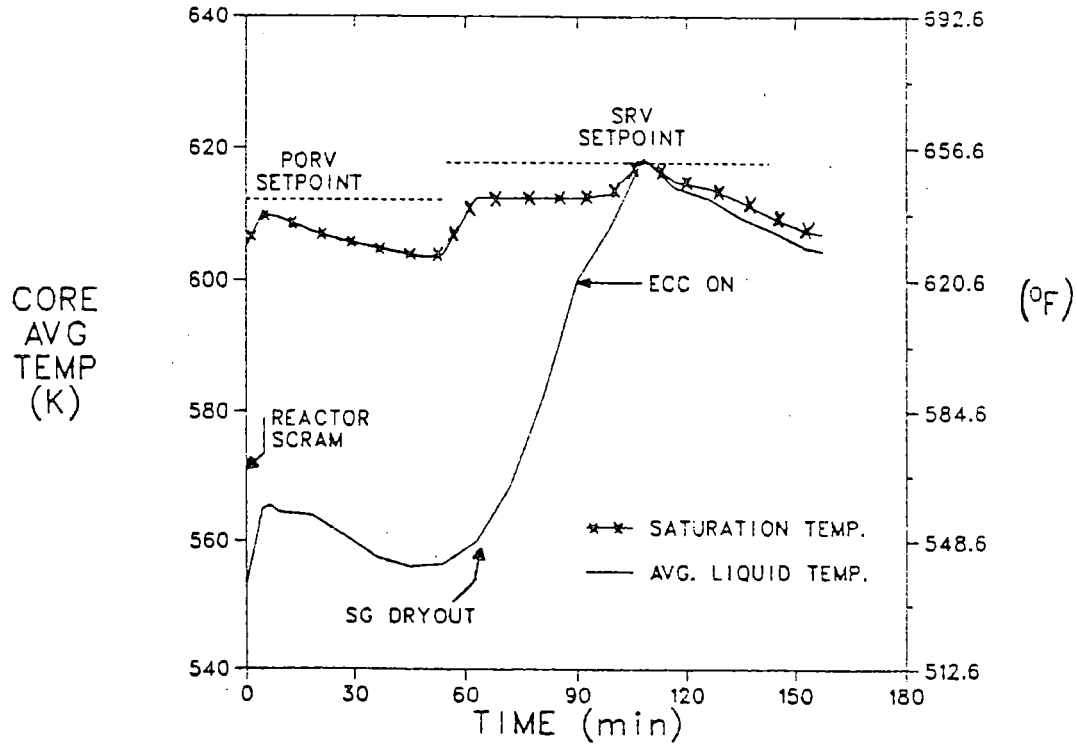

FAN COOLERS PREVENT CONTAINMENT
OVERPRESSURIZATION DURING LOFW TRANSIENT

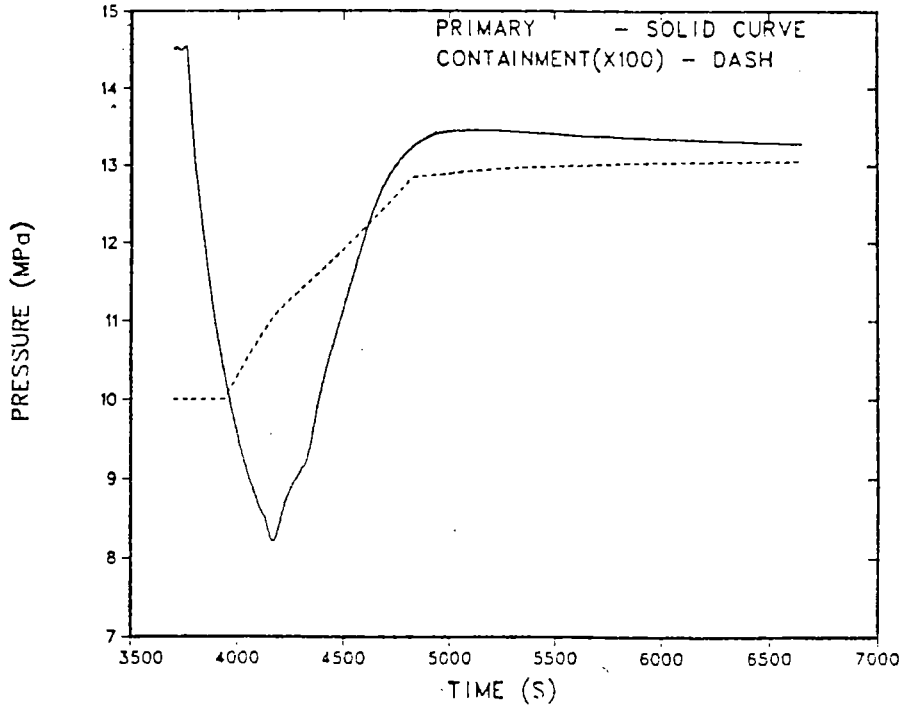

BLEED–AND–FEED DEMONSTRATED AS
VIABLE RECOVERY MODE

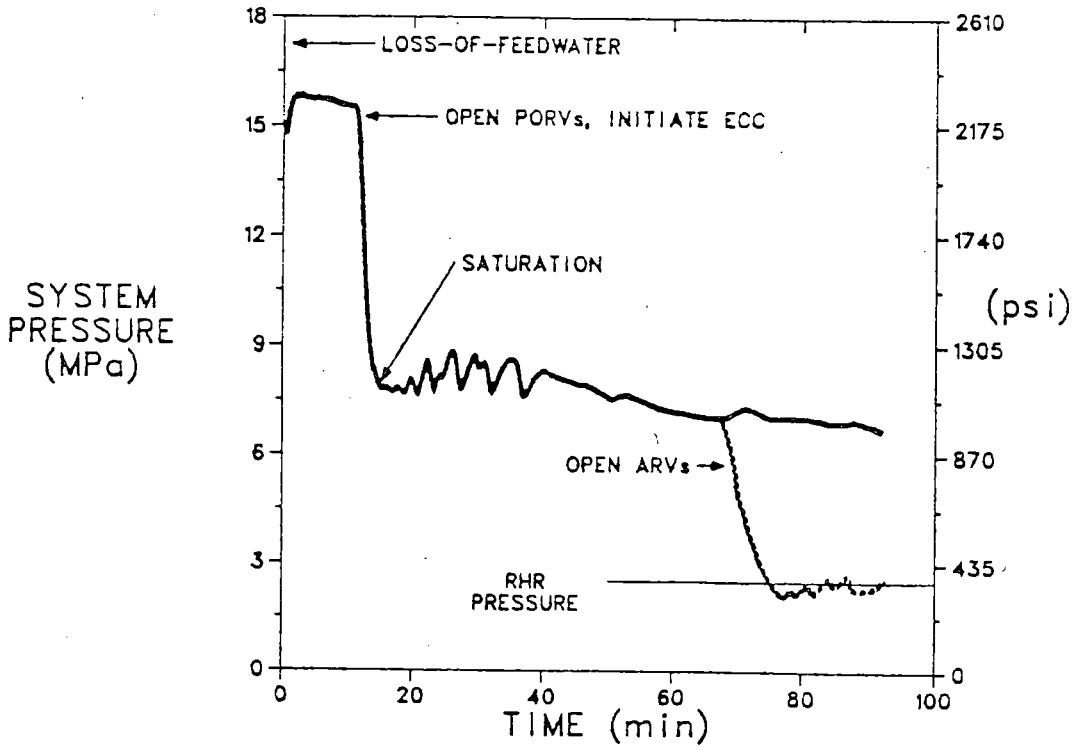

RESULTS FOR SEVERE FEEDWATER TRANSIENTS

1. NOMINAL SCENARIO
   (a) ABOUT 1 h FOR AFW RECOVERY BEFORE SG DRYOUT
   (b) PRIMARY SATURATION REACHED ABOUT 2 h
   (c) ABOUT 2.5 h FOR ECCS INITIATION BEFORE CLAD HEATUP

2. ECCS ACTUATED BY CONTAINMENT OVERPRESSURE
   (a) SRVs OPEN BRIEFLY TO RELIEVE SATURATED EXPANSION
   (b) CORE REMAINS COVERED; PRIMARY INVENTORY GRADUALLY BEING DEPLETED
   (c) DECAY HEAT REMOVAL AFTER 4 h BY ONCE-THROUGH ECCS FLOW

LOS ALAMOS

RESULTS FOR SEVERE FEEDWATER TRANSIENTS (cont.)

3. SYMPTOM ORIENTED EMERGENCY PROCEDURES
   (a) OPERATOR ACTIONS ENHANCE CORE COOLING
   (b) THREE FAN COOLERS PREVENT SPRAY INITIATION
   (c) RWST DEPLETED IN ABOUT 11 h
   (d) RWST DEPLETED IN ABOUT 4 h WITH SPRAYS

4. OPERATOR STRATEGIES FOR MITIGATION
   (a) EARLY OPERATOR ACTIONS PERMIT DEPRESSURIZATION TO RHR PRESSURE SETPOINT
   (b) DECAY HEAT REMOVAL BY ONCE-THROUGH HPI FLOW
   (c) DECAY HEAT GENERATION GREATER THAN RHR CAPACITY

LOS ALAMOS

STEAM GENERATOR TUBE RUPTURE ANALYSES

– NOMINAL SCENARIO –

INITIATOR : SECONDARY DEPRESSURIZATION CAUSED BY MAIN STEAM LINE BREAK

PARAMETER : NUMBER OF BROKEN TUBES (1, 5 AND 10)

SAFETY SYSTEMS : EMERGENCY CORE COOLING INITIATED BY LOW PRIMARY PRESSURE

LOS ALAMOS

STEAM GENERATOR TUBE RUPTURE MODEL

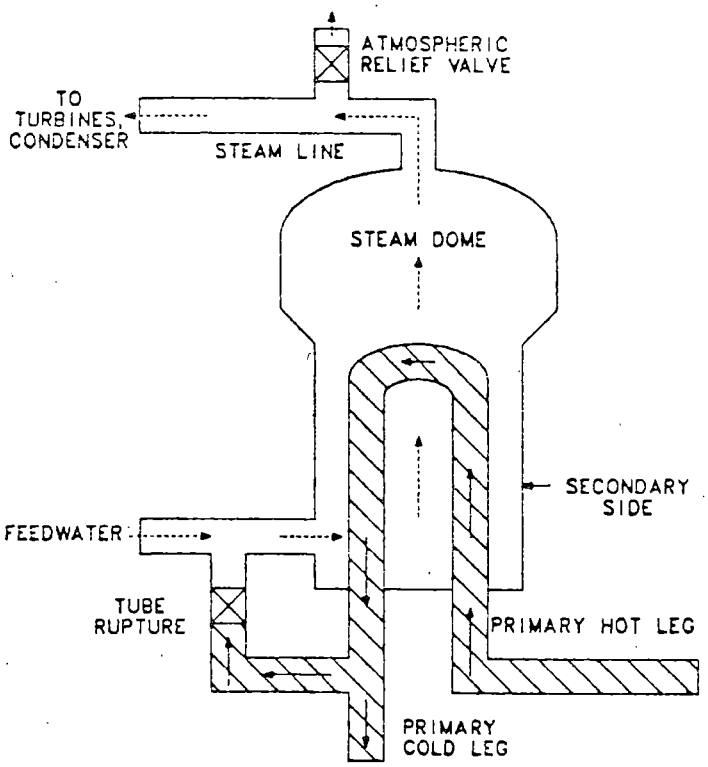

SYSTEM PRESSURE INDICATES PLANT RESPONSE

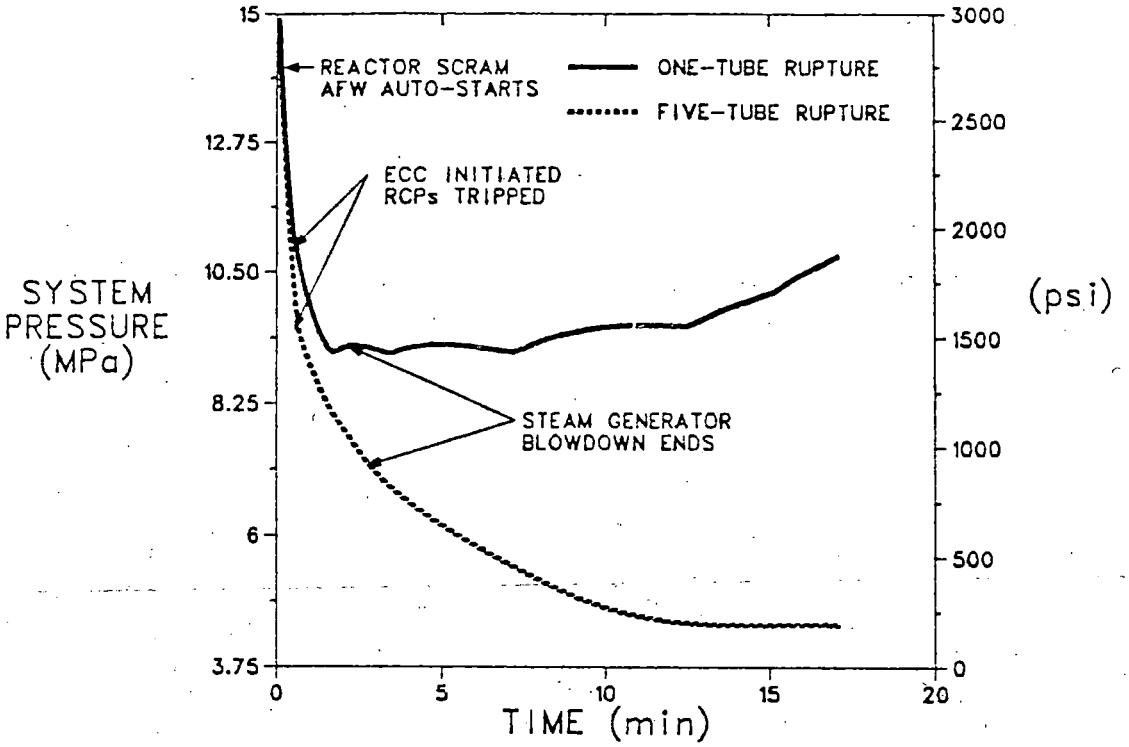

RESULTS FOR TUBE RUPTURE TRANSIENTS

ECCS FLOW EQUILIBRATES WITH LEAKAGE FLOW AND PREVENTS CORE UNCOVERY

PRIMARY PRESSURE DROPS BELOW ACCUMULATOR SETPOINT FOR MORE THAN FIVE RUPTURED TUBES

LOS ALAMOS

BWR STATION BLACKOUT STUDIES ACCIDENT SEQUENCE ANALYSIS*

S. A. Hodge

Oak Ridge National Laboratory
Oak Ridge, Tennessee 37830

presented at

NINTH WATER REACTOR SAFETY RESEARCH
Information Meeting
Gaithersburg, Maryland
October 30, 1981

*Research sponsored by the Office of Nuclear Regulatory Research, Nuclear Regulatory Commission under Interagency Agreement 40-551-75 with the U.S. Department of Energy under contract W-7405-eng-26 with the Union Carbide Corporation.

BWR STATION BLACKOUT STUDIES
ACCIDENT SEQUENCE ANALYSIS

S. A. Hodge

Oak Ridge National Laboratory

This paper is a summary of a report[1] describing the predicted response of Unit 1 at the Tennessee Valley Authority (TVA) Browns Ferry Nuclear Plant to a hypothetical Station Blackout. This accident would be initiated by a loss of offsite power concurrent with a failure of all onsite diesel-generators to start and load; the only remaining electrical power at this three-unit plant would be that derived from the station batteries. It is assumed that the Station Blackout occurs at a time when each of the Browns Ferry units is operating at 100% power so that there is no opportunity for use of the batteries for units 2 or 3 in support of unit 1.

The 250 volt DC battery system at Browns Ferry was not designed for the case of a prolonged Station Blackout. In response to AEC inquiry in 1971, during the period of plant construction, TVA estimated that the steam-driven High Pressure Coolant Injection (HPCI) and Reactor Core Isolation Cooling (RCIC) systems, which use DC power for turbine control and valve operation, could remain operational for a period of four to six hours. A period of four hours was assumed for this study.*

The initial phase of a Station Blackout extends from the time of reactor vessel isolation following scram until battery exhaustion. During this period the operator would maintain reactor vessel water level in the normal operating range by intermittent operation of the RCIC system, with the HPCI system available as a backup. Each of these systems is normally aligned to pump water from the condensate storage tank into the reactor vessel via a feedwater line. The operator would also control reactor vessel pressure by means of remote-manual operation of the primary relief valves; sufficient stored control air would remain available to permit the desired valve operations for well over four hours. The Control Room instrumentation necessary to monitor reactor vessel level and pressure and for operation of the RCIC and HPCI systems would also remain available during this period.

The plant response during the initial phase of a Station Blackout can be summarized as an open cycle. Water would be pumped from the condensate storage tank into the reactor vessel by the RCIC system as necessary to maintain level in the normal operating range. The injected water would be heated by the reactor decay heat and subsequently passed to the pressure suppression pool as steam when the operator remote-manually opens the relief valves as necessary to maintain the desired reactor vessel pressure.

---

* In reviewing the results of this study, TVA performed a battery capacity calculation showing that the unit batteries could last as long as seven hours under blackout conditions. Events subsequent to battery failure are relatively insensitive to the time at which failure occurs because of the slow variance of the decay heat several hours after shutdown.

The initial phase of a Station Blackout has been analyzed by use of a relatively simple computer code developed specifically for this purpose. This coding uses the Continuous Systems Modeling Program (CSMP) language of the IBM computer system to simulate the plant response to postulated operator actions. The analysis shows, because of the loss of the drywell coolers, that it is necessary for the operator to begin to reduce the reactor vessel pressure to about 0.791 MPa (100 psig) within one hour of the inception of the Station Blackout. This depressurization reduces the temperature of the saturated fluid within the reactor vessel and thereby decreases the driving potential for heat transfer into the drywell, yet keeps the vessel pressure high enough for continued operation of the RCIC system steam turbine. With this action, the drywell average ambient temperature can be kept below 149°C (300°F) throughout the initial phase of a Station Blackout; tests have shown that both the drywell structure and the equipment located therein can be expected to survive temperatures of this magnitude.

The analysis also reveals an important second reason for operator action to depressurize the reactor vessel early in the initial phase of a Station Blackout. This depressurization removes a great deal of steam and the associated stored energy from the reactor vessel at a time when the RCIC system is available to inject replacement water and thereby maintain the vessel level. Subsequently, when water injection capability is lost, remote-manual relief valve operation would be terminated and there would be no further water loss from the reactor vessel until the pressure has been restored to the setpoint (7.72 MPa (1105 psig)) for automatic relief valve actuation. Because of the large amount of water to be reheated and the reduced level of decay heat, this repressurization would require a significant period of time. In addition, the subsequent boiloff would begin from a very high vessel level because of the increase in the specific volume of the water as it is heated and repressurized. Thus, an early depressurization will provide valuable additional time for preparative and possible corrective action before core uncovery after injection capability is lost.

The MARCH code was used for the analysis of the second phase of the blackout, i.e., the period following inception of boiloff of the reactor vessel water inventory due to loss of injection capability. The MARCH results predict core melting to begin about one hour after the top of the core is uncovered. The model provides that the melted core slumps down to the bottom of the reactor vessel resulting in a predicted failure of the vessel bottom head at about two hours after core uncovery. The corium leaves the vessel, and breaching of the primary containment because of failure of the electrical penetration assembly (EPA) seals by overtemperature is predicted to occur about one and one-third hours later.

An estimate of the magnitude and timing of the noble gas and iodine fission products to the environment is provided in a follow-on report.[2] The thermo-hydraulic parameters needed for the fission product transport analysis were taken from the MARCH results for the blackout sequence.

References

1. D. H. Cook, et al, "Station Blackout at Browns Ferry Unit One - Accident Sequence Analysis," NUREG/CR-2182, ORNL/TM-455/V1.

2. W. J. Armento, et al, "Station Blackout at Browns Ferry Unit One - Fission Product Transport Analysis," NUREG/CR-2182, ORNL/TM-455/V2.

UNION CARBIDE ORNL

BWR STATION BLACKOUT STUDIES – ACCIDENT SEQUENCE ANALYSIS

S. A. HODGE
SASA PROGRAM MANAGER
OAK RIDGE NATIONAL LABORATORY

PRESENTED AT
NINTH WATER REACTOR SAFETY RESEARCH INFORMATION MEETING
NATIONAL BUREAU OF STANDARDS
GAITHERSBURG, MARYLAND
30 OCTOBER 1981

UNION CARBIDE ORNL

THE OBJECTIVE OF THE ORNL BLACKOUT STUDIES IS A "BEST ESTIMATE" ANALYSIS OF A STATION BLACKOUT AT A TYPICAL BWR

- TIME-DEPENDENT PROGRESSION OF EVENTS CONSIDERING:
  - PHYSICAL PLANT AT BROWNS FERRY UNIT 1
  - NO ADDITIONAL INDEPENDENT EQUIPMENT FAILURES BEYOND THE LOSS OF OFFSITE AND ONSITE ac POWER
  - EXISTING INSTRUMENTATION TO DISPLAY PLANT STATUS
  - PROBABLE OPERATOR ACTIONS GIVEN EXISTING EOIs AND STATE OF TRAINING
- ESTIMATE MAGNITUDE AND TIMING OF FISSION PRODUCT TRANSPORT

UNION CARBIDE ORNL

STATION BLACKOUT AT BROWNS FERRY HAS NOT BEEN PREVIOUSLY STUDIED

- BROWNS FERRY OPERATING PROCEDURES DO **NOT** CONSIDER STATION BLACKOUT
- OPERATOR TRAINING DOES NOT INCLUDE STATION BLACKOUT SCENARIOS

"THE TOTAL LOSS OF ac POWER COULD ONLY RESULT FROM MULTIPLE FAILURE WITHIN THE OFFSITE POWER SYSTEM AND THE STANDBY ac POWER SYSTEM. THIS EVENT IS CONSIDERED HIGHLY IMPROBABLE AND IS NOT A DESIGN REQUIREMENT FOR BROWNS FERRY"

— RESPONSE TO AEC QUESTION 14.2 OF MARCH 25, 1971

UNION CARBIDE ORNL

THE STATION BLACKOUT ACCIDENT SEQUENCE ANALYSIS EMPLOYED THE "BEST-ESTIMATE" APPROACH FOR

- THE INITIATING LOSS OF OFFSITE POWER AND FAILURE OF ALL ONSITE DIESEL GENERATORS TO START AND LOAD
- THE PERIOD BEFORE CORE UNCOVERY
  - ORNL-DEVELOPED PLANT RESPONSE CODE AND THE TVA SIMULATOR
- THE PERIOD AFTER CORE UNCOVERY
  - THE MARCH CODE
- REALISTIC VALUES FOR COMPUTER CODE INPUT

UNION CARBIDE
ORNL

RESULTS: THE REACTOR CORE ISOLATION COOLING (RCIC) SYSTEM PROVIDES ADEQUATE LEVEL CONTROL IN AN OPEN CYCLE

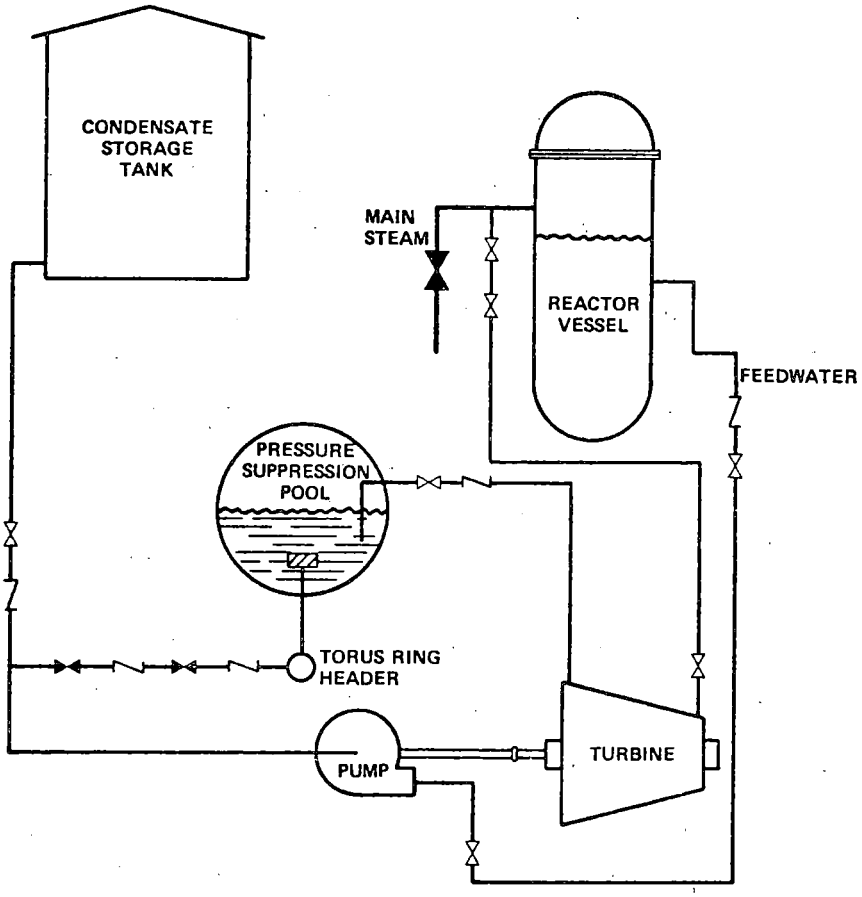

UNION CARBIDE
ORNL

RESULTS: THE INSTALLED BATTERY SYSTEM WOULD PERMIT REACTOR VESSEL PRESSURE AND LEVEL CONTROL FOR OVER SIX HOURS

- INSTRUMENTATION AND CONTROL SYSTEMS ADEQUATE
- REACTOR VESSEL LEVEL MAINTAINED IN THE NORMAL OPERATING RANGE
- REACTOR VESSEL SHOULD BE DEPRESSURIZED TO ~ 100 psig WITHIN ONE HOUR
  - LOW ENOUGH TO AVOID EXCESSIVE DRYWELL TEMPERATURES
  - HIGH ENOUGH TO PERMIT CONTINUED OPERATION OF TURBINE-DRIVEN INJECTION SYSTEM

UNION CARBIDE
ORNL

DEPRESSURIZATION ALSO PROVIDES ADDITIONAL TIME FOLLOWING BATTERY EXHAUSTION BEFORE CORE UNCOVERY

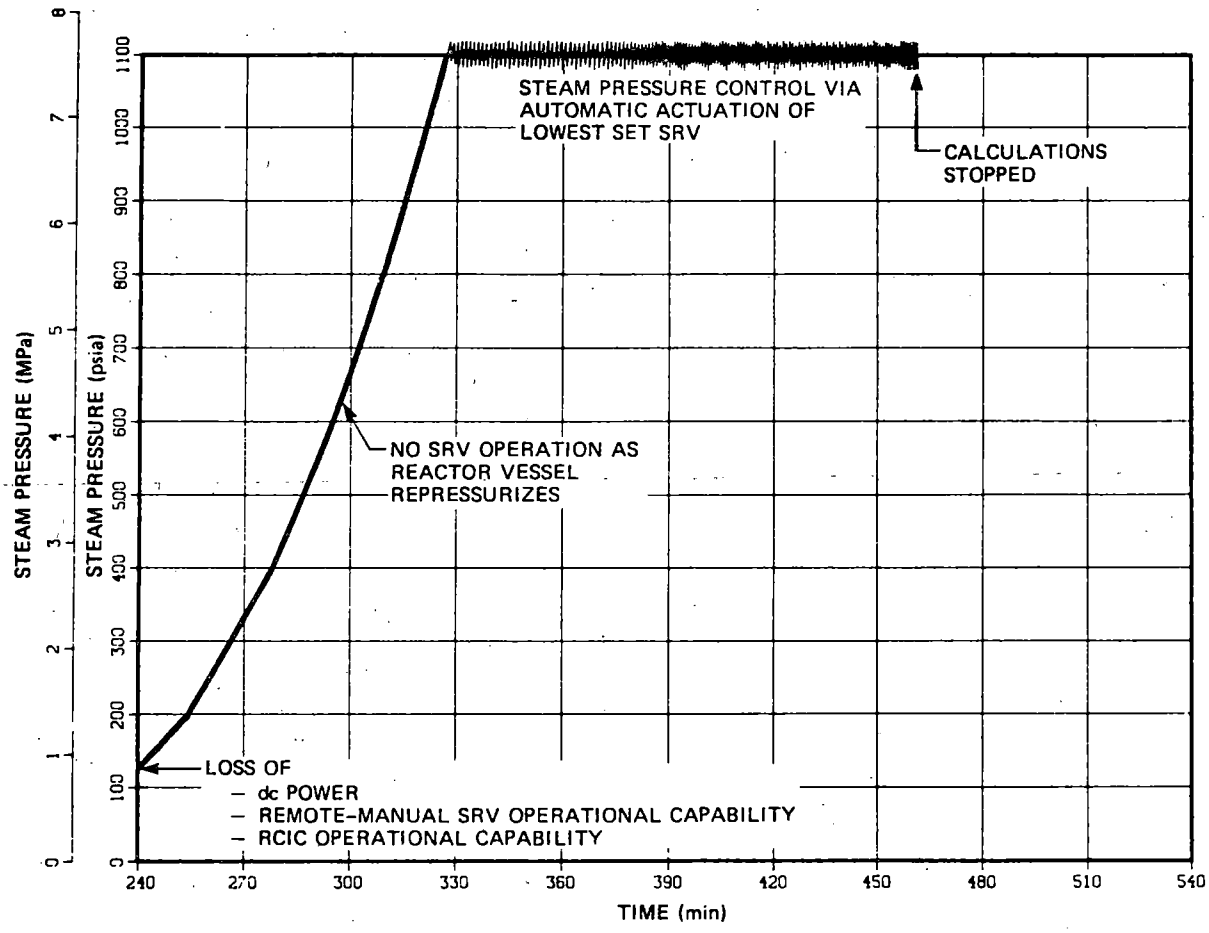

UNION CARBIDE
ORNL

ONCE THE VESSEL IS REPRESSURIZED, THE BOILOFF BEGINS FROM A VERY HIGH LEVEL

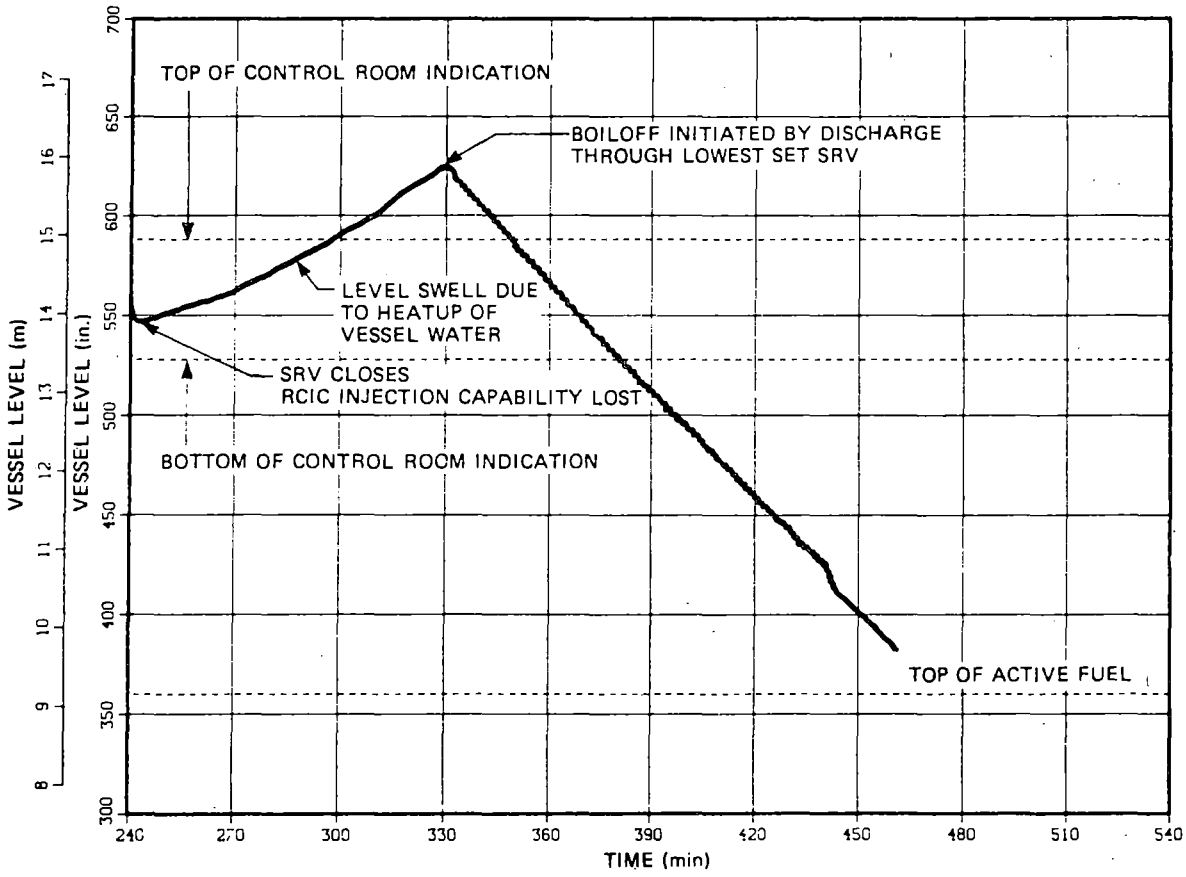

UNION CARBIDE ORNL

THE MARCH CODE WAS USED TO STUDY THE SEQUENCE OF EVENTS FOLLOWING CORE UNCOVERY AND TO PROVIDE NEEDED PARAMETERS FOR THE FISSION PRODUCT TRANSPORT ANALYSIS

EVENT	TIME AFTER TOP OF CORE UNCOVERED
FIRST FUEL RODS FAIL (1300°C)	43 min
FIRST FUEL RODS MELT (2280°C)	1 h
CENTRAL CORE COLLAPSES INTO LOWER PLENUM	1 h 17 min
VESSEL LOWER HEAD FAILS AND CORE DROPS TO DRYWELL FLOOR	1 h 52 min

---

UNION CARBIDE ORNL

CONTAINMENT WAS ASSUMED TO FAIL BY TEMPERATURE-INDUCED DEGRADATION OF ELECTRICAL PENETRATION ASSEMBLY (EPA) SEALS

- EPA SEALS HAVE SHORT-TERM RATING OF 163°C (325°F) AND LONG-TERM RATING OF 138°C (281°F)
- SEALS ASSUMED TO FAIL AT 260°C (500°F)
- FAILURE AREA 1.95 m^2 (21 ft^2)
- FLOW IS THROUGH EPAs INTO REACTOR BUILDING
- FAILURE OCCURS AT 1 hr 17 min AFTER CORIUM LEAVES VESSEL

UNION CARBIDE
ORNL

THE CONTAINMENT PRESSURE AT EPA SEAL FAILURE IS 0.9 MPa (130 psia)

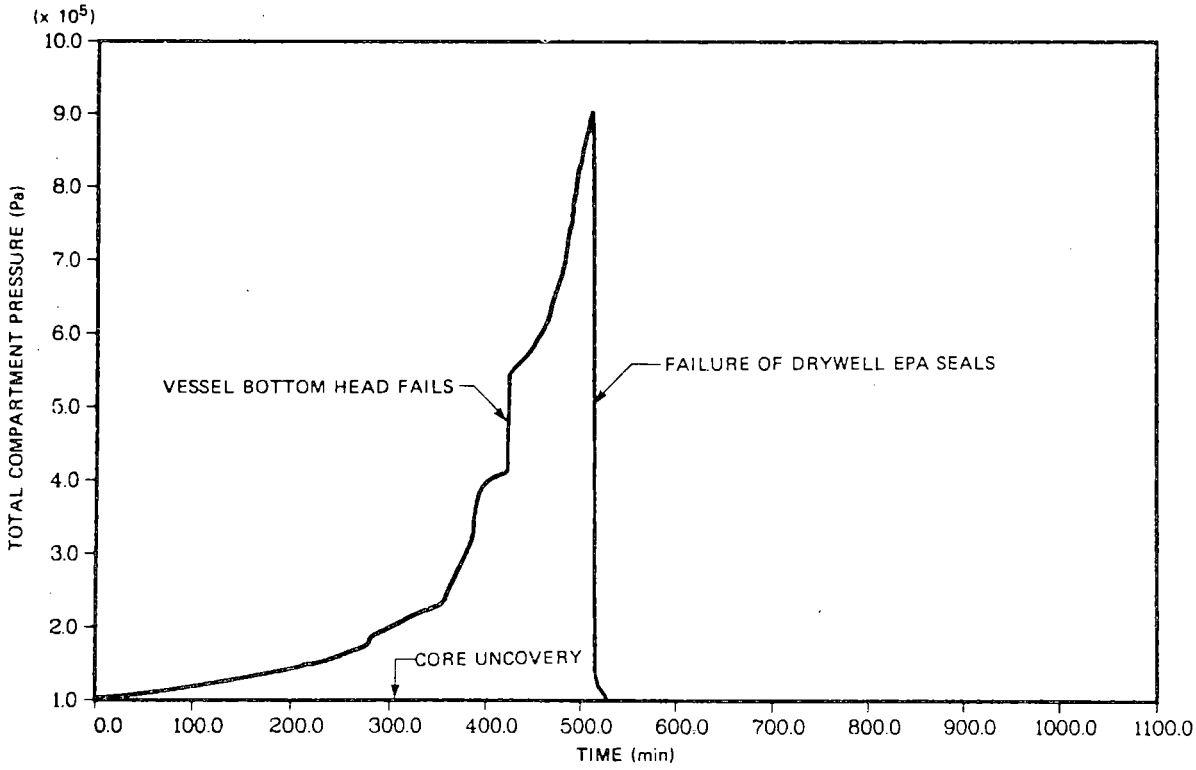

"STATION BLACKOUT AT BROWNS FERRY UNIT 1"

Part 2

ANALYSIS OF FISSION PRODUCT TRANSPORT *

R. P. Wichner
A. D. Mitchell
R. A. Lorenz
W. J. Armento
C. W. Weber

For presentation at the 9th Water Reactor Safety Meeting
Washington, DC, October 26–30, 1981

* Research sponsored in part by the Office of Nuclear Regulatory Research, U.S. Nuclear Regulatory Commission under Interagency Agreements 40-511-75 and 40-552-75 with the U.S. Department of Energy under contract W-7405-eng-26 with the Union Carbide Corporation.

"STATION BLACKOUT AT BROWNS FERRY UNIT 1"

Part 2

ANALYSIS OF FISSION PRODUCT TRANSPORT

R. P. Wichner
A. D. Mitchell
R. A. Lorenz
W. J. Armento
C. W. Weber

This report deals with the analysis of noble gas and iodine transport within a specific reactor (Browns Ferry Unit 1) and for a specified accident sequence. The postulated accident is a serious one, beginning with a loss of ac power and a failure to initiate the onsite source of emergency ac. This completely powerless state (after battery run-down), leads to core uncovery (60 m), cladding failure (103 m), fuel melt (120 m), core slump (137 m), pressure vessel failure (172 m), and drywell vent (238 m). The listed times are estimated using MARCH and measured from time of battery run-down.

The principal fission product pathways for this accident sequence are illustrated in three of the accompanying figures for the situations (1) prior to pressure vessel failure, (2) following pressure vessel failure but prior to drywell failure, and (3) following drywell failure.

For the first case, convection by steam and hydrogen carries the fission products through the steam separators and driers into the upper main steam lines and down through the open S/RV and tailpipe into the suppression pool. Pressure in the wetwell becomes sufficient to open the vacuum relief check valves on the vent headers well before any fuel failure occurs. The open vacuum reliefs allow flow from the suppression pool atmosphere back into the drywell causing the drywell temperature and pressure to rise. Projected leakage rates from the drywell to the reactor building in this initial phase have been estimated based on integrated leak rate tests performed on the Unit 1 drywell during 1980. The wetwell leaks into the lower reactor building via the wetwell vacuum breakers, while the drywell leaks into the higher levels of the reactor building. The pathway is altered following pressure vessel failure, as shown in the next figure. Here the S/RV's are closed, but the increased drywell pressure caused by the presence of the core in the drywell drives vapor flow from the drywell into the suppression pool via vent headers and the downcomers. We should note that the reactor pedestal and the biological shield form only a minor flow obstruction since there are large openings in these structures.

The electrical seals are projected to begin venting when the drywell temperature reaches 204°C and to fail completely at 260°C. Following this event, a large gas flow from the drywell to the reactor building occurs.

The situation in the reactor building is illustrated in the next figure. As noted, the failure of the electrical penetration assembly seals allows flow into the lower portion of the reactor building. (Flow into the wetwell cavity would be nil following electrical seal failure.) Since the reactor building floors contain large open areas, there is little to impede vertical flow in the reactor building and into the refueling bay situated above the building. As noted, the refueling bay contains 18 blowout panels acuated by 50 lb/ft^2 interior room pressure.

Determination of the degree of fission product transport consisted of the following steps:

1. Specification of the accident sequence and the behavior of the core, pressure vessel, wetwell, drywell, and reactor building. Key parameters such as fuel temperature, coolant temperature, surface temperature of various structures, water level in the core, steam and hydrogen partial pressures, total pressure, and volumetric flowrates are computed by the MARCH program.

2. Specification of reactor geometry. The core, pressure vessel, wetwell, drywell and reactor building were subdivided to represent an approximation of the actual geometry.

3. Calculation of nuclide inventories. Inventories of all key noble gas and iodine nuclides plus their significant precursors were estimated using the ORIGEN program employing as input core operational and loading data obtained from TVA and the FSAR.

4. Release rates from fuel were estimated by models based on an experimental value of a temperature dependent release rate coefficient.

5. Iodine chemical species alterations were followed under the influence of changing environmental conditions along the pathway.

6. Convective transport was assumed between communicating control volumes at a rate specified by flows acquired from the MARCH program. Complete mixing was assumed in each control volume.

7. Deposition and revaporization rates of iodine species on various surfaces were estimated.

8. Estimates of aerosol formation rates from overheated fuel and structure and from the interaction of molten core and concrete materials were estimated. Aerosol behavior under the complex primary system conditions was examined parametrically. Aerosol behavior in the containment vessel for the core concrete reaction was modeled using HAARM-3 which is incorporated as a subroutine.

9. The decontamination affected by the suppression pool was modeled by methods based on published values.

Some preliminary results for iodine are presented in the last three figures. About 11% of the iodine in this accident sequence is projected to ramain in unfailed fuel elements located around the periphery of the core. Afterheat estimates for these zones are estimated to be insufficient to fail the cladding. The degree to which iodine remains within the upper pressure zone after PV failure depends in large part on the degree of aerosol deposition. For the present case, we assumed 50% aerosol deposition in the pressure vessel which resulted in ∿13% of the iodine inventory remaining in the pressure vessel. Our estimate is that ∿66% of the iodine is more-or-less permanently captured in the suppression pool, and ∿5% escapes to the atmosphere. We emphasize that these results are highly preliminary until both the technical review process as well as the sensitivity study of the key transport assumptions are completed.

SYNOPSIS OF KEY EVENTS

	TIME FROM BATTERY LOSS (m)
BATTERY EXHAUSTION	0
CORE UNCOVERY BEGINS	60
FIRST CLADDING FAILURE	103
FUEL MELT INITIATION	120
CORE SLUMPS	137
PRESSURE VESSEL FAILURE	172
DRYWELL VENT INITIATION	238
DRYWELL SEAL FAILURE	249

OUTLINE

- FISSION PRODUCT PATHWAYS
- RELEASE RATES FROM FUEL
- AEROSOL PRODUCTION RATES
  - OVERHEATED CORE
  - CORE/CONCRETE
- TRANSPORT PHENOMENA
  - DEPOSITION/REEVAPORATION
  - SOLUBILITY
- CHEMICAL CHANGE ALONG PATHWAY

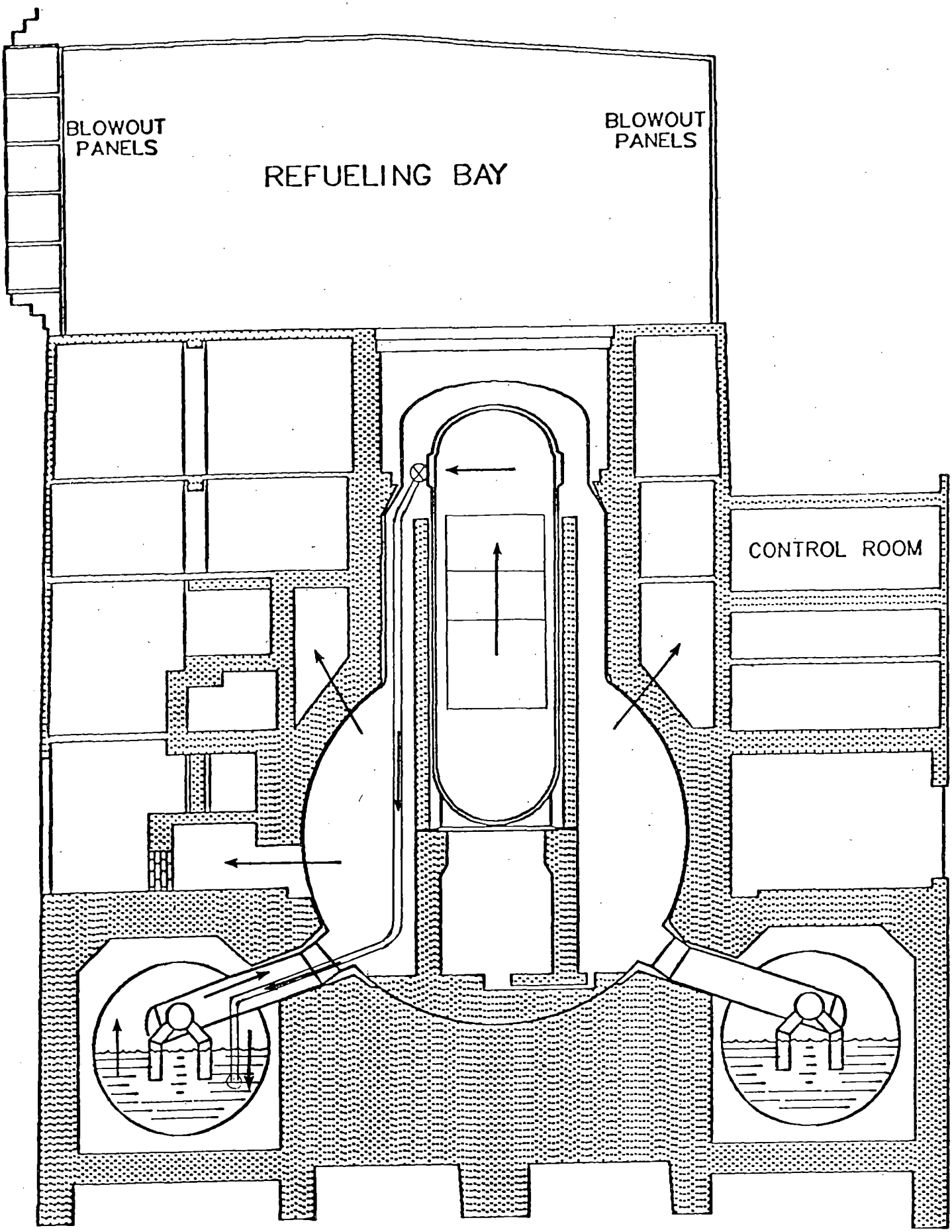

PATHWAYS PRIOR TO PV FAILURE

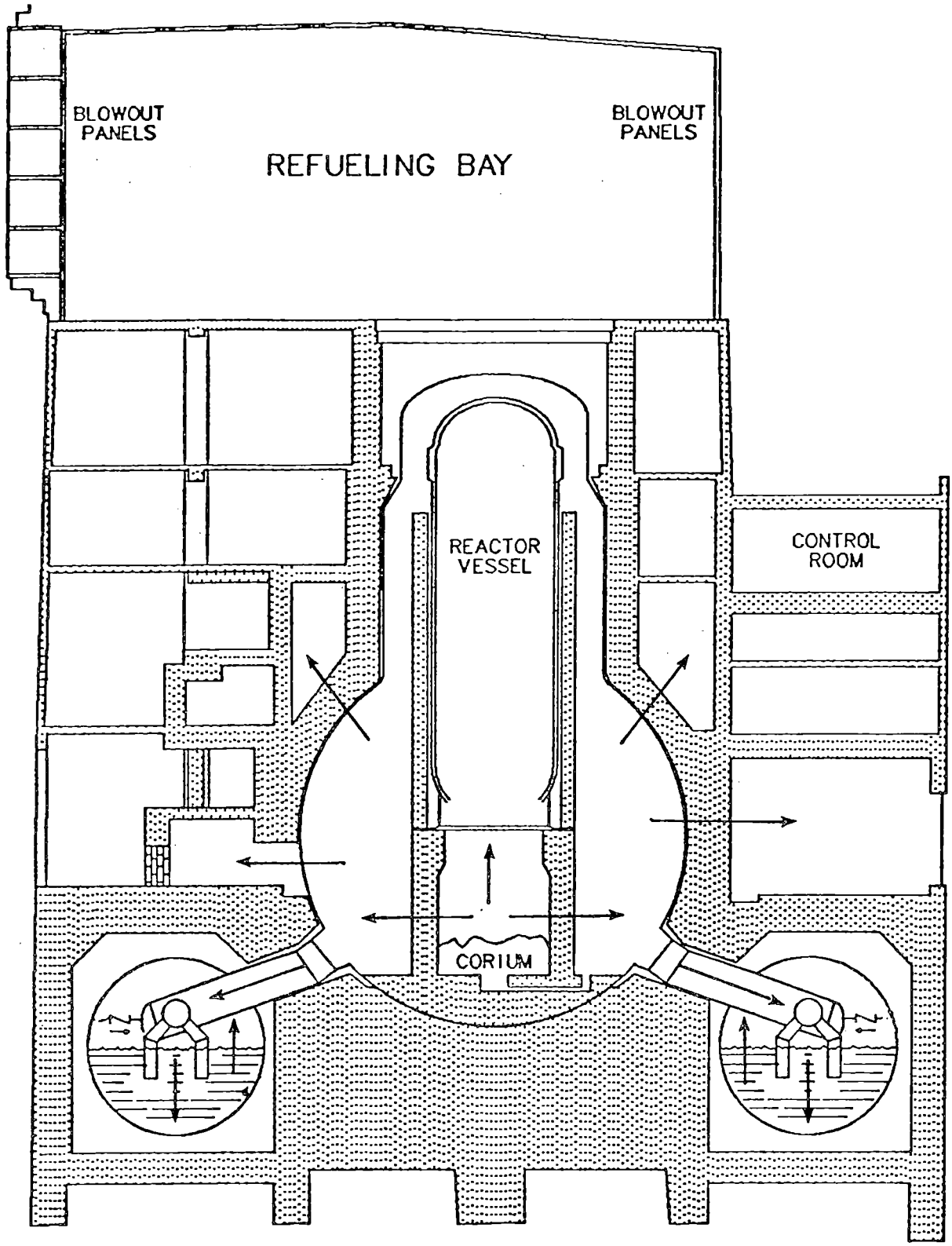

PATHWAYS FOLLOWING PV FAILURE

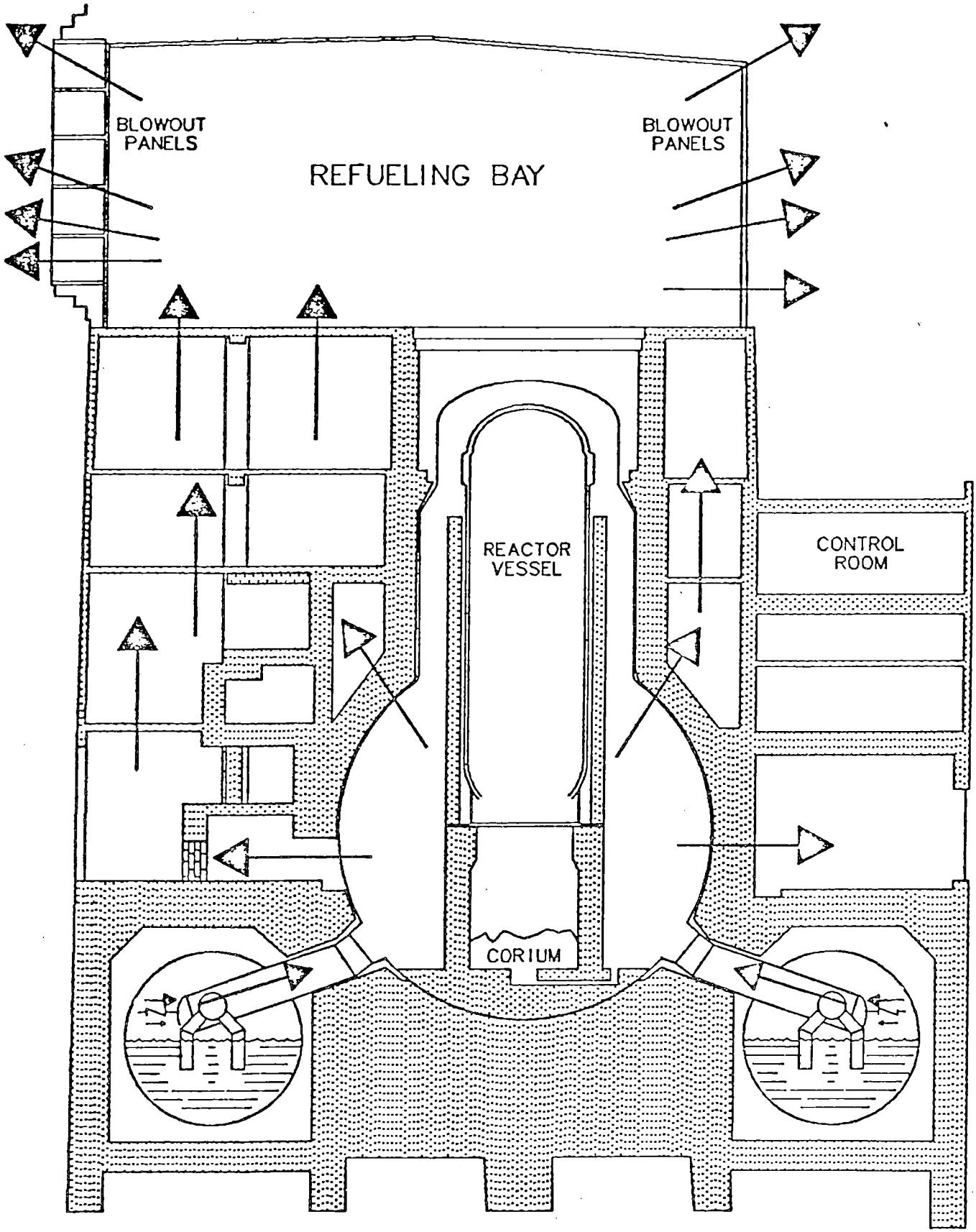

PATHS FOLLOWING DW FAILURE

ALTERNATE FISSION PRODUCT PATHWAYS

- EXAMINED REACTOR, SAFETY AND AUXILIARY SYSTEMS, ASSUMING NO INDEPENDENT FAILURES

- ACCIDENTS WHICH DO NOT RESULT IN PRIMARY CONTAINMENT FAILURE AND COMPLETE POWER LOSS REQUIRE DETAILED SYSTEMS STUDY TO DEFINE PATHWAYS TO ENVIRONMENT

- FOR THE CSB SEQUENCE AND ALTERNATE PATHWAY EXISTS VIA

$$\text{MSIV'S} \rightarrow \begin{matrix}\text{HPCI}\\ \text{RCIC}\end{matrix} \text{ STEAM TRAPS} \rightarrow \text{MAIN CONDENSER}$$

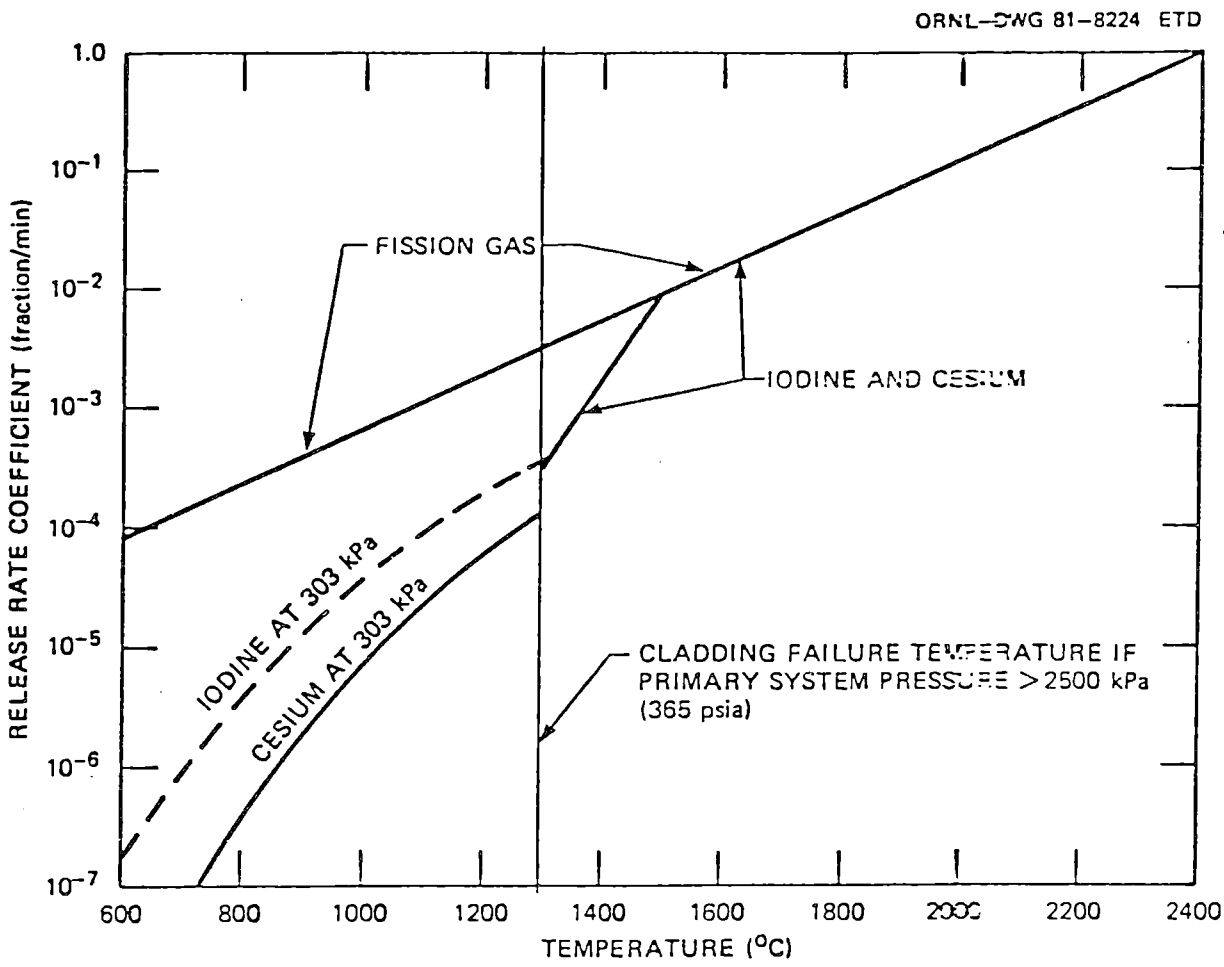

Release rate coefficients for fission gas, iodine and cesium

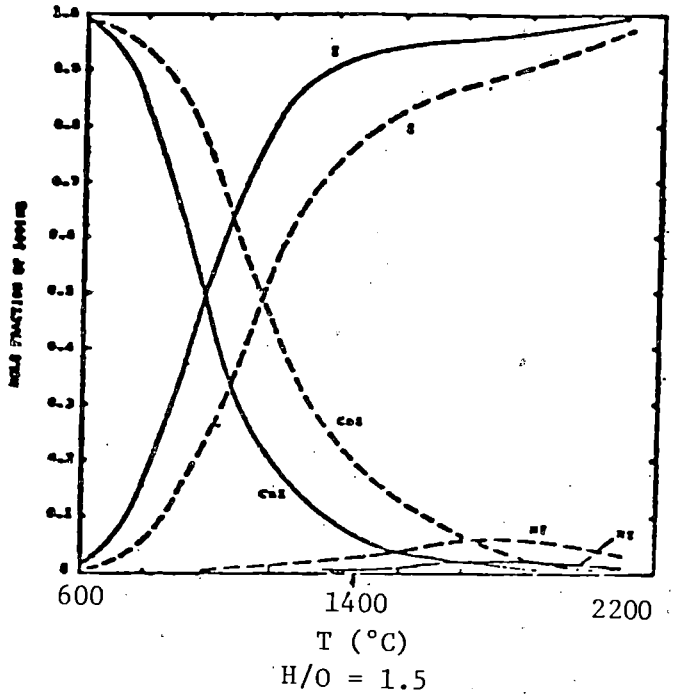

H/O = 1.5

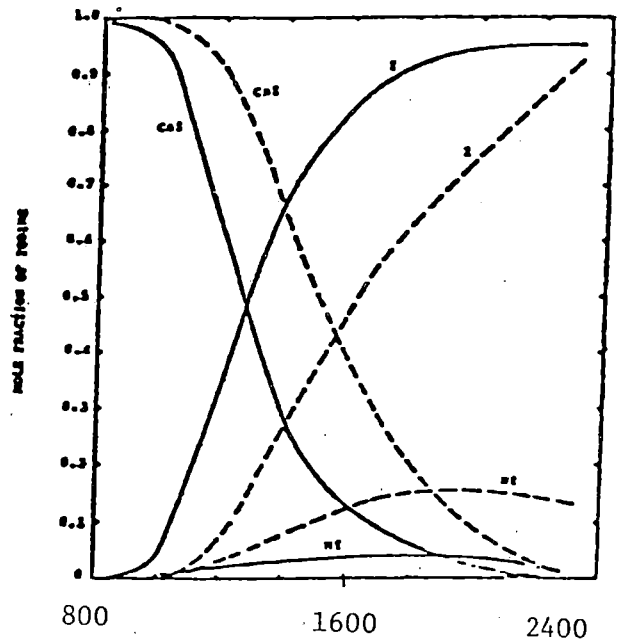

H/O = 2

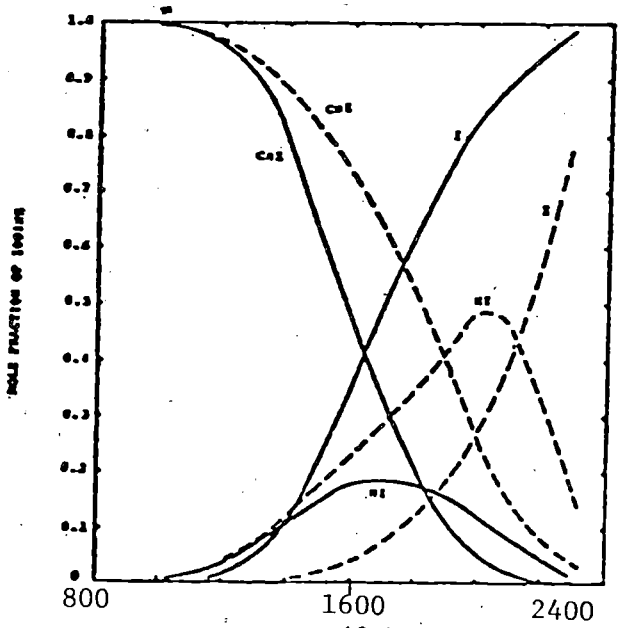

H/O = 3

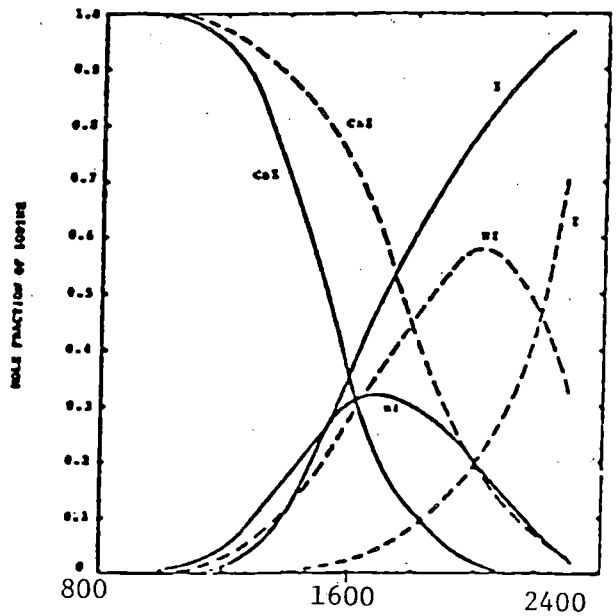

H/O = 10

GAS PHASE EQUILIBRIA: Cs-I-H-O, $Cs/_{I} = 10$, $I/H_2O = 2 \times 10^{-9}$

———— 1 bar

---------- 150 bar

MOLECULAR FORMS OF IODINE

	GROUP [1]	GROUP [2]
GAS PHASE, T > 700°C Cs, H_2 EXCESS	CsI	I, HI
GAS PHASE, T < 700°C SLOW KINETICS	CsI	I_2, HI, I
WATER SOLUTION T > 200°C (PV)	I_2	I^-, IO_3^-
WATER SOLUTION T < 160°C	I_2, HOI, ORG-I	I^-, IO_3^-
GAS PHASE CONTAINMENT	ORG-I	I_2

METHOD AND MAJOR ASSUMPTIONS

- CONVECTIVE TRANSPORT; TIME STEPS THROUGH CONTROL VOLUMES; CONDITIONS FROM MARCH.

- CHEMICAL CHANGE ALONG PATHWAY; IODINE SPECIES IN TWO GROUPS.

- MODELS FOR FP RELEASE FROM FUEL AND AEROSOL GENERATION.

- AEROSOL DEPOSITION IN PV DONE PARAMETRICALLY. USE HAARM-3 IN CV.

- MODELS FOR I-SORPTION/DESORPTION AND ORG-I PRODUCTION.

- MODELS FOR S.P. DF'S.

- NO FLOW COMMUNICATION BETWEEN PV AND DW FOLLOWING PV FAILURE.

FORM OF RESULTS

- TOTAL Kr, Xe, I INVENTORY IN EACH CONTROL VOLUME AS f(t).

- CONTROL VOLUMES ARE:
  - 6 IN PV
  - 2 IN DW
  - 5 IN BUILDING
  - ATMOSPHERE IS FINAL CONTROL VOLUME.

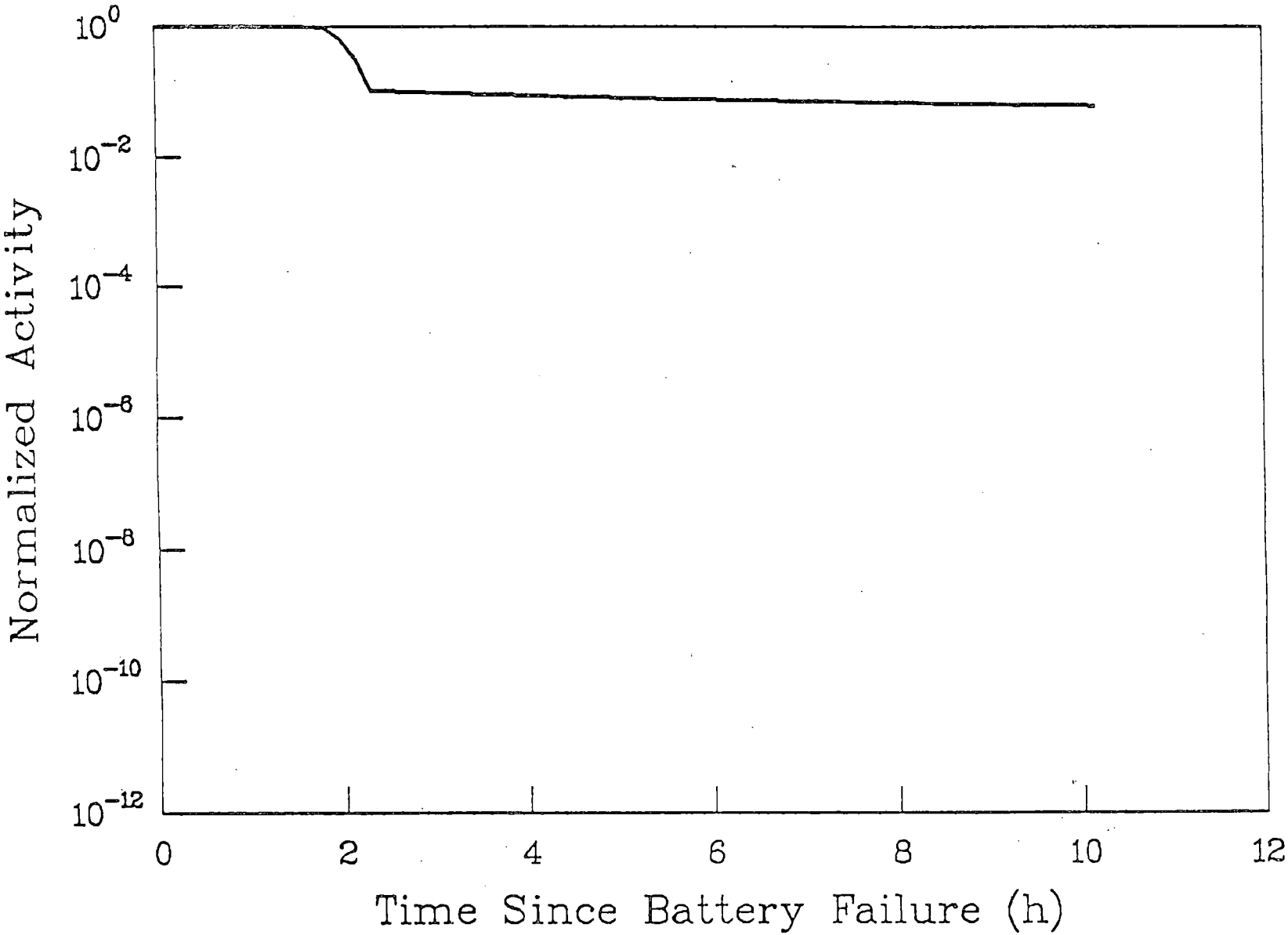

IODINE REMAINING IN CORE, PRELIMINARY

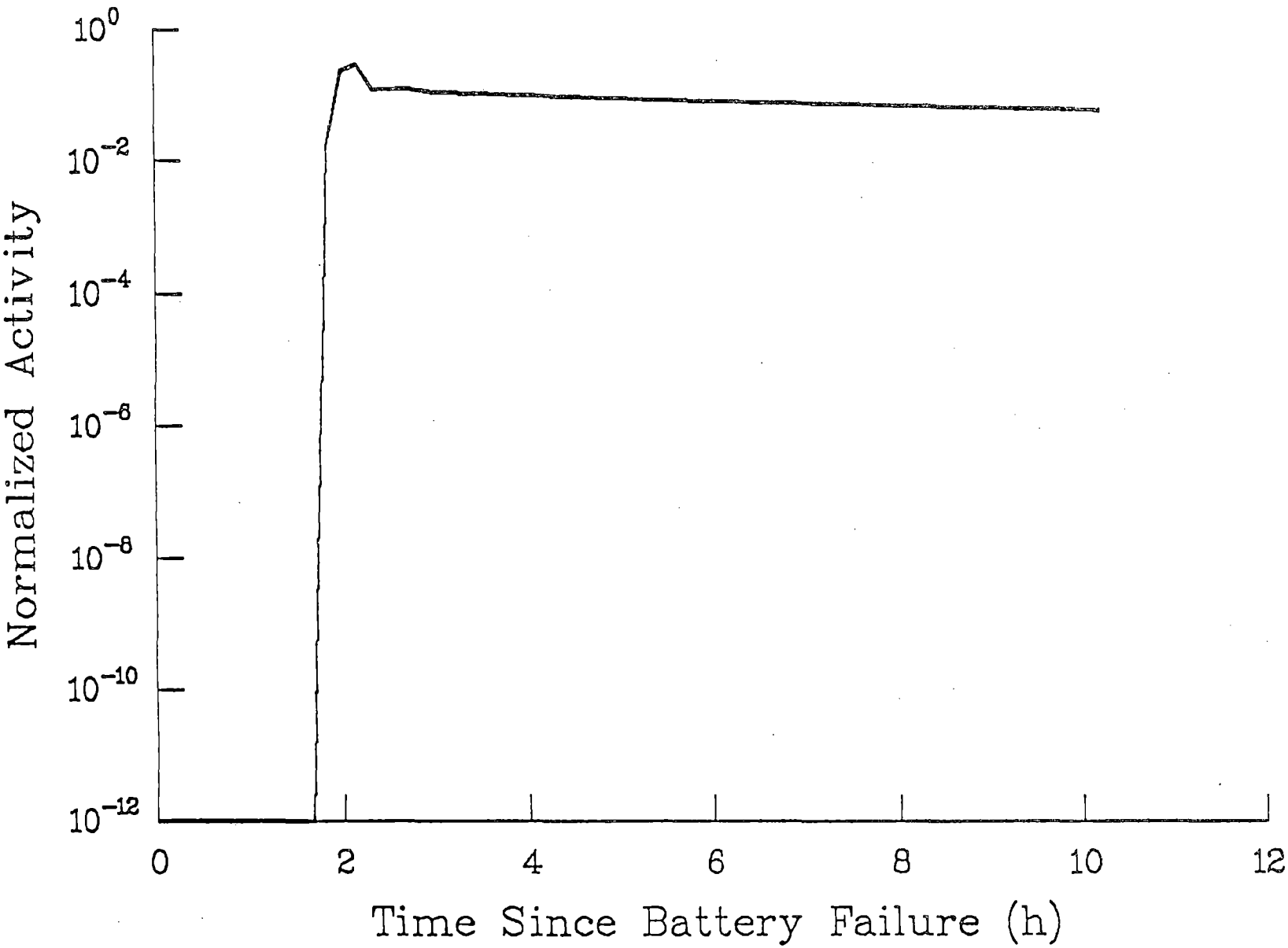

IODINE IN UPPER PV (EXCLUDING FUEL), PRELIMINARY

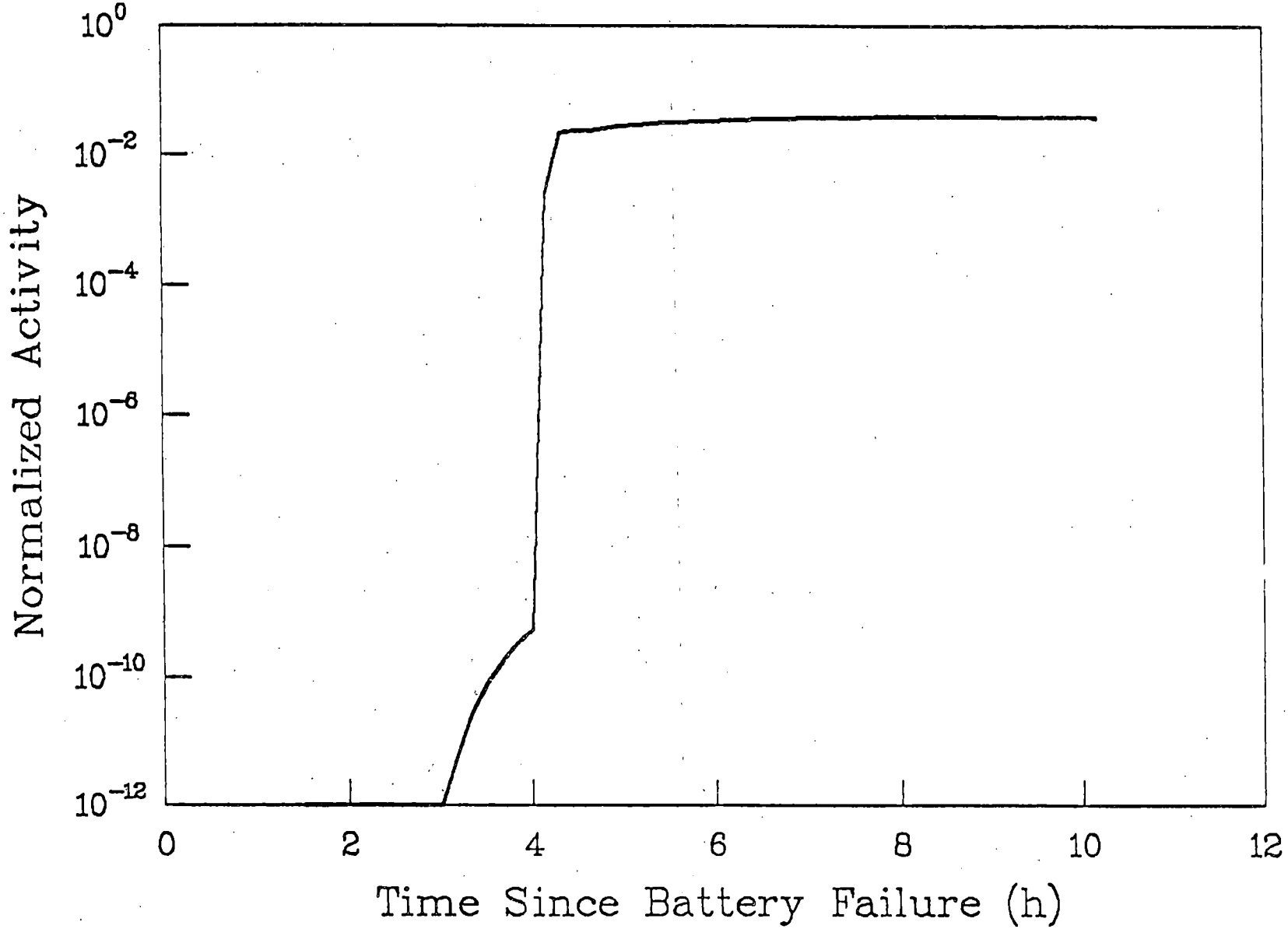

IODINE RELEASE TO ATMOSPHERE (ON AEROSOLS), PRELIMINARY

CONCLUSIONS

- NG RELEASED FROM FUEL ENCOUNTERS ONLY SMALL OBSTACLES IN PATH TO ATMOSPHERE. DEPRESSURIZATION AND CORE/CONCRETE GASES FLUSH OUT NG'S.

- PRINCIPAL FACTORS EFFECTING I-RELEASE ARE:
  1. S.P. DF
  2. FLOW COMMUNICATION BETWEEN FAILED PV AND THE DW.
  2a. AEROSOL DEPOSITION IN PV.

- PRELIMINARY RESULTS INDICATE $\sim$5% I-RELEASE; MAINLY AS I_2 SORBED ON CORE/CONCRETE AEROSOLS.

POST-MELTDOWN ANALYSES FOR PWR's

F. E. Haskin
J. L. Darby

Sandia National Laboratories
Albuquerque, New Mexico 87185
USA

Presented at
The Ninth Water Reactor Safety Research Information Meeting
October 26-30, 1981
Gaithersburg, Maryland

Post-Meltdown Analyses for PWR's

F. E. Haskin and J. L. Darby

Sandia National Laboratories
Albuquerque, New Mexico 87185, USA

Sandia National Laboratories (Sandia), Idaho National Engineering Laboratory (INEL), and Los Alamos National Laboratory (Los Alamos) are cooperating in an investigation of Pressurized Water Reactor (PWR) plants for the Severe Accident Sequence Analysis (SASA) program. INEL and Los Alamos are analyzing the primary and secondary system responses before core degradation. Sandia is analyzing the "backend"; that is, the time from the beginning of sustained core uncovering until recovery or meltdown and (if applicable) containment failure.

Maximum radiological consequences would occur for accidents involving both core melting and a direct pathway to the outside environment. For this reason, our backend analyses have primarily attempted to ascertain the integrity of containment for accidents which, in the absence of operator action, would lead to core meltdown. We have also examined possible operator actions for terminating core degradation and mitigating radiological consequences. Our analyses have been based on best-estimate inputs and available computer codes. Examples of best-estimates include realistic containment failure pressures which may be 2.2 to 2.7 times the respective design pressures, no containment failure due to in-vessel steam explosions, and hydrogen deflagrations initiated at 8 to 10 mole percent hydrogen (detonations are not considered). The computer codes we have used include MARCH[1,2], CORRAL[3], and CRAC[4].

Many physical phenomena associated with meltdown accidents are not well understood and modeling of such accidents is clearly in an evolutionary stage[2]; therefore, it is important that uncertainties involved in SASA be recognized. SASA uncertainties fall into three broad categories: uncertainties which could be reduced by developing better input data for use with existing models, uncertainties whose resolution would require further verification, improvement, or development of models based on existing phenomenological knowledge, and uncertainties which result primarily from incomplete information about physical phenomena. References 2, 5, 6, 7 and 8 assess numerous SASA uncertainties. Often the treatment is qualitative; however, limited sensitivity analyses have been performed where practical. We believe that the SASA findings discussed below are consistent with identified uncertainties.

Thusfar our analyses have been for the Zion plan only. We have examined the following accident sequences:[5,6] station blackout with failure of auxiliary feedwater (TMLB'), loss of coolant accidents (LOCA's) of various sizes inside containment, and the V-sequence interfacing system LOCA which involves direct blowdown of primary coolant through a pipe break in the auxiliary building thereby bypassing containment. The Zion containment has a large free volume (2.715E6 ft^3), a high failure pressure (150 psia, best estimate), and diverse and redundant heat removal systems

(5 fan coolers and 3 spray trains). Our analyses indicate that the probability of gross containment failure due to overpressure or hydrogen burning is low at Zion. Therefore, the degree of containment isolation strongly influences the radiological consequences for most meltdown accidents at Zion. The V-sequence LOCA bypasses containment and leads to high radiological consequences if the break is not isolated in time to prevent core melting. The V-sequence is the worst of the sequences analyzed for Zion in terms of potential radiological consequences and time available for operator action.

The Zion TMLB' sequence[5] would lead to core meltdown if cooling were not restored within 2-1/2 hours. However, containment failure due to overpressure is not predicted until several hours after the primary vessel is breached. Restoration of AC power in the interim would permit the operator to reduce containment pressure using the containment sprays or fan coolers. Using WASH-1400[3] data on power restoration, the probability of gross containment failure was found to be less than 10% for the Zion TMLB'. Operator actions appropriate for the Zion TMLB' include manual assurance of containment isolation and preservation of DC power for instrumentation. The operator could attempt in-vessel quenching of molten fuel if emergency core cooling capability were restored in time. Such quenching should be carefully controlled because it could lead to rapid containment pressurization especially if containment sprays or fan coolers were not yet operating. Following core meltdown and vessel breach, containment pressure reductions should be carefully controlled to avoid hydrogen burns which could result in containment failure. Use of containment sprays rather than containment fan coolers for this purpose would result in lower pressure rises should hydrogen burns occur.

The fan coolers at Zion would be very effective in decreasing the likelihood of gross containment failure in LOCA's.[6] We estimate that one fan cooler could prevent containment failure due to overpressure and three fan coolers could prevent containment failure due to hydrogen burning (by reducing pre-burn pressures). A total failure of containment heat removal capability (fan coolers and residual-heat-removal heat exchangers) would eventually lead to recirculation failure (by pump overheating) followed by core meltdown and, at 12 hours or more (time depends on break size), containment failure due to overpressure. For any LOCA in which emergency core cooling is functional in the injection mode, the potential for recirculation failure and subsequent core meltdown can be reduced by preserving refueling water storage tank inventory and delaying switchover to recirculation from the containment sump.

References 5 and 6 discuss the potential implications of our SASA studies to instrumentation and control, operator preparedness, systems design, and emergency response. We feel that accident signatures such as we have generated can provide significant inputs to operator training programs and to programs addressing emergency response actions. Desirable design features may also be identfied via SASA studies; however, design recommendations are beyond the scope of SASA in most cases since they require detailed cost-benefit analyses.

References

1. R. O. Wooten and H. I. Avci, MARCH (Meltdown Accident Response Characteristics) Code Description and User's Manual, NUREG/CR-1711 (BMI-2064), Battelle Columbus Laboratories, 1980.

2. J. B. Rivard, et al., Interim Technical Assessment of the MARCH Code, NUREG/CR-2285, Sandia National Laboratories, 1981.

3. Reactor Safety Study, WASH-1400 (NUREG-75/014), US Nuclear Regulatory Commission, 1975.

4. I. B. Wall, et al., Overview of the Reactor Safety Study Consequence Model, NUREG-0340, US Nuclear Regulatory Commission, 1977.

5. F. E. Haskin, W. B. Murfin, J. B. Rivard, and J. L. Darby, Analysis of a Hypothetical Core Meltdown Accident Initiated by Loss of Offsite Power for the Zion Pressurized Water Reactor, NUREG/CR-1988 (SAND81-0504), Sandia National Laboratories, 1981.

6. W. B. Murfin, F. E. Haskin, and J. L. Darby, Analysis of Hypothetical Severe Core Damage Accidents for the Zion Pressurized Water Reactors, NUREG/CR-1989 (SAND81-0504), Sandia National Laboratories, in process.

7. J. B. Rivard, Review of In-Vessel Meltdown Models, NUREG/CR-1493 (SAND80-0455), Sandia National Laboratories, 1980.

8. J. B. Rivard and F. E. Haskin, "LWR Meltdown Analyses and Uncertainties," Proceedings, ANS/ENS Topical Meeting on Reactor Safety Aspects of Fuel Behavior, August 2-6, 1981, Sun Valley, Idaho.

SEVERE ACCIDENT ANALYSIS (SASA)
RELATIONSHIP TO RISK

- RISK (CONSEQUENCES/UNIT TIME)
  = FREQUENCY (EVENTS/UNIT TIME)
  x MAGNITUDE (CONSEQUENCES/EVENT)

- SASA PRIMARILY SEEKS BEST-ESTIMATE INFORMATION AFFECTING THE MAGNITUDE FACTOR

- MAGNITUDE IS PRIMARILY DETERMINED BY
  - EXTENT OF CORE DEGRADATION
  - STATE OF CONTAINMENT

KEY QUESTIONS

- WOULD POSTULATED EVENTS LEAD TO CORE DAMAGE?

- WOULD POSTULATED EVENTS LEAD TO A DIRECT PATHWAY TO THE OUTSIDE ATMOSPHERE?

- WHAT ACTIONS WOULD RESULT IN
  1. TERMINATION?
  2. MITIGATION?
  3. EXACERBATION?

EVENT TREE FOR RADIOLOGICAL CONSEQUENCES

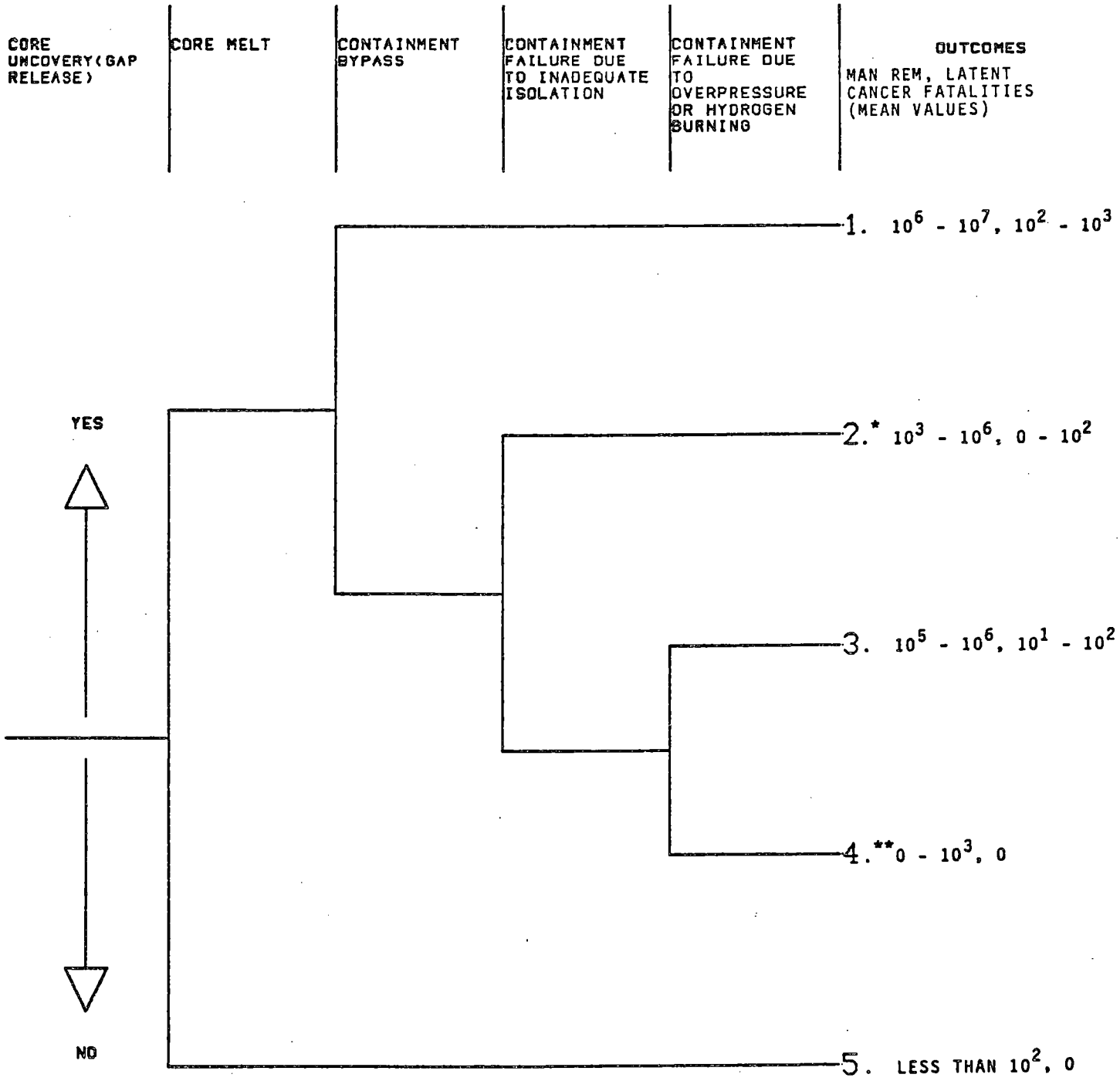

*LOWER BOUND FOR DESIGN LEAKAGE, UPPER BOUND FOR LARGE HOLE.

**LOWER BOUND FOR NO LEAKAGE, UPPER BOUND FOR DESIGN LEAKAGE (0.1 VOL % PER DAY).

PWR SASA "BACKEND" EMPHASIS

USE AVAILABLE COMPUTER CODES TO PERFORM BEST-ESTIMATE ANALYSES FOR SPECIFIC PLANTS AND ACCIDENT SEQUENCES IDENTIFYING

- HANDS-OFF MELTDOWN ACCIDENT SIGNATURES
- ASSOCIATED RADIOLOGICAL CONSEQUENCES
- POSSIBLE OPERATOR ACTIONS
- INFORMATION NEEDED BY EMERGENCY RESPONSE TEAMS
- UNCERTAINTIES

EXAMPLES OF "BEST-ESTIMATE" ASSUMPTIONS

- REALISTIC CONTAINMENT FAILURE PRESSURE
- NO CONTAINMENT FAILURE DUE TO IN-VESSEL STEAM EXPLOSIONS
- HYDROGEN DEFLAGRATION INITIATED AT 8 TO 10 MOLE PERCENT
- NO HYDROGEN DETONATION
- WASH-1400 DATA ON RESTORATION OF POWER
- RELEASES ADJUSTED FOR REMOVAL BY FAN COOLERS

NOTE: "BEST-ESTIMATES" ARE SUBJECTIVE AND EVOLVING.

Zion Sequences Analyzed	WASH-1400 Nomenclature
Loss of AC Power and AFW	TMLB'
Small LOCA's	S1 & S2
Large LOCA's	A
LPIS Check Valve Failure	V

ZION TMLB', KEY FINDINGS WITH RESPECT TO

- Gross Containment Failure
- Containment Isolation
- Restoration of Reactor Coolant Makeup
- Restoration of Containment ESF's
- DC Instrumentation

ZION SMALL LOCA'S, KEY FINDING WITH RESPECT TO

- ECC and Spray Injection Failures
- Containment Air Coolers
- Gross Containment Failure
- Switchover to Recirculation

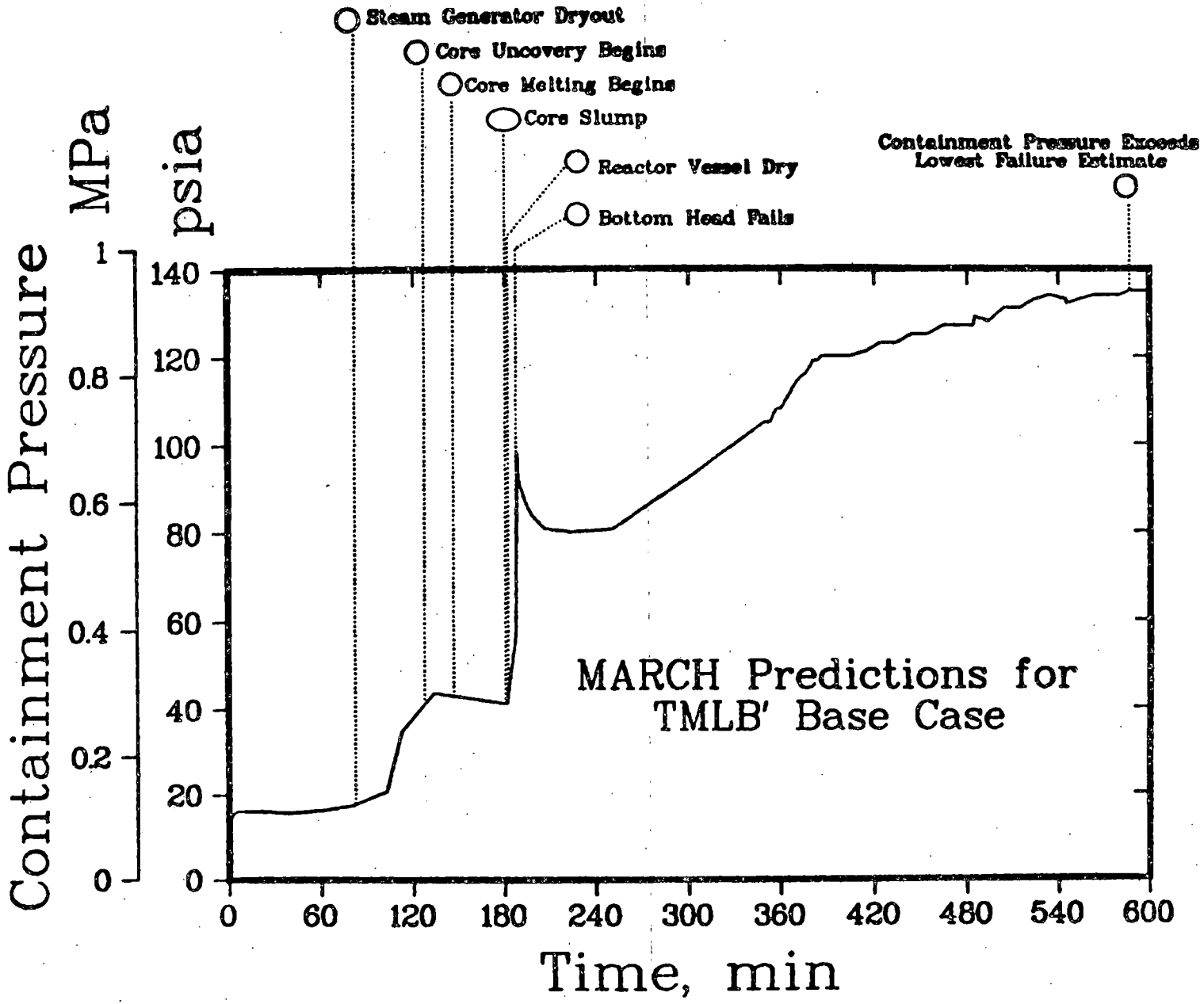
Steam Generator Dryout
Core Uncovery Begins
Core Melting Begins
Core Slump
Reactor Vessel Dry
Bottom Head Fails
Containment Pressure Exceeds Lowest Failure Estimate
Containment Pressure
MPa
psia
1
0.8
0.6
0.4
0.2
0
140
120
100
80
60
40
20
0
0
60
120
180
240
300
360
420
480
540
600
Time, min
MARCH Predictions for
TMLB' Base Case

SUMMARY OF ACCIDENT SEQUENCE CALCULATIONS

ACCIDENT	MEAN CONSEQUENCES MAN-REM	LATENT CANCER FATALITIES
• TMLB'		
-- NO CONTAINMENT OVERPRESSURE; DESIGN LEAKAGE	2×10^3	0
• LOCA'S		
-- ADH, S1DH, S2DH; DESIGN LEAKAGE OF CONTAINMENT	8×10^2	0
-- S1DHF; FAILURE TO ISOLATE CONTAINMENT (100 x DESI N LEAK RATE)	6×10^4	4×10^0
-- S1GHF; CONTAINMENT OVERPRESSURE AT 12 HOURS	2×10^6	1×10^2
• INTERFACING SYSTEM LOCA'S		
-- V; 1.5 INCH BREAK; CONTAINMENT BYPASSED	4×10^6	2×10^2
-- V; 1.5 INCH BREAK; CONTAINMENT ISOLATED; PRIMARY COOLANT RELEASED	3×10^2	0

STRATEGY FOR TREATING SASA UNCERTAINTIES

- USE AVAILABLE, STATE-OF-THE-ART COMPUTER CODES AND BEST-ESTIMATE INPUTS TO DEVELOP BASE CASES.
- IDENTIFY SIGNIFICANT UNCERTAINTIES
  - DATA UNCERTAINTIES
  - MODELING UNCERTAINTIES
  - PHENOMENOLOGICAL UNCERTAINTIES
- WHERE APPROPRIATE, USE LIMITED PARAMETRIC ANALYSES
- ASSURE THAT FINDINGS AND RECOMMENDATIONS ARE CONSISTENT WITH THE IDENTIFIABLE UNCERTAINTIES
- INCLUDE EXPLICIT TREATMENT OF UNCERTAINTIES IN REPORTS

INPUT (DATA) UNCERTAINTIES

- UNCERTAINTIES WHICH COULD BE REDUCED BY DEVELOPING BETTER INPUT DATA FOR USE WITH EXISTING MODELS
- EXAMPLES:
  - LINER TO CONCRETE HEAT TRANSFER COEFFICIENT
  - PASSIVE HEAT SINKS
  - REACTOR CAVITY GEOMETRY
  - BASEMAT CONCRETE PROPERTIES

MODELING UNCERTAINTIES

- REDUCTION OR BOUNDING OF MODELING UNCERTAINTIES WOULD REQUIRE FURTHER VERIFICATION, IMPROVEMENT, OR DEVELOPMENT OF MODELS BASED ON EXISTING PHENOMENOLOGICAL KNOWLEDGE.

- EXAMPLES:
  - HEAT TRANSFER CORRELATIONS
  - STEAM PROPERTIES MODEL
  - DECAY HEAT MODEL
  - CRITICAL FLOW MODEL

PHENOMENOLOGICAL UNCERTAINTIES

- PHENOMENOLOGICAL UNCERTAINTIES RESULT PRIMARILY FROM INCOMPLETE INFORMATION ABOUT PHYSICAL PHENOMENA.

- EXAMPLES:
  - MELT PROGRESSION (COMPOSITION, GEOMETRY, ETC.)
  - IN-VESSEL MELT-WATER INTERACTIONS (STEAM GENERATION, FRAGMENTATION, ZR/H_2O, ETC.)
  - VESSEL BREACH & MATERIALS DISCHARGE
  - MELT-WATER INTERACTIONS IN REACTOR CAVITY
  - FISSION PRODUCT RELEASE, TRANSPORT, AND REMOVAL
  - HYDROGEN GENERATION TRANSPORT & BURNING

ZION TMLB' SENSITIVITY STUDIES

	CONTAINMENT PRESSURE AT 600 MIN (PSIA)	TIME TO VESSEL BREACH (MIN)
• LINER TO CONCRETE HEAT TRANSFER COEFFICIENT		
4 BTU/HR/FT^2/F	135	187
100 BTU/HR/FT^2/F	127	188
• PASSIVE HEAT SINKS		
ZION FSAR	135	187
BTP CSB 6-1	108	187
• OVERFLOW INTO REACTOR CAVITY		
AT 2000 FT^3	135	187
AT 7000 FT^3 (NONE)	110	187
• DECAY HEAT		
ANS 5.1 +10%	136	164
ANS 5.1	135	187
ANS 5.1 -10%	128	216

IMPLICATIONS OF PWR "BACKEND" SASA

- Instrumentation and Control
- Operator Preparedness
- System Design
- Emergency Response

SEVERE ACCIDENT MITIGATION STUDIES

H. J. Reilly

Presented at

The Ninth Water Reactor Safety Research

Information Meeting

October 26 - 30, 1981

Gaithersburg, Maryland

Idaho National Engineering Laboratory

Idaho Falls, Idaho 83415

EG&G Idaho

Idaho Falls, Idaho 83415

SEVERE ACCIDENT MITIGATION STUDIES

H. J. Reilly
EG&G Idaho, Inc.

EG&G Idaho is performing studies of systems to mitigate severe accidents in light water reactors. The purpose of this work is to assist NRC in its considerations of proposed degraded-core rulemaking by defining potential requirements for core melt mitigation systems that could be retrofitted to existing facilities. The scope of work includes identification of recommended systems, development of design requirements, and conceptual systems designs. The Sequoyah-1 reactor was selected as representative of ice condenser PWRs, and Grand Gulf-1 as representative of Mark III BWRs for study purposes.

Work was started on this task in late FY-1980. EG&G Idaho divided the work on each reactor into three phases: literature review and fault tree development (Phase 1), development of design requirements (Phase 2), conceptual design and project report (Phase 3). Phase 1 for Sequoyah was completed in January 1981. Phase 2 was completed at the end of September 1981. Phase 3 completion is planned for end of first quarter FY-1982. Work on Grand Gulf was started early--in July 1981--to accommodate delays in obtaining information on Sequoyah. Phase 1 for Grand Gulf will be completed by the end of first quarter FY-1982. Completion of all work on Grand Gulf is planned for the end of FY-1982.

The Phase 1 work identified that most public risk from hypothetical Class 9 accidents at Sequoyah was due to small break events (reactor coolant system piping failures 1/2 inch to 6 inches in diameter) coupled with emergency core cooling system failures. Some risk was also identified due to the V sequence (failure of check valves separating high and low pressure systems) and a possible common mode failure due to drains shared by the containment spray recirculation system and the emergency core

cooling recirculation system. The predominant failure mode of the containment would be overpressure due to uncontrolled hydrogen burning, although it appeared that containment failure due to overpressure by other sources could occur if failure by uncontrolled hydrogen burning did not occur first. These conclusions were based principally on review of other work, especially the Reactor Safety Study Methods Application Program conducted by Sandia Laboratories.

EG&G Idaho performed further analysis to extend these results from other studies. Risk calculations showed that risk reduction for Sequoyah would require several elements: probability reductions of certain difficult-to-mitigate sequences, control of hydrogen burning, control of contact mode between fuel and water outside the vessel, and prevention of basemat attack. The first two of these items are of high priority and will accomplish a large risk reduction (factor of 20 to 80) if only these two are completed. The third item is recommended because of the large uncertainty in what will happen if such contact between water and molten fuel, cladding, and structural support metal (corium) is uncontrolled. The fourth is recommended because of the desirability of preventing containment failure even by the relatively low consequence failure modes associated with long-term pressure buildup and basemat melt-through.

EG&G Idaho has recommended design solutions which appear to accomplish these objectives. A gas turbine to burn the oxygen in the containment was identified as being the least problematical of the provable methods of hydrogen control. A water management system to control the mode of contact between corium and water below the vessel is proposed, combined with either a wetted rubble bed system to control basemat attack or a vent-holding tank system to prevent overpressurization from basemat attack. As of September 1981, conceptual design of the water management system, vent-holding system, and wetted rubble bed system was proceeding. Because of the perceived advantages and the advanced status of the distributed ignition system, design of the gas turbine system will not proceed, pending NRC indication of a desire to have this information.

Completion of the report on Phase 2 activities for Sequoyan is expected by the end of FY-1981. The report will contain the EG&G analysis, the identification of proposed core melt mitigation systems, and the preliminary design requirements for those subsystems. Work has begun on conceptual design of these subsystems and on calculations of the reduction in public risk that installation of these subsystems would accomplish.

Status of Severe Accident Mitigation Study

H.J. Reilly

EG&G Idaho, Inc.

IDAHO NATIONAL ENGINEERING LABORATORY

Scope-of-Work

- Conceptual design studies of core melt mitigation systems
  - Identify needed systems
  - Develop design requirements
  - Perform conceptual designs and cost estimates
- Sequoyah-1 (PWR with ice-condenser containment)
- Grand Gulf-1 (BWR Mark III)
- Other reactors as identified by NRC

INEL-S-34 971

Schedule Status

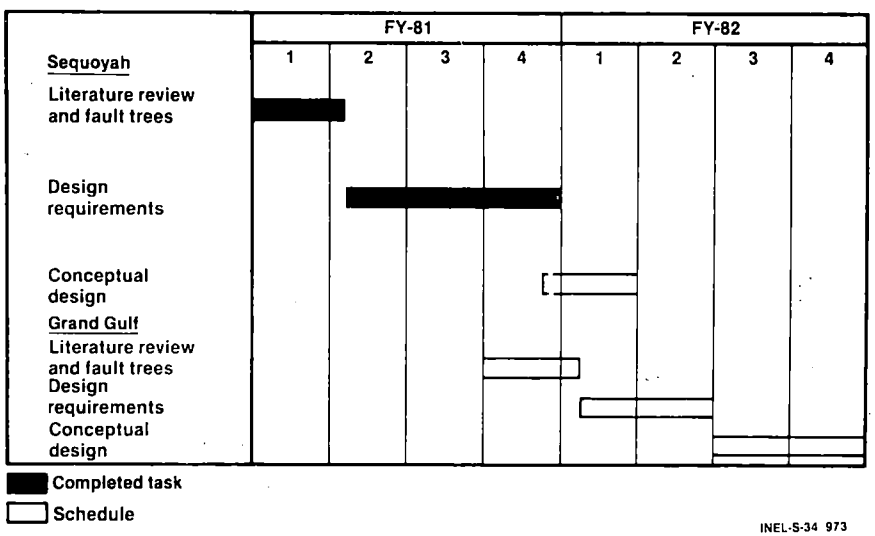

INEL-S-34 973

Sequoyah - S2D Accident

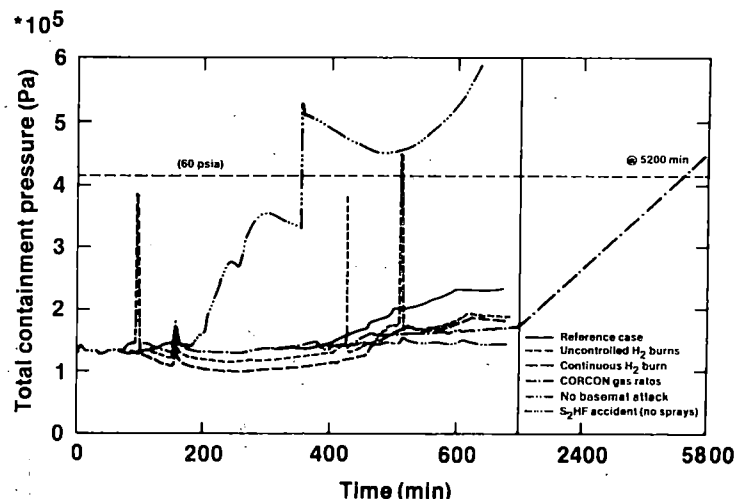

INEL-S-34 972

Estimated Public Risks*

Containment Failure Mode	Early Fatalities	Latent Cancer Fatalities**	Property Damage, $
V	2×10^{-4}	0.05	56,000
γ	2×10^{-4}	0.27	201,000
α	1×10^{-6}	~ 0	~ 0
(γ δ)	6×10^{-6}	0.02	15,000
δ (If γ does not occur)	4×10^{-6}	0.02	10,000

* Expected consequences due to 5 reactor-years of operation

** Assuming a plateau incidence rate between 10 and 40 years after an accident

INEL-S-34 978

Candidate Device Evaluations
Hydrogen Control Systems

Deliberate ignition

- Proving capability for class 9 accidents is beyond present state-of-the-art
- Otherwise nearly ideal system if capability can be proved
- Effort by TVA on D.I.S. successful to date

Pre-inerting

- Proven method, know how to design
- Adds personnel risk
- Unacceptable operating costs due to policy prohibiting work in inerted spaces

INEL-S-34 968

Candidate Device Evaluations
Hydrogen Control Systems (cont'd)

Hydrogen recombiners

- Capacity problem leading to high installation and maintenance costs

Post-inerting

- Inert gas injection (CO_2, N_2) increases containment pressure
- Foams not proven for this application. Continuous injection required.
- Halons unacceptable because of corrosion problems
- Spray-inerting not proven for this application. Continuous injection required
- Gas turbine has least disadvantages for Sequoyah
- In all cases, a timing problem (when to inject)

INEL-S-34 969

Candidate Device Evaluations
Filter-Vent Systems

- Probably cannot reduce risk from hydrogen burn, most important for Sequoyah
- Does not reduce risk from basemat penetration
- Undesirable to deliberately release radioactivity (noble gasses)
- If spray failure is to be accommodated, systems become large and expensive
- With filters, tends to become expensive
- Typical systems tend to have significant failure modes, design difficulties
- Active pumping of noncondensible gases to a high pressure underground tank could reduce expense, remove risk of containment failure to long term overpressure

INEL-S-34 962

Candidate Device Evaluations
Core Retention Systems

- Relatively small gain in risk by core retention, but qualitatively important
- Insufficient data to merely flood cavity before vessel failure
- Passive devices inadequate because only provide a small added delay
- Active devices problematical because of vulnerability to vessel failure event, dependence on power source, near-impossibility of retrofit
- Literature on rubble beds shows compatibility problems
- Wetted rubble bed could combine best features of passive and active devices, and be retrofittable. Looks good based on engineering judgement because data is lacking

INEL-S-34 963

CMMS Subsystems

Subsystem	Purpose	Risk Improvement Factor*		
		EF	LC	PD
Gas turbine	Control hydrogen burning	5	7	3
Rubble bed or vent-holding system	Prevent basemat attack	~1	~1	3
	Control long-term pressure buildup	~1	~1	3
Water management system	Control corium-water contact mode			
		16	3	4

* Assuming reductions in P(V), P(HF), P(H)

INEL-S-34 966

Candidate Device Evaluations
Other Concepts

- Strengthening containment probably not retrofittable; expensive; would not change results qualitatively for Sequoyah
- Relatively minor modifications could give operator the capability to control the entry of water into the bottom cavity

INEL-S-34 970

Principal Design Requirements

Gas turbine system

- Outside containment. One turbine serves two units
- Capable of inerting containment within 30 minutes of demand
- Heat rejection outside. Return gas inside
- Not compromise existing containment
- Independent power supply
- Operator-actuated. Audible/visual alarms when operating

INEL-S-34 976

Principal Design Requirements (cont'd)

Water management system

- Capable of maintaining cavity dry in all dominant accident sequences
- Flooding of cavity at controllable amount and rate at operator demand
- All-passive systems preferred

INEL-S-34 977

Principal Design Requirements (cont'd)

Vent-hold system

- Vent and hold maximum rate of noncondensible gas formation
- High pressure underground tank
- Independent power supply
- One pump, tank, etc., serve both units
- Operator actuated
- Not compromise existing containment

INEL-S-34 975

Principal Design Requirements (cont'd)

Core retention system

- Sufficient depth (~1 m?) to prevent basemat attack
- Retrofittable
- Spheres of same composition as corium. At least as dense
- Normally dry. Capability to fill bed with water when vessel failure is imminent
- Capability to gravity feed sufficient water to bed to makeup boiloff
- Capability to fill in with water on top of molten core
- Accommodate existing instrument leads with compartments or etc.

INEL-S-34 974

ASSESSMENT OF THE MARCH COMPUTER CODE

Presented at
the Ninth Water Reactor Safety Research Information Meeting

October 26-31, 1981
Gaithersburg, MD

J. B. Rivard
Sandia National Laboratories
Albuquerque, NM 87185, U.S.A.

ASSESSMENT OF THE MARCH COMPUTER CODE

J. B. Rivard
Sandia National Laboratories
Albuquerque, NM 87185

The focus of LWR safety concerns has recently expanded beyond the large LOCA design-basis accident to consideration of system response to severe core damage accidents (including meltdown) of several hours duration. The MARCH computer code[1] was developed as a tool for use in early risk assessments; however, because MARCH models severe core damage sequences, it has been used to satisfy previously unanticipated, but pressing, analysis needs. The expanded usage of MARCH has generated questions regarding the extent, appropriateness, and accuracy level of the modeling in the code, and the application and interpretation of MARCH results. As assessment of MARCH was prepared[2] in response to a request by NRC to clarify the capabilities and limitations of MARCH within the context of current applications, to evaluate the major modeling and phenomenological uncertainties, and to recommend how MARCH should be used and/or improved.

Project constraints included the requirement that the assessment be based primarily upon existing information (available from the NRC and its contractors). New evaluations were initiated only where the information needed was deemed essential and where the necessary resources and time were available.

Findings

To a large extent, MARCH was found to integrate recent understanding of the many complex phenomenologies, engineered systems, and events into a fast-running code applicable to a wide variety of LWR systems and accident sequences involving core melt. Accomplishing this has often required that phenomena and systems be modeled very simply and with a minimum of detail. This approach was justified during code development on the basis of the intended application, i.e., risk analysis. The approach may also have been partly due to limited resources for code development and/or the limited phenomenological knowledge base.

However, some of the models in MARCH are overly simplified; they reduce phenomena and systems to a degree that ignores complicating--and often important--factors. This modeling approach restricts the usefulness of the code for many applications and can result in code predictions which are not physically realizable. Examples include a single volume primary model, lumped fuel/clad nodes, and nonmechanistic heat transfer modeling.

A considerable number of phenomena are not modeled in MARCH at all. Examples include the oxidation of steel structures and other hydrogen sources (other than oxidation of zircaloy), the downward

*This work supported by the U. S. Nuclear Regulatory Commission.

relocation of fuel as it melts and freezes, phenomena accompanying steam explosions (fragmentation, dispersal), and core barrel heatup/failure in PWRs.

Significant improvement in the level of modeling in MARCH is possible, but would in some cases be limited by inadequate knowledge concerning specific phenomena.

The design of MARCH did not anticipate assessment and verification requirements. In particular, the nonmodular structure (one subroutine exceeds 2400 statements), inadequate code comments, lack of systematic and global mass/energy balance information, and incomplete and misleading documentation, provide significant deterrents to understanding the detailed calculational procedures. The limited code documentation and the lack of several fully-documented sample problems provide an inadequate basis for most MARCH applications.

In applications requiring a consensus regarding the course and effects of a meltdown accident, it is necessary that diverse users of a code (such as MARCH) obtain similar results when calculating a given accident sequence for a certain reactor plant. However, different users of MARCH with identical plant and sequence parameters may easily obtain significantly different results. This is due to the sensitivity of MARCH predictions to modeling parameters which are neither fixed by the plant nor accident sequence but which must be specified by the user. In most cases, these parameters represent input which are made necessary by modeling limitations within the code.

Taken together, the limitations, errors, and deficiencies identified in MARCH may seriously compromise the validity of some code predictions. A much more thorough study would be required to provide a comprehensive evaluation of MARCH. (Most of the limitations discussed herein have been uncovered in the use of MARCH for the study of PWRs and large dry containments. Very little information was available to the assessment group concerning the modeling of BWRs and other containment types.)

The evidence uncovered during the assessment does not support the sometimes-heard opinion that MARCH accident sequence predictions are "conservative" (more severe than realistically expected), although some features of MARCH, individually considered, do appear to give "conservative" results.

Although an NRC-sponsored program designed to more comprehensively assess the capabilities and limitations of MARCH would have intrinsic merit and would provide a better basis for application (especially to containments other than large dry and to BWRs generally) of the version of MARCH discussed in this report, it is the opinion of the assessment project group that the resources which would be required would be better allocated to the improvement of MARCH or the development of alternatives.

In terms of current computing costs, MARCH is very inexpensive to run. A large (i.e., an order of magnitude) increase in execution time, if coupled with a corresponding increase in model complexity, detail, and algorithmic rigor, would not seriously hinder the bulk of current applications of MARCH.

Some modifications of MARCH to improve its capabilities would be difficult. One significant deterrent to modification is the sequential processing structure of the code which prevents the treatment of some parallel (and coupled) phenomena. However, the clear need of NRC for severe accident sequence calculations appears to us to require the early implementation of a robust NRC program for the improvement of MARCH or the development of alternatives.

Assuming that a program at some level will be instituted by the NRC to improve MARCH, an organizational structure to support this effort is recommended in the assessment report. Included would be a forum for MARCH users, both inside and external to the NRC, to provide comprehensive and balanced review, discussion, and recommendation of MARCH improvements.

Because the deficiencies identified in MARCH may seriously compromise the validity of some code predictions, the project group recommends that the applications of MARCH to formal safety evaluations by subject to two conditions:

a. Code results be accompanied by explicit evaluation and discussion of code limitations with regard to their potential for invalidating the conclusions drawn from the code results.

b. Calculations be made using a documented version of the code with data input appropriate to the plant and accident sequence, and with a fully accessible set of values for the modeling parameters and options used.

References

1. R. O. Wooten and H. I. Avci, "MARCH (Meltdown Accident Response Characteristics) Code Description and User's Manual," NUREG/CR-1711, BMI-2064, Battelle Columbus Laboratories (1980).

2. J. B. Rivard et al., "Interim Technical Assessment of the MARCH Code," SAND81-1672, NUREG/CR-2285, Sandia National Laboratories (in publication).

MARCH ASSESSMENT

- BACKGROUND
- FINDINGS
- RECOMMENDATIONS

BACKGROUND

- MARCH Developed by BCL as Follow-On Code for WASH-1400-Type Risk Analysis.

- Features

  Integrated Accident Responses

  Wide Variety of Plants, Systems, & Sequences

  FORTRAN

  Relatively Small (12,500 Statements)

  Fast Running (~$10-50/Run)

MARCH APPLICATIONS

- Risk Assessments
- TMI-2 Analysis
- Hydrogen Behavior & Control
- Z/IP Task Action Studies
- Severe Accident Sequence Analysis (SASA)
- Filtered-Vented Containment Systems Studies
- Steam Explosion Research
- Degraded Core Rulemaking Research

NEED FOR ASSESSMENT

- Implications for Applications to Current Risk Assessment
- Implications for Applications Other Than Risk Assessment
- Is MARCH "Conservative"?
- Is MARCH "State-of-the-Art"?
- What Improvements are Needed?
  (What Priority)
- Alternatives to MARCH

ASSESSMENT PROJECT

- SPONSOR: NRC-RES
- LIMITED SCOPE ~ 3 MO. STUDY
- USE EXISTING INFORMATION AND EXPERIENCE
- IDENTIFY LIMITATIONS IN CONTEXT OF CURRENT APPLICATIONS
- MAKE RECOMMENDATIONS
- START JANUARY 1981

ASSESSMENT PROJECT

- ORGANIZATION
  - -- PROJECT LEADER, J. B. RIVARD, SNL
  - -- AUTHORS AND CONTRIBUTORS FROM

    NRC
    SNL
    BCL
    UKAEA
    EI
    ORNL
    BNL

- IDENTIFY AND COLLATE MARCH INFORMATION AND EXPERIENCE
- PREPARE REPORT

ASSESSMENT TECHNIQUES

1. COMPARISON WITH EXPERIMENT
2. COMPARISON WITH OTHER CODES
3. USE OF EXPERT JUDGMENT
4. SENSITIVITY STUDIES
5. COMPARISON OF RESULTS WITH AUXILIARY CALCULATIONS
6. BOTTOM-UP CODE EVALUATION

FINDINGS

Limitations Identified

33	General
29	Chemical, Nuclear or Thermal Interactions or Reactions
44	Transport Phenomena
6	Structural Deformations, etc.
11	Safety Systems, Equipment
123	

22	Rated Important
50	Importance Unknown
17	Rated Moderately Important
34	Rated Least Important
123	

EXAMPLES

Limitations Due to Modeling Simplifications

- Primary System Nodalization
- Lumped Fuel/Clad Nodalization
- Nonmechanistic Fuel Pin Quenching
- No Downward Relocation of Melting Fuel/Clad
- Steam Generation and Debris Oxidation in Reactor Cavity
- Steam Explosions
- Fission Product Release and Tracking

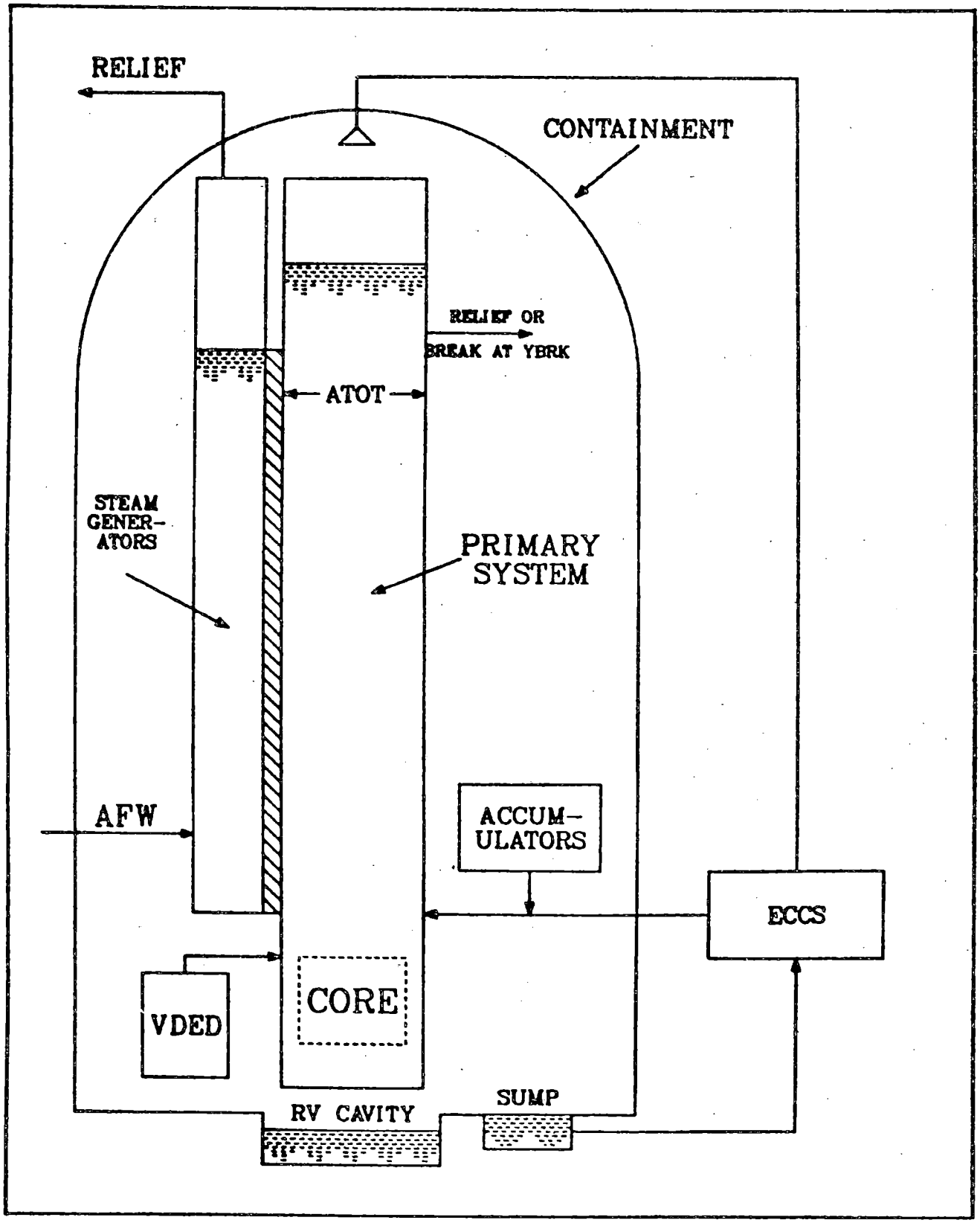
RELIEF
CONTAINMENT
RELIEF OR
BREAK AT YBRK
ATOT
STEAM
GENER-
ATORS
PRIMARY
SYSTEM
AFW
ACCUM-
ULATORS
ECCS
VDED
CORE
RV CAVITY
SUMP

EXAMPLES

Limitations Due to Lack of Models

- Debris Bed Formation, Cooling
- Radial Thermal Radiation, In-Core and Ex-Core
- Engineered Systems for H_2 Control, Filtered Vents
- In-Vessel Steel Oxidation
- Heavy Element Decay Heating
- CO Burning

EXAMPLES

Limitations Due to Errors and Problems

- Fuel-to-Vapor/Gas Heat Transfer
- Core Water Not Heated by Partly-Covered Nodes
- Core Node Heat Transfer to Liquid Limited to < Decay Heat
- Film Boiling Model (HOTDROP)
- Convergence Problems w/BOIL Timestep
- Nonphysical (numerical) Oscillations
- ECCS ΔP Incorrect in Injection Mode

EXAMPLES

Phenomenological Data Base Limitations

- Core Relocation Dynamics During Meltdown
- Fission Product Release and Transport
- Fragmentation, Heat Transfer, Oxidation During Melt-water Interactions (including steam explosions)
- Debris Bed Formation/Cooling
- Fuel Flow/Dispersal During Discharge From Vessel
- Sources, Transport and Burning of Combustible Gases
- Component/Equipment Survivability
- Core-Concrete Interactions
- Aerosol Deposition and Consequences
- Containment Failure Mechanisms

DOCUMENTATION PROBLEMS

- USER'S MANUAL INADEQUATE, SOMETIMES INSCRUTABLE
- WELL-DOCUMENTED SAMPLE PROBLEMS NEEDED
- CONSTRAINTS DUE TO MODELING, ALGORITHMS AND PROGRAM DESIGN NOT DISCUSSED
- MODELING EQUATIONS OFTEN UNSUPPORTED BY DERIVATION OR REFERENCE
- MANY DEFAULT VALUES HAVE NO PRACTICAL SIGNIFICANCE
- CODING SPARSELY AND INADEQUATELY COMMENTED

SOME NONCONSERVATISMS EXIST IN MARCH

- No Heavy Element Decay Heat
- No Steel Oxidation (H_2 Source)
- Clad Temperature Underestimated During Oxidation
- Critical Flowrate of Liquid can be Underestimated for Small LOCAs
- Film Boiling Model in HOTDROP

Impact of Phenomenological Uncertainty on Modeling

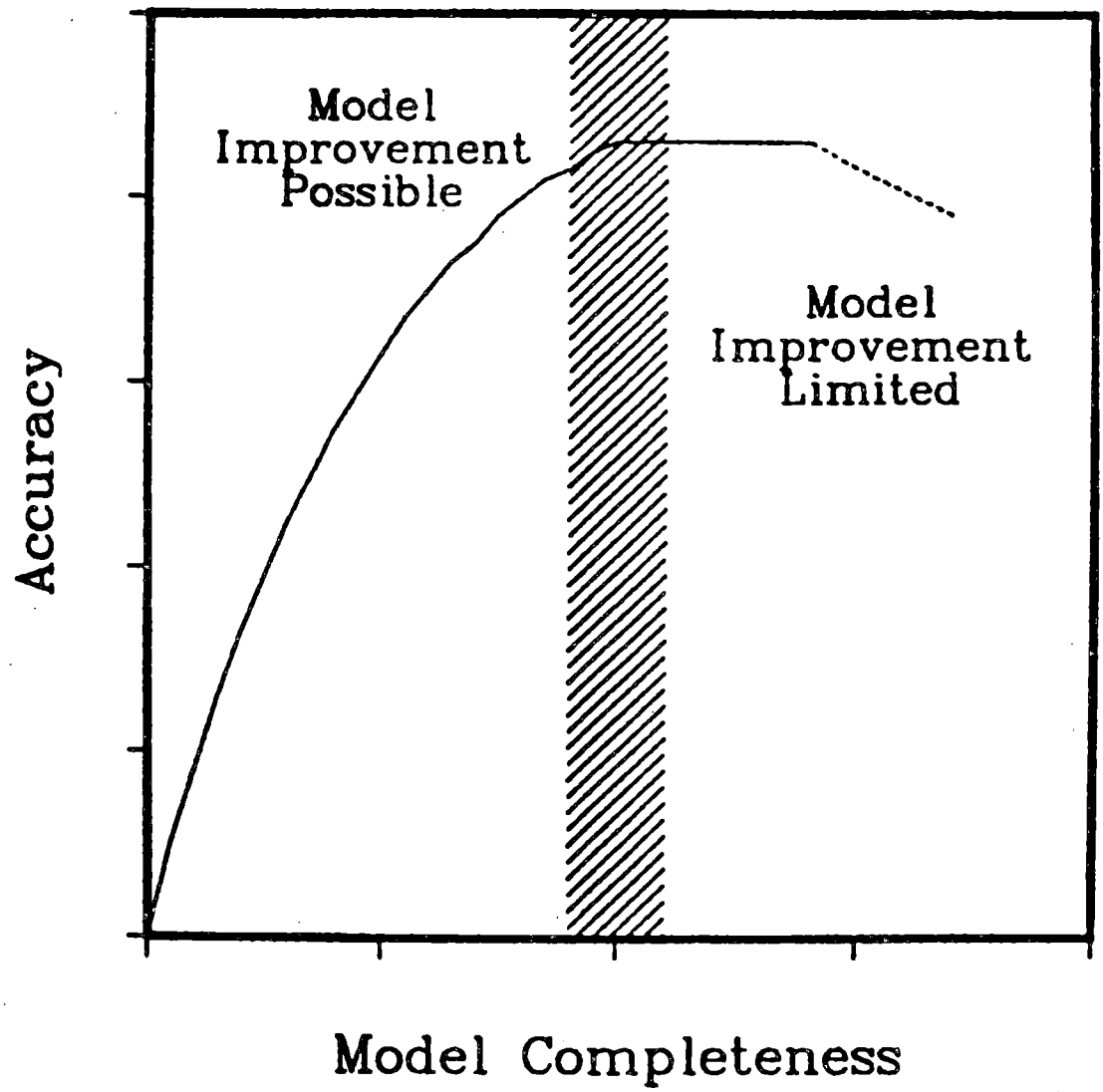

MARCH IMPROVEMENTS

- Many Models Could be Improved
- Lack of Phenomenological Data Base Limits Extent of Many Improvements
- Some Models not Appropriate for Inclusion in MARCH
  - -- Kinetics
  - -- Detailed Steam Explosion Modeling

SENSITIVITY

- MARCH Results are Sensitive to User-Selected Modeling Options and Parameters

- Consensus Results Regarding Reactor Safety Assessments may be Difficult to Achieve

RECOMMENDATIONS

- Robust Program for MARCH Improvement or Development of Alternatives
- Further Assessment of MARCH Capabilities, Especially for BWRs, and Small Containments
- Priorities for Improvement

  (See Report)

ORGANIZATION

To Provide the Necessary Organization for Maintaining and Improving MARCH, the NRC Should:

Designate a Contractor to Provide Code Support with Responsibility To

- Make Changes to MARCH
- Issue Standard Versions of the Code on a Timely Basis,
- Provide Adequate and Updated Documentation for Each Standard Version,
- Provide Documented Sample Problems Run On Each Standard Version,
- Test MARCH and Document Results
- Provide Information Exchange Services For, and Respond to the Needs of, the MARCH Users' Group.

- Sponsor a MARCH Users' Group with Responsibility To

  - Recommend Code Changes to the Code Support Organization,

  - Review User-Proposed Changes,

  - Review the Code Status and Set Priorities for Major Code Modifications,

  - Perform a Continuing Peer Review of MARCH Versions and Associated Documentation,

  - Provide a Forum for Continuing Information Exchange on MARCH Usage and Problems.

RECOMMENDATIONS

APPLICATION OF CURRENT MARCH TO FORMAL SAFETY EVALUATIONS

- EXPLICIT EVALUATION AND DISCUSSION OF CODE LIMITATIONS WITH REGARD TO POTENTIAL FOR INVALIDATING CONCLUSIONS.

- CALCULATIONS USE DOCUMENTED VERSION WITH APPROPRIATE PLANT AND SEQUENCE DATA AND ACCESSIBLE VALUES OF MODELING OPTIONS AND PARAMETERS.

NUREG-0772"

"TECHNICAL BASES FOR ESTIMATING FISSION PRODUCT BEHAVIOR DURING LWR ACCIDENT"

OBJECTIVE: TO PRESENT A DESCRIPTION OF THE BEST TECHNICAL INFORMATION CURRENTLY AVAILABLE FOR ESTIMATING THE RELEASE OF RADIOACTIVE MATERIAL FROM A COMMERCIAL LWR POWER PLANT TO THE ENVIRONMENT DURING POSTULATED SEVERE ACCIDENTS AND TO IDENTIFY WHERE GAPS EXIST IN THE AVAILABLE DATA BASE.

PRESENTED BY

R. R. SHERRY

DIVISION OF ACCIDENT EVALUATION

USNRC

REPORT STRUCTURE

CHAPTER 1 INTRODUCTION, SUMMARY, AND CONCLUSIONS

CHAPTER 2 FISSION PRODUCT FORMATION

CHAPTER 3 ACCIDENT SEQUENCE CHARACTERISTICS

CHAPTER 4 FISSION PRODUCT RELEASE FROM THE FUEL

CHAPTER 5 FISSION PRODUCT CHEMISTRY

CHAPTER 6 FISSION PRODUCT TRANSPORT THROUGH THE PRIMARY CONTAINMENT SYSTEM

CHAPTER 7 FISSION PRODUCT TRANSPORT BEHAVIOR IN CONTAINMENT

CHAPTER 8 PERFORMANCE OF ENGINEERED SAFETY FEATURES

ACKNOWLEDGEMENTS

M. SILBERBERG - REPORT COORDINATOR - NRC

CHAPTER 1.0	R. R. SHERRY, CHAPTER LEAD, NRC M. A. CUNNINGHAM, NRC C. N. KELBER, NRC M. SILBERBERG, NRC
CHAPTER 2.0	R. S. DENNING, CHAPTER LEAD, BATTELLE COLUMBUS LABORATORIES (BCL)
CHAPTER 3.0	R. S. DENNING, CHAPTER LEAD, BCL
CHAPTER 4.0	R. P. WICHNER, CHAPTER LEAD, OAK RIDGE NATIONAL LABORATORY (ORNL) T. S. KRESS, ORNL R. A. LORENZ, ORNL
CHAPTER 5.0	R. M. ELRICK, CHAPTER CO-LEADER, SANDIA NATIONAL LABORATORY (SECTION 5.1 AND 5.2) J. T. BELL, CHAPTER CO-LEADER, ORNL (SECTION 5.3) R. A. SALLACH, SANDIA L. M. TOTH, ORNL D. O. CAMPBELL, ORNL A. P. MALINAUSKAS, ORNL
CHAPTER 6.0	J. A. GIESEKE, CHAPTER LEAD, BCL M. R. KUHLMAN, BCL
CHAPTER 7.0	J. A. GIESEKE, CHAPTER LEAD, BCL R. S. DENNING, BCL K. W. LEE, BCL H. JORDAN, BCL T. C. DAVIS, BCL T. C. KRESS, ORNL
CHAPTER 8.0	W. F. PASEDAG, CHAPTER LEAD, NRC A. K. POSTMA (NRC CONSULTANT) R. ADAMS, ORNL

RECENT ISSUES

CAMPBELL, MALINAUSKAS, AND STRATTON

- IODINE WILL BE RELEASED FROM FUEL AND TRANSPORTED AS A METAL IODIDE (CsI) RATHER THAN AS THE MORE VOLATILE MOLECULAR IODINE (I_2).

- SINCE CsI IS LESS VOLATILE THAN I_2 AND IS MUCH MORE SOLUABLE IN WATER, RELEASES OF IODINE UNDER CERTAIN ACCIDENT CONDITIONS ARE CURRENTLY BEING OVERPREDICTED.

LEVENSON AND RAHN

- CURRENT FISSION PRODUCT RELEASE ESTIMATES FOR THE MOST SEVERE ACCIDENTS ARE ONE TO TWO ORDERS OF MAGNITUDE GREATER THAN THE REALISTIC MAGNITUDE WHICH MIGHT OCCUR.

- NATURAL PROCESSES SUCH AS CHEMICAL REACTIONS, AEROSOL SETTLING, EFFECTS OF MOISTURE, ETC., WILL LIMIT THE RELEASE MAGNITUDE. THESE PHENOMENA WERE NOT ADEQUATELY ACCOUNTED FOR IN PAST ANALYSES (E.G., WASH-1400).

SPECIFIC CONCLUSIONS - NUREG-0772

- CsI SHOULD BE THE PREDOMINANT IODINE FORM UNDER SEVERE ACCIDENT CONDITIONS.

- CsI ATTENUATION WITHIN THE RCS WILL BE GREATER THAN I_2.

- PARTICULATE (FISSION PRODUCT) RETENTION WITHIN RCS CAN BE SUBSTANTIAL FOR CERTAIN SEQUENCES - TRANSIENTS AND SMALL BREAK LOCA'S.

- AEROSOL REMOVAL MECHANISMS WITHIN CONTAINMENT WILL SUBSTANTIALLY REDUCE ATMOSPHERIC RELEASES IF CONTAINMENT FAILURE IS DELAYED.

RESULTS - FP RELEASE FROM FUEL

- EXPERIMENTAL EVIDENCE IS INCONCLUSIVE AS TO CHEMICAL FORM OF IODINE WITHIN THE FUEL ROD OR RELEASED FROM A FUEL ROD.

- THERMODYNAMIC CALCULATION INDICATE CsI SHOULD BE IODINE FORM IN FUEL-CLADDING GAP.

- UPDATED FISSION PRODUCT (AND STRUCTURAL MATERIAL AEROSOL) RELEASE ESTIMATES DEVELOPED FROM DATA OF:

    - o LORENZ
    - o ALBRECHT
    - o PARKER

ORNL DWG 81-178

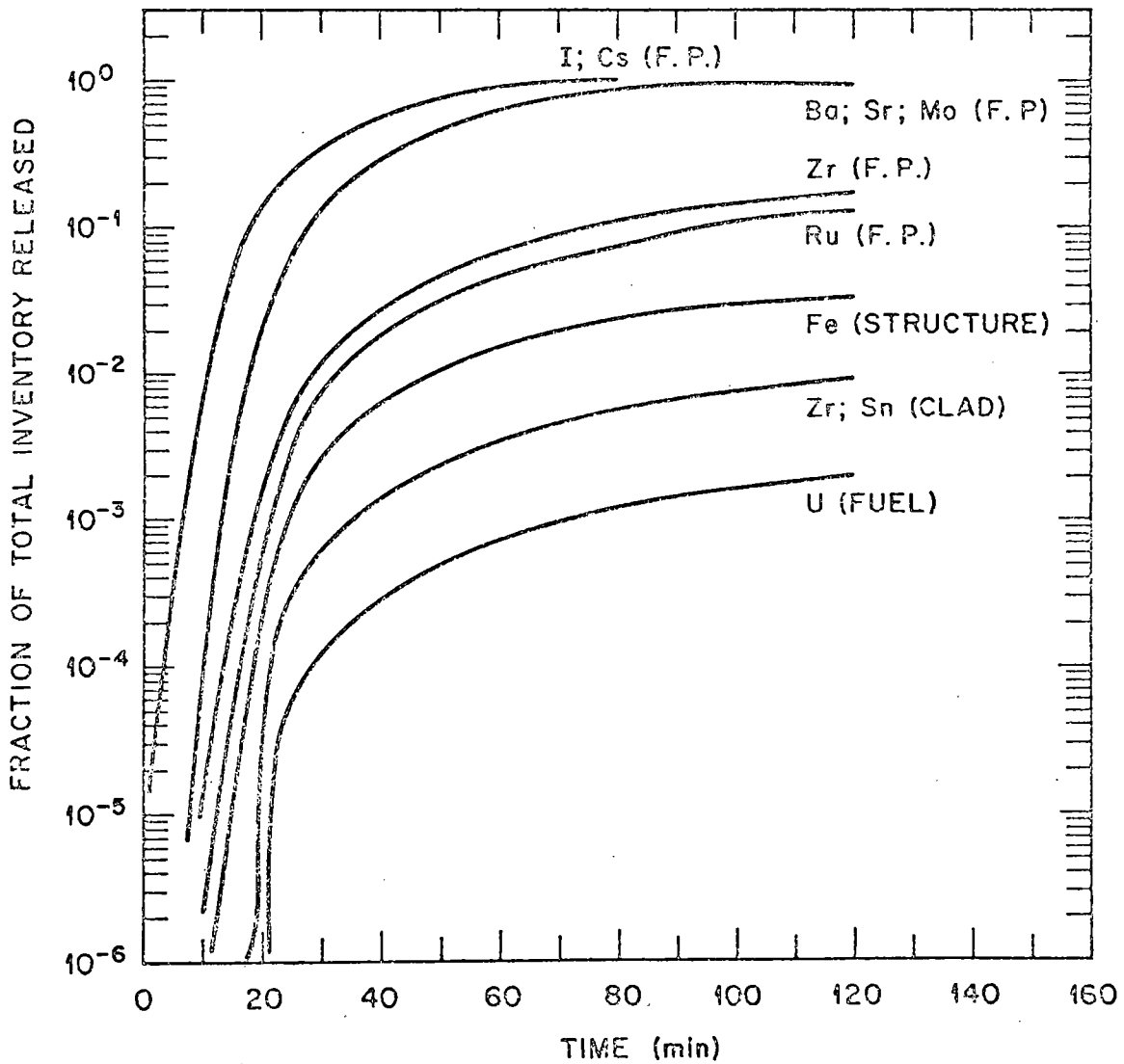

Table I. Comparison of Fraction Release Estimates

NUREG-0772		RSS	
Fission Product Group	20 Min Release Fraction for AB Sequence	Fission Product Group	Melt Release Fraction
I	1.0	I, Br	0.9
Cs	1.0	Cs, Rb	0.8
Te, Ag, Sb	1.0	Te, Sb, Se	0.15
Ba	0.5		
Sr	0.3	Ba, Sr	0.1
Zr	0.03		
Ru	0.02	Noble metals	0.03
Structure	0.005		
Clad	0.002	Rare earths	0.003
Fuel	0.003		

FISSION PRODUCT CHEMISTRY

HIGH TEMPERATURE VAPOR PHASE

- THERMODYNAMIC CALCULATIONS FOR THE SYSTEM (CESIUM-IODINE-STEAM-AND HYDROGEN OR OXYGEN) INDICATE THE FOLLOWING BEHAVIOR:

  - o UNDER REDUCING CONDITIONS -

    CsI IS PREDOMINANT IODINE SPECIES AT LOWER TEMPERATURES

    HI AND I OCCUR AT HIGHER TEMPERATURES

    CsOH AND Cs ARE PREDOMINANT Cs FORMS (IN ADDITION TO CsI)

  - o UNDER OXIDIZING CONDITIONS -

    I IS DOMINANT IODINE SPECIES

    CsOH IS DOMINANT CESIUM SPECIES

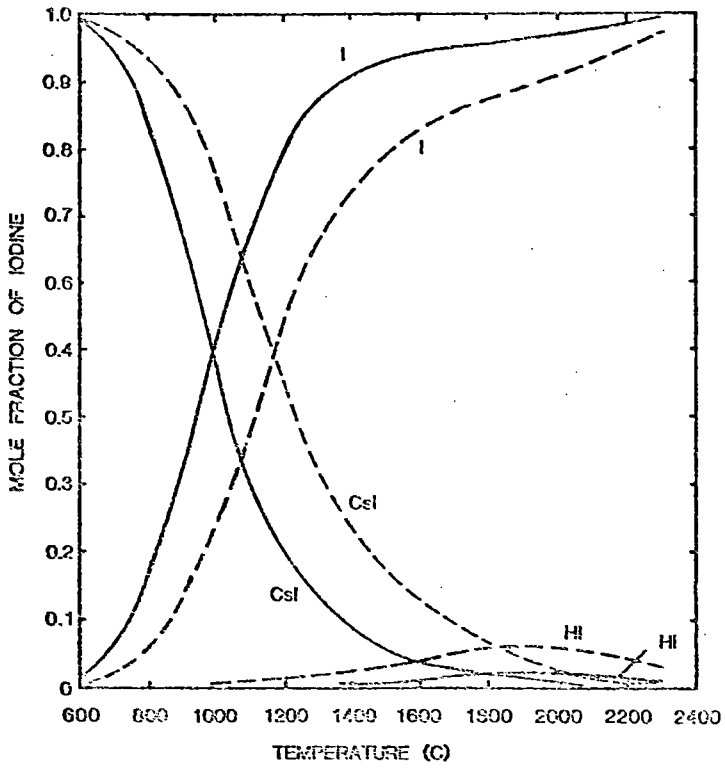

Fig. 5.a $I/H_2O = 2 \times 10^{-5}$; H/O = 1.5; Cs/I = 10;
(——) PRESSURE EQUALS 1 BAR.
(- - - -) PRESSURE EQUALS 150 BARS.

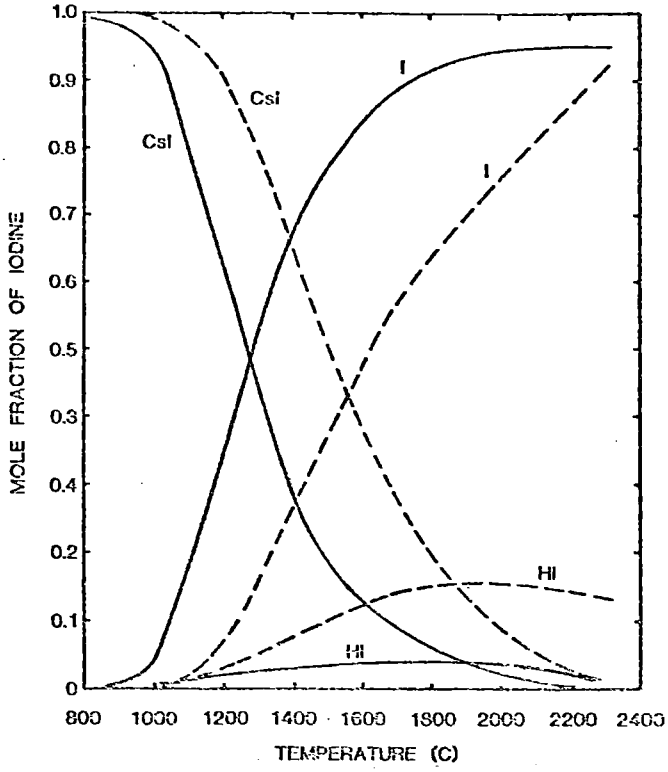

Fig. 5.b $I/H_2O = 2 \times 10^{-5}$; H/O = 2.0; Cs/I = 10;
(——) PRESSURE EQUALS 1 BAR.
(- - - -) PRESSURE EQUALS 150 BARS.

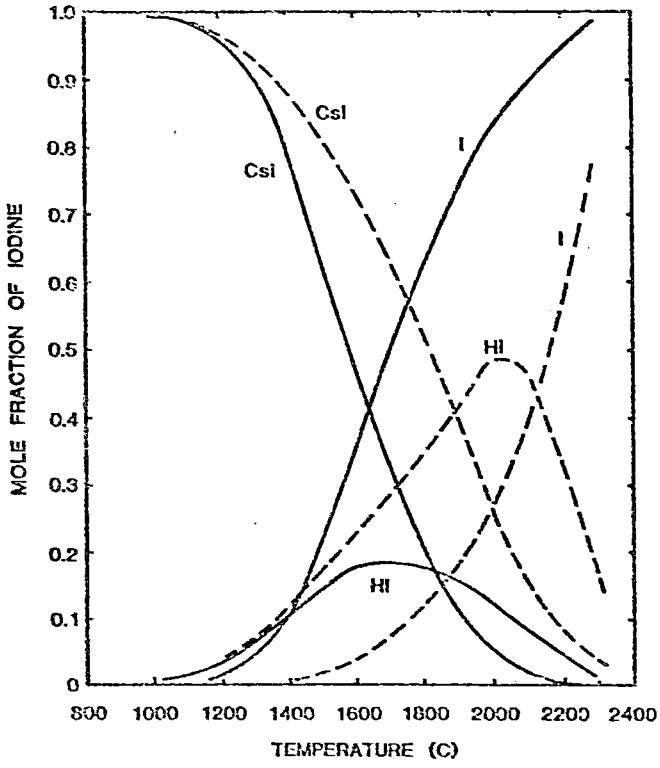

Fig. 5.c $I/H_2O = 2 \times 10^{-5}$; H/O = 3.0; Cs/I = 10;
(——) PRESSURE EQUALS 1 BAR.
(- - - -) PRESSURE EQUALS 150 BARS.

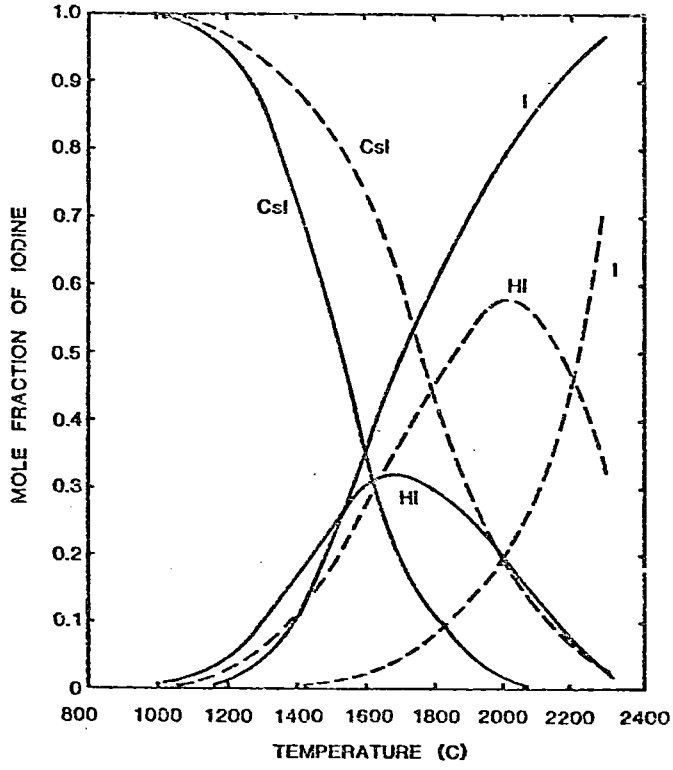

Fig. 5.d $I/H_2O = 2 \times 10^{-5}$; H/O = 30; Cs/I = 10;
(——) PRESSURE EQUALS 1 BAR.
(- - - -) PRESSURE EQUALS 150 BARS.

AQUEOUS PHASE CHEMISTRY

- IODINE AT EQUILIBRIUM IN AQUEOUS REACTOR COOLANT SOLUTIONS WILL EXIST PRIMARILY AS THE STABLE IODIDE (I^-) AND IODATE (IO^-_3) SPECIES.

- I_2 REACTS RAPIDLY WITH WATER VIA:

$$I_2 + H_2O = H^+ + I^- + HOI \qquad (1)$$

$$3HOI = 2I^- + 3H^+ + IO^-_3 \qquad (2)$$

- IODINE ALREADY IN THE REDUCED FORM AS CsI WILL RAPIDLY DISOLVE AND ENTER SOLUTION AS THE IONIC IODIDE (I^-) SPECIES.

ORNL-DWG 81-14791

PARTITION COEFFICIENTS for AQUEOUS IODINE

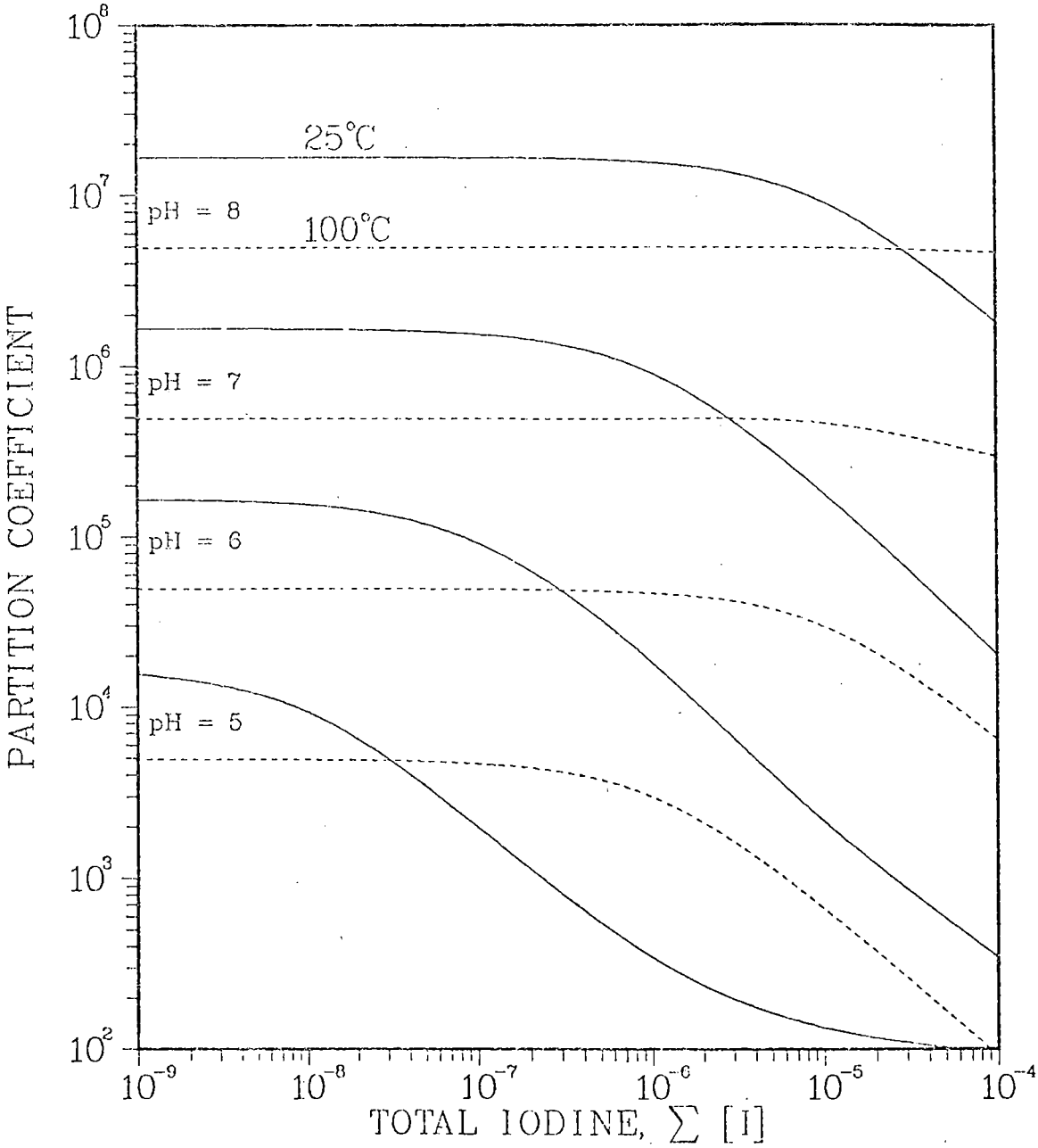

ORNL-DWG 81-14752

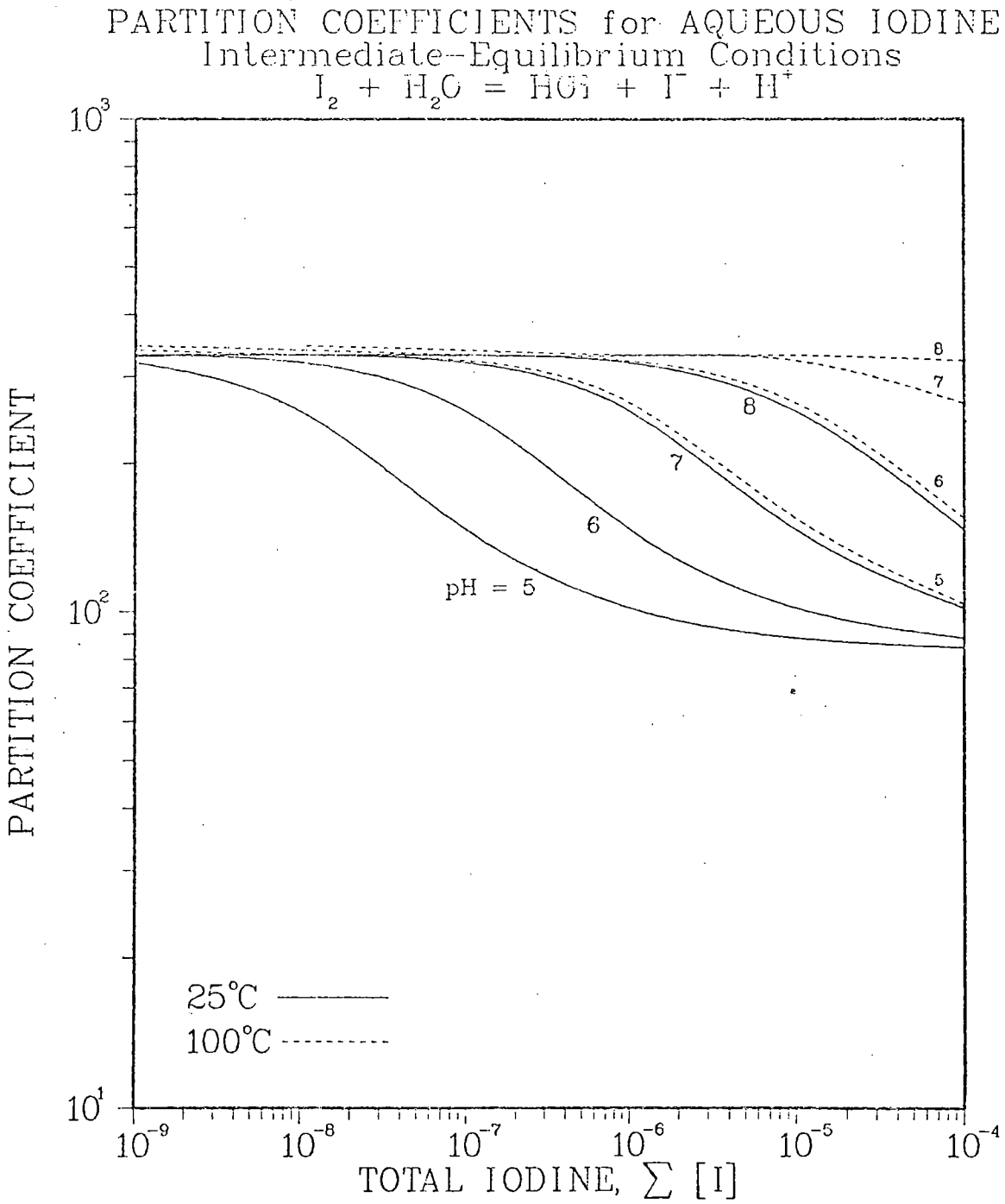

RESULTS - PRIMARY COOLANT SYSTEM TRANSPORT

- RCS FISSION PRODUCT TRANSPORT BEHAVIOR ANALYSES WERE PERFORMED USING THE TRAP-MELT AND QUICK CODES.

- I_2 DEPOSITION IN RCS WILL BE LOW FOR SEQUENCES WHERE PATHWAY IS DRY.

- FOR FLOWPATHS CONTACTING WATER, I_2 REMOVAL FROM THE GAS PHASE CAN BE SIGNIFICANT.

- CsI RETENTION IN RCS IS HIGHLY VARIABLE AND DEPENDS UPON:

    (1) SYSTEM TEMPERATURES

    (2) AVAILABILITY OF WATER

    (3) AEROSOL CHARACTERISTICS

- RETENTION OF CsI WITHIN RCS SIGNIFICANTLY GREATER THAN I_2 RETENTION.

RESULTS - PRIMARY SYSTEM TRANSPORT (CONTINUED)

- RETENTION WITHIN THE RCS OF LESS VOLATILE FISSION PRODUCTS BEING TRANSPORTED AS AEROSOLS CAN BE SUBSTANTIAL FOR SEQUENCES WHERE AEROSOL MASS CONCENTRATIONS ARE HIGH, RCS RETENTION TIMES ARE LONG, AND SYSTEM FLOW RATES ARE LOW, E.G., TRANSIENT AND SMALL BREAK INITIATED CORE MELT ACCIDENT SEQUENCES.

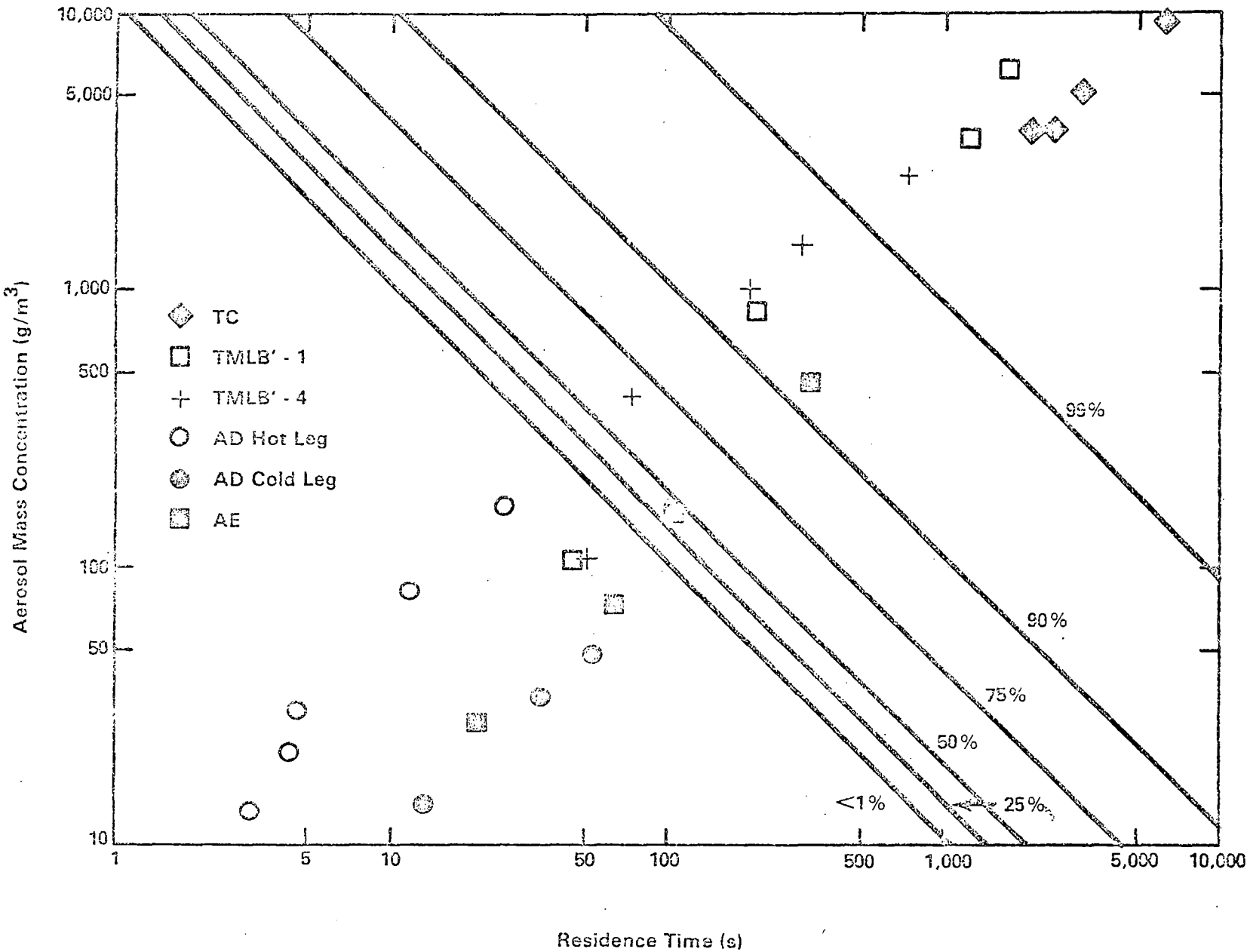
10,000
5,000
1,000
500
100
50
10
1
5
10
50
100
500
1,000
5,000
10,000
Aerosol Mass Concentration (g/m3)
Residence Time (s)
TC
TMLB' - 1
TMLB' - 4
AD Hot Leg
AD Cold Leg
AE
99%
90%
75%
50%
25%
<1%

RESULTS - CONTAINMENT FISSION PRODUCT TRANSPORT

- CONTAINMENT FISSION PRODUCT TRANSPORT BEHAVIOR ANALYSES WERE PERFORMED USING THE CORRAL-2, QUICK, HAARM-3, AND NAUA-4 CODES.

- FOR THE MOST SEVERE ACCIDENT SEQUENCES (I.E., A CORE MELT ACCIDENT WITH EARLY, ABOVE GROUND CONTAINMENT FAILURE AND IMPAIRMENT OF CONTAINMENT FISSION PRODUCT MITIGATION FEATURES) THE RETENTION OF IODINE IN EITHER VAPOR (I_2) OR PARTICULATE FORM WITHIN CONTAINMENT WAS APPROXIMATELY 50%.

- FOR A SEVERE CORE DAMAGE ACCIDENT (~50% FUEL MELT) WITH DELAYED ECCS OPERATION, NO LOSS OF CONTAINMENT INTEGRITY AND CONTAINMENT SAFETY FEATURES OPERABLE, THE ATTENUATION FACTOR FOR ALL FPs (EXCEPT NOBLE GASES) WAS GREATER THAN 100,000.

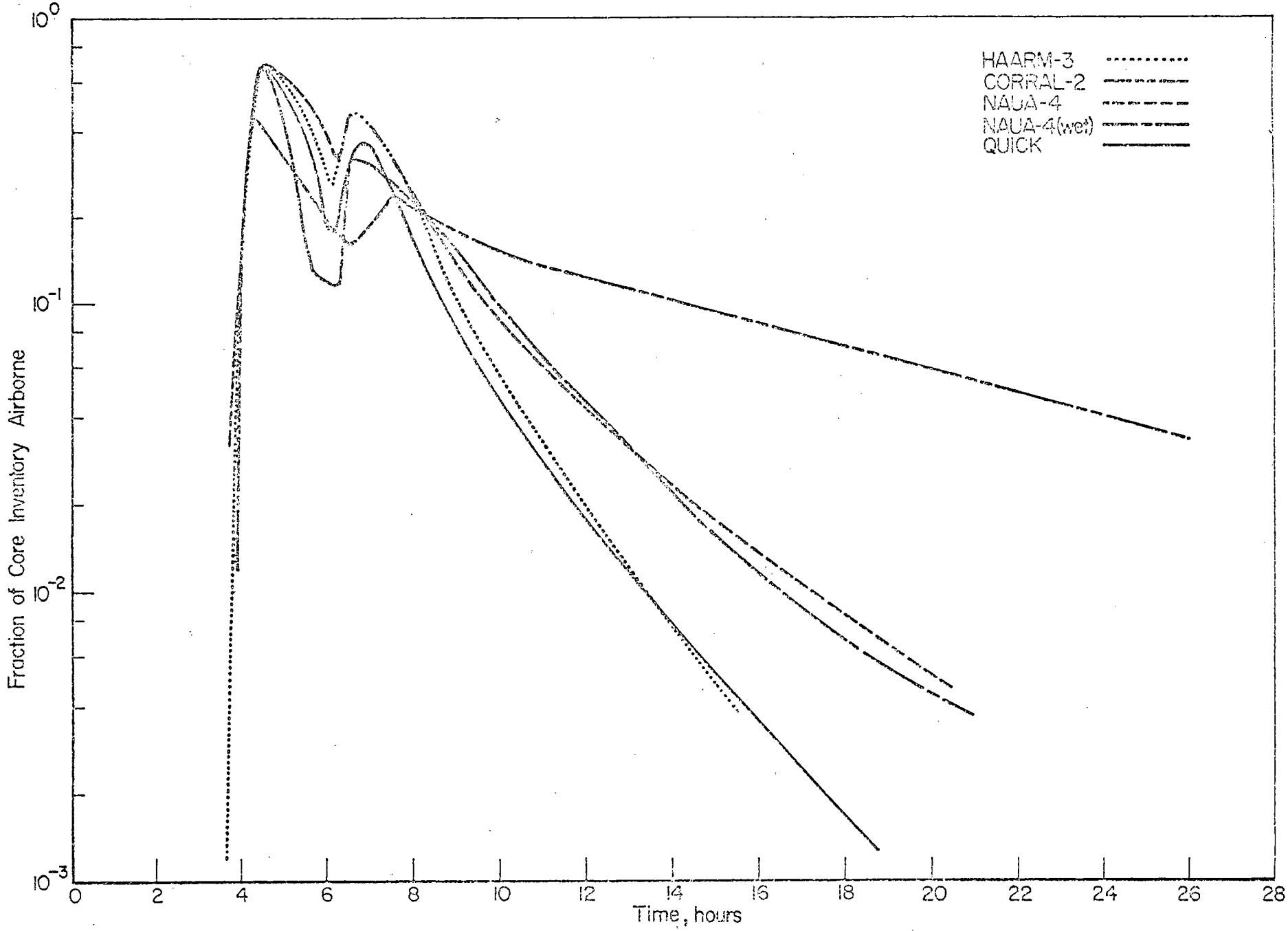
HAARM-3
CORRAL-2
NAUA-4
NAUA-4(wet)
QUICK
Fraction of Core Inventory Airborne
10^{0}
10^{-1}
10^{-2}
10^{-3}
0
2
4
6
8
10
12
14
16
18
20
22
24
26
28
Time, hours

RESULTS - ENGINEERED SAFETY FEATURES EVALUATION

EIGHT SYSTEMS EVALUATED -

(A) EFFECTIVE UNDER SEVERE ACCIDENT CONDITIONS

(1) CONTAINMENT SPRAYS

(2) BWR SUPPRESSION POOLS

(3) PWR ICE CONDENSERS

(B) LESS EFFECTIVE FOR SEVERE ACCIDENTS FOR NOTED REASONS

(4) RECIRCULATING FILTER SYSTEM (PLUGGING BY AEROSOLS)

(5) BWR MSIV LEAKAGE CONTROL SYSTEMS (LEAKPATH BYPASSES SYSTEM)

(6) AUXILIARY BUILDING FILTER SYSTEM (LEAKPATH BYPASS OR AUXILIARY BUILDING FAILURE)

(7) DUAL CONTAINMENTS AND STANDBY GAS TREATMENT SYSTEMS (LEAKPATH BYPASS AND STRUCTURAL FAILURE)

(8) CONTAINMENT LEAKAGE REQUIREMENTS

MAJOR CONCLUSIONS

1) UNCERTAINTIES IN PREDICTING ATMOSPHERIC RELEASE SOURCE TERMS ARE VERY LARGE (AT LEAST AN ORDER OF MAGNITUDE).

2) SOURCE TERMS FOR CERTAIN ACCIDENT SEQUENCES MAY HAVE BEEN OVERESTIMATED IN PAST STUDIES (E.G., WASH-1400).

   - SMALL BREAKS AND TRANSIENTS
   - SEQUENCES WITH DELAYED CONTAINMENT FAILURE

3) CsI SHOULD BE PREDOMINANT CHEMICAL FORM OF IODINE.

MAJOR UNCERTAINTIES AND DATA NEEDS

IDENTIFIED IN NUREG-0772

1) RCS AEROSOL BEHAVIOR (EXPERIMENTAL DATA FOR MODEL VERIFICATION).

2) RCS THERMAL/HYDRAULIC MODELS UNDER CORE MELT ACCIDENT CONDITIONS.

3) CONTAINMENT FAILURE TIME, MODE, LOCATION (EXPERIMENTAL DATA AND ANALYSIS).

4) FISSION PRODUCT CHEMISTRY (EXPERIMENTAL DATA).

5) LESS VOLATILE FISSION PRODUCT, CONTROL MATERIAL, AND STRUCTURAL MATERIAL AEROSOL FORMATION RATES (IN-VESSEL AND DURING INTERACTION WITH CONCRETE) - (EXPERIMENTAL DATA).

6) AEROSOL BEHAVIOR IN CONDENSING STEAM ATMOSPHERES (EXPERIMENTAL DATA).

7) REMOVAL OF PARTICULATE FISSION PRODUCTS IN WATER POOLS AND ICE BEDS (EXPERIMENTAL DATA AND MODELS).

8) THE EFFECT OF A HYDROGEN BURN ON FP PHYSICAL AND CHEMICAL FORMS (EXPERIMENTAL).

9) COUPLED MODELS OF CONTAINMENT FISSION PRODUCT VAPOR TRANSPORT, AEROSOL BEHAVIOR, STEAM EFFECTS, AND EFFECTS OF ESFs.

NRC FORM 335 (11-81)

U.S. NUCLEAR REGULATORY COMMISSION

BIBLIOGRAPHIC DATA SHEET

1. REPORT NUMBER *(Assigned by DDC)*
NUREG/CP-0024, Vol. 3

4. TITLE AND SUBTITLE *(Add Volume No., if appropriate)*
Ninth Water Reactor Safety Research Information Meeting

2. *(Leave blank)*

3. RECIPIENT'S ACCESSION NO.

7. AUTHOR(S)

5. DATE REPORT COMPLETED
MONTH | YEAR

9. PERFORMING ORGANIZATION NAME AND MAILING ADDRESS *(Include Zip Code)*
U.S. Nuclear Regulatory Commission
Office of Nuclear Regulatory Research
Washington, DC 20555

DATE REPORT ISSUED
MONTH | YEAR
March 1982

6. *(Leave blank)*

8. *(Leave blank)*

12. SPONSORING ORGANIZATION NAME AND MAILING ADDRESS *(Include Zip Code)*
Same as 9, above.

10. PROJECT/TASK/WORK UNIT NO.

11. FIN NO.

13. TYPE OF REPORT

PERIOD COVERED *(Inclusive dates)*

15. SUPPLEMENTARY NOTES

14. *(Leave blank)*

16. ABSTRACT *(200 words or less)*

This is a compilation of papers which were presented at the Ninth Water Reactor Safety Research Information Meeting. It consists of three volumes.

17. KEY WORDS AND DOCUMENT ANALYSIS

17a. DESCRIPTORS

17b. IDENTIFIERS/OPEN-ENDED TERMS

18. AVAILABILITY STATEMENT
Unlimited

19. SECURITY CLASS *(This report)*
Unclassified

21. NO. OF PAGES

20. SECURITY CLASS *(This page)*
Unclassified

22. PRICE
S

UNITED STATES
NUCLEAR REGULATORY COMMISSION
WASHINGTON, D. C. 20555

OFFICIAL BUSINESS
PENALTY FOR PRIVATE USE, $300

POSTAGE AND FEES PAID
U.S. NUCLEAR REGULATORY
COMMISSION

Name Mail Stop Due Date

Return to: 823 LIBRARY/SNL, MS 0731